THE BACTERIAL CELL: COUPLING BETWEEN GROWTH, NUCLEOID REPLICATION, CELL DIVISION AND SHAPE

EDITED BY: Arieh Zaritsky, Conrad L. Woldringh and Jaan Männik
PUBLISHED IN: Frontiers in Microbiology

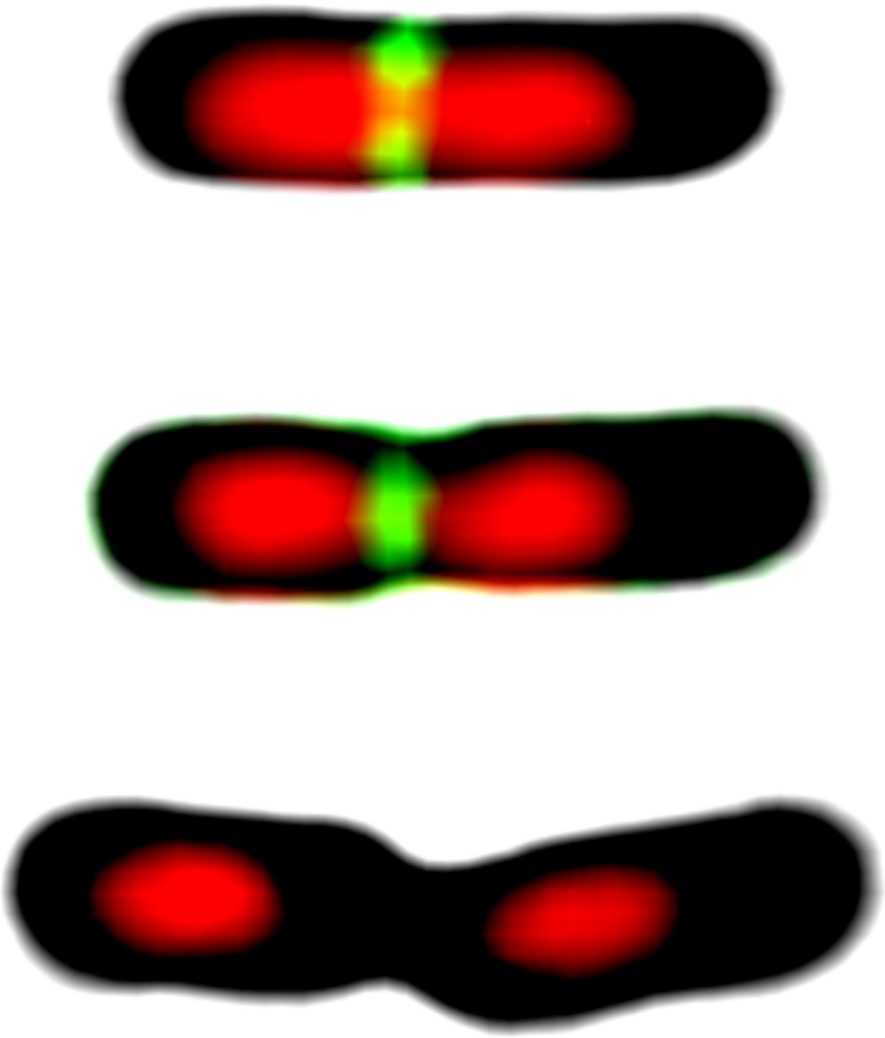

frontiers Research Topics

frontiers

Frontiers Copyright Statement

© Copyright 2007-2016 Frontiers Media SA. All rights reserved.

All content included on this site, such as text, graphics, logos, button icons, images, video/audio clips, downloads, data compilations and software, is the property of or is licensed to Frontiers Media SA ("Frontiers") or its licensees and/or subcontractors. The copyright in the text of individual articles is the property of their respective authors, subject to a license granted to Frontiers.

The compilation of articles constituting this e-book, wherever published, as well as the compilation of all other content on this site, is the exclusive property of Frontiers. For the conditions for downloading and copying of e-books from Frontiers' website, please see the Terms for Website Use. If purchasing Frontiers e-books from other websites or sources, the conditions of the website concerned apply.

Images and graphics not forming part of user-contributed materials may not be downloaded or copied without permission.

Individual articles may be downloaded and reproduced in accordance with the principles of the CC-BY licence subject to any copyright or other notices. They may not be re-sold as an e-book.

As author or other contributor you grant a CC-BY licence to others to reproduce your articles, including any graphics and third-party materials supplied by you, in accordance with the Conditions for Website Use and subject to any copyright notices which you include in connection with your articles and materials.

All copyright, and all rights therein, are protected by national and international copyright laws.

The above represents a summary only. For the full conditions see the Conditions for Authors and the Conditions for Website Use.

ISSN 1664-8714
ISBN 978-2-88919-817-7
DOI 10.3389/978-2-88919-817-7

About Frontiers

Frontiers is more than just an open-access publisher of scholarly articles: it is a pioneering approach to the world of academia, radically improving the way scholarly research is managed. The grand vision of Frontiers is a world where all people have an equal opportunity to seek, share and generate knowledge. Frontiers provides immediate and permanent online open access to all its publications, but this alone is not enough to realize our grand goals.

Frontiers Journal Series

The Frontiers Journal Series is a multi-tier and interdisciplinary set of open-access, online journals, promising a paradigm shift from the current review, selection and dissemination processes in academic publishing. All Frontiers journals are driven by researchers for researchers; therefore, they constitute a service to the scholarly community. At the same time, the Frontiers Journal Series operates on a revolutionary invention, the tiered publishing system, initially addressing specific communities of scholars, and gradually climbing up to broader public understanding, thus serving the interests of the lay society, too.

Dedication to Quality

Each Frontiers article is a landmark of the highest quality, thanks to genuinely collaborative interactions between authors and review editors, who include some of the world's best academicians. Research must be certified by peers before entering a stream of knowledge that may eventually reach the public - and shape society; therefore, Frontiers only applies the most rigorous and unbiased reviews.
Frontiers revolutionizes research publishing by freely delivering the most outstanding research, evaluated with no bias from both the academic and social point of view.
By applying the most advanced information technologies, Frontiers is catapulting scholarly publishing into a new generation.

What are Frontiers Research Topics?

Frontiers Research Topics are very popular trademarks of the Frontiers Journals Series: they are collections of at least ten articles, all centered on a particular subject. With their unique mix of varied contributions from Original Research to Review Articles, Frontiers Research Topics unify the most influential researchers, the latest key findings and historical advances in a hot research area! Find out more on how to host your own Frontiers Research Topic or contribute to one as an author by contacting the Frontiers Editorial Office: **researchtopics@frontiersin.org**

THE BACTERIAL CELL: COUPLING BETWEEN GROWTH, NUCLEOID REPLICATION, CELL DIVISION AND SHAPE

Topic Editors:
Arieh Zaritsky, Ben-Gurion University of the Negev, Israel
Conrad L. Woldringh, University of Amsterdam, Netherlands
Jaan Männik, University of Tennessee, USA

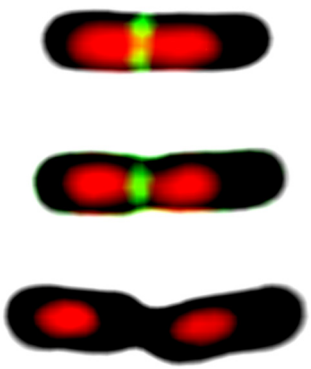

Progression of nucleoid replication, cell growth and division in *Escherichia coli* (from top to bottom). The exponentially growing cell is chosen from a mutant strain lacking *slmA* and *min* genes. The nucleoids are labelled red (HupA-mCherry) and the cytokinetic ring, green (ZipA-GFP).
Image by: J. Männik and M. W. Bailey

Bacterial Physiology was inaugurated as a discipline by the seminal research of Maaløe, Schaechter and Kjeldgaard published in 1958. Their work clarified the relationship between cell composition and growth rate and led to unravel the temporal coupling between chromosome replication and the subsequent cell division by Helmstetter et al. a decade later. Now, after half a century this field has become a major research direction that attracts interest of many scientists from different disciplines. The outstanding question how the most basic cellular processes - mass growth, chromosome replication and cell division - are inter-coordinated in both space and time is still unresolved at the molecular level. Several particularly pertinent questions that are intensively studied follow: (a) what is the primary signal to place the Z-ring precisely between the two replicating and segregating nucleoids? (b) Is this coupling related to the structure and position of the nucleoid itself? (c) How does a bacterium determine and maintain its shape and dimensions? Possible answers include gene expression-based mechanisms, self-organization of protein assemblies and physical principles such as micro-phase separations by excluded volume interactions, diffusion ratchets and membrane stress or curvature. The relationships between biochemical reactions and physical forces are yet to be conceived and discovered.

This e-book discusses the above mentioned and related questions. The book also serves as an important depository for state-of-the-art technologies, methods, theoretical simulations and innovative ideas and hypotheses for future testing. Integrating the information gained

from various angles will likely help decipher how a relatively simple cell such as a bacterium incorporates its multitude of pathways and processes into a highly efficient self-organized system. The knowledge may be helpful in the ambition to artificially reconstruct a simple living system and to develop new antibacterial drugs.

Citation: Zaritsky, A., Woldringh, C. L., Männik, J., eds. (2016). The Bacterial Cell: Coupling between Growth, Nucleoid Replication, Cell Division and Shape. Lausanne: Frontiers Media. doi: 10.3389/978-2-88919-817-7

Table of Contents

06 ***Editorial: The bacterial cell: coupling between growth, nucleoid replication, cell division, and shape***
Jaan Männik, Conrad L. Woldringh and Arieh Zaritsky

1. Historical overview

09 ***A brief history of bacterial growth physiology***
Moselio Schaechter

14 ***A balanced perspective on unbalanced growth and thymineless death***
Philip C. Hanawalt

21 ***A ten-year search for synchronous cells: obstacles, solutions, and practical applications***
Charles E. Helmstetter

31 ***Chromosome replication, cell growth, division and shape: a personal perspective***
Arieh Zaritsky and Conrad L. Woldringh

2. The nucleoid

42 ***The orisome: structure and function***
Alan C. Leonard and Julia E. Grimwade

55 ***A Replisome's journey through the bacterial chromosome***
Thomas R. Beattie and Rodrigo Reyes-Lamothe

67 ***Segregation of chromosome arms in growing and non-growing* Escherichia coli *cells***
Conrad L. Woldringh, Flemming G. Hansen, Norbert O. E. Vischer and Tove Atlung

79 ***The spatial biology of transcription and translation in rapidly growing* Escherichia coli**
Somenath Bakshi, Heejun Choi and James C. Weisshaar

94 ***The dynamic nature and territory of transcriptional machinery in the bacterial chromosome***
Ding J. Jin, Cedric Cagliero, Carmen M. Martin, Jerome Izard and Yan N. Zhou

108 ***The nucleoid as a smart polymer***
Vittore F. Scolari, Bianca Sclavi and Marco Cosentino Lagomarsino

112 **Thymineless death*, at the origin***
Elena C. Guzmán and Carmen M. Martín

119 ***Perturbed states of the bacterial chromosome: a thymineless death case study***
Lev Ostrer, Bree L. Hamann and Arkady Khodursky

3. Cell envelope and shape

126 ***Light-dependent governance of cell shape dimensions in cyanobacteria***
Beronda L. Montgomery

134 ***Molecular mechanisms for the evolution of bacterial morphologies and growth modes***
Amelia M. Randich and Yves V. Brun

147 ***Structural constraints and dynamics of bacterial cell wall architecture***
Miguel A. de Pedro and Felipe Cava

157 ***The membrane: transertion as an organizing principle in membrane heterogeneity.***
Kouji Matsumoto, Hiroshi Hara, Itzhak Fishov, Eugenia Mileykovskaya and Vic Norris

4. The divisome

178 ***Why do bacteria divide?***
Vic Norris

188 ***How much territory can a single* E. coli *cell control?***
Ziad W. El-Hajj and Elaine B. Newman

200 ***The stoichiometric divisome: a hypothesis.***
Alexander J. F. Egan and Waldemar Vollmer

206 ***Cell age dependent concentration of* Escherichia coli *divisome proteins analyzed with ImageJ and ObjectJ***
Norbert O. E. Vischer, Jolanda Verheul, Marten Postma, Bart van den Berg van Saparoea, Elisa Galli, Paolo Natale, Kenn Gerdes, Joen Luirink, Waldemar Vollmer, Miguel Vicente and Tanneke den Blaauwen

224 ***Tetracycline hypersensitivity of an* ezrA *mutant links GalE and TseB (YpmB) to cell division***
Pamela Gamba, Eva Rietkötter, Richard A. Daniel and Leendert W. Hamoen

239 ***MioC and GidA proteins promote cell division in* E. coli**
Mark Lies, Bryan J. Visser, Mohan C. Joshi, David Magnan and David Bates

251 ***Interaction sites of DivIVA and RodA from* Corynebacterium glutamicum**
Boris Sieger and Marc Bramkamp

262 ***Multi-color imaging of the bacterial nucleoid and division proteins with blue, orange, and near-infrared fluorescent proteins***
Fabai Wu, Erwin Van Rijn, Bas G. C. Van Schie, Juan E. Keymer and Cees Dekker

5. Mechanisms for spatial and temporal couplings

277 ***Spatial coordination between chromosomes and cell division proteins in* Escherichia coli**
Jaan Männik and Matthew W. Bailey

285 ***The Min system and other nucleoid-independent regulators of Z ring positioning.***
Veronica W. Rowlett and William Margolin

295 ***Simultaneous regulation of cell size and chromosome replication in bacteria.***
Po-Yi Ho and Ariel Amir

305 ***Size sensors in bacteria, cell cycle control, and size control.***
Lydia Robert

314 ***Self-consistent examination of Donachie's constant initiation size at the single-cell level***
Sattar Taheri-Araghi

frontiers in Microbiology

EDITORIAL
published: 15 February 2016
doi: 10.3389/fmicb.2016.00116

Editorial: The Bacterial Cell: Coupling between Growth, Nucleoid Replication, Cell Division, and Shape

Jaan Männik[1]*, *Conrad L. Woldringh*[2] *and Arieh Zaritsky*[3]

[1] Department of Physics and Astronomy, Department of Biochemistry and Molecular and Cellular Biology, University of Tennessee, Knoxville, TN, USA, [2] Bacterial Cell Biology, Faculty of Science, Swammerdam Institute for Life Sciences, University of Amsterdam, Amsterdam, Netherlands, [3] Faculty of Natural Sciences, Ben-Gurion University of the Negev, Be'er-Sheva, Israel

Keywords: chromosome replication, nucleoid, cell division, divisome, envelope, cell shape, *Escherichia coli*, cell cycle

The Editorial on the Research Topic

The Bacterial Cell: Coupling between Growth, Nucleoid Replication, Cell Division, and Shape

INTRODUCTION

The nucleoid and cell envelope are two unique macromolecules that define a bacterium. To ensure that the essential genetic information is carried faithfully from one generation to the next their duplications must be coupled. Research dating back more than half a century established that this is realized at the level of replication-initiation and cell division. These seminal investigations demonstrated that cell size determines when replication starts and that, in turn, the progress in replication determines when cell division processes occur. Moreover, cell division was later established to be spatially controlled by the structure and position of the nucleoid. Despite extensive research over the past 60 years, detailed understanding on how these spatio-temporal couplings are realized at the molecular level is yet to emerge. The aim in creating this e-book has been to bring together scientists from different backgrounds spanning biology, chemistry and physics to address these fundamental mechanisms in a bacterial cell. The book starts with a historical overview of the research that has established the field. It then advances through series of reviews and research articles devoted to the nucleoid, cell envelope, and their temporary hyper-structures, the orisome, replisome, and divisome. Finally, coupling between them is discussed in the last set of contributions.

HISTORICAL OVERVIEW

The first evidence of coupling between duplications of the bacterial cell envelope and the nucleoid was revealed in the 1950s and 1960s. Milestones in this research were demonstrations of replication initiation at a constant cell mass per *oriC* and constant *C* and *D*, dissociated from growth dynamics, where *C* denotes replication time and *D* time from replication–termination to the separation between the subsequent daughter cells. These findings form the basis of our understanding of physiology of bacterial cell duplication and guide the current research. Historical accounts of how these ideas came about are covered in the e-book by the scientists who were instrumental in developing these concepts (Hanawalt; Helmstetter; Schaechter; Zaritsky and Woldringh). The articles dwell on scientific achievements and personal experiences, which endows the new generation of scientists valuable perspective.

OPEN ACCESS

Edited and reviewed by:
Marc Strous,
University of Calgary, Canada

***Correspondence:**
Jaan Männik
jmannik@utk.edu

Specialty section:
This article was submitted to Microbial Physiology and Metabolism, a section of the journal Frontiers in Microbiology

Received: *01 December 2015*
Accepted: *22 January 2016*
Published: *15 February 2016*

Citation:
Männik J, Woldringh CL and Zaritsky A (2016) Editorial: The Bacterial Cell: Coupling between Growth, Nucleoid Replication, Cell Division, and Shape. Front. Microbiol. 7:116. doi: 10.3389/fmicb.2016.00116

THE NUCLEOID

The nucleoid as a central macromolecular complex of bacterial cell harbors several hyper-structures that are essential to its organization and coupling to the envelope. These hyperstructures include orisomes, replisomes, transcriptional assemblies, and transertional linkages that connect DNA through transcribed mRNA and coupled translated membrane protein to the plasma membrane of the cell. Leonard and Grimwade describe how a timing mechanism, based on unwinding of *oriC* by the highly conserved DnaA, starts the orisome assembly. Next, the composition and architecture of the replisome is discussed with emphasis on dynamics and stability during its "journey" from origin to terminus (Beattie and Reyes-Lamothe). Despite detailed knowledge of the orisome and replisome components from both *in vivo* and *in vitro* studies, we have little understanding of how these structures are spatially correlated and physically positioned in the cell. Regarding this aspect, Woldringh et al. present new data on movement and positioning of fluorescently tagged chromosome arms in slow-growing *Escherichia coli* cells. Remarkably, the observed segregation patterns were similar to those obtained during run-off DNA replication in rifampicin-inhibited cells, suggesting that segregation is passively driven by *de novo* DNA synthesis.

Analysis of super-resolution fluorescence images of ribosomes and RNA polymerase in rapidly growing *E. coli* cells enabled Bakshi et al. to propose a "translation-centric" view of the compartmentalization of cytoplasm and nucleoid. Their observations are supported by time-dependent effects of rifampicin and chloramphenicol inhibition on nucleoid-ribosome morphology and could be simulated by a physical model assuming entropic contributions and excluded volume interactions between ribosomal subunits and DNA. In a more "transcription-centric" view of nucleoid morphology, Jin et al. describe how multiple ribosomal RNA operons form a nucleolus-like structure at the periphery of the nucleoid.

How these cytological observations of nucleoid behavior can be understood in a more quantitative, physical perspective remains to be seen. For instance, following a well-known concept in material science, Scolari et al. provoke us to think of the bacterial nucleoid as a smart polymer—a gel-like substance that shows a variety of responsive behaviors to external stimuli such as temperature, pH, and ionic strength.

Coupling between mass growth and chromosome replication has been studied for six decades using mutants defective in thymine biosynthesis (Guzmán and Martín). Yet, what leads to thymineless death and whether this process is actively controlled are still open questions (Ostrer et al).

CELL ENVELOPE AND SHAPE

Different bacteria display different cell shapes in reaction to environmental changes, including light-dependent responses (Montgomery). The underlying shape changes depend on the peptidoglycan synthesizing machinery, which is largely conserved and modular as reviewed by Randich and Brun. On the other hand, as emphasized by De Pedro and Cava, the structural diversity of the peptidoglycan wall is larger than expected on the basis of *E. coli* data. An intriguing hypothesis that tries to connect the structure and organization of the nucleoid with growth of the cell envelope is the transertion mechanism, i.e., coupled transcription, translation, and insertion of membrane proteins. Matsumoto et al. review how transertion may induce heterogeneity of lipids and proteins in the membrane that might ultimately influence local peptidoglycan synthesis leading to cell division.

THE DIVISOME

Life requires cell division. Norris argues that division is essential to maintain the connectivity of cellular components. However, some bacteria can grow surprisingly large and apparently still retain all their essential functions except division (El-Hajj and Newman). One of the biggest, *Epulopiscium fishelsoni*, clearly defies limits expected to be set by diffusive transport.

On a molecular level, the divisome is a busy factory that involves over 30 proteins in *E. coli*. How these proteins come together and form this hyper-structure is still unclear. Here, both Egan and Vollmer, and Vischer et al. address the stoichiometry of the divisome components. New interactions among the components are reported in three research articles (Gamba et al; Lies et al; Sieger and Bramkamp), and a thorough review of new fluorescent probes for labeling the divisome is presented by Wu et al.

SPATIO-TEMPORAL COUPLING MECHANISMS

The last set of articles in the e-book investigates spatio-temporal coupling between the nucleoid, divisome, and cell size. The divisome positioning in *E. coli* is realized by two partially redundant mechanisms that use chromosome as a structural scaffold (Männik and Bailey) but also in an apparently chromosome-independent manner by the Min proteins (Rowlett and Margolin). None of these molecular systems is essential provided that cell division occurs sufficiently infrequently (Männik and Bailey). The bacteria may be even capable of propagating without any spatial coupling between the nucleoids and the divisome although at the expense of much lower fitness.

Seminal studies in the 1960s established a relationship between initiation of replication and cell size using population average measurements. A series of recent analyzes of large numbers of individual cells have shown that they grow by adding a constant length/volume from one division to the next. Taheri-Araghi argues that an incremental growth model is consistent with the old ideas of initiation at a constant cell mass per *oriC* and finds a consistency between the model and experiment in an analysis that assumes invariant *C* and *D* periods for all cells. The new findings also raise the question of how a cell senses that it has added a constant length increment since its birth. Ho and Amir propose that the size increment is realized by constant accumulation of replication initiator factors. When the concentration of these factors reaches a threshold they trigger

new round of replication. The authors assume that the initiation factors are degraded immediately after start of replication and that their accumulation then starts anew. The model accounts for experimentally observed incremental length control but it leaves open the molecular origin of the initiator factor. According to Robert, the factor could be DnaA but as pointed out by the author, several experimental findings argue against realization of this essential control mechanism through this single factor alone.

CONCLUDING REMARKS

At the phenomenological level, "the facts on the ground" are mostly established now, yet the molecular details of how the coupling between nucleoid replication, cell growth, and division are realized remain to be clarified. Localized molecular interactions are playing major roles in these couplings, but large-scale global dynamics resulting from entropic forces, phase separation, self-assembly, and pattern formation are as important. An interdisciplinary approach is necessary to link all these processes into a coherent understanding. We hope that this e-book will spur further research in this fundamental area of biology and foster new collaborations between cell biologists, chemists, and physicists. A follow-up series of articles on this field is likely to arise as new results emerge in future studies.

AUTHOR CONTRIBUTIONS

All authors listed contributed to the writing of this article, and approved it for publication.

ACKNOWLEDGMENTS

The work was supported in part by University of Tennessee start-up funds and NSF research grant MCB-1252890.

Conflict of Interest Statement: The authors declare that the research was conducted in the absence of any commercial or financial relationships that could be construed as a potential conflict of interest.

Copyright © 2016 Männik, Woldringh and Zaritsky. This is an open-access article distributed under the terms of the Creative Commons Attribution License (CC BY). The use, distribution or reproduction in other forums is permitted, provided the original author(s) or licensor are credited and that the original publication in this journal is cited, in accordance with accepted academic practice. No use, distribution or reproduction is permitted which does not comply with these terms.

frontiers in Microbiology

REVIEW
published: 21 April 2015
doi: 10.3389/fmicb.2015.00289

A brief history of bacterial growth physiology

Moselio Schaechter *

Biology Department, San Diego State University, and Division of Biological Sciences, University of California, San Diego, San Diego, CA, USA

Arguably, microbial physiology started when Leeuwenhoek became fascinated by observing a Vorticella beating its cilia, my point being that almost any observation of microbes has a physiological component. With the advent of modern microbiology in the mid-19th century, the field became recognizably distinctive with such discoveries as anaerobiosis, fermentation as a biological phenomenon, and the nutritional requirements of microbes. Soon came the discoveries of Winogradsky and his followers of the chemical changes in the environment that result from microbial activities. Later, during the first half of the 20th century, microbial physiology became the basis for much of the elucidation of central metabolism. Bacterial physiology then became a handmaiden of molecular biology and was greatly influenced by the discovery of cellular regulatory mechanisms. Microbial growth, which had come of age with the early work of Hershey, Monod, and others, was later pursued by studies on a whole cell level by what became known as the "Copenhagen School." During this time, the exploration of physiological activities became coupled to modern inquiries into the structure of the bacterial cell. Recent years have seen the development of a further phase in microbial physiology, one seeking a deeper quantitative understanding of phenomena on a whole cell level. This pursuit is exemplified by the emergence of systems biology, which is made possible by the development of technologies that permit the gathering of information in huge amounts. As has been true through history, the research into microbial physiology continues to be guided by the development of new methods of analysis. Some of these developments may well afford the possibility of making stunning breakthroughs.

Keywords: growth physiology, Copenhagen school, balanced growth, bacterial physiology, bacterial growth and physiology

OPEN ACCESS

Edited by:
Arieh Zaritsky, Ben-Gurion University of the Negev, Israel

Reviewed by:
Kelly Bidle, Rider University, USA
Lawrence Rothfield, University of Connecticut, USA
Alexandra L. Blinkova, University of Texas at Austin, USA

***Correspondence:**
Moselio Schaechter, Biology Department, San Diego State University, and Division of Biological Sciences, University of California, San Diego, San Diego, CA, USA
elios179@gmail.com

Specialty section:
This article was submitted to Microbial Physiology and Metabolism, a section of the journal Frontiers in Microbiology

Received: *10 February 2015*
Accepted: *23 March 2015*
Published: *21 April 2015*

Citation:
Schaechter M (2015) A brief history of bacterial growth physiology. Front. Microbiol. 6:289. doi: 10.3389/fmicb.2015.00289

Ancient History

Arguably, the science of microbial physiology began when Leeuwenhoek first became fascinated by the sight of *Vorticella* beating its cilia. I propose that like most observations of microbes, from the simplest to the most sophisticated, this one has a physiological component. With the advent of modern microbiology in the mid-19th century, this new field of inquiry became conspicuous and recognizable with discoveries of processes such as anaerobiosis and sporulation, along with the recognition of fermentation as a microbiological phenomenon. Soon thereafter came the studies of Winogradsky and his followers on the chemical changes in the environment that result from microbial activities. Later still, during the first half of the 20th century, microbial physiology was a major contributor to biochemistry and played a key role in the elucidation of central metabolism.

The understanding of the physiology of *bacterial growth*, however, lagged behind. Even in the early 1950s, a student of microbiology, like myself, who wished to understand what happens when bacteria grow, was hard put to find useful guideposts. In the textbooks of the day, the focus was on the growth curve, with its depressingly unintelligible sequence of phases and the implication that they represented stages of an obligatory life cycle. Yet, even from the earliest days of microbiology, there were beacons of lucid thinking on the subject. One of Pasteur's first students, Raulin (1869), carried out quantitative growth experiments with the mold *Aspergillus niger* that revealed, surprisingly, its ability to grow on a simple sugar and a few mineral salts. Raulin's minimal medium is not very different from those used today. Pasteur himself believed almost obsessively that the morphology and activities of microbes are conditioned by their environment.

In time, a vast literature on growth experiments accumulated, some fanciful, others exact in intent and meticulous in execution. Notable for its clarity of thought is Henrici's classic (Henrici, 1928) report on how bacteria change in size throughout their growth cycle. Despite such examples of astute insight, a fog continued to envelop growth physiology, fueled by quirky notions. For example, some thought that the yield of bacterial cultures was limited by an entity called "biological space." Others saw the growth curve as inexorably S-shaped, thus determined by the logistic equation first published by Pierre Verhulst (1845). (I have run into people who believe this to this day.) Throughout this period, the sanctity of the growth curve prevailed. In a 1949 review on growth, even Van Niel (1949) stated: "Nearly all that it is known about the kinetics of growth of microorganisms has been learned from studies of so-called growth curves."

Recent History

The fog began to lift with the work of, among others, two people who later went on to become fathers of molecular biology, Alfred Hershey in the late 1930's and Jacques Monod in the 1940's (**Figures 1**, **2**). Hershey (Hershey, 1939) (collaborating with his chairman, Jacques Bronfenbrenner) countenanced the use of a culture in the log phase of growth as the inoculum to start a new culture, thus dispelling the inviolable sanctity of the growth curve. Monod (1942) consigned the growth response of whole cultures to enzyme kinetics and showed that the rate of growth was dependent, in Michaelis–Menten fashion, on substrate concentration, while the yield was proportional to the amount of substrate available. These experiments were carried out with cultures growing in a steady state, a key point that I will return to shortly. Monod, probably dissatisfied by the prevailing view of the field as being superficial, soon looked elsewhere in his quest for molecular mechanisms. It is noteworthy that his studies on the regulation of gene expression originated from his growth physiological work on "diauxic growth," a phenomenon wherein having glucose in the medium impedes the growth on other sugars. He left behind an encompassing yet dismissive parting shot (Monod, 1949): "The study of the growth of bacterial cultures does not constitute a specialized subject or branch of research: it is the basic method of microbiology." As a discipline, physiology of bacterial growth came close to passing from confusion to oblivion in a single leap.

As is sometimes the case, subsequent work was facilitated by a clear definition. In Campbell (1957) proposed that the steady state growth condition be referred to as "balanced growth." In so doing, he elevated what was previously just one phase in the growth curve (the log phase) into a general concept. In a sense, moving from the observation of log phase to the concept of balanced growth is like going from watching apples fall to thinking of gravity. Cells in balanced growth attain the maximum growth rate possible for that particular medium. One may fantasize a bacterium's most cherished ambition is to grow as fast as possible, thereby outpacing less productive competitors. But balanced growth has another important and unique attribute: it is the only *readily reproducible* growth condition. Consider how variable over time all the other states in the growth of a culture are. Sample now and sample a few minutes later, and you find

FIGURE 1 | Alfred Hershey (1908–1997). Source http://scarc.library.oregonstate.edu/coll/pauling/dna/people/hershey.html.

FIGURE 2 | Jacques Monod (1910–1976). Source: http://todayinsci.com/2/2_09.htm#MonodJacques.

that the cells already have different properties. Alas, even now this simple point is not always taken into consideration when defining research protocols. See a reasoned excoriation aimed at the practitioners of sloppy culturing by Neidhardt (2006). An untold amount of work carried out with cultures at undefined stages of growth is not reproducible, thus it is wasted.

The importance of growth at a steady state had been realized earlier, but Campbell's novel and precise term helped remove the aura of immutability from the growth curve. It provided the freedom to manipulate cultures by, for instance, repeatedly diluting them so as to maintain them in balanced growth. One of the most interesting of these manipulations in the early 1950s was the development of continuous cultures in chemostats (Monod, 1949; Novick and Szilard, 1950).

Come the mid-1950s, growth physiology was extended to one of the main concerns of the day: the relationship of nucleic acids to protein synthesis. Here this narrative changes to a rather selective, personal account. It was in 1956 that I joined the lab of Ole Maaløe in Copenhagen (**Figure 3**). Eventually much work on growth physiology was to come from his lab and the people who had been there became known collectively as the "Copenhagen School" (Maaløe and Kjeldgaard, 1966; Cooper, 2008). The earliest finding, on which subsequent work relied, was that cells of one species growing at different rates (in balanced growth, of course!) differed in size depending on the growth rate, with the faster ones growing being larger. Consequently, cells growing in two different media but at the same growth rate have the same cell size. The Copenhagen lab was not alone in such studies (Schaechter et al., 1958). Extensive experiments relating RNA content to growth rate were also reported by Neidhardt and Magasanik (1960), Neidhardt (1963) and Herbert (1961). Thus, a sizable window was opened to molecular mechanisms and Monod was proven wrong to some degree.

I should mention that this work was made possible, as much as anything, by the rigor that Maaløe brought to experimental measurements. In his lab, viable counts were carried out so precisely that the experimental error was consistently smaller than random sampling error (and that was before accurate pipetting gadgets). Or, to determine the growth rate of a culture, optical density (mass) measurements were made *at least 10 times* in the course of each doubling of the culture. But the deeper point was a striving for a quantitative approach to studying growth.

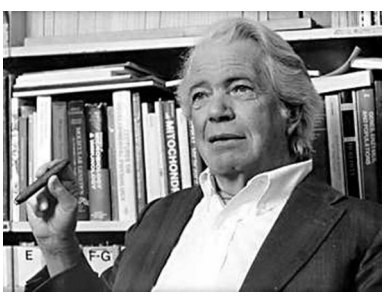

FIGURE 3 | Ole Maaløe (1914–1988). Source: http://www.denstoredanske.dk/Krop,_psyke_og_sundhed/Sundhedsvidenskab/L%C3%A6ger/Ole_Maal%C3%B8e.

Why would bacterial cells of the same species differ in size? Bacteria by dry weight consist mainly of proteins, so could fast growing cells be larger because they contain more protein-synthesizing ribosomes? When we measured the content of ribosomes in cells growing at different rates, we found, to our delight, that there was also a simple relationship here: the faster the growth rate, the more ribosomes per cell mass (Ecker and Schaechter, 1963). In other words, the concentration of ribosomes turned out to be a linear function of the growth rate. As if to test the rule, this relationship breaks down at very slow rates. This makes sense because otherwise cells growing infinitely slowly would have no ribosomes and would not be able to make proteins when placed in a richer medium. Eventually, the concentration of many other cellular components as a function of the growth rate became known in some detail (Bremer and Dennis, 1996). Because of such a dependency, bacteria obey the maxim of the Spanish philosopher José Ortega y Gasset that I am fond of quoting: "I am I and my circumstance" (*Yo soy yo y mi circunstancia*).

These studies deal with bacterial populations. How about single cells? Their life span is described by their cell cycle and is distinct from the growth curve. It depends instead on what happens between one division and the next. What events transpire during the cell cycle? It was observed early on using fairly simple microscopy and confirmed more recently by more sophisticated tools that the increase in mass in growing bacteria is exponential. In other words, growth is due to an autocatalytic expansion of most cell components. Constituents such as ribosomes and proteins are usually present in a large number of copies; therefore they need not all initiate their synthesis at once. One ribosome can be made now, another one an instant later, and yet their population will, in the aggregate expand exponentially. But the situation differs for elements that are present in one or a small number of copies, to wit, the chromosome and the cell itself. Being unitary events, both of these processes have to be regulated quite precisely, lest the population of cells become errantly heterogeneous. But in the 1950s and early 1960s, there were few tools with which to study the timing of DNA replication in single cells. Division synchronization of a culture could not readily be achieved without disturbing normal growth, e.g., by subjecting the culture to temperature shifts.

The earliest model for the regulation of the chromosome cycle was proposed by Helmstetter et al. (1968), Cooper and Helmstetter (1968) based on an expressly non-intrusive method to synchronize bacterial cells. They made use of the "baby machine," a device to unobtrusively collect "newborn" cells. It was known that the *Escherichia coli* chromosome is composed of a single DNA molecule and that its replication starts at one site, the origin, and ends at another, the terminus. The H&C model proposed that the interval between initiation and termination is nearly constant at a given temperature, regardless of the growth rate and the richness of the medium. Regulation, therefore, is principally concerned with initiation, and this became the focus of such studies. But in fast growing cells, the time required for chromosome replication can be longer than the cell cycle. This led to the proposal that initiation need not wait for termination but can take place before the previous replication finishes, thus leading to multiple

concurrent replication events on a chromosome—the so-called "multifork replication" (Yoshikawa and Sueoka, 1963).

These ways of thinking led to subsequent investigations into the mechanisms that control bacterial gene expression and chromosome replication. How is the synthesis of the ribosomal RNAs and proteins regulated? What might this have to do with the control of gene expression? How is chromosome replication regulated? And so on. I have participated in this work and derive much pleasure from the sophisticated understanding of the mechanisms that have been unraveled. However, I still stand in awe of the central marvel—the ability of such seemingly simple cells to grow in such perfect rhythm. For a lucid manifesto of this outlook, see the commentary by Neidhardt (1999).

Studies on the mechanisms that regulate growth were greatly aided by genetic analysis. A large number of conditional mutants, especially of *E. coli*, were constructed, e.g., some heat sensitive (see Hirota et al., 1968), some cold sensitive (see Ingraham, 1969). Studying their phenotype at the restrictive temperatures revealed much about the biochemical basis for growth and became an essential complement to the purely physiological experiments.

The Present Day

Although the Copenhagen School emphasized a quantitative approach, early on at least, the mechanistic understanding of growth phenomena was undeniably limited. Francis Crick figured that out that appallingly fast. When I visited him at the Cavendish Laboratory in Cambridge University in 1958, he blurted out: "Congratulations! You people started a new field, but it's over!" Gulp! In a narrow sense, this was true for the time, although even then I could have timidly argued that the physiological focus on the growing cell had contributed a needed counterpoint to molecular reductionism. But it took time. For some 50 years, until around the turn of the 20th century, growth physiology remained more or less in a latent state.

Recently, microbial growth physiology has seen a rebirth in a form that seeks a deeper *quantitative* understanding of phenomena on a whole cell level. This is exemplified by the emergence of systems biology: an approach made possible by technologies that can gather and analyze colossal amounts of information to disclose how intracellular transactions are interrelated. In fact, I have heard it said that systems biology is just an all-embracing view of cell physiology, or, if you wish, a continuation of the escape from biochemical reductionism. As has been true throughout history, research into microbial physiology continues to be guided by the development of new methods of experimental and mathematical analysis. A few examples (of many) can be seen in the exciting papers by Edwards et al. (2001), Wang et al. (2010), Valgepea et al. (2013), Klumpp and Hwa (2014), and Scott et al. (2014).

How is the bacterial growth physiology of old connected to the systems biology of today? Both historical and conceptual threads are clearly visible (Schaechter, 2006). Old questions, such as how many macromolecular components are in a cell, how rapidly are they made, and how do their interactions result in cell growth, can now be studied with modern tools. Yet, the newer methods still have a direct connection with the older ones. An example is the proteomic measurement of growing versus stressed *E. coli*, first done on a large scale in Neidhardt's lab (2011). The initial impetus for this work was to determine the number of proteins made at different growth rates of the culture, which was soon directed to looking at the effects of physiological stresses. But this approach was quickly replaced when these researchers realized that such studies had been focused largely on what *the investigator* thought interesting, useful, or potentially vital to the cell. Soon, they saw that the new methods of surveying the global production of proteins, notably two-dimensional gel electrophoresis, enabled the investigator to put the ball in the microbe's court and discover what *the cell* deemed important. Many such studies of the proteins made at different growth rates and temperatures, as well as when under various stresses, led to a nuanced appreciation of the cell as a dynamic system, with an expanded universe of rules and relationships governing its physiology and metabolism.

A major value of systems biology lies in its ability to create predictive models, something that has been achieved to a considerable extent with yeast and is being realized with bacteria. We are beginning to get a multidimensional view of the complex network of interactions that leads to the growth of a cell. As ever, the experimental basis for this work must be growing the cells under reproducible and readily assayable conditions, in other words, using cultures in balanced growth as the baseline condition. This is but one of the concepts that systems biology inherits from growth physiology.

Enfin, aficionados of balanced growth, such as myself, are often reminded that this state is unusual in nature. This is not the fault of the cells. Most planktonic cells and possibly many sessile ones grow as rapidly as conditions permit (although the abundant cyanobacteria in the ocean respond to non-nutritional inducements, such as their diel clock). Microbial environments are highly variable and usually allow only short spurts of unhindered growth that follow the infusion of foodstuff. Balanced growth over protracted periods is found mainly in the laboratory. But the experimenter who provides conditions that permit balanced growth is doing no more than letting cells put into action their fundamental yearning to grow. The cells take care of everything else.

Acknowledgments

I gratefully acknowledge the help of Doug Berg, John Ingraham, Fred Neidhardt, Irwin Rubenstein, and Christoph Weigel in writing this article.

References

Bremer, H., and Dennis, P. P. (1996). "Modulation of chemical composition and other parameters of the cell by growth rate," in *Escherichia coli and Salmonella, 2nd Edn.*, ed F. C. Neidhardt (Washington, DC: ASM Press), 1553–1569.

Campbell, A. (1957). Synchronization of cell division. *Bacteriol Rev*. 21, 263–272.

Cooper, S., and Helmstetter, C. E. (1968). Chromosome replication and division cycle of *Escherichia coli* B/r. *J. Mol. Biol.* 31, 519–540.

Cooper, S. (2008). On the fiftieth anniversary of the Schaechter, Maaløe, Kjeldgaard experiments: implications for cell-cycle and cell-growth control. *Bioessays* 30, 1019–1024. doi: 10.1002/bies.20814

Ecker, R. E., and Schaechter, M. (1963). Ribosome content and the rate of growth of *Salmonella typhimurium*. *Biochim. Biophys Acta* 76, 275–279.

Edwards, J. S., Ibarra, R. U., and Palsson, B. O. (2001). *In silico* predictions of *Escherichia coli* metabolic capabilities are consistent with experimental data. *Nat. Biotechnol.* 19, 125–130. doi: 10.1038/84379

Helmstetter, C., Cooper, S., Pierucci, O., and Revelas, E. (1968). On the bacterial life sequence. *Cold Spring Harb. Symp. Quant. Biol*. 33, 809–822.

Henrici, A. T. (1928). *Morphologic Variation and the Rate of Growth of Bacteria*. Baltimore, MD: Charles C. Thomas, Publisher; Springfield, ILL.

Herbert, D. (1961). The chemical composition of micro-organisms as a function of their environment. *Symp. Soc. Gen. Microbiol*. 11, 391–416.

Hershey, A. D. (1939). Factors limiting bacterial growth: IV. The age of the parent culture and the rate of growth of transplants of *Escherichia coli*. *J. Bacteriol*. 37, 285–299.

Hirota, Y., Ryter, A., and Jacob, F. (1968). Thermosensitive mutants of *E. coli* affected in the processes of DNA synthesis and cellular division. *Cold Spring Harb. Symp. Quant. Biol.* 33, 677–693.

Ingraham, J. L. (1969). Factors which preclude growth of bacteria at low temperature. *Cryobiology* 6, 188–193. doi: 10.1016/S0011-2240(69)80348-2

Klumpp, S., and Hwa, T. (2014). Bacterial growth: global effects on gene expression, growth feedback and proteome partition. *Curr. Opin. Biotechnol*. 28, 96–102. doi: 10.1016/j.copbio.2014.01.001

Maaløe, O., and Kjeldgaard, N. O. (1966). *Control of Macromolecular Synthesis*. New York, NY: Benjamin, Inc.

Monod, J. (1942). *Recherches sur la Croissance des Cultures Bactériennes*. Paris: Hermann & Cie.

Monod, J. (1949). The growth of bacterial cultures. *Annu. Rev. Microbiol*. 3, 371–394.

Neidhardt, F. C., and Magasanik, B. (1960). Studies on the role of ribonucleic acid in the growth of bacteria. *Biochim. Biophys. Acta* 42, 99–116. doi: 10.1016/0006-3002(60)90757-5

Neidhardt, F. C. (1963). Effects of environment on the composition of bacterial cells. *Annu. Rev. Microbiol*. 17, 61–86.

Neidhardt, F. C. (1999). Bacterial growth: constant obsession with dN/dt. *J. Bacteriol*. 181, 7405–7408.

Neidhardt, F. C. (2006). Apples, oranges and unknown fruit. *Nat Rev Microbiol*. 4, 876. doi: 10.1038/nrmicro1554

Neidhardt, F. C. (2011). How microbial proteomics got started. *Proteomics* 11, 2943–2946. doi: 10.1002/pmic.201000780

Novick, A., and Szilard, L. (1950). Experiments with the chemostat on spontaneous mutations of bacteria. *Proc. Natl. Acad. Sci. U.S.A*. 36, 708–719.

Raulin, J. (1869). Chemical studies on growth. *Ann. Sci. Nat. Bot*. 11, 93–299.

Schaechter, M., Maaløe, O., and Kjeldgaard, N. O. (1958). Dependency on medium and temperature of cell size and chemical composition during balanced grown of *Salmonella typhimurium*. *J. Gen. Microbiol*. 19, 607–616.

Schaechter, M. (2006). From growth physiology to systems biology. *Int. Microbiol*. 9, 157–161.

Scott, M., Klumpp, S., Mateescu, E. M., and Hwa, T. (2014). Emergence of robust growth laws from optimal regulation of ribosome synthesis. *Mol. Syst. Biol*. 10, 747. doi: 10.15252/msb.20145379

Valgepea, K., Adamberg, K., Seiman, A., and Vilu, R. (2013). *Escherichia coli* achieves faster growth by increasing catalytic and translation rates of proteins. *Mol. Biosyst*. 9, 2344–2358. doi: 10.1039/c3mb70119k

Van Niel, C. B. (1949). *The Chemistry and Physiology of Growth*. Princeton, NJ: Princeton University Press.

Verhulst, P.-F. (1845). Recherches mathématiques sur la loi d'accroissement de la population. *Nouveaux Mémoires de l'Académie Royale des Sciences et Belles-Lettres de Bruxelles* 18, 1–42.

Wang, P., Robert, L., Pelletier, J., Dang, W. L., Taddei, F., Wright, A., et al. (2010). Robust growth of *Escherichia coli*. *Curr. Biol.* 20, 1099–1103. doi: 10.1016/j.cub.2010.04.045

Yoshikawa, H., and Sueoka, N. (1963). Sequential replication of *Bacillus subtilis* chromosome. I. Comparison of marker frequencies in exponential and stationary growth phases. *Proc. Natl. Acad. Sci. U.S.A*. 49, 559–566.

Conflict of Interest Statement: The author declares that the research was conducted in the absence of any commercial or financial relationships that could be construed as a potential conflict of interest.

Copyright © 2015 Schaechter. This is an open-access article distributed under the terms of the Creative Commons Attribution License (CC BY). The use, distribution or reproduction in other forums is permitted, provided the original author(s) or licensor are credited and that the original publication in this journal is cited, in accordance with accepted academic practice. No use, distribution or reproduction is permitted which does not comply with these terms.

frontiers in Microbiology

REVIEW
published: 05 June 2015
doi: 10.3389/fmicb.2015.00504

A balanced perspective on unbalanced growth and thymineless death

*Philip C. Hanawalt**

Department of Biology, Stanford University, Stanford, CA, USA

The early history of the esoteric phenomenon of thymineless death (TLD) is recounted, from the pioneering discovery by Seymour Cohen and Hazel Barner, through my graduate studies at Yale and postdoctoral research in Copenhagen. My principal contribution was the discovery that restricted synthesis of protein and RNA permits cultures of *Escherichia coli* to complete their DNA replication cycles without initiating new ones, and that cells held in this physiological state are immune to the lethality of thymine deprivation; unbalanced growth is not the fundamental cause of TLD. The successful synchronization of the DNA replication cycle contributed to formulation of the replicon concept. Studies at Stanford revealed a specific requirement for transcription and led to the discovery of a TLD-resistant mutant in a new gene, termed *recQ*, with important homologs in humans and most other organisms. The lessons learned from research on TLD underscore the value of basic research in bacterial systems that can have profound implications for human health.

Keywords: DNA replication cycle, DNA degradation, replication origin, DNA repair, thymine starvation, transcription, genomic uracil, RecQ

OPEN ACCESS

Edited by:
Arieh Zaritsky, Ben-Gurion University of the Negev, Israel

Reviewed by:
Conrad L. Woldringh, University of Amsterdam, Netherlands (retired)
Charles E. Helmstetter, Florida Institute of Technology, USA
Moselio Schaechter, San Diego State University, USA
Mutsuo Sekiguchi, Fukuoka Dental College, Japan

***Correspondence:**
Philip C. Hanawalt, Department of Biology, Stanford University, 371 Serra Mall, Stanford, CA 94305-5020, USA
hanawalt@stanford.edu

Specialty section:
This article was submitted to Microbial Physiology and Metabolism, a section of the journal Frontiers in Microbiology

Received: *08 April 2015*
Accepted: *07 May 2015*
Published: *05 June 2015*

Citation:
Hanawalt PC (2015) A balanced perspective on unbalanced growth and thymineless death. Front. Microbiol. 6:504. doi: 10.3389/fmicb.2015.00504

Introduction

This review constitutes a reflection upon my early experiences in biomedical research, with particular focus upon the enigmatic phenomenon of thymineless death (TLD) that began during my graduate study and that still commands my intrigue. I came to appreciate how advances in science and their promotion are coupled to the personalities and aspirations of the investigators. While a discovery may incorporate novel insights, it always builds upon the contributions from predecessors and usually includes elements of serendipity. I will candidly relate the collaborative interactions among some pioneering investigators who have strived to achieve a mechanistic understanding of TLD, while the ultimate comprehension still eludes their grasp.

Upon graduation from Oberlin College with a major in physics, I joined the biophysics program at Yale for graduate study in 1954. That was an exciting era; the Watson–Crick DNA structure and a plausible model for DNA replication had just emerged, but we did not have a clue about the functions of RNA or its relationships to DNA. My first research mentor, Harold Morowitz, suggested that I should synchronize the division cycle in cultures of the bacterium, *Escherichia coli* (*E. coli*), so that we could study the time-course of biochemical events from one division to the next. Unfortunately, a published synchronization procedure involving glucose starvation was not reproducible by us or by anyone else. Although I retained my interest in the cell cycle, I then joined the laboratory of Richard Setlow, with whom I had just completed an outstanding spectroscopy course. I wanted to explore the application of short-wavelength ultraviolet light (UV) to probe macromolecular activities

in bacterial cells through action spectra. I developed an approach to resolve the cellular components of DNA, RNA, and phospholipids so that I could follow their respective syntheses by labeling with ^{32}P orthophosphate (Hanawalt, 1959). However, I also wanted to follow DNA synthesis at higher specificity with ^{14}C-labeled thymine, so I needed to improve the efficiency of its exogenous incorporation. In a literature search I found a timely paper describing a thymine-requiring bacterium (Barner and Cohen, 1954).

Seymour Cohen was characterizing *E. coli* 15T−, later shown to lack functional thymidylate synthetase. This auxotrophic mutant, originally isolated by Raymond Roepke from UV-irradiated *E. coli* strain 15, had been acquired from Joseph Gots at the University of Pennsylvania. Unlike the biostatic consequences of starvation for most required growth factors, such as uracil or cytosine, *E. coli* 15T− suffered a striking loss of viability when thymine was omitted from the defined growth medium, which may explain the scarcity of this type of mutant. The lethality was initially attributed to "unbalanced growth," since the bacteria continued to grow in mass while cell division was curtailed and hardly any DNA synthesis was evident (Cohen and Barner, 1954); however, the cells in minimal medium survived if the sole carbon source, glucose, was omitted, indicating that metabolism was required for TLD. The suggestion that the inhibition of DNA synthesis by UV might also kill cells by unbalanced growth sparked my interest. Balanced growth, in contrast to unbalanced growth, was defined as the physiological condition over a time interval during which every extensive property of the growing system increased by the same factor (Campbell, 1957).

TLD Studies at Yale

Cohen generously provided *E. coli* 15T−, and my research followed upon his work, with an eventual thesis entitled: "Macromolecular synthesis in *Escherichia coli* during conditions of unbalanced growth," in which I compared the effects of thymine starvation to those caused by short-wavelength UV irradiation (Hanawalt, 1958). I confirmed that during thymine starvation the bacteria stopped dividing and formed long filaments, similar to those observed following UV irradiation (Deering and Setlow, 1957). The optical density (turbidity) continued to follow that of cultures in balanced growth for one division period or a little longer, while viability remained constant for about 30 min before it decreased exponentially at roughly 90% per division period. RNA synthesis in the absence of thymine was linear for two division periods before declining, while protein synthesis (followed by labeling with ^{14}C-proline or $^{35}SO_4$) leveled off earlier. Unlike the case for thymine starvation, DNA synthesis eventually recovered following low doses of UV (Hanawalt and Setlow, 1960) and the lag in recovery could be shortened by exposing the cells to photoreactivating light (Hanawalt and Buehler, 1960). Of course, the ^{32}P labeling protocol was needed to confirm that there was very little DNA synthesis in the thymine-starved cells (Hanawalt, 1959). Cohen and Barner had also established that the thymine analog, 5-bromouracil (5BU), could partially fulfill the thymine requirement and prolong the viability of *E. coli* 15T− (Cohen and Barner, 1956). The incorporation of deoxyuridine or 5BU during DNA synthesis *in vitro* was documented by Bessman et al. (1958). At that point in history we were unaware of any effects of thymine starvation on DNA structure or function and we did not yet know the nature of the DNA damage produced by UV.

TLD Studies in Denmark

Upon completion of my Ph.D., I wanted to return to my earlier interest in synchronous growth, so I obtained an NIH postdoctoral fellowship to join Ole Maaløe in Denmark, where Gordon Lark, Elio Schaechter, and others had collaborated in studies of bacterial growth and division patterns upon changing media or shifting temperature. Maaløe was considered the international expert in bacterial synchronous growth, and he had just been appointed Professor/Chair of a newly established Department of Microbiology at the University of Copenhagen. Shortly before leaving Yale I received from Cohen a triple-mutant derivative of *E. coli* 15T− called "TAU," auxotrophic for arginine (A) and uracil (U), as well as for thymine (T; Barner and Cohen, 1958). Maaløe offered no immediate suggestions for a research project upon my arrival in his lab, so I simply continued with the TLD studies I had begun at Yale. Although I recorded some interesting effects of incubation temperature on TLD, the most exciting results were those obtained when A and U were withheld (henceforth, "AU," since both requirements were due to the same mutation in carbamoyl phosphate synthase). The first thing I noted was that although mass (turbidity) did not increase in the absence of AU, nearly all of the cells (∼97%) still suffered TLD. Thus, unbalanced growth at the level of cell mass in relation to DNA content could not be responsible for the lethality. In the presence of T but absence of AU, DNA synthesis continued for over an hour to achieve roughly a 40% increase before it leveled off. Interestingly, the fraction of the population resistant to TLD in the absence of AU also increased during that period of allowed DNA synthesis. By the time DNA synthesis had ceased, the entire population of cells had become immune to TLD, unless protein and RNA syntheses were again permitted (**Figure 1**). These results prompted me to suggest that the cellular DNA replication cycle could be completed in the absence of protein and RNA synthesis, but that protein and/or RNA synthesis were required for re-initiation of the cycle; and furthermore, that cells are only susceptible to TLD if they are actively replicating DNA. (This made logical sense: why would they need thymine if they were not replicating DNA? Of course, we did not yet know about *repair replication*!) I had inadvertently discovered a simple approach for synchronizing the DNA replication cycle in bacteria. At this point Maaløe became intensely interested in my project and I enjoyed more frequent discussions with him. We decided that we would need to use autoradiography to learn the status of DNA replication in individual cells in order to verify the model. Elio Schaechter had previously employed single cell autoradiography in Maaløe's group to demonstrate that *E. coli* normally replicates DNA throughout most of the cell cycle (Schaechter et al., 1959). Unfortunately, the technology had not been retained in Maaløe's lab when Schaechter departed. However, my graduate colleague from Yale, Bob Van Tubergen, was an expert in single cell autoradiography and had just joined Roy Markham's group in

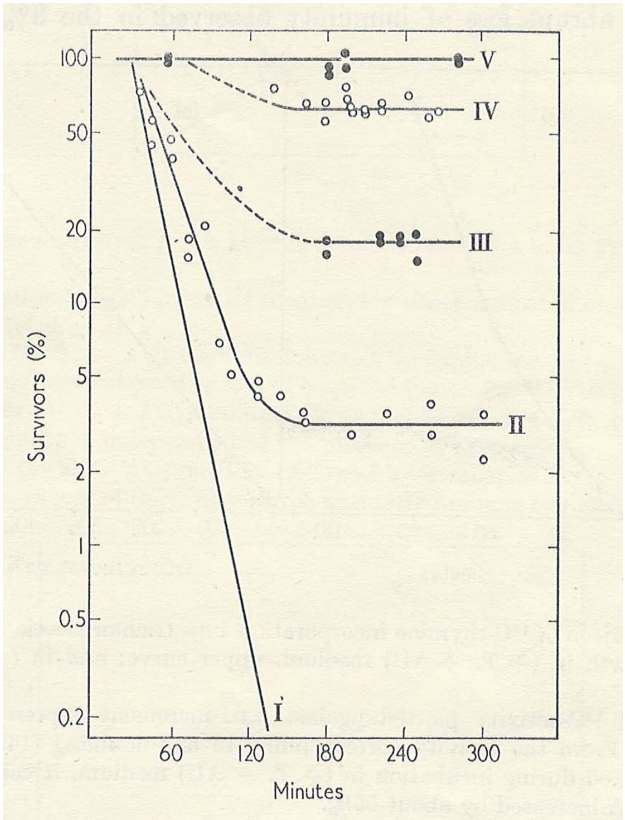

FIGURE 1 | Effect of pre-incubation with T but without AU on survival of *E. coli* TAU during subsequent incubation, −T − AU. II; −T − AU (no pre-incubation): III; 30 min pre-incubation +T − AU: IV; 60 min pre-incubation +T − AU: V; 90 min pre-incubation +T − AU: I; Comparison curve for −T + AU, from another experiment. From Maaløe and Hanawalt (1961).

Cambridge (Van Tubergen, 1961). That afforded an opportunity for me to visit England, to learn the autoradiographic procedures from Bob, and to carry out several preliminary experiments under his guidance. I then completed the single cell autoradiographic studies to confirm our model that individual cells terminated DNA synthesis at different times during incubation with T in the absence of AU. A new postdoc, Donald Cummings, soon joined Maaløe's group and contributed experience in density-labeling DNA with 5BU to follow DNA synthesis. I was pleased to have Don as a collaborator because I appreciated the unique advantages of density-labeling for analysis of DNA replication (Meselson and Stahl, 1958). Density-labeling nascent DNA could tell us whether the DNA that had replicated in the absence of AU was able to begin a new round of synthesis before AU was again supplied. The studies of TLD in Copenhagen provided early insights into control of the normal DNA replication cycle in bacteria and contributed to the formulation of the concept of the replicon (Jacob et al., 1963).

Other researchers were also attracted to the TLD field, while Barner and Cohen (1956) continued their leadership with many additional contributions, including evidence for at least one synchronous division when thymine was re-added 30 min after starvation, the report that a single amino acid deficiency does not completely block TLD although it inhibits growth (Barner and Cohen, 1957), and the finding that deprivation of uracil (in a double-mutant for T and U) prolongs the lag period for TLD and induces RNA turnover (Barner and Cohen, 1958). The UV irradiation of cells prior to thymine starvation was shown to shorten the lag period before the onset of TLD, suggesting some similarities in the "cellular units" affected by the respective treatments (Gallant and Suskind, 1961). However, there was still no information on the nature of DNA damage due to either UV or thymine starvation.

TLD Studies at Caltech

With an interest in learning more about biophysical approaches for characterizing nucleic acids, and hoping to discover what thymine starvation actually did to DNA, I joined the group of Robert Sinsheimer at the California Institute of Technology for a third-year postdoc. Shortly after my arrival at Caltech in late 1960 I heard about an upcoming Cold Spring Harbor Symposium on "Cellular Regulatory Mechanisms," for which Maaløe was an invited speaker. Unfortunately, the conference had been oversubscribed so it was too late for me to attend. I learned later that my mentor had featured our TLD project in his lecture and in the published proceedings as sole author, and had acknowledged his research assistant, Jens Ole Rostock, for the autoradiography (Maaløe, 1961). The results were simultaneously published in two journal articles (Hanawalt et al., 1961; Maaløe and Hanawalt, 1961). The authorship of the second paper included not only Don Cummings for the 5BU studies but also Elio Schaechter, who had not participated in the project and whom I had not even met. (That was my first encounter with "courtesy authorship.") Although these were disappointing experiences, I learned important lessons from them about appropriate attribution of contributions in the dissemination of scientific advances. Seven years later, at the 1968 Cold Spring Harbor Symposium on "Replication of DNA in Microorganisms," two of my graduate students gave invited talks on their own work, and I included four additional graduate students and two postdocs as co-authors for my presentation (Hanawalt et al., 1968). I also convened a reunion of alumni from Maaløe's group for beer and informal discussions during the conference (**Figure 2**).

Although I learned a lot at Caltech from productive interactions with Sinsheimer, Max Delbrück, Matt Meselson, Jerry Vinograd, and their students, my search for DNA alterations during TLD did not reveal anything significant. The most exciting new information that year was the report that UV irradiation caused thymine to form covalent dimers (Beukers and Berends, 1960), and these were soon shown to be the predominant photoproducts in cellular DNA; so there was finally a specific lesion to study in relation to DNA synthesis inhibition and damage processing in UV-irradiated bacteria.

TLD Studies at Stanford

I joined the Biophysics Laboratory at Stanford University in September 1961 with a primary focus on DNA replication in

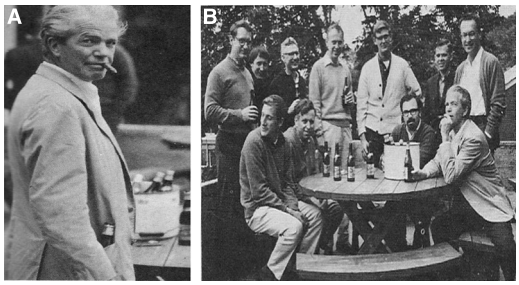

FIGURE 2 | Photos from Cold Spring Harbor Symposium Vol. XXXIII on "Replication of DNA in Micro-organisms" (1968). (A) Professor Ole Maaløe, with his ever-present cigar. **(B)** Reunion of alumni from Ole Maaløe's research group Standing: P. Hanawalt, J. Clark, C. Levinthal, J. Watson, P. Kuempel, C. Helmstetter, D. Glaser Seated: K. G. Lark, M. Schaechter, S. Cooper, O. Maaløe, with cigar.

UV-irradiated *E. coli*, but also with ongoing TLD studies. I then acquired a new multiple auxotroph of *E. coli* 15T− from Richard Wax that required methionine, tryptophan, proline, and arginine as well as thymine, and had a more stringent uracil requirement than that in strain TAU. (I named it TAU-bar, simply to avoid confusion with TAU). The removal of uracil greatly reduced TLD and implicated mRNA transcription in the lethality; however, I emphasized that one must distinguish between the event that causes killing and an event that converts the cell from the immune state to the susceptible state (Hanawalt, 1963). Gallant and Suskind (1962), in studies of *E. coli B3,* had concluded that TLD is correlated with unbalanced synthesis of RNA. In later studies we showed that the transcription inhibitor, rifampicin, essentially eliminates TLD, while also preventing the DNA strand breaks we had observed during thymine deprivation (Nakayama and Hanawalt, 1975). The accumulation of strand breaks had been seen, or not, by a number of other researchers using different bacterial strains and different conditions, but it was difficult to assess whether this could be a cause or an effect of TLD, in part because some of the strains carried inducible prophage or colicin factors (Freifelder, 1969; Ahmad et al., 1998 for review). Following upon our discovery of repair replication in UV-irradiated *E. coli* (Pettijohn and Hanawalt, 1964), we documented the non-conservative repair mode of DNA replication in thymine-starved bacteria (Pauling and Hanawalt, 1965), and we speculated that transcription was somehow responsible for introducing strand breaks or gaps that required thymine for their repair. An obvious hypothesis was that, in the absence of thymidine, DNA polymerases incorporated deoxyuridine and this would lead to a futile cycle of removal and resynthesis, as the uracil in DNA is recognized by glycosylases (e.g., Ung) for repair. The pool of deoxyuridylate was reported to increase markedly during thymine starvation (Goulian and Beck, 1966). Meanwhile, adding to the complexity of models, it was shown that initiation of replication from the chromosomal origin occurred before completion of the previous replication cycle during thymine starvation, and that amino acid starvation prevented what was called "*premature* initiation" (Pritchard and Lark, 1964). Cells growing in very low thymine concentrations exhibited increased *thymineless mutagenesis* and required an extended period for completion of chromosomal DNA synthesis (Zaritsky and Pritchard, 1971). Since thymine limitation can be seen as the *approach* to thymine exhaustion, some features of thymine deficiency may already be apparent, as exemplified by the more recent (40 years later!) results of Zaritsky et al. (2011), in which delayed initiations during thymine limitation are ascribed to possible "collapsing replisomes" and double strand breaks in the origin region.

Donachie and Hobbs (1967) had proposed that the lethality during TLD could result from sensitivity to plating on nutrient agar, but Nakayama and Couch (1973) established that the lethal event must occur *during the period of thymine starvation*, as they assayed viability entirely in the liquid phase, through application of the Poisson distribution to dilute suspensions of the bacteria.

Thymineless death was demonstrated in a member of the simplest class of living cells, *Mycoplasma laidlawii B* (Smith and Hanawalt, 1968) and in the most UV-resistant of known bacteria, *Deinococcus radiodurans*, which suffered TLD with roughly the same kinetics as *E. coli*, thereby challenging the hypothesis that the DNA damage due to thymine deprivation was similar to that due to UV (Little and Hanawalt, 1973). TLD was also documented in the eukaryote, *Saccharomyces cerevisiae* (Barclay and Little, 1978; Little, 1985), and of course, eventually in cultured mammalian cells. Goulian et al. (1985) studied mammalian cells treated with methotrexate, which inhibits dihydrofolate reductase to result in thymidine deficiency, and found a greater than 1000-fold increase in dUTP (normally <0.3 nM) associated with the drop in intracellular dTTP. They documented the incorporation of uracil and fragmentation of newly replicated DNA together with lethality, supporting the hypothesis that an elevated concentration of dUTP in mammalian cells resulted in TLD through a mechanism of uracil incorporation and removal during DNA repair (Goulian et al., 1985). For current reviews on uracil in DNA and its processing, see Krokan et al. (2014)and Williams and Kunkel (2014).

An undergraduate from Cornell University, Jack Nunberg, spent the summer of 1971 in our laboratory to study the DNA degradation associated with thymine deprivation, following the report of selective degradation of nascent DNA during TLD in *Bacillis subtilis* (Reiter and Ramareddy, 1970). Breitman et al. (1972) had also documented loss of thymine from DNA and an early increase in deoxyribose during thymine starvation in *E. coli* TAU-bar. We had previously documented preferential loss of nascent DNA in UV-irradiated *E. coli* (Hanawalt and Brempelis, 1967), and many years later we learned that the RecQ helicase and RecJ 5′–3′ exonuclease were responsible for that specific degradation of the lagging DNA strand (Courcelle and Hanawalt, 1999). Nunberg found that the *E. coli* CR34/74 temperature-sensitive DNA synthesis mutant (deficient in the DnaB helicase that operates at the replication fork), exhibited nascent DNA degradation at the restrictive temperature but without loss of viability. However, TLD at the restrictive temperature in CR34/74 did not differ significantly from that at the normal growth temperature; thus, active DNA replication forks are not required for TLD! Using *E. coli* TAU-bar prelabeled with ^{14}C-thymine and pulse labeled with ^{3}H-thymine, Nunberg also found that "bulk" DNA degradation but not nascent DNA degradation was

eliminated by rifampicin, in parallel with the protection from TLD (Nunberg, 1971). We had previously documented turnover of deoxyribonucleotides in DNA at ∼0.02% per generation period at the restrictive temperature in *E. coli* CR34/74, and this was markedly suppressed by rifampicin, in support of our hypothesis that transcription may sometimes result in repairable single-strand breaks (Grivell et al., 1975).

Hiroaki Nakayama selected survivors from a thymine-starved *E. coli K12* strain to isolate a mutant that was remarkably resistant to TLD. Upon return to Kyushu University from Stanford, he named the gene *recQ* (for *Kyushu*!) and identified the product as a helicase (Nakayama et al., 1984). RecQ participates in the RecF recombination pathway, and it turns out that mutants in other genes in this pathway are also resistant to TLD, whereas *recBC* mutants are unusually sensitive (Nakayama et al., 1982, 1988). RecQ is the prototype for the large family of RecQ helicases found in many bacterial strains and most eukaryotes, and its discovery is one of many examples that validate the importance of basic research on seemingly esoteric topics for future advances in biomedical science. Human cells have 5 *RecQ* homologs; mutation in one causes premature aging, mutation in another causes high levels of sister-chromatid exchanges and mutation in a third also has a cancer prone phenotype. For reviews of RecQ, see Nakayama (2005) and Larsen and Hickson (2013).

Structural changes in DNA from thymine-starved *E. coli* were revealed by pulsed field gel electrophoresis following cell lysis in agarose gels and post-lysis treatment with restriction endonucleases. Non-migrating DNA fragments accumulated in cells during thymine deprivation. Interestingly, the amounts of specific migrating DNA fragments were reduced inversely in relation to their map distances from the replication origin (*oriC*). Electron microscopy of the non-migrating DNA revealed convoluted structures, with branching and single-strand tails. The accumulation of non-migrating DNA was largely dependent upon RecA and *recF*-family genes, including *recQ*, implying links between the non-migrating DNA and TLD (Nakayama et al., 1994). However, the question remained as to whether these observations were revealing causes or consequences of TLD.

In the early 1990s the TLD field went into "eclipse" for a decade, with sparse publication of bacterial work, although the number of clinically relevant papers began to increase (for examples, see Canman et al., 1992; Houghton et al., 1997; Ladner, 2001; Liao et al., 2005). The *stalemate* in mechanistic comprehension is highlighted by the fact that a drafted review on TLD by Shamim Ahmad, Raymond Devoret, Hiroaki Nakayama, and myself in 1988, was eventually completed and published by Ahmad and several other co-authors 10 years later (Ahmad et al., 1998).

Re-Awakened Interest in TLD

Periodically, I would suggest to a student that there were many interesting things yet to be learned from the study of TLD, but very few took the "bait" until an undergraduate, Pam Morganroth, joined my group in her junior year to study genetic control of TLD, for graduation with Honors (Morganroth and Hanawalt, 2006). TLD was characterized in *E. coli* mutants deficient in DNA synthesis (*dnaA, dnaB, dnaC,* and *dnaE*) and in cells treated with hydroxyurea (HU) to inhibit replication. Substantial resistance to TLD was observed when replication initiation was inhibited (*dnaA* and *dnaC*), but little resistance was noted when only replication elongation was inhibited (*dnaE* and HU). Morganroth's results confirmed those of Bouvier and Sicard (1975), who had reported TLD resistance in several other temperature sensitive *dnaA* and *dnaC* mutants at the non-permissive temperature. It was concluded that active replication elongation is not required for the major TLD pathway, consistent with the findings of Nunberg (1971). A *uvrA* mutant, deficient in both global and transcription coupled nucleotide excision repair, exhibited normal TLD, ruling out participation of that ubiquitous pathway. In addition, the *lexA3* mutation, causing deficient activation of the SOS genomic stress response, did not affect TLD. However, the later studies of Fonville et al. (2010) indicated that part of the sensitivity to thymine starvation is dependent upon the SOS response, through activation of *sulA* to block cell division, in contrast to Morganroth's results. Further study resolved the discrepancy by establishing different genotypes in the respective strains employed and by showing inexplicably that TLD is inhibited by CsrA, a *c*arbon *s*torage *r*egulator, in cells lacking the SOS response (Hamilton et al., 2013). Reflecting upon the roles of the *recF*-family genes, it is provocative to consider the paradoxical observation that while RecF proteins operate at arrested replication forks in UV-irradiated cells to enhance survival, their *absence* enhances survival in thymine-starved cells (Courcelle, 2005).

A major breakthrough in our understanding of TLD resulted from the application of genome wide DNA microarrays by Sangurdekar et al. (2010), who revealed a striking loss of genetic material, spreading outward from the origin (*oriC*), that correlated with lethality during thymine starvation. TLD resistant mutants in the RecFORJQ pathway had correspondingly less damage in the origin region. Using the same approach, the loss of origin-specific DNA during TLD has been confirmed by Kuong and Kuzminov (2012). Fonville et al. (2010) employed FISH analyses to record loss of DNA near the origin during thymine deprivation as well as eventual loss near the replication terminus at late times. Martín and Guzmán (2011) have confirmed the initiation of new replication initiations at the origin during thymine deprivation that correlate with TLD, and that are inhibited by rifampicin. Chapters from the groups of Guzmân and Khodursky follow in this special collection of articles on The Bacterial Cell (Guzmân and Martîn, 2015; Ostrer et al., 2015). It is exciting as we appear to be closing in on the prime culprit for TLD at the replication origin. The ultimate answer to the mechanism of TLD will surely implicate the essential role of RNA polymerase in initiating the DNA replication cycle (Lark, 1972; Martîn et al., 2014) as well as the genomic instability due to incorporation of uracil into DNA during the initiation of DNA synthesis at *oriC*. TLD underlies the mechanisms of action of a number of clinically important drugs such as methotrexate, trimethoprim, and fluorouracil. It is more than likely that the insights derived from the continuing studies of TLD in bacteria will have translational impact for chemotherapies that depend upon TLD-like responses.

Acknowledgments

I wish to dedicate this review to the memory of my graduate mentor, Richard (Dick) Setlow, who passed away April 6, 2015 at age 94. Dick was largely responsible for my graduate training and ultimate scientific career in the fields of UV photobiology and DNA repair. We are all indebted to Seymour Cohen and Hazel Barner for initiating the TLD field, and for the ideas and efforts of many talented students and their mentors over the past 60 years. I apologize to those whose contributions were overlooked or not cited for lack of space and time. The work in my laboratory has been supported by the National Institutes of Health, most recently by a grant CA077712 from the National Cancer Institute.

References

Ahmad, S. I., Kirk, S. H., and Eisenstark, A. (1998). Thymine metabolism and thymineless death in prokaryotes and eukaryotes. *Annu. Rev. Microbiol.* 52, 591–625. doi: 10.1146/annurev.micro.52.1.591

Barclay, B. J., and Little, J. G. (1978). Genetic damage during thymidylate starvation in *Saccharomyces cerevisiae*. *Mol. Gen. Genet.* 160, 33–40.

Barner, H. D., and Cohen, S. S. (1954). The induction of thymine synthesis by T2 infection of a thymine requiring mutant of *Escherichia coli*. *J. Bacteriol.* 68, 80–88.

Barner, H. D., and Cohen, S. S. (1956). Synchronization of division of a thymineless mutant of *Escherichia coli*. *J. Bacteriol.* 72, 115–123.

Barner, H. D., and Cohen, S. S. (1957). The isolation and properties of amino acid requiring mutants of a thymineless bacterium. *J. Bacteriol.* 74, 350–355.

Barner, H. D., and Cohen, S. S. (1958). Protein synthesis and RNA turnover in a pyrimidine-deficient bacterium. *Biochim. Biophys. Acta* 30, 12–20. doi: 10.1016/0006-3002(58)90234-8

Bessman, M. J., Lehman, I. R., Adler, J., Zimmerman, S. B., Simms, E. S., and Kornberg, A. (1958). Enzymatic synthesis of deoxoribonucleic acide III. The incorporation of pyrimidine and purine analogues into deoxyribonucleic acid. *Proc. Natl. Acad. Sci. U.S.A.* 44, 633–640. doi: 10.1073/pnas.44.7.633

Beukers, R., and Berends, W. (1960). Isolation and identification of the irradiation product of thymine. *Biochim. Biophys. Acta* 41, 550–551. doi: 10.1016/0006-3002(60)90063-9

Bouvier, F., and Sicard, N. (1975). Interference of dna-ts mutations of *Escherichia coli* with thymineless death. *J. Bacteriol.* 124, 1198–1204.

Breitman, T. R., Maury, P. B., and Toal, J. N. (1972). Loss of deoxyribonucleic acid-thymine during thymine starvation of *Escherichia coli*. *J. Bacteriol.* 112, 646–648.

Campbell, A. (1957). Synchronization of cell division. *Bacteriol. Rev.* 21, 263–272.

Canman, C. E., Tang, H.-Y., Normolle, D. P., Lawrence, T. S., and Maybaum, J. (1992). Variations in patterns of DNA damage induced in human colorectal tumor cells by 5-fluorodeoxyuridine: implications for mechanisms of resistance and cytotoxicity. *Proc. Natl. Acad. Sci. U.S.A.* 89, 10474–10478. doi: 10.1073/pnas.89.21.10474

Cohen, S. S., and Barner, H. D. (1954). Studies on unbalanced growth in *E. coli*. *Proc. Natl. Acad. Sci. U.S.A.* 40, 885–893. doi: 10.1073/pnas.40.10.885

Cohen, S. S., and Barner, H. D. (1956). Studies on the induction of thymine deficiency and on the effects of thymine and thymidine analogues in *Escherichia coli*. *J. Bacteriol.* 71, 588–597.

Courcelle, J. (2005). Recs preventing wrecks. *Mutat. Res.* 577, 217–227. doi: 10.1016/j.mrfmmm.2005.03.019

Courcelle, J., and Hanawalt, P. C. (1999). RecQ and RecJ process blocked replication forks prior to the resumption of replication in UV-irradiated *Escherichia coli*. *Mol. Gen. Genet.* 262, 543–551. doi: 10.1007/s004380051116

Deering, R. A., and Setlow, R. B. (1957). Inhibition of cell division of *Escherichia coli* by low doses of ultraviolet light. *Science* 126, 397–398. doi: 10.1126/science.126.3270.397

Donachie, W. D., and Hobbs, D. G. (1967). Recovery from "thymineless death" in *Escherichia coli* 15T-. *Biochem. Biophys. Res. Commun.* 29, 172–177. doi: 10.1016/0006-291X(67)90582-7

Fonville, N., Bates, D., Hastings, P. J., Hanawalt, P. C., and Rosenberg, S. M. (2010). Role of RecA and the SOS response in thymineless death in *Escherichia coli*. *PLoS Genet.* 6:e1000865. doi: 10.1371/journal.pgen.1000865

Freifelder, D. (1969). Single-strand breaks in bacterial DNA associated with thymine starvation. *J. Mol. Biol.* 45, 1–7. doi: 10.1016/0022-2836(69)90205-8

Gallant, J., and Suskind, S. R. (1961). Relationship between thymineless death and ultraviolet inactivation in *Escherichia coli*. *J. Bacteriol.* 82, 187–194.

Gallant, J., and Suskind, S. R. (1962). Ribonucleic acid synthesis and thymineless death. *Biochim. Biophys.* 55, 627–638. doi: 10.1016/0006-3002(62)90841-7

Goulian, M., and Beck, W. (1966). Variations of intracellular deoxyribosyl compounds in deficiencies of vitamin B12, folic acid and thymine. *Biochim. Biophys. Acta* 129, 336–349. doi: 10.1016/0005-2787(66)90376-5

Goulian, M., Ingraham, H., Tseng, B., Dickey, L., Bleile, B., and Neynaber, S. (1985). Mechanisms of thymineless death. *Pediatr. Res.* 19, 756–762. doi: 10.1203/00006450-198507000-00093

Grivell, A. R., Grivell, M. B., and Hanawalt, P. C. (1975). Turnover in bacterial DNA containing thymine or 5-bromouracil. *J. Mol. Biol.* 98, 219–233. doi: 10.1016/S0022-2836(75)80110-0

Guzmân, E. C., and Martîn, C. M. (2015). Death at the origin. *Front. Microbiol.* 6:499. doi: 10.3389/fmicb.2015.00499

Hamilton, H. M., Wilson, R., Blythe, M., Nehring, R. B., Fonville, N. C., Louis, E. J., et al. (2013). Thymineless death is inhibited by CsrA in *Escherichia coli* lacking the SOS response. *DNA Repair* 12, 993–999. doi: 10.1016/j.dnarep.2013.08.011

Hanawalt, P. C. (1958). *Macromolecular Synthesis in E. coli Under Conditions of Unbalanced Growth*. Ph.D. thesis, Yale University.

Hanawalt, P. C. (1959). Use of phosphorus-32 in microassay for nucleic acid synthesis in *E. coli*. *Science* 130, 386–387. doi: 10.1126/science.130.3372.386

Hanawalt, P. C. (1963). Involvement of synthesis of RNA in thymineless death. *Nature* 198, 286. doi: 10.1038/198286a0

Hanawalt, P. C., and Brempelis, I. (1967). "Selective degradation of newly-replicated DNA after inhibition of DNA synthesis in *E. coli*," in *Proceedings of Seventh International Congress of Biochemistry*, Japan, 650.

Hanawalt, P. C., and Buehler, J. (1960). Photoreactivation of macromolecular synthesis in *E. coli*. *Biochim. Biophys. Acta* 37, 141–143. doi: 10.1016/0006-3002(60)90088-3

Hanawalt, P. C., Maaløe, O., Cummings, O., and Schaechter, M. (1961). The normal DNA replication cycle II. *J. Mol. Biol.* 3, 156–165. doi: 10.1016/S0022-2836(61)80042-9

Hanawalt, P. C., Pettijohn, D. E., Pauling, C. E., Brunk, C. F., Smith, D. W., Kanner, L. C., et al. (1968). Repair replication of DNA in vivo. *Cold Spring Harb. Symp. Quant. Biol.* 36, 187–194. doi: 10.1101/SQB.1968.033.01.022

Hanawalt, P. C., and Setlow, R. B. (1960). Effect of monochromatic UV on macromolecular synthesis in *E. coli*. *Biochim. Biophys. Acta* 41, 283–294. doi: 10.1016/0006-3002(60)90011-1

Houghton, J. A., Harwood, F. G., and Tillman, D. M. (1997). Thymineless death in colon carcinoma cells is mediated by fas signaling. *Proc. Natl. Acad. Sci. U.S.A.* 94, 8144–8149. doi: 10.1073/pnas.94.15.8144

Jacob, F., Brenner, S., and Cuzin, F. (1963). On the regulation of DNA replication in bacteria. *Cold Spring Harb. Symp. Quant. Biol.* 28, 329–438. doi: 10.1101/SQB.1963.028.01.048

Krokan, H. E., Sætrom, P., Aas, P. A., Pettersen, H. S., Kavli, B., and Slupphaug, G. (2014). Error-free versus mutagenic processing of genomic uracil-relevance to cancer. *DNA Repair* 19, 38–47. doi: 10.1016/j.dnarep.2014.03.028

Kuong, K. J., and Kuzminov, A. (2012). Disintegration of nascent replication bubbles during thymine starvation triggers RecA- and RecBCD-dependent replication origin destruction. *J. Biol. Chem.* 287, 23958–23970. doi: 10.1074/jbc.M112.359687

Ladner, R. D. (2001). The role of dUTPase and uracil-DNA repair in cancer chemotherapy. *Curr. Protein Peptide Sci.* 2, 361–370. doi: 10.2174/1389203013380991

Lark, K. G. (1972). Evidence for the direct involvement of RNA in the initiation of DNA replication in *E. coli* 15T-. *J. Mol. Biol.* 64, 47–60. doi: 10.1016/0022-2836(72)90320-8

Larsen, N. B., and Hickson, I. D. (2013). RecQ helicases: conserved guardians of genomic integrity. *Adv. Exp. Med. Biol.* 767, 161–184. doi: 10.1007/978-1-4614-5037-5_8

Liao, Z. Y., Sordet, O., Zhang, H. L., Kohlhagen, G., Antony, S., Gmeiner, W. H., et al. (2005). A novel polypyrimidine antitumor agent FdUMP[10] induces thymineless death with topoisomerase I-DNA complexes. *Cancer Res.* 65, 4844–4851. doi: 10.1158/0008-5472.CAN-04-1302

Little, J. G. (1985). Genetic and biochemical effects of thymidylate stress in yeast. *Basic Life Sci.* 31, 211–231. doi: 10.1007/978-1-4613-2449-2_13

Little, J. G., and Hanawalt, P. C. (1973). Thymineless death and ultraviolet sensitivity in *Micrococcus radiodurans*. *J. Bacteriol.* 113, 233–240.

Maaløe, O. (1961). The control of normal DNA replication in bacteria. *Cold Spring Harb. Symp. (Quant.) Biol.* 26, 45–52. doi: 10.1101/SQB.1961.026.01.010

Maaløe, O., and Hanawalt, P. C. (1961). Thymine deficiency and the normal DNA replication cycle I. *J. Mol. Biol.* 3, 144–155. doi: 10.1016/S0022-2836(61)80041-7

Martín, C. M., and Guzmán, E. C. (2011). DNA replication initiation as a key element in thymineless death. *DNA Repair* 10, 94–101. doi: 10.1016/j.dnarep.2010.10.005

Martîn, C. M., Viguera, E., and Guzmân, E. C. (2014). Rifampicin suppresses thymineless death by blocking the transcription-dependent step of chromosome initiation. *DNA Repair* 18, 10–17. doi: 10.1016/j.dnarep.2014.03.004

Meselson, M., and Stahl, F. (1958). The replication of DNA in *Escherichia coli*. *Proc. Natl. Acad. Sci. U.S.A.* 44, 671–682. doi: 10.1073/pnas.44.7.671

Morganroth, P., and Hanawalt, P. (2006). Role of DNA replication and repair in thymineless death in *Escherichia coli*. *J. Bacteriol.* 188, 5286–5288. doi: 10.1128/JB.00543-06

Nakayama, H. (2005). *Escherichia coli* RecQ helicase: a player in thymineless death. *Mutat. Res.* 577, 228–236. doi: 10.1016/j.mrfmmm.2005.02.015

Nakayama, H., and Couch, J. (1973). Effects of thymine deprivation in thymine auxotrophs of *E. coli*; thymineless death in liquid assay system. *J. Bacteriol.* 114, 228–232.

Nakayama, H., and Hanawalt, P. C. (1975). Sedimentation analysis of deoxyribonucleic acid from thymine-starved *Escherichia coli*. *J. Bacteriol.* 121, 537–547.

Nakayama, H., Nakayama, K., Nakayama, R., Irino, N., Nakayama, Y., and Hanawalt, P. C. (1984). Isolation and genetic characterization of a thymineless death-resistant mutant of *Escherichia coli* K-12: identification of a new mutation (recQ1) that blocks the RecF recombination pathway. *Mol. Gen. Genet.* 195, 474–480. doi: 10.1007/BF00341449

Nakayama, H., Nakayama, K., Nakayama, R., and Nakayama, Y. (1982). Recombination-deficient mutations and thymineless death in *Escherichia coli* K12: reciprocal effects of recBC and recF and indifference of recA mutations. *Can. J. Microbiol.* 28, 425–430. doi: 10.1139/m82-064

Nakayama, K., Kusano, K., Irino, N., and Nakayama, H. (1994). Thymine starvation-induced structural changes in *Escherichia coli* DNA. Detection by pulsed field gel electrophoresis and evidence for involvement of homologous recombination. *J. Mol. Biol.* 243, 611–620. doi: 10.1016/0022-2836(94)90036-1

Nakayama, K., Shiota, S., and Nakayama, H. (1988). Thymineless death in *Escherichia coli* mutants deficient in the RecF recombination pathway. *Can. J. Microbiol.* 34, 905–907. doi: 10.1139/m88-157

Nunberg, J. (1971). *On the Correlation of DNA Degradation with Thymineless Death*. Undergraduate Honors Thesis, Division of Biological Sciences, Cornell University.

Ostrer, L., Hamann, B. L., and Khodursky, A. (2015). Perturbed states of the bacterial chromosome: a thymineless death case study. *Front. Microbiol.* 6:363. doi: 10.3389/fmicb.2015.00363

Pauling, C., and Hanawalt, P. C. (1965). Nonconservative DNA replication in bacteria after thymine starvation. *Proc. Natl. Acad. Sci. U.S.A.* 54, 1728–1735. doi: 10.1073/pnas.54.6.1728

Pettijohn, D., and Hanawalt, P. C. (1964). Evidence for repair-replication of ultraviolet damaged DNA in bacteria. *J. Mol. Biol.* 9, 395–410. doi: 10.1016/S0022-2836(64)80216-3

Pritchard, R. H., and Lark, K. G. (1964). Induction of replication by thymine starvation at the chromosome origin in *Escherichia coli*. *J. Mol. Biol.* 9, 288–307. doi: 10.1016/S0022-2836(64)80208-4

Reiter, H., and Ramareddy, G. (1970). Loss of DNA behind the growing point of thymine-starved *Bacillus subtilis* 168. *J. Mol. Biol.* 50, 533–548. doi: 10.1016/0022-2836(70)90210-X

Sangurdekar, D. P., Hamann, B. L., Smirnov, D., Srienc, F., Hanawalt, P. C., and Khodursky, A. B. (2010). Thymineless death is associated with loss of essential genetic information from the replication origin. *Mol. Microbiol.* 6, 1455–1467. doi: 10.1111/j.1365-2958.2010.07072.x

Schaechter, M., Bentson, M. W., and Maaløe, O. (1959). Synthesis of deoxyribonucleic acid during the division cycle of bacteria. *Nature* 183, 1207–1208. doi: 10.1038/1831207a0

Smith, D., and Hanawalt, P. C. (1968). Macromolecular synthesis and thymineless death in *Mycoplasma laidlawii* B. *J. Bacteriol.* 96, 2066–2076.

Van Tubergen, R. P. (1961). The use of radioautography and electron microscopy for the localization of tritium label in bacteria. *J. Biophys. Biochem. Cytol.* 9, 219–222. doi: 10.1083/jcb.9.1.219

Williams, J. S., and Kunkel, T. A. (2014). Ribonucleotides in DNA: origins, repair and consequences. *DNA Repair* 19, 27–37. doi: 10.1016/j.dnarep.2014.03.029

Zaritsky, A., and Pritchard, R. (1971). Replication time of the chromosome in thymineles mutants of *Escherichia coli*. *J. Mol. Biol.* 60, 65–74. doi: 10.1016/0022-2836(71)90447-5

Zaritsky, A., Wang, P., and Vischer, N. O. E. (2011). Instructive simulation of the bacterial division cycle. *Microbiology* 157, 1876–1885. doi: 10.1099/mic.0.049403-0

Conflict of Interest Statement: The author declares that the research was conducted in the absence of any commercial or financial relationships that could be construed as a potential conflict of interest.

Copyright © 2015 Hanawalt. This is an open-access article distributed under the terms of the Creative Commons Attribution License (CC BY). The use, distribution or reproduction in other forums is permitted, provided the original author(s) or licensor are credited and that the original publication in this journal is cited, in accordance with accepted academic practice. No use, distribution or reproduction is permitted which does not comply with these terms.

frontiers in Microbiology

REVIEW
published: 25 March 2015
doi: 10.3389/fmicb.2015.00238

A ten-year search for synchronous cells: obstacles, solutions, and practical applications

Charles E. Helmstetter *

Department of Biological Sciences, Florida Institute of Technology, Melbourne, FL, USA

My effort to use synchronously dividing cultures to examine the *Escherichia coli* cell cycle involved a 10-year struggle with failure after failure punctuated by a few gratifying successes, especially at the end. In this essay, I recount my personal journey in this obsessive experimental pursuit. That narrative is followed by a description of a simplified version of the "baby machine," a technique that was developed to obtain minimally disturbed, synchronously growing *E. coli* cells. Subsequent studies with this methodology led to an understanding of the basic properties of the relationship between chromosome replication and cell division. Accordingly, I end this reminiscence with a simple, fool-proof graphical strategy for deducing the pattern of chromosome replication during the division cycle of cells growing at any rate.

Keywords: synchronous cells, cell cycle, cell division, chromosome replication, *E. coli*, cellular baby machine

OPEN ACCESS

Edited by:
Arieh Zaritsky, Ben-Gurion University of the Negev, Israel

Reviewed by:
Kevin D. Young, University of Arkansas for Medical Science, USA
Karl Drlica, Rutgers University, USA

***Correspondence:**
Charles E. Helmstetter, Department of Biological Sciences, 150 W. University Blvd., Melbourne, FL 32937, USA
chelmste@fit.edu

Specialty section:
This article was submitted to Microbial Physiology and Metabolism, a section of the journal Frontiers in Microbiology

Received: *11 February 2015*
Accepted: *11 March 2015*
Published: *25 March 2015*

Citation:
Helmstetter CE (2015) A ten-year search for synchronous cells: obstacles, solutions, and practical applications. Front. Microbiol. 6:238. doi: 10.3389/fmicb.2015.00238

Introduction

Frank Sinatra once famously sang about age thirty-five being a very good year. For me, that happened in 1968. It marked the end of a long, exhausting, but ultimately satisfying expedition to decipher the growth-rate-dependent coordination between chromosome replication and cell division in *E. coli*. Here I describe the backstory to the development of the "baby machine" technique that ultimately led to our description of the *E. coli* cell cycle published in 1968 (Cooper and Helmstetter, 1968; Helmstetter and Cooper, 1968; Helmstetter et al., 1968). At the conclusion of this personal account, I attempt to dispel any impression that there are major complexities associated with either performing the baby machine procedure, or perhaps of more pertinence, with deciphering the growth-rate dependency of chromosomal replication patterns. Both undertakings are actually quite simple to carry out, as I endeavor to explain with a few relatively painless illustrations.

A Research Plan

My interest in the bacterial division cycle began in 1958 while a graduate student with Robert B. Uretz in the Committee on Biophysics at the University of Chicago. It was an unexpected shift in direction because I had previously become fascinated with atomic and radiation physics as a physics major at Johns Hopkins University. My penchant for physics continued and expanded while in masters programs in biophysics at the University of Michigan and in radiological physics at the University of Chicago. As a consequence, I entered the Ph.D. program at Chicago, and joined Bob's laboratory, with the intent of becoming a radiation biologist. The shift in career plans came about after reading some of the stunning work on bacterial

conjugation produced at the Pasteur Institute in the 1950s (e. g., Wollman and Jacob, 1955; Wollman et al., 1956). I had no idea scientific research could be so exciting. So after reading everything I could find on the topic, it was clear that I had to study some aspect of *E. coli* DNA.

The decision to focus on chromosomal DNA in the cell cycle came about naturally because Bob Uretz and the Committee on Biophysics at Chicago were renowned for microbeam irradiation of mitotic chromosomes (Uretz et al., 1954), and I had already spent many hours observing and filming the response of newt heart cell chromosomes to UV microbeams. Furthermore, the surprising paucity of information available on the cell cycle of bacteria, compared to that of eukaryotes, was obvious and intriguing. Plus, I could then combine my new interest in bacterial genetics with the laboratory's interest in radiobiology by investigating cell cycle-dependent sensitivity to photo-inactivation by DNA intercalating agents. It seemed quite straightforward at the time. To initiate my career in cell cycle research, all I needed to do was synchronize *E. coli* and I was off. How naïve.

Synchronous Cells

My search for synchronously dividing *E. coli* began in late 1958. Unfortunately, it took 4 years to come up with an acceptable technique, another 4 years to finally figure out an optimal way to apply it, and two additional years to generate and correctly interpret key data on the division cycle. What an unexpectedly long and difficult experience that was. Of course there were personal milestones along the way, including the births of sons Charlie and Michael, but without sheer stubbornness in the face of endless setbacks, my research career would have collapsed on more than one occasion.

The first step was to choose a strain of *E. coli*. I don't recall how I came to the decision to choose *E. coli* B/r, but it was likely because Aaron Novick had been running a bank of chemostats containing strain B in an adjacent laboratory (Novick and Szilard, 1950). I was also aware of Evelyn Witkin's radiation resistant mutant B/r (Witkin, 1946) and felt comparing a radiation resistant mutant with the parental strain might be useful. Also, strain B/r appeared to form fewer filaments during exponential growth, a seemingly advantageous property. That decision turned out to be the first of two incredible strokes of pure good luck during this investigation. If the far more popular strain K-12 had been chosen, most of the crucial experiments I will mention later would likely have failed and the baby machine technique would not have been developed, at least by me[1] .

In the late 1950s there were basically three different approaches reported for bacterial synchronization: single or multiple temperature shifts, single or multiple nutritional deprivations, and size selection by filtration or centrifugation (Helmstetter, 1969). I tried all of them over and over with limited success. These were not trivial efforts because cell concentrations were all determined using agar plates, requiring pouring, plating, counting, and cleaning hundreds of glass Petri dishes every week. That was the case until 1 day a guy named Joe Coulter, who along with his brother had started a small electronics firm in Chicago, walked into the laboratory carrying a machine he claimed could accurately count thousands of bacteria in seconds. After he had considerable difficulty getting mercury to fill the new manometer during set-up of the instrument (not uncommon for an inexperienced user but a bit surprising in retrospect for someone named Coulter), it worked! This was, of course, the original Coulter Counter model A. Now I was able to not only get rapid, accurate cell concentrations, but I was also able to simultaneously see the "sizes" of the cells on the integrated oscilloscope. With the model A amplifiers and a 30-μm aperture tube, the size distributions of exponential-phase, newborn and synchronously growing cells were readily distinguishable. This instrument proved to be invaluable for my work, and the work of many others who dared try to employ synchronously dividing cells.

Since the goal in studies of this sort was to examine the cell cycle properties of cells in exponentially growing cultures undergoing unrestricted growth, the technique for producing the synchrony must cause little if any disturbance to growth. At a minimum, it was required that the cells undergo at least two cycles of detectable synchrony, that whatever is observed in the first cycle repeats in the second, and that the fundamental properties of the synchronous cultures, such as cell sizes and growth rates, mimic the initial exponential-phase populations. All methods I tested caused some level of disturbance. Many methods produced a single burst of seemingly synchronized division after a delay period, but these were deemed to be nothing more than a reflection of the recovery from the sometimes harsh treatments employed. The method that appeared to cause the least disturbance involved filtration of a culture through a stack of Whatman cellulose filter papers. In this procedure, the smaller newborn cells pass through the stack into the effluent, and can be collected, while the larger, older cells are retained within the stack (Maruyama and Yanagita, 1956; Abbo and Pardee, 1960). With some modifications from the original reports, such as pressure rather than vacuum filtration, this technique enabled me to perform a few simple irradiation experiments on cells at very low concentrations.

During this time, two fellow graduate students with whom I had close contact, and who would eventually play important roles in this work, were Donald J. Cummings and David Friefelder. Don was working on T2 bacteriophage structure with Lloyd Kozloff, and Dave was a member of the Uretz lab. Don and I became very close friends and spent many hours gabbing about our work, often during endless games of bridge in smoke-filled living rooms. This friendship with Don proved invaluable after graduation. Don received his degree before I, did a postdoc with Ole Maaløe at the University Institute of Microbiology in Copenhagen, and then accepted a position at the National Institutes of Health in Bethesda to continue his work with T2 in a unit headed by Ernst Freese. I, on the other hand, was committed to 2 years

[1]The K-12 strains commonly employed at the time were generally motile, filament-forming and weakly adherent to the surfaces used for cell attachment, all of which would have caused experiments to fail or perform poorly. Once the technology was developed with the nonmotile, non-filamentous, strongly-adhesive strain B/r, the modifications necessary for use with K-12 became possible (Helmstetter et al., 1992).

of active duty service after being enrolled in the Army Reserved Officers' Training Corps at Johns Hopkins. Fortunately I was able to transfer from the Army to the Commissioned Corps of the U. S. Public Health Service, and to serve my time at NIH, thanks to a convincing letter to whomever makes these transfer decisions and the blessing of Freese. So in the fall of 1961, I was given a desk in Don's laboratory, as well as a small room down the hall with a walk-in incubator and an indispensable model A Coulter Counter in order to continue developing the filtration synchrony technique.

Origin of the Baby Machine

At NIH my plan was to increase the quantity of small cells produced with the filtration technique, while minimizing perturbations, by employing a larger vessel capable of rapidly pushing liters of cells through a thick stack of filter papers. To accomplish this, a skilled machinist constructed a filter holder from a large stainless steel pipe, 12 cm in diameter and 40 cm long. A removable cap was clamped to the top and attached to a cylinder of compressed air to produce the pressure needed to push the culture through the filter stack. When it was completed, Don and I walked across campus to the machine shop to run the first test. After it was all set up and the top was clamped securely and attached to the air cylinder, we all stood as far back as we could and one of us, the machinist I believe, turned the valve on the cylinder. There was an immediate sound of a canon having been fired in this cavernous, high-ceilinged room. At the time I thought the entire apparatus had been blown into the air with a thunderous roar. We all dove for cover. It turned out to be just the cap. The only subsequent sound was my voice saying "has it come down yet?" a comment Don joked about for many years thereafter with anyone willing to listen to this story about our underestimation of the importance of pressure regulation. The device was eventually properly strengthened and regulated, and I began running tests with it.

Everything changed in early 1963 while at a meeting of the Biophysical Society in New York. After one of the sessions I was standing at the back of a room with a small group talking about synchronizing cells. I believe Philip Hanawalt was amongst us, and I certainly recall David Friefelder being there too because he asked me a question that completely changed the course of the work. Dave loved back-and-forth banter, perhaps originating early in life while he was one of the teenage stars of a very popular radio show in the U. S. called Quiz Kids. After describing the technique I was using, Dave asked a number of questions including how long the filtration took. I said, "a few minutes." He then said, as I distinctly recall, "well then, the cells must be growing in the filter stack." Although I felt at the time that Dave's comment was intended to be a criticism of the method, it turned out to be the second incredible stroke of good luck during this pursuit of synchrony.

The story of what happened later that night has been told previously (Cooper, 1997), but I will recount it from my perspective. I couldn't sleep as I mulled over Dave's comment while staring at the ceiling in the dark hotel room. I was thinking about the larger cells stuck in the filter stack growing and dividing while the medium passed through for those short few minutes. Then for reasons unknown, since I know nothing about poultry farming, I began visualizing chickens attached all over the ceiling of the room and thinking that the only (living) objects that would fall from the surface would be eggs. That was it. I thought that if cells became stuck within the filter stack while culture medium passed through, the only cells that could be released from the stack would be newborn cells originating from the portion of the adhered cells that was not involved in their adherence I realized that many of the dividing rod-shaped cells might not release progeny at all, or that some newborn cells might reattach, but in the ideal case in which attachment was permanent, only new daughter cells would be released, no matter how few. Experimentally, strong attachment and good flushing with culture medium ought to yield a highly pure population of newborn cells. The best part was that this could be a truly minimally disturbed synchronous population because the process of preparing the synchronous cells simply involved collecting cells falling from a surface-bound culture growing under undisturbed conditions.

I was feeling euphoric during the train ride back to Bethesda and I very likely went to the lab that night to set up a culture to test the idea the next day. I don't recall the precise filter configuration for the first test, but in essence I performed the usual filtration of cells through the filter stack. However, instead of collecting the first small cells released I simply kept fresh medium flushing slowly through the filter containing whatever cells remained bound. During the first few minutes of the experiment, the concentration of cells in the effluent decreased to almost background. (At that time, it had not yet occurred to me that the cells close to division might be so completely attached that neither daughter would release at division). Then, to my relief, the concentration began to increase gradually. I could see in the oscilloscope of the Coulter Counter that most of the cells were at the size expected for newborn cells. Soon the cell number rose rapidly, reaching a peak at about 40 min with a thick pattern of spikes in the oscilloscope, seemingly all at newborn size. What a moment. I had to stop the experiment earlier than I would have liked due to an appointment for a haircut in a shop in the basement of the NIH Clinical Center. So the first person I told about this successful experiment was a very disinterested barber.

Development and testing of this new approach progressed rapidly, with the final configuration consisting of simply filtering the cells onto a nitrocellulose membrane filter, inverting the filter apparatus, pumping medium through the filter, and collecting the cells that fell off (Helmstetter and Cummings, 1964). It eventually became known as the "baby machine," and depicted with humor (**Figure 1**). I don't recall who first called it by that name, but it wasn't me since I continued to dub it "membrane elution," true to my conservative writing style.

A Key Experiment in Copenhagen

With the method a success and my tour with the Public Health Service ending in the fall 1963, I headed to Ole Maaløe's laboratory in Copenhagen on a 1-year NIH postdoctoral fellowship. This was a big deal for me since I was well aware that Ole's lab was at the top of my new field of microbial physiology, and Don

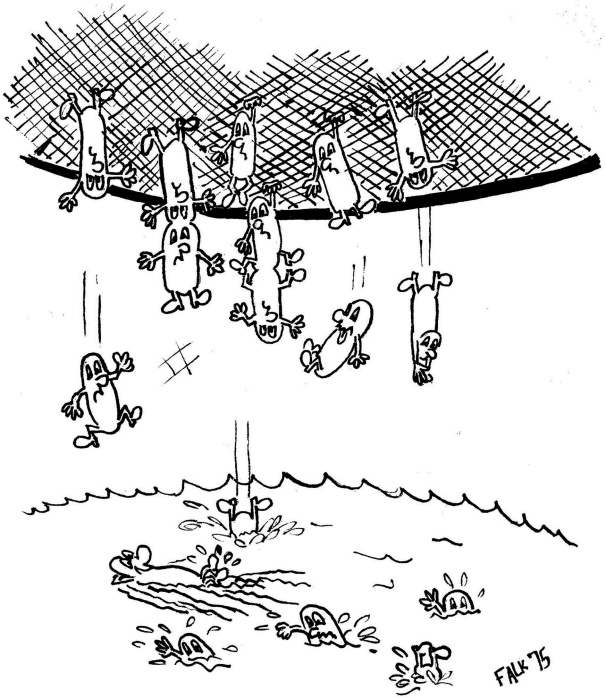

FIGURE 1 | Bacterial baby machine cartoon. Caricature of the technique sketched by Avshalom Falk while a student in the laboratory of Eliora Ron at Tel Aviv University.

Cummings had raved about his experiences there. I also assumed, correctly, that Maaløe would have keen interest in having this new minimally disturbing synchrony technique introduced into his lab. It was a scientifically stimulating year with an eclectic group of North Americans: James Friesen, Steven Cooper, D. Joseph Clark and Kivie Moldave, along with Danish colleagues Niels Ole Kjeldgaard and Knuth Rasmussen. I was able to absorb much of the beautiful ground-breaking work on bacterial physiology that had come out of the laboratory (e.g., Schaechter et al., 1958; Hanawalt et al., 1961). The Copenhagen School motto of "look but don't touch" when investigating microbial physiology became embedded for life. I also developed a multi-year fascination with possible explanations for the "rate maintenance" phenomenon, that is, the finding that after a shift of exponentially growing *Salmonella typhymurium* to a richer culture medium, the rate of division remained essentially unchanged for 60–70 min at 37°C before shifting suddenly to the rate expected in the new medium (Kjeldgaard et al., 1958).

Shortly after arriving, I set up the baby machine apparatus in an incubator room that contained a small opening hatch in one wall of the laboratory Joe Clark and I occupied, thereby enabling me to collect samples in comfort. For health reasons I accomplished very little, and did not interact with Maaløe as much as anticipated, except for some discussions on drafts of the monograph on macromolecular synthesis he and Kjeldgaard were writing (Maaløe and Kjeldgaard, 1966). However, he was enormously kind and helpful to me when I became ill, ferrying me around town to find the best physicians, even to the extent of going into examining rooms with me to "participate" in the physical exams.

But one experiment was performed that would eventually prove to be very important on the way to deciphering the replication-division coordination in *E. coli*. We all spent a good deal of time in scientific bull-sessions discussing what we thought we knew about the cell cycle. One day Steve Cooper and I decided to do an unusual experiment with the baby machine. We decided to pulse-label the cells with ^{14}C-thymidine immediately prior to binding them to the membrane filter, rather than labeling the synchronous cells eluted from the surface in the usual manner, with the idea that we could learn something about chromosome segregation. So we pulse-labeled glucose-grown *E. coli* B/r, collected newborn cells eluted from the membrane for about three generations, and measured radioactivity per cell. The results were very clear. The radioactivity per cell decreased in a step-wise pattern, with horizontal plateaus followed by sudden two-fold decreases every generation. As I remember, we concluded that the two-fold reduction in radioactivity per cell each generation was the relatively uninteresting consequence of semiconservative replication followed by random distribution of chromosomal DNA into daughter cells, and that we had learned little of real value. What a mistake. The mistake was probably a consequence of our inability at that time to accurately measure, and thus interpret, the characteristic fluctuation in concentration of newborn cells eluted from a surface-bound population. Unfortunately it would take me two more years to think about this experiment again and interpret it correctly.

Dealing with Adversity

In the fall of 1964, when it became time to find a job as my year in Copenhagen neared an end, I was pleasantly surprised to find that the mid 1960s was a time when positions in science were plentiful. Due to my obsession with using the baby machine to study basic properties of chromosome replication in *E. coli*, I preferred a full-time research position rather than a university appointment. One day I got a letter from someone at Roswell Park Cancer Institute describing a research position that included the option of joining the graduate faculty at what would become the State University of New York at Buffalo. I had not heard of the place so I looked on a map of Buffalo for a park named Roswell, without success. (I soon learned that in 1898 Dr. Roswell Park founded the nation's first research facility devoted exclusively to cancer research at the University of Buffalo). With some trepidation I accepted an offer to fly to Buffalo, see the facilities, and meet faculty. After being convinced I could focus on the research of my choosing while an active member of the graduate program, and after meeting several first-rate researchers such as Kenneth Paigen, David Pressman, Theodore Hauschka and David Harker, I accepted the position. It didn't hurt that I was offered a salary that was about 50% higher than I had anticipated.

The NIH grant application I submitted while in Copenhagen was funded before I arrived in Buffalo, and that, along with some small start-up funding, got me going. The next 2 years were enjoyable personally but painful scientifically. My students, technicians and I must have performed several hundred experiments

with synchronous cells obtained with the baby machine. Some worked quite nicely but the ones I really cared about were never as pristine as required. The questionable experiments all involved pulse-labeling synchronous cultures with radioactive precursors of various macromolecules, with primary interest in nucleic acids. I was distressed by what appeared to be minor but persistent inconsistencies in the uptake patterns in the first and second cycles of synchronous growth. Nothing I tried solved the problem. I vividly remember the very cold Buffalo night when I finally came to the decision, while leaving the lab and heading to the basically deserted car park to scrape the ice from my windshield, that I, at least, was incapable of growing *E. coli* synchronously without noticeable disturbance. What a miserable night. I simply could not understand why a technique that seemed so sound theoretically was not working properly[2]. That night I became firmly convinced that I had better do something else with my life because 8 years of beating my head against the wall was enough.

Of course that is not what happened. I spent the next few days mulling over the concept behind the baby machine and what fundamental flaw I might be missing. For whatever reason, the experiment Cooper and I did in Copenhagen crossed my mind, and something just snapped. I finally realized what the experimental result was telling us; namely, the rate of ^{14}C-thymidine incorporation during the division cycle. It can be understood by considering the following simple facts with reference to that experiment. The first newborn cells to fall from the surface at the start of elution were progeny of the oldest cells in the culture at the time of pulse-labeling with ^{14}C-thymidine. The cells eluted at the end of the first generation of growth on the surface were progeny of the youngest cells in the culture at the time of labeling. Thus, the radioactivity in the newborn cells eluted during the first generation reflected the rate of thymidine incorporation during the division cycle of their parents, in reverse. Similar analysis applied to subsequent generations of elution (see Helmstetter, 1967 for a detailed illustration of this reasoning). What a feeling it was to suddenly realize how powerful this application of the technique would be to study a host of cycle-dependent phenomena with virtually no disturbance of the cells. As with the chicken epiphany, I was fully convinced it would work because all treatments, including labeling, would be done in untouched cultures. All we were asking was for the cells to divide on the membrane surface in the same sequence as they would have divided in the original exponentially growing culture. The first experiment was done the next day. I pulse-labeled a culture with radioactive thymidine, filtered it onto the membrane in the usual way, and I then had to head off to teach a class while a technician collected the samples and prepared them for counting. That experiment failed because I had added too much label, but it was repeated the next day with great success showing unequivocally that in glucose-grown cells, the rate of DNA replication appeared constant for the first half of the cycle, doubled at mid-cycle, and was constant at twice the rate for the second half of the cycle.

[2]It was eventually assumed to be a culture media preparation problem, likely associated with the production of preconditioned media, which was not discovered until our laboratory moved to a new location 2 years later and the problem miraculously disappeared. Use of preconditioned medium was determined to be unnecessary, irreproducible and thus not recommended.

Deciphering the Coordination between Chromosome Replication and Cell Division

This time my barber wasn't the first to be told about an experimental success. I immediately wrote Steve Cooper a very long letter explaining the benefit and potential of this application of the technique along with numerous sketches of the data. Steve responded with 43 pages of typical enthusiastic verbal eurekas that literally jumped off the pages with ideas for many year's worth of experiments, presumably for me to do. It turned out, however, that by pure chance, Steve, who was in Kivie Moldave's laboratory at Tufts University at that time, had accepted a position with Robert Guthry at Childrens Hospital in Buffalo. Upon arriving in Buffalo in the summer of 1966 his facilities were not yet ready at Childrens so he came to my lab at Roswell with the idea that we could work together for a month or two, since cell cycle research had continued to be one of his interests. By that time I had completed work on chromosome replication in slower-growing *E. coli* B/r, finding a G2-like gap in DNA synthesis (Helmstetter, 1967), and the obvious next step was to extend the analyses to rapid growth in an effort to generalize the findings.

After a few ups and downs, humorously described in Cooper (1997), the relationship between chromosome replication and cell division became obvious. Two papers were then written and published in 1968 (Cooper and Helmstetter, 1968; Helmstetter and Cooper, 1968). The first contained new data on ^{3}H-thymidine incorporation during the cycle of rapidly growing cells, and the second described a "model" to explain the general relationship between replication and division. The writing was a joint effort although I took primary responsibility for the first and Steve for the second. That division of labor proved wise due to Steve's skill at inventive prose. The first paper reflects my traditional, generally accepted writing style, segmented into: Introduction, Methods, Results, and Discussion. Steve simply wrote in a manner he felt was most informative, irrespective of expected norms. I have to believe his compositional skills are one reason the basic ideas in the second paper came across so easily to readers and are so frequently cited. Another reason lies in the presentation of the findings as a "model" when in fact it was primarily a description of our data and not a generalized model. The "model" states that the time for a round of chromosome replication (C) and the time between the end of a round of replication and cell division (D) are constants over a specific range of growth rates. Thus, cell division takes place $C + D$ min after initiation of each round of chromosome replication. Subsequently, the model was extended to include (I), defined as the interinitiation time, i.e., the time required for the cell to achieve the potential to initiate chromosome replication (Helmstetter et al., 1968). Accordingly, in a purely phenomenological sense, *E. coli* duplication can be described as $I + C + D$, irrespective of the durations of I, C, and D. Later that same year, Ole Maaløe and I reconnected at Argonne National Laboratory during a presentation of the model (**Figure 2**).

I was not entirely comfortable with emphasizing that *C* and especially *D* were constants at growth rates between 1 and 3 doublings/h at 37°C (although that turned out to be a reasonable and useful concept), but I was convinced of the "*ICD*" idea. I was also gratified that the model explained the previously mentioned "rate maintenance" phenomenon, since it stipulated that the rate of cell division would be expected to remain unchanged for $C + D$ min after a shift-up (Helmstetter et al., 1968). Plus, being a novice physicist, I saw the possibility of using this simple idea to develop quantitative expressions for the chromosomal DNA contents of cells in exponentially growing cultures. I was not particularly skilled in calculus but I loved the challenge. So while simultaneously listening to the Indianapolis 500 auto race in May 1967, I set out to calculate the genome equivalents of DNA per cell as a function of growth rate in log-phase cultures. It was great fun for someone with modest ability in math, and if you glance at the equations shown in Cooper and Helmstetter (1968), the derivations might seem fairly simple, but it wasn't easy for me. As I thought about the preliminary equations that do not appear in the paper, I found the need to simultaneously envision expressions for the three distinct DNA replication intervals present in the more complex division cycles. Exasperatingly, one or two kept slipping away until at last I was able to retain all three at once, saw the formula, and quickly wrote it down. From there on, and in concert with Steve and Olga Pierucci, the equations flowed out and it was done. I suppose the process of holding multiple mathematical expressions in one's head when deriving equations is common for those with expertise in this area, but it was new to me. I tell this anecdote because I enjoyed doing these and subsequent calculations using the model, but also because it echoes a story I read a while ago about Isaac Newton during the time he was developing calculus. The story I recall is that the staggering genius of Newton was reflected in his apparent ability to hold several mathematical expressions in his brain simultaneously for days at a time, while walking around in London or on his mother's farm, as he meshed them together until the problem of interest was solved. Having been able to retain only three expressions for probably less than a second with considerable effort, I was amazed by this account of an incomprehensible talent of an unquestioned genius.

The preceding was intended to describe some of the activities that went into our early contributions to research on specific aspects of the bacterial division cycle. It is not comprehensive and it only reflects our work and not those of numerous others whose studies during the same time frame all contributed to the accomplishments in this field in the late 1960s. In particular, the design of our experiments was made possible by the critical discoveries of Schaechter et al. (1958) on the relationship between cellular properties and culture conditions. Additionally, interpretation of our findings in rapidly growing cells was facilitated by the earlier report of multifork DNA replication in *Bacillus subtilis* (Yoshikawa et al., 1964). I will never know whether the work described here would have been performed, or interpreted correctly, absent these prior findings. Steve Cooper left Buffalo in 1970 for the University of Michigan, but we remained in touch for years, including at the occasional meeting (**Figure 3**). Several colleagues whose published work, private discussions and encouragement were of great help during this time have already been mentioned, but I also wish to especially acknowledge my long-term collaboration with Olga Pierucci, a number of valuable inputs from K. Gordon Lark, Arthur Pardee and Joe Clark, and the important insightful subsequent contributions of Alan C. Leonard.

A Simplified Baby Machine

My primary reasons for agreeing to write this exhumation of the past are contained in this and the following section. So if you have skimmed through the preceding, but have a developing interest in synchronous cells or the bacterial cell cycle, this is the point

FIGURE 2 | Argonne National Laboratory, 1968. Ole Maaløe facilitating discussion after a presentation by Charles Helmstetter at a Division of Biological and Medical Sciences symposium.

FIGURE 3 | Charles Helmstetter and Steve Cooper during a reception at a conference in 1987.

at which you might consider reading more slowly. I completely understand why someone might be reluctant to embark on studies with minimally disturbed synchronous cells if it is believed that the baby machine device is too complex to construct and use. In my biased opinion, this notion is inaccurate. The baby machine process for generating synchronous cells is remarkably simple to perform.

What is actually needed to get minimally disturbed synchronous cells? Nothing very special. In fact, if you would like to try the technique, or perform a few experiments, or test some cells, it is very easy to construct and operate a minimalistic but functional baby machine. The primary requirements are the following:

(1) A 150-mm ID porcelain Buchner funnel.
(2) A 142-mm diameter, 0.22-μm Millipore MF membrane filter, or equivalent.
(3) A mesh screen to place underneath the membrane filter.
(4) A means to hold the membrane filter in place in the funnel.

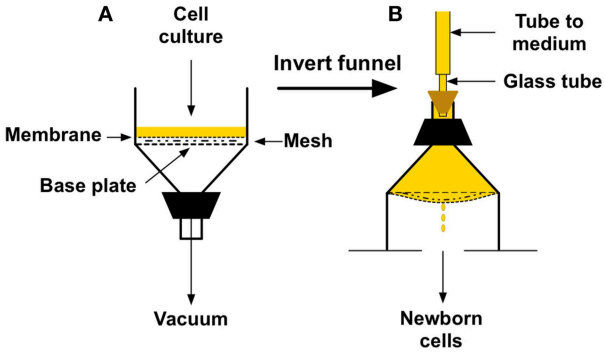

FIGURE 4 | Buchner funnel version of a cellular baby machine. (A) Funnel set-up for binding cells to a membrane filter surface. **(B)** Orientation and appearance of the funnel during elution of newborn cells from the membrane filter surface.

Figure 4 shows the basic set-up and procedure using a Buchner funnel with a 150-mm diameter perforated base plate (Scientific Equipment of Houston). To prepare the funnel as shown in **Figure 4A**, the membrane filter must be sealed to the bottom plate of the funnel. This is most easily accomplished by first running a narrow bead of biologically safe silicone sealant (such as Factor II A-4100 or aquarium-safe silicone) around the bottom of the funnel just inside the 142-mm circumference of a membrane filter. Next, place the mesh screen loosely inside the bead. I recommend using a 120-mm diameter screen cut from a Buchner polyethylene disc (Avogadro's Lab Supply, Inc.). Lastly, place the membrane filter on top of the bead and press down on the edge. I have used the top portion of 130-mm two-piece polypropylene Buchner funnel for this purpose (Avogadro's Lab Supply, Inc.), but any ring of that approximate diameter should work well. After curing, this procedure yields a perfect seal, produces a surface of about 120 mm in diameter for attachment of the cells, and enables culture medium to flow uniformly across the membrane after inversion of the apparatus. The seal is easily removed with a razor blade for the next experiment.

To perform the procedure, a total of 0.5 to 1.0 $\times$ 10^{10} bacteria growing in 100–200 ml of minimal defined medium are filtered slowly (1–2 min) under vacuum onto the membrane filter at the appropriate temperature in a warm room or any convenient table-top incubator (**Figure 4A**). The entire filter holder is then inverted (**Figure 4B**), culture medium is poured into the top of the inverted holder (about 300 ml), and tubing from a reservoir of medium is connected to the stem of the funnel with a stopper. To produce a sealed system, the tubing should be attached to a narrow glass or rigid plastic tube installed in a hole bored through a stopper of appropriate size, as shown. It is helpful to have most of the stem of the funnel cut off, as indicated in the figure, to ease pouring of the medium and connection of the stopper. A peristaltic pump can be used to regulate the rate of medium flow into the apparatus after inversion. It should be set at about 15 ml/min for a few minutes to flush off weakly attached cells and then reduced to 2 ml/min thereafter. Alternatively, if you wish to perform tests before obtaining a pump, a reservoir bottle with a bottom outlet can be placed above the apparatus with a hose clamp acting as the flow regulator. In either case, once medium flow begins, the underside of the membrane will become convex with drops coming from the center as seen in **Figure 4B**. The smooth, convex shape of the membrane is VERY important because it enables the medium to flow uniformly over the surface of the attached cells, and to form drops that fall exclusively from a single point at the center of the membrane.

The procedure is so simple that anyone with an interest in obtaining minimally disturbed synchronous cells should try it. There are, however, a few nuances that can be generalized. Of course it is essential to try the method first with a strain known to work effectively. For bacteria, it works best with *E. coli* B/r (ATCC 12407) and wild-type K12 (Helmstetter et al., 1992). It has also been shown to work very well with some other *E. coli* strains, *B. subtilis,* and *S. typhimurium* (Shehata and Marr, 1970; Holmes et al., 1980; Helmstetter et al., 1992). That said, any rod-shaped bacterium that does not aggregate or filament extensively during liquid culture is worth trying (after establishing adequate skill level with B/r). For cells other than *E. coli* B/r, the membrane filter might need to be pre-coated with an adhesive such as poly-D-lysine before use (Helmstetter et al., 1992). If a decision is made to perform long-term work with the technique, a specialized apparatus can be lathed from 15-cm diameter acrylic rods and cylinders as pictured in Thornton et al. (2002) and Helmstetter et al. (2003).

A video of the method, entitled "Cellular Baby Machine," can be seen at (https://m.youtube.com/watch?v=hfGwetVg2gM). The video demonstrates the technique for mammalian cells using the specialized acrylic set-up, but it is performed in the same basic manner with bacteria and when using a Buchner funnel. In fact, the procedure is significantly easier for bacteria since sterilization of the apparatus is generally unnecessary.

Fun with the Cell Cycle

Making babies can be fun, but it is not the only fun thing to try, as I hope to demonstrate in this final section. Visualizing the

chromosome replication pattern during the division cycle of cells growing under a given set of conditions can sometimes seem so baffling that it is not worth the effort. However, understanding cellular responses to various treatments often demands that the replication pattern be taken into consideration. I suspect that the impression of complexity regarding this topic is related to the unfortunate abstruseness of some of the figures we and others have used to describe the cycle. The publication that contains the most complete description of the $I+C+D$ model and its applications (Helmstetter et al., 1968) also contains, in retrospect, some impossibly complex figures. It is sometimes difficult and tiresome to look at a complex figure and plow through each aspect to get to the bottom line. Furthermore, the figure may not apply directly to the question at hand. Therefore, in this section I will describe the very simple method I use to determine replication patterns. This is exactly what I draw either on a lined pad for my own benefit or on a white board for students. In fact, the beginning of such a drawing appears on the chalkboard in **Figure 2**.

We will determine the moderately complex relationship between chromosome replication and cell division for the average *E. coli* B/r cell in a population growing with a doubling time of 35 min at 37°C. At this growth rate, reasonable values for *C* and *D* would be 40 min and 20 min, respectively. Referring to **Figure 5**, start at the top left by imagining a hypothetical cell with no initiation potential and draw a squiggly horizontal line, 35 min in duration, to represent *I*. *I* must be 35 min under these conditions because, as will be seen at the end of this exercise, *I* determines the doubling time. At the end of the *I* period, replication initiates, so draw a 40-min horizontal line to represent *C*, followed by a 20-min interrupted line to represent *D*. Then draw a long vertical line to represent cell fission. Now start the second $I + C + D$ sequence below the first. Since *I* is continuous by definition, begin the next squiggly line at the time the *I* period ends in the first sequence, and then draw *C* for another 40 min, *D* for 20 min and another vertical line. At this point I would normally shout at the students, saying something like: "DON'T THINK! Just draw $I+C+D$, $I+C+D$, over and over until you have gone past the second vertical division line. If you try to think you will surely mess up, especially at more rapid growth rates." Now we are done, and the division cycle for a cell with the given characteristics is shown between the two vertical lines representing division. It is important to note that the duplication process of *E. coli* can be described as a simple overlapping series of $I + C + D$ sequences. Furthermore, the time between divisions is determined exclusively by *I* and independent of the durations of *C* and *D*.

Thinking is now permitted to complete the exercise because the correctly drawn cycle is in front of us. The first step is to add chromosome configurations during the cycle to the sequences drawn in **Figure 5**. This process is presented in red in **Figure 6**, above the $I + C + D$ sequences. Chromosomes are represented by straight lines rather than circles because circles are too hard to draw and unnecessary in this schematic representation. Again start at the beginning of the first sequence at the upper left by drawing a short horizontal line to represent a chromosome with no initiation potential residing in a hypothetical cell. The origin of replication is at the left end of the line, and the terminus at the right. Now, progress to the right, looking vertically as you go, to observe where the cell is located in each of the overlapping $I + C + D$ sequences. At the end of the first *I* period, the chromosome initiates replication, as indicated by a small filled circle at the left end, and preparation begins for the next initiation event as shown in the second $I + C + D$ sequence. After 20 min of the first *C* period, the chromosome is half replicated. After 35 min of the first *C* period, the chromosome is 35/40 replicated and new rounds of replication have initiated due to the second sequence, as indicated by two filled circles at the left end. Thus, the cell has begun to progress through two *C* periods simultaneously. Replication along the first sequence ends

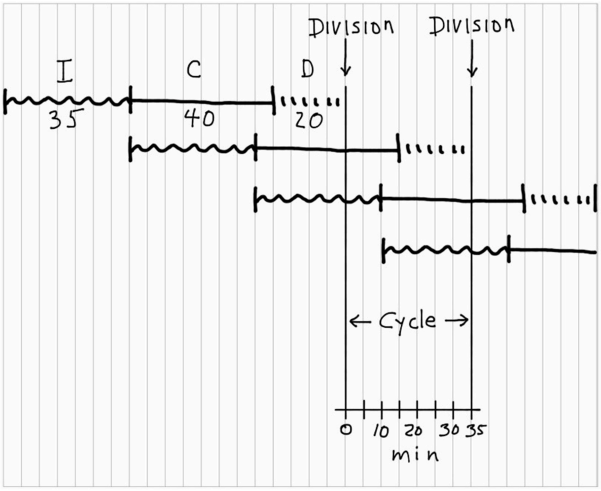

FIGURE 5 | Construction of a chromosomal replication pattern during the bacterial division cycle. The construction, starting at the top left, is based on the $(I + C + D)$ rule with $I = 35$ min, $C = 40$ min, and $D = 20$ min.

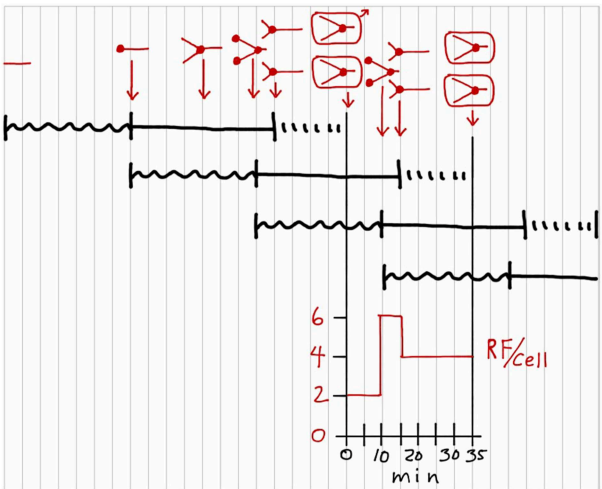

FIGURE 6 | Addition of chromosome configurations to a division cycle construction. Chromosomal DNA is represented by red lines, with small filled circles indicating replication sites. The configurations in rectangles indicate cell divisions. Only one cell is followed after the first division. Number of replication forks per cell (RF/cell) is shown during the division cycle.

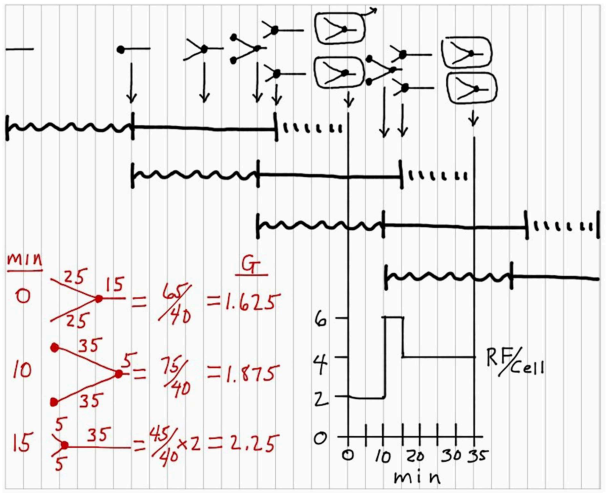

FIGURE 7 | Genome equivalents of DNA per cell (*G*) during the division cycle. Calculations of the values for *G* are shown in red for three select times in the division cycle: 0, 10, and 15 min.

5 min later so the cell now contains two chromosomes each 5/40 replicated. Twenty minutes later the cell divides due to the first sequence. Each daughter cell contains one chromosome that is 25/40 replicated due to the second sequence, and is also 25/35 of the way along preparation for the next initiation event due to the third sequence. This then is the chromosome configuration in a newborn cell in a culture growing with the given parameters. Chromosome replication during the division cycle of these cells is given by the chromosome configurations between the two vertical division lines. Configurations are shown for three key time points in the cycle, again determined by observing what is happening, vertically, in each $I + C + D$ sequence. Note that cells growing at this rate are progressing along three reproductive paths simultaneously, such that the processes leading to a specific cell division began two division cycles in advance.

With the chromosome configurations completed, two additional aspects of the cycle can be determined. The graph beneath the division cycle in **Figure 6** shows replication forks per cell (RF/cell) during the cycle, determined by counting the number of forks in the chromosome drawings and multiplying by two to account for bidirectional replication on the circular chromosome. Assuming the rate of DNA polymerization is constant during *C*, this graph shows the rate of chromosomal DNA synthesis during the cycle. For the first 10 min of the cycle, there are 2 RF/cell due to the single round of bidirectional replication on the chromosome. Then the RF/cell increases three-fold due to initiation of new rounds of bidirectional replication at the two origins on the replicating chromosome. Five minutes later, the intial round of replication finishes, and the cell is left with two chromosomes replicating bidirectionally for the last 15 min of the cycle, i.e., 4 RF/cell.

Finally, it is sometimes of interest to determine chromosomal DNA content per cell at various times in the cycle in terms of genome equivalents (*G*) (Cooper and Helmstetter, 1968). This calculation is shown in red in **Figure 7** for three select times in the division cycle (0, 10, and 15 min). Again based on the idea that the replication rate is constant during *C*, this calculation is most easily visualized by recording the extent of chromosomal replication based on time rather than distance, and then dividing the sum of the times by *C* (40 min in this case) as shown. The average chromosomal DNA content in an exponentially growing culture can be determined with the equation: $G = \tau/Cln2\left[2^{(C+D)/\tau} - 2^{D/\tau}\right]$, where τ equals doubling time.

The preceding shows an example of a simple method to sketch the division cycle of cells growing at any rate. Slower growing cells are easier to draw due to less overlap of $I + C + D$ sequences, and more rapidly growing cells are more complex due to increased overlap but are still easy to do if you follow the rule of just drawing the $I + C + D$ sequences without overthinking the issue. Simply change the values for *I*, *C*, and *D*, and follow the instructions in the preceding paragraphs. Should a difficulty be encountered, additional examples of this procedure can be found in Helmstetter (1996). It can be entertaining to consider cells with odd values for *I*, *C*, and *D* and then determine how they must behave.

A few additional points need to be made. The idea of overlapping $I + C + D$ sequences for duplication appears to apply to many bacteria that divide by binary fission, but the durations of each step can vary considerably with temperature and culture conditions (e.g., Helmstetter et al., 1992, and references therein). For many *E. coli* strains, the values for *C* and *D* are roughly 40 and 20 min growing with doubling times between about 20 and 80 min at 37°C. Under these circumstances it is only necessary to measure τ to determine the chromosome replication pattern since τ equals *I*, and *C* and *D* are constants. On the other hand, in some strains *C* and *D* can be quite different, usually longer. During slow growth, one and sometimes two gaps in DNA synthesis appear in the cycle. When τ is between *C* and $C + D$ min in duration, a gap exists at the end of the cycle during part or all of *D*. When τ is longer than $C + D$ min, a gap also exists at the start of the cycle, designated the *B* period. But again, all of this can be seen by simply drawing the sequences as shown here with the appropriate values for the parameters. This analysis disregards dispersions in the values for the parameters in individual cells in a culture, but the purpose of the preceding was merely to display what happens in a single, average cell without regard to population variability.

My hope is that anyone who would like to run some experiments on synchronously dividing bacteria will try the procedure described here and see how simple yet useful the baby machine can be. I also hope the handy method for visualizing chromosome replication during the cell cycle will be found useful.

Acknowledgments

I wish to thank Valerie LeBleu for preparation of the video of the baby machine procedure and for her advice on the technology.

References

Abbo, F. E., and Pardee, A. B. (1960). Synthesis of macromolecules in synchronously dividing bacteria. *Biochim. Biophys. Acta* 39, 478–485. doi: 10.1016/0006-3002(60)90201-8

Cooper, S. (1997). DNA replication: the 30th anniversary of the bacterial model and the "baby Machine." *Trends Biol. Sci.* 22, 490–494. doi: 10.1016/S0968-0004(97)01126-2

Cooper, S., and Helmstetter, C. E. (1968). Chromosome replication and the division cycle of *Escherichia coli* B/r. *J. Mol. Biol.* 31, 519–540. doi: 10.1016/0022-2836(68)90425-7

Hanawalt, P. C., Maaløe, O., Cummings, D. J., and Schaechter, M. (1961). The normal DNA replication cycle II. *J. Mol. Biol.* 3, 156–165. doi: 10.1016/S0022-2836(61)80042-9

Helmstetter, C., Cooper, S., Pierucci, O., and Revelas, E. (1968). On the bacterial life sequence. *Cold Spring Harbor Symp. Quant. Biol.* 33, 809–822. doi: 10.1101/SQB.1968.033.01.093

Helmstetter, C. E. (1967). Rate of DNA synthesis during the division cycle of *Escherichia coli* B/r. *J. Mol. Biol.* 24, 417–427. doi: 10.1016/0022-2836(67)90228-8

Helmstetter, C. E. (1969). "Methods for studying the microbial division cycle," in *Methods in Microbiology*, eds J. R. Norris and D. W. Ribbons (New York, NY Academic Press), 327–363.

Helmstetter, C. E. (1996). "Timing of synthetic activities in the cell cycle," in *Escherichia coli and Salmonella Typhimurium*: *Cellular and Molecular Biology*, eds F. C. Neidhardt, R. Curtiss III, J. L. Ingraham, E. C. C. Lin, K. B. Magasanik, W. S. Resnikoff, et al. (Washington, DC: ASM Press), 1627–1639.

Helmstetter, C. E., and Cooper, S. (1968). DNA synthesis during the division cycle of rapidly growing *Escherichia coli* B/r. *J. Mol. Biol.* 31, 507–518. doi: 10.1016/0022-2836(68)90424-5

Helmstetter, C. E., and Cummings, D. J. (1964). An improved method for selection of bacterial cells at division. *Biochim. Biophys. Acta* 82, 608–610. doi: 10.1016/0304-4165(64)90453-2

Helmstetter, C. E., Eenhuis, C., Theisen, P., Grimwade, J., and Leonard, A. C. (1992). Improved bacterial baby machine: application to *Escherichia coli* K-12. *J. Bacteriol.* 174, 3445–3449.

Helmstetter, C. E., Thornton, M., Romero, A., and Eward, K. L. (2003). Synchrony in human, mouse and bacterial cell cultures. *Cell Cycle* 2, 42–45. doi: 10.4161/cc.2.1.185

Holmes, M., Rickert, M., and Pierucci, O. (1980). Cell division cycle of *Bacillus subtilis*: evidence of variability in period D. *J. Bacteriol.* 103, 789–792.

Kjeldgaard, N. O., Maaløe, O., and Schaechter, M. (1958). The transition between different physiological states during balanced growth of *Salmonella typhimurium*. *J. Gen. Microbiol.* 19, 607–619. doi: 10.1099/00221287-19-3-607

Maaløe, O., and Kjeldgaard, N. O. (1966). *Control of Macromolecular Synthesis*. New York. NY: W. A. Benjamin.

Maruyama, Y., and Yanagita, T. (1956). Physical methods for obtaining synchronous culture of *Escherichia coli*. *J. Bacteriol.* 71, 542–546.

Novick, A., and Szilard, L. (1950). Experiments with the chemostat on spontaneous mutants of bacteria. *Proc. Natl. Acad. Sci. U.S.A.* 36, 708–719. doi: 10.1073/pnas.36.12.708

Schaechter, M., Maaløe, O., and Kjeldgaard, N. O. (1958). Dependency on medium and temperature of cell size and chemical composition during balanced growth of *Salmonella typhimurium*. *J. Gen. Microbiol.* 19, 592–606. doi: 10.1099/00221287-19-3-592

Shehata, T. E., and Marr, A. G. (1970). Synchronous growth of enteric bacteria. *J. Bacteriol.* 103, 789–792.

Thornton, M., Eward, K. L., and Helmstetter, C. E. (2002). Production of minimally disturbed synchronous cultures of hematopoietic cells. *Biotechniques* 32, 1098–1105.

Uretz, R. B., Bloom, W., and Zirkle, R. E. (1954). Irradiation of parts of individual cells II. Effects of an ultraviolet microbeam focused on parts of chromosomes. *Science* 120, 197–199. doi: 10.1126/science.120.3110.197

Witkin, E. M. (1946). Inherited differences in sensitivity to radiation in *Escherichia coli*. *Proc. Natl. Acad. Sci. U.S.A.* 32, 59–68. doi: 10.1073/pnas.32.3.59

Wollman, E. L., and Jacob, F. (1955). Mechanism of the transfer of genetic material during recombination in *Escherichia coli* K12. *CR Hebd. Seances Acad. Sci.* 240, 2449–2451.

Wollman, E. L., Jacob, F., and Hayes, W. (1956). Conjugation and genetic recombination in *Escherichia coli* K-12. *Cold Spring Harb. Symp. Quant. Biol.* 21, 141–162. doi: 10.1101/SQB.1956.021.01.012

Yoshikawa, H., O'Sullivan, A., and Sueoka, N. (1964). Sequential replication of the *Bacillus subtilis* chromosome. III. Regulation of initiation. *Proc. Natl. Acad. Sci. U.S.A.* 52, 973–980.

Conflict of Interest Statement: The authors declare that the research was conducted in the absence of any commercial or financial relationships that could be construed as a potential conflict of interest.

Copyright © 2015 Helmstetter. This is an open-access article distributed under the terms of the Creative Commons Attribution License (CC BY). The use, distribution or reproduction in other forums is permitted, provided the original author(s) or licensor are credited and that the original publication in this journal is cited, in accordance with accepted academic practice. No use, distribution or reproduction is permitted which does not comply with these terms.

frontiers in Microbiology

REVIEW
published: 03 August 2015
doi: 10.3389/fmicb.2015.00756

Chromosome replication, cell growth, division and shape: a personal perspective

Arieh Zaritsky[1]* *and Conrad L. Woldringh*[2]*

[1] Faculty of Natural Sciences, Ben-Gurion University of the Negev, Be'er-Sheva, Israel, [2] Swammerdam Institute for Life Sciences, University of Amsterdam, Amsterdam, Netherlands

OPEN ACCESS

Edited by:
Julie A. Maupin-Furlow, University of Florida, USA

Reviewed by:
Jason W. Cooley, University of Missouri, USA
Jolanta Zakrzewska, University of Wroclaw, Poland
Iain Duggin, University of Technology Sydney, Australia

***Correspondence:**
Arieh Zaritsky, Faculty of Natural Sciences, Ben-Gurion University of the Negev, Kiryat Bergman N2 (2110), PO Box 653, Be'er-Sheva 85105, Israel
ariehzar@gmail.com;
Conrad L. Woldringh, Swammerdam Institute for Life Sciences, University of Amsterdam, Science Park 904, NL-1098 XH Amsterdam, Netherlands
c.woldringh@gmail.com

Specialty section:
This article was submitted to Microbial Physiology and Metabolism, a section of the journal Frontiers in Microbiology

Received: *11 February 2015*
Accepted: *10 July 2015*
Published: *03 August 2015*

Citation:
Zaritsky A and Woldringh CL (2015) Chromosome replication, cell growth, division and shape: a personal perspective. Front. Microbiol. 6:756. doi: 10.3389/fmicb.2015.00756

The origins of Molecular Biology and Bacterial Physiology are reviewed, from our personal standpoints, emphasizing the coupling between bacterial growth, chromosome replication and cell division, dimensions and shape. Current knowledge is discussed with historical perspective, summarizing past and present achievements and enlightening ideas for future studies. An interactive simulation program of the bacterial cell division cycle (BCD), described as "The Central Dogma in Bacteriology," is briefly represented. The coupled process of transcription/translation of genes encoding membrane proteins and insertion into the membrane (so-called transertion) is invoked as the functional relationship between the only two unique macromolecules in the cell, DNA and peptidoglycan embodying the nucleoid and the sacculus respectively. We envision that the total amount of DNA associated with the replication terminus, so called "nucleoid complexity," is directly related to cell size and shape through the transertion process. Accordingly, the primary signal for cell division transmitted by DNA dynamics (replication, transcription and segregation) to the peptidoglycan biosynthetic machinery is of a physico-chemical nature, e.g., stress in the plasma membrane, relieving nucleoid occlusion in the cell's center hence enabling the divisome to assemble and function between segregated daughter nucleoids.

Keywords: bacterial cell division cycle, nucleoid complexity and segregation, size and shape determination, transertion, peptidoglycan biosynthesis

Bacteriology and the Molecular Biology Revolution

Bacteriology was conceived by the Dutch Scientist Antony van Leeuwenhoek in the 17th Century (Porter, 1976), but considered "The Last Stronghold of Lamarckism" until 1943, when the ingenious Fluctuation Test was performed (Luria and Delbrück, 1943). The Phage Group of reductionists led by Max Delbrück (Cairns et al., 1966) revolutionized Basic Genetics to explain the flow of genetic information from Mendelian genes to proteins in molecular terms. This transformation was preceded by the era of protein biochemistry that could not easily pass the concept hurdle of enzyme-cannot-make-enzyme paradox (Stent and Calendar, 1978). Pure logic supported by simple, clear-cut experiments forced them to conclude that the long, seemingly monotonous DNA macromolecule is the storehouse of genetic information.

Molecular Biology developed quickly by clarifying that the transforming principle (Avery et al., 1944) was DNA: its structure was deciphered (Watson and Crick, 1953), semi-conservative replication demonstrated (Measelson and Stahl, 1958), functions in transcription/translation into proteins disclosed (Nirenberg, 2004), and manipulations crossed species barriers (Balbás et al., 1986).

Two mutually-exclusive groups that hardly exchanged information were responsible for the revolution: those mentioned above led by Physicist Max Delbrück and Chemists led by Arthur Kornberg (Kornberg and Baker, 1992). Exposing the DNA's symmetrical beauty and crucial role required seminal studies by persistent scientists such as Erwin Chargaff and Rosalind Franklin, who were in the frontier's cutting edge but individualistic and less lucky (Watson, 1996).

There were unavoidable diversions: some excellent scientists considered penicillin resistance to be an adaptive response, others described enzyme induction in terms of kinetics, still others thought of bacterial conjugation as zygote formation, but these and many more failed attempts were indispensable for the main thrust of advance. Furthermore, the absolute acceptance of the operon model (Jacob and Monod, 1961) for example, misled others to consider *lon* mutants as regulatory (Markovitz, 1964).

Merging molecular biology with general bacteriology, basic genetics and sophisticated microscopic and physical techniques discovered the sexuality and circularity of the bacterial chromosome (Jacob and Wollman, 1956; Cairns, 1963; Hayes, 1968), its replication schedule (Helmstetter et al., 1968), and the nucleoid structure (Kellenberger et al., 1958; Woldringh and Odijk, 1999).

The Origins of Bacterial Physiology

Until the late 1920's, bacterial cultures were thought to be composed of cells that constantly change size, form and structure in a meaningless fashion. In his book, Henrici (1928) noted that these changes during a single growth cycle "*occur with great regularity and are governed by simple laws which,... may probably be very precisely formulated*." It took 30 years to achieve this goal in descriptive terms, and additional decades to begin deciphering the fundamental laws anticipated by Henrici (1928) in robust, molecular terms. The multitude of forms and sizes in a random, single-species pure culture could only be explained when age distribution (Powell, 1956) and balanced growth (Campbell, 1957) were defined, and the Copenhagen School (Maaløe and Kjeldgaard, 1966; Schaechter, 2006) described how cell size and composition change with the medium (Schaechter et al., 1958) and during transitions between growth rates (Kjeldgaard et al., 1958).

Ole Maaløe was working at The State Serum Institute (Cooper, 1993) until he was named a Professor and started, late in 1958, The Institute of Microbiology. It seems to some of us that Ole entertained the idea to imitate Niels Bohr's Physics Institute, likely because he held Bohr in the highest admiration and was a good friend of his son Aage, also a Nobel laureate in Physics. This Institute and Ole's strong personality influenced dramatically several generations of scientists involved in investigating physiological aspects of the bacterial cell, nicknaming it The Copenhagen School. The numerous scientists who passed through it during their careers (Anderson et al., 2006), mostly young, promising and subsequently influential, demonstrate that it was a success.

The seminal series of experiments with *Salmonella typhimurium* published in 1958 in two back-to-back articles (Kjeldgaard et al., 1958; Schaechter et al., 1958), established the field of Bacterial Physiology and turned into its main hallmark. The stream of articles stemming from the Institute became a flood of crucial information published in the most prestigious periodicals of the time. One major motto of Ole in understanding the cell was "Look–Do Not Touch" hence studies were performed with minimal perturbations of the so-called steady-state of exponential growth (Fishov et al., 1995). After physiological manipulations were seemingly exhausted, the use of drugs and mutants became common when the mechanisms of their actions were, or thought to be deciphered. The multi-faceted phenotypes exerted by these (lack of specificity and pleiotropism, respectively) occasionally remind us to stick to this rule-of-thumb in order to keep interpretations of results as crystal-clear as possible.

This first leg of the journey to understand the logic behind the duplication of a bacterial cell, which took place in the 1950s, is described in this collection by Schaechter (2015), and the other two, partially overlapping legs in the 1960s–by Hanawalt (2015) and Helmstetter (2015). Phil studied the phenomenon of thymineless-death (TLD) in thymine-starved populations of *thyA* mutants (Cohen and Barner, 1954) employing it to better understand the connection between chromosome replication and cell growth and viability (Hanawalt et al., 1961), and Charles exploited the neat, so-called "baby-machine" that he devised (Helmstetter and Cummings, 1964) to derive the temporal aspects of the bacterial cell cycle (Helmstetter et al., 1968).

Being students during the early 1970's, here we try to fill-in the development in a perspective of half a century and in line with our view-points. To this effect, we acknowledge with admiration the ingenuity of Noboru Sueoka and Hirosho Yoshikawa, whose results with *Bacillus subtilis* (Yoshikawa and Sueoka, 1963) revealed Ole's prediction (Maaløe, 1961) that replication initiates from a single point (later defined as *oriC*) and is sequential and multi-forked at fast growth rates (Oishi et al., 1964). Thinking rigorously, they derived marker frequency equations (Sueoka and Yoshikawa, 1965) that survived the test of time. Bidirectionality of the replication has later been demonstrated by various genetic, physiological and microscopic means (e.g., Masters and Broda, 1971; Bird et al., 1972; Prescott and Kuempel, 1972; Wake, 1972).

Experiments that investigated the fractional increase of DNA (ΔG) in amino acids-starved cultures of *Escherichia coli* $15T^-$ (so-called "runout") using dense and radioactive isotopes of thymine (Lark et al., 1963) led to the discovery of the so-called premature initiation (Pritchard and Lark, 1964), distinguishing between the two independent processes of replication, initiation and elongation. This distinction had clearly been indicated by Phil's classical experiments (Hanawalt et al., 1961), and was later supported by isolating two groups of conditional-lethal replication mutants (Hirota et al., 1968) that either stopped replication immediately upon transfer to the restrictive temperature (elongation) or allowed completion of the ongoing cycle but not new initiations.

Growth, Chromosome Replication and Cell Division; the BCD

Two essential, unique macromolecules (structures) exist in a bacterium: DNA (nucleoid) that stores the genetic information, and the shape-maintaining peptidoglycan (sacculus), which also protects the cell from rupture by its osmotic pressure (turgor). To survive, the cell must divide after its genome doubles and in a plane between the two emerging sets, hence duplications of the two are coupled, temporally and spatially. Much effort is expended to discover the mechanism responsible for this coupling, which raises the efficacy of competition among species. To study this coupling, reproducible steady-state conditions and well-defined perturbations (Maalφe and Kjeldgaard, 1966) have been exploited.

Wild-type *E. coli* can synthesize all of its component macromolecules necessary for duplication from aqueous salts solution. Multiplication rate is carbon source-dependent, the most efficient of which is glucose, supporting doubling time τ of about 40 min at 37°C. Slower rates are obtained on poorer sources, whereas adding organic building blocks result in faster rates, the maximum achievable being about 3 h^{-1} (i.e., $\tau_{min} \approx 20$ min). Irrespectively, the time C taken to duplicate the chromosome (of ∼4.6 Mb) is constant, *ca*. 40 min (Helmstetter et al., 1968). A cell divides into two morphologically-identical daughters (Trueba and Woldringh, 1980) about 20 min (designated D) after termination of replication hence division follows replication-initiation by about 1 h. This model was experimentally confirmed for cells growing at τ ranging 20–70 min (growth rate μ of 3–0.9 h^{-1}, respectively). Situations with $\tau < C$ are achieved by initiating new replication rounds before completing the previous ones. Under slow growth rates, on the other hand, the cycle includes a period B [$= \tau - (C+D)$] in which cells have not initiated yet hence they continue to grow—much like in the G_1 period of the eukaryotic cell division cycle. This (B, C, D, τ) model has survived over 40 years with minor modifications of parameter values (e.g., Bipatnath et al., 1998; Michelsen et al., 2003), and many of its conclusions have been confirmed in other eubacteria (Helmstetter, 1996; Toro and Shapiro, 2010). It can thus be termed (Zaritsky et al., 2011, 2012) as "*The Central Dogma of The Bacterial Cell Division Cycle*" (two meanings for *BCD*). A cell cycle is divided in 3 (or 4) periods by two major events between successive fissions, initiation and termination of replication that can occur in reverse order depending on the values of C, D, and τ (Jiménez Sánchez, 2015).

Combining the noted constancy of C and D values (Helmstetter et al., 1968) with the way mean cell mass change with τ (Schaechter et al., 1958) resulted in an important insight: cell mass M_i at the time of replication-initiation is roughly constant per replication origin *oriC* (Donachie, 1968; Pritchard, 1968; Pritchard et al., 1969). The molecular mechanism regulating initiation of replication, occurring synchronously from all existing *oriC* copies and once per cell cycle, is under investigation (e.g., Leonard and Grimwade, 2010), but the apparent constancy of the *Mi*/*oriC* ratio is very useful, conferring a quantitative description of the bacterial cell. The cycle ends $C+D$ min after initiation, when cell mass reaches $M_i \times 2^{(C+D)/\tau}$. The changing exponential rate of mass growth in different media is not matched by the linear, constant DNA elongation rate ($1/C$), but the faster increase of cell mass in richer media leads to increased initiation frequency as prescribed by the constant M_i/*oriC*. BCD thus explains changes in cell composition and size with τ and predicts the consequences of perturbations such as nutritional shifts (Kjeldgaard et al., 1958). These basic features and other examples are illustrated and can be followed by the user-friendly Cell Cycle Simulation program (CCSim) at https://sils.fnwi.uva.nl/bcb/ that was partially described before (Zaritsky et al., 2006, 2007, 2011, 2012) and will be re-mentioned below. It must be noted that the values of these constants do change slightly with τ—more so at longer values, can be manipulated experimentally by various means (e.g., Meacock and Pritchard, 1975; Zaritsky and Zabrovitz, 1981; Wold et al., 1994; Bipatnath et al., 1998), and inserted in the CCSim program to confirm or reject working hypotheses.

Dissociating Rates of Replication and Growth

Capitalizing on Helmstetter's "baby machine" (Helmstetter and Cummings, 1964) and just before the description of BCD (Helmstetter et al., 1968), Clark and Maalφe (1967) demonstrated a constant rate of replication along the chromosome, with distinct discontinuities in DNA synthesis rate during the cell cycle interpreted as occurring due to initiation and completion of replication cycles. Chromosomes with multiple replication forks (also termed dichotomously replicating) is the reason for bigger ΔG added DNA in amino acids-starved, faster growing cells (Schaechter, 1961). This was the current knowledge at the end of 1968, upon the arrival of one of us (AZ) at Leicester University for graduate studies, supervised by Robert Pritchard, who had established the Genetics Department there merely 4 years earlier[1].

Digressing to some personal involvements, one of us (AZ) was very lucky to enter the atmosphere inspired by Bob and at the right time to be assigned a project in the just-opened BCD field, about which I had no clue. During 6-years of previous studies (1962–1968) at the Hebrew University of Jerusalem, my M.Sc. (with distinction but no publication) in Bacterial Genetics was supervised by Amiram Ronen, I finished 4 full years of Pre-Medical studies and attended several courses in Mathematics (my ever-lasting love). The latter was helpful to sharpen rigorous thinking, to derive the equation relating DNA concentration to the number of replication positions (Sueoka and Yoshikawa, 1965) n ($= C/\tau$) irrespective of the value of D (Pritchard and Zaritsky, 1970; Zaritsky, 1971) and to program the huge computer at Leicester University (using card-punching). It may have been important for my active participation in developing CCSim, as described below. Bob and his large team of students were instrumental for my learning both, proper English and the BCD, mainly in the tea/coffee/seminar room that was inhabited during many hours, days and nights.

Simultaneously, the other (CLW) extended his biological and microscopic skills at the University of Amsterdam. There are at least three at that time commonly-accepted ideas that I ruled out

[1] http://www2.le.ac.uk/news/blog/2014-archive-1/october/50th-anniversary-of-department-of-genetics-celebrates-world-changing-research-1

during my Ph.D. studies and beyond namely, existence of direct DNA-membrane attachments (Woldringh, 1974), of peri-septal annuli (Woldringh, 1994) and rapid nucleoid displacement (van Helvoort and Woldringh, 1994), all has meanwhile disappeared from our knowledge-base, justifiably so. My close association with Nanne Nanninga (e.g., Woldringh and Nanninga, 1985), who in the late 1960's demonstrated the artifactual origin of mesosomes (Nanninga, 1971), enabled the establishment of a department that attracted distinguished students and scientists from all over the world, microbiologists as well as physicists and engineers. In their search to define the structural changes occurring during fixation and dehydration necessary for visualizing the bacterial nucleoid in the electron microscope, the possibilities to study live cells were improved with the reinvention and development of the confocal scanning light microscope (CSLM) by Brakenhoff (see Valkenburg et al., 1985).

Back to the main subject, at Leicester, Bob realized existence of literature-recorded contradictory results, the common feature of most is that they were obtained in thymine-requiring strains. These observations (e.g., Maaløe and Rasmussen, 1963; Friesen and Maaloe, 1965; Lark and Lark, 1965; Beacham et al., 1968) led him to hypothesize that the replication time of the chromosome in *thyA* strains depends on the external concentration of thymine [T] present in their growth medium (Pritchard, 1974). This hypothesis could explain all discrepancies and is consistent with lack of active thymine-transport, in *E. coli* (Itsko and Schaaper, 2011) and other bacterial species (Carmody and Herriott, 1970; Reinhart and Copeland, 1973). It was strongly confirmed by four physiological methods, more or less independent of each other (Pritchard and Zaritsky, 1970; Zaritsky, 1971), and later supported by various means in other laboratories (reviewed in Zaritsky et al., 2006).

Thus, the dissociation between syntheses rates of mass and DNA, originally observed by changing the former alone (Helmstetter et al., 1968), was confirmed by exclusively manipulating *C* by limiting [T] in *thyA* strains (Pritchard and Zaritsky, 1970), affected through the intracellular [dTTP] (Beacham et al., 1971). This method is more amenable to analysis than nutritional shifts because modulating [dTTP] by changing [T] occurs abruptly, without affecting the multitude of metabolic pathways and interactions between them that accompany nutritional shifts (Scott and Hwa, 2011).

Dissociating Cell Growth and Division; the Eclipse

In a steady-state exponentially growing culture, concentrations of all cell components increase in parallel to each other and in pace with divisions (Campbell, 1957; Fishov et al., 1995). The puzzling phenomenon of division rate-maintenance after a nutritional shift-up (Kjeldgaard et al., 1958) was instantly explained by the BCD model (Helmstetter et al., 1968): a cell divides a constant time, $C+D$ min after initiation of chromosome replication, which in turn follows mass growth. The division-rate therefore changes $C+D$ (*ca.* 65) min after the change in growth rate is affected by enriching the medium. Most perturbations, by chemical/physical agents or under restrictive conditions of *ts* mutants, cause immediate block of division (Slater and Schaechter, 1974)—one that is usually restored upon transfer back to permissive conditions. Specific inhibition of protein or DNA synthesis, however, allows divisions to continue during the *D* period; these so-called residual divisions cause a decrease in average cell length (cf. entry into stationary phase) and enable estimation of the *D* period (Dix and Helmstetter, 1973; Kubitschek, 1974; Woldringh et al., 1977).

Determination of *C* and *D* periods for batch cultures of *E. coli* cells have also been performed by flow cytometry (Michelsen et al., 2003) or by image cytometry (cf. Huls et al., 1999). From these studies it becomes clear how these cell cycle periods can vary with different strains and growth conditions. The measurements indicate that the *D* period is especially variable, making it difficult to generalize the *E. coli* cell cycle.

When thymine-limited *thyA* mutants grow at fast growth rates, another puzzling phenomenon appears, namely dissociation between growth and division that is related to replication. Under these conditions, the inter-division time is longer than mass doubling time (i.e., $\tau_d > \tau_m$) thus cell size increases continuously (Zaritsky and Pritchard, 1973), and seemingly indefinitely. The 40 years-old observation (Zaritsky, 1975a) that indicated existence of a minimal possible distance l_{min} between two successive replisomes, promptly explains this phenomenon (Zaritsky et al., 2007). The question whether the mechanism involved is structural (replisome size; Norris et al., 2007) or chemical (sequestration of membrane-attached hemi-methylated DNA; Olsson et al., 2002) remains moot, but breaching this distance would extend the inter-initiation time I ($= \tau_i$) beyond the mass doubling time (τ_m) thus delay initiations, and cumulatively so (Zaritsky et al., 2007). Such a breach can be achieved by enhanced initiation frequency (Simmons et al., 2004) or slowed replication rate (Zaritsky and Pritchard, 1973). This distance is estimated to be about half of the chromosome length (l_{chr}), termed the Eclipse (l_{min}/l_{chr}) and can be expressed in units of time depending on the rate of replication (l_{min}/l_{chr}) $\times$ C (e.g., how long it takes to reach this fraction of chromosome at a given, constant rate C^{-1}). Release from this situation by restoring the permissive conditions causes a transient increase in the frequency of divisions (Zaritsky et al., 2011) thus substantiating this concept and facilitating its investigation.

The Cell Cycle Simulation Program

Our fortuitous encounter at the Luntern Conference in November 1974 was very fortunate. We had apparently met 3 years earlier in a previous meeting there, but being students it hadn't engendered significant mutual impressions. In 1974, both of us had already acquired results related to morphometric variations of *E. coli* cells under different growth conditions, theoretical (Zaritsky, 1975b) and experimental (Woldringh, 1974), and ideas about joint research sprang in the air during a long night of extensive discussions. It was just 7 months later that EMBO financed a 3-month visit for CLW in Be'er-Sheva (**Figure 1**), followed by another short-term fellowship for AZ to visit Amsterdam a couple of years later. These and follow-up visits culminated in detailed descriptions of cell dimensional rearrangements during nutritional shift-up experiments (Grover et al., 1980; Woldringh

FIGURE 1 | Conrad (R) and Arieh (L) at the unique "Chezi" 30 mm-film projector, manually measuring cell dimensions and constrictions, Be'er-Sheva, Summer 1976. This primitive, bulky "machine" was designed and constructed by the Workshop of the Natural Sciences Faculty at Ben-Gurion University, led by Mr. Yechezkel Tahori in the "pre-history" of computer visualization, initiated in the University of Amsterdam by (Trueba and Woldringh, 1980) and developed further into a versatile measuring plugin "ObjectL," which runs under ImageJ (see Vischer et al., 2015).

et al., 1980; Zaritsky et al., 1982), organization of two EMBO Workshops on Duplication of Bacteria (1980 in Holland; 1984 in Israel[2]), and 40 years of continuous cooperation. One notable outcome of our interactions was implementation of an interactive simulation program (Zaritsky et al., 2011) that integrates all quantitative knowledge about the BCD (Helmstetter et al., 1968), including the anticipated behavior of various existing and prospective mutants. This program implementation was enabled by the recruitment of Norbert Vischer, a computer engineer, by the Amsterdam department chair and faculty dean Nanne Nanninga. The lab in Swammerdam Institute is thus frequently referred to as The Amsterdam School (*à la* the Copenhagen School mentioned above).

All considerations described so far and by the CCSim (**Figure 2**) do not relate to cell dimensions and shape nor to nucleoid segregation. Future versions of CCSim may be extended to incorporate these aspects.

Cell Size and Dimensions

An exponentially growing bacillary cell elongates with unnoticeable change in width, and divides evenly at a perpendicular plane (Trueba and Woldringh, 1980). The seminal observation (Schaechter et al., 1958) that larger cells at faster growth rates in richer media are both longer *and* wider led to the proposal (Zaritsky and Pritchard, 1973; Pritchard, 1974; Zaritsky, 1975b) that cell dimensions and cell shape could be directly coupled to the process of DNA replication and segregation. It was initially interpreted to involve active regulation of length *L* (Grover et al., 1977) or surface area *S* (Rosenberger et al., 1978a,b) extension, and passive response of width *W* to the changes of volume *V* and *L* (or *S*), the so-called linear/log model. Cell elongation was assumed to proceed at a constant rate (either dependent on μ or not) that is proportional to the number of *oriC*s, *terC*s (replication termini) or replisomes (Zaritsky and Pritchard, 1973). This view was later abandoned when peptidoglycan synthesis was demonstrated to be diffuse throughout the cylindrical periphery and only localized during the division process (Woldringh et al., 1987).

With such models in mind, we measured (**Figure 1**) the dimensions of *E. coli* cells cultured under steady-state of exponential growth in different media supporting various rates, prepared for electron microscopy by the agar filtration method (Woldringh et al., 1977; **Figure 3**), and compared the results with the various models (Zaritsky et al., 1982). Our nutritional-upshift experiment (Woldringh et al., 1980) revealed that the increase in cell diameter was slow and occurred mainly during the division process in the vicinity of the deepening constriction site, forming transiently tapered cells (**Figure 4**). Consequent to this slow adaptation and almost immediate change in the rate of mass synthesis, cell length overshoots, but the mechanism governing this diameter change is still enigmatic. A diameter increase during the constriction process has also been implied in populations growing in steady state where the cells showed a diameter decrease during elongation (see Figure 4 in Trueba and Woldringh, 1980). It should be noted that in all these preparations the cells had been fixed with osmium tetroxide and were air-dried, causing their flattening (Vardi and Grover, 1993). Nevertheless, the measurements compared well with those obtained from hydrated cells with phase-contrast microscopy (cf. Table 3 in Trueba and Woldringh, 1980).

Associated with cell widening, the nucleoids (bright areas in **Figure 4**) start replicating in planes tilted to the long cell axis (**Figure 4**), rather than parallel to it as during slow growth conditions. The differences in cell dimensions and nucleoids replication-planes are pronounced when *thyA* cells grow under identical conditions but with limiting [T] that impose slow replication rate (compare, e.g., panels A and B of Figure 6 of Zaritsky et al., 2006; and see Figure 1 in Woldringh et al., 1994).

Homeostasis of Cell Size and Shape

In the 1970's, the period of DNA replication during a division cycle was determined by pulse-labeling cells with ^{3}[H]-thymidine and measuring size distributions of cells prepared for radio-autographic electron microscopy (Koppes et al., 1978). These studies clarified that individual cells elongate exponentially (i.e., at a rate proportional to their length) and provided information about length variations at different events in the cycle as well as size and time correlations between these events (Koppes and Nanninga, 1980). The results led Koppes et al. (1978) in The

[2]http://ariehz.weebly.com/uploads/2/9/6/1/29618953/emboworkshop1984.pdf

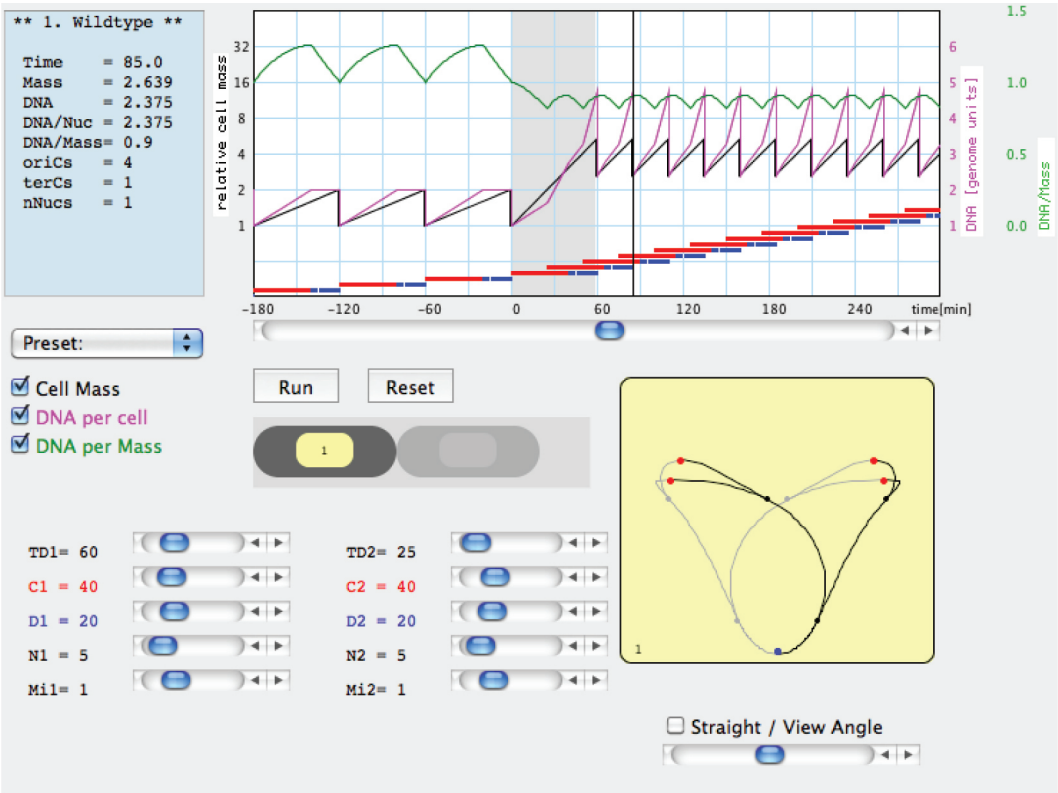

FIGURE 2 | Example of a work window of the Cell Cycle Simulation program (CCSim) for a nutritional shift-up from a doubling time $\tau_1 = 60$ min to $\tau_2 = 25$ min. The interactive program can be downloaded from: https://sils.fnwi.uva.nl/bcb/.

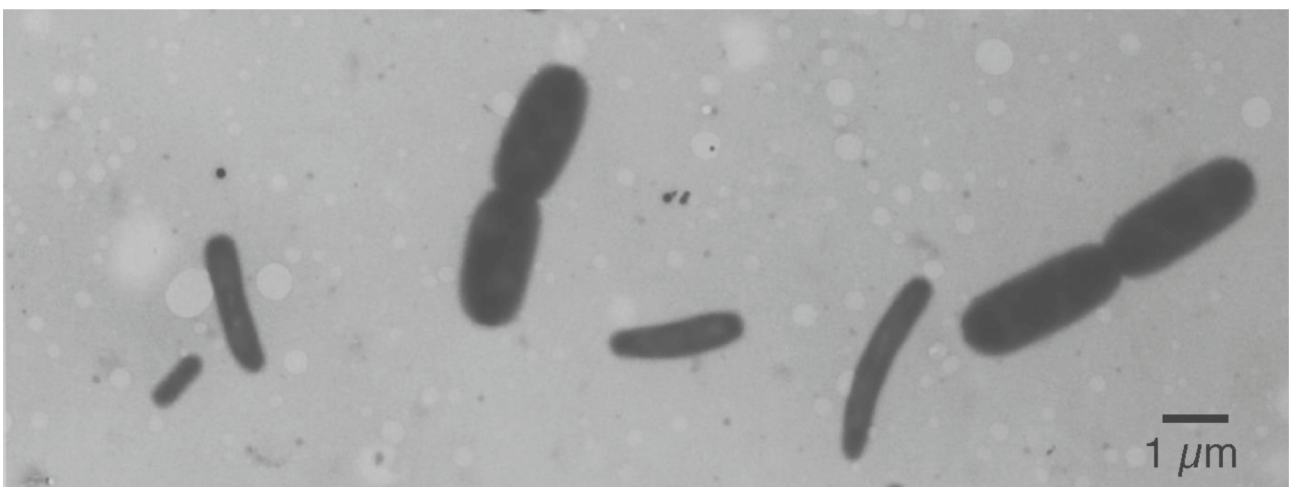

FIGURE 3 | Electron micrograph of a mixture of two *E. coli* B/r cultures prepared by agar filtration. The big cells were grown in trypton broth with a doubling time of 22 min; the small cells were grown in synthetic alanine-medium with a doubling time of 150 min. Compare with a similar preparation of mixed populations in Figure 2 of Nanninga and Woldringh (1985).

Amsterdam School to propose that cells initiate constriction after a constant length increment ΔL following initiation of DNA replication (**Figure 5**) thus establishing a correlation between cell sizes at replication initiation and at initiation of visible constriction C min later. This model of constant ΔL was recently revived (Amir, 2014) and supported by measurements of live cells (Campos et al., 2014; Iyer-Biswas et al., 2014; Taheri-Araghi et al., 2015) confirming that a growing bacterium maintains stable size by adding a constant incremental length ΔL each generation irrespective of its size at birth. This automatically leads to size

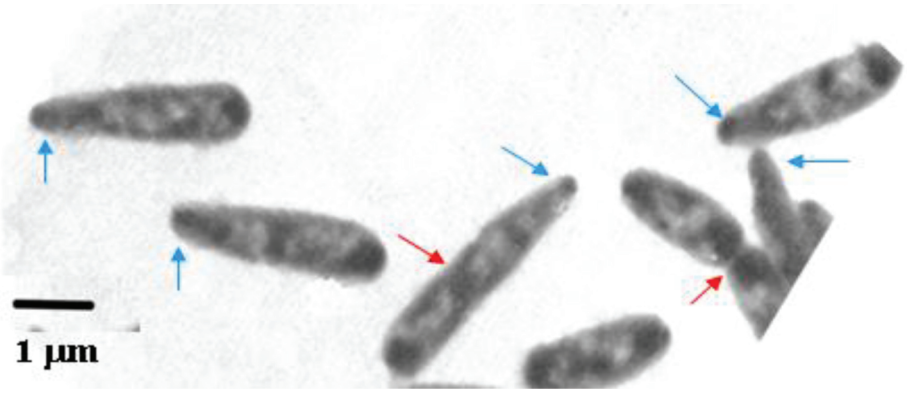

FIGURE 4 | *Escherichia coli* B/r cells prepared for electron microscopy by agar filtration, 60 min after a nutritional shift-up from $\tau_1 = 72$ to $\tau_2 = 24$ min (cf. Figure 3 in Nanninga and Woldringh, 1985). The nucleoids show up as electron-transparent regions in the air-dried cells, flattened by surface tension (cf. Woldringh et al., 1977). Red arrows indicate constriction sites, blue arrows, tapered tips.

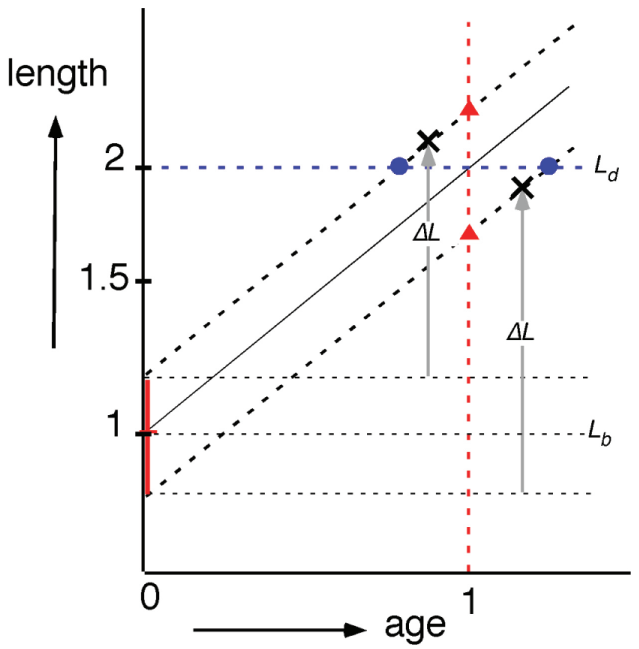

FIGURE 5 | Semi-log plot of cell length as a function of cell age (cf. Figure 6 in Koppes et al., 1978). Irrespective of newborn cell size (vertical, red bar; $L_b \pm$ SD) cells elongate exponentially (same specific elongation rate). According to the "timer" model (red triangles), newborn cells divide (at age 1) after a constant period; according to the "sizer" model (blue circles, L_d), newborn cells divide after reaching a critical size (at length 2); according to the "adder" model (black crosses) newborn cells divide after elongating with a constant length increment ΔL.

homeostasis that is valid at all growth rates obtained in different media, and since faster growing cells are longer, ΔL changes accordingly.

Jun and colleagues (Jun and Taheri-Araghi, 2014; Taheri-Araghi et al., 2015) proposed that the molecular mechanism underlying the size homeostasis by the so-called "adder" model (**Figure 5**) is related to the P-sector proteins of the *E. coli* proteome of which the total number per cell is relatively constant at different growth conditions. According to this hypothesis, accumulation of these proteins to a fixed threshold each generation would serve as a trigger for cell division. This proposal, however, does not relate mass growth to the DNA replication cycle, as suggested four decades ago (Zaritsky, 1975b). If P-sector proteins are at a fixed number per cell, then they would become diluted during the interdivision time (molecules fixed, but cell volume increases). Therefore, it is not clear how it could result in their accumulation to trigger division. Other aspects of this idea have recently been rebutted in more details (Zaritsky, 2015).

Coupling between DNA replication and cell elongation could be obtained by the nucleoid occlusion mechanism that is being relieved when daughter nucleoids are segregating apart (Mulder and Woldringh, 1989; Nanninga et al., 1990; Woldringh et al., 1990). This would require that newborn cells contain nucleoids with the same amount of DNA (*G/terC*) irrespective of their size at birth and that the state of nucleoid segregation parallels the cell's length increase. In other words, a length increment of the nucleoid would be sensed rather than a length increment of the cell. That DNA replication and segregation go hand in hand with cell elongation is supported by observations on the movement of duplicated *oriC's* (Elmore et al., 2005) and of segregating chromosome arms (cf. Youngren et al., 2014; Woldringh et al., 2015). However, while during slow growth all newborn cells can be assumed to contain nucleoids with the same amount of DNA, this will not hold for fast growth showing multifork replication. Here, stochastic premature or postponed division of mother cells will produce small and large daughter cells, respectively, with different amounts of DNA per nucleoid and thus different stages of segregation. Such cells will not signal division after a constant length increment as predicted by the "adder" model.

Another proposal (Ho and Amir, 2015; see also Robert, 2015) couples DNA replication and cell elongation to the time of initiation of DNA replication. Here, sensing of a constant length increment is starting at the last initiation of DNA replication. How a size increment rather than a critical size is monitored and whether nucleoid segregation is involved in such a model

remains to be seen. Presently, information is lacking on the size of the nucleoids in newborn cells at different growth rates at the individual cell level. Better DNA staining techniques are required to observe nucleoid growth and segregation in individual cells growing in microfluidic systems.

Whatever property a cell is sensing to enable it to divide after a constant size increment irrespective of its size at birth, some communication will be necessary between the dynamics of DNA (transcription, replication and segregation) and the biosynthetic activities of peptidoglycan (elongation and constriction at perpendicular angles). It has been proposed (Rabinovitch et al., 2003) that DNA could exert stress on the membrane through the transertion mechanism (Woldringh, 2002): coupled transcription/translation of genes encoding membrane proteins and inserting these proteins into the membrane. The strength of this interaction varies along cell length with a minimum in between the segregating nucleoids. By a yet-unknown mechanism, this stress-change signal that is relayed to initiate division is proposed to be sensed by the peptidoglycan-synthetic machinery. As described by Typas et al. (2012), this may involve stretching of the peptidoglycan network hence influencing the activity of outer membrane-anchored lipoproteins. These proteins reach through the pores of the peptidoglycan network to interact with peptidoglycan synthases (penicillin binding proteins) as required for constriction (Woldringh et al., 1987). Proteins interfering with FtsZ-ring formation were recently also related to the NO phenomenon (reviewed by Wu and Errington, 2012).

The notion that a functional relationship exists between DNA dynamics and peptidoglycan biosynthesis is supported by the high correlations found between cell dimensions and the amount of DNA per nucleoid (*G*/*terC*) over a wide range of conditions (Zaritsky, 2015). Moreover, the constant aspect ratio (cell length/width ratio) supports the view that the expansion of the nucleoid during replication and segregation (and cell mass growth) occurs equally in three dimensions.

Concluding Remarks

It is well known that the formulas describing cell mass and DNA content, as well as nucleoid complexity (amount of DNA per nucleoid), can only be applied in populations that grow under steady-state conditions (Campbell, 1957; Fishov et al., 1995). However, confirmation of steady state is seldom mentioned or documented. In many studies, bacterial batch cultures growing in rich media are used after a 100- to 1000-fold dilution of an overnight culture. In such populations the steady state has probably not been reached as it requires unperturbed, exponential growth at the same rate for some 20 generations (e.g., Maalφe and Kjeldgaard, 1966).

How do single-cell growth studies in microfluidic channels measure up to the requirements for steady state growth? It appears that constancy of growth rate and length distributions of newborn cells dividing in the channels can accurately be monitored (Wang et al., 2010; Campos et al., 2014; Osella et al., 2014; Taheri-Araghi et al., 2015). If in addition the growth experiments could include observations on nucleoid extension and segregation after labeling with, for instance, fluorescent DNA binding proteins (e.g., Männik et al., 2012; Pelletier et al., 2012), it would be possible to test the present proposal, that DNA replication and cell growth are coupled via a segregation signal for cell division. If the presumed segregation signal could be related to forces exerted by the nucleoid on the plasma membrane (Rabinovitch et al., 2003) and on the peptidoglycan network (Typas et al., 2012), it would support a belief expressed by Bob Pritchard more than 50 years ago: "...that an understanding of the determination of cell size and shape will not be possible without taking into account the physical forces to which the cell boundary is exposed." (Pritchard, 1974). We believe that the task of Physicists in expanding and deepening understanding of Cell Biology, bacteria included of course, is as critical as it was for Molecular Biology during the last Century, and similar, tight cooperation with Biologists is as crucial. The novel technologies continuously developed to enhance this end, as exemplified in the whole series of articles of this *Research Topic*, facilitate the study on both levels, single cells and single molecules in real-time.

In this memoir-style review, we try to bridge between past achievements and future prospects in the relatively-young field of Bacterial Physiology through present knowledge; scientists and students who are involved can exploit the information, which by no means is exhaustive, for the benefit of their current investigations, in the never-ending endeavor to understand Nature.

Acknowledgments

This review is a personal tribute to our mentors and inspiring colleagues Robert H Pritchard, Nanne Nanninga, Ole Maalφe and Charles E Helmstetter. Appropriate remarks by the Editor and Reviewers, particularly lain Duggin, have improved the article.

References

Amir, A. (2014). Cell size regulation in bacteria. *Phys. Rev. Lett.* 112, 208102. doi: 10.1103/PhysRevLett.112.208102

Anderson, K. B., Atlung, T., Bennett, P. M., Cooper, S., Dennis, P., Diderichsen, B., et al. (2006). Honoring Ole Maalφe. *Microbe* 1, 210–211.

Avery, O. T., MacLeod, C. M., and McCarty, M. (1944). Studies on the chemical nature of the substance inducing transformation of pneumococcal types. Induction of transformation by a desoxyribonucleic acid fraction isolated from pneumococcus type III. *J. Cell Biol.* 79, 137–158. doi: 10.1084/jem.79.2.137

Balbás, P., Soberón, X., Merino, E., Zurita, M., Lomeli, H., Fernando, V., et al. (1986). Plasmid vector pBR322 and its special-purpose derivatives—a review. *Gene* 50, 3–40. doi: 10.1016/0378-1119(86)90307-0

Beacham, I. R., Barth, P. T., and Pritchard, R. H. (1968). Constitutivity of thymidine phosphorylase in deoxyriboaldolase negative strains: dependence on thymine requirement and concentration. *Biochim. Biophys. Acta* 166, 589–592. doi: 10.1016/0005-2787(68)90251-7

Beacham, I. R., Beacham, K., Zaritsky, A., and Pritchard, R. H. (1971). Intracellular thymidine triphosphate concent-ration in wild-type and thymine-requiring mutants of *Escherichia coli* 15 and K12. *J. Mol. Biol.* 60, 75–86. doi: 10.1016/0022-2836(71)90448-7

Bipatnath, M., Dennis, P. P., and Bremer, H. (1998). Initiation and velocity of chromosome replication in *Escherichia coli* B/r and K-12. *J. Bacteriol.* 180, 265–273.

Bird, R. E., Louarn, J., Martuscelli, J., and Caro, L. (1972). Origin and sequence of chromosome replication in *Escherichia coli*. *J. Mol. Biol.* 70, 549–566. doi: 10.1016/0022-2836(72)90559-1

Cairns, J. (1963). The chromosome of *Escherichia coli*. *Cold Spring Harbor Symp. Quant. Biol.* 33, 43–45. doi: 10.1101/SQB.1963.028.01.011

Cairns, J., Stent, G. S., and Watson, J. D. (1966). *Phage and the Origins of Molecular Biology*. New York: Cold Spring Harbor Laboratory Press.

Campbell, A. (1957). Synchronization of cell division. *Bacteriol. Rev.* 21, 263–272.

Campos, M., Surovtsev, I. V., Kato, S., Paintdakhi, A., Beltran, B., Ebmeier, S. E., et al. (2014). A constant size extension drives bacterial cell size homeostasis. *Cell* 159, 1433–1446. doi: 10.1016/j.cell.2014.11.022

Carmody, J. M., and Herriott, R. M. (1970). Thymine and thymidine uptake by *Haemophilus influenzae* and the labeling od deoxyribonucleic acid. *J. Bacteriol.* 101, 525–530.

Clark, D. J., and Maaløe, O. (1967). DNA replication and the division cycle in *Escherichia coli*. *J. Mol. Biol.* 23, 99–112. doi: 10.1016/S0022-2836(67)80070-6

Cohen, S. S., and Barner, H. D. (1954). Studies on unbalanced growth in *Escherichia coli*. *Proc. Natl. Acad. Sci. U.S.A.* 40, 885–893. doi: 10.1073/pnas.40.10.885

Cooper, S. (1993). The origins and meaning of the Schaechter-Maaløe-Kjeldgaard experiments. *J. Gen. Microbiol.* 139, 1117–1124. doi: 10.1099/00221287-139-6-1117

Dix, D. E., and Helmstetter, C. E. (1973). Coupling between chromosome completion and cell division in *Escherichia coli*. *J. Bacteriol.* 115, 786–795.

Donachie, W. (1968). Relationships between cell size and time of initiation of DNA replication. *Nature* 219, 1077–1079. doi: 10.1038/2191077a0

Elmore, S., Müller, M., Vischer, N., Odijk, T., and Woldringh, C. L. (2005). Single-particle tracking of oriC-GFP fluorescent spots during chromosome segregation in *Escherichia coli*. *J. Struct. Biol.* 151, 275–287. doi: 10.1016/j.jsb.2005.06.004

Fishov, I., Grover, N. B., and Zaritsky, A. (1995). On microbial states of growth. *Mol. Microbiol.* 15, 789–794. doi: 10.1111/j.1365-2958.1995.tb02349.x

Friesen, J. D., and Maaløe, O. (1965). On the control of DNA synthesis by amino acids in *E. coli*. *Biochim. Biophys. Acta* 95, 436–445. doi: 10.1016/0005-2787(65)90190-5

Grover, N. B., Woldringh, C. L., Zaritsky, A., and Rosenberger, R. F. (1977). Elongation of rod-shaped bacteria. *J. Theor. Biol.* 67, 181–193. doi: 10.1016/0022-5193(77)90192-8

Grover, N. B., Zaritsky, A., Woldringh, C. L., and Rosenberger, R. F. (1980). Dimensional rearrangement of rod-shaped bacteria following nutritional shift-up. I. Theory. *J. Theor. Biol.* 86, 421–439. doi: 10.1016/0022-5193(80)90343-4

Hanawalt, P. C. (2015). A balanced perspective on unbalanced growth and thymineless death. *Front. Microbiol.* 6:504. doi: 10.3389/fmicb.2015.00504

Hanawalt, P. C., Maaløe, O., Cummings, D. J., and Schaechter, M. (1961). The normal DNA replication cycle. II. *J Mol. Biol.* 3, 156–165. doi: 10.1016/S0022-2836(61)80042-9

Hayes, W. (1968). *The Genetics of Bacteria and their Viruses*, 2nd Edn. Oxford: Blackwell Scientific Publications. 925.

Helmstetter, C. E. (1996). "Timing and synthetic activities in the cell cycle," in *Escherichia coli and Salmonella Typhimurium: Cellular and Molecular Biology*, eds F. C. Neidhardt, R. III, Curtiss, J. L. Ingraham, K. B. Low, B. Magasanik, M. Schaechter, and H. E. Umbarger (Washington, DC: ASM Press), 1627–1649.

Helmstetter, C. E. (2015). A ten-year search for synchronous cells: obstacles, solutions and practical applications. *Front. Microbiol.* 6:238. doi: 10.3389/fmicb.2015.00238

Helmstetter, C. E., and Cummings, D. J. (1964). An improved method for the selection of bacterial cells at division. *Biochim. Biophys. Acta* 82, 608–610. doi: 10.1016/0304-4165(64)90453-2

Helmstetter, H. E., Cooper, S., Pierucci, O., and Revelas, E. (1968). On the bacterial life sequence. *Cold Spring Harb. Symp. Quant. Biol.* 33, 809–822. doi: 10.1101/SQB.1968.033.01.093

Henrici, A. T. (1928). *Morphological Variations and the Rate of Growth of Bacteria*. London: Bailliere, Tindall & Cox. doi: 10.5962/bhl.title.7269

Ho, P.-Y., and Amir, A. (2015). Simultaneous regulation of cell size and chromosome replication in bacteria. *Front. Microbiol.* 6:662. doi: 10.3389/fmicb.2015.00662

Hirota, Y., Ryter, A., and Jacob, F. (1968). Thermosensitive mutants of *E. coli* affected in the processes of DNA synthesis and cellular division. *Cold Spring Harb. Symp. Quant. Biol.* 33, 677–694. doi: 10.1101/SQB.1968.033.01.077

Huls, P. G., Vischer, N. O. E., and Woldringh, C. L. (1999). Delayed nucleoid segregation in *Escherichia coli*. *Mol. Microbiol.* 33, 959–970. doi: 10.1046/j.1365-2958.1999.01535.x

Itsko, M., and Schaaper, R. M. (2011). The dgt gene of *E. coli* facilitates thymine utilization in thymine-requiring strains. *Mol. Microbiol.* 81, 1221–1232. doi: 10.1111/j.1365-2958.2011.07756.x

Iyer-Biswas, S., Wright, C. S., Henry, J. T., Lo, K., Burov, S., Lin, Y., et al. (2014). Scaling laws governing stochastic growth and division of single bacterial cells. *Proc. Natl. Acad. Sci. U.S.A.* 111, 15912–15917. doi: 10.1073/pnas.1403232111

Jacob, F., and Monod, J. (1961). Genetic regulatory mechanisms in the synthesis of proteins. *J. Mol. Biol.* 3, 318–356. doi: 10.1016/S0022-2836(61)80072-7

Jacob, F., and Wollman, E. L. (1956). Processes of conjugation and recombination in *Escherichia coli*. I. Induction by conjugation or zygotic induction. *Ann. Inst. Pasteur* 91, 486–510.

Jiménez Sánchez, A. (2015). Chromosome replication status and DNA content at any cell age in a bacterial cell cycle. *J. Theor. Biol*. doi: 10.1016/j.jtbi.2015.06.008 [Epub ahead of print].

Jun, S., and Taheri-Araghi, S. (2014). Cell-size maintenance: universal strategy revealed. *Trends Microbiol.* 23, 4–6. doi: 10.1016/j.tim.2014.12.001

Kellenberger, E., Ryter, A., and Séchaud, J. (1958). Electron microscope study of DNA-containing plasms. II. Vegetative and mature phage DNA as compared with normal bacterial nucleoids in different physiological states. *J. Cell Biol.* 4, 671–678. doi: 10.1083/jcb.4.6.671

Kjeldgaard, N. O., Schaechter, M., and Maaløe, O. (1958). The transition between different physiological states during balanced growth of *Salmonella typhimurium*. *J. Gen. Microbiol.* 19, 607–616. doi: 10.1099/00221287-19-3-607

Koppes, L. J. H., Woldringh, C. L., and Nanninga, N. (1978). Size variations and correlation on different cell cycle events in slow-growing *Escherichia coli*. *J. Bacteriol.* 134, 423–433.

Koppes, L. J. H., and Nanninga, N. (1980). Positive correlation between size at initiation of chromosome replication in *Escherichia coli* and cell size at initiation of cell constriction. *J. Bacteriol.* 143, 89–99.

Kornberg, A., and Baker, T. A. (1992). *DNA Replication*, 2nd Edn. New York: WH Freeman and Company. 952.

Kubitschek, H. E. (1974). Estimation of the D period from residual division after exposure of exponential phase bacteria to chloramphenicol. *Mol. Gen. Genet.* 135, 123–130. doi: 10.1007/BF00264780

Lark, K. G., Repko, T., and Hoffman, E. J. (1963). The effect of amino acid deprivation on subsequent DNA replication. *Biochim. Biophys. Acta* 79, 9–24. doi: 10.1016/0926-6550(63)90003-3

Lark, K. G., and Lark, C. (1965). Regulation of chromosome replication in *Escherichia coli*: alternate replication of two chromosomes at slow growth rates. *J. Mol. Biol.* 13, 105–126. doi: 10.1016/S0022-2836(65)80083-3

Leonard, A. C., and Grimwade, J. E. (2010). "Initiation of DNA replication," in *EcoSal—Escherichia coli and Salmonella: Cellular and Molecular Biology*, eds A. Böck, R. III. Curtiss, J. B. Kaper, P. D. Karp, F. C. Neidhardt, T. Nyström, et al. (Washington, DC: ASM Press).

Luria, S. E., and Delbrück, M. (1943). Mutations of bacteria from virus sensitivity to virus resistance. *Genetics* 28, 491–511.

Maaløe, O. (1961). The control of normal DNA replication in bacteria. *Cold Spring Harb. Symp. Quant. Biol.* 26, 45–52. doi: 10.1101/SQB.1961.026.01.010

Maaløe, O., and Kjeldgaard, N. O. (1966). *Control of Macromolecular Synthesis*. New York: WA Benjamin Inc. 284.

Maaløe, O., and Rasmussen, K. V. (1963). On the *in vivo* replication of bacterial DNA. *Colloq. Intern. Centre Nat. Rech. Sci.* 124, 165–168.

Männik, J., Wua, F., Hol, F. J. H., Bisicchia, P., Sherratt, D. J., Keymer, J. E., et al. (2012). Robustness and accuracy of cell division in *Escherichia coli* in diverse cell shapes. *Proc. Natl. Acad. Sci. U.S.A.* 109, 6957–6962. doi: 10.1073/pnas.1120854109

Markovitz, A. (1964). Regulatory mechanisms for synthesis of capsular polysaccharide in mucoid mutants of *Escherichia coli* K-12. *Proc. Natl. Acad. Sci. U.S.A.* 51, 239–246. doi: 10.1073/pnas.51.2.239

Masters, M., and Broda, P. (1971). Evidence for the bidirectional replication of the *Escherichia coli* chromosome. *Nat. New Biol.* 232, 137–140. doi: 10.1038/newbio232137a0

Measelson, M., and Stahl, F. W. (1958). The replication of DNA in *Escherichia coli*. *Proc. Natl. Acad. Sci. U.S.A.* 44, 671–682. doi: 10.1073/pnas.44.7.671

Meacock, P. A., and Pritchard, R. H. (1975). Relationship between chromosome replication and cell division in a thymineless mutant of *Escherichia coli* B/r. *J. Bacteriol.* 122, 931–942.

Michelsen, O., de Mattos, M. J. T., Jensen, P. R., and Hansen, F. G. (2003). Precise determinations of C and D periods by flow cytometry in *E. coli K*-12 and B/r. *Microbiology* 149, 1001–1010. doi: 10.1099/mic.0.26058-0

Mulder, E., and Woldringh, C. L. (1989). Actively replicating nucleoids influence the positioning of division sites in DNA-less cell forming filaments of *Escherichia coli*. *J. Bacteriol.* 171, 4303–4314.

Nanninga, N. (1971). The mesosome of *Bacillus subtilis* as affected by chemical and physical fixation. *J. Cell Biol.* 48, 219–224. doi: 10.1083/jcb.48.1.219

Nanninga, N., and Woldringh, C. L. (1985). "Cell growth, genome duplication and cell division in *Escherichia coli*," in *Molecular Cytology of Escherichia coli*, ed. N. Nanninga (London: Academic Press Inc.), 259–318.

Nanninga, N., Wientjes, F. B., de Jonge, B. L. M., and Woldringh, C. L. (1990). Polar cap formation during cell division in *Escherichia coli*. *Res. Microbiol.* 141, 103–118. doi: 10.1016/0923-2508(90)90102-V

Nirenberg, M. (2004). Historical review: deciphering the genetic code—a personal account. *Trends Biochem. Sci.* 29, 46–54. doi: 10.1016/j.tibs.2003.11.009

Norris, V., den Blaauwen, T., Cabin-Flaman, A., Doi, R. H., Harshey, R., Janniere, L., et al. (2007). Functional taxonomy of bacterial hyperstructures. *Microbiol. Mol. Biol. Rev.* 71, 230–253. doi: 10.1128/MMBR.00035-06

Oishi, M., Yoshikawa, H., and Sueoka, N. (1964). Synchronous and dichotomous replication of the *Bacillus subtilis* chromosome during spore germination. *Nature* 204, 1069–1073. doi: 10.1038/2041069a0

Olsson, J., Dasgupta, S., Berg, O. G., and Nordström, K. (2002). Eclipse period without sequestration in *Escherichia coli*. *Mol. Microbiol.* 44, 1429–1440. doi: 10.1046/j.1365-2958.2002.02954.x

Osella, M., Nugent, E., and Cosentino Lagomarsino, M. (2014). Concerted control of *Escherichia coli* cell division. *Proc. Natl. Acad. Sci. U.S.A.* 111, 3431–3435. doi: 10.1073/pnas.1313715111

Pelletier, J., Halvorsen, K., Ha, B.-Y., Paparcone, R., Sandler, S. J., Woldringh, C. L., et al. (2012). Physical manipulation of the *Escherichia coli* chromosome reveals its soft nature. *Proc. Natl. Acad. Sci. U.S.A.* 109, E2649–E2656. doi: 10.1073/pnas.1208689109

Porter, J. R. (1976). Antony van Leeuwenhoek: tercentenary of his discovery of bacteria. *Bacteriol. Rev.* 40, 260–269.

Powell, E. O. (1956). Growth rate and generation time in bacteria with special reference to continuous culture. *J. Gen. Microbiol.* 15, 492–511. doi: 10.1099/00221287-15-3-492

Prescott, D. M., and Kuempel, P. L. (1972). Bidirectional replication of the chromosome of *Escherichia coli*. *Proc. Natl. Acad. Sci. U.S.A.* 69, 2842–2845. doi: 10.1073/pnas.69.10.2842

Pritchard, R. H. (1968). Control of DNA synthesis in bacteria. *Heredity* 23, 472–473.

Pritchard, R. H. (1974). On the growth and form of a bacterial cell. *Phil. Trans. R. Soc. London Ser B* 267, 303–336. doi: 10.1098/rstb.1974.0003

Pritchard, R. H., Barth, P. T., and Collins, J. (1969). Control of DNA synthesis in bacteria. *Microbial Growth. Symp. Soc. Gen. Microbiol.* 19, 263–297.

Pritchard, R. H., and Lark, K. G. (1964). Induction of replication by thymine starvation at the chromosome origin in *Escherichia coli*. *J. Mol. Biol.* 9, 288–307. doi: 10.1016/S0022-2836(64)80208-4

Pritchard, R. H., and Zaritsky, A. (1970). Effect of thymine concentration on the replication velocity of DNA in a thymineless mutant of *Escherichia coli*. *Nature* 226, 126–131. doi: 10.1038/226126a0

Rabinovitch, A., Zaritsky, A., and Feingold, M. (2003). DNA-membrane interactions can localize bacterial cell center. *J. Theor. Biol.* 225, 393–396. doi: 10.1016/S0022-5193(03)00292-3

Reinhart, K. V., and Copeland, J. C. (1973). Evidence that thymine is not a normal metabolite in wild-type *Bacillus subtilis*. *Biochim. Biophys. Acta* 294, 1–7. doi: 10.1016/0005-2787(73)90308-0

Robert, L. (2015). Size sensors in bacteria, cell cycle control, and size control. *Front. Microbiol.* 6:515. doi: 10.3389/fmicb.2015.00515

Rosenberger, R. F., Grover, N. B., Zaritsky, A., and Woldringh, C. L. (1978a). Surface growth in rod-shaped bacteria. *J. Theor. Biol.* 73, 711–721. doi: 10.1016/0022-5193(78)90132-7

Rosenberger, R. F., Grover, N. B., Zaritsky, A., and Woldringh, C. L. (1978b). Control of microbial surface growth by density. *Nature* 271, 244–245. doi: 10.1038/271244a0

Schaechter, M. (1961). Pattern of cellular control during unbalanced growth. *Cold Spring Harb. Symp. Quant. Biol.* 26, 53–62. doi: 10.1101/SQB.1961.026.01.011

Schaechter, M. (2006). From growth physiology to systems biology. *Int. Microbiol.* 9, 157–161.

Schaechter, M. (2015). A brief history of bacterial growth physiology. *Front. Microbiol.* 6:289. doi: 10.3389/fmicb.2015.00289

Schaechter, M., Maalφe, O., and Kjeldgaard, N. O. (1958). Dependency on medium and temperature of cell size and chemical composition during balanced growth of *Salmonella typhimurium*. *J. Gen. Microbiol.* 19, 592–606. doi: 10.1099/00221287-19-3-592

Scott, M., and Hwa, T. (2011). Bacterial growth laws and their applications. *Curr. Opin. Biotechnol.* 22, 559–565. doi: 10.1016/j.copbio.2011.04.014

Simmons, L. A., Breier, A. M., Cozzarelli, N. R., and Kaguni, J. M. (2004). Hyperinitiation of DNA replication in *Escherichia coli* leads to replication forks collapse and invariability. *Mol. Microbiol.* 51, 349–358. doi: 10.1046/j.1365-2958.2003.03842.x

Slater, M., and Schaechter, M. (1974). Control of cell division in bacteria. *Bacteriol. Rev.* 38, 199–221.

Stent, G. S., and Calendar, R. (1978). *Molecular Genetics—An Introductory Narrative*. 2nd Edn. San Francisco: W. H. Freeman and Company. 773.

Sueoka, N., and Yoshikawa, H. (1965). The chromosome of *Bacillus subtilis*. I. Theory of marker frequency analysis. *Genetics* 52, 747–757.

Taheri-Araghi, S., Bradde, S., Sauls, J. T., Hill, N. S., Levin, P. A., Paulsson, J., et al. (2015). Size-control and homeostasis in bacteria. *Curr. Biol.* 25, 385–391. doi: 10.1016/j.cub.2014.12.009

Toro, E., and Shapiro, L. (2010). Bacterial chromosome organization and segregation. *Cold Spring Harb. Perspect. Biol.* 2, a000349. doi: 10.1101/cshperspect.a000349

Trueba, F. J., and Woldringh, C. L. (1980). Changes in cell diameter during the division cycle of *Escherichia coli*. *J. Bacteriol.* 142, 869–878.

Typas, A., Banzhaf, M., Gross, C. A., and Vollmer, W. (2012). From the regulation of peptidoglycan synthesis to bacterial growth and morphology. *Nat. Rev. Microbiol.* 10, 123–135. doi: 10.1038/nrmicro2677

Valkenburg, J. A. C., Woldringh, C. L., Brakenhoff, G. J., van der Voort, H. T. M., and Nanninga, N. (1985). Confocal scanning light microscopy of the *Escherichia coli* nucleoid: comparison with phase-contrast and electron microscope images. *J. Bacteriol.* 161, 478–483.

van Helvoort, J. M. L. M., and Woldringh, C. L. (1994). Nucleoid partitioning in *Escherichia coli* during steady state growth and upon recovery from chloramphenicol treatment. *Mol. Microbiol.* 13, 577–583. doi: 10.1111/j.1365-2958.1994.tb00452.x

Vardi, E., and Grover, N. B. (1993). Shape changes in *Escherichia coli* B/rA during agar filtration. *Cytometry* 14, 173–178. doi: 10.1002/cyto.990140209

Vischer, N. O. E., Verheul, J., Postma, M., Bart van den Berg van Saparoea, B., Galli, E., Natale, P., et al. (2015). Cell age dependent concentration of *Escherichia coli* divisome proteins analyzed with ImageJ and ObjectJ. *Front. Microbiol.* 6:586. doi: 10.3389/fmicb.2015.00586

Wake, R. G. (1972). Visualization of reinitiated chromosomes in *Bacillus subtilis*. *J. Mol. Biol.* 68, 501–509. doi: 10.1016/0022-2836(72)90102-7

Wang, P., Robert, L., Pelletier, J., Dang, W.-L., Taddei, F., Wright, A., et al. (2010). Robust growth of *Escherichia coli*. *Curr. Biol.* 20, 1099–1103. doi: 10.1016/j.cub.2010.04.045

Watson, J. D. (1996). *The Double Helix—A Personal Account of the Discovery of the Structure of DNA*. New York: Scribner.

Watson, J., and Crick, F. H. C. (1953). Molecular structure of nucleic acids. *Nature* 171, 737–738. doi: 10.1038/171737a0

Wold, S., Skarstad, K., Steen, H. B., Stokke, T., and Boye, E. (1994). The initiation mass for DNA replication in *Escherichia coli* K-12 is dependent on growth rate. *EMBO J.* 13, 2097–2102.

Woldringh, C. L. (1974). *The Nucleoplasm of Escherichia coli*. Ph.D. thesis, University of Amsterdam (NL), Amsterdam, 129.

Woldringh, C. L. (1994). Significance of plasmolysis spaces as markers for periseptal annuli and adhesion sites. *Mol. Microbiol.* 14, 597–607. doi: 10.1111/j.1365-2958.1994.tb01299.x

Woldringh, C. L. (2002). The role of co-transcriptional translation and protein translocation (transertion) in bacterial chromosome segregation. *Mol. Microbiol.* 45, 17–29. doi: 10.1046/j.1365-2958.2002.02993.x

Woldringh, C. L., de Jong, M. A., van den Berg, W., and Koppes, L. (1977). Morphological analysis of the division cycle of two *Escherichia coli* substrains during slow growth. *J. Bacteriol.* 131, 270–279.

Woldringh, C. L., Grover, N. B., Rosenberger, R. F., and Zaritsky, A. (1980). Dimensional rearrangement of rod-shaped bacteria following nutritional shift-up. II. Experiments with *Escherichia coli* B/r. *J. Theor. Biol.* 86, 441–454. doi: 10.1016/0022-5193(80)90344-6

Woldringh, C. L., Hansen, F. G., Vischer, N. O. E., and Atlung, T. (2015). Segregation of chromosome arms in growing and non-growing *Escherichia coli* cells. *Front. Microbiol.* 6:448. doi: 10.3389/fmicb.2015.00448

Woldringh, C. L., Huls, P., Pas, E., Brakenhoff, G. J., and Nanninga, N. (1987). Topography of peptidoglycan synthesis during elongation and polar cap formation in a cell division mutant of *Escherichia coli* MC4100. *J. Gen. Microbiol.* 133, 575–586. doi: 10.1099/00221287-133-3-575

Woldringh, C. L., Mulder, E., Valkenburg, J. A. C., Wientjes, F. B., Zaritsky, A., and Nanninga, N. (1990). Role of nucleoid in toporegulation of division. *Res. Microbiol.* 141, 39–49. doi: 10.1016/0923-2508(90)90096-9

Woldringh, C. L., and Nanninga, N. (1985). "Structure of nucleoid and cytoplasm in the intact cell," in *Molecular Cytology of Escherichia coli*, ed. N. Nanninga (London: Academic Press), 161–197.

Woldringh, C. L., and Odijk, T. (1999). "Structure of DNA within the bacterial cell: physics and physiology," in *Organization of the Prokaryotic Genome*, ed. R. L. Charlebois (Washington, DC: ASM Press), 171–187.

Woldringh, C. L., Zaritsky, A., and Grover, N. B. (1994). Nucleoid partitioning and the division plane in *Escherichia coli*. *J. Bacteriol.* 176, 6030–6038.

Wu, L. J., and Errington, J. (2012). Nucleoid occlusion and bacterial cell division. *Nat. Rev. Microbiol.* 10, 8–12. doi: 10.1038/nrmicro2671

Yoshikawa, H., and Sueoka, N. (1963). Sequential replication of the *Bacillus subtilis* chromosome. I. Comparison of marker frequencies in exponential and stationary growth phases. *Proc. Natl. Acad. Sci. U.S.A.* 49, 559–566. doi: 10.1073/pnas.49.4.559

Youngren, B., Nielsen, H. J., Jun, S., and Austin, S. (2014). The multifork *Escherichia coli* chromosome is a self-duplicating and self-segregating thermodynamic ring polymer. *Genes Dev.* 28, 71–84. doi: 10.1101/gad.231050.113

Zaritsky, A. (1971). *Studies on DNA Replication and Cell Division in Bacteria*. Ph.D. thesis, The University of Leicester (UK), Leicester, 97.

Zaritsky, A. (1975a). Rate stimulation of DNA synthesis after inhibition. *J. Bacteriol.* 122, 841–846.

Zaritsky, A. (1975b). On dimensional determination of rod-shaped bacteria. *J. Theor. Biol.* 54, 243–248. doi: 10.1016/S0022-5193(75)80129-9

Zaritsky, A. (2015). Cell shape homeostasis in *Escherichia coli* is driven by growth, division, and nucleoid complexity. *Biophys. J.* 109, 178–181. doi: 10.1016/j.bpj.2015.06.026

Zaritsky, A., and Pritchard, R. H. (1973). Changes in cell size and shape associated with changes in the replication time of the chromosome of *Escherichia coli*. *J. Bacteriol.* 114, 824–837.

Zaritsky, A., Vischer, N., and Rabinovitch, A. (2007). Changes of initiation mass and cell dimensions by the 'eclipse'. *Mol. Microbiol.* 63, 15–21. doi: 10.1111/j.1365-2958.2006.05501.x

Zaritsky, A., Wang, P., and Vischer, N. O. E. (2011). Instructive simulation of the bacterial cell cycle. *Microbiology* 157, 1876–1885. doi: 10.1099/mic.0.049403-0

Zaritsky, A., Woldringh, C. L., Einav, M., and Alexeeva, S. (2006). Thymine limitation and thymine starvation to study bacterial physiology and cytology. *J. Bacteriol.* 188, 1667–1679. doi: 10.1128/JB.188.5.1667-1679.2006

Zaritsky, A., Woldringh, C. L., Grover, N. B., Naaman, J., and Rosenberger, R. F. (1982). Growth and form in bacteria. *Comments Mol. Cell. Biophys.* 1, 237–260.

Zaritsky, A., Woldringh, C. L., Vischer, N. O. E., Wang, P., and Helmstetter, C. E. (2012). Simulation of the prokaryotic cell cycle at http://simon.bio.uva.nl/cellcycle/. *J. Sytem. Cybernet. Informat.* 10, 18–23.

Zaritsky, A., and Zabrovitz, S. (1981). DNA synthesis in *Escherichia coli* during a nutritional shiftup. *Mol. Gen. Genet.* 181, 564–565. doi: 10.1007/BF00428756

Conflict of Interest Statement: The authors declare that the research was conducted in the absence of any commercial or financial relationships that could be construed as a potential conflict of interest.

Copyright © 2015 Zaritsky and Woldringh. This is an open-access article distributed under the terms of the Creative Commons Attribution License (CC BY). The use, distribution or reproduction in other forums is permitted, provided the original author(s) or licensor are credited and that the original publication in this journal is cited, in accordance with accepted academic practice. No use, distribution or reproduction is permitted which does not comply with these terms.

frontiers in Microbiology

REVIEW
published: 02 June 2015
doi: 10.3389/fmicb.2015.00545

The orisome: structure and function

Alan C. Leonard and Julia E. Grimwade*

Department of Biological Sciences, Florida Institute of Technology, Melbourne, FL, USA

During the cell division cycle of all bacteria, DNA-protein complexes termed orisomes trigger the onset of chromosome duplication. Orisome assembly is both staged and stringently regulated to ensure that DNA synthesis begins at a precise time and only once at each origin per cycle. Orisomes comprise multiple copies of the initiator protein DnaA, which oligomerizes after interacting with specifically positioned recognition sites in the unique chromosomal replication origin, *oriC*. Since DnaA is highly conserved, it is logical to expect that all bacterial orisomes will share fundamental attributes. Indeed, although mechanistic details remain to be determined, all bacterial orisomes are capable of unwinding *oriC* DNA and assisting with loading of DNA helicase onto the single-strands. However, comparative analysis of *oriC*s reveals that the arrangement and number of DnaA recognition sites is surprisingly variable among bacterial types, suggesting there are many paths to produce functional orisome complexes. Fundamental questions exist about why these different paths exist and which features of orisomes must be shared among diverse bacterial types. In this review we present the current understanding of orisome assembly and function in *Escherichia coli* and compare the replication origins among the related members of the Gammaproteobacteria. From this information we propose that the diversity in orisome assembly reflects both the requirement to regulate the conformation of origin DNA as well as to provide an appropriate cell cycle timing mechanism that reflects the lifestyle of the bacteria. We suggest that identification of shared steps in orisome assembly may reveal particularly good targets for new antibiotics.

Keywords: *oriC*, DnaA, DNA replication, replication origin, DNA binding proteins, orisomes, pre-replication complexes

OPEN ACCESS

Edited by:
Conrad L. Woldringh, University of Amsterdam, Netherlands

Reviewed by:
Dhruba Chattoraj, National Institutes of Health, USA
Elliott Crooke, Georgetown University Medical Center, USA

****Correspondence:***
Alan C. Leonard, Department of Biological Sciences, Florida Institute of Technology, LSB 234, 150 West University Boulevard, Melbourne, FL 32901, USA
aleonard@fit.edu

Specialty section:
This article was submitted to Microbial Physiology and Metabolism, a section of the journal Frontiers in Microbiology

Received: *30 March 2015*
Accepted: *18 May 2015*
Published: *02 June 2015*

Citation:
Leonard AC and Grimwade JE (2015) The orisome: structure and function. Front. Microbiol. 6:545. doi: 10.3389/fmicb.2015.00545

Introduction

As the commitment step for proliferation, initiating new rounds of chromosomal DNA synthesis is arguably the paramount event in the life of a bacterial cell. It is also a precarious step, which must rely on sophisticated regulatory mechanisms to ensure that new replication forks are established with sufficient time and number to provide every daughter cell with at least one complete genome copy, regardless of cellular growth rate. Many of these regulatory mechanisms are focused on orisomes, the large multimeric complexes of the bacterial initiator protein, DnaA, that assemble along the unique chromosomal replication origin, *oriC*.

DnaA is a highly conserved protein whose activity is regulated by the binding and hydrolysis of ATP, with initiation requiring the ATP-bound form (Sekimizu et al., 1987). The crystal structure of a truncated version (domains III and IV) of *Aquifex aeolicus* has been determined (Erzberger et al., 2002, 2006), revealing that DnaA is not only conserved among bacteria, but also has structural similarity to archaeal and eukaryotic initiatior proteins. Additionally, several

laboratories have used reverse genetics to introduce targeted mutations in Domains I, III, and IV, and use of these mutants has revealed key roles for these domains in DnaA recruitment (I), binding (IV), oligomerization (I, III), and helicase loading (I, III; see below and representative reviews; Kaguni, 1997; Zawilak-Pawlik et al., 2005; Mott and Berger, 2007; Ozaki and Katayama, 2009; Leonard and Grimwade, 2011).

Insightful studies on how orisomes assemble, function, and are regulated have come from many laboratories over the course of several decades, mostly using *Escherichia coli*. Cloning of *E. coli oriC* onto plasmids (minichromosomes) allowed determination that all instructions for normal orisome assembly are contained in the *oriC* nucleotide sequence (Leonard and Helmstetter, 1986). Sequencing the cloned *oriC* (Meijer et al., 1979) identified repeated 9 mer sequences that were determined to be DnaA recognition site (Fuller et al., 1984; Matsui et al., 1985), providing the framework that allowed analysis of how DnaA contacted DNA (Speck et al., 1997; Fujikawa et al., 2003; Yoshida et al., 2003). Seminal studies done by the Kornberg lab provided evidence that initiation could be studied *in vitro* using crude extracts and purified proteins (Fuller et al., 1981; Kaguni and Kornberg, 1984) and revealed the major stages of orisome assembly (Sekimizu et al., 1988). More recently, high-resolution mapping of DnaA-*oriC* interactions (McGarry et al., 2004; Rozgaja et al., 2011), biochemical analysis of ordered orisome assembly (Margulies and Kaguni, 1996), and characterization of key subassemblies (Ozaki and Katayama, 2012; Ozaki et al., 2012) have given a clearer picture of how orisomes assemble in *E. coli*, and, to a lesser extent, in other bacterial types [reviewed in Wolanski et al. (2014)]. However, fundamental questions remain about the relationship between DnaA oligomer formation and the DnaA-directed changes in DNA conformation necessary to unwind the origin, as well as the manner by which orisome assembly is precisely timed in during cell cycle.

The majority of studies on orisomes have been done *in vitro*, using either DNA fragments or plasmid templates. Plasmids are also useful tools for site-specific mutagenesis, which is essential for dissection of the roles of individual DnaA recognition sites and other *oriC* sequence elements. However, when the effects of *oriC* mutations on orisome function were examined *in vivo*, it became apparent that mutations in cloned *oriC* do not always have the same effect when placed into the chromosomal context (Weigel et al., 2001). Although the regulatory factors and timing during the cell cycle are identical for plasmid and chromosomal *oriC*s, there are obvious differences in DNA topology, and intracellular location (Niki and Hiraga, 1999). Most importantly, functional studies of mutant cloned *oriCs* were usually performed in hosts that harbored wild-type *oriC* on their chromosomes, setting up a potential competition for available DnaA (Grimwade et al., 2007). Under these conditions the winner ultimately excludes the *oriC* that loses (does not meet the threshold requirement for DnaA) and causes either death of the host or replacement of the wild-type chromosomal origin with the mutant cloned version. Thus it seems preferable to dissect orisome function *in vivo* by introducing mutations in chromosomal *oriC*, but this has, in the past, been a difficult, and labor-intensive process.

The development of *E. coli* recombineering strains that express inducible lambda phage recombination proteins (RED strains; Datsenko and Wanner, 2000; Sharan et al., 2009) has streamlined the introduction of mutations into chromosomal *oriC* or anywhere else on the genome. Short PCR fragments containing mutant *oriC* can now be easily inserted as perfect replacements on the chromosome without any additional genetic alterations. Furthermore, these replacements can be performed in strains whose chromosomal replication is under the control of an DnaA-independent, integrated R1 plasmid (Hansen and Yarmolinsky, 1986; Koppes and Nordström, 1986) so that even mutations that render *oriC* non-functional can be introduced into a DnaA null strain (Kaur et al., 2014). Recently, recombineering strains were constructed with the *sacB* gene from *Bacillus* within *oriC* to permit selection for *oriC* replacements on sucrose-containing plates (only strains that lack *sacB* will grow; **Figure 1**). Since the *oriC* replacement strains still contain an integrated R1 plasmid origin, it is possible to quickly test for function of the mutant *oriC* by measuring cell viability in the presence of a plasmid that expresses both DnaA and the R1*ori* repressor (*copA*) RNA (Stougaard et al., 1981). Once the mutation is

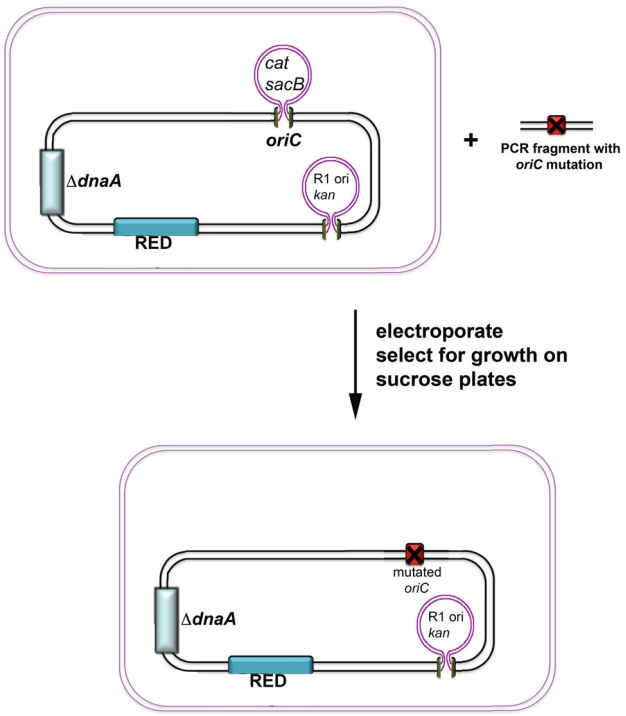

FIGURE 1 | Scheme of the *oriC*-specific recombineering method. Recombineering strains harbor *sacB* and *cat* genes replacing all of the *oriC* sequence, inducible genes encoding the lambda RED system, and a plasmid origin of replication (R1*ori*) linked to a kanamycin resistance determinant. The strain also has a deletion in the *dnaA* gene. For insertion of *oriC* mutants into the chromosome, a PCR fragment carrying the desired mutation is electroporated to transform cells in which the RED system was induced. Recombination results in replacement of the *sacB* and *cat* genes with the mutated *oriC*. Successful recombineering confers the ability to grow in the presence of sucrose, and sensitivity to chloramphenicol.

confirmed by nucleotide sequence analysis, functional *oriC*s can be transduced into strains with clean genetic backgrounds to study the effect of the mutation on cell growth or cell cycle timing.

Escherichia coli recombineering strains also show promise for the development of novel heterologous systems that will allow *in vivo* examination of DnaA-*oriC* interactions that are difficult to perform in native strains, particularly for slow growers or pathogens. Since *E. coli* DnaA is not required to drive chromosome replication in the recombineering strains, any heterologous *oriC* and DnaA combination (and any other proteins associated with orisome function) can be introduced at any chromosomal location desired.

Getting Started: The Multifunctional Bacterial Origin Recognition Complex (bORC)

In order to build orisomes reproducibly during every cell division cycle, there needs to be an invariant starting scaffold that is capable of not only recruiting additional orisome components for later stages of assembly, but also of arranging origin DNA into an appropriate configuration that prohibits DnaA-independent *oriC* DNA unwinding. This latter feature may be unexpected, but when they are in the supercoiled topology that is required for origin function (Funnell et al., 1986; Von Freiesleben and Rasmussen, 1992), *oriC* templates contain single-stranded DNA in the absence of any associated protein (Kowalski and Eddy, 1989). Unwinding is observed in an A-T rich region (DNA Unwinding Element, or DUE; **Figure 2A**; Kowalski and Eddy, 1989), which is identical to the region which unwinds following orisome assembly (Bramhill and Kornberg, 1988). In *E. coli*, the DUE contains three 13 mer repeats with consensus sequence 5′-GATCTnTTnTTTT-3′, although the nucleotide sequences of DUEs can be quite variable among other bacterial types (Zawilak-Pawlik et al., 2005).

To avoid premature unwinding, bacterial *oriC* is usually not naked in cells, but rather is bound to DnaA at high affinity (K_d in the range of 4–20 nM) recognition sites (5′-TTATC/ACACA-3′), via a helix-turn-helix (HTH)-type DNA binding motif located within the C-terminal domain (domain IV; Speck et al., 1997; Erzberger et al., 2002; Fujikawa et al., 2003). Three such sites (R1, R2, and R4) are found in *E. coli oriC* (**Figure 2A**). DnaA occupies these sites as soon as they becomes accessible, usually after the origin DNA is replicated, and remains bound to them throughout the majority of the cell cycle (Samitt et al., 1989; Nievera et al., 2006). One consequence of this binding is prevention of strand separation, since unwinding of the *E. coli* DUE, detected by susceptibility to single-strand DNA-specific endonucleases, is completely eliminated when DnaA occupies all three high affinity sites. Endonuclease cutting returns when any single site is unoccupied as a result of mutation (Kaur et al., 2014). This observation is consistent with the idea that supercoiled *oriC* is constrained by the direct interaction among the bound DnaA molecules. Although the nature of the interaction region is not yet known, a logical candidate is a globular K-homology (KH)-type fold mapped to the N-terminus (domain I; Weigel et al., 1999; Simmons et al., 2003). Domain I is attached to the rest of DnaA by a long flexible linker (domain II; Nozaki and

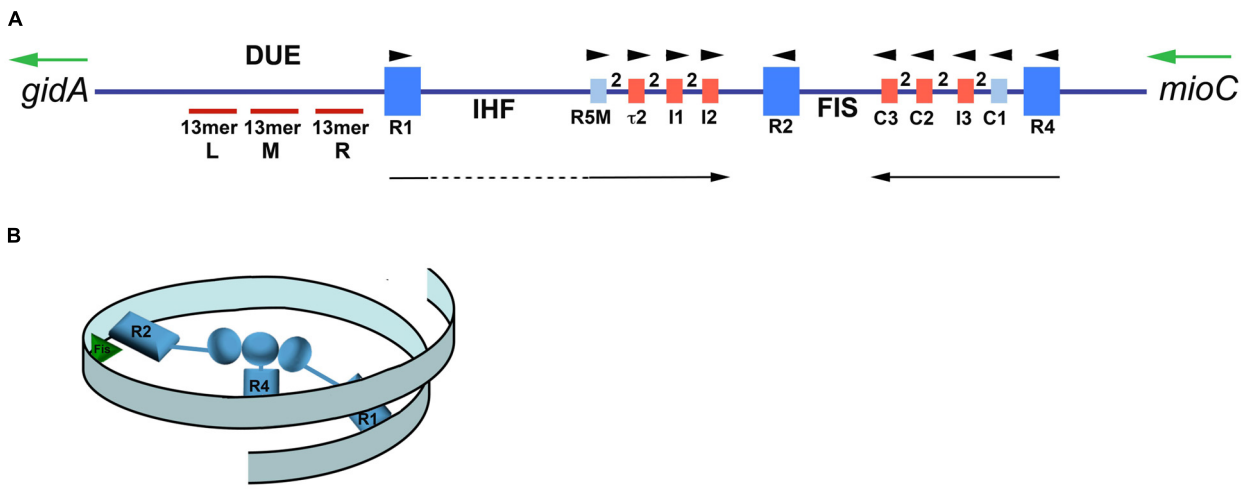

FIGURE 2 | Map of *Escherichia coli oriC* and conformation of bORC. (A) The *oriC* region is mapped, showing positions of binding sites for DnaA, IHF, and Fis, as well as the right (R), middle (M), and left (L) 13mer sequences in the DNA unwinding element (DUE). The three high-affinity sites R1, R2, and R4 are designated by royal blue squares, and the low-affinity sites are marked by small light blue or red rectangles. The red rectangles designate sites that preferentially bind DnaA–ATP, while the sites marked by light blue rectangles bind both nucleotide forms of DnaA equivalently. Small arrowheads show orientation of sites, the two between sites indicates the number of bp separating the sites. Arrows under the map indicate growth direction of DnaA oligomers. The dotted line marks that the oligomer does not span the region between R1 and R5M. Two genes, *gidA* and *mioC,* flanking *oriC* are shown, with the green arrows marking the direction of transcription. **(B)** Proposed looped conformation of bORC in *E. coli*. *OriC* DNA (ribbon) is constrained by DnaA (gray-blue figures in center of loop) bound at R1, R2, and R4 sites, as labeled. Interaction among the three bound DnaAs proposed to be via domain I. The green triangle represents Fis bound to its cognate site.

Ogawa, 2008) that could facilitate association of bound DnaA molecules. The high affinity recognition sites in *E. coli* are widely separated (**Figure 2A**), and even using the flexible linker, it is difficult to conceive of a way for all the bound DnaA molecules to interact without the formation of DNA loops. An example of a looped bORC is shown in **Figure 2B**, although this structure is still hypothetical. Since the orisome of *E. coli* appears as a nucleosome-like structure when observed using the electron microscope (Crooke et al., 1993), an intriguing possibility is that as orisome assembly progresses, newly recruited DnaA is added to loosely looped DNA, and then forms oligomers that tighten the loops to form a quasi-nucleosome.

The minimal trimeric DnaA complex bound to *E. coli oriC* is temporally equivalent to the persistent and well-characterized hexameric eukaryotic origin recognition complex (ORC) that resides at eukaryotic replication origins (Duncker et al., 2009), and we will refer to the bacterial version as bORC. An important difference is that in eukaryotes, ORC is preassembled prior to interacting with replication origins and specific nucleotide motifs are not usually recognized (Bell, 2002; Kawakami and Katayama, 2010). Although DnaA can aggregate in solution, *oriC* recognition sites are occupied by monomers (Schaper and Messer, 1995; Weigel et al., 1997), with DnaA–DnaA interactions taking place after monomers have bound to DNA.

In additional to being temporally analogous, bORC has functional similarity to the eukaryotic ORC. Like ORC, which recruits additional components of the eukaryotic pre-replication complex, the DnaA in bORC also acts as a scaffold for the recruitment of more copies of DnaA to form subsequent stages of the orisome (Miller et al., 2009; Smits et al., 2011). DnaA molecules are recruited to bORC via domain I (Miller et al., 2009) and a separate DnaA oligomerization region in domain III, encompassing the AAA+ (ATPases associated with various cellular activities) fold (Felczak and Kaguni, 2004; Kawakami et al., 2005). Mutations in either domain I or III that abolish DnaA–DnaA interactions also prevent progression of orisome assembly beyond bORC.

Although all three high affinity sites in *E. coli oriC* are required to constrain the origin, any combination of two high affinity sites are sufficient to assemble orisomes that are functional, albeit with timing defects (Kaur et al., 2014). However, orisomes lacking either R1 or R4 become dependent on two DNA bending proteins that bind to *oriC* (Fis and IHF, **Figure 2** and see below; Kaur et al., 2014), suggesting that there are conformational requirements for bORC. The ability of orisomes to function without DnaA-binding to R1 also counters previous models that proposed that R1 is essential for DnaA-dependent DNA helicase loading (Speck and Messer, 2001; Soultanas, 2012), and this finding suggests that either R1 is not required for this step, or that another component of the orisome can provide a back-up function when R1 is inactivated.

The nature of bORC in other bacterial types is not well characterized. Clustering of high affinity DnaA recognition sites near A-T rich regions is used as a criteria for mapping bacterial replication origins on newly sequenced genomes (Gao and Zhang, 2007), but the numbers, positions, and orientations of these sites is remarkably variable. Most bacteria carry between 3 and 8 high affinity DnaA recognition sites, but *oriC* geography is distinctive for each genus (Marczynski and Shapiro, 1993; Zawilak-Pawlik et al., 2005; Gao and Zhang, 2007; Leonard and Mechali, 2013; see also **Figure 4**). While larger origins usually have higher numbers of high affinity recognition sites, there are, as yet, no hard and fast rules that can be used to predict the configuration of initiator binding sites in *oriC*s. For example, the thermophile *Thermus thermophilus* carries a 300 bp *oriC* with 13 consensus or near consensus recognition sites (Schaper et al., 2000). In *Caulobacter*, there is only one high affinity DnaA recognition site, but many recognition sites for the regulatory protein CtrA (Marczynski and Shapiro, 1992). This arrangement allows the initiation step to remain DnaA-dependent, but under the control of an additional regulator that ensures the initiation step is restricted to a particular stage of the cell cycle. In some bacteria, for example, *Helicobacter* (Donczew et al., 2012), *Mycoplasma* (Cordova et al., 2002; Lartigue et al., 2003), and *Bacillus* (Moriya et al., 1999), there are two separated clusters of high affinity DnaA recognition sites. This arrangement produces a bipartite configuration whereby DnaA bound at each cluster can interact, but this interaction becomes dependent on DNA bending.

Filling the Gaps: Ordered Orisome Assembly is Determined by Low Affinity DnaA-*oriC* Interactions

Since DnaA occupies high affinity sites throughout the cell cycle, mechanisms regulating progression of orisome assembly beyond bORC must be focused on lower affinity DnaA-*oriC* interactions. Low affinity DnaA recognition sites are mapped in a variety of bacterial *oriC*s (Charbon and Lobner-Olesen, 2011; Leonard and Mechali, 2013) but these sites are often difficult to identify because they deviate substantially (two or more bases) from the consensus sequence. Thus, direct measurement of DnaA contacts with these sites is often required to confirm their role in orisome assembly (Rozgaja et al., 2011). In *E. coli*, the recognition sites that are not bound in the bORC have at least a 50-fold lower DnaA binding affinity than do R1, R2, and R4 (Schaper and Messer, 1995). Most importantly, low affinity DnaA recognition sites cannot become occupied unless DnaA is recruited by bound DnaA at a nearby site, and this assistance requires DnaA's domain I (Schaper and Messer, 1995; Rozgaja et al., 2011). For this reason, it is not surprising that the low affinity DnaA recognition sites in *E. coli oriC* lie in the two DNA gaps (Leonard and Grimwade, 2010) flanked by high affinity recognition sites (see **Figure 2A**). The arrangement of the low affinity recognition sites within these gaps was unexpected, but provides insight into how cooperative binding leading to DnaA occupation of low affinity sites is achieved. Each of two distinct arrays contains four sites, one in each half of *oriC* (**Figure 2A**; R5M, t2, I1, and I2 in the left half and C3, C2, I3, and C1 in the right half; Rozgaja et al., 2011). Notably, each low affinity site within an array is separated from its neighbor by exactly two base pairs, which positions DnaA on the same face of the DNA helix. All the recognition sites in an individual array face in the same direction

in *E. coli*, and the arrays in each half of *oriC* are also oriented in opposite directions relative to one another (Rozgaja et al., 2011; see **Figure 2**). This arrangement allows a DnaA bound to a high affinity site to assist loading at the proximal low affinity site, with the other sites in the array being filled by progressive cooperative binding between two low affinity sites (Rozgaja et al., 2011).

Spacing between adjacent DnaA recognition sites is critical for these cooperative interactions (Hansen et al., 2007). Since the spacing between high and low affinity sites in *oriC* varies among bacterial types, and since domain I interactions play a key role in cooperative binding at *oriC* (Miller et al., 2009), this stringency in spacing implies that the length of the flexible linker region in DnaA's domain II may contribute to the efficiency of orisome assembly. Consistent with this idea, deletions that shorten domain II result in an under-initiation phenotype (Molt et al., 2009). Thus, it is not surprising that the length and amino acid sequence of domain II is the least conserved property of DnaA, and it is likely that among different bacterial types, there is a direct relationship between linker length/flexibility and placement of recognition sites in *oriC* (Nozaki and Ogawa, 2008).

It should be noted that in some bacterial types, the affinity for DnaA may not be as high as is measured for R1 and R4 in *E. coli oriC*, and many closely spaced consensus recognition sites may be required for co-operative DnaA binding, as exemplified by the *oriC* of *Thermus* (Schaper et al., 2000), and *Streptomyces* (Jakimowicz et al., 2000). Specific spacing requirements will become more apparent as new low affinity sites are identified in different bacterial origins, and this will necessitate substantial revisions of existing *oriC* maps, as has happened for *E. coli* (Leonard and Grimwade, 2011). It is also important to not rule out the role of DNA topology in the ability of DnaA to access its recognition sites, and supercoiling dependent DnaA binding in *oriC* is reported for the *oriC* of *Helicobacter pylori* (Donczew et al., 2014).

Dynamic Conformational Switching in *oriC*: Regulation of Staged Orisome Assembly

The precise positioning and spacing of DnaA recognition sites encoded into *E. coli oriC,* described above, provides the instructions for ordered orisome assembly. Starting from bORC, the first cooperative binding that should take place, based on proximity, is between DnaA bound at R4 and the adjacent low affinity site C1 (**Figure 2A**), which nucleates a DnaA oligomer that grows by progressive binding of the low affinity sites in the gap between R4 and R2 (Rozgaja et al., 2011; **Figure 3**). Given the positions and orientations of DnaA recognition sites in the left half of *oriC*, assembly of a similar DnaA oligomer in the gap region between R1 and R2 was predicted and then detected (Rozgaja et al., 2011). Experimental evidence is consistent with both left and right oligomers growing toward R2 (Rozgaja et al., 2011), and this arrangement means that the DnaA occupying R2 primarily acts to anchor the converging oligomers. Complete loss of DnaA binding at R2 is well tolerated (Weigel et al., 2001) so anchoring of the DnaA oligomers does not appear to be a critical step in orisome assembly. The observation that *E. coli oriC* retains function in the absence of binding to R1 or R4 implies that the DnaA occupying R2 is capable of nucleating oligomers, and this was shown to be true (Kaur et al., 2014), although R2-bound DnaA does not nucleate as efficiently as the DnaA occupying the peripheral sites, particularly in the right half of *oriC*.

Despite the appealing symmetry of converging DnaA oligomers, there is an obvious difference in the nucleation of oligomers from DnaA bound at R1 and R4, due to their distance from their proximal sites. Extension of DnaA from R4 is easily accomplished, due to close spacing (3 bp) of R4 and C1 (Rozgaja et al., 2011), but there is a 45 bp gap between R1 and the nearest low affinity recognition site, R5M, and there is evidence that DnaA oligomers nucleated at R1 do not extend into this region (Rozgaja et al., 2011). Rather, to span this 45 bp space, *E. coli oriC* DNA is bent to bring R1 and R5 into proximity, and the DnaA oligomer that grows by progressive binding of DnaA monomers to the left array of low affinity sites is most likely nucleated by cross-strand DnaA–DnaA interactions via domain I (**Figure 3**). A DNA bending protein, integration host factor (IHF) recognizes a site placed in the gap between R1and R5M (Polaczek, 1990; **Figure 2A**) and facilitates the interaction between DnaAs bound at R1 and R5M. IHF binding is not essential for R1 to nucleate a DnaA oligomer or for assembly of functional orisomes (Von Freiesleben et al., 2000; Weigel et al., 2001), presumably because the DNA between R1 and R5M is intrinsically flexible, but loss of IHF binding results in perturbed initiation timing.

In rapidly growing cells, assembly of oligomers nucleated by DnaA bound to R1 and R4 is nearly coincident, and correlates closely with the time that IHF binding to its cognate site in *oriC* can be detected, and with the time of initiation of DNA synthesis (Cassler et al., 1995). Thus, *in vivo*, assembly of the right and left DnaA oligomers must be both coordinated and precisely timed. This coupled oligomer assembly appears to be critical, since any loss of precisely ordered orisome assembly causes defects in initiation efficiency or timing (Kaur et al., 2014), especially for bacteria undergoing rapid growth, where new rounds of DNA replication must initiate before previous rounds are completed. In rapidly growing *E. coli* where multiple copies of *oriC* exist, all origins are activated synchronously to ensure that replication is completed for all chromosomes at the correct time (Skarstad et al., 1986).

To ensure orderly DnaA oligomerization, *E. coli* uses a DnaA-dependent switch mechanism that is built around the successive activity of IHF and another DNA bending protein, Fis (Factor for inversion stimulation), whose recognition site is placed in the gap regions between R2 and C3 (**Figure 2A**; Filutowicz et al., 1992; Ryan et al., 2004). In rapidly growing *E. coli*, Fis binds to bORC and places a bend in the constrained bORC loop (Cassler et al., 1995; **Figure 3**). This bend acts as a long distance inhibitor of IHF binding (Ryan et al., 2004), most likely because it prevents additional bending within the loop (Kaur et al., 2014). Close to the time of initiation, DnaA bound to R4 nucleates assembly of the DnaA oligomer bound to the right array of low affinity sites. Fis is displaced from its site during this process (Ryan et al., 2004;

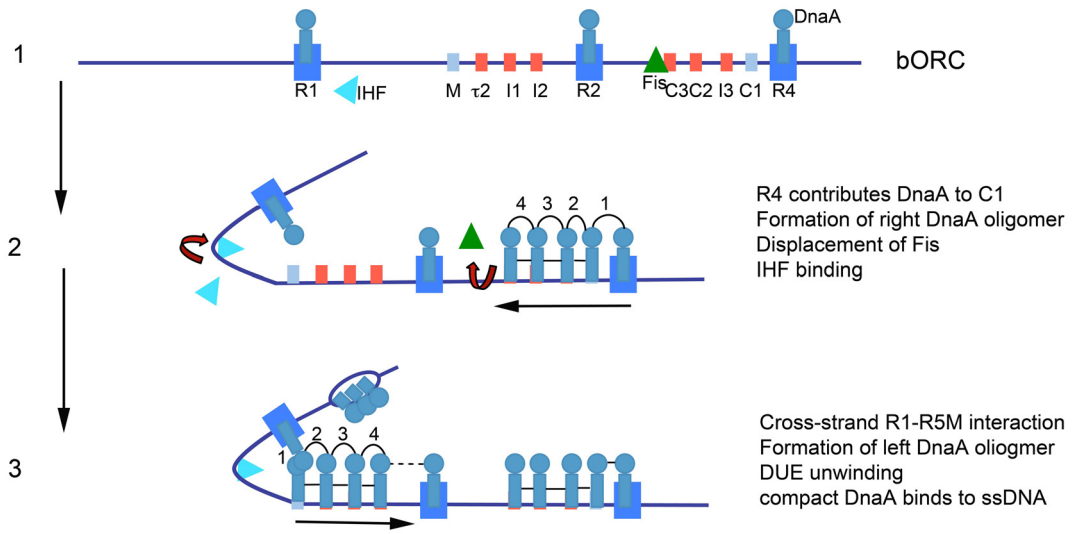

FIGURE 3 | Model of staged orisome assembly. Stage 1 (bORC): after initiation of chromosome replication, DnaA rebinds to high affinity R1, R2, and R4 sites. Fis is also bound at this stage, but IHF is not. Low affinity sites are unoccupied. Stage 2: DnaA bound to R4 recruits DnaA for binding to C1. DnaA then progressively fills the remaining arrayed sites, forming an oligomer in the gap region between R2 and R4. The DnaA oligomer displaces Fis, and loss of Fis allows IHF to bind to its cognate site. Stage 3: the bend induced by IHF binding allows DnaA, recruited by R1, to bind to R5M, and form a cross-strand DnaA interaction. A DnaA oligomer then progressively grows toward R2, bound to arrayed low affinity sites, and anchored by R2. In this configuration, oriC DNA is unwound in the DUE, and DnaA in the form of a compact filament binds to the ssDNA.

Figure 3), and it is possible that interactions between high affinity sites are also broken, although this has yet to be determined. Displacement of Fis allows IHF to bind and bring DnaA bound to R1 into proximity to R5M (Cassler et al., 1995), resulting in nucleation of the left side oligomer (Ryan et al., 2004; **Figure 3**). Full occupation of *oriC* with DnaA is coincident with origin unwinding in the DUE (Grimwade et al., 2000).

The possibility that DNA bending itself may promote unwinding of the DUE was suggested by the timing of the IHF-induced bend. However, in the absence of DnaA, IHF is not capable of creating a single-strand DNA bubble (Grimwade et al., 2000), so some feature of the left oligomer is also required. One possibility is that DNA bending is sufficient for unwinding, but the unwinding is not sustainable, and so the left oligomer is needed to stabilize the unwound single-stranded DNA, and/or participate in DNA helicase loading (Duderstadt et al., 2011; Ozaki and Katayama, 2012). It should be noted that the IHF-induced bend places the DUE in closer proximity to the DnaA bound to the left array of low affinity sites (**Figure 3**). Alternatively, if bending alone is not sufficient to separate DNA strands in the DUE, then the left oligomer may play a direct role in unwinding, and this has been suggested based on *in vitro* studies (Ozaki et al., 2012). How left oligomer formation might mediate strand separation is not clearly understood. One model suggests that the DnaA oligomer induces positive supertwists in *oriC* DNA that result in compensatory negative supercoiling that promotes DNA unwinding of the DUE (Erzberger et al., 2006; Zorman et al., 2012). There is less evidence for a role of the right oligomer in unwinding, since *oriC* deletion mutants lacking the right half of *oriC* are viable at slow growth rates, albeit with severely perturbed initiation (Stepankiw et al., 2009). However, the right oligomer cannot be ruled out as a contributor to events in the late stages of orisome assembly, particularly in the loading of DnaB helicase (Ozaki et al., 2012).

The nucleation of DnaA oligomers from high affinity sites is a critical step, and requires domain I-domain I interactions between DnaA molecules (Miller et al., 2009). Given the importance of this stage of orisome assembly, it is logical that it would be a target for regulation. While this remains to be determined, there are several good candidates for regulatory factors. In particular, DiaA (Ishida et al., 2004) and its structural analog HobA (Natrajan et al., 2009; Zawilak-Pawlik et al., 2011), are both positive effectors of orisome assembly, and stimulate the assembly of DnaA oligomers. Both proteins form homotetramers that bind to domain I directly (Keyamura et al., 2009; Zawilak-Pawlik et al., 2011). *E. coli* DiaA interacts with a subgroup of DnaA molecules binding to *oriC,* although the position of these molecules is not known (Keyamura et al., 2007). DnaB helicase and DiaA interact with DnaA domain I at the same location, suggesting that DiaA plays a negative role in the regulation of DNA helicase loading (Keyamura et al., 2009). Although the protein is dispensable, *E. coli* mutants of DiaA show delayed initiation of chromosome replication (Ishida et al., 2004). HobA is an essential factor in *H. pylori* (Zawilak-Pawlik et al., 2007), and tetramers of HobA are required for domain I-domain I DnaA oliogmerization (Natrajan et al., 2009). Despite their structural similarity, DiaA and HobA are not interchangeable suggesting a high degree of specificity for the DnaA regulating factors among bacterial types (Zawilak-Pawlik et al., 2011), possibly due to differences in domain I.

Some factors that interact with DnaA domain I are repressors of chromosome replication. This is the case for the *E. coli*

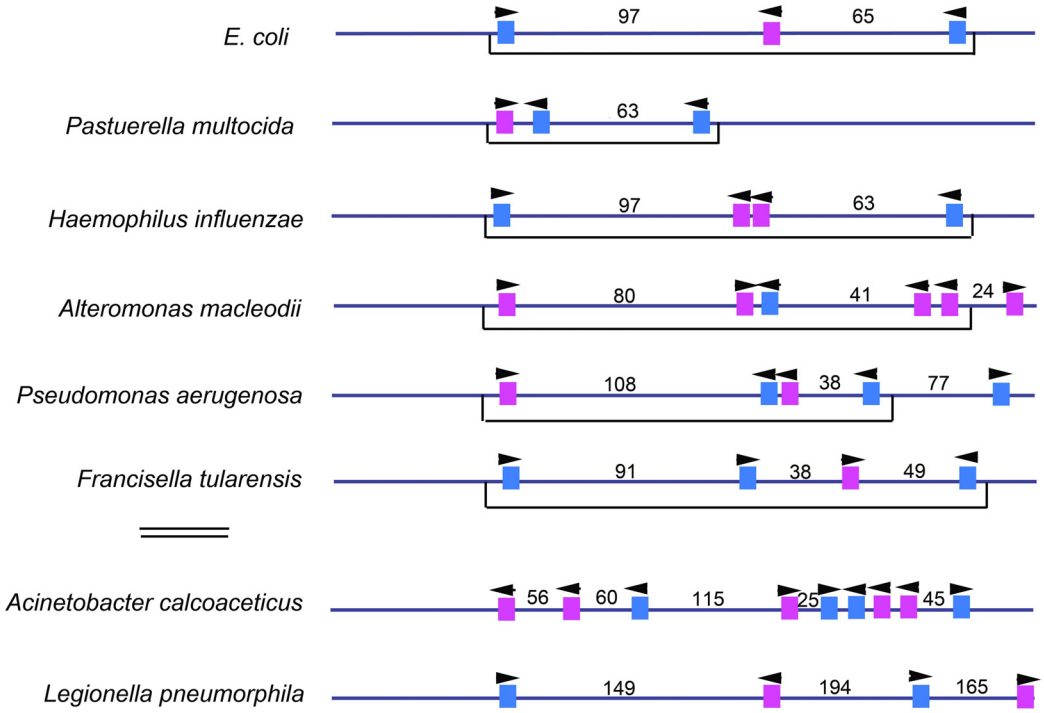

FIGURE 4 | Comparison of the number and placement of high affinity DnaA binding sites in *oriC*s in related members of the Gammaproteobacteria family. The high affinity sites in the *oriC* regions of *E. coli* and several related bacterial types are shown. Blue rectangles indicate sites that match the consensus 5′-TTATCCACA, and the pink rectangles mark sites which deviate from this sequence at one or two bases. The arrowheads mark the presumptive orientation of the sites, and the numbers designate the number of base pairs in the gap regions between sites. The brackets below the maps show an *E. coli*-like arrangement of high affinity sites (see text for details). The two bacterial types below the double line are larger than those above, but it should be noted that the maps are not drawn to scale.

ribosomal protein L2 (Chodavarapu et al., 2011), the *E. coli* starvation protein, Dps (Chodavarapu et al., 2008), and the sporulation-related regulator of *Bacillus subtilis*, SirA (Rahn-Lee et al., 2011). SirA is an important regulator of ploidy in *Bacillus* and during sporulation, (Wagner et al., 2009) cells lacking this protein will over-initiate the replication of their chromosomes.

Dissecting the Role of DnaA–ATP in Orisome Assembly and in Timing of Initiation of Chromosome Replication

New rounds of chromosome replication in most bacteria are dependent on newly synthesized DnaA–ATP and DnaA–ATP is commonly considered to be the "active form" of the initiator. *In vitro* studies also identified an additional requirement for ATP in the mM range (Sekimizu et al., 1987); this is much higher than is needed for DnaA to bind ATP (μM range; Sekimizu et al., 1987), and the reason for this requirement has not yet been determined. Additionally, experimental evidence from both *in vitro* and *in vivo* studies indicates that some DnaA–ADP is permitted in a functional orisome in *E. coli* (Yung et al., 1990; McGarry et al., 2004; Grimwade et al., 2007), and it is not yet fully understood what features of orisome assembly and function specifically require DnaA–ATP. One possibility is that DnaA–ATP forms a specific structure on DNA that is required for orisome function. In the absence of DNA, a truncated version (domains III and IV) of *Aquifex aeolicus* DnaA–ATP assembles into an open ended, compact, right handed, helical filament (Erzberger et al., 2006). In this configuration, an arginine finger in one molecule's domain III contacts the ATP bound to the adjacent protomer. The DNA-binding domain (domain IV) also folds up to contact domain III in the helical filament, implying that a crosstalk mechanism exists between domains III and IV (Duderstadt et al., 2010). These compact DnaA–ATP filaments can interact directly with single-stranded DNA through a central channel formed by domains III and IV. Two distinct roles, in helicase loading and unwinding, have been proposed for the compact DnaA–ATP filament. Evidence to support these roles comes from *in vitro* studies, where this structure has been reported to bind the helicase loader, DnaC, and possibly mediate asymmetric loading of the replicative helicase, DnaB (Mott et al., 2008). The filament has also been shown to melt short DNA duplexes, presumably by stretching the helix (Duderstadt et al., 2011). However, the compact filament has very low affinity for double-stranded DNA (Duderstadt et al., 2010), and it is unclear how its assembly could be started in the DUE unless the first protomer was recruited to DNA that was already unwound.

Although the crystal structure of DnaA–ATP oligomers is compatible with only single-stranded DNA binding, there is also experimental evidence that DnaA–ATP filaments assemble on double-stranded DNA in the gap regions between high affinity site, where they are proposed to mediate unwinding (left gap region) and assist in helicase loading (right gap region; Ozaki and Katayama, 2012). DnaA–ATP oligomers have also been shown to play a key role in *Bacillus* orisome function *in vivo*, although it is not known where in *oriC* these oligomers are formed. Oligomerization of *Bacillus* DnaA–ATP is stimulated by either single-stranded DNA or double-stranded DNA (Scholefield et al., 2012), but stimulation does not require site-specific DnaA binding and the role of DNA in this reaction remains unclear.

It is also not clear if the oligomers formed on double-stranded DNA must contain only DnaA–ATP. In *E. coli*, DnaA–ADP and a mutant version of DnaA (R285A), defective in domain III oligomerization, do not fill low affinity binding sites (McGarry et al., 2004; Kawakami et al., 2005), but it is not yet known if this is because only DnaA–ATP can participate in the DnaA–DnaA interactions required for cooperative binding, or because the nucleotide sequence of some of the low affinity 9 mer recognition sites preferentially binds DnaA–ATP (McGarry et al., 2004; Saxena et al., 2011). In support of the latter idea, a single base pair in the 9 mer recognition sequences of I2 and I3 is sufficient to convert these sites into ones that bind both nucleotide forms, without increasing their affinity for DnaA–ATP (McGarry et al., 2004). It is not known if low affinity sites that discriminate between DnaA's nucleotide forms are common among different bacterial types.

The structure of the DnaA oligomer associated with double-stranded DNA has not been determined. Duderstadt et al. (2010) suggested that DnaA–ATP forms a less compact oligomer on double-stranded DNA, and single molecule studies examining interaction of DnaA with *E. coli oriC* are consistent with DnaA–ATP, but not DnaA–ADP, forming a right handed helical filament on double-stranded DNA (Zorman et al., 2012). However, since *E. coli oriC* was used as the DNA substrate for the single molecule studies, it is possible the DnaA–ADP did not oligomerize because it was not bound to the origin fragment.

Despite the lack of clarity on how DnaA–ATP participates in orisome function and structure, it is clear that properly timed initiations require tight control of DnaA–ATP binding to *oriC*. In *E. coli*, multiple mechanisms, reviewed in Katayama et al. (2010) ensure that the availability of active initiator at *oriC* fluctuates appropriately during the cell cycle (Kurokawa et al., 1999), and that full occupation of *oriC* by DnaA is restricted to a short period of time during the cell cycle. These mechanisms, described below, include: (1) converting active DnaA–ATP into the inactive ADP-bound form, (2) titrating DnaA by binding it to sites outside *oriC*, (3) blocking DnaA access to *oriC*, and when necessary, (4) reactivating DnaA–ADP into active DnaA–ATP.

Mechanisms that inactivate DnaA–ATP activity are often coupled to the elongation phase of DNA replication. In *E. coli*, conversion of DnaA–ATP to DnaA–ADP is accomplished primarily by interactions with a replisome-associated protein, Hda, which stimulates DnaA's hydrolytic activity in a process termed regulatory inactivation of DnaA (RIDA; Katayama et al., 1998; Katayama and Sekimizu, 1999; Keyamura and Katayama, 2011). Since the nucleotide exchange rate for DnaA in many Gram positives is much higher than in Gram negatives, stimulating DnaA's hydrolysis activity is apparently not an effective regulatory mechanism in all bacteria (Bonilla and Grossman, 2012), and consistent with this idea, Hda is not a conserved protein.

In several bacterial types, DnaA is titrated away from *oriC* by individual high affinity recognition sites dispersed around the chromosome (Roth and Messer, 1998; Christensen et al., 1999), or by localized clusters of DnaA recognition sites at one, or more positions on the genome. One well-characterized cluster in *E. coli*, *datA*, resides over 450,000 bp away from *oriC* (Kitagawa et al., 1996; Ogawa et al., 2002) and can titrate large amounts of DnaA–ATP. At *datA*, DnaA assembles into a higher order complex that promotes DnaA–ATP hydrolysis (Kasho and Katayama, 2013). Clusters of DnaA are also found at eight intergenic regions on the *Bacillus* chromosome (Ishikawa et al., 2007). The conserved YabA protein found in several Gram-positive bacteria may represent a replisome-associated DnaA titration mechanism (Noirot-Gros et al., 2006; Soufo et al., 2008), but YabA is also reported to inhibit cooperative DnaA binding to *oriC* (Merrikh and Grossman, 2011; Scholefield and Murray, 2013).

Multiple factors in many different bacterial types are reported to bind to *oriC* and either block DnaA accessibility or affect its cooperative binding/oligomerization. These include CtrA in *Caulobacter* (Quon et al., 1998), AdpA in *Streptomyces* (Wolanski et al., 2012), MtrA in *Mycobacteria* (Rajagopalan et al., 2010), HP1021 in *Helicobacter* (Donczew et al., 2015), as well as SirA (Rahn-Lee et al., 2011), Soj (Scholefield et al., 2012), and DnaD (Bonilla and Grossman, 2012; Scholefield and Murray, 2013) in *Bacillus*. The master regulator of *Bacillus* sporulation, Spo0A, is also reported to bind to *oriC,* and block rounds of chromosome replication (Boonstra et al., 2013). In *E. coli*, direct blocking of access to low affinity sites is performed during every cell cycle by the sequestration protein, SeqA (Lu et al., 1994; Slater et al., 1995; Nievera et al., 2006), which recognizes and binds to newly replicated hemimethylated GATC sites that are clustered in *oriC* and in the *dnaA* promoter. High affinity recognition sites in *oriC* are not sequestered and can remain occupied throughout the cell cycle (Nievera et al., 2006), but low affinity *oriC* recognition sites and transcription of *dnaA* are blocked for about 1/3 of the cell cycle (Campbell and Kleckner, 1990). It is important to note that mechanisms of these types may play an important role in returning *oriC* to its correct bORC form, and thereby might turn out to be positive effectors of orisome assembly in addition to repressors.

In rapidly growing *E. coli*, where new rounds of DNA replication are triggered prior to the completion of previous rounds, there is insufficient new of DnaA–ATP synthesis to allow for proper initiation timing at all copies of *oriC*. A DnaA–ADP recharging system, dependent on two chromosomal loci termed DnaA reactivating sequences (DARSs) raises the levels of DnaA–ATP, although the exact mechanism remains unclear (Fujimitsu et al., 2009). DARS sites contain a specific arrangement of DnaA recognition sites, which must produce specific interactions

between bound DnaA–ADP that promotes nucleotide exchange. Interestingly, DARS2 activity is regulated by both Fis and IHF (Kasho et al., 2014), the same DNA bending proteins that regulate orisome assembly. DARS are identified in a number of Gammaproteobacteria and this may be a common regulator for bacteria in this group that are capable of fast growth (Fujimitsu et al., 2009). There is also long standing evidence that DnaA interacts with the acidic phospholipids of the cytoplasmic membrane in *E. coli* (Crooke, 2001; Regev et al., 2012; Saxena et al., 2013) and like DARS, membranes recharge DnaA–ADP (Garner and Crooke, 1996).

In addition to the multiple mechanisms used to regulate DnaA–ATP levels and *oriC* accessibility, the existence of sites that preferentially bind DnaA–ATP suggest that the *oriC* sequence itself is an important component of the cell cycle timing mechanism for chromosome replication in *E. coli* and any other bacteria with similar sites. To test this idea, several obvious questions must be considered. Is the occupation of DnaA–ATP preferential recognition sites a rate-limiting step for initiation? If so, does each site play an equivalent role in determining the amount of DnaA–ATP needed for initiation, or is accessibility differentially regulated among sites? To answer these questions, it will be necessary to convert each discriminatory site into one that binds both nucleotide forms of DnaA equivalently. From preliminary studies, it appears that such conversion may alter the time of initiation in the cell cycle. For example, changing I2 and I3 into non-discriminatory sites on plasmid origins resulted in an origin that was more efficient that the chromosomal *oriC*, resulting in rapid integration of the cloned version into the host chromosome as a replacement for the wild-type *oriC* (Grimwade et al., 2007). Further analysis of mutations in individual and combinations of sites will determine their contribution to the cell cycle timing mechanism, but the possibility exists that all of the low affinity DnaA–ATP discriminatory sites in *E. coli oriC* can be changed into a form that binds DnaA–ADP, while maintaining orisome activity. If this is the case, it would provide strong evidence that that DnaA–ATP is not required for the assembly of the oligomeric filament along double-stranded DNA or even for initial DNA unwinding, but is required for correct cell cycle timing of initiation. In this scenario, the version of the DnaA–ADP oligomer assembled along *oriC* would be functionally equivalent to the DnaA–ATP version and it will be necessary to re-evaluate the pervading view of orisome assembly. It is important to note that regardless of the oligomers assembled along the arrayed low affinity sites, DnaA–ATP is also likely to be required later in orisome assembly for single-stranded DNA binding and helicase loading. Further studies should reveal the different roles of DnaA–ATP as a structural component and as a timing feature for the orisome.

Orisomes are an Underexploited Drug Target

As a component of an essential machine for bacterial growth, and with regulatory proteins that are distinctly different from their eukaryotic counterparts, the orisome might be expected to be an excellent target for antibiotics. However, the orisome, like the replisome, remains under-exploited as a target for new drug development (Robinson et al., 2010). There are no known naturally occurring antibiotics that affect orisomes and perhaps this should be expected for an assemblage comprising a protein that is as highly conserved as DnaA. However, despite the dearth of orisome-specific inhibitors, DnaA activity has been be used as the basis for an antibiotic screen. Robust and high throughput *in vivo* assays (Fossum et al., 2008) were performed using *E. coli* conditional lethal, cold-sensitive strains (COS mutants) of DnaA which over-initiate new replication forks (Katayama and Kornberg, 1994). An inhibitor of orisome activity or replication fork movement will restore growth at the non-permissive temperature (Fossum et al., 2008). The strain also contained an alternative mode of chromosome replication to allow cell survival in the presence of an inhibitor that completely blocked DnaA activity. Using this assay, a novel benzazepine-derived, DNA gyrase inhibitor was identified from the Library of Pharmacologically Active Compounds (LOPACs; Johnsen et al., 2010). Although no direct inhibitors of DnaA were identified, over-expression of portions of the *E. coli* DnaA molecule (domain I or domain IV) were also shown to permit growth at low temperature in a similar assay, presumably by forming inactive hetero-oligomers and blocking orisome assembly (Weigel et al., 1999). Drugs modeled on these domains of DnaA may worth investigating in the future.

Successful orisome inhibitors may be most effective if they are directed toward specific stages or subassemblies of the orisome. Candidate sub-assemblies include the cross-strand DnaA–DnaA structures, promoted by DNA bending proteins like IHF, that may be "Achilles heel" stages that may require more time to assemble, or are less stable than other orisome assembly stages. These stages are likely already to be targets of cellular orisome assembly regulators such as DiaA (Ishida et al., 2004) or HobA (Zawilak-Pawlik et al., 2007).

Another important aspect of targeting inhibitors of orisome assembly is to identify shared steps in orisome assembly among bacterial types. Fortunately, a large *oriC* database, DoriC, is available for comparative orisome analysis (Gao et al., 2013), but it is obvious from the diverse arrangements of consensus DnaA recognition sites that there are many different ways to assemble orisomes. Furthermore, there is a lack of information on low affinity DnaA recognition sites in bacteria other than *E. coli*. Although it appears that these sites exist in the well-studied origins of *Helicobacter*, *Mycobacteria*, *Bacillus,* and *Caulobacter* (Charbon and Lobner-Olesen, 2011; Taylor et al., 2011; Leonard and Mechali, 2013), for comparative analysis, it may be more informative to examine the origins of close relatives (for an example see, Shaheen et al., 2009). The *oriC* geography for relatives of *E. coli* (members of the Gammaproteobacteria) is shown in **Figure 4**. Even among the closely related members of this group, the arrangement, number, and orientation of consensus (high affinity) sites is variable. However, a shared, *E. coli*-like, motif appears with high affinity sites at the boundaries of gap regions (40–100 bp) where low affinity recognition sites would be expected to reside. This motif includes

E. coli's orientation of high affinity sites and may reflect the common assembly pattern of DnaA oligomers. Interestingly, some members (such as *Haemophilus influenza, Pseudomonas aerugenosa, and Alteromonas macleodii*) of this group carry extra high affinity sites that are centralized and extremely closely spaced. This arrangement suggests that in these origins, each DnaA oligomer may be anchored at its own high affinity site, rather than sharing one central site (R2) as is the case for *E. coli*. Other members (such as *Acinetobacter calcoaceticus*) have multiple high affinity sites downstream or upstream from the shared motif. Although the minimal requirement for high affinity sites remains to be determined for any member of this group other than *E. coli* (Kaur et al., 2014), additional high affinity sites may be required to build bORCs capable of forming larger or smaller DNA loops or to provide for synthesis of additional DnaA oligomers during staged orisome assembly. Some *oriCs* in this group (such as *A. calcoaceticus*) may also reflect a bipartite arrangement. Targeting these interesting versions of *oriC* that deviate from *E. coli* should provide valuable information to set the rules for orisome assembly and identify shared steps for inhibitor targeting.

It is worth noting that the *E. coli* recombineering strains mentioned above should be useful in developing heterologous systems to map DnaA-*oriC* interactions *in vivo* without having to study pathogenic organisms. Any replication origin can be introduced into the *E. coli* chromosome along with appropriate *dnaA* the gene as replacements for the *E. coli* versions. The heterologous origin does not need to be functional in these strains, since valuable information on orisome assembly can be obtained by examining origin binding to its cognate DnaA and, in the case of non-functional origins, where this process is halted. With a few modifications, a heterologous system of this type should also be useful for orisome inhibitor screening.

In summary, although more challenging experiments await, one can't help but admire the versatility of the instruction set that is encoded into the bacterial origin of replication. Although some of its features are hidden within cryptic nucleotide sequence motifs, these instructions are sufficient to direct the addition of each DnaA subunit to produce staged orisome assembly, as well as encode recognition sites for proteins the produce regulatory switches for orisome assembly as well as binding sites for the regulatory proteins needed for origin resetting. Specific nucleotide sequences are likely to be involved in timing of orisome assembly in the cell cycle and it will be interesting to identify new roles for *oriC* sequences as different bacterial types are examined and compared. Clearly, despite the intense scrutiny that orisomes have received over the years, they still hold secrets that are worth uncovering.

Acknowledgments

The work in our laboratories was supported by Public Health Service grant GM54042. Publication of this article was funded in part by the Open Access Subvention Fund and the Florida Tech Libraries.

References

Bell, S. P. (2002). The origin recognition complex: from simple origins to complex functions. *Genes Dev.* 16, 659–672. doi: 10.1101/gad.969602

Bonilla, C. Y., and Grossman, A. D. (2012). The primosomal protein DnaD inhibits cooperative DNA binding by the replication initiator DnaA in *Bacillus subtilis*. *J. Bacteriol.* 194, 5110–5117. doi: 10.1128/JB.00958-12

Boonstra, M., de Jong, I. G., Scholefield, G., Murray, H., Kuipers, O. P., and Veening, J. W. (2013). Spo0A regulates chromosome copy number during sporulation by directly binding to the origin of replication in *Bacillus subtilis*. *Mol. Microbiol.* 87, 925–938. doi: 10.1111/mmi.12141

Bramhill, D., and Kornberg, A. (1988). Duplex opening by dnaA protein at novel sequences in initiation of replication at the origin of the *E. coli* chromosome. *Cell* 52, 743–755. doi: 10.1016/0092-8674(88)90412-6

Campbell, J. L., and Kleckner, N. (1990). *E. coli* oriC and the dnaA gene promoter are sequestered from dam methyltransferase following the passage of the chromosomal replication fork. *Cell* 62, 967–979. doi: 10.1016/0092-8674(90)90271-F

Cassler, M. R., Grimwade, J. E., and Leonard, A. C. (1995). Cell cycle-specific changes in nucleoprotein complexes at a chromosomal replication origin. *EMBO J.* 14, 5833–5841.

Charbon, G., and Lobner-Olesen, A. (2011). A role for the weak DnaA binding sites in bacterial replication origins. *Mol. Microbiol.* 82, 272–274. doi: 10.1111/j.1365-2958.2011.07840.x

Chodavarapu, S., Felczak, M. M., and Kaguni, J. M. (2011). Two forms of ribosomal protein L2 of *Escherichia coli* that inhibit DnaA in DNA replication. *Nucleic Acids Res.* 39, 4180–4191. doi: 10.1093/nar/gkq1203

Chodavarapu, S., Gomez, R., Vicente, M., and Kaguni, J. M. (2008). *Escherichia coli* Dps interacts with DnaA protein to impede initiation: a model of adaptive mutation. *Mol. Microbiol.* 67, 1331–1346. doi: 10.1111/j.1365-2958.2008.06127.x

Christensen, B. B., Atlung, T., and Hansen, F. G. (1999). DnaA boxes are important elements in setting the initiation mass of *Escherichia coli*. *J. Bacteriol.* 181, 2683–2688.

Cordova, C. M., Lartigue, C., Sirand-Pugnet, P., Renaudin, J., Cunha, R. A., and Blanchard, A. (2002). Identification of the origin of replication of the *Mycoplasma pulmonis* chromosome and its use in oriC replicative plasmids. *J. Bacteriol.* 184, 5426–5435. doi: 10.1128/JB.184.19.5426-5435.2002

Crooke, E. (2001). *Escherichia coli* DnaA protein–phospholipid interactions: in vitro and in vivo. *Biochimie* 83, 19–23. doi: 10.1016/S0300-9084(00)01224-4

Crooke, E., Thresher, R., Hwang, D. S., Griffith, J., and Kornberg, A. (1993). Replicatively active complexes of DnaA protein and the *Escherichia coli* chromosomal origin observed in the electron microscope. *J. Mol. Biol.* 233, 16–24. doi: 10.1006/jmbi.1993.1481

Datsenko, K. A., and Wanner, B. L. (2000). One-step inactivation of chromosomal genes in *Escherichia coli* K-12 using PCR products. *Proc. Natl. Acad. Sci. U.S.A.* 97, 6640–6645. doi: 10.1073/pnas.120163297

Donczew, R., Makowski, L., Jaworski, P., Bezulska, M., Nowaczyk, M., Zakrzewska-Czerwińska, J., et al. (2015). The atypical response regulator HP1021 controls formation of the *Helicobacter pylori* replication initiation complex. *Mol. Microbiol.* 95, 297–312. doi: 10.1111/mmi.12866

Donczew, R., Mielke, T., Jaworski, P., Zakrzewska-Czerwinska, J., and Zawilak-Pawlik, A. (2014). Assembly of *Helicobacter pylori* initiation complex is determined by sequence-specific and topology-sensitive DnaA-oriC interactions. *J. Mol. Biol.* 426, 2769–2782. doi: 10.1016/j.jmb.2014.05.018

Donczew, R., Weigel, C., Lurz, R., Zakrzewska-Czerwinska, J., and Zawilak-Pawlik, A. (2012). *Helicobacter pylori* oriC – the first bipartite origin of chromosome replication in Gram-negative bacteria. *Nucleic Acids Res.* 40, 9647–9660. doi: 10.1093/nar/gks742

Duderstadt, K. E., Chuang, K., and Berger, J. M. (2011). DNA stretching by bacterial initiators promotes replication origin opening. *Nature* 478, 209–213. doi: 10.1038/nature10455

Duderstadt, K. E., Mott, M. L., Crisona, N. J., Chuang, K., Yang, H., and Berger, J. M. (2010). Origin remodeling and opening in bacteria rely on distinct assembly states of the DnaA initiator. *J. Biol. Chem.* 285, 28229–28239. doi: 10.1074/jbc.M110.147975

Duncker, B. P., Chesnokov, I. N., and McConkey, B. J. (2009). The origin recognition complex protein family. *Genome Biol.* 10:214. doi: 10.1186/gb-2009-10-3-214

Erzberger, J. P., Mott, M. L., and Berger, J. M. (2006). Structural basis for ATP-dependent DnaA assembly and replication-origin remodeling. *Nat. Struct. Mol. Biol.* 13, 676–683. doi: 10.1038/nsmb1115

Erzberger, J. P., Pirruccello, M. M., and Berger, J. M. (2002). The structure of bacterial DnaA: implications for general mechanisms underlying DNA replication initiation. *EMBO J.* 21, 4763–4773. doi: 10.1093/emboj/cdf496

Felczak, M. M., and Kaguni, J. M. (2004). The box VII motif of *Escherichia coli* DnaA protein is required for DnaA oligomerization at the *E. coli* replication origin. *J. Biol. Chem.* 279, 51156–51162. doi: 10.1074/jbc.M409695200

Filutowicz, M., Ross, W., Wild, J., and Gourse, R. L. (1992). Involvement of Fis protein in replication of the *Escherichia coli* chromosome. *J. Bacteriol.* 174, 398–407.

Fossum, S., De Pascale, G., Weigel, C., Messer, W., Donadio, S., and Skarstad, K. (2008). A robust screen for novel antibiotics: specific knockout of the initiator of bacterial DNA replication. *FEMS Microbiol. Lett.* 281, 210–214. doi: 10.1111/j.1574-6968.2008.01103.x

Fujikawa, N., Kurumizaka, H., Nureki, O., Terada, T., Shirouzu, M., Katayama, T., et al. (2003). Structural basis of replication origin recognition by the DnaA protein. *Nucleic Acids Res.* 31, 2077–2086. doi: 10.1093/nar/gkg309

Fujimitsu, K., Senriuchi, T., and Katayama, T. (2009). Specific genomic sequences of *E. coli* promote replicational initiation by directly reactivating ADP-DnaA. *Genes Dev.* 23, 1221–1233. doi: 10.1101/gad.1775809

Fuller, R. S., Funnell, B. E., and Kornberg, A. (1984). The dnaA protein complex with the *E. coli* chromosomal replication origin (oriC) and other DNA sites. *Cell* 38, 889–900. doi: 10.1016/0092-8674(84)90284-8

Fuller, R. S., Kaguni, J. M., and Kornberg, A. (1981). Enzymatic replication of the origin of the *Escherichia coli* chromosome. *Proc. Natl. Acad. Sci. U.S.A.* 78, 7370–7374. doi: 10.1073/pnas.78.12.7370

Funnell, B. E., Baker, T. A., and Kornberg, A. (1986). Complete enzymatic replication of plasmids containing the origin of the *Escherichia coli* chromosome. *J. Biol. Chem.* 261, 5616–5624.

Gao, F., Luo, H., and Zhang, C. T. (2013). DoriC 5.0: an updated database of oriC regions in both bacterial and archaeal genomes. *Nucleic Acids Res.* 41, D90–D93. doi: 10.1093/nar/gks990

Gao, F., and Zhang, C. T. (2007). DoriC: a database of oriC regions in bacterial genomes. *Bioinformatics* 23, 1866–1867. doi: 10.1093/bioinformatics/btm255

Garner, J., and Crooke, E. (1996). Membrane regulation of the chromosomal replication activity of *E. coli* DnaA requires a discrete site on the protein. *EMBO J.* 15, 3477–3485.

Grimwade, J. E., Ryan, V. T., and Leonard, A. C. (2000). IHF redistributes bound initiator protein, DnaA, on supercoiled oriC of *Escherichia coli*. *Mol. Microbiol.* 35, 835–844. doi: 10.1046/j.1365-2958.2000.01755.x

Grimwade, J. E., Torgue, J. J., McGarry, K. C., Rozgaja, T., Enloe, S. T., and Leonard, A. C. (2007). Mutational analysis reveals *Escherichia coli* oriC interacts with both DnaA-ATP and DnaA-ADP during pre-RC assembly. *Mol. Microbiol.* 66, 428–439. doi: 10.1111/j.1365-2958.2007.05930.x

Hansen, E. B., and Yarmolinsky, M. B. (1986). Host participation in plasmid maintenance: dependence upon dnaA of replicons derived from P1 and F. *Proc. Natl. Acad. Sci. U.S.A.* 83, 4423–4427. doi: 10.1073/pnas.83.12.4423

Hansen, F. G., Christensen, B. B., and Atlung, T. (2007). Sequence characteristics required for cooperative binding and efficient in vivo titration of the replication initiator protein DnaA in *E. coli*. *J. Mol. Biol.* 367, 942–952. doi: 10.1016/j.jmb.2007.01.056

Ishida, T., Akimitsu, N., Kashioka, T., Hatano, M., Kubota, T., Ogata, Y., et al. (2004). DiaA, a novel DnaA-binding protein, ensures the timely initiation of *Escherichia coli* chromosome replication. *J. Biol. Chem.* 279, 45546–45555. doi: 10.1074/jbc.M402762200

Ishikawa, S., Ogura, Y., Yoshimura, M., Okumura, H., Cho, E., Kawai, Y., et al. (2007). Distribution of stable DnaA-binding sites on the *Bacillus subtilis* genome detected using a modified ChIP-chip method. *DNA Res.* 14, 155–168. doi: 10.1093/dnares/dsm017

Jakimowicz, D., Majkadagger, J., Konopa, G., Wegrzyn, G., Messer, W., Schrempf, H., et al. (2000). Architecture of the *Streptomyces lividans* DnaA protein-replication origin complexes. *J. Mol. Biol.* 298, 351–364. doi: 10.1006/jmbi.2000.3686

Johnsen, L., Weigel, C., von Kries, J., Møller, M., and Skarstad, K. (2010). A novel DNA gyrase inhibitor rescues *Escherichia coli* dnaAcos mutant cells from lethal hyperinitiation. *J. Antimicrob. Chemother.* 65, 924–930. doi: 10.1093/jac/dkq071

Kaguni, J. M. (1997). *Escherichia coli* DnaA protein: the replication initiator. *Mol. Cells* 7, 145–157.

Kaguni, J. M., and Kornberg, A. (1984). Replication initiated at the origin (oriC) of the *E. coli* chromosome reconstituted with purified enzymes. *Cell* 38, 183–190. doi: 10.1016/0092-8674(84)90539-7

Kasho, K., Fujimitsu, K., Matoba, T., Oshima, T., and Katayama, T. (2014). Timely binding of IHF and Fis to DARS2 regulates ATP-DnaA production and replication initiation. *Nucleic Acids Res.* 42, 13134–13149. doi: 10.1093/nar/gku1051

Kasho, K., and Katayama, T. (2013). DnaA binding locus datA promotes DnaA-ATP hydrolysis to enable cell cycle-coordinated replication initiation. *Proc. Natl. Acad. Sci. U.S.A.* 110, 936–941. doi: 10.1073/pnas.1212070110

Katayama, T., and Kornberg, A. (1994). Hyperactive initiation of chromosomal replication in vivo and in vitro by a mutant initiator protein, DnaAcos, of *Escherichia coli*. *J. Biol. Chem.* 269, 12698–12703.

Katayama, T., Kubota, T., Kurokawa, K., Crooke, E., and Sekimizu, K. (1998). The initiator function of DnaA protein is negatively regulated by the sliding clamp of the *E. coli* chromosomal replicase. *Cell* 94, 61–71. doi: 10.1016/S0092-8674(00)81222-2

Katayama, T., Ozaki, S., Keyamura, K., and Fujimitsu, K. (2010). Regulation of the replication cycle: conserved and diverse regulatory systems for DnaA and oriC. *Nat. Rev. Microbiol.* 8, 163–170. doi: 10.1038/nrmicro2314

Katayama, T., and Sekimizu, K. (1999). Inactivation of *Escherichia coli* DnaA protein by DNA polymerase III and negative regulations for initiation of chromosomal replication. *Biochimie* 81, 835–840. doi: 10.1016/S0300-9084(99)00213-8

Kaur, G., Vora, M. P., Czerwonka, C. A., Rozgaja, T. A., Grimwade, J. E., and Leonard, A. C. (2014). Building the bacterial orisome: high-affinity DnaA recognition plays a role in setting the conformation of oriC DNA. *Mol. Microbiol.* 91, 1148–1163. doi: 10.1111/mmi.12525

Kawakami, H., and Katayama, T. (2010). DnaA, ORC, and Cdc6: similarity beyond the domains of life and diversity. *Biochem. Cell Biol.* 88, 49–62. doi: 10.1139/o09-154

Kawakami, H., Keyamura, K., and Katayama, T. (2005). Formation of an ATP-DnaA-specific initiation complex requires DnaA Arginine 285, a conserved motif in the AAA+ protein family. *J. Biol. Chem.* 280, 27420–27430. doi: 10.1074/jbc.M502764200

Keyamura, K., Abe, Y., Higashi, M., Ueda, T., and Katayama, T. (2009). DiaA dynamics are coupled with changes in initial origin complexes leading to helicase loading. *J. Biol. Chem.* 284, 25038–25050. doi: 10.1074/jbc.M109.002717

Keyamura, K., Fujikawa, N., Ishida, T., Ozaki, S., Su'etsugu, M., Fujimitsu, K., et al. (2007). The interaction of DiaA and DnaA regulates the replication cycle in *E. coli* by directly promoting ATP DnaA-specific initiation complexes. *Genes Dev.* 21, 2083–2099. doi: 10.1101/gad.1561207

Keyamura, K., and Katayama, T. (2011). DnaA protein DNA-binding domain binds to Hda protein to promote inter-AAA+ domain interaction involved in regulatory inactivation of DnaA. *J. Biol. Chem.* 286, 29336–29346. doi: 10.1074/jbc.M111.233403

Kitagawa, R., Mitsuki, H., Okazaki, T., and Ogawa, T. (1996). A novel DnaA protein-binding site at 94.7 min on the *Escherichia coli* chromosome. *Mol. Microbiol.* 19, 1137–1147. doi: 10.1046/j.1365-2958.1996.453983.x

Koppes, L., and Nordström, K. (1986). Insertion of an R1 plasmid into the origin of replication of the *E.* coli chromosome: random timing of replication of the hybrid chromosome. *Cell* 44, 117–124. doi: 10.1016/0092-8674(86)90490-3

Kowalski, D., and Eddy, M. J. (1989). The DNA unwinding element: a novel, cis-acting component that facilitates opening of the *Escherichia coli* replication origin. *EMBO J.* 8, 4335–4344.

Kurokawa, K., Nishida, S., Emoto, A., Sekimizu, K., and Katayama, T. (1999). Replication cycle-coordinated change of the adenine nucleotide-bound

forms of DnaA protein in *Escherichia coli*. *EMBO J.* 18, 6642–6652. doi: 10.1093/emboj/18.23.6642

Lartigue, C., Blanchard, A., Renaudin, J., Thiaucourt, F., and Sirand-Pugnet, P. (2003). Host specificity of mollicutes oriC plasmids: functional analysis of replication origin. *Nucleic Acids Res.* 31, 6610–6618. doi: 10.1093/nar/gkg848

Leonard, A. C., and Grimwade, J. E. (2010). Regulating DnaA complex assembly: it is time to fill the gaps. *Curr. Opin. Microbiol.* 13, 766–772. doi: 10.1016/j.mib.2010.10.001

Leonard, A. C., and Grimwade, J. E. (2011). Regulation of DnaA assembly and activity: taking directions from the genome. *Annu. Rev. Microbiol.* 65, 19–35. doi: 10.1146/annurev-micro-090110-102934

Leonard, A. C., and Helmstetter, C. E. (1986). Cell cycle-specific replication of *Escherichia coli* minichromosomes. *Proc. Natl. Acad. Sci. U.S.A.* 83, 5101–5105. doi: 10.1073/pnas.83.14.5101

Leonard, A. C., and Mechali, M. (2013). DNA replication origins. *Cold Spring Harb. Perspect. Biol.* 5:a010116. doi: 10.1101/cshperspect.a010116

Lu, M., Campbell, J. L., Boye, E., and Kleckner, N. (1994). SeqA: a negative modulator of replication initiation in *E. coli*. *Cell*. 77, 413–426. doi: 10.1016/0092-8674(94)90156-2

Marczynski, G. T., and Shapiro, L. (1992). Cell-cycle control of a cloned chromosomal origin of replication from *Caulobacter crescentus*. *J. Mol. Biol.* 226, 959–977. doi: 10.1016/0022-2836(92)91045-Q

Marczynski, G. T., and Shapiro, L. (1993). Bacterial chromosome origins of replication. *Curr. Opin. Genet. Dev.* 3, 775–782. doi: 10.1016/S0959-437X(05)80098-X

Margulies, C., and Kaguni, J. M. (1996). Ordered and sequential binding of DnaA protein to oriC, the chromosomal origin of *Escherichia coli*. *J. Biol. Chem.* 271, 17035–17040. doi: 10.1074/jbc.271.29.17035

Matsui, M., Oka, A., Takanami, M., Yasuda, S., and Hirota, Y. (1985). Sites of dnaA protein-binding in the replication origin of the *Escherichia coli* K-12 chromosome. *J. Mol. Biol.* 184, 529–533. doi: 10.1016/0022-2836(85)90299-2

McGarry, K. C., Ryan, V. T., Grimwade, J. E., and Leonard, A. C. (2004). Two discriminatory binding sites in the *Escherichia coli* replication origin are required for DNA strand opening by initiator DnaA-ATP. *Proc. Natl. Acad. Sci. U.S.A.* 101, 2811–2816. doi: 10.1073/pnas.0400340101

Meijer, M., Beck, E., Hansen, F. G., Bergmans, H. E., Messer, W., von Meyenburg, K., et al. (1979). Nucleotide sequence of the origin of replication of the *Escherichia coli* K-12 chromosome. *Proc. Natl. Acad. Sci. U.S.A.* 76, 580–584. doi: 10.1073/pnas.76.2.580

Merrikh, H., and Grossman, A. D. (2011). Control of the replication initiator DnaA by an anti-cooperativity factor. *Mol. Microbiol.* 82, 434–446. doi: 10.1111/j.1365-2958.2011.07821.x

Miller, D. T., Grimwade, J. E., Betteridge, T., Rozgaja, T., Torgue, J. J., and Leonard, A. C. (2009). Bacterial origin recognition complexes direct assembly of higher-order DnaA oligomeric structures. *Proc. Natl. Acad. Sci. U.S.A.* 106, 18479–18484. doi: 10.1073/pnas.0909472106

Molt, K. L., Sutera, V. A., Moore, K. K., and Lovett, S. T. (2009). A role for non-essential domain II of initiator protein, DnaA, in replication control. *Genetics* 183, 39–49. doi: 10.1534/genetics.109.104760

Moriya, S., Imai, Y., Hassan, A. K., and Ogasawara, N. (1999). Regulation of initiation of *Bacillus subtilis* chromosome replication. *Plasmid* 41, 17–29. doi: 10.1006/plas.1998.1381

Mott, M. L., and Berger, J. M. (2007). DNA replication initiation: mechanisms and regulation in bacteria. *Nat. Rev. Microbiol.* 5, 343–354. doi: 10.1038/nrmicro1640

Mott, M. L., Erzberger, J. P., Coons, M. M., and Berger, J. M. (2008). Structural synergy and molecular crosstalk between bacterial helicase loaders and replication initiators. *Cell* 135, 623–634. doi: 10.1016/j.cell.2008.09.058

Natrajan, G., Noirot-Gros, M. F., Zawilak-Pawlik, A., Kapp, U., and Terradot, L. (2009). The structure of a DnaA/HobA complex from *Helicobacter pylori* provides insight into regulation of DNA replication in bacteria. *Proc. Natl. Acad. Sci. U.S.A.* 106, 21115–21120. doi: 10.1073/pnas.0908966106

Nievera, C., Torgue, J. J., Grimwade, J. E., and Leonard, A. C. (2006). SeqA blocking of DnaA-oriC interactions ensures staged assembly of the *E. coli* pre-RC. *Mol. Cell* 24, 581–592. doi: 10.1016/j.molcel.2006.09.016

Niki, H., and Hiraga, S. (1999). Subcellular localization of plasmids containing the oriC region of the *Escherichia coli* chromosome, with or without the sopABC partitioning system. *Mol. Microbiol.* 34, 498–503. doi: 10.1046/j.1365-2958.1999.01611.x

Noirot-Gros, M. F., Velten, M., Yoshimura, M., McGovern, S., Morimoto, T., Ehrlich, S. D., et al. (2006). Functional dissection of YabA, a negative regulator of DNA replication initiation in *Bacillus subtilis*. *Proc. Natl. Acad. Sci. U.S.A.* 103, 2368–2373. doi: 10.1073/pnas.0506914103

Nozaki, S., and Ogawa, T. (2008). Determination of the minimum domain II size of *Escherichia coli* DnaA protein essential for cell viability. *Microbiology* 154, 3379–3384. doi: 10.1099/mic.0.2008/019745-0

Ogawa, T., Yamada, Y., Kuroda, T., Kishi, T., and Moriya, S. (2002). The datA locus predominantly contributes to the initiator titration mechanism in the control of replication initiation in *Escherichia coli*. *Mol. Microbiol.* 44, 1367–1375. doi: 10.1046/j.1365-2958.2002.02969.x

Ozaki, S., and Katayama, T. (2012). Highly organized DnaA-oriC complexes recruit the single-stranded DNA for replication initiation. *Nucleic Acids Res.* 40, 1648–1665. doi: 10.1093/nar/gkr832

Ozaki, S., and Katayama, T. (2009). DnaA structure, function, and dynamics in the initiation at the chromosomal origin. *Plasmid* 62, 71–82. doi: 10.1016/j.plasmid.2009.06.003

Ozaki, S., Noguchi, Y., Hayashi, Y., Miyazaki, E., and Katayama, T. (2012). Differentiation of the DnaA-oriC subcomplex for DNA unwinding in a replication initiation complex. *J. Biol. Chem.* 287, 37458–37471. doi: 10.1074/jbc.M112.372052

Polaczek, P. (1990). Bending of the origin of replication of *E. coli* by binding of IHF at a specific site. *New Biol.* 2, 265–271.

Quon, K. C., Yang, B., Domian, I. J., Shapiro, L., and Marczynski, G. T. (1998). Negative control of bacterial DNA replication by a cell cycle regulatory protein that binds at the chromosome origin. *Proc. Natl. Acad. Sci. U.S.A.* 95, 120–125. doi: 10.1073/pnas.95.1.120

Rahn-Lee, L., Merrikh, H., Grossman, A. D., and Losick, R. (2011). The sporulation protein SirA inhibits the binding of DnaA to the origin of replication by contacting a patch of clustered amino acids. *J. Bacteriol.* 193, 1302–1307. doi: 10.1128/JB.01390-10

Rajagopalan, M., Dziedzic, R. A., Zayer, M., Stankowska, D., Ouimet, M. C., Bastedo, D. P., et al. (2010). The Mycobacterium tuberculosis origin of replication and the promoter for immunodominant secreted antigen 85B are the targets of MtrA, the essential response regulator. *J. Biol. Chem.* 285, 15816–15827. doi: 10.1074/jbc.M109.040097

Regev, T., Myers, N., Zarivach, R., and Fishov, I. (2012). Association of the chromosome replication initiator DnaA with the *Escherichia coli* inner membrane in vivo: quantity and mode of binding. *PLoS ONE* 7:e36441. doi: 10.1371/journal.pone.0036441

Robinson, A., Brzoska, A. J., Turner, K. M., Withers, R., Harry, E. J., Lewis, P. J., et al. (2010). Essential biological processes of an emerging pathogen: DNA replication, transcription, and cell division in *Acinetobacter* spp. *Microbiol. Mol. Biol. Rev.* 74, 273–297. doi: 10.1128/MMBR.00048-09

Roth, A., and Messer, W. (1998). High-affinity binding sites for the initiator protein DnaA on the chromosome of *Escherichia coli*. *Mol. Microbiol.* 28, 395–401. doi: 10.1046/j.1365-2958.1998.00813.x

Rozgaja, T. A., Grimwade, J. E., Iqbal, M., Czerwonka, C., Vora, M., and Leonard, A. C. (2011). Two oppositely oriented arrays of low-affinity recognition sites in oriC guide progressive binding of DnaA during *Escherichia coli* pre-RC assembly. *Mol. Microbiol.* 82, 475–488. doi: 10.1111/j.1365-2958.2011.07827.x

Ryan, V. T., Grimwade, J. E., Camara, J. E., Crooke, E., and Leonard, A. C. (2004). *Escherichia coli* prereplication complex assembly is regulated by dynamic interplay among Fis, IHF and DnaA. *Mol. Microbiol.* 51, 1347–1359. doi: 10.1046/j.1365-2958.2003.03906.x

Samitt, C. E., Hansen, F. G., Miller, J. F., and Schaechter, M. (1989). In vivo studies of DnaA binding to the origin of replication of *Escherichia coli*. *EMBO J.* 8, 989–993.

Saxena, R., Fingland, N., Patil, D., Sharma, A. K., and Crooke, E. (2013). Crosstalk between DnaA Protein, the initiator of *Escherichia coli* chromosomal replication, and acidic phospholipids present in bacterial membranes. *Int. J. Mol. Sci.* 14, 8517–8537. doi: 10.3390/ijms14048517

Saxena, R., Rozgaja, T., Grimwade, J., and Crooke, E. (2011). Remodeling of nucleoprotein complexes is independent of the nucleotide state of a mutant AAA+ protein. *J. Biol. Chem.* 286, 33770–33777. doi: 10.1074/jbc.M111.223495

Schaper, S., and Messer, W. (1995). Interaction of the initiator protein DnaA of *Escherichia coli* with its DNA target. *J. Biol. Chem.* 270, 17622–17626. doi: 10.1074/jbc.270.29.17622

Schaper, S., Nardmann, J., Lüder, G., Lurz, R., Speck, C., and Messer, W. (2000). Identification of the chromosomal replication origin from *Thermus thermophilus* and its interaction with the replication initiator DnaA. *J. Mol. Biol.* 299, 655–665. doi: 10.1006/jmbi.2000.3764

Scholefield, G., Errington, J., and Murray, H. (2012). Soj/ParA stalls DNA replication by inhibiting helix formation of the initiator protein DnaA. *EMBO J.* 31, 1542–1555. doi: 10.1038/emboj.2012.6

Scholefield, G., and Murray, H. (2013). YabA and DnaD inhibit helix assembly of the DNA replication initiation protein DnaA. *Mol. Microbiol.* 90, 147–159. doi: 10.1111/mmi.12353

Sekimizu, K., Bramhill, D., and Kornberg, A. (1987). ATP activates dnaA protein in initiating replication of plasmids bearing the origin of the *E. coli* chromosome. *Cell* 50, 259–265. doi: 10.1016/0092-8674(87)90221-2

Sekimizu, K., Bramhill, D., and Kornberg, A. (1988). Sequential early stages in the in vitro initiation of replication at the origin of the *Escherichia coli* chromosome. *J. Biol. Chem.* 263, 7124–7130.

Shaheen, S. M., Ouimet, M. C., and Marczynski, G. T. (2009). Comparative analysis of *Caulobacter chromosome* replication origins. *Microbiology* 155, 1215–1225. doi: 10.1099/mic.0.025528-0

Sharan, S. K., Thomason, L. C., Kuznetsov, S. G., and Court, D. L. (2009). Recombineering: a homologous recombination-based method of genetic engineering. *Nat. Protoc.* 4, 206–223. doi: 10.1038/nprot.2008.227

Simmons, L. A., Felczak, M., and Kaguni, J. M. (2003). DnaA Protein of *Escherichia coli*: oligomerization at the *E. coli* chromosomal origin is required for initiation and involves specific N-terminal amino acids. *Mol. Microbiol.* 49, 849–858. doi: 10.1046/j.1365-2958.2003.03603.x

Skarstad, K., Boye, E., and Steen, H. B. (1986). Timing of initiation of chromosome replication in individual *Escherichia coli* cells. *EMBO J.* 5, 1711–1717.

Slater, S., Wold, S., Lu, M., Boye, E., Skarstad, K., and Kleckner, N. (1995). *E. coli* SeqA protein binds oriC in two different methyl-modulated reactions appropriate to its roles in DNA replication initiation and origin sequestration. *Cell* 82, 927–936. doi: 10.1016/0092-8674(95)90272-4

Smits, W. K., Merrikh, H., Bonilla, C. Y., and Grossman, A. D. (2011). Primosomal proteins DnaD and DnaB are recruited to chromosomal regions bound by DnaA in *Bacillus subtilis*. *J. Bacteriol.* 193, 640–648. doi: 10.1128/JB.01253-10

Soufo, C. H., Soufo, H. J., Noirot-Gros, M. F., Steindorf, A., Noirotand, P., and Graumann, P. L. (2008). Cell-cycle-dependent spatial sequestration of the DnaA replication initiator protein in *Bacillus subtilis*. *Dev. Cell* 15, 935–941. doi: 10.1016/j.devcel.2008.09.010

Soultanas, P. (2012). Loading mechanisms of ring helicases at replication origins. *Mol. Microbiol.* 84, 6–16. doi: 10.1111/j.1365-2958.2012.08012.x

Speck, C., and Messer, W. (2001). Mechanism of origin unwinding: sequential binding of DnaA to double- and single-stranded DNA. *EMBO J.* 20, 1469–1476. doi: 10.1093/emboj/20.6.1469

Speck, C., Weigel, C., and Messer, W. (1997). From footprint to toeprint: a close-up of the DnaA box, the binding site for the bacterial initiator protein DnaA. *Nucleic Acids Res.* 25, 3242–3247. doi: 10.1093/nar/25.16.3242

Stepankiw, N., Kaidow, A., Boye, E., and Bates, D. (2009). The right half of the *Escherichia coli* replication origin is not essential for viability, but facilitates multi-forked replication. *Mol. Microbiol.* 74, 467–479. doi: 10.1111/j.1365-2958.2009.06877.x

Stougaard, P., Molin, S., and Nordstrom, K. (1981). RNAs involved in copy-number control and incompatibility of plasmid R1. *Proc. Natl. Acad. Sci. U.S.A.* 78, 6008–6012. doi: 10.1073/pnas.78.10.6008

Taylor, J. A., Ouimet, M. C., Wargachuk, R., and Marczynski, G. T. (2011). The *Caulobacter crescentus* chromosome replication origin evolved two classes of weak DnaA binding sites. *Mol. Microbiol.* 82, 312–326. doi: 10.1111/j.1365-2958.2011.07785.x

Von Freiesleben, U., and Rasmussen, K. V. (1992). The level of supercoiling affects the regulation of DNA replication in *Escherichia coli*. *Res. Microbiol.* 143, 655–663. doi: 10.1016/0923-2508(92)90060-2

Von Freiesleben, U., Rasmussen, K. V., Atlung, T., and Hansen, F. G. (2000). Rifampicin-resistant initiation of chromosome replication from oriC in ihf mutants. *Mol. Microbiol.* 37, 1087–1093. doi: 10.1046/j.1365-2958.2000.02060.x

Wagner, J. K., Marquis, K. A., and Rudner, D. Z. (2009). SirA enforces diploidy by inhibiting the replication initiator DnaA during spore formation in *Bacillus subtilis*. *Mol. Microbiol.* 73, 963–974. doi: 10.1111/j.1365-2958.2009.06825.x

Weigel, C., Messer, W., Preiss, S., Welzeck, M., Morigen, and Boye, E. (2001). The sequence requirements for a functional *Escherichia coli* replication origin are different for the chromosome and, a minichromosome. *Mol. Microbiol.* 40, 498–507. doi: 10.1046/j.1365-2958.2001.02409.x

Weigel, C., Schmidt, A., Rückert, B., Lurz, R., and Messer, W. (1997). DnaA protein binding to individual DnaA boxes in the *Escherichia coli* replication origin, oriC. *EMBO J.* 16, 6574–6583. doi: 10.1093/emboj/16.21.6574

Weigel, C., Schmidt, A., Seitz, H., Tüngler, D., Welzeck, M., and Messer, W. (1999). The N-terminus promotes oligomerization of the *Escherichia coli* initiator protein DnaA. *Mol. Microbiol.* 34, 53–66. doi: 10.1046/j.1365-2958.1999.01568.x

Wolanski, M., Donczew, R., Zawilak-Pawlik, A., and Zakrzewska-Czerwinska, J. (2014). oriC-encoded instructions for the initiation of bacterial chromosome replication. *Front. Microbiol.* 5:735. doi: 10.3389/fmicb.2014.00735

Wolanski, M., Jakimowicz, D., and Zakrzewska-Czerwinska, J. (2012). AdpA, key regulator for morphological differentiation regulates bacterial chromosome replication. *Open Biol.* 2, 120097. doi: 10.1098/rsob.120097

Yoshida, Y., Obita, T., Kokusho, Y., Ohmura, T., Katayama, T., Ueda, T., et al. (2003). Identification of the region in *Escherichia coli* DnaA protein required for specific recognition of the DnaA box. *Cell Mol. Life Sci.* 60, 1998–2008. doi: 10.1007/s00018-003-3176-7

Yung, B. Y., Crooke, E., and Kornberg, A. (1990). Fate of the DnaA initiator protein in replication at the origin of the *Escherichia coli* chromosome in vitro. *J. Biol. Chem.* 265, 1282–1285.

Zawilak-Pawlik, A., Donczew, R., Szafranski, S., Mackiewicz, P., Terradot, L., and Zakrzewska-Czerwinska, J. (2011). DiaA/HobA and DnaA: a pair of proteins co-evolved to cooperate during bacterial orisome assembly. *J. Mol. Biol.* 408, 238–251. doi: 10.1016/j.jmb.2011.02.045

Zawilak-Pawlik, A., Kois, A., Majka, J., Jakimowicz, D., Smulczyk-Krawczyszyn, A., Messer, W., et al. (2005). Architecture of bacterial replication initiation complexes: orisomes from four unrelated bacteria. *Biochem. J.* 389, 471–481. doi: 10.1042/BJ20050143

Zawilak-Pawlik, A., Kois, A., Stingl, K., Boneca, I. G., Skrobuk, P., Piotr, J., et al. (2007). HobA–a novel protein involved in initiation of chromosomal replication in *Helicobacter pylori*. *Mol. Microbiol.* 65, 979–994. doi: 10.1111/j.1365-2958.2007.05853.x

Zorman, S., Seitz, H., Sclavi, B., and Strick, T. R. (2012). Topological characterization of the DnaA-oriC complex using single-molecule nanomanipuation. *Nucleic Acids Res.* 40, 7375–7383. doi: 10.1093/nar/gks371

Conflict of Interest Statement: The authors declare that the research was conducted in the absence of any commercial or financial relationships that could be construed as a potential conflict of interest.

Copyright © 2015 Leonard and Grimwade. This is an open-access article distributed under the terms of the Creative Commons Attribution License (CC BY). The use, distribution or reproduction in other forums is permitted, provided the original author(s) or licensor are credited and that the original publication in this journal is cited, in accordance with accepted academic practice. No use, distribution or reproduction is permitted which does not comply with these terms.

frontiers in Microbiology

REVIEW
published: 05 June 2015
doi: 10.3389/fmicb.2015.00562

A Replisome's journey through the bacterial chromosome

*Thomas R. Beattie and Rodrigo Reyes-Lamothe**

Department of Biology, McGill University, Montreal, QC, Canada

Genome duplication requires the coordinated activity of a multi-component machine, the replisome. In contrast to the background of metabolic diversity across the bacterial domain, the composition and architecture of the bacterial replisome seem to have suffered few changes during evolution. This immutability underlines the replisome's efficiency in copying the genome. It also highlights the success of various strategies inherent to the replisome for responding to stress and avoiding problems during critical stages of DNA synthesis. Here we summarize current understanding of bacterial replisome architecture and highlight the known variations in different bacterial taxa. We then look at the mechanisms in place to ensure that the bacterial replisome is assembled appropriately on DNA, kept together during elongation, and disassembled upon termination. We put forward the idea that the architecture of the replisome may be more flexible that previously thought and speculate on elements of the replisome that maintain its stability to ensure a safe journey from origin to terminus.

Keywords: DNA replication, replisome, bacteria, chromosome, evolution, DNA polymerase, *Escherichia coli*, *Bacillus subtilis*

OPEN ACCESS

Edited by:
Jaan Männik,
University of Tennessee, USA

Reviewed by:
Hua Xiang,
Institute of Microbiology, Chinese Academy of Sciences, China
Alan Leonard,
Florida Institute of Technology, USA
Nicholas E. Dixon,
University of Wollongong, Australia

***Correspondence:**
Rodrigo Reyes-Lamothe,
Department of Biology, McGill University, 3649 Sir William Osler, Montreal, QC H3G 0B1, Canada
rodrigo.reyes@mcgill.ca

Specialty section:
This article was submitted to Microbial Physiology and Metabolism, a section of the journal Frontiers in Microbiology

Received: *30 March 2015*
Accepted: *21 May 2015*
Published: *05 June 2015*

Citation:
Beattie TR and Reyes-Lamothe R (2015) A Replisome's journey through the bacterial chromosome. Front. Microbiol. 6:562. doi: 10.3389/fmicb.2015.00562

The Architecture of the Bacterial Replisome

Replication of chromosomal DNA is fundamental to the propagation of all bacterial species. This essential process faces many complex mechanistic challenges. Parental DNA must be unwound, and the resulting template strands replicated simultaneously with great efficiency and accuracy. Furthermore, because these two template strands have opposing polarity, the two new DNA strands are synthesized differently, with one strand—the leading strand—synthesized continuously, and the other—the lagging strand—synthesized as a series of short Okazaki fragments. A multi-protein complex known as the replisome has evolved to coordinate all the core enzymatic activities required for these coupled processes into a single molecular machine.

Replisome Structure in *E. coli*

Replisome structure is currently best understood in the Gram-negative bacterium *Escherichia coli*. Decades of genetic and biochemical research have enabled all the essential components of the replisome in this organism to be identified, and a series of protein-protein interactions which link them into a single entity to be mapped. Indeed, it is possible to reconstitute a fully functional replisome *in vitro* from purified *E. coli* proteins (Wu et al., 1992). At the core of the replisome is the DnaB homohexameric helicase, which encircles single-stranded DNA (ssDNA) on the lagging strand and unwinds the parental DNA duplex. Copying of the resulting template strands is performed by DNA polymerase III (Pol III), which consists of a catalytic subunit α, a proofreading exonuclease subunit ε, and a poorly conserved non-essential subunit θ. The exact function of θ is still unclear, but it may moderately stimulate the exonuclease activity of ε (Slater et al., 1994). To achieve the processivity needed to synthesize the entire chromosome, Pol III associates with the dimeric β sliding

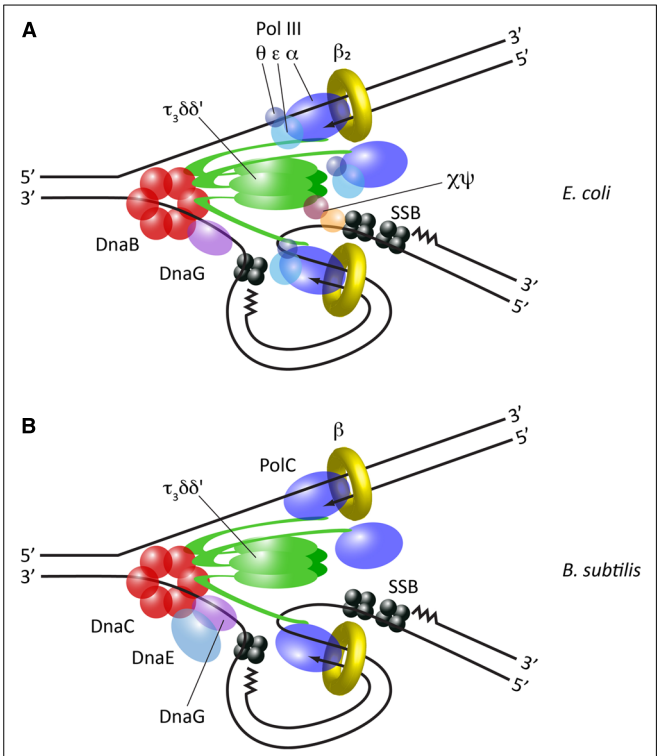

FIGURE 1 | Replisome architecture in bacteria. (A) Architecture of the *E. coli* replisome, derived from *in vitro* studies and direct observation *in vivo*. **(B)** Architecture of the *B. subtilis* replisome, predominantly derived from *in vitro* reconstitution studies.

clamp, which is assembled around DNA by the pentameric $\tau_3\delta\delta'$ clamp loader complex. Crucially, both DnaB and Pol III α directly interact with the C-terminal domain of τ, and thus the clamp loader additionally provides an architectural function, physically coupling template unwinding with DNA synthesis (**Figure 1A**).

It was previously assumed that only two Pol III complexes were present within the replisome, divided between the leading and lagging strands. However, elegant *in vitro* reconstitution experiments surprisingly demonstrated that the *E. coli* replisome can incorporate three Pol III complexes, multimerised by the trimeric τ within the clamp loader (McInerney et al., 2007). More recently, an unprecedented level of detail has been obtained by directly visualizing individual components of the replisome in living *E. coli* cells by fluorescence microscopy (Reyes-Lamothe et al., 2010). This work has confirmed the presence of three active polymerases within a single replisome. Further *in vitro* studies have suggested the third replicative polymerase may serve as a backup to support efficient synthesis of the lagging strand (Georgescu et al., 2011).

A trimeric polymerase architecture was previously unanticipated because the clamp loader was thought to consist of $\tau_2\gamma\delta\delta'$, γ being an alternative C-terminally truncated form of τ which is unable bind to Pol III and derives from a frameshift during translation of the dnaX gene. The role of γ is now unclear; like *E. coli*, clamp loader complexes from a number of other bacterial species appear to possess a τ-only structure (Bruck and O'Donnell, 2000; Bruck et al., 2002, 2005; Bullard et al., 2002; Jarvis et al., 2005a; Sanders et al., 2010). However, although the generation of γ by a frameshift mechanism appears to be limited to enterobacteria (Blinkova et al., 1997), γ-like subunits have been detected in *Thermus thermophilus* and *Caulobacter crescentus*, and furthermore these arise from distinct mechanisms for truncating the dnaX gene product—transcriptional slippage and controlled proteolysis, respectively (Yurieva et al., 1997; Vass and Chien, 2013). This hints at convergent evolution for generating γ, suggesting that in at least some bacterial species a clamp loader containing this truncated product may play a specialized role. It has been suggested for example that γ may be important in dealing with DNA damage (Reyes-Lamothe et al., 2010; Vass and Chien, 2013), but its precise role remains to be elucidated.

Multimerisation of Pol III within the *E. coli* replisome presents a potential topological problem as polymerases must track in opposite directions on the leading and lagging strands, but yet are arranged symmetrically through their interaction with the clamp loader. The replisome has evolved to ensure that DNA unwinding and synthesis proceed uninterrupted by allowing the transient accumulation of ssDNA loops between Pol III and the helicase on the lagging strand. These loops are rapidly bound by the tetrameric ssDNA binding protein, SSB, which protects them from damage. The cyclical assembly, growth and disassembly of these loops, which accompanies the synthesis of each Okazaki fragment, has been compared to the slide of a trombone (trombone model; Sinha et al., 1980). The presence of such trombone loops has been directly observed in simpler bacteriophage replisomes by electron microscopy and single-molecule biophysical studies (Park et al., 1998; Hamdan et al., 2009).

Initiation of each Okazaki fragment requires the synthesis of an RNA primer, which is subsequently extended by Pol III following loading of the β clamp onto the primer-template junction. In *E. coli* this is performed by the DnaG primase, which interacts directly with DnaB, thus facilitating primer deposition on the emerging lagging strand template. However, biochemical studies suggest that DnaG is not a constitutive component of the replisome, but rather associates with DnaB transiently; indeed it has been suggested that each primer is synthesized by a new DnaG molecule recruited from solution (Wu et al., 1992). In contrast, biophysical measurements on bacteriophage T4 replisomes have shown that primase behavior is stochastic, sometimes dissociating from the helicase following primer synthesis, but sometimes remaining tightly bound (Manosas et al., 2009). Unlike other replisome components, it has so far not been possible to observe DnaG *in vivo* by microscopy. It will be interesting in the future to directly determine the nature of the DnaG-DnaB interaction in its native environment of the living cell.

Since the predicted number of Okazaki fragments generated during chromosomal replication in *E. coli* exceeds the number of β clamps available in the cell, these clamps must be reused throughout replication (Leu et al., 2000). While some *in vitro* data suggests that clamps may be immediately recycled with Pol III between successive Okazaki fragments (Tanner et al., 2011), live cell microscopy data from both *E. coli* and *Bacillus subtilis* has demonstrated that clamps accumulate on DNA behind the replisome (Su'etsugu and Errington, 2011; Moolman et al., 2014).

TABLE 1 | A comparison of replication protein nomenclature in *E. coli* and *B. subtilis*.

Protein function	*E. coli*	*B. subtilis*
Origin activator	DnaA	DnaA
Helicase loader	DnaC	DnaI
Helicase	DnaB	DnaC
Primase	DnaG	DnaG
Clamp loader	$\tau_3\delta\delta'\chi\psi$	$\tau_3\delta\delta'$
Primary replicative polymerase	Pol III ($\alpha\varepsilon\theta$)	PolC
Accessory replicative polymerase	–	DnaE
ssDNA binding protein	SSB	SSB
Sliding clamp	β_2	β_2

This therefore supports an alternative model whereby clamps are reloaded from a pool left on the lagging strand. Such an accumulation of β clamps may serve as an important landing platform on DNA for the recruitment of DNA modifying enzymes following the passage of the replisome. Indeed, it has even been proposed that it is for this function, rather than their role as processivity factors, that clamp molecules originally evolved (Georgescu et al., 2015).

Replisome Structure in *B. subtilis*

To date, the replisome has only been characterized in detail in one organism other than *E. coli*: the low-GC Gram-positive bacterium *Bacillus subtilis* (**Figure 1B** and **Table 1**). A fully functional replisome with physiological rates of coupled leading and lagging strand synthesis has been reconstituted *in vitro* from purified *B. subtilis* proteins, defining its minimal protein requirements (Sanders et al., 2010). This study demonstrated a conserved core replisome structure with *E. coli*, consisting of a homohexameric helicase (DnaC) which interacts with both a distributive primase (DnaG) and a pentameric $\tau_3\delta\delta'$ clamp loader complex. Replication is also similarly dependent on a dimeric β clamp and SSB.

However, the *B. subtilis* replisome also exhibits some notable differences compared to *E. coli*. Two distinct C-type DNA polymerases—DnaE and PolC—are required for chromosomal replication in this organism (Dervyn et al., 2001), a feature common to many species of Gram-positive bacteria (Timinskas et al., 2014). DnaE is related to *E. coli* Pol III α, while PolC is significantly different in domain organization and additionally possesses an intrinsic exonuclease activity. Initial genetic analysis suggested that the activities of PolC and DnaE may be divided between the leading and lagging strands respectively (Dervyn et al., 2001), but more recent biochemical analysis suggests that DnaE may in fact purely be used to extend RNA primers a short distance on the lagging strand, before PolC rapidly displaces it to synthesize the majority of DNA on both lagging and leading strands (Sanders et al., 2010). This division of function may be enforced by differences in the mode of interaction of the two polymerases with other components of the replisome; while PolC is linked to the helicase via τ, as in *E. coli* (Bruck and O'Donnell, 2000), it has been reported that DnaE interacts directly with the helicase and DnaG, forming a "primosome" complex (Rannou et al., 2013).

A mechanism of primer extension through the sequential action of two distinct DNA polymerases is also used in eukaryotic organisms. However, it has been noted that this mechanism is inherently wasteful, as the short stretch of error-prone DNA synthesized by the first DNA polymerase is entirely removed later in replication anyway (Forterre, 2013). This is also likely to be the case in *B. subtilis* since DnaE lacks a proofreading activity, although it is unclear which polymerase replaces the DNA synthesized by DnaE; it is possible that DNA Pol I fulfils this function as it removes RNA primers prior to Okazaki fragment ligation. Since the respective proteins involved in lagging strand synthesis in eukaryotes and bacteria are non-orthologous this dual polymerase mechanism likely arose through convergent evolution. At present however, it is still unclear what selective advantage, if any, DnaE-PolC coordination on the lagging strand provides.

While the core replisome components have been identified in *B. subtilis*, their relative stoichiometry within the complex has yet to be fully determined. In particular it is unknown how many polymerases are typically present within the *B. subtilis* replisome. The role of PolC on both leading and lagging strands suggests that at least two molecules of this polymerase must be simultaneously present within the replisome. Furthermore, given the interaction between PolC and the trimeric τ of the clamp loader it is possible that three molecules of PolC may be present, similar to *E. coli* Pol III. Rapid displacement of non-proofreading DnaE by PolC on the lagging strand is presumably important for genome integrity, and therefore it may be speculated that maintaining a high relative local concentration of PolC within the replisome would be a mechanism for achieving this. It should be noted that the interaction between τ and PolC is significantly weaker than the equivalent interaction in *E. coli* (Bruck and O'Donnell, 2000). It is currently unclear whether this represents a physiological property of the *B. subtilis* replisome with implications for its architecture or is due to the absence of other stabilizing components that have yet to be identified. Further characterisation of the *B. subtilis* replisome both *in vitro* and *in vivo* will be important for determining the precise structure of the replisome in this organism and how its multiple polymerases are efficiently coordinated.

Notably, an analysis of polymerase distribution across bacterial genomes has demonstrated that a third major combination of replicative polymerases is found in some organisms: PolC together with a DnaE distinct from that of both *E. coli* and *B. subtilis* (Timinskas et al., 2014). The DNA replication machinery has yet to be examined in any of these species, and it will be interesting in the future to determine if their replisomes employ similar or different strategies to those already described for coordinating multiple DNA polymerases.

Replisome Structure in Other Bacterial Organisms

Despite the extreme diversity present across the bacterial kingdom in many areas of cell biology, a relatively high degree of

conservation has been noted for many DNA replication proteins, highlighting the central importance of this cellular process. However, it is not clear whether the assembly of these proteins into a higher order replisome complex also follows a conserved architecture. Beyond *E. coli* and *B. subtilis* this question has not been extensively addressed.

Replisome subassemblies have been successfully reconstituted using purified proteins from *Aquifex aeolicus* (Bruck et al., 2002), *Streptococcus pyogenes* (Bruck and O'Donnell, 2000), *Staphylococcus aureus* (Bruck et al., 2005), *Thermus thermophilus* (Bullard et al., 2002), and *Pseudomonas aeruginosa* (Jarvis et al., 2005a). These studies demonstrate that the core replisome structure of a $\tau_3\delta\delta'$ clamp loader linked to the catalytic subunit of the replicative polymerase is likely to be a conserved feature among bacteria. In the case of *T. thermophilus* the clamp loader can also incorporate γ, although the same caveats should apply as in *E. coli*. However, the organisms examined to date still constitute a tiny sample of total bacterial diversity. Furthermore, it is still unclear if the mode of interaction between this replisome core and other components such as the helicase, primase, and additional polymerases is similarly conserved.

For example, two additional clamp loader subunits, χ and ψ, are present in *E. coli*. While not essential, χ and ψ are required for normal growth. These two components form a tight dimer and interact with both τ and SSB, resulting in both the stabilization of the clamp loader complex and the replisome overall (Olson et al., 1995; Marceau et al., 2011). The $\chi\psi$ subassembly has also been proposed to play a role in promoting the access of Pol III to newly synthesized primers (Yuzhakov et al., 1999). However, sequence analysis suggests these two subunits are only present in proteobacteria, and it is unclear what, if anything, fulfils their replisome function in other bacterial lineages. It should be noted that in *P. aeruginosa* a ψ subunit was identified through its co-purification with χ despite it being unidentifiable on the basis of sequence homology alone (Jarvis et al., 2005b). This raises the possibility that highly diverged functional homologs of these subunits may indeed exist in other organisms where they have not yet been detected, and highlights the importance of empirical research to describing replisome composition across the bacterial kingdom.

In vivo characterisation of replisome architecture is still lacking outside of *E. coli*. Tools are gradually being developed to study the DNA replication machinery in living cells of other species, such as *Helicobacter pylori* (Sharma et al., 2014), *Mycobacterium smegmatis* (Santi and McKinney, 2015; Trojanowski et al., 2015), and *B. subtilis* (Lemon and Grossman, 1998), and it is hoped that in the future determining replisome stoichiometries *in vivo* will enable a better assessment of replisome structure conservation.

Mechanisms of Replisome Assembly

Assembly of the bacterial replisome is a tightly regulated process. DNA replication is normally initiated at a specific origin locus by the assembly of just two replisomes, each of which synthesizes half of the circular chromosome. It is important to restrict replisome assembly beyond this specific initiation event, to prevent over-replication of DNA and chromosome instability. Different mechanisms exist to ensure specificity in replisome assembly, but they appear to converge at the level of controlling the loading of the DnaB helicase onto ssDNA (Fang et al., 1999). Once this loading step has been overcome, DnaB can serve as the platform upon which the rest of the replisome is assembled, through its direct interactions with the primase and clamp loader. Interestingly, a similar strategy is observed in eukaryotic organisms, despite the use of completely non-orthologous proteins, whereby loading and activation of the replicative helicase Mcm2-7 is also the limiting step in replisome assembly (Yeeles et al., 2015).

Replisome Assembly During Initiation

Initiation of replication is best understood in *E. coli*, where replication originates from the *oriC* locus. *oriC* is recognized and melted through sequence-specific binding of the AAA+ protein, DnaA (Leonard and Grimwade, 2011). The prevailing current model proposes that DnaA oligomerizes into a helical filament, around which bound *oriC* DNA is wrapped (Erzberger et al., 2006). This destabilizes the neighboring duplex unwinding element (DUE), leading to DNA melting as the DnaA filament extends onto transiently exposed ssDNA (Duderstadt et al., 2011). The resulting bubble of SSB-coated ssDNA is a substrate for the assembly of two DnaB helicases (Fang et al., 1999). Crucially, however, DnaB loading onto such structures is not spontaneous; it is restricted to the *oriC* locus through a dependence on the helicase loader protein, DnaC (**Figure 2A**).

DnaC has been shown to interact with both DnaA and DnaB, and thus serves as link to recruit DnaB to melted origins (Mott et al., 2008). Furthermore, it appears to play an active role in loading the helicase. Structural analysis of DnaC has shown that this protein resembles DnaA and similarly adopts a helical filament when bound to ssDNA (Mott et al., 2008). More recently, it has been demonstrated that this spiral configuration enables DnaC to break open the DnaB hexameric ring as the two proteins interact, allowing ssDNA to enter the central chamber of the helicase (Arias-Palomo et al., 2013). Association of DnaG primase with DnaB triggers the release of DnaC and thus activates the helicase, beginning the process of replisome assembly (Davey et al., 2002; Makowska-Grzyska and Kaguni, 2010). Interestingly, it has been shown that while two DnaB helicases must be loaded at *oriC* (Fang et al., 1999), the first of these is always deposited on the lower strand (Weigel and Seitz, 2002). A model for asymmetric loading of DnaB has thus been proposed, whereby DnaC-DnaB on one strand is loaded via the interaction of DnaC with DnaA, while on the other strand DnaC-DnaB is loaded via a direct interaction observed between DnaB and DnaA (Mott et al., 2008). Such a loading mechanism is attractive because it accounts for the need for the two helicases—and their associated replisomes—to proceed bidirectionally from *oriC*.

This helicase loading pathway may not be well conserved across bacterial organisms. *B. subtilis* for example possesses orthologs of DnaA, DnaC (called DnaI) and DnaB (called DnaC) but also requires two additional proteins for helicase loading that have no orthologs in *E. coli*: DnaB, and DnaD (Smits et al., 2010). The precise role of these additional proteins is still unclear. Furthermore, despite being related to *E. coli* DnaC, the *B. subtilis*

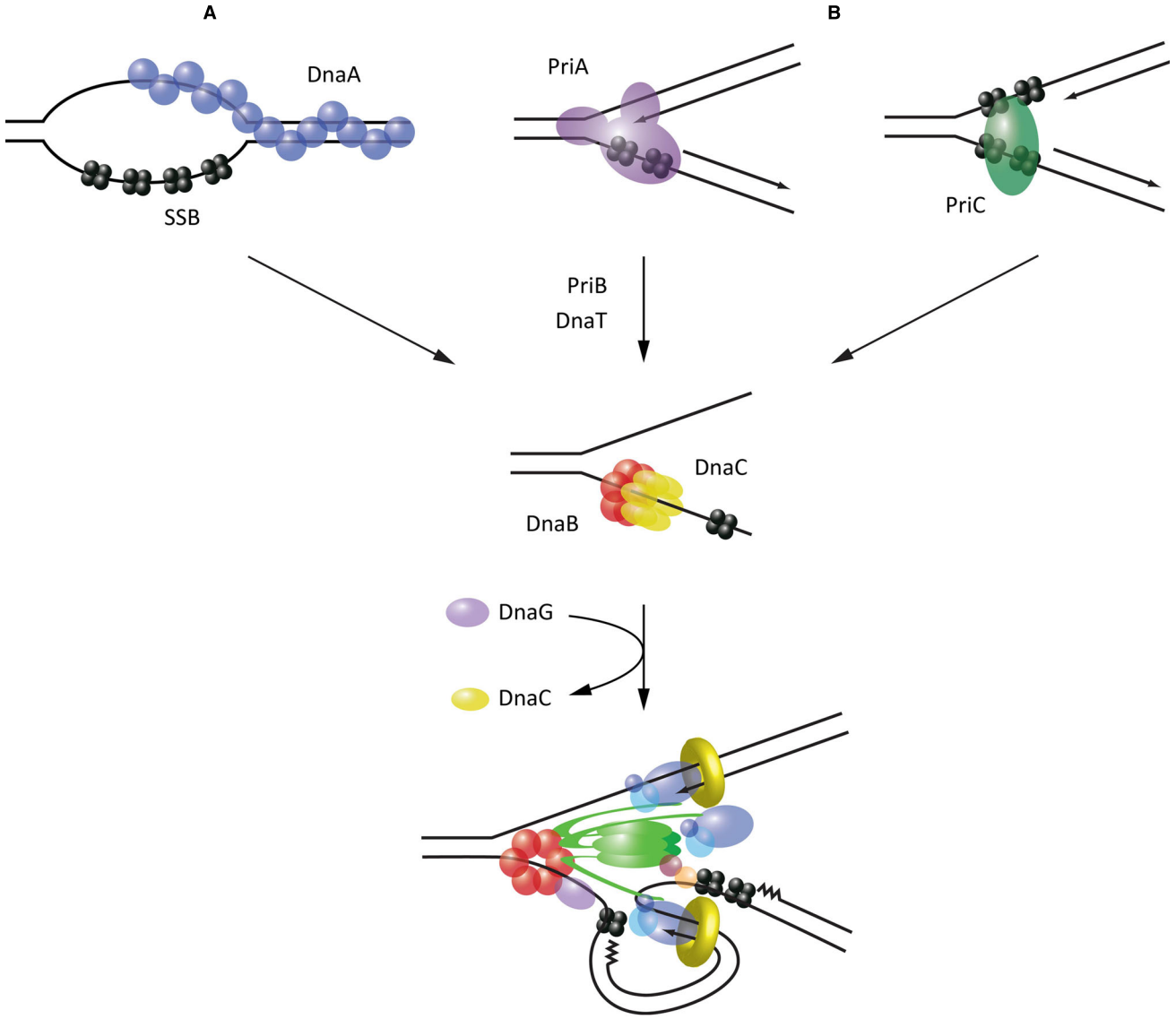

FIGURE 2 | Mechanisms of helicase loading leading to replisome assembly in *E. coli*. (A) Recognition and melting of the *oriC* locus during initiation by DnaA. **(B)** Recognition of abandoned fork structures during replisome reloading by PriA and PriC. All pathways converge on the loading of the replicative helicase DnaB, which acts as an assembly platform for the remaining replisome components.

helicase loader DnaI may employ a different mechanism to load the helicase on DNA; structural and biochemical data suggest that rather than acting as a ring-opener, DnaI may act as a template for the assembly of the hexameric helicase around ssDNA from individual monomers (Velten et al., 2003; Liu et al., 2013). It has been proposed from sequence analysis that some bacterial species including *A. aeolicus* posses a helicase loader distinct from that present in either *E. coli* or *B. subtilis* (Robinson et al., 2012). However, a low-resolution structural comparison suggests that *E. coli* and *A. aeolicus* DnaC form similar spiral oligomers and therefore may employ the same mechanism for opening the DnaB hexameric ring (Arias-Palomo et al., 2013).

Helicase loading may differ even further in other bacterial organisms, since many species lack an identifiable DnaC homolog. For example, helicases from *Pseudomonas* species can be loaded *in vitro* in the absence of a loader protein, in contrast to *E. coli* (Caspi et al., 2001). Similarly, the helicase from *H. pylori* is sufficient to complement *E. coli* lacking DnaC, suggesting it is functionally loaded onto DNA without a loader (Soni et al., 2005). Interestingly, this correlates with the ability of this helicase to uniquely form a double hexamer (Stelter et al., 2012). Thus it may be speculated that in some bacterial species at least, the replicative helicase possesses structural adaptations that confer intrinsic self-loading ability. It is unclear how site-specific loading would be maintained in such cases.

Replisome Assembly Following Fork Collapse

It is now apparent that replication fork structures can frequently break down during chromosomal replication, leading to collapse of the replisome. This is especially the case under stress conditions, when lesions in DNA become more prevalent, but is also likely to be the case during unperturbed replication in healthy cells (Maisnier-Patin et al., 2001). Thus to ensure complete replication of the chromosome, there is a requirement for systems that can efficiently reload replisomes at sites where they have collapsed. Crucially, these mechanisms must be specific enough to ensure that replisomes aren't simply loaded indiscriminately onto any ssDNA structure.

In *E. coli*, this reloading process is restricted to abandoned replication forks through the activity of two proteins, PriA and PriC, which recognize specific DNA structures (**Figure 2B**). PriA possesses a modular arrangement of DNA-binding domains which allow it to specifically bind the three arms of forked DNA structures, with a preference for those possessing a fully extended leading strand (Heller and Marians, 2005a; Bhattacharyya et al., 2014). PriC provides complementary activity by recognizing fork structures lacking a leading strand; these can arise when the leading strand polymerase stalls at a lesion and becomes uncoupled from the continuing lagging strand polymerase (Heller and Marians, 2005a). PriC probably recognizes such fork structures through an interaction with SSB (Wessel et al., 2013). In some cases the presence of SSB may rely on prior unwinding of the lagging strand by Rep or even PriA (Heller and Marians, 2005b).

Supported by genetic analysis, reconstitution of helicase reloading *in vitro* has demonstrated that these different modes of substrate recognition lead to two distinct pathways of helicase reloading. PriA substrate recognition leads to the sequential recruitment of PriB, DnaT and finally the DnaC-DnaB complex for loading (Lopper et al., 2007). Alternatively, substrate recognition by PriC leads directly to the recruitment of DnaC-DnaB (Heller and Marians, 2006). Notably, while the components of these pathways have been characterized extensively, the precise mechanisms that lead to the recruitment of DnaC and loading of the helicase specifically onto the lagging strand, are still unknown. Intriguingly, DnaT has been suggested from structural studies to form a helical filament on DNA (Liu et al., 2014), raising the possibility that it could act analogously to DnaA in recruiting DnaC. The mode of interaction between PriC and DnaC-DnaB has yet to be characterized, although high-throughput studies have identified a potential interaction between PriC and DnaB (Butland et al., 2005).

Notably, many bacteria lack an ortholog of *E. coli* PriC and thus it is unclear what, if anything, fulfils its function in these species. Furthermore, while PriA does seem to be relatively well-conserved, its mode of action may not be; reconstitution of helicase reloading in *B. subtilis* suggests that PriA acts to recruit the helicase through the DnaD, DnaB and DnaI proteins used during initiation, rather than a specialized set of proteins as in *E. coli* (Manhart and McHenry, 2013). The exact mechanism of replisome assembly both at origins of replication and following replication fork collapse may therefore differ significantly between bacterial species. Nonetheless, it appears that these different pathways converge on the limiting step of loading of the replicative helicase, which serves as the core replisome component upon which other replication proteins are assembled.

Dynamics and Stability of the Replisome

Looking at the replisome in action must surely be like looking at a beehive. Like bees performing their collection duties, multiple replisome components are continuously arriving and leaving with every cycle of synthesis on the lagging strand. One new copy of primase and the β clamp dimer is needed to start every Okazaki fragment, and multiple copies of SSB are recruited and displaced as a result of DNA melting by helicase and synthesis by Pol III respectively (Wu et al., 1992).

A long-standing debate on the coordination of replisome activities has been over how Pol III, evolved for high processivity, frequently dissociates from the lagging strand to ensure efficient cycles of Okazaki fragment synthesis. The collision model hypothesizes that Pol III dissociates upon encountering the previous Okazaki fragment. It has been suggested that Pol III senses elimination of template ssDNA as it approaches the end of each Okazaki fragment, which weakens its affinity for the β clamp through an unknown mechanism, thus decreasing the stability of the polymerase on DNA (Georgescu et al., 2009). In contrast, the signaling model proposes that a specific signal intrinsic to the replisome triggers Pol III dissociation following synthesis of each new primer (Wu et al., 1992). This is supported by the fact that Pol III dissociation rates following collision *in vitro* are insufficient to support the rate of synthesis required during chromosomal replication—at least in the context of a dimeric Pol III replisome (Dohrmann et al., 2011). Recent single-molecule data has suggested that the source of this dissociation signal may be the accumulation of topological stress at the replication fork as the physically coupled polymerases track around helical DNA during synthesis (Kurth et al., 2013). Although their relative importance is still contested, some *in vitro* experiments have suggested that in fact both mechanisms operate redundantly to maximize the efficiency of Okazaki fragment synthesis (Li and Marians, 2000; Hamdan et al., 2009).

In contrast with this dynamic picture, the replisome also needs to be a very stable assembly to accomplish replication of the long chromosomal DNA molecules. In *E. coli*, chromosome duplication takes the replisome over forty minutes of continuous work even at synthesis rates of 1 kb per second (Kubitschek and Newman, 1978; Kornberg and Baker, 1992). The importance of keeping the replisome active and in one piece is demonstrated by the observation that the majority of double strand breaks, which are potentially lethal lesions to the cell, occur during DNA replication (Cox et al., 2000; Pennington and Rosenberg, 2007) often as a result of extended pauses in replication fork progression (Michel et al., 2004). Judging by relatively infrequent replisome collapse events—once every five generations in *E. coli* (Maisnier-Patin et al., 2001)—high stability seems to be inherent to the replisome.

Stability may be the result of the extended lifetime of some of the subassemblies of the active replisome. The idea of tight binding between its components is intimately linked to the

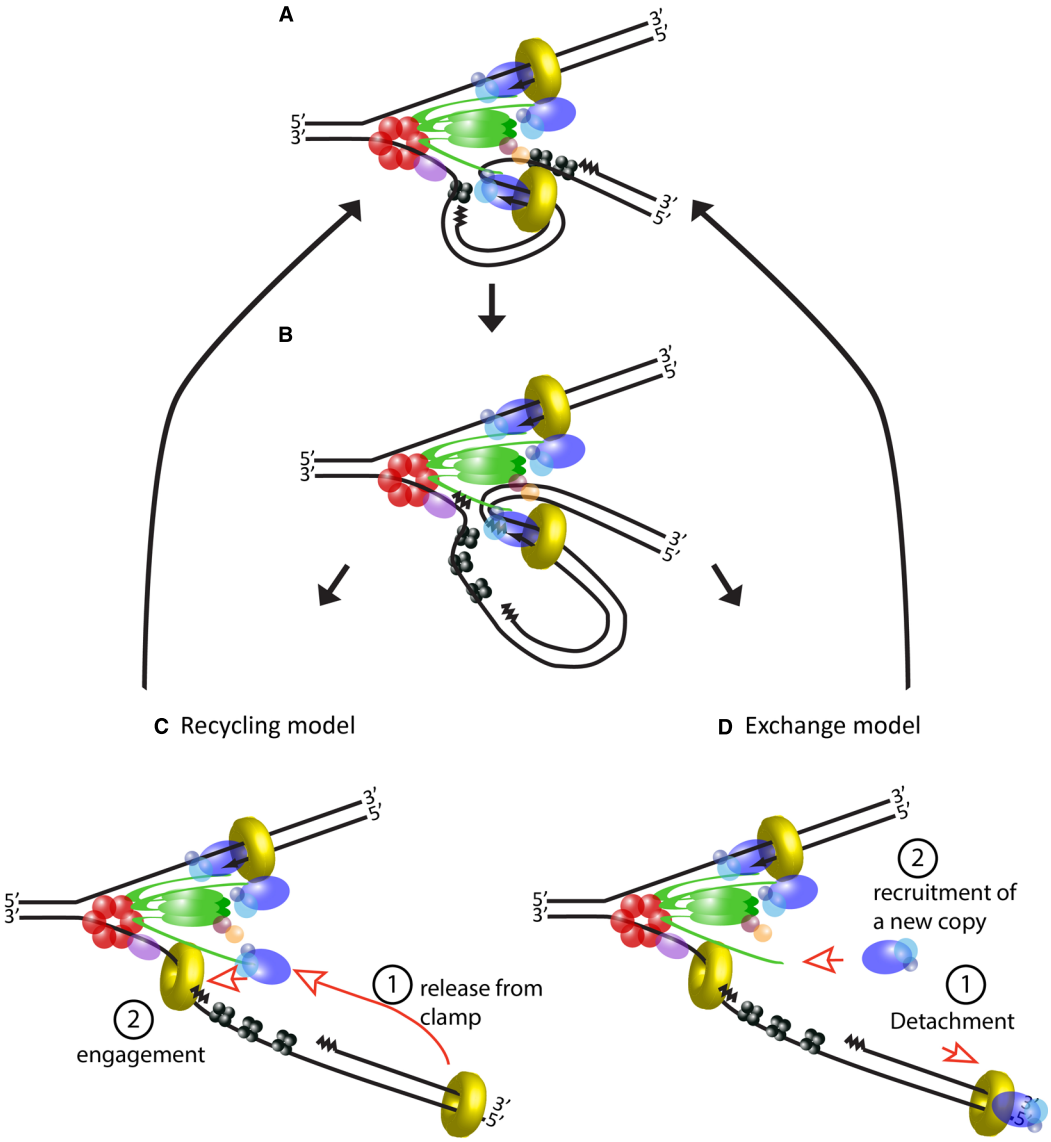

FIGURE 3 | Usage of DNA polymerase during lagging strand synthesis. (A) Schematic of the *E. coli* replisome during the elongation step of an Okazaki fragment. **(B)** Lagging strand polymerase meets the RNA primer of the previous Okazaki fragment and stops synthesis. **(C)** Current model of events following completion of an Okazaki fragment. DNA polymerase is released from the β clamp (step 1) and the same molecule rebinds to a new β clamp to start the next Okazaki fragment (step 2). **(D)** An alternative model based on evidence from T4 and T7 replisomes. After completing the Okazaki fragment, the DNA polymerase detaches from the rest of the replisome (step 1). A new molecule of DNA polymerase is recruited to the replisome (step 2) and engages in the synthesis of a new Okazaki fragment. In this tentative model, a local pool of "spare" polymerases may facilitate their exchange and additional components may exchange along with the polymerase (not depicted).

trombone model of DNA replication. At its conception, this model arose to explain synchronous action of polymerases on both strands, and postulated a physical coupling between polymerases at the leading and lagging strands during synthesis. Importantly, it also suggested that the same copy of Pol III is recycled for multiple rounds of synthesis at the lagging strand (Sinha et al., 1980). Validation of this model came from experimental evidence showing that the replisome in *E. coli* can contain two polymerases (Maki et al., 1988; Onrust et al., 1995), and that they synthesize the two strands simultaneously (Yuzhakov et al., 1996). Long residence times of core replisome components have been demonstrated by ensemble and single-molecule *in vitro* studies of the *E. coli* replisome that show processive DNA synthesis in the absence of any free helicase, clamp loader or Pol III in the buffer (Li and Marians, 2000; Yao et al., 2009). From this data it is inferred that helicase, clamp loader and polymerases form a tight structure in the replisome, so that the same molecules of these proteins may be used over long periods, potentially even the whole replication event (**Figures 3A–C**).

However, this model of the replisome contrasts with evidence from T4 and T7 phages, which shows that the replicative polymerase is frequently replaced during fork progression (Yang

et al., 2004; Johnson et al., 2007). Although the number and nature of their components differ, both of these systems have a similar architecture to the replisome of *E. coli*, indeed the trombone model was originally proposed for T4. Similarly to *E. coli*, coordination between leading and lagging strand synthesis has been extensively validated in these systems, and their replisomes can also carry out DNA synthesis in the absence of excess polymerase in the buffer (Debyser et al., 1994; Yang et al., 2004). Nevertheless, polymerase exchange can be detected shortly after addition of mutant polymerase to a reaction where the replisome is engaged in DNA synthesis (Yang et al., 2004; Johnson et al., 2007). How can we reconcile frequent polymerase turnover with efficient recycling on the lagging strand? At least in the case of the T7 replisome, which has been studied using elegant single-molecule studies, this seems to be achieved by creating a local pool of "spare" polymerases available for fast switching. The replisome in this phage consists of only four proteins: gp5, the DNA polymerase; gp4, which acts as helicase and primase; gp2.5, a ssDNA binding protein; and *E. coli*'s thioredoxin which serves as processivity factor for the polymerase (serving the same function as the β clamp in the bacterial replisome). The gp5 polymerase interacts directly with gp4, but importantly, these proteins have two modes of interaction resulting in tight or loose association, respectively (Hamdan et al., 2005; Kulczyk et al., 2012). The tight interaction has a greater contribution to the processivity of the polymerase, but the weak interaction additionally permits the presence of up to six polymerases at the replication fork (Loparo et al., 2011; Geertsema et al., 2014).

The dynamics of phage replisomes are relevant to *E. coli* since they both show different behaviors depending on the concentration of their components in solution. Studies performed *in vitro* in the absence of excess components show the *E. coli* replisome can function without exchange of its subunits, but it is currently unclear if a different behavior will be observed inside the cell (**Figure 3D**), where the diffusing pool of replisome components is one-to-two orders of magnitude higher than the number of active molecules (Leu et al., 2000; Reyes-Lamothe et al., 2010). It is easy to imagine how the capacity to detach polymerases from the replisome would be advantageous in order to rapidly respond to lesions and roadblocks on DNA. Multiple studies have shown that after encountering an obstacle, polymerase can unbind from DNA and subsequently re-engage via alternative mechanisms, leaving a gap in the double strand (Pomerantz and O'Donnell, 2008, 2010; Yeeles and Marians, 2011). The high processivity of polymerase bound to the β clamp conflicts with the observed "hopping" over obstacles on DNA, but complete detachment from the replisome would reconcile the long residence of polymerase on DNA with progression of the replication fork, potentially providing greater flexibility to the replisome.

In this scenario, replisome components otherwise thought to be stable are actually moving parts that actively exchange; one wonders what would then help maintain the stability of the replisome as an assembly. Reiterating its central role in the control of DNA replication, the most likely candidate would be DnaB helicase. Indeed, measurements on the processivity of the replisome show that helicase is its most stable component, although multiple contacts to DNA from engaged polymerases seem to also help increase the processivity of the replisome (Yao et al., 2009). Whatever strategy the replisome may use, work still needs to be done to shed light on the interplay between its dynamics and stability.

Disassembly of the Replisome

A key mechanistic challenge faces the bacterial replisome during termination of DNA replication. The circular nature of the bacterial chromosome dictates that a pair of replisomes that initiate from a single origin of replication will eventually converge on each other in a head-to-head orientation. Positive supercoiling accumulates between the two replisomes as they converge, but the activity of DNA gyrase, which normally removes positive supercoils, becomes limited by the decreasing amount of template DNA available. Instead, supercoils may diffuse behind the replisomes, forming precatenanes between newly replicated DNA; in *E. coli* these must be resolved by Topoisomerase IV for chromosome segregation to occur (Wang et al., 2008). Alternatively, it has been shown *in vitro* that a combination of the 3′-5′ helicase RecQ and Topoisomerase III is sufficient to directly resolve topological stress ahead of converging replication forks, in the presence of SSB (Suski and Marians, 2008).

In at least some bacteria, the progression of replisomes is modulated to ensure that their convergence is restricted to a specific terminus region of the chromosome. This is best characterized in *E. coli*, where the Tus protein binds tightly to specific DNA sequences in the terminus, designated *ter* sites, and halts progression of the replisome. Crucially this effect is dependent on the orientation of *ter* sites, such that replisomes can enter but not exit the terminus region (**Figure 4**). The exact mechanism by which Tus-*ter* is able to block the replisome is still a matter of debate. Biochemical and structural studies have demonstrated that DnaB-catalyzed unwinding of *ter* DNA in the blocking orientation results in flipping of a specific cytosine into a binding pocket in Tus, strengthening its interaction with DNA and blocking further helicase progression. In contrast, unwinding from the opposing direction does not trigger this base flipping and results in displacement of the Tus protein from DNA (Neylon et al., 2000; Mulcair et al., 2006). However, an alternative model proposes that Tus mediates its effect on the replisome through direct protein-protein interactions with DnaB (Mulugu et al., 2001). This argument is supported by the fact that Tus can arrest DnaB translocation on dsDNA *in vitro* independently of *ter* unwinding (Bastia et al., 2008). However, given that DnaB within the replisome translocates on ssDNA, the relevance of this observation is unclear.

Regardless of the precise mechanism by which Tus operates, its regulation of the replisome does not appear to play a direct role in the process of termination, since it can be deleted from *E. coli* without producing a detectable phenotype (Roecklein et al., 1991). Furthermore, the Tus-*ter* system is poorly conserved among bacteria; while *B. subtilis* possesses a functional homolog of Tus (RTP) the two proteins lack any significant sequence or structural homology. The role of these replisome

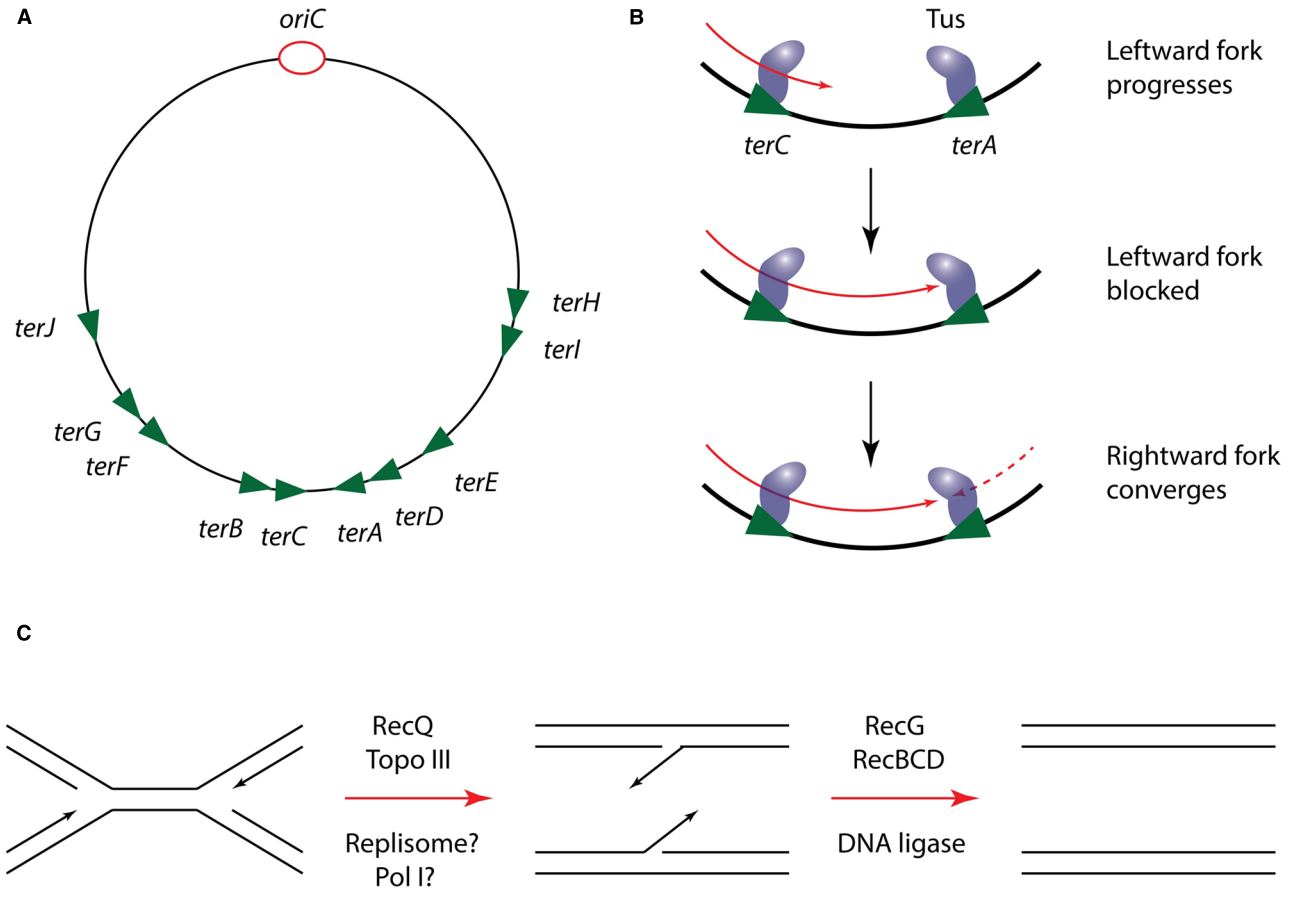

FIGURE 4 | Mechanism of replication termination in *E. coli*. (A) Schematic of the *E. coli* chromosome showing the approximate location of *ter* sites relative to *oriC*. Arrowheads indicate the permitted direction of replisome progression. Adapted from Duggin et al., 2008. **(B)** Mechanism of replisome trapping in the terminus region by Tus-*ter*. Just two *ter* sites are shown for clarity but the same mechanism can operate at any *ter* site. **(C)** Resolution of DNA structures following replisome convergence during termination.

"traps" is thus more likely to be in coordinating termination with other processes localized to the terminus region of the chromosome, such as chromosome dimer resolution by XerCD (Duggin et al., 2008).

Genetic analysis suggests that the actual site of replication termination contains regions of overlapping DNA sequence that must be resolved into single daughter strands through the action of the RecG DNA translocase and the helicase-nuclease RecBCD (Rudolph et al., 2013; Wendel et al., 2014). Crucially however, it is unclear exactly how these termination structures are generated. Some analysis has suggested that DNA Pol I may play a role in replicating DNA at the terminus, but it is unclear if this occurs in coordination with the Pol III machinery or following its disassembly (Markovitz, 2005). Thus in particular, the role of the replisome in the final stages of chromosomal replication, and the fate of the replisome during termination are poorly understood.

Failure to disassemble replisomes in a timely manner is likely to result in genome instability; *in vitro* studies have demonstrated that *E. coli* replisomes can switch strands after converging upon each other, resulting in chromosome over-replication (Hiasa and Marians, 1994). However, it has not been addressed whether replisomes simply dissociate upon converging, or whether their disassembly is an active process. It has recently been shown that disassembly of the replisome in eukaryotic organisms is an active process, triggered by post-translational modification of the replicative helicase, Mcm2-7 (Maric et al., 2014; Moreno et al., 2014). Given the extensive regulation of bacterial helicase loading during initiation and replisome re-loading, it may be speculated that the bacterial replisome is subject to similar mechanisms of regulated disassembly.

Future Perspectives

The information summarized in this work suggests that replisome organization and function follow a common theme with minor variations across bacteria, underlying the importance of DNA replication as a basic metabolic function of the cell. However, more work is needed in order to assess if these conclusions can be extended to all bacteria. Novel technologies in imaging,

sequencing and genome editing will likely help us in the study of the replisome at a single-molecule level and *in vivo*, and to extend this analysis to non-classical model organisms. Future research promises a greater understanding of the composition of the replisome; how it is assembled; how it remains assembled; and how it comes apart. Furthermore, work in other bacteria will be especially revealing in understanding how specialized additions to the replisome help adapt organisms to their particular physiological needs. In turn, this information can catalyze the discovery of a set of basic considerations that any replisome must meet in order to achieve fast and efficient genome duplication.

Acknowledgments

This work was supported by the Natural Sciences and Engineering Research Council of Canada (NSERC# 435521-2013), the Canada Research Chairs program and McGill University.

References

Arias-Palomo, E., O'Shea, V. L., Hood, I. V., and Berger, J. M. (2013). The bacterial DnaC helicase loader is a DnaB ring breaker. *Cell* 153, 438–448. doi: 10.1016/j.cell.2013.03.006

Bastia, D., Zzaman, S., Krings, G., Saxena, M., Peng, X., and Greenberg, M. M. (2008). Replication termination mechanism as revealed by Tus-mediated polar arrest of a sliding helicase. *Proc. Natl. Acad. Sci. U.S.A.* 105, 12831–12836. doi: 10.1073/pnas.0805898105

Bhattacharyya, B., George, N. P., Thurmes, T. M., Zhou, R., Jani, N., Wessel, S. R., et al. (2014). Structural mechanisms of PriA-mediated DNA replication restart. *Proc. Natl. Acad. Sci. U.S.A.* 111, 1373–1378. doi: 10.1073/pnas.1318001111

Blinkova, A., Burkart, M. F., Owens, T. D., and Walker, J. R. (1997). Conservation of the *Escherichia coli* dnaX programmed ribosomal frameshift signal in *Salmonella typhimurium*. *J. Bacteriol.* 179, 4438–4442.

Bruck, I., Georgescu, R. E., and O'Donnell, M. (2005). Conserved interactions in the *Staphylococcus aureus* DNA PolC chromosome replication machine. *J. Biol. Chem.* 280, 18152–18162. doi: 10.1074/jbc.M413595200

Bruck, I., and O'Donnell, M. (2000). The DNA replication machine of a gram-positive organism. *J. Biol. Chem.* 275, 28971–28983. doi: 10.1074/jbc.M003565200

Bruck, I., Yuzhakov, A., Yurieva, O., Jeruzalmi, D., Skangalis, M., Kuriyan, J., et al. (2002). Analysis of a multicomponent thermostable DNA polymerase III replicase from an extreme thermophile. *J. Biol. Chem.* 277, 17334–17348. doi: 10.1074/jbc.M110198200

Bullard, J. M., Williams, J. C., Acker, W. K., Jacobi, C., Janjic, N., and McHenry, C. S. (2002). DNA polymerase III holoenzyme from *Thermus thermophilus* identification, expression, purification of components, and use to reconstitute a processive replicase. *J. Biol. Chem.* 277, 13401–13408. doi: 10.1074/jbc.M110833200

Butland, G., Peregrin-Alvarez, J. M., Li, J., Yang, W., Yang, X., Canadien, V., et al. (2005). Interaction network containing conserved and essential protein complexes in *Escherichia coli*. *Nature* 433, 531–537. doi: 10.1038/nature03239

Caspi, R., Pacek, M., Consiglieri, G., Helinski, D. R., Toukdarian, A., and Konieczny, I. (2001). A broad host range replicon with different requirements for replication initiation in three bacterial species. *EMBO J.* 20, 3262–3271. doi: 10.1093/emboj/20.12.3262

Cox, M. M., Goodman, M. F., Kreuzer, K. N., Sherratt, D. J., Sandler, S. J., and Marians, K. J. (2000). The importance of repairing stalled replication forks. *Nature* 404, 37–41. doi: 10.1038/35003501

Davey, M. J., Fang, L., McInerney, P., Georgescu, R. E., and O'Donnell, M. (2002). The DnaC helicase loader is a dual ATP/ADP switch protein. *EMBO J.* 21, 3148–3159. doi: 10.1093/emboj/cdf308

Debyser, Z., Tabor, S., and Richardson, C. C. (1994). Coordination of leading and lagging strand DNA synthesis at the replication fork of bacteriophage T7. *Cell* 77, 157–166. doi: 10.1016/0092-8674(94)90243-7

Dervyn, E., Suski, C., Daniel, R., Bruand, C., Chapuis, J., Errington, J., et al. (2001). Two essential DNA polymerases at the bacterial replication fork. *Science* 294, 1716–1719. doi: 10.1126/science.1066351

Dohrmann, P. R., Manhart, C. M., Downey, C. D., and McHenry, C. S. (2011). The rate of polymerase release upon filling the gap between Okazaki fragments is inadequate to support cycling during lagging strand synthesis. *J. Mol. Biol.* 414, 15–27. doi: 10.1016/j.jmb.2011.09.039

Duderstadt, K. E., Chuang, K., and Berger, J. M. (2011). DNA stretching by bacterial initiators promotes replication origin opening. *Nature* 478, 209–213. doi: 10.1038/nature10455

Duggin, I. G., Wake, R. G., Bell, S. D., and Hill, T. M. (2008). The replication fork trap and termination of chromosome replication. *Mol. Microbiol.* 70, 1323–1333. doi: 10.1111/j.1365-2958.2008.06500.x

Erzberger, J. P., Mott, M. L., and Berger, J. M. (2006). Structural basis for ATP-dependent DnaA assembly and replication-origin remodeling. *Nat. Struct. Mol. Biol.* 13, 676–683. doi: 10.1038/nsmb1115

Fang, L., Davey, M. J., and O'Donnell, M. (1999). Replisome assembly at oriC, the replication origin of *E. coli*, reveals an explanation for initiation sites outside an origin. *Mol. Cell* 4, 541–553. doi: 10.1016/S1097-2765(00)80205-1

Forterre, P. (2013). Why are there so many diverse replication machineries? *J. Mol. Biol.* 425, 4714–4726. doi: 10.1016/j.jmb.2013.09.032

Geertsema, H. J., Kulczyk, A. W., Richardson, C. C., and van Oijen, A. M. (2014). Single-molecule studies of polymerase dynamics and stoichiometry at the bacteriophage T7 replication machinery. *Proc. Natl. Acad. Sci. U.S.A.* 111, 4073–4078. doi: 10.1073/pnas.1402010111

Georgescu, R. E., Kurth, I., and O'Donnell, M. (2011). Single-molecule studies reveal the function of a third polymerase in the replisome. *Nat. Struct. Mol. Biol.* 19, 113–116. doi: 10.1038/nsmb.2179

Georgescu, R. E., Kurth, I., Yao, N. Y., Stewart, J., Yurieva, O., and O'Donnell, M. (2009). Mechanism of polymerase collision release from sliding clamps on the lagging strand. *EMBO J.* 28, 2981–2991. doi: 10.1038/emboj.2009.233

Georgescu, R., Langston, L., and O'Donnell, M. (2015). A proposal: evolution of PCNA's role as a marker of newly replicated DNA. *DNA Repair* 29, 4–15. doi: 10.1016/j.dnarep.2015.01.015

Hamdan, S. M., Loparo, J. J., Takahashi, M., Richardson, C. C., and van Oijen, A. M. (2009). Dynamics of DNA replication loops reveal temporal control of lagging-strand synthesis. *Nature* 457, 336–339. doi: 10.1038/nature07512

Hamdan, S. M., Marintcheva, B., Cook, T., Lee, S. J., Tabor, S., and Richardson, C. C. (2005). A unique loop in T7 DNA polymerase mediates the binding of helicase-primase, DNA binding protein, and processivity factor. *Proc. Natl. Acad. Sci. U.S.A.* 102, 5096–5101. doi: 10.1073/pnas.0501637102

Heller, R. C., and Marians, K. J. (2005a). The disposition of nascent strands at stalled replication forks dictates the pathway of replisome loading during restart. *Mol. Cell* 17, 733–743. doi: 10.1016/j.molcel.2005.01.019

Heller, R. C., and Marians, K. J. (2005b). Unwinding of the nascent lagging strand by Rep and PriA enables the direct restart of stalled replication forks. *J. Biol. Chem.* 280, 34143–34151. doi: 10.1074/jbc.M507224200

Heller, R. C., and Marians, K. J. (2006). Replication fork reactivation downstream of a blocked nascent leading strand. *Nature* 439, 557–562. doi: 10.1038/nature04329

Hiasa, H., and Marians, K. J. (1994). Tus prevents overreplication of oriC plasmid DNA. *J. Biol. Chem.* 269, 26959–26968.

Jarvis, T. C., Beaudry, A. A., Bullard, J. M., Janjic, N., and McHenry, C. S. (2005a). Reconstitution of a minimal DNA replicase from *Pseudomonas aeruginosa* and stimulation by non-cognate auxiliary factors. *J. Biol. Chem.* 280, 7890–7900. doi: 10.1074/jbc.M412263200

Jarvis, T. C., Beaudry, A. A., Bullard, J. M., Ochsner, U., Dallmann, H. G., and McHenry, C. S. (2005b). Discovery and characterization of the cryptic psi subunit of the pseudomonad DNA replicase. *J. Biol. Chem.* 280, 40465–40473. doi: 10.1074/jbc.M508310200

Johnson, D. E., Takahashi, M., Hamdan, S. M., Lee, S. J., and Richardson, C. C. (2007). Exchange of DNA polymerases at the replication fork of bacteriophage T7. *Proc. Natl. Acad. Sci. U.S.A.* 104, 5312–5317. doi: 10.1073/pnas.0701062104

Kornberg, A., and Baker, T. (1992). *DNA Replication*. New York, NY: Freeman.

Kubitschek, H. E., and Newman, C. N. (1978). Chromosome replication during the division cycle in slowly growing, steady-state cultures of three *Escherichia coli* B/r strains. *J. Bacteriol.* 136, 179–190.

Kulczyk, A. W., Akabayov, B., Lee, S. J., Bostina, M., Berkowitz, S. A., and Richardson, C. C. (2012). An interaction between DNA polymerase and helicase is essential for the high processivity of the bacteriophage T7 replisome. *J. Biol. Chem.* 287, 39050–39060. doi: 10.1074/jbc.M112.410647

Kurth, I., Georgescu, R. E., and O'Donnell, M. E. (2013). A solution to release twisted DNA during chromosome replication by coupled DNA polymerases. *Nature* 496, 119–122. doi: 10.1038/nature11988

Lemon, K. P., and Grossman, A. D. (1998). Localization of bacterial DNA polymerase: evidence for a factory model of replication. *Science* 282, 1516–1519. doi: 10.1126/science.282.5393.1516

Leonard, A. C., and Grimwade, J. E. (2011). Regulation of DnaA assembly and activity: taking directions from the genome. *Annu. Rev. Microbiol.* 65, 19–35. doi: 10.1146/annurev-micro-090110-102934

Leu, F. P., Hingorani, M. M., Turner, J., and O'Donnell, M. (2000). The δ subunit of DNA polymerase III holoenzyme serves as a sliding clamp unloader in *Escherichia coli*. *J. Biol. Chem.* 275, 34609–34618. doi: 10.1074/jbc.M005495200

Li, X., and Marians, K. J. (2000). Two distinct triggers for cycling of the lagging strand polymerase at the replication fork. *J. Biol. Chem.* 275, 34757–34765. doi: 10.1074/jbc.M006556200

Liu, B., Eliason, W. K., and Steitz, T. A. (2013). Structure of a helicase-helicase loader complex reveals insights into the mechanism of bacterial primosome assembly. *Nat. Commun.* 4, 2495. doi: 10.1038/ncomms3495

Liu, Z., Chen, P., Wang, X., Cai, G., Niu, L., Teng, M., et al. (2014). Crystal structure of DnaT84-153-dT10 ssDNA complex reveals a novel single-stranded DNA binding mode. *Nucleic Acids Res.* 42, 9470–9483. doi: 10.1093/nar/gku633

Loparo, J. J., Kulczyk, A. W., Richardson, C. C., and van Oijen, A. M. (2011). Simultaneous single-molecule measurements of phage T7 replisome composition and function reveal the mechanism of polymerase exchange. *Proc. Natl. Acad. Sci. U.S.A.* 108, 3584–3589. doi: 10.1073/pnas.1018824108

Lopper, M., Boonsombat, R., Sandler, S. J., and Keck, J. L. (2007). A hand-off mechanism for primosome assembly in replication restart. *Mol. Cell* 26, 781–793. doi: 10.1016/j.molcel.2007.05.012

Maisnier-Patin, S., Nordstrom, K., and Dasgupta, S. (2001). Replication arrests during a single round of replication of the *Escherichia coli* chromosome in the absence of DnaC activity. *Mol. Microbiol.* 42, 1371–1382. doi: 10.1046/j.1365-2958.2001.02718.x

Maki, H., Maki, S., and Kornberg, A. (1988). DNA Polymerase III holoenzyme of *Escherichia coli*. IV. The holoenzyme is an asymmetric dimer with twin active sites. *J. Biol. Chem.* 263, 6570–6578.

Makowska-Grzyska, M., and Kaguni, J. M. (2010). Primase directs the release of DnaC from DnaB. *Mol. Cell* 37, 90–101. doi: 10.1016/j.molcel.2009.12.031

Manhart, C. M., and McHenry, C. S. (2013). The PriA replication restart protein blocks replicase access prior to helicase assembly and directs template specificity through its ATPase activity. *J. Biol. Chem.* 288, 3989–3999. doi: 10.1074/jbc.M112.435966

Manosas, M., Spiering, M. M., Zhuang, Z., Benkovic, S. J., and Croquette, V. (2009). Coupling DNA unwinding activity with primer synthesis in the bacteriophage T4 primosome. *Nat. Chem. Biol.* 5, 904–912. doi: 10.1038/nchembio.236

Marceau, A. H., Bahng, S., Massoni, S. C., George, N. P., Sandler, S. J., Marians, K. J., et al. (2011). Structure of the SSB-DNA polymerase III interface and its role in DNA replication. *EMBO J.* 30, 4236–4247. doi: 10.1038/emboj.2011.305

Maric, M., Maculins, T., De Piccoli, G., and Labib, K. (2014). Cdc48 and a ubiquitin ligase drive disassembly of the CMG helicase at the end of DNA replication. *Science* 346, 1253596. doi: 10.1126/science.1253596

Markovitz, A. (2005). A new *in vivo* termination function for DNA polymerase I of *Escherichia coli* K12. *Mol. Microbiol.* 55, 1867–1882. doi: 10.1111/j.1365-2958.2005.04513.x

McInerney, P., Johnson, A., Katz, F., and O'Donnell, M. (2007). Characterization of a triple DNA polymerase replisome. *Mol. Cell* 27, 527–538. doi: 10.1016/j.molcel.2007.06.019

Michel, B., Grompone, G., Flores, M. J., and Bidnenko, V. (2004). Multiple pathways process stalled replication forks. *Proc. Natl. Acad. Sci. U.S.A.* 101, 12783–12788. doi: 10.1073/pnas.0401586101

Moolman, M. C., Krishnan, S. T., Kerssemakers, J. W., van den Berg, A., Tulinski, P., Depken, M., et al. (2014). Slow unloading leads to DNA-bound β2-sliding clamp accumulation in live *Escherichia coli* cells. *Nat. Commun.* 5, 5820. doi: 10.1038/ncomms6820

Moreno, S. P., Bailey, R., Campion, N., Herron, S., and Gambus, A. (2014). Polyubiquitylation drives replisome disassembly at the termination of DNA replication. *Science* 346, 477–481. doi: 10.1126/science.1253585

Mott, M. L., Erzberger, J. P., Coons, M. M., and Berger, J. M. (2008). Structural synergy and molecular crosstalk between bacterial helicase loaders and replication initiators. *Cell* 135, 623–634. doi: 10.1016/j.cell.2008.09.058

Mulcair, M. D., Schaeffer, P. M., Oakley, A. J., Cross, H. F., Neylon, C., Hill, T. M., et al. (2006). A molecular mousetrap determines polarity of termination of DNA replication in *E. coli*. *Cell* 125, 1309–1319. doi: 10.1016/j.cell.2006.04.040

Mulugu, S., Potnis, A., Shamsuzzaman, Taylor, J., Alexander, K., and Bastia, D. (2001). Mechanism of termination of DNA replication of *Escherichia coli* involves helicase-contrahelicase interaction. *Proc. Natl. Acad. Sci. U.S.A.* 98, 9569–9574. doi: 10.1073/pnas.171065898

Neylon, C., Brown, S. E., Kralicek, A. V., Miles, C. S., Love, C. A., and Dixon, N. E. (2000). Interaction of the *Escherichia coli* replication terminator protein (Tus) with DNA: a model derived from DNA-binding studies of mutant proteins by surface plasmon resonance. *Biochemistry* 39, 11989–11999. doi: 10.1021/bi001174w

Olson, M. W., Dallmann, H. G., and McHenry, C. S. (1995). DnaX complex of *Escherichia coli* DNA polymerase III holoenzyme. The χ ψ complex functions by increasing the affinity of τ and γ for δ.δ′ to a physiologically relevant range. *J. Biol. Chem.* 270, 29570–29577. doi: 10.1074/jbc.270.49.29570

Onrust, R., Finkelstein, J., Turner, J., Naktinis, V., and O'Donnell, M. (1995). Assembly of a chromosomal replication machine: two DNA polymerases, a clamp loader, and sliding clamps in one holoenzyme particle. III. Interface between two polymerases and the clamp loader. *J. Biol. Chem.* 270, 13366–13377. doi: 10.1074/jbc.270.22.13366

Park, K., Debyser, Z., Tabor, S., Richardson, C. C., and Griffith, J. D. (1998). Formation of a DNA loop at the replication fork generated by bacteriophage T7 replication proteins. *J. Biol. Chem.* 273, 5260–5270. doi: 10.1074/jbc.273.9.5260

Pennington, J. M., and Rosenberg, S. M. (2007). Spontaneous DNA breakage in single living *Escherichia coli* cells. *Nat. Genet.* 39, 797–802. doi: 10.1038/ng2051

Pomerantz, R. T., and O'Donnell, M. (2008). The replisome uses mRNA as a primer after colliding with RNA polymerase. *Nature* 456, 762–766. doi: 10.1038/nature07527

Pomerantz, R. T., and O'Donnell, M. (2010). Direct restart of a replication fork stalled by a head-on RNA polymerase. *Science* 327, 590–592. doi: 10.1126/science.1179595

Rannou, O., Le Chatelier, E., Larson, M. A., Nouri, H., Dalmais, B., Laughton, C., et al. (2013). Functional interplay of DnaE polymerase, DnaG primase and DnaC helicase within a ternary complex, and primase to polymerase hand-off during lagging strand DNA replication in *Bacillus subtilis*. *Nucleic Acids Res.* 41, 5303–5320. doi: 10.1093/nar/gkt207

Reyes-Lamothe, R., Sherratt, D. J., and Leake, M. C. (2010). Stoichiometry and architecture of active DNA replication machinery in *Escherichia coli*. *Science* 328, 498–501. doi: 10.1126/science.1185757

Robinson, A., Causer, R. J., and Dixon, N. E. (2012). Architecture and conservation of the bacterial DNA replication machinery, an underexploited drug target. *Curr. Drug Targets* 13, 352–372. doi: 10.2174/138945012799424598

Roecklein, B., Pelletier, A., and Kuempel, P. (1991). The tus gene of *Escherichia coli*: autoregulation, analysis of flanking sequences and identification of a complementary system in *Salmonella typhimurium*. *Res. Microbiol.* 142, 169–175. doi: 10.1016/0923-2508(91)90026-7

Rudolph, C. J., Upton, A. L., Stockum, A., Nieduszynski, C. A., and Lloyd, R. G. (2013). Avoiding chromosome pathology when replication forks collide. *Nature* 500, 608–611. doi: 10.1038/nature12312

Sanders, G. M., Dallmann, H. G., and McHenry, C. S. (2010). Reconstitution of the B. subtilis replisome with 13 proteins including two distinct replicases. *Mol. Cell* 37, 273–281. doi: 10.1016/j.molcel.2009.12.025

Santi, I., and McKinney, J. D. (2015). Chromosome organization and replisome dynamics in *Mycobacterium smegmatis*. *MBio* 6, e01999-01914. doi: 10.1128/mBio.01999-14

Sharma, A., Kamran, M., Verma, V., Dasgupta, S., and Dhar, S. K. (2014). Intracellular locations of replication proteins and the origin of replication during

chromosome duplication in the slowly growing human pathogen *Helicobacter pylori*. *J. Bacteriol.* 196, 999–1011. doi: 10.1128/JB.01198-13

Sinha, N. K., Morris, C. F., and Alberts, B. M. (1980). Efficient *in vitro* replication of double-stranded DNA templates by a purified T4 bacteriophage replication system. *J. Biol. Chem.* 255, 4290–4293.

Slater, S. C., Lifsics, M. R., O'Donnell, M., and Maurer, R. (1994). holE, the gene coding for the θ subunit of DNA polymerase III of *Escherichia coli*: characterization of a *holE* mutant and comparison with a *dnaQ* (ϵ-subunit) mutant. *J. Bacteriol.* 176, 815–821.

Smits, W. K., Goranov, A. I., and Grossman, A. D. (2010). Ordered association of helicase loader proteins with the *Bacillus subtilis* origin of replication *in vivo*. *Mol. Microbiol.* 75, 452–461. doi: 10.1111/j.1365-2958.2009.06999.x

Soni, R. K., Mehra, P., Mukhopadhyay, G., and Dhar, S. K. (2005). *Helicobacter pylori* DnaB helicase can bypass *Escherichia coli* DnaC function *in vivo*. *Biochem. J.* 389, 541–548. doi: 10.1042/BJ20050062

Stelter, M., Gutsche, I., Kapp, U., Bazin, A., Bajic, G., Goret, G., et al. (2012). Architecture of a dodecameric bacterial replicative helicase. *Structure* 20, 554–564. doi: 10.1016/j.str.2012.01.020

Su'etsugu, M., and Errington, J. (2011). The replicase sliding clamp dynamically accumulates behind progressing replication forks in *Bacillus subtilis* cells. *Mol. Cell* 41, 720–732. doi: 10.1016/j.molcel.2011.02.024

Suski, C., and Marians, K. J. (2008). Resolution of converging replication forks by RecQ and topoisomerase III. *Mol. Cell* 30, 779–789. doi: 10.1016/j.molcel.2008.04.020

Tanner, N. A., Tolun, G., Loparo, J. J., Jergic, S., Griffith, J. D., Dixon, N. E., et al. (2011). *E. coli* DNA replication in the absence of free β clamps. *EMBO J.* 30, 1830–1840. doi: 10.1038/emboj.2011.84

Timinskas, K., Balvociute, M., Timinskas, A., and Venclovas, C. (2014). Comprehensive analysis of DNA polymerase III alpha subunits and their homologs in bacterial genomes. *Nucleic Acids Res.* 42, 1393–1413. doi: 10.1093/nar/gkt900

Trojanowski, D., Ginda, K., Pioro, M., Holowka, J., Skut, P., Jakimowicz, D., et al. (2015). Choreography of the *Mycobacterium* replication machinery during the cell cycle. *MBio* 6, e02125-02114. doi: 10.1128/mBio.02125-14

Vass, R. H., and Chien, P. (2013). Critical clamp loader processing by an essential AAA+ protease in Caulobacter crescentus. *Proc. Natl. Acad. Sci. U.S.A.* 110, 18138–18143. doi: 10.1073/pnas.1311302110

Velten, M., McGovern, S., Marsin, S., Ehrlich, S. D., Noirot, P., and Polard, P. (2003). A two-protein strategy for the functional loading of a cellular replicative DNA helicase. *Mol. Cell* 11, 1009–1020. doi: 10.1016/S1097-2765(03)00130-8

Wang, X., Reyes-Lamothe, R., and Sherratt, D. J. (2008). Modulation of *Escherichia coli* sister chromosome cohesion by topoisomerase IV. *Genes Dev.* 22, 2426–2433. doi: 10.1101/gad.487508

Weigel, C., and Seitz, H. (2002). Strand-specific loading of DnaB helicase by DnaA to a substrate mimicking unwound oriC. *Mol. Microbiol.* 46, 1149–1156. doi: 10.1046/j.1365-2958.2002.03232.x

Wendel, B. M., Courcelle, C. T., and Courcelle, J. (2014). Completion of DNA replication in *Escherichia coli*. *Proc. Natl. Acad. Sci. U.S.A.* 111, 16454–16459. doi: 10.1073/pnas.1415025111

Wessel, S. R., Marceau, A. H., Massoni, S. C., Zhou, R., Ha, T., Sandler, S. J., et al. (2013). PriC-mediated DNA replication restart requires PriC complex formation with the single-stranded DNA-binding protein. *J. Biol. Chem.* 288, 17569–17578. doi: 10.1074/jbc.M113.478156

Wu, C. A., Zechner, E. L., and Marians, K. J. (1992). Coordinated leading- and lagging-strand synthesis at the *Escherichia coli* DNA replication fork. I. Multiple effectors act to modulate Okazaki fragment size. *J. Biol. Chem.* 267, 4030–4044.

Yang, J., Zhuang, Z., Roccasecca, R. M., Trakselis, M. A., and Benkovic, S. J. (2004). The dynamic processivity of the T4 DNA polymerase during replication. *Proc. Natl. Acad. Sci. U.S.A.* 101, 8289–8294. doi: 10.1073/pnas.0402625101

Yao, N. Y., Georgescu, R. E., Finkelstein, J., and O'Donnell, M. E. (2009). Single-molecule analysis reveals that the lagging strand increases replisome processivity but slows replication fork progression. *Proc. Natl. Acad. Sci. U.S.A.* 106, 13236–13241. doi: 10.1073/pnas.0906157106

Yeeles, J. T., Deegan, T. D., Janska, A., Early, A., and Diffley, J. F. (2015). Regulated eukaryotic DNA replication origin firing with purified proteins. *Nature* 519, 431–435. doi: 10.1038/nature14285

Yeeles, J. T., and Marians, K. J. (2011). The *Escherichia coli* replisome is inherently DNA damage tolerant. *Science* 334, 235–238. doi: 10.1126/science.1209111

Yurieva, O., Skangalis, M., Kuriyan, J., and O'Donnell, M. (1997). *Thermus thermophilis* dnaX homolog encoding γ- and τ-like proteins of the chromosomal replicase. *J. Biol. Chem.* 272, 27131–27139. doi: 10.1074/jbc.272.43.27131

Yuzhakov, A., Kelman, Z., and O'Donnell, M. (1999). Trading places on DNA—a three-point switch underlies primer handoff from primase to the replicative DNA polymerase. *Cell* 96, 153–163. doi: 10.1016/S0092-8674(00)80968-X

Yuzhakov, A., Turner, J., and O'Donnell, M. (1996). Replisome assembly reveals the basis for asymmetric function in leading and lagging strand replication. *Cell* 86, 877–886. doi: 10.1016/S0092-8674(00)80163-4

Conflict of Interest Statement: The authors declare that the research was conducted in the absence of any commercial or financial relationships that could be construed as a potential conflict of interest.

Copyright © 2015 Beattie and Reyes-Lamothe. This is an open-access article distributed under the terms of the Creative Commons Attribution License (CC BY). The use, distribution or reproduction in other forums is permitted, provided the original author(s) or licensor are credited and that the original publication in this journal is cited, in accordance with accepted academic practice. No use, distribution or reproduction is permitted which does not comply with these terms.

frontiers in Microbiology

ORIGINAL RESEARCH
published: 12 May 2015
doi: 10.3389/fmicb.2015.00448

Segregation of chromosome arms in growing and non-growing *Escherichia coli* cells

Conrad L. Woldringh[1]*, *Flemming G. Hansen*[2], *Norbert O. E. Vischer*[1] and *Tove Atlung*[3]

[1] Bacterial Cell Biology, Faculty of Science, Swammerdam Institute for Life Sciences, University of Amsterdam, Amsterdam, Netherlands, [2] Department of Systems Biology, Technical University of Denmark, Lyngby, Denmark, [3] Department of Science, Systems and Models, Roskilde University, Roskilde, Denmark

In slow-growing *Escherichia coli* cells the chromosome is organized with its left (L) and right (R) arms lying separated in opposite halves of the nucleoid and with the origin (O) in-between, giving the pattern L-O-R. During replication one of the arms has to pass the other to obtain the same organization in the daughter cells: L-O-R L-O-R. To determine the movement of arms during segregation six strains were constructed carrying three colored loci: the left and right arms were labeled with red and cyan fluorescent-proteins, respectively, on loci symmetrically positioned at different distances from the central origin, which was labeled with green-fluorescent protein. In non-replicating cells with the predominant spot pattern L-O-R, initiation of replication first resulted in a L-O-O-R pattern, soon changing to O-L-R-O. After replication of the arms the predominant spot patterns were, L-O-R L-O-R, O-R-L R-O-L or O-L-R L-O-R indicating that one or both arms passed an origin and the other arm. To study the driving force for these movements cell growth was inhibited with rifampicin allowing run-off DNA synthesis. Similar spot patterns were obtained in growing and non-growing cells, indicating that the movement of arms is not a growth-sustained process, but may result from DNA synthesis itself. The distances between loci on different arms (LR-distances) and between duplicated loci (LL- or RR-distances) as a function of their distance from the origin, indicate that in slow-growing cells DNA is organized according to the so-called sausage model and not according to the doughnut model.

Keywords: ***Escherichia coli,*** **nucleoid, DNA segregation, chromosome arms (replichores), ordering pattern, rifampicin-treatment, run-off DNA synthesis**

OPEN ACCESS

Edited by:
Thomas E. Hanson, University of Delaware, USA

Reviewed by:
Rodrigo Reyes, McGill University, Canada
Mohan C. Joshi, Baylor College of Medicine, USA

***Correspondence:**
Conrad L. Woldringh, Swammerdam Institute for Life Sciences, University of Amsterdam, Science Park 904, 1098 XH Amsterdam, Netherlands
c.woldringh@gmail.com

Specialty section:
This article was submitted to Microbial Physiology and Metabolism, a section of the journal Frontiers in Microbiology

Received: *30 November 2014*
Accepted: *24 April 2015*
Published: *12 May 2015*

Citation:
Woldringh CL, Hansen FG, Vischer NOE and Atlung T (2015) Segregation of chromosome arms in growing and non-growing Escherichia coli cells. Front. Microbiol. 6:448. doi: 10.3389/fmicb.2015.00448

Introduction

The chromosome of *Escherichia coli* can be readily visualized in living cells by phase contrast microscopy as a separate and dynamic structure (Mason and Powelson, 1956; Yamaichi and Niki, 2004). We now know that within this nucleoid structure the DNA is confined as a single branched, plectonemic supercoil formed and maintained by topoisomerases (Zechiedrich et al., 2000) and by nucleoid associated proteins (NAPs; Luijsterburg et al., 2006). The primary cause for the phase separation between nucleoid and cytoplasm is the physical phenomenon of excluded-volume interactions between DNA and soluble proteins (Odijk, 1998). Studies of the physical structure of isolated bacterial DNA (Cunha et al., 2001; Pelletier et al., 2012) have indicated that the

DNA segments behave as entropic springs showing diffusive motion within a visco-elastic network (Cunha et al., 2005).

Against this physical background we must consider the process of bacterial segregation and the dynamics of replicated DNA strands collapsed or confined into the nucleoid of living cells. Do these strands become entangled or mixed as is to be expected for such polymer chains? It is now well accepted that DNA daughter strands segregate as they are replicated and that in slow growing *E. coli* cells the two chromosome arms move to different halves of the nucleoid with the origin in-between (Nielsen et al., 2006a; Wang et al., 2006). This organization suggests that the replicated daughter strands do not entangle or mix, but stay separated as Left and Right arms of the chromosome during the entire replication-segregation process (review Jun and Wright, 2010).

Can such an organization and movement be explained without the help of an underlying biological structure as suggested by several authors (Wiggins et al., 2010; Le Chat and Espéli, 2012; Yazdi et al., 2012), a hypothetical structure that, in its turn, has to become organized? This question has recently been considered by Youngren et al. (2014) for the even more complicated situation in fast growing *E. coli* cells undergoing multifork replication. These authors propose that in the wider cells replicating chromosomes are thermodynamically driven into ring polymers in which replicated strands segregate spontaneously by entropic demixing without the help of any additional, biological mechanism.

Nevertheless, it has been proposed that segregation proceeds in growing cells with the help of transcription/transertion processes (Woldringh, 2002). In addition, it was suggested that the demixing process may be sustained by regulatory interactions between transcription factors and target genes that help to self-organize the chromosome into topological domains that do not mix (Fritsche et al., 2011). According to Fisher et al. (2013), the non-intermingling of sister strands occurs in pulses of nucleoid elongation at defined times in the cycle of slowly grown cells while cell elongation continues monotonically. The periodical movements are proposed to depend on the accumulation and release of tethers between sister strands, processes that can be expected to depend on cell growth.

In view of these growth-sustained, active processes proposed to organize and segregate the replicating chromosome we analyzed the positions of fluorescently tagged loci in either growing *E. coli* cells or in rifampicin-treated cells that do not grow but only carry out run-off DNA synthesis. The measurements indicate that separation and migration of loci is very similar in growing and non-growing cells suggesting that the process of segregation continues in the absence of RNA synthesis without cellular or nucleoid elongation. The measurements are discussed in the light of two segregation models proposed in the literature, the so-called doughtnut and sausage model.

Materials and Methods

Strains and Growth Conditions

Strains of *E. coli* MG1655 Δ*lacIZYA* (Nielsen et al., 2006b) carrying three different ParB/*parS* systems were constructed by recombineering. The strains with the three different *parS* sequences were transformed with plasmid pFH4034 which carry three different *parB* gene fusions to three different genes for fluorescent proteins with different colors (green (G), cyan (C), and red (R); see Supplementary Data Figure S1) to give the strains depicted in **Figure 1A**. See for strain construction Supplementary Material and Table S1.

The strains were grown in minimal glycerol medium supplemented with lysine (20 μg/ml) and ampicillin (100 μg/ml). Strain FH4035 has a lysine requirement while the strains FH404056-4060 are *lysA*$^+$. We add 10 μg/ml uracil due to a possible mutation in the *rph* gene which might affect the expression of the *pyrE* gene. Cell growth was monitored with a spectrophotometer at 450 nm. Cells were grown undisturbed at 32°C (doubling time about 150 min) for about 16 h while the OD was kept below 0.5 by periodical dilutions.

Strain FH4035 was grown in a slightly different growth medium at 28°C, with a doubling time of ∼180 min. For unknown reasons these cells were shorter than those of the other constructs while showing the same cell diameter (0.7 μm). The smaller cell length leading to smaller segregation distances is evident from the Tables, but in our view does not influence our

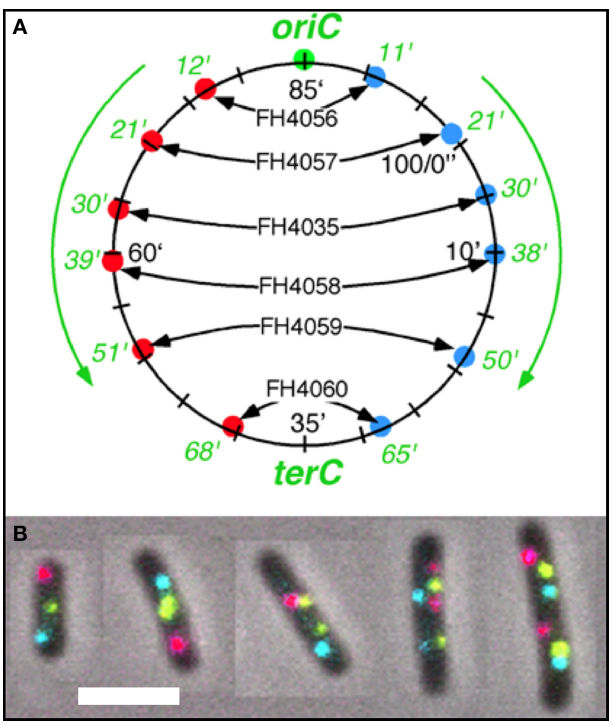

FIGURE 1 | Fluorescent loci and spots. (A) Schematic representation of the chromosome of the 6 strains showing the positions of the 3 probes. Green fluorescent protein labels a locus ∼1 kb to the right of the origin (O). The chromosome arms are labeled, respectively, with red (L, left arm) and cyan (R, right arm) fluorescent protein on opposite sites and at different distances from *oriC*. Green numbers indicate the theoretical time when the loci are replicated during progression of the replication forks, based on their distance in kb from *oriC* and on the replication velocity, assuming the replication time to be 75 min (Nielsen et al., 2006a). **(B)** Composite image of the 4 channels (phase contrast, red, green, and cyan filters) of cells of *E. coli* FH4035 showing the most abundant pattern of 3-spot cells (LOR) and 6-spot cells (LOR LOR), as well as some replicative intermediates. Magnification bar 2 μm.

interpretation of patterns and movement of the chromosome arms.

Microscopy

Cell samples (1 ml) were concentrated about 20x by centrifugation, prepared on an agar slab or a poly-lysine coated microscope slide and photographed within 30 min after sampling.

For the constructs FH4056, 4057, 4058, 4059, and 4060 pictures were taken on a Zeiss Axioplan microscope equipped with a Kappa DX 2 camera using an ImageBase capture program. For construct FH4035 an Olympus BX microscope was used in combination with programs ImageJ and MicroManager. Both microscopes had 100 × 1.3 oil immersion lens (PH3) giving a magnification of 15 pixels per μm. Four pictures of each field were obtained using the respective capture programs. Both microscopes had filters for detecting red, cyan, and green fluorescence.

Measurement of Cells and Spots

Image analysis was performed with Coli-Inspector, which is a set of scripts packed in a "project file" running under the ImageJ plugin ObjectJ. After spatial alignment of the 4 channels, cell length and diameter were automatically measured. The positions of the three kinds of spots were automatically measured using different thresholds. Cells in which one kind of spot was lacking were manually discarded. In some cells missing spots could be manually added after better adjusting brightness and contrast of the image. After checking all cells by eye, the spot positions along the long and short axis of the cell, their pattern, the frequency of each pattern and the (half-) distance between duplicated spots were calculated by Coli-Inspector (see: https://sils.fnwi.uva.nl/bcb/oblectj/examples/). By making use of the so-called Qualifier-possibility the distribution of, for instance, cells that show a specific spot pattern can be obtained (cf. **Table 3**).

Results

Analysis of Three- and Four-Spot Patterns in Growing Cells

The segregation of chromosome arms in slowly growing *E. coli* cells (doubling time at 28°C or 32°C Td = 180/150 min), was studied by measuring the cellular positions of three fluorescently labeled loci. The chromosomes contain one locus of green fluorescent-protein near *oriC* (O) and two loci on opposite positions on the chromosome arms at different distances from *oriC* in six constructs. Red fluorescent-protein tags the left arm (L) and cyan fluorescent-protein the right arm (R). See **Figure 1A** for a schematic representation of the chromosome in the different strains. **Figure 1B** shows composite images of the 4 channels for typical cells of *E. coli* FH4035.

In non-replicating cells with only 3 spots the most prominent pattern is LOR (46–78% of cells containing 3 spots; **Table 1A**, column I). This reflects the occurrence of unmixed chromosome arms in the two halves of the nucleoid as originally described by Nielsen et al. (2006b) and Wang et al. (2006). However, in many cells the origin is lying outside the two arms, giving the patterns OLR or ORL (column II in **Table 1A**). This pattern is more prominent in the constructs with loci close to the terminus (strains FH4059 and FH4060), where it increases to 50 per cent of the cells. It does not necessarily mean that the origin lies at the end of the nucleoid as depicted in the cells of **Table 1A**. In these constructs (FH4059 and FH4060), origin proximal loci may well have passed the origin. On average the origin in the 3 spot cells showing the LOR configuration is located in the middle of the cell with a standard deviation of 0.08–0.16 (Figure S2A) in agreement with a previous study (Nielsen et al., 2006a).

We measured the distance between the L and R loci in the 3 spot cells (**Figure 2**, Table S2). The distances were small for the origin proximal loci increasing with increasing distance from the origin, except for the most terminus proximal pair; these two loci are closer together, but not as close as for the origin proximal one's and with larger cell to cell variation (Figure S2). The trends were the same for LOR cells and for OLR/ORL cells, but L-R distances were shorter for the latter cells in all six constructs. Also in 4-spot cells the L-R distances were found to increase for the 4 first constructs in all ordering patterns (see Table S3).

Initiation of DNA replication occurs after a significant increase in cell length (compare lengths indicated in columns I and II with those in columns IIIA and B in **Table 1A**) and results in cells with 4 spots. In general, the duplicated O-spots are found adjacent to each other, either in between the L- and R-arm spots (column III-A) or in rare cases on the outside (column III-B in **Table 1A**). The relatively low percentage of this latter pattern suggests that the origins soon move apart and pass either one or both of the other labeled loci giving the patterns as depicted in column IV and V in **Table 1A**. The relatively high percentage of cells in which the duplicated O-spots occur on the outside of spots on both chromosome arms in some of the constructs (column V in **Table 1A**) shows that some unreplicated loci stay relatively close to the mid of the long axis of the cell. It should be kept in mind that for the constructs with origin proximal loci 4 spot cells are a fairly homogeneous cohort, whereas the 4 spot cells of constructs with origin distal loci are a mixture of cells with different amounts of replicated DNA.

Analysis of the O-O distances (Table S3) as a function of LR locus position shows that soon after initiation the origins are lying close together (strains FH4056 and FH4057), and when later replicated loci are duplicated the origins have moved further apart (strains FH4035 and FH4058). Comparison of the L-R distances in the 3-spot cells (**Figure 2**) with the distances in the 4-spot cells (Table S3) suggests that upon initiation the un-replicated LR loci first move apart (LOOR pattern), but move inward again when the origin passes one (OLOR/OROL) or two (OLRO) arms, causing smaller distances. Table S3 further indicates that while the distance between origins (O-O) increases gradually in the origin-distal constructs, the L-R distances show, after an initial increase, a decrease in the terminal-proximal constructs (FH4059 and FH4060). This could be ascribed to the association of the terminus region with the divisome (Espéli et al., 2012).

Cells with a 5-spot pattern are obtained when a locus on only one of the chromosome arms has duplicated. The relatively low percentage of these cells (last column in **Table 1A**) indicates that the oppositely positioned loci on the two arms are replicated and segregated more or less synchronously, directly

TABLE 1A | Percentages of most abundant patterns in non-replicating cells with 3 spots (column I and II) and in replicating cells with 4 spots that have a replicated origin (O; column III–V).

Strains	Total number cells with spots (mean cell length, μm)	Number cells with 3 spots (% of total population)	Non-replicating cells. % of 3-spot cells (mean cell length, μm)		nr. cells with 4 spots (% of total population)	Replicating cells with only the origin (O) duplicated. % of 4-spot cells (mean cell length, μm)				nr cells with 5 spots (% of total population)
			I LOR	II OLR/ORL		III-A LOOR	III-B OOLR/OORL	IV OLOR/OLOR	V OLRO	
4056[a]	1376 (3.27)	527 (33)	62 (2.61)	38 (2.56)	63 (5)	35 (3.27)	6 (2.65)	40 (3.04)	19 (2.89)	80 (6)
4057[a]	1099 (3.30)	487 (44)	74 (2.75)	26 (2.63)	138 (13)	32 (3.21)	9 (3.11)	42 (3.21)	15 (3.17)	56 (5)
4035[b]	1003 (2.55)	384 (38)	77 (2.07)	23 (2.57)	129 (13)	36 (2.27)	1 (2.31)	36 (2.33)	26 (2.36)	48 (5)
4058[a]	1166 (3.04)	617 (53)	78 (2.61)	22 (2.54)	191 (16)	44 (3.03)	8 (2.88)	35 (3.14)	13 (3.25)	33 (3)
4059[a]	705 (3.09)	448 (64)	46 (2.75)	54 (2.80)	56 (8)	43 (3.16)	7 (2.75)	32 (3.48)	20 (3.38)	41 (6)
4060[a]	989 (2.98)	306 (31)	50 (2.49)	50 (2.37)	412 (42)	14 (2.92)	11 (2.83)	43 (2.88)	32 (3.17)	85 (9)

The average cell length (μm) in each subpopulation is given within brackets.

[a]*Cells grown at 32°C; doubling time Td = ~150 min.*

[b]*Cells grown at 28°C (Td = 180 min) showing smaller cell lengths (see Materials and Methods).*

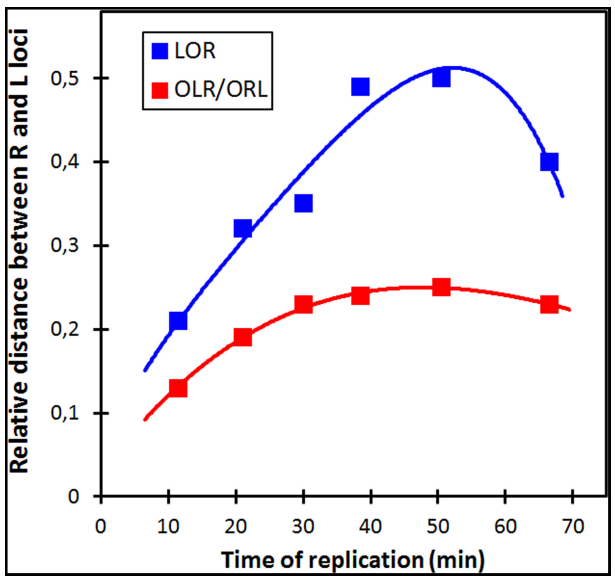

FIGURE 2 | Relative distances between L and R loci for the two different configurations of 3-spot cells. See Table S2 for SD values. For each strain the distances between the L and R spots in the two different configuration types were measured and normalized to the average cell length. The distances are plotted as a function of the time of replication of the loci (see legend to **Figure 1A**).

giving rise to the cells with 6 spots, discussed in the next section.

Analysis of Six-Spot Patterns in Growing Cells

Table 1B presents the cells which have replicated and segregated the three loci thus containing 6 spots. The spot patterns appeared to be very variable. With the 3 spots doubling to 6 spots, a range of 40–70 different patterns were obtained for the six constructs. Except for strain FH4060 the most predominant patterns are those shown in columns VI and VIII of **Table 1B**. The pattern in column VIII will upon division give rise to LOR cells shown in column I of **Table 1A** and the patterns shown in column VI will give rise to the 3-spot patterns shown in column I (LOR) and II (OLR/ORL) of **Table 1A**.

Cells which still have the origins lying outside (ORL LRO) occur in relatively low percentages (column VII in **Table 1B**) and are in all cases the smallest of the 6 spot cells. This suggests that origins which are located at the quarter position relatively early in the cell cycle soon are passed by one or both of the newly replicated loci. Only in construct FH4060, where the loci lie close to the terminus, many of the duplicated L- and R- spots did not pass the origins probably reflecting that these loci, which have the terminus located in between them, remain close for some time after replication. This may reflect a slow movement of loci in the terminal region of the nucleoid up to the division of the cell.

Patterns where the loci on either the Left or Right arm remain adjacent are less frequent (columns IX and X in **Table 1B**). Patterns where loci on both the Left and Right arm remain adjacent (e.g. OLL RRO) are rarely observed (<1% of the cells with 6 spots), indicating a fast separation of duplicated spots along the length axis of the cell, thereby passing loci on the other chromosome arm. However, patterns with adjacent LL or RR spots do occur with an average of 4% in subpopulations of long cells (>3.5 μm). This could indicate that such cells may have experienced an unusual difficulty in replication (and thus segregation) or an extended cohesion time (see Wang et al., 2008), that postponed cell division.

While a minority of the cells show either ajacent loci on the Left or Right arm (columns IX and X in **Table 1B**), cells with all three duplicated loci remaining next to each other (LLOORR) have not been observed. We conclude that both the origin and the loci at different positions on the chromosome arms separate soon after their replication. The observed patterns are well in agreement with movements of chromosome arms as previously described by Nielsen et al. (2006a,b) and Wang et al. (2006).

Segregation Patterns during Run-off DNA Replication in Non-Growing Cells

When cell growth is stopped by inhibiting protein synthesis (Maaløe and Hanawalt, 1961) or RNA synthesis (Lark, 1972), ongoing rounds of DNA replication terminate as is seen by both flow cytometry (Michelsen et al., 2003; Nielsen et al., 2006a), and image cytometry (Huls et al., 1999) of similar samples. To investigate whether segregation of chromosome arms still takes place under such conditions, spot patterns were determined in cells of *E. coli* strain FH4035 treated with 300 μg/ml rifampicin for 210 min at 28°C (cf. Skarstad et al., 1986). If replicated spots would not segregate in rifampicin treated cells we would expect to observe a high percentage of cells with adjacent spots (LLOORR).

For comparison of nucleoid sizes and shapes, cells were also treated with chloramphenicol under the same conditions. **Figure 3** shows the various cell samples fixed with osmium tetroxide and stained with DAPI for visualizing and measuring nucleoids. In contrast to the control cells showing a skewed distribution of nucleoid lengths (average 1.21 μm), the rifampicin-treated cells showed a bimodal distribution with peaks at 0.77 and 1.5 μm (results not shown). It seems probable that these peaks represent 1 and 2 chromosome equivalents.

We performed three independent growth experiments in which cells of strain FH4035 were treated with 300 μg/ml rifampicin for 210 min. These populations were analyzed for spot patterns and the combined results are shown in **Table 2**, together with the data of strain FH4035 given in **Tables 1A,B**, as a reference.

Rifampicin treatment caused a decrease of average cell length from 2.55 to 2.37 μm. This can be attributed to residual divisions, also indicated by the decrease in the percentage of cells with divided nucleoids (from 15 to 9%) and of constricted cells from 14% in the control to 3% in the rifampicin-treated samples (results not shown). Also because of residual division, the percentage of cells with 3 spots increased (3rd column in **Table 2**). In these 3-spot cells the distributions of individual spots in the rifampicin-treated cells are similar to those in the control (results not shown). The nucleoid organization in the 3-spot cells is also very similar to that in the untreated cells, the L-O-R configuration being found in 74% of the rifampicin cells (data not shown) vs. 77% for the control cells (**Table 1A**, column I).

TABLE 1B | Percentages of most abundant patterns of 6 spots in cells with replicating or replicated chromosomes of the different constructs (see Figure 1A).

Strains	Number cells with 6 spots (mean cell length, μm)	% of total population	Percentage of 6-spot patterns					
			VI ORL ROL/OLR LOR	VII OLR LRO	VIII LOR LOR	IX LOR RLO/ROL LRO	X ROL LOR/LOR ROL	Other combi-nations (% of total population)
			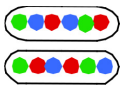	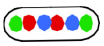		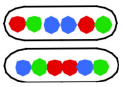	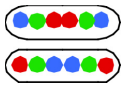	
4056[a] 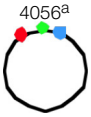	603 (3.80)	44	20 (3.85)	5 (3.64)	22 (3.92)	10 (3.67)	9 (3.96)	34 (2)
4057[a] 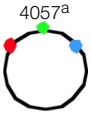	318 (4.04)	29	27 (4.11)	4 (3.92)	28 (4.19)	8 (3.99)	8 (4.04)	25 (2)
4035[b]	412 (3.02)	41	23 (2.89)	7 (2.79)	22 (3.23)	17 (3.02)	15 (3.10)	16 (2)
4058[a]	243 (3.89)	21	28 (3.82)	7 (3.60)	24 (4.07)	14 (3.88)	10 (4.31)	17 (2)
4059[a]	120 (3.97)	17	15 (4.05)	5 (3.75)	15 (3.82)	12 (4.16)	7 (4.14)	46 (7)
4060[a] 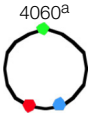	132 (3.85)	13	32 (4.05)	21 (3.66)	11 (4.24)	12 (4.01)	0	24 (2)

The average cell length (μm) in each subpopulation is given within brackets.
[a]Cells grown at 32°C; doubling time Td = ~150 min.
[b]Cells grown at 28°C (Td = 180 min) showing smaller cell lengths (see Materials and Methods.

Due to continued replication, the percentage of cells with 4 spots (only the origin replicated) and 5 spots decreased dramatically causing an increase in the percentage of 6-spot cells (6th column in **Table 2**).

To better compare the patterns in cells with replicated arms (6 spots), **Table 2** shows the same numbering of columns VI–X as used in **Table 1B**. The percentages of cells in **Table 2** showing either one (column VI or IX) or two origin spots (column VII) lying outside of the Left- and Right-arm loci have decreased in comparison to the control cells, whereas the percentage of cells showing the LOR LOR pattern (column VIII) or other patterns with the origin spot between the Left and Right arm (column X) have increased. The percentages in columns IX and X reflect the same trend as in the control. Apparently, the patterns in columns VIII and X can be considered to be a final stage of segregation, while the patterns in column VI, VII, and IX reflect a class of cells that is still in the process of segregation.

In view of (i) the significantly decreased percentage of cells with 4 or 5 spots, (ii) the absence of cells with adjacent LL, OO, RR spots, and (iii) the decrease in percentage of cells showing the origin lying outside of the other loci (columns VI and VII in **Table 2**), we conclude that chromosome movements in non-growing cells occur in a similar way as in growing cells, placing the two arms in different halves of the nucleoid with the origin in between.

Analysis of Segregation Distances between Spot Pairs (LL, RR) and Loci on Different Arms (LR)

The schematic cell images included in **Tables 1**, **2** suggest a seemingly ordered, lengthwise distribution of duplicated loci.

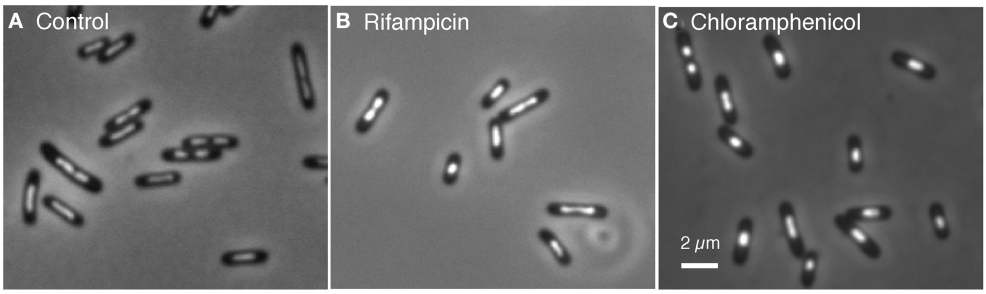

FIGURE 3 | Cells of *E. coli* FH4035, grown in glycerol minimal medium at 28°C, were treated during 100 min with the indicated inhibitors, fixed with 0.1% OsO4 and stained with 10 μg/ml DAPI. (A) In the control cells divided and well separated nucleoids occur in 15% of the cells. **(B)** In rifampicin-treated cells only 9% of the cells show divided nucleoids. **(C)** In chloramphenicol-treated cells the nucleoids (only 3% divided) have a more spherical shape.

TABLE 2 | Percentages of most abundant patterns in cells of strain FH4035, during growth (cf. Tables 1A,B) and after inhibition with rifampicin (300 μg/ml for 210 mi.

Cells	Total nr. cells with spots	% cells with 3 spots	% cells with 4 spots	% cells with 5 spots	% cells with 6 spots	Percentage of patterns in cells with 6 spots					
						VI ROL RLO/LOR LRO	VII ORL RLO	VIII LOR LOR	IX ORL LOR/OLR ROL	X ROL LOR/LOR ROL	Other combinations
Control[a]	1003 (2.55)	38	13	5	41	23 (2.89)	7 (2.79)	22 (3.23)	17 (3.02)	15 (3.10)	16
Rifampicin[b]	2065 (2.37)	46	1	1	49	13 (2.69)	2 (2.34)	25 (2.86)	12 (2.72)	20 (2.82)	28

The average cell length (μm) for each subpopulation s given within brackets.

[a] *Strain FH4035; compare with data in* ***Tables 1A,B****.*

[b] *Cells of strain FH4035 treated with rifampicin; data from three independent growth experiments have been averaged.*

However, in many cells the two groups of duplicated L-, O-, and R-spots are irregularly positioned along the length axis (see **Figure 1B**). To get a better insight in the positioning and movement of the loci, we determined the distances over which duplicated spots, i.e., spot pairs replicated from the same chromosome arm (L-L and R-R distances), have migrated to opposite cell halves. Depending on the spot pattern and thus the Left/Right arm configuration, the distances between spot pairs will differ. But how will the segregation distance between spot pairs differ in dependence of the distance of the loci from the origin? **Table 3** shows that for the LRLR pattern these distances remain more or less constant in the first 5 constructs. For the RLLR pattern the R-R distances tend to increase, while the L-L distances decrease with their distance from the origin. For the LRRL pattern the opposite behavior is observed (see also Figure S3). For all arm configurations the distances in the last construct (FH4060) are smaller. A possible explanation is that these terminus-proximal loci remain tethered together by the terminus region (see Espéli et al., 2012).

As to be expected, in cells with the RLLR or LRRL configuration, the mean distance between spot pairs on the outer arms is significantly larger than on the inner arms (see **Table 3**). For the LRLR ordering the mean segregation distance between the origins (O-O distance) is slightly larger (1.57 μm) than between the loci on either the Right arm (R-R distance) or the Left arm (L-L distance), which are similar for the first 5 constructs (**Table 3**).

For the rifampicin-treated cells (last row in **Table 3**) it can be seen that all segregation distances are about 0.3 μm smaller than in the growing cells, and cell length is also 0.3 μm smaller. The percentage of cells showing the LRLR ordering pattern has decreased from 57% in the control cells of FH4035, to an average of 52% in the FH4035 cultures treated with rifampicin (**Table 3**). This could indicate a more random segregation with respect to whether either the leading or the lagging strand moves faster (Wang et al., 2005) in growth-inhibited cells.

We conclude that in the majority of cells showing the LRLR configuration, spot pairs segregate over equal distances independent of their distance from the origin (Figure S3). This is in accordance to the movements of chromosome arms as previously described by Nielsen et al. (2006a,b) and Wang et al. (2006). Also in rifampicin-treated cells with the LRLR configuration different spot pairs segregate during run-off DNA synthesis over equal but slightly shorter distances. In contrast, the L-R distances show an increase as a function of the time of replication, except for the latest replicated loci (68 min; **Figure 2**

TABLE 3 | Average distances between spot pairs (LL, OO and RR) in 6-spot cells for the three ordering patterns of Left (L) and Right (R) chromosome arms in the different constructs[a].

Strains	Mean length 6-spot cells (μm)	Number 6-spot cells	LRLR				RLLR				LRRL			
			%	Mean distance spot pairs (μm)			%	Mean distance spot pairs (μm)			%	Mean distance spot pairs (μm)		
				L-L	O-O	R-R		L-L	O-O	R-R		L-L	O-O	R-R
4056[b]	3.80 ± 0.78	625	65	1.39 ± 0.54	1.43 ± 0.55	1.33 ± 0.53	14	1.12 ± 0.52	1.43 ± 0.57	1.67 ± 0.60	21	1.83 ± 0.6	1.54 ± 0.64	1.18 ± 0.51
4057[b] 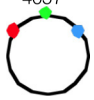	4.04 ± 0.87	326	72	1.49 ± 0.51	1.63 ± 0.54	1.49 ± 0.50	17	1.11 ± 0.44	1.76 ± 0.65	1.91 ± 0.61	12	2.10 ± 0.7	1.63 ± 0.68	1.06 ± 0.51
4035[c]	3.02 ± 0.49	420	57	1.28 ± 0.44	1.49 ± 0.43	1.29 ± 0.47	17	0.96 ± 0.36	1.57 ± 0.46	1.73 ± 0.53	26	1.68 ± 0.5	1.50 ± 0.42	0.91 ± 0.34
4058[b] 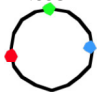	3.89 ± 0.71	243	68	1.51 ± 0.57	1.77 ± 0.57	1.46 ± 0.55	12	0.85 ± 0.44	1.86 ± 0.65	2.21 ± 0.79	20	2.26 ± 0.5	1.91 ± 0.53	0.98 ± 0.34
4059[b]	3.89 ± 0.75	123	65	1.47 ± 0.50	1.53 ± 0.47	1.44 ± 0.50	24	0.81 ± 0.25	1.55 ± 0.55	1.97 ± 0.54	11	1.92 ± 0.5	1.69 ± 0.52	0.68 ± 0.32
4060[b]	3.85 ± 0.61	131	70	1.01 ± 0.46	1.79 ± 0.51	1.10 ± 0.40	16	0.66 ± 0.29	1.68 ± 0.57	1.41 ± 0.60	15	1.37 ± 0.5	1.83 ± 0.49	0.67 ± 0.39
4035 +rifampicin[d]	2.73 ± 0.48	1036	52	1.07 ± 0.36	1.12 ± 0.38	1.07 ± 0.35	30	0.64 ± 0.28	1.09 ± 0.37	1.45 ± 0.42	18	1.51 ± 0.4	1.08 ± 0.41	0.72 ± 0.27

[a] *Spot patterns were qualified using the ObjectJ qualification mode, (cf.* ***Table 1B****).*

[b] *Cells grown at 32°C; doubling time Td = ~150 min.*

[c] *Cells grown at 28°C (Td = 180 min) showing smaller cell lengths (see Materials and Methods).*

[d] *The data of three populations treated with rifampicin have been averaged (cf.* ***Table 2****).*

and Tables S2, S3). In the Discussion below we will consider these results in the light of two proposed segregation models, the doughnut- and the sausage-model.

Discussion

Segregation in Non-Growing Cells

The main conclusion from the present study is that segregation of chromosome arms continues in non-growing cells during run-off DNA replication. This result falsifies a previous proposal that the process of transertion drives DNA segregation (Woldringh, 2002) and supports the hypothesis that segregation is merely driven by the process of *de novo* DNA synthesis and accumulation. Ideas of a replication-driven segregation have been proposed previously by Grossman (Lemon and Grossman, 2001), Hansen (Nielsen et al., 2006a,b), Sherratt (Wang et al., 2006), Austin (Nielsen et al., 2007; Youngren et al., 2014), and Wiggins (Wiggins et al., 2010). A direct link between DNA replication and chromosome organization has been demonstrated and emphasized by the group of Sherratt (Liu et al., 2010), who also presented evidence that transertion played no role in *E. coli* chromosome segregation (Wang and Sherratt, 2010).

Doughnut and Sausage Models for Segregation

Two different models have been suggested for explaining observations on the position and movement of fluorescent DNA loci in *E. coli* cells, the doughnut model (Niki et al., 2000) and the sausage model (Wang et al., 2006; Liu et al., 2010).

In the doughnut model newly replicated DNA is deposited in parallel by the replisomes resulting in a separation of the arms in the short axis of the cell (**Figure 4A**, panels 2, 3). This mode of segregation is reminiscent of the situation in *Caulobacter* (Toro and Shapiro, 2010), but has also been observed in fast-growing *E. coli* cells (Youngren et al., 2014).

As depicted for the doughnut model (**Figure 4A**), the replicated origins move to and remain positioned at the polar ends of the developing nucleoid until division (**Figure 4A**, panel 4). In rapidly growing cells this polar position of the origins and the parallel orientation of the chromosome arms in the short axis is maintained during the next round of replication. In these cells replication occurs at their quarter positions (see Figure 7 in Youngren et al., 2014), giving rise to a branched doughnut structure with partial overlap of chromosome arms of different replication cycles. However, in slow-growing cells, replication initiates in the center of the cell (Reyes-Lamothe et al., 2008). The doughnut model therefore requires a reorientation of the origin by a "sliding movement" that places the two chromosome arms in the two halves of the nucleoid along the cell length axis with the origin in the cell center (Niki et al., 2000; see **Figure 4A**, panels 1a,b). The developing nucleoid arms have the earliest replicated loci (colored circles in **Figure 4**) moved further

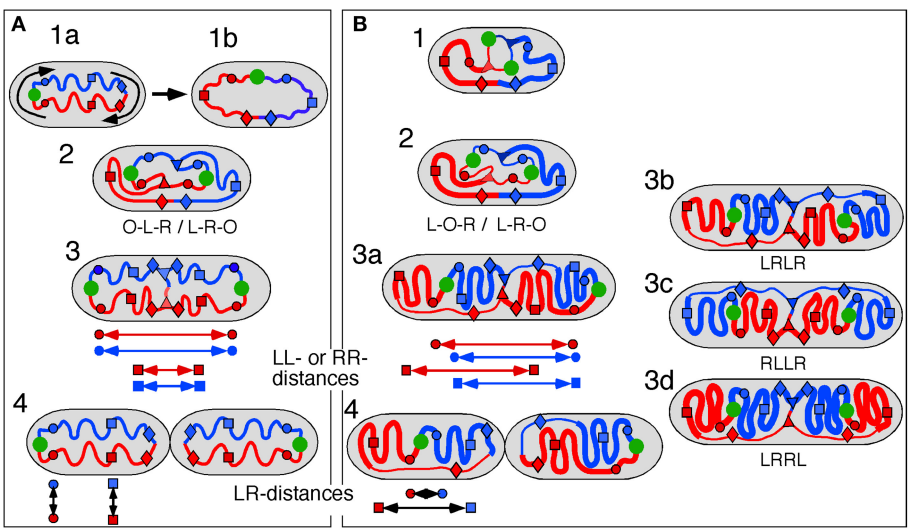

FIGURE 4 | Schematic representation of doughnut and sausage models. Green circle, origin; red and blue circles, origin-proximal loci; red and blue squares, origin-distal loci; red and blue diamonds, terminus-proximal loci; red and blue triangles, replisomes; double arrows indicate distances between loci. **(A)** Doughnut model. The drawings are based on the assumption of parallel, symmetric deposition of the daughter strands leading to a configuration with both origins at the end of the nucleoid (OLR/LRO; panels 3, 4). The circular nucleoid (panel 1a) has to be re-arranged to bring the origin and terminus to the cell center before replication initiates (panel 1b). The model illustrates distances between spot pairs (LL-distances; panel 3) decreasing with their distance from the origin, whereas LR-distances (panel 4) remain constant for origin-proximal and origin-distal loci. **(B)** Sausage model. Replicating chromosome leading to both LOR and LRO configurations (panel 2). The drawings are based on the assumption of an alternating, asymmetric deposition of the daughter strands, which requires stretched regions of replicated DNA to feed the newly developing nucleoids (thin lines). The model illustrates equal distances between spot pairs (LL-distances; panels 3a,b) and an increase in LR-distance for origin-distal loci (panel 4). Cells with the arm configuration LRLR, show LL- and RR-distances that are the same (cf. panels 3a,b); cells with the LRRL configuration show that the LL-distance increases and the RR-distance decreases with distance from the origin (panel 3c); cells with the RLLR configuration, show the LL-distance to decrease and the RR-distance to increase with distance from the origin (panel 3d).

apart than later replicated loci (colored squares in **Figure 4**). This causes a decrease in the distance between replicated loci pairs (LL and RR) with their distance from the origin (**Figure 4A**, panel 3). In contrast, the distances between loci on the parallel arms (L-R-distances) remain constant (**Figure 4A**, panel 4).

In the sausage model, depicted in **Figure 4B**, the replicated origins remain in the center of the nucleoid (**Figure 4B**, panel 2), although a polar positioning can also be observed (**Table 1A**, column II; see also **Figure 4B**, panel 3a). To obtain the alternating orientation of chromosome arms in the long axis, newly replicated DNA of each arm is layered to both inner and outer edges of the newly developing nucleoids. This implies that newly replicated DNA of one arm passes the origin and the other arm, possibly by means of a thread-like structure (**Figure 4B**, panels 2, 3b). In this way, both the earliest and the later replicated loci show similar distances between loci pairs (LL and RR), independent of their distance from the origin (**Figure 4B**, arrows in panel 3a). In contrast, the distances between loci on either arm (LR-distance) increase with their distance from the origin (**Figure 4B**, arrows in panel 4).

Comments on the Doughnut Model

As discussed above, the doughnut model requires a rearrangement of the ring-shaped chromosome before initiation of replication (Niki et al., 2000). A somewhat different reorganization has been proposed by Fisher et al. (2013). In their model, initiation of DNA replication first starts at the polar origin region before one of the daughter strands switches place with unreplicated, parental DNA, placing the terminus in the central part of the nucleoid (see Figure 5B in Fisher et al., 2013). Our data on the 4 spot cells argue against this proposal as we observed very few cells with the OORL configuration even for the most origin proximal RL pair (**Table 1A**).

The high percentage of cells showing the origin outside of the loci on one or two arms (columns II, IIIB and V in **Table 1A** and VI and VII in **Table 1B**) would support the doughnut model (**Figure 4A**). However, an origin lying outside the other loci (OLR-pattern) can still be envisaged to occur from asymmetric, alternating deposition of chromosome arms (see **Figure 4B**, right cell half in panels 2–4). In the 3-spot cells of Figure S2B showing the RLO-pattern, the long axis distributions of L- and R-loci are not fully overlapping as to be expected for the doughnut model (**Figure 4A**, panel 1a).

Comments on the Sausage Model

In the sausage model (Liu et al., 2010; Wiggins et al., 2010) the alternating deposition of replicated DNA to the inner and outer edges of the newly developing nucleoids requires that at least one of the replicated chromosome arms passes the other arm (and the origin). This remote deposition could occur through a thread-like structure (thin lines as depicted in **Figure 4B**). We do not know whether such "feeding threads" exist or how much DNA they contain. They may be revealed by a faster (Brownian) movement of DNA segments through these narrow threads. In the case of a LRLR arm configuration, each replisome forms feeding threads of unequal length resulting in an alternating arm pattern (**Figure 4B**, panel 3b). Presently, indications for the existence of such threads are still lacking.

Concluding Remarks

The results in **Table 3** (see also Figure S3) show that the distances measured between loci pairs (LL and RR) for the different arm configurations stay either constant (LRLR) or show an increase or decrease (LRRL or RLLR) as predicted by the sausage model (**Figure 4B**, panel 3a). Likewise, the distances between loci on the two arms (LR-distances) in the non-replicating (3 spot) cells showing an increase as a function of their distance from the origin (**Figure 3**), conform clearly to the sausage model (**Figure 4B**, panel 4) rather than to the doughnut model (**Figure 4A**, panel 1b). In addition, it should be noted that distributions of spots in the short axis of the present cells did not show the bi-modality as expected for the doughnut model (**Figure 4A**) and as observed in the wide cells of Youngren et al. (2014) (results not shown).

The large variation in the ordering patterns of loci in all constructs suggests that the position and orientation of the nucleoid in the cell is not fixed, so sometimes the origin can lie outside the L and R loci, with a thin thread of DNA extending to the origin close to one pole (**Figure 4B**, panel 3a). This variation is in agreement with the images of nucleoid shape and dynamics obtained by Fisher et al. (2013). Such a flexibility of nucleoid organization and loci positioning is necessary when considering the shape and size changes cells undergo during nutritional shift-up.

At some point during the transition to multifork replication and wider cells, the linear, sausage-like nucleoid will obtain a ring-shaped doughnut structure. Future theoretical work on ring- and linear-polymers will help to understand how, during nutritional shift-up, these two structures move from one state into one another. At present, it only seems clear that in both structures the duplicated origins are separated spontaneously along the cell's long axis by *de novo* DNA synthesis and accumulation and thermodynamic demixing of the newly replicated strands (Youngren et al., 2014).

Segregation can be considered to occur in two stages, (i) the separation of daughter strands or replicated loci as considered here in growing and non-growing cells and (ii) the division of the nucleoid. Because under conditions of inhibited growth nucleoid divisions do not seem to occur (**Figure 3**) it remains possible that an active mechanism like transertion or cell constriction functions in the second stage, the division of the nucleoid in growing cells (see also discussion in Woldringh and Nanninga, 2006).

Acknowledgments

We thank Suckjoon Jun for comments on the manuscript; Alan Leonard, Theo Odijk, Norman Grover, Tanneke

den Blaauwen, Arieh Zaritsky, and Mogens Kilstrup for discussions and Jolanda Verheul and Søs Koefoed for practical help. Some of this work was supported by a grant to FH and TA by the Danish National Science Foundation.

Supplementary Material

The Supplementary Material for this article can be found online at: http://journal.frontiersin.org/article/10.3389/fmicb.2015.00448/abstract

References

Cunha, S., Woldringh, C. L., and Odijk, T. H. (2001). Polymer-mediated compaction and internal dynamics of isolated *Escherichia coli* nucleoids. *J. Struct. Biol.* 136, 53–66. doi: 10.1006/jsbi.2001.4420

Cunha, S., Woldringh, C. L., and Odijk, T. H. (2005). Restricted diffusion of DNA segments within the isolated *Escherichia coli* nucleoid. *J. Struct. Biol.* 150, 226–232. doi: 10.1016/j.jsb.2005.02.004

Espéli, O., Borne, R., Dupaigne, P., Thiel, A., Gigant, E., Mercier, R., et al. (2012). A MatP-divisome interaction coordinates chromosome segregation with cell division in *E. coli*. *EMBO J.* 31, 3198–3211. doi: 10.1038/emboj.2012.128

Fisher, J. K., Bourniquel, A., Witz, G., Weiner, B., Prentiss, M., and Kleckner, N. (2013). Four-dimensional imaging of *E. coli* nucleoid organization and dynamics in living cells. *Cell* 153, 882–895. doi: 10.1016/j.cell.2013.04.006

Fritsche, M., Li, S., Heermann, D. W., and Wiggins, P. A. (2011). A model for *Escherichia coli* chromosome packaging supports transcription factor-induced DNA domain formation. *Nucleic Acids Res.* 40, 972–9801-9. doi: 10.1093/nar/gkr779

Huls, P. G., Vischer, N. O. E., and Woldringh, C. L. (1999). Delayed nucleoid segregation in *Escherichia coli*. *Mol. Microbiol.* 33, 959–970. doi: 10.1046/j.1365-2958.1999.01535.x

Jun, S., and Wright, A. (2010). Entropy as the driver of chromosome segregation. *Nat. Rev. Microbiol.* 8, 600–607. doi: 10.1038/nrmicro2391

Lark, K. G. (1972). Evidence for the direct involvement of RNA in the initiation of DNA replication in *Escherichia coli* 15T-. *J. Mol. Biol.* 64, 47–60. doi: 10.1016/0022-2836(72)90320-8

Le Chat, L., and Espéli, O. (2012). Let's get "Fisical" with bacterial nucleoid. *Mol. Microbiol.* 86, 1285–1290. doi: 10.1111/mmi.12073

Lemon, K. P., and Grossman, A. D. (2001). The extrusion-capture model for chromosome partitioning in bacteria. *Genes Dev.* 15, 2031–2041. doi: 10.1101/gad.913301

Liu, X., Wang, X., Reyes-Lamothe, R., and Sherratt, D. (2010). Replication-directed sister chromosome alignment in *Escherichia coli*. *Mol. Microbiol.* 75, 1090–1097. doi: 10.1111/j.1365-2958.2009.06791.x

Luijsterburg, M. S., Noom, M. C., Wuite, G. J., and Dame, R. T. (2006). The architectural role of nucleoid-associated proteins in the organization of the bacterial chromatin: a molecular perspective. *J. Struct. Biol.* 156, 262–272. doi: 10.1016/j.jsb.2006.05.006

Maaløe, O., and Hanawalt, P. C. (1961). Thymine deficiency and the normal DNA replication cycle. I. *J. Mol. Biol.* 3, 144–155. doi: 10.1016/S0022-2836(61)80041-7

Mason, D. J., and Powelson, D. M. (1956). Nuclear division as observed in live bacteria by a new technique. *J. Bacteriol.* 71, 474–479.

Michelsen, O., Teixeira de Mattos, M. J., Jensen, P. R., and Hansen, F. G. (2003). Precise determinations of C and D periods by flow cytometry in *Escherichia coli* K-12 and B/r. *Microbiology* 149, 1001–1010. doi: 10.1099/mic.0.26058-0

Nielsen, H. J., Li, Y., Youngren, B., Hansen, F. G., and Austin, S. J. (2006a). Progressive segregation of the *Escherichia coli* chromosome. *Mol. Microbiol.* 61, 383–393. doi: 10.1111/j.1365-2958.2006.05245.x

Nielsen, H. J., Ottesen, J. R., Youngren, B., Austin, S. J., and Hansen, F. G. (2006b). The *Escherichia coli* chromosome is organized with the left and right chromosome arms in separate cell halves. *Mol. Microbiol.* 62, 331–338. doi: 10.1111/j.1365-2958.2006.05346.x

Nielsen, H. J., Youngren, B., Hansen, F. G., and Austin, S. (2007). Dynamics of *Escherichia coli* chromosome segregation during multifork replication. *J. Bacteriol.* 189, 8660–8666. doi: 10.1128/JB.01212-07

Niki, H., Yamaichi, Y., and Hiraga, S. (2000). Dynamic organization of chromosomal DNA in *Escherichia coli*. *Genes Dev.* 14, 212–223. doi: 10.1101/gad.14.2.212

Odijk, T. (1998). Osmotic compaction of supercoiled DNA into a bacterial nucleoid. *Biophys. Chem.* 73, 23–29. doi: 10.1016/S0301-4622(98)00115-X

Pelletier, J., Halvorsen, K., Ha, B.-Y., Paparcone, R., Sandler, S. J., Woldringh, C. L., et al. (2012). Physical manipulation of the *Escherichia coli* chromosome reveals its soft nature. *Proc. Natl. Acad. Sci. U.S.A.* 109, E2649–E2656. doi: 10.1073/pnas.1208689109

Reyes-Lamothe, R., Possoz, C., Danilova, O., and Sherratt, D. J. (2008). Independent positioning and action of *Escherichia coli* replisomes in live cells. *Cell* 133, 90–102. doi: 10.1016/j.cell.2008.01.044

Skarstad, K., Boye, E., and Steen, H. B. (1986). Timing of initiation of chromosome replication in individual *Escherichia coli* cells. *EMBO J.* 5, 1711–1717.

Toro, E., and Shapiro, L. (2010). Bacterial chromosome organization and segregation. *Cold Spring Harb. Perspect. Biol.* 2:a000349. doi: 10.1101/cshperspect.a000349

Wang, X., Liu, X., Possoz, C., and Sherratt, D. J. (2006). The two *Escherichia coli* chromosome arms locate to separate cell halves. *Genes Dev.* 20, 1727–1731. doi: 10.1101/gad.388406

Wang, X., Possoz, C., and Sherratt, D. J. (2005). Dancing around the divisome: asymmetric chromosome segregation in *Escherichia coli*. *Genes Dev.* 19, 2367–2377. doi: 10.1101/gad.345305

Wang, X., Reyes-Lamothe, R., and Sherratt, D. J. (2008). Modulation of *Escherichia coli* sister chromosome cohesion by topoisomerase IV. *Genes Dev.* 22, 2426–2433. doi: 10.1101/gad.487508

Wang, X., and Sherratt, D. J. (2010). Independent segregation of the two arms of the *Escherichia coli ori* region requires neither RNA synthesis nor MreB dynamics. *J. Bacteriol.* 192, 6143–6153. doi: 10.1128/JB.00861-10

Wiggins, P. A., Cheveralls, K. C., Martin, J. S., Lintner, R., and Kondev, J. (2010). Strong intranucleoid interactions organize the *Escherichia coli* chromosome into a nucleoid filament. *Proc. Natl. Acad. Sci. U.S.A.* 107, 4991–4995. doi: 10.1073/pnas.0912062107

Woldringh, C. L. (2002). The role of co-transcriptional translation and protein translocation (transertion) in bacterial chromosome segregation. *Mol. Microbiol.* 45, 17–29. doi: 10.1046/j.1365-2958.2002.02993.x

Woldringh, C. L., and Nanninga, N. (2006). Structural and physical aspects of bacterial chromosome segregation. *J. Struct. Biol.* 156, 273–283. doi: 10.1016/j.jsb.2006.04.013

Yamaichi, Y., and Niki, H. (2004). *migS*, a cis-acting site that affects bipolar positioning of *oriC* on the *Escherichia coli* chromosome. *EMBO J.* 23, 221–233. doi: 10.1038/sj.emboj.7600028

Yazdi, N. H., Guet, C. C., Johnson, R. C., and Marko, J. F. (2012). Variation of the folding and dynamics of the *Escherichia coli* chromosome with growth conditions. *Mol. Microbiol.* 86, 1318–1333. doi: 10.1111/mmi.12071

Youngren, B., Nielsen, H. J., Jun, S., and Austin, S. (2014). The multifork *Escherichia coli* chromosome is a self-duplicating and self-segregating thermodynamic ring polymer. *Genes Dev.* 28, 71–84. doi: 10.1101/gad.231050.113

Zechiedrich, E. L., Khodursky, A. B., Bachellier, S., Schneider, R., Chen, D., Lilley, D. M. J., et al. (2000). Roles of topoisomerases in maintaining steady-state

DNA supercoiling in *Escherichia coli*. *Biol. Chem.* 275, 8103–8113. doi: 10.1074/jbc.275.11.8103

Conflict of Interest Statement: The authors declare that the research was conducted in the absence of any commercial or financial relationships that could be construed as a potential conflict of interest.

Copyright © 2015 Woldringh, Hansen, Vischer and Atlung. This is an open-access article distributed under the terms of the Creative Commons Attribution License (CC BY). The use, distribution or reproduction in other forums is permitted, provided the original author(s) or licensor are credited and that the original publication in this journal is cited, in accordance with accepted academic practice. No use, distribution or reproduction is permitted which does not comply with these terms.

frontiers in Microbiology

REVIEW
published: 02 July 2015
doi: 10.3389/fmicb.2015.00636

The spatial biology of transcription and translation in rapidly growing *Escherichia coli*

*Somenath Bakshi†, Heejun Choi and James C. Weisshaar**

Department of Chemistry and Molecular Biophysics Program, University of Wisconsin-Madison, Madison, WI, USA

Single-molecule fluorescence provides high resolution spatial distributions of ribosomes and RNA polymerase (RNAP) in live, rapidly growing *Escherichia coli*. Ribosomes are more strongly segregated from the nucleoids (chromosomal DNA) than previous widefield fluorescence studies suggested. While most transcription may be co-translational, the evidence indicates that most translation occurs on free mRNA copies that have diffused from the nucleoids to a ribosome-rich region. Analysis of time-resolved images of the nucleoid spatial distribution after treatment with the transcription-halting drug rifampicin and the translation-halting drug chloramphenicol shows that both drugs cause nucleoid contraction on the 0–3 min timescale. This is consistent with the transertion hypothesis. We suggest that the longer-term (20–30 min) nucleoid expansion after Rif treatment arises from conversion of 70S-polysomes to 30S and 50S subunits, which readily penetrate the nucleoids. Monte Carlo simulations of a polymer bead model built to mimic the chromosomal DNA and ribosomes (either 70S-polysomes or 30S and 50S subunits) explain spatial segregation or mixing of ribosomes and nucleoids in terms of excluded volume and entropic effects alone. A comprehensive model of the transcription-translation-transertion *system* incorporates this new information about the spatial organization of the *E. coli* cytoplasm. We propose that transertion, which radially expands the nucleoids, is essential for recycling of 30S and 50S subunits from ribosome-rich regions back into the nucleoids. There they initiate co-transcriptional translation, which is an important mechanism for maintaining RNAP forward progress and protecting the nascent mRNA chain. Segregation of 70S-polysomes from the nucleoid may facilitate rapid growth by shortening the search time for ribosomes to find free mRNA concentrated outside the nucleoid and the search time for RNAP concentrated within the nucleoid to find transcription initiation sites.

Keywords: single-molecule tracking live cell, *E. coli*, ribosomes, RNA polymerase, nucleoid structure, DNA-ribosome spatial segregation

OPEN ACCESS

Edited by:
Conrad L. Woldringh, University of Amsterdam, Netherlands

Reviewed by:
Vic Norris, University of Rouen, France
Suckjoon Jun, University of California, San Diego, USA

****Correspondence:***
James C. Weisshaar, Department of Chemistry and Molecular Biophysics Program, University of Wisconsin-Madison, Madison, WI 53706, USA
weisshaar@chem.wisc.edu

†Present address:
Somenath Bakshi, Department of Systems Biology, Harvard Medical School, Boston, MA 02115, USA
somenath_bakshi@hms.harvard.edu

Specialty section:
This article was submitted to Microbial Physiology and Metabolism, a section of the journal Frontiers in Microbiology

Received: *30 March 2015*
Accepted: *12 June 2015*
Published: *02 July 2015*

Citation:
Bakshi S, Choi H and Weisshaar JC (2015) The spatial biology of transcription and translation in rapidly growing Escherichia coli. Front. Microbiol. 6:636. doi: 10.3389/fmicb.2015.00636

Introduction

Super-resolution fluorescence methods (Betzig et al., 2006; Hess et al., 2006; Rust et al., 2006) enable detailed exploration of the ways in which the central dogma of molecular biology plays out in *Escherichia coli*. "Photoactivation-localization microscopy" (PALM) can locate and track 1000s of copies of single, specific proteins *in live cells* with ~30 nm spatial resolution and low-ms

time resolution. This has enabled detailed, quantitative studies of how ribosomes (Bakshi et al., 2012), chromosomal DNA (Wang et al., 2011), and RNA polymerase (RNAP; Bakshi et al., 2012, 2013; Endesfelder et al., 2013) are distributed in space and move in time within the cytoplasm of single cells. In addition, time-resolved widefield fluorescence imaging after drug treatment has provided new insight into the ways in which transcription and translation determine the internal organization of cytoplasm (Bakshi et al., 2014a). Transcription, translation, and the spatial organization of *E. coli* cytoplasm act as a coupled biochemical–biophysical system. Here, we describe the delicate balance of forces that enables the system to drive rapid cell growth.

In *E. coli*, the chromosomal DNA occupies the region of space called the *nucleoids* (Kellenberger, 1991). During rapid growth, ribosomes are concentrated outside the nucleoids in *ribosome-rich regions* comprising the two polar end-caps, the space between nucleoid lobes, and the thin region proximal to the cytoplasmic membrane (**Figure 1**; Bakshi et al., 2012). The spatial extent of the nucleoids evidently arises from a balance of compacting and expanding forces (Woldringh et al., 1995; Zimmerman, 2006). Likely compacting forces include depletion-attraction of DNA arising from macromolecular crowding by myriad small proteins (Zimmerman and Murphy, 1996); conformational entropy of the confined DNA polymer, which causes the polymer to avoid walls (Mondal et al., 2011; Bakshi et al., 2014a); inter-strand coupling by DNA binding proteins such as H-NS (Dame, 2005; Wang et al., 2011); bending of DNA by IHF (Dame, 2005); and net supercoiling of the DNA by Gyrase and Topoisomerase I (Woldringh et al., 1995). The hypothesized primary expanding force is "*transertion,*" which is the simultaneous co-transcriptional translation *and insertion* of membrane proteins via the translocon machinery (Woldringh, 2002). Transertion implies the existence of DNA-RNAP-mRNA-ribosome-polypeptide-membrane *"transertion chains"* directly linking DNA to the membrane (**Figure 1**). A sufficient number of these chains would radially expand the overall nucleoid. The main evidence for transertion had been the dramatic contraction of the nucleoids on treatment with translation-halting drugs such as chloramphenicol (van Helvoort et al., 1996; Zimmerman, 2002). Treatment with transcription-halting drugs such as rifampicin should have the same effect, but this was not observed on the 30-min timescale studied (Fishov and Woldringh, 1999; Cabrera et al., 2009). Our recent time-dependent imaging study

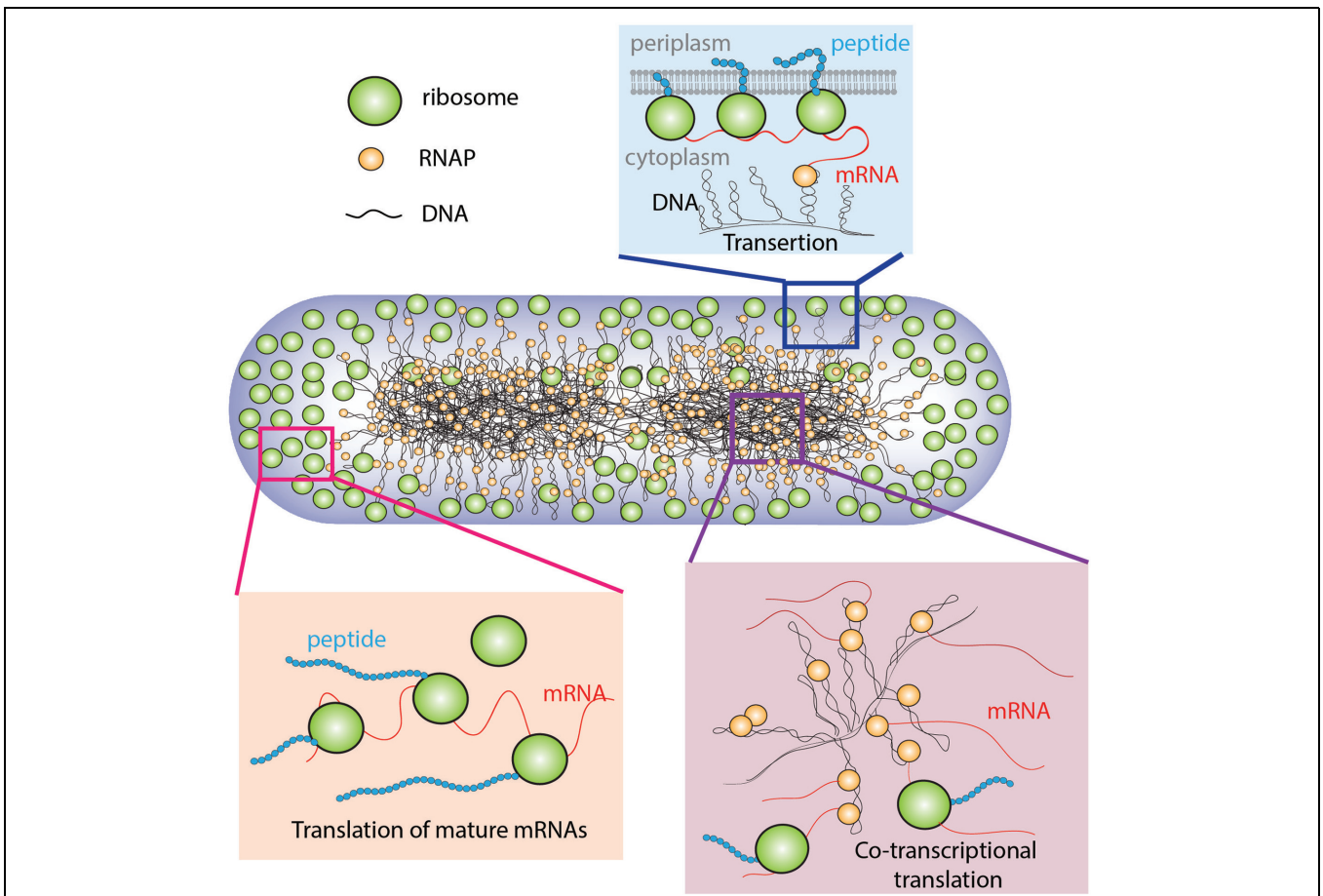

FIGURE 1 | Schematic of the coupled transcription–translation–transertion system in rapidly growing *Escherichia coli*. Adapted from Bakshi et al. (2014a).

discovered nucleoid contraction on a 3-min timescale after rifampicin treatment, placing the transertion hypothesis on solid footing (Bakshi et al., 2014a).

In rapidly growing *E. coli*, only 10–15% of ribosomal subunits lie within the nucleoids (Bakshi et al., 2012). Single-30S subunit tracking studies suggest that most 30S subunits in the ribosome-rich regions are engaged as slowly diffusing 70S-polysomes. The majority of the translation events are presumably carried out on mature, freely diffusing mRNAs within the ribosome-rich regions. While *co-transcriptional* translation (coupled transcription and translation; Miller et al., 1970) is essential for protecting nascent mRNA and ensuring efficient transcription (Burmann et al., 2010, 2012; Proshkin et al., 2010; Svetlov and Nudler, 2012; McGary and Nudler, 2013), it is apparently not the primary means of protein production. The 70S-polysome diffusion coefficient $D_{70S-poly} \sim 0.02\ \mu m^2\ s^{-1}$ is large enough to enable nascent mRNA to diffusively find a ribosome-rich region in ∼1 s (Bakshi et al., 2012), a short period compared with the ∼6–7 min lifetime of mRNA against degradation (Bernstein et al., 2002).

A number of earlier studies used physical models to explain the formation of compact nucleoids that occupy only a fraction of the entire bacterial cytoplasm. A statistical mechanical model used the osmotic effects of myriad small proteins to explain the apparent phase separation (Odijk, 1998). A recent experimental study of free bacterial nucleoids confined in a microfluidic channel showed that crowding by added polyethylene glycine chains (PEG) led to reversible, first-order "coil-to-globule" collapse of the nucleoids (Pelletier et al., 2012). This study augmented the earlier statistical model to include the entropic spring nature of the nucleoids. A very recent coarse-grained simulation showed that small, spherical crowding agents can induce compaction of a DNA polymer, modeled as a freely jointed chain (Shendruk et al., 2015).

We have found that a simple physical model using Monte Carlo simulations of DNA and ribosome spatial distributions in a confining cytoplasmic space enhances our understanding of the observed ribosome-nucleoid segregation (Mondal et al., 2011). In the model, entropic and excluded volume effects cause strong segregation of the unperturbed nucleoid from 70S-polysomes. The biochemical state of ribosomes (70S-polysomes vs. free 30S and 50S subunits) plays an essential role in ribosome-nucleoid segregation. When the model 70S-polysomes are converted to 30S and 50S subunits, the components mix quite thoroughly with the DNA and the nucleoid expands (Bakshi et al., 2014a). This suggests that the fraction of 70S-polysomes vs. 30S and 50S subunits strongly affects the relative compactness of the nucleoid.

Based on these new experimental and computational results, we are developing a comprehensive model of the spatial organization within the *E. coli* cytoplasm and how it may work to optimize cell growth. Our present view encompasses a variety of inter-related phenomena: (1) In rapidly growing cells, *most translation occurs in the ribosome-rich regions*, not within the nucleoids. (2) Yet there is direct evidence of co-transcriptional translation (Miller et al., 1970), and this is important for protecting nascent mRNA from degradation and for efficient transcription. *Evidently most or all transcription is co-translational, but only ∼10–15% of translation is co-transcriptional*. (3) Therefore 30S and 50S subunits must be able to penetrate the nucleoid where they initiate co-transcriptional translation (Sanamrad et al., 2014). This picture implies a *circulation* of 30S and 50S subunits between the nucleoids and the ribosome-rich regions. (4) Transertion expands the nucleoids beyond their relaxed, highly compacted state (Woldringh, 2002). The evidence suggests that transertion plays an essential role, enabling 30S and 50S subunits to move into the nucleoids where they initiate co-transcriptional translation and form nascent 70S-polysomes.

In this view, the transcription and translation machinery and the spatial organization of the cytoplasm act as a coupled biochemical–biophysical system. Effective compartmentalization of the cytoplasm into ribosome-rich regions and DNA- and RNAP-rich nucleoids may enhance the efficiency of protein synthesis and the utilization of RNAP. Segregation of 70S-polysomes from the nucleoid may facilitate rapid growth by minimizing the search time for ribosomes to find the free mRNA concentrated outside the nucleoid and for RNAP concentrated within the nucleoid to find transcription initiation sites. This review describes the evidence behind the comprehensive picture, briefly compares *E. coli* with *Caulobacter crescentus*, and contrasts our "translation-centric" view of nucleoid morphology with a "transcription-centric" view (Jin et al., 2013) presented in another chapter of this volume.

Super-Resolution Imaging of Single Protein Copies in Live Bacterial Cells

Overview

Super-resolution fluorescence microscopy of specific proteins in live cells (**Figure 2**) was enabled by three key technical advances. First, genetic manipulations enable replacement of the gene for the target protein by a gene that appends a fluorescent protein to the target. This "GFP revolution" enables imaging of a specific target protein in a live cell (Zhang et al., 2002). But caution is needed. The fluorescent protein tags may affect the function, aggregation state, spatial distribution, or movement of the target protein (Landgraf et al., 2012).

Second, on a dark background a single fluorescent molecule can produce a punctal, high signal-to-noise image on a sensitive EMCCD camera (Vrljic et al., 2007). However, the full width at half maximum height (FWHM) of this image is broadened to $\sim\lambda/2 = 260$ nm for detection of green light with wavelength $\lambda = 520$ nm. This defines the diffraction limit of light for an optical microscope. Nevertheless, a well-isolated, slowly moving single fluorophore can be located and tracked far more accurately than the diffraction-limited width of its image. In a 1 μm diameter × 3 μm long *E. coli* cell, the localization accuracy for fluorescent proteins is photon- and background-limited to ∼30 nm in each of the two projected dimensions (Bakshi et al., 2011).

Third, the super-resolution fluorescence methods use "photoswitchable" fluorescent proteins as the labels to overcome

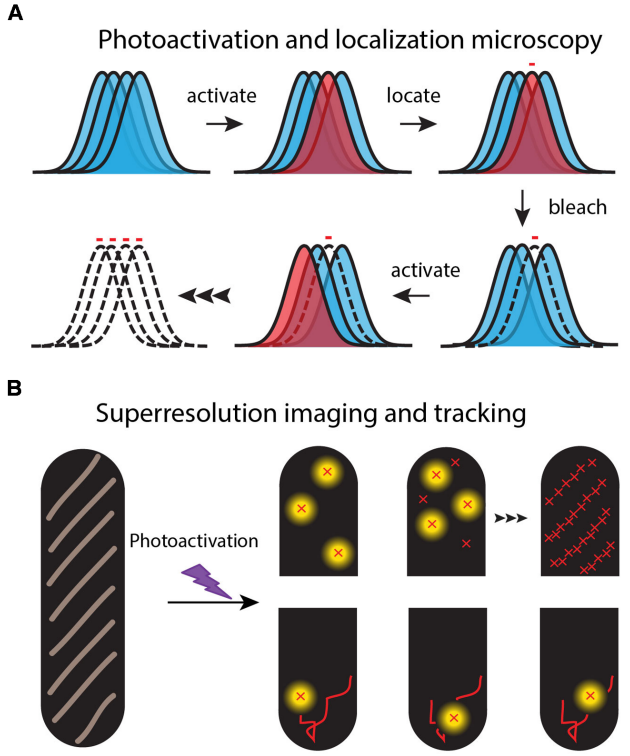

FIGURE 2 | Schematic of the super-resolution imaging method. **(A)** Each fluorescent molecule makes a diffraction-limited, essentially Gaussian image on the camera. A dense set of normal labels (blue images) makes overlapping images. In each imaging cycle, a sparse set of labels is photoactivated (red image) and localized from the well-isolated, single-molecule images. **(B)** An image of the spatial distribution is built up one molecule at a time over 100s or 1000s of optical cycles (upper "half-cells"). Successive images of the same molecule form a diffusive trajectory (lower "half-cells").

the problem of spatial overlap of the myriad images of high copy number fluorescent proteins in small cells (**Figure 2**). For example, PALM and its variations enable sub-diffraction-limit imaging of the ~50,000 labeled 30S-mEos2 ribosomal subunits, essentially by imaging them one or a few copies at a time (Betzig et al., 2006; Rust et al., 2006; Gould et al., 2008). In a widefield fluorescence image, all the 30S images would overlap in space, severely limiting the precision of spatial information (**Figure 2**). Following excitation at shorter wavelengths (typically near 405 nm), photoswitchable proteins undergo photochemistry that shifts their absorption and emission spectra toward longer wavelengths. For the photoswitchable label mEos2, PALM uses weak excitation at 405 nm to create a sparse set of new fluorophores that emit at 584 nm. In each PALM cycle, the few photoswitched copies are located and tracked by excitation with a second probe laser at 561 nm (where the unswitched copies do not absorb). The photoswitched copies bleach all too quickly, after which a new sparse set is photoswitched and tracked. Over several-minutes, literally 1000s of short, 5–15 step trajectories with ~30 nm localization accuracy can be acquired. The stored individual locations are used to reconstruct a PALM image of the two-dimensional spatial distribution of the target protein, averaged over a typical 1–2 min of data acquisition.

The diffusive behavior of each individual copy then provides clues to its biochemical state (Lippincott-Schwartz and Patterson, 2009). For ribosomes, 70S-polysomes diffuse somewhat more slowly than 30S subunits searching for a translation initiation site (Bakshi et al., 2012). Those RNAP copies that are searching for a transcription initiation site diffuse much more rapidly than copies engaged in transcription and thus bound to the DNA polymer (Bakshi et al., 2013). Thus PALM provides not only much more precise spatial distributions than widefield microscopy, but also new information about where specific biochemical processes are carried out within the bacterial cell and the fraction of proteins engaged in each process.

Cell Growth and Preparation

Our preferred *E. coli* strain VH1000 is a modification of MG1655 with the PyrE defect repaired. VH1000 grown in EZRDM ("EZ rich, defined medium"; Neidhardt et al., 1974), MBM (MOPS-buffered minimal medium) using glucose as carbon source, or MBM with glycerol, provides access to a wide range of doubling time (30, 60, and 120 min, respectively, at 37°C). Most of the experiments described here were carried out in EZRDM at 30°C.

We maintain cells at well-defined, constant levels of nutrition and aeration throughout the imaging experiments (Bakshi et al., 2011, 2012). Cells are harvested from exponential growth and plated on a polylysine coated coverslip that forms the base of a microfluidics device providing a continuous flow of fresh, aerated growth medium during imaging. This enables us to study 50–100 cells simultaneously. Length vs. time measurements of single cells shows that they grow at the same rate as in bulk medium to within 5%; evidently there are no harmful effects of the polylysine surface. Visible light can be toxic (Bakshi et al., 2012). It is essential to minimize total photon dosage at 514 or 561 nm. We always ensure that the laser exposure does not alter the property being measured.

Labeling Strategies

The use of λ-Red mediated recombination (Datsenko and Wanner, 2000) to replace wild-type genes on the chromosome with genes for mEos2-labeled proteins has become routine. P1 transduction then transfers the new genes back to the parent strain to eliminate unwanted mutations. Our VH1000 strains expressing the ribosomal protein S2 labeled by mEos2 or the RNAP subunit β′ labeled with mEos2 grow normally. The long time required for mEos2 to achieve its fluorescent state (~130 min) compared to the assembly time of ribosome/RNAP core enzymes (a few min) ensures that we are almost always tracking assembled 30S ribosomal subunits (Bakshi et al., 2012) or complete RNAP enzymes (Bakshi et al., 2013). As a test for possible adverse effects of the labels (Landgraf et al., 2012), we showed that for both β′ and S2, the mEos2 and yGFP labeling schemes produce indistinguishable spatial distributions and diffusive properties.

To image the overall spatial distribution of DNA in growing cells, we strongly prefer the non-perturbative stain SYTOX

Orange over the more standard DAPI imaging (Bakshi et al., 2014a,b). DAPI staining plus UV light perturbs growth rate and nucleoid morphology. SYTOX Orange staining enables normal growth and widefield imaging over 100s of camera frames.

Single-Molecule Localization and Tracking Methodology

The mEos2 constructs yield trajectories of mean length 10 frames and enable control of the time between frames. For each 1000 trajectories, we obtain ~150 trajectories of length >18 frames. We spatially filter the images and fit single-molecule locations using a centroid algorithm (Wang et al., 2010; Bakshi et al., 2011, 2012). Images of cells are rotated so that the long axis is x and the short, transverse axis is y. By plotting a point at the (x, y) coordinates of each centroid, we produce a high-resolution, two-dimensional (2D) projection of the 3D spatial distribution, averaged over the several-minute acquisition period.

A sequence of locations for a particular particle forms a diffusive trajectory. We analyze single-molecule diffusion data in a variety of ways. Plots of mean-square displacement vs. lag time τ, $MSD(\tau)$, are obtained as a running average over each trajectory and over all molecules. To test for sub-diffusion effects due to tethering or caging, $MSD(\tau)$ is compared with Monte Carlo random walk (free diffusion) model calculations within an appropriate confinement volume. To test for heterogeneity of diffusion, we compute histograms of single-molecule diffusion coefficients, estimated as $D_i = \mathrm{msd}_i(\tau)/4\tau$, where $\mathrm{msd}_i(\tau)$ is the single-molecule mean-square displacement averaged over *one trajectory*. The aspect ratio of trajectories can also help distinguish sub-diffusion from free diffusion of single-molecules (Bakshi et al., 2013).

Ribosome-Nucleoid Segregation in Rapid, Exponential Growth

Background

Miller et al. (1970), in their EM study of the contents of the *E. coli* cytoplasm observed long DNA strands to which chains of ribosomes ("70S-polysomes") were attached, direct evidence of translation coupled to transcription ("co-transcriptional translation"). That study inferred that *all* bacterial protein synthesis was co-transcriptional. The total amount of mRNA per cell and the ribosome copy number confirm the importance of polysomes and suggest their typical length to be about ten 70S per mRNA. Co-transcriptional translation evidently assists optimal cell growth. It helps protect nascent mRNA against early termination by Rho and against premature degradation by ribonucleases (Proshkin et al., 2010; McGary and Nudler, 2013). In addition, specific proteins bind simultaneously to both RNAP and the lead ribosome in a polysome chain (Burmann et al., 2012; Svetlov and Nudler, 2012). The translating lead ribosome helps to prevent undesirable RNAP backtracking (Burmann et al., 2010).

However, evidence from EM studies of sections of fixed *E. coli* cells (Kellenberger, 1991) and from widefield immuno-staining of whole, fixed cells (Azam et al., 2000) argued against a model in which all translation is co-transcriptional. The images showed a strong tendency of ribosomes to avoid the nucleoids. Early widefield fluorescence studies in fixed *Bacillus subtilis* co-imaged DNA and ribosomes and again demonstrated strong segregation of ribosomes from DNA (Lewis et al., 2000).

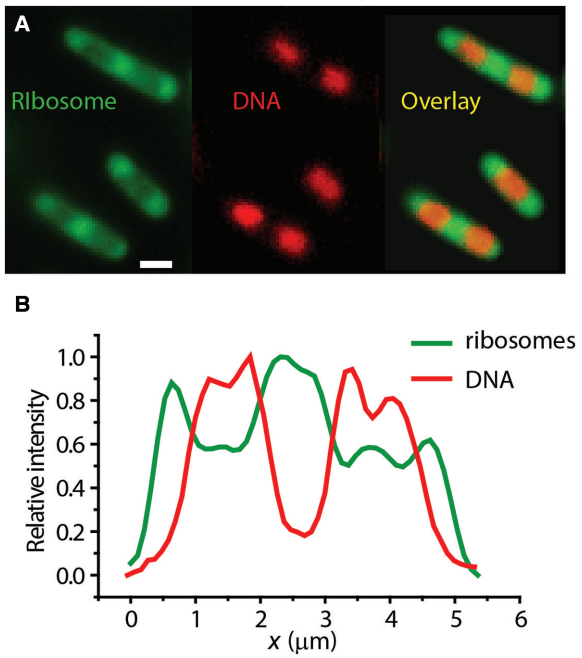

FIGURE 3 | (A) Widefield images of ribosomes (S2-YFP labeling) and DNA (DRAQ5 staining) in single *E. coli* cells. **(B)** Axial linescans of ribosome and DNA intensity vs. the long-axis coordinate x. Anti-correlation is evident. Adapted from Bakshi et al. (2012).

Our own widefield images of live *E. coli* with DNA stained with DRAQ5 and ribsosomes labeled with S2-YFP show clear anti-correlation in the axial spatial distributions of the two species (**Figure 3**). The "peak-to-valley" ratio of the ribosomes is about 1.5:1. Intriguingly, in the slow-growing species *C. crescentus*, ribosomes and DNA appear to be much more thoroughly mixed (Llopis et al., 2010).

Superresolution Imaging of RNAP and Ribosomes

In Bakshi et al. (2012), we reported super-resolution images of RNAP (β′-yGFP, **Figures 4A–C**) and ribosome (30S-YFP, **Figures 4D–G**) spatial distributions. RNAP spends almost all of its time bound to DNA, either specifically or non-specifically. The experiments revealed a much greater degree of RNAP/ribosome spatial segregation than suggested by the earlier widefield work.

In our study of RNAP motion, we labeled RNAP as β′-mEos2 expressed from the chromosome (Bakshi et al., 2013). Single-molecule diffusive trajectories of 1-s duration cleanly distinguish two states of motion of RNAP. In **Figure 5**, compare the compact purple trajectory with the extended yellow one. Specifically bound copies jiggle in place (sub-diffusion), much like DNA foci, while copies searching for transcription initiation sites undergo apparently free diffusion (a combination of 3D hopping

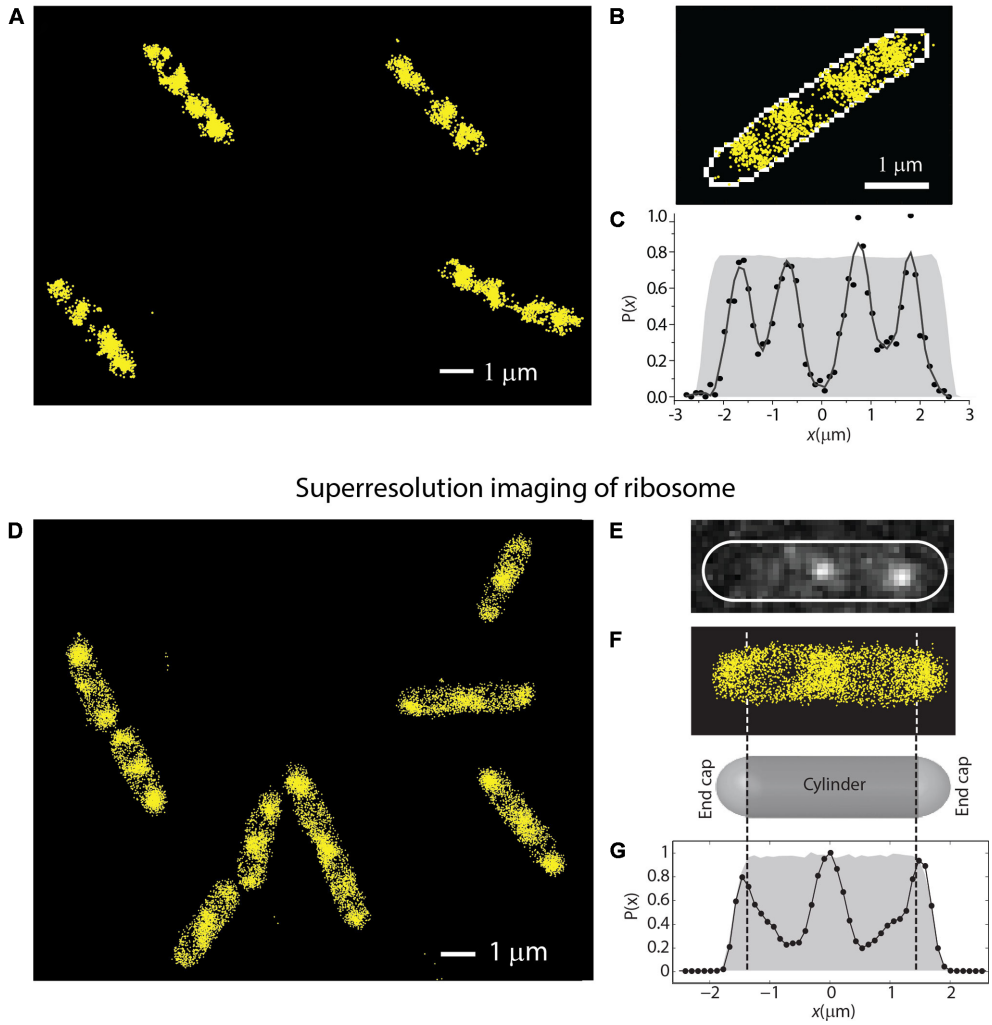

FIGURE 4 | (A–C) Super-resolution imaging of the spatial distributions of RNA polymerase (β′-YFP labeling) in live *E. coli*. **(C)** Shows a histogram of locations projected onto the long axis of the cell in **(B)**. **(D–G)** Super-resolution imaging of the spatial distributions of ribosomes (30S-YFP labeling) in live *E. coli*. **(E)** Shows two single copies imaged in one camera frame. **(G)** Shows an axial histogram of locations for the cell shown in **(F)**. The gray regions in **(C,G)** are simulated histograms for a uniformly filled spherocylinder matching the length and radius of the single cell. Adapted from Bakshi et al. (2012).

and non-specific binding) within the nucleoids. For growth in EZRDM at 37°C, about 50% of RNAP copies are evidently specifically bound to DNA (including all stages of transcription). According to classic estimates (Dennis et al., 2004), about 1/2 to 2/3 of this 50% should be transcribing stable RNA (rRNA and tRNA); the remainder should be transcribing protein genes. In rapidly growing cells, both widefield (Jin and Cabrera, 2006; Bratton et al., 2011) and super-resolution (Endesfelder et al., 2013) fluorescence studies find highly concentrated clusters of RNAP copies. These "transcription foci" presumably comprise RNAP copies engaged in transcription of *rrn* operons.

In the ribosome imaging studies, we found that some 85–90% of the 30S-YFP copies lie in the "ribosome-rich regions" (Bakshi et al., 2012). This suggests that only ∼10–15% of translation is co-transcriptional. The diffusive behavior of single 30S-mEos2 copies (**Figure 6**) reveals two distinguishable sub-populations. This enabled us to roughly divide the 30S behavior into 20–30% free 30S with diffusion coefficient $D_{30S} \sim 0.14\ \mu m^2\ s^{-1}$ and 80–70% 70S-polysomes with $D_{70S-poly} \sim 0.02\ \mu m^2\ s^{-1}$. The latter value describes the diffusive motion of mRNA decorated by a variable number of 70S-ribosomes. For comparison, the timescale of transcription of mRNA for a typical protein is ∼20 s and the degradation time for messages is ∼5 min (Bernstein et al., 2002). These data in *E. coli* are consistent with the view that most transcription of protein genes is co-translational. However, mRNA copies spend most of their lifetime separated from RNAP and DNA. After completion of transcription, $D_{70S-poly}$ is large enough to enable free mRNA decorated with translating 70S ribosomes to diffuse to a ribosome-rich region in ∼1 s. There each message can be translated repeatedly before degradation.

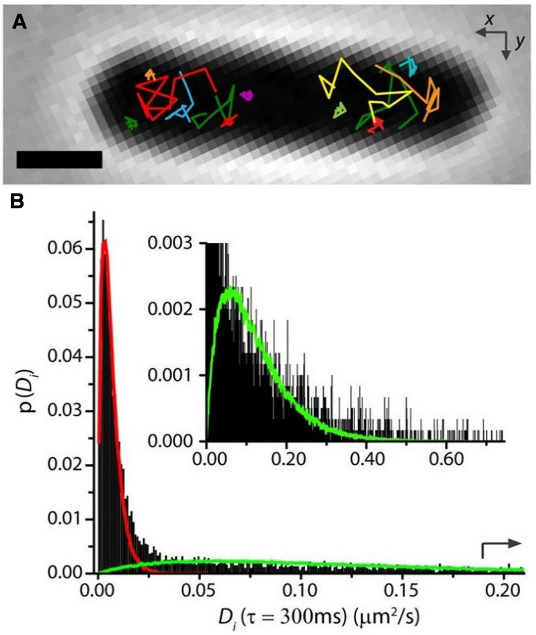

FIGURE 5 | (A) Single-RNAP diffusive trajectories in live *E. coli* growing in EZRDM at 37°C. Labeling was β′-mEos2. Note two types of trajectory. **(B)** Distribution of estimated diffusion coefficients D_i from single-RNAP trajectories. Fast and slow sub-populations are evident. Red and green curves are model distributions for the two components. Adapted from Bakshi et al. (2013).

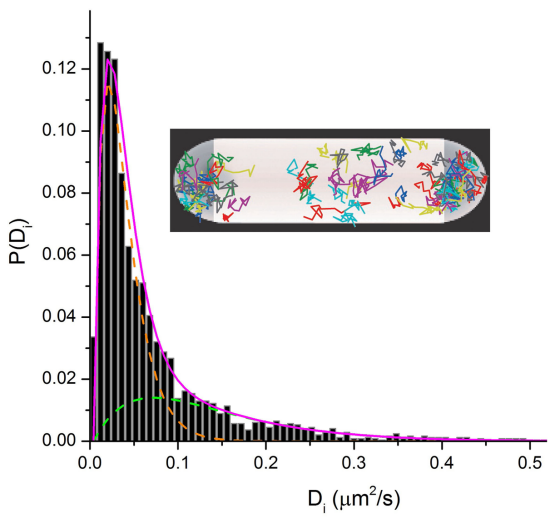

FIGURE 6 | Inset: Single-ribosome diffusive trajectories from a live *E. coli* cell growing in EZRDM at 30°C. Labeling is S2-YFP. **Main figure:** Distribution of estimated single-ribosome diffusion coefficients D_i. S2-mEos2 labeling. Two sub-populations are evident. Model sub-distributions are shown as green and orange dashed lines. Magenta line is their sum.

After complete synthesis of a protein in a ribosome-rich region, the newly free 30S and 50S subunits may engage in repeated rounds of translation in the ribosome-rich region, or "escape" back to the nucleoid region where they can re-initiate co-transcriptional translation (**Figure 7**). Accordingly, the Elf lab recently showed that the more rapidly diffusing 30S and 50S subunits penetrate the nucleoids while the slower 70S-polysomes are largely excluded (Sanamrad et al., 2014). This picture implies a circulation of ribosomal subunits from the nucleoids (where co-transcriptional translation occurs) to the ribosome-rich regions (where most protein synthesis occurs) and back again.

In fast growth conditions, concentration of 70S-polysomes in ribosome-rich regions may enhance the rate of protein synthesis by shortening the search time for translation initiation sites by newly freed 30S and 50S subunits that have just completed synthesis of a protein. Such spatial separation of transcription from most translation in *E. coli* is somewhat reminiscent of eukaryotic cells. However, it occurs without compartmentalization of DNA within a nuclear membrane. The Monte Carlo simulations described below suggest that the underlying segregation mechanism may be primarily physical in nature.

What Driving Forces Induce Nucleoid-Ribosome Mixing or Segregation?

In spite of the 1.5 mm contour length of an *E. coli* chromosome, the nucleoids do not fill the entire volume of the 3–4 μm long, 1 μm diameter cytoplasm (Pettijohn, 1982; Robinow and Kellenberger, 1994). The irregular shape of the *E. coli* nucleoids may be governed by the ring topology of DNA and spatial confinement effects on the ring polymer (Jung et al., 2012; Fisher et al., 2013; Youngren et al., 2014). In *C. crescentus*, chromosome conformation capture (3C) data suggest the nucleoids adopt a "bottle brush" geometry with plectonemes radiating outward from a central spine (Le et al., 2013). Less detail is presently available for the *E. coli* chromosome (Cagliero et al., 2013). Our focus here is on the coarse spatial extent of the nucleoids under different conditions, not the finer details.

Long-Term Effects of Chloramphenicol and Rifampicin on Nucleoid-Ribosome Morphology

It has long been known that transcription- and translation-halting drugs strongly affect nucleoid morphology. Typical imaging experiments have compared nucleoid morphology before and 20–30 min after drug treatment, usually using DAPI as the DNA stain. We used the non-perturbative DNA stain SYTOX Orange (Bakshi et al., 2014b) to study *time-dependent*, *quantitative* effects of Rif and Cam on nucleoid length and width in live cells over 20 min (Bakshi et al., 2014a). To describe the overall spatial distribution of the chromosomal DNA vs. time, we defined two parameters measured from the SYTOX Orange fluorescence intensity distributions projected along the *x*- and *y*-axes (**Figure 8A**). The axial distribution was characterized by the overall length L_{DNA}, measured as the "outside" full-width at half-maximum height (FWHM) of the projected intensity distribution along *x*. The width W_{DNA}, a rough measure of the mean nucleoid diameter, was defined as

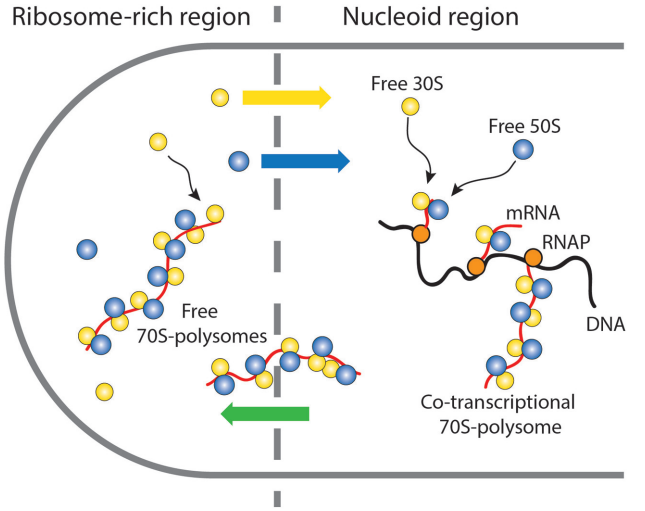

FIGURE 7 | Schematic showing the suggested circulation of ribosomal subunits into and out of the nucleoids and the ribosome-rich regions.

the FWHM of the projection of intensity along the transverse coordinate *y*. We believe this definition of nucleoid length and width is more quantitative than the "relative nucleoid size" used in other work (Jin et al., 2013). We also measured single-ribosome diffusive motion vs. time after drug treatment, using the 30S-mEos2 labeling scheme (Bakshi et al., 2014a). This helps distinguish 70S-polysomes from free 30S subunits after drug treatment.

On the 10–20 min timescale, the nucleoids of Cam-treated cells have become much more compact axially than normally growing cells, while the nucleoids of Rif-treated cells have expanded in both dimensions (**Figures 8B,C**). Similar long-term drug effects were observed in earlier work (Cabrera and Jin, 2006; Zimmerman, 2006). Ribosomes are evidently maintained as 70S-polysomes on a 20-min timescale after Cam treatment, as inferred from the distribution of ribosome diffusion coefficients (Bakshi et al., 2014a). We further suggest that the long-term nucleoid expansion induced by Rif is due to slow degradation of existing mRNA, after transcription initiation is halted by the drug. Imaging of the putative mRNA stain SYTO RNASelect vs. time is consistent with this suggestion. As mRNA is degraded, 70S-polysomes that dissociate to 30S and 50S subunits after completion of translation find fewer and fewer translation initiation sites. The resulting free subunits diffuse much more rapidly than 70S-polysomes. Unlike 70S-polysomes, the free subunits mix thoroughly with the nucleoids.

Nucleoid-Ribosome Mixing Hypothesis

These long-term drug effects have motivated a new nucleoid-ribosome mixing hypothesis (**Figure 9**; Bakshi et al., 2014a). We view the ribosomes and the chromosomal DNA as a *composite biochemical–biophysical system*. Cell physiology and drug treatments dictate the partitioning of ribosomal components between 70S-polysomes and free 30S and 50S subunits. Overall nucleoid spatial extent is then governed by the tendency for nucleoids to segregate from 70S-polysomes and to mix with free 30S and 50S subunits. The Monte Carlo modeling (Mondal et al., 2011; Bakshi et al., 2014a) described next suggests that the underlying driving forces for mixing or segregation are *excluded volume effects* combined with *maximal total entropy* of the composite DNA-ribosome system.

In this view, the drug studies reveal three "states" of the nucleoid-ribosome system. For normally growing, untreated cells, transertion expands the nucleoids, imposing a state of *intermediate DNA density* that prevents 70S polysomes and the chromosomal DNA from mixing while permitting 30S and 50S subunits to penetrate the nucleoids. Transertion may thus be essential for the initiation and maintenance of co-transcriptional translation of nascent mRNA in the dense regions of the nucleoids. Cam freezes ribosomal subunits as 70S-polysomes. Completion of transcription events will break the transertion chains and the 70S-polysomes will then be unable to make new chains. Over 20 min, the chromosomal DNA relaxes to a *fully condensed state* that excludes both 70S-polysomes and 30S and 50S subunits. The fraction of free 30S and 50S subunits becomes even smaller than in normal growth, enabling very strong compaction of the nucleoids. We suggest that this represents the relaxed volume of the nucleoids in the absence of the expanding force of transertion and in the near absence of free ribosomal subunits. Rif treatment also breaks the transertion links on the same timescale as Cam, the time over which transcription events are completed. Again, new transertion chains are prevented from forming. This leads to similar short-term contraction (see below). DNA mixing with 30S and 50S ribosomal subunits eventually occurs on the longer, 10–20 min timescale of mRNA degradation. This leads to the third, *fully expanded* state of the nucleoids, in which few 70S-polysomes exist and DNA and the 30S and 50S ribosomal subunits mix extensively. However, the nucleoids continue to avoid the cylindrical walls and especially the endcaps.

Simple Physical Model of Ribosomes and Nucleoids

In Mondal et al. (2011), we developed a simple physical model of plectonemic DNA and 70S-polysomes confined in a spherocylinder (as pictured in **Figure 10A**). DNA was modeled as a hyperbranched polymer (hard spheres and connecting rods). Based on estimates at the time (Bremer and Dennis, 1996), the model placed two chromosome equivalents of plectonemic DNA (comprising 7000 plectoneme rods) plus 20,000 70S particles organized as freely jointed 70S-polysome 13-mers into a spherocylinder (350 nm radius, 3.0 μm length). DNA–DNA, polysome–DNA, and polysome–polysome excluded volume effects were modeled realistically. There are no attractive interactions between particles. The free energy of the composite system was minimized using Monte Carlo methods. This minimalist, coarse-grained model does not include the effects of transertion, nor does it attempt to describe the level of geometric detail revealed by recent chromosome conformational capture data (Cagliero et al., 2013; Le et al., 2013; Le and Laub, 2014). Instead, it seeks to understand the effects of excluded volume

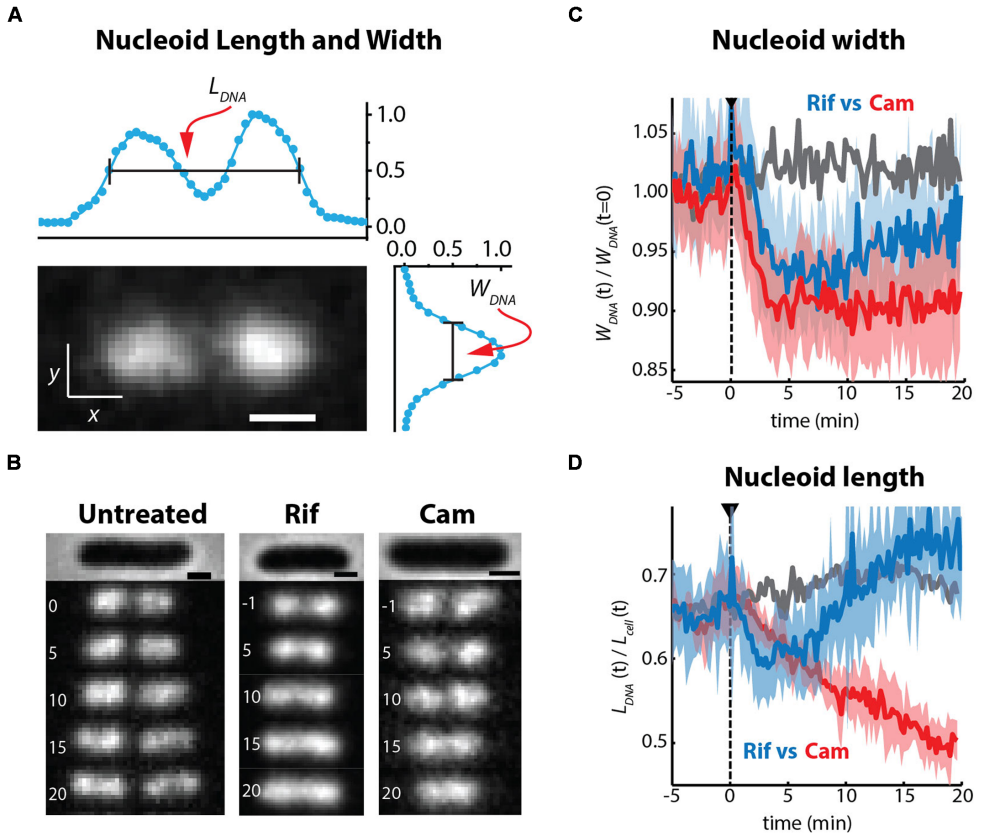

FIGURE 8 | (A) SYTOX orange-stained image of chromosomal DNA in a live *E. coli* cell growing in EZRDM at 30°C. The nucleoid spatial extent is characterized by length L_{DNA} and width W_{DNA} measured as the full width at half-maximum height (FWHM) of intensity distributions projected onto the *x* and *y* axes. **(B)** Time-lapse sequences of images of nucleoids stained by SYTOX Orange. Times in minutes, scale bars are 1 mm. Untreated cells, Rif-treated cells, and Cam-treated cells as indicated. **(C)** Quantitative nucleoid width W_{DNA} vs. time. *Gray:* mean behavior of a set of untreated cells. *Blue:* behavior of Rif-treated cells. *Red:* behavior of Cam-treated cells. For blue and red, heavy lines are averages of traces from many cells; shaded regions show the envelope of single-cell results that were averaged. Dashed line shows time of initiation of flow of drug. **(D)** Same as **(C)**, but with relative nucleoid length plotted as L_{DNA}/L_{cell}. Adapted from Bakshi et al. (2014a).

and entropy on the overall spatial distributions of DNA and ribosomes.

Translational entropy is the entropy of movement in space. It increases with the number of free particles and with the volume available to the particles. DNA conformational entropy is determined by the number of conformational states available to the DNA polymer. *In the model, these entropic plus excluded volume effects lead to strong segregation of DNA from 70S-polysomes* (**Figure 10B**). The model DNA polymer, comprising beads connected by rods, avoids the walls and does not fill the cytoplasm. This is because placing a bead near a wall would eliminate many potential conformations of the polymer and hence decrease conformational entropy.

To help understand why Rif-induced dissociation of 70S-polysomes into 30S and 50S subunits enables mixing of free subunits with the DNA and nucleoid expansion, we have recently performed a new set of simulations based on the same simplified model of DNA (**Figure 10C**; Bakshi et al., 2014a). The 20,000 70S ribosomes engaged as 1538 polysome 13-mers were converted to 20,000 30S spheres and 20,000 50S spheres. Excluded volume effects were adjusted appropriately. *The free 30S and 50S subunits mix with the DNA polymer*. In addition, the nucleoid becomes more expanded, while continuing to avoid the confining walls. Both features are reminiscent of experimental results (Bakshi et al., 2014a; Sanamrad et al., 2014).

The model suggests that the primary driving force for mixing of chromosomal DNA with ribosomal subunits after Rif treatment is *increased translational entropy*. Each 70S-polysome 13-mer has become 26 independent subunits, each "demanding" its own translational entropy. We suggest that the nucleoid expands to provide the 30S and 50S subunits with access to more volume in which to move.

In real cells, the nucleoids adopt their most compact form after Cam treatment, which preserves most ribosomal subunits as 70S-polysomes. Importantly, in this highly compacted form the nucleoids exclude not only 70S-polysomes, but also free 30S subunits (Sanamrad et al., 2014), LacI (Kuhlman and Cox, 2012), and the Kaede tetramer (Bakshi et al., 2011). Accordingly, we believe that it is *transertion* that expands the nucleoids

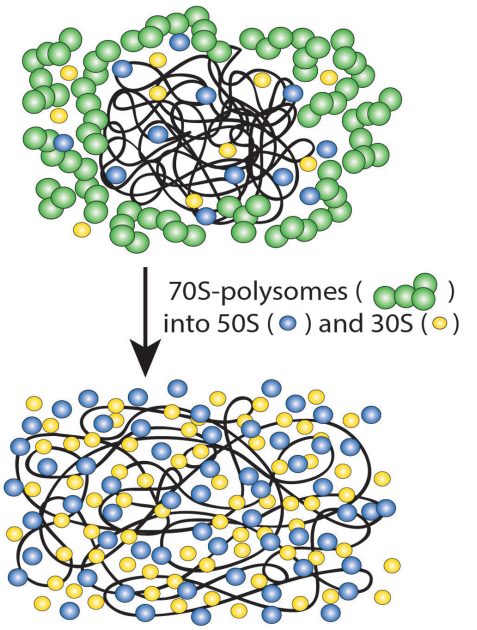

FIGURE 9 | Schematic of ribosome-nucleoid mixing hypothesis. 70S-polysomes and DNA strongly avoid each other, while free 30S and 50S subunits readily penetrate into the nucleoids. Adapted from Bakshi et al. (2014a).

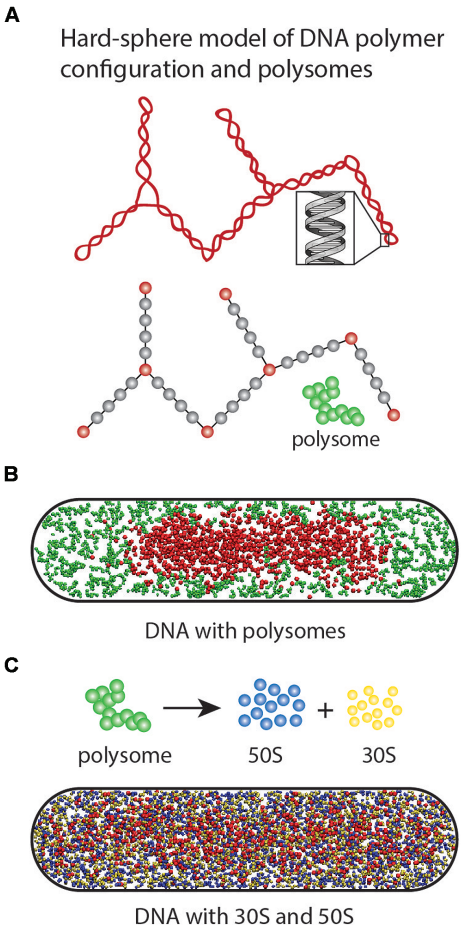

FIGURE 10 | (A) Hyper-branched polymer bead model of plectonemic DNA and 70S-polysomes. The red DNA beads exclude each other; the gray beads are invisible to the DNA beads but act as volume appropriately excluded to the polysomes. Polysomes are represented as freely jointed chains of spheres of appropriate size. **(B)** In Monte Carlo simulations, 70S-polysomes and DNA strongly avoid each other. **(C)** When the 70S-polysomes are dissociated into 50S and 30S monomers, the simulations show strong mixing and nucleoid expansion. Adapted from Bakshi et al. (2014a).

sufficiently to enable 30S and 50S subunits to penetrate and initiate co-transcriptional translation.

Co-transcriptional translation in turn is biologically important for preventing premature degradation of mRNA by endonucleases, termination of transcription by Rho, and excessive backtracking by RNAP. *Thus transertion, whose very existence has long been debated, may be essential to optimal cell growth.*

In our view, the overall physiological state of the cell (slow growth, fast growth, stationary phase, stress response, etc.) determines the number of ribosomal subunits and their partitioning between 70S-polysomes and 30S and 50S subunits. The Monte Carlo modeling then suggests that at least in rapid growth, the corresponding coarse nucleoid morphology is dictated by the tendency of the combined nucleoid-ribosome *system* to maximize total conformational and translational entropy. The modeling further suggests that in the presence of free 30S and 50S subunits, the tendency to maximize translational entropy of ribosomal subunits provides a second expanding force on the nucleoids, in addition to transertion. This tendency is most evident after treatment with the transcription-halting drug Rif. It is less evident, but may still be a significant effect, in normal growth when 30S and 50S subunits are minority ribosomal species. Our model of the factors controlling the overall DNA spatial distribution might be called "translation-centric," because it emphasizes the importance of the DNA-ribosome system.

It is difficult to compare our model of DNA-ribosome interactions with other physical models of DNA confinement and compaction. The two most recent models treat the DNA polymer as a freely jointed chain of beads (Pelletier et al., 2012; Shendruk et al., 2015), whereas we represent DNA as plectonemes modeled as a hyper-branched chain of sticks connecting beads. The other models include small-protein crowders but not ribosomes, whereas we include ribosomes explicitly and neglect small-protein crowders. With its 7000 connecting rods, our hyper-branched chain has many more internal degrees of freedom than a freely jointed chain of several 100 beads, and so may have a greater tendency to avoid walls. We anticipate more detailed physical models in the future, perhaps including crowders of all sizes, the effects of transertion, and new information about specific DNA conformations from chromosome-capture experiments (Cagliero et al., 2013; Le et al., 2013).

New Evidence for Transertion

Background

Transertion is viewed as a dynamic process in which numerous membrane-DNA linkages are constantly forming and breaking during normal transcription and translation events (Norris and Madsen, 1995). The transertion hypothesis implies DNA-RNAP-mRNA-ribosome-polypeptide-membrane "transertion chains" that tether the chromosomal DNA to the cytoplasmic membrane and provide a radially expanding force on the nucleoids (**Figure 1**). The primary evidence for transertion had long been the dramatic contraction of the nucleoids after treatment with drugs that halt translation (e.g., chloramphenicol; van Helvoort et al., 1996; Zimmerman, 2002). Such treatment should break the transertion chains on the timescale of completion of transcription events (∼20 s). However, transertion chains should also be broken by drugs such as rifampicin ("Rif"), which prevents transcription initiation. Yet cells observed 20–30 min after Rif treatment showed nucleoid *expansion*, in contradiction of the transertion hypothesis (Jin and Cabrera, 2006).

Recent additional support for transertion came from the Goulian lab. Libby et al. (2012), they discovered a net outward migration of genes encoding cytoplasmic membrane proteins within minutes of induction of transcription. They measured the 2D spatial distribution of fluorescent markers of genes encoding two soluble proteins (*mcherry*, coding the fluorescent protein mCherry; and *aadA*, spectinomycin adenylyltransferase) and of genes encoding two membrane proteins (*lacY*, lactose permease; and *tetA*, the tetracycline efflux pump). For the two membrane-protein genes (but not for the soluble protein genes), induction caused a substantial outward shift in the distribution (toward the membrane), consistent with the transertion hypothesis. The shift occurred within 1–3 min of gene induction.

Short-Time Imaging of Drug Effects on Nucleoid Morphology

Our recent time-resolved drug studies have resolved the Rif dilemma (Bakshi et al., 2014a). The non-perturbative DNA stain SYTOX Orange allows monitoring of nucleoid morphology in growing cells using widefield time-lapse microscopy. We are able follow the size and shape of the nucleoids at 10 s intervals over 25 min after cells are treated with drugs. *On the 0–5 min timescale, both Cam and Rif shrink both the length and width of the nucleoids* (**Figures 8B–D**). This is consistent with the transertion hypothesis. Both Cam and Rif should cause radial contraction of the nucleoids on the timescale of completion of transcription events within the transertion chains. On the 10–20 min timescale following Rif treatment, the nucleoids of the Rif-treated cells expand axially, becoming longer than in the unperturbed state. As described above, we believe the expansion is due to converstion of 70S-polysomes to 30S and 50S subunits, which freely mix with the nucleoids. However, the nucleoid width remains smaller than that of the unperturbed state, consistent with wall avoidance by the DNA polymer, which is no longer tethered to the plasma membrane.

A "Transcription-Centric" Model of *E. coli* Organization

In a separate chapter of this compendium, Ding Jin presents a very different view of the factors governing the overall DNA spatial distribution. The model from the Jin lab might be called "transcription-centric." Jin et al. (2013) labeled RNAP using a GFP tag on the β′ subunit and imaged fixed *E. coli* cells harvested from rapidly growing cultures. They discovered that each cell exhibits several bright puncta of RNAP-GFP intensity, which they dubbed "transcription foci" (Cabrera et al., 2009). Similar foci have been observed in a recent super-resolution study (Endesfelder et al., 2013). The Jin lab studied the presence or absence of transcription foci as well as the overall nucleoid spatial extent in a wide variety of growth and stress conditions (Jin et al., 2013). Transcription foci dissipate rapidly when fast-growing cells are starved or treated with Rif, among other conditions. The foci are not evident in slowly growing cells.

The transcription foci are very likely concentrated centers of transcription of *rrn* operons, the predominant type of transcription in rapidly growing cells. The seven *rrn* operons are distributed broadly within the half of the chromosome closest to *oriC*. Rapidly growing cells containing perhaps four genome equivalents of DNA can easily harbor ∼40 *rrn* operons, a number that far exceeds the number of transcription foci observed. This strongly suggests *clustering* of *rrn* operons into hubs of rRNA transcription, perhaps analogous to the nucleolus of eukaryotic cells. The cause of such clustering is unknown. Cook and co-workers developed a statistical model that suggested that a strong depletion-attraction force would arise between two *rrn* operons heavily decorated with RNAP copies (Marenduzzo et al., 2006).

Across a variety of growth conditions, mutant strains, and drug treatments, Jin et al. (2013) observed a strong, positive *correlation* between the presence of transcription foci and the occurrence of relatively compact states of the nucleoids. This led to the suggestion that binding of a large fraction of RNAP copies within transcription foci somehow *causes* the nucleoid to compact.

The most recent concept involves the redistribution of RNAP copies that occurs in conditions that "dissolve" transcription foci. Imaging evidence indicates that the transcription foci tend to lie at or near the nucleoid periphery (Jin et al., 2013). In rapidly growing cells, RNAP may thus be depleted from the bulk of the nucleoids. When the RNAP previously concentrated in peripheral *rrn* clusters are dispersed by Rif treatment or by inducing the stringent response, they bind specifically and non-specifically to numerous sites within the bulk of the DNA. The suggestion is that this expands the nucleoids. However, such expansion cannot be due to insertion of the extra volume of RNAPs into the bulk of the nucleoids. The nucleoids occupy roughly half of the total cytoplasmic volume, or ∼2 μm^3 in rapid growth. The RNAP copy number per cell is ∼5000 (Bakshi et al., 2012). Even if we place all the RNAP copies within the nucleoids, their total volume is only ∼0.003 μm^3. Insertion of RNAP copies into the bulk of the nucleoids in and of itself cannot induce anything like the observed volume expansion induced

by Rif. Similarly, the presence in the nucleoid of 10–15% of the ribosomes has only a minor effect on overall nucleoid volume (Bakshi et al., 2012). The total volume of 7,500 70S ribosomes is only $\sim$0.03 μm^3.

Instead, we believe it is the translational entropy of free ribosomal subunits that drives the expansion of the nucleoid (Bakshi et al., 2014a). The fraction of ribosomes involved in active translation as 70S polysomes decreases upon Rif treatment or induction of the stringent response. The increased contribution of translational entropy from the increased fraction of free, non-translating ribosomal subunits causes the nucleoid to expand, making the entire the cytoplasm accessible to the 30S and 50S subunits (**Figures 9** and **10**).

It might be suggested that the gathering of multiple *rrn* operons into a single *rrn* cluster, whatever the underlying cause, constrains the entire nucleoid to be more compact. A critical test of this suggestion would use dual-color fluorescence reporter–operator systems (FROS) to label two different *rrn* operons and test whether *rrn* clusters persist or disperse in slow growth. If they disperse and the nucleoids expand, the idea may have merit. At present, a counter-argument is that the linear contour of one genome measures 1.5 mm in length. Whatever causes *rrn* operons to cluster, it seems likely to us that there is plenty of "slack" in the overall chromosome to accommodate clustering of distant operons without compacting the overall nucleoid morphology. Additional study of the confined DNA polymer model, including pinning together of distant beads to each other, may be informative here.

Also relevant is a recent study of DAPI-stained nucleoid morphology in different growth conditions (Kuhlman and Cox, 2012). From a quantitative comparison of the integrated curvature of 2D images of the nucleoids, they inferred that the nucleoids are substantially *more condensed* (have higher density) in slowly growing cells than in rapidly growing cells. Since transcription foci do not occur in slowly growing cells, this would appear to oppose the trend predicted by the transcription-centric model of Jin et al. (2013).

We plan to extend our ribosome, RNAP, and nucleoid imaging and tracking studies to very slow growth conditions to test the nucleoid-ribosome mixing hypothesis in a very different physiological context.

Does mRNA Co-localize with Ribosomes or with the Gene from Which it was Transcribed?

According to our model of *E. coli* spatial organization, in rapid growth most translation is physically separated from most transcription. The exception is the small fraction of co-transcriptional translation (perhaps 10–15%), which should co-localize with the chromosomal DNA. If this picture is essentially correct, then the spatial distribution of total mRNA should mimic that of the ribosomes more closely than that of the chromosomal DNA.

As reviewed by Amster-Choder and co-workers (Buskila et al., 2014), there are two primary methods for labeling specific mRNAs: fluorescence *in situ* hybridization ("FISH," which requires fixation and permeabilization of the cells) and tagging of mRNA with a sequence to which a fluorescently labeled protein such as MS2-GFP binds specifically (which can be carried out on live cells). That review describes the current evidence on mRNA localization. The resulting picture is complicated and far from complete. It is possible that the picture of strong ribosome-nucleoid segregation and rapid diffusion of mRNA-70S polysomes away from their point of origin after completion of transcription holds only for rapidly growing cells.

Results in Rapidly Growing *E. coli* and *B. subtilis*

Early on, Golding and Cox (2004) used the MS2 scheme to label a very large, artificial mRNA transcribed from a plasmid. The resulting MS2-coated mRNA copies have mass of several MDa, comparable to a ribosome. They localized near the cell poles, much like ribosomes. The diffusive and localization properties of such large objects are not closely related to those of normal gene transcripts.

Amster-Choder and co-workers labeled specific *E. coli* genes in live cells under fast growth conditions using the MS2-GFP procedure (Nevo-Dinur et al., 2011). They found that the mRNA coding for the membrane proteins *lacY* and *bglF* was *localized at the membrane*. This behavior persisted even after treatment with translation-halting drugs such as Cam. The interpretation was that the mRNA itself contains information that targets the transcript to the location where the protein will ultimately be used, analogous to what occurs in eukaryotic cells. However, if the lead ribosome (i.e., the one connected to the RNA polymerase) is indeed necessary to prevent premature intrinsic or Rho-dependent termination of transcription (Burmann et al., 2010), then Cam may prevent efficient transcription as well. We suggest that this result might be interpreted as further evidence of transertion chains. The ribosome-mRNA-membrane linkages would persist after Cam treatment, so the localization of mRNA at the membrane would also persist.

In contrast, the mRNAs coding for the cytoplasmic proteins *cat* and *bglB* were distributed throughout the cytoplasm in a pattern that was described as helical (Nevo-Dinur et al., 2011). However, to our eyes the *cat* and *bglB* mRNA distributions look like the strongly segregated ribosomal spatial distributions in fast growth conditions (**Figure 4**).

We recently used the fluorescent stain SYTO RNASelect to monitor the degradation of total mRNA following Rif treatment (Bakshi et al., 2014a). SYTO RNASelect purportedly stains RNA in preference to DNA. For normally growing cells in EZRDM at 30°C, the resulting images look qualitatively similar to widefield images of ribosomes labeled by S2-YFP in the same growth conditions (**Figure 3**; Bakshi et al., 2012). The *caveat* here is the possibility that SYTO RNASelect is actually staining ribosomal RNA, not mRNA. However, most rRNA is buried in the ribosome interior and not accessible to the stain. In addition, the SYTO RNASelect signal decayed on a 10-min timescale after Rif treatment, consistent with the timescale of degradation of mRNA. Ribosomes are still present after the decay of SYTO RNASelect fluorescence.

Allowing for some re-interpretation of the Amster-Choder results, the available data on mRNA distributions from live, rapidly growing *E. coli* cells seems quite consistent with our overall picture of strong ribosome-DNA spatial segregation in rapidly growing cells.

Rapidly growing *B. subtilis* cells also exhibit strong nucleoid-ribosome segregation (Lewis et al., 2000). The first two-color widefield studies of cells with DNA stained and ribosomes labeled showed two or three ribosome-rich regions with interleaved regions of concentrated DNA. We know of no data on mRNA spatial distribution in *B. subtilis*, but we expect the distribution would closely mimic the ribosome distribution.

Results in Slowly Growing *C. crescentus* and *E. coli*

Using FISH in the slowly growing species *C. crescentus*, the Jacobs-Wagner lab found that six different mRNA messages formed images comprising one or a few *puncta* (Llopis et al., 2010). Remarkably, each of these puncta co-localized with the corresponding gene (also detected by FISH). In addition, the ribosomes and DNA mix extensively in *C. crescentus*. The mixing means that there is no contradiction between retention of mRNA near the site of its transcription and repeated translation of the same message. In slowly growing *E. coli*, similar mRNA and gene co-localization was observed for *lacZ*. This suggests that in slow growth conditions, mRNA diffusion away from the gene from which it was transcribed is very slow, in contrast to our picture of facile mRNA escape from the nucleoids in rapid growth conditions.

In a similar vein, Kuhlman and Cox (2012) used DAPI staining, "FROS" (a fluorescent reporter–operator system), FISH, and Venus labeling in *E. coli* to measure the spatial distributions (averaged over many cells) of the overall nucleoid, the *lacI* gene, its *lacI* mRNA product, and its LacI-Venus protein product. In slow growth, they varied the position of the *lacI* gene, either on an extrachromosomal plasmid, near *oriC*, or near *ter*. The gene and mRNA distributions are non-uniform and quite different in the three cases, exhibiting two, one, and three axial peaks, respectively. In all three cases, the mRNA distribution closely mimicked the gene distribution, again suggesting that the mRNA is not readily diffusing away from the location where it was transcribed. It is perhaps worth noting that the three different *lacI* gene and mRNA spatial distributions in slow growth conditions all have strong peaks in locations that would match our three ribosome-rich regions in rapidly growing cells. However, in rapidly growing *E. coli*, Kuhlman and Cox (2012) found that the *lacI* mRNA spatial distributions from FISH mimic the overall nucleoid distributions, again suggesting that the mRNA does not readily escape the nucleoids. That is, the *lacI* mRNA does not form a pattern mimicking the *ribosome* spatial distributions of **Figures 3** and **4**.

In slowly growing *E. coli* the evidence for two different genes (*lac Z* and *lacI*) indicates that the corresponding mRNA message remains in the vicinity of the gene itself rather than diffusing away (Kuhlman and Cox, 2012). It is possible that the behavior of *lacZ* and *lacI* mRNA in slowly growing cells is somehow not representative of the predominant mRNA behavior. It is also possible that strong DNA-ribosome segregation only occurs in rapidly growing cells. However, facile DNA-ribosome mixing in slow growth would seem contrary to the Kuhlman and Cox (2012) inference of higher DNA density in slowly growing cells than in rapidly growing cells. According to our Monte Carlo modeling, higher DNA density in slowly growing cells would exclude 70S-polysomes to a greater extent, assuming that they can escape the nucleoid interior in the first place.

At present, the mRNA data on slowly growing cells, both *E. coli* and *C. crescentus*, stand in opposition to a picture of strong DNA-ribosome segregation and diffusion of free mRNA to ribosome-rich regions where the bulk of translation occurs. We have not carried out detailed super-resolution studies of ribosomes in slowly growing *E. coli*. We plan to repeat the spatial distribution and diffusion studies to measure the degree of nucleoid-ribosome segregation and the diffusive properties of the ribosomes. Studies of the SYTO RNASelect staining pattern in slow growth are also of interest.

Returning to rapidly growing *E. coli* cells, it seems highly implausible to us that the nucleoids and ribosomes would be strongly segregated while the *overall* mRNA spatial distribution would mimic that of the chromosomal DNA. If that were the case, then what are the ∼80% of ribosomes doing while they are so far from the majority of the mRNA that they must translate? The situation could be quite different in slowly growing *E. coli*. Additional work is needed.

Summary

We have presented a comprehensive model whose goal is to explain the coarse spatial organization of the *E. coli* transcription and translation machinery in rapid growth conditions with and without the influence of transcription- or translation-halting drugs. This builds on a great deal of earlier work from other labs (Odijk, 1998; Pelletier et al., 2012). Our model takes account of both the biochemical state of the cell (fraction of ribosomes engaged in translation, presence or absence of transertion chains) and the important underlying physical effects of excluded volume and conformational and translational entropy. By treating the ribosomes and DNA as a coupled biochemical–biophysical *system*, the model explains a wide variety of experimental results.

A wise cell biologist once complained that the trouble with physics-based hypotheses attempting to explain aspects of cellular behavior is that they can never be critically tested. There are no appropriate negative controls—you cannot turn the physics off. Our response would be that neither should the physics be neglected in our thinking. Physical models that make experimentally testable predictions have real value in cell biology. Our physical model can explain why in normal, rapid growth conditions 70S-polysomes and the nucleoids segregate, while free 30S and 50S subunits mix with the nucleoids. The model is oversimplified to be sure, but we believe it captures essential interactions that must not be ignored.

From the time-dependent drug studies, we further infer that transertion maintains the nucleoids in a sufficiently expanded state to enable recycling of 30S and 50S subunits between ribosome-rich regions and the nucleoid interior, where they initiate co-transcriptional translation. This in turn protects the nascent mRNA and prevents undesirable backtracking of RNA polymerase.

These concepts suggest how the strongly coupled transcription-translation-transertion *system* may enhance the maximum growth rate of *E. coli*. Strong segregation of DNA and RNAP from 70S-polysomes in rapid growth may significantly decrease the search times of RNAP for transcription initiation sites and of free 30S and 50S ribosomal subunits for translation initiation sites. Future work will provide additional quantitative detail in rapid growth and seek a better understanding of the situation in slowly growing cells.

Acknowledgments

Different aspects of this research were supported by the grants CHE-1213860 from the US National Science Foundation and R01-GM094510 and R01-GM093265 from the National Institutes of Health (NIGMS). We are deeply indebted to our co-workers and collaborators, including Dr. Jagannath Mondal, Prof. Arun Yethiraj, Prof. Mark Goulian, Dr. Albert Siryaporn, Dr. Benjamin Bratton, Dr. Renee Dalrymple, and Ms. Wenting Li.

References

Azam, T. A., Hiraga, S., and Ishihama, A. (2000). Two types of localization of the DNA-binding proteins within the *Escherichia coli* nucleoid. *Genes Cells* 5, 613–626. doi: 10.1046/j.1365-2443.2000.00350.x

Bakshi, S., Bratton, B. P., and Weisshaar, J. C. (2011). Subdiffraction-limit study of Kaede diffusion and spatial distribution in live *Escherichia coli*. *Biophys. J.* 101, 2535–2544. doi: 10.1016/j.bpj.2011.10.013

Bakshi, S., Choi, H., Mondal, J., and Weisshaar, J. C. (2014a). Time-dependent effects of transcription- and translation-halting drugs on the spatial distributions of the *E. coli*, chromosome and ribosomes. *Mol. Microbiol.* 94, 871–887. doi: 10.1111/mmi.12805

Bakshi, S., Choi, H., Rangarajan, N., Barns, K. J., Bratton, B. P., and Weisshaar, J. C. (2014b). Nonperturbative imaging of nucleoid morphology in live bacterial cells during an antimicrobial peptide attack. *Appl. Environ. Microbiol.* 80, 4977–4986. doi: 10.1128/AEM.00989-14

Bakshi, S., Dalrymple, R. M., Li, W., Choi, H., and Weisshaar, J. C. (2013). Partitioning of RNA polymerase activity in live *Escherichia coli* from analysis of single-molecule diffusive trajectories. *Biophys. J.* 105, 2676–2686. doi: 10.1016/j.bpj.2013.10.024

Bakshi, S., Siryaporn, A., Goulian, M., and Weisshaar, J. C. (2012). Superresolution imaging of ribosomes and RNA polymerase in live *Escherichia coli* cells. *Mol. Microbiol.* 85, 21–38. doi: 10.1111/j.1365-2958.2012.08081.x

Bernstein, J. A., Khodursky, A. B., Lin, P. H., Lin, S.,-C., and Cohen, S. N. (2002). Global analysis of mRNA decay and abundance in *Escherichia coli* at single-gene resolution using two-color fluorescent DNA microarrays. *Proc. Natl. Acad. Sci. U.S.A.* 99, 9697–9702. doi: 10.1073/pnas.112318199

Betzig, E., Patterson, G. H., Sougrat, R., Lindwasser, O. W., Olenych, S., Bonifacino, J. S., et al. (2006). Imaging intracellular fluorescent proteins at nanometer resolution. *Science* 313, 1642–1645. doi: 10.1126/science.1127344

Bratton, B. P., Mooney, R. A., and Weisshaar, J. C. (2011). Spatial distribution and diffusive motion of RNA polymerase in live *Escherichia coli*. *Bacteriol. J.* 193, 5138–5146. doi: 10.1128/JB.00198-11

Bremer, H., and Dennis, P. (1996). "Modulation of chemical composition and other parameters of the cell by growth rate," in *Escherichia coli and Salmonella: Cellular and Molecular Biology*, eds F. C. Neidhardt and R. Curtiss (Washington, DC: ASM Press), 1553–1569.

Burmann, B. M., Knauer, S. H., Sevostyanova, A., Schweimer, K., Mooney, R. A., Landick, R., et al. (2012). An alpha helix to beta barrel domain switch transforms the transcription factor RfaH into a translation factor. *Cell* 150, 291–303. doi: 10.1016/j.cell.2012.05.042

Burmann, B. M., Schweimer, K., Luo, X., Wahl, M. C., Stitt, B. L., Gottesman, M. E., et al. (2010). A NusE:NusG complex links transcription and translation. *Science* 328, 501–504. doi: 10.1126/science.1184953

Buskila, A. A., Kannaiah, S., and Amster, O.-C. (2014). RNA localization in bacteria. *RNA Biol.* 11, 1051–1060. doi: 10.4161/rna.36135

Cabrera, J. E., Cagliero, C., Quan, S., Squires, C. L., and Jin, D. J. (2009). Active transcription of rRNA operons condenses the nucleoid in *Escherichia coli*: examining the effect of transcription on nucleoid structure in the absence of transertion. *J. Bacteriol.* 191, 4180–4185. doi: 10.1128/JB.01707-08

Cabrera, J. E., and Jin, D. J. (2006). Active transcription of rRNA operons is a driving force for the distribution of RNA polymerase in bacteria: effect of extrachromosomal copies of rrnB on the in vivo localization of RNA polymerase. *J. Bacteriol.* 188, 4007–4014. doi: 10.1128/JB.01893-05

Cagliero, C., Grand, R. S., Jones, M. B., Jin, D. J., and O'Sullivan, J. M. (2013). Genome conformation capture reveals that the *Escherichia coli* chromosome is organized by replication and transcription. *Nucleic Acid Res.* 41, 6058–6071. doi: 10.1093/nar/gkt325

Dame, R. T. (2005). The role of nucleoid-associated proteins in the organization and compaction of bacterial chromatin. *Mol. Microbiol.* 56, 858–870. doi: 10.1111/j.1365-2958.2005.04598.x

Datsenko, K. A., and Wanner, B. L. (2000). One-step inactivation of chromosomal genes in *Escherichia coli* K-12 using PCR products. *Proc. Natl. Acad. Sci. U.S.A.* 97, 6640–6645. doi: 10.1073/pnas.120163297

Dennis, P. P., Ehrenberg, M., and Bremer, H. (2004). Control of rRNA synthesis in *Escherichia coli*: a systems biology approach. *Microbiol. Mol. Biol. Rev.* 68, 639–668. doi: 10.1128/MMBR.68.4.639-668.2004

Endesfelder, U., Finan, K., Holden, S. J., Cook, P. R., Kapanidis, A. N., and Heilemann, M. (2013). Multiscale spatial organization of RNA polymerase in *Escherichia coli*. *Biophys. J.* 105, 172–181. doi: 10.1016/j.bpj.2013.05.048

Fisher, J. K., Bourniquel, A., Witz, G., Weiner, B., Prentiss, M., and Kleckner, N. (2013). Four-dimensional imaging of *E. coli*, nucleoid organization and dynamics in living cells. *Cell* 153, 882–895. doi: 10.1016/j.cell.2013.04.006

Fishov, I., and Woldringh, C. L. (1999). Visualization of membrane domains in *Escherichia coli*. *Mol. Microbiol.* 32, 1166–1172. doi: 10.1046/j.1365-2958.1999.01425.x

Golding, I., and Cox, E. C. (2004). RNA dynamics in live *Escherichia coli* cells. *Proc. Natl. Acad. Sci. U.S.A.* 101, 11310–11315. doi: 10.1073/pnas.0404443101

Gould, T. J., Gunewardene, M. S., Gudheti, M. V., Verkhusha, V. V., Yin, S. R., Gosse, J. A., et al. (2008). Nanoscale imaging of molecular positions and anisotropies. *Nat. Methods* 5, 1027–1030. doi: 10.1038/nmeth.1271

Hess, S. T., Girirajan, T. P., and Mason, M. D. (2006). Ultra-high resolution imaging by fluorescence photoactivation localization microscopy. *Biophys. J.* 91, 4258–4272. doi: 10.1529/biophysj.106.091116

Jin, D. J., and Cabrera, J. E. (2006). Coupling the distribution of RNA polymerase to global gene regulation and the dynamic structure of the bacterial nucleoid in *Escherichia coli*. *Struct. J. Biol.* 156, 284–291. doi: 10.1016/j.jsb.2006.07.005

Jin, D. J., Cagliero, C., and Zhou, Y. N. (2013). Role of RNA polymerase and transcription in the organization of the bacterial nucleoid. *Chem. Rev.* 113, 8662–8682. doi: 10.1021/cr4001429

Jung, Y., Jeon, C., Kim, J., Jeong, H., Jun, S., and Ha, B.-Y. (2012). Ring polymers as model bacterial chromosomes: confinement, chain topology, single chain statistics, and how they interact. *Soft Matter* 8, 2095–2102. doi: 10.1039/C1SM05706E

Kellenberger, E. (1991). Functional consequences of improved structural information on bacterial nucleoids. *Res. Microbiol.* 142, 229–238. doi: 10.1016/0923-2508(91)90035-9

Kuhlman, T. E., and Cox, E. C. (2012). Gene location and DNA density determine transcription factor distributions in *Escherichia coli*. *Mol Syst. Biol.* 8:610. doi: 10.1038/msb.2012.42

Landgraf, D., Okumus, B., Chien, P., Baker, T. A., and Paulsson, J. (2012). Segregation of molecules at cell division reveals native protein localization. *Nat. Methods* 9, 480–498. doi: 10.1038/nmeth.1955

Le, T. B., Imakaev, M. V., Mirny, L. A., and Laub, M. T. (2013). High-resolution mapping of the spatial organization of a bacterial chromosome. *Science* 342, 731–734. doi: 10.1126/science.1242059

Le, T. B., and Laub, M. T. (2014). New approaches to understanding the spatial organization of bacterial genomes. *Curr. Opin. Microbiol.* 22C, 15–21. doi: 10.1016/j.mib.2014.09.014

Lewis, P. J., Thaker, S. D., and Errington, J. (2000). Compartmentalization of transcription and translation in *Bacillus subtilis*. *EMBO J.* 19, 710–718. doi: 10.1093/emboj/19.4.710

Libby, E. A., Roggiani, M., and Goulian, M. (2012). Membrane protein expression triggers chromosomal locus repositioning in bacteria. *Proc. Natl. Acad. Sci. U.S.A.* 109, 7445–7450. doi: 10.1073/pnas.1109479109

Lippincott-Schwartz, J., and Patterson, G. H. (2009). Photoactivatable fluorescent proteins for diffraction-limited and super-resolution imaging. *Trends Cell Biol.* 19, 555–565. doi: 10.1016/j.tcb.2009.09.003

Llopis, P. M., Jackson, A. F., Sliusarenko, O., Surovtsev, I., Heinritz, J., Emonet, T., et al. (2010). Spatial organization of the flow of genetic information in bacteria. *Nature* 466, U77–U90. doi: 10.1038/nature09152

Marenduzzo, D., Micheletti, C., and Cook, P. R. (2006). Entropy-driven genome organization. *Biophys. J.* 90, 3712–3721. doi: 10.1529/biophysj.105.077685

McGary, K., and Nudler, E. (2013). RNA polymerase and the ribosome: the close relationship. *Curr. Opin. Microbiol.* 16, 112–117. doi: 10.1016/j.mib.2013.01.010

Miller, O. L., Hamkalo, B. A., and Thomas, C. A. (1970). Visualization of bacterial genes in action. *Science* 169, 392–395. doi: 10.1126/science.169.3943.392

Mondal, J., Bratton, B. P., Li, Y., Yethiraj, A., and Weisshaar, J. C. (2011). Entropy-based mechanism of ribosome-nucleoid segregation in *E. coli*, cells. *Biophys. J.* 100, 2605–2613. doi: 10.1016/j.bpj.2011.04.030

Neidhardt, F. C., Bloch, P. L., and Smith, D. F. (1974). Culture medium for enterobacteria. *J. Bacteriol.* 119, 736–747.

Nevo-Dinur, K., Nussbaum, A.,-Shochat, Ben, S.,-Y., and Amster, O.-C. (2011). Translation-independent localization of mRNA in *E. coli*, *Science* 331, 1081–1084. doi: 10.1126/science.1195691

Norris, V., and Madsen, M. S. (1995). Autocatalytic gene expression occurs via transertion and membrane domain formation and underlies differentiation in bacteria: a model. *Mol. J. Biol.* 253, 739–748. doi: 10.1006/jmbi.1995.0587

Odijk, T. (1998). Osmotic compaction of supercoiled DNA into a bacterial nucleoid. *Biophys. Chem.* 73, 23–29. doi: 10.1016/S0301-4622(98)00115-X

Pelletier, J., Halvorsen, K., Ha, B. Y., Paparcone, R., Sandler, S. J., Woldringh, C. L., et al. (2012). Physical manipulation of the *Escherichia coli* chromosome reveals its soft nature. *Proc. Natl. Acad. Sci. U.S.A.* 109, E2649–E2656. doi: 10.1073/pnas.1208689109

Pettijohn, D. E. (1982). Structure and properties of the bacterial nucleoid. *Cell* 30, 667–669. doi: 10.1016/0092-8674(82)90269-0

Proshkin, S., Rahmouni, A. R., Mironov, A., and Nudler, E. (2010). Cooperation between translating ribosomes and RNA polymerase in transcription elongation. *Science* 328, 504–508. doi: 10.1126/science.1184939

Robinow, C., and Kellenberger, E. (1994). The bacterial nucleoid revisited. *Microbiol. Rev.* 58, 211–232.

Rust, M. J., Bates, M., and Zhuang, X. (2006). Sub-diffraction-limit imaging by stochastic optical reconstruction microscopy (STORM). *Nat. Methods* 3, 793–795. doi: 10.1038/nmeth929

Sanamrad, A., Persson, F., Lundius, E. G., Fange, D., Gynna, A. H., and Elf, J. (2014). Single-particle tracking reveals that free ribosomal subunits are not excluded from the *Escherichia coli* nucleoid. *Proc. Natl. Acad. Sci. U.S.A.* 111, 11413–11418. doi: 10.1073/pnas.1411558111

Shendruk, T. N., Bertrand, M., de Haan, H. W., Harden, J. L., and Slater, G. W. (2015). Simulating the entropic collapse of coarse-grained chromosomes. *Biophys. J.* 108, 810–820. doi: 10.1016/j.bpj.2014.11.3487

Svetlov, V., and Nudler, E. (2012). Unfolding the bridge between transcription and translation. *Cell* 150, 243–245. doi: 10.1016/j.cell.2012.06.025

van Helvoort, J. M., Kool, J., and Woldringh, C. L. (1996). Chloramphenicol causes fusion of separated nucleoids in *Escherichia coli* K-12 cells and filaments. *J. Bacteriol.* 178, 4289–4293.

Vrljic, M., Nishimura, S. Y., and Moerner, W. E. (2007). Single-molecule tracking. *Methods Mol. Biol.* 398, 193–219. doi: 10.1007/978-1-59745-513-8_14

Wang, T., Ingram, C., and Weisshaar, J. C. (2010). Model lipid bilayer with facile diffusion of lipids and integral membrane proteins. *Langmuir* 26, 11157–11164. doi: 10.1021/la101046r

Wang, W. Q., Li, G. W., Chen, C. Y., Xie, X. S., and Zhuang, X. W. (2011). Chromosome organization by a nucleoid-associated protein in live bacteria. *Science* 333, 1445–1449. doi: 10.1126/science.1204697

Woldringh, C. L. (2002). The role of co-transcriptional translation and protein translocation (transertion) in bacterial chromosome segregation. *Mol. Microbiol.* 45, 17–29. doi: 10.1046/j.1365-2958.2002.02993.x

Woldringh, C. L., Jensen, P. R., and Westerhoff, H. V. (1995). Structure and partitioning of bacterial DNA: determined by a balance of compaction and expansion forces? *FEMS Microbiol. Lett.* 131, 235–242. doi: 10.1111/j.1574-6968.1995.tb07782.x

Youngren, B., Nielsen, H. J., Jun, S., and Austin, S. (2014). The multifork *Escherichia coli* chromosome is a self-duplicating and self-segregating thermodynamic ring polymer. *Genes Dev.* 28, 71–84. doi: 10.1101/gad.231050.113

Zhang, J., Campbell, R. E., Ting, A. Y., and Tsien, R. Y. (2002). Creating new fluorescent probes for cell biology. *Nat. Rev. Mol. Cell Biol.* 3, 906–918. doi: 10.1038/nrm976

Zimmerman, S. B. (2002). Toroidal nucleoids in *Escherichia coli* exposed to chloramphenicol. *Struct. J. Biol.* 138, 199–206. doi: 10.1016/S1047-8477(02)00036-9

Zimmerman, S. B. (2006). Shape and compaction of *Escherichia coli* nucleoids. *J. Struct. Biol.* 156, 255–261. doi: 10.1016/j.jsb.2006.03.022

Zimmerman, S. B., and Murphy, L. D. (1996). Macromolecular crowding and the mandatory condensation of DNA in bacteria. *FEBS Lett.* 390, 245–248. doi: 10.1016/0014-5793(96)00725-9

Conflict of Interest Statement: The authors declare that the research was conducted in the absence of any commercial or financial relationships that could be construed as a potential conflict of interest.

Copyright © 2015 Bakshi, Choi and Weisshaar. This is an open-access article distributed under the terms of the Creative Commons Attribution License (CC BY). The use, distribution or reproduction in other forums is permitted, provided the original author(s) or licensor are credited and that the original publication in this journal is cited, in accordance with accepted academic practice. No use, distribution or reproduction is permitted which does not comply with these terms.

frontiers in Microbiology

REVIEW
published: 21 May 2015
doi: 10.3389/fmicb.2015.00497

The dynamic nature and territory of transcriptional machinery in the bacterial chromosome

Ding J. Jin, Cedric Cagliero, Carmen M. Martin, Jerome Izard and Yan N. Zhou*

Transcription Control Section, Gene Regulation and Chromosome Biology Laboratory, National Cancer Institute, National Institutes of Health, Frederick, MD, USA

Our knowledge of the regulation of genes involved in bacterial growth and stress responses is extensive; however, we have only recently begun to understand how environmental cues influence the dynamic, three-dimensional distribution of RNA polymerase (RNAP) in *Escherichia coli* on the level of single cell, using wide-field fluorescence microscopy and state-of-the-art imaging techniques. Live-cell imaging using either an agarose-embedding procedure or a microfluidic system further underscores the dynamic nature of the distribution of RNAP in response to changes in the environment and highlights the challenges in the study. A general agreement between live-cell and fixed-cell images has validated the formaldehyde-fixing procedure, which is a technical breakthrough in the study of the cell biology of RNAP. In this review we use a systems biology perspective to summarize the advances in the cell biology of RNAP in *E. coli*, including the discoveries of the bacterial nucleolus, the spatial compartmentalization of the transcription machinery at the periphery of the nucleoid, and the segregation of the chromosome territories for the two major cellular functions of transcription and replication in fast-growing cells. Our understanding of the coupling of transcription and bacterial chromosome (or nucleoid) structure is also summarized. Using *E. coli* as a simple model system, co-imaging of RNAP with DNA and other factors during growth and stress responses will continue to be a useful tool for studying bacterial growth and adaptation in changing environment.

Keywords: RNA polymerase, bacterial nucleolus, replisome, chromosome territories, growth rate regulation, stress responses, superresolution imaging, *E. coli*

OPEN ACCESS

Edited by:
Arieh Zaritsky, Ben-Gurion University of the Negev, Israel

Reviewed by:
Moselio Schaechter, San Diego State University, USA
Long Cai, California Institute of Technology, USA
Bianca Sclavi, National Center for Scientific Research, France
Lucia B. Rothman-Denes, The University of Chicago, USA

****Correspondence:***
Ding J. Jin, Transcription Control Section, Gene Regulation and Chromosome Biology Laboratory, National Cancer Institute, PO Box B, Frederick, MD 21702, USA
jind@mail.nih.gov

Specialty section:
This article was submitted to Microbial Physiology and Metabolism, a section of the journal Frontiers in Microbiology

Received: *27 February 2015*
Accepted: *06 May 2015*
Published: *21 May 2015*

Citation:
Jin DJ, Cagliero C, Martin CM, Izard J and Zhou YN (2015) The dynamic nature and territory of transcriptional machinery in the bacterial chromosome. Front. Microbiol. 6:497. doi: 10.3389/fmicb.2015.00497

Features of E. Coli Genome That Are Important for Cell Growth and Chromosome Replication

Genome, Gene, and Growth Rate Regulation

Escherichia coli cells, such as the prototype K-12 strain MG1655, are small rod-shaped, gram-negative bacteria. The *E. coli* genome contains ∼4.6 million base pairs (bp). If fully stretched, a single *E. coli* genomic DNA is ∼1600 μm long, ∼1000-fold longer than the length of the cell; therefore the genome must be fully compacted to fit into a cell. The genome encodes 4453 genes, which are organized into about 2390 operons (Blattner et al., 1997; Riley et al., 2006). Not all genes are equal in terms of growth (or growth rate) regulation: *E. coli* genes can be broadly categorized in two functional classes: growth-promoting genes, represented by ribosomal RNA (rRNA) operons (for simplicity hereafter called *rrn*) and other genes.

The bacterial growth rate is determined by the growth medium (Kjeldgaard et al., 1958; Schaechter et al., 1958). Growth-promoting genes are few in number and mainly involved the synthesis of the translationary machinery, primarily *rrn* that encodes different species of rRNA and tRNA. Synthesis of rRNA is a rate-limiting step for the production of ribosomes (Gausing, 1980), as ribosomes are assembled onto nascent rRNAs. The number of ribosomes in the cell is proportional to the growth rate, which is needed to meet the demand for protein synthesis (Bremer and Dennis, 1996; Keener and Nomura, 1996). Because of the important role of rRNA synthesis in growth-rate regulation, the regulation of *rrn* has been extensively studied (Condon et al., 1995; Gourse et al., 1996; Wagner, 2002; Paul et al., 2004; Potrykus et al., 2011; Jin et al., 2012; Ross et al., 2013). The promoters of *rrn* are the most actively transcribed, accounting for >80% of total RNA synthesis in cells growing in nutrient-rich media (Bremer and Dennis, 1996), but become marginal under poor growth conditions or by the treatment of serine hydroxamate (SHX), a serine analog that triggers amino acid starvation (Tosa and Pizer, 1971) and induces the stringent response (Cashel et al., 1996). In addition, transcription of *rrn* is also regulated by an antitermination system containing NusA and NusB as well as other factors. While NusA binds to RNAP *in vitro* (Greenblatt and Li, 1981), NusB does not. NusB is thought to bind *in vivo* to the BoxA RNA sequences of nascent rRNA molecules and is also involved in rRNA processing (Torres et al., 2004; Bubunenko et al., 2013). Another difference between the two functional classes of genes is their respective genomic DNA content (see below): while the seven *rrn* operons (each ~5.5 kb in length) represent only ~1% of genomic DNA, other genes represent 99% of the genome.

Bacterial Growth and Chromosome Replication

The *E. coli* genetic map is shown in **Figure 1A**. The chromosome is a circular DNA molecule with a specific origin of chromosome replication (*oriC*). After initiation, DNA replication proceeds bidirectionally as a pair of replication forks toward the terminus region (*ter*). As an integral component of replisomes (Yao and O'Donnell, 2010), single-stranded DNA binding protein (SSB) (Reyes-Lamothe et al., 2008; Marceau et al., 2011) coats the single-stranded DNA at the replication forks and interacts with the DNA polymerase III holoenzyme (O'Donnell, 2006). SeqA protein polymerizes with the nascent hemimethylated DNA at or near the DNA replication forks (Slater et al., 1995; Yamazoe et al., 2005; Waldminghaus et al., 2012).

Several features related to the *E. coli* lifestyle and the location of growth-promoting genes in the genome are important with respect to bacterial growth and chromosome replication.

First, the cell size and the copy number of the bacterial chromosome in a cell are sensitive to growth rate (Jin et al., 2013) (**Figure 1B**). The combined time required to complete a round of replication and subsequently chromosome segregation and cell division varies from ~70 to 150 min, depending on growth conditions (Stokke et al., 2012). Consequently, there are 1.5 genome equivalents (displaying one nucleoid surrounded by ribosomes) in a small slow-growing cell (doubling time 135 min) in M63 nutrient-poor media, containing glycerol as the carbon source at 30°C. When a cell's doubling time is shorter than the combined time required for replication and segregation, multiple initiations from *oriC* occur in preceding generations, manifesting "multi-fork replication" to ensure that at least one completed genome is passed onto each of the two newly formed daughter cells (Cooper and Helmstetter, 1968). For example, in a cell growing in nutrient-rich Lennox Broth (LB) at 37°C with a doubling time of ~20 min, the cell is large and there are up

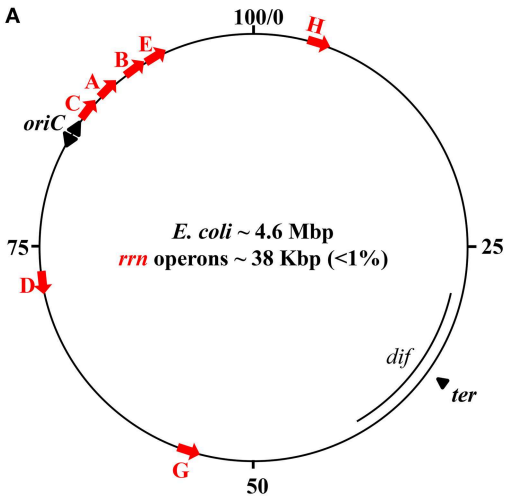

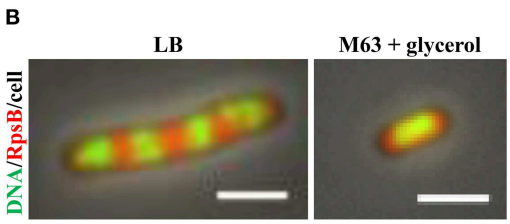

Doubling time	20min	135min
Genome equivalent	5.0	1.5
Copy of *rrn*	50	12

FIGURE 1 | *E. coli* chromosome map and features important for growth rate regulation and genome replication. (A) The genetic map of *E. coli* K-12. Positions of the *rrn* operons, along with *oriC,* and *ter* regions, are indicated. The red arrows represent each of the seven *rrn* operons, all of which are localized in the *oriC* proximal half of the chromosome; four are near the *oriC*, from which replication initiates and elongates bidirectionally, as indicated by black arrowheads. Transcription of *rrn* occurs in the same direction as replication. **(B)** Cell size and the number of genome equivalents and the *rrn* gene copies in a cell are sensitive to growth rate, as determined by growth medium. Images are overlays of nucleoid (green)/ribosome (red)/cell. Exponential-phase cells were prepared for imaging as described (Cabrera and Jin, 2003b). Ribosomes are tracked by 30S ribosomal subunit protein S2 fused with mCherry at the carboxy terminus (*rpsB-mCherry*). The nucleoid (DNA) is stained with Hoescht 33342. The cell growing in nutrient-rich LB (37°C) is large and has four apparent nascent nucleoids surrounded by ribosomes. The cell growing in minimal M63 + glycerol (30°C) is small and has only one apparent nucleoid surrounded with ribosomes. The scale bar represents 2 μm.

to five genome equivalents (displaying four nascent nucleoids surrounded by plentiful of ribosomes), and 8–16 copies of the *oriC* (Nielsen et al., 2007).

The second feature is the location of the seven *rrn* operons. All seven are located in the *oriC* half of the genome, and four of these are close to *oriC*. Because of the unique location of *rrn* relative to *oriC*, the gene dosage of *rrn* magnifies as the growth rate increases. For example, it can be calculated, based on the growth rate and the location of the *rrn* in the genetic map (Condon et al., 1993; Bremer and Dennis, 1996), that when cells are growing in LB at 30°C, with a doubling time of 45 min, the copy number for *rrn* is 18 per cell with more than two genome equivalents; however, with a doubling time of 20 min (LB, 37°C), the copy number of *rrn* approaches 50 per cell. This feature is particularly significant, as it dictates the differential allocation of RNAP between *rrn* and other genes genome-wide in response to changes in the environment, as described below. In addition, the transcription of *rrn* and most of the components of the translational machinery is in the same direction as that of chromosome replication (Rocha and Danchin, 2003; Lin et al., 2010). This co-directionality has likely evolved to minimize replication–transcription conflicts in bacteria (Merrikh et al., 2012).

Differential Allocation of RNA Polymerase between *rrn* and Other Genes Genome-Wide in Response to a Changing Environment: Evidence from Genetic and Genomic Studies

Competition for Limited RNAP between *rrn* and Other Genes Genome-Wide in Fast-Growing Cells

It becomes evident that RNAP is limiting in the cell for the simultaneous active expression of *rrn* and the broad transcription of other genes genome-wide. This notion was first suggested by the study of a class of RNAP mutants that altered growth rate regulation: these mutants grew slowly in LB because of reduced transcription of *rrn*, as if they were partially starved for amino acids, even in nutrient-rich medium. In contrast, the expression of some other genes that are activated only during starvation in wild type was elevated in those mutants grown in LB (Zhou and Jin, 1997, 1998). Combined with the biochemical studies of these RNAP mutants, it was proposed that RNAP is limiting in the cell for simultaneous active transcription of *rrn* and other genes involved in the stress response and thus RNAP redistributes from *rrn* to other genes in the genome during the stringent response induced by amino acid starvation (Zhou and Jin, 1998). Analysis of these RNAP mutants motivated the initiation of research on the cell biology of RNAP as described below.

RNAP is primarily allocated to the active transcription of *rrn* in cells growing in nutrient-rich media. Micrographs of chromatin spreads of fast-growing cells revealed that RNAP molecules are packed during *rrn* synthesis, at an estimated 65 RNAP molecules per *rrn* (French and Miller, 1989). The estimated number of RNAP molecules in a cell varies by quantitative Western blot analysis (Ishihama, 2000; Grigorova et al., 2006; Piper et al., 2009), but direct counting of single molecules using photoactivated localization microscopy (PALM) yields an independent measurement of ∼5000 RNAP molecules in a fast-growing cell (Bakshi et al., 2012; Endesfelder et al., 2013). Consequently, in a fast-growing cell with a doubling time of 20 min (LB, 37°C), active transcription of the estimated 50 copies of *rrn* will consume 3250 RNAP molecules, indicating that ∼65% of the total RNAP (assuming ∼5000 molecules per cell) is allocated for rRNA synthesis. To use an analogy, in fast-growing cells, most of the bacterial RNAP functions as eukaryotic Pol I/III activities to promote growth. In eukaryotic cells Pol I is responsible for the synthesis of rRNA at the nucleolus (O'Sullivan et al., 2013) and Pol III makes small RNAs including tRNAs. Consequently, only a small fraction of *E. coli* RNAP engages in transcription of other genes in the remaining ∼99% of the genome, consistent with the finding that most regions of the chromatin spreads appeared to be "naked," or devoid of RNAP (French and Miller, 1989).

Redistribution of RNAP from *rrn* to Other Genes Genome-Wide during Stress Responses

When fast-growing cells are exposed to nutrient limitation/starvation or to stresses, the immediate response of cells is to "turn off" *rrn* expression, leading to the decrease and/or arrest of growth, and concomitantly to "turn on" other genes involved in the response. The "feast or famine" or "thrive or survive" lifestyle not only reflects the amazing ability of *E. coli* to rapidly respond and/or adapt to changing environments but also represents the two ends of the spectrum in bacterial growth rate regulation. Global transcriptional profiling of cells grown on different carbon sources has indicated that there is an apparent inverse correlation between the growth potential of the environment and the number of genes expressed systematically genome-wide (Liu et al., 2005). The poorer the quality of carbon source used, the larger the number of genes that are expressed genome-wide. Similarly, when fast-growing cells are subject to amino acid starvation with the addition of SHX, leading to the stringent response (Cashel et al., 1996), transcription of *rrn* becomes minimal and the cells' growth arrests, whereas the number of other genes expressed across the genome increases systematically (Durfee et al., 2008; Traxler et al., 2008). To use another analogy, in cells undergoing stress responses, most of the bacterial RNAP functions as eukaryotic Pol II activities for bulk mRNA synthesis at the expense of the *rrn* expression.

This apparent inverse relationship between the expression of *rrn* and the number of other genes expressed genome-wide in response to changes in the environment indicates that growth regulation and stress responses can be explained by genome-wide competition between *rrn* and other genes for limited RNAP in the cell (Jin et al., 2012). The differential allocation of RNAP between the two functional classes of genes in response to changes in the environment also argues against the notion that there are a significant number of "inactive" RNAP molecules in the cell (Bremer and Dennis, 1996).

Extensive studies with different approaches have pointed to the special role of rRNA synthesis in both cell growth and the competition for the limited RNAP in the transcription of other genes genome-wide in response to environmental cues. These studies have provided an intellectual foundation for understanding the cell biology of RNAP in cells under different growth conditions.

Imaging the Dynamic Distribution of RNAP in Cells Responding Rapidly to Environmental Cues: Challenge and a Breakthrough Solution

The Distribution of RNAP in Fast-Growing Cells Undergoes Continuous Change during Sampling Preparation and Live-Cell Imaging

Shortly after green fluorescent protein (GFP) technology was introduced into bacteria (Gordon et al., 1997; Lewis et al., 2000; Margolin, 2000), an *E. coli* chromosomal *rpoC-gfp* fusion as the RNAP-GFP reporter was constructed to study the cell biology of RNAP in fast-growing cells and in cells undergoing an amino acid starvation–induced stress response (Cabrera and Jin, 2003a,b). Since then, many derivatives of the RNAP-GFP reporter have been constructed in *E. coli* to study the distribution of RNAP under different conditions using wide-field microscopy and other cutting-edge imaging techniques (Cabrera et al., 2009; Bakshi et al., 2012; Cagliero and Jin, 2013; Endesfelder et al., 2013; Jin et al., 2013).

It soon became evident that the distribution of RNAP is extremely sensitive to physiological perturbations, including those caused by the sampling and imaging processes; such a property has not been reported for other GFP reporters, such as the *parS*-ParB-GFP system (Nielsen et al., 2007) and the SSB-GFP fusion used in tracking the replisome (Reyes-Lamothe et al., 2008). Initially, no difference was observed in the RNAP distribution in living cells under different growth conditions. **Figure 2A** shows a set of images of living cells growing in a rapidly shaking flask (LB, 37°C), a condition in which most RNAP molecules are engaged in active rRNA synthesis. These cells were imaged after sampling from the flask and then agarose-embedded on coverslips at room temperature (25°C). The pattern of RNAP distribution changes depending on the length of time between sampling preparation and imaging. For example, RNAP foci could be observed in some cells after a short time (3 min); however, as the length of time increases (6 min), only few cells have RNAP foci, and RNAP is homogeneously distributed in the nucleoid in the cell population after 12 min. Note that nucleoid structure also changes in parallel and becomes expanded as time increases during the imaging process, indicating also the dynamic nature of the nucleoid. Experimentally, the time elapsed between sampling and image acquisition is usually longer than 10 min. The same distribution pattern was also observed in fast-growing cells treated either with rifampicin (**Figure 3A**, living cell), or with SHX (**Figure 3B**, living cell), which inhibit *rrn* transcription. RNAP is distributed homogeneously in the nucleoid regardless of growth conditions and status of *rrn* synthesis in living cells under the conditions used.

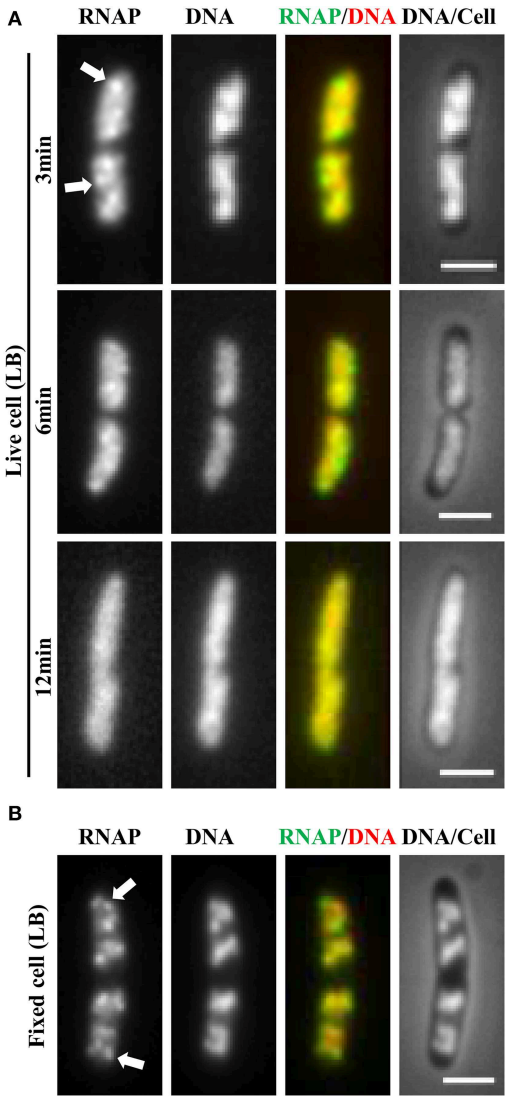

FIGURE 2 | Challenge of imaging RNAP in fast-growing living cells and a breakthrough technique using a formaldehyde-fixed cell procedure. **(A)** Rapidly disappearing RNAP foci during sampling and imaging of fast-growing living cells (LB, 37°C). Exponential-phase cells (*rpoC-venus*) in a rapidly shaking flask in a water bath were sampled and agarose embedded on coverslips for imaging at different time intervals as indicated. The sampling and preparation were performed as described (Cabrera and Jin, 2003b), except that there was no formaldehyde treatment. The nucleoid (DNA) was stained with Hoescht 33342. **(B)** Same as in **(A)**, except that the cells were fixed with formaldehyde immediately after sampling. RNAP foci were stable in the formaldehyde-fixed cells for a few hr before imaging. Foci are indicated by arrows. The scale bar represents 2 μm.

Using Formaldehyde-Fixed Cells Revolutionizes the Imaging of RNAP

Realizing that fast-growing cells in a rapidly shaking flask quickly adapt to slow-growth or growth arrest on coverslips during

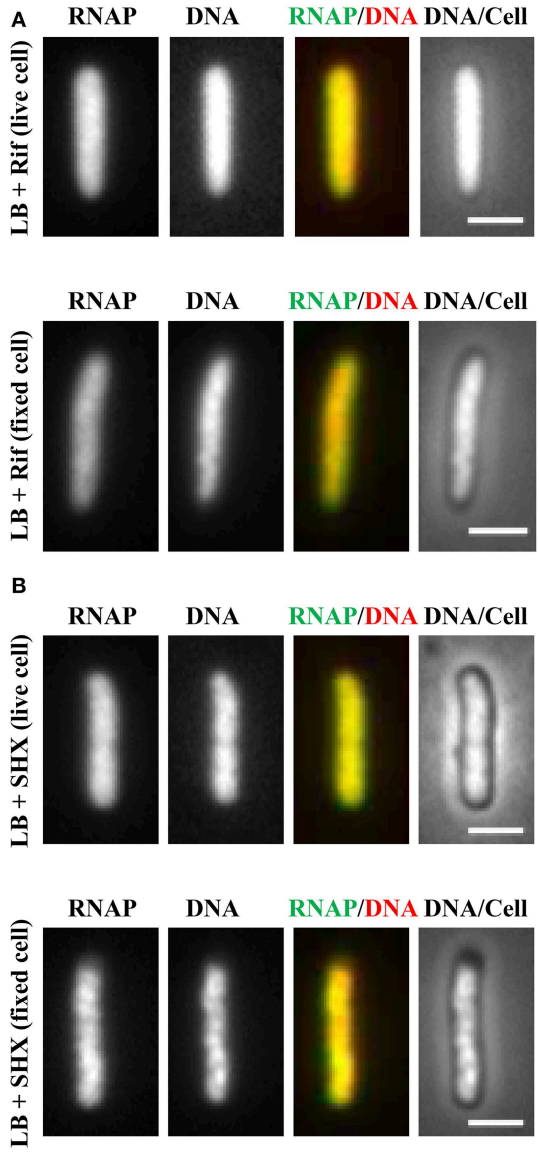

FIGURE 3 | Inhibition of *rrn* expression leads to homogeneous distribution of RNAP across the nucleoid in both living and fixed cells. Fast-growing cells (LB, 37°C) were treated with either rifampicin (100 μg/ml) for 15 min **(A)** or with SHX (500 μg/ml) for 30 min **(B)**. Cells were sampled and agarose embedded on coverslips. Live-cell imaging (live cell); Fixed-cell imaging (fixed cell), cells were fixed by formaldehyde. The scale bar represents 2 μm.

the sampling procedure, which usually takes between 10 and 15 min, and that sequential imaging would capture only the adapted states of RNAP, thereby missing the "true" state of RNAP in fast-growing cells, it became essential to develop a new sampling procedure. To this end, a formaldehyde-fixed cell procedure was developed, in which cells under different physiological conditions are immediately fixed or cross-linked with formaldehyde to "freeze" RNAP and subcellular structures before embedding them in agarose on coverslips for imaging. Formaldehyde is a cell-permeable, small four-atom molecule that penetrates cells rapidly and cross-links stably bound proteins to DNA (Schmiedeberg et al., 2009). This breakthrough technique has enabled the capture of dynamic states of RNAP in *E. coli* as snapshots in changing environments; the results have been shown to be consistent with the genetics and physiology of *E. coli* cells (Cabrera and Jin, 2003b). For example, RNAP forms prominent foci (**Figure 2B**, fixed cell) at the clustering of *rrn*, resembling a bacterial nucleolus in fast-growing cells (LB, 37°C) (more below). In contrast, there are no RNAP foci in cells treated with either rifampicin (**Figure 3A**, fixed cell) or SHX (**Figure 3B**, fixed cell); instead, RNAP distributes homogeneously across the nucleoid. These images have provided the first biological evidence, at a single-cell level, of the redistribution of RNAP from the clustering of *rrn* in fast-growing cells to a broad genome-wide transcription (or RNAP binding) in cells undergoing stresses. Intriguingly, changes in the distribution of RNAP accompany changes in nucleoid structure (see **Figures 2**, **3**), revealing the role of RNAP and transcription in the organization of the bacterial chromosome (Jin and Cabrera, 2006; Jin et al., 2013) (more below). On a cautionary note, the dynamic nature of the nucleoid, which responds to changes in the environment and sampling and imaging processes, should be taken into consideration when studying cell cycles using live-cell imaging.

Live-Cell Imaging Using Continuous-Flow Microfluidics Has Further Validated the Use of Formaldehyde in the Study of the Cell Biology of RNAP

Recently, continuous-flow microfluidics has been introduced for live cell imaging of *E. coli* (Wang et al., 2010). This technique has the advantage of enabling continuous live-cell imaging of RNAP in fast-growing and/or in changing environments without sampling interruptions. Time-lapse images from a set of such experiments are shown in **Figure 4**. RNAP foci are evident in fast-growing living cells in LB (RNAP and RNAP/nucleoid overlay), and the foci disappear shortly (~3 min) after the culture is downshifted from LB (at time 0) to nutrient-poor, minimal medium, M9 + glycerol; the process is reversible, as RNAP foci reappear after the culture is upshifted back to LB (RNAP and RNAP/Nucleoid overlay). Treatment of fast-growing cells in LB with SHX for 30 min (**Figure 5**) causes the RNAP foci to disappear (RNAP and RNAP/Nucleoid overlay) almost completely. In addition, RNAP foci are preserved after formaldehyde treatment of fast-growing cells in microfluidics (**Figure 6A**), whereas RNAP maintains a homogenous distribution pattern after the formaldehyde treatment of cells that were starved for amino acid by the SHX treatment (**Figure 6B**). Together, these findings demonstrated that formaldehyde does not cause "artificial" perturbations in the organization of RNAP and DNA in cells, as has been shown in ChIP-chip assays (Davis et al., 2011), and that the distribution of RNAP from fixed-cell images (Cabrera and Jin, 2003b, 2006; Cabrera et al., 2009; Cagliero and Jin, 2013; Endesfelder et al., 2013; Jin et al., 2013), reflects the true dynamic states of RNAP in living cells, thus validating the use of formaldehyde in the study of the cell biology of RNAP.

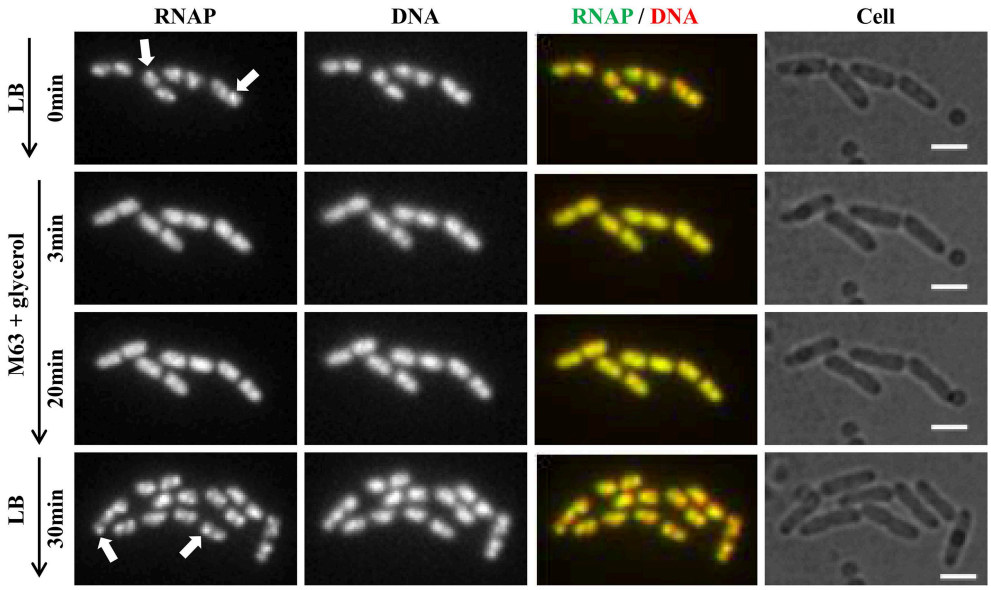

FIGURE 4 | RNAP foci are evident in fast-growing cells and dynamic in response to nutrient downshift and upshift using live-cell imaging with continuous-flow microfluidics. Cells (*rpoC-venus, hupA-mCherry*) were growing in a microfluidic device controlled by the CellASIC ONIX microfluidic perfusion system (EMD Millipore) with continuous flow of LB. After exponential-phase cells in LB were imaged (LB, 0 min), LB was replaced with M63 + glycerol, and time-lapse images were taken, two of which, at 3 min and 20 min, are shown. At 20 min, the minimal medium was replaced with LB, and 30 min later, the image shown was taken. The experiments with microfluidics were performed at 30°C because LB has high background autofluorescence at 37°C. It took about 1 min to complete a medium change in the system. Hu-mCherry was used as a proxy for DNA staining because the microfluidic device used has high autofluorescence in the range of 460–488 nm, which interferes with the detection of DNA-bind dye DAPI or Hoescht 33342. The scale bar represents 2 μm. RNAP foci are indicated by arrows. Note the changes in the cells' position and size during the imaging process.

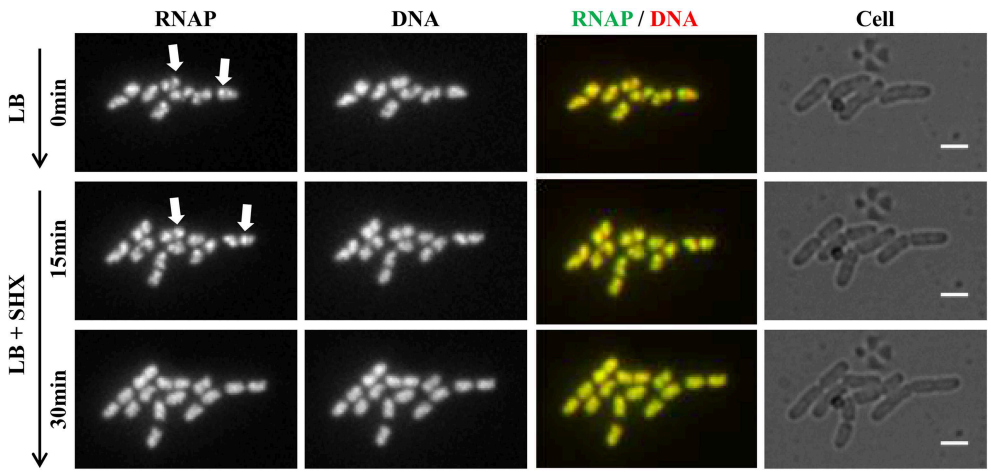

FIGURE 5 | Live-cell imaging using microfluidics confirms that RNAP foci disappear in cells treated with SHX, causing amino acid starvation. Cells (*rpoC-venus, hupA-mCherry*) were grown in LB using the CellASIC ONIX microfluidic system, as described in **Figure 4**. After exponential-phase cells in LB were imaged (LB, 0 min), LB was replaced with LB + SHX (500 μg/ml), and cells were imaged at different intervals after the SHX treatment. Images taken at 15 and 30 min after the addition of SHX are shown. The scale bar represents 2 μm. RNAP foci are indicated by arrows. Note the changes in the cells' position and size during the imaging process.

Imaging of RNAP in formaldehyde-fixed cells has significant advantages over live-cell imaging. Living cells, particularly fast-growing cells, undergo high metabolic activities, such as DNA replication and cell division, which constantly generate internal motions and may also change cells' positions in microfluidics during the imaging process (**Figures 4**, **5**). Also, because LB has high background autofluorescence, the quality of RNAP live-cell images, particularly in fast-growing cells in microfluidics,

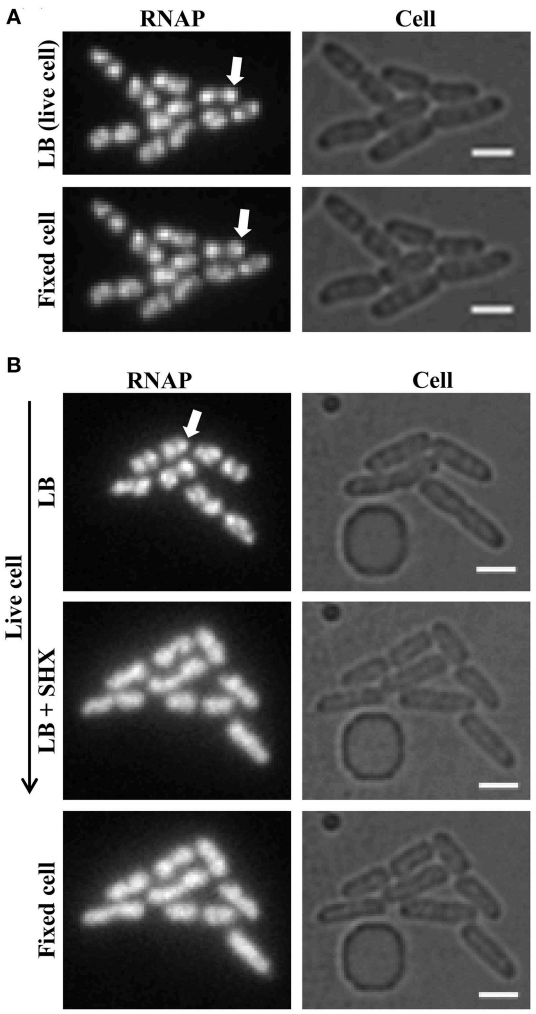

FIGURE 6 | Formaldehyde freezes the dynamic states of RNAP in living cells. (A) RNAP foci in fast-growing cells are preserved by formaldehyde treatment. Live-cell imaging with continuous-flow microfluidics was performed as described in **Figure 4**. After exponential-phase cells in LB were imaged (LB, live cell), LB was replaced with LB + formaldehyde (final concentration 3.7% v/v) for 10 min to fix the cells, followed by flushing with M63 + glycerol for 10 min before imaging (fixed cell). **(B)** Homogenous distribution of RNAP across the nucleoid is maintained in amino acid-starved cells by formaldehyde treatment. The early steps of live-cell imaging, including LB and LB + SHX for 30 min to induce amino acid starvation, were performed as described in **Figure 5**. The subsequent formaldehyde treatment steps were performed as described in **(A)** for fixed-cell imaging. For simplicity, only images of RNAP and cells are shown. RNAP foci are indicated by arrows. The scale bar represents 2 μm.

is rather poor. In addition, for some studies, the physiology of cells in a continuous-flow microfluidic device may be different from that of cells in shaking flasks in a water bath. In contrast, formaldehyde-fixed cells are immobile, and this characteristic is critical and mandatory for acquiring sharp superresolution co-images of RNAP and DNA, as demonstrated below.

It is noteworthy that the formaldehyde-fixed cell procedure has also been widely used in ChIP-chip assays to study the distribution of *E. coli* RNAP genome-wide in one dimension (Grainger et al., 2005; Herring et al., 2005; Davis et al., 2011) and in various chromosome conformation capture assays to probe chromosome organization in living cells (Dekker et al., 2002; Dostie et al., 2006; Umbarger et al., 2011; Cagliero et al., 2013). It is expected that the formaldehyde-fixed cell procedure will also be useful for the capture of dynamic states of other cellular machineries in *E. coli*.

Chromosome Territories in *E. Coli*: A Landscape of Transcription Machinery and Replisome

Significance of the Study of the Cell Biology of RNAP

Significant progress has been made in imaging the distribution of RNAP in *E. coli* in response to changing environments and these studies have shed new light on the differential allocation of RNAP in during bacterial growth and stress responses. Findings from the images of RNAP at the single-cell level complement other genomic analyses of transcription and RNAP binding, including gene arrays and ChIP-chip assays, which are used in population studies and in which the data involved in rRNA synthesis or RNAP binding at the *rrn* regions are purposely deleted to "simplify" the analyses. Consequently, these analyses have missed a significant part of the whole story in the lifestyle of *E. coli*, as transcription of *rrn* plays a key role in growth rate regulation. Specifically, as described below, recent co-imaging of RNAP with DNA and components of the replisome in a single cell has revealed some important features related to the spatial organization of the transcription machinery as well as the landscape of the transcription machinery and replisome (Cagliero et al., 2014). Features of the chromosome territories in bacteria are analogous to those of eukaryotes (Cremer et al., 2006; Meaburn and Misteli, 2007), indicating that *E. coli* is a useful simple model system to study chromosome biology in response to changes in the environment.

Bacterial Nucleolus

In fast-growing cells, most RNAP molecules are concentrated, forming foci at the clustering of *rrn*, which resembles the eukaryotic nucleolus. The presence of the bacterial nucleolus is inferred from the finding using wide-field microscopy, that the number of RNAP foci is significantly lower than the number of copies of *rrn* in a fast-growing cell (Cabrera and Jin, 2003b). Subsequent super-resolution images have further confirmed this finding (Endesfelder et al., 2013; Cagliero et al., 2014). For example, super-resolution structured illumination microscopy (SIM) of RNAP and DNA (Cagliero et al., 2014) (**Figure 7**) reveals that the median number of RNAP foci is eight per cell in fast-growing cells (LB at 37°C, doubling time 20 min) (**Figure 7C**). Compared with the estimated average of 50 *rrn* copies, then, each RNAP focus occurs, on average, at approximately six copies of *rrn*. The resolution (∼140 nm lateral and ∼300 nm axial for a typical Venus fluorophore) of SIM would be as effective as PALM in detecting small transcription foci in fast-growing cells. Indeed, analysis of PALM images

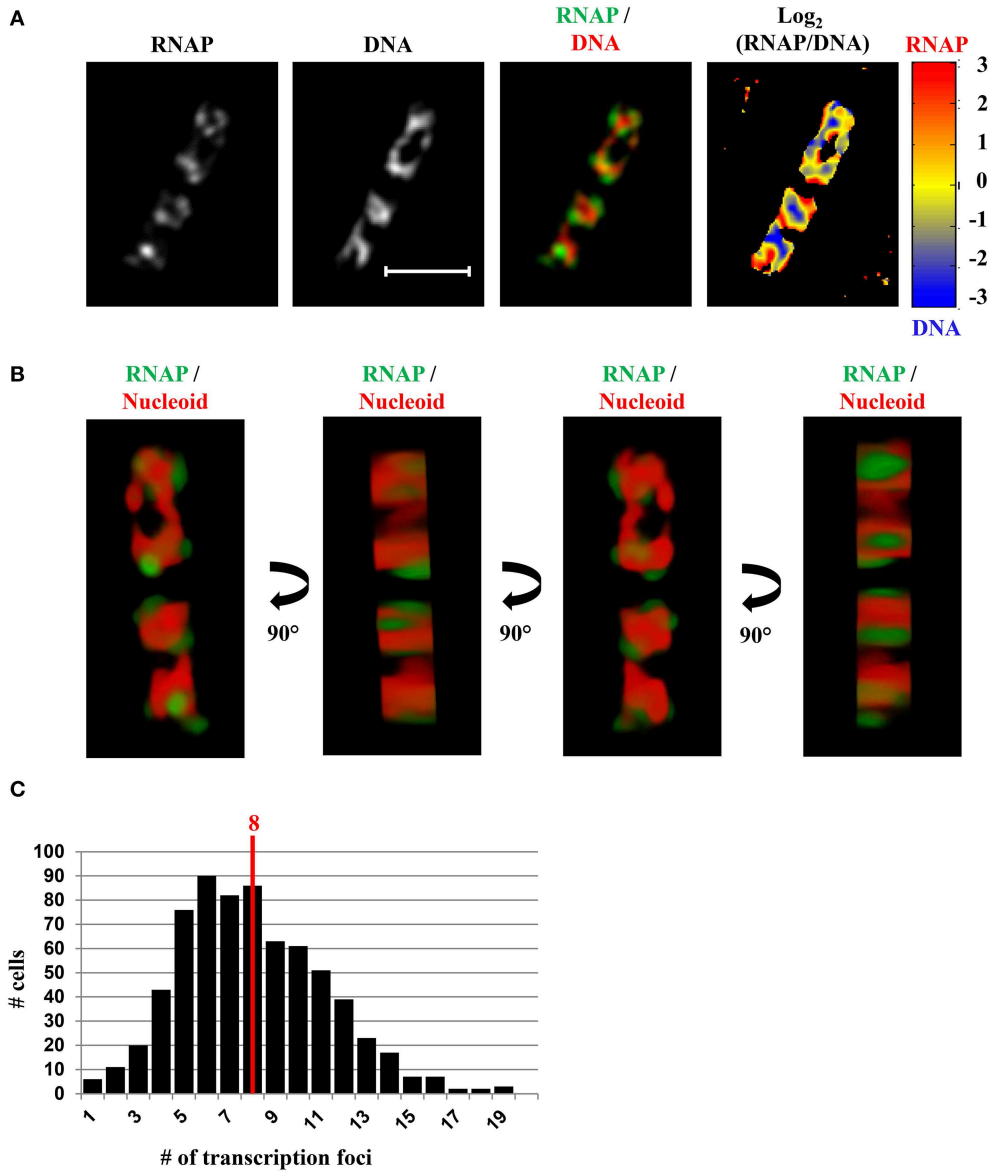

FIGURE 7 | SIM co-imaging of RNAP and DNA reveals spatial compartmentalization of transcription foci in fast-growing cells. **(A)** Images of RNAP, DNA (nucleoid), and an overlay of RNAP (green) and DNA (red) from a representative fast-growing *E. coli* cell (LB, 37°C). The scale bar represents 2 μm. The $\log_2$(RNAP/DNA) plot (heat map) is a quantitative representation of the relationship between RNAP and DNA, which is represented by a color scale bar with values ranging from −3 to 3. Note that regions enriched in RNAP up to eightfold over DNA are at the periphery of the nucleoid (red foci), and regions enriched in DNA up to eightfold over RNAP are in the center of the nucleoid (blue regions). **(B)** 3D representation of the overlay image of RNAP (green) and nucleoid (DNA) (red) in the cell, as shown in **(A)**. Compared with the first and the third panels (x–y axis), the second and fourth panels reflect the limited Z-stacking due to the short axis of the cell. **(C)** Histogram showing the distribution of apparent RNAP-Venus foci in fast-growing cells. The red line indicates the median number of transcription foci in the population of cells. Modified and adapted from Cagliero et al. (2014).

reveals that even small clusters (foci) of 70 RNAPs form a sphere of ∼160 nm in diameter (Endesfelder et al., 2013), which is larger than the resolution detectable by SIM. Whether *rrn* from different locations in the chromosome are clustered with RNAP foci remain to be determined experimentally.

There are up to four nascent nucleoids in a fast-growing cell; thus, on average, there are two RNAP foci per nascent nucleoid in the cell. The size of RNAP foci in fast-growing cells varies, probably reflecting the dynamic nature of the foci, as they are likely undergoing disassembly and reassembly when replication forks pass through the *rrn* region. The size variation of RNAP foci is consistent with the super-resolution images, using PALM, of both large clusters of RNAP (up to 800 molecules), which are likely engaging in rRNA synthesis from multiple *rrn* operons, and small clusters of RNAP (∼70 molecules), which are attributed to the transcription of a single *rrn* operon (Endesfelder et al.,

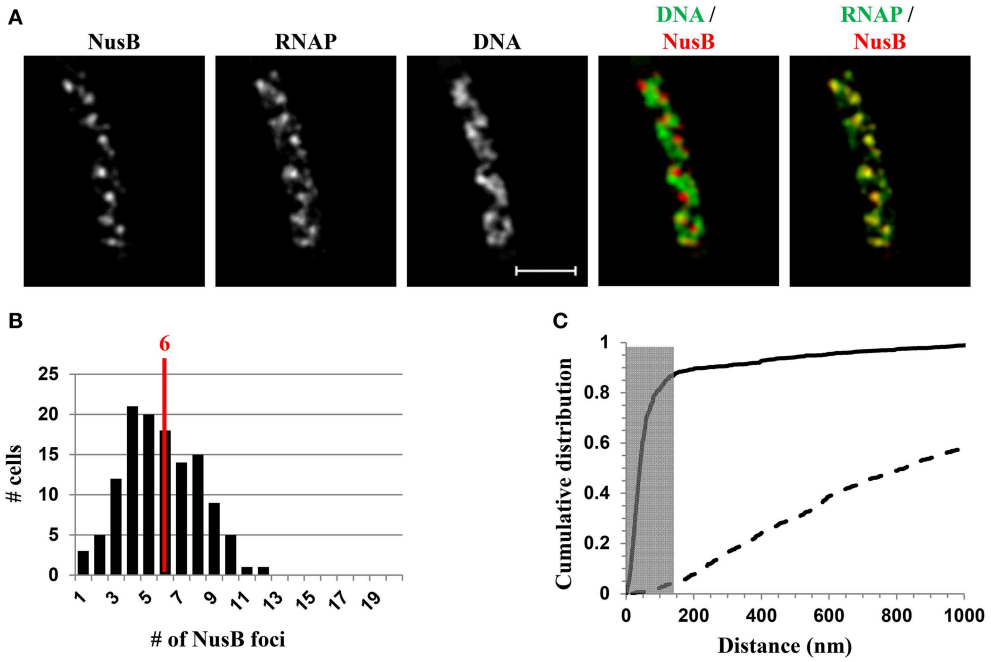

FIGURE 8 | Nascent rRNA-binding protein NusB forms foci and colocalizes with transcription foci in fast-growing cells. (A) Images of NusB, RNAP, DNA (nucleoid), overlay of NusB (red) and DNA (green), and overlay of RNAP (green) and NusB (red) from a representative fast-growing *E. coli* cell, as described in the legend to **Figure 7**. NusB foci are at the periphery of the nucleoid (separate red and green colors on the RNAP/NusB overlay) and the NusB signals perfectly colocalize with RNAP signals (overall yellow color on the RNAP/NusB overlay). **(B)** The distribution of apparent NusB-mCherry foci in fast-growing cells. The red line in the histogram indicates the median number of NusB foci in the population of cells. Note that the median number of NusB foci is close to that of RNAP foci in fast-growing cells. **(C)** Cumulative distribution of the distances between NusB foci and their closest RNAP foci in the population of cells. (—) NusB-mCherry RNAP-Venus, and (- - -) NusB-mCherry RNAP-Venus random. The gray rectangle represents the colocalization area (≤140 nm), as the theoretical SIM microscope resolution for the mCherry is 140 nm. 87.1% of the NusB foci are within 140 nm of the closest transcription foci. Adapted from Cagliero et al. (2014).

2013). As each nascent nucleoid has RNAP foci in place, each of the two newly formed daughter cells will "inherit" the functional transcription machinery without the need for *de novo* synthesis and/or assembly. Because transcription foci at the bacterial nucleolus are critical for growth rate regulation in *E. coli* (Jin et al., 2012), this feature can explain, in part, why newly formed daughter cells maintain the same fast growth rate as the parental cells.

Compartmentalization of RNAP Foci at the Periphery of the Nucleoid

A significant advantage of co-imaging RNAP with DNA is that it enables the determination of the spatial relationship between the transcription machinery and DNA. In a fast-growing cell, RNAP foci appear to be located at the periphery or surroundings of the nucleoid (RNAP/DNA overlay), either in two-dimensional SIM pictures (**Figure 7A**) or reconstituted three-dimensional SIM images (**Figure 7B**). The quantitative heat map, as a normalized Log_2(RNAP/DNA) density plot, further illustrates an inverse relationship between the intensities of RNAP and DNA (**Figure 7A**), indicating that RNAP foci at the clustering of *rrn* are low in DNA density or at loops at the surface of the nucleoid. Such a spatial organization has logistical advantages, including coupling of rRNA synthesis with rRNA processing and ribosome assembly, as well as reducing the traffic jams with other cellular functions.

RNAP foci are likely to be networking hubs for transcription of growth-promoting genes, because genome conformation capture assays have shown that those genes, which are down-regulated during amino acid starvation, are in a highly interactive environment and are present in large clusters (Cagliero et al., 2013). The spatial compartmentalization of RNAP foci suggests that transcription foci could be used as RNAP pools to effectively interact with DNA loops containing non-*rrn* growth-promoting genes located a distance away by hopping three-dimensionally, rather than by traveling linearly or laterally (Wang et al., 2013). Such an organization would reduce the transcription traffic jam and allow for maximum use of limited RNAP in the cell (Jin et al., 2012). It would be interesting to identify other non-*rrn* genes and RNAs as well as proteins in these potential transcription hubs. Other subcellular hyperstructures in bacteria have been described (Norris et al., 2007).

Components of *rrn* Antitermination and rRNA Processing Systems Are Colocalized with RNAP Foci

NusA and NusB are involved in *rrn* antitermination and rRNA processing systems. SIM co-imaging of RNAP-Venus with DNA

and NusA-mCherry or NusB-mCherry in fast-growing cells has demonstrated that, (i) like RNAP, NusA, or NusB forms foci at the periphery of the nucleoid, and the median number of NusA or NusB foci per cell is similar to that of the RNAP foci, and (ii) the NusA or NusB foci are co-localized with RNAP foci (Cagliero et al., 2014). For example, **Figure 8** shows the SIM images of NusB and its spatial relationship with DNA (DNA/NusB overlay) and with RNAP (RNAP/NusB) in a typical fast-growing cell (LB at 37°C) (**Figure 8A**). There were six NusB foci per cell on average in a population of fast-growing cells (**Figure 8B**), a value that is close to that of RNAP foci. The cumulative distribution of NusB foci and RNAP foci from a population of fast-growing cells has confirmed that most of NusB foci (>87%) are colocalized with RNAP foci at the clustering of *rrn* or bacterial nucleolus (**Figure 8C**), demonstrating that rRNA synthesis and processing are intimately coupled in space. It remains to be determined what other components are associated with transcription foci in fast-growing cells.

Spatial Segregation of Transcription Machinery and Replisome

Unlike a eukaryotic cell that has defined phases in the cell cycle (S, G2, M, and G1), all processes–such as transcription, replication, and chromosome segregation, are intimately entangled in a rapidly growing *E. coli* cell. Therefore, maximum expression of growth-promoting genes and multiple genome replications are occurring concurrently in a fast-growing cell. A long-standing interest in the field relates to understanding how the two major cellular functions, transcription and replication, maintain harmony to avoid conflicts between the two processes (Merrikh et al., 2012), particularly in fast-growing cells.

Recent SIM co-images of RNAP-Venus with DNA as well as with SeqA-mCherry or SSB-mCherry serving as proxies for replisomes have revealed chromosome landscapes for the two major functions of transcription and replication, which could explain why they remain in harmony in fast-growing cells. The major transcription machinery and replisome are mostly located in different chromosome territories or spatially segregated in the nucleoid (Cagliero et al., 2014). For example, **Figure 9A** shows the SIM images of SeqA and its spatial relationship with DNA (DNA/SeqA overlay) and with RNAP (RNAP/SeqA) in a typical fast-growing cell (LB at 37°C). Similar to RNAP foci and foci of NusA/NusB, SeqA foci also are located at the periphery of the nucleoid (DNA/SeqA overlay), indicating that the replisome is also compartmentalized in regions low in density of DNA or at DNA loops. Image analyses of populations of fast-growing cells showed that on average, each cell contains 10 SeqA foci (**Figure 9B**). In contrast to NusA/NusB, the cumulative distribution of SeqA foci and RNAP foci in the population of fast-growing cells has shown that most (~80%) of the SeqA foci

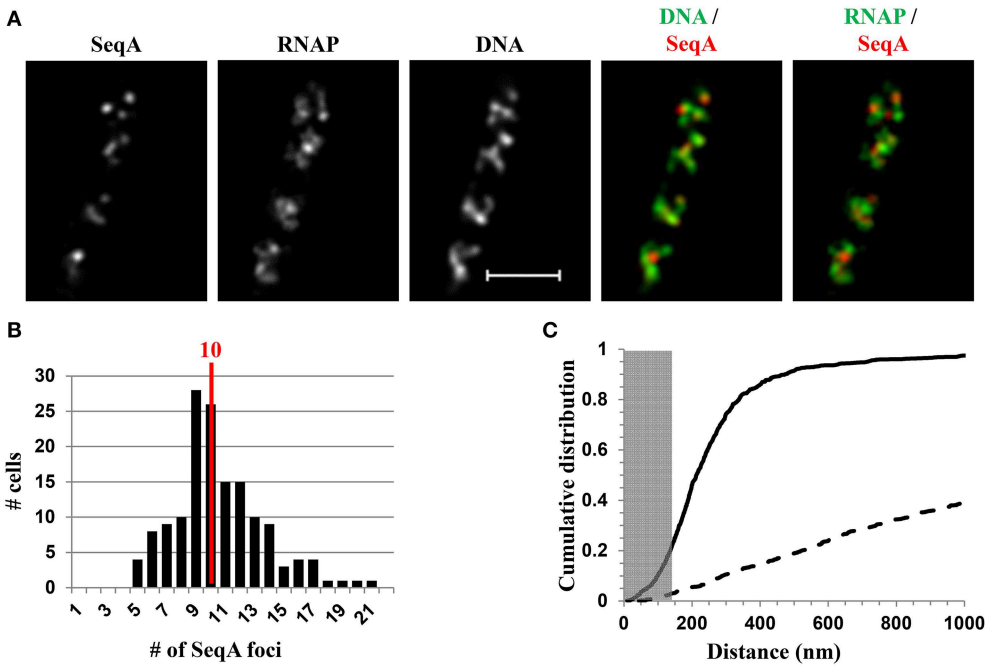

FIGURE 9 | Spatial segregation of transcription foci and replication forks tracked by SeqA in fast-growing cells. (A) Images of SeqA, RNAP, DNA (nucleoid), overlays of SeqA (red) and DNA (green), and RNAP (green) and SeqA (red) from a representative fast-growing *E. coli* cell, as described in the legend to **Figure 7**. SeqA foci and transcription foci are largely located at different positions (red and green colors on the overlay of SeqA and RNAP). Note also that most of the SeqA foci appear to be separated from high intensities of DNA signals in the nucleoids (red and green colors on the overlay of SeqA and DNA). **(B)** The distribution of apparent SeqA-mCherry foci in a population of fast-growing cells. The red line in the histogram indicates the median number of SeqA foci in these cells. **(C)** Cumulative distribution of the distances between SeqA foci and their closest RNAP foci in the population of cells. (—) SeqA-mCherry RNAP-Venus, and (- - -) SeqA-mCherry RNAP-Venus random. The gray rectangle represents the colocalization area (≤140 nm). Only 21.5% of the SeqA foci are within 140 nm of the closest transcription foci. Adapted from Cagliero et al. (2014).

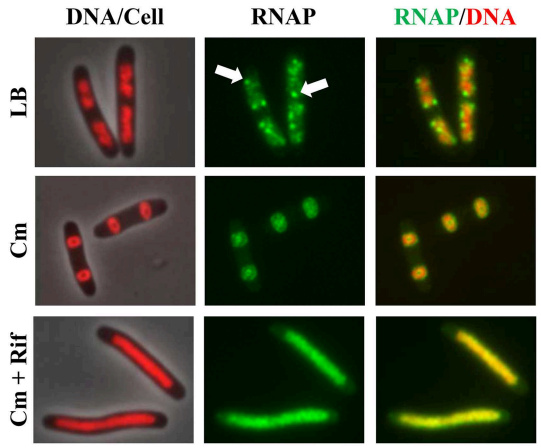

FIGURE 10 | Active *rrn* expression is required to condense the nucleoid in the presence of chloramphenicol. Images of overlay of DNA (nucleoid) and cell, RNAP, and overlay of RNAP and DNA are shown. DNA in the DNA/cell overlay is shown in red (left column), RNAP is shown in green (middle column), and the RNAP (green) and DNA (red) overlay is shown (right column). The panels on the top row show rapidly growing cells (*rpoC-gfp*) in LB, at 30°C, and RNAP foci are indicated by arrows; panels in the center row show cells treated with chloramphenicol (100 μg/ml) for 100 min; panels in the bottom row show cells sequentially treated with chloramphenicol (100 μg/ml, 10 min) and rifampicin (100 μg/ml, 90 min). Modified and adapted from Cabrera et al. (2009).

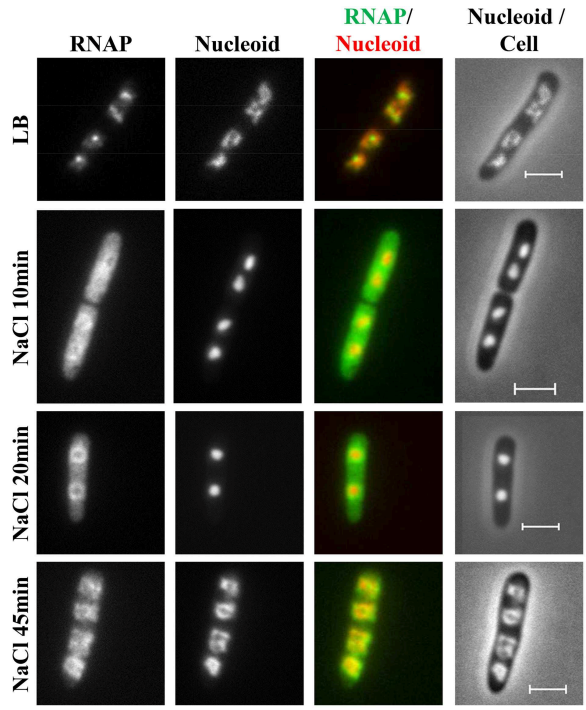

FIGURE 11 | Dynamic interaction of RNAP and DNA during the osmotic stress response. Images of RNAP, nucleoid, overlays of RNAP (green) and nucleoid (red), and nucleoid and cell (*rpoC-venus*) before LB or after osmotic shock (NaCl 10 min to NaCl 45 min). The RNAP rapidly dissociates from the nucleoid, and the released RNAP occupies the entire cytoplasmic space shortly after osmotic shock (NaCl 10 min). The nucleoid becomes hyper-condensed at the same time. Subsequently, the freed RNAP gradually re-associates with the genome by first forming a ring at the periphery of the hyper-condensed nucleoid (NaCl 20 min to NaCl 30 min) before penetrating the interior (NaCl 45 min). The scale bar represents 2 μm. Adapted from Cagliero and Jin (2013).

are not colocalized with the RNAP foci, i.e., the two cellular functions are mostly segregated in space (**Figure 9C**). The low co-localization frequency of SeqA foci and RNAP foci suggests transient overlapping of transcription and replication of *rrn* regions. It is conceivable that during replication of *rrn* operons, RNAP foci are somehow disassembled, allowing replication forks to pass through the region, followed by reassembly of transcription machinery at the *rrn* clusters. Development of fast, super-resolution, time-lapse, live-cell imaging techniques will be necessary to address the dynamic interaction and segregation of the two active cellular functions in fast-growing cells.

Coupling the Distribution of RNAP to the Organization of the Bacterial Nucleoid

Active rRNA Synthesis at the Clustering of *rrn* Causes Nucleoid Compaction

Co-imaging of RNAP and DNA in cells undergoing physiological perturbations has also revealed that global changes in the distribution of RNAP accompany alterations in nucleoid structure, indicating an important role of RNAP and transcription in the organization of the bacterial chromosome (Jin and Cabrera, 2006; Jin et al., 2013). The changes are stress-dependent and in most cases studied, as shown in **Figures 2**, **3**, redistribution of RNAP from a few prominent foci at the clustering of *rrn* to the nucleoid homogeneously leads to nucleoid expansion. In an effort to determine whether active rRNA synthesis is required to condense the nucleoid, the effects of the antibiotics chloramphenicol and rifampin as well as two mutations that decrease rRNA synthesis, on the nucleoid structure have been reexamined (Cabrera et al., 2009). The nucleoids are condensed in fast-growing cells (LB) treated with the translation inhibitor chloramphenicol (Woldringh et al., 1995; van Helvoort et al., 1996); however, if cells are treated sequentially with chloramphenicol first and then rifampicin, the nucleoids become expanded and RNAP foci disappear (**Figure 10**). Moreover, the nucleoids remain expanded in the above-described RNAP mutant cells defective in the transcription of *rrn* in LB when treated with chloramphenicol. Similarly, even with chloramphenicol treatment, the nucleoids remain expanded in the Δ6*rrn* cells that have only one copy of *rrn* remaining in the chromosome. Together, these results support the role of active rRNA synthesis from the clustering of *rrn* in nucleoid compaction in fast-growing cells. Because transcription and supercoiling are coupled (Liu and Wang, 1987), it is possible that transcription-induced supercoiling at the clustering of *rrn* (Jin et al., 2012) contributes to the nucleoid compaction in fast-growing cells.

The mechanisms underlying the apparent coupling of the distribution of RNAP with the organization of the bacterial chromosome remain to be determined. Multiple factors are likely

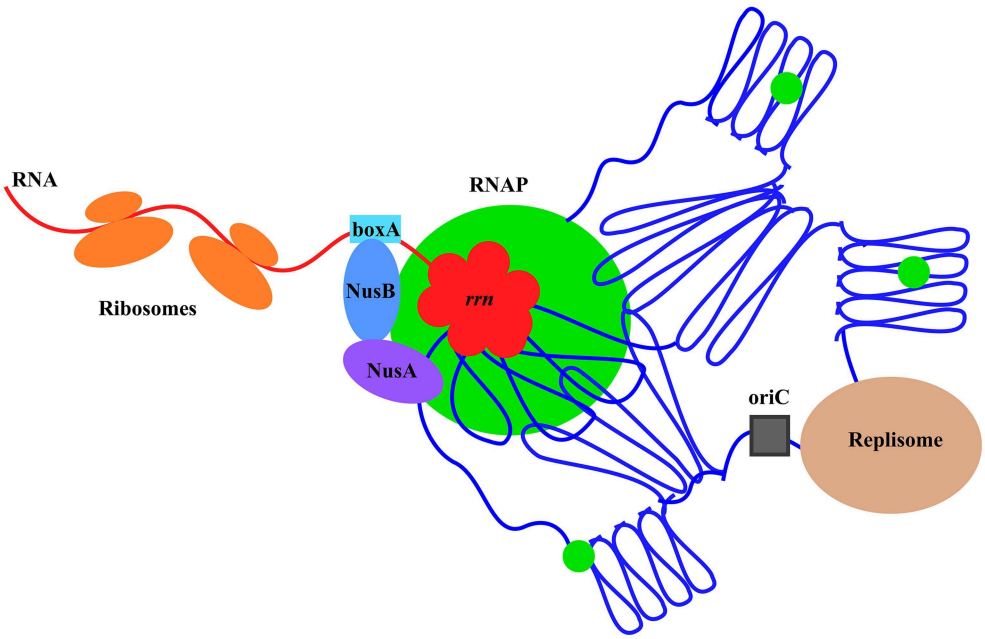

FIGURE 12 | Model illustrating the chromosome territories of the major transcription machinery and replisome in a fast-growing cell. The *E. coli* chromosome is represented by the blue lines folded in loops, the *oriC* by a black square, and the RNAP molecules by green circles. For simplicity, only one of the prominent transcription foci and the replisome are shown. RNAP foci at the clustering of *rrn* (red), resembling a bacterial nucleolus, are spatially organized at the periphery of the nucleoid for compartmentalization. Foci of NusA and NusB co-localize with RNAP foci, indicating the coupling of the synthesis and processing of rRNA, and, possibly, ribosomal assembly. Compartmentalization of the replisome is also shown, but the two major cellular functions of transcription and replication are largely spatially segregated. See text for the details and advantages of the landscapes of transcription machinery and replisome in fast-growing cells.

to be responsible for the organization of the bacterial nucleoid (Woldringh et al., 1995; Cagliero et al., 2013; Jin et al., 2013). Other small nucleoid-associated proteins (NAPs) or "histone-like" proteins, such as FIS, H-NS, HU, and IHF, play important architectural roles and are transcription factors (Luijsterburg et al., 2006; Browning et al., 2010; Dillon and Dorman, 2010; Liu et al., 2010; Pul and Wagner, 2012). The distribution of RNAP will likely to be affected by these NAPs and vice versa; together, they determine the organization of the nucleoid.

Temporal Changes in the Distribution of RNAP and the Nucleoid Structure in Response to Osmotic Stress

During hyperosmotic stress response, the changes in RNAP distribution and nucleoid compaction are temporally manifested (Cagliero and Jin, 2013). Initially, significant numbers of RNAP molecules dissociate from the nucleoid into the cytoplasmic space because of the transient accumulation of the cytoplasmic K^+, and, concomitantly, the nucleoid becomes hyper-condensed (**Figure 11**). Subsequently, when the cytoplasmic K^+ levels decrease during the osmoadaptation phase, the free RNAP re-associates with DNA and initially forms a ring at the periphery of the nucleoid, and the nucleoid gradually expands to a size approaching that prior to the salt shock. The ring of RNAP surrounding the hyper-condensed nucleoid during the early osmoadaptation phase (NaCl 20 min) is thought to indicate the location of DNA loops for the expression of responsive genes. The causes of temporal changes of the nucleoid structure during the osmotic stress response are not clear.

Summary

Co-imaging of RNAP with DNA as well as with other proteins in cells under different growth conditions has been an important tool and a new approach in the long-standing journey to understanding growth rate regulation and stress responses in *E. coli*. Significant progress has been made, including new concepts and findings from these studies, particularly in fast-growing cells (**Figure 12**). It is expected that more will be learned using wide-field and state-of-the-art imaging systems in future studies. In addition, as a simple model system, *E. coli* will have many advantages in seeking fundamental knowledge of the chromosome biology including chromosome territories, a frontier in biology research.

Acknowledgments

This research was supported by the Intramural Research Program of the NIH, National Cancer Institute, Center for Cancer Research. DJJ would like to thank the four reviewers and the editor for critical reading of the manuscript and productive interactions in the reviewing process.

References

Bakshi, S., Siryaporn, A., Goulian, M., and Weisshaar, J. C. (2012). Superresolution imaging of ribosomes and RNA polymerase in live *Escherichia coli* cells. *Mol. Microbiol.* 85, 21–38. doi: 10.1111/j.1365-2958.2012.08081.x

Blattner, F. R., Plunkett, G. III, Bloch, C. A., Perna, N. T., Burland, V., Riley, M., et al. (1997). The complete genome sequence of *Escherichia coli* K-12. *Science* 277, 1453–1474. doi: 10.1126/science.277.5331.1453

Bremer, H., and Dennis, P. P. (1996). "Modulation of chemical composition and other parameters of the cell by growth rate," in *Escherichia coli and Salmonella,* eds F. C. Neidhardt, R. Curtiss III, J. L. Ingraham, E. C. C. Lin, K. B. Low, B. Magasanik, W. S. Reznikoff, M. Riley, M. Schaechter, and H. E. Umbarger (Washington, DC: ASM Press), 1553–1569.

Browning, D. F., Grainger, D. C., and Busby, S. J. (2010). Effects of nucleoid-associated proteins on bacterial chromosome structure and gene expression. *Curr. Opin. Microbiol.* 13, 773–780. doi: 10.1016/j.mib.2010.09.013

Bubunenko, M., Court, D. L., Al Refaii, A., Saxena, S., Korepanov, A., Friedman, D. I., et al. (2013). Nus transcription elongation factors and RNase III modulate small ribosome subunit biogenesis in *Escherichia coli*. *Mol. Microbiol.* 87, 382–393. doi: 10.1111/mmi.12105

Cabrera, J. E., Cagliero, C., Quan, S., Squires, C. L., and Jin, D. J. (2009). Active transcription of rRNA operons condenses the nucleoid in *Escherichia coli*: examining the effect of transcription on nucleoid structure in the absence of transertion. *J. Bacteriol.* 191, 4180–4185. doi: 10.1128/JB.01707-08

Cabrera, J. E., and Jin, D. J. (2003a). Construction, purification, and characterization of *Escherichia coli* RNA polymerases tagged with different fluorescent proteins. *Methods Enzymol.* 370, 3–10. doi: 10.1016/S0076-6879(03)70001-9

Cabrera, J. E., and Jin, D. J. (2003b). The distribution of RNA polymerase in *Escherichia coli* is dynamic and sensitive to environmental cues. *Mol. Microbiol.* 50, 1493–1505. doi: 10.1046/j.1365-2958.2003.03805.x

Cabrera, J. E., and Jin, D. J. (2006). Active transcription of rRNA operons is a driving force for the distribution of RNA polymerase in bacteria: effect of extrachromosomal copies of rrnB on the *in vivo* localization of RNA polymerase. *J. Bacteriol.* 188, 4007–4014. doi: 10.1128/JB.01893-05

Cagliero, C., Grand, R. S., Jones, M. B., Jin, D. J., and O'Sullivan, J. M. (2013). Genome conformation capture reveals that the *Escherichia coli* chromosome is organized by replication and transcription. *Nucleic Acids Res.* 41, 6058–6071. doi: 10.1093/nar/gkt325

Cagliero, C., and Jin, D. J. (2013). Dissociation and re-association of RNA polymerase with DNA during osmotic stress response in *Escherichia coli*. *Nucleic Acids Res.* 41, 315–326. doi: 10.1093/nar/gks988

Cagliero, C., Zhou, Y. N., and Jin, D. J. (2014). Spatial organization of transcription machinery and its segregation from the replisome in fast-growing bacterial cells. *Nucleic Acids Res.* 42, 13696–13705. doi: 10.1093/nar/gku1103

Cashel, M., Gentry, D. R., Hernandez, V. J., and Vinella, D. (1996). "The stringent response," in *Escherichia coli and Salmonella,* eds F. C. Neidhardt, R. Curtiss III, J. L. Ingraham, E. C. C. Lin, K. B. Low, B. Magasanik, W. S. Reznikoff, M. Riley, M. Schaechter, and H. E. Umbarger (Washington, DC: ASM Press), 1458–1496.

Condon, C., French, S., Squires, C., and Squires, C. L. (1993). Depletion of functional ribosomal RNA operons in *Escherichia coli* causes increased expression of the remaining intact copies. *EMBO J.* 12, 4305–4315.

Condon, C., Squires, C., and Squires, C. L. (1995). Control of rRNA transcription in *Escherichia coli*. *Microbiol. Rev.* 59, 623–645.

Cooper, S., and Helmstetter, C. E. (1968). Chromosome replication and the division cycle of *Escherichia coli* B/r. *J. Mol. Biol.* 31, 519–540. doi: 10.1016/0022-2836(68)90425-7

Cremer, T., Cremer, M., Dietzel, S., Muller, S., Solovei, I., and Fakan, S. (2006). Chromosome territories–a functional nuclear landscape. *Curr. Opin. Cell Biol.* 18, 307–316. doi: 10.1016/j.ceb.2006.04.007

Davis, S. E., Mooney, R. A., Kanin, E. I., Grass, J., Landick, R., and Ansari, A. Z. (2011). Mapping *E. coli* RNA polymerase and associated transcription factors and identifying promoters genome-wide. *Methods Enzymol.* 498, 449–471. doi: 10.1016/B978-0-12-385120-8.00020-6

Dekker, J., Rippe, K., Dekker, M., and Kleckner, N. (2002). Capturing chromosome conformation. *Science* 295, 1306–1311. doi: 10.1126/science.1067799

Dillon, S. C., and Dorman, C. J. (2010). Bacterial nucleoid-associated proteins, nucleoid structure and gene expression. *Nat. Rev. Microbiol.* 8, 185–195. doi: 10.1038/nrmicro2261

Dostie, J., Richmond, T. A., Arnaout, R. A., Selzer, R. R., Lee, W. L., Honan, T. A., et al. (2006). Chromosome Conformation Capture Carbon Copy (5C): a massively parallel solution for mapping interactions between genomic elements. *Genome Res.* 16, 1299–1309. doi: 10.1101/gr.5571506

Durfee, T., Hansen, A. M., Zhi, H., Blattner, F. R., and Jin, D. J. (2008). Transcription profiling of the stringent response in *Escherichia coli*. *J. Bacteriol.* 190, 1084–1096. doi: 10.1128/JB.01092-07

Endesfelder, U., Finan, K., Holden, S. J., Cook, P. R., Kapanidis, A. N., and Heilemann, M. (2013). Multiscale spatial organization of RNA polymerase in *Escherichia coli*. *Biophys. J.* 105, 172–181. doi: 10.1016/j.bpj.2013.05.048

French, S. L., and Miller, O. L. Jr. (1989). Transcription mapping of the *Escherichia coli* chromosome by electron microscopy. *J. Bacteriol.* 171, 4207–4216.

Gausing, K. (1980). "Regulation of ribosome production in *Escherichia coli*," in *Ribosomes: Structure, Function and Genetics*, eds G. Chambliss, G. R. Craven, J. Davies, K. Davis, and M. Nomura (Baltimore, MD: University Park Press), 693–718.

Gordon, G. S., Sitnikov, D., Webb, C. D., Teleman, A., Straight, A., Losick, R., et al. (1997). Chromosome and low copy plasmid segregation in *E. coli:* visual evidence for distinct mechanisms. *Cell* 90, 1113–1121. doi: 10.1016/S0092-8674(00)80377-3

Gourse, R. L., Gaal, T., Bartlett, M. S., Appleman, J. A., and Ross, W. (1996). rRNA transcription and growth rate-dependent regulation of ribosome synthesis in *Escherichia coli*. *Annu. Rev. Microbiol.* 50, 645–677. doi: 10.1146/annurev.micro.50.1.645

Grainger, D. C., Hurd, D., Harrison, M., Holdstock, J., and Busby, S. J. (2005). Studies of the distribution of *Escherichia coli* cAMP-receptor protein and RNA polymerase along the *E. coli* chromosome. *Proc. Natl. Acad. Sci. U.S.A.* 102, 17693–17698. doi: 10.1073/pnas.0506687102

Greenblatt, J., and Li, J. (1981). Interaction of the sigma factor and the nusA gene protein of *E. coli* with RNA polymerase in the initiation-termination cycle of transcription. *Cell* 24, 421–428. doi: 10.1016/0092-8674(81)90332-9

Grigorova, I. L., Phleger, N. J., Mutalik, V. K., and Gross, C. A. (2006). Insights into transcriptional regulation and sigma competition from an equilibrium model of RNA polymerase binding to DNA. *Proc. Natl. Acad. Sci. U.S.A.* 103, 5332–5337. doi: 10.1073/pnas.0600828103

Herring, C. D., Raffaelle, M., Allen, T. E., Kanin, E. I., Landick, R., Ansari, A. Z., et al. (2005). Immobilization of *Escherichia coli* RNA polymerase and location of binding sites by use of chromatin immunoprecipitation and microarrays. *J. Bacteriol.* 187, 6166–6174. doi: 10.1128/JB.187.17.6166-6174.2005

Ishihama, A. (2000). Functional modulation of *Escherichia coli* RNA polymerase. *Annu. Rev. Microbiol.* 54, 499–518. doi: 10.1146/annurev.micro.54.1.499

Jin, D. J., and Cabrera, J. E. (2006). Coupling the distribution of RNA polymerase to global gene regulation and the dynamic structure of the bacterial nucleoid in *Escherichia coli*. *J. Struct. Biol.* 156, 284–291. doi: 10.1016/j.jsb.2006.07.005

Jin, D. J., Cagliero, C., and Zhou, Y. N. (2012). Growth rate regulation in *Escherichia coli*. *FEMS Microbiol. Rev.* 36, 269–287. doi: 10.1111/j.1574-6976.2011.00279.x

Jin, D. J., Cagliero, C., and Zhou, Y. N. (2013). Role of RNA polymerase and transcription in the organization of the bacterial nucleoid. *Chem. Rev.* 113, 8662–8682. doi: 10.1021/cr4001429

Keener, J., and Nomura, M. (1996). "Regulation of ribosome synthesis," in *Escherichia coli and Salmonella,* ed F. C. Neidhardt (Washington, DC: ASM Press), 1417–1431.

Kjeldgaard, N. O., Maaloe, O., and Schaechter, M. (1958). The transition between different physiological states during balanced growth of *Salmonella typhimurium*. *J. Gen. Microbiol.* 19, 607–616. doi: 10.1099/00221287-19-3-607

Lewis, P. J., Thaker, S. D., and Errington, J. (2000). Compartmentalization of transcription and translation in Bacillus subtilis. *EMBO J.* 19, 710–718. doi: 10.1093/emboj/19.4.710

Lin, Y., Gao, F., and Zhang, C. T. (2010). Functionality of essential genes drives gene strand-bias in bacterial genomes. *Biochem. Biophys. Res. Commun.* 396, 472–476. doi: 10.1016/j.bbrc.2010.04.119

Liu, L. F., and Wang, J. C. (1987). Supercoiling of the DNA template during transcription. *Proc. Natl. Acad. Sci. U.S.A.* 84, 7024–7027. doi: 10.1073/pnas.84.20.7024

Liu, M., Durfee, T., Cabrera, J. E., Zhao, K., Jin, D. J., and Blattner, F. R. (2005). Global transcriptional programs reveal a carbon source foraging strategy by *Escherichia coli*. *J. Biol. Chem.* 280, 15921–15927. doi: 10.1074/jbc.M414050200

Liu, Y., Chen, H., Kenney, L. J., and Yan, J. (2010). A divalent switch drives H-NS/DNA-binding conformations between stiffening and bridging modes. *Genes Dev.* 24, 339–344. doi: 10.1101/gad.1883510

Luijsterburg, M. S., Noom, M. C., Wuite, G. J., and Dame, R. T. (2006). The architectural role of nucleoid-associated proteins in the organization of bacterial chromatin: a molecular perspective. *J. Struct. Biol.* 156, 262–272. doi: 10.1016/j.jsb.2006.05.006

Marceau, A. H., Bahng, S., Massoni, S. C., George, N. P., Sandler, S. J., Marians, K. J., et al. (2011). Structure of the SSB-DNA polymerase III interface and its role in DNA replication. *EMBO J.* 30, 4236–4247. doi: 10.1038/emboj.2011.305

Margolin, W. (2000). Green fluorescent protein as a reporter for macromolecular localization in bacterial cells. *Methods* 20, 62–72. doi: 10.1006/meth.1999.0906

Meaburn, K. J., and Misteli, T. (2007). Cell biology: chromosome territories. *Nature* 445, 379–781. doi: 10.1038/445379a

Merrikh, H., Zhang, Y., Grossman, A. D., and Wang, J. D. (2012). Replication-transcription conflicts in bacteria. *Nat. Rev. Microbiol.* 10, 449–458. doi: 10.1038/nrmicro2800

Nielsen, H. J., Youngren, B., Hansen, F. G., and Austin, S. (2007). Dynamics of *Escherichia coli* chromosome segregation during multifork replication. *J. Bacteriol.* 189, 8660–8666. doi: 10.1128/JB.01212-07

Norris, V., den Blaauwen, T., Cabin-Flaman, A., Doi, R. H., Harshey, R., Janniere, L., et al. (2007). Functional taxonomy of bacterial hyperstructures. *Microbiol. Mol. Biol. Rev.* 71, 230–253. doi: 10.1128/MMBR.00035-06

O'Donnell, M. (2006). Replisome architecture and dynamics in *Escherichia coli*. *J. Biol. Chem.* 281, 10653–10656. doi: 10.1074/jbc.R500028200

O'Sullivan, J. M., Pai, D. A., Cridge, A. G., Engelke, D. R., and Ganley, A. R. (2013). The nucleolus: a raft adrift in the nuclear sea or the keystone in nuclear structure? *Biomol. Concepts* 4, 277–286. doi: 10.1515/bmc-2012-0043

Paul, B. J., Ross, W., Gaal, T., and Gourse, R. L. (2004). rRNA transcription in *Escherichia coli*. *Annu. Rev. Genet.* 38, 749–770. doi: 10.1146/annurev.genet.38.072902.091347

Piper, S. E., Mitchell, J. E., Lee, D. J., and Busby, S. J. (2009). A global view of *Escherichia coli* Rsd protein and its interactions. *Mol. Biosyst.* 5, 1943–1947. doi: 10.1039/b904955j

Potrykus, K., Murphy, H., Philippe, N., and Cashel, M. (2011). ppGpp is the major source of growth rate control in *E. coli*. *Environ. Microbiol.* 13, 563–575. doi: 10.1111/j.1462-2920.2010.02357.x

Pul, U., and Wagner, R. (2012). "Nucleoid-associated proteins: structural properties," in *Bacterial Chromatin*, eds R. T. Dame and C. J. Dorman (New York, NY: Springer), 149–173.

Reyes-Lamothe, R., Possoz, C., Danilova, O., and Sherratt, D. J. (2008). Independent positioning and action of *Escherichia coli* replisomes in live cells. *Cell* 133, 90–102. doi: 10.1016/j.cell.2008.01.044

Riley, M., Abe, T., Arnaud, M. B., Berlyn, M. K., Blattner, F. R., Chaudhuri, R. R., et al. (2006). *Escherichia coli* K-12: a cooperatively developed annotation snapshot–2005. *Nucleic Acids Res.* 34, 1–9. doi: 10.1093/nar/gkj405

Rocha, E. P., and Danchin, A. (2003). Gene essentiality determines chromosome organisation in bacteria. *Nucleic Acids Res.* 31, 6570–6577. doi: 10.1093/nar/gkg859

Ross, W., Vrentas, C. E., Sanchez-Vazquez, P., Gaal, T., and Gourse, R. L. (2013). The magic spot: a ppGpp binding site on *E. coli* RNA polymerase responsible for regulation of transcription initiation. *Mol. Cell* 50, 420–429. doi: 10.1016/j.molcel.2013.03.021

Schaechter, M., Maaloe, O., and Kjeldgaard, N. O. (1958). Dependency on medium and temperature of cell size and chemical composition during balanced grown of *Salmonella typhimurium*. *J. Gen. Microbiol.* 19, 592–606. doi: 10.1099/00221287-19-3-592

Schmiedeberg, L., Skene, P., Deaton, A., and Bird, A. (2009). A temporal threshold for formaldehyde crosslinking and fixation. *PLoS ONE* 4:e4636. doi: 10.1371/journal.pone.0004636

Slater, S., Wold, S., Lu, M., Boye, E., Skarstad, K., and Kleckner, N. (1995). *E. coli* SeqA protein binds oriC in two different methyl-modulated reactions appropriate to its roles in DNA replication initiation and origin sequestration. *Cell* 82, 927–936. doi: 10.1016/0092-8674(95)90272-4

Stokke, C., Flatten, I., and Skarstad, K. (2012). An easy-to-use simulation program demonstrates variations in bacterial cell cycle parameters depending on medium and temperature. *PLoS ONE* 7:e30981. doi: 10.1371/journal.pone.0030981

Torres, M., Balada, J. M., Zellars, M., Squires, C., and Squires, C. L. (2004). *In vivo* effect of NusB and NusG on rRNA transcription antitermination. *J. Bacteriol.* 186, 1304–1310. doi: 10.1128/JB.186.5.1304-1310.2004

Tosa, T., and Pizer, L. I. (1971). Biochemical bases for the antimetabolite action of L-serine hydroxamate. *J. Bacteriol.* 106, 972–982.

Traxler, M. F., Summers, S. M., Nguyen, H. T., Zacharia, V. M., Hightower, G. A., Smith, J. T., et al. (2008). The global, ppGpp-mediated stringent response to amino acid starvation in *Escherichia coli*. *Mol. Microbiol.* 68, 1128–1148. doi: 10.1111/j.1365-2958.2008.06229.x

Umbarger, M. A., Toro, E., Wright, M. A., Porreca, G. J., Bau, D., Hong, S. H., et al. (2011). The three-dimensional architecture of a bacterial genome and its alteration by genetic perturbation. *Mol. Cell* 44, 252–264. doi: 10.1016/j.molcel.2011.09.010

van Helvoort, J. M., Kool, J., and Woldringh, C. L. (1996). Chloramphenicol causes fusion of separated nucleoids in *Escherichia coli* K-12 cells and filaments. *J. Bacteriol.* 178, 4289–4293.

Wagner, R. (2002). Regulation of ribosomal RNA synthesis in *E. coli*: effects of the global regulator guanosine tetraphosphate (ppGpp). *J. Mol. Microbiol. Biotechnol.* 4, 331–340.

Waldminghaus, T., Weigel, C., and Skarstad, K. (2012). Replication fork movement and methylation govern SeqA binding to the *Escherichia coli* chromosome. *Nucleic Acids Res.* 40, 5465–5476. doi: 10.1093/nar/gks187

Wang, F., Redding, S., Finkelstein, I. J., Gorman, J., Reichman, D. R., and Greene, E. C. (2013). The promoter-search mechanism of *Escherichia coli* RNA polymerase is dominated by three-dimensional diffusion. *Nat. Struct. Mol. Biol.* 20, 174–181. doi: 10.1038/nsmb.2472

Wang, P., Robert, L., Pelletier, J., Dang, W. L., Taddei, F., Wright, A., et al. (2010). Robust growth of *Escherichia coli*. *Curr. Biol.* 20, 1099–1103. doi: 10.1016/j.cub.2010.04.045

Woldringh, C. L., Jensen, P. R., and Westerhoff, H. V. (1995). Structure and partitioning of bacterial DNA: determined by a balance of compaction and expansion forces? *FEMS Microbiol. Lett.* 131, 235–242. doi: 10.1111/j.1574-6968.1995.tb07782.x

Yamazoe, M., Adachi, S., Kanaya, S., Ohsumi, K., and Hiraga, S. (2005). Sequential binding of SeqA protein to nascent DNA segments at replication forks in synchronized cultures of *Escherichia coli*. *Mol. Microbiol.* 55, 289–298. doi: 10.1111/j.1365-2958.2004.04389.x

Yao, N. Y., and O'Donnell, M. (2010). SnapShot: the replisome. *Cell* 141, 1088, 1088.e1081. doi: 10.1016/j.cell.2010.05.042

Zhou, Y. N., and Jin, D. J. (1997). RNA polymerase beta mutations have reduced sigma70 synthesis leading to a hyper-temperature-sensitive phenotype of a sigma70 mutant. *J. Bacteriol.* 179, 4292–4298.

Zhou, Y. N., and Jin, D. J. (1998). The rpoB mutants destabilizing initiation complexes at stringently controlled promoters behave like "stringent" RNA polymerases in *Escherichia coli*. *Proc. Natl. Acad. Sci. U.S.A.* 95, 2908–2913. doi: 10.1073/pnas.95.6.2908

Conflict of Interest Statement: The authors declare that the research was conducted in the absence of any commercial or financial relationships that could be construed as a potential conflict of interest.

Copyright © 2015 Jin, Cagliero, Martin, Izard and Zhou. This is an open-access article distributed under the terms of the Creative Commons Attribution License (CC BY). The use, distribution or reproduction in other forums is permitted, provided the original author(s) or licensor are credited and that the original publication in this journal is cited, in accordance with accepted academic practice. No use, distribution or reproduction is permitted which does not comply with these terms.

frontiers in Microbiology

OPINION
published: 08 May 2015
doi: 10.3389/fmicb.2015.00424

The nucleoid as a smart polymer

Vittore F. Scolari[1†], *Bianca Sclavi*[2] *and Marco Cosentino Lagomarsino*[1,3*]

[1] Computational and Quantitative Biology, Sorbonne Universités, UPMC Univ Paris 06, UMR 7238, Paris, France, [2] Centre National de la Recherche Scientifique, LBPA, UMR 8113, ENS Cachan, Cachan, France, [3] Centre National de la Recherche Scientifique, UMR 7238, Paris, France

Keywords: genome organization, bacterial nucleoid, nucleoid-associated proteins, supercoiling, smart-polymers, polymer sensors

Science has a close but very complex relationship with technology (Latour, 1987). A simple phenomenon is that technology enables science by offering tools that provide new data or new kinds of data. In other cases, aspects or views of the empirical world may remain invisible until technology builds something that unveils them to the eyes of the scientific community. On a deeper level, building something may be a form of understanding. For example "complex networks" became prominent in all sectors of science in the late 1990s, at the time that the Internet became a common tool for research and for society at large. Before then, networks had been restricted for decades to smaller niches. This change was accompanied by a thrust of high throughput technologies to collect new data, but arguably many of the "network" data had already been available for many years.

On a smaller scale, we want to suggest here that so called "smart polymers" (Galaev and Mattiasson, 1999; Kumar et al., 2007) could be a promising technological metaphor for the behavior of the bacterial nucleoid. We want to explore the analogy with the similarly "intelligent" behavior shaped into bacterial nucleoids by natural selection.

But first, what is a smart polymer, and what does it do? In soft-matter physics, "smart," or "stimulus-responsive," polymers are technological polymer systems designed to effect a variety of responsive behaviors to external stimuli (**Figure 1**). Smart polymers respond to the environment they are in. They are engineered to be sensitive to a number of factors, such as solvency, temperature, humidity, pH, light, electrical and magnetic field, and to effect mechanical and chemical changes (Galaev and Mattiasson, 1999; Kumar et al., 2007; Chen and Chang, 2014). They can be realized as linear free chains in solution, or as surface-grafted brushes or gels. Usually, response to stimuli is achieved through the addition of specific reactive functional groups and side chains, or by the use of graft-and-block copolymers (two different polymers grafted together) with different chemical properties (e.g., hydrophyly). Effective smart polymers typically undergo large changes (e.g., conformational transitions) in response to just small changes in the environment (e.g., pH, temperature, ionic strength). One way to achieve this behavior is through the introduction of "pre-programmed" phase transitions. For example, the polymer undergoes a reversible collapse after an external stimulus is applied. The reversibility of this change may also be an important property, allowing to detect changes in both directions. To fix the ideas, a prevalent use for smart polymers is targeted drug delivery. A smart-polymer system may control the release of drugs until the desired target is reached, and it is sensed by either a chemical or physical response triggering the release of the drug by "uncaging" it. For example, a polymer site-specific conjugation to specific amino acid sites may induce a trigger in the concentration of a targeted protein (Hoffman et al., 2000). It is then evident that the bacterial nucleoid can be seen as a smart polymer (Dillon and Dorman, 2010; Muskhelishvili et al., 2010; Benza et al., 2012; Kleckner et al., 2014). Its degree of compaction and conformation are modulated by the cell's growth conditions and in response to specific external cues (**Figure 1**). It is a complex system made of a long DNA polymer associated with RNA and proteins that may play at least two roles: adapt the shape of the nucleoid through both specific and non-specific DNA binding, and change the physical properties of DNA through dynamic changes in DNA topology.

OPEN ACCESS

Edited by:
Conrad L. Woldringh, University of Amsterdam, Netherlands

Reviewed by:
Remus T. Dame, Leiden University, Netherlands
Georgi Muskhelishvili, Jacobs University, Germany

****Correspondence:***
Marco Cosentino Lagomarsino, marco.cosentino-lagomarsino@upmc.fr

†Present Address:
Vittore F. Scolari, Spatial Regulation of Genomes Group, Department of Genomes and Genetics, Institut Pasteur, Paris, France

Specialty section:
This article was submitted to Microbial Physiology and Metabolism, a section of the journal Frontiers in Microbiology

Received: *27 February 2015*
Accepted: *21 April 2015*
Published: *08 May 2015*

Citation:
Scolari VF, Sclavi B and Cosentino Lagomarsino M (2015) The nucleoid as a smart polymer. Front. Microbiol. 6:424. doi: 10.3389/fmicb.2015.00424

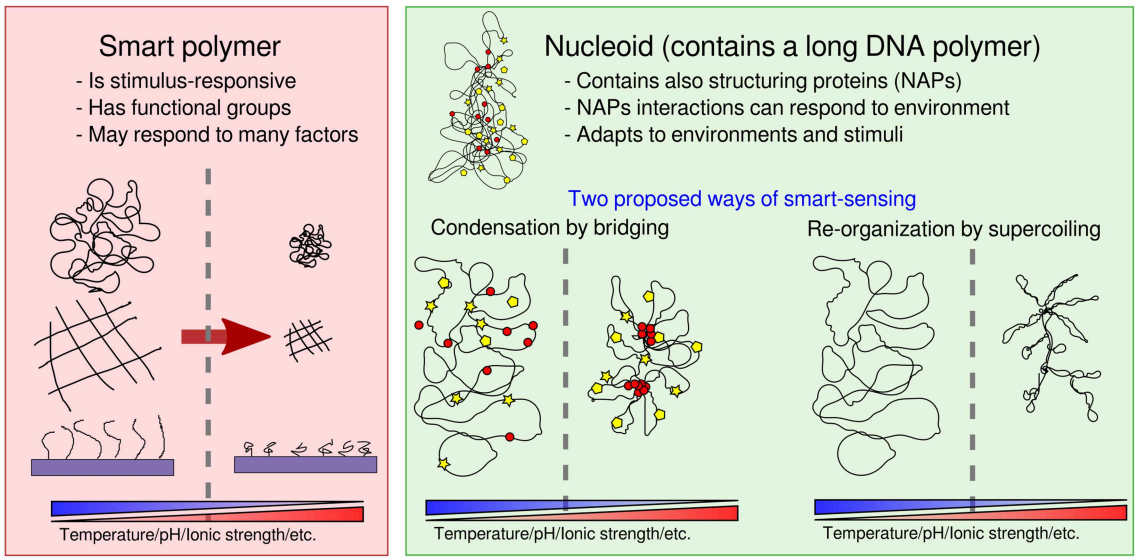

FIGURE 1 | "Smart-polymer" functionality of the nucleoid.

First, the abundant nucleoid associated proteins ("NAPs," e.g., focusing on *E. coli*, Dps, Fis, H-NS, IHF, HU, and the condensin MukBEF), can act as "functional groups" (Luijsterburg et al., 2006; Dillon and Dorman, 2010; Ohniwa et al., 2011) to plastically modify the genome conformation. Of particular interest are NAP-mediated bridging interactions (Wiggins et al., 2009) (e.g., from Fis, H-NS, and MukBEF in *E. coli*), which can thus act as "functional groups" in the nucleoid. In particular, H-NS is known respond to temperature, salt concentration and pH (La Teana et al., 1991; Atlung and Ingmer, 1997; Amit et al., 2003; Dorman, 2004; Ono et al., 2005; Stella et al., 2006). and Fis has been implicated in adaptation to favorable growth conditions and quorum sensing (Lenz and Bassler, 2007). Additionally, some NAPs may operate both as monomers and as oligomers, introducing the possibility of cooperativity in the formation of higher order complexes (Luijsterburg et al., 2006; Skoko et al., 2006; Lim et al., 2012). On theoretical grounds, looped domain formation offers the opportunity of producing a very rich phase behavior (Leibler, 1980; Borisov and Halperin, 1996, 1997; Kantor and Kardar, 1996; Camacho and Schanke, 1997), as exploited in recent models motivated by the study of the organization of chromatin (Junier et al., 2010; Barbieri et al., 2013; Brackley et al., 2013). Biologically, one can imagine that the collapse and swelling of selected genomic regions by bridging proteins may be tuned to be switch-like (Scolari and Cosentino Lagomarsino, 2015) in order to be differentially controlled by the cell. While the mechanisms has not yet been studied in detail, domain formation is well-documented in bacterial chromosomes (Espéli and Boccard, 2006; Espéli et al., 2008; Dame et al., 2011). Such mechanism may account for the observed correlation between the position of genetic loci along the chromosome and their position in the cell (Mercier et al., 2008; Wiggins et al., 2010), it may help the resolution of the identity of segregating sister chromosomes (Lesterlin et al., 2012; Junier et al., 2014), as well as play a role in explaining observed "abrupt" transitions in chromosome arrangements (Joshi et al., 2011; Fisher et al., 2013; Javer et al., 2014). Additionally, NAPs that do not bridge specifically such as Dps may also trigger switch-like collapse (Zimmerman, 2006), and NAPs that do not bridge but exhibit cooperative clustering may also affect the global nucleoid state by affecting key parameters such as effective stiffness (Luijsterburg et al., 2006).

Second, the action of specific DNA enzymes such as topoisomerases and gyrases changes the polymer's mechanical properties through changes in DNA topology. Nucleoids are composed of topologically unlinked dynamic domain structures, forming plectonemes and toroids (Trun and Marko, 1998). Torsional constraints can be generated by active processes, such as DNA replication and transcription (Le et al., 2013), and stabilized by bridging NAPs, such as Fis and H-NS (Schneider et al., 2001). Together, supercoiling and nucleoid organization can affect gene expression (Breier and Cozzarelli, 2004; Postow et al., 2004; Travers and Muskhelishvili, 2005; Blot et al., 2006; Dillon and Dorman, 2010) and, in turn, expression of specific regulators may affect the concentration or the activity of the genes setting nucleoid conformation resulting in feedback loops that can lead to more robust nucleoid conformations. Also, NAPs and supercoiling regulation by enzymes may interact in complex ways (Dorman, 2013a). Clearly, such an object has higher computational power than any current technological smart polymer, because it is also able to control the elements leading to its self-organization, which may inspire new technology. The coexistence of two parallel mechanisms of regulation through polymer organization (mainly supercoiling and growth) and through conventional protein binding may be an important feature of the nucleoid. A

series of studies on *E. coli* investigated the interactions between these mechanisms arguing the presence of two different codes overlapped at different at levels on DNA, and possibly evolving at different time-scales, carrying, respectively, a "digital" and an "analog" information (Sobetzko et al., 2012; Dorman, 2013b; Muskhelishvili and Travers, 2013; Sobetzko et al., 2013). Finally this system is able to rapidly evolve in response to adaptation to recurring changes (Crozat et al., 2010), possibly improving the efficiency and the speed of the programmed conformational changes.

We propose that this technological parallel could also be useful in the reverse direction, to reframe the current biological knowledge in a physical perspective. Indeed, the smart polymer analogy does not by itself add new knowledge to the long list of biological information already acquired on the nucleoid. However, it may help us putting the same knowledge in a different perspective, and treat the same information in more precise and quantitative ways using the tools of soft-matter physics. This may lead to defining new questions, and ultimately to reaching new knowledge. For example, new biomimetic "constructive" approaches using purified DNA and NAPs may be defined to explore the resulting phase diagram in a controlled fashion (Maurer et al., 2009; Pelletier et al., 2012; Thacker et al., 2014), and to achieve a physical understanding of how robustness and response to changes are encoded in such structures.

Funding

This work was supported by the International Human Frontier Science Program Organization, grants RGY0069/2009-C and RGY0070/2014.

References

Amit, R., Oppenheim, A. B., and Stavans, J. (2003). Increased bending rigidity of single DNA molecules by h-ns, a temperature and osmolarity sensor. *Biophys. J.* 84, 2467–2473. doi: 10.1016/S0006-3495(03)75051-6

Atlung, T., and Ingmer, H. (1997). H-ns: a modulator of environmentally regulated gene expression. *Mol. Microbiol.* 24, 7–17. doi: 10.1046/j.1365-2958.1997.3151679.x

Barbieri, M., Chotalia, M., Fraser, J., Lavitas, L.-M., Dostie, J., Pombo, A. et al. (2013). A model of the large-scale organization of chromatin. *Biochem. Soc. Trans.* 41, 508–512. doi: 10.1042/BST20120238

Benza, V. G., Bassetti, B., Dorfman, K. D., Scolari, V. F., Bromek, K., Cicuta, P., et al. (2012). Physical descriptions of the bacterial nucleoid at large scales, and their biological implications. *Rep. Prog. Phys.* 75:076602. doi: 10.1088/0034-4885/75/7/076602

Blot, N., Mavathur, R., Geertz, M., Travers, A., and Muskhelishvili, G. (2006). Homeostatic regulation of supercoiling sensitivity coordinates transcription of the bacterial genome. *Embo. Rep.* 7, 710–715. doi: 10.1038/sj.embor.7400729

Borisov, O. V., and Halperin, A. (1996). Micelles of polysoaps: the role of bridging interactions. *Macromolecules* 29, 2612–2617. doi: 10.1021/ma951565w

Borisov, O. V., and Halperin, A. (1997). Polysoaps: the signatures of intrachain self assembly in solvents. *Macromol. Symp.* 117, 99–107. doi: 10.1002/masy.19971170114

Brackley, C. A., Taylor, S., Papantonis, A., Cook, P. R., and Marenduzzo, D. (2013). Nonspecific bridging-induced attraction drives clustering of DNA-binding proteins and genome organization. *Proc. Natl. Acad. Sci. U.S.A.* 110, E3605–E3611. doi: 10.1073/pnas.1302950110

Breier, A. M., and Cozzarelli, N. R. (2004). Linear ordering and dynamic segregation of the bacterial chromosome. *Proc. Natl. Acad. Sci. U.S.A.* 101, 9175–9176. doi: 10.1073/pnas.0403722101

Camacho, C. J., and Schanke, T. (1997). From collapse to freezing in random heteropolymers. *Europhys. Lett.* 37, 603. doi: 10.1209/epl/i1997-00197-2

Chen, J.-K., and Chang, C.-J. (2014). Fabrications and applications of stimulus-responsive polymer films and patterns on surfaces: a review. *Materials* 7, 805–875. doi: 10.3390/ma7020805

Crozat, E., Winkworth, C., Gaffé, J., Hallin, P. F., Riley, M. A., Lenski, R. E., et al. (2010). Parallel genetic and phenotypic evolution of DNA superhelicity in experimental populations of *Escherichia coli*. *Mol. Biol. Evol.* 27, 2113–2128. doi: 10.1093/molbev/msq099

Dame, R. T., Kalmykowa, O. J., and Grainger, D. C. (2011). Chromosomal macrodomains and associated proteins: implications for DNA organization and replication in gram negative bacteria. *PLoS Genet.* 7:e1002123. doi: 10.1371/journal.pgen.1002123

Dillon, S. C., and Dorman, C. J. (2010). Bacterial nucleoid-associated proteins, nucleoid structure and gene expression. *Nat. Rev. Microbiol.* 8, 185–195. doi: 10.1038/nrmicro2261

Dorman, C. J. (2004). H-ns: a universal regulator for a dynamic genome. *Nat. Rev. Microbiol.* 2, 391–400. doi: 10.1038/nrmicro883

Dorman, C. J. (2013a). Co-operative roles for DNA supercoiling and nucleoid-associated proteins in the regulation of bacterial transcription. *Biochem. Soc. Trans.* 41, 542–547. doi: 10.1042/BST20120222

Dorman, C. J. (2013b). Genome architecture and global gene regulation in bacteria: making progress towards a unified model? *Nat. Rev. Microbiol.* 11, 349–355. doi: 10.1038/nrmicro3007

Espéli, O., and Boccard, F. (2006). Organization of the *Escherichia coli* chromosome into macrodomains and its possible functional implications. *J. Struct. Biol.* 156, 304–310. doi: 10.1016/j.jsb.2006.07.010

Espéli, O., Mercier, R., and Boccard, F. (2008). DNA dynamics vary according to macrodomain topography in the *E. coli* chromosome. *Mol. Microbiol.* 68, 1418–1427. doi: 10.1111/j.1365-2958.2008.06239.x

Fisher, J. K., Bourniquel, A., Witz, G., Weiner, B., Prentiss, M., and Kleckner, N. (2013). Four-dimensional imaging of *E. coli* nucleoid organization and dynamics in living cells. *Cell* 153, 882–895. doi: 10.1016/j.cell.2013.04.006

Galaev, I. Y., and Mattiasson, B. (1999). 'Smart' polymers and what they could do in biotechnology and medicine. *Trends Biotechnol.* 17, 335–340. doi: 10.1016/S0167-7799(99)01345-1

Hoffman, A. S., Stayton, P. S., Bulmus, V., Chen, G., Chen, J., Cheung, C., et al. (2000). Really smart bioconjugates of smart polymers and receptor proteins. *J. Biomed. Mater. Res.* 52, 577–586. doi: 10.1002/1097-4636(20001215)52:4<577::AID-JBM1>3.0.CO;2-5

Javer, A., Kuwada, N. J., Long, Z., Benza, V. G., Dorfman, K. D., Wiggins, P. A., et al. (2014). Persistent super-diffusive motion of *Escherichia coli* chromosomal loci. *Nat. Commun.* 5:3854. doi: 10.1038/ncomms4854

Joshi, M. C., Bourniquel, A., Fisher, J., Ho, B. T., Magnan, D., Kleckner, N., et al. (2011). *Escherichia coli* sister chromosome separation includes an abrupt global transition with concomitant release of late-splitting intersister snaps. *Proc. Natl. Acad. Sci. U.S.A.* 108, 2765–2770. doi: 10.1073/pnas.1019593108

Junier, I., Boccard, F., and Espli, O. (2014). Polymer modeling of the *E. coli* genome reveals the involvement of locus positioning and macrodomain structuring for the control of chromosome conformation and segregation. *Nucleic Acids Res.* 42, 1461–1473. doi: 10.1093/nar/gkt1005

Junier, I., Martin, O., and Képès, F. (2010). Spatial and topological organization of DNA chains induced by gene co-localization. *PLoS Comput. Biol.* 6:e1000678. doi: 10.1371/journal.pcbi.1000678

Kantor, Y., and Kardar, M. (1996). Collapse of randomly linked polymers. *Phys. Rev. Lett.* 77:4275. doi: 10.1103/PhysRevLett.77.4275

Kleckner, N., Fisher, J. K., Stouf, M., White, M. A., Bates, D., and Witz, G. (2014). The bacterial nucleoid: nature, dynamics and sister segregation. *Curr. Opin. Microbiol.* 22C, 127–137. doi: 10.1016/j.mib.2014.10.001

Kumar, A., Srivastava, A., Galaev, I. Y., and Mattiasson, B. (2007). Smart polymers: physical forms and bioengineering applications. *Prog. Polym. Sci.* 32, 1205–1237. doi: 10.1016/j.progpolymsci.2007.05.003

La Teana, A., Brandi, A., Falconi, M., Spurio, R., Pon, C. L., and Gualerzi, C. (1991). Identification of a cold shock transcriptional enhancer of the *Escherichia coli* gene encoding nucleoid protein h-ns. *Proc. Natl. Acad. Sci. U.S.A.* 88, 10907–10911. doi: 10.1073/pnas.88.23.10907

Latour, B. (1987). *Science in Action: How to Follow Scientists and Engineers through Society*. Cambridge, MA: Harvard University Press.

Le, T. B. K., Imakaev, M. V., Mirny, L. A., and Laub, M. T. (2013). High-resolution mapping of the spatial organization of a bacterial chromosome. *Science* 342, 731–734. doi: 10.1126/science.1242059

Leibler, L. (1980). Theory of microphase separation in block copolymers. *Macromolecules* 13, 1602–1617. doi: 10.1021/ma60078a047

Lenz, D. H., and Bassler, B. L. (2007). The small nucleoid protein fis is involved in *Vibrio cholerae* quorum sensing. *Mol. Microbiol.* 63, 859–871. doi: 10.1111/j.1365-2958.2006.05545.x

Lesterlin, C., Gigant, E., Boccard, F., and Espeli, O. (2012). Sister chromatid interactions in bacteria revealed by a site-specific recombination assay. *EMBO J.* 31, 3468–3479. doi: 10.1038/emboj.2012.194

Lim, C. J., Whang, Y. R., Kenney, L. J., and Yan, J. (2012). Gene silencing h-ns paralogue stpa forms a rigid protein filament along DNA that blocks DNA accessibility. *Nucleic Acids Res.* 40, 3316–3328. doi: 10.1093/nar/gkr1247

Luijsterburg, M. S., Noom, M. C., Wuite, G. J., and Dame, R. T. (2006). The architectural role of nucleoid-associated proteins in the organization of bacterial chromatin: a molecular perspective. *J. Struct. Biol.* 156, 262–272. doi: 10.1016/j.jsb.2006.05.006

Maurer, S., Fritz, J., and Muskhelishvili, G. (2009). A systematic *in vitro* study of nucleoprotein complexes formed by bacterial nucleoid-associated proteins revealing novel types of DNA organization. *J. Mol. Biol.* 387, 1261–1276. doi: 10.1016/j.jmb.2009.02.050

Mercier, R., Petit, M.-A., Schbath, S., Robin, S., Karoui, M. E., Boccard, F., et al. (2008). The matp/mats site-specific system organizes the terminus region of the *E. coli* chromosome into a macrodomain. *Cell* 135, 475–485. doi: 10.1016/j.cell.2008.08.031

Muskhelishvili, G., Sobetzko, P., Geertz, M., and Berger, M. (2010). General organisational principles of the transcriptional regulation system: a tree or a circle? *Mol. BioSyst.* 6, 662–676. doi: 10.1039/b909192k

Muskhelishvili, G., and Travers, A. (2013). Integration of syntactic and semantic properties of the DNA code reveals chromosomes as thermodynamic machines converting energy into information. *Cell. Mol. Life Sci.* 70, 4555–4567. doi: 10.1007/s00018-013-1394-1

Ohniwa, R. L., Ushijima, Y., Saito, S., and Morikawa, K. (2011). Proteomic analyses of nucleoid-associated proteins in *Escherichia coli*, *Pseudomonas aeruginosa*, *Bacillus subtilis*, and *Staphylococcus aureus*. *PLoS ONE* 6:e19172. doi: 10.1371/journal.pone.0019172

Ono, S., Goldberg, M. D., Olsson, T., Esposito, D., Hinton, J. C. D., and Ladbury, J. E. (2005). H-ns is a part of a thermally controlled mechanism for bacterial gene regulation. *Biochem. J.* 391(Pt 2), 203–213. doi: 10.1042/BJ20050453

Pelletier, J., Halvorsen, K., Ha, B.-Y., Paparcone, R., Sandler, S. J., Woldringh, C. L., et al. (2012). Physical manipulation of the *Escherichia coli* chromosome reveals its soft nature. *Proc. Natl. Acad. Sci. U.S.A.* 109, E2649–E2656. doi: 10.1073/pnas.1208689109

Postow, L., Hardy, C., Arsuaga, J., and Cozzarelli, N. (2004). Topological domain structure of the *Escherichia coli* chromosome. *Genes Dev.* 18, 1766–1779. doi: 10.1101/gad.1207504

Schneider, R., Lurz, R., Lder, G., Tolksdorf, C., Travers, A., and Muskhelishvili, G. (2001). An architectural role of the *Escherichia coli* chromatin protein fis in organising DNA. *Nucleic Acids Res.* 29, 5107–5114. doi: 10.1093/nar/29.24.5107

Scolari, V. F., and Cosentino Lagomarsino, M. (2015). Combined collapse by bridging and self-adhesion in a prototypical polymer model inspired by the bacterial nucleoid. *Soft. Matter.* 11, 1677–1687. doi: 10.1039/C4SM02434F

Skoko, D., Yoo, D., Bai, H., Schnurr, B., Yan, J., McLeod, S. M., et al. (2006). Mechanism of chromosome compaction and looping by the *Escherichia coli* nucleoid protein fis. *J. Mol. Biol.* 364, 777–798. doi: 10.1016/j.jmb.2006.09.043

Sobetzko, P., Glinkowska, M., Travers, A., and Muskhelishvili, G. (2013). DNA thermodynamic stability and supercoil dynamics determine the gene expression program during the bacterial growth cycle. *Mol. BioSyst.* 9, 1643–1651. doi: 10.1039/c3mb25515h

Sobetzko, P., Travers, A., and Muskhelishvili, G. (2012). Gene order and chromosome dynamics coordinate spatiotemporal gene expression during the bacterial growth cycle. *Proc. Natl. Acad. Sci. U.S.A.* 109, E42–E50. doi: 10.1073/pnas.1108229109

Stella, S., Falconi, M., Lammi, M., Gualerzi, C. O., and Pon, C. L. (2006). Environmental control of the in vivo oligomerization of nucleoid protein h-ns. *J. Mol. Biol.* 355, 169–174. doi: 10.1073/pnas.1108229109

Thacker, V. V., Bromek, K., Meijer, B., Kotar, J., Sclavi, B., Cosentino Lagomarsino, M., et al. (2014). Bacterial nucleoid structure probed by active drag and resistive pulse sensing. *Integr. Biol.* 6, 184–191. doi: 10.1039/c3ib40147b

Travers, A., and Muskhelishvili, G. (2005). DNA supercoiling - a global transcriptional regulator for enterobacterial growth? *Nat. Rev. Microbiol.* 3, 157–169. doi: 10.1038/nrmicro1088

Trun, N. J., and Marko, J. F. (1998). Architecture of a bacterial chromosome (review). *Am. Soc. Microbiol. News* 64:276.

Wiggins, P. A., Cheveralls, K. C., Martin, J. S., Lintner, R., and Kondev, J. (2010). Strong intranucleoid interactions organize the *Escherichia coli* chromosome into a nucleoid filament. *Proc. Natl. Acad. Sci. U.S.A.* 107, 4991–4995. doi: 10.1073/pnas.0912062107

Wiggins, P. A., Dame, R. T., Noom, M. C., and Wuite, G. J. L. (2009). Protein-mediated molecular bridging: a key mechanism in biopolymer organization. *Biophys. J.* 97, 1997–2003. doi: 10.1016/j.bpj.2009.06.051

Zimmerman, S. B. (2006). Cooperative transitions of isolated *Escherichia coli* nucleoids: implications for the nucleoid as a cellular phase. *J. Struct. Biol.* 153, 160–175. doi: 10.1016/j.jsb.2005.10.011

Conflict of Interest Statement: The authors declare that the research was conducted in the absence of any commercial or financial relationships that could be construed as a potential conflict of interest.

Copyright © 2015 Scolari, Sclavi and Cosentino Lagomarsino. This is an open-access article distributed under the terms of the Creative Commons Attribution License (CC BY). The use, distribution or reproduction in other forums is permitted, provided the original author(s) or licensor are credited and that the original publication in this journal is cited, in accordance with accepted academic practice. No use, distribution or reproduction is permitted which does not comply with these terms.

frontiers in Microbiology

MINI REVIEW
published: 19 May 2015
doi: 10.3389/fmicb.2015.00499

Thymineless death, at the origin

Elena C. Guzmán and Carmen M. Martín*

Departamento de Bioquímica Biología Molecular y Genética, Facultad de Ciencias, Universidad de Extremadura, Badajoz, Spain

Thymineless death (TLD) in bacteria has been a focus of research for decades. Nevertheless, the advances in the last 5 years, with *Escherichia coli* as the model organism, have been outstanding. Independent research groups have presented compelling results that establish that the initiation of chromosome replication under thymine starvation is a key element in the scenario of TLD. Here we review the experimental results linking the initiation of replication to the lethality under thymine starvation and the proposed mechanisms by which TLD occurs. The concept of this relationship was 'in the air,' but approaches were not sufficiently developed to demonstrate the crucial role of DNA initiation in TLD. Genome-wide marker frequency analysis and Two Dimensional agarose gel electrophoresis have been critical methods employed to reveal that initiation events and the degradation of the *oriC* region occur during thymine starvation. The relationships between these events and TLD have established them to be the main underlying causes of the lethality under thymine starvation. Furthermore, we summarize additional important findings from the study of different mutant strains, which support the idea that the initiation of chromosomal replication and TLD are connected.

Keywords: TLD, replication fork, initiation, *oriC*, rifampicin, DSBs, 2D gel DNA

OPEN ACCESS

Edited by:
Arieh Zaritsky, Ben-Gurion University of the Negev, Israel

Reviewed by:
Arkady Khodursky, University of Minnesota, USA
David Bates, Baylor College of Medicine, USA
Andrei Kuzminov, University of Illinois at Urbana-Champaign, USA

****Correspondence:***
Elena C. Guzmán, Departamento de Bioquímica Biología Molecular y Genética, Facultad de Ciencias, Universidad de Extremadura, Badajoz 06071, Spain
eguzmac@gmail.com

Specialty section:
This article was submitted to Microbial Physiology and Metabolism, a section of the journal Frontiers in Microbiology

Received: *23 February 2015*
Accepted: *06 May 2015*
Published: *19 May 2015*

Citation:
Guzmán EC and Martín CM (2015) Thymineless death, at the origin. Front. Microbiol. 6:499. doi: 10.3389/fmicb.2015.00499

Introduction

Thymineless death (TLD) is defined by the loss of viability that occurs in a culture of a *thyA* defective mutant strain when deprived of thymine (**Figure 1A**). It was first reported by Barner and Cohen 60 years ago (Barner and Cohen, 1954). In the ensuing 60 years a number of other laboratory groups have studied this phenomenon and have attempted to elucidate its mechanism. Throughout the years, TLD has been associated with DNA damage and DNA recombination structures, as well as their outcomes: SOS induction, filamentation, mutagenesis, loss of plasmids, or induction of suicide modules and prophages, among others (Ahmad et al., 1998). However, the relative contribution of these factors, individually or in combination, to TLD remains unknown. A novel and critical aspect has emerged in the last 5 years: the initiation of chromosomal replication. Abortive events in attempted initiation during thymine starvation may be associated with the observed degradation of the *oriC* DNA sequence that eventually leads to TLD.

The goal of this minireview is to detail the experiments and various approaches that establish the initiation of replication as a key element in the continuously evolving story of TLD.

The Unbalanced Growth Model

The first general model to explain TLD was the recognition of *unbalanced growth* generated under thymine starvation (Barner and Cohen, 1954). Certainly, DNA replication eventually stops

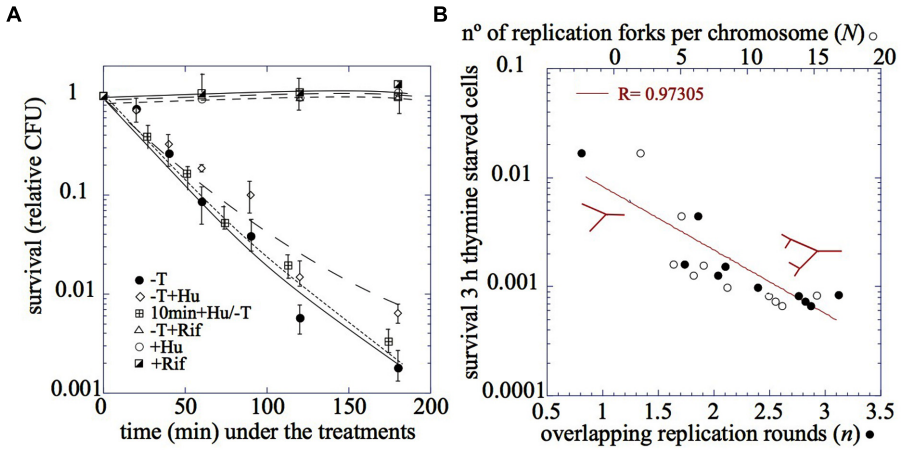

FIGURE 1 | (A) The relative cell survival after (●) thymine starvation, (◇) in the presence of hydroxyurea, (△) in the presence of rifampicin, (⊞) 10 min pretreatment with hydoxyurea and after addition of hydroxyurea 75 mM, (○) addition of hydroxyurea 75 mM, (◪) addition of rifampicin. **(B)** The relationship between the number of replication rounds per chromosome, *n*, or the number of replication forks per chromosome, *N*, and the relative viability after 3 h of thymine starvation. The red drawing corresponds to the chromosome configuration with one or two cycles of chromosome replication. (adapted from Martín and Guzmán, 2011; Martín, 2014).

in thymine-starved cells, while the processes of DNA recombination and repair may continue (Nakayama et al., 1994), and neither RNA nor protein synthesis are greatly affected (Hanawalt et al., 1961; Maaloe and Hanawalt, 1961; Nakayama and Hanawalt, 1975). Nevertheless, the notion of *unbalanced growth* was too vague, and it was shown that it cannot be the sole cause of TLD. Various experimental conditions suppressed TLD while maintaining an imbalance between DNA and protein synthesis. Examples of these conditions include the starvation of thymine in the presence of chloramphenicol (Okagaki et al., 1960) during which RNA synthesis remains active, or the heat inactivation of the proteins required for chromosomal initiation, DnaA or DnaC, (Bouvier and Sicard, 1975) during which RNA and protein synthesis are not affected. None of these conditions would predict the suppression of TLD according to the *unbalanced growth* model.

TLD is Related to DNA Replication

Thymine is exclusively incorporated into DNA during the replication process; therefore, TLD has been associated for many years with DNA replication. Early observations described conditions under which TLD was suppressed in cells that had completed replication rounds (Maaloe and Hanawalt, 1961). Additionally, TLD has been shown to be affected differently under inactivation of several replication proteins (Bouvier and Sicard, 1975; Nakayama et al., 1994). Thus, a direct involvement of the chromosomal replication process in TLD is apparent.

TLD Correlates with the Number of Replication Forks, but they are Not Required to be Fully Active

A relationship between the magnitude of the lethality under thymine starvation and the number of replication forks has been well established. Both parameters were determined in the strain MG1693 *thyA175* grown under various conditions to achieve different numbers of replication rounds per chromosome, *n*, (Sueoka and Yoshikawa, 1965). Survival after thymine starvation (**Figure 1A**) was found to inversely correlate with *n* and the number of forks per cell, *N*, before thymine starvation (**Figure 1B**; Martín and Guzmán, 2011; Martín, 2014). However, it is not clear whether the activity of the replication forks is required for the lethality. TLD is not suppressed when thymine starvation is accomplished under conditions of DNA inhibition, such as the addition of hydroxyurea (Morganroth and Hanawalt, 2006; Kuong and Kuzminov, 2009; Martín and Guzmán, 2011; **Figure 1A**) or the incubation of a *dnaBts* mutant at 42°C (Bouvier and Sicard, 1975). Controversy has arisen because the two approaches used to inactivate the replication forks do not show a clear-cut inhibition of DNA synthesis (Kuong and Kuzminov, 2009, 2010). Nevertheless, the complete absence of effect on TLD either after hydroxyurea addition or incubation of *dnaBts* at 42°C suggests that TLD is not dependent on the level of activity of the replication forks. Furthermore, the observation that the addition of hydroxyurea 10 min before thymine starvation does not change the kinetics of TLD supports this idea (**Figure 1A**; Martín and Guzmán, 2011; Martín, 2014).

DNA Fragmentation and Recombinant DNA Intermediates are Not Sufficient to Account for TLD

When considering the idea that the replication forks are targeted during thymine starvation, the primary assumption is that TLD results from DNA damage brought about by thymine starvation on its target. What effects could thymine starvation produce on the replication forks? Different models have suggested two primary sources of TLD that are not mutually exclusive: DNA breakage and DNA recombination intermediates, which have

been associated either with RNA synthesis during thymine starvation (Nakayama and Hanawalt, 1975) or to different recombination pathways such as RecA/RecBCD or RecFOR (Fonville et al., 2010; Kuong and Kuzminov, 2010).

DNA breakage has been observed under thymine starvation; thus, the occurrence of single-strand breaks (SSBs), DNA single-strand gaps (DNA ss-gaps; Nakayama and Hanawalt, 1975), and double strand breaks (DSBs; Guarino et al., 2007; Kuong and Kuzminov, 2010; Martín and Guzmán, 2011) have been shown to occur during *thymineless* incubation of bacteria. Furthermore, Nakayama et al. (1994) demonstrated the presence of DNA recombination intermediates, known as "non-migrating DNA" (nmDNA), in thymine-starved cells. Nevertheless, Martín and Guzmán (2011) have shown that neither the number of DSBs nor the level of nmDNA correlated with TLD. DSBs appeared in the DNA of thymine-starved cells in the presence of rifampicin, a drug that prevents TLD. Thus, DSBs might be necessary but not sufficient to cause TLD. In addition, DNA recombination intermediates (nmDNA) were not observed under thymine starvation when hydroxyurea was present (Martín and Guzmán, 2011). Because death still occurs under thymine starvation in the presence of hydroxyurea (**Figure 1A**), DNA recombination intermediates may be associated with, but are not essential for, TLD. Thus, what is the critical condition for TLD to occur?

Initiation of Replication is a Key Element in TLD

Although TLD has been associated for many years with replicating cells, and recent results have demonstrated a correlation between TLD and the number of replication forks, two results have suggested that additional components of the replication process are involved in TLD. First, TLD is suppressed by inhibiting RNA or protein synthesis, or both, as is observed in experimental conditions including the presence of rifampicin (Hanawalt, 1963; Martín and Guzmán, 2011; Martín et al., 2014) or chloramphenicol or in amino acid-starved cells (Martín, 2014). Second, TLD is avoided by inactivating the DnaA protein (Bouvier and Sicard, 1975; Nakayama et al., 1994; Martín et al., 2014). The nexus between these three conditions (RNA and protein synthesis and the active form of DnaA protein) is their requirement at the initiation of replication. The inhibition of initiation by any of these treatments does not affect elongating replication forks, which can progress until the replication of the chromosome is completed. Thus, a correlation has been found between initiation of new replication rounds under thymine starvation and TLD. The causative link between DNA initiation and TLD has been established by several lines of evidence detailed below.

New Initiations Occur Under Thymine Starvation

The occurrence of new initiation events after restoring thymine to thymine-starved cells was first reported in the 1960s (Pritchard and Lark, 1964) and confirmed within the past 5 years (Martín and Guzmán, 2011; Martín et al., 2014). Furthermore, it has been shown by different approaches that initiation events do occur during thymine starvation.

(i) Replication runouts – This approach is based on the ΔG and the $\Delta G'$ values. Briefly, ΔG refers to the relative increase in the amount of DNA after the inhibition of new rounds of chromosome replication, a condition achieved by adding 150 μg ml^{-1} of rifampicin to an exponentially growing culture (Sueoka and Yoshikawa, 1965; Zaritsky and Pritchard, 1971). $\Delta G'$ represents the relative increment of DNA in a culture subjected to 10 min of thymine starvation followed by restoration of thymine in the presence of 150 μg ml^{-1} of rifampicin to inhibit new initiations. Thus, if new initiations occur in the thymine-starved cells, then the $\Delta G'$ value is expected to be higher than the ΔG value (Jiménez-Sánchez and Guzmán, 1988). The results in **Figure 2A** show that the value of $\Delta G'$ after the addition of thymine to 10-min thymine-starved cultures is higher than ΔG. These results show that new initiations occurred at a number of origins (*i*) under thymine starvation. Initiation events also occurred in the presence of hydroxyurea, but they were suppressed when the 10-min period of thymine starvation was performed in the presence of rifampicin or chloramphenicol. These results show a correlation between chromosomal initiation and lethality under thymine starvation (Martín and Guzmán, 2011; Martín et al., 2014).

Furthermore, it was shown that the number of initiations at *oriC* increased with the amount of treatment time (**Figure 2B**), correlating with a loss of colony-forming units on solid medium (**Figure 1A**). Flow cytometry profiles of the replication runouts after thymine addition to cultures previously exposed to increasing time periods of thymine starvation indicated that only the *thymineless*-initiations that had occurred during the first 30 min could be repaired to allow complete chromosome replications (Martín et al., 2014).

(ii) Visualization of the oriC replication intermediates under thymine starvation by 2D gels – The analysis of the replication fork progression at one specific position of the chromosome can be resolved by performing two-dimensional DNA gel electrophoresis (2D gels; Brewer and Fangman, 1987; Schwartzman et al., 2012). The results with 2D gels show the different DNA structures that occur in the *oriC* region during thymine starvation (**Figure 2C**). The bubble arcs detected after 40 min indicate initiation events at *oriC*, while the double-Y structures are most likely produced by two forks encountering each other at *oriC*. These structures indicate that replication rounds are initiated during thymine starvation in the *oriC* region, although the possibility of initiations at different locations cannot be excluded. A simple-Y arc, corresponding to accumulated Y-shaped replication intermediates, was clearly detected after 10 min of thymine starvation. This indicates the arrest of replication forks within the *oriC* region and also strongly suggests that some initiations occur outside of the restriction fragment but still in the vicinity of *oriC*.

The experiments using the mutant strains confirmed the occurrence of initiation during thymine starvation. Consistent with the suppression of TLD, none of the DNA intermediates observed in wild type strains under TLD

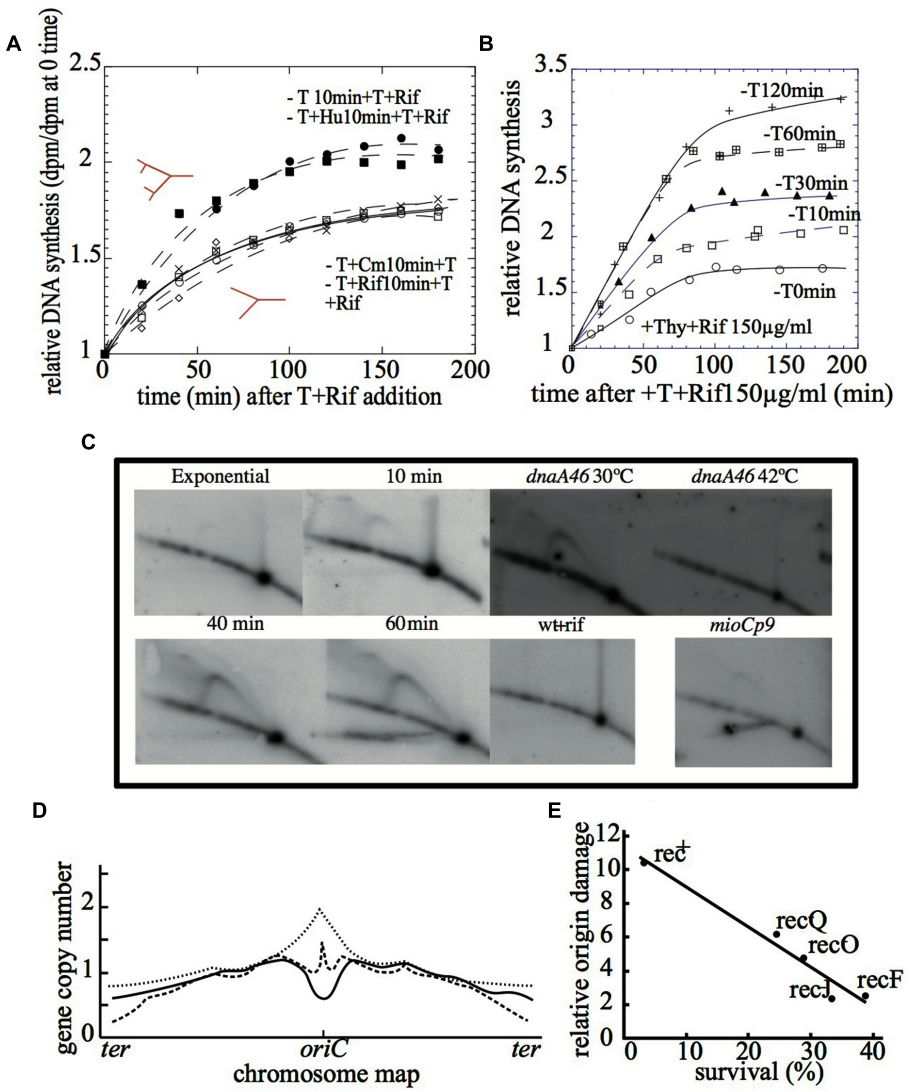

FIGURE 2 | (A) The relative DNA accumulation in the presence of rifampicin after thymine restoration to 10 min thymine-starved cells in the presence of rifampicin, chloramphenicol, hydroxyurea, or any drugs (Martín and Guzmán, 2011). **(B)** The relative DNA accumulation in the presence of rifampicin after thymine restoration to cells under thymine starvation for different extents of time (Martín et al., 2014). **(C)** The 2D gel DNA analysis of exponentially growing cells at 0, 10, 40, and 60 min of thymine starvation in the wild type strain; at 60 min and 30 or 42°C in the *dnaA46* thermosensitive mutant; in the presence of rifampicin and in the *mioCp9* mutant (adapted from Martín et al., 2014). **(D)** The Marker Frequency Analysis of the wild type strain (solid line), the *recA* (dotted line) mutant, or the *recBC* mutant (broken line) after 4 h of thymine starvation (adapted from Kuong and Kuzminov, 2012). **(E)** The correlation between the relative *origin* damage and percent of survival after 3 h of thymine starvation in the wild type strain and Rec defective mutants (*recQ, recO, recJ,* and *recF*) (adapted from Sangurdekar et al., 2010).

conditions were detected by 2D gels when initiations were inhibited by rifampicin or by DnaA inactivation (**Figure 2C**; Martín et al., 2014).

(iii) Copy number of oriC sequences increases during first 30 min under thymine starvation – The third approach providing evidence that new initiations occur during thymine starvation has been the quantification of the *ori/ter* ratio by performing either quantitative PCR (Sangurdekar et al., 2010) or Marker Frequency Analysis (dot-blot hybridization; Kuong and Kuzminov, 2012). The frequency of a gene along the chromosome, *f(a)*, follows a function that depends upon the number of replication rounds per chromosome, *n*, and the position of the gene relative to the origin of replication, *x*, being $f(a) = 2^{n(1-x)}$ (Sueoka and Yoshikawa, 1965).

Determination of the *ori/ter* ratio after 30 min of thymine starvation yielded a value higher than that obtained when the cells were growing exponentially (Kuong and Kuzminov, 2012). The overall results show that *thymineless*-initiation events do occur. With the passage of time, the number of origins decreases, revealing a progressive loss of DNA in the *oriC* sequence (Sangurdekar et al., 2010; Kuong and Kuzminov, 2012) as detailed below.

oriC is Degraded Under Thymine Starvation in a Rec-Dependent Manner

Marker Frequency Analysis on the scale of the whole chromosome by gene arrays is becoming the standard method of analyzing the replication pattern in bacteria. The results of the comparative genomic hybridization of chromosomal DNA after 3–4 h of thymine starvation revealed the loss of the *oriC* region (Sangurdekar et al., 2010; Kuong and Kuzminov, 2012; **Figure 2D**). Furthermore, this conclusion is supported by the loss of *oriC*-containing foci during TLD, which was revealed by fluorescence *in situ* hybridization (FISH; Fonville et al., 2010). An explanation for these observations could rely upon the degradation of the *oriC* region originated from DSBs nearby. An interesting question arises at this point: why and how is the *oriC* sequence preferentially degraded? One of the better-known triggers of chromosomal fragmentation is the incorporation of uracil into DNA. This occurs *dut* mutants, in such a way that the chromosome fragmentation exhibits a gradient that parallels the replication gradient (Kouzminova and Kuzminov, 2008). Thus, it may be possible that the distinctive degradation of the *oriC* region is explained by the AT-rich feature of the *oriC* sequence, which could allow for a very significant incorporation of uracil in the absence of thymine.

Several defective repair/recombination mutant strains have been assayed for DNA damage impacting the *oriC* region (Sangurdekar et al., 2010). These include those affecting enzymes that process and repair single-stranded gaps such a *recFOR, recJ,* or *recQ*. All of them are, to some extent, resistant to TLD and contain quantitatively lower origin DNA damage than in wild type strains (**Figure 2E**), thus connecting the extent of DNA damage at the *oriC* region to the lethality under thymine starvation. Interestingly, *recA* defective mutant starved for thymine for 4 h displayed an *ori/ter* ratio even higher than the initial value before treatment (Kuong and Kuzminov, 2012; **Figure 2D**). RecA is a protein that plays a central role in homologous DNA recombination and repair. Nevertheless, it has been reported that either it is not required for TLD (Nakayama et al., 1982) or it may partially palliate it (Fonville et al., 2010; Kuong and Kuzminov, 2010). Thus, the reported absence of *oriC* degradation in a *recA* mutant during thymine starvation would support the alleviated TLD observed in the *recA* mutant (Kuong and Kuzminov, 2012), consistent with the idea that TLD would depend on the origin degradation triggered by RecA-promoted recombinational misrepair.

The provocative exception is the feature exhibited by a *recBC* defective mutant, which has been described to be hypersensitive to TLD, although no *oriC* degradation is observed in this genetic background (Kuong and Kuzminov, 2010, 2012). The RecBCD complex has both helicase and exonuclease activities, and it initiates the repair of DSBs by homologous recombination in combination with RecA protein (Michel et al., 2007; Dillingham and Kowalczykowski, 2008). Because *recBC* mutant cells do not degrade double-strand DNA ends and cannot repair DSBs, the TLD in this defective mutant likely could be related to its inability to repair DSBs at the original replication forks, even though the *oriC* region is not degraded (**Figure 2D**).

The Transcription-Dependent Step of Initiation is the Target for Rifampicin Suppression of TLD

Thymineless death suppression by rifampicin was observed in early studies (Nakayama and Hanawalt, 1975), but its mechanism of action has not yet been elucidated. This problem has been analyzed by two different approaches.

(i) The effects of different concentrations of rifampicin – It has been shown that the activity of the RNA polymerase in thymine-starved cells modulates both the initiation of DNA replication under thymine starvation and TLD (Martín et al., 2014). Interestingly, suppression of TLD by rifampicin in a Δ*datA* mutant was achieved when treated with 1,000 $\mu g\ ml^{-1}$ of the drug but not with 150 $\mu g\ ml^{-1}$ (Martín and Guzmán, 2011). It has been suggested that in a Δ*datA* strain, less RNA transcription around *oriC* would be required for initiation to occur because more DnaA protein would be available to open the *oriC* sequence during initiation in this mutant (Morigen et al., 2005). Accordingly, the Δ*datA* strain initiates chromosome replication in the presence of 150 $\mu g\ ml^{-1}$ rifampicin, explaining the observed TLD, while addition at 1,000 $\mu g\ ml^{-1}$ completely inhibits the transcription requirement for initiation, hence suppressing TLD.

(ii) mioC and gid defective mutant strains – The importance of *mioC* and *gid* gene transcription for the initiation of chromosomal replication at *oriC* is widely accepted (Messer, 1972; Baker and Kornberg, 1988). Nevertheless, neither the deletion of *PmioC112* or *Pgid113* promoters, nor the constitutive transcription from the *mioCp9* promoter have a large effect on the cell cycle. However, reduction in initiation efficiency has been observed in rich medium (Bates et al., 1997; Molina et al., 1999; Su'etsugu et al., 2003). Under thymine starvation, altered *mioC* and *gid* transcription limited the initiation process and TLD was alleviated (Martín et al., 2014). The relevance of these results relies on the fact that TLD alleviation in these mutants must be related to the alteration of the normal transcription levels around *oriC*. This effect on TLD, combined with the broad reduction in chromosome initiation intermediates in these mutants (**Figure 2C**), strongly suggests that the transcription-dependent step of the initiation is the target for rifampicin suppression of TLD, hence being critical for TLD.

Conclusion

Overall, these experimental approaches pinpoint the initiations at the *oriC* region as the main targets for TLD in wild type strains. Thus, if DNA initiation is allowed under thymine starvation, death occurs likely due to the lethal consequences of the presence of DSBs, DNAss gaps, and DNA recombination intermediates at the *origin* that eventually result in *oriC* region degradation. If initiation is inhibited (*dnaA46* mutant, rifampicin, chloramphenicol) or impaired (*mioC, gid,* Δ*datA*, sub-inhibitory rifampicin concentrations), TLD is subsequently suppressed or alleviated, respectively. Thus, the observed correlation between TLD and the number of replication forks could reflect not only the importance of the forks as targets, but also the

quantitative relationship between TLD, and the number of *origins* per chromosome, 2^n.

Regarding *thymineless*-initiation events in *thyA* mutants that are otherwise wild type cells, the observations could be divided into two stages. During the first 30–60 min following thymine starvation the instability of DNA ss-gaps and the resulting DNA degradation behind the replication forks (and/or different source; Kuong and Kuzminov, 2012), might provide the dNTPs necessary to support new initiations, residual DNA elongation and the repair of the replication forks. According to the results from different authors, initiation events (supposed to occur at the first stage) are required to yield TLD, as lethality has not been observed in thymine-starved cells under conditions inhibiting DNA initiation.

The second stage would proceed after 30–60 min when the new thymineless-initiation events would generate unrepaired DSBs or DNAss gaps together with unresolved DNA recombination intermediaries at the origin, somehow triggering the unique degradation of the *oriC* region that acts as the major lethal effect of thymine starvation. Supporting this explanation, it also has been shown that the extent of *origin* degradation (supposed to occur at the second stage) correlates with the magnitude of TLD (Sangurdekar et al., 2010). At this point, the role of the recombination/repair enzymes reflects the different sensitivities to thymine starvation described above. Accordingly, several independent pathways accounting for TLD has been proposed (Courcelle, 2005; Nakayama, 2005; Kuong and Kuzminov, 2010) and also supported by Rosenberg's lab (Fonville et al., 2010, 2011; Hamilton et al., 2013).

Several questions arise from this tentative model. The first one is whether new DNA initiation is a requisite for origin degradation. Second, what is the mechanism by which the *oriC* region is selectively degraded? Third, according to this proposal the DSBs located outside the origin region do not seem to be lethal or, alternatively, the inhibition of DNA initiation is counteracting their potentially lethal effect. Therefore, what is the mechanism of that phenomenon?

The advances in knowledge about TLD mechanisms have been impressive in the past 5 years. New technologies and approaches have evolved to provide novel insights, but TLD is still like a black hole – you know how you got into it but you never know where you will end up as time passes.

Acknowledgments

We wish to specially thank Phil Hanawalt, Arkady Khodursky, Alfonso Jiménez-Sánchez, and the reviewers for critically reading this manuscript, promoting constructive discussion and, especially to Andrei Kuzminov for providing such a wording suggestions. We thank the Servicio de Técnicas Aplicadas a la Biociencia (STAB) of the Universidad de Extremadura and Encarna Ferrera for technical assistance. This work was supported by grants GRU10058 from the Junta de Extremadura and BFU2007-63942 from the Ministerio de Educación y Ciencia to ECG.

References

Ahmad, S. I., Kirk, S. H., and Eisenstark, A. (1998). Thymine metabolism and thymineless death in prokaryotes and eukaryotes. *Annu. Rev. Microbiol.* 52, 591–625. doi: 10.1146/annurev.micro.52.1.591

Baker, T. A., and Kornberg, A. (1988). Transcriptional activation of initiation of replication from the E. *coli* chromosomal origin: an RNA-DNA hybrid near *oriC*. *Cell* 55, 113–123. doi: 10.1016/0092-8674(88)90014-1

Barner, H. D., and Cohen, S. S. (1954). The induction of thymine synthesis by T2 infection of a thymine requiring mutant of *Escherichia coli*. *J. Bacteriol.* 68, 80–88.

Bates, D., Boye, E., Asai, T., and Kogoma, T. (1997). The absence of effect of *gid* or *mioC* transcription on the initiation of chromosomal replication in *Escherichia coli*. *Proc. Natl. Acad. Sci. U.S.A.* 94, 12497–12502. doi: 10.1073/pnas.94.23.12497

Bouvier, F., and Sicard, N. (1975). Interference of *dna-ts* mutations of *Escherichia coli* with *thymineless death*. *J. Bacteriol.* 124, 1198–1204.

Brewer, B. J., and Fangman, W. L. (1987). The localization of replication origins on ARS plasmids in *S. cerevisiae*. *Cell* 51, 463–471. doi: 10.1016/0092-8674(87)90642-8

Courcelle, J. (2005). Recs preventing wrecks. *Mutant. Res.* 557, 217–227. doi: 10.1016/j.mrfmmm.2005.03.019

Dillingham, M. S., and Kowalczykowski, S. C. (2008). RecBCD enzyme and the repair of Double-Stranded DNA Breaks. *Microbiol. Mol. Biol. Rev.* 72, 642–671. doi: 10.1128/MMBR.00020-08

Fonville, N. C., Bates, D., Hastings, P. J., Hanawalt, P. C., and Rosenberg, S. M. (2010). Role of RecA and the SOS response in thymineless death in *Escherichia coli*. *PLoS Genet.* 6:e1000865. doi: 10.1371/journal.pgen.1000865

Fonville, N., Vaksman, Z., DeNapoli, J., Hastings, P. J., and Rosenberg, S. M. (2011). Pathways of resistance to thymineless death in *Escherichia coli* and the function of UvrD. *Genetics* 189, 23–36. doi: 10.1534/genetics.111.130161

Guarino, E., Salguero, I., Jiménez-Sánchez, A., and Guzmán, E. C. (2007). Double-strand break generation under deoxyribonucleotide starvation in *Escherichia coli*. *J. Bacteriol.* 189, 5782–5786. doi: 10.1128/JB.00411-07

Hamilton, H. M, Wilson, R., Blythe, M., Nehring, R. B., Fonville, N. C., Louis, E. J., et al. (2013). Thymineless death is inhibited by CsrA in Escherichia coli lacking the SOS response. *DNA Repair (Amst)* 12, 993–999. doi: 10.1016/j.dnarep.2013.08.011

Hanawalt, P. C. (1963). Involvement of synthesis of RNA in *thymineless death*. *Nature* 198, 286. doi: 10.1038/198286a0

Hanawalt, P. C., Maaløe, O., Cummings, D. J., and Schaechter, M. (1961). The normal DNA replication cycle. II. *J. Mol. Biol.* 3, 156–165. doi: 10.1016/S0022-2836(61)80042-9

Jiménez-Sánchez, A., and Guzmán, E. C. (1988). Direct procedure for the determination of the number of replication forks and the reinitiation fraction in bacteria. *Comput. Appl. Biosci.* 4, 431–433.

Kouzminova, E. A., and Kuzminov, A. (2008). Patterns of chromosomal fragmentation due to uracil-DNA incorporation reveal a novel mechanism of replication-dependent double-stranded breaks. *Mol. Microbiol.* 68, 202–215. doi: 10.1111/j.1365-2958.2008.06149.x

Kuong, K. J., and Kuzminov, A. (2009). Cyanide, peroxide and nitric oxide formation in solutions of hydroxyurea causes cellular toxicity and may contribute to its therapeutic potency. *J. Mol. Biol.* 390, 845–862. doi: 10.1016/j.jmb.2009.05.038

Kuong, K. J., and Kuzminov, A. (2010). Stalled replication fork repair and misrepair during thymineless death in *Escherichia coli*. *Genes Cells* 15, 619–634. doi: 10.1111/j.1365-2443.2010.01405.x

Kuong, K. J., and Kuzminov, A. (2012). Disintegration of nascent replication bubbles during thymine starvation triggers RecA- and RecBCD-dependent replication origin destruction. *J. Biol. Chem.* 287, 23958–23970. doi: 10.1074/jbc.M112.359687

Maaloe, O., and Hanawalt, P. C. (1961). Thymine deficiency and the normal DNA replication cycle. *I. J. Mol. Biol.* 3, 144–155. doi: 10.1016/S0022-2836(61)80041-7

Martín, C. M. (2014). *Role of DNA Replication Initiation on the Lethality Caused by Thymine Starvation*. Ph.D. thesis, Universidad de Extremadura, Badajoz.

Martín, C. M., and Guzmán, E. C. (2011). DNA replication initiation as a key element in thymineless death. *DNA Repair (Amst.)* 10, 94–101. doi: 10.1016/j.dnarep.2010.10.005

Martín, C. M., Viguera, E., and Guzmán, E. (2014). Rifampicin suppresses thymineless death by blocking the transcription-dependent step of chromosome initiation. *DNA Repair* 18, 10–71. doi: 10.1016/j.dnarep.2014.03.004

Messer, W. (1972). Initiation of deoxyribonucleic acid replication in *Escherichia coli* B-r: chronology of events and transcriptional control of initiation. *J. Bacteriol.* 112, 7–12.

Michel, B., Boubakri, H, Baharoglu, Z, LeMasson, M, and Lestini, R. (2007). Recombination proteins and rescue of arrested replication forks. *DNA Repair* 6, 967–980. doi: 10.1016/j.dnarep.2007.02.016

Molina, F., Jiménez-Sánchez, A., Zyskind, J. W., and Guzmán, E. C. (1999). Chromosomal insertions localized around *oriC* affect the cell cycle in *Escherichia coli*. *Biochimie* 81, 811–818. doi: 10.1016/S0300-9084(99)00216-3

Morganroth, P. A., and Hanawalt, P. C. (2006). Role of DNA replication and repair in thymineless death in *Escherichia coli*. *J. Bacteriol.* 188, 5286–5288. doi: 10.1128/JB.00543-06

Morigen, Molina, F., and Skarstad, K. (2005). Deletion of the *datA* site does not affect once-per-cell-cycle timing but induces rifampin-resistant replication. *J. Bacteriol.* 187, 3913–3920. doi: 10.1128/JB.187.12.3913-3920.2005

Nakayama, H. (2005). *Escherichia coli* RecQ helicase: a player in *thymineless death*. *Mutat. Res.* 577, 228–236. doi: 10.1016/j.mrfmmm.2005.02.015

Nakayama, H., and Hanawalt, P. C. (1975). Sedimentation analysis of deoxyribonucleic acid from thymine-starved *Escherichia coli*. *J. Bacteriol.* 121, 537–547.

Nakayama, H., Nakayama, K., Nakayama, R., and Nakayama, Y. (1982). Recombination-deficient mutations and thymineless death in *Escherichia coli*: reciprocal effects of *recBC* and *recF* and indifference of *recA* mutations. *Can. J. Microbiol.* 28, 425–430. doi: 10.1139/m82-064

Nakayama, K., Kusano, K., Irino, N., and Nakayama, H. (1994). Thymine starvation-induced structural changes in *Escherichia coli* DNA. Detection by pulsed field gel electrophoresis and evidence for involvement of homologous recombination. *J. Mol. Biol.* 243, 611–620. doi: 10.1016/0022-2836(94)90036-1

Okagaki, H., Tsubota, Y., and Sibataini, A. (1960). Unbalanced growth and bacterial death in thymine-deficient and ultraviolet irradiated *Escherichia coli*. *J. Bacteriol.* 80, 762–771.

Pritchard, R. H., and Lark, K. G. (1964). Induction of replication by thymine starvation at the chromosome origin in *Escherichia coli*. *J. Mol. Biol.* 9, 288–307. doi: 10.1016/S0022-2836(64)80208-4

Sangurdekar, D. P., Hamann, B. L., Smirnov, D., Srienc, F., Hanawalt, P. C., and Khodursky, A. B. (2010). *Thymineless death* is associated with loss of essential genetic information from the replication origin. *Mol. Microbiol.* 75, 1455–1467. doi: 10.1111/j.1365-2958.2010.07072.x

Schwartzman, J. B., Martínez-Robles, M. L., López, V., Hernández, P., and Krimer, D. B. (2012). 2D gel and their third-dimensional potential. *Methods* 57, 170–178. doi: 10.1016/j.ymeth.2012.03.013

Sueoka, N., and Yoshikawa, H. (1965). The chromosome of Bacillus subtilis. I. Theory of marker frequency analysis. *Genetics* 52, 747–757.

Su'etsugu, M., Emoto, A., Fujimitsu, K., Keyamura, K., and Katayama, T. (2003). Transcriptional control for initiation of chromosomal replication in *Escherichia coli*: fluctuation of the level of origin transcription ensures timely initiation. *Genes Cells* 8, 731–745. doi: 10.1046/j.1365-2443.2003.00671.x

Zaritsky, A., and Pritchard, R. (1971). Replication time of the chromosome in *thymineles* mutants of *Escherichia coli*. *J. Mol. Biol.* 60, 65–74. doi: 10.1016/0022-2836(71)90447-5

Conflict of Interest Statement: The authors declare that the research was conducted in the absence of any commercial or financial relationships that could be construed as a potential conflict of interest.

Copyright © 2015 Guzmán and Martín. This is an open-access article distributed under the terms of the Creative Commons Attribution License (CC BY). The use, distribution or reproduction in other forums is permitted, provided the original author(s) or licensor are credited and that the original publication in this journal is cited, in accordance with accepted academic practice. No use, distribution or reproduction is permitted which does not comply with these terms.

frontiers in Microbiology

MINI REVIEW
published: 24 April 2015
doi: 10.3389/fmicb.2015.00363

Perturbed states of the bacterial chromosome: a thymineless death case study

*Lev Ostrer, Bree L. Hamann† and Arkady Khodursky**

Department of Biochemistry, Molecular Biology and Biophysics, Biotechnology Institute, University of Minnesota, St. Paul, MN, USA

OPEN ACCESS

Edited by:
Arieh Zaritsky, Ben-Gurion University of the Negev, Israel

Reviewed by:
Norman P. Higgins, University of Alabama at Birmingham, USA
Andrei Kuzminov, University of Illinois at Urbana–Champaign, USA
Georgi Muskhelishvili, Jacobs University, Germany

****Correspondence:***
Arkady Khodursky, Department of Biochemistry, Molecular Biology and Biophysics, Biotechnology Institute, University of Minnesota, 244 Gortner Lab, 1479 Gortner Avenue, St. Paul, MN 55108, USA
khodu001@umn.edu

† Formerly associated with Biotechnology Institute, University of Minnesota, St. Paul, MN, USA

Specialty section:
This article was submitted to Microbial Physiology and Metabolism, a section of the journal Frontiers in Microbiology

Received: *24 February 2015*
Accepted: *10 April 2015*
Published: *24 April 2015*

Citation:
Ostrer L, Hamann BL and Khodursky A (2015) Perturbed states of the bacterial chromosome: a thymineless death case study. Front. Microbiol. 6:363. doi: 10.3389/fmicb.2015.00363

Spatial patterns of transcriptional activity in the living genome of *Escherichia coli* represent one of the more peculiar aspects of the *E. coli* chromosome biology. Spatial transcriptional correlations can be observed throughout the chromosome, and their formation depends on the state of replication in the cell. The condition of thymine starvation leading to thymineless death (TLD) is at the "cross-roads" of replication and transcription. According to a current view, e.g., (Cagliero et al., 2014), one of the cellular objectives is to segregate the processes of transcription and replication in time and space. An ultimate segregation would take place when one process is inhibited and another is not, as it happens during thymine starvation, which results in numerous molecular and physiological abnormalities associated with TLD. One of such abnormalities is the loss of spatial correlations in the vicinity of the origin of replication. We review the transcriptional consequences of replication inhibition by thymine starvation in a context of the state of DNA template in the starved cells and opine about a possible significance of normal physiological coupling between the processes of replication and transcription.

Keywords: transcription, replication, spatial correlations, thymine starvation, thymineless death

Introduction

Replication and transcription are intertwined in a number of ways, as molecular reactions and biological processes. In the cell, the two polymerization reactions utilize, and compete for, the same DNA template. That may force local interactions between DNA and RNA polymerase complexes (Liu and Alberts, 1995; Felipe-Abrio et al., 2014), which may be a part of the normal replication process (French, 1992; Merrikh et al., 2011) or, under special circumstances, may be a source of chromosome pathology (Merrikh et al., 2012). The reactions are also linked at a deep evolutionary level via the activity of the enzyme ribonucleoside di(tri)phosphate reductase which converts ribonucleotides, precursors of substrates (or substrates) for the reaction of transcription, into deoxyribonucleotides, substrates for DNA polymerization reaction (Reichard, 2010).

The biological processes of replication and transcription are also coupled via a number of regulatory mechanisms, some of which are still unexplained or/and whose physiological significance is not yet understood. First, DNA replication determines intrinsic levels of gene expression by establishing gene dosage gradients along the chromosome (Chandler and Pritchard, 1975; Schmid and Roth, 1987; Couturier and Rocha, 2006; Slager et al., 2014). Second, transcription is required for initiation of chromosomal DNA replication (Lark, 1972; Messer, 1972). Third, DNA replication is required for establishing normal spatial patterns of chromosomal transcription (Jeong et al., 2006). Fourth, interference with DNA replication results in a specialized DNA damage transcriptional response (Simmons et al., 2008; Kreuzer, 2013). Fifth, the replication initiator protein DnaA

(Kaguni, 2006) controls, as an activator and repressor, transcription of the ribonucleotide reductase operon (Olliver et al., 2010). Sixth, activity of both processes can be modulated by (p)ppGpp (Chiaramello and Zyskind, 1990; Levine et al., 1991; Denapoli et al., 2013) and by changes in DNA supercoiling (Kowalski and Eddy, 1989; Crooke et al., 1991; von Freiesleben and Rasmussen, 1992; Peter et al., 2004; Rovinskiy et al., 2012), two molecular sensors that can relay information about critical fluctuations in the cell's environment to the parts of the replication and transcription machineries (Dorman, 2006; Jin et al., 2012; Sobetzko et al., 2012). Last and perhaps more of a fortuitous link is a genetic one, exemplified by the evolutionarily conserved arrangement of genes encoding the DNA primase DnaG and the main sigma factor RpoD in one operon (Burton et al., 1983; Versalovic et al., 1993).

All these interactions have been shaped and calibrated by the evolutionary forces to accommodate species specific differences in genome organization and physiology. Disruption of normal temporal and spatial relationships between replication and transcription may have detrimental consequences for the cell. And nowhere such consequences are more pronounced than during thymine starvation.

Thymine Starvation and Transcription

Thymine is one of the five common nucleobases and it is found primarily in DNA where it makes a Watson-Crick pair with Adenine. Active thymine compound in the cell is TTP: it is a precursor of DNA as well as of thymidine nucleotide sugars that serve as intermediates in O-antigen biosynthesis (Samuel and Reeves, 2003). In most organisms, cells synthesize thymine on the level of a nucleotide as thymidine monophosphate from deoxyuridine monophosphate (www.kegg.jp, www.ecocyc.org). Thymine dependency, or auxotrophy, can be established by mutating a gene encoding thymidylate synthase (Belfort et al., 1983). Thymine requiring mutants can only grow in presence of the exogenous base or nucleoside (Barner and Cohen, 1954). Starving cells for thymine results in a rapid decay in colony counts (Barner and Cohen, 1954). The decay is preceded by a near complete cessation of DNA synthesis (Barner and Cohen, 1958; Kuong and Kuzminov, 2010) and it is paralleled by increase in the cell size (Barner and Cohen, 1954), which is indicative of division arrest. However, inhibition of RNA and protein synthesis across a population of starved cells lags significantly behind the drop in colony formation (Barner and Cohen, 1958; McFall and Magasanik, 1960). Thus, cells deprived of thymine go through temporally ordered events: 1-inhibition of bulk DNA synthesis; 2-cell elongation and division arrest; 3-decrease in colony formation; 4-inhibition of protein and RNA synthesis. The overall phenomenon of thymine starvation leading to an exponential decrease in colony counts is known as thymineless death (Cohen and Barner, 1954), or TLD. It was postulated that the cause of death is "inhibition of DNA synthesis under conditions of continued cytoplasmic synthesis" (Barner and Cohen, 1957), including RNA, protein and overall biomass. Such uncoupling between biosynthetic processes was termed an "unbalanced growth" (Cohen and Barner, 1954) and it was proposed to be the underlying macro-mechanism of the bactericidal effect of not only thymine starvation, but also of a number of antibiotics (Barner and Cohen, 1956). However, the pathology of TLD has been associated with the transcriptional activity of the starved cells and not with other aspects of the unbalanced growth (Gallant and Suskind, 1962; Hanawalt, 1963; Rolfe, 1967; Morganroth and Hanawalt, 2006; Martin et al., 2014).

Transcriptional activity of a population of bacterial cells is a sum of the activities of individual cells. Even when growth rate of a population is kept constant, cells making up that population may have different microenvironments, may come from different stages of the cell cycle, and may be of different sizes and ages. As a result, transcriptional activity across a population of cells in a steady state can be viewed as a type of noise that must be deconvoluted on the basis of physiological parameters in order to make sense of the activity. In part because transcriptional activity is noisy, even under controlled conditions, transcriptional states of the cell have been traditionally characterized in terms of dominant differences in transcript abundances, or in promoter activities, which could be associated with physiological or/and environmental changes. Activation of the DNA damage sensitive promoter of the *recA* gene was originally shown to be one of such dominant changes elicited by thymine deprivation (Casaregola et al., 1982).

Introduction of whole-genome microarray technology (Schena et al., 1995) made monitoring transcriptional activity less biased and more quantitative. Genome-wide surveys of changes in transcript abundances elicited by thymine deprivation confirmed that the condition induces the SOS regulon (Sangurdekar et al., 2010, 2011), a collection of genetically unlinked genes whose transcription is primarily controlled by the LexA repressor and whose activities allow the cell to repair or bypass DNA lesions in time before the delayed cell division (Simmons et al., 2008). The surveys also found that activity of the SOS regulon contrasts thymine limitation and thymine deprivation: whereas both limitation and starvation result in transcriptional upregulation of genes of the deoxyribose salvage pathway and downregulation of genes whose products are involved in pyrimidine biosynthesis, only the starvation induces transcription of the SOS regulon (Sangurdekar et al., 2010, 2011).

Relative transcript abundances measured for nearly every gene in a genome can be used to correlate transcriptional activities of genes over time or conditions (Eisen et al., 1998; Tamayo et al., 1999).The resulting correlation patterns can be explained in terms of underlying regulatory mechanisms, e.g., (van Helden et al., 1998). Co-transcriptional patterns in prokaryotic genomes result primarily from organization of genes in operons (Gutierrez-Rios et al., 2003) and regulons (Khodursky et al., 2000a; Courcelle et al., 2001). However, an operonal organization can be inferred not only from multidimensional comparative profiles of transcriptional activity of genomes, but also from one dimensional spatial series of transcript abundances, strongly suggesting that transcriptional signals recorded across a population of cells, despite being a product of multiple sources of biological variation, contain biologically relevant structural information (Jeong et al., 2004). In fact, the spatial transcriptional signal can be used to model geometric features of the chromosomal DNA superstructure, assuming juxtaposition of co-regulated genes in 3-D space (Xiao et al., 2011). Mapping of contacts between linearly

non-adjacent DNA segments in the *Caulobacter crescentus* chromosome using the high-resolution chromosome capture methodology (Lieberman-Aiden et al., 2009) revealed the general properties of physical organization of chromosomal DNA inside the cell (Le et al., 2013). These properties, including the dimensions of short- and medium-range features, were consistent with the estimates obtained from the geometric model which was based on expression data alone. This concordance bolsters the notion that spatial transcriptional profiles contain information about underlying structure of the chromosomal DNA inside the cell (Jeong et al., 2004).

Phenomenologically, transcriptional activity of any two genes can be up or down relative to some baseline level. If activities of multiple pairs of genes vary in the same direction, and genes in the pairs are situated the same or nearly the same distance apart, then the transcriptional signal can be viewed as spatially regular with a characteristic distance between genes with co-varying activity. Such characteristic distance, or spatial frequency, can be evaluated using conventional signal processing techniques, including autocorrelation or the Fourier transform. Using these methods, it was demonstrated that, independently of growth conditions, transcriptional signal from the *E. coli* chromosome can be characterized by several statistically significant spatial frequencies: 1 kbp, 4 ± 2 kbp, 16 ± 4 kbp, 32 ± 6 kbp, 128 ± 12 kbp, and 570 ± 50 kbp (Jeong et al., 2004). However, co-variations in transcriptional activities do not have to be spatially regular or have the same regularity across the entire chromosome. To account for that the signal can be analyzed using the wavelet transform which provides space-frequency representation of original spatial series (Torrence and Compo, 1998). Moreover, it may be useful to know what spectral components occur in which chromosomal intervals, especially for the purposes of comparative analysis (Allen et al., 2006). As expected, chromosome wide transcriptional signals are not stationary; all spatial frequency components, from short- (up to 16 kbp) to long-range are found in certain regions of the chromosome but not in others (Jeong et al., 2004; Allen et al., 2006). Furthermore, different parts of the chromosome may contain different amount of spectral information. For example, nearly all spatial frequency components can be found in a region of the chromosome proximal to the origin of replication in the counter-clockwise replichore (Jeong et al., 2004). In fact, the presence of multiple frequency components, up to 128 ± 12 kbp, in this region is a characteristic feature of spatial transcriptional profiles obtained under dozens of conditions, including growth phase transitions, nutritional shifts, recoveries, antibiotic treatments, etc. (Jeong et al., 2004, 2006; Sangurdekar et al., 2006; Xiao et al., 2011). The exceptions were DNA damaging conditions causing inhibition of DNA replication, including treatment with a quinolone antibiotic, norfloxacin (Jeong et al., 2004, 2006), and thymine starvation leading to TLD (**Figure 1**). A study by Jeong et al. (2006) demonstrated, using mutants with conditionally defective initiation of chromosomal DNA replication, that ongoing replication is required for observing spatial patterns across scales. Both the quinolone treatment (Goss et al., 1965; Benbrook and Miller, 1986; Khodursky and Cozzarelli, 1998) and thymine starvation (Barner and Cohen, 1958; Kuong and Kuzminov, 2010) result in rapid inhibition of DNA replication, which in turn likely brings about structural changes in the chromosome that disfavor spatial pattern formation.

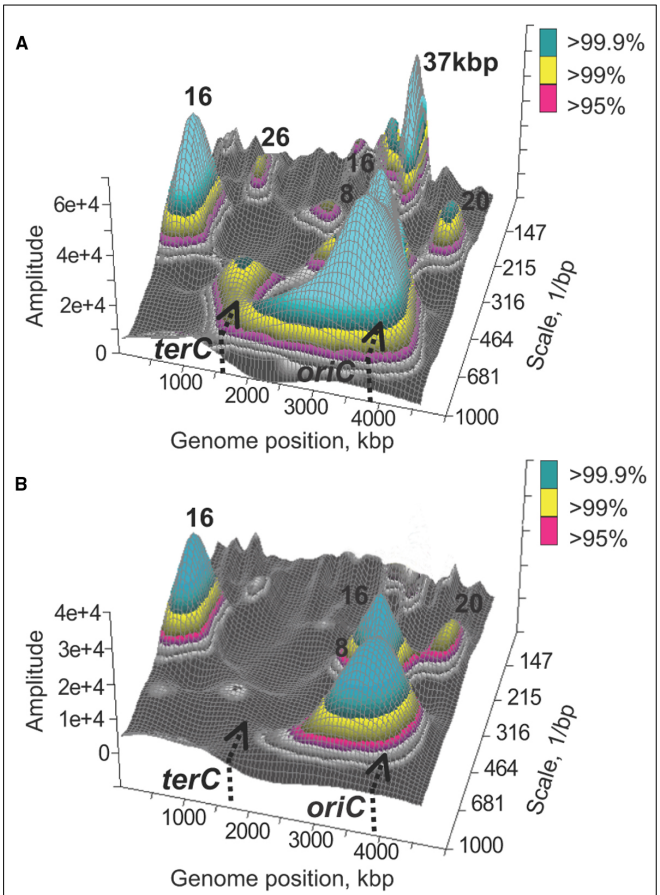

FIGURE 1 | Spatial correlations in transcript abundances along the *E. coli* chromosome. Significant wavelets with corresponding main frequencies are shown for a genome-wide transcriptional signal recorded prior to thymine starvation **(A)** and 30 min into starvation **(B)**. The figure was obtained using publicly available data as previously described (Jeong et al., 2004).

State of DNA in Thymine Starved Cells

Observations of the dissolution of spatial transcriptional patterns may be confounded in part by the fact that the loss of the patterns occurs under conditions that induce DNA damage. The damaged DNA may serve as a poor template for transcription, thereby providing an almost trivial reason for the loss of the spatial correlations in transcriptional activity.

Indeed, several types of DNA damage have been observed in cells starved for thymine, some of which may culminate in the template destruction: single strand breaks in DNA (Freifelder, 1969; Hill and Fangman, 1973; Nakayama and Hanawalt, 1975); double strand breaks (Yoshinaga, 1973; Guarino et al., 2007; Kuong and Kuzminov, 2010, 2012); geographically limited degradation of *Bacillus subtilis* chromosomal DNA behind the replication fork (Ramareddy and Reiter, 1970; Reiter and Ramareddy, 1970) and on one side of the origin of replication

(Regamey et al., 2000); partial unstructuring of the *E. coli* chromosome in a region around the origin of replication (Nakayama et al., 1994). It was shown that DNA from thymine starved cells is indeed susceptible to a single strand endonuclease activity *in vitro* and that thymine starvation induces transcription of the ssb gene, encoding the single strand DNA binding protein, which is consistent with an increase in the fraction of single strand DNA *in vivo* (Sangurdekar et al., 2010). Furthermore, investigations of DNA metabolism indicated that the starvation not only inhibits normal elongation of DNA replication (Maaloe and Hanawalt, 1961) but also results in a residual DNA synthesis (Kuong and Kuzminov, 2010) and small but quantifiable increase in the amount of bulk DNA (Barner and Cohen, 1958; Breitman et al., 1972; Kuong and Kuzminov, 2012), which is concomitant with the loss of thymine from DNA (Breitman et al., 1972) and is followed by contained DNA degradation (Kuong and Kuzminov, 2012).

Thus DNA degradation appears to be the main confounding factor in interpreting the loss of spatial transcriptional patterns in the vicinity of the origin of replication. In their attempt to map single strand DNA regions and/or regions of unstructured DNA, Sangurdekar et al. used the array comparative genomic hybridization (aCGH) method (Sangurdekar et al., 2010), which was earlier adapted (Khodursky et al., 2000b) for genetic marker frequency analysis (Sueoka and Yoshikawa, 1965) with a single gene resolution. Hybridization of labeled genomic DNA to microarray probes representing nearly every single gene and intergenic sequence in the *E. coli* genome (Khodursky et al., 2003) results in a characteristic profile of average abundances of sequences along the chromosome in a population of cells. It was shown that thymine starvation triggers gradual loss of DNA in the 500 kbp region surrounding the origin of replication (Sangurdekar et al., 2010): in the course of starvation the average dosage of DNA at and in the immediate vicinity of the origin of replication is reduced to the dosage of the replication terminus, the area of the chromosome present at the lowest frequency in an exponentially growing bacterial population (**Figure 2A**). Comparable localized variations in gene dosage have been observed by Rosenberg and colleagues (Fonville et al., 2010) and by Kuong and Kuzminov (2012). These results are consistent with a model according to which DNA template collapses at the replication origin and its neighborhood either as a result of degradation of nascent leading and lagging DNA strands in both chromatids or from a random, relatively short patch degradation of parental and nascent DNA, also in both chromatids (Sangurdekar et al., 2010). Both interpretations imply that DNA in the region may be degenerated to a point where it can no longer be used as a template in the reaction of transcription, explaining why any transcriptional patterns in that region might also be degraded. This view however, is complicated by an observation that thymine deprived cells continue transcribing genes in the region of the lesion well into starvation and even during the killing phase of TLD (Sangurdekar et al., 2010): half-life of a representative *E. coli* mRNA is about 60 times shorter than the timeline of a typical thymine starvation experiment (Bernstein et al., 2002) and there is no indication that mRNA stability is affected under conditions of thymine starvation, and the average abundance of transcripts from the region in question changes less than 50% in the course of the starvation (Sangurdekar et al., 2010). Thus an alternative model of the formation of the origin-centric lesion must be entertained, in which at least one DNA template remains intact.

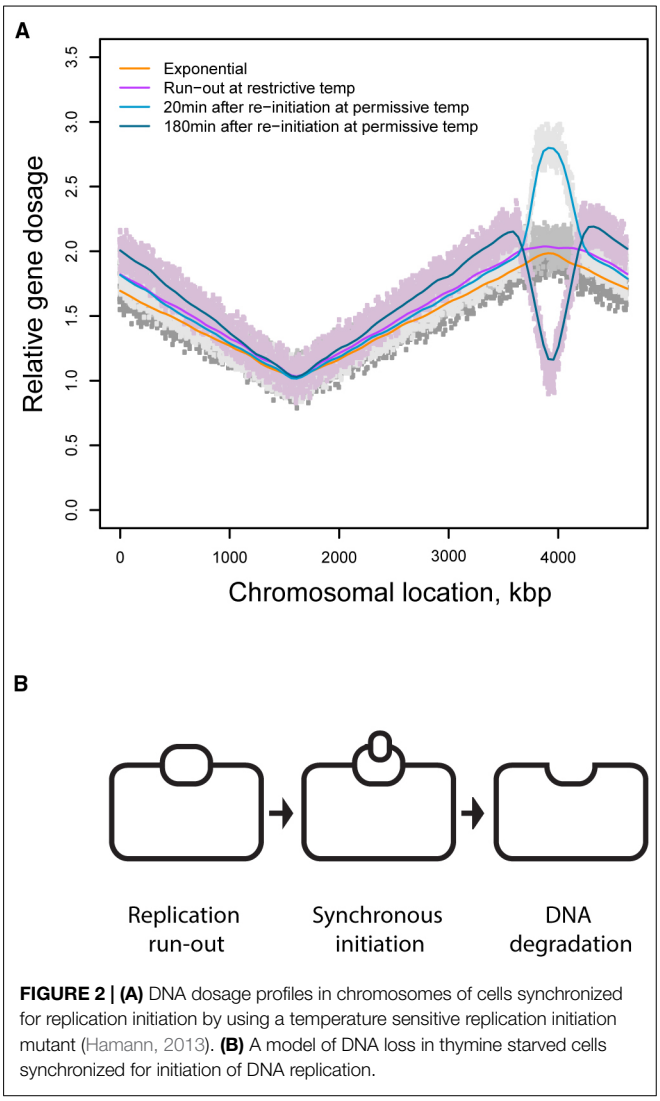

FIGURE 2 | (A) DNA dosage profiles in chromosomes of cells synchronized for replication initiation by using a temperature sensitive replication initiation mutant (Hamann, 2013). **(B)** A model of DNA loss in thymine starved cells synchronized for initiation of DNA replication.

Figure 2A depicts DNA dosage variations in a population of the thymine starved cells synchronized for initiation of DNA replication using a dnaC^{ts} mutant (Hamann, 2013); a similar profile with analogous interpretation was independently obtained by Kuong and Kuzminov (2012) in an asynchronous population of starved cells. Three conclusions can be drawn from this observation. First, following thymine withdrawal from a population of cells that can no longer initiate new rounds of replication, replication continues at least in a fraction of cells for a short period of time and then stops, resulting in a characteristic plateau spanning the stretch of the chromosome that underwent residual replication. Second, upon return to the permissive temperature, starved cells can initiate new rounds of replication even though the cells were deprived of thymine and could only support limited

extension of the ongoing replication rounds. Third, new rounds of replication are initiated only on one of two partially replicated sister chromatids followed by complete destruction of the newly established replication bubble. (Although the increase in DNA dosage may be interpreted as a variation in a fraction of the population, the decrease cannot be explained in fractional terms.). Such sequence of events would result in one intact DNA template (**Figure 2B**). Although this template is transcriptionally active, its activity is spatially disorganized.

Concluding Remarks

Spatial regularity is one of the attributes of transcriptional activity of living genomes. The nature of spatial correlations at linear distances greater than the average size of an operon is poorly understood. The patterns somewhat coincide with the purported structural features of the chromosomal DNA and may in small part be explained by co-regulation of genes that are spaced with some periodicity on the chromosome (Kepes, 2004). The correlations are particularly sensitive to the state of DNA. Conditions that interfere with either DNA supercoiling or DNA replication result in diminishment or dissolution of the patterns, suggesting that the correlations are set, or modulated, by the moving replication fork.

Thymine starvation is one of the conditions that inhibit spatial pattern formation in the region of the chromosome adjacent to the origin of replication. However, this condition not merely inhibits DNA replication but also results in structural, copy number variations in the same region of the chromosome that loses the spatial pattern and yet does not become transcriptionally silent. It raises a formal possibility that, if spatial transcriptional correlations are the result of chromosomal DNA folding behind the replication fork, the normal folding of the chromosome in a region may also depend on the regional gene dosage or ploidy of the region. Moreover, the behind-the-fork organization of the chromosomal DNA into supercoiled loops (Postow et al., 2004) or rosettes of similar size loops (Kavenoff and Bowen, 1976) may result in a coordinated, basal transcriptional activity along the newly replicated stretch of DNA. This activity may facilitate further chromosomal folding which in turn may be required for the following round of replication initiation and nucleoid segregation. Consistent with this view are observations that global inhibition of transcription results in chromosome decondensation (Pettijohn and Hecht, 1974) and precludes initiation of DNA replication without a need for locus-specific transcription (Bates et al., 1997).

Acknowledgments

AK would like to thank Anrei Kuzminov, Pat Higgins and Georgi Muskhelishvili for positive reviews and critical reading of the manuscript.

References

Allen, T. E., Price, N. D., Joyce, A. R., and Palsson, B. O. (2006). Long-range periodic patterns in microbial genomes indicate significant multi-scale chromosomal organization. *PLoS Comput. Biol.* 2:e2. doi: 10.1371/journal.pcbi.0020002

Barner, H. D., and Cohen, S. S. (1954). The induction of thymine synthesis by T2 infection of a thymine requiring mutant of *Escherichia coli*. *J. Bacteriol.* 68, 80–88.

Barner, H. D., and Cohen, S. S. (1956). The relation of growth to the lethal damage induced by ultraviolet irradiation in *Escherichia coli*. *J. Bacteriol.* 71, 149–157.

Barner, H. D., and Cohen, S. S. (1957). The isolation and properties of amino acid requiring mutants of a thymineless bacterium. *J. Bacteriol.* 74, 350–355.

Barner, H. D., and Cohen, S. S. (1958). Protein synthesis and RNA turnover in a pyrimidine-deficient bacterium. *Biochim. Biophys. Acta* 30, 12–20. doi: 10.1016/0006-3002(58)90234-8

Bates, D. B., Boye, E., Asai, T., and Kogoma, T. (1997). The absence of effect of gid or mioC transcription on the initiation of chromosomal replication in *Escherichia coli*. *Proc. Natl. Acad. Sci. U.S.A.* 94, 12497–12502. doi: 10.1073/pnas.94.23.12497

Belfort, M., Maley, G., Pedersen-Lane, J., and Maley, F. (1983). Primary structure of the *Escherichia coli* thyA gene and its thymidylate synthase product. *Proc. Natl. Acad. Sci. U.S.A.* 80, 4914–4918. doi: 10.1073/pnas.80.16.4914

Benbrook, D. M., and Miller, R. V. (1986). Effects of norfloxacin on DNA metabolism in *Pseudomonas aeruginosa*. *Antimicrob. Agents Chemother.* 29, 1–6. doi: 10.1128/AAC.29.1.1

Bernstein, J. A., Khodursky, A. B., Lin, P. H., Lin-Chao, S., and Cohen, S. N. (2002). Global analysis of mRNA decay and abundance in *Escherichia coli* at single-gene resolution using two-color fluorescent DNA microarrays. *Proc. Natl. Acad. Sci. U.S.A.* 99, 9697–9702. doi: 10.1073/pnas.112318199

Breitman, T. R., Maury, P. B., and Toal, J. N. (1972). Loss of deoxyribonucleic acid-thymine during thymine starvation of *Escherichia coli*. *J. Bacteriol.* 112, 646–648.

Burton, Z. F., Gross, C. A., Watanabe, K. K., and Burgess, R. R. (1983). The operon that encodes the sigma subunit of RNA polymerase also encodes ribosomal protein S21 and DNA primase in *E. coli* K12. *Cell* 32, 335–349. doi: 10.1016/0092-8674(83)90453-1

Cagliero, C., Zhou, Y. N., and Jin, D. J. (2014). Spatial organization of transcription machinery and its segregation from the replisome in fast-growing bacterial cells. *Nucleic Acids Res.* 42, 13696–13705. doi: 10.1093/nar/gku1103

Casaregola, S., D'ari, R., and Huisman, O. (1982). Role of DNA replication in the induction and turn-off of the SOS response in *Escherichia coli*. *Mol. Gen. Genet.* 185, 440–444. doi: 10.1007/BF00334136

Chandler, M. G., and Pritchard, R. H. (1975). The effect of gene concentration and relative gene dosage on gene output in *Escherichia coli*. *Mol. Gen. Genet.* 138, 127–141. doi: 10.1007/BF02428117

Chiaramello, A. E., and Zyskind, J. W. (1990). Coupling of DNA replication to growth rate in *Escherichia coli*: a possible role for guanosine tetraphosphate. *J. Bacteriol.* 172, 2013–2019.

Cohen, S. S., and Barner, H. D. (1954). Studies on Unbalanced Growth in *Escherichia Coli*. *Proc. Natl. Acad. Sci. U.S.A.* 40, 885–893. doi: 10.1073/pnas.40.10.885

Courcelle, J., Khodursky, A., Peter, B., Brown, P. O., and Hanawalt, P. C. (2001). Comparative gene expression profiles following UV exposure in wild-type and SOS-deficient *Escherichia coli*. *Genetics* 158, 41–64.

Couturier, E., and Rocha, E. P. (2006). Replication-associated gene dosage effects shape the genomes of fast-growing bacteria but only for transcription and translation genes. *Mol. Microbiol.* 59, 1506–1518. doi: 10.1111/j.1365-2958.2006.05046.x

Crooke, E., Hwang, D. S., Skarstad, K., Thony, B., and Kornberg, A. (1991). *E. coli* minichromosome replication: regulation of initiation at *oriC*. *Res. Microbiol.* 142, 127–130. doi: 10.1016/0923-2508(91)90019-7

Denapoli, J., Tehranchi, A. K., and Wang, J. D. (2013). Dose-dependent reduction of replication elongation rate by (p)ppGpp in *Escherichia coli* and *Bacillus subtilis*. *Mol. Microbiol.* 88, 93–104. doi: 10.1111/mmi.12172

Dorman, C. J. (2006). DNA supercoiling and bacterial gene expression. *Sci. Prog.* 89, 151–166. doi: 10.3184/003685006783238317

Eisen, M. B., Spellman, P. T., Brown, P. O., and Botstein, D. (1998). Cluster analysis and display of genome-wide expression patterns. *Proc. Natl. Acad. Sci. U.S.A.* 95, 14863–14868. doi: 10.1073/pnas.95.25.14863

Felipe-Abrio, I., Lafuente-Barquero, J., Garcia-Rubio, M. L., and Aguilera, A. (2014). RNA polymerase II contributes to preventing transcription-mediated replication fork stalls. *EMBO J.* 34, 236–250. doi: 10.15252/embj.201488544

Fonville, N. C., Bates, D., Hastings, P. J., Hanawalt, P. C., and Rosenberg, S. M. (2010). Role of RecA and the SOS response in thymineless death in *Escherichia coli*. *PLoS Genet.* 6:e1000865. doi: 10.1371/journal.pgen.1000865

Freifelder, D. (1969). Single-strand breaks in bacterial DNA associated with thymine starvation. *J. Mol. Biol.* 45, 1–7. doi: 10.1016/0022-2836(69)90205-8

French, S. (1992). Consequences of replication fork movement through transcription units *in vivo*. *Science* 258, 1362–1365. doi: 10.1126/science.1455232

Gallant, J., and Suskind, S. R. (1962). Ribonucleic acid synthesis and thymineless death. *Biochim. Biophys. Acta* 55, 627–638. doi: 10.1016/0006-3002(62)90841-7

Goss, W. A., Deitz, W. H., and Cook, T. M. (1965). Mechanism of action of nalidixic acid on *Escherichia Coli*. ii. inhibition of deoxyribonucleic acid synthesis. *J. Bacteriol.* 89, 1068–1074.

Guarino, E., Salguero, I., Jimenez-Sanchez, A., and Guzman, E. C. (2007). Double-strand break generation under deoxyribonucleotide starvation in *Escherichia coli*. *J. Bacteriol.* 189, 5782–5786. doi: 10.1128/JB.00411-07

Gutierrez-Rios, R. M., Rosenblueth, D. A., Loza, J. A., Huerta, A. M., Glasner, J. D., Blattner, F. R., et al. (2003). Regulatory network of *Escherichia coli*: consistency between literature knowledge and microarray profiles. *Genome Res.* 13, 2435–2443. doi: 10.1101/gr.1387003

Hamann, B. L. (2013). *Elucidating the Mechanism of Thymineless Death in Escherichia coli*. Ph.D. thesis, University of Minnesota, Minnesota.

Hanawalt, P. C. (1963). Involvement of synthesis of RNA in thymineless death. *Nature* 198, 286. doi: 10.1038/198286a0

Hill, W. E., and Fangman, W. L. (1973). Single-strand breaks in deoxyribonucleic acid and viability loss during deoxyribonucleic acid synthesis inhibition in *Escherichia coli*. *J. Bacteriol.* 116, 1329–1335.

Jeong, K. S., Ahn, J., and Khodursky, A. B. (2004). Spatial patterns of transcriptional activity in the chromosome of *Escherichia coli*. *Genome Biol.* 5, R86. doi: 10.1186/gb-2004-5-11-r86

Jeong, K. S., Xie, Y., Hiasa, H., and Khodursky, A. B. (2006). Analysis of pleiotropic transcriptional profiles: a case study of DNA gyrase inhibition. *PLoS Genet.* 2:e152. doi: 10.1371/journal.pgen.0020152

Jin, D. J., Cagliero, C., and Zhou, Y. N. (2012). Growth rate regulation in *Escherichia coli*. *FEMS Microbiol. Rev.* 36, 269–287. doi: 10.1111/j.1574-6976.2011.00279.x

Kaguni, J. M. (2006). DnaA: controlling the initiation of bacterial DNA replication and more. *Annu. Rev. Microbiol.* 60, 351–375. doi: 10.1146/annurev.micro.60.080805.142111

Kavenoff, R., and Bowen, B. C. (1976). Electron microscopy of membrane-free folded chromosomes from *Escherichia coli*. *Chromosoma* 59, 89–101. doi: 10.1007/BF00328479

Kepes, F. (2004). Periodic transcriptional organization of the *E.coli* genome. *J. Mol. Biol.* 340, 957–964. doi: 10.1016/j.jmb.2004.05.039

Khodursky, A. B., Bernstein, J. A., Peter, B. J., Rhodius, V., Wendisch, V. F., and Zimmer, D. P. (2003). *Escherichia coli* spotted double-strand DNA microarrays: RNA extraction, labeling, hybridization, quality control, and data management. *Methods Mol. Biol.* 224, 61–78. doi: 10.1385/1-59259-364-X:61

Khodursky, A. B., and Cozzarelli, N. R. (1998). The mechanism of inhibition of topoisomerase IV by quinolone antibacterials. *J. Biol. Chem.* 273, 27668–27677. doi: 10.1074/jbc.273.42.27668

Khodursky, A. B., Peter, B. J., Cozzarelli, N. R., Botstein, D., Brown, P. O., and Yanofsky, C. (2000a). DNA microarray analysis of gene expression in response to physiological and genetic changes that affect tryptophan metabolism in *Escherichia coli*. *Proc. Natl. Acad. Sci. U.S.A.* 97, 12170–12175. doi: 10.1073/pnas.220414297

Khodursky, A. B., Peter, B. J., Schmid, M. B., Derisi, J., Botstein, D., Brown, P. O., et al. (2000b). Analysis of topoisomerase function in bacterial replication fork movement: use of DNA microarrays. *Proc. Natl. Acad. Sci. U.S.A.* 97, 9419–9424. doi: 10.1073/pnas.97.17.9419

Kowalski, D., and Eddy, M. J. (1989). The DNA unwinding element: a novel, *cis*-acting component that facilitates opening of the *Escherichia coli* replication origin. *EMBO J.* 8, 4335–4344.

Kreuzer, K. N. (2013). DNA damage responses in prokaryotes: regulating gene expression, modulating growth patterns, and manipulating replication forks. *Cold Spring Harb. Perspect. Biol.* 5, a012674. doi: 10.1101/cshperspect.a012674

Kuong, K. J., and Kuzminov, A. (2010). Stalled replication fork repair and misrepair during thymineless death in *Escherichia coli*. *Genes Cells* 15, 619–634. doi: 10.1111/j.1365-2443.2010.01405.x

Kuong, K. J., and Kuzminov, A. (2012). Disintegration of nascent replication bubbles during thymine starvation triggers RecA- and RecBCD-dependent replication origin destruction. *J. Biol. Chem.* 287, 23958–23970. doi: 10.1074/jbc.M112.359687

Lark, K. G. (1972). Evidence for the direct involvement of RNA in the initiation of DNA replication in *Escherichia coli* 15T. *J. Mol. Biol.* 64, 47–60. doi: 10.1016/0022-2836(72)90320-8

Le, T. B., Imakaev, M. V., Mirny, L. A., and Laub, M. T. (2013). High-resolution mapping of the spatial organization of a bacterial chromosome. *Science* 342, 731–734. doi: 10.1126/science.1242059

Levine, A., Vannier, F., Dehbi, M., Henckes, G., and Seror, S. J. (1991). The stringent response blocks DNA replication outside the ori region in *Bacillus subtilis* and at the origin in *Escherichia coli*. *J. Mol. Biol.* 219, 605–613. doi: 10.1016/0022-2836(91)90657-R

Lieberman-Aiden, E., Van Berkum, N. L., Williams, L., Imakaev, M., Ragoczy, T., Telling, A., et al. (2009). Comprehensive mapping of long-range interactions reveals folding principles of the human genome. *Science* 326, 289–293. doi: 10.1126/science.1181369

Liu, B., and Alberts, B. M. (1995). Head-on collision between a DNA replication apparatus and RNA polymerase transcription complex. *Science* 267, 1131–1137. doi: 10.1126/science.7855590

Maaloe, O., and Hanawalt, P. C. (1961). Thymine deficiency and the normal DNA replication cycle. I. *J. Mol. Biol.* 3, 144–155. doi: 10.1016/S0022-2836(61)80041-7

Martin, C. M., Viguera, E., and Guzman, E. C. (2014). Rifampicin suppresses thymineless death by blocking the transcription-dependent step of chromosome initiation. *DNA Repair (Amst)* 18, 10–17. doi: 10.1016/j.dnarep.2014.03.004

McFall, E., and Magasanik, B. (1960). Thymine starvation and enzyme synthesis. *Biochim. Biophys. Acta* 45, 610–612. doi: 10.1016/0006-3002(60)91505-5

Merrikh, H., Machon, C., Grainger, W. H., Grossman, A. D., and Soultanas, P. (2011). Co-directional replication-transcription conflicts lead to replication restart. *Nature* 470, 554–557. doi: 10.1038/nature09758

Merrikh, H., Zhang, Y., Grossman, A. D., and Wang, J. D. (2012). Replication-transcription conflicts in bacteria. *Nat. Rev. Microbiol.* 10, 449–458. doi: 10.1038/nrmicro2800

Messer, W. (1972). Initiation of deoxyribonucleic acid replication in *Escherichia coli* B-r: chronology of events and transcriptional control of initiation. *J. Bacteriol.* 112, 7–12.

Morganroth, P. A., and Hanawalt, P. C. (2006). Role of DNA replication and repair in thymineless death in *Escherichia coli*. *J. Bacteriol.* 188, 5286–5288. doi: 10.1128/JB.00543-06

Nakayama, H., and Hanawalt, P. (1975). Sedimentation analysis of deoxyribonucleic acid from thymine-starved *Escherichia coli*. *J. Bacteriol.* 121, 537–547.

Nakayama, K., Kusano, K., Irino, N., and Nakayama, H. (1994). Thymine starvation-induced structural changes in *Escherichia coli* DNA. Detection by pulsed field gel electrophoresis and evidence for involvement of homologous recombination. *J. Mol. Biol.* 243, 611–620. doi: 10.1016/0022-2836(94)90036-1

Olliver, A., Saggioro, C., Herrick, J., and Sclavi, B. (2010). DnaA-ATP acts as a molecular switch to control levels of ribonucleotide reductase expression in *Escherichia coli*. *Mol. Microbiol.* 76, 1555–1571. doi: 10.1111/j.1365-2958.2010.07185.x

Peter, B. J., Arsuaga, J., Breier, A. M., Khodursky, A. B., Brown, P. O., and Cozzarelli, N. R. (2004). Genomic transcriptional response to loss of chromosomal supercoiling in *Escherichia coli*. *Genome Biol.* 5, R87. doi: 10.1186/gb-2004-5-11-r87

Pettijohn, D. E., and Hecht, R. (1974). RNA molecules bound to the folded bacterial genome stabilize DNA folds and segregate domains of supercoiling. *Cold Spring Harb. Symp. Quant. Biol.* 38, 31–41. doi: 10.1101/SQB.1974.038.01.006

Postow, L., Hardy, C. D., Arsuaga, J., and Cozzarelli, N. R. (2004). Topological domain structure of the *Escherichia coli* chromosome. *Genes Dev.* 18, 1766–1779. doi: 10.1101/gad.1207504

Ramareddy, G., and Reiter, H. (1970). Sequential loss of loci in thymine-starved *Bacillus subtilis* 168 cells. Evidence for a circular chromosome. *J. Mol. Biol.* 50, 525–532. doi: 10.1016/0022-2836(70)90209-3

Regamey, A., Harry, E. J., and Wake, R. G. (2000). Mid-cell Z ring assembly in the absence of entry into the elongation phase of the round of replication in bacteria: co-ordinating chromosome replication with cell division. *Mol. Microbiol.* 38, 423–434. doi: 10.1046/j.1365-2958.2000.02130.x

Reichard, P. (2010). Ribonucleotide reductases: substrate specificity by allostery. *Biochem. Biophys. Res. Commun.* 396, 19–23. doi: 10.1016/j.bbrc.2010.02.108

Reiter, H., and Ramareddy, G. (1970). Loss of DNA behind the growing point of thymine-starved *Bacillus subtilis* 168. *J. Mol. Biol.* 50, 533–548. doi: 10.1016/0022-2836(70)90210-X

Rolfe, R. (1967). On the mechanism of thymineless death in *Bacillus subtilis*. *Proc. Natl. Acad. Sci. U.S.A.* 57, 114–121. doi: 10.1073/pnas.57.1.114

Rovinskiy, N., Agbleke, A. A., Chesnokova, O., Pang, Z., and Higgins, N. P. (2012). Rates of gyrase supercoiling and transcription elongation control supercoil density in a bacterial chromosome. *PLoS Genet.* 8:e1002845. doi: 10.1371/journal.pgen.1002845

Samuel, G., and Reeves, P. (2003). Biosynthesis of O-antigens: genes and pathways involved in nucleotide sugar precursor synthesis and O-antigen assembly. *Carbohydr. Res.* 338, 2503–2519. doi: 10.1016/j.carres.2003.07.009

Sangurdekar, D. P., Hamann, B. L., Smirnov, D., Srienc, F., Hanawalt, P. C., and Khodursky, A. B. (2010). Thymineless death is associated with loss of essential genetic information from the replication origin. *Mol. Microbiol.* 75, 1455–1467. doi: 10.1111/j.1365-2958.2010.07072.x

Sangurdekar, D. P., Srienc, F., and Khodursky, A. B. (2006). A classification based framework for quantitative description of large-scale microarray data. *Genome Biol.* 7, R32. doi: 10.1186/gb-2006-7-4-r32

Sangurdekar, D. P., Zhang, Z., and Khodursky, A. B. (2011). The association of DNA damage response and nucleotide level modulation with the antibacterial mechanism of the anti-folate drug trimethoprim. *BMC Genomics* 12:583. doi: 10.1186/1471-2164-12-583

Schena, M., Shalon, D., Davis, R. W., and Brown, P. O. (1995). Quantitative monitoring of gene expression patterns with a complementary DNA microarray. *Science* 270, 467–470. doi: 10.1126/science.270.5235.467

Schmid, M. B., and Roth, J. R. (1987). Gene location affects expression level in *Salmonella typhimurium*. *J. Bacteriol.* 169, 2872–2875.

Simmons, L. A., Foti, J. J., Cohen, S. E., and Walker, G. C. (2008). The SOS regulatory network. *Ecosal Plus* 2008, 1–48. doi: 10.1128/ecosalplus.5.4.3

Slager, J., Kjos, M., Attaiech, L., and Veening, J. W. (2014). Antibiotic-induced replication stress triggers bacterial competence by increasing gene dosage near the origin. *Cell* 157, 395–406. doi: 10.1016/j.cell.2014.01.068

Sobetzko, P., Travers, A., and Muskhelishvili, G. (2012). Gene order and chromosome dynamics coordinate spatiotemporal gene expression during the bacterial growth cycle. *Proc. Natl. Acad. Sci. U.S.A.* 109, E42–E50. doi: 10.1073/pnas.1108229109

Sueoka, N., and Yoshikawa, H. (1965). The chromosome of *Bacillus subtilis*. I. Theory of marker frequency analysis. *Genetics* 52, 747–757.

Tamayo, P., Slonim, D., Mesirov, J., Zhu, Q., Kitareewan, S., Dmitrovsky, E., et al. (1999). Interpreting patterns of gene expression with self-organizing maps: methods and application to hematopoietic differentiation. *Proc. Natl. Acad. Sci. U.S.A.* 96, 2907–2912. doi: 10.1073/pnas.96.6.2907

Torrence, C., and Compo, G. (1998). A practical guide to wavelet analysis. *Bull. Amer. Met. Soc.* 79, 61–78. doi: 10.1175/1520-0477(1998)079<0061:APGTWA>2.0.CO;2

van Helden, J., Andre, B., and Collado-Vides, J. (1998). Extracting regulatory sites from the upstream region of yeast genes by computational analysis of oligonucleotide frequencies. *J. Mol. Biol.* 281, 827–842. doi: 10.1006/jmbi.1998.1947

Versalovic, J., Koeuth, T., Britton, R., Geszvain, K., and Lupski, J. R. (1993). Conservation and evolution of the rpsU-dnaG-rpoD macromolecular synthesis operon in bacteria. *Mol. Microbiol.* 8, 343–355. doi: 10.1111/j.1365-2958.1993.tb01578.x

von Freiesleben, U., and Rasmussen, K. V. (1992). The level of supercoiling affects the regulation of DNA replication in *Escherichia coli*. *Res. Microbiol.* 143, 655–663. doi: 10.1016/0923-2508(92)90060-2

Xiao, G., Wang, X., and Khodursky, A. B. (2011). Modeling three-dimensional chromosome structures using gene expression data. *J. Am. Stat. Assoc.* 106, 61–72. doi: 10.1198/jasa.2010.ap09504

Yoshinaga, K. (1973). Double-strand scission of DNA involved in thymineless death of *Escherichia coli* 15 TAU. *Biochim. Biophys. Acta* 294, 204–213. doi: 10.1016/0005-2787(73)90293-1

Conflict of Interest Statement: The authors declare that the research was conducted in the absence of any commercial or financial relationships that could be construed as a potential conflict of interest.

Copyright © 2015 Ostrer, Hamann and Khodursky. This is an open-access article distributed under the terms of the Creative Commons Attribution License (CC BY). The use, distribution or reproduction in other forums is permitted, provided the original author(s) or licensor are credited and that the original publication in this journal is cited, in accordance with accepted academic practice. No use, distribution or reproduction is permitted which does not comply with these terms.

frontiers in Microbiology

REVIEW
published: 26 May 2015
doi: 10.3389/fmicb.2015.00514

Light-dependent governance of cell shape dimensions in cyanobacteria

Beronda L. Montgomery [1,2]*

[1] Department of Energy-Plant Research Laboratory, Michigan State University, East Lansing, MI, USA, [2] Department of Biochemistry and Molecular Biology, Michigan State University, East Lansing, MI, USA

The regulation of cellular dimension is important for the function and survival of cells. Cellular dimensions, such as size and shape, are regulated throughout the life cycle of bacteria and can be adapted in response to environmental changes to fine-tune cellular fitness. Cell size and shape are generally coordinated with cell growth and division. Cytoskeletal regulation of cell shape and cell wall biosynthesis and/or deposition occurs in a range of organisms. Photosynthetic organisms, such as cyanobacteria, particularly exhibit light-dependent regulation of morphogenes and generation of reactive oxygen species and other signals that can impact cellular dimensions. Environmental signals initiate adjustments of cellular dimensions, which may be vitally important for optimizing resource acquisition and utilization or for coupling the cellular dimensions with the regulation of subcellular organization to maintain optimal metabolism. Although the involvement of cytoskeletal components in the regulation of cell shape is widely accepted, the signaling factors that regulate cytoskeletal and other distinct components involved in cell shape control, particularly in response to changes in external light cues, remain to be fully elucidated. In this review, factors impacting the inter-coordination of growth and division, the relationship between the regulation of cellular dimensions and central carbon metabolism, and consideration of the effects of specific environment signals, primarily light, on cell dimensions in cyanobacteria will be discussed. Current knowledge about the molecular bases of the light-dependent regulation of cellular dimensions and cell shape in cyanobacteria will be highlighted.

Keywords: cell division, cellular morphology, cyanobacteria, morphogenes, photomorphogenesis

OPEN ACCESS

Edited by:
Arieh Zaritsky, Ben-Gurion University of the Negev, Israel

Reviewed by:
Patrick Hallenbeck, University of Montreal, Canada
Lydia Robert, Institut National de la Recherche Agronomique, France

***Correspondence:**
Beronda L. Montgomery, Department of Energy-Plant Research Laboratory, Michigan State University, 612 Wilson Road, Room 106, East Lansing, MI 48824-1312, USA
montg133@msu.edu

Specialty section:
This article was submitted to Microbial Physiology and Metabolism, a section of the journal Frontiers in Microbiology

Received: *07 March 2015*
Accepted: *09 May 2015*
Published: *26 May 2015*

Citation:
Montgomery BL (2015) Light-dependent governance of cell shape dimensions in cyanobacteria. Front. Microbiol. 6:514. doi: 10.3389/fmicb.2015.00514

Introduction

Cyanobacteria and other photosynthetic organisms, which have limited mobility in their environment, are exquisitely sensitive to changes in environmental conditions. Cues that impact growth, development, and metabolism of these organisms include light, nutrients, and other factors such as inter-organismal interactions, including predation. As photosynthetic organisms depend upon light for driving energy-producing photosynthesis, these organisms are finely tuned to perceive changes in the photoenvironment. Properties of light that impact organismal form and function include light quality or prevalent wavelengths (visible and ultraviolet or UV), light intensity, daily cycles of dark/light cues, and interactions of light with other factors such as the availability of nutrients.

Light can positively promote organismal development; however, in excess it can also induce light-associated damage or phototoxicity, particularly in photosynthetic organisms (reviewed by Busch and Montgomery, 2015). Thus, changes in growth, development, or metabolism in response to light can be photomorphogenic or photoprotective in nature. Morphological changes can be linked to

the optimization of the utilization of resources to support growth and development in bacterial generally (Young, 2006, 2007). A role for light in regulating cell shape or morphology occurs across many organisms, including prokaryotes (Bennett and Bogorad, 1973; Bordowitz and Montgomery, 2008; Singh and Montgomery, 2011) and eukaryotes (Daniel and Rusch, 1962; Desnos et al., 1996; Gendreau et al., 1997; Marwan, 2001; Nishihama et al., 2015). The specific mechanisms by which light impacts morphology have not been vastly studied; however, in some cases photomorphogenesis is linked to the regulation of cytoskeleton proteins (Putzer et al., 1984; Poetsch et al., 1989; Kadota and Wada, 1992; Dyachok et al., 2011; Lindeboom et al., 2013; Singh and Montgomery, 2014). Notably, the regulation of cell shape is correlated with cytoskeletal components and/or function across a range of organisms (Smith, 2003; Mathur, 2004; Cabeen and Jacobs-Wagner, 2005, 2007; Stewart, 2005; Carballido-López, 2006; Osborn and Rothfield, 2007; Terenna et al., 2008; Margolin, 2009; Ueki and Nishii, 2009).

Changes in cyanobacterial shape specifically can be directly linked to growth and/or development—light-dependent changes in vegetative cell shape (Bennett and Bogorad, 1973) or cellular differentiation, e.g., nitrogen fixation-associated development of heterocysts (Kumar et al., 2010), spore-like akinete formation for surviving harsh or stressful environments (Rippka et al., 1979; Flores and Herrero, 2010; Kaplan-Levy et al., 2010), or motility-associated hormogonium induction (Rippka et al., 1979; Meeks and Elhai, 2002; Wong and Meeks, 2002; Adams and Duggan, 2008). These developmentally induced changes in cellular morphology can be tuned by environmental cues, which include light and/or nutrient availability (Singh and Montgomery, 2011; Vadia and Levin, 2015). Stress-induced changes in cellular morphology also occur frequently in bacterial cells. UV, temperature, salt, osmotic, and biotic stresses have known impacts on the morphology of cyanobacterial cells (reviewed Singh and Montgomery, 2011). Knowledge about the mechanisms by which developmental- or stress-related cues result in morphological changes has only recently begun to emerge. Such mechanisms include light-and photoreceptor-dependent regulation of morphogene expression and cytoskeletal protein accumulation (Pattanaik and Montgomery, 2010; Singh and Montgomery, 2014), regulation of reactive oxygen species (ROS) levels that are associated with morphological determination (Singh and Montgomery, 2012; Singh et al., 2013) and light-driven changes in second messenger homeostasis that have the potential to modulate cell shape or dimensions (Neunuebel and Golden, 2008; Agostoni and Montgomery, 2014). Also noted are nutrient-associated, cell division-related cues (Goclaw-Binder et al., 2012; Osanai et al., 2013), among others.

Light-Modulated Regulators Drive Adaptation of Cellular Morphology in Cyanobacteria

Light quality- or wavelength-dependent changes in physiology and development occur in some cyanobacteria (Bennett and Bogorad, 1973; Bordowitz and Montgomery, 2008). The well-studied, freshwater filamentous cyanobacerium *Fremyella diplosiphon* exhibits an acclimatory phenomenon, which is historically known as complementary chromatic adaptation or CCA, during which the photosynthetic pigment content is tuned to the external environment (Bennett and Bogorad, 1973; Tandeau de Marsac, 1991). The organism accumulates red-colored, green wavelength-absorbing pigment phycoerythrin (PE) in green-enriched environments, and conversely blue-green-colored, red wavelength-absorbing pigment phycocyanin (PC) in red-enriched environments (Gutu and Kehoe, 2012). The PE and PC pigments are contained in peripheral light-harvesting complexes called phycobilisomes (PBS). The PBS antennae are associated with the thylakoid membranes generally found at the periphery of cyanobacterial cells (**Figure 1**). As the availability of red vs. green wavelengths vary significantly at difference depths in a water column, CCA-dependent tuning of photosynthetic pigmentation is linked to environmental adaptation and tuning of photosynthetic efficiency in natural contexts (Campbell, 1996; Postius et al., 2001). This process is regulated by a soluble, light-absorbing photoreceptor known as RcaE in *F. diplosiphon* (Kehoe and Grossman, 1996). As a part of CCA, there are noted changes in cellular morphology, in addition to pigmentation. Spherical cells and shorter filaments are characteristic of growth under red light (RL), whereas rectangular cells and long filaments are associated with growth under green light (GL; Bennett and Bogorad, 1973; Bordowitz and Montgomery, 2008). RcaE is the regulator for cell shape and filament morphology changes, in addition to its previously mentioned role in fine-tuning photosynthetic pigment levels in *F. diplosiphon* (Bordowitz and Montgomery, 2008). RcaE mutant cells exhibit a rounded cell shape independent of the external light conditions, in contrast to the light-regulated switch between spherical- and rod-shaped cells observed for wild-type (Bennett and Bogorad, 1973; Bordowitz and Montgomery, 2008).

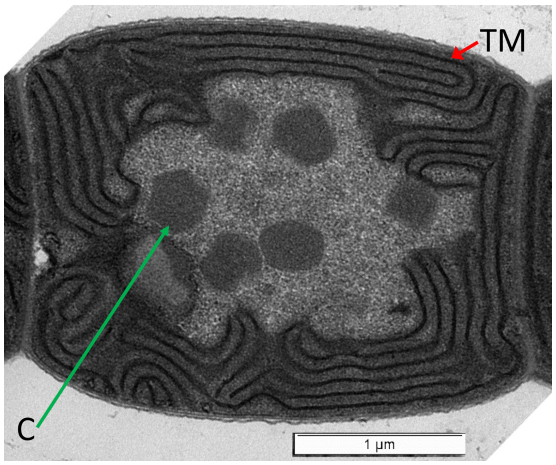

FIGURE 1 | Transmission electron micrograph of wild-type *Fremyella diplosiphon* cell grown in BG-11 medium. Thylakoid membranes (TM; red arrow) are at the periphery of the cell. Carboxysomes (C; green arrow) are found in the center cytoplasmic region of the cell. Bar is 1 micrometer.

Apart from RcaE which is linked to the regulation of pigmentation and morphology in *F. diplosiphon*, another regulator cpeR has also been linked to the regulation of both pigmentation and morphology in this organism (Pattanaik et al., 2011b). CpeR

induces synthesis of the photosynthetic pigment PE in GL (Cobley et al., 2002; Seib and Kehoe, 2002; Alvey et al., 2003). However, it was also shown that a Δ*cpeR* mutant in *F. diplosiphon* exhibits an altered cellular morphology compared to wild-type cells (Pattanaik et al., 2011b). Thus, the CpeR regulator, which appears to serve as a transcriptional activator for PE genes (Cobley et al., 2002), also likely controls genes important for photoregulation of cellular morphology. Notably, many other pigment mutants isolated in *F. diplosiphon* impact pigmentation of cells with no measurable impact on cellular morphology (Whitaker et al., 2009, 2011; Bordowitz et al., 2010; Pattanaik et al., 2011a,b).

Light intensity has been shown to impact cellular morphology in cyanobacteria (Bittencourt-Oliveira et al., 2012; Pattanaik et al., 2012; Walters et al., 2013). *Cylindrospermopsis raciborskii* exhibits trichome elongation under reduced light intensity (Bittencourt-Oliveira et al., 2012). In *F. diplosiphon*, lower intensity light results in elongated cells, whereas light of increased intensity results in cells which are more spherical and with reduced length (Pattanaik et al., 2012; Walters et al., 2013). In natural environmental contexts, elongated *F. diplosiphon* cells are prevalent in low light intensities, whereas spherical cells exist in higher intensity regions of the water column (Montgomery, 2008). Thus, it was proposed that cells may regulate cellular morphology in natural contexts under different light intensities to control cellular volume and associated capacity for total photosynthetic membrane content that is correlated with regulation of cellular photosynthetic capacity (Montgomery, 2008; Pattanaik et al., 2012; Walters et al., 2013). As related photoreceptors serve as potent light quality and intensity sensors (e.g., Reed et al., 1994; Rausenberger et al., 2010), it is proposed that RcaE serves as a mediator of light intensity-dependent regulation of morphology in *F. diplosiphon*.

Visible and UV light exposure can result in trichome spiral compression in *Arthrospira platensis* (Wu et al., 2005; Ma and Gao, 2009). The mechanism of this morphological regulation has been implicated as a periplasmic protein of undetermined function (Ma and Gao, 2009). Spiral compression in this organism may serve a role in self-shading that can protect cells against damaging UV exposure (Wu et al., 2005). Thus, the smaller, compressed state under UV has been correlated with reduced surface area that has been hypothesized to serve as a photoprotective state associated with the maintenance of photosynthetic capacity (Singh and Montgomery, 2011). Relatedly, trichome breakage or filament fragmentation under UV light also occurs in *A. platensis* and other cyanobacteria (Gao et al., 2007; Ma and Gao, 2010; Rastogi et al., 2010, 2014). Similar to trichome compression, these responses may be associated with reduced surface area potentially exposed to UV and a potential reduction in UV-associated damage.

Light-Dependent Regulation of Morphogenes is One Mechanism for Regulating Cellular Morphology in Cyanobacteria

Although distinct links between environmental signals and modulation of cellular morphology are clear in cyanobacteria (Singh and Montgomery, 2011), knowledge about the mechanisms by which these changes are mediated is limited. TonB is important for regulating GL-dependent cellular morphology in *F. diplosiphon* (Pattanaik and Montgomery, 2010). Although its exact biochemical function has not been elucidated, the protein has sequence similarity to both iron-associated TonB proteins and a glycine-rich region related to domains in proteins involved in cellular elongation (Sachetto-Martins et al., 2000; Pattanaik and Montgomery, 2010). However, the GL-associated disruption in photoregulation of morphology in a Δ*tonB* mutant in *F. diplosiphon* was shown to be independent of responses to iron limitation (Pattanaik and Montgomery, 2010). This observation, thus, suggests a more direct role for TonB in modulating cell shape in response to GL in this organism.

Recently, photoregulation of morphogenes has emerged as a key mechanism for tuning cellular morphology to light cues in cyanobacteria (Singh and Montgomery, 2014). Morphogene function in the regulation of cellular morphology generally is well known. The bacterial actin MreB is associated with rod-shaped bacteria, and is nearly always absent in spherical bacterial cells (reviewed by Cabeen and Jacobs-Wagner, 2007). MreB has functional homologs in cyanobacteria, both filamentous (Hu et al., 2007; González et al., 2010; Singh and Montgomery, 2014) and unicellular (Koksharova et al., 2007; Savage et al., 2010; Singh and Montgomery, unpublished data), which are associated with rod-shaped cells. Mutation of *mreB* in cyanobacterial systems leads to a loss of shape regulation, thus resulting in the adoption of spherical cells in Δ*mreB* mutants (Hu et al., 2007; Savage et al., 2010). In *F. diplosiphon*, in which rod-shaped cells are prevalent under GL, it appears that photoregulation of *mreB* expression corresponds to the induction of rod-shaped morphology (Singh and Montgomery, 2014).

A well-characterized regulator of MreB is the morphogene BolA (Aldea et al., 1989; Santos et al., 1999). Accumulation of BolA is associated with a spherical cell shape, and imparts this morphology in part through transcriptional downregulation of *mreB* (Aldea et al., 1988, 1989; Santos et al., 1999; Freire et al., 2009). In the first reported functional characterization of a cyanobacterial BolA protein, we recently showed that photoregulation of *bolA* expression in *F. diplosiphon* is correlated with RL-dependent BolA accumulation that is associated with spherical morphology (Singh and Montgomery, 2014). Similar to *E. coli* BolA (Freire et al., 2009), BolA from *F. diplosiphon* binds the promotor of *mreB* to maintain low levels of *mreB* expression in RL (Singh and Montgomery, 2014). Lower levels of BolA are found in GL which are correlated with derepression of *mreB* expression, thereby resulting in the induction of a rod-shaped morphology in *F. diplosiphon* under these conditions (Singh and Montgomery, 2014).

Additional Signals that Impact Cyanobacterial Morphology or Cellular Dimensions—ROS, Second Messengers, and Cell Cycle Factors

Additional factors apart from morphogenes have been correlated with the regulation of cellular morphology in response to

environmental cues in cyanobacteria. Some factors induced by environmental cues, including light, that impact cellular dimensions include reactive oxygen species (ROS), second messengers, and cell cycle or division cues.

ROS as a Signal that Impacts Cellular Morphology of Cyanobacteria

Reactive oxygen species are potent cues that can arise from photooxidative stress. When light absorption by the photosynthetic light-harvesting complexes exceeds the need for carbon fixation or the capacity of the photosynthetic electron transfer chains, absorbed light energy can be transferred to other targets resulting in production of ROS (reviewed by Busch and Montgomery, 2015). Generated ROS can then result in cellular photodamage and/or ROS molecules can serve as signals that impact cellular function or development (Busch and Montgomery, 2015). In cyanobacteria, light-generated ROS have been associated with the adoption of particular cellular morphologies. In *F. diplosiphon*, ROS levels are elevated in RL and this light-induced ROS accumulation is associated with spherical morphology (Singh and Montgomery, 2012; Singh et al., 2013). ROS levels are lower in GL and associated with rod-shaped *F. diplosiphon* cells (Singh and Montgomery, 2012; Singh et al., 2013). ROS specifically appear to be the signal impacting morphological adaptation as treatment of cells grown in RL with ROS-scavenging antioxidants reverses the ROS-associated impacts on cellular dimensions (Singh and Montgomery, 2012). In addition to the impact of ROS on cellular morphology, filament length is regulated by photoregulation of ROS. RL-associated elevated ROS accumulation is correlated with shorter filaments, presumably due to filament fragmentation (Singh and Montgomery, 2012). Notably, the RL vs. GL effects on ROS levels are regulated by the RL-responsive RcaE photoreceptor (Singh and Montgomery, 2012), a photoreceptor which regulates pigmentation and the photoregulation of morphology as described above (Kehoe and Grossman, 1996; Bordowitz and Montgomery, 2008). ROS levels are also elevated when light intensity is increased, which also is associated with the induction of a spherical cellular morphology (Walters et al., 2013). ROS have been associated with the regulation of cellular morphology in other systems, including non-photosynthetic organisms such as *Aspergillus nidulans* (Semighini and Harris, 2008) and specific phenotypes such as pollen germination and development, root elongation and cell expansion in plants (Foreman et al., 2003; Carol and Dolan, 2006; Li et al., 2007; Potocký et al., 2007; Müller et al., 2009; Speranza et al., 2012). One function of ROS in this regard is in cell wall loosening (Müller et al., 2009), potentially due to lipid peroxidation (He and Häder, 2002). This ROS-dependent impact could be linked to observed changes in cellular morphology.

The role of UV irradiation in spiral breakage or filament fragmentation in cyanobacteria has been associated with ROS formation (Ma and Gao, 2010; Rastogi et al., 2010, 2014). The accumulation of ROS has been implicated in the induction of lipid oxidation, which ultimately is hypothesized to lead to cellular damage and/or lysis (Ma and Gao, 2010; Rastogi et al., 2010). Thus, as in other systems, ROS molecules have the potential to serve as signaling molecules as proposed for the regulation of cellular morphology in *F. diplosiphon* or as molecules that cause potential damage such as cellular lysis (Busch and Montgomery, 2015). Ultimately, however, the morphology changes and/or filament fragmentation may be associated with improved fitness of strains in some cases. Early experiments with cyanobacteria demonstrated that targeted cell lysis at specialized cells along a filament can result in fragmentation or breakage of filaments into shorter filaments (Lamont, 1969; Bennett and Bogorad, 1973). Such filament fragmentation due to targeted cell lysis during the transition of *F. diplosiphon* cultures to RL was proposed to facilitate a reduction in the content of phycobiliproteins in the culture that are not optimal for growth in RL (Bennett and Bogorad, 1973). This morphological adaptation, thus, is associated with temporal tuning of the pigment content of the organism to the external light environment, which has been associated with optimizing photosynthetic efficiency (Campbell, 1996). Additionally, filament length regulation has been associated with fitness implications in a heterocyst-forming cyanobacterium, whereby the ability to restrict filament length under nitrogen-fixing conditions is associated with improved survival of *Anabaena* sp. strain PCC 7120 (Merino-Puerto et al., 2013).

Second Messengers are Correlated with the Regulation of Cyanobacterial Cell Shape

Second messengers serve as key signaling molecules used in cellular responses to external (or first messenger) cues. These molecules can be rapidly turned over in an energetically conservative manner to facilitate rapid changes in response to environmental fluctuations. Cyanobacteria contain a wide range of second messengers (Agostoni and Montgomery, 2014). Calcium is a ubiquitous second messenger utilized in response to a number of environmental cues that has been implicated in several cyanobacterial responses, including heterocyst development and homorgonia differentiation (reviewed by Agostoni and Montgomery, 2014). The second messengers guanosine pentaphosphate or tetraphosphate [(p)ppGpp] and cyclic AMP (cAMP) have been implicated specifically as mediators of cellular differentiation during cellular responses to nutrient availability (reviewed by Agostoni and Montgomery, 2014). Cyclic dimeric guanosine 3′,5′-monophosphate, i.e., c-di-GMP, presumably contributes to cell shape maintenance and cellular development in the filamentous cyanobacterium *Anaebaena* sp. PCC 7120 as deletion of putative c-di-GMP synthesis enzyme-encoding gene *all2874* results in reduced heterocyst development and smaller vegetative cells under high light intensity (Neunuebel and Golden, 2008). Notably, cAMP (Ohmori et al., 1988, 2002; Ohmori and Okamoto, 2004; Okamoto et al., 2004; Terauchi and Ohmori, 2004) and c-di-GMP (Agostoni et al., 2013) levels are controlled by light in cyanobacteria. As many of these molecules have only recently begun to be the focus of studies in cyanobacteria (Agostoni and Montgomery, 2014), many additional second messenger-regulated responses are expected to emerge.

Coordination of Cell Cycle, Cell Division, and Central Carbon Metabolism with Cell Dimensions

Cellular dimensions are largely heritable across a range of organisms, including prokaryotes and eukaryotes (Zaritsky, 1975;

Fantes, 1977; Koch, 1996; Chien et al., 2012; Marshall et al., 2012; Turner et al., 2012; Lloyd, 2013; Campos et al., 2014). Cell size control is a core feature of the bacterial cell cycle under defined growth conditions (Campos et al., 2014). Bacterial cell size homeostasis appears to be regulated by reproducible and constant cell size extension (Campos et al., 2014; Soifer et al., 2014; Taheri-Araghi et al., 2015). Coordination of cell growth or elongation and division during the cell cycle maintains and/or regulates cell size in bacteria, and can be impacted by nutrient availability or central metabolism (Weart et al., 2007; Siegal-Gaskins and Crosson, 2008; Chien et al., 2012; Yao et al., 2012; Hill et al., 2013; Robert et al., 2014).

Cell division and elongation in cyanobacteria have also been correlated (Koksharova and Wolk, 2002; Mazouni et al., 2004; Miyagishima et al., 2005; Marbouty et al., 2009; Gorelova et al., 2013). Although disruptions in cell division can result in elongated or filamentous cells, in some cases, the reversion of the impairment in cell division results in the restoration of the original cellular dimensions, providing evidence for the recognized strong regulation over cell size (Goclaw-Binder et al., 2012). Environmental cues such as nutrient availability can impact cell division and thereby impact cellular morphology in cyanobacteria (Goclaw-Binder et al., 2012), as described above for other bacterial systems.

An impact of central carbon metabolism on the cell cycle can affect cell size (reviewed by Vadia and Levin, 2015). While definitive experiments linking central carbon metabolism with cell size in cyanobacteria lag behind assessment in other systems, interesting phenomena have been reported. Cell division regulation that is associated with alterations in cell size has been shown to be impacted by sugar metabolism in *Synechocystis* (Osanai et al., 2013). This observed phenotype is driven by overexpression of a sigma factor gene, i.e., *sigE*, which impacts gene expression through interacting with the RNA polymerase (Osanai et al., 2013).

Carbon-Concentrating Mechanism and Correlations with Cell Shape

In cyanobacteria, carboxysomes are subcellular microcompartments centrally located in the cytoplasm of cells (**Figure 1**) and which are associated with the carbon-concentrating mechanism (CCM) and carbon fixation in cyanobacteria (Rae et al., 2013). In some studies, changes in carboxysome quantity and carboxysomal structural defects are apparent in elongated cell division mutants lacking *ftn2* and *ftn6* (Gorelova et al., 2013). Additionally, a disruption of apposite spatial distribution of carboxysomes in a mutant with cytoskeleton-associated defects in cellular morphology has been observed (Savage et al., 2010). Such observations suggest interactions between cellular shape and/or division with the spatial organization of carboxysomes central to carbon metabolism.

The CCM can also include alterations to inorganic carbon (Ci) uptake or active transport. Low Ci levels result in a reduced trichome size in *Arthrospira platensis* (Ma and Gao, 2014). This reduction of trichome size is hypothesized to increase the surface area to cellular volume ratio. Such a response may serve in part to sustain photochemical efficiency and reduce potential damage under high light conditions, which are associated with an increased CCM (Beardall, 1991; Qiu and Liu, 2004).

Conclusion

Cyanobacteria and other cells can alter cellular dimensions and/or shape in response to environmental cues. In some cases this morphological adaptation is linked to the production of cells tuned to the external environment to increase fitness. In other cases, the fitness implications of the energy-requiring morphological adaptations are less clear or only beginning to emerge. For example, *F. diplosiphon* can alter cellular morphology in response to wavelength- or intensity-dependent cues that appear to be correlated with regulating cellular capacity for photosynthetic protein accumulation, which is linked to tuning the capacity of photosynthetic efficiency and associated carbon metabolism to external cues. Other cyanobacteria can alter trichome spiral length and/or filament morphology to reduce surface area exposed to potential damaging light, such as UV or high intensity light. Cells such as *A. platensis* and *C. raciborskii* can alter trichome size in response to cues such as light intensity and Ci availability, presumably to limit damage and alter surface to volume ratios that may alter resource acquisition to sustain photosynthesis. Additional analyses of the mechanisms by which morphological changes are regulated and the potential fitness costs and/or benefits may result in targets for engineering cyanobacterial strains for use in biotechnological applications, in addition to providing greater insight into the roles of these adaptations in natural contexts.

Acknowledgments

Work in the author's laboratory on the impacts of light on growth and development of cyanobacteria is supported by the National Science Foundation (grant no. MCB-1243983 to BM), whereas work on adapting cyanobacterial cultures for biotechnological applications is supported by the U.S. Department of Energy, Chemical Sciences, Geosciences and Biosciences Division, Office of Basic Energy Sciences, Office of Science (grant no. DE-FG02-91ER20021 to BL). I would like to thank Dr. Bagmi Pattanaik for obtaining the transmission electron micrograph of *Fremyella diplosiphon*.

References

Adams, D. G., and Duggan, P. S. (2008). Cyanobacteria–bryophyte symbioses. *J. Exp. Bot.* 59, 1047–1058. doi: 10.1093/jxb/ern005

Agostoni, M., Koestler, B. J., Waters, C. M., Williams, B. L., and Montgomery, B. L. (2013). Occurrence of cyclic di-GMP-modulating output domains in cyanobacteria: an illuminating perspective. *mBio* 4, e00451-00413. doi: 10.1128/mBio.00451-13

Agostoni, M., and Montgomery, B. (2014). Survival strategies in the aquatic and terrestrial world: the impact of second messengers on cyanobacterial processes. *Life* 4, 745–769. doi: 10.3390/life4040745

Aldea, M., Garrido, T., Hernandez-Chico, C., Vicente, M., and Kushner, S. (1989). Induction of a growth-phase-dependent promoter triggers transcription of bolA, an *Escherichia coli* morphogene. *EMBO J.* 8, 3923–3931.

Aldea, M., Hernández-Chico, C., De La Campa, A. G., Kushner, S. R., and Vicente, M. (1988). Identification, cloning, and expression of bolA, an

ftsZ-dependent morphogene of *Escherichia coli*. *J. Bacteriol.* 170, 5169–5176.

Alvey, R. M., Karty, J. A., Roos, E., Reilly, J. P., and Kehoe, D. M. (2003). Lesions in phycoerythrin chromophore biosynthesis in *Fremyella diplosiphon* reveal coordinated light regulation of apoprotein and pigment biosynthetic enzyme gene expression. *Plant Cell* 15, 2448–2463. doi: 10.1105/tpc.015016

Beardall, J. (1991). Effects of photon flux density on the 'CO_2-concentrating mechanism' of the cyanobacterium *Anabaena variabilis*. *J. Plankton Res.* 13, 133–141.

Bennett, A., and Bogorad, L. (1973). Complementary chromatic adaptation in a filamentous blue-green alga. *J. Cell Biol.* 58, 419–435.

Bittencourt-Oliveira, M., Buch, B., Hereman, T., Arruda-Neto, J., Moura, A., and Zocchi, S. (2012). Effects of light intensity and temperature on *Cylindrospermopsis raciborskii* (cyanobacteria) with straight and coiled trichomes: growth rate and morphology. *Braz. J. Biol.* 72, 343–351. doi: 10.1590/S1519-69842012000200016

Bordowitz, J. R., and Montgomery, B. L. (2008). Photoregulation of cellular morphology during complementary chromatic adaptation requires sensor-kinase-class protein RcaE in *Fremyella diplosiphon*. *J. Bacteriol.* 190, 4069–4074. doi: 10.1128/jb.00018-08

Bordowitz, J. R., Whitaker, M. J., and Montgomery, B. L. (2010). Independence and interdependence of the photoregulation of pigmentation and development in *Fremyella diplosiphon*. *Commun. Integr. Biol.* 3, 151–153. doi: 10.4161/cib.3.2.10367

Busch, A. W. U., and Montgomery, B. L. (2015). Interdependence of tetrapyrrole metabolism, the generation of oxidative stress and the mitigative oxidative stress response. *Redox Biol.* 4, 260–271. doi: 10.1016/j.redox.2015.01.010

Cabeen, M. T., and Jacobs-Wagner, C. (2005). Bacterial cell shape. *Nat. Rev. Microbiol.* 3, 601–610. doi: 10.1038/nrmicro1205

Cabeen, M. T., and Jacobs-Wagner, C. (2007). Skin and bones: the bacterial cytoskeleton, cell wall, and cell morphogenesis. *J. Cell Biol.* 179, 381–387. doi: 10.1083/jcb.200708001

Campbell, D. (1996). Complementary chromatic adaptation alters photosynthetic strategies in the cyanobacterium Calothrix. *Microbiology* 142, 1255–1263.

Campos, M., Surovtsev, I. V., Kato, S., Paintdakhi, A., Beltran, B., Ebmeier, S. E., et al. (2014). A constant size extension drives bacterial cell size homeostasis. *Cell* 159, 1433–1446. doi: 10.1016/j.cell.2014.11.022

Carballido-López, R. (2006). Orchestrating bacterial cell morphogenesis. *Mol. Microbiol.* 60, 815–819. doi: 10.1111/j.1365-2958.2006.05161.x

Carol, R. J., and Dolan, L. (2006). The role of reactive oxygen species in cell growth: lessons from root hairs. *J. Exp. Bot.* 57, 1829–1834. doi: 10.1093/jxb/erj201

Chien, A.-C., Hill, N. S., and Levin, P. A. (2012). Cell size control in bacteria. *Curr. Biol.* 22, R340–R349. doi: 10.1016/j.cub.2012.02.032

Cobley, J. G., Clark, A. C., Weerasurya, S., Queseda, F. A., Xiao, J. Y., Bandrapali, N., et al. (2002). CpeR is an activator required for expression of the phycoerythrin operon (cpeBA) in the cyanobacterium *Fremyella diplosiphon* and is encoded in the phycoerythrin linker-polypeptide operon (cpeCDESTR). *Mol. Microbiol.* 44, 1517–1531. doi: 10.1046/j.1365-2958.2002.02966.x

Daniel, J. W., and Rusch, H. P. (1962). Method for inducing sporulation of pure cultures of the myxocmycete *Physarum polycephalum*. *J. Bacteriol.* 83, 234–240.

Desnos, T., Orbović, V., Bellini, C., Kronenberger, J., Caboche, M., Traas, J., et al. (1996). Procuste1 mutants identify two distinct genetic pathways controlling hypocotyl cell elongation, respectively in dark- and light-grown *Arabidopsis* seedlings. *Development* 122, 683–693.

Dyachok, J., Zhu, L., Liao, F., He, J., Huq, E., and Blancaflor, E. B. (2011). SCAR mediates light-induced root elongation in *Arabidopsis* through photoreceptors and proteasomes. *Plant Cell* 23, 3610–3626. doi: 10.1105/tpc.111.088823

Fantes, P. A. (1977). Control of cell size and cycle time in *Schizosaccharomyces pombe*. *J. Cell Sci.* 24, 51–67.

Flores, E., and Herrero, A. (2010). Compartmentalized function through cell differentiation in filamentous cyanobacteria. *Nat. Rev. Microbiol.* 8, 39–50. doi: 10.1038/nrmicro2242

Foreman, J., Demidchik, V., Bothwell, J. H. F., Mylona, P., Miedema, H., Torres, M. A., et al. (2003). Reactive oxygen species produced by NADPH oxidase regulate plant cell growth. *Nature* 422, 442–446. doi: 10.1038/nature01485

Freire, P., Moreira, R. N., and Arraiano, C. M. (2009). BolA inhibits cell elongation and regulates MreB expression levels. *J. Mol. Biol.* 385, 1345–1351. doi: 10.1016/j.jmb.2008.12.026

Gao, K., Yu, H., and Brown, M. T. (2007). Solar PAR and UV radiation affects the physiology and morphology of the cyanobacterium *Anabaena* sp. *PCC* 7120. *J. Photochem. Photobiol.* B 89, 117–124. doi: 10.1016/j.jphotobiol.2007.09.006

Gendreau, E., Traas, J., Desnos, T., Grandjean, O., Caboche, M., and Höfte, H. (1997). Cellular basis of hypocotyl growth in *Arabidopsis thaliana*. *Plant Physiol.* 114, 295–305.

Goclaw-Binder, H., Sendersky, E., Shimoni, E., Kiss, V., Reich, Z., Perelman, A., et al. (2012). Nutrient-associated elongation and asymmetric division of the cyanobacterium *Synechococcus* PCC 7942. *Environ. Microbiol.* 14, 680–690. doi: 10.1111/j.1462-2920.2011.02620.x

González, A., Teresa Bes, M., Barja, F., Peleato, M. L., and Fillat, M. F. (2010). Overexpression of FurA in *Anabaena* sp. *PCC* 7120 reveals new targets for this regulator involved in photosynthesis, iron uptake and cellular morphology. *Plant Cell Physiol.* 51, 1900–1914. doi: 10.1093/pcp/pcq148

Gorelova, O. A., Baulina, O. I., Rasmussen, U., and Koksharova, O. A. (2013). The pleiotropic effects of ftn2 and ftn6 mutations in cyanobacterium *Synechococcus* sp. PCC 7942. *Protoplasma* 250, 931–942. doi: 10.1007/s00709-012-0479-2

Gutu, A., and Kehoe, D. M. (2012). Emerging perspectives on the mechanisms, regulation, and distribution of light color acclimation in cyanobacteria. *Mol. Plant* 5, 1–13. doi: 10.1093/mp/ssr054

He, Y. Y., and Häder, D. P. (2002). Involvement of reactive oxygen species in the UV-B damage to the cyanobacterium *Anabaena* sp. *J. Photochem. Photobiol. B* 66, 73–80. doi: 10.1016/S1011-1344(01)00278-0

Hill, N. S., Buske, P. J., Shi, Y., and Levin, P. A. (2013). A moonlighting enzyme links *Escherichia coli* cell size with central metabolism. *PLoS Genet.* 9:e1003663. doi: 10.1371/journal.pgen.1003663

Hu, B., Yang, G., Zhao, W., Zhang, Y., and Zhao, J. (2007). MreB is important for cell shape but not for chromosome segregation of the filamentous cyanobacterium *Anabaena* sp. *PCC* 7120. *Mol. Microbiol.* 63, 1640–1652. doi: 10.1111/j.1365-2958.2007.05618.x

Kadota, A., and Wada, M. (1992). Reorganization of the cortical cytoskeleton in tip-growing fern protonemal cells during phytochrome-mediated phototropism and blue light-induced apical swelling. *Protoplasma* 166, 35–41. doi: 10.1007/bf01320140

Kaplan-Levy, R., Hadas, O., Summers, M., Rücker, J., and Sukenik, A. (2010). "Akinetes: dormant cells of cyanobacteria," in *Dormancy and Resistance in Harsh Environments*, eds E. Lubzens, J. Cerda, and M. Clark (Berlin: Springer), 5–27.

Kehoe, D. M., and Grossman, A. R. (1996). Similarity of a chromatic adaptation sensor to phytochrome and ethylene receptors. *Science* 273, 1409–1412.

Koch, A. L. (1996). What size should a bacterium be? A question of scale. *Annu. Rev. Microbiol.* 50, 317–348. doi: 10.1146/annurev.micro.50.1.317

Koksharova, O. A., Klint, J., and Rasmussen, U. (2007). Comparative proteomics of cell division mutants and wild-type of *Synechococcus* sp. strain *PCC* 7942. *Microbiology* 153, 2505–2517. doi: 10.1099/mic.0.2007/007039-0

Koksharova, O. A., and Wolk, C. P. (2002). A novel gene that bears a DnaJ motif influences cyanobacterial cell division. *J. Bacteriol.* 184, 5524–5528. doi: 10.1128/JB.184.19.5524-5528.2002

Kumar, K., Mella-Herrera, R. A., and Golden, J. W. (2010). Cyanobacterial heterocysts. *Cold Spring Harb. Perspect. Biol.* 2, a000315. doi: 10.1101/cshperspect.a000315

Lamont, H. (1969). Sacrificial cell death and trichome breakage in an oscillatoriacean blue-green alga: the role of murein. *Arch. Mikrobiol.* 69, 237–259. doi: 10.1007/bf00408976

Li, H. B., Qin, Y. M., Pang, Y., Song, W. Q., Mei, W. Q., and Zhu, Y. X. (2007). A cotton ascorbate peroxidase is involved in hydrogen peroxide homeostasis during fibre cell development. *New Phytol.* 175, 462–471. doi: 10.1111/j.1469-8137.2007.02120.x

Lindeboom, J. J., Nakamura, M., Hibbel, A., Shundyak, K., Gutierrez, R., Ketelaar, T., et al. (2013). A mechanism for reorientation of cortical microtubule arrays driven by microtubule severing. *Science* 342, 1245533. doi: 10.1126/science.1245533

Lloyd, A. C. (2013). The regulation of cell size. *Cell* 154, 1194–1205. doi: 10.1016/j.cell.2013.08.053

Ma, Z., and Gao, K. (2009). Photoregulation of morphological structure and its physiological relevance in the cyanobacterium *Arthrospira* (Spirulina) *platensis*. *Planta* 230, 329–337. doi: 10.1007/s00425-009-0947-x

Ma, Z., and Gao, K. (2010). Spiral breakage and photoinhibition of *Arthrospira platensis* (Cyanophyta) caused by accumulation of reactive oxygen species

under solar radiation. *Environ. Exp. Bot.* 68, 208–213. doi: 10.1016/j.envexpbot.2009.11.010

Ma, Z., and Gao, K. (2014). Carbon limitation enhances CO_2 concentrating mechanism but reduces trichome size in *Arthrospira platensis* (cyanobacterium). *J. Appl. Phycol.* 26, 1465–1472. doi: 10.1007/s10811-013-0181-6

Marbouty, M., Saguez, C., Cassier-Chauvat, C., and Chauvat, F. (2009). ZipN, an FtsA-like orchestrator of divisome assembly in the model cyanobacterium *Synechocystis* PCC 6803. *Mol. Microbiol.* 74, 409–420. doi: 10.1111/j.1365-2958.2009.06873.x

Margolin, W. (2009). Sculpting the bacterial cell. *Curr. Biol.* 19, R812–R822. doi: 10.1016/j.cub.2009.06.033

Marshall, W., Young, K., Swaffer, M., Wood, E., Nurse, P., Kimura, A., et al. (2012). What determines cell size? *BMC Biol.* 10:101. doi: 10.1186/1741-7007-10-101

Marwan, W. (2001). "Photomovement and photomorphogenesis in *Physarum polycephalum*: targeting of cytoskeleton and gene expression by light," in *Comprehensive Series in Photosciences*, eds D. P. Häder and A. M. Breure (Amsterdam: Elsevier), 561–587.

Mathur, J. (2004). Cell shape development in plants. *Trends Plant Sci.* 9, 583–590. doi: 10.1016/j.tplants.2004.10.006

Mazouni, K., Domain, F., Cassier-Chauvat, C., and Chauvat, F. (2004). Molecular analysis of the key cytokinetic components of cyanobacteria: FtsZ, ZipN and MinCDE. *Mol. Microbiol.* 52, 1145–1158. doi: 10.1111/j.1365-2958.2004.04042.x

Meeks, J. C., and Elhai, J. (2002). Regulation of cellular differentiation in filamentous cyanobacteria in free-living and plant-associated symbiotic growth states. *Mol. Microbiol. Biol. Rev.* 66, 94–121. doi: 10.1128/mmbr.66.1.94-121.2002

Merino-Puerto, V., Herrero, A., and Flores, E. (2013). Cluster of genes that encode positive and negative elements influencing filament length in a heterocyst-forming cyanobacterium. *J. Bacteriol.* 195, 3957–3966. doi: 10.1128/JB.00181-13

Miyagishima, S. Y., Wolk, C. P., and Osteryoung, K. W. (2005). Identification of cyanobacterial cell division genes by comparative and mutational analyses. *Mol. Microbiol.* 56, 126–143. doi: 10.1111/j.1365-2958.2005.04548.x

Montgomery, B. L. (2008). Shedding new light on the regulation of complementary chromatic adaptation. *Cent. Eur. J. Biol.* 3, 351–358. doi: 10.2478/s11535-008-0039-0

Müller, K., Linkies, A., Vreeburg, R. A., Fry, S. C., Krieger-Liszkay, A., and Leubner-Metzger, G. (2009). In vivo cell wall loosening by hydroxyl radicals during cress seed germination and elongation growth. *Plant Physiol.* 150, 1855–1865. doi: 10.1104/pp.109.139204

Neunuebel, M. R., and Golden, J. W. (2008). The *Anabaena* sp. strain *PCC* 7120 gene all2874 encodes a diguanylate cyclase and is required for normal heterocyst development under high-light growth conditions. *J. Bacteriol.* 190, 6829–6836. doi: 10.1128/jb.00701-08

Nishihama, R., Ishizaki, K., Hosaka, M., Matsuda, Y., Kubota, A., and Kohchi, T. (2015). Phytochrome-mediated regulation of cell division and growth during regeneration and sporeling development in the liverwort *Marchantia polymorpha*. *J. Plant Res.* 1–15. doi: 10.1007/s10265-015-0724-9

Ohmori, M., Ohmori, K., and Hasunuma, K. (1988). Rapid change in cyclic 3′, 5′-AMP concentration triggered by a light-off or light-on signal in *Anabaena cylindrica*. *Arch. Microbiol.* 150, 203–204.

Ohmori, M., and Okamoto, S. (2004). Photoresponsive cAMP signal transduction in cyanobacteria. *Photochem. Photobiol. Sci.* 3, 503–511. doi: 10.1039/b401623h

Ohmori, M., Terauchi, K., Okamoto, S., and Watanabe, M. (2002). Regulation of cAMP-mediated photosignaling by a phytochrome in the cyanobacterium *Anabaena cylindrica*. *Photochem. Photobiol.* 75, 675–679. doi: 10.1562/0031-8655(2002)075<0675:ROCMPB>2.0.CO;2

Okamoto, S., Kasahara, M., Kamiya, A., Nakahira, Y., and Ohmori, M. (2004). A phytochrome-like protein AphC triggers the cAMP signaling induced by far-red light in the cyanobacterium *Anabaena* sp. strain *PCC*7120. *Photochem. Photobiol.* 80, 429–433. doi: 10.1562/0031-8655(2004)080<0429:APPATT>2.0.CO;2

Osanai, T., Kuwahara, A., Iijima, H., Toyooka, K., Sato, M., Tanaka, K., et al. (2013). Pleiotropic effect of sigE over-expression on cell morphology, photosynthesis and hydrogen production in *Synechocystis* sp. *PCC* 6803. *Plant J.* 76, 456–465. doi: 10.1111/tpj.12310

Osborn, M. J., and Rothfield, L. (2007). Cell shape determination in *Escherichia coli*. *Curr. Opin. Microbiol.* 10, 606–610. doi: 10.1016/j.mib.2007.09.004

Pattanaik, B., and Montgomery, B. L. (2010). A novel role for a TonB-family protein and photoregulation of iron acclimation in *Fremyella diplosiphon*. *Plant Signal. Behav.* 5, 851–853. doi: 10.4161/psb.5.7.11827

Pattanaik, B., Whitaker, M. J., and Montgomery, B. L. (2011a). Convergence and divergence of the photoregulation of pigmentation and cellular morphology in *Fremyella diplosiphon*. *Plant Signal. Behav.* 6, 2038–2041. doi: 10.4161/psb.6.12.18239

Pattanaik, B., Whitaker, M. J., and Montgomery, B. L. (2011b). Regulation of phycoerythrin synthesis and cellular morphology in *Fremyella diplosiphon* green mutants. *Biochem. Biophys. Res. Commun.* 413, 182–188. doi: 10.1016/j.bbrc.2011.08.051

Pattanaik, B., Whitaker, M. J., and Montgomery, B. L. (2012). Light quantity affects the regulation of cell shape in *Fremyella diplosiphon*. *Front. Microbiol.* 3:170. doi: 10.3389/fmicb.2012.00170

Poetsch, B., Schreckenbach, T., and Werenskiold, A. K. (1989). Photomorphogenesis in *Physarum polycephalum*: temporal expression pattern of actin, α- and β-tubulin. *Eur. J. Biochem.* 179, 141–146. doi: 10.1111/j.1432-1033.1989.tb14531.x

Postius, C., Neuschaefer-Rube, O., Haid, V., and Böger, P. (2001). N2-fixation and complementary chromatic adaptation in non-heterocystous cyanobacteria from Lake Constance. *FEMS Microbiol. Ecol.* 37, 117–125. doi: 10.1111/j.1574-6941.2001.tb00859.x

Potocký, M., Jones, M. A., Bezvoda, R., Smirnoff, N., and Žárský, V. (2007). Reactive oxygen species produced by NADPH oxidase are involved in pollen tube growth. *New Phytol.* 174, 742–751. doi: 10.1111/j.1469-8137.2007.02042.x

Putzer, H., Verfuerth, C., Claviez, M., and Schreckenbach, T. (1984). Photomorphogenesis in *Physarum*: induction of tubulins and sporulation-specific proteins and of their mRNAs. *Proc. Natl. Acad. Sci. U.S.A.* 81, 7117–7121.

Qiu, B., and Liu, J. (2004). Utilization of inorganic carbon in the edible cyanobacterium Ge–Xian–Mi (Nostoc) and its role in alleviating photo-inhibition. *Plant Cell Environ.* 27, 1447–1458. doi: 10.1111/j.1365-3040.2004.01248.x

Rae, B. D., Long, B. M., Whitehead, L. F., Forster, B., Badger, M. R., and Price, G. D. (2013). Cyanobacterial carboxysomes: microcompartments that facilitate CO_2 fixation. *J. Mol. Microbiol. Biotechnol.* 23, 300–307. doi: 10.1159/000351342

Rastogi, R. P., Incharoensakdi, A., and Madamwar, D. (2014). Responses of a rice-field cyanobacterium *Anabaena siamensis* TISTR-8012 upon exposure to PAR and UV radiation. *J. Plant Physiol.* 171, 1545–1553. doi: 10.1016/j.jplph.2014.07.011

Rastogi, R. P., Singh, S. P., Häder, D.-P., and Sinha, R. P. (2010). Detection of reactive oxygen species (ROS) by the oxidant-sensing probe 2′,7′-dichlorodihydrofluorescein diacetate in the cyanobacterium *Anabaena variabilis* PCC 7937. *Biochem. Biophys. Res. Commun.* 397, 603–607. doi: 10.1016/j.bbrc.2010.06.006

Rausenberger, J., Hussong, A., Kircher, S., Kirchenbauer, D., Timmer, J., Nagy, F., et al. (2010). An integrative model for phytochrome B mediated photomorphogenesis: from protein dynamics to physiology. *PLoS ONE* 5:e10721. doi: 10.1371/journal.pone.0010721

Reed, J. W., Nagatani, A., Elich, T. D., Fagan, M., and Chory, J. (1994). Phytochrome A and phytochrome B have overlapping but distinct functions in *Arabidopsis* development. *Plant Physiol.* 104, 1139–1149.

Rippka, R., Deruelles, J., Waterbury, J. B., Herdman, M., and Stanier, R. Y. (1979). Generic assignments, strain histories and properties of pure cultures of cyanobacteria. *Microbiology* 111, 1–61. doi: 10.1099/00221287-111-1-1

Robert, L., Hoffmann, M., Krell, N., Aymerich, S., Robert, J., and Doumic, M. (2014). Division in *Escherichia coli* is triggered by a size-sensing rather than a timing mechanism. *BMC Biol.* 12:17. doi: 10.1186/1741-7007-12-17

Sachetto-Martins, G., Franco, L. O., and De Oliveira, D. E. (2000). Plant glycine-rich proteins: a family or just proteins with a common motif? *Biochim. Biophys. Acta* 1492, 1–14. doi: 10.1016/S0167-4781(00)00064-6

Santos, J. M., Freire, P., Vicente, M., and Arraiano, C. M. (1999). The stationary-phase morphogene bolA from *Escherichia coli* is induced by stress during early stages of growth. *Mol. Microbiol.* 32, 789–798.

Savage, D. F., Afonso, B., Chen, A. H., and Silver, P. A. (2010). Spatially ordered dynamics of the bacterial carbon fixation machinery. *Science* 327, 1258–1261. doi: 10.1126/science.1186090

Seib, L. O., and Kehoe, D. M. (2002). A turquoise mutant genetically separates expression of genes encoding phycoerythrin and its associated linker peptides. *J. Bacteriol.* 184, 962–970. doi: 10.1128/jb.184.4.962-970.2002

Semighini, C. P., and Harris, S. D. (2008). Regulation of apical dominance in *Aspergillus nidulans* hyphae by reactive oxygen species. *Genetics* 179, 1919–1932. doi: 10.1534/genetics.108.089318

Siegal-Gaskins, D., and Crosson, S. (2008). Tightly regulated and heritable division control in single bacterial cells. *Biophys. J.* 95, 2063–2072. doi: 10.1529/biophysj.108.128785

Singh, S. P., Miller, H. L., and Montgomery, B. L. (2013). Temporal dynamics of changes in reactive oxygen species (ROS) levels and cellular morphology are coordinated during complementary chromatic acclimation in *Fremyella diplosiphon*. *Photosyn. Res.* 1–10. doi: 10.1007/s11120-013-9938-7 [Epub ahead of print].

Singh, S. P., and Montgomery, B. L. (2011). Determining cell shape: adaptive regulation of cyanobacterial cellular differentiation and morphology. *Trends Microbiol.* 19, 278–285. doi: 10.1016/j.tim.2011.03.001

Singh, S. P., and Montgomery, B. L. (2012). Reactive oxygen species are involved in the morphology-determining mechanism of *Fremyella diplosiphon* cells during complementary chromatic adaptation. *Microbiology* 158, 2235–2245. doi: 10.1099/mic.0.060475-0

Singh, S. P., and Montgomery, B. L. (2014). Morphogenes bolA and mreB mediate the photoregulation of cellular morphology during complementary chromatic acclimation in *Fremyella diplosiphon*. *Mol. Microbiol.* 93, 167–182. doi: 10.1111/mmi.12649

Smith, L. G. (2003). Cytoskeletal control of plant cell shape: getting the fine points. *Curr. Opin. Plant Biol.* 6, 63–73. doi: 10.1016/S1369-5266(02)00012-2

Soifer, I., Robert, L., Barkai, N., and Amir, A. (2014). Single-cell analysis of growth in budding yeast and bacteria reveals a common size regulation strategy. arXiv preprint. arXiv:1410.4771

Speranza, A., Crinelli, R., Scoccianti, V., and Geitmann, A. (2012). Reactive oxygen species are involved in pollen tube initiation in kiwifruit. *Plant Biol. (Stuttg.)* 14, 64–76. doi: 10.1111/j.1438-8677.2011.00479.x

Stewart, G. C. (2005). Taking shape: control of bacterial cell wall biosynthesis. *Mol. Microbiol.* 57, 1177–1181. doi: 10.1111/j.1365-2958.2005.04760.x

Taheri-Araghi, S., Bradde, S., Sauls, J. T., Hill, N. S., Levin, P. A., Paulsson, J., et al. (2015). Cell-size control and homeostasis in bacteria. *Curr. Biol.* 25, 385–391. doi: 10.1016/j.cub.2014.12.009

Tandeau de Marsac, N. (1991). "Chromatic adaptation by cyanobacteria," in *Cell Culture and Somatic Cell Genetics of Plants*, eds L. Bogorad and I. K. Vasil (New York: Academic Press), 417–446.

Terauchi, K., and Ohmori, M. (2004). Blue light stimulates cyanobacterial motility via a cAMP signal transduction system. *Mol. Microbiol.* 52, 303–309. doi: 10.1111/j.1365-2958.2003.03980.x

Terenna, C. R., Makushok, T., Velve-Casquillas, G., Baigl, D., Chen, Y., Bornens, M., et al. (2008). Physical mechanisms redirecting cell polarity and cell shape in fission yeast. *Curr. Biol.* 18, 1748–1753. doi: 10.1016/j.cub.2008.09.047

Turner, J. J., Ewald, J. C., and Skotheim, J. M. (2012). Cell size control in yeast. *Curr. Biol.* 22, R350–R359. doi: 10.1016/j.cub.2012.02.041

Ueki, N., and Nishii, I. (2009). Controlled enlargement of the glycoprotein vesicle surrounding a *Volvox* embryo requires the InvB nucleotide-sugar transporter and is required for normal morphogenesis. *Plant Cell* 21, 1166–1181. doi: 10.1105/tpc.109.066159

Vadia, S., and Levin, P. A. (2015). Growth rate and cell size: a re-examination of the growth law. *Curr. Opin. Microbiol.* 24, 96–103. doi: 10.1016/j.mib.2015.01.011

Walters, K. J., Whitaker, M. J., Singh, S. P., and Montgomery, B. L. (2013). Light intensity and reactive oxygen species are centrally involved in photoregulatory responses during complementary chromatic adaptation in *Fremyella diplosiphon*. *Commun. Integr. Biol.* 6, e25005. doi: 10.4161/cib.25005

Weart, R. B., Lee, A. H., Chien, A. C., Haeusser, D. P., Hill, N. S., and Levin, P. A. (2007). A metabolic sensor governing cell size in bacteria. *Cell* 130, 335–347. doi: 10.1016/j.cell.2007.05.043

Whitaker, M. J., Bordowitz, J. R., and Montgomery, B. L. (2009). CpcF-dependent regulation of pigmentation and development in *Fremyella diplosiphon*. *Biochem. Biophys. Res. Commun.* 389, 602–606. doi: 10.1016/j.bbrc.2009.09.030

Whitaker, M. J., Pattanaik, B., and Montgomery, B. L. (2011). Characterization of green mutants in *Fremyella diplosiphon* provides insight into the impact of phycoerythrin deficiency and linker function on complementary chromatic adaptation. *Biochem. Biophys. Res. Commun.* 404, 52–56. doi: 10.1016/j.bbrc.2010.11.056

Wong, F. C. Y., and Meeks, J. C. (2002). Establishment of a functional symbiosis between the cyanobacterium *Nostoc punctiforme* and the bryophyte *Anthoceros punctatus* requires genes involved in nitrogen control and initiation of heterocyst differentiation. *Microbiology* 148, 315–323.

Wu, H., Gao, K., Villafane, V. E., Watanabe, T., and Helbling, E. W. (2005). Effects of solar UV radiation on morphology and photosynthesis of filamentous cyanobacterium *Arthrospira platensis*. *Appl. Environ. Microbiol.* 71, 5004–5013. doi: 10.1128/aem.71.9.5004-5013.2005

Yao, Z., Davis, R. M., Kishony, R., Kahne, D., and Ruiz, N. (2012). Regulation of cell size in response to nutrient availability by fatty acid biosynthesis in *Escherichia coli*. *Proc. Natl. Acad. Sci. U.S.A.* 109, E2561–E2568. doi: 10.1073/pnas.1209742109

Young, K. D. (2006). The selective value of bacterial shape. *Microbiol. Mol. Biol. Rev.* 70, 660–703. doi: 10.1128/MMBR.00001-06

Young, K. D. (2007). Bacterial morphology: why have different shapes? *Curr. Opin. Microbiol.* 10, 596–600. doi: 10.1016/j.mib.2007.09.009

Zaritsky, A. (1975). On dimensional determination of rod-shaped bacteria. *J. Theor. Biol.* 54, 243–248.

Conflict of Interest Statement: The author declares that the research was conducted in the absence of any commercial or financial relationships that could be construed as a potential conflict of interest.

Copyright © 2015 Montgomery. This is an open-access article distributed under the terms of the Creative Commons Attribution License (CC BY). The use, distribution or reproduction in other forums is permitted, provided the original author(s) or licensor are credited and that the original publication in this journal is cited, in accordance with accepted academic practice. No use, distribution or reproduction is permitted which does not comply with these terms.

frontiers in Microbiology

REVIEW
published: 09 June 2015
doi: 10.3389/fmicb.2015.00580

Molecular mechanisms for the evolution of bacterial morphologies and growth modes

*Amelia M. Randich and Yves V. Brun**

Department of Biology, Indiana University, Bloomington, IN, USA

Bacteria exhibit a rich diversity of morphologies. Within this diversity, there is a uniformity of shape for each species that is replicated faithfully each generation, suggesting that bacterial shape is as selectable as any other biochemical adaptation. We describe the spatiotemporal mechanisms that target peptidoglycan synthesis to different subcellular zones to generate the rod-shape of model organisms *Escherichia coli* and *Bacillus subtilis*. We then demonstrate, using the related genera *Caulobacter* and *Asticcacaulis* as examples, how the modularity of the core components of the peptidoglycan synthesis machinery permits repositioning of the machinery to achieve different growth modes and morphologies. Finally, we highlight cases in which the mechanisms that underlie morphological evolution are beginning to be understood, and how they depend upon the expansion and diversification of the core components of the peptidoglycan synthesis machinery.

Keywords: bacterial shape, bacterial morphology, peptidoglycan synthesis, *Caulobacter*, *Asticcacaulis*, FtsZ, MreB

OPEN ACCESS

Edited by:
Jaan Männik,
University of Tennessee, USA

Reviewed by:
Miguel A. De Pedro,
Consejo Superior de Investigaciones Científicas, Spain
Waldemar Vollmer,
Newcastle University, UK

***Correspondence:**
Yves V. Brun,
Department of Biology, Indiana University, 1001 E 3rd Street, Bloomington, IN 47405-7005, USA
ybrun@indiana.edu

Specialty section:
This article was submitted to Microbial Physiology and Metabolism, a section of the journal Frontiers in Microbiology

Received: *31 March 2015*
Accepted: *26 May 2015*
Published: *09 June 2015*

Citation:
Randich AM and Brun YV (2015) Molecular mechanisms for the evolution of bacterial morphologies and growth modes. Front. Microbiol. 6:580. doi: 10.3389/fmicb.2015.00580

Introduction

The typical of bacterial shapes as simply rods, variations of rods, or cocci belies the great diversity of bacterial morphologies. Within these simple classifications, bacteria exhibit a broad range of morphologies—helical or vibrioid twists, filaments, hyphae or branched filaments, prosthecae or stalks (thin cylindrical extensions of the cell envelope)—as well as distinct growth modes, forms of cellular differentiation, and life cycles (**Figure 1**, Young, 2006). The mechanisms by which bacteria achieve these morphologies, much less evolve them, has remained unclear. Historically, the murein sacculus, or peptidoglycan layer, has been posited as the underlying determinant of bacterial shape (Vollmer et al., 2008a). A heteropolymer of peptide cross-linked glycan strands, the sacculus confers strength to the cell wall and maintains cell shape and size. It is becoming clear that the sacculus in and of itself is not the only determinant of cell shape; rather it is the spatiotemporal regulation of the enzymes that build the sacculus and modify it in response to environmental changes that drives morphogenesis (Young, 2010; Cava and de Pedro, 2014).

In bacteria, morphologies and growth modes are interconnected (Brown et al., 2011). In many taxa, maintenance of the rod shape itself requires at least two well-studied modes of growth: lateral elongation (**Figure 2A**), or incorporation of peptidoglycan along the sidewalls; and septation (**Figure 2B**), the generation of nascent poles, usually at the cell center. In these canonical cases, which are exemplified by model organisms *Escherichia coli* and *Bacillus subtilis*, material at the poles remains inert, with no evidence of new peptidoglycan incorporation or turnover (Mobley et al., 1984; Schlaeppi et al., 1985; de Pedro et al., 1997; Janakiraman and Goldberg, 2004). However, other, less understood approaches to achieving rod-shaped morphologies exist. Actinobacteria exhibit polar

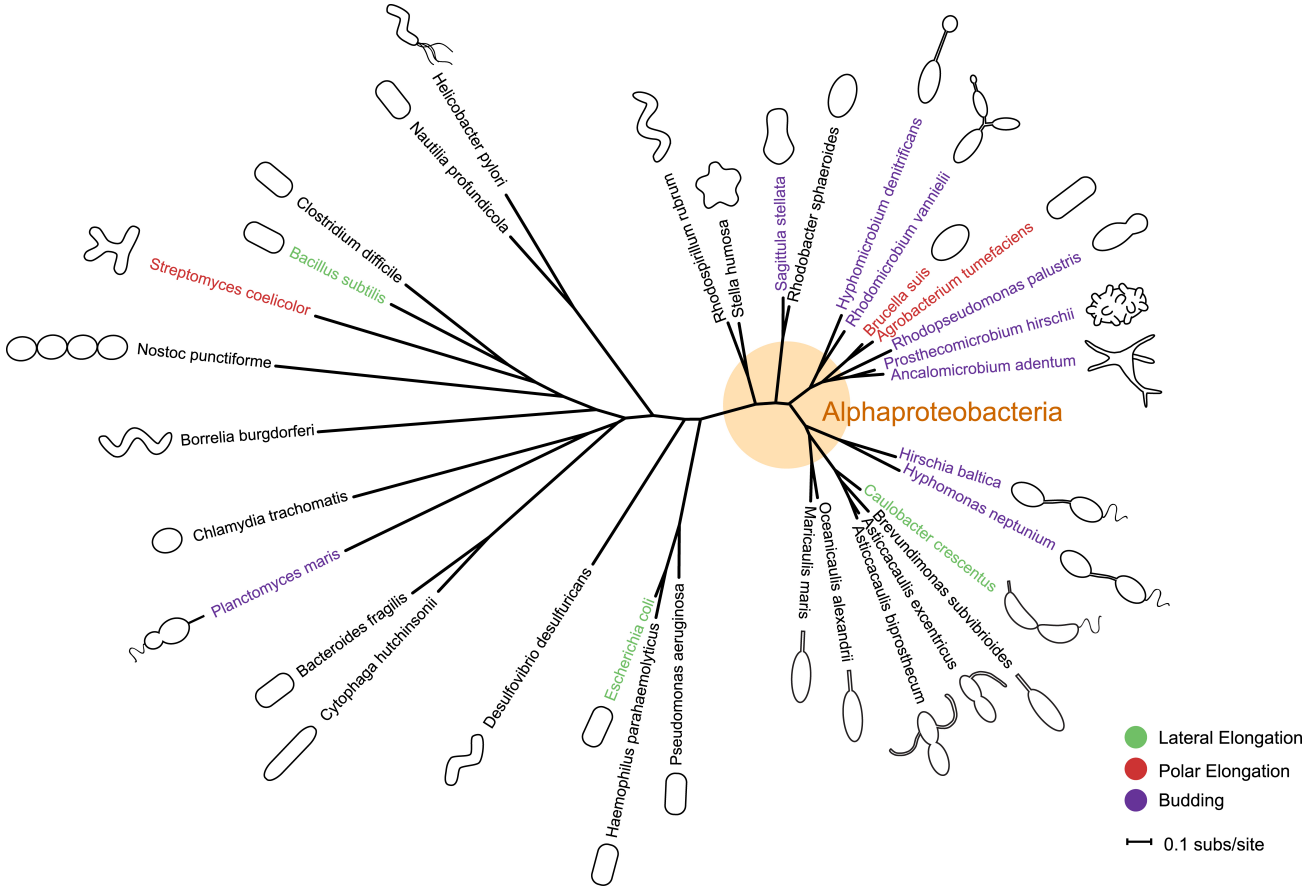

FIGURE 1 | Phylogeny and morphology of bacteria exhibiting different modes of growth. *rpoC* sequences were aligned using MUSCLE v3.8.31 (Edgar, 2004). RAxML v7.0.4 (Stamatakis, 2006) reconstructed the maximum likelihood phylogeny using the JTT amino acid substitution matrix with rate variation among sites modeled by a four-category discrete gamma distribution and an additional invariant category. Note that the stalk of *Planctomyces maris* is composed of several parallel fibrils (Bauld and Staley, 1976), and is not bound by cell envelop layers like that of the Caulobacterales. Bacteria are not drawn to scale. Scale bar reflects numbers of substitutions per site.

growth (**Figure 2C**), where elongation occurs strictly at one or both poles, leaving the sidewalls, instead of the poles, inert (Umeda and Amako, 1983; Daniel and Errington, 2003; Chauhan et al., 2006; Flärdh and Buttner, 2009; Flärdh, 2010). Alphaproteobacteria (the superfamily highlighted in **Figure 1**), exhibit a diverse mix of growth strategies including lateral elongation and polar growth, but also the unknown mechanisms of zonal growth to produce buds and/or stalks (**Figures 2D,E**; Brown et al., 2011). In a striking example, bacteria in the family *Hyphomicrobiaceae* not only produce a stalk, but also bud daughter cells from the end of the stalk (**Figure 2D**) via an unknown mechanism (Whittenbury and Dow, 1977; Moore, 1981). The life cycle of these cells involves at least three separate modes of growth: stalk elongation at the junction of the cell body and stalk, daughter cell elongation at the tip of the stalk, and septum formation within the stalk to complete division (Moore and Hirsch, 1973; Whittenbury and Dow, 1977; Moore, 1981).

In comparison to lateral elongation and septation, much less is known genetically or mechanistically about polar growth or budding, making it hard to rigorously distinguish between these growth modes. The next section will describe how, although lateral elongation and septation differ at the genetic level, they ultimately drive distinct growth modes by positioning functionally similar peptidoglycan synthesis machineries at specific locations in the cell. It is likely that polar growth, budding, and stalk growth also result from the repositioning of yet to be described peptidoglycan synthesis machineries. In this way, all growth modes can be described as zonal growth (Brown et al., 2011). Already with these few examples, a great plurality of growth modes clearly has evolved to generate a "common" rod shape, as well as to achieve novel morphologies and life cycles. This review aims to summarize the spatiotemporal mechanisms that target peptidoglycan synthesis to different subcellular zones to generate the rod-shape of model organisms *E. coli* and *B. subtilis* and to then describe how the modularity of the core components of the peptidoglycan synthesis machinery permits repositioning of the growth machinery to achieve different growth modes and morphologies. Because of space limitations, we were unable to cover the septal elongation mechanisms that generate round and ovoid cells and we refer the reader to excellent

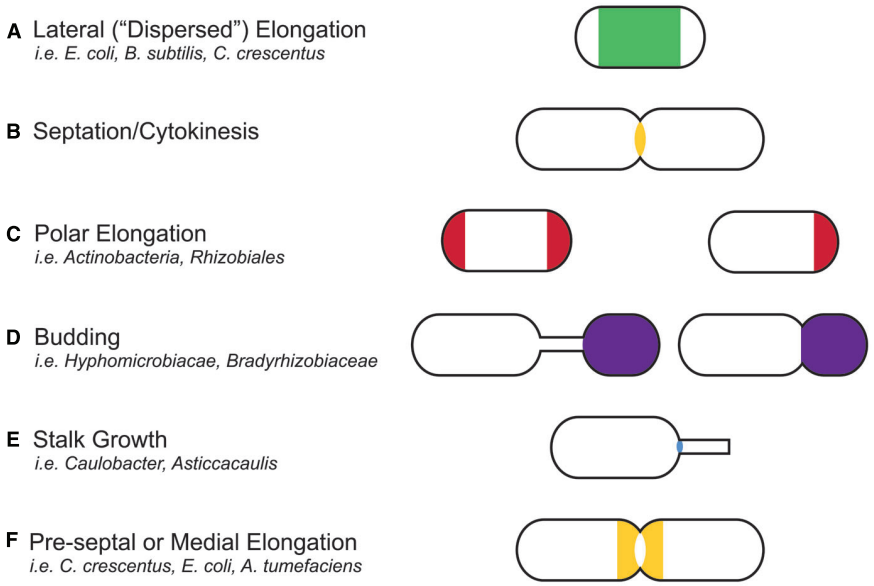

FIGURE 2 | Growth modes in rod-shaped bacteria. Several growth modes with the regions of active peptidoglycan synthesis are schematized. Colors indicate regions of active peptidoglycan synthesis. **(A)** Lateral elongation is well-studied in *E. coli*, *B. subtilis*, and *C. crescentus*, and often assumed for many rod-shaped bacteria. **(B)** A majority of bacterial families divide in a FtsZ-dependent manner. Notable exceptions are members of the PVC (Planctomycetes, Verrucomicrobia, and Chlamydiae) superfamily. **(C)** Polar elongation is characteristic of Actinobacteria, where it is bipolar. It has recently been demonstrated in Rhizobiales (Brown et al., 2012) where it is unipolar. **(D)** Budding occurs both at the ends of stalks and off the cell body in Alphaproteobacteria. **(E)** Stalks are wide-spread in Alphaproteobacteria. While the exact mechanism for growth may differ among families, all depend on zonal growth of the peptidoglycan at the cell-stalk junction. **(F)** Some species exhibit medial (pre-septal) growth, which appears to be peptidoglycan synthesis near the division plane before full assembly of the Z-ring.

recent reviews on this topic (Sham et al., 2012; Pinho et al., 2013).

Molecular Machinery of Bacterial Growth and Division in Rod-shaped Bacteria

The molecular underpinnings of how bacteria grow, divide, and maintain shape are slowly emerging, especially in model rod-shaped bacteria such as *E. coli* and *B. subtilis*. In these species, two protein assemblies direct the modification and synthesis of the sacculus at specific times and locations during the cell cycle: the elongasome inserts new peptidoglycan along the length of the rod during growth, and the divisome completes the steps of constriction and new peptidoglycan synthesis at the cell center during cell division (Typas et al., 2012). Both of these assemblies utilize similar components and likely share a common evolutionary history (Szwedziak and Löwe, 2013). The preponderance of conserved protein classes for peptidoglycan synthesis machinery across gram-negative and positive bacteria, as well as between the elongasome and divisome assemblies, suggests a general strategy for shaping the bacterial cell as well as molecular mechanisms for the evolution of novel morphologies.

The divisome and elongasome have long been hypothesized to form large complexes (Höltje, 1998). Both consist of cytoplasmic scaffolding cytoskeletal-like proteins; inner membrane-spanning elements; and a host of periplasmic enzymes including peptidoglycan synthases and hydrolases (**Figure 3**; Margolin, 2009; Typas et al., 2012; Egan and Vollmer, 2013). This machinery works in concert to create the sacculus, a meshwork consisting of chains of two alternating sugar types, *N*-acetyl glucosamine and *N*-acetyl muramic acid, joined through beta-(1,4)-glycosidic bonds that are cross-linked together via peptide chains. The steps in peptidoglycan synthesis proceed as follows: a series of enzymes generates a pool of nucleotide precursors in the cytoplasm, a flippase then transfers the lipidated monomers over the inner membrane, and finally, peptidoglycan synthases polymerize the monomers into glycan chains and cross-link them through peptide bonds, thus forming the sacculus. Other peptidoglycan-modifying enzymes further diversify the periplasmic/extracellular components, such as the carboxypeptidases that trim peptide chains and the lytic transglycosylases that reduce the length of glycan strands. Moreover, peptidoglycan hydrolases, which cleave either the glycosidic or amide bonds of peptidoglycan, play important roles in turning over old peptidoglycan to allow insertion of new material in the growing cell and help shape the new poles (Priyadarshini et al., 2007; Vollmer et al., 2008b; Frirdich and Gaynor, 2013; Lee and Huang, 2013).

The cytoplasmic scaffold FtsZ organizes and regulates the activity and localization of various divisome components. Much progress has been made in elucidating how the divisome is spatiotemporally regulated in canonical rod-shaped bacteria.

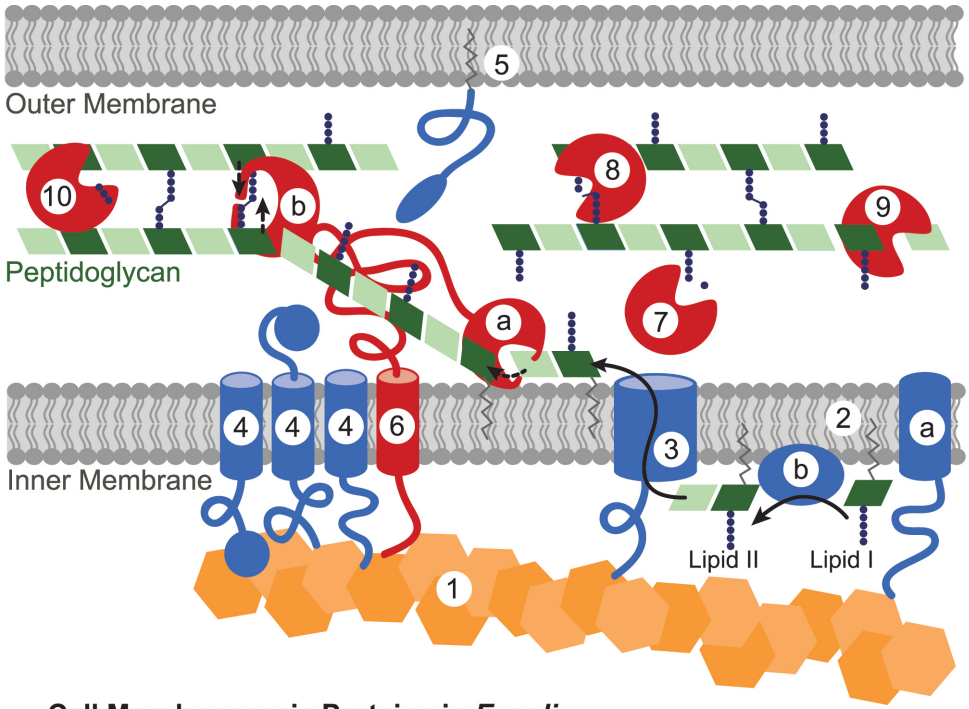

Cell Morphogenesis Proteins in *E. coli*

		Divisome	Elongasome
1	**Cytoplasmic Scaffolds**	FtsZ, FtsA	MreB
	Membrane-Spanning Elements		
2	Pecursor Synthesis	(a) MraY, (b) MurG	
3	Flippase	FtsW/MurJ?	RodA/MurJ?
4	Associated Proteins	FtsEX, FtsK, FtsN	MreCD, RodZ
5	(OM) PG Synthase Activator	LpoB	LpoA
	PG-Modifying Enzymes		
6	PG-Synthase (Bifunctional)	PBP1B	PBP1A
	a Glycosyltransferase	MtgA	
	b Transpeptidase	PBP3	PBP2
7	Carboxypeptidase	PBP5, PBP4B, PBP6, PBP6B	
8	Endopeptidase	PBP4, PBP7	Spr, YdhO, YebA
9	Lytic Transglycosylase	Slt70, MltABCDEF	?
10	Amidase	AmiABCD	?

FIGURE 3 | Peptidoglycan synthesis machinery schematic. The divisome and elongasome both consist of cytoplasmic scaffolds (orange), membrane-spanning elements that include regulatory proteins as well as peptidoglycan precursor synthesis machinery (blue), and peptidoglycan-modifying enzymes (red). Each assembly has genetic components that are biochemically distinct despite retaining similar functions (Table). In general, (1) cytoplasmic scaffolds such as FtsZ or MreB direct the location of peptidoglycan synthesis and recruit various cytoplasmic and inner-membrane components. (2) Cytoplasmic and inner membrane enzymes synthesize peptidoglycan monomers (lipid II) in the cytoplasm [only (a) MraY and (b) MurG shown] and (3) a flippase flips them across the inner membrane. (4, 5) Various membrane proteins function to regulate or organize the divisome or elongasome protein assemblies. (6) Bifunctional or monofunctional peptidoglycan synthases (a) polymerize lipid II into glycan strands and (b) crosslink the peptide chains to form the sacculus. Various enzymes modify the peptidoglycan after synthesis: (7) carboxypeptidases trim peptide chains, (8) endopeptidases cleave crosslinks, (9) lytic transglycosylases cleave the glycan strand, (10) and amidases remove peptide chains from the glycan strand. Question marks in the table indicate that elongasome proteins responsible for the indicated activities remain to be identified. Some proteins essential to the divisome have been omitted: ZipA, ZapABCD, FtsQ, FtsL, and FtsB.

During division, the GTP-dependent polymerization of the tubulin-like FtsZ creates a ring-shaped structure called the Z ring at the cytoplasmic face of the membrane at the center of the cell (Bi and Lutkenhaus, 1991; Löwe and Amos, 1998; Mukherjee and Lutkenhaus, 1998). The exact architecture of the Z-ring has recently been the subject of intense study (Li et al., 2007; Fu et al., 2010; Strauss et al., 2012; Szwedziak et al., 2014). Once assembled, the Z-ring recruits over 10 essential divisome components (Egan and Vollmer, 2013). In *E. coli*, the mechanism for targeting the Z-ring to the center of the cell involves the well-characterized Min system, which prevents Z-ring assembly at the cell poles (Raskin and de Boer, 1999; Hale et al., 2001), and nucleoid occlusion protein SlmA (Bernhardt and de Boer, 2005). *B. subtilis* appears to maintain many of the same essential division proteins with the exception of utilizing DivIVA to regulate the septation site by positioning and stabilizing Min proteins at the cell poles (Edwards and Errington, 1997; Marston et al., 1998; Hamoen and Errington, 2003) and using a nucleoid occlusion mechanism mediated by a different protein, Noc (Wu and Errington, 2004). Other species also utilize different systems for positioning FtsZ, such as the MipZ system in *Caulobacter crescentus* (Thanbichler and Shapiro, 2006), the MapZ/LocZ system in *Streptococcus pneumoniae* (Fleurie et al., 2014; Holečková et al., 2015), and the SsgB system in *Streptomyces* (Willemse et al., 2011). Each of these systems (with the exception of SsgB) faithfully localizes the Z ring to the division plane with high precision at onset of division (Trueba, 1982; Yu and Margolin, 1999; Männik et al., 2012).

Much less is known about the spatiotemporal regulation of the elongasome, for which MreB appears to be the major scaffold for coordinating peptidoglycan precursor synthesis and peptidoglycan polymerization. MreB is an actin-like protein that forms membrane-associated filaments (Esue et al., 2005, 2006; Salje et al., 2011; Ozyamak et al., 2013). Once thought to form a cytoskeletal meshwork, MreB has since been shown to form discrete, motile patches that move, independently of MreB polymerization or treadmilling, near-perpendicularly to the long cell axis in *E. coli*, *B. subtilis*, and *C. crescentus* (Dominguez-Escobar et al., 2011; Garner et al., 2011; van Teeffelen et al., 2011). MreB interacts with inner membrane proteins MreC, MreD, RodZ (Kruse et al., 2004; van den Ent et al., 2006; Shiomi et al., 2008; Alyahya et al., 2009; Bendezú et al., 2009), as well as lipid II synthesis enzymes MraY and MurG (Mohammadi et al., 2007), and its movement during elongation depends on both the synthesis of essential peptidoglycan components and the activity of peptidoglycan synthases (Dominguez-Escobar et al., 2011; Garner et al., 2011; van Teeffelen et al., 2011). Other components of the elongasome, such as MreB-associated proteins MreCD and certain PBPs, have been shown to exhibit the same motile, spatiotemporal localization as MreB (Dominguez-Escobar et al., 2011; Garner et al., 2011), suggesting that parts of the elongasome indeed travel as a complex. MreB could function to coordinate elongasome complexes and perhaps restrict their mobility to ensure a uniform distribution of peptidoglycan insertion. Recent work combining time-lapse and 3D-imaging with computational analysis indicates that MreB preferentially localizes to and directs peptidoglycan synthesis at regions of negative curvature in *E. coli* cells (Ursell et al., 2014). Therefore MreB could selectively drive peptidoglycan growth away from the positive curvature of the cell poles to straighten the cell and create the rod shape. Possibly, other factors remain to be discovered that could regulate the localization and dynamics of MreB to in turn direct the activity of the elongasome. For example, as will be covered in the next sections, MreB interacts with *Caulobacter crescentus*-specific genes TipN and CreS.

While both the divisome and elongasome depend on similar molecular components, they clearly drive disparate morphological changes: cutting the cell in half versus lengthening the cell. These particular growth modes are achieved by the distinct localization patterns of their respective cytoplasmic scaffolds. During division, FtsZ forms a ring at the site of septation and thereby directs peptidoglycan growth and hydrolysis to shape the new poles of the daughter cells. In contrast, MreB distributes along the sidewalls of the cell to drive homogeneous insertion of new peptidoglycan in the lengthening cell. While these assemblies appear to share a similar strategies for growth, their respective components make them biochemically distinguishable (Table in **Figure 3**) and allow for independent regulation and incorporation into specific cell events. This modularity—evident here in the cytoplasmic scaffolds—permits wholesale repositioning of the growth machinery to achieve different growth modes and morphologies.

Mechanisms for Evolving Novel Morphologies and Growth Modes

One can imagine multiple ways in which complexes such as the elongasome and divisome could be repurposed or retooled to evolve new morphologies and modes of growth. Theoretically, expansion and diversification of any of the core elements of the peptidoglycan synthesis assembly—cytoskeletal-like proteins, inner membrane-spanning elements, periplasmic or extracellular enzymes and outer membrane proteins—present opportunities for such evolution. The spatiotemporal interdependency of peptidoglycan synthesis machinery components in both the elongasome and divisome suggests that new relationships can evolve between different components. Moreover, the addition of new regulatory or recruitment components to the complexes may drive species-specific morphologies. Recent studies in non-canonical rod-shaped bacteria indicate that different modes of growth depend upon the same core machinery, but that these are organized or regulated differently by species-specific components.

A large diversity of bacterial cytoskeletal elements appears to underlie species-specific lifestyles and morphologies. Besides FtsZ and MreB, other self-oligomerizing protein scaffolds have been identified and shown to be widespread in bacteria (Bagchi et al., 2008; Kühn et al., 2010). In many cases, these scaffolds have roles in driving morphology. For example, intermediate filament-like crescentin (CreS) forms a single filamentous structure in *Caulobacter crescentus* that produces the characteristic vibrioid shape of the bacterium by inducing differential growth of the sides of the rod-shaped sacculus (Ausmees et al., 2003; Cabeen et al., 2009). In contrast, *Helicobacter pylori* utilizes a family of coiled-coil rich proteins (Ccrp) that form extended filamentous

structures to maintain a helical rod shape (Waidner et al., 2009; Specht et al., 2011). These examples demonstrate how two scaffolding proteins, unrelated in sequence, have arisen in two different species to create twists in the rod shape. In contrast to the eukaryotic cytoskeleton, in which classes of scaffolding proteins such as actin or microtubules have been adapted to suit multiple processes by using adaptor proteins, it appears bacteria may have developed larger numbers of species- and process-specific scaffolding proteins (Ozyamak et al., 2013).

Although FtsZ and MreB comprise the core of the canonical divisome and elongasome, there are many cases in which their roles have changed or they have been eliminated from genomes completely. For example, MreB plays a role in chromosome segregation but not growth in *H. pylori* (Waidner et al., 2009), and is absent in the majority of Actinobacteria, some Firmicutes, and a minority of Proteobacteria (Margolin, 2009; Brown et al., 2011; Jiang et al., 2015). It is tantalizing to infer that MreB delineates specific growth modes since bacteria lacking MreB, such as Actinobacteria and many Alphaproteobacteria—*Agrobacterium*, *Hyphomicrobium*, and *Rhizobium*—utilize polar growth mechanisms (Brown et al., 2012, 2011). However, the story appears to be much more complex than associating MreB with lateral elongation of rod-shaped bacteria. Members of the *Chlamydiae* family represent an interesting family of bacteria that lack FtsZ while maintaining a nearly complete suite of other peptidoglycan synthesis machinery components, including MreB (Stephens et al., 1998; McCoy and Maurelli, 2006; Pilhofer et al., 2008; Bertelli et al., 2010). This is in contrast to the great majority of bacterial phyla that utilize FtsZ for cell division (Erickson et al., 2010). In fact, the presence of peptidoglycan in the *Chlamydiae* cell wall was long debated and has only recently been demonstrated in several members of the family (Pilhofer et al., 2013; Liechti et al., 2014). Localization studies in *Waddlia chondrophila* suggest that MreB acts in lieu of FtsZ to facilitate division in this species (Jacquier et al., 2014). Other studies have demonstrated that various components of the peptidoglycan synthesis pathway from FtsZ-independent species function *in vitro* and in complementation studies (Henrichfreise et al., 2009; Frandi et al., 2014). Therefore, even in genera that have diverged greatly, the overarching mechanism of peptidoglycan synthesis remains.

The expansion of various classes of peptidoglycan-modifying enzymes is becoming a common theme in studies of alternative morphologies and growth modes as less studied genera come to the forefront. *H. pylori* appears to employ a diverse cast of endo- and carboxypeptidases that likely shape the helical sacculus through alternative cross-linking (Bonis et al., 2010; Sycuro et al., 2010, 2012, 2013). In *Agrobacterium tumefaciens*, which has been recently shown to grow polarly (Brown et al., 2012), polar growth appears to depend on a class of alternative L,D-transpeptidases (Cameron et al., 2014). Overall, the modularity of the common core components of the peptidoglycan synthesis machinery provides ample flexibility for new growth modes and morphologies. Although some bacterial families have clearly shifted their dependence from central components such as MreB or FtsZ to other scaffolds, the general mechanism for assembling core peptidoglycan synthesis machineries appears to remain intact.

Cell Growth and Morphology of *Caulobacter crescentus*

The dimorphic alphaproteobacterium *Caulobacter crescentus* represents an excellent case study in understanding how new morphologies arise from the diversification of the common core peptidoglycan synthesis machinery. *C. crescentus* divides asymmetrically, producing a swarmer cell with a polar flagellum and a DNA replication-competent cell with a polar stalk. This process of division requires strict coordination in time and space with other cell cycle events such as cell growth, chromosome segregation, and differentiation. Therefore it is unsurprising that although *C. crescentus* maintains similar core peptidoglycan synthesis machinery components in its divisome and elongasome, it has evolved discrete scaffolds, regulatory proteins, and cell cycle control mechanisms to adapt the machinery to its specific lifestyle. Determining exactly how *C. crescentus* has repurposed conserved peptidoglycan synthesis components for elongation, division, and stalk synthesis will help to expand our understanding of bacterial morphology.

The diversification of proteins interacting with and regulating FtsZ and MreB allows for strict control of asymmetric division and morphological development in *C. crescentus*. One significant difference between *C. crescentus* and the canonical rod-shaped bacteria *E. coli* and *B. subtilis* is that *C. crescentus* does not utilize a Min system or nucleoid occlusion proteins. Instead, *C. crescentus* uses MipZ gradients to position the FtsZ ring at the division plane (Thanbichler and Shapiro, 2006). MipZ directly interacts with FtsZ to inhibit ring polymerization. When MipZ associates with ParB at the stalk pole prior to S phase, it drives FtsZ monomers to the new, non-stalked pole (**Figure 4B**). During initiation of chromosome replication and origin duplication, some of the MipZ-ParB complex binds the new origin and migrates with it to the new pole, displacing FtsZ from the new pole to the division plane. Although MipZ shares some distant domain similarity with MinD, it likely evolved from ParA-like DNA partitioning proteins and is conserved amongst all Alphaproteobacteria without MinCD orthologues (Thanbichler and Shapiro, 2006).

Other polar regulators have been shown to influence cell morphology and interact with peptidoglycan synthesis machinery (**Figure 4B**). TipN, a polytopic membrane protein with a large coiled-coil cytoplasmic domain, ensures transmission of cell polarity to the daughter cell by marking the new pole and regulating MreB dynamics at the division plane (Lam et al., 2006). PopZ forms oligomeric networks at the poles to form polar ribosome exclusion zones and serves two roles during the cell cycle, switching function during the swarmer to stalk transition: it first interacts with the parS/ParB centromere at the stalked pole prior to the initiation of DNA replication, and later, during polar maturation, it recruits remodeling factors, such as peptidoglycan synthesis machinery, to transform the flagellated pole into a stalked pole (Bowman et al., 2010; Laloux and Jacobs-Wagner, 2013; Ptacin et al., 2014). All of these regulatory polar protein systems serve as examples of alternative networks that regulate the otherwise conserved core peptidoglycan synthesis machinery.

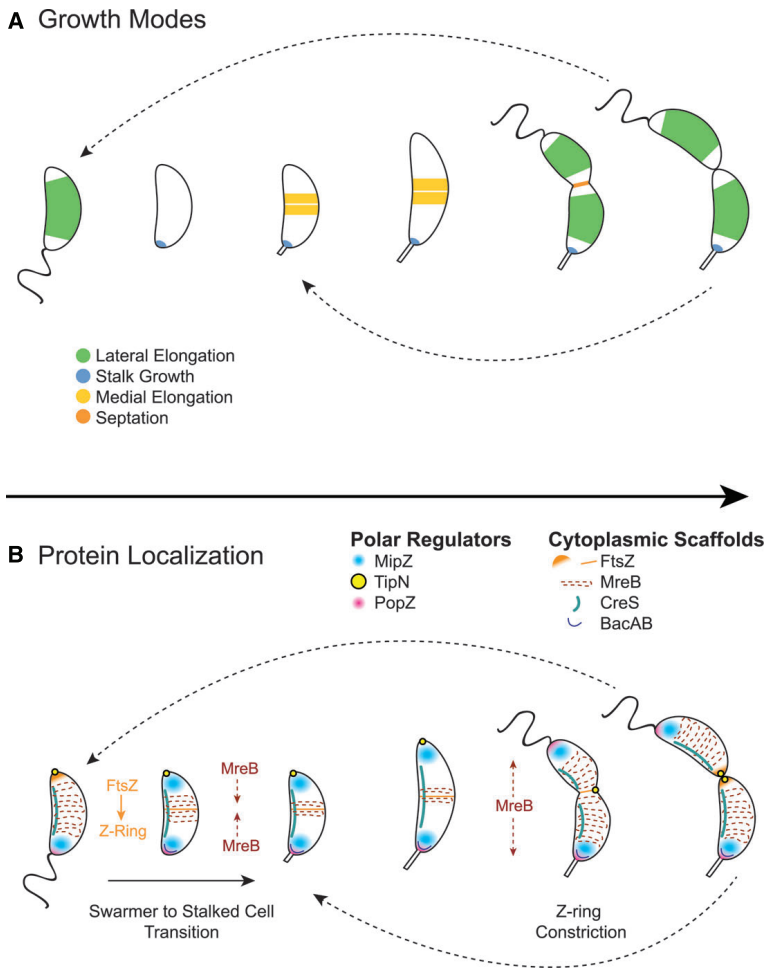

FIGURE 4 | Cytoplasmic scaffold localization dynamics and growth modes in *Caulobacter crescentus*. (A) *C. crescentus* exhibits four growth modes over the course of its dimorphic cell cycle: lateral elongation (swarmer and stalked cells), stalk synthesis and elongation (stalked cells), medial elongation (stalked cells), and septation. Colors indicate regions of active peptidoglycan synthesis. **(B)** The activity and dynamics of various peptidoglycan synthesis machineries, which are regulated by polar regulators, underlie the different growth modes. In swarmer cells, MipZ localizes at the flagellar pole, driving FtsZ to the opposite pole, and MreB is dispersed along the length of the cell. During the swarmer to stalked cell transition, the flagellar pole undergoes remodeling to become the stalked pole. This transition involves the recruitment of bactofilin and peptidoglycan synthesis machinery to the stalked pole by the PopZ network to initiate stalk synthesis. During initiation of chromosome replication and origin duplication, some of the MipZ-ParB complex binds the new origin and migrates with it to the new pole, displacing FtsZ from the new pole to the division plane, where it forms the Z-ring. MreB condenses at the division plane before dispersing again during constriction due to regulation by TipN. After septation, FtsZ reassembles into the Z-ring quickly in stalked cells, making medial elongation the primary mode of elongation in this morphology.

Another difference between *C. crescentus* and canonical rod-shaped bacteria is that it exhibits at least four peptidoglycan synthesis modes over its cell cycle: lateral elongation, elongation at the division plane before division (also called "pre-septal" or "medial" elongation, **Figure 2F**), septation, and stalk synthesis/elongation (**Figure 4A**). As in canonical rod-shaped cells, cell elongation in *C. crescentus* is MreB-dependent. Early studies showed that depletion of MreB disrupts cell morphology and results in lemon-shaped cells (Figge et al., 2004; Gitai et al., 2004). However, the role of MreB has expanded in *C. crescentus* to accommodate the cell cycle and additional growth modes. For example, MreB appears to influence cell polarity and division, as its depletion disturbs the localization of origins of replication as well as the localization of polar regulatory proteins PleC, DivJ, CckA, and DivK (Gitai et al., 2004). Moreover, MreB exhibits dynamic localization throughout the cell cycle, cycling between dispersed helical patterns in swarmer cells (similar to that seen in *E. coli* and *B. subtilis*) and an intense band at the division plane in pre-divisional cells (**Figure 4B**).

The dynamic localization of MreB drives a shift in growth mode from dispersed, lateral elongation mediated by MreB to zonal, medial elongation mediated by both MreB and FtsZ. The condensation of MreB at the division plane requires assembly of the FtsZ ring (Figge et al., 2004; Aaron et al., 2007), and high-resolution temporal studies have shown that MreB recruitment to the FtsZ ring coincides with medial elongation (Goley et al., 2011). *E. coli* also exhibits a transient pre-septal elongation mode (de Pedro et al., 1997; Aarsman et al., 2005;

Potluri et al., 2012), in which FtsZ and MreB interact directly to transfer peptidoglycan synthesis machinery from the elongasome to the divisome (Fenton and Gerdes, 2013). However, in *C. crescentus,* this growth mode predominates a portion of the cell cycle. Because the FtsZ quickly reassembles after division in stalked cells, stalked cells likely elongate primarily via medial elongation (Aaron et al., 2007). Therefore, a similar medial elongation growth mode has been extended in *C. crescentus* to accommodate the asymmetric cell cycle.

MreB appears to have species-specific functions in *C. crescentus*. For example, it appears to interact directly or indirectly with CreS, and is required for proper attachment of the CreS filament to the membrane (Ausmees et al., 2003; Cabeen et al., 2009). Mutations along one surface of MreB alter cell curvature and disrupt the association of the CreS filament with the membrane (Charbon et al., 2009; Dye et al., 2011). Therefore MreB may organize CreS during cell growth, facilitating the attachment of the filament in a stretched conformation (Charbon et al., 2009). Another set of MreB mutations, which occur within the nucleotide-binding pocket, result in morphological defects and affect the localization pattern and dynamics of MreB (Dye et al., 2011). The nucleotide binding site mutants suggest that the ATP hydrolysis cycle of MreB could be coupled to the *C. crescentus* cell cycle to spatiotemporally regulate specific growth modes. The regulation of MreB by ATP could drive its relocation from the sides of the elongating cell to the division plane during the cell cycle.

Some MreB mutants have interesting implications for understanding how *C. crescentus* may remodel polar peptidoglycan. For a subset of the nucleotide binding site MreB mutants (E213G, D16G, N21D, and A325P), cells exhibit a variable width phenotype in which the ends of the cells become extremely tapered and pointed (Dye et al., 2011; Harris et al., 2014). In these mutants, although MreB still exhibits wild type function, it localizes to the cell poles instead of dispersing or condensing at the division plane (Harris et al., 2014). This behavior presumably drives aberrant peptidoglycan synthesis to create elongated cell poles. These MreB mutants may be trapped in a phase of the ATP cycle in which MreB localizes to the poles for a specific polar growth mode in wild type *C. crescentus* cells (Dye et al., 2011). Previous observations that the tapered shape of the wild type *C. crescentus* cell pole develops during the next cell cycle, not during septation or medial elongation (Aaron et al., 2007), corroborates the idea that MreB could participate in remodeling the cell wall at the poles. That the polar cell wall in *C. crescentus* undergoes remodeling instead of remaining entirely inert contradicts what is typically assumed for rod-shaped bacteria. Given that *C. crescentus* belongs to the Alphaproteobacteria class, many members of which exhibit polar growth (Brown et al., 2011, 2012), it may not be surprising if its poles do not follow the same rules as *E. coli* and *B. subtilis*.

In addition to its diversified polar regulators and various growth modes, *C. crescentus* hosts an expanded repertoire of bifunctional peptidoglycan synthases (penicillin-binding proteins, or PBPs). *E. coli* has three bifunctional PBPs. Although PBP1A and PBP1B exhibit semi-redundancy in function, PBP1A appears to preferentially associate with the elongasome (Banzhaf et al., 2012) and PBP1B with the divisome (Bertsche et al., 2006; Müller et al., 2007). The function of PBP1C remains unknown (Schiffer and Höltje, 1999). In contrast, *C. crescentus* has five predicted bifunctional PBPs (PBP1A, PbpC, PbpX, PbpY, PbpZ) which appear to be largely redundant, with any of them capable of functioning as the sole bifunctional PBP with the exception of PbpZ (Yakhnina and Gitai, 2013; Strobel et al., 2014). The same four enzymes were shown to be capable of interacting with divisome components FtsN, FtsL, and DipM (Strobel et al., 2014). Despite this redundancy, each PBP has a specific localization pattern during the cell cycle, suggesting specific cellular functions and roles: Pbp1A and PbpZ localize to the cell periphery; PbpY and PbpX to the periphery, division plane, and stalk; and PbpC to the stalk. Therefore, with the exception of PbpZ, these bifunctional PBPs have retained the ability to interact with both the elongasome and divisome while also evolving distinct affinities for specific localization factors.

Caulobacter crescentus exemplifies how the core peptidoglycan synthesis machinery can be adapted to create its specific morphology and to fit its lifestyle. While it retains an MreB-dependent elongasome and an FtsZ-dependent divisome, it has diversified its growth modes by adding what appears to be a dual MreB- and FtsZ-mediated zonal growth mode at the division plane. These growth modes are strictly regulated in order to synchronize them with the cell cycle and to accommodate asymmetric division. The vibrioid shape arises from diversifying cytoplasmic scaffolds (CreS) and changing the interacting partners of MreB to achieve cell cycle-dependent dynamics. In addition, *C. crescentus* has expanded its suite of bifunctional PBPs and may have additional peptidoglycan-modifying enzymes. Finally, *C. crescentus* has evolved a specialized growth mode, stalk synthesis, which is described in the next section.

The Stalk as a Model System for Understanding Zonal Growth

Stalk synthesis and elongation constitutes one growth mode unique to *C. crescentus* among model rod-shaped bacteria (although not among Alphaproteobacteria). A thin extension of the inner membrane, peptidoglycan, and outer membrane layers (Poindexter, 1964), the stalk is a morphologically distinct organelle thought to improve the nutrient scavenging ability of the cell (Poindexter, 1978; Ireland et al., 2002; Wagner et al., 2006). The narrow cytoplasm of the stalk is free of DNA, ribosomes and most cytoplasmic proteins (Poindexter and Cohen-Bazire, 1964; Ireland et al., 2002; Wagner et al., 2006) and compartmentalized by cross-bands, disk-like, proteinaceous structures that intersect the width of the stalk perpendicular to the long axis of the cell (Jones and Schmidt, 1973; Schlimpert et al., 2012). Cross-bands prevent exchange of membrane and soluble proteins between the stalk and cell body (Schlimpert et al., 2012). As a nonessential organelle, the stalk serves as a convenient model for zonal, or targeted, peptidoglycan growth (Wagner and Brun, 2007).

Stalk synthesis initiates at the cell pole during the swarmer to stalked cell transition phase of the cell cycle, and elongation occurs at the cell-stalk junction during pre-divisional cell elongation (Schmidt and Stanier, 1966; Aaron et al., 2007). MreB and RodA

(an MreB-associated protein) depletion, or treatment with the PBP2 inhibitor mecillinam (Seitz and Brun, 1998), result in the loss or shortening of stalks, and recovery from depletion leads to the growth of ectopic stalked poles, suggesting that MreB, in concert with RodA and a PBP2 homolog, plays a role in recruiting peptidoglycan synthesis machinery for stalk synthesis (Wagner et al., 2005). Overexpression of RodZ (another MreB-associated protein) resulted in multiple stalks forming at the same pole, opposite pole, or on the cell body (Alyahya et al., 2009). RodZ localization dynamics coincided with FtsZ during the cell cycle but appeared to depend on MreB. Overall, these data suggest that stalk synthesis and elongation in *C. crescentus* potentially depends on a similar core apparatus as elongation, utilizing MreB as a scaffold. The mechanism for cross-band formation may have interesting intersections with the processes of stalk synthesis and elongation. Early on, electron micrographs of *C. crescentus* stalks showed that cross-bands consisted of concentric circular striations, possibly of peptidoglycan and membranes (Jones and Schmidt, 1973). Because the stalk continues to elongate as the stalked cell participates in increasing rounds of division, it was postulated that stalk length and number of cross-bands could indicate cell age. Quantitative analysis suggested that one cross-band is added to the stalk toward the end of each reproductive cycle, possibly accompanying division (Poindexter and Staley, 1996; Schlimpert et al., 2012). The idea that cross-bands consist of peptidoglycan has been challenged by the discovery that cross-bands are the product of the macromolecular assembly of least four proteins, StpABCD (Schlimpert et al., 2012). However, a relationship between cross-band assembly and the peptidoglycan synthesis machinery may still exist.

Like septation, lateral, or medial elongation in *C. crescentus*, stalk synthesis and elongation appear to be highly tuned to cell cycle regulation and polar positioning mechanisms. Moreover, the mechanism for stalk synthesis appears to depend on the expansion and diversification of the core machinery. Bactofilins BacA and BacB constitute a class of scaffolding proteins with proline-rich terminal regions that localize to the stalked pole of the cell during the swarmer to stalked cell transition (Kühn et al., 2010). Deletion of these genes led to a 45% reduction in stalk length, suggesting a recruitment role in stalk assembly. Indeed, the localization of the stalk-specific bifunctional peptidoglycan synthase PbpC to the stalk was shown to be dependent on BacA and BacB. PbpC potentially acts in conjunction with PbpX in stalk elongation (Yakhnina and Gitai, 2013; Strobel et al., 2014), however, it has also been shown to have a role in recruiting and modifying a stalk-specific protein. StpX is a stalk-specific membrane protein that promotes the elongation of the stalk in nutrient-limiting conditions (Hughes et al., 2010). PbpC is not only required for localizing StpX to the stalk-cell junction at onset of stalk synthesis, but appears to be directly or indirectly involved in the process of tethering StpX to the outer membrane or to an outer membrane protein (Hughes et al., 2013). That this phenomenon takes place regardless of PbpC's transglycosylase or transpeptidase activities suggests alternative roles for various PBPs and other enzyme classes in regulating the peptidoglycan synthesis machinery, opening up the diversity of mechanisms for the evolution of novel functions.

Phylogenic studies indicate that stalk positioning evolved from an ancestral, single polar stalk in the order *Caulobacteraceae*, to a single sub-polar stalk in *Asticcacaulis excentricus*, and subsequently to bilateral stalks in *Asticcacaulis biprosthecum* (Jiang et al., 2014). The stalk structure appears identical in *Caulobacter* and *Asticcacaulis* (Pate and Ordal, 1965) and all three species appear to share the same stalk synthesis mechanism of inserting peptidoglycan at the base of the stalk (Jiang et al., 2014). The natural variation and evolution of stalk positioning in these species correlates with the localization of SpmX, a developmental regulator (Radhakrishnan et al., 2008) that has been shown to be necessary for stalk synthesis in *Asticcacaulis* but not in *Caulobacter* (Radhakrishnan et al., 2008; Jiang et al., 2014). Therefore, in *Asticcacaulis* SpmX has been co-opted as a stalk-positioning factor. SpmX consists of three defined regions: a highly conserved N-terminal muramidase domain, an unstructured intermediate region that has been expanded by over 370 amino acids in the *Asticcacaulis* genus, and a two-pass transmembrane domain. Recent work has demonstrated that either the intermediate region or the transmembrane domain contain the residues responsible for SpmX's new role in sub-polar and bilateral stalk positioning (Jiang et al., 2014). The muramidase domain, while necessary for overall function and localization, is interchangeable amongst species. How a murein hydrolase participates in SpmX's function and localization will be an interesting question for future studies.

The recent discovery that SpmX coordinates stalk placement in the *Asticcacaulis* genus underscores the utility of not only studying the stalk as a model system for zonal growth, but of exploiting the natural diversity of stalked morphologies observed in Alphaproteobacteria. In marked contrast to division and elongation genes, which require depletion strains, stalk-less mutants are far easier to identify in a genetic screen. *Asticcacaulis* provides an opportunity for screening stalkless mutants with fewer chances of impacting elements critical for cell viability, since stalk synthesis no longer overlaps with polar regulation. Finally, altering the location of the stalk may prove to be a far more advantageous phenotype than losing the stalk entirely in terms of discovering localization and recruitment factors for stalk initiation and maintenance. Therefore studying stalk localization, initiation, and maintenance in *Asticcacaulis* will likely make significant inroads into understanding how bacteria can redirect the core peptidoglycan machinery to create novel morphologies.

Conclusion and Summary

Critical advances in studying bacterial growth and division in model bacteria such as *E. coli*, *B. subtilis*, and *C. crescentus* have identified and characterized the fundamental components of the molecular machinery responsible for creating and shaping the sacculus. This expanding body of work reveals a general strategy for growing and shaping the bacterial cell wall. Moreover, it suggests ways in which the core can be adapted for various bacterial lifestyles as well as molecular mechanisms for the evolution of novel morphologies. The peptidoglycan synthesis machinery consists of a central core of cytoskeletal-like scaffolding proteins, inner membrane-spanning elements, and periplasmic or extracellular peptidoglycan-modifying elements.

The modularity and evolvability of this system is inherent in how different elements have been retuned or repurposed in each genus for species-specific growth modes and morphologies. As different species of bacteria become genetically tractable, it is becoming clear that the diversification and expansion of any of the core elements of the peptidoglycan synthesis assembly underlie morphological diversity and alternate growth modes.

As studies in *C. crescentus* and the closely related genus *Asticcacaulis* demonstrate, much can be learned about general growth strategies using comparative approaches with related families. The great diversity of morphologies and growth modes in Alphaproteobacteria (**Figure 4**) offers an opportunity to exploit natural diversity to dissect mechanisms for stalk localization and synthesis, as well as polar growth. The recent advances in expressing fluorescent fusions in *Hyphomonas neptunium* open up yet another opportunity for discovering genes responsible for polar growth and stalk development (Jung et al., 2014). The increasing ease and affordability of genome sequencing allows further investigation into the suites of genes underlying uncharacterized growth modes in other genera. New reagents that fluorescently label sites of peptidoglycan synthesis are providing simple methods to determine growth modes, even in understudied species and environmental samples (Kuru et al., 2012; Pilhofer et al., 2013; Liechti et al., 2014). Determining how bacteria actively restructure their morphologies, or how they have evolved various morphologies over time, remains a major goal in bacteriology. Expanding investigations into understudied genera with novel morphologies and growth modes will complement and enrich our understanding of how bacteria grow and proliferate.

Acknowledgments

Our research on morphogenesis is supported by National Institutes of Health Grants GM051986 and GM113172 to YB AR was supported by National Institutes of Health National Research Service Award F32GM112362. We thank David Kysela for the phylogenetic tree, and Kevin Young and members of the Brun laboratory for critical reading of the manuscript.

References

Aaron, M., Charbon, G., Lam, H., Schwarz, H., Vollmer, W., and Jacobs-Wagner, C. (2007). The tubulin homologue FtsZ contributes to cell elongation by guiding cell wall precursor synthesis in *Caulobacter crescentus*. *Mol. Microbiol.* 64, 938–952. doi: 10.1111/j.1365-2958.2007.05720.x

Aarsman, M. E. G., Piette, A., Fraipont, C., Vinkenvleugel, T. M. F., Nguyen-Distèche, M., and den Blaauwen, T. (2005). Maturation of the *Escherichia coli* divisome occurs in two steps. *Mol. Microbiol.* 55, 1631–1645. doi: 10.1111/j.1365-2958.2005.04502.x

Alyahya, S. A., Alexander, R., Costa, T., Henriques, A. O., Emonet, T., and Jacobs-Wagner, C. (2009). RodZ, a component of the bacterial core morphogenic apparatus. *Proc. Natl. Acad. Sci. U.S.A.* 106, 1239–1244. doi: 10.1073/pnas.0810794106

Ausmees, N., Kuhn, J. R., and Jacobs-Wagner, C. (2003). The bacterial cytoskeleton: an intermediate filament-like function in cell shape. *Cell* 115, 705–713. doi: 10.1016/S0092-8674(03)00935-8

Bagchi, S., Tomenius, H., Belova, L. M., and Ausmees, N. (2008). Intermediate filament-like proteins in bacteria and a cytoskeletal function in *Streptomyces*. *Mol. Microbiol.* 70, 1037–1050. doi: 10.1111/j.1365-2958.2008.06473.x

Banzhaf, M., van den Berg van Saparoea, B., Terrak, M., Fraipont, C., Egan, A., Philippe, J., et al. (2012). Cooperativity of peptidoglycan synthases active in bacterial cell elongation. *Mol. Microbiol.* 85, 179–194. doi: 10.1111/j.1365-2958.2012.08103.x

Bauld, J., and Staley, J. T. (1976). Planctomyces maris sp. nov: a marine isolate of the planctomyces-blastocaulis group of budding bacteria. *J. Gen. Microbiol.* 97, 45–55. doi: 10.1099/00221287-97-1-45

Bendezú, F. O., Hale, C. A., Bernhardt, T. G., and de Boer, P. A. J. (2009). RodZ (YfgA) is required for proper assembly of the MreB actin cytoskeleton and cell shape in *E. coli*. *EMBO J.* 28, 193–204. doi: 10.1038/emboj.2008.264

Bernhardt, T. G., and de Boer, P. A. J. (2005). SlmA, a nucleoid-associated, FtsZ binding protein required for blocking septal ring assembly over chromosomes in *E. coli*. *Mol. Cell* 18, 555–564. doi: 10.1016/j.molcel.2005.04.012

Bertelli, C., Collyn, F., Croxatto, A., Rückert, C., Polkinghorne, A., Kebbi-Beghdadi, C., et al. (2010). The waddlia genome: a window into chlamydial biology. *PLoS ONE* 5:e10890. doi: 10.1371/journal.pone.0010890

Bertsche, U., Kast, T., Wolf, B., Fraipont, C., Aarsman, M. E. G., Kannenberg, K., et al. (2006). Interaction between two murein (peptidoglycan) synthases, PBP3 and PBP1B, in *Escherichia coli*. *Mol. Microbiol.* 61, 675–690. doi: 10.1111/j.1365-2958.2006.05280.x

Bi, E. F., and Lutkenhaus, J. (1991). FtsZ ring structure associated with division in *Escherichia coli*. *Nature* 354, 161–164. doi: 10.1038/354161a0

Bonis, M., Ecobichon, C., Guadagnini, S., Prévost, M.-C., and Boneca, I. G. (2010). A M23B family metallopeptidase of *Helicobacter pylori* required for cell shape, pole formation and virulence. *Mol. Microbiol.* 78, 809–819. doi: 10.1111/j.1365-2958.2010.07383.x

Bowman, G. R., Comolli, L. R., Gaietta, G. M., Fero, M., Hong, S.-H., Jones, Y., et al. (2010). *Caulobacter* PopZ forms a polar subdomain dictating sequential changes in pole composition and function. *Mol. Microbiol.* 76, 173–189. doi: 10.1111/j.1365-2958.2010.07088.x

Brown, P. J. B., de Pedro, M. A., Kysela, D. T., Van der Henst, C., Kim, J., De Bolle, X., et al. (2012). Polar growth in the Alphaproteobacterial order Rhizobiales. *Proc. Natl. Acad. Sci. U.S.A.* 109, 1697–1701. doi: 10.1073/pnas.1114476109

Brown, P. J. B., Kysela, D. T., and Brun, Y. V. (2011). Polarity and the diversity of growth mechanisms in bacteria. *Semin. Cell Dev. Biol.* 22, 790–798. doi: 10.1016/j.semcdb.2011.06.006

Cabeen, M. T., Charbon, G., Vollmer, W., Born, P., Ausmees, N., Weibel, D. B., et al. (2009). Bacterial cell curvature through mechanical control of cell growth. *EMBO J.* 28, 1208–1219. doi: 10.1038/emboj.2009.61

Cameron, T. A., Anderson-Furgeson, J., Zupan, J. R., Zik, J. J., and Zambryski, P. C. (2014). Peptidoglycan synthesis machinery in *Agrobacterium tumefaciens* during unipolar growth and cell division. *MBio* 5, e01219–14. doi: 10.1128/mBio.01219-14

Cava, F., and de Pedro, M. A. (2014). Peptidoglycan plasticity in bacteria: emerging variability of the murein sacculus and their associated biological functions. *Curr. Opin. Microbiol.* 18, 46–53. doi: 10.1016/j.mib.2014.01.004

Charbon, G., Cabeen, M. T., and Jacobs-Wagner, C. (2009). Bacterial intermediate filaments: *in vivo* assembly, organization, and dynamics of crescentin. *Genes Dev.* 23, 1131–1144. doi: 10.1101/gad.1795509

Chauhan, A., Lofton, H., Maloney, E., Moore, J., Fol, M., Madiraju, M. V. V. S., et al. (2006). Interference of Mycobacterium tuberculosis cell division by Rv2719c, a cell wall hydrolase. *Mol. Microbiol.* 62, 132–147. doi: 10.1111/j.1365-2958.2006.05333.x

Daniel, R. A., and Errington, J. (2003). Control of cell morphogenesis in bacteria. *Cell* 113, 767–776. doi: 10.1016/S0092-8674(03)00421-5

de Pedro, M. A. Quintela, J. C., Höltje, J. V., and Schwarz, H. (1997). Murein segregation in *Escherichia coli*. *J. Bacteriol.* 179, 2823–2834.

Dominguez-Escobar, J., Chastanet, A., Crevenna, A. H., Fromion, V., Wedlich-Soldner, R., and Carballido-Lopez, R. (2011). Processive movement of MreB-associated cell wall biosynthetic complexes in bacteria. *Science* 333, 225–228. doi: 10.1126/science.1203466

Dye, N. A., Pincus, Z., Fisher, I. C., Shapiro, L., and Theriot, J. A. (2011). Mutations in the nucleotide binding pocket of MreB can alter cell curvature and polar morphology in *Caulobacter*: modifying morphology with mutations in mreB. *Mol. Microbiol.* 81, 368–394. doi: 10.1111/j.1365-2958.2011.07698.x

Edgar, R. C. (2004). MUSCLE: multiple sequence alignment with high accuracy and high throughput. *Nucleic Acids Res.* 32, 1792–1797. doi: 10.1093/nar/gkh340

Edwards, D. H., and Errington, J. (1997). The *Bacillus subtilis* DivIVA protein targets to the division septum and controls the site specificity of cell division. *Mol. Microbiol.* 24, 905–915.

Egan, A. J. F., and Vollmer, W. (2013). The physiology of bacterial cell division. *Ann. N. Y. Acad. Sci.* 1277, 8–28. doi: 10.1111/j.1749-6632.2012.06818.x

Erickson, H. P., Anderson, D. E., and Osawa, M. (2010). FtsZ in bacterial cytokinesis: cytoskeleton and force generator all in one. *Microbiol. Mol. Biol. Rev.* 74, 504–528. doi: 10.1128/MMBR.00021-10

Esue, O., Cordero, M., Wirtz, D., and Tseng, Y. (2005). The assembly of MreB, a prokaryotic homolog of actin. *J. Biol. Chem.* 280, 2628–2635. doi: 10.1074/jbc.M410298200

Esue, O., Wirtz, D., and Tseng, Y. (2006). GTPase activity, structure, and mechanical properties of filaments assembled from bacterial cytoskeleton protein MreB. *J. Bacteriol.* 188, 968–976. doi: 10.1128/JB.188.3.968-976.2006

Fenton, A. K., and Gerdes, K. (2013). Direct interaction of FtsZ and MreB is required for septum synthesis and cell division in *Escherichia coli*. *EMBO J.* 32, 1953–1965. doi: 10.1038/emboj.2013.129

Figge, R. M., Divakaruni, A. V., and Gober, J. W. (2004). MreB, the cell shape-determining bacterial actin homologue, co-ordinates cell wall morphogenesis in *Caulobacter crescentus*: MreB-dependent regulation of cell shape. *Mol. Microbiol.* 51, 1321–1332. doi: 10.1111/j.1365-2958.2003.03936.x

Flärdh, K. (2010). Cell polarity and the control of apical growth in *Streptomyces*. *Curr. Opin. Microbiol.* 13, 758–765. doi: 10.1016/j.mib.2010.10.002

Flärdh, K., and Buttner, M. J. (2009). *Streptomyces* morphogenetics: dissecting differentiation in a filamentous bacterium. *Nat. Rev. Microbiol.* 7, 36–49. doi: 10.1038/nrmicro1968

Fleurie, A., Lesterlin, C., Manuse, S., Zhao, C., Cluzel, C., Lavergne, J.-P., et al. (2014). MapZ marks the division sites and positions FtsZ rings in *Streptococcus pneumoniae*. *Nature* 516, 259–262. doi: 10.1038/nature13966

Frandi, A., Jacquier, N., Théraulaz, L., Greub, G., and Viollier, P. H. (2014). FtsZ-independent septal recruitment and function of cell wall remodelling enzymes in chlamydial pathogens. *Nat. Commun.* 5, 4200. doi: 10.1038/ncomms5200

Frirdich, E., and Gaynor, E. C. (2013). Peptidoglycan hydrolases, bacterial shape, and pathogenesis. *Curr. Opin. Microbiol.* 16, 767–778. doi: 10.1016/j.mib.2013.09.005

Fu, G., Huang, T., Buss, J., Coltharp, C., Hensel, Z., and Xiao, J. (2010). *In vivo* structure of the *E. coli* FtsZ-ring revealed by photoactivated localization microscopy (PALM). *PLoS ONE* 5:e12682. doi: 10.1371/journal.pone.0012680

Garner, E. C., Bernard, R., Wang, W., Zhuang, X., Rudner, D. Z., and Mitchison, T. (2011). Coupled, circumferential motions of the cell wall synthesis machinery and MreB filaments in *B. subtilis*. *Science* 333, 222–225. doi: 10.1126/science.1203285

Gitai, Z., Dye, N., and Shapiro, L. (2004). An actin-like gene can determine cell polarity in bacteria. *Proc. Natl. Acad. Sci. U.S.A.* 101, 8643–8648. doi: 10.1073/pnas.0402638101

Goley, E. D., Yeh, Y.-C., Hong, S.-H., Fero, M. J., Abeliuk, E., McAdams, H. H., et al. (2011). Assembly of the *Caulobacter* cell division machine. *Mol. Microbiol.* 80, 1680–1698. doi: 10.1111/j.1365-2958.2011.07677.x

Hale, C. A., Meinhardt, H., and de Boer, P. A. J. (2001). Dynamic localization cycle of the cell division regulator MinE in *Escherichia coli*. *EMBO J.* 20, 1563–1572. doi: 10.1093/emboj/20.7.1563

Hamoen, L. W., and Errington, J. (2003). Polar targeting of DivIVA in *Bacillus subtilis* is not directly dependent on FtsZ or PBP 2B. *J. Bacteriol.* 185, 693–697. doi: 10.1128/JB.185.2.693-697.2003

Harris, L. K., Dye, N. A., and Theriot, J. A. (2014). A *Caulobacter* MreB mutant with irregular cell shape exhibits compensatory widening to maintain a preferred surface area to volume ratio. *Mol. Microbiol.* 94, 988–1005. doi: 10.1111/mmi.12811

Henrichfreise, B., Schiefer, A., Schneider, T., Nzukou, E., Poellinger, C., Hoffmann, T.-J., et al. (2009). Functional conservation of the lipid II biosynthesis pathway in the cell wall-less bacteria Chlamydia and Wolbachia: why is lipid II needed? *Mol. Microbiol.* 73, 913–923. doi: 10.1111/j.1365-2958.2009.06815.x

Holečková, N., Doubravová, L., Massidda, O., Molle, V., Buriánková, K., Benada, O., et al. (2015). LocZ is a new cell division protein involved in proper septum placement in *Streptococcus pneumoniae*. *mBio* 6, e01700–14. doi: 10.1128/mBio.01700-14

Höltje, J.-V. (1998). Growth of the stress-bearing and shape-maintaining murein sacculus of *Escherichia coli*. *Microbiol. Mol. Biol. Rev.* 62, 181–203.

Hughes, H. V., Huitema, E., Pritchard, S., Keiler, K. C., Brun, Y. V., and Viollier, P. H. (2010). Protein localization and dynamics within a bacterial organelle. *Proc. Natl. Acad. Sci. U.S.A.* 107, 5599–5604. doi: 10.1073/pnas.0909119107

Hughes, H. V., Lisher, J. P., Hardy, G. G., Kysela, D. T., Arnold, R. J., Giedroc, D. P., et al. (2013). Co-ordinate synthesis and protein localization in a bacterial organelle by the action of a penicillin-binding-protein. *Mol. Microbiol.* 90, 1162–1177. doi: 10.1111/mmi.12422

Ireland, M. M. E., Karty, J. A., Quardokus, E. M., Reilly, J. P., and Brun, Y. V. (2002). Proteomic analysis of the *Caulobacter crescentus* stalk indicates competence for nutrient uptake. *Mol. Microbiol.* 45, 1029–1041. doi: 10.1046/j.1365-2958.2002.03071.x

Jacquier, N., Frandi, A., Pillonel, T., Viollier, P. H., and Greub, G. (2014). Cell wall precursors are required to organize the chlamydial division septum. *Nat. Commun.* 5, 3578. doi: 10.1038/ncomms4578

Janakiraman, A., and Goldberg, M. B. (2004). Recent advances on the development of bacterial poles. *Trends Microbiol.* 12, 518–525. doi: 10.1016/j.tim.2004.09.003

Jiang, C., Brown, P. J. B., Ducret, A., and Brun, Y. V. (2014). Sequential evolution of bacterial morphology by co-option of a developmental regulator. *Nature* 506, 489–493. doi: 10.1038/nature12900

Jiang, C., Caccamo, P. D., and Brun, Y. V. (2015). Mechanisms of bacterial morphogenesis: evolutionary cell biology approaches provide new insights. *Bioessays* 37, 413–425. doi: 10.1002/bies.201400098

Jones, H. C., and Schmidt, J. M. (1973). Ultrastructural study of crossbands occurring in the stalks of *Caulobacter crescentus*. *J. Bacteriol.* 116, 466–470.

Jung, A., Eisheuer, S., Cserti, E., Leicht, O., Strobel, W., Möll, A., et al. (2014). A molecular toolbox for the genetic manipulation of the stalked budding bacterium *Hyphomonas neptunium*. *Appl. Environ. Microbiol.* 81, 736–744. doi: 10.1128/AEM.03104-14

Kruse, T., Bork-Jensen, J., and Gerdes, K. (2004). The morphogenetic MreBCD proteins of *Escherichia coli* form an essential membrane-bound complex: MreBCD proteins form an essential membrane complex. *Mol. Microbiol.* 55, 78–89. doi: 10.1111/j.1365-2958.2004.04367.x

Kühn, J., Briegel, A., Mörschel, E., Kahnt, J., Leser, K., Wick, S., et al. (2010). Bactofilins, a ubiquitous class of cytoskeletal proteins mediating polar localization of a cell wall synthase in *Caulobacter crescentus*. *EMBO J.* 29, 327–339. doi: 10.1038/emboj.2009.358

Kuru, E., Hughes, H. V., Brown, P. J., Hall, E., Tekkam, S., Cava, F., et al. (2012). *In situ* probing of newly synthesized peptidoglycan in live bacteria with fluorescent D-amino acids. *Angew. Chem. Int. Ed.* 51, 12519–12523. doi: 10.1002/anie.201206749

Laloux, G., and Jacobs-Wagner, C. (2013). Spatiotemporal control of PopZ localization through cell cycle–coupled multimerization. *J. Cell Biol.* 201, 827–841. doi: 10.1083/jcb.201303036

Lam, H., Schofield, W. B., and Jacobs-Wagner, C. (2006). A landmark protein essential for establishing and perpetuating the polarity of a bacterial cell. *Cell* 124, 1011–1023. doi: 10.1016/j.cell.2005.12.040

Lee, T. K., and Huang, K. C. (2013). The role of hydrolases in bacterial cell-wall growth. *Curr. Opin. Microbiol.* 16, 760–766. doi: 10.1016/j.mib.2013.08.005

Li, Z., Trimble, M. J., Brun, Y. V., and Jensen, G. J. (2007). The structure of FtsZ filaments *in vivo* suggests a force-generating role in cell division. *EMBO J.* 26, 4694–4708. doi: 10.1038/sj.emboj.7601895

Liechti, G. W., Kuru, E., Hall, E., Kalinda, A., Brun, Y. V., VanNieuwenhze, M., et al. (2014). A new metabolic cell-wall labelling method reveals peptidoglycan in *Chlamydia trachomatis*. *Nature* 506, 507–510. doi: 10.1038/nature12892

Löwe, J., and Amos, L. A. (1998). Crystal structure of the bacterial cell-division protein FtsZ. *Nature* 391, 203–206. doi: 10.1038/34472

Männik, J., Wu, F., Hol, F. J. H., Bisicchia, P., Sherratt, D. J., Keymer, J. E., et al. (2012). Robustness and accuracy of cell division in *Escherichia coli* in diverse cell shapes. *Proc. Natl. Acad. Sci. U.S.A.* 109, 6957–6962. doi: 10.1073/pnas.1120854109

Margolin, W. (2009). Sculpting the bacterial cell. *Curr. Biol.* 19, R812–R822. doi: 10.1016/j.cub.2009.06.033

Marston, A. L., Thomaides, H. B., Edwards, D. H., Sharpe, M. E., and Errington, J. (1998). Polar localization of the MinD protein of *Bacillus subtilis* and its role in selection of the mid-cell division site. *Genes Dev.* 12, 3419–3430.

McCoy, A. J., and Maurelli, A. T. (2006). Building the invisible wall: updating the chlamydial peptidoglycan anomaly. *Trends Microbiol.* 14, 70–77. doi: 10.1016/j.tim.2005.12.004

Mobley, H. L., Koch, A. L., Doyle, R. J., and Streips, U. N. (1984). Insertion and fate of the cell wall in *Bacillus subtilis*. *J. Bacteriol.* 158, 169–179.

Mohammadi, T., Karczmarek, A., Crouvoisier, M., Bouhss, A., Mengin-Lecreulx, D., and den Blaauwen, T. (2007). The essential peptidoglycan glycosyltransferase MurG forms a complex with proteins involved in lateral envelope growth as well as with proteins involved in cell division in *Escherichia coli*. *Mol. Microbiol.* 65, 1106–1121. doi: 10.1111/j.1365-2958.2007.05851.x

Moore, R. L. (1981). The biology of *Hyphomicrobium* and other prosthecate, budding bacteria. *Annu. Rev. Microbiol.* 35, 567–594. doi: 10.1146/annurev.mi.35.100181.003031

Moore, R., and Hirsch, P. (1973). First generation synchrony of isolated *Hyphomicrobium* swarmer populations. *J. Bacteriol.* 116, 418–423.

Mukherjee, A., and Lutkenhaus, J. (1998). Dynamic assembly of FtsZ regulated by GTP hydrolysis. *EMBO J.* 17, 462–469. doi: 10.1093/emboj/17.2.462

Müller, P., Ewers, C., Bertsche, U., Anstett, M., Kallis, T., Breukink, E., et al. (2007). The essential cell division protein FtsN interacts with the murein (peptidoglycan) synthase PBP1B in *Escherichia coli*. *J. Biol. Chem.* 282, 36394–36402. doi: 10.1074/jbc.M706390200

Ozyamak, E., Kollman, J. M., and Komeili, A. (2013). Bacterial actins and their diversity. *Biochemistry* (*Mosc.*) 52, 6928–6939. doi: 10.1021/bi4010792

Pate, J. L., and Ordal, E. J. (1965). The fine structure of two unusual stalked bacteria. *J. Cell Biol.* 27, 133–150.

Pilhofer, M., Aistleitner, K., Biboy, J., Gray, J., Kuru, E., Hall, E., et al. (2013). Discovery of chlamydial peptidoglycan reveals bacteria with murein sacculi but without FtsZ. *Nat. Commun.* 4:2856. doi: 10.1038/ncomms3856

Pilhofer, M., Rappl, K., Eckl, C., Bauer, A. P., Ludwig, W., Schleifer, K. -H., et al. (2008). Characterization and evolution of cell division and cell wall synthesis genes in the bacterial phyla verrucomicrobia, lentisphaerae, chlamydiae, and planctomycetes and phylogenetic comparison with rRNA genes. *J. Bacteriol.* 190, 3192–3202. doi: 10.1128/JB.01797-07

Pinho, M. G., Kjos, M., and Veening, J. -W. (2013). How to get (a)round: mechanisms controlling growth and division of coccoid bacteria. *Nat. Rev. Microbiol.* 11, 601–614. doi: 10.1038/nrmicro3088

Poindexter, J. L. S., and Cohen-Bazire, G. (1964). The fine structure of stalked bacteria belonging to the family *Caulobacteraceae*. *J. Cell Biol.* 23, 587–607. doi: 10.1083/jcb.23.3.587

Poindexter, J. S. (1964). Biological properties and classification of the *Caulobacter* group1. *Bacteriol. Rev.* 28, 231–295.

Poindexter, J. S. (1978). Selection for nonbuoyant morphological mutants of *Caulobacter crescentus*. *J. Bacteriol.* 135, 1141–1145.

Poindexter, J. S., and Staley, J. T. (1996). *Caulobacter* and *Asticcacaulis* stalk bands as indicators of stalk age. *J. Bacteriol.* 178, 3939–3948.

Potluri, L. -P., Kannan, S., and Young, K. D. (2012). ZipA is required for FtsZ-dependent preseptal peptidoglycan Synthesis prior to Invagination during cell division. *J. Bacteriol.* 194, 5334–5342. doi: 10.1128/JB.00859-12

Priyadarshini, R., de Pedro, M. A., and Young, K. D. (2007). Role of peptidoglycan amidases in the development and morphology of the division septum in *Escherichia coli*. *J. Bacteriol.* 189, 5334–5347. doi: 10.1128/JB.00415-07

Ptacin, J. L., Gahlmann, A., Bowman, G. R., Perez, A. M., Diezmann, A. R. S., von, Eckart, M. R., et al. (2014). Bacterial scaffold directs pole-specific centromere segregation. *Proc. Natl. Acad. Sci. U.S.A.* 111, E2046–E2055. doi: 10.1073/pnas.1405188111

Radhakrishnan, S. K., Thanbichler, M., and Viollier, P. H. (2008). The dynamic interplay between a cell fate determinant and a lysozyme homolog drives the asymmetric division cycle of *Caulobacter crescentus*. *Genes Dev.* 22, 212–225. doi: 10.1101/gad.1601808

Raskin, D. M., and de Boer, P. A. J. (1999). Rapid pole-to-pole oscillation of a protein required for directing division to the middle of *Escherichia coli*. *Proc. Natl. Acad. Sci. U.S.A.* 96, 4971–4976.

Salje, J., van den Ent, F., de Boer, P., and Löwe, J. (2011). Direct membrane binding by bacterial actin MreB. *Mol. Cell* 43, 478–487. doi: 10.1016/j.molcel.2011.07.008

Schiffer, G., and Höltje, J. V. (1999). Cloning and characterization of PBP 1C, a third member of the multimodular class A penicillin-binding proteins of *Escherichia coli*. *J. Biol. Chem.* 274, 32031–32039.

Schlaeppi, J. M., Schaefer, O., and Karamata, D. (1985). Cell wall and DNA cosegregation in *Bacillus subtilis* studied by electron microscope autoradiography. *J. Bacteriol.* 164, 130–135.

Schlimpert, S., Klein, E. A., Briegel, A., Hughes, V., Kahnt, J., Bolte, K., et al. (2012). General protein diffusion barriers create compartments within bacterial cells. *Cell* 151, 1270–1282. doi: 10.1016/j.cell.2012.10.046

Schmidt, J. M., and Stanier, R. Y. (1966). The development of cellular stalks in bacteria. *J. Cell Biol.* 28, 423–436.

Seitz, L. C., and Brun, Y. V. (1998). Genetic analysis of mecillinam-resistant mutants of *Caulobacter crescentus* deficient in stalk biosynthesis. *J. Bacteriol.* 180, 5235–5239.

Sham, L.-T., Tsui, H.-C. T., Land, A. D., Barendt, S. M., and Winkler, M. E. (2012). Recent advances in pneumococcal peptidoglycan biosynthesis suggest new vaccine and antimicrobial targets. *Curr. Opin. Microbiol.* 15, 194–203. doi: 10.1016/j.mib.2011.12.013

Shiomi, D., Sakai, M., and Niki, H. (2008). Determination of bacterial rod shape by a novel cytoskeletal membrane protein. *EMBO J.* 27, 3081–3091. doi: 10.1038/emboj.2008.234

Specht, M., Schätzle, S., Graumann, P. L., and Waidner, B. (2011). *Helicobacter pylori* possesses four coiled-coil-rich proteins that form extended filamentous structures and control cell shape and motility. *J. Bacteriol.* 193, 4523–4530. doi: 10.1128/JB.00231-11

Stamatakis, A. (2006). RAxML-VI-HPC: maximum likelihood-based phylogenetic analyses with thousands of taxa and mixed models. *Bioinforma. Oxf. Engl.* 22, 2688–2690. doi: 10.1093/bioinformatics/btl446

Stephens, R. S., Kalman, S., Lammel, C., Fan, J., Marathe, R., Aravind, L., et al. (1998). Genome sequence of an obligate intracellular pathogen of humans: *Chlamydia trachomatis*. *Science* 282, 754–759.

Strauss, M. P., Liew, A. T. F., Turnbull, L., Whitchurch, C. B., Monahan, L. G., and Harry, E. J. (2012). 3D-SIM super resolution microscopy reveals a bead-like arrangement for FtsZ and the division machinery: implications for triggering cytokinesis. *PLoS Biol.* 10:e1001389. doi: 10.1371/journal.pbio.1001389

Strobel, W., Möll, A., Kiekebusch, D., Klein, K. E., and Thanbichler, M. (2014). Function and localization dynamics of bifunctional penicillin-binding proteins in *Caulobacter crescentus*. *J. Bacteriol.* 196, 1627–1639. doi: 10.1128/JB.01194-13

Sycuro, L. K., Pincus, Z., Gutierrez, K. D., Biboy, J., Stern, C. A., Vollmer, W., et al. (2010). Peptidoglycan crosslinking relaxation promotes *Helicobacter pylori*'s helical shape and stomach colonization. *Cell* 141, 822–833. doi: 10.1016/j.cell.2010.03.046

Sycuro, L. K., Rule, C. S., Petersen, T. W., Wyckoff, T. J., Sessler, T., Nagarkar, D. B., et al. (2013). Flow cytometry-based enrichment for cell shape mutants identifies multiple genes that influence *Helicobacter pylori* morphology. *Mol. Microbiol.* 90, 869–883. doi: 10.1111/mmi.12405

Sycuro, L. K., Wyckoff, T. J., Biboy, J., Born, P., Pincus, Z., Vollmer, W., et al. (2012). Multiple peptidoglycan modification networks modulate *Helicobacter pylori*'s cell shape, motility, and colonization potential. *PLoS Pathog.* 8:e1002603. doi: 10.1371/journal.ppat.1002603

Szwedziak, P., and Löwe, J. (2013). Do the divisome and elongasome share a common evolutionary past? *Curr. Opin. Microbiol.* 16, 745–751. doi: 10.1016/j.mib.2013.09.003

Szwedziak, P., Wang, Q., Bharat, T. A. M., Tsim, M., and Löwe, J. (2014). Architecture of the ring formed by the tubulin homologue FtsZ in bacterial cell division. *eLife* 3, e04601. doi: 10.7554/eLife.04601

Thanbichler, M., and Shapiro, L. (2006). MipZ, a spatial regulator coordinating chromosome segregation with cell division in *Caulobacter*. *Cell* 126, 147–162. doi: 10.1016/j.cell.2006.05.038

Trueba, F. J. (1982). On the precision and accuracy achieved by *Escherichia coli* cells at fission about their middle. *Arch. Microbiol.* 131, 55–59. doi: 10.1007/BF00451499

Typas, A., Banzhaf, M., Gross, C. A., and Vollmer, W. (2012). From the regulation of peptidoglycan synthesis to bacterial growth and morphology. *Nat. Rev. Microbiol.* 10, 123–136. doi: 10.1038/nrmicro2677

Umeda, A., and Amako, K. (1983). Growth of the surface of *Corynebacterium diphtheriae*. *Microbiol. Immunol.* 27, 663–671. doi: 10.1111/j.1348-0421.1983.tb00629.x

Ursell, T. S., Nguyen, J., Monds, R. D., Colavin, A., Billings, G., Ouzounov, N., et al. (2014). Rod-like bacterial shape is maintained by feedback between cell curvature and cytoskeletal localization. *Proc. Natl. Acad. Sci. U.S.A.* 111, E1025–E1034. doi: 10.1073/pnas.1317174111

van den Ent, F., Leaver, M., Bendezu, F., Errington, J., de Boer, P., and Löwe, J. (2006). Dimeric structure of the cell shape protein MreC and its functional implications. *Mol. Microbiol.* 62, 1631–1642. doi: 10.1111/j.1365-2958.2006.05485.x

van Teeffelen, S., Wang, S., Furchtgott, L., Huang, K. C., Wingreen, N. S., Shaevitz, J. W., et al. (2011). The bacterial actin MreB rotates, and rotation depends on cell-wall assembly. *Proc. Natl. Acad. Sci. U.S.A.* 108, 15822–15827. doi: 10.1073/pnas.1108999108

Vollmer, W., Blanot, D., and de Pedro, M. A. (2008a). Peptidoglycan structure and architecture. *FEMS Microbiol. Rev.* 32, 149–167. doi: 10.1111/j.1574-6976.2007.00094.x

Vollmer, W., Joris, B., Charlier, P., and Foster, S. (2008b). Bacterial peptidoglycan (murein) hydrolases. *FEMS Microbiol. Rev.* 32, 259–286. doi: 10.1111/j.1574-6976.2007.00099.x

Wagner, J. K., and Brun, Y. V. (2007). Out on a limb: how the *Caulobacter* stalk can boost the study of bacterial cell shape. *Mol. Microbiol.* 64, 28–33. doi: 10.1111/j.1365-2958.2007.05633.x

Wagner, J. K., Galvani, C. D., and Brun, Y. V. (2005). *Caulobacter crescentus* requires RodA and MreB for stalk synthesis and prevention of ectopic pole formation. *J. Bacteriol.* 187, 544–553. doi: 10.1128/JB.187.2.544-553.2005

Wagner, J. K., Setayeshgar, S., Sharon, L. A., Reilly, J. P., and Brun, Y. V. (2006). A nutrient uptake role for bacterial cell envelope extensions. *Proc. Natl. Acad. Sci. U.S.A.* 103, 11772–11777. doi: 10.1073/pnas.0602047103

Waidner, B., Specht, M., Dempwolff, F., Haeberer, K., Schaetzle, S., Speth, V., et al. (2009). A novel system of cytoskeletal elements in the human pathogen *Helicobacter pylori*. *PLoS Pathog.* 5:e1000669. doi: 10.1371/journal.ppat.1000669

Whittenbury, R., and Dow, C. S. (1977). Morphogenesis and differentiation in Rhodomicrobium vannielii and other budding and prosthecate bacteria. *Bacteriol. Rev.* 41, 754–808.

Willemse, J., Borst, J. W., de Waal, E., Bisseling, T., and van Wezel, G. P. (2011). Positive control of cell division: FtsZ is recruited by SsgB during sporulation of *Streptomyces*. *Genes Dev.* 25, 89–99. doi: 10.1101/gad.600211

Wu, L. J., and Errington, J. (2004). Coordination of cell division and chromosome segregation by a nucleoid occlusion protein in *Bacillus subtilis*. *Cell* 117, 915–925. doi: 10.1016/j.cell.2004.06.002

Yakhnina, A. A., and Gitai, Z. (2013). Diverse functions for six glycosyltransferases in *Caulobacter crescentus* cell wall assembly. *J. Bacteriol.* 195, 4527–4535. doi: 10.1128/JB.00600-13

Young, K. D. (2006). The selective value of bacterial shape. *Microbiol. Mol. Biol. Rev.* 70, 660–703. doi: 10.1128/MMBR.00001-06

Young, K. D. (2010). Bacterial shape: two-dimensional questions and possibilities. *Annu. Rev. Microbiol.* 64, 223–240. doi: 10.1146/annurev.micro.112408.134102

Yu, X. C., and Margolin, W. (1999). FtsZ ring clusters in min and partition mutants: role of both the Min system and the nucleoid in regulating FtsZ ring localization. *Mol. Microbiol.* 32, 315–326.

Conflict of Interest Statement: The authors declare that the research was conducted in the absence of any commercial or financial relationships that could be construed as a potential conflict of interest.

Copyright © 2015 Randich and Brun. This is an open-access article distributed under the terms of the Creative Commons Attribution License (CC BY). The use, distribution or reproduction in other forums is permitted, provided the original author(s) or licensor are credited and that the original publication in this journal is cited, in accordance with accepted academic practice. No use, distribution or reproduction is permitted which does not comply with these terms.

frontiers in Microbiology

REVIEW
published: 08 May 2015
doi: 10.3389/fmicb.2015.00449

Structural constraints and dynamics of bacterial cell wall architecture

*Miguel A. de Pedro[1,2] and Felipe Cava[2]**

[1] Centro de Biología Molecular "Severo Ochoa" – Consejo Superior de Investigaciones Científicas, Universidad Autónoma de Madrid, Madrid, Spain, [2] Laboratory for Molecular Infection Medicine Sweden, Department of Molecular Biology, Umeå Center for Microbial Research, Umeå University, Umeå, Sweden

The peptidoglycan wall (PG) is a unique structure which confers physical strength and defined shape to bacteria. It consists of a net-like macromolecule of peptide interlinked glycan chains overlying the cell membrane. The structure and layout of the PG dictates that the wall has to be continuously modified as bacteria go through division, morphological differentiation, and adaptive responses. The PG is poorly known in structural terms. However, to understand morphogenesis a precise knowledge of glycan strand arrangement and of local effects of the different kinds of subunits is essential. The scarcity of data led to a conception of the PG as a regular, highly ordered structure which strongly influenced growth models. Here, we review the structure of the PG to define a more realistic conceptual framework. We discuss the consequences of the plasticity of murein architecture in morphogenesis and try to define a set of minimal structural constraints that must be fulfilled by any model to be compatible with present day information.

Keywords: cell wall, peptidoglycan, structure, cross-link, chain length, HPLC, muropeptides

OPEN ACCESS

Edited by:
Arieh Zaritsky, Ben-Gurion University of the Negev, Israel

Reviewed by:
Waldemar Vollmer, Newcastle University, UK
Kevin D. Young, University of Arkansas for Medical Sciences, USA

****Correspondence:***
Felipe Cava, Laboratory for Molecular Infection Medicine Sweden, Department of Molecular Biology, Umeå Center for Microbial Research, Umeå University, 90187 Umeå, Sweden
felipe.cava@molbiol.umu.se

Specialty section:
This article was submitted to Microbial Physiology and Metabolism, a section of the journal Frontiers in Microbiology

Received: *05 March 2015*
Accepted: *25 April 2015*
Published: *08 May 2015*

Citation:
de Pedro MA and Cava F (2015) Structural constraints and dynamics of bacterial cell wall architecture. Front. Microbiol. 6:449. doi: 10.3389/fmicb.2015.00449

Introduction

The bacterial cell wall was first described as a region of specific staining behavior wrapping the cell body (Churchman, 1927). This structure was soon associated with the processes of cell division and growth (Knaysi, 1930, 1941). Introduction of electron microscopy in conjunction with the development of cell wall purification methods, demonstrated the ability of purified walls to retain cell shape (Salton and Horne, 1951a,b), and characterized cell walls as mesh bag-like macromolecules called sacculi (from the Latin for small bags, sing. sacculus; Weidel et al., 1960). These early techniques were also critical to define the glyco-peptidic nature of the cell wall, which became also known as the peptidoglycan (PG) layer, and led to the establishment of its polymeric nature (Salton, 1952, 1953, 1956, 1960; Weidel, 1960; Primosigh et al., 1961; Salton, 1961; Weidel and Pelzer, 1964). Schleifer and Kandler (1972) neatly summarized the knowledge on the structure of bacterial walls accumulated until the early 1970s and sort of wrote in stone most of the basic notions that still hold today, namely: the universality of the basic structural subunit; the long-glycan/short peptide idea; the chemical uniformity of PG and its planar, ordered, net-like organization in Gram-negative bacteria, among others. Unavoidably, some of these ideas derived into a geometric and static perception of the PG layer as depicted in so many articles and textbooks.

An aspect of PG studies important to stress at an early point is quantification. Most studies present the abundance of the individual kinds of PG subunits (muropeptides) as a percentage of the total number because this makes measurements independent of the absolute amount of sample. However, this practice makes it easy to underestimate the relevance of minor components.

The amount of PG in an *Escherichia coli* cell is around 3.5×10^6 monomeric units (Wientjes et al., 1991). Therefore, values as low as 0.1% mean that each cell has about 3×10^3 molecules of that particular muropeptide, a meaningful number on biological terms.

Here, we will review the experimental evidence accumulated on PG structure and metabolism in an attempt to define a series of basic structural constraints that can help us to revisit current models of the bacterial cell wall. In this study we will center on the features of Gram-negatives because of the relative abundance of studies, and the (apparently) simpler organization of their sacculi. However, most of the information available comes from a very limited number of bacterial species and generalizations have to be taken with great precaution. Particular emphasis will be made on the influence of individual muropeptides on local structure and on how subtle changes in the subunits might influence the properties of the cell wall.

The Structure of the PG Monomers and Linear Polymers

The primary structure of PG monomers was defined in the early 1960s and it was soon found out that most Gram-negatives shared as common basic subunit the disaccharide pentapeptide: GlcNAc-(β,1⟶4)MurNAc-(L)ala-(D)glu-(γ)-(*meso*)Dap-(D)ala-(D)ala (M5; Schleifer and Kandler, 1972). The monomeric subunit might suffer a number of chemical modifications, but in most instances, the alternancy of L- and D-amino acids, as well as the presence of a terminal D-ala-D-ala dipeptide is respected (Vollmer, 2008; Vollmer et al., 2008).

The PG monomer is a molecule with rather unusual biochemical and structural properties (**Figure 1A**) that, according to molecular modeling studies, results in the peptide moiety adopting a curled, compact disposition with the terminal D-ala interacting with the L-ala at position 2 by means of hydrogen bonds (**Figure 1B**; Barnickel et al., 1979; Meroueh et al., 2006; Gumbart et al., 2014). This disposition of the amino acid residues means that the stem peptides can potentially span considerably larger distances, from *ca.* 10 Å up to *ca.* 25 Å when stretched (up to 2.5 fold), as predicted by molecular modeling (Barnikel et al., 1983).

Although some species as *Caulobacter crescentus* retain the terminal D-ala-D-ala in a high proportion of PG subunits (Takacs et al., 2010), most species contain mostly tetrapeptides and tripeptides following the sequential elimination of the D-ala residues to variable extents (Quintela et al., 1995). The kinetics of elimination of the terminal D-ala have been measured in *E. coli* (Glauner and Höltje, 1990). Assuming every monomer is added as a pentapeptide, nascent PG accumulated for as little as 20 s exhibits only about 25% pentapeptides, 60 s later it drops to about 5% and in a further few minutes goes well below 0.5%. As the terminal D-ala is required for the polymerization of PG the modified muropeptides are disabled to act as donors in DD-transpeptidation reactions (see below). Elimination of the terminal D-ala also affects folding of the stem peptides favoring a more extended conformation and displacements of the potential NH_2 acceptor sites in the *(meso)*DAP residue (**Figure 2**).

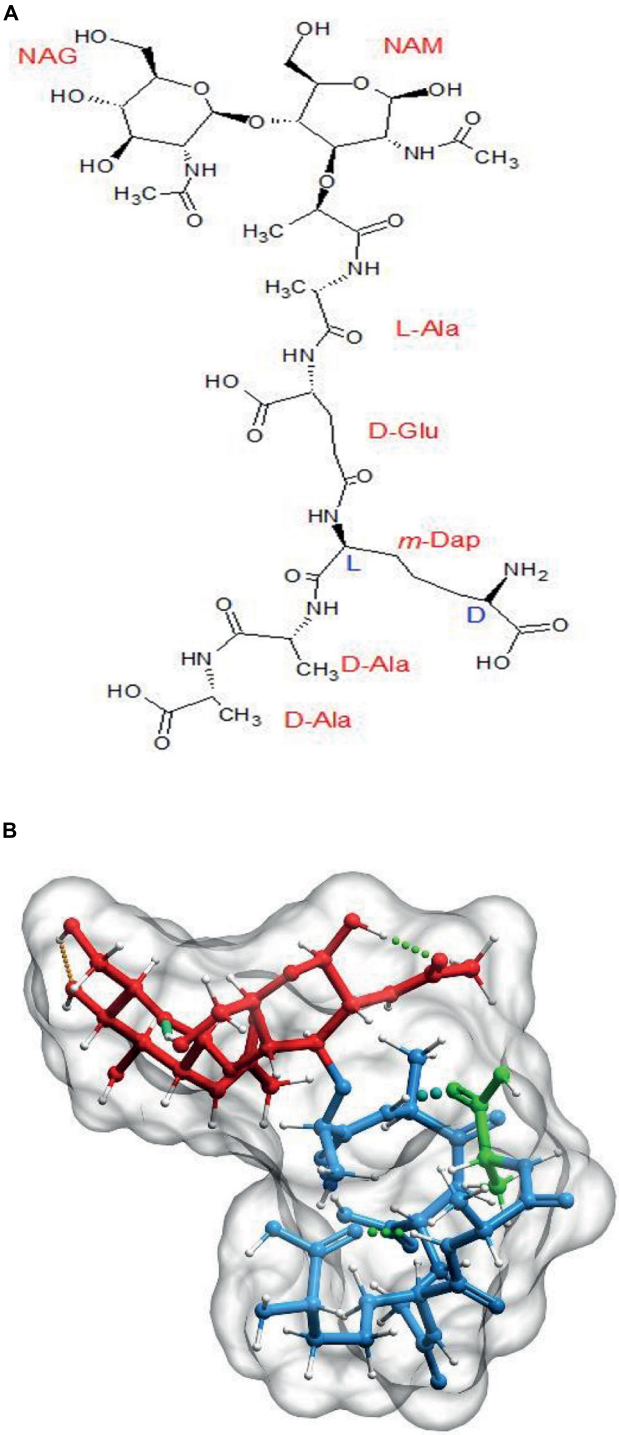

FIGURE 1 | The basic PG subunit. (A) Explicit formula for *N*-acetyl-glucosaminyl-(β,1⟶4)-*N*-acetyl-muramyl-L-Alanyl-D-Glutaminyl(γ)-L-*(meso)*diaminopimelyl-D-alanyl-D-alanine (disaccharide–pentapeptide or M5). **(B)** Computer generated 3D representation of the same molecule after energy optimization. Red signals the glycan part, blue the stem peptide and green the terminal D-ala residue. Molecules were generated with Chemsketch (http://www.acdlabs.com/resources/freeware/chemsketch/), subjected to geometry and molecular mechanics optimization with Avogadro

(continued)

FIGURE 1 | Continued

software (http://avogadro.cc/) using the MMFF94s field force, the steepest descent algorithm and a convergence of 10^{-7}. Muropeptides were modeled in the absence of solvent. The optimized molecular structure was visualized and prepared for publication with Molsoft ICM software (http://www.molsoft.com/).

In order to weave the polymeric cell wall the subunits must first form linear polymers, a reaction performed by bifunctional DD-transpeptidase-transglycosylase enzymes, the Class A Penicillin-Binding Proteins (PBP's; Typas et al., 2012). The polymerization reaction happens in the periplasmic space and occurs by the transfer of a molecule of the activated precursor M5-P-Bactoprenol (lipid-II) to the C_4-OH of the GlcNAc moiety in a second lipid-II molecule to generate a (β, 1⟶4) glycosidic bond (van Heijenoort, 2001). The growing glycan is then reiteratively transferred to new molecules of lipid-II causing longitudinal extension of the PG strand. The mechanism for the termination and release of newly made glycan strands remains unclear. In most bacteria, glycan strands display a molecule of (1⟶6) anhydro MurNAc (Anh-MurNAc) as the C1 terminal sugar, suggesting the participation of a transglycosylase activity in the process. However, there is no reason to discard the existence of alternative mechanisms. Indeed, *Agrobacterium tumefaciens* and *Mesorhizobium meliloti* either lack Anh-MurNAc or have amounts undetectable by HPLC and MALDI-MS techniques (Quintela et al., 1995; Brown et al., 2012).

The sugar backbone of a PG linear polymer tends to adopt a right-handed helical structure (Leps et al., 1987; Meroueh et al., 2006; Gumbart et al., 2014). Calculations derived from actual NMR analysis of a linear dimer indicate three disaccharides per turn with consecutive subunits at roughly 120°, and a pitch of *ca.* 3 nm (**Figure 3B**; Meroueh et al., 2006; Gumbart et al., 2014) although a certain degree of variation in the helicity looks likely (Gumbart et al., 2014). This disposition implies that in a state of minimal energy, the sugar backbone is almost fully stretched, therefore when subjected to tensile forces the glycan polymer remains essentially unyielding. This fact contrasts with the relaxed disposition of the peptide moieties and makes the cell wall anisotropic respect to some properties (Gumbart et al., 2014). **Figure 3**, shows a likely conformation for a linear dodecamer as calculated by computer modeling. Other than the compact disposition of the stem peptides, is interesting to note that the critical regions, the D-ala-D-ala dipeptides and the D-NH_2 groups of (*meso*)DAP molecules, involved in the all-important cross-linking reactions occupy rather accessible positions at the surface of the molecule (**Figure 3B**).

Length of Glycan Strands

Length of the glycan strands is an important structural parameter of PG. Because the glycan backbone of PG strands is inextensible, the longer the strands the more rigid the structure of the sacculus. The PG can be compared to a composite material in that the global properties of the structure depend to

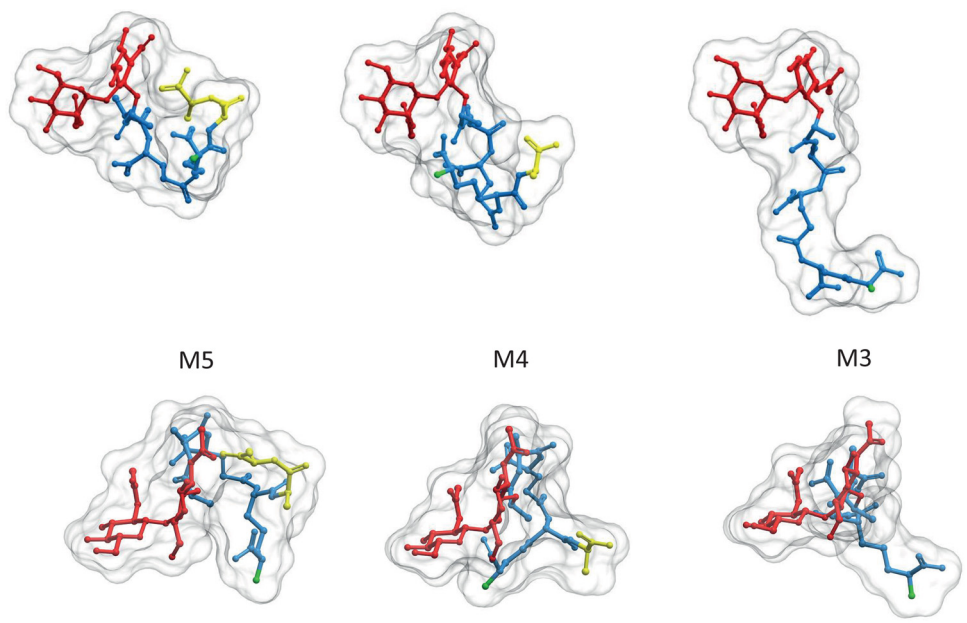

FIGURE 2 | Elimination of the terminal D-ala residue has strong influence on the 3D structure of PG subunits. PG monomeric subunits derived from the M5 by elimination of the terminal D-ala (M4) or the terminal D-ala-D-ala (M3) are compared in two orientations, transversal to (upper panel) and from above (lower panel) the surface of the sacculus. To facilitate comparison muropeptides were rotated until GlcNAc residues overlap. Red designates the glycan moiety and blue the stem peptide. Terminal D-ala residues are highlighted in yellow. The 3D structures were calculates as in **Figure 1**. Hydrogen atoms were removed in the image, but considered for the calculation of the molecular surface.

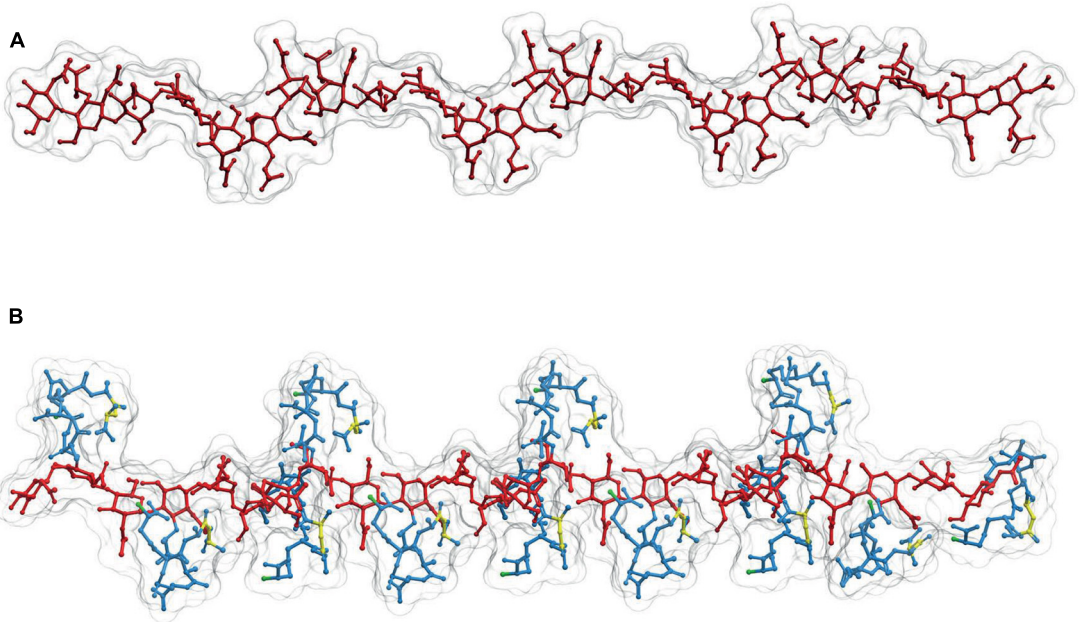

FIGURE 3 | Structure of linear PG polymers. (A) Sugar backbone for a 12-mer linear PG polymer, with a helical pitch of three subunits/turn. The backbone is derived from the structure of **(B)** a PG strand made up of 12 M5 subunits. Red designates the glycan moiety and blue the stem peptides. The D-ala-D-ala dipeptides are highlighted in yellow, and the *(meso)*DAP free NH_2 groups in green. The 3D structures were calculated as in **Figures 1** and **2**.

a large extent on the length, orientation, and bonding of the fibers.

Because of the specific presence of Anh-MurNAc at the glycan ends (van Heijenoort, 2001), it is possible to calculate experimentally the average length (AL) of PG strands as the inverse of the molar fraction of Anh-MurNAc-containing subunits in the PG (Glauner, 1988). Available information supports a large variability in the AL of glycan strands amongst different bacteria. In *E. coli* the AL for cells actively growing in rich media is around 30 monomers/strand (M/S; Glauner et al., 1988). Most Gram-negatives analyzed so far fall in the 20–100 M/S range with a preference for the lower values (10–40 M/S). However, values lower than 10 M/S have been measured in *C. crescentus* and *Helicobacter pylori* (Costa et al., 1999; Takacs et al., 2010). AL is not constant but strongly influenced by the state of growth (Pisabarro et al., 1985; Lam et al., 2009; Cava et al., 2011), and by mutational or chemical alterations of cell wall metabolism (Romeis et al., 1991; Varma et al., 2007). In *E. coli* growth arrest causes a progressive reduction in AL (25–30%) until a constant value is reached in resting cells. Resumption of growth is accompanied by a progressive rise in AL which reaches its characteristic value after 2–3 doublings in mass. However, measurements of AL in newly made *vs.* total PG in *E. coli*, showed that AL was essentially constant for the new PG made during the transitions (Pisabarro et al., 1985). These observations support the idea that AL variations are not due to a change in the frequency of glycan chain terminating events, but rather to processing of macromolecular PG. Therefore, bacteria must have some modulatory mechanisms able to modify the AL of PG in response to environmental conditions.

An important aspect is that although the length of average PG strands (∼10–100 nm) is very small when compared to the dimensions of the cell, in most cases the strands are considerably longer than the thickness of the sacculus, which is between 2.5 and 7 nm for hydrated sacculi (Yao et al., 1999).

Although AL certainly gives important structural information, it is the distribution of glycan chain lengths that really influences the properties of the sacculus. However, experimental determination of length distributions has been achieved in a very limited number of cases. The only extensive study was performed in *E. coli* (Harz et al., 1990). Whether or not the information obtained is representative for other bacteria is uncertain. The analysis showed a very wide and positively skewed size distribution with a modal value of eight M/S (Harz et al., 1990). However, this distribution only accounts for about 70% of the total PG. The remaining 30% could not be resolved into individual length classes but presents an AL equivalent of 45 M/S (Harz et al., 1990). At present, there are no data to choose a particular distribution of lengths for the longer fraction. However, as the shorter strands have to be at least 31 disaccharides long, and the AL is 45, the existence of extremely long (>500 disaccharides or roughly 500 nm) glycans is not very likely. The determination of both the AL and length distribution indicates that the sacculus is mostly made of rather short glycan strands but covering a very wide range of lengths, an aspect often neglected in cell wall models.

There have been a limited number of attempts to study how different conditions affect the glycan strand length distribution (Romeis et al., 1991; Obermann and Holtje, 1994; Ishidate et al.,

1998; Ursinus et al., 2004). Particularly interesting is the comparison of regular rods and mini-cells in a mini-cell producing *E. coli* mutant (Obermann and Holtje, 1994). The results showed moderately shorter strands in the mini-cells with a reduction in AL from 28 to 25 M/S and a drift toward shorter lengths in the size distribution. A similar study performed with *E. coli* cell division mutants is also enlightening about local variations in glycan length distributions (Ishidate et al., 1998). This study showed that PG associated with the initiation of septation is likely made of relatively long glycan strands, and interestingly, the cell division protein FtsN requires strands >25 M/S to interact with septal PG (Ursinus et al., 2004).

Most of the information above is consistent with the existence of mechanisms able to make glycan strands of adequate lengths as a function of environmental conditions and surface topology.

Cross-Linking of Glycan Strands

Formation of the sacculus requires glycan strands to be cross-linked to each other in a net-like fashion. Cross-linking is catalyzed by specific peptidyl-transferases which are able to transfer a peptide bond from a stem peptide (donor) to the free NH_2 group at the D-center of the *(meso)*DAP residue of a second stem peptide (acceptor) from a nearby glycan strand. Most bacteria are capable of cross-linking reactions mediated by DD-transpeptidase activities residing in the bifunctional class A PBPs (Typas et al., 2012). These enzymes catalyze the transfer of the peptide bond linking the two terminal D-ala residues of the donor moiety, to generate a new peptide bond with a DD configuration. DD-transpeptidation seems to be a universal mechanism to interlink glycan strands, but it is not necessarily unique. Indeed, a few alternative cross-linking reactions have been described (Vasstrand et al., 1982; Glauner et al., 1988; Boniface et al., 2009; Bui et al., 2009). The more extended "accessory" cross-linking reaction is mediated by LD-peptidyl transferases (LD-TPases) which transfer the L–D peptide bond between the L-center of *(meso)*DAP and the D-ala at position 4 in the donor stem peptide to the NH_2 group of the acceptor *(meso)*DAP (the very same as for the DD-reaction), generating a L-*(meso)*DAP → D-*(meso)*DAP peptide bond (Glauner and Höltje, 1990). LD-TPases are monofunctional enzymes, structurally unrelated to the PBPs, and are involved in a number of functions such as attachment of PG-bound lipoprotein (Magnet et al., 2007) and incorporation of D-amino acids (Cava et al., 2011). Although *E. coli* and most other Gram-negatives that have been analyzed have both kinds of cross-links, LD cross-linking is neither universal (Cava et al., 2011) nor essential for bacteria with both LD and DD cross-linkage (Magnet et al., 2008; Cava et al., 2011). The relative abundances of LD and DD cross-linking are very variable, but in some species can be equally abundant (Lavollay et al., 2008; Brown et al., 2012). Why some species have both kinds of cross-links is not clear yet. The fact that LD-enzymes are, in most cases, insensitive to beta-lactams has led to the proposal of LD-cross-links as contributors to escape antibiotic action (Gupta et al., 2010).

DD cross-linking of new strands is coupled to linear polymerization and is the reaction responsible for the incorporation of nascent strands into the sacculus. Indeed, analysis of nascent PG shows that right after incorporation, the new material already exhibits a content of DD-cross-links that is close to the average value for total PG (Glauner and Höltje, 1990). However, LD cross-links are initially absent (or below experimental detection limits) and then increase in a progressive way as PG ages (typically hours). This difference in kinetics supports the idea that LD cross-links are not involved primarily in the insertion of new precursors, but rather as part of PG maturation (Glauner and Höltje, 1990; Brown et al., 2012). However, LD-TPases involved in LD cross-linking work preferentially on those regions where incorporation of precursors occurs (Kuru et al., 2012; Siegrist et al., 2013), suggesting a close association between PG synthesis and LD-TPase activity. These considerations suggest that LD cross-links are an accessory feature of PG and may play important physiological and structural functions, particularly in those species where they are more abundant (Cameron et al., 2014).

Comparison of computer models suggests important differences between LD and DD cross-links. The absence of the D-ala residue linking the two *(meso)*DAP molecules in LD cross-links makes the stem peptide more rigid, with a more extended conformation reaching a longer distance than the equivalent DD cross-link (1 nm *vs.* 0.7 nm distance between the MurNAc-C3 carbons of each strand, respectively; **Figure 4**). The possibility of additional hydrogen bonds in the DD cross-links affects the preferred orientations of the disaccharide moieties, and favors a more compact folding of the stem peptides. These differences imply that each kind of cross-link might fit optimally into subtly different relative orientations and distances between the glycans, and that local accumulations of one or the other crosslink should influence the local properties of PG differently. The longer range of LD cross-links might be especially well suited to connect glycans which are already under stress, as expected from the apparently post-insertional nature of this kind of cross-linkage.

Cross-linking most frequently takes place between the stem peptides of muropeptides belonging to two glycan strands. However, in a variable but often considerable number of cases, three or, more rarely, four glycan strands become interconnected by their stem peptides generating cross-linked trimers and tetramers, respectively (**Figure 5**). Cross-linked trimers seem to be rather universal and have been detected in most Gram-negatives studied in relatively high proportions. Cross-linked tetramers are rarer than trimers. In most cases tetramers are not detected, but in a few instances sizable amounts have been measured, as in the case of *C. crescentus* (Takacs et al., 2010). Most abundant trimers are fully DD cross-linked. However, smaller amounts of hybrid (DD plus LD) and full LD cross-linked trimers are present in PG from bacteria able to LD cross-link PG (Glauner and Höltje, 1990; Brown et al., 2012).

According to Glauner and Höltje (1990), in *E. coli* DD trimers are readily detected in nascent PG with an age of 1 min. As the proportion of trimers in PG is rather low (about

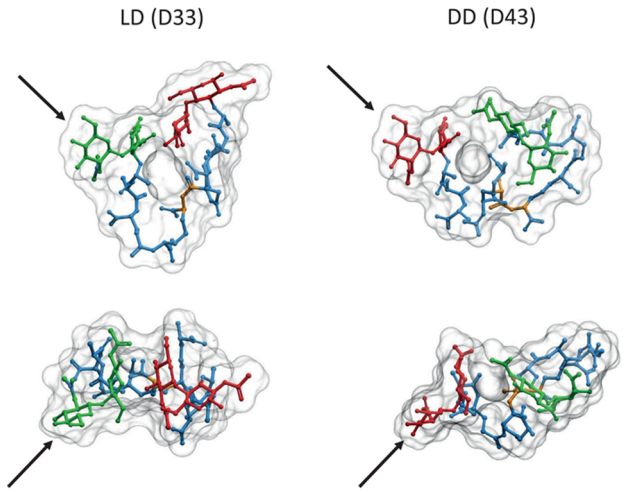

FIGURE 4 | Comparison of LD and DD cross-linked PG dimers. 3D representations of molecules from the LD cross-linked *bis*-disaccharide-tripeptide (D33), and the DD cross-linked disaccharide-tetrapeptide-disaccharide-tripeptide (D43) dimers were generated as described in **Figures 1** and **2**. Upper images correspond to a transversal view, and lower images to a view from above. Each pair was oriented according to the GlcNAc residues indicated by the black arrows. Red, green, and blue designate the disaccharide for the donor moiety, the disaccharide for the acceptor moiety and the stem peptide, respectively. Yellow highlights the position of the cross-link. Note the inverted orientation predicted for the donor and acceptor moieties.

3–4% of total muropeptides), this supports the idea of DD-trimers being synthesized concomitantly with the incorporation of new glycans into the pre-existing PG fabric. This is further supported by the kinetics of D-ala-D-ala elimination from nascent PG. Formation of DD-trimers should depend on the presence of subunits with a pentapeptide stem peptide in the donor moiety. The terminal D-ala is quickly removed from nascent PG. Therefore, DD-trimers should be made concomitantly or very shortly (<2 min) after incorporation of new subunits into a growing strand. With respect to how, when and where DD/LD hybrids or full LD trimers are made, there are no experimental data reported.

The presence of sizable proportions of cross-linked trimers and tetramers in the PG has deep structural consequences. As illustrated in **Figure 5A**, in the case of trimers the geometric constraints imposed by the nature of the molecule mean that the three glycan strands cross each other in a non-planar configuration. Indeed, at least one of the glycans has to follow a trajectory on a markedly different plane to that defined by the other two strands. A similar, even more complex situation is generated by the presence of tetramers (**Figure 5B**) which force a disposition of the strands in different planes. The normal abundance of trimers is rather variable, but taking *E. coli* as a reference (4–5% of total muropeptides) a sacculus would contain roughly 6×10^4 such glycan-strand knots. As the number of strands per sacculus is *ca.* 1.1×10^5 (3.5×10^6 monomers per sacculus with an AL of *ca.* 30 M/S) (Harz et al., 1990; Wientjes et al., 1991) on average, each glycan chain participates in 1–2 of these knots. The contribution of tetramers is more difficult to estimate, as their presence in many species is doubtful. In *E. coli* their amount is close to the detection limit (0.2% of total muropeptides). This apparently low abundance still means about 2×10^3 tetramers/sacculus, or that roughly one out of 16 strands is cross-linked by one tetramer. In those species were they are present in larger amounts as in *C. crescentus* (>3%; Takacs et al., 2010), their effect should lead to a very disordered orientation of the strands. Such a situation indicates that most strands weave over and under other strands and therefore, cannot form the kind of ordered, planar net often presented in representations and models of the cell wall.

Knitting the Net, Cross-Links, and Glycan Strands

Escherichia coli PG has a considerable proportion (about 30%) of strands shorter than eight disaccharide subunits (DSs; Harz et al., 1990). The degree of cross-linkage is about 30% for *E. coli*. How this value is calculated means that there are 30 peptide bridges for each 100 muropeptides. Therefore, most strands equal or shorter than eight DS would statistically be cross-linked at two or fewer points. Such a structure would behave like a single long cross-link when subjected to stress (Costa et al., 1999), unless one of the cross-linking points were a trimer or tetramer connecting the short strand to two or three other strands, respectively. Quite interestingly, the terminal muropeptides of PG strands are hyper cross-linked (Glauner and Höltje, 1990; Lam et al., 2009; Takacs et al., 2010). Most strands terminate in a cross-linked dimer, but many in trimers and tetramers. The preference for a particular kind of terminal muropeptide could work as a compensating mechanism to ensure the continuity of the net-like structure under such circumstances. For similar reasons strands shorter than four DS (still about 10% of total PG) would be cross-linked at only one point and could not contribute to the strength of the stress bearing structure. These extremely short "strands" could represent material being recycled on its way out of the sacculus. Nevertheless, the above arguments assume a homogeneous distribution of cross-links, but this assumption could be wrong. An alternative would be that short chains were proportionally more cross-linked than long ones. Under these circumstances the short strands could play the role of staples joining longer chains at certain locations, whereas the long, under-cross linked, strands could deform more easily.

In some cases low AL values are associated with elevated proportions of cross-linked muropeptides, in particular trimers and tetramers (Takacs et al., 2010). The high proportions of trimers and tetramers might compensate for the shortness of the strands increasing the probability that they will cross-link to more than two other strands and therefore help create a relatively tight net made up of short strands. *H. pylori* represents an extreme case, with an AL of about 7 M/S in actively growing cells, but with a PG that lacks trimers and has a low degree of cross-linking (27% of dimers). In cases like this the NAc-muraminyl end of a short strand could be linked to the NAc-glucosaminyl end of another

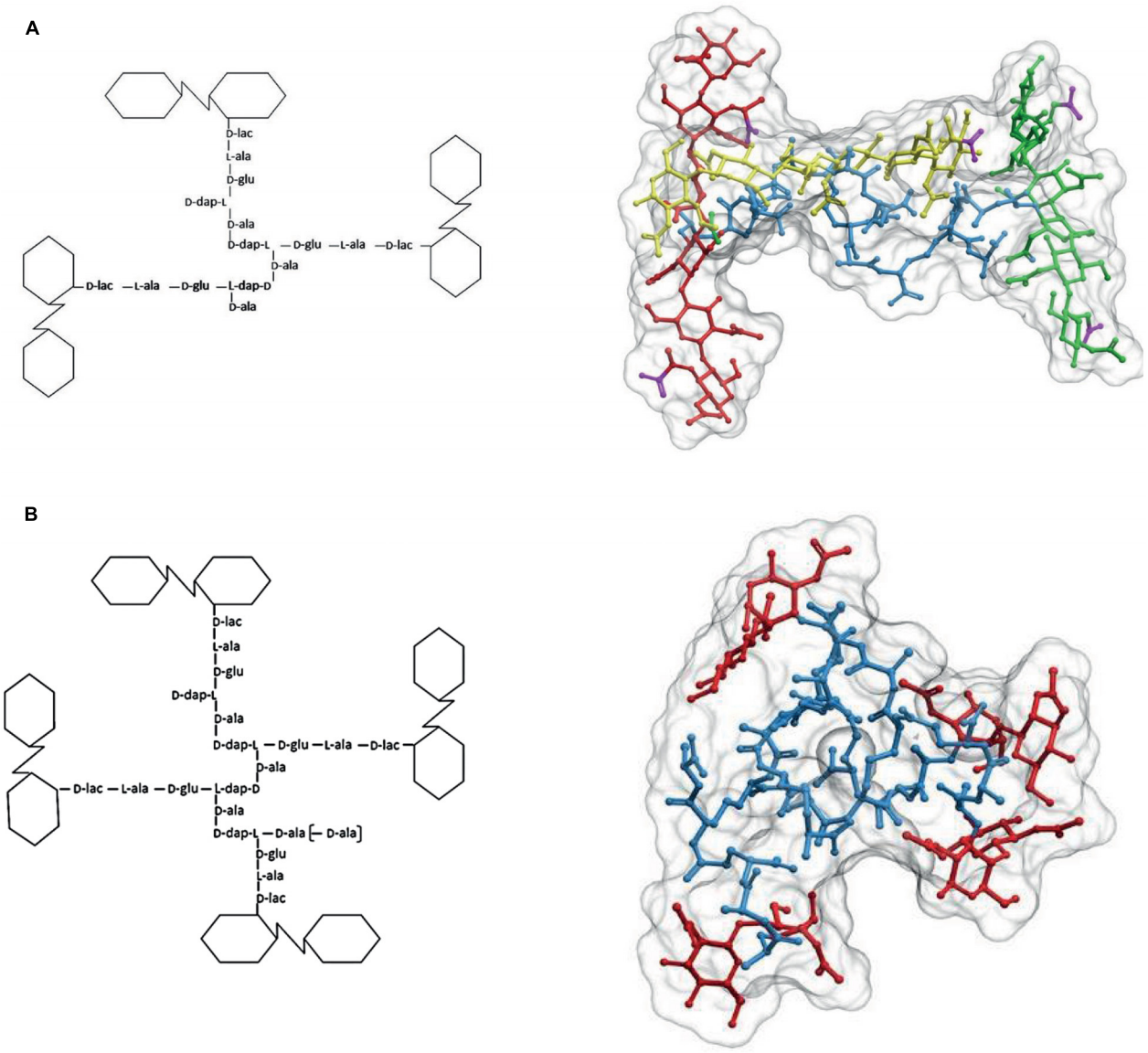

FIGURE 5 | The structure of cross-linked trimers and tetramers. **(A)** Simplified formula and 3D representation of a molecule of the DD cross-linked trimer *tris*-disaccharide tetrapeptide. For a better visualization of the relative orientation of the strands, the glycans were extended by the addition of two disaccharides, one at each side, to each of the cross-linked moieties. Red, yellow, and green designate each of the glycan strands, and blue the peptide moiety. **(B)** Simplified formula and 3D representation of a molecule of the DD cross-linked tetramer *tetra*-disaccharide tetrapeptide. Red designates the glycan moieties and blue the stem peptides. The 3D structure was calculated as in **Figures 1** and **2**.

by a peptide cross-link, generating a longer linear polymer with alternating glycan and peptidic regions that could interconnect relatively distant strands and contribute to the strength of the sacculus (Costa et al., 1999).

Organization and Orientation of PG Strands

Two important parameters define the structure of the sacculus: the total amount of PG subunits available, and the orientation of the glycan strands. Indeed, how PG is stretched to cover the area of the cell and how many PG layers exist in Gram-negatives have been matters of debate since the earliest works on cell walls (Wientjes et al., 1991).

Small-angle neutron diffraction experiments on purified *E. coli* sacculi (Labischinski et al., 1991) indicated that the thickness of PG in *E. coli* is non-homogeneous, with about one third of the surface thick enough (7 nm) to accommodate a triple layer of PG, whilst the rest has a thickness (2.5 nm) compatible with a single layered structure. However, the method only estimates the proportion of areas with each thickness, but gives no data about

their distribution. These data are compatible with the distortions expected from the presence of cross-linked trimers and tetramers, as discussed above (Labischinski et al., 1991). Further support for a (partially) multilayered organization was obtained from cryo-EM (Hobot et al., 1984) and AFM (Yao et al., 1999). The later methodology provided the first measurements of PG thickness in the hydrated state and showed that hydration strongly influences this parameter. Direct determination of the amount of PG per cell ($3.5 \pm 0.6 \times 10^6$ monomers/cell) and per unit of cell surface area (PG density) was also compatible with the kind of partially multilayered ordering suggested by other techniques (Wientjes et al., 1991). However, the calculations were based on a rather primitive model for the PG network (Oldmixon et al., 1974), and ignored the size distribution of strands and its possible relaxation effects on the PG fabric (Huang et al., 2012).

A second very important, and often neglected, observation from the AFM work was the demonstration that purified sacculi from Gram-negatives could have different thicknesses. Indeed, sacculi from *Pseudomonas aeruginosa* were about half the thickness of those from *E. coli* (Yao et al., 1999). This result clearly indicates that PG thickness might be a variable parameter. Indeed, studies on the effects of specific mutations (Lam et al., 2009), partial starvation for PG precursors (Prats and de Pedro, 1989) and the effects of D-amino acids on the structure of PG (Caparros et al., 1994; Cava et al., 2011) indicate that, at least some bacteria can accommodate large variations in the amount of PG per unit of cell surface, without apparent consequences for morphology, growth, and division. A relevant observation in *E. coli* is that the only significant variation detected in the composition of PG from cells with low PG content was a shortening in the AL of glycan strands (from 28 down to 19 M/S), a change that might change the elasticity of the sacculus to favor stretching (Huang et al., 2008). The surface density of PG seems to suffer large changes not only in response to harsh treatments, but also during the regular life cycle of bacteria (leaving aside those having specialized resistance forms), with resting cells accumulating considerably more PG per unit area than their actively growing counterparts (Caparros et al., 1994; Cava et al., 2011). Therefore, in at least some bacteria, the organization of the sacculus has to be compatible with drastic alterations in the PG surface density without causing macroscopic alteration in the shape and growth of the cell.

The relative orientation of the glycan strands with respect to the axes of the cell is another "hot topic" in cell wall biology. Because PG is not isotropic with respect to some characteristics, particularly elasticity (Gumbart et al., 2014), the disposition of strands in the sacculus has an important influence on cell wall properties. Measurements of the mechanical characteristics of sacculi show that they behave as a perfectly elastic material but with a high anisotropy (Yao et al., 1999). In fact, the elastic modulus for hydrated PG sacculi from either *P. aeruginosa* or *E. coli*, was 2–3 times larger in the longitudinal dimension (the long axis of the cell) than in the transverse direction, meaning that under pressure the sacculus would become proportionally longer. Such a behavior is a strong indication that the glycan strands transverse the long axis of the cell. In contrast, a perfectly (or close to perfect) perpendicular orientation of the glycan chains would be difficult to reconcile with arguments against a planar organization of these strands. Instead, analysis of purified sacculi by cryo-electron tomography supports a disordered circumferential arrangement of the glycan strands, which show a preferential, but not strict, transverse alignment relative to the cell axis (Gan et al., 2008). This disposition is also supported by advanced computational approaches, which find that such a layout best fits the mechanical properties of sacculi (Huang et al., 2008; Gumbart et al., 2014).

Concluding Remarks

The arguments discussed above indicate that there is not such a thing as a "Gram-negative sacculus" and if there were, it would be quite far from a regular or highly ordered structure. Nonetheless, the most important point we wish to make is how little real structural information is available. Many readers will be surprised by the age of the citations in this review. The reason is simply that many important lines of work have been abandoned or not pursued with the intensity that is required to acquire more comprehensive information on cell wall biology. The biological diversity of the cell wall seems to be much larger than initially expected in terms of structure and composition, questioning the universality of the models developed on the basis of *E. coli* data. To explore the real range of cell wall structural variability an "omics" approach looks like the best direction to go. Recent methodological advances make fast analysis of large numbers of PG samples feasible, and open the way to a methodical, large scale survey of bacterial cell walls. New techniques in electron, atomic force, and optical (fluorescence) microscopy are also demonstrating enough resolving power to contribute substantially to the unraveling of the fine structure of cell sacculi. Further development and systematic application of these new capabilities should provide the data required for a realistic understanding of bacterial cell wall structure and biology.

Acknowledgments

This work was supported by the Laboratory for Infection Medicine Sweden (MIMS), the Knut and Alice Wallenberg Foundation (KAW), and the Swedish Research Council to FC, and UCMR Linneus professorship to MAP.

References

Barnickel, G., Labischinski, H., Bradaczek, H., and Giesbrecht, P. (1979). Conformational energy calculation on the peptide part of murein. *Eur. J. Biochem.* 95, 157–165. doi: 10.1111/j.1432-1033.1979.tb12950.x

Barnikel, G., Naumann, D., Bradaczek, H., Labischinski, H., and Giesbrecht, P. (1983). "Computer-aided molecular modelling of the three dimensional structure of bacterial peptidoglycan," in *The Target of Penicillin: The Murein Sacculus of Bacterial Cell Walls, Architecture and Growth*, eds J.-V. H. R. Hakenbeck and H. Labischinski (Berlin: de Gruyter), 61–66.

Boniface, A., Parquet, C., Arthur, M., Mengin-Lecreulx, D., and Blanot, D. (2009). The elucidation of the structure of *Thermotoga maritima* peptidoglycan reveals two novel types of cross-link. *J. Biol. Chem.* 284, 21856–21862. doi: 10.1074/jbc.M109.034363

Brown, P. J., de Pedro, M. A., Kysela, D. T., Van Der Henst, C., Kim, J., De Bolle, X., et al. (2012). Polar growth in the Alphaproteobacterial order Rhizobiales. *Proc. Natl. Acad. Sci. U.S.A.* 109, 1697–1701. doi: 10.1073/pnas.1114476109

Bui, N. K., Gray, J., Schwarz, H., Schumann, P., Blanot, D., and Vollmer, W. (2009). The peptidoglycan sacculus of *Myxococcus xanthus* has unusual structural features and is degraded during glycerol-induced myxospore development. *J. Bacteriol.* 191, 494–505. doi: 10.1128/JB.00608-08

Cameron, T. A., Anderson-Furgeson, J., Zupan, J. R., Zik, J. J., and Zambryski, P. C. (2014). Peptidoglycan synthesis machinery in *Agrobacterium tumefaciens* during unipolar growth and cell division. *MBio* 5, e01219–e01214. doi: 10.1128/mBio.01219-14

Caparros, M., Quintela, J. C., and de Pedro, M. A. (1994). Variability of peptidoglycan surface density in *Escherichia coli*. *FEMS Microbiol. Lett.* 121, 71–76. doi: 10.1016/0378-1097(94)90147-3

Cava, F., de Pedro, M. A., Lam, H., Davis, B. M., and Waldor, M. K. (2011). Distinct pathways for modification of the bacterial cell wall by non-canonical D-amino acids. *EMBO J.* 30, 3442–3453. doi: 10.1038/emboj.2011.246

Churchman, J. W. (1927). The structure of *B. anthracis* and reversal of the Gram Reaction. *J. Exp. Med.* 46, 1007–1029. doi: 10.1084/jem.46.6.1007

Costa, K., Bacher, G., Allmaier, G., Dominguez-Bello, M. G., Engstrand, L., Falk, P., et al. (1999). The morphological transition of *Helicobacter pylori* cells from spiral to coccoid is preceded by a substantial modification of the cell wall. *J. Bacteriol.* 181, 3710–3715.

Gan, L., Chen, S., and Jensen, G. J. (2008). Molecular organization of Gram-negative peptidoglycan. *Proc. Natl. Acad. Sci. U.S.A.* 105, 18953–18957. doi: 10.1073/pnas.0808035105

Glauner, B. (1988). Separation and quantification of muropeptides with high-performance liquid chromatography. *Anal. Biochem.* 172, 451–464. doi: 10.1016/0003-2697(88)90468-X

Glauner, B., and Höltje, J. V. (1990). Growth pattern of the murein sacculus of *Escherichia coli*. *J. Biol. Chem.* 265, 18988–18996.

Glauner, B., Holtje, J. V., and Schwarz, U. (1988). The composition of the murein of *Escherichia coli*. *J. Biol. Chem.* 263, 10088–10095.

Gumbart, J. C., Beeby, M., Jensen, G. J., and Roux, B. (2014). *Escherichia coli* peptidoglycan structure and mechanics as predicted by atomic-scale simulations. *PLoS Comput. Biol.* 10:e1003475. doi: 10.1371/journal.pcbi.1003475

Gupta, R., Lavollay, M., Mainardi, J. L., Arthur, M., Bishai, W. R., and Lamichhane, G. (2010). The *Mycobacterium tuberculosis* protein LdtMt2 is a nonclassical transpeptidase required for virulence and resistance to amoxicillin. *Nat. Med.* 16, 466–469. doi: 10.1038/nm.2120

Harz, H., Burgdorf, K., and Holtje, J. V. (1990). Isolation and separation of the glycan strands from murein of *Escherichia coli* by reversed-phase high-performance liquid chromatography. *Anal. Biochem.* 190, 120–128. doi: 10.1016/0003-2697(90)90144-X

Hobot, J. A., Carlemalm, E., Villiger, W., and Kellenberger, E. (1984). Periplasmic gel: new concept resulting from the reinvestigation of bacterial cell envelope ultrastructure by new methods. *J. Bacteriol.* 160, 143–152.

Huang, K. C., Ehrhardt, D. W., and Shaevitz, J. W. (2012). The molecular origins of chiral growth in walled cells. *Curr. Opin. Microbiol.* 15, 707–714. doi: 10.1016/j.mib.2012.11.002

Huang, K. C., Mukhopadhyay, R., Wen, B., Gitai, Z., and Wingreen, N. S. (2008). Cell shape and cell-wall organization in Gram-negative bacteria. *Proc. Natl. Acad. Sci. U.S.A.* 105, 19282–19287. doi: 10.1073/pnas.0805309105

Ishidate, K., Ursinus, A., Holtje, J. V., and Rothfield, L. (1998). Analysis of the length distribution of murein glycan strands in ftsZ and ftsI mutants of *E. coli*. *FEMS Microbiol. Lett.* 168, 71–75. doi: 10.1111/j.1574-6968.1998.tb13257.x

Knaysi, G. (1930). The cell structure and cell division of *Bacillus subtilis*. *J. Bacteriol.* 19, 113–115.

Knaysi, G. (1941). Observations on the cell division of some yeasts and bacteria. *J. Bacteriol.* 41, 141–153.

Kuru, E., Hughes, H. V., Brown, P. J., Hall, E., Tekkam, S., Cava, F., et al. (2012). In Situ probing of newly synthesized peptidoglycan in live bacteria with fluorescent D-amino acids. *Angew Chem. Int. Ed. Engl.* 51, 12519–12523. doi: 10.1002/anie.201206749

Labischinski, H., Goodell, E. W., Goodell, A., and Hochberg, M. L. (1991). Direct proof of a "more-than-single-layered" peptidoglycan architecture of *Escherichia coli* W7: a neutron small-angle scattering study. *J. Bacteriol.* 173, 751–756.

Lam, H., Oh, D. C., Cava, F., Takacs, C. N., Clardy, J., de Pedro, M. A., et al. (2009). D-amino acids govern stationary phase cell wall remodeling in bacteria. *Science* 325, 1552–1555. doi: 10.1126/science.1178123

Lavollay, M., Arthur, M., Fourgeaud, M., Dubost, L., Marie, A., Veziris, N., et al. (2008). The peptidoglycan of stationary-phase *Mycobacterium tuberculosis* predominantly contains cross-links generated by L,D-transpeptidation. *J. Bacteriol.* 190, 4360–4366. doi: 10.1128/JB.00239-08

Leps, B., Labischinski, H., and Bradaczek, H. (1987). Conformational behavior of the polysaccharide backbone of murein. *Biopolymers* 26, 1391–1406. doi: 10.1002/bip.360260813

Magnet, S., Bellais, S., Dubost, L., Fourgeaud, M., Mainardi, J. L., Petit-Frere, S., et al. (2007). Identification of the L,D-transpeptidases responsible for attachment of the Braun lipoprotein to *Escherichia coli* peptidoglycan. *J. Bacteriol.* 189, 3927–3931. doi: 10.1128/JB.00084-07

Magnet, S., Dubost, L., Marie, A., Arthur, M., and Gutmann, L. (2008). Identification of the L,D-transpeptidases for peptidoglycan cross-linking in *Escherichia coli*. *J. Bacteriol.* 190, 4782–4785. doi: 10.1128/JB.00025-08

Meroueh, S. O., Bencze, K. Z., Hesek, D., Lee, M., Fisher, J. F., Stemmler, T. L., et al. (2006). Three-dimensional structure of the bacterial cell wall peptidoglycan. *Proc. Natl. Acad. Sci. U.S.A.* 103, 4404–4409. doi: 10.1073/pnas.0510182103

Obermann, W., and Holtje, J. V. (1994). Alterations of murein structure and of penicillin-binding proteins in minicells from *Escherichia coli*. *Microbiology* 140(Pt 1), 79–87. doi: 10.1099/13500872-140-1-79

Oldmixon, E. H., Glauser, S., and Higgins, M. L. (1974). Two proposed general configurations for bacterial cell wall peptidoglycans shown by space-filling molecular models. *Biopolymers* 13, 2037–2060. doi: 10.1002/bip.1974.360131008

Pisabarro, A. G., de Pedro, M. A., and Vazquez, D. (1985). Structural modifications in the peptidoglycan of *Escherichia coli* associated with changes in the state of growth of the culture. *J. Bacteriol.* 161, 238–242.

Prats, R., and de Pedro, M. A. (1989). Normal growth and division of *Escherichia coli* with a reduced amount of murein. *J. Bacteriol.* 171, 3740–3745.

Primosigh, J., Pelzer, H., Maass, D., and Weidel, W. (1961). Chemical characterization of mucopeptides released from the *E. coli* B cell wall by enzymic action. *Biochim. Biophys. Acta* 46, 68–80. doi: 10.1016/0006-3002(61)90647-3

Quintela, J. C., Caparros, M., and de Pedro, M. A. (1995). Variability of peptidoglycan structural parameters in gram-negative bacteria. *FEMS Microbiol. Lett.* 125, 95–100. doi: 10.1111/j.1574-6968.1995.tb07341.x

Romeis, T., Kohlrausch, U., Burgdorf, K., and Holtje, J. V. (1991). Murein chemistry of cell division in *Escherichia coli*. *Res. Microbiol.* 142, 325–332. doi: 10.1016/0923-2508(91)90048-F

Salton, M. R. (1952). Studies of the bacterial cell wall. III. Preliminary investigation of the chemical constitution of the cell wall of *Streptococcus faecalis*. *Biochim. Biophys. Acta* 8, 510–519. doi: 10.1016/0006-3002(52)90082-6

Salton, M. R. (1953). Studies of the bacterial cell wall. IV. The composition of the cell walls of some Gram-positive and Gram-negative bacteria. *Biochim. Biophys. Acta* 10, 512–523. doi: 10.1016/0006-3002(53)90296-0

Salton, M. R. (1956). Studies of the bacterial cell wall. V. The action of lysozyme on cell walls of some lysozyme-sensitive bacteria. *Biochim. Biophys. Acta* 22, 495–506. doi: 10.1016/0006-3002(56)90060-9

Salton, M. R. (1960). Studies of the bacterial cell wall. VII. Monosaccharide constituents of the walls of gram-negative bacteria. *Biochim. Biophys. Acta* 45, 364–371. doi: 10.1016/0006-3002(60)91459-1

Salton, M. R. (1961). Studies of the bacterial cell wall. VIII. Reaction of walls with hydrazine and with fluorodinitrobenzene. *Biochim. Biophys. Acta* 52, 329–342. doi: 10.1016/0006-3002(61)90682-5

Salton, M. R., and Horne, R. W. (1951a). Studies of the bacterial cell wall. I. Electron microscopical observations on heated bacteria. *Biochim. Biophys. Acta* 7, 19–42. doi: 10.1016/0006-3002(51)90003-0

Salton, M. R., and Horne, R. W. (1951b). Studies of the bacterial cell wall. II. Methods of preparation and some properties of cell walls. *Biochim. Biophys. Acta* 7, 177–197. doi: 10.1016/0006-3002(51)90017-0

Schleifer, K. H., and Kandler, O. (1972). Peptidoglycan types of bacterial cell walls and their taxonomic implications. *Bacteriol. Rev.* 36, 407–477.

Siegrist, M. S., Whiteside, S., Jewett, J. C., Aditham, A., Cava, F., and Bertozzi, C. R. (2013). (D)-Amino acid chemical reporters reveal peptidoglycan dynamics of an intracellular pathogen. *ACS Chem. Biol.* 8, 500–505. doi: 10.1021/cb300 4995

Takacs, C. N., Poggio, S., Charbon, G., Pucheault, M., Vollmer, W., and Jacobs-Wagner, C. (2010). MreB drives de novo rod morphogenesis in *Caulobacter crescentus* via remodeling of the cell wall. *J. Bacteriol.* 192, 1671–1684. doi: 10.1128/JB.01311-09

Typas, A., Banzhaf, M., Gross, C. A., and Vollmer, W. (2012). From the regulation of peptidoglycan synthesis to bacterial growth and morphology. *Nat. Rev. Microbiol.* 10, 123–136. doi: 10.1038/nrmicro2677

Ursinus, A., Van Den Ent, F., Brechtel, S., de Pedro, M., Holtje, J. V., Lowe, J., et al. (2004). Murein (peptidoglycan) binding property of the essential cell division protein FtsN from *Escherichia coli*. *J. Bacteriol.* 186, 6728–6737. doi: 10.1128/JB.186.20.6728-6737.2004

van Heijenoort, J. (2001). Formation of the glycan chains in the synthesis of bacterial peptidoglycan. *Glycobiology* 11, 25R–36R. doi: 10.1093/glycob/11.3.25R

Varma, A., de Pedro, M. A., and Young, K. D. (2007). FtsZ directs a second mode of peptidoglycan synthesis in *Escherichia coli*. *J. Bacteriol.* 189, 5692–5704. doi: 10.1128/JB.00455-07

Vasstrand, E. N., Jensen, H. B., Miron, T., and Hofstad, T. (1982). Composition of peptidoglycans in Bacteroidaceae: determination and distribution of lanthionine. *Infect. Immun.* 36, 114–122.

Vollmer, W. (2008). Structural variation in the glycan strands of bacterial peptidoglycan. *FEMS Microbiol. Rev.* 32, 287–306. doi: 10.1111/j.1574-6976.2007.00088.x

Vollmer, W., Blanot, D., and de Pedro, M. A. (2008). Peptidoglycan structure and architecture. *FEMS Microbiol. Rev.* 32, 149–167. doi: 10.1111/j.1574-6976.2007.00094.x

Weidel, W. (1960). Mucopolymers of the cell-wall of *E. coli* B. *Bull. Soc. Chim. Biol.* (*Paris*) 42, 1833–1835.

Weidel, W., Frank, H., and Martin, H. H. (1960). The rigid layer of the cell wall of *Escherichia coli* strain B. *J. Gen. Microbiol.* 22, 158–166. doi: 10.1099/00221287-22-1-158

Weidel, W., and Pelzer, H. (1964). Bagshaped macromolecules – a new outlook on bacterial cell walls. *Adv. Enzymol. Relat. Areas Mol. Biol.* 26, 193–232.

Wientjes, F. B., Woldringh, C. L., and Nanninga, N. (1991). Amount of peptidoglycan in cell walls of gram-negative bacteria. *J. Bacteriol.* 173, 7684–7691.

Yao, X., Jericho, M., Pink, D., and Beveridge, T. (1999). Thickness and elasticity of gram-negative murein sacculi measured by atomic force microscopy. *J. Bacteriol.* 181, 6865–6875.

Conflict of Interest Statement: The authors declare that the research was conducted in the absence of any commercial or financial relationships that could be construed as a potential conflict of interest.

Copyright © 2015 de Pedro and Cava. This is an open-access article distributed under the terms of the Creative Commons Attribution License (CC BY). The use, distribution or reproduction in other forums is permitted, provided the original author(s) or licensor are credited and that the original publication in this journal is cited, in accordance with accepted academic practice. No use, distribution or reproduction is permitted which does not comply with these terms.

frontiers in Microbiology

REVIEW
published: 12 June 2015
doi: 10.3389/fmicb.2015.00572

The membrane: transertion as an organizing principle in membrane heterogeneity

Kouji Matsumoto[1], Hiroshi Hara[1], Itzhak Fishov[2], Eugenia Mileykovskaya[3] and Vic Norris[4]*

[1] Department of Biochemistry and Molecular Biology, Graduate School of Science and Engineering, Saitama University, Saitama, Japan, [2] Department of Life Sciences, Ben-Gurion University of the Negev, Beer-Sheva, Israel, [3] Department of Biochemistry and Molecular Biology, University of Texas Medical School at Houston, Houston, TX, USA, [4] Laboratory of Microbiology Signals and Microenvironment EA 4312, Department of Science, University of Rouen, Mont-Saint-Aignan, France

OPEN ACCESS

Edited by:
Arieh Zaritsky, Ben-Gurion University of the Negev, Israel

Reviewed by:
Marc Bramkamp, Ludwig Maximilians University of Munich, Germany
Ding J. Jin, National Institutes of Health, USA
Germán Rivas, Consejo Superior de Investigaciones Científicas, Spain

***Correspondence:**
Kouji Matsumoto, Department of Biochemistry and Molecular Biology, Graduate School of Science and Engineering, Saitama University, 255 Shimo-ohkubo, Sakura-ku, Saitama-shi, Saitama 338-8570, Japan
koumatsu@mail.saitama-u.ac.jp

Specialty section:
This article was submitted to Microbial Physiology and Metabolism, a section of the journal Frontiers in Microbiology

Received: *26 March 2015*
Accepted: *25 May 2015*
Published: *12 June 2015*

Citation:
Matsumoto K, Hara H, Fishov I, Mileykovskaya E and Norris V (2015) The membrane: transertion as an organizing principle in membrane heterogeneity. Front. Microbiol. 6:572. doi: 10.3389/fmicb.2015.00572

The bacterial membrane exhibits a significantly heterogeneous distribution of lipids and proteins. This heterogeneity results mainly from lipid–lipid, protein–protein, and lipid–protein associations which are orchestrated by the coupled transcription, translation and insertion of nascent proteins into and through membrane (transertion). Transertion is central not only to the individual assembly and disassembly of large physically linked groups of macromolecules (*alias* hyperstructures) but also to the interactions between these hyperstructures. We review here these interactions in the context of the processes in *Bacillus subtilis* and *Escherichia coli* of nutrient sensing, membrane synthesis, cytoskeletal dynamics, DNA replication, chromosome segregation, and cell division.

Keywords: membrane, transertion, hyperstructures, lipid domain, *Escherichia coli, Bacillus subtilis*

Introduction

The laterally heterogeneous distribution of the lipid and the protein components of bacterial cell membranes is the current paradigm, having replaced the homogeneous distribution of these components that is assumed in the fluid mosaic membrane model. This heterogeneity is involved in producing the specific environments needed for membrane proteins to participate in the many important processes that are associated with cell membranes. This raises the question of the nature of the mechanisms responsible for membrane heterogeneity.

One of the main causes of large-scale heterogeneity in bacterial membranes is the coupled transcription, translation and insertion of nascent proteins into and through membrane, *alias* transertion (Norris and Madsen, 1995; Binenbaum et al., 1999; Bakshi et al., 2014; **Figure 1**). The tethering of nascent proteins orchestrates interactions that result in the formation of membrane domains. These interactions include protein–protein interactions and lipid–protein interactions – and therefore also include lipid–lipid interactions (Vereb et al., 2003). The multitude of processes in which transertion is implicated has led to it being proposed as a powerful force in maintaining the nucleoid in expanded state, in the integrative sensing of metabolic activity and in coupling chromosome segregation to cell division (Norris and Amar, 2012; Fishov and Norris, 2012b).

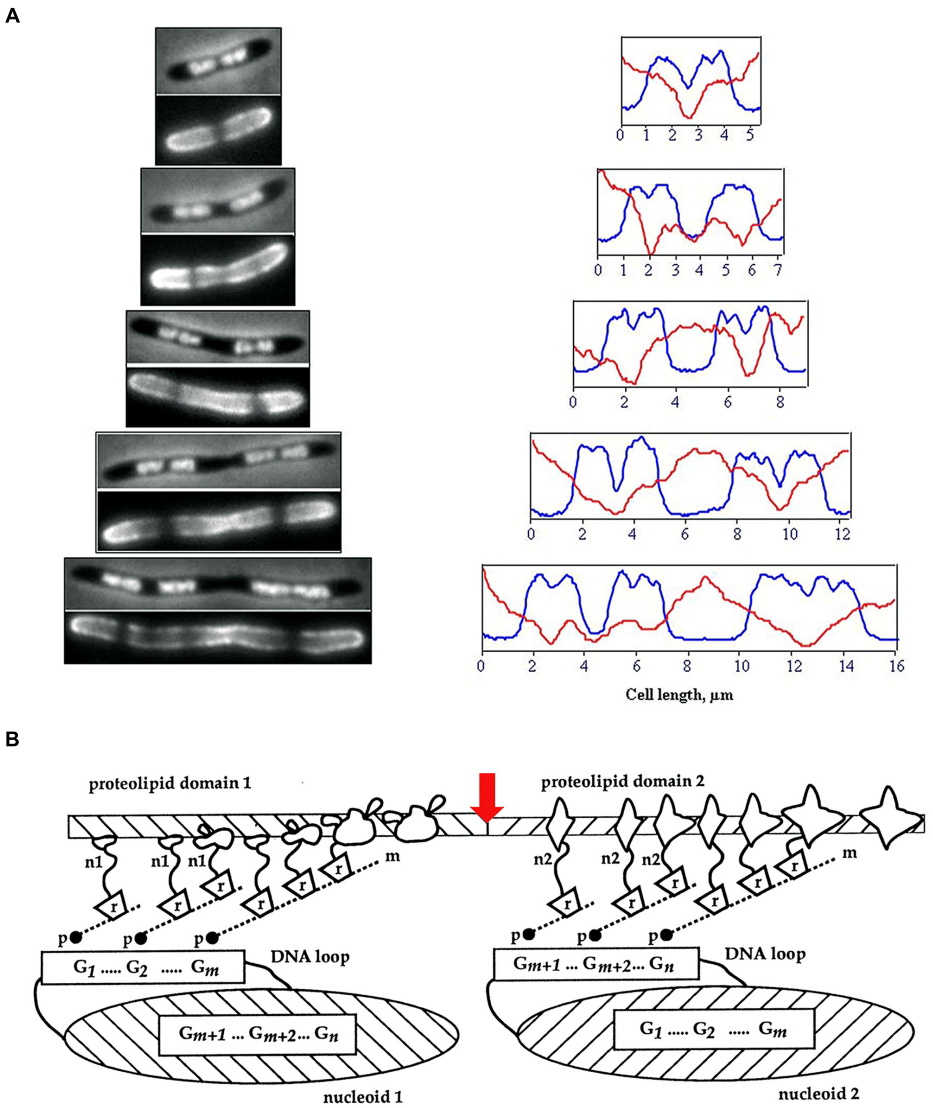

FIGURE 1 | (A) Visualization of membrane heterogeneity in *Escherichia coli* cells by fluorescent microscopy. Left: image of an *E. coli* cell division mutant *pbpB*(ts) transferred to the non-permissive temperature (time zero, bacterium at the top), double-stained with DAPI (top half of image) and FM4-64 (bottom half of image) for visualization of nucleoids and membrane, respectively; adapted from Fishov and Woldringh (1999), © John Wiley and Sons. On the right, plots of fluorescence intensity profiles along filaments (DAPI, blue line; FM4-64, red). **(B)** The relationship between proteolipid domains, transertion, and clusters of genes either "looped out" from or buried within the nucleoid. n1, n2, nascent proteins; m, mRNA; r, ribosomes; p, RNA polymerase; G, gene clusters; red arrow indicates division site; adapted from Norris and Madsen (1995), © Elsevier.

It has long been evident that bacteria are highly structured (for references see Norris et al., 1994). It is now emerging that this structuring is in the form of *hyperstructures* which are large, physically linked, assemblies of macromolecules that serve specific functions (Norris et al., 2007a). Transertion plays a central role in the formation of one class of hyperstructures and also in the dialog between these hyperstructures that determines the behavior of the cell itself. Here, we review membrane heterogeneity focussing on transertion hyperstructures and their relationships with the processes of nutrient sensing, membrane synthesis, cytoskeletal dynamics, DNA replication, chromosome segregation, and cell division.

Lipid Domains

Cardiolipin and Other Anionic Phospholipid Domains

Although the lipids present in the inner membrane of *Escherichia coli* will spontaneously separate into domains *in vitro* (Zerrouk et al., 2008), until fairly recently, the lipid molecules in the membranes of bacterial cells were assumed to be homogeneously distributed, since the fluidity of biological membranes had become generally accepted following the publication of the fluid mosaic model (Singer and Nicolson, 1972). However, cell membranes must be laterally polarized to

produce specific environments for certain membrane proteins, in particular, chemoreceptor proteins and proteins that promote polymerization of actin in eukaryotic hosts, as well as proteins involved in cell division at mid-cell and at asymmetric positions (Shapiro et al., 2002). Microscopic visualization of membrane lipids in cells has reinforced the view that bacterial membranes do possess structural heterogeneity. Uneven distribution of fluorescent lipophilic dyes and selective staining of septal regions has been observed in mycobacteria and an uneven distribution of fluorescence has been observed in lipophilic dye (FM4-64)-stained *E. coli* cells (Christensen et al., 1999; Fishov and Woldringh, 1999; **Figure 1**).

Unequivocal visualization of cardiolipin (CL) domains in the septal region and in the poles in the membranes of *E. coli* cells has been accomplished by means of the CL-specific fluorescent dye 10-*N*-nonyl-3,6-bis(dimethylamino)acridine (10-*N*-nonyl-acridine orange: NAO; Mileykovskaya and Dowhan, 2000, 2009; Mileykovskaya, 2007; **Figures 2A–C**). Time-lapse microscopy of *E. coli* cells showed positioning of NAO stained domains at nascent division sites and their gradual development into septal domains (Mileykovskaya and Dowhan, 2009; Mileykovskaya and Margolin, 2012; **Figure 2D**). NAO only binds to anionic phospholipids owing to an interaction between its quaternary amine and the phosphate residue of phospholipids and an intercalation of the hydrophobic acridine moiety into the membrane bilayer (Petit et al., 1992). The stoichiometry between NAO and monoacidic phospholipids is 1:1 and the emitted fluorescence is green whilst with CL, which contains two phosphate groups per molecule, NAO forms a dimer and the emitted fluorescence of the CL complex shifts to red due to the metachromatic effect of acridine molecules (Petit et al., 1994; Mileykovskaya et al., 2001; **Figure 2G**). CL domains have also been observed in *Bacillus subtilis* cells, both during exponential growth in the septal region and the poles and during sporulation in the engulfment and the forespore membranes (Kawai et al., 2004, 2006; **Figures 2E,F**). Note that in *B. subtilis* cells PE is also localized in polar and septal membranes (Nishibori et al., 2005). The CL localization to the polar membranes in *E. coli* is consistent with the increase in the content of CL in the membranes of minicells, which are rich in polar membranes (Koppelman et al., 2001).

An *E. coli*Δ*pgsA* mutant lacks phosphatidylglycerophosphate synthase, which catalyzes the committed step of biosynthesis of the major acidic phospholipids, and thus lacks phosphatidylglycerol (PG) and CL (both < 0.01% of total phospholipids); this mutant, which is viable if it also has an *lpp* mutation, accumulates the anionic biosynthetic precursors, phosphatidic acid (PA) and CDP-diacylglycerol (4.0 and 3.2%, respectively; Kikuchi et al., 2000; Shiba et al., 2004). PG is required for modification of prolipoprotein (the precursor of Braun's lipoprotein, the product of *lpp*); cells lacking PG in an lpp^+ background are not viable because the accumulation of unmodified prolipoprotein in the inner membrane causes a tight membrane fusion (Suzuki et al., 2002). The viability of a Δ*pgsA* lpp^- mutant suggests that the anionic phospholipids can substitute for one another in essential biological functions that include (1) the initiation of DNA replication, which depends on the rejuvenation of the DnaA protein by CL, and (2) the selection of the division site, which depends on the inhibition of inappropriate FtsZ polymerization in the polar regions by a complex, MinCD, with a high affinity for anionic phospholipids (Matsumoto, 2001; Szeto et al., 2002; Mileykovskaya et al., 2003; Norris et al., 2004; Mileykovskaya and Dowhan, 2005; Mazor et al., 2008; Vecchiarelli et al., 2014). In the Δ*pgsA* mutant cells, *N*-acyl-phosphatidylethanolamine (*N*-acyl-PE) and PA have been localized to polar and septal membrane domains (Mileykovskaya et al., 2009), indicating that these normally minor anionic phospholipids are segregated, like CL, into similar anionic lipid domains. Thus, *E. coli* has a mechanism for preferential segregation of anionic phospholipids to the polar and septal regions. One possible segregation mechanism depends on the shape of lipid molecules. 'Cone-shaped' lipid molecules, in which the cross-sectional area of the polar head group is less than the cross-sectional area of the hydrophobic domain, prefer regions of membranes that have a negative curvature; hence CL and PA are concentrated in negatively curved regions of the inner leaflet of the bacterial membranes (Cullis et al., 1983; Gennis, 1989; Seddon, 1990; Renner and Weibel, 2011; Jouhet, 2013; Renner et al., 2013). Using a mathematical model, this sensing of membrane curvature – and consequent positioning in the poles – has been attributed to stable, conical clusters of CL molecules forming due to the membrane being pinned to the cell wall, which is itself the result of the balance between the osmotic-pressure difference across the membrane and the inward pressure of the cell wall (Huang et al., 2006; Huang and Ramamurthi, 2010; **Figure 2F**).

A recent report from Weibel's lab has claimed that there is no clear preference of NAO for binding to CL compared to PG and other anionic phospholipids, and that NAO produces an intense red-shifted fluorescence emission with PG, PA, and phosphatidylserine (PS) that is comparable to that with CL (Oliver et al., 2014). They suggested that not only CL but also PG is concentrated in the polar regions of *E. coli* cell membranes. However, they used much higher concentrations of NAO than previous authors used for bacterial staining (Mileykovskaya and Dowhan, 2000; Kawai et al., 2004; Romantsov et al., 2007, 2008; Rosch et al., 2007; Lobasso et al., 2009, 2013; Maloney et al., 2011; Muchová et al., 2011; Kicia et al., 2012; Tran et al., 2013). Moreover, PG microdomains, in contrast to CL domains, cannot sense membrane curvature, since the cross-sectional area of PG molecule is cylindrical and lamellar structures are preferred (Cullis et al., 1983; Gennis, 1989; Seddon, 1990). As Weibel's lab had already demonstrated that the location of NAO-stained domains depends directly on membrane curvature (Renner and Weibel, 2011; Renner et al., 2013), this group did not propose a specific physical mechanism responsible for localizing anionic phospholipid domains stained by NAO (Oliver et al., 2014). In *B. subtilis*, phospholipid-specific dyes including FM4-64 are localized in a helical pattern extending along the long axis (Barák et al., 2008). Helical FM4-64 domains are missing in cells depleted of MurG, an enzyme involved in peptidoglycan synthesis, indicating a link between the helical

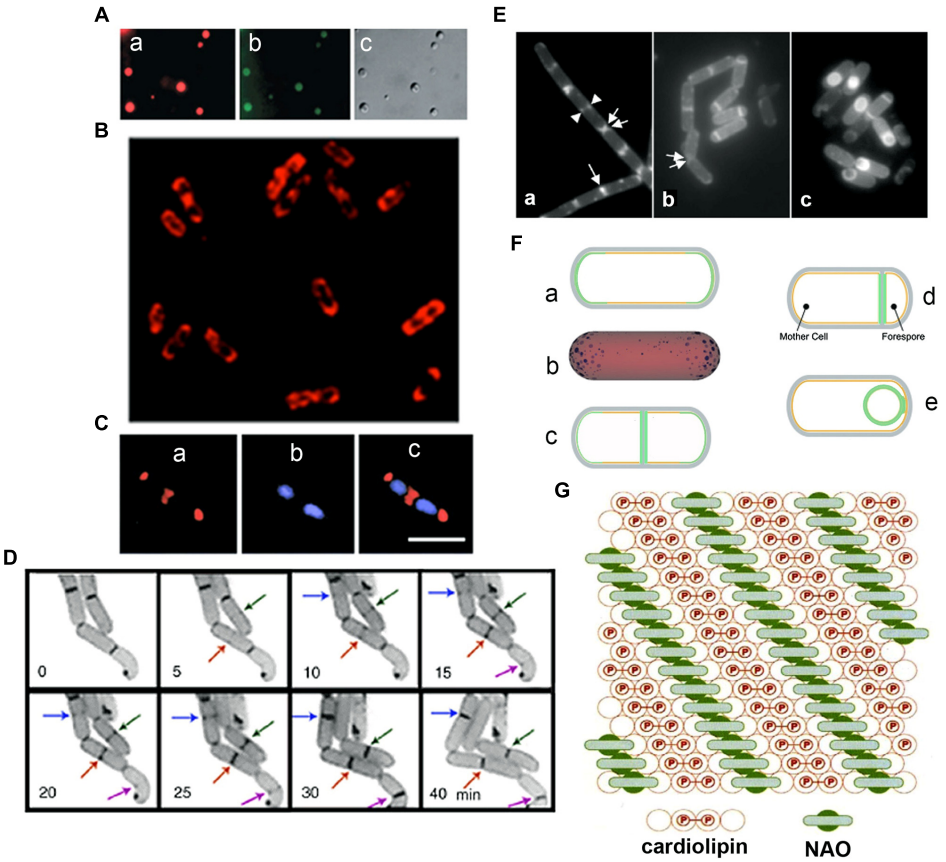

FIGURE 2 | Anionic phospholipid domains in *E. coli* and *B. subtilis* cells revealed by NAO staining. (A) Fluorescence microscopy of cardiolipin (CL)-containing liposomes stained with NAO. Liposomes composed of CL and phosphatidylcholine (60 mol%/40 mol%). Excitation: 490 nm, emission: 617 nm (a) and 528 (b), DIC (c); modified from Mileykovskaya (2007), © John Wiley and Sons. **(B)** Deconvolved images of an optical section of *E. coli* W3899 stained with NAO. Cells were grown in LB media in the presence of 200 nM NAO to OD_{600} 1.5, and then immobilized on a microscope slide cover glass with poly-L-lysine; modified from Mileykovskaya and Dowhan (2009), © Elsevier. Excitation is 490 nm and emission is 617 nm. **(C)** *E. coli* cells stained with NAO (red) for CL (a) and DAPI (blue) for the nucleoid (b). Overlay of images (c) demonstrates localization of CL at the cell poles and at the division site; scale bar, 2.5 μM; modified from Mileykovskaya and Dowhan (2000), © American Society for Microbiology. **(D)** The dynamics of CL domain formation during the cell cycle of growing *E. coli*. Arrows of the same color indicate the progression of the corresponding NAO-stained structures with time; adapted from Mileykovskaya and Dowhan (2009). **(E)** Staining of wild type *B. subtilis* cells with NAO. Wild type *B. subtilis* 168 cells were harvested in exponential growth and sporulation phase (at T2 and T4) and stained with 100 nM NAO for 20 min. Fluorescence images of exponential growth (a) and sporulation phase cells at T2 (b) and T4 (c). An arrow indicates a sharp fluorescence band in the center of the cell. Two fluorescence dot structures in the cell center are indicated by a pair of arrowheads. Regions of NAO stained nascent poles in the cells that are separating are indicated with a pair of arrows. Panels are adapted from Kawai et al. (2004), © American Society for Microbiology. **(F)** Osmotic pressure and turgor-induced localization of lipid clusters during cell division and sporulation. During exponential growth, high-intrinsic-curvature clusters of CL localize to the poles of the inner leaflet [green curve (a) or blue clusters in (b)], driven by differences in membrane curvature. A lower osmotic-pressure differential across the septal/forespore-engulfing membrane [green area, (c)/(d), respectively] induces relocalization of the lipid clusters to the septal membrane; (d) CL clusters migrate along the continuous leaflet consisting of the inner leaflet of the mother cell and the outer leaflet of the forespore-engulfing membrane to localize around the spore due to low osmotic-pressure differential (green circle); modified from Huang et al. (2006) and Huang and Ramamurthi (2010), © John Wiley and Sons with permission. **(G)** The proposed arrangement of CL in the presence of NAO. A top view of the bilayer in which the hexagonal array of large circles represents the fatty acid chains is shown. The small internal circles containing P represent the phosphate groups, hydrogen-bonded tightly by the hydroxyl of the connecting glycerol, above the two central circles of the four fatty acid chains of CL (red). This tight array provides room for the NAO molecules (green) to stack in between the rows of CL head groups; adapted from Mileykovskaya et al. (2001), © Elsevier.

domains and peptidoglycan synthesis (Muchová et al., 2011). As the helical structures are absent from the cells with repressed *pgsA* expression (in which the levels of PG and CL are much reduced; Hashimoto et al., 2009), the dyes are considered to be associated with the anionic phospholipids (Barák et al., 2008). As the CL-specific NAO dye is located in the septal regions and the poles of *B. subtilis* cells (Kawai et al., 2004), the principal component of the FM4-64 helical structures is likely to be PG (Barák et al., 2008). It has, however, been suggested that experiments showing changes in FM 4-64 staining of *B. subtilis* cells with repressed *pgsA* expression cannot serve as unambiguous evidence of FM 4-64 specificity for PG since,

first, changes in the distribution of FM 4-64 resulted from the dissipation of membrane potential by the uncoupler CCCP and, second, the membrane potential was much lower in *B. subtilis* cells with repressed *pgsA* expression (Strahl et al., 2014). In *E. coli* no discernible helical structures were observed with FM4-64 staining (Barák et al., 2008) as reported previously (Fishov and Woldringh, 1999).

Microdomains that are functionally similar to the lipid rafts of eukaryotic cells have recently been found in *B. subtilis* membranes (Lopez and Kolter, 2010). These microdomains contain homologues of eukaryotic flotillins, YuaG and YqfA, referred to as FloT and FloA, respectively (see Heterogeneous Distribution of Envelope and Envelope-Associated Proteins). The distribution of these microdomains was in a punctuated pattern along the cytoplasmic membrane (Donovan and Bramkamp, 2009; Lopez and Kolter, 2010), which differs from the patterns of FM4-64-stained helices and of CL-domains in the septal region and the poles. YisP is involved in biofilm formation in *B. subtilis* and has been predicted to produce C30 isoprenoids; the enzyme acts as a phosphatase, catalyzing formation of farnesol from farnesyl diphosphate (Feng et al., 2014). Inhibition of formation of these microdomains using zaragozic acid impaired biofilm formation and protein secretion but not cell viability and it has been suggested that polyisoprenoids are constituents of the microdomains (Lopez and Kolter, 2010; Feng et al., 2014; Bramkamp and Lopez, 2015).

Lipid Synthases and Membrane Domains

The septal and polar locations of specific phospholipids may be related to the subcellular location of the enzymes involved in their synthesis. In *E. coli*, a relationship between the location of CL (Mileykovskaya and Dowhan, 2009; Mileykovskaya and Margolin, 2012; see Cardiolipin and Other Anionic Phospholipid Domains) and that of CL synthase (ClsA) and phosphatidylglycerolphosphate synthase (PgsA; Tan et al., 2012; Dowhan, 2013) has yet to be reported. In *B. subtilis*, green fluorescent protein (GFP) fusions to ClsA and PssA, a PS synthase that catalyzes the committed step of biosynthesis of PE, are located in the septal membranes even when the corresponding genes are expressed at a low level from their natural promoters (Nishibori et al., 2005). Thus, ClsA is probably concentrated in the septal membranes under natural conditions thereby playing an important role in the septal localization of CL in *B. subtilis* (**Figure 3**). Localizing the enzymes involved in the synthesis of other lipids has yielded unexpected, interesting results. GFP fusions to several phospholipid synthases were localized to the septum in a thick, bright fluorescence band. These synthases include PgsA, PssA, Psd, which converts PS into PE, CdsA, which produces CDP-diacylglycerol, MprF, which transfers lysine to PG to produce lysylPG, and UgtP, which is responsible for glucolipid synthesis. The dot-pair distribution of UgtP corresponds to its role in regulating FtsZ assembly and hence differs from the distribution of the phospholipid synthases

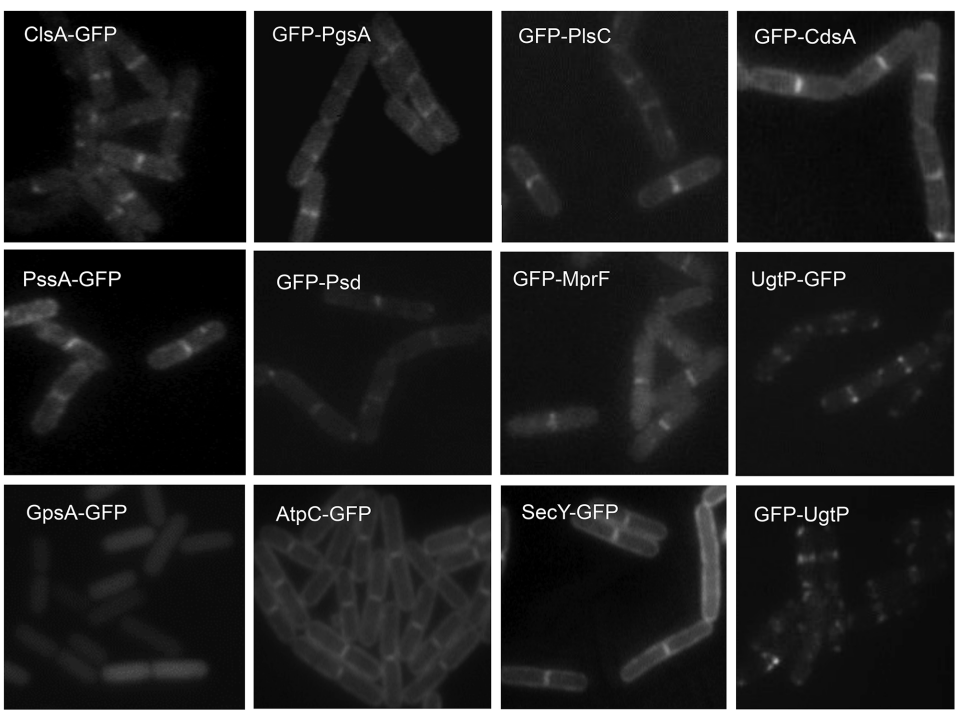

FIGURE 3 | Septal localization of lipid synthases in *B. subtilis* cells. Typical florescence images from cells harboring *gfp* fusions in the *amyE* locus cultivated in sporulation medium (DSM) up to late logarithmic growth phase are shown. Green fluorescence from the GFP-fusions was detected by using a standard GFP(R)-BP filter unit. For the name of the enzymes and their catalytic activities refer to the figure of the biosynthetic pathway (**Figure 5B**). Panels are from Figures 4 and 5 of Nishibori et al. (2005), © American Society for Microbiology. GFP-fusions of ClsA and PssA are located in the septal membranes even when the corresponding genes are expressed from their natural promoters (see Figure 4 of Nishibori et al., 2005).

(see Sensing). The locations of these enzymes thus differ from the cytoplasmic location of GpsA, which catalyzes the production of G3P (Nishibori et al., 2005; **Figure 3**), and the uniformly distributed locations of the membrane proteins AtpC, a subunit of ATP synthase, and SecY (Matsumoto et al., 2012). It has also been shown that the enzymes for lipoteichoic acid (LTA) synthesis, LtaS and YfnI, are septally localized (Schirner et al., 2009; Matsuoka et al., 2011b), but DG kinase (DgkB), which converts DG that is produced in LTA synthesis into PA, is not localized (Matsuoka et al., 2011b).

How are the lipid synthases targeted to the septal membranes? These enzymes presumably have specific regions responsible either directly for their localization or indirectly via interaction with certain cell division proteins. Selective inactivation of putative targeting regions has shown that ClsA has regions of amphipathic α-helices at its COOH-terminus that are responsible for its septal localization (Kusaka et al., manuscript in preparation). PgsA has no such amphipathic α-helices at its COOH-terminus, suggesting that the system for its septal localization is different from that of ClsA. Many other proteins with amphipathic α-helices, including MinD (see Lipid–Protein Interactions), have membrane binding properties that depend on electrostatic interactions, *via* their net positive charges, and on hydrophobicity. In addition, the catalytic domains (or consensus sequences) of *B. subtilis* PssA (Saha et al., 1996b) and *E. coli* and *B. subtilis* PgsA (Usui et al., 1994; Matsumoto, 1997) have an amphipathic α-helix structure which allows them to access their hydrophilic substrates, serine and G3P, in the cytoplasm (Matsumoto et al., 2012). The septal location of the phospholipid synthases in *B. subtilis* cells implies that most phospholipids are synthesized at the septal membranes, and, given the septal location of PE and CL, it is likely that these newly synthesized lipids are somehow prevented from diffusing into the lateral membranes (Matsumoto et al., 2006).

Chemical Basis for Generation of Lipid Domains

What then is the chemical basis for the generation of lipid domains? How do the lipid molecules form domains in membranes that are fluid? Both lipid–lipid interactions and lipid–membrane protein interactions are suspected to induce the formation of microdomains, which comprise at most some tens of molecules of a specific lipid (for a review, see Edidin, 1997). The following properties of phospholipid molecules may account for the formation of microdomains through lipid–lipid interactions.

Cardiolipin, which is a diphosphatidylglycerol, has a unique head group, with a tightly locked, surprisingly small configuration and only one negative charge (Haines and Dencher, 2002); this result contradicts the previous view reported in textbooks. The two phosphates in the head group trap a proton and are locked in a bicyclic array held together by the hydroxyl residue of the glycerol which connects the two halves. This small polar head group makes for a tighter packing of hydrophobic acyl chains between CL molecules by van der Waals force interactions than is found in lipids with larger polar head groups. It has also been suggested (Haines and Dencher, 2002) that interaction between adjacent head-groups creates a compact array of CL molecules, which becomes manifest in the presence of associated NAO arrays (Mileykovskaya et al., 2001).

Recently, a microtechnology for manipulating bacterial membrane curvature and quantitatively measuring its effect on the localization of CL in spheroplasts has been developed (Renner and Weibel, 2011). CL domains were localized to regions of high intrinsic negative curvature and MinD was found to be associated to the region of large negative curvature (see below). This localization of CL to membranes of highly negative curvature is ascribable to its cone-like molecular configuration (Gennis, 1989; Jouhet, 2013; see Cardiolipin and Other Anionic Phospholipid Domains). Polar localization of PA domains found in *E. coli*Δ*pgsA* cells lacking both CL and PG can also be ascribable to the cone-like configuration of PA molecule (Norris et al., 2002; Mileykovskaya et al., 2009).

Polar head groups of PG molecules interact by an extensive network of hydrogen bonds, ionic bonds, and coordination bonds between glycerol hydroxyls and the unesterified phosphate oxygen both in the anhydrous crystal and the hydrated gel state (Boggs, 1987; Pascher et al., 1987; Seddon, 1990). In fact, PG is probably segregated into distinct domains, in both *B. subtilis* and *E. coli* membranes, according to studies using pyrene-labeled phospholipids (Vanounou et al., 2003). This extensive and tight network of PG molecules may cause exclusion of CL molecules to produce patches of CL in the membranes (Mileykovskaya et al., 2001), since the small and tightly locked head group of CL cannot interact with PG.

The head group of the PE molecule has both a cationic amine residue and an anionic phosphate residue. Each amine and unesterified phosphate oxygen can participate in short distance intermolecular hydrogen bonds. The ethanolamine groups thus form a linkage between phosphorus groups of adjacent PE molecules and the tendency to be hydrated must be less than that of phosphatidylcholine, so producing a very compact, rigid head-group network of PE molecules (Elder et al., 1977; Hauser et al., 1981; Boggs, 1987; Seddon, 1990), and giving PE substantially higher T_m values than phosphatidylcholine which has an identical acyl chain structure. This compact head-group network of PE may well suffice to explain the formation of PE microdomains. Interactions with certain membrane proteins might then modify the lipid organization and further stabilize the head-group network, as suggested (Edidin, 1997). Polar and septal localization of PE in *B. subtilis* cells (Nishibori et al., 2005) is likely ascribable to its cone-like molecular shape (see Cardiolipin and Other Anionic Phospholipid Domains). For details refer to the previous review (Matsumoto et al., 2006).

The potential role for polyamines in lipid domain formation is largely unexplored although it has been suggested that polyamine binding to the acidic groups of phospholipids in membranes could lead to clusters forming (Schuber, 1989). Ionic interactions between polyamines and acidic phospholipids are strongest between the polyamine with the highest positive charges and the phospholipid with the highest content of negative groups (Yung and Green, 1986). Interaction with polyamines is believed to reduce the repulsive forces between negatively charged membrane components by bridging proteins and lipids

and by shielding the surface charges (Schuber, 1989). The binding of ions such as calcium to anionic phospholipids can also result in domain formation (Haverstick and Glaser, 1987) and for references see Cannon et al. (2003), but, again, this is relatively unexplored.

Transertion and Membrane Heterogeneity

Heterogeneous Distribution of Envelope and Envelope-Associated Proteins

A heterogeneous distribution of proteins in the cell envelope of bacteria, despite their size, has been widely demonstrated (see reviews, Shapiro et al., 2002; Fishov and Norris, 2012b; Govindarajan et al., 2012). During the course of investigation of specific biological functions and processes, this heterogeneity has been revealed mainly by visualization with GFP-fusions and immunofluorescence to take the form of polar, patchy and helix-like distributions in the membranes. Examples of proteins localized to the septal regions include lipid synthases in *B. subtilis* (Nishibori et al., 2005; Matsumoto et al., 2012; Takada et al., 2014; described in Lipid Synthases and Membrane Domains). Reciprocally, ATP synthase and succinate dehydrogenase are at low levels in (or absent from) the mid-cell region at the onset of cell division in *B. subtilis*, which may reflect an association with lipid domains elsewhere that are rich in PG or other lipids rather than with lipid domains in the mid-cell region (i.e., the division site) where these lipids may be at low levels (Meredith et al., 2008). Recently, FloT and FloA, homologues of eukaryotic flotillin proteins found exclusively in lipid rafts along with proteins involved in signaling and transport have been localized to discrete microdomains in the membrane of *B. subtilis* (see Cardiolipin and Other Anionic Phospholipid Domains); significantly, these microdomains, which are likely to be present in many other bacteria, also contain other proteins involved in signal transduction and cell–cell communication such as the sensor kinase, KinC, and protein secretion such as SecY in *B. subtilis* (Donovan and Bramkamp, 2009; Lopez and Kolter, 2010; Bach and Bramkamp, 2013; Bramkamp and Lopez, 2015). Flotillins are believed to play a large part in maintaining the overall physical heterogeneity of the membrane since, in their absence, lipid-ordered domains coalesce (Bach and Bramkamp, 2013; Bramkamp and Lopez, 2015). Cytoplasmic membrane proteins located in the polar regions of *E. coli* cells include ProP, LacY, and MscS (Romantsov et al., 2010) and the MCPs (methyl-accepting chemotaxis proteins; Alley et al., 1992; Sourjik and Armitage, 2010) whilst proteins located at the sites of cell constriction in *E. coli* include the components of *trans*-envelope Tol-Pal complex, TolA, TolQ, and TolR (in the cytoplasmic membrane), the peptidoglycan-associated lipoprotein Pal, (anchored to the outer membrane), and TolB (a soluble periplasmic protein; Gerding et al., 2007).

Two systematic approaches have been taken to find proteins that are preferentially located in the poles. Using two-dimensional gel electrophoresis, Lai et al. (2004) identified proteins preferentially located in *E. coli* minicells and created a catalog of polar proteins; these included the inner membrane proteins MCPs, AtpA, AtpB, YiaF, and AcrA, the membrane-associated protein FtsX, and the outer membrane proteins YbhC, OmpW, Tsx, Pal, FadL, OmpT, and BtuB. In a complementary, cataloging approach, Li and Young (2012) used FLAG peptide-tagged Tar, a known polar MCP, to isolate by affinity capture those inner membrane vesicles that originated from the poles. These vesicles were enriched in over 30 proteins. Most were in or associated with the inner membrane and included Aer, PBP1B, TnaA, DcuA, PutP, TrxA, FliP, AccD, CpxA, FliC, RpsD, YcbC, GlnP, GroEL, MlaF, NarZ, YqjD, YniB, MCPs, CheA, YijP, PBP1A, SppA, LepB, NupC, and YiaF, although a few exceptions, TolC, Pal, and BamA, were in the outer membrane. In following up the latter catalog by fusing proteins to GFP and expressing the gene from their own promoters, Aer, TnaA, GroES (rather than GroEL), YqjD, and YiaF were found to form polar foci that were distinct from inclusion bodies, thereby suggesting that these proteins are located in polar membranes *in vivo*. Moreover, the MCPs and Pal figure in the polar membrane class in both cataloges, thus lending some confidence to the results. Extensions of approaches like these should identify the remaining proteins with polar preference using the full list of *E. coli* proteins, which includes as many as 1,133 predicted integral inner membrane proteins (Bernsel and Daley, 2009) and 503 peripheral, inner membrane-associated ones (Papanastasiou et al., 2013).

GFP-fusions and immunofluorescence have provided many examples of specific proteins in polar and helix-like distributions in the membranes of *E. coli* and *B. subtilis* cells; these proteins include MreB (as well as homologues MreBH and Mbl) and the Sec translocon (for the list and references see Table 1 in Fishov and Norris, 2012a). These results have, however, been questioned due to recent findings showing that artefactual distributions can be generated by high levels of expression. The translocon in *E. coli* includes the SecYEG translocon which can associate with SecDF–YajC–YidC and SecA to enable protein transport in a reaction that is stimulated by CL (Gold et al., 2010; Schulze et al., 2014). The GFP-fusions of SecA and SecY over-expressed using 1% xylose are helically distributed in *B. subtilis* (Campo et al., 2004) whilst expression from the native promoter Psec-*secA* gives a peripherally homogeneous and septal distribution of the fusion products in conditions in which careful high-level expression controls show helices (Carballido-Lopez et al., 2006-Supplementary Figure S6; Halbedel et al., 2014). This peripherally homogeneous distribution of SecA in *B. subtilis* is different from that of *E. coli* GFP-SecE which has a patchy subcellular distribution (Shiomi et al., 2006). Localization of FlAsH-tagged SecY and SecE in *E. coli* also shows quite different patterns from that of *B. subtilis* SecA, with helix-like (patchy), polar dots and a diffuse distribution in cells under conditions of no induction (Gold et al., 2010); that said, the cells still have higher levels of tagged products from the high copy number plasmid pBAD22, even in the absence of the inducer, compared with those from their native promoter on the chromosome, i.e., single copy. The translocon distributions in *B. subtilis* and *E. coli* also differ from that of the *Streptococcus pyogenes* translocon, which

forms a single microdomain (Rosch and Caparon, 2005; Rosch et al., 2007) and that of *S. pneumonia* D39, expressed from the native chromosomal loci, which localizes dynamically to different places (Tsui et al., 2011). GFP-fusions of MreB have been shown to move, as fragmented discrete patches, perpendicular to the long axis of *B. subtilis* cells using highly sensitive time-lapse imaging (Dominguez-Escobar et al., 2011; Garner et al., 2011). This movement of MreB did not, as one would have expected, follow a helical pattern. Recent reports and reviews suggest that the distribution pattern reported for *E. coli* MreB mainly resembles that reported for *B. subtilis* MreB: a punctuated pattern with pairs of dots or small bands generally described as helical (van Teeffelen et al., 2011; Chastanet and Carballido-Lopez, 2012; Margolin, 2012; Errington, 2015). Indeed, MreB proteins form elongated filamentous structures when over-produced or when observed in late phases of growth. In virtually all older reports describing MreB localization, inducible, mostly over-expressed, GFP fusions were used, and observations were often made during the late exponential stage, when the structures were easier to visualize. This could be the case for other fusion proteins showing polar and helix-like distributions under highly expressed conditions. Thus, it is difficult at present to decide how many of the proteins do indeed form long-range, helical structures at the membrane, as noted by Margolin (2012).

Lipid–Protein Interactions

The last stage of transertion (see below) involves interaction of nascent proteins with the polar head groups of lipids followed by insertion into non-polar acyl-chain layer of the membrane. Proteins with a preference for a specific polar head group interact to form a specific domain in the membrane. Integral inner membrane proteins with specific lipid preferences could therefore be located in specific membrane domains (for the list of proteins see Table 2 in the review of Fishov and Norris, 2012a). In addition, peripheral membrane proteins that associate weakly with specific lipids could help form specific domains and, if these proteins bind other proteins, could bring them into the domain too. Among the peripheral membrane proteins, there are amphitropic proteins that have two apparent locations: one form of the protein is in the aqueous compartment of the cytosol whilst the other form is weakly associated with the cell membrane. Amphitropic proteins can be classified into three major categories (Johnson and Cornell, 1999), based on the way they associate with membranes. The first class (A) contains motifs with binding pockets for a lipid monomer, called lipid clamps. The second class (B) contains lipid covalent anchors embedded in the lipid bilayer; this class includes lipoproteins such as the major outer membrane lipoprotein (Braun's lipoprotein), LolB, components of Bam complexes and RcsF with an *N*-acyl chain and a diacylglyceryl moiety at the NH_2-terminus (Sankaran and Wu, 1994; Matsumoto, 2001; Suzuki et al., 2002; Okuda and Tokuda, 2011; Shiba et al., 2012; Konovalova et al., 2014). *E. coli* has 96 lipoproteins, 58% of which have completely unknown functions (Brokx et al., 2004). The third class (C) of amphitropic proteins contains amphipathic α-helices, which bind to a membrane by partitioning into the membrane bilayer such that the hydrophobic face of the protein is sequestered away from water, yet its polar face can contact the aqueous phase (Johnson and Cornell, 1999). The helix axis lies parallel to the membrane surface. The weak (reversible) interaction of the proteins with amphipathic α-helices plays an important role in regulation of their functions. Representatives of this class include a family of prokaryotic cytoskeletal proteins such as MreB, MinD, and FtsA, having an amphipathic α-helix at their NH_2- or COOH-terminus (Szeto et al., 2003; Pichoff and Lutkenhaus, 2005; Salje et al., 2011; Szwedziak et al., 2012; **Figure 4**). Membrane anchoring with amphipathic helices has yet to be reported for any eukaryotic filament (Salje et al., 2011). It has been demonstrated recently that the nucleoid occlusion protein of *B. subtilis*, Noc, also associates with the cell membrane via an NH_2-terminal amphipathic α-helix. It occludes assembly of the division machinery by simultaneous binding to DNA and the membrane (Adams et al., 2015). PgsA, *B. subtilis* PssA (Matsumoto, 1997), and the well-understood mammalian CTP: phosphocholine cytidylyltransferase (CCT) have an amphipathic α-helical structure in the middle of the protein (Cornell and Taneva, 2006). The amphipathic α-helices that were found in DnaA (Garner and Crook, 1996; Makise et al., 2001) are not involved in membrane association; instead, the results of membrane retention experiment obtained with various fragments of the protein indicated that the association is through a concerted interaction of distant residues forming a surface (Regev et al., 2012).

MreB is one of the key components of the bacterial cytoskeleton that lies just underneath the membrane and organizes the cell wall synthesis machinery. In *E. coli*, MreB has an amphipathic α-helix (an 11 amino acid residue sequence which includes two methionine, two phenylalanine, one leucine on one face of the helical wheel and three basic residues on the other face) at its NH_2-terminus that is responsible for its location underneath the membrane. In gram-positive bacteria and the thermotrophic archaeum *Thermotoga maritima*, the counterpart of MreB has no such helix (Salje et al., 2011) and the membrane binding of *T. maritima* MreB is mediated by a small insertion loop that contains leucine and phenylalanine (residue 93 and 94), two other hydrophobic residues, the start methionine and a leucine (residues 1 and 2; Salje et al., 2011). MinD, plays a key role in division site selection by protecting the poles from aberrant positioning of FtsZ ring, and has a small amphipathic α-helix of 8–12 residues, termed the membrane targeting sequence or MTS, at its COOH-terminus that is conserved across eubacteria, archaea, and chloroplasts; this MTS is essential for association with anionic phospholipid-enriched membrane from which, in the case of *E. coli*, it can be easily detached by MinE at the appropriate time in the Min oscillation cycle (Raskin and de Boer, 1999; Szeto et al., 2002, 2003; Mileykovskaya et al., 2003; Vecchiarelli et al., 2014). The actin-like protein FtsA has an MTS that comprises a conserved COOH-terminal amphipathic α-helix of 13–14 residues (Pichoff and Lutkenhaus, 2005); FtsA polymerizes to form an "FtsA ring." The tubulin-like protein FtsZ is tethered to FtsA through a COOH-terminal tail of 16 residues to polymerize to form an FtsZ ring underneath the A-ring (Szwedziak et al., 2012; **Figure 4**). Work on liposome division has shown the importance of the MTS in division. ATP

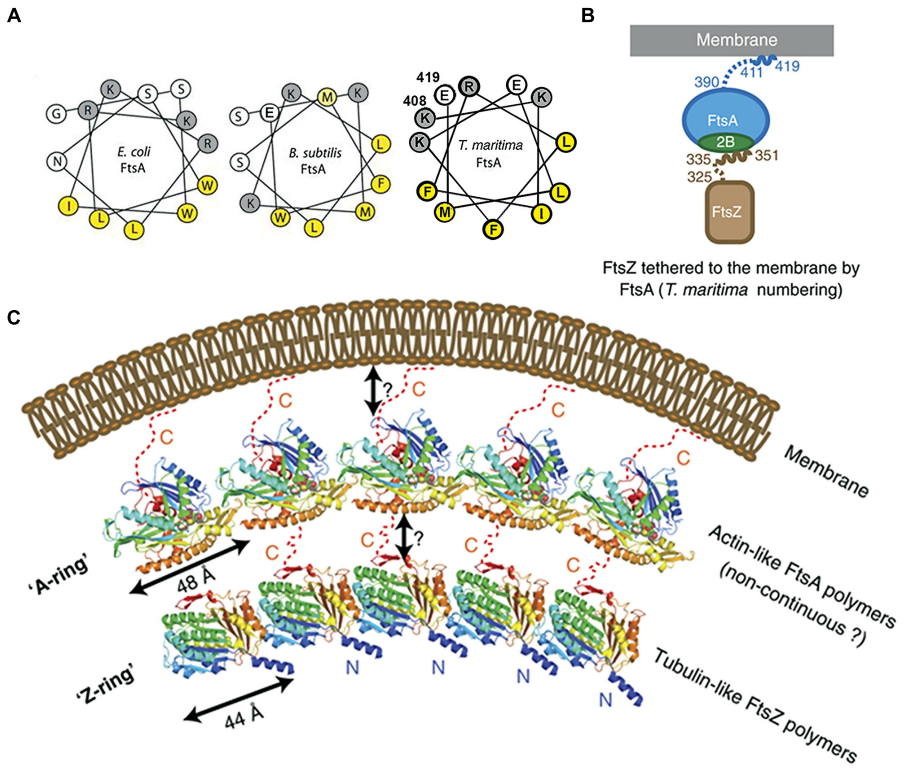

FIGURE 4 | Crucial role of the COOH-terminal amphipathic α-helix of FtsA in tethering FtsZ to the membrane. (A) Helical wheel diagrams of the COOH-terminal domains of FtsA from *E. coli, B. subtilis* (Pichoff and Lutkenhaus (2005), © John Wiley and Sons with permission.) and *Thermotoga maritima* (prepared using Helixator-TCDB: www.tcdb.org/progs/helical_wheel.php). Hydrophobic residues are highlighted in yellow and negatively charged residues are highlighted in gray. **(B)** FtsA/FtsZ membrane-bound complex of *T. maritima*. **(C)** The Z-ring made of polymerized tubulin-like FtsZ may be attached to the membrane by an A-ring, made of actin-like FtsA polymers. The two cartoons are adapted from Szwedziak et al. (2012), © John Wiley and Sons with permission.

is needed not only for the polymerization of FtsA and also for its attachment via its MTS to lipid monolayers and to vesicle membranes; this polymerization of FtsA caused vesicle shrinkage, consistent with the protein facilitating division both indirectly by interacting with FtsZ and directly by altering the membrane (Krupka et al., 2014). A fusion of FtsZ-YFP-mts was constructed with an MTS at its COOH-terminus to tether it directly to the membrane; this allowed Z-rings to assemble in multi-lamellar tubular liposomes and to generate a constriction force in the presence of GTP without the need for any other protein (Osawa et al., 2008). Uni-lamellar liposomes incorporating FtsA and FtsZ-YFP produced more natural Z-rings, which constricted liposomes and in some cases appeared to complete the division (Osawa and Erickson, 2013). The co-polymerization of FtsZ and FtsA is proposed to lead to bending, curvature and membrane constriction because the subunit repeat lengths of FtsZ and FtsA are different, being roughly 4 and 5 nm, respectively (Szwedziak et al., 2014; **Figure 4**).

Membrane Curvature and Protein Location

In rod-shaped bacterial cells, negatively curved membranes characterize the poles and parts of the developing septum. In *B. subtilis*, it has been suggested that this curvature is sensed by DivIVA (Lenarcic et al., 2009; Ramamurthi and Losick, 2009), which is located at the septum and at mature poles and which is responsible for the polar location of the division inhibitor MinC/MinD via MinJ, a system different from the Min system of *E. coli* (Marston et al., 1998; Bramkamp et al., 2008; Patrick and Kearns, 2008). In cells with engineered curvature, DivIVA is indeed located preferentially in regions of high negative curvature (Renner et al., 2013; **Figure 2F**). The location of DivIVA depends on SecA although DivIVA does not contain a signal sequence (Halbedel et al., 2014). Instead, SecA is considered to act as a chaperone in the folding of DivIVA, which has essentially an α-helical structure with several coiled-coil helices that contribute to the curvature of the DivIVA tetramer (Halbedel et al., 2014). The crystal structure of this tetramer resembles the crescent shape of eukaryotic BAR domains which bind to curved membranes and also introduce curvature (Lemmon, 2008; Oliva et al., 2010; Mim and Unger, 2012). Enzyme I (EI), which is a part of the phosphoenolpyruvate-phosphotransferase system (PTS) responsible for the sensing and uptake of many extracellular sugars, is located in the poles of *E. coli* and *B. subtilis* due, it is proposed, to its affinity for negatively curved membrane, an affinity shared by DivIVA (Govindarajan et al., 2013). Conversely, SpoVM, a small peripheral membrane protein with an amphipathic α-helix, associates with the positively curved (convex) membrane surfaces of the forespore to form

the spore coat complex with SpoVA, in the mother cell during sporulation (Ramamurthi, 2010; **Figure 2F**). Recently, it has been suggested that the actual amphipathic α-helix region of SpoVM (26 aa) is atypical; this region is short with only 13 residues (from 11 to 23), contains only one positively charged residue (Arg) and three Gly residues, and inserts deeply into the membrane, unlike many amphipathic α-helix molecules that only insert shallowly into the membrane (Gill et al., 2015). The authors hypothesize that deep insertion of SpoVM into membrane, which involves extensive interactions with acyl chains to sense packing differences in differently curved membranes and which may involve cooperative interactions with other SpoVM proteins, drives its preferential localization onto slightly convex membranes surface such as the outer surface of the forespore.

Transertion

In the transertion hypothesis, it is proposed that the coupled transcription-translation of genes encoding membrane proteins (1) structures the membranes, both physically and chemically, and (2) positions these genes close to the membrane (Norris and Madsen, 1995; Woldringh, 2002; **Figure 1**). Despite early evidence in its favor (Binenbaum et al., 1999), this hypothesis lacked further evidence to support it for long time. Recently, Libby et al. (2012) have shown that the synthesis of membrane proteins expression affects the position of chromosome loci in *E. coli* cells. They observed that two genetic loci, *lacY* and *tetA*, which encode membrane proteins, were rapidly shifted toward the membrane upon induction whilst the chromosomal locus for a cytoplasmic protein was not shifted; in addition, antibiotics that block transcription and translation prevented these shifts toward the membrane. More recently still, a radial contraction of the *E. coli* nucleoids was observed immediately after the addition of inhibitors of either transcription or translation, again consistent with transertion normally exerting an expanding force on the nucleoid (Bakshi et al., 2014). In the case of inhibition of transcription and hence transertion by Rifampicin, the eventual expansion of the nucleoid has recently been attributed to the penetration of the nucleoid by the ribosomal subunits (Bakshi et al., 2014; Sanamrad et al., 2014). That said, it should be noted that transcription is the essential source of supercoiling (particularly at high growth rates when 50–80% of active RNA polymerases are transcribing *rrn* genes) which is a major cause of nucleoid compaction; hence, inhibition of transcription initiation with Rifampicin results in RNA polymerase run-off, less supercoiling, and nucleoid expansion; this expansion can happen even after nucleoid compaction by chloramphenicol when transertion is absent (for a review, see Jin et al., 2013).

Over 1,100 genes distributed throughout the *E. coli* genome are predicted to encode integral inner membrane proteins (Bernsel and Daley, 2009) and therefore their expression could maintain the chromosome in an expanded and dynamic state, consistent with the transertion hypothesis. Significant numbers of ribosome and RNA polymerase copies have been shown by superresolution imaging to extend from the nucleoid to the cytoplasmic membrane (Bakshi et al., 2012), indicating that transertion exerts a direct radially expanding force on the nucleoid (Woldringh, 2002; Woldringh and Nanninga, 2006). In this study, however, few copies of RNA polymerase were found near the polar caps, indicating that transertion could not occur in the regions away from the nucleoid (polar caps) and therefore it might seem that the radially expanding force on the nucleoid of transertion could not be a direct axially expanding force. Such axial expansion might, however, result from the penetration of the nucleoid by the 30S and 50S subunits released from the 70S ribosomes following treatment with inhibitors of translation (Bakshi et al., 2014; Sanamrad et al., 2014). It should be noted that although less than 15% of *E. coli*'s ribosomes are reported to be available to participate in transertion (Bakshi et al., 2012; Gahlmann and Moerner, 2014), this figure does not necessarily reflect the percentage of the ribosomes that are actually engaged in translation. A higher percentage is likely to be available in *C. crescentus* where genes and mRNA have been found to be close to one another (Llopis et al., 2010).

There are plenty of polar membrane proteins as noted in the previous section (see Heterogeneous Distribution of Envelope and Envelope-Associated Proteins). Transertion is unlikely to be an important factor in directly controlling their location since, firstly, RNA polymerase is relatively scarce near the polar caps and, secondly, the Sec machinery responsible for inserting integral membrane proteins into membranes is not specifically located in the poles in either *B. subtilis* (Carballido-Lopez et al., 2006-Supplementary Figure S6) or *E. coli* (Shiomi et al., 2006; Gold et al., 2010; see Heterogeneous Distribution of Envelope and Envelope-Associated Proteins). Thus, some integral membrane proteins (e.g., the MCPs) are inserted into the cytoplasmic membrane around the nucleoid via the Sec machinery and then freely migrate in the membrane to the polar regions (Shiomi et al., 2006). One possibility is that integral membrane proteins such as the MCPs are excluded from the transertion domains around the chromosome because they have no affinity for the lipids in which those domains are enriched. The reason for this is that transertion may create a problem if it leads to the formation of an array of MCPs of the wrong size in the wrong place. Another, recently proposed, possibility is that polar localization of the diffused MCPs occurs independently of the phospholipid composition of the cytoplasmic membrane and is not be dictated by the curvature of the cell poles, instead, MCPs interact with components of the trans-envelope Tol-Pal complex which restricts the diffusion of MCP arrays (Santos et al., 2014; see Transertion Problems).

In the original transertion hypothesis, the structuring of the membrane and the tethering of genes was restricted to those genes encoding proteins inserted into or through membranes. Although the role of the former class of proteins (i.e., integral membrane proteins) is easy to imagine, the latter class (i.e., secreted and exported proteins) is also of interest. For example, there could be a role in transertion for Braun's lipoprotein if the lipid modification at the NH_2-terminus of the lipoprotein were to occur before the synthesis of the rest of the protein. Moreover, the transertion hypothesis could be extended to genes encoding peripheral membrane proteins such as SeqA (Slater et al., 1995; Shakibai et al., 1998) and DnaA in *E. coli* (Regev et al., 2012) and Noc in *B. subtilis* (Adams et al., 2015).

Finally, it has been proposed recently on entropic grounds that transertion enables ribosomal subunits to penetrate the nucleoids

and to initiate the more general process of co-transcriptional translation (Bakshi et al., 2014). Co-transcriptional translation would then protect nascent mRNA (Deana and Belasco, 2005; Deneke et al., 2013) and prevent the backtracking of RNA polymerases (McGary and Nudler, 2013), thereby giving transertion a key role in the optimization of transcription and translation (Bakshi et al., 2014). In the context in which two chemically identical chromosomes are in competition for the transcriptional and translational apparatuses, such optimization constitutes a positive feedback that could underpin differentiation (Norris and Madsen, 1995; Norris and Amar, 2012).

Hyperstructures

A hyperstructure is an assembly of elements (such as genes, RNA, proteins, small molecules and ions) that performs a function and that constitutes a substantial proportion of the cellular material (Norris et al., 2007a; Saier, 2013; Meyer et al., 2014). The accumulating evidence for their existence allows them to be classed in several ways (Norris et al., 2007b). In the case of the membrane, the best known include those involved in motility (such as the MCPs and flagella), lactose metabolism, energy generation, and cell division. It has been further proposed that a dialog between hyperstructures determines the phenotype of the cell (Norris et al., 2014a). Here we focus on some of the hyperstructures involved with the membrane.

Transertion Hyperstructures

The coupled transcription-translation-insertion of membrane proteins (transertion) has been proposed to tether networks of nascent proteins, mRNAs and genes to the cytoplasmic membrane thereby attaching DNA dynamically to the bacterial cell envelope (Norris, 1995; Norris and Madsen, 1995; Woldringh, 2002; **Figure 1**). This means that the high level expression of a gene encoding a membrane protein could lead to the formation of a domain in the membrane enriched by the nascent proteins, possibly specific lipids, and translocon complexes, along with an adjacent, highly structured cytoplasm to give a transertion hyperstructure (Norris, 1995; Norris and Madsen, 1995; Binenbaum et al., 1999; Woldringh, 2002).

The *lac* operon is an obvious candidate for giving rise to a transertion hyperstructure. In *E. coli*, full induction of this operon has been calculated to give 23 RNA polymerases on *lacZ* and 5 or 6 on *lacY* and *lacA* with the ensemble of the nascent, full length and decaying mRNAs being translated by several hundred ribosomes (Kennell and Riezman, 1977). *lacY* encodes the membrane-bound permease with an average of four ribosomes calculated as translating the corresponding full length mRNA (Kennell and Riezman, 1977). LacZ-encoding mRNA has been shown to remain close to the *lacZYA* locus, consistent with both transcription and translation occurring in the same place (Llopis et al., 2010). Expression of the *lac* operon brings the locus closer to the membrane and this movement depends on the presence in the operon of *lacY*, consistent with transertion (Libby et al., 2012). Hence, calculations and experiments suggest that a transertion hyperstructure exists that comprises the *lac* genes dynamically attached to tens of nascent mRNAs and to 100s of ribosomes and the nascent enzymes some of which would be inserted into the membrane. This does not, of course, mean that the Lac proteins once synthesized remain within the transertion hyperstructure. Indeed, a tagged version of LacY – albeit expressed from a plasmid – was localized to the poles (Romantsov et al., 2010).

RNA degradation may also play a part in the dynamics of transertion hyperstructures. Using epifluorescence microscopy and molecular dynamics simulation, RNase E, the backbone of the RNA degradosome, was shown to diffuse over the entire inner membrane of *E. coli* to form, along with other proteins, short-lived hyperstructures (Strahl et al., 2015). The existence of these hyperstructures depends on the presence of the RNA substrate (Strahl et al., 2015) so they may be considered as *functioning-dependent* structures, that is, structures that form due to their activity (Norris et al., 2007a). It should be noted that such separation of the degradosomes from the sites of transcription would favor nascent transcripts being translated by polyribosomes, that is, would favor the coupling of transcription and translation over the separation of these processes (Strahl et al., 2015).

Transertion Problems

Transertion is not only a likely solution to many of the problems that confront cells but also a source of potential problems. One problem would occur if a transertion hyperstructure were to determine, inappropriately, the size, position or composition of another class of hyperstructure. Consider, for example, the importance in signal transduction of the distribution of the MCPs and related proteins into many small clusters or into one giant cluster (Bray et al., 1998). These distribution confer different sensitivities but this relationship could be lost if transertion were to dominate by creating a large chemosignaling hyperstructure. In *E. coli*, part of the solution may be that the genes that encode chemotaxis proteins are located on the chromosome so that their transertion associates them with another major hyperstructure, that of the flagellum; it is then conceivable that differences in the affinities of the chemotaxis and flagellar proteins for the chemical or physical properties of lipids are responsible for the chemotaxis proteins relocating from the flagellar hyperstructure(s) to the poles (Cabin-Flaman et al., 2005). Consistent with this, Tar-GFP does diffuse away from the sites where this MCP is synthesized to the poles (Shiomi et al., 2006). It has been recently found that this polar localization of the diffused MCPs does not depend on either the phospholipid composition of the cytoplasmic membrane or the curvature of the cell poles; instead, MCPs interact with components of the trans-envelope Tol-Pal complex which restricts the diffusion of MCP arrays (Santos et al., 2014). The Tol-Pal complex is also part of the cell division hyperstructure, to which it is recruited by FtsN so as to play a role in the invagination of the outer membrane during division (Gerding et al., 2007).

A second problem would arise if the lipid preferences of the constituents of the transertion hyperstructure were to menace the planar, bilayer structure of the cytoplasmic membrane. The

reality of this danger is evident from the proteo-lipid structures that result from the overproduction of peripheral and integral membrane proteins (Weiner et al., 1984; Arechaga et al., 2000; van den Brink-van der Laan et al., 2003; Eriksson et al., 2009). In mitochondria, the bioenergetic supercomplexes are indeed in specific membrane structures whilst in bacteria such as *E. coli*, fluorescent fusions suggest that the complexes are spatially dispersed in mobile 100–200 nm domains containing 10s–100s of complexes (Erhardt et al., 2014; Llorente-Garcia et al., 2014). A possible solution would be for an abundant structure such as the ATP synthase to have subunits with complementary lipid preferences (Arechaga et al., 2000) since even overproduction of all eight subunits results in morphological changes (von Meyenburg et al., 1984). Extending this argument, one might expect different proteins to have preferences for different lipids, which may help explain why cells have so many different lipids. An alternative or complementary solution would be the creation by a large, dynamic hyperstructure of many mobile domains with an affinity for ATP synthase.

Finally, problems due to the formation of an inappropriate transertion hyperstructure might be avoided by reducing the time during its synthesis in which the nascent protein interacts with the membrane; this might be achieved if, for example, evolution were to have selected for the membrane-interacting sequences (such as amphipathic helices) to be located at the COOH-terminus rather than at the NH_2-terminus.

Sensing

The membrane is the final frontier between the cell and its environment so membrane-based hyperstructures are in the right place to sense and to respond to environmental changes. This task is not trivial. Not only do new mRNAs and proteins have to be made but many existing mRNAs and proteins must be degraded. There are, for example, probably over a 1000 membrane proteins in *E. coli* (Bernsel and Daley, 2009) and a similar number in *B. subtilis* (Hahne et al., 2008; Otto et al., 2010; van Dijl et al., 2012) and the functioning of these proteins must be coordinated; this task is particularly difficult when major changes in the protein composition of the membrane must occur as during changes in growth conditions. On the entry of *B. subtilis* to stationary phase, the levels of the many proteins that increase include those involved in the uptake of glycerol, ribose, lactate, nucleoside, succinate, fumarate and zinc whilst the levels of those that decrease include transporters of malate, Fe^{3+} citrate, Fe^{3+} hydroxamate, and hydroxymethylthiamine (HMP)/thiamine transport (Otto et al., 2010). In *E. coli* cells supplemented with glucose, which is the preferred carbon and energy source, the transcriptional levels of the many genes that increase include those involved in the import of polyamines, inorganic phosphate and Mg^{2+} whilst the levels of those that are repressed (in other words, upregulated upon glucose–starvation), are of transporters and periplasmic receptor proteins related to the import of alternative carbon and carbon–nitrogen sources, which include amino acids, carbohydrates, lactate, glycerol, peptides, dipeptides, and nucleotides (Gutierrez-Ríos et al., 2007). This transcriptome pattern is consistent with the consequences of carbon catabolite repression exerted by glucose (Saier et al., 1996). The phosphoenolpyruvate-dependent PTS controls the uptake of a large number of energetically preferred sugars. It comprises proteins, EI and HPr, which are common to all substrates, as well as sugar-specific permeases, enzymes II (EIIs). Interestingly, EI and HPr are mainly located near the poles of *E. coli* cell (Patel et al., 2004; Lopian et al., 2010; Govindarajan et al., 2012). Upon addition of the sugar to the growth medium, HPr is phosphorylated by EI; HPr-P produced is released from the polar membranes and distributes in the cell, though EI remains located near the poles of negatively curved sites (Govindarajan et al., 2013; see Membrane Curvature and Protein Location). A fraction of HPr-P gets near the membrane to phosphorylate the permeases, allowing them to transport the sugars into the cell and to phosphorylate them (Govindarajan et al., 2012).

Common affinities for molecules and ions within and between hyperstructures may help in this task of coordination. These molecules include polyamines, poly-(R)-3-hydroxybutyrate, polyphosphate and, of course, lipids (Norris et al., 2014b). Polyamines, for example, bind to nucleic acids, ribosomes and porins, and stimulate the synthesis of around 300 proteins in *E. coli* that include the sigma factors RpoS, FecI, RpoN, and related RNA polymerase omega subunit RpoZ, Cya, Cra, Fis, H-NS and SpoT (Igarashi and Kashiwagi, 2006). These multiple actions may allow polyamines to play an important, coordinating, role in the survival of *E. coli* in the transition to stationary phase (Terui et al., 2012; Norris et al., 2014b) and during osmotic changes (Munro et al., 1972).

Similar global regulatory roles can be ascribed to CL and an increase in CL levels has been proposed as a general physiological response that protects microorganisms from lysis due to osmotic stress (Catucci et al., 2004) and, in line with this, an increase in osmolality leads to transcriptional activation of the *cls* gene in *E. coli* (Romantsov et al., 2007). This increase in CL and its distribution to the poles was correlated with the polar distribution of the osmosensory transporter ProP which actively transports osmo-protectants into the cell (Mileykovskaya, 2007; Romantsov et al., 2007). In such coordination of lipid metabolism with the environment, the formation of a hyperstructure containing membrane components may help. Acyl carrier protein (ACP), a small protein of 9 kDa, interacts with diverse proteins associated with many biosynthetic pathways, including enzymes involved in synthesis of fatty acid in the cytoplasm as well as enzymes on or in the membrane involved in phospholipid or LPS synthesis; the latter assocations could account for the partial localization of ACP with *E. coli* membranes. Two enzymes involved in phospholipid synthesis, PlsB, a *sn*-glycerol-3-phosphate acyltransferase and PssA, a PS synthase, have been shown to interact with ACP and YbgC, an acyl-CoA thioesterase involved in fatty acid synthesis, using a tandem affinity purification method (Gully and Bouveret, 2006). *E. coli* PssA, which has a preference for acidic phospholipids, exists as both a membrane-associated active form and a cytoplasmic latent form and is at the heart of a cross-feedback regulation of the synthesis of zwitterionic (PE) and acidic phospholipids (Shibuya, 1992; Okada et al., 1994; Saha et al., 1996a; Matsumoto, 1997; Rilfors et al., 1999; **Figure 5A**). Bacterial two-hybrid analysis has

shown that the enzymes in the phospholipid synthetic pathway, PlsB-PssA and ACP, form a complex in/on the inner membrane and further that YbgC, a fatty acid synthesis enzyme, and PlsB, form a complex in association with ACP (Gully and Bouveret, 2006). Thus, physical interactions between many of the enzymes responsible for fatty acid synthesis and phospholipid synthesis could form a hyperstructure to help coordinate lipid metabolism.

Sensing changes in nutrient availability entails bacteria transmitting this information to flagella hyperstructures to perform chemotaxis (see Transertion Problems) and to the division apparatus to regulate their size, grow faster and become larger when they are grown in nutrient-rich media. UgtP, a glucosyltransferase responsible for the synthesis of glucosylated diacylglycerols, one of which is the anchor of LTA synthesis, is localized, in a dot-pair structure similar to that of the open ring of FtsZ, to the division site in *B. subtilis* (Nishibori et al., 2005). UgtP is a division inhibitor, which prevents assembly of FtsZ and which results in an increase in the length of the cells under nutrient-rich conditions (Shiomi and Margolin, 2007; Weart et al., 2007; **Figure 5**). It has been proposed that UDP-glucose acts as a proxy for nutrient availability and modulates the equilibrium between the UgtP–UgtP oligomer and the UgtP-FtsZ complex thereby serving as a molecular rheostat to help ensure that cell size is precisely co-ordinated with growth rate and nutrient availability (Chien et al., 2012). OpgH, a glucosyltransferase, is an integral membrane protein in the inner membrane of *E. coli* that is involved in the synthesis of osmoregulated periplasmic glucans, OPG (MDO); recently, OpgH has been localized to the division ring and shown to inhibit FtsZ assembly in the presence of UDP-glucose so as to delay the timing of cell division (Hill et al., 2013; **Figure 5A**). These two, very different, bacteria employ unrelated glucosyltransferases – a peripheral membrane enzyme for LTA synthesis in *B. subtilis* and an integral inner membrane enzyme for OPG synthesis in *E. coli* – that both have the second, "moonlighting," function of coupling nutrient availability to cell division by regulating FtsZ assembly (Hill et al., 2013). Disruptions of the moonlighting function of UgtP not only affect cell length: *ugtP* null mutants, which lack glucolipid products of the UgtP-catalyzed reaction, membrane glucolipids, are rounder (Price et al., 1997) and abnormally bent and distended (Lazarevic et al., 2005; Matsuoka et al., 2011a). Moreover, the extracytoplasmic function (ECF) σ factors, σ^M, σ^V, and σ^X are constitutively activated (Salzberg and Helmann, 2008; Matsuoka et al., 2011a; Hashimoto et al., 2013), consistent with glucolipids directly influencing anti-σ^M and anti-σ^V factors by stabilizing conformations that sequester the respective ECF σ factors (Seki et al., 2015).

A two-hybrid-based investigation of interactions between the components of cell division machinery (27 proteins) and the enzymes involved in lipid synthesis (12 enzymes) in *B. subtilis* has revealed that FtsA interacts with PlsX (Takada et al., 2014). PlsX is an acyl-ACP:phosphate acyltransferase that synthesizes acyl-phosphate, an essential substrate for lysophosphatidic acid (LPA) production by PlsY, an acyltransferase that uses acyl-phosphate for the first acylation of *sn*-glycerol-3-phosphate (G3P); these are novel enzymes in a unique LPA synthesis pathway found in prokaryotic but not in eukaryotic cells (Lu et al., 2006;

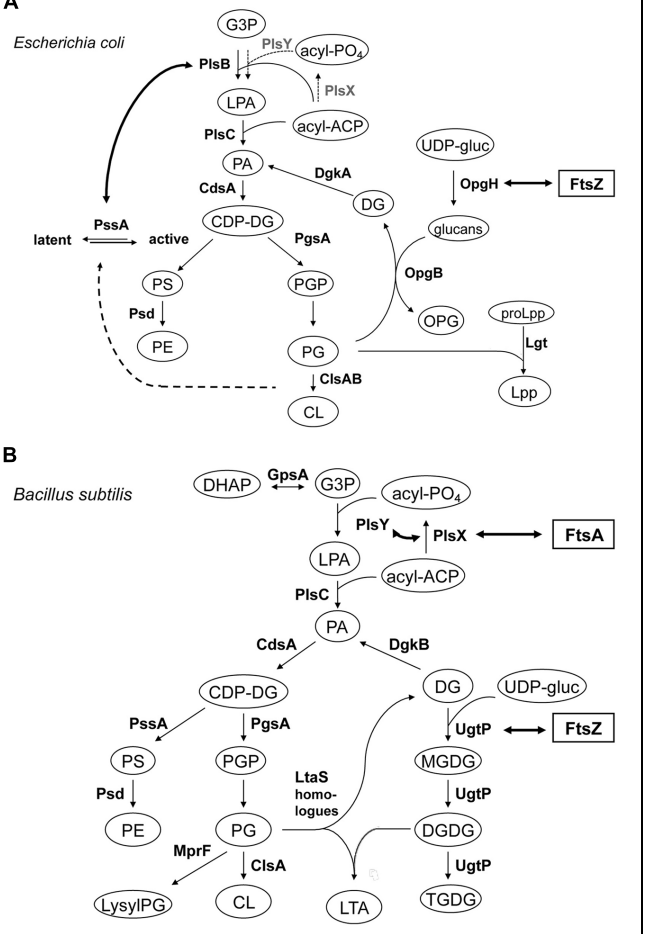

FIGURE 5 | Lipid biosynthetic pathways and interactions of phospholipid synthases and proteins involved in cell division. **(A)** Phospholipid biosynthetic pathway in *E. coli.* The gene product catalyzing each step is indicated. Abbreviations used are: G3P, glycerol-3-phosphate; LPA, lysophosphatidic acid; PA, phosphatidic acid; acyl-PO_4, acylphosphate; acyl-ACP, acyl acyl-carrier protein; CDP-DG, (d)CDP-diacylglycerol; PS, phosphatidylserine; PE, phosphatidylethanolamine; PGP, phosphatidylglycerophosphate; PG, phosphatidylglycerol; CL, cardiolipin; OPG, osmoregulated periplasmic glucans (or MDO); UDP-gluc, UDP-glucose; DG, diacylglycerol; Lpp, major outer membrane lipoprotein; proLpp, prolipoprotein. Trace activities of PlsX-PlsY for LPA synthesis in *E. coli* (Lu et al., 2006/Hara et al., 2008) were indicated with thin letters and dotted arrows, different from those of the major pathway in *B. subtilis*. For Cls homologues, ClsA and ClsB, refer to Tan et al. (2012). Interaction of OpgH (a glucosyltransferase) and FtsZ indicated with thick arrow is from Hill et al. (2013); see Sensing). Activation of phosphatidylserine synthase, PssA, with acidic phospholipids indicated with thick dotted arrow is adapted from Shibuya (1992) and Matsumoto (1997). Interaction of PlsB and PssA is from Gully and Bouveret (2006), but to avoid apparent complexity the interactions between PlsB, ACP and YbgC, an Acyl-CoA thioesterase, shown by the authors, are not depicted. **(B)** Biosynthetic pathways for phospholipids, glucolipids and LTA in *B. subtilis*. Abbreviations used are: lysylPG, lysylphosphatidylglycerol; MGDG, monoglucosyldiacylglycerol; DGDG, diglucosyldiacylglycerol; TGDG, triglucosyldiacylglycerol; LTA, lipoteichoic acid; DHAP, dihydroxyacetone phosphate. For other abbreviations refer to (A) for *E. coli*. The pathway is adapted and compiled from Jerga et al. (2007) and Matsuoka et al. (2011b). For LtaS homologues (YflE, YfnI, YqgS and YvgJ) refer to Gründling and Schneewind (2007), Matsuoka et al. (2011b) and

(Continued)

FIGURE 5 | Continued

Hashimoto et al. (2013). Interactions of FtsA and PlsX, and PlsY, both indicated with thick arrows, are from Hara et al. (2008) and Takada et al. (2014), respectively, but to avoid apparent complexity the interaction of PlsX with EzrA, DivIA and others, shown by the authors, are not depicted. Interaction of UgtP (a glucosyltransferase) and FtsZ indicated with thick arrow is from Weart et al. (2007) and Chien et al. (2012); see Sensing).

Paoletti et al., 2007; Yoshimura et al., 2007, and Hara et al., 2008; **Figure 5B**). *In vivo* cross-linking shows that PlsX interacts with cell division proteins (EzrA, DivIVA), cytoskeletal proteins and several metabolic enzymes, in addition to FtsA. PlsX is in a punctuated pattern in the peripheral membrane and is present at potential division sites independently of FtsA and FtsZ. Inactivation of PlsX leads to aberrant Z-ring formation. Thus, the key enzyme for phospholipid metabolism interacts with the cell division machinery in order to complete septum assembly (Takada et al., 2014). Although PlsX interacts with PlsY, many other enzymes involved in phospholipid synthesis, which localize in the septal region (Nishibori et al., 2005), do not interact with it, except MprF that synthesizes lysylPG (Takada et al., 2014). Depletion of PlsX leads to the cessation of both fatty acid and phospholipid biosynthesis (Paoletti et al., 2007; Yao and Rock, 2013).

Cell Cycle

Transertion may help provide solutions to the problems of coupling growth to the cell cycle, of triggering chromosome replication, and of coupling chromosome segregation spatially and temporally to cell division. The first problem, the way in which growth is coupled to the cell cycle, has been a mystery that has lasted for over half a century (Schaechter et al., 1958; Osella et al., 2014). Many different metabolic processes occur during growth and these processes are needed for the synthesis of RNA, proteins and lipids. These processes come together in transertion, which is therefore well-placed to integrate metabolic information (Fishov and Norris, 2012b). Moreover, transertion is a primary determinant of the structure and composition of the membrane, which is central to the initiation of DNA replication, segregation and cell division, as well as to the structure of the chromosome, which is kept in an expanded state (Woldringh et al., 1995; Libby et al., 2012). Hence transertion is also well-placed to couple growth to the cell cycle. Consistent with this, major effects of transertion on the microviscosity of the membrane have been shown via inhibition of transcription and translation (Binenbaum et al., 1999). The second problem, the nature of the mechanism that initiates chromosome replication, is another long-standing mystery (Eliasson and Nordström, 1997; Wang et al., 2011). This mechanism in *E. coli* is generally attributed to the relative proportions of the DnaA 'initiator' protein in the ATP-DnaA form, which is active in initiation, and the ADP-DnaA, which is inactive (Castuma et al., 1993). The reasons to invoke lipids in a DnaA-based control of initiation include the involvement of unsaturated fatty acids in initiation (Fralick and Lark, 1973), the promotion of formation of ATP-DnaA *in vitro* by anionic phospholipids (Castuma et al., 1993) and the association of 10% of the DnaA in a cell with the membrane (Regev et al., 2012). Given its role in determining membrane dynamics, transertion may well lie at the heart of the initiator mechanism and act via DnaA and, more generally, via promoting strand separation (Norris and Amar, 2012).

The third problem, the coupling between chromosome segregation and cell division, is essentially a membrane problem in the sense that the cell must arrange for the membrane to invaginate and separate segregated chromosomes. One role for transertion may be to create membrane domains in a particular physico-chemical state around the segregating chromosomes such that a different, 'septal' domain forms by default between them (Norris, 1995; Woldringh, 2002; Norris et al., 2004). This septal domain might then generate tubular or other structures that would recruit and activate division proteins. This hypothesis is supported by evidence for cell cycle variations in the lipid composition of *E. coli* (Mozharov et al., 1985) and in the spatial distribution of the lipids of *Micrococcus luteus* (Welby et al., 1996), for the CL-rich domains at the division sites of *E. coli* (Mileykovskaya and Dowhan, 2000; Koppelman et al., 2001) and *B. subtilis* (Kawai et al., 2004), and the septal location of the polyunsaturated fatty acid eicosapentaenoic acid of *Shewanella livingstonensis Ac10* (Sato et al., 2012). Significantly, distinct domains appear around and between the segregating chromosomes at a very early stage of the cell cycle in *E. coli* and these domains disappear when translation – and hence transertion – is abolished (Fishov and Woldringh, 1999). Division is inhibited by the Min system and lipids are again important (Suefuji et al., 2002; Kretschmer and Schwille, 2014). The NH_2-terminal domain of MinC perturbs the interactions between FtsZ monomers within an FtsZ polymer, while the COOH-terminal domain perturbs the lateral association of FtsZ protofilaments as well as interacting with MinD, for references see Kretschmer and Schwille (2014); MinD is a peripheral membrane-binding protein with an ATPase activity that is activated by MinE and that triggers the detachment of MinD from the membrane to prevent MinCD from inhibiting division; MinE may self-assemble on the membrane via an N-terminal helix that acts as an MTS. The idea is that, in *E. coli*, MinD binds cooperatively to the membrane at one pole with MinE forming an "E-ring" on the rim of this MinD zone that induces its disassembly leading to the diffusion of MinD and MinE and repetition of this assembly disassembly process at the other pole; MinC follows these oscillations of MinD and MinE to inhibit division (Rowlett and Margolin, 2013; Zheng et al., 2014 and references therein). *In vitro* and *in vivo*, MinD interacts with anionic lipids, which determine its distribution (Mileykovskaya et al., 2003), as does MinE (Vecchiarelli et al., 2014). In the case of the *E. coli* MinD introduced into *B. subtilis*, MinD makes spirals that coincide with the spirals of what are probably anionic phospholipids (Pavlendova et al., 2010). Moreover, MinD can convert phospholipid vesicles into tubes (Hu et al., 2002), consistent with the possible importance of phospholipid structures in nucleating division (Norris et al., 2004; Li et al., 2011). Finally, in spherical *E. coli* cells, FtsZ is associated with intracellular membraneous structures and MinD accumulates and oscillates between the places where these structures form (Bendezú and de Boer, 2008).

The 2 min or *dcw* cluster includes 16 genes, such as *ftsZ*, involved in peptidoglycan synthesis and cell division, and the promoter at the start of the cluster probably contributes to the transcription of the whole cluster, leading to the synthesis of a quite long mRNA (Hara et al., 1997; Mengin-Lecreulx et al., 1998; Vicente et al., 1998). Transertion of this cluster may therefore be an important factor in the spatio-temporal control of division. Transertion structures not only the membrane but also the cytoplasm thereby raising the possibility that chromosome segregation is accompanied by a phase separation in the cytoplasm that affects membrane dynamics and drives cell division. Hence, it is significant that phase separation of dextran and polyethylene glycol within giant vesicles leads to tubes of membrane forming at their interface (Li et al., 2011).

If transertion from the *dcw* cluster is indeed important, what is the consequence of having transertion from two clusters (one per segregating chromosome)? Are the lipid preferences of the secretion machinery different from those of the proteins encoded by this cluster so that the domain-producing potential of transertion is reduced? In bacterial L-forms, which lack a cell wall, it might be supposed that the requirement for many of the *dcw* genes would be reduced and less transertion would occur. This would be consistent with the findings that, in L-forms of *E. coli*, some of the genes were mutated (Siddiqui et al., 2006) and the levels of FtsZ were fivefold lower (Onoda et al., 2000) whilst in an L-form of *B. subtilis* FtsZ could be eliminated altogether (Leaver et al., 2009).

Discussion

The different ways of making membrane domains include lipid–lipid, lipid–protein, protein–protein, and polyamine–lipid interactions. By integrating these interactions, transertion plays a central role in the organization of the bacterial cell. It might even be argued that transertion helps provide a conceptual context for thinking about a plethora of intracellular events, structures and processes including the regulation and execution of the cell cycle, hyperstructure dynamics and the origins of life. In 1989, the term 'nucleoid occlusion' was coined to describe the inhibitory effect of the nucleoids on cell division (Cook et al., 1989) and it was suggested that nucleoid occlusion "may be related to a transcription or translation activity of the nucleoid" (Mulder and Woldringh, 1989). A few years later, it was proposed that the coupled transcription-translation-insertion of nascent proteins into and through membrane (i.e., transertion) is the mechanism responsible for nucleoid occlusion (Norris, 1995; Norris and Madsen, 1995; Woldringh, 2002). In this proposal, transertion creates membrane domains at the right times and in the right places not only to control chromosome replication, segregation and cell division but also to create the positive feedback needed for differentiation (Norris, 1995; Norris and Madsen, 1995; Binenbaum et al., 1999; Norris et al., 2004; Norris and Amar, 2012). Recently, it has been suggested that the role of transertion in nucleoid occlusion is complemented by the recruitment of Noc nucleoprotein complexes and associated DNA to the membrane (Adams et al., 2015).

Transertion can generate hyperstructures (Norris et al., 2007a; Llopis et al., 2010). Such transertion hyperstructures form a large class that, along with the other classes of hyperstructures, constitute the bacterial cell. The exact conformation of transertion hyperstructures is unknown but could be very important in bacterial cell physiology if, as proposed, interactions between hyperstructures were to be the primary determinants of the phenotype (Norris et al., 2007a). For example, interactions based on the condensation and decondensation of ions (Manning, 2007) might enable transertion hyperstructures containing membrane domains and/or linear assemblies of macromolecules to drive the cell cycle (Norris and Amar, 2012) whilst the kinetics of the reactions in the vicinity of a membrane domains are likely to be different from elsewhere, possibly due to the structuring of water (Wichmann et al., 2003).

Transertion may help explain the controversial existence of many spiral hyperstructures (Errington, 2015). Suppose a particular protein has a tendency to form a spiral via protein–protein and protein–lipid interactions. In the absence of transertion, this tendency may result in a spiral whereas, in the presence of transertion, the high concentration of nascent proteins and associated lipids in a circular membrane domain may compete effectively for the mature proteins and thereby prevent a spiral forming. Alternatively, transertion might help generate a protein spiral if the ensemble of gene, nascent RNA (and perhaps mature RNA) were constrained to be essentially linear via RNA–RNA interactions etc. Given the potential of a transertion hyperstructure for altering the morphology of the membrane or for directing a protein to the wrong location, avoidance of these inappropriate results of transertion may act as a powerful factor in evolution that affects both the position in a protein of membrane-interacting sequences and the type of translocon with which the nascent protein interacts.

Finally, several coupled processes in addition to transertion exist in modern bacteria. These include transcription-translation-assembly as in the case of ribosome synthesis (Woldringh and Nanninga, 1985; French and Miller, 1989; Norris et al., 2007a; Cabrera et al., 2009) and transcription-replication as in the case of initiation of DNA replication and DNA repair (Kogoma, 1997; McGlynn, 2010). It might therefore be expected that these processes in their coupled forms would have played a role in the origins of the first cells. This has been suggested for transertion based on its force-generating properties, which are responsible for expanding the nucleoid in modern bacteria (Woldringh et al., 1995; Cabrera et al., 2009; Libby et al., 2012; Bakshi et al., 2014): in this scenario, transertion would have helped maintain membrane integrity in early cells and have been of selective value even without the advantages of coding (Norris et al., 1999).

Acknowledgments

KM and HH would like to thank professors emeriti Isao Shibuya and Yoshito Sadaie for discussion and encouragement. We would also like to thank the editor, Arieh Zaritsky and the reviewers, Marc Bramkamp, Ding J. Jin, and Germán Rivas for helpful comments and guidance.

References

Adams, D. W., Wu, L. J., and Errington, J. (2015). Nucleoid occlusion protein Noc recruit DNA to the bacterial cell membrane. *EMBO J.* 34, 491–501. doi: 10.15252/embj.201490177

Alley, M. R. K., Maddock, J. R., and Shapiro, L. (1992). Polar localization of a bacterial chemoreceptor. *Genes Dev.* 6, 825–836. doi: 10.1101/gad.6.5.825

Arechaga, I., Miroux, B., Karrasch, S., Huijbregts, R., de Kruijff, B., Runswick, M. J., et al. (2000). Characterization of new intracellular membranes in *Escherichia coli* accompanying large scale over-production of the b subunit of F(1)F(o) ATP synthase. *FEBS Lett.* 482, 215–219. doi: 10.1016/S0014-5793(00)02054-8

Bach, J. N., and Bramkamp, M. (2013). Flotillins functionally organize the bacterial membrane. *Mol. Microbiol.* 88, 1205–1217. doi: 10.1111/mmi.12252

Bakshi, S., Choi, H., Mondai, J., and Weisshaar, J. C. (2014). Time-dependent effects of transcription- and translation-halting drugs on the spatial distributions of the *Escherichia coli* chromosome and ribosomes. *Mol. Microbiol.* 94, 871–887. doi: 10.1111/mmi.12805

Bakshi, S., Siryaporn, A., Goulian, M., and Weisshaar, J. C. (2012). Superresolution imaging of ribosomes and RNA polymerase in live *Escherichia coli* cells. *Mol. Microbiol.* 85, 21–38. doi: 10.1111/j.1365-2958.2012.08081.x

Barák, I., Muchová, K., Wilkinson, A. J., O'Toole, P. J., and Pavlendova, N. (2008). Lipid spirals in *Bacillus subtilis* and their role in cell division. *Mol. Microbiol.* 68, 1315–1327. doi: 10.1111/j.1365-2958.2008.06236.x

Bendezú, F. O., and de Boer, P. A. (2008). Conditional lethality, division defects, membrane involution, and endocytosis in mre and mrd shape mutants of *Escherichia coli*. *J. Bacteriol.* 190, 1792–1811. doi: 10.1128/JB.01322-07

Bernsel, A., and Daley, D. O. (2009). Exploring the inner membrane proteome of *Escherichia coli*: which proteins are eluding detection and why? *Trends Microbiol.* 17, 444–449. doi: 10.1016/j.tim.2009.07.005

Binenbaum, Z., Parola, A. H., Zaritsky, A., and Fishov, I. (1999). Transcription- and translation- dependent changes in membrane dynamics in bacteria: testing the transertion model for domain formation. *Mol. Microbiol.* 32, 1173–1182. doi: 10.1046/j.1365-2958.1999.01426.x

Boggs, J. M. (1987). Lipid intermolecular hydrogen bonding: influence on structural organization and membrane function. *Biochim. Biophys. Acta* 906, 353–404. doi: 10.1016/0304-4157(87)90017-7

Bramkamp, M., Emmins, R., Weston, L., Donovan, C., Daniel, R. A., and Errington, J. (2008). A novel component of the division-site selection system of Bacillus sutilis and a new mode of action for the division inhibitor MinCD. *Mol. Microbiol.* 70, 1556–1569. doi: 10.1111/j.1365-2958.2008.06501.x

Bramkamp, M., and Lopez, D. (2015). Exploring the existence of lipid rafts in bacteria. *Microbiol. Mol. Biol. Rev.* 79, 81–100. doi: 10.1128/MMBR.00036-14

Bray, D., Levin, M. D., and Morton-Firth, C. J. (1998). Receptor clustering as a cellular mechanism to control sensitivity. *Nature* 393, 85–88. doi :10.1038/30018

Brokx, S. J., Ellison, M., Locke, T., Bottorff, D., Frost, L., and Weiner, J. H. (2004). Genome-wide analysis of lipoprotein expression in *Escherichia coli* MG1655. *J. Bacteriol.* 186, 3254–3258. doi: 10.1128/JB.186.10.3254–3258.2004

Cabin-Flaman, A., Ripoll, C., Saier, M. H. Jr., and Norris, V. (2005). Hypothesis: chemotaxis in *Escherichia coli* results from hyperstructure dynamics. *J. Mol. Microbiol. Biotechnol.* 10, 1–14. doi: 10.1159/000090343

Cabrera, J. E., Cagliero, C., Quan, S., Squires, C. L., and Jin, D. J. (2009). Active transcription of rRNA operons condenses the nucleoid in *Escherichia coli*: examining the effect of transcription on nucleoid structure in the absence of transertion. *J. Bacteriol.* 191, 4180–4185. doi: 10.1128/JB.01707-08

Campo, N., Tjalsma, H., Buist, G., Stepniak, D., Meijer, M., Veenhuis, M., et al. (2004). Subcellular sites for bacterial protein export. *Mol. Microbiol.* 53, 1583–1599. doi: 10.1111/j.1365-2958.2004.04278.x

Cannon, B., Hermansson, M., Gyorke, S., Somerharju, P., Virtanen, J. A., and Cheng, K. H. (2003). Regulation of calcium channel activity by lipid domain formation in planar lipid bilayers. *Biophys. J.* 85, 933–942. doi: 10.1016/S0006-3495(03)74532-9

Carballido-Lopez, R., Formstone, A., Li, Y., Ehrlich, S. D., Noirot, P., and Errington, J. (2006). Actin homolog MreBH governs cell morphogenesis by localization of the cell wall hydrolase LytE. *Dev. Cell* 11, 399–409. doi: 10.1016/j.devcel.2006.07.017

Castuma, C. E., Crooke, E., and Kornberg, A. (1993). Fluid membranes with acidic domains activate DnaA, the initiator protein of replication in *Escherichia coli*. *J. Biol. Chem.* 268, 24665–24668.

Catucci, L., Depalo, N., Lattanzio, V. M. T., Agostiano, A., and Corcelli, A. (2004). Neosynthesis of cardiolipin in Rhodobacter sphaeroides under osmotic stress. *Biochemistry* 43, 15066–15072. doi: 10.1021/bi048802k

Chastanet, A., and Carballido-Lopez, R. (2012). The actin-like MreB proteins in *Bacillus subtilis*: a new turn. *Front. Biosci.* S4:1582–1606. doi: 10.2741/S354

Chien, A. C., Zareh, S. K., Wang, Y. M., and Levin, P. A. (2012). Changes in the oligomerization potential of the division inhibitor UgtP co-ordinate *Bacillus subtilis* cell size with nutrient availability. *Mol. Microbiol.* 86, 594–610. doi: 10.1111/mmi.12007

Christensen, H., Garton, N. J., Horobin, R. W., Minnikin, D. E., and Barer, M. R. (1999). Lipid domains of mycobacteria studied with fluorescent molecular probes. *Mol. Microbiol.* 31, 1561–1572. doi: 10.1046/j.1365-2958.1999.01304.x

Cook, W. R., de Boer, P. A. J., and Rothfield, L. I. (1989). Differentiation of the bacterial cell division site. *Int. Rev. Cytol.* 118, 1–31.

Cornell, R. B., and Taneva, S. G. (2006). Amphipathic helices as mediators of the membrane interaction of amphitropic proteins, and as modulators of bilayer physical properties. *Curr. Protein Pept. Sci* 7, 539–552. doi: 10.2174/138920306779025675

Cullis, P. R., de Kruijff, B., Hope, M. J., Verkleij, A. J., Nayar, R., Farren, S. B., et al. (1983). "Structure properties of lipids and their functional roles in biological membranes," in *Membrane Fluidity in Biology*, ed. R. C. Aloia (New York, NY: Academic Press), 39–81.

Deana, A., and Belasco, J. G. (2005). Lost in translation: the influence of ribosomes on bacterial mRNA decay. *Genes Dev.* 19, 2526–2533. doi: 10.1101/gad.1348805

Deneke, C., Lipowsky, R., and Valleriani, A. (2013). Effect of ribosome shielding on mRNA stability. *Phys. Biol.* 10, 046008. doi: 10.1088/1478-3975/10/4/046008

Dominguez-Escobar, J., Chastanet, A., Crevenna, A. H., Fromion, V., Wedlich-Soldner, R., and Carballido-Lopez, R. (2011). Processive movement of MreB-associated cell wall biosynthetic complexes in bacteria. *Science* 333, 225–228. doi: 10.1126/science.1203466

Donovan, C., and Bramkamp, M. (2009). Characterization and subcellular localization of a bacterial flotillin homologue. *Microbiology* 155, 1786–1799. doi: 10.1099/mic.0.025312-0

Dowhan, W. (2013). A retrospective: use of *Escherichia coli* as a vehicle to study phospholipid synthesis and function. *Biochim. Biophys. Acta* 1831, 471–494. doi: 10.1016/j.bbalip.2012.08.007

Edidin, M. (1997). Lipid microdomains in cell surface membranes. *Curr. Opin. Struct. Biol.* 7, 528–532. doi: 10.1016/S0959-440X(97)80117-0

Elder, M., Hitchcock, P., Mason, F. R. S., and Shipley, G. G. (1977). A refinement analysis of crystallography of the phospholipid, 1,2-dilauroyl-DL-phosphatidylethanolamine, and some remarks on lipid–lipid and lipid–protein interactions. *Proc. R. Soc. London A* 354, 157–170. doi: 10.1098/rspa.1977.0062

Eliasson, A., and Nordström, K. (1997). Replication of minichromosomes in a host in which chromosome replication is random. *Mol. Microbiol.* 23, 1215–1220. doi: 10.1046/j.1365-2958.1997.2981663.x

Erhardt, H., Dempwolff, F., Pfreundschuh, M., Riehle, M., Schäfer, C., Pohl, T., et al. (2014). Organization of the *Escherichia coli* aerobic enzyme complexes of oxidative phosphorylation in dynamic domains within the cytoplasmic membrane. *Microbiol. Open* 3, 316–326. doi: 10.1002/mbo3.163

Eriksson, H. M., Wessman, P., Ge, C., Edwards, K., and Wieslander, Å. (2009). Massive formation of intracellular membrane vesicles in *Escherichia coli* by a monotopic membrane-bound lipid glycosyltransferase. *J. Biol. Chem.* 284, 33904–33914. doi: 10.1074/jbc.M109.021618

Errington, J. (2015). Bacterial morphogenesis and the enigmatic MreB helix. *Nat. Rev. Microbiol.* 13, 241–248. doi: 10.1038/nrmicro3398

Feng, X., Hu, Y., Zheng, Y., Zhu, W., Li, K., Guo, R. T., et al. (2014). Structural and functional analysis of *Bacillus subtilis* YisP reveals a role of its product in biofilm production. *Chem. Biol.* 21, 1557–1563. doi: 10.1016/j.chembiol.2014.08.018

Fishov, I., and Norris, V. (2012a). "Membrane structure and heterogeneity," in *Escherichia coli and Bacillus subtilis*: *The Frontiers of Molecular Microbiology Revisited*, eds Y. Sadaie and K. Matsumoto (Kerara: Research Signpost), 93–113.

Fishov, I., and Norris, V. (2012b). Membrane heterogeneity created by transertion is a global regulator in bacteria. *Curr. Opin. Microbiol.* 15, 724–730. doi: 10.1016/j.mib.2012.11.001

Fishov, I., and Woldringh, C. L. (1999). Visualization of membrane domains in *Escherichia coli*. *Mol. Microbiol.* 32, 1166–1172. doi: 10.1046/j.1365-2958.1999.01425.x

Fralick, J. A., and Lark, K. G. (1973). Evidence for the involvement of unsaturated fatty acids in the initiation of chromosome replication in *Escherichia coli*. *J. Mol. Biol.* 80, 459–475. doi: 10.1016/0022-2836(73)90416-6

French, S. L., and Miller, O. L. Jr. (1989). Transcription mapping of the *Escherichia coli* chromosome by electron microscopy. *J. Bacteriol.* 171, 4207–4216.

Gahlmann, A., and Moerner, W. E. (2014). Exploring bacterial cell biology with single-molecule tracking and super-resolution imaging. *Nat. Rev. Microbiol.* 12, 9–22. doi: 10.1038/nrmicro3154

Garner, E. C., Bernard, R., Wang, W., Zhuang, X., Rudner, D. Z., and Mitchison, T. (2011). Coupled, circumferential motions of the cell wall synthesis machinery and MreB filaments in *B. subtilis*. *Science* 333, 222–225. doi: 10.1126/science.1203285

Garner, J., and Crook, E. (1996). Membrane regulation of the chromosomal replication activity of *E. coli DnaA requires a discrete site on the protein*. *EMBO J.* 15, 1313–2321.

Gennis, R. (1989). *Biomembranes*. New York: Springer-Verlag. doi: 10.1007/978-1-4757-2065-5

Gerding, M. A., Ogata, Y., Pecora, N. D., Niki, H., and de Boer, P. A. J. (2007). The trans-envelope Tol–Pal complex is part of the cell division machinery and required for proper outer-membrane invagination during cell constriction in *E. coli*. *Mol. Microbiol.* 63, 1008–1025. doi: 10.1111/j.1365-2958.2006.05571.x

Gill, R. L. Jr., Castaing, J.-P., Hsin, J., Tan, I. S., Wang, X., Huang, K. C., et al. (2015). Structural basis for the geometry-driven localization of a small protein. *Proc. Natl. Acad. Sci. U.S.A.* 112, E1908–E1915. doi: 10.1073/pnas.1423868112

Gold, V. A. M., Robson, A., Bao, H., Romantsov, T., Duong, F., and Collinson, I. (2010). The action of cardiolipin on the bacterial translocon. *Proc. Natl. Acad. Sci. U.S.A.* 107, 10044–10049. doi: 10.1073/pnas.0914680107

Govindarajan, S., Elisha, Y., Nevo-Dinur, K., and Amster-Choder, O. (2013). The general phosphotransferase system proteins localize to sites of strong negative curvature in bacterial cells. *mBio* 4:e00443-13. doi: 10.1128/mBio.00443-13

Govindarajan, S., Nevo-Dinur, K., and Amster-Choder, O. (2012). Compartmentalization and spatiotemporal organization of macromolecules in bacteria. *FEMS Microbiol. Rev.* 36, 1005–1022. doi: 10.1111/j.1574-6976.2012.00348.x

Gründling, A., and Schneewind, O. (2007). Synthesis of glycerol phosphate lipoteichoic acid in *Staphylococcus aureus*. *Proc. Natl. Acad. Sci. U.S.A.* 104, 8478–8483. doi: 10.1073/pnas.0701821104

Gully, D., and Bouveret, E. (2006). A protein network for phospholipid synthesis uncovered by a variant of the tandem affinity purification method in *Escherichia coli*. *Proteomis* 6, 282–293. doi: 10.1002/pmic.200500115

Gutierrez-Ríos, R. M., Freyre-Gonzalez, J. A., Resendis, O., Collado-Vides, J., Saier, M., and Gosset, G. (2007). Identification of regulatory network topological units coordinating the genome-wide transcriptional response to glucose in *Escherichia coli*. *BMC Microbiol.* 7:53. doi: 10.1186/1471-2180-7-53

Hahne, H., Wolff, S., Hecker, M., and Becher, D. (2008). From complementarity to comprehensiveness–targeting the membrane proteome of growing Bacillus subtilis by divergent approaches. *Proteomics* 8, 4123–4136. doi: 10.1002/pmic.200800258

Haines, T. H., and Dencher, N. A. (2002). Cardiolipin: a proton trap for oxidative phosphorylation. *FEBS Lett.* 528, 35–39. doi: 10.1016/S0014-5793(02)03292-1

Halbedel, S., Kawai, M., Breitling, R., and Hamoen, L. (2014). SecA is required for membrane targeting of the cell division protein DivIVA in vivo. *Front. Microbiol.* 5:58. doi: 10.3389/fmicb.2014.00058

Hara, H., Yasuda, S., Horiuchi, K., and Park, J. T. (1997). A promoter for the first nine genes of the *Escherichia coli* mra cluster of cell division and cell envelope biosynthesis genes, including ftsI and ftsW. *J. Bacteriol.* 179, 5802–5811.

Hara, Y., Seki, M., Matsuoka, S., Hara, H., Yamashita, A., and Matsumoto, K. (2008). Involvement of PlsX and the acyl-phosphate dependent sn-glycerol-3-phosphate acyltransferase PlsY in the initial stage of glycerolipid synthesis in *Bacillus subtilis*. *Genes Genet. Syst.* 83, 433–442. doi: 10.1266/ggs.83.433

Hashimoto, M., Seki, T., Matsuoka, S., Hara, H., Asai, K., Sadaie, Y., et al. (2013). Induction of extracytoplasmic function sigma factors in *Bacillus subtilis* cells with defects in lipoteichoic acid synthesis. *Microbiology* 159, 23–35. doi. 10.1099/mic.0.063420-0

Hashimoto, M., Takahashi, H., Hara, Y., Hara, H., Asai, K., Sadaie, Y., et al. (2009). Induction of extracytoplasmic function sigma factors in *Bacillus subtilis* cells with membranes of reduced phosphatidylglycerol content. *Genes Genet. Syst.* 84, 191–198. doi: 10.1266/ggs.84.191

Hauser, H., Pascher, I., Pearson, R. H., and Sundell, S. (1981). Preferred conformation and molecular packing of phosphatidylethanolamine and phosphatidylcholine. *Biochim. Biophys. Acta* 650, 21–51. doi: 10.1016/0304-4157(81)90007-1

Haverstick, D. M., and Glaser, M. (1987). Visualization of Ca^{2+}-induced phospholipid domains. *Proc. Natl. Acad. Sci. U.S.A.* 84, 4475–4479. doi: 10.1073/pnas.84.13.4475

Hill, N. S., Buske, P. J., Shi, Y., and Levine, P. A. (2013). A moonlighting enzyme links *Escherichia coli* cell size with central metabolism. *PLoS Genetics* 9:e1003663. doi: 10.1371/journal.pgen.1003663

Hu, Z., Gogol, E. P., and Lutkenhaus, J. (2002). Dynamic assembly of MinD on phospholipid vesicles regulated by ATP and MinE. *Proc. Natl. Acad. Sci. U.S.A.* 99, 6761–6766. doi: 10.1073/pnas.102059099

Huang, K. C., Mukhopadhyay, R., and Wingreen, N. S. (2006). A curvature-mediated mechanism for localization of lipids to bacterial poles. *PLoS Comput. Biol.* 2:e151. doi: 10.1371/journal.pcbi.0020151

Huang, K. C., and Ramamurthi, K. S. (2010). Macromolecules that prefer their membranes curvy. *Mol. Microbiol.* 76, 822–832. doi: 10.1111/j.1365-2958.2010.07168.x

Igarashi, K., and Kashiwagi, K. (2006). Polyamine modulon in *Escherichia coli*: genes involved in the stimulation of cell growth by polyamines. *J. Biochem.* 139, 11–16. doi: 10.1093/jb/mvj020

Jerga, A., Miller, D. J., White, S. W., and Rock, C. O. (2007). Molecular determinants for interfacial binding and conformational change in a soluble diacylglycerol kinase. *J. Biol. Chem.* 284, 7246–7254. doi: 10.1074/jbc.M805962200

Jin, D. J., Cagliero, C., and Zhou, Y. N. (2013). Role of RNA polymerase and transcription in the organization of the bacterial nucleoid. *Chem. Rev.* 113, 8662-8682. doi: 10.1021/cr4001429

Johnson, J. E., and Cornell, R. B. (1999). Amphitropoic proteins: regulation by reversible membrane interactions (review). *Molec. Membr. Biol.* 16, 217–235. doi: 10.1080/096876899294544

Jouhet, J. (2013). Importance of the hexagonal lipid phase in biological membrane organization. *Front. Plant Sci.* 4:494. doi: 10.3389/fpls.2013.00494

Kawai, F., Hara, H., Takamatsu, H., Watabe, K., and Matsumoto, K. (2006). Cardiolipin enrichment in spore membranes and its involvement in germination of *Bacillus subtilis* Marburg. *Genes Genet. Syst.* 81, 69–76. doi: 10.1266/ggs.81.69

Kawai, F., Shoda, M., Harashima, R., Sadaie, Y., Hara, H., and Matsumoto, K. (2004). Cardiolipin domains in *Bacillus subtilis* Marburg membranes. *J. Bacteriol.* 186, 1475–1483. doi: 10.1128/JB.186.5.1475-1483.2004

Kennell, D., and Riezman, H. (1977). Transcription and translation frequencies of the *Escherichia coli* lac operon. *J. Mol. Biol.* 114, 1–21. doi: 10.1016/022-2836(77)90279-0

Kicia, M., Janeczko, N., Lewicka, J., and Hendrich, A. B. (2012). Comparison of the effects of subinhibitory concentrations of ciprofloxacin and colistin on the morphology of cardiolipin domains in *Escherichia coli* membranes. *J. Med. Microbiol.* 61, 520–524. doi: 10.1099/jmm.0.037788-0

Kikuchi, S., Shibuya, I., and Matsumoto, K. (2000). Viability of an *Escherichia coli* pgsA null mutant lacking detectable phosphatidylglycerol and cardiolipin. *J. Bacteriol.* 182, 371–376. doi: 10.1128/JB.182.2.371-376.2000

Kogoma, T. (1997). Stable DNA replication: interplay between DNA replication, homologous recombination and transcription. *Microbiol. Molec. Biol. Rev.* 61, 212–238.

Konovalova, A., Perlman, D. H., Coweles, C. E., and Silhavy, T. J. (2014). Transmembrane domain of surface-exoised outer membrane lipoprotein RcsF is threaded through the lumen of β-barrel proteins. *Proc. Natl. Acad. Sci. U.S.A.* 111, E4350-8. doi: 10.1073/pnas.1417138111

Koppelman, C.-M., den Blaauwen, T., Duursma, M. C., Heeren, R. M. A., and Nanninga, N. (2001). *Escherichia coli* minicell membranes are enriched in cardiolipin. *J. Bacteriol.* 183, 6144–6147. doi: 10.1128/JB.183.20.6144-6147.2001

Kretschmer, S., and Schwille, P. (2014). Toward spatially regulated division of protocells: insights into the *E. coli Min System from in vitro studies. Life* (*Basel*) 4, 915–928. doi: 10.3390/life4040915

Krupka, M., Cabré, E. J., Jiménez, M., Rivas, G., Rico, A. I., and Vicente, M. (2014). Role of the FtsA C terminus as a switch for polymerization and membrane association. *mBio* 5:e02221-14. doi: 10.1128/mBio.02221-14

Lai, E. M., Nair, U., Phadke, N. D., and Maddock, J. R. (2004). Proteomic screening and identification of differentially distributed membrane proteins in *Escherichia coli*. *Mol. Microbiol.* 52, 1029–1044. doi: 10.1111/j.1365–2958.2004.04040.x

Lazarevic, V., Soldo, B., Médico, N., Pooley, H., Bron, S., and Karamata, D. (2005). *Bacillus subtilis* α-phosphoglucomutase is required for normal cell morphology and biofilm formation. *Appl. Environ. Microbiol.* 71, 39–45. doi: 10.1128/AEM.71.1.39–45.2005

Leaver, M., Dominguez-Cuevas, P., Coxhead, J. M., Daniel, R. A., and Errington, J. (2009). Life without a wall or division machine in *Bacillus subtilis*. *Nature* 457, 849–853. doi: 10.1038/nature07742

Lemmon, M. A. (2008). Membrane recognition by phospholipid-binding domains. *Nat. Rev. Molec. Cell Biol.* 9, 99–111. doi: 10.1038/nrm2328

Lenarcic, R., Halbedel, S., Visser, L., Shaw, M., Wu, L. J., and Errington, J. (2009). Localization of DivIVA by targeting to negatively curved membranes. *EMBO J.* 28, 2272–2282. doi: 10.1038/emboj.2009.129

Li, G., and Young, K. (2012). Isolation and identification of new inner membrane-associated proteins that localize to cell poles in *Escherichia coli*. *Mol. Microbiol.* 84, 276–295. doi: 10.1111/j.1365-2958.2012.08021.x

Li, Y., Lipowsky, R., and Dimova, R. (2011). Membrane nanotubes induced by aqueous phase separation and stabilized by spontaneous curvature. *Proc. Natl. Acad. Sci. U.S.A.* 108, 4731–4736. doi: 10.1073/pnas.1015892108

Libby, E., Roggiani, M., and Goulian, M. (2012). Membrane protein expression triggers chromo-somal locus repositioning in bacteria. *Proc. Natl. Acad. Sci. U.S.A.* 109, 7445–7450. doi: 10.1073/pnas.1109479109

Llopis, P. M., Jackson, A. F., Sliusarenko, O., Surovtsev, I., Heinritz, J., Emonet, T., et al. (2010). Spatial organization of the flow of genetic information in bacteria. *Nature* 466, 77–82. doi: 10.1038/nature09152

Llorente-Garcia, I., Lenn, T., Erhardt, H., Harriman, O. L., Liu, L. N., Robson, A., et al. (2014). Single-molecule in vivo imaging of bacterial respiratory complexes indicates delocalized oxidative phosphorylation. *Biochim. Biophys. Acta* 1837, 811–824. doi: 10.1016/j.bbabio.2014.01.020

Lobasso, S., Palese, L. L., Angelini, R., and Corcelli, A. (2013). Relationship between cardiolipin metabolism and oxygen availability in *Bacillus subtilis*. *FEBS Open Bio* 3, 151–155. doi: 10.1016/j.fob.2013.02.002

Lobasso, S., Saponetti, M. S., Polidoro, F., Lopalco, P., Urbanija, J., Kralj-Iglic, V., et al. (2009). Archaebacterial lipid membranes as models to study the interaction of 10-N-nonyl acridine orange with phospholipids. *Chem. Phys. Lipids* 157, 12–20. doi: 10.1016/j.chemphyslip.2008.09.002

Lopez, D., and Kolter, R. (2010). Functional microdomains in bacterial membranes. *Genes Dev.* 24, 1893–1902. doi: 10.1101/gad.1945010

Lopian, L., Elisha, Y., Nussbaum-Shochat, A., and Amster-Choder, O. (2010). Spatial and temporal organization of the *E. coli PTS components. EMBO J.* 29, 3630–3645. doi: 10.1038/emboj.2010.240

Lu, Y. J., Zhang, Y. M., Grimes, K. D., Qi, J., Lee, R. E., and Rock, C. O. (2006). Acyl-phosphates initiate membrane phospholipid synthesis in gram-positive pathogens. *Molec. Cell* 23, 765–772. doi: 10.1016/j.molcel.2006.06.030

Makise, M., Mima, S., Tsuchiya, T., and Mizushima, T. (2001). Molecular mechanism for functional interaction between DnaA protein and acidic phospholipids: identification of important amino acids. *J. Biol. Chem.* 276, 7450–7456. doi: 10.1074/jbc.M009643200

Maloney, E., Madiraju, S. C., Rajagopalan, M., and Madiraju, M. (2011). Localization of acidic phospholipid cardiolipin and DnaA in mycobacteria. *Tuberculosis* (*Edinb*) 1, S150–S155. doi: 10.1016/j.tube.2011.10.025

Manning, G. S. (2007). Counterion condensation on charged spheres, cylinders, and planes. *J. Phys. Chem.* 111, 8554–8559. doi: 10.1021/jp067084417

Margolin, W. (2012). The price of tags in protein localization studies. *J. Bacteriol.*194, 6369–6371. doi: 10.1128/JB.01640-12

Marston, A. L., Thomaides, H. B., Edwards, D. H., Sharpe, M. E., and Errington, J. (1998). Polar localization of the MinD protein of *Bacillus subtilis* and its role in selection of the mid-cell division site. *Genes Dev.* 12, 3419–3430. doi: 10.1101/gad.12.21.3419

Matsumoto, K. (1997). Phosphatidylserine synthase from bacteria. *Biochim. Biophys. Acta* 1348, 214–227. doi: 10.1016/S0005-2760(97)00110-0

Matsumoto, K. (2001). Dispensable nature of phosphatidylglycerol in *Escherichia coli*: dual roles of anionic phospholipids. *Mol. Microbiol.* 39, 1427–1433. doi: 10.1046/j.1365-2958.2001.02320.x

Matsumoto, K., Kusaka, J., Nishibori, A., and Hara, H. (2006). Lipid domains in bacterial membranes. *Mol. Microbiol.* 61, 1110–1117. doi: 10.1111/j.1365-2958.2006.05317.x

Matsumoto, K., Matsuoka, S., and Hara, H. (2012). "Membranes and lipids," in *Escherichia coli and Bacillus subtilis: The Frontiers of Molecular Microbiology Revisited*, eds Y. Sadaie and K. Matsumoto (Kerala: Research Signpost), 61–91.

Matsuoka, S., Chiba, M., Tanimura, Y., Hashimoto, M., Hara, H., and Matsumoto, K. (2011a). Abnormal morphology of *Bacillus subtilis* ugtP mutant cells lacking glucolipids. *Genes Genet. Syst.* 86, 295–304. doi: 10.1266/ggs.86.295

Matsuoka, S., Hashimoto, M., Kamiya, Y., Miyazawa, T., Ishikawa, K., Hara, H., et al. (2011b). The *Bacillus subtilis* essential gene dgkB is dispensable in mutants with defective lipoteichoic acid synthesis. *Genes Genet. Syst.* 86, 365–376. doi: 10.1266/ggs.86.365

Mazor, S., Regev, T., Mileykovskaya, E., Margolin, W., Dowhan, W., and Fishov, I. (2008). Mutual effects of MinD-membrane interaction: II. Domain structure of the membrane enhances MinD binding. *Biochim. Biophys. Acta* 1778, 2505–2511. doi: 10.1016/j.bbamem.2008.08.004

McGary, K., and Nudler, E. (2013). RNA polymerase and the ribosome: the close relationship. *Curr. Opin. Microbiol.* 16, 112–117. doi: 10.1016/j.mib.2013.01.010

McGlynn, P. (2010). Linking transcription with DNA repair, damage tolerance, and genome duplication. *Proc. Natl. Acad. Sci. U.S.A.* 107, 15314–15315. doi: 10.1073/pnas.1010659107

Mengin-Lecreulx, D., Ayala, J., Bouhss, A., van Heijenoort, J., Parquet, C., and Hara, H. (1998). Contribution of the P*mra* promoter to expression of genes in the *Escherichia coli mra* cluster of cell envelope biosynthesis and cell division genes. *J. Bacteriol.* 180, 4406–4412.

Meredith, D. H., Plank, M., and Lewis, P. J. (2008). Different patterns of integral membrane protein localization during cell division in *Bacillus subtilis*. *Microbiology* 154, 64–71. doi: 10.1099/mic.0.2007/013268-0

Meyer, P., Cecchi, G., and Stolovitzky, G. (2014). Spatial localization of the first and last enzymes effectively connects active metabolic pathways in bacteria. *BMC Syst. Biol.* 8:131. doi: 10.1186/s12918-014-0131-1

Mileykovskaya, E. (2007). Subcellular localization of *Escherichia coli* osmosensory transporter ProP: focus on cardiolipin membrane domains. *Mol. Microbiol.* 64, 1419–1422. doi: 10.1111/j.1365-2958.2007.05766.x

Mileykovskaya, E., and Dowhan, W. (2000). Visualization of phospholipid domains in *Escherichia coli* by using the cardiolipin-specific fluorescent dye 10-N-nonyl acridineorange. *J. Bacteriol.* 182, 1172–1175. doi: 10.1128/JB.182.4.1172-1175.2000

Mileykovskaya, E., and Dowhan, W. (2005). Role of membrane lipids in bacterial division-site selection. *Curr. Opin. Microbiol.* 8, 135–142. doi: 10.1016/j.mib.2005.02.012

Mileykovskaya, E., and Dowhan, W. (2009). Cardiolipin membrane domains in prokaryotes and eukaryotes. *Biochim. Biophys. Acta* 1788, 2084–2091. doi: 10.1016/j.bbamem.2009.04.003

Mileykovskaya, E., Dowhan, W., Birke, R. L., Zheng, D., Lutterodt, L., and Haines, T. H. (2001). Cardiolipin binds nonyl acridine orange by aggregating the dye at exposed hydrophobic domains on bilayer surfaces. *FEBS Lett.* 507, 187–190. doi: 10.1016/S0014-5793(01)02948-9

Mileykovskaya, E., Fishov, I., Fu, X., Corbin, B. D., Margolin, W., and Dowhan, W. (2003). Effects of phospholipids composition on MinD-membrane interaction in vitro and in vivo. *J. Biol. Chem.* 278, 22193–22198. doi: 10.1074/jbc.M302603200

Mileykovskaya, E., and Margolin, W. (2012). "Cell division" in *Escherichia coli and Bacillus subtilis*: *The frontiers of Molecular Microbiology Revisited*, eds Y. Sadaie and K. Matsumoto (Kerala: Research Signpost), 149–177.

Mileykovskaya, E., Ryan, A. C., Mo, X., Lin, C. C., Khalaf, K. I., Dowhan, W., et al. (2009). Phosphatidic acid and N-acylphosphatidylethanolamine from membrane domains in *Escherichia coli* mutant lacking cardiolipin and phosphatidylglycerol. *J. Biol. Chem.* 284, 2990–3000. doi. 10.1074/jbc.M805189200

Mim, C., and Unger, V. M. (2012). Membrane curvature and its generation by BAR proteins. *Trends Bichem. Sci.* 37, 526–533. doi: 10.1016/j.tibs.2012.09.001

Mozharov, A. D., Shchipakin, V. N., Fishov, I. L., and Evtodienko, Y. V. (1985). Changes in the composition of membrane phospholipids during the cell cycle of *E. coli*. *FEBS Lett.* 186, 103–106. doi: 10.1016/0014-5793(85)81348-X

Muchová, K., Wilkinson, A., and Barak, I. (2011). Change of lipid domains in *Bacillus subtilis* cells with disrupted cell wall peptidoglycan. *FEMS Microbiol. Lett.* 325, 92–98. doi: 10.1111/j.1574-6968.2011.02417

Mulder, E., and Woldringh, C. (1989). Actively replicating nucleoids influence positioning of division sites in *Escherichia coli* filaments forming cells lacking DNA. *J. Bacteriol.* 171, 4303–4314.

Munro, G. F., Hercules, K., Morgan, J., and Sauerbier, W. (1972). Dependence of the putrescine content of *Escherichia coli* on the osmotic strength of the medium. *J. Biol. Chem.* 247, 1272–1280.

Nishibori, A., Kusaka, J., Hara, H., Umeda, M., and Matsumoto, K. (2005). Phosphatidylethanolamine domains and localization of phospholipids synthases in *Bacillus subtilis* membranes. *J. Bacteriol.* 187, 2163–2174. doi: 10.1128/JB.187.6.2163-2174.2005

Norris, V. (1995). Hypothesis: chromosome separation in *Escherichia coli* involves autocatalytic gene expression, transertion and membrane-domain formation. *Mol. Microbiol.* 16, 1051–1057. doi: 10.1111/j.1365-2958.1995.tb02330.x

Norris, V., and Amar, P. (2012). Chromosome replication in *Escherichia coli*: life on the scales. *Life* 2, 286–312. doi: 10.3390/life2040286

Norris, V., Ayala, J. A., Begg, K., Bouché, J. P., Bouloc, P., Boye, E., et al. (1994). Cell cycle control: prokaryotic solutions to eukaryotic problems? *J. Theor. Biol.* 168, 227–230. doi: 10.1006/jtbi.1994.1102

Norris, V., den Blaauwen, T., Doi, R. H., Harshey, R. M., Janniere, L., Jiménez-Sánchez, A., et al. (2007a). Toward a hyperstructure taxonomy. *Annu. Rev. Microbiol.* 61, 309–329. doi: 10.1146/annurev.micro.61.081606.103348

Norris, V., den Blaauwen, T., Cabin-Flaman, A., Doi, R. H., Harshey, R., Janniere, L., et al. (2007b). Functional taxonomy of bacterial hyperstructures. *Microbiol. Mol. Biol. Rev.* 71, 230–253. doi: 10.1128/MMBR.00035-06

Norris, V., and Madsen, M. S. (1995). Autocatalytic gene expression occurs via transertion and membrane domain formation and underlies differentiation in bacteria: a model. *J. Mol. Biol.* 253, 739–748. doi: 10.1006/jmb.1995.0587

Norris, V., Misevic, G., Delosme, J.-M., and Oshima, A. (2002). Hypothesis: a phospholipid translocase couples lateral and transverse bilayer asymmetries in dividing bacteria. *J. Mol. Biol.* 318, 455–462. doi: 10.1016/S0022-2836(02)00098-0

Norris, V., Nana, G. G., and Audinot, J. N. (2014a). New approaches to the problem of generating coherent, reproducible phenotypes. *Theory Biosci.* 133, 47–61. doi: 10.1007/s12064-013-0185-4

Norris, V., Reusch, R. N., Igarashi, K., and Root-Bernstein, R. (2014b). Molecular complementarity between simple, universal molecules and ions limited phenotype space in the precursors of cells. *Biol. Direct.* 10, 28. doi: 10.1186/s13062-014-0028-3

Norris, V., Onoda, T., Pollaert, H., and Grehan, G. (1999). The mechanical advantages of DNA. *BioSystems* 49, 71–78. doi: 10.1016/S0303-2647(98)00031-8

Norris, V., Woldringh, C. L., and Mileykovskaya, E. (2004). Hypothesis: a hypothesis to explain division site selection in *Escherichia coli* by combining nucleoid occlusion and min. *FEBS Lett.* 561, 3–10. doi: 10.1016/S0014-5793(04)00135-8

Okada, M., Matsuzaki, H., Shibuya, I., and Matsumoto, K. (1994). Cloning, sequencing, and expression in *Escherichia coli* of the *Bacillus subtilis* gene for phosphatidylserine synthase. *J. Bacteriol.* 176, 7456–7461.

Okuda, S., and Tokuda, H. (2011). Lipoprotein sorting in bacteria. *Annu. Rev. Microbiol.* 65, 239–259. doi: 10.1146/annurev-micro-090110-102859

Oliva, M. A., Halbedel, S., Freund, S. M., Dutow, P., Leonard, T. A., Veprintsev, D. B., et al. (2010). Features critical for membrane binding reveal ed by DivIVA crystal structure. *EMBO J.* 29, 1988–2001. doi: 10.1038/emboj.2010.99

Oliver, P. M., Crooks, J. A., Leidl, M., Yoon, E. J., Saghatelian, A., and Weibel, D. B. (2014). Localization of anionic phospholipids in *Escherichia coli* cells. *J. Bacteriol.* 196, 3386–3398. doi: 10.1128/JB.01877-14

Onoda, T., Enokizono, J., Kaya, H., Oshima, A., Freestone, P., and Norris, V. (2000). Effects of calcium and calcium chelators on growth and morphology of *Escherichia coli* L-form NC-7. *J. Bacteriol.* 182, 1419–1422. doi: 10.1128/JB.182.5.1419-1422.2000

Osawa, M., Anderson, D. E., and Erickson, H. P. (2008). Reconstitution of contractile FtsZ rings in liposomes. *Science* 320, 792–794. doi: 10.1126/science.1154520

Osawa, M., and Erickson, H. P. (2013). Liposome division by a simple bacterial division machinery. *Proc. Natl. Acad. Sci. U.S.A.* 110, 11000–11004. doi: 10.1073/pnas.1222254110

Osella, M., Nugent, E., and Lagomarsino, M. C. (2014). Concerted control of *Escherichia coli* cell division. *Proc. Natl. Acad. Sci. U.S.A.* 111, 3431–3435. doi: 10.1073/pnas.1313715111

Otto, A., Bernhardt, J., Meyer, H., Schaffer, M., Herbst, F.-A., Siebourg, J., et al. (2010). Systems-wide temporal proteomic profiling in glucose-starved *Bacillus subtilis*. *Nat. Commun.* 1, 137. doi: 10.1038/ncomms1137

Paoletti, L., Lu, Y. J., Schujman, G., de Mendoza, and Rock, C. O. (2007). Coupling of fatty acid and phospholipid synthesis in *Bacillus subtilis*. *J. Bacteriol.* 189, 5816–5842. doi: 10.1128/JB.00602-07

Papanastasiou, M., Orfanoudaki, G., Koukaki, M., Kountourakis, N., Frantzeskos Sardis, M. F., Aivaliotis, M., et al. (2013). The *Escherichia coli* peripheral inner membrane proteome. *Molec. Cell Proteom.* 12, 599–610. doi: 10.1074/mcp.M112.024711

Pascher, I., Sundell, S., Harlos, K., and Eibl, H. (1987). Conformation and packing properties of membrane lipids: the crystal structure of sodium dimyristoylphosphatidylglycerol. *Biochim. Biophys. Acta* 896, 77–88. doi: 10.1016/0005-2736(87)90358-0

Patel, H. V., Vyas, K. A., Li, X., Savtchenko, R., and Roseman, S. (2004). Subcellular distribution of enzyme I of the *Escherichia coli* phosphoenolpyruvate: glucose phosphotransferase system depends on growth conditions. *Proc. Natl. Acad. Sci. U.S.A.* 102, 17486–17491. doi: 10.1073/pnas.0407865101

Patrick, J. E., and Kearns, D. B. (2008). MinJ(YvjD) is a topological determinant of cell division in *Bacillus subtilis*. *Mol. Microbiol.* 70, 1166–1179. doi: 10.1111/j.1365-2958.2008.06469.x

Pavlendova, N., Muchova, K., and Barak, I. (2010). Expression of *Escherichia coli* Min system in *Bacillus subtilis* and its effect on cell division. *FEMS Microbiol. Lett.* 302, 58–68. doi: 10.1111/j.1574-6968.2009.01832.x

Petit, J. M., Huet, O., Gallet, P. F., Maftah, A., Ratinaud, M. H., and Julien, R. (1994). Direct analysis and significance of cardiolipin transverse distribution in mitochondrial inner membranes. *Eur. J. Biochem.* 220, 871–879. doi: 10.1111/j.1432-1033.1994.tb18690.x

Petit, J. M., Maftah, A., Ratinaud, M. H., and Julien, R. (1992). 10-N-nonyl acridine orange interacts with cardiolipin and allows the quantification of this phospholipid in isolated mitochondria. *Eur. J. Biochem.* 209, 267–273. doi: 10.1111/j.1432-1033.1992.tb17285.x

Pichoff, S., and Lutkenhaus, J. (2005). Tethering the Z ring to the membrane through a conserved membrane targeting sequence in FtsA. *Mol. Microbiol.* 55, 1722–1734. doi: 10.1111/j.1365-2958.2005.04522.x

Price, K. D., Roels, S., and Losick, R. (1997). A *Bacillus subtilis* gene encoding a protein similar to nucleotide sugar transferases influences cell shape and viability. *J. Bacteriol.* 179, 4959–4961.

Ramamurthi, K. S. (2010). Protein localization by recognition of membrane curvature. *Curr. Opin. Microbiol.* 13, 753–757. doi: 10.1016/j.mib.2010.09.14

Ramamurthi, K. S., and Losick, R. (2009). Negative membrane curvature as a cue for subcellular localization of a bacterial protein. *Proc. Natl. Acad. Sci. U.S.A.* 106, 13541–13545. doi: 10.1073/pnas.0906851106

Raskin, D. M., and de Boer, P. A. J. (1999). Rapid pole-to-pole oscillation of a protein required for directing division to the middle of *Escherichia coli*. *Proc. Natl. Acad. Sci. U.S.A.* 96, 4971–4976. doi: 10.1073/pnas.96.9.4971

Regev, T., Myers, N., Zarivach, R., and Fishov, I. (2012). Association of the chromosome replication initiator DnaA with the *Escherichia coli* inner membrane in vitro: quantity and mode of binding. *PLoS ONE* 7:e36441. doi: 10.1371/journal.pone.0036441

Renner, L. D., Eswaramoorthy, P., Ramamurthi, K. S., and Weibel, D. B. (2013). Studying biomolecule localization by engineering bacterial cell wall curvature. *PLoS ONE* 8:e84143. doi: 10.1371/journal.pone.0084143

Renner, L. D., and Weibel, D. B. (2011). Cardiolipin microdomains localize to negatively curved regions of *Escherichia coli* membranes. *Proc. Natl. Acad. Sci. U.S.A.* 108, 6264–6269. doi: 10.1073/pnas.1015757108

Rilfors, L., Niemi, A., Haraldsson, S., Edwards, K., Andersson, A.-S., and Dowhan, W. (1999). Reconstituted phosphatidylserine synthase from *Escherichia coli* is activated by anionic phospholipids and micelle-forming amphiphiles. *Biochim. Biophys. Acta* 1438, 281–294. doi: 10.1016/S1388-1981(99)00060-8

Romantsov, T., Battle, A. R., Hendel, J. L., Martinac, B., and Wood, J. M. (2010). Protein localization in *Escherichia coli* cells: comparison of the cytoplasmic membrane protein ProP, LacY, ProW, AqpZ, MscS, and MscL. *J. Bacteriol.* 192, 912–924. doi: 10.1128/JB.00967-09

Romantsov, T., Helbig, S., Culham, D. E., Gill, C., Stalker, L., and Wood, J. (2007). Cardiolipin promotes polar localization of osmosensory transporter ProP in *Escherichia coli*. *Mol. Microbiol.* 64, 1455–1465. doi: 10.1111/j.1365-2958.2007.05727.x

Romantsov, T., Stalker, L., Culham, D. E., and Wood, J. M. (2008). Cardiolipin controls the osmotic stress response and the subcellular location of transporter ProP in *Escherichia coli*. *J. Biol. Chem.* 283, 12314–12323. doi: 10.1074/jbc.M709871200

Rosch, J. W., and Caparon, M. G. (2005). The ExPortal: an organelle dedicated to the biogenesis of secreted proteins in *Streptococcus pyogenes*. *Mol. Microbiol.* 58, 959–968. doi: 10.1111/j.1365-2958.2005.04887.x

Rosch, J. W., Hsu, F. F., and Caparon, M. G. (2007). Anionic lipids enriched at the exportal of *Streptococcus pyogenes*. *J. Bacteriol.* 189, 801–806. doi: 10.1128/JB.01549-06

Rowlett, V. W., and Margolin, W. (2013). The bacterial Min system. *Curr. Biol.* 23, R553–R556. doi: 10.1016/j.cub.2013.05.024

Saha, S. K., Furukawa, Y., Matsuzaki, H., Shibuya, I., and Matsumoto, K. (1996b). Directed mutagenesis, Ser-56 to Pro, of *Bacillus subtilis* phosphatidylserine synthase drastically lowers enzymatic activity and relieves amplification toxicity in *Escherichia coli*. *Biosci. Biotech. Biochem.* 60, 630–633. doi: 10.1271/bbb.60.630

Saha, S. K., Nishijima, S., Matsuzaki, H., Shibuya, I., and Matsumoto, K. (1996a). A regulatory mechanism for the balanced synthesis of membrane phospholipid species in *Escherichia coli*. *Biosci. Biotech. Biochem.* 60, 111–116. doi: 10.1271/bbb.60.111

Saier, M. H. Jr. (2013). Microcompartments and protein machines in prokaryotes. *J. Mol. Microbiol. Biotechnol.* 23, 243–269. doi: 10.1271/bbb.60.630

Saier, M. H. Jr., Ramseier, T. M., and Reizer, J. (1996). "Regulation of carbon utilization," in *Escherichia coli and Salmonella*. *Cellular and Molecular Biology*, eds F. C. Neidhardt, R. Curtiss, J. L. Ingraham, E.C.C. Lin, K. B. Low, B. Magasanik, et al. (Washington, DC: American Society for Microbiology), 1325–1343.

Salje, J., van den Ent, F., de Boer, P., and Löwe, J. (2011). Direct membrane binding by bacterial actin MreB. *Molec. Cell* 43, 478–487. doi: 10.1016/j.molec.2011.07.008

Salzberg, L. I., and Helmann, J. D. (2008). Phenotypic and transcriptomic characterization of *Bacillus subtilis* mutants with grossly altered membrane composition. *J. Bacteriol.* 190, 7797–7807. doi: 10.1128/JB.00720-08

Sanamrad, A., Persson, F., Lundius, E. G., Fange, D., Gynnå, A. H., and Elf, J. (2014). Single-particle tracking reveals that free ribosomal subunits are not excluded from the *Escherichia coli* nucleoid. *Proc. Natl. Acad. Sci. U.S.A.* 111, 11413–11418. doi: 10.1073/pnas.1411558111

Sankaran, K., and Wu, H. C. (1994). Lipid modification of bacterial prolipoprotein. Transfer of diacylglycerol moiety from phosphatidylglycerol. *J. Biol. Chem.* 269, 19701–19706.

Santos, T. M. A., Lin, T. Y., Rajendran, M., Anderson, S. M., and Weibel, D. B. (2014). Polar localization of *Escherichia coli* chemoreceptors requires an intact Tol-Pal complex. *Moelc. Microbiol.* 92, 985–1004. doi: 10.1111/mm.12609

Sato, S., Kawamoto, J., Sato, S. B., Watanabe, B., Hiratake, J., Esaki, N., et al. (2012). Occurrence of a bacterial membrane microdomain at the cell division site enriched in phospholipids with polyunsaturated hydrocarbon chains. *J. Biol. Chem.* 287, 24113–24121. doi: 10.1074/jbc.M111.318311

Schaechter, M., Maaloe, O., and Kjeldgaard, N. O. (1958). Dependency on medium and temperature of cell size and chemical composition during balanced grown of *Salmonella typhimurium*. *J. Gen. Microbiol.* 19, 592–606. doi: 10.1099/00221287-19-3-592

Schirner, K., Marles-Wright, J., Lewis, R. J., and Errington, J. (2009). Distinct and essential morphogenic functions for wall- and lipoteichoic acids in *Bacillus subtilis*. *EMBO J.* 28, 830–842. doi: 10.1038/emboj.2009.25

Schuber, F. J. (1989). Influence of polyamines on membrane functions. *Biochemistry* 260, 1–10.

Schulze, R. J., Komar, J., Botte, M., Allen, W. J., Whitehouse, S., Gold, V. A., et al. (2014). Membrane protein insertion and proton-motive-force-dependent secretion through the bacterial holo-translocon SecYEG-SecDF-YajC-YidC. *Proc. Natl. Acad. Sci. U.S.A.* 111, 4844–4849. doi: 10.1073/pnas.1315901111

Seddon, J. M. (1990). Structure of the inverted hexagonal (HII) phase, and non-lamellar phase transitions of lipids. *Biochim. Biophys. Acta* 1031, 1–69. doi: 10.1016/0304-4157(90)90002-T

Seki, T., Mineshima, R., Hashimoto, M., Matsumoto, K., Hara, H., and Matsuoka, S. (2015). Repression of the activities of extracytoplasmic function σ factors, σM and σV of *Bacillus subtilis* by glucolipids in *Escherichia coli* cells. *Genes Genet. Syst.* (in press).

Shakibai, N., Ishidate, K., Reshetnyak, E., Gunji, S., Kohiyama, M., and Rothfield, L. (1998). High-affinity binding of hemimethylated oriC by *Escherichia coli* membranes is mediated by a multiprotein system that includes SeqA and a newly identified factor, SeqB. *Proc. Natl. Acad. Sci. U.S.A.* 95, 11117–11121. doi: 10.1073/pnas.95.19.11117

Shapiro, L., McAdams, H. H., and Losick, R. (2002). Generating and exploiting polarity in bacteria. *Science* 298, 1942–1946. doi: 10.1126/science.1072163

Shiba, Y., Miyagawa, H., Nagahama, H., Matsumoto, K., Kondo, D., Matsuoka, S., et al. (2012). Exploring the relationship between lipoprotein mislocalization and activation of the Rcs signal transduction system in *Escherichia coli*. *Microbiology* 158, 1238–1248. doi: 10.1099/mic.0.056945-0

Shiba, Y., Yokoyama, Y., Aono, Y., Kiuchi, T., Kusaka, J., Matsumoto, K., et al. (2004). Activation of the Rcs signal transduction system is responsible for the thermosensitive growth defect of an *Escherichia coli* mutant lacking phosphatidylglycerol and cardiolipin. *J. Bacteriol.* 186, 6526–6535. doi: 10.1128/JB.186.19.6526–6535.2004

Shibuya, I. (1992). Metabolic regulations and biological functions of phospholipids in *Escherichia coli*. *Prog. Lipid Res.* 31, 245–299. doi: 10.1016/0163-7827(92)90010-G

Shiomi, D., and Margolin, W. (2007). Sweet sensor for size-conscious bacteria. *Cell* 130, 21–218. doi: 10.1016/j.cell.2007.07.011

Shiomi, D., Yoshimoto, M., Homma, M., and Kawagishi, I. (2006). Helical distribution of the bacterial chemoreceptor via colocalization with the Sec protein translocation machinery. *Mol. Microbiol.* 60, 894–906. doi: 10.1111/j.1365-2958.2006.05145.x

Siddiqui, R. A., Hoischen, C., Holst, O., Heinze, I., Schlott, B., Gumpert, J., et al. (2006). The analysis of cell division and cell wall synthesis genes reveals mutationally inactivated ftsQ and mraY in a protoplast-type L-form of *Escherichia coli*. *FEMS Microbiol. Lett.* 258, 305–311. doi: 10.1111/j.1574-6968.2006.00237.x

Singer, S. J., and Nicolson, G. L. (1972). The fluid mosaic model of the structure of cell membranes. *Science* 175, 720–731. doi: 10.1126/science.175.4023.720

Slater, S., Wold, S., Lu, M., Boye, E., Skarstad, K., and Kleckner, N. (1995). *E. coli* SeqA protein binds oriC in two different methyl-modulated reactions appropriate to its roles in DNA replication initiation and origin sequestration. *Cell* 82, 927–936. doi: 10.1016/0092-8674(95)90272-4

Sourjik, V., and Armitage, J. P. (2010). Spatial organization in bacterial chemotaxis. *EMBO J.* 29, 2724–2733. doi: 10.1038/emboj.2010.178

Strahl, H., Bürmann, F., and Hamoen, L. W. (2014). The actin homologue MreB organizes the bacterial cell membrane. *Nat. Commun.* 5, 3442. doi: 10.1038/ncomms4442

Strahl, H., Turlan, C., Khalid, S., Bond, P. J., Kebalo, J. M., Peyron, P., et al. (2015). Membrane recognition and dynamics of the RNA degradosome. *PLoS Genet.* 11:e1004961. doi: 10.1371/journal.pgen.1004961

Suefuji, K., Valluzzi, R., and RayChaudhuri, D. (2002). Dynamic assembly of MinD into filament bundles modulated by ATP, phospholipids, and MinE. *Proc. Natl. Acad. Sci. U.S.A.* 99, 16776–16781. doi: 10.1073/pnas.262671699

Suzuki, M., Hara, H., and Matsumoto, K. (2002). Envelope disorder of *Escherichia coli* cells lacking phosphatidylglycerol. *J. Bacteriol.* 184, 5418–5425. doi: 10.1128/JB.184.19.5418-5425.2002

Szeto, T. H., Rowland, S. L., Habrukowich, C. L., and King, G. F. (2003). The MinD membrane targeting sequence is a transdplantable lipid-binding helix. *J. Biol. Chem.* 278, 40050–40056. doi: 10.74/jbc.M306876200

Szeto, T. H., Rowland, S. L., Rothfield, L. I., and King, G. F. (2002). Membrane localization of MinD is mediated by a C-terminal motif that is conserved across eubacteria, archaea, and chloroplasts. *Proc. Natl. Acad. Sci. U.S.A.* 99, 15693–15698. doi: 10.1073/pnas.232590599

Szwedziak, P., Wang, Q., Bharat, T. A. M., Tsim, M., and Löwe, J. (2014). Architecture of the ring formed by the tubulin homologue FtsZ in bacterial cell division. *elife* 3:e04601. doi: 10.7554/eLife.04601

Szwedziak, P., Wang, Q., Freund, S. M. V., and Löwe, J. (2012). FtsA forms actin-like protofilaments. *EMBO J.* 31, 2249–2260. doi: 10.1038/emboj.2012.76

Takada, H., Fukushima-Tanaka, S., Morita, M., Kasahara, Y., Watanabe, S., Chibazakura, T., et al. (2014). An essential enzyme for phospholipid synthesis associates with the *Bacillus subtilis* divisome. *Mol. Microbiol.* 91, 242–255. doi: 10.1111/mmi.12457

Tan, B. K., Bogdanov, M., Zhao, J., Dowhan, W., Raetz, C. R. H., and Guan, Z. (2012). Discovery of a cardiolipin synthase utilizing phosphatidylethanolamine and phosphatidylglycerol as substrates. *Proc. Natl. Acad. Sci. U.SA.* 109, 16504–16509. doi: 10.1073/pnas.1212797109

Terui, Y., Akiyama, M., Sakamoto, A., Tomitori, H., Yamamoto, K., Ishihama, A., et al. (2012). Increase in cell viability by polyamines through stimulation of the synthesis of ppGpp regulatory protein and ω protein of RNA polymerase in *Escherichia coli*. *Int. J. Biochem. Cell Biol.* 44, 412–422. doi: 10.1016/j.biocel.2011.11.017

Tran, T. T., Panesso, D., Mishra, N. N., Mileykovskaya, E., and Arias, C. A. (2013). Daptomycin-resistant *Enterococcus faecalis* diverts the antibiotic molecule from the division septum and remodels cell membrane phospholipids. *mBio* 4:e00281-13. doi: 10.1128/mBio.00281-13

Tsui, H. C. T., Keen, S., Sham, L. T., Wayne, K. J., and Winkler, M. E. (2011). Dynamic distribution of the SecA and SecY translocase subunits and septal localization of the HtrA surfacee chaperon/protease during *Streptococcus pneumoniae* D39 cell division. *mBio* 2:e00202-11. doi: 10.1128/mBio.00202-11

Usui, M., Sembongi, H., Matsuzaki, H., Matsumoto, K., and I Shibuya, I. (1994). Primary structures of the wild-type and mutant alleles encoding the phosphatidylglycerophosphate synthase of *Escherichia coli*. *J. Bacteriol.* 176, 3389–3392.

van den Brink-van der Laan, E., Boots, J. W. P., Spelbrink, R. E. J., Kool, G. M., Breukink, E. J., Killian, A., et al. (2003). Membrane interaction of the glycosyltransferase MurG: a special role for cardiolipin. *J. Bacteriol.* 185, 3773–23779. doi: 10.1128/JB.185.13.3773-3779.2003

van Dijl, J. M., Dreisbach, A., Skwark, M. J., Sibbald, M. J. J. B., Tjalsma, H., Zweers, J. C., et al. (2012). "Ins and outs of the *Bacillus subtilis* membrane proteome," in *Bacillus Cellular and Molecular Biology*, ed. P. Graumann (Norfolk: Caister Academic Press), 253–283.

van Teeffelen, S., Wang, S., Furchtgott, L., Huang, K. H., Wingreen, N. S., Shaevitz, J. W., et al. (2011). The bacterial actin MreB rotates, and rotation depends on cell-wall assembly. *Proc. Natl. Acad. Sci. U.S.A.* 108, 15822–15827. doi: 10.1073/pnas.1108999108

Vanounou, S., Parola, A. H., and Fishov, I. (2003). Phosphatidylethanolamine and phosphatidyl-glycerol are segregated into different domains in bacterial membrane. *A* study with pyren-labelled phospholipids. *Mol. Microbiol.* 49, 1067–1079. doi: 10.1046/j.1365-2958.2003.03614.x

Vecchiarelli, A. G., Li, M., Mizuuchi, M., and Mizuuchi, K. (2014). Differential affinities of MinD and MinE to anionic phospholipid influence Min pattering dynamics in vitro. *Mol. Microbiol.* 93, 453–463. doi: 10.1111/mmi.12669

Vereb, G., Szöllösi, J., Matkó, J., Nagy, P., Farkas, T., Vigh, L., et al. (2003). Dynamic, yet structure: the cell membrane three decades after the Singer-Nicolson model. *Proc. Natl. Acad. Sci. U.S.A.* 100, 8053–8058. doi: 10.1073/ pnas.1332550100

Vicente, M., Gomez, M. J., and Ayala, J. A. (1998). Regulation of transcription of cell division genes in the *Escherichia coli* dcw cluster. *Cell. Mol. Life Sci.* 54, 317–324. doi: 10.1007/s000180050158

von Meyenburg, K., Jørgsen, B. B., and van Deurs, B. (1984). Physiological and morphological effects of overproduction of membrane-bound ATP synthase in *Escherichia coli* K-12. *EMBO J.* 3, 1791–1797.

Wang, X., Lesterlin, C., Reyes-Lamothe, R., Ball, G., and Sherratt, D. J. (2011). Replication and segregation of an *Escherichia coli* chromosome with two replication origins. *Proc. Natl. Acad. Sci. U.S.A.* 108, E243–E250. doi: 10.1073/pnas.1100874108

Weart, R. B., Lee, A. H., Chien, A. C., Haeusser, D. P., Hill, N. S., and Levin, P. A. (2007). A metabolic sensor governing cell size in bacteria. *Cell* 130, 335–347. doi: 10.1016/j.cell.2007.05.043

Weiner, J. H., Lemire, B. D., Elmes, M. L., Bradley, R. D., and Scraba, D. G. (1984). Overproduction of fumarate reductase in *Escherichia coli* induces a novel intracellular lipid-protein organelle. *J. Bacteriol.* 158, 590–596.

Welby, M., Poquet, Y., and Tocanne, J.-F. (1996). The spatial distribution of phospholipids and glycolipids in the membrane of the bacterium *Micrococcus luteus* varies during the cell cycle. *FEBS Lett.* 384, 107–111. doi. 10.1016/0014-5793(96)00278-5

Wichmann, C., Naumann, P. T., Spangenberg, O., Konrad, M., Mayer, F., and Hoppert, M. (2003). Liposomes for microcompartmentation of enzymes and their influence on catalytic activity. *Biochem. Biophys. Res. Commun.* 310, 1104–1110. doi: 10.1016/j.bbrc.2003.09.128

Woldringh, C. L. (2002). The role of co-transcriptional translation and protein translocation (transertion) in bacterial chromosome segregation. *Mol. Microbiol.* 45, 17–29. doi: 10.1046/j.1365-2958.2002.02993.x

Woldringh, C. L., Jensen, P. R., and Westerhoff, H. V. (1995). Structure and partitioning of bacterial DNA: determined by a balance of compaction and expansion forces? *FEMS Microbiol. Lett.* 131, 235–242. doi: 10.1111/j.1574-6968.1995.tb07782.x

Woldringh, C. L., and Nanninga, N. (1985). "Structure of the nucleoid and cytoplasm in the intact cell," in *Molecular Cytology of Escherichia coli*. ed. N. Nanninga (London: Academic Press), 161–197.

Woldringh, C. L., and Nanninga, N. (2006). Structural and physical aspects of bacterial chromosome segregation. *J. Struct. Biol.* 156, 273–283. doi: 10.1016/j.jsb.2006.04.013

Yao, J., and Rock, C. O. (2013). Phosphatidic acid synthesis in bacteria. *Biochim. Biophys. Acta* 1831, 495–502. doi: 10.1016/j.bbalip.2012.08.018

Yoshimura, M., Oshima, T., and Ogasawara, N. (2007). Involvement of the YneS/YgiH and PlsX proteins in phospholipid biosynthesis in both *Bacillus subtilis* and *Escherichia coli*. *BMC Microbiol.* 7:69. doi: 10.1186/1471-2180-7-69

Yung, M. W., and Green, C. (1986). The binding of polyamines to phospholipid bilayers. *Biochem. Pharmacol.* 35, 4037–4041. doi: 10.1016/0006-2952(86)90024-9

Zerrouk, Z., Alexandre, S., Lafontaine, C., Norris, V., and Valleton, J. M. (2008). Inner membrane lipids of *Escherichia coli* form domains. *Colloids and Surfaces B Biointerfaces* 63, 306–310. doi: 10.1016/j.colsurfb.2007.12.016

Zheng, M., Chiang, Y. L., Lee, H. L., Kong, L. R., Hsu, S.-T. D., Hwang, I.-S., et al. (2014). Self-assembly of MinE on the membrane underlies formation of the MinE ring to sustain function of the *Escherichia coli* Min system. *J. Biol. Chem.* 289, 21252–21266. doi: 10.1074/jbc.M114.571976

Conflict of Interest Statement: The Associate Editor Arieh Zaritsky declares that, despite being affiliated with the same institution as author Itzhak Fishov, the review process was handled objectively and no conflict of interest exists. The authors declare that the research was conducted in the absence of any commercial or financial relationships that could be construed as a potential conflict of interest.

Copyright © 2015 Matsumoto, Hara, Fishov, Mileykovskaya and Norris. This is an open-access article distributed under the terms of the Creative Commons Attribution License (CC BY). The use, distribution or reproduction in other forums is permitted, provided the original author(s) or licensor are credited and that the original publication in this journal is cited, in accordance with accepted academic practice. No use, distribution or reproduction is permitted which does not comply with these terms.

frontiers in Microbiology

HYPOTHESIS AND THEORY
published: 16 April 2015
doi: 10.3389/fmicb.2015.00322

Why do bacteria divide?

*Vic Norris**

Laboratory of Microbiology Signals and Microenvironment, Theoretical Biology Unit, University of Rouen, Mont Saint Aignan, France

The problem of not only how but also *why* cells divide can be tackled using recent ideas. One idea from the origins of life – *Life as independent of its constituents* – is that a living entity like a cell is a particular pattern of connectivity between its constituents. This means that if the growing cell were just to get bigger the average connectivity between its constituents per unit mass – its *cellular connectivity* – would decrease and the cell would lose its identity. The solution is division which restores connectivity. The corollary is that the cell senses decreasing cellular connectivity and uses this information to trigger division. A second idea from phenotypic diversity – *Life on the Scales of Equilibria* – is that a bacterium must find strategies that allow it to both survive and grow. This means that it has learnt to reconcile the opposing constraints that these strategies impose. The solution is that the cell cycle generates daughter cells with different phenotypes based on sufficiently complex equilibrium (**E**) and non-equilibrium (**NE**) cellular compounds and structures appropriate for survival and growth, respectively, *alias* 'hyperstructures.' The corollary is that the cell senses both the quantity of **E** material and the intensity of use of **NE** material and then uses this information to trigger the cell cycle. A third idea from artificial intelligence – *Competitive Coherence* – is that a cell selects the *active* subset of elements that actively determine its phenotype from a much larger set of available elements. This means that the selection of an active subset of a specific size and composition must be done so as to generate both a coherent cell state, in which the cell's contents work together harmoniously, and a coherent sequence of cell states, each coherent with respect to itself and to an unpredictable environment. The solution is the use of a range of mechanisms ranging from hyperstructure dynamics to the cell cycle itself.

Keywords: neural net, FtsZ, connectivity, heterogeneity, molecular assembly, dualism, competitive coherence, hyperstructure

OPEN ACCESS

Edited by:
Arieh Zaritsky, Ben-Gurion University of the Negev, Israel

Reviewed by:
Luyan Zulie Ma, Institute of Microbiology–Chinese Academy of Sciences, China
Charles Edward Helmstetter, Florida Institute of Technology, USA

***Correspondence:**
Vic Norris, Laboratory of Microbiology Signals and Microenvironment, Theoretical Biology Unit, University of Rouen, Mont Saint Aignan 76821, France
victor.norris@univ-rouen.fr

Specialty section:
This article was submitted to Microbial Physiology and Metabolism, a section of the journal Frontiers in Microbiology

Received: *24 February 2015*
Accepted: *31 March 2015*
Published: *16 April 2015*

Citation:
Norris V (2015) Why do bacteria divide? Front. Microbiol. 6:322. doi: 10.3389/fmicb.2015.00322

Introduction

The very fact of growing is a source of many serious problems that bacteria somehow have to solve. These problems include DNA becoming a limiting factor (thereby disrupting patterns of expression and preventing exponential growth), positive feedback (thereby leading to a single phenotype), over-reliance on fragile, non-equilibrium (**NE**) structures such as those created by the coupling of transcription, translation (thereby making the cell vulnerable to changes in its environment), and unbalanced production of RNA, protein and lipid (Norris, 2011). The problems do not stop there. More generally, bacteria must have found ways to avoid incoherence at the level of both the individual cell and the population so as to be able to not only grow but also survive (arguably, the more important of the two behaviors since a dead cell can never grow)

in what we have called 'Life on the Scales' (Norris and Amar, 2012a). More generally still, bacteria – like all living objects – risk losing the connectivity between their constituents as they get bigger (Norris, 2015). This is particularly serious because patterns of connectivity are often claimed to define pretty well everything – as testified by the claims of universality made for self-organized criticality (Bak, 1996) and small world networks (Watts and Strogatz, 1999) – so that a bacterium that continued to grow would eventually lose its identity.

The above problems are intimately related to the cell cycle. In non-differentiating bacteria such as *Escherichia coli*, the cell cycle was long considered to have only the function of replicating the hereditary material and distributing it into two cells that would be effectively identical unless driven down the path of differentiation. This fitted with the idea that the laws underlying cell growth – and, in particular, those directly relevant to the cell cycle – could be found not by studying single cells but rather by studying cells as an aggregate (Cooper, 2006). However, it is now clear that even *E. coli* generates substantial phenotypic diversity (Godin et al., 2010; Wang et al., 2010; Kiviet et al., 2014; Osella et al., 2014; Taheri-Araghi et al., 2015) with cell division playing the key role. It is not therefore surprising that connections have been found between the replication of the bacterial chromosome and processes that include central carbon metabolism (Janniere et al., 2007; Baranska et al., 2013), phospholipid synthesis (Sekimizu and Kornberg, 1988; Xia and Dowhan, 1995), respiration, lipoteichoic acid synthesis, and ribosome biosynthesis (Murray and Koh, 2014). Other connections have also been found between cell division and processes that include fatty acid synthesis (Yao et al., 2012), glycolysis and its offshoots (Weart et al., 2007; Hill et al., 2013; Monahan et al., 2014), and polyphosphate metabolism (Rao et al., 2009; Boutte et al., 2012).

In the above context, it is interesting to revisit cell division in terms of concepts, such as *hyperstructures* or *competitive coherence*, that are either new or under development. The concept of *hyperstructures* is directly relevant to the problem of maintaining connectivity. A hyperstructure is an assembly of elements (such as genes, RNA, proteins, small molecules, and ions) that performs a function and that constitutes a substantial proportion of the cellular material (Norris et al., 2007a; Saier, 2013; Meyer et al., 2014). The existence of the hyperstructure level is a partial solution to the problem of reducing the enormity of phenotype space from the combinations of 1000s of types of macromolecules to combinations of a 100 or so hyperstructures, thereby allowing Darwinian selection to operate (Kauffman, 1996; Norris et al., 2014). Hyperstructures exist in **NE** and equilibrium (**E**) forms with the ratio between these forms proposed to control the cell cycle and to generate phenotype diversity by sensing both the intensity with which **NE** hyperstructures are working and the quantity of **E** hyperstructures that has accumulated (Norris, 2011; Norris and Amar, 2012a); the importance of cell division to the related stability of cellular constituents has been demonstrated by simulation (Kamimura and Kaneko, 2014). The concept of *competitive coherence*, which relies on patterns of connections, has been developed to explain the behavior of biological systems, which include, of course, bacteria (Norris et al., 2014). This behavior is determined by a relatively small, phenotypically *active*, subset of all the constituents available to the bacterium; selection of this subset entails competition between (1) those constituents whose activities are coherent with one another and with the environment and (2) those constituents whose activities are coherent with the previous history of the bacterium. Simulation has shown that a system based on competitive coherence can adapt to growth and stress conditions (Norris et al., 2012). Moreover, the concept can be extended to include the role of **NE** and **E** hyperstructures and the role of the cell cycle in the nature and size of the active subset (Norris et al., 2014).

According to Krakauer (2014) at the Santa Fe Institute, this institute "is about circling a phenomenon, considering all the angles and unique perspectives to see a thing in a completely new light." Such circling could be likened to someone preparing to climb a mountain shrouded in fog who tries many routes that may be useful-even if they do not lead to the summit-because they give new views. This is the approach to cell division that I adopt here.

Maintenance of Connectivity

A bacterium is a physical object but what exactly is a physical object? Put differently, what makes one physical object different from another. A crab-like alien examining the Earth from orbit might mistake me and the chair on which I am sitting for an eight-legged crab. The reason the alien would be wrong is that there is a frontier between my chair and me. My constituent bits or elements are more connected to one another than they are to the chair's bits and *vice versa*. More generally, a physical object can be said to exist in some space if there is a topologically closed (or nearly closed) discontinuity in the connectivity of the elements in that space; this discontinuity constitutes a frontier of connectivity that makes the object different from its environment. The exact nature of this object is defined by the pattern of connectivity of its constituent elements and by the pattern of connectivity of these elements to its environment. In other words, a physical object owes its identity and its very existence to patterns of connectivity. This is one interpretation that can be made of the picture by Mary Cassatt of her dying sister, Lydia (**Figure 1**).

A bacterium is, of course, more than just a physical object, it is a *living* physical object. One of the characteristics of living objects such as bacteria is that at some stage they grow (or, at least, their ancestors grew). Growth entails an increase in mass *via* the addition of new elements or constituents. In the case of a bacterium, these constituents may be the same as those already there (as shown for the constituents numbered 1–6 in **Figure 2A**); hence, the addition of these new constituents may leave the average connectivity unchanged, where connectivity, L/E, equals the number of links or physical associations, L, divided by the number of constituents or elements, **E** (**Figure 2A**). In other words, growth does not necessarily change the number or nature of the connections between the constituents themselves and L/E either remains constant (**Figure 2A**) or even drops (**Figure 2B**). Growth does, of course, mean an increase in the mass of the bacterium and this in turn means that the average connectivity

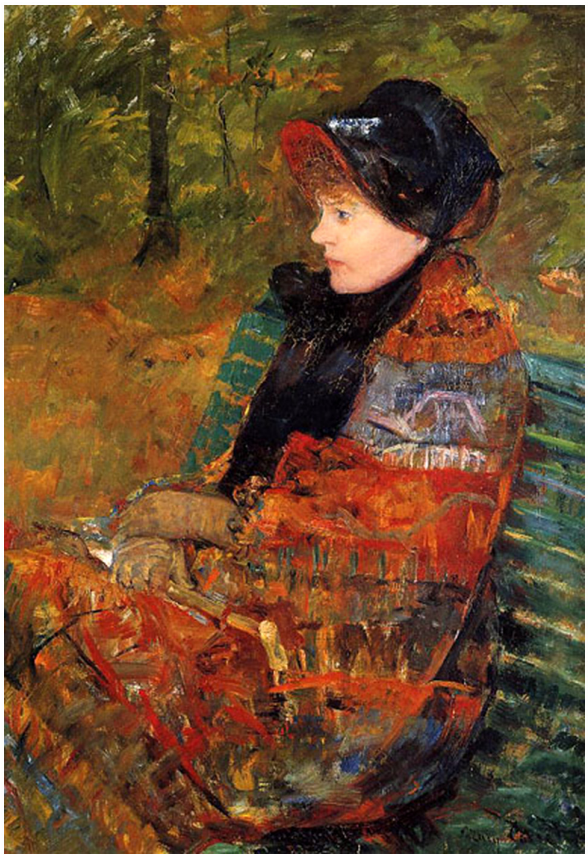

FIGURE 1 | Profile of Lydia Cassatt (1880). This portrait entitled Autumn of the seriously ill Lydia by her sister, Mary Cassatt, can be interpreted as showing her losing her identity (copied from http://hoocher.com/Mary_Cassatt/Mary_Cassatt.htm original in the Musee du Petit Palais, Paris, France).

per mass M of the bacterium, (L/E)/M *alias cellular connectivity*, decreases. To make this clearer, consider a toy cell that comprises six different elements each of which binds to two other elements (such that the connectivity, L/E, is one). Consider too that this cell manages to grow so as to duplicate exactly its six constituents, as shown by the two sets of differently colored constituents in **Figure 2A**. Its L/E either remains one or, if this duplication is not exact, drops below one, as shown by the relative excess of constituents number 1 in **Figure 2B**. However, connectivity divided by mass has halved. Why does this matter?

Scaling up a process or a structure often results in a changed connectivity and a changed behavior. This is one of the dangers posed by growth: identity is changed. Consider a bacterium that has grown much bigger than normal. It would have different mechanical properties (and different resistance to mechanical stresses), a different motility, differences in regulatory networks (the behavior of the ensemble of two identical networks can be qualitatively different from that of one of these networks on its own), possibly differences in the surface/volume ratio (see, Bendezu and de Boer, 2008), etc. Not surprisingly, the changing connections that accompany increased hydration create problems for cells (Lang, 2011). The change in identity that accompanies extensive growth is not always negative. Such growth is, for example, fundamental to the change in the identity of an *E. coli* cell as it becomes a filamentous, multinucleate, hyperflagellate cell that can swarm over the surface of solid media (Harshey and Matsuyama, 1994). That said, the reduction of cellular connectivity that accompanies growth generally constitutes a serious problem constraining the evolution of cells.

It turns out that there are several possible solutions to the problem of how to maintain cellular connectivity despite growth. One of them involves the creation or the expansion of an additional level of organization. Multi-level structuring is a fundamental characteristic of living systems. Each new emergent level of organization in the dynamics of a complex self-organizing system – such as a living system – re-organizes variety on the level below so that it has meaning for the level above (Salthe, 1985; Lemke, 2000). The physical nature of the processes, the spatio-temporal scales, and connections at a particular level may be characteristic of that level (Norris et al., 2007a). In the case of the individual bacterium, I would argue that the level of

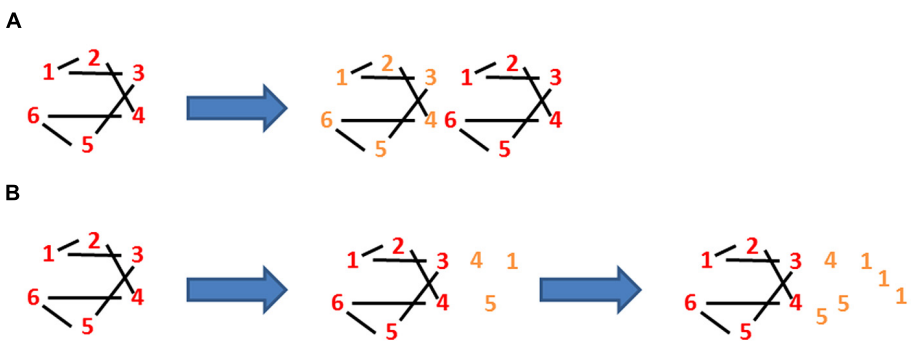

FIGURE 2 | Loss of identity through growth. There are six elements in the autocatalytic set linked by two links per element. **(A)** The links:elements ratio (L:E) is 1 and stays 1 in the above case as the cell grows. However, this ratio per mass goes down with growth as (L:E)/M goes to (L:E)/2M. **(B)** After the first stage of growth (50% increase in mass), the (L:E)/M has gone down from 1 to (6:9)/1.5M, i.e., 0.4444 whilst after continuing but unbalanced growth (100% increase in mass), the (L:E)/M has gone down from 1 to (6:12)/2M, i.e., 0.25.

organization that is relevant to the cellular connectivity problem is that of hyperstructures, which is the level intermediate between macromolecules and the bacterial cell itself (Norris et al., 2007a). There are several types of hyperstructure (Norris et al., 2007a). In the case of enzymic hyperstructures, a recent study suggests that a quarter of known cytoplasmic enzymes are in hyperstructures in which they have a higher within-group connectivity than enzymes that appear to be outside hyperstructures (Meyer et al., 2014). The relevance of the hyperstructure concept to growth is that, as the bacterium grows, the dynamics of hyperstructures changes such that some hyperstructures are born and others are consolidated; in other words, connectivity at the level of hyperstructures increases, thereby compensating for the decrease in connectivity at the level of macromolecules and maintaining the average connectivity per mass (i.e., cellular connectivity). A prime candidate for a hyperstructure that is born during growth would be the initiation hyperstructure based on the DnaA protein whilst candidates for hyperstructures that are consolidated during growth would include the ribosomal hyperstructure or microcompartment where ribosomal constituents are made and perhaps assembled (see, Intensity Sensing and Quantity Sensing; Norris and Amar, 2012a). These different hyperstructures and their dynamics may be in part responsible for the relationship between the fluidity of the cytoplasm and metabolism (Parry et al., 2014).

Another possible solution to the cellular connectivity problem involves cell division. To simplify it, cell division produces two daughter cells in which the average connectivity per constituent per mass is restored to that of the parental cell when it was born. A population of bacteria such as *E. coli* usually has a size distribution – characteristic of the rate of growth – that is the culmination of the cell cycle in which mass plays an important regulatory role (see below; Schaechter et al., 1958). It has been proposed that the timing and locating of the division site are the result of what is essentially a local reduction in the connectivity of the membrane *alias* the frontier of discontinuity with the environment (Norris et al., 2004). Evidence for this includes the appearance of membrane domains at the site of division (Mileykovskaya and Dowhan, 2000; Kawai et al., 2004), which constitutes the earliest known step of the formation of the division site in *E. coli* (Fishov and Woldringh, 1999). These anionic lipid-rich domains form in the regions outside (including between) the chromosomes, presumably by default because the membrane around the chromosomes is both enriched in other lipids and structured by the coupling between the processes of transcription, translation, and insertion of nascent proteins into membrane *alias transertion* which increases the microviscosity of the membrane (Binenbaum et al., 1999). Such relatively unconnected domains at the division site may have a propensity to invaginate as shown in phase separation experiments (Li et al., 2011). Moreover, excess production of membrane – which I would argue results in a region of relatively unconnected membrane – results in division in wall-less bacteria (Mercier et al., 2013) and can titrate division enzymes such as FtsZ and MinD in certain shape mutants of *E. coli* (Bendezu and de Boer, 2008). A lower density of connections between envelope proteins, peptidoglycan, and the inner membrane has been proposed to explain the release of membrane vesicles from Gram-negative bacteria and, in particular, from their the division sites (Deatherage et al., 2009). Despite my focus here on the membrane as the important frontier of connectivity, it should be noted that two classes of models of the cell are proposed to exist, one in which the membrane is all-important in defining the cell and a second in which the entire cell is in a different phase relative to its surroundings (Jaeken and Vasilievich Matveev, 2012). Hence, a division site might result not only from a local reduction in the connectivity of the membrane but also from a frontier of discontinuity forming in the interior of the cell (as might be argued in the case of the phragmoplast in plant cells). Indeed, when two liquid phases are in contact with a membrane, their interactions with that membrane can lead to budding (Li et al., 2012).

Dualism

An apparently intractable dilemma often confronts bacteria: either to interact, take risks and grow, or to minimize interactions, avoid risks, shut down, and survive. A bacterium that tries to grow forever will eventually run out of resources and to survive must abandon this strategy. Conversely, a bacterium that refuses to grow whilst others grow successfully must abandon this strategy if it is not to be out-competed. A strong evolutionary pressure therefore exists to compel bacteria to choose between at least two apparently incompatible strategies or, to put it differently, to navigate in phenotype space between the two basins of growth and survival. This is the problem of *Life on the Scales* (Norris and Amar, 2012b).

The solution adopted by bacteria is to generate a phenotypically diverse population (Smits et al., 2006; Maisonneuve and Gerdes, 2014; Serra et al., 2014). This diversity extends to the growth rate itself such that, within a growing population of *E. coli*, non-growing persisters are produced at a low frequency (Balaban et al., 2004). Growth rate diversity is, however, much greater than this. Measurements of the buoyant mass of individual *E. coli* reveal a considerable variation in 'instantaneous' growth rates (Godin et al., 2010) as do measurements of the elongation rates of individual *E. coli* (Wang et al., 2010; Kiviet et al., 2014; Osella et al., 2014).

The many ways to achieve a phenotypically diverse population include multi-stationarity in networks (Thomas, 1980; Dubnau and Losick, 2006), noise (Silva-Rocha and de Lorenzo, 2010), spontaneous gene amplification (Anderson and Roth, 1977), and chemical communication (Vega et al., 2012). These mechanisms may not necessarily lead to the satisfaction of two requirements: the phenotypes generated need to be both (1) internally coherent and (2) coherent with respect to the other phenotypes in the population. In the case of the former requirement, if an evolutionarily useful, phenotypic diversity is to be generated, each phenotype must be coherent with respect to the set of genes expressed (Norris and Amar, 2012a). This requirement for coherence is strong in the case of the growth rate since growth and survival strategies are incompatible at the level of the individual cell.

An evident mechanism to generate coherent phenotypic diversity is the cell cycle itself. Each division in differentiating, bacterial species such as *Caulobacter crescentus* generates two cells with very different metabolisms (Bowman et al., 2013). It is therefore conceivable that even in non-differentiating bacteria such as *E. coli*, the cell cycle is the primary mechanism for generating daughter cells with different growth rates. Indeed, the authors' interpretation of the results of a microfluidics-based experiment on the growth rate distribution of *E. coli* is that the cell "forgets" on division its growth rate in the previous cell cycle (Wang et al., 2010); further analysis of these results confirms the importance of cell division in generating diversity (Osella et al., 2014). The question is how.

The answer is that differentiation far from being difficult to achieve is difficult to avoid. Differentiation is almost inescapable in systems where negative feedback operates globally and positive feedback operates locally (Norris, 1995b; Norris and Madsen, 1995). Consider two similar research laboratories competing with others for limited funds (i.e., a globally negative feedback); if one of these laboratories is actually funded and the other is not, in the next competition, the previously funded laboratory is at an advantage (i.e., a locally positive feedback). During the cell cycle of modern bacteria, two – what are for my purpose here – essentially identical chromosomes compete for limiting factors like RNA polymerases and ribosomes; this constitutes negative regulation *in trans*. At the same time, a region of one chromosome that is being expressed by polymerases is pulled by these polymerases out of the nucleoid (where it would otherwise be buried and relatively inaccessible) and this expression increases the region's accessibility to more polymerases; this constitutes positive regulation *in cis*; in addition, transertion allows ribosomal subunits to penetrate the nucleoid and to perform co-transcriptional translation (Bakshi et al., 2014), which in turn would protect nascent mRNA (Deana and Belasco, 2005; Deneke et al., 2013), limit the formation of the RNA degradosome (Strahl et al., 2015) and stop RNA polymerases backtracking (McGary and Nudler, 2013). The two chromosomes therefore spontaneously have different patterns of expression (Norris, 1995b; Norris and Madsen, 1995). This 'globally negative, locally positive' mechanism might explain the generation of daughters with different phenotypes but not the coherence of these phenotypes.

There are many ways to achieve a diversity that is coherent (Norris et al., 2014). One of them is *dualism* (Norris, 2011). It works like this: the cell cycle generates two daughter cells with different ratios of **NE** and **E** hyperstructures; these different ratios confer different properties on the daughter cells such that those with higher **NE**:**E** ratios grow fast to profit from nutrient availability whilst those with lower **NE**:**E** ratios grow slowly or cease growth so as to resist stresses. These ratios give rise to coherent phenotypes because one of the parental strands of DNA is physically associated with the **NE** hyperstructures appropriate for growth whilst the other strand is physically associated with the **E** hyperstructures appropriate for survival (Rocha et al., 2003). The logic here is that, in a competitive cytoplasm, an old strand associated with a particular hyperstructure (e.g., *via* coupled transcription–translation) has more chance of retaining that hyperstructure than a chemically identical, newly replicated (and therefore unexpressed) strand has of acquiring that hyperstructure (**Figure 3**). Hence, the older strands have the advantage in terms of making the major contribution to the phenotypes of the daughter cells. Evidence consistent with dualism includes the different locations of the leading and lagging strands (White et al., 2008) and the colocation of genes and their products (Llopis et al., 2010). In the dualism hypothesis, it is essential to achieving a phenotypically diverse population that the replication of the chromosome be followed by cell division since this puts these chromosomes into separate cells. Coherent separation leading to division can, of course, be achieved by several, complementary, physical mechanisms as shown by lipid vesicles that encapsulate an aqueous two-phase system of polyethylene glycol and dextran within a membrane of liquid-disordered and liquid-ordered domains (Andes-Koback and Keating, 2011). The philosophical rationale behind this physical separation is that the regulatory and metabolic networks that depend on these chromosomes can disrupt one another if they are not separated, as illustrated by a simple model based on artificial chemistry (Demarty et al., 2003).

In discussing the maintenance of cellular connectivity, I proposed above that cell division maintains identity or phenotype by regenerating the original patterns of connectivity. This can now be seen to be an over-simplification. More exactly, division is fundamental to generating the two classes of patterns of connectivity that allow a population to live on the scales. In other words, even in steady-state conditions, growth, and division create a bacterial population with a constant distribution of varied but coherent phenotypes that interchange over successive generations.

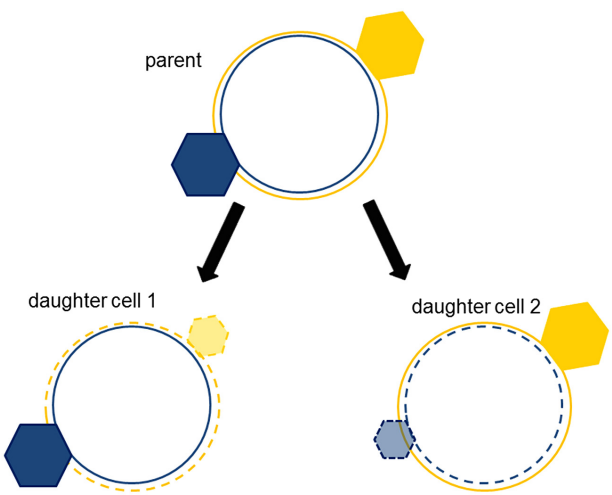

FIGURE 3 | Strand segregation of hyperstructures creates complementary, coherent phenotypes. The hyperstructure (hexagon) associated with an old strand (continuous circle) is segregated with the old strand into the daughter cell. New hyperstructures (translucent hexagons) associated with the new strands (dotted circles) are smaller because they must compete with the parent cell's hyperstructures (solid hexagons).

Intensity Sensing and Quantity Sensing

The cell cycle is also the solution to another two fundamental problems. The *intensity* problem that confronts bacteria during growth is that the **NE** constituents that do the work, like enzymes, eventually work with such intensity that they can do no more; the cell can then do no better than grow linearly. The *quantity* problem that also confronts bacteria during growth is that the quantity of unused, **E** material – be it lipids or macromolecules – accumulates; this material risks being a waste of resources. By sensing both intensity and quantity, a bacterium could decide when it was time to increase the number of enzymes and to convert the unused macromolecules into another form. In the case of *E. coli*, we have proposed that this combination of intensity and quantity sensing reaches a threshold that triggers the cell cycle and it is then the events of the cell cycle that solve both intensity and quantity problems (Norris, 2011; Norris and Amar, 2012a; Norris et al., 2014). The idea is that the state of one or more **NE** hyperstructures reflects the intensity of metabolism at that *particular moment in time* and that when this intensity is sufficiently high for growth to risk growth being limited, one or more signals are emitted by these hyperstructures to initiate chromosome replication. In addition, the state of one or more **E** hyperstructures senses the quantity of accumulated material and when this is likely to be sufficient for daughter cells to be generated, a complementary, initiation signal is emitted. These signals trigger the cell cycle which has the function of converting **E** into **NE** material and redistributing this material into the daughter cells.

There are several mechanisms that might be responsible for intensity sensing; one attractive mechanism could be based on interactions between cytoskeletal hyperstructures and metabolic enzymes such that, for example, an enzyme that is catalyzing its reaction has a greater affinity for the replication and/or cytoskeletal hyperstructures and helps to stabilize/destabilize them (Norris et al., 2013). This actually occurs in *Bacillus subtilis* where assembly of FtsZ into an effective division structure is inhibited by interaction between FtsZ and the glucosyltransferase UgtP, which depends on the concentration of UDP-glucose (Weart et al., 2007); a similar system exists in *E. coli* where the interaction is between FtsZ and the functional homolog of UgtP, OpgH (Hill et al., 2013). FtsZ dynamics are also affected by the location of pyruvate dehydrogenase E1α, which depends on the concentration of pyruvate (Monahan et al., 2014). Another mechanism might involve sensing the density of RNA polymerases transcribing genes and of ribosomes translating mRNA (Norris, 1995c); in line with this, a correlation exists between attaining a particular growth rate per unit mass in mouse lymphoblasts and their entry into S phase (Son et al., 2012). There are also several mechanisms that might be responsible for quantity sensing and that, for example, might be based on the possible accumulation of proteins and lipids (Norris and Amar, 2012a). In the former case, examples might include the wall synthesis enzyme, MurG, which is stored in an inactive form in the cell poles (Michaelis and Gitai, 2010) and the CTP synthetase, CtpS, which is stored in an inactive form as a polymer (Barry et al., 2014). In the latter case, accumulation of cardiolipin would be an attractive candidate given its roles in initiation of replication (Sekimizu and Kornberg, 1988; Makise et al., 2002) and in cell division (Mileykovskaya and Dowhan, 2000; Koppelman et al., 2001; Kawai et al., 2004). Finally, there are molecules of major physiological importance that are often overlooked (Norris et al., 2015); these include polyphosphate which, in some bacteria, has been shown to play a role in the cell cycle (Boutte et al., 2012) and to exist in both soluble and insoluble forms (Klauth et al., 2006).

Competitive Coherence

Competitive coherence is a particular way of choosing a temporal series of subsets of elements from a much larger set (Norris et al., 2012). These subsets are *active* subsets insofar as a subset actively determines the behavior of the entire system at a particular time. Such a subset (*alias* the phenotype) is selected by a competition between (1) those elements that have a relationship with the elements in the previous subset and (2) those elements that have a relationship with the elements already selected to be part of the new, emerging subset. At the level of a bacterium, growth and survival require selection of an active subset of macromolecules in response to external and internal conditions; such responses entail both the generation of a coherent cell state, in which the cell's contents work together efficiently and harmoniously, and the generation of a coherent sequence of cell states. Incoherence within a cell state is punished since, for example, a cell that simultaneously induces the expression of genes for growth at high temperature and at low temperature is likely to be outcompeted by rival cells that induce each set of genes only when needed. Incoherence in the succession of cell states is also punished since a cell that goes from one cell state to another very different one (without good environmental reason) is wasting resources. A strong selective pressure, therefore, exists to generate active subsets of elements to provide both coherent cell states and a coherent sequence of such states (Norris et al., 2014). In response to this pressure, the process of competitive coherence has evolved to reconcile two sorts of coherence in generating the active subset. Note that the active subset is not the same as the bacterium's entire set of genes, set of mRNAs and/or set of proteins: the active subset is the set of elements that determines the behavior of the cell at a particular time. Hence, a gene that is not expressed or an mRNA that is not translated or an enzyme that is not in the right hyperstructure might have no effect on the phenotype at a particular time and therefore would not be part of the active subset. The question therefore arises as to whether the concept of competitive coherence can provide an insight into the cell cycle.

One of the important parameters in competitive coherence is the nature and size of the active subset. It is far from clear, however, how the size of the active subset should vary with conditions. In a bacterium growing rapidly, the need for it to be ready to adapt to new opportunities or stresses might be better served by a large active subset containing mainly **NE** elements whilst in a non-growing bacterium the need for it to maintain its structures (rather than abandon them too readily so as to profit from a growth opportunity) may require a small active

subset containing mainly **E** elements. It might be argued that in stress conditions, the active subset may be smaller in order to conserve energy and to lose diversity as the system concentrates on a limited number of **E** hyperstructures in which the elements are tightly connected with one another (Norris et al., 2014). In changing conditions, however, we predict that the active subset would also change and go through a period when it changes in size, as proposed for *Streptomyces coelicolor* as it goes through changes in nutrient availability and population density (Vohradsky and Ramsden, 2001).

Changes in the active subset is where the cell cycle comes in. Cell division permits activity subsets not just with different contents but also of different sizes. One question here is what would happen to the active subset if a bacterium were to grow without going through the cell cycle. Presumably, RNA and protein production would eventually become limited by the relative scarcity of DNA so that exponential growth could not be sustained (Zaritsky, 1975; Norris, 2011). It is tempting to think that, since many different genes compete for an increasing number of RNA polymerases (Stickle et al., 1994), continuation of growth in the absence of a cell cycle would lead to the inappropriate transcription of an increasing number of genes and to an incoherent phenotype, but this must depend to some extent on how the regulatory network would change. Assuming an increase in transcriptional and translational machinery relative to unit DNA, growth without cell cycle progress should lead to a gene encoding a repressor reaching a maximum level of expression and the repressor eventually being diluted by growth and becoming insufficient to repress its targets. It is therefore conceivable that the absence of the cell cycle would result in an increase in the size of the active subset such that all the phenotypes in the population converged onto a single phenotype. Inhibition of chromosome replication in *B. subtilis*, accompanied by continued growth led to significant alterations in the expression of over a 100 genes, around a half being regulated by DnaA, which is both an initiator of replication and a transcription factor (Goranov et al., 2005). In this experiment, the period of unbalanced growth lasted for a maximum of 90 min and only the mRNA levels of the entire population could be measured. To explore the ideas outlined above would require following the global patterns of transcription and translation in individual cells growing over several hours without cell cycle progress. Unfortunately, this is at present impossible. In summary, once again, the cell cycle is about the preservation of the coherence of individual phenotypes and the coherence of the population of phenotypes.

Discussion

It is somewhat surprising that after decades of intense research into the cell cycle of some of biology's best understood model organisms, the fundamental nature of the control over the cell cycle remains elusive and, in particular, the coupling between the cell cycle and the growth rate (Marshall et al., 2012; Campos et al., 2014; Taheri-Araghi et al., 2015). One explanation is that the paradigm that has guided this research is wrong. If so, a new paradigm is required. This is easier said than done. The approach to generating new paradigms that I advocate here is to ask the question "why do bacteria divide?" Such 'existentialist' questions are fundamental and attempts to answer them can lead to new insights. Some of us have considered explanations for cell division in terms of the maintenance of cellular connectivity, the reconciliation of growth and survival strategies, and combining present coherence with past coherence. Could these ideas lead to a new paradigm and, if so, would we know if it were a good one?

A new paradigm might be evaluated on grounds that include its esthetic qualities, its testability, its difference with the current paradigm, and the breadth of its fields of application (Norris, 1995a). In other words, does the new paradigm result in a rapid advance in a specific field of science, and does it help us understand other fields? One approach is to focus on those *unifying* problems that recur in different fields, for example, how to limit the enormity of phenotype space so that Darwinian selection can act (Kauffman, 1996). To solve this problem, we have invoked a key role for simple, universal molecules and inorganic ions, termed SUMIs, which include polyphosphate, polyhydroxybutyrate, polyamines, and calcium (Norris et al., 2015). A complementary approach is to ask whether the paradigm would help elucidate another field, for example, could a hypothesis developed for the origins of life help with cell division? This may be the case for the SUMIs, all of which have major roles in the growth, cell cycle, and differentiation of bacteria (Huang and Reusch, 1996; Igarashi and Kashiwagi, 2006; Naseem et al., 2009; Rao et al., 2009; Boutte et al., 2012). It may also be that case for **NE** and **E** hyperstructures, dualism, and life on the scales, which we would argue are as important to the division of modern cells as they were to the origins of protocells in the prebiotic ecology (Norris and Raine, 1998; Hunding et al., 2006; Norris et al., 2007b). Indeed, concepts such as life on the scales and competitive coherence are essentially scale-free and substance-free, and are applicable to life elsewhere in the cosmos (Norris, 2015).

In discussing the maintenance of cellular connectivity, we proposed that cell division maintains identity by regenerating the original patterns of connectivity. This is clearly an oversimplification since division is fundamental to generating the two patterns of connectivity that allow a population to live on the scales. The point is that growth and division create a population of individuals with a constant distribution of phenotypes or identities that interchange over successive generations. Ironically, this fundamental role for the cell cycle may have been obscured by the importance – admittedly understandable – attributed to only studying the cell cycle of bacteria growing in steady-state conditions which minimize differentiation (Schaechter et al., 1958; Fishov et al., 1995).

Acknowledgments

I thank Andreas Dress, Alex Grossman, Marie Beurton-Aimar and the reviewers for helpful comments.

References

Anderson, R. P., and Roth, J. R. (1977). Tandem genetic duplications in phage and bacteria. *Annu. Rev. Microbiol.* 31, 473–505. doi: 10.1146/annurev.mi.31.100177.002353

Andes-Koback, M., and Keating, C. D. (2011). Complete budding and asymmetric division of primitive model cells to produce daughter vesicles with different interior and membrane compositions. *J. Am. Chem. Soc.* 133, 9545–9555. doi: 10.1021/ja202406v

Bak, P. (1996). *How Nature Works: The Science of Self-Organized Criticality*. New York: Copernicus. doi: 10.1007/978-1-4757-5426-1

Bakshi, S., Choi, H., Mondal, J., and Weisshaar, J. C. (2014). Time-dependent effects of transcription- and translation-halting drugs on the spatial distributions of the *Escherichia coli* chromosome and ribosomes. *Mol. Microbiol.* 94, 871–887. doi: 10.1111/mmi.12805

Balaban, N. Q., Merrin, J., Chait, R., Kowalik, L., and Leibler, S. (2004). Bacterial persistence as a phenotypic switch. *Science* 305, 1622–1625. doi: 10.1126/science.1099390

Baranska, S., Glinkowska, M., Herman-Antosiewicz, A., Maciag-Dorszynska, M., Nowicki, D., Szalewska-Palasz, A., et al. (2013). Replicating DNA by cell factories: roles of central carbon metabolism and transcription in the control of DNA replication in microbes, and implications for understanding this process in human cells. *Microb. Cell Fact.* 12:55. doi: 10.1186/1475-2859-12-55

Barry, R. M., Bitbol, A. F., Lorestani, A., Charles, E. J., Habrian, C. H., Hansen, J. M., et al. (2014). Large-scale filament formation inhibits the activity of CTP synthetase. *Elife* 3:e03638. doi: 10.7554/eLife.03638

Bendezu, F. O., and de Boer, P. A. (2008). Conditional lethality, division defects, membrane involution, and endocytosis in mre and mrd shape mutants of *Escherichia coli*. *J. Bacteriol.* 190, 1792–1811. doi: 10.1128/JB.01322-07

Binenbaum, Z., Parola, A. H., Zaritsky, A., and Fishov, I. (1999). Transcription- and translation-dependent changes in membrane dynamics in bacteria: testing the transertion model for domain formation. *Mol. Microbiol.* 32, 1173–1182. doi: 10.1046/j.1365-2958.1999.01426.x

Boutte, C. C., Henry, J. T., and Crosson, S. (2012). ppGpp and polyphosphate modulate cell cycle progression in *Caulobacter crescentus*. *J. Bacteriol.* 194, 28–35. doi: 10.1128/JB.05932-11

Bowman, G. R., Perez, A. M., Ptacin, J. L., Ighodaro, E., Folta-Stogniew, E., Comolli, L. R., et al. (2013). Oligomerization and higher-order assembly contribute to sub-cellular localization of a bacterial scaffold. *Mol. Microbiol.* 90, 776–795. doi: 10.1111/mmi.12398

Campos, M., Surovtsev, I. V., Kato, S., Paintdakhi, A., Beltran, B., Ebmeier, S. E., et al. (2014). A constant size extension drives bacterial cell size homeostasis. *Cell* 159, 1433–1446. doi: 10.1016/j.cell.2014.11.022

Cooper, S. (2006). Distinguishing between linear and exponential cell growth during the division cycle: single-cell studies, cell-culture studies, and the object of cell-cycle research. *Theor. Biol. Med. Model* 3:10. doi: 10.1186/1742-4682-3-10

Deana, A., and Belasco, J. G. (2005). Lost in translation: the influence of ribosomes on bacterial mRNA decay. *Genes Dev.* 19, 2526–2533. doi: 10.1101/gad.1348805

Deatherage, B. L., Lara, J. C., Bergsbaken, T., Rassoulian Barrett, S. L., Lara, S., and Cookson, B. T. (2009). Biogenesis of bacterial membrane vesicles. *Mol. Microbiol.* 72, 1395–1407. doi: 10.1111/j.1365-2958.2009.06731.x

Demarty, M., Gleyse, B., Raine, D., Ripoll, C., and Norris, V. (2003). Modelling autocatalytic networks with artificial microbiology. *C. R. Biol.* 326, 459–466. doi: 10.1016/S1631-0691(03)00097-0

Deneke, C., Lipowsky, R., and Valleriani, A. (2013). Effect of ribosome shielding on mRNA stability. *Phys. Biol.* 10:046008. doi: 10.1088/1478-3975/10/4/046008

Dubnau, D., and Losick, R. (2006). Bistability in bacteria. *Mol. Microbiol.* 61, 564–572. doi: 10.1111/j.1365-2958.2006.05249.x

Fishov, I., and Woldringh, C. L. (1999). Visualization of membrane domains in *Escherichia coli*. *Mol. Microbiol.* 32, 1166–1172. doi: 10.1046/j.1365-2958.1999.01425.x

Fishov, I., Zaritsky, A., and Grover, N. B. (1995). On microbial states of growth. *Mol. Microbiol.* 15, 789–794. doi: 10.1111/j.1365-2958.1995.tb02349.x

Godin, M., Delgado, F. F., Son, S., Grover, W. H., Bryan, A. K., Tzur, A., et al. (2010). Using buoyant mass to measure the growth of single cells. *Nat. Methods* 7, 387–390. doi: 10.1038/nmeth.1452

Goranov, A. I., Katz, L., Breier, A. M., Burge, C. B., and Grossman, A. D. (2005). A transcriptional response to replication status mediated by the conserved bacterial replication protein DnaA. *Proc. Natl. Acad. Sci. U.S.A.* 102, 12932–12937. doi: 10.1073/pnas.0506174102

Harshey, R. M., and Matsuyama, T. (1994). Dimorphic transition in *Escherichia coli* and *Salmonella typhimurium*: surface-induced differentiation into hyperflagellate swarmer cells. *Proc. Natl. Acad. Sci. U.S.A.* 91, 8631–8635. doi: 10.1073/pnas.91.18.8631

Hill, N. S., Buske, P. J., Shi, Y., and Levin, P. A. (2013). A moonlighting enzyme links *Escherichia coli* cell size with central metabolism. *PLoS Genet.* 9:e1003663. doi: 10.1371/journal.pgen.1003663

Huang, R., and Reusch, R. N. (1996). Poly(3-hydroxybutyrate) is associated with specific proteins in the cytoplasm and membranes of *Escherichia coli*. *J. Biol. Chem.* 271, 22196–22202. doi: 10.1074/jbc.271.36.22196

Hunding, A., Kepes, F., Lancet, D., Minsky, A., Norris, V., Raine, D., et al. (2006). Compositional complementarity and prebiotic ecology in the origin of life. *Bioessays* 28, 399–412. doi: 10.1002/bies.20389

Igarashi, K., and Kashiwagi, K. (2006). Polyamine Modulon in *Escherichia coli*: genes involved in the stimulation of cell growth by polyamines. *J Biochem* (*Tokyo*) 139, 11–16. doi: 10.1093/jb/mvj020

Jaeken, L., and Vasilievich Matveev, V. (2012). Coherent behavior and the bound state of water and K(+) imply another model of bioenergetics: negative entropy instead of high-energy bonds. *Open Biochem. J.* 6, 139–159. doi: 10.2174/1874091X01206010139

Janniere, L., Canceill, D., Suski, C., Kanga, S., Dalmais, B., Lestini, R., et al. (2007). Genetic evidence for a link between glycolysis and DNA replication. *PLoS ONE* 2:e447. doi: 10.1371/journal.pone.0000447

Kamimura, A., and Kaneko, K. (2014). Compartmentalization and cell division through molecular discreteness and crowding in a catalytic reaction network. *Life* (*Basel*) 4, 586–597. doi: 10.3390/life4040586

Kauffman, S. (1996). *At Home in the Universe, the Search for the Laws of Complexity*. London: Penguin.

Kawai, F., Shoda, M., Harashima, R., Sadaie, Y., Hara, H., and Matsumoto, K. (2004). Cardiolipin domains in *Bacillus subtilis* marburg membranes. *J. Bacteriol.* 186, 1475–1483. doi: 10.1128/JB.186.5.1475-1483.2004

Kiviet, D. J., Nghe, P., Walker, N., Boulineau, S., Sunderlikova, V., and Tans, S. J. (2014). Stochasticity of metabolism and growth at the single-cell level. *Nature* 514, 376–379. doi: 10.1038/nature13582

Klauth, P., Pallerla, S. R., Vidaurre, D., Ralfs, C., Wendisch, V. F., and Schoberth, S. M. (2006). Determination of soluble and granular inorganic polyphosphate in *Corynebacterium glutamicum*. *Appl. Microbiol. Biotechnol.* 72, 1099–1106. doi: 10.1007/s00253-006-0562-8

Koppelman, C.-M., Den Blaauwen, T., Duursma, M. C., Heeren, R. M. A., and Nanninga, N. (2001). *Escherichia coli* minicell membranes are enriched in cardiolipin. *J. Bacteriol.* 183, 6144–6147. doi: 10.1128/JB.183.20.6144-6147.2001

Krakauer, D. (2014). *David Krakauer Selected as SFI's Next President*. Available at: http://www.santafe.edu/news/item/krakauer-selected-sfis-next-president/

Lang, F. (2011). Effect of cell hydration on metabolism. *Nestle Nutr. Inst. Workshop Ser.* 69, 115–126. doi: 10.1159/000329290

Lemke, J. L. (2000). Opening up closure. *Semiotics across scales. Ann. N. Y. Acad. Sci.* 901, 100–111. doi: 10.1111/j.1749-6632.2000.tb06269.x

Li, Y., Kusumaatmaja, H., Lipowsky, R., and Dimova, R. (2012). Wetting-induced budding of vesicles in contact with several aqueous phases. *J. Phys. Chem. B* 116, 1819–1823. doi: 10.1021/jp211850t

Li, Y., Lipowsky, R., and Dimova, R. (2011). Membrane nanotubes induced by aqueous phase separation and stabilized by spontaneous curvature. *Proc. Natl. Acad. Sci. U.S.A.* 108, 4731–4736. doi: 10.1073/pnas.1015892108

Llopis, P. M., Jackson, A. F., Sliusarenko, O., Surovtsev, I., Heinritz, J., Emonet, T., et al. (2010). Spatial organization of the flow of genetic information in bacteria. *Nature* 466, 77–81. doi: 10.1038/nature09152

Maisonneuve, E., and Gerdes, K. (2014). Molecular mechanisms underlying bacterial persisters. *Cell* 157, 539–548. doi: 10.1016/j.cell.2014.02.050

Makise, M., Mima, S., Katsu, T., Tsuchiya, T., and Mizushima, T. (2002). Acidic phospholipids inhibit the DNA-binding activity of DnaA protein, the initiator of chromosomal DNA replication in *Escherichia coli*. *Mol. Microbiol.* 46, 245–256. doi: 10.1046/j.1365-2958.2002.03161.x

Marshall, W. F., Young, K. D., Swaffer, M., Wood, E., Nurse, P., Kimura, A., et al. (2012). What determines cell size? *BMC Biol.* 10:101. doi: 10.1186/1741-7007-10-101

McGary, K., and Nudler, E. (2013). RNA polymerase and the ribosome: the close relationship. *Curr. Opin. Microbiol.* 16, 112–117. doi: 10.1016/j.mib.2013.01.010

Mercier, R., Kawai, Y., and Errington, J. (2013). Excess membrane synthesis drives a primitive mode of cell proliferation. *Cell* 152, 997–1007. doi: 10.1016/j.cell.2013.01.043

Meyer, P., Cecchi, G., and Stolovitzky, G. (2014). Spatial localization of the first and last enzymes effectively connects active metabolic pathways in bacteria. *BMC Syst. Biol.* 8:131. doi: 10.1186/s12918-014-0131-1

Michaelis, A. M., and Gitai, Z. (2010). Dynamic polar sequestration of excess MurG may regulate enzymatic function. *J. Bacteriol.* 192, 4597–4605. doi: 10.1128/JB.00676-10

Mileykovskaya, E., and Dowhan, W. (2000). Visualization of phospholipid domains in *Escherichia coli* by using the cardiolipin-specific fluorescent dye 10-N-nonyl acridine orange. *J. Bacteriol.* 182, 1172–1175. doi: 10.1128/JB.182.4.1172-1175.2000

Monahan, L. G., Hajduk, I. V., Blaber, S. P., Charles, I. G., and Harry, E. J. (2014). Coordinating bacterial cell division with nutrient availability: a role for glycolysis. *MBio* 5:e00935-14. doi: 10.1128/mBio.00935-14

Murray, H., and Koh, A. (2014). Multiple regulatory systems coordinate DNA replication with cell growth in *Bacillus subtilis*. *PLoS Genet.* 10:e1004731. doi: 10.1371/journal.pgen.1004731

Naseem, R., Wann, K. T., Holland, I. B., and Campbell, A. K. (2009). ATP regulates calcium efflux and growth in *E. coli*. *J. Mol. Biol.* 391, 42–56. doi: 10.1016/j.jmb.2009.05.064

Norris, V. (1995a). Hypotheses and the regulation of the bacterial cell cycle. *Mol. Microbiol.* 15, 785–787. doi: 10.1111/j.1365-2958.1995.tb02385.x

Norris, V. (1995b). Hypothesis: chromosome separation in *Escherichia coli* involves autocatalytic gene expression, transertion and membrane-domain formation. *Mol. Microbiol.* 16, 1051–1057. doi: 10.1111/j.1365-2958.1995.tb02330.x

Norris, V. (1995c). Hypothesis: transcriptional sensing and membrane-domain formation initiate chromosome replication in *Escherichia coli*. *Mol. Microbiol.* 15, 985–987. doi: 10.1111/j.1365-2958.1995.tb02367.x

Norris, V. (2011). Speculations on the initiation of chromosome replication in *Escherichia coli*: the dualism hypothesis. *Med. Hypotheses* 76, 706–716. doi: 10.1016/j.mehy.2011.02.002

Norris, V. (2015). What properties of life are universal? Substance-free, Scale-free Life. *Orig. Life Evol. Biosph.* doi: 10.1007/s11084-015-9432-7 [Epub ahead of print].

Norris, V., and Amar, P. (2012a). Chromosome replication in *Escherichia coli*: life on the scales. *Life* 2, 286–312. doi: 10.3390/life2040286

Norris, V., and Amar, P. (2012b). "Life on the scales: initiation of replication in *Escherichia coli*," in *Modelling Complex Biological Systems in the Context of Genomics*, eds P. Amar, F. Képès, and V. Norris (Strasbourg: EDF Sciences), 55–77.

Norris, V., Amar, P., Legent, G., Ripoll, C., Thellier, M., and Ovadi, J. (2013). Sensor potency of the moonlighting enzyme-decorated cytoskeleton: the cytoskeleton as a metabolic sensor. *BMC Biochem.* 14:3. doi: 10.1186/1471-2091-14-3

Norris, V., Blaauwen, T. D., Doi, R. H., Harshey, R. M., Janniere, L., Jimenez-Sanchez, A., et al. (2007a). Toward a hyperstructure taxonomy. *Annu. Rev. Microbiol.* 61, 309–329. doi: 10.1146/annurev.micro.61.081606.103348

Norris, V., Hunding, A., Kepes, F., Lancet, D., Minsky, A., Raine, D., et al. (2007b). Question 7: the first units of life were not simple cells. *Orig. Life Evol. Biosph.* 37, 429–432. doi: 10.1007/s11084-007-9088-z

Norris, V., Engel, M., and Demarty, M. (2012). Modelling biological systems with competitive coherence. *Adv. Artif. Neural Syst.* 2012, 1–20. doi: 10.1155/2012/703878

Norris, V., and Madsen, M. S. (1995). Autocatalytic gene expression occurs via transertion and membrane domain formation and underlies differentiation in bacteria: a model. *J. Mol. Biol.* 253, 739–748. doi: 10.1006/jmbi.1995.0587

Norris, V., Nana, G. G., and Audinot, J. N. (2014). New approaches to the problem of generating coherent, reproducible phenotypes. *Theory Biosci.* 133, 47–61. doi: 10.1007/s12064-013-0185-4

Norris, V., and Raine, D. J. (1998). A fission-fusion origin for life. *Orig. Life Evol. Biosph.* 28, 523–537. doi: 10.1023/A:1006568226145

Norris, V., Reusch, R. N., Igarashi, K., and Root-Bernstein, R. (2015). Molecular complementarity between simple, universal molecules and ions limited phenotype space in the precursors of cells. *Biol. Direct* 10:28. doi: 10.1186/s13062-014-0028-3

Norris, V., Woldringh, C., and Mileykovskaya, E. (2004). A hypothesis to explain division site selection in *Escherichia coli* by combining nucleoid occlusion and Min. *FEBS Lett.* 561, 3–10. doi: 10.1016/S0014-5793(04)00135-8

Osella, M., Nugent, E., and Lagomarsino, M. C. (2014). Concerted control of *Escherichia coli* cell division. *Proc. Natl. Acad. Sci. U.S. A.* 111, 3431–3435. doi: 10.1073/pnas.1313715111

Parry, B. R., Surovtsev, I. V., Cabeen, M. T., O'hern, C. S., Dufresne, E. R., and Jacobs-Wagner, C. (2014). The bacterial cytoplasm has glass-like properties and is fluidized by metabolic activity. *Cell* 156, 183–194. doi: 10.1016/j.cell.2013.11.028

Rao, N. N., Gomez-Garcia, M. R., and Kornberg, A. (2009). Inorganic polyphosphate: essential for growth and survival. *Annu. Rev. Biochem.* 78, 605–647. doi: 10.1146/annurev.biochem.77.083007.093039

Rocha, E. P., Fralick, J., Vediyappan, G., Danchin, A., and Norris, V. (2003). A strand-specific model for chromosome segregation in bacteria. *Mol. Microbiol.* 49, 895–903. doi: 10.1046/j.1365-2958.2003.03606.x

Saier, M. H. Jr. (2013). Microcompartments and protein machines in prokaryotes. *J. Mol. Microbiol. Biotechnol.* 23, 243–269. doi: 10.1159/000351625

Salthe, S. (1985). *Evolving Hierarchical Systems*. New York: Columbia University Press.

Schaechter, M., Maaloe, O., and Kjeldgaard, N. O. (1958). Dependency on medium and temperature of cell size and chemical composition during balanced grown of *Salmonella typhimurium*. *J. Gen. Microbiol.* 19, 592–606. doi: 10.1099/00221287-19-3-592

Sekimizu, K., and Kornberg, A. (1988). Cardiolipin activation of dnaA protein, the initiation protein of replication in *Escherichia coli*. *J. Biol. Chem.* 263, 7131–7135.

Serra, C. R., Earl, A. M., Barbosa, T. M., Kolter, R., and Henriques, A. O. (2014). Sporulation during growth in a gut isolate of *Bacillus subtilis*. *J. Bacteriol.* 196, 4184–4196. doi: 10.1128/JB.01993-14

Silva-Rocha, R., and de Lorenzo, V. (2010). Noise and robustness in prokaryotic regulatory networks. *Annu. Rev. Microbiol.* 64, 257–275. doi: 10.1146/annurev.micro.091208.073229

Smits, W. K., Kuipers, O. P., and Veening, J. W. (2006). Phenotypic variation in bacteria: the role of feedback regulation. *Nat. Rev. Microbiol.* 4, 259–271. doi: 10.1038/nrmicro1381

Son, S., Tzur, A., Weng, Y., Jorgensen, P., Kim, J., Kirschner, M. W., et al. (2012). Direct observation of mammalian cell growth and size regulation. *Nat. Methods* 9, 910–912. doi: 10.1038/nmeth.2133

Stickle, D. F., Vossen, K. M., Riley, D. A., and Fried, M. G. (1994). Free DNA concentration in *E. coli* estimated by an analysis of competition for DNA binding proteins. *J. Theor. Biol.* 168, 1–12. doi: 10.1006/jtbi.1994.1082

Strahl, H., Turlan, C., Khalid, S., Bond, P. J., Kebalo, J. M., Peyron, P., et al. (2015). Membrane recognition and dynamics of the RNA degradosome. *PLoS Genet.* 11:e1004961. doi: 10.1371/journal.pgen.1004961

Taheri-Araghi, S., Bradde, S., Sauls, J. T., Hill, N. S., Levin, P. A., Paulsson, J., et al. (2015). Cell-size control and homeostasis in bacteria. *Curr. Biol.* 25, 385–391. doi: 10.1016/j.cub.2014.12.009

Thomas, R. (1980). On the relation between the logical structure of systems and their ability to generate multiple steady states or sustained oscillations. *Ser. Synerg.* 9, 180–193.

Vega, N. M., Allison, K. R., Khalil, A. S., and Collins, J. J. (2012). Signaling-mediated bacterial persister formation. *Nat. Chem. Biol.* 8, 431–433. doi: 10.1038/nchembio.915

Vohradsky, J., and Ramsden, J. J. (2001). Genome resource utilization during prokaryotic development. *FASEB J.* 15, 2054–2056. doi: 10.1096/fj.00-0889fje

Wang, P., Robert, L., Pelletier, J., Dang, W. L., Taddei, F., Wright, A., et al. (2010). Robust growth of *Escherichia coli*. *Curr. Biol.* 20, 1099–1103. doi: 10.1016/j.cub.2010.04.045

Watts, D. J., and Strogatz, S. H. (1999). Collective dynamics of 'small-world' networks. *Nature* 393, 440–442. doi: 10.1038/30918

Weart, R. B., Lee, A. H., Chien, A. C., Haeusser, D. P., Hill, N. S., and Levin, P. A. (2007). A metabolic sensor governing cell size in bacteria. *Cell* 130, 335–347. doi: 10.1016/j.cell.2007.05.043

White, M. A., Eykelenboom, J. K., Lopez-Vernaza, M. A., Wilson, E., and Leach, D. R. (2008). Non-random segregation of sister chromosomes in *Escherichia coli*. *Nature* 455, 1248–1250. doi: 10.1038/nature07282

Xia, W., and Dowhan, W. (1995). In vivo evidence of the involvement of anionic phospholipids in initiation of DNA replication in *Escherichia coli*. *Proc. Natl. Acad. Sci. U.S.A.* 92, 783–787. doi: 10.1073/pnas.92.3.783

Yao, Z., Davis, R. M., Kishony, R., Kahne, D., and Ruiz, N. (2012). Regulation of cell size in response to nutrient availability by fatty acid biosynthesis in *Escherichia coli*. *Proc. Natl. Acad. Sci. U.S.A.* 109, E2561–E2568. doi: 10.1073/pnas.1209742109

Zaritsky, A. (1975). Rate stimulation of deoxyribonucleic acid synthesis after inhibition. *J. Bacteriol.* 122, 841–846.

Conflict of Interest Statement: The author declares that the research was conducted in the absence of any commercial or financial relationships that could be construed as a potential conflict of interest.

Copyright © 2015 Norris. This is an open-access article distributed under the terms of the Creative Commons Attribution License (CC BY). The use, distribution or reproduction in other forums is permitted, provided the original author(s) or licensor are credited and that the original publication in this journal is cited, in accordance with accepted academic practice. No use, distribution or reproduction is permitted which does not comply with these terms.

frontiers in Microbiology

REVIEW
published: 21 April 2015
doi: 10.3389/fmicb.2015.00309

How much territory can a single *E. coli* cell control?

Ziad W. El-Hajj and Elaine B. Newman*

Department of Biology, Concordia University, Montreal, QC, Canada

Bacteria have been traditionally classified in terms of size and shape and are best known for their very small size. *Escherichia coli* cells in particular are small rods, each 1–2 μ. However, the size varies with the medium, and faster growing cells are larger because they must have more ribosomes to make more protoplasm per unit time, and ribosomes take up space. Indeed, Maaløe's experiments on how *E. coli* establishes its size began with shifts between rich and poor media. Recently much larger bacteria have been described, including *Epulopiscium fishelsoni* at 700 μm and *Thiomargarita namibiensis* at 750 μm. These are not only much longer than *E. coli* cells but also much wider, necessitating considerable intracellular organization. *Epulopiscium* cells for instance, at 80 μm wide, enclose a large enough volume of cytoplasm to present it with major transport problems. This review surveys *E. coli* cells much longer than those which grow in nature and in usual lab cultures. These include cells mutated in a single gene (*metK*) which are 2–4× longer than their non-mutated parent. This *metK* mutant stops dividing when slowly starved of *S*-adenosylmethionine but continues to elongate to 50 μm and more. FtsZ mutants have been routinely isolated as long cells which form during growth at 42°C. The SOS response is a well-characterized regulatory network that is activated in response to DNA damage and also results in cell elongation. Our champion elongated *E. coli* is a *metK* strain with a further, as yet unidentified mutation, which reaches 750 μm with no internal divisions and no increase in width.

Keywords: *E. coli*, cell length, cell division, giant bacteria, metabolism

OPEN ACCESS

Edited by:
Arieh Zaritsky,
Ben-Gurion University of the Negev, Israel

Reviewed by:
Moselio Schaechter,
San Diego State University, USA
William Margolin,
University of Texas Health Science Center at Houston, USA
James R. Walker,
University of Texas at Austin, USA

****Correspondence:***
Ziad W. El-Hajj,
Department of Biology, Concordia University, 1455 De Maisonneuve Boulevard, Montreal, QC H3G 1M8, Canada
ziad.elhajj@concordia.ca

Specialty section:
This article was submitted to Microbial Physiology and Metabolism, a section of the journal Frontiers in Microbiology

Received: *24 February 2015*
Accepted: *29 March 2015*
Published: *21 April 2015*

Citation:
El-Hajj ZW and Newman EB (2015) How much territory can a single E. coli cell control? Front. Microbiol. 6:309. doi: 10.3389/fmicb.2015.00309

Introduction

Escherichia coli has astonished investigators with its remarkable metabolic efficiency packed into such a small size. In its 0.5–2 μ length, it packs its genetic material, its metabolic machinery, and an impressive variety of adaptive strategies. It can make a new cell as fast as every 30 min with scarcely an error. The brilliant analysis of *E. coli* function by Jacob, Monod, and Lwoff excited the entire field and led to the amazing detail with which *E. coli* is now understood (Cohn, 2014).

In order to produce a new cell, *E. coli* must approximately double its cell contents and distribute them between 2 daughter cells. It must exactly duplicate and segregate its DNA, and it must double its length and divide itself at midcell. It becomes longer using a cell wall synthesizing system based on penicillin binding protein 2 (PBP2) to elongate. This elongation is the result of the combined activity of peptidoglycan synthesis and hydrolysis enzymes, which constantly remodel the cell wall, but the net result is an increase in cell length (Johnson et al., 2013). The direction of cell wall synthesis changes when the length has doubled, uses a different enzyme system based on PBP3, and coincides with synthesis of a septum at midcell. This system, known as binary fission, is thus an alternation between elongation via a PBP2 complex and division via a PBP3 complex (Lutkenhaus et al., 2012).

Initiation of the septum at midcell involves spatial inhibitors that prevent septum formation elsewhere, such as SlmA involved in nucleoid occlusion (Du and Lutkenhaus, 2014), and the well-known MinCD complex (Ghosal et al., 2014). Although the mechanisms by which they inhibit division are relatively well understood, how *E. coli* finds its mid-point in the first place has been a long standing problem. This was settled very recently by the lab of Suckjoon Jun, who showed that it divides when it has added a constant volume, the rate depending on how fast its environment allows it to do so (Taheri-Araghi et al., 2015). The cell alters its volume and length according to its environment. However in whatever conditions it can grow, it makes viable cells and wastes nothing, i.e., except for the end products of metabolism, it does not overproduce and excrete metabolic products.

Various Ways to Grow Very Long *E. coli*

It would make sense that if one were to inhibit the activation of the PBP3 divisome in such a way that everything else functions, the cell would not divide, nor would it stop growing. It would continue its various metabolic functions and become very long. This is indeed what seems to occur in our strain MNR2 (see Extremely Elongated *E. coli* Cells). In this section we will discuss the problems that such an elongating cell might face, and assess the role of two amino acids (methionine and L-serine) and of alternative cell envelope components in promoting elongation.

Potential Problems in Elongation

The elongating cell has a number of problems, and some might be expected to increase in severity the longer it gets. Among these, it has to add peptidoglycan to the wall, it has to synthesize and distribute DNA, it has to transcribe from the new and old DNA, make new ribosomes and distribute those, and use them to make new proteins and enzymes, and form new enzyme complexes and distribute them.

As the cell lengthens, its mass clearly must increase and each addition it makes to its protoplasm and its peptidoglycan must be pushing against more mass and more wall. If this caused it problems, one might expect it to grow more slowly than a cell which divides every time it doubles, and perhaps more important, to slow down as it becomes longer. This effect might be lessened by the saving in time and energy occasioned by not making the vertical cell wall.

However, a cell elongates by adding many short lengths of new peptidoglycan at many points along its surface, thus providing new space for the macromolecules it is making, and for the duplicating DNA to move into. Because the additions are many and short, rather than few and long, elongation may require less forces. If the sites are numerous enough, they may not even have to have a fixed pattern to maintain a linear form overall. Otherwise there must be some pattern to where PBP2 acts. In any case this forms an unobstructed tube within which cytoplasmic components can move.

Many physical chemists, and others, suggest that *E. coli* cytoplasm is extremely crowded, and this is often supposed to interfere with diffusion and distribution of cell contents. By one estimate, its cytoplasm contains 200 mg/ml protein, 11–18 mg/ml DNA and 75–120 mg/ml RNA occupying 20–40% of the cell volume and affecting transit though much more "excluded volume" (Hasnain et al., 2014). They suggest this implies that it is not easy for even small molecules to make their way through the cytoplasm, and even harder for large molecules.

The effects of crowding are considered in interesting detail in a 1999 review (Hoppert and Mayer, 1999). These authors suggest that bacterial cells have functional compartments but they are not bounded by membranes. Instead they are formed from the nucleoid, from multienzyme complexes, from storage granules, and cytoskeletal elements all of which affect the properties of water in the cell (Hoppert and Mayer, 1999).

These papers, and many others, make it clear that the cell is crowded with respect to macromolecules. However, the rapidity of elongation suggests that this apparent crowding does not actually slow synthesis much or inhibit function of newly synthesized and distributed material, no doubt because of the continuous elongation of the tube. This is perhaps another example of *E. coli* being able to solve its problems better than we can understand them.

Indeed one of the problems of "crowded cytoplasm" considerations is that it does not allow for the nature of growing cells and turbulence within expanding cytoplasm. While the wall is being extended by hundreds of insertions, the DNA is being synthesized and segregated, and causing turbulence in the cytoplasm around it, which must aid the motion of other molecules in the cytoplasm. Small molecules can probably move with very little obstruction.

Involvement of Methionine

We have found several cases in which production of long cells in *E. coli* is associated with alterations in methionine and *S*-adenosylmethionine (SAM) metabolism. The first long *E. coli* isolated in the Newman lab was derived from a supposed *metK* mutant described in R. C. Greene's lab (Greene et al., 1973). This carried a point mutation in *metK* together with an *lrp* mutation which decreased Lrp expression and increased *metK* expression just enough to permit growth (Newman et al., 1998). We showed that a strain carrying only the *metK* mutation required leucine for growth, as an inducer of the *lrp* gene. When grown overnight with limiting leucine, e.g., 5 μg/ml, the cells did not divide but elongated up to 100-fold with imperfectly segregated nuclei and no visible constriction (Newman et al., 1998). Whereas other cell division mutants (such as strain MNR2 or *ftsZ84* mutants) made no septum at all, the SAM-starved cells incorporated three proteins into the septum, FtsZ, ZipA, and FtsA, but continued to elongate with these partial septa (Wang et al., 2005).

These cultures probably did not represent the full potential for elongation of the *metK* strain. The cells could elongate only once they reduced the leucine sufficiently to inhibit division, but then quickly ran out of leucine for protein synthesis. The 100-fold elongation is thus quite prodigious. We conclude that a supply of SAM is needed for complete activation of septum formation, and suggest that this is due to the need for one or more methyltransferase reactions in activating division.

We could not make a strain carrying a deletion of *metK* because *E. coli* cannot transport SAM, but we did construct a deletion

compensated by a plasmid-carried inducible *metK* (Wei and Newman, 2002). However, the group of D. O. Wood created a SAM-transporting *E. coli* strain by isolating a SAM transporter from *Rickettsia prowazekii* (Tucker et al., 2003) and cloning it into an *E. coli* plasmid, allowing a mutant deficient in *metK* to grow in rich medium with an exogenous SAM supply (Driskell et al., 2005). They kindly allowed us to use this transport gene for all our work on SAM utilization including strain MNR2.

Using the *metK* deletion strain of Wei Yuhong, and the Wood plasmid, with some modifications, we were able to determine the growth requirements of an *E. coli metK* mutant (El-Hajj et al., 2013). The mutant in fact had two requirements, SAM because of the deletion, and methionine because in the presence of SAM, methionine synthesis is inhibited.

As we discovered with considerable difficulty and chagrin, using externally provided SAM is a matter of real complexity. We have described these problems in DETAIL (El-Hajj et al., 2013) and anyone wishing to use commercial SAM should read that description. We used commercial SAM, purified of course, for our experiments (before understanding all these complexities) but would make our own enzymatically for any further experiments.

After a year on the lab shelf, commercial SAM is a 1:1 mixture of its enantiomers *(R)*-SAM and *(S)*-SAM, even if it was provided as pure *(S)*-SAM. Enzymatic SAM is purely *(S)*-SAM when first made but isomerizes relatively quickly. Only *(S)*-SAM is a methyl donor for most *E. coli* methyltransferases. However, *(R)*-SAM provided exogenously is a methyl donor for one reaction, the methylation of homocysteine to methionine by the enzyme MmuM, a third methionine synthase.

We found then that the SAM deletion strain requires both SAM and methionine, but the amount of methionine it requires depends on the proportion of SAM which is in the form of *(R)*-SAM and that proportion varies greatly. However with more *(R)*-SAM than it needs, the cell still needs methionine though very little—about 100 ng/ml rather than 20–40 μg usually provided to a methionine-requiring mutant such as a *metB*. We do not understand what the cell needs the small amount of methionine for, when it is getting so much methionine from *(R)*-SAM and is not actually blocked in methionine biosynthesis.

We conclude that methionine metabolism is less well understood than generally thought, and that *(R)*-SAM can serve *E. coli* as a methyl donor for conversion of homocysteine to methionine via the enzyme MmuM. We suggest further that the switch from PBP2 elongation to PBP3 division requires the availability of methyl donors.

Involvement of L-Serine

Among the oddities of L-serine metabolism is that *E. coli* codes for three different very specific high K_m L-serine deaminases (L-SDs) but cannot use L-serine as carbon source. These enzymes, SdaA, SdaB, and TdcG (Su and Newman, 1991; Shao and Newman, 1993; Burman et al., 2004), use a [4Fe-4S] cluster to catalyze the deamination of serine to pyruvate (Cicchillo et al., 2004). They are so highly specific for L-serine that even TdcG, which is coded by a gene in an anaerobic threonine utilization operon, does not deaminate threonine but is a dedicated L-SD (Burman et al., 2004). However, they only work on high concentrations of L-serine, preventing interference with peptidoglycan synthesis (Zhang et al., 2010).

Deleting all three genes from *E. coli* of course greatly increased the availability of L-serine and it also severely impeded the ability of the mutant to grow in minimal medium with amino acids, where the deletion mutant made very large, abnormally shaped cells (Zhang and Newman, 2008). In Luria broth, the triple mutant made long filaments—not as long as strain MNR2 but nonetheless an average of 10× normal length and up to 80×. Most surprising, even though SAM normally cannot enter the *E. coli* cell, it prevents filament formation in the triple mutant equipped with the Rickettsial transporter (Zhang and Newman, 2008).

We suggest that high serine interferes with the serine/glycine/C1 balance of the cell and decreases the availability of C1 units and SAM for the cell division specific methylation resulting in production of long cells. On the other hand, overproduction of L-SD also produced long cells. The mutant with the highest serine deaminase activity recorded, the *ssd* mutant now shown to be a subclass of *cpxA* mutants (Rainwater and Silverman, 1990; Monette, 2006), grows in glucose minimal medium expressing high L-SD, with 50% of its cells as small rods and the other 50% as a few enormously long rods. This suggests that every now and then the cell cannot divide and does not recover from this but instead goes on elongating.

Neither of these cases is well understood. However, we suggest that when the balance of serine, glycine and C1 is not maintained, some methylation associated with cell division does not occur.

Interference with Cell Division by Provision of Alternative Cell Wall Components

If the cell is provided with the means to make an entirely different cell wall, e.g., not peptidoglycan, it may go ahead and do it, and then find that it has problems breaking the alternative wall down into smaller cells. Like so many of us, Lederer et al. (2011) used *E. coli* to clone and express proteins of interest to them in *E. coli*. In this case, they cloned S-layer proteins from *Lysinibacillus sphaericus* JG-A12 into *E. coli* BL21(DE3). These are mostly protein and glycoprotein, forming the S-layer envelope of various organisms. *E. coli* can express them, grow well and produce viable cultures. However, its morphology is entirely changed (Lederer et al., 2011).

In early exponential phase these cells form filaments 100 μm long or more. Later these appear as transparent filaments with small *E. coli* rods lined up inside them. For the moment, there is not enough information to analyze these in detail. Nonetheless it is obvious that adding alternative cell wall components to the cell's possibilities has interfered with peptidoglycan synthesis and allowed it to construct an alternative cell envelope of considerable length.

Extremely Elongated *E. coli* Cells

Isolation of a Mutant that Does Not Activate PBP3

Escherichia coli divides every 0.5 h or so in Luria broth with or without added sodium chloride (LB, LBNoSalt), and about every 58 min in minimal medium with glucose, all at 37°C. In our attempts to understand the requirement for methionine in the

metK deletion mutant (see Involvement of Methionine), we have recently isolated a mutant which divides every 80 min in minimal medium but divides rarely in LB and almost not at all in LBNS. That is, it can elongate via PBP2 and divide with PBP3 when growing in minimal medium, but in LB or LBNS it can only use PBP2 and thus continues to elongate indefinitely. The longest cell we have seen so far was is 750 μ long (El-Hajj and Newman, 2015, Figure 1).

When the mutant, known as MNR2, is grown in minimal medium it makes the rods one expects, but they are considerably longer than the parent cell. When the population is subcultured into LBNS, every cell continues to elongate and cannot divide, so that they gradually grow longer over the next 15–24 h. This elongation occurs at many points along the cell (Woldringh et al., 1987). The exact pattern of elongation points is not known (den Blaauwen, 2013). However, even our longest cells show no distortion, so that points of elongation must be chosen according to some pattern. A biophysical simulation by Sean Sun and colleagues suggests that MreB stabilizes the peptidoglycan tube, and provides a framework for the localization of the PBP2 complex and its function (Jiang et al., 2011).

We attributed the elongation in MNR2 to the much lower osmotic pressure of LB and LBNS (El-Hajj and Newman, 2015). This was based on the fact that adding the components of LB to minimal medium produced a medium which had a high osmolality (349 vs. 342 mOSm/kg) and did not prevent division. Also, cells were much longer in LBNS than in LB (93 vs. 256 mOsm/kg). This may indicate that the elongation rate is faster at low osmolality. However, it is also possible that the elongation rate does not change but the probability of transient PBP3 activation is higher at the osmolality of LB.

The size of wild-type *E. coli* is larger the faster it grows (Chien et al., 2012). The larger size is required in order for the cell to contain all the machinery it needs to make cell components, among others, ribosomes to make protein at an increased rate. Thus when *E. coli* is taken from minimal to rich medium, it responds by growing wider and longer (Grover and Woldringh, 2001). Strain MNR2 of course grows longer, but the mechanism for this may be different since its width did not change in any of the thousands of cells we examined.

Cells subcultured in LBNS all elongate for the first few hours, with some extremely elongated (eel) cells reaching lengths up to 200 μm. These cells could be made to grow even longer by plating them on LBNS agar slide cultures, which provides them with fresh nutrients and is how we isolated the longest cell we have seen, 750 μm long. However, when plating these cells on the agar slides and examining them by time-lapse photography, a few produced a new rod at the end of the long cell (El-Hajj and Newman, 2015). These rods are about the size of the usual MNR2 rods in minimal medium, but they immediately begin to elongate again. This predilection for division near the ends is also seen in filaments formed in other ways (Dajkovic et al., 2010, movie S1 early frames). We conclude that PBP3 is normally inactive in the mutants in Luria media, and if it happens to function, it is quickly re-inactivated.

When we instead plated the eel cells on minimal medium slide cultures, we expected that PBP3 would immediately reactivate and they would start dividing promptly. Much to our surprise, the long cells continued elongating at multiple points along the cells, forming loops that pushed outward from the long axis of the cell (El-Hajj and Newman, 2015). This suggests that there are pre-requisites for PBP3 activation even when cells are over the length required to divide. How PBP3 function is activated is currently unknown. However, two separate studies have suggested that peptidoglycan synthesis is altered at the division point even before PBP3 activity begins. One group suggest that there may be PBP3 independent synthesis at midcell of a narrow band of new peptidoglycan, a process involving only two very early septation proteins, FtsZ and ZipA (Potluri et al., 2012). A second group shows that PBP2 and PBP3 interact directly for a short time, and suggests an association between them to synthesize a new area of peptidoglycan prior to the actual septation, so that both enzymes work concurrently for a short time as peptidoglycan synthesis shifts from PBP2 to PBP3 (van der Ploeg et al., 2013). The loops we have seen could be this new peptidoglycan being synthesized. In a small rod-shaped cell, this synthesis would simply push the poles apart and the cell would elongate in a straight line. However, the eel cells are much longer, and the adherence of the cell to the agar on the slide culture would require enough force to push away the entire length of the cell on either side, which could be up to 100 μm of cellular content. Peptidoglycan synthesis does not produce sufficient force to do this, so instead the force pushes in a direction perpendicular to the long axis of the cell and the area where it occurs loops outward.

The cell wall of *E. coli* is usually considered to protect the cell against osmotic pressure by virtue of its rigidity, and this applies to the usual small rods. The peptidoglycan at the poles (which is always the result of a former PBP3-driven lateral peptidoglycan synthesis during division) is thought to be inert. That is, old peptidoglycan is not degraded and replaced by newly-synthesized peptidoglycan (Koch and Woldringh, 1994). This is in contrast to the longitudinal peptidoglycan synthesized by PBP2, which undergoes constant recycling as older peptidoglycan is degraded by and newer peptidoglycan is incorporated in its place (reviewed in Johnson et al., 2013). In a small *E. coli cell* 1 or 2 μ long, the rigidity of the inert polar peptidoglycan maintains the characteristic unbending rod shape. However in the much longer MNR2 eel cells, the rigid poles are frequently separated by over 100 μm and as a result the cells are remarkably flexible. In fact we found cells can be intertwined even by the forces of pipetting a drop of a diluted culture onto a slide! This can be seen in **Figure 1A**, where the free ends of cells are aligned by the flow caused by the falling cover slip. The flexibility can also be seen in a single cell twisting around itself into corkscrew shapes (**Figure 1B**). Long chains of small *Bacillus subtilis* cells form similar corkscrew macrofibers of astounding flexibility, and their elasticity generates enough torque and force to allow self-propulsion when their natural unwinding is hindered (Mendelson et al., 2000). Neil Mendelson recorded a remarkable video of these bacterial macrofibers on his website (www.neilhmendelson.com), which unfortunately seems unavailable at the time of writing.

Whether the high flexibility of the MNR2 eel cells makes it more difficult to produce a crosswall away from the poles, or whether the inability of the cells to form the crosswall in the first place is

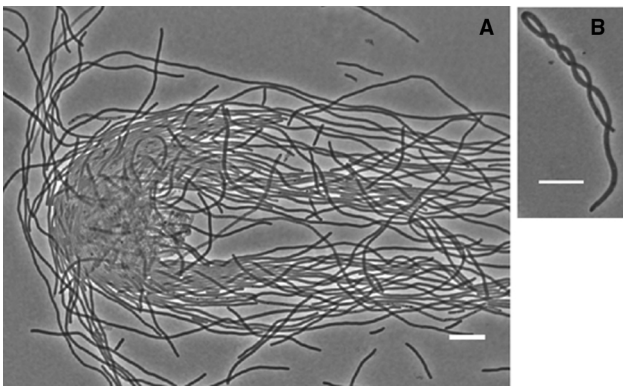

FIGURE 1 | Flexibility of the MNR2 eel cells. (A) Intertwined eel cells of strain MNR2 incubated in liquid LBNS for 16 h. **(B)** Example of a corkscrew-shaped filament from a 24 h LBNS slide culture. Scale bars are 10 μm.

what lends them this remarkable flexibility, seems to be a chicken-or-egg question. What is clear is that the ends of the cell somehow alleviate this problem, as seen by the transient activation of PBP3 on LBNS slide cultures discussed earlier. At the pole, the cell can take advantage of the rigidity conferred by the end wall, and using that, it requires constriction at only one point one normal cell length away to form a rod of the usual *E. coli* size. This would also allow for the MinCD complex to shuttle within its usual length (Lutkenhaus et al., 2012) and help in accurate placement of the division site, as well as subsequent formation of a functional divisome.

Characteristics of Long Cells

We did not attempt to find conditions which allowed the cells to grow particularly long. The 750 μ cell we photographed (El-Hajj and Newman, 2015) extended over three microscope fields, and was simply the longest we happened to find with our usual growth media. There is no reason to suppose that this is the longest possible, though physical problems may eventually make lengthening more difficult.

It is odd that the diameter of the cell does not increase on subculture into LB or LBNS. One of the earliest findings in studies of *E. coli* adaptation is that wild type *E. coli* transferred from minimal to rich medium, gets both longer and wider (Schaechter et al., 1958). Though there are many circumstances in which *E. coli* can get wider, reviewed in a fascinating review of bacterial shape (Young, 2010), this widening is not seen with this mutant when grown on enriched medium. Strains derived from the same parent do become very much wider when overexposed to L-serine (Zhang et al., 2010) so this does not seem to be simply a strain difference.

The long cells are remarkably flexible, as seen in the corkscrew pictured here (**Figure 1B**). They nonetheless occasionally lyse, as is particularly visible on solid medium. Lysis could be due to adherence to or to other cells pulling them in a different direction from the one in which they elongate. When they lyse, the entire contents pour out leaving an empty tube. In one of our photographs (El-Hajj and Newman, 2015, Figure 2B), the point of lysis fell at a point where the cell formed a closed loop on an agar surface, and one could see the cell contents within that loop. Clearly we could adapt this to collect the entire content of a single cell, perhaps by micromanipulation with a microsyringe.

We assume that as elongation goes on, new DNA is made and transcribed throughout the length of the cell (El-Hajj and Newman, 2015). As an example of "games" which become possible with cells of this size, it might be interesting to add an inducer like X-gal at different times and see if it can induce at all parts of the cell, or to streak inducer on the plate and let cells grow toward it. Similarly we plated cells on slides coated with turmeric powder and found that the cells appeared much thicker due to the negative staining, which would allow us to search for even longer cells at lower magnifications.

What is clear, and surprising, is how well these cells grow and metabolize even after many hours. They do not show signs of metabolic problems and the majority of the long cells can give rise to a colony (El-Hajj and Newman, 2015). This does not inform us as to how many of the DNA molecules in a long cell can give rise to colonies. It does tell us that the long cells remain alive and their metabolism lets them continue to elongate—i.e., their metabolic capacity is remarkable. As long as they are in LB or LBNS, we do not see any localized defect other than occasional lysis. As seen below, this is no longer the case when we transfer the cells to glucose minimal medium where they might be able to subdivide and multiply thereafter as rods.

The Return of Elongated Cells to Minimal Medium

The elongated cells can reach the size of the largest bacteria known (see Giant Bacteria). As long as they are kept in enriched medium, the entire cell appears intact and functional. When they occasionally form rod-shaped cells at the ends of the long cells, these rods maintain the same characteristics, i.e., they elongate once again if left in rich medium. The remaining long cell also continues to elongate. There is no indication that there are non-functional areas in these long cells, with the possible exception that DNA does not segregate perfectly in all cells. However, even cells with smears of DNA elongate.

The situation is very different when the elongated cells are plated on minimal medium, where most of the cells give rise to a colony. However, this new colony is not derived from all parts of the elongated cells. Some parts do not grow at all, and some grow and die off, but each long cell has at least one area in which cells grow into a microcolony of rod shaped cells and ultimately into a colony with the same characteristics as MNR2.

We did not follow these in the detail they deserve but intend to do so. When plated on minimal plates, the cells did not immediately produce rods. As seen in **Figure 2**, the eel cell began to elongate, but by 2.5 h incubation, showed the problems we expected but did not see in rich medium. The new lengths of cells could not push the old cell mass to the sides but instead grew outward making irregularly spaced loops. These loops were randomly placed but the same process was seen in all dividing cells.

We have not found other mentions of these loops in *E. coli*. This is the first evidence that the long cells are not entirely homogeneous, and this becomes obvious by 4.5 h when the cells

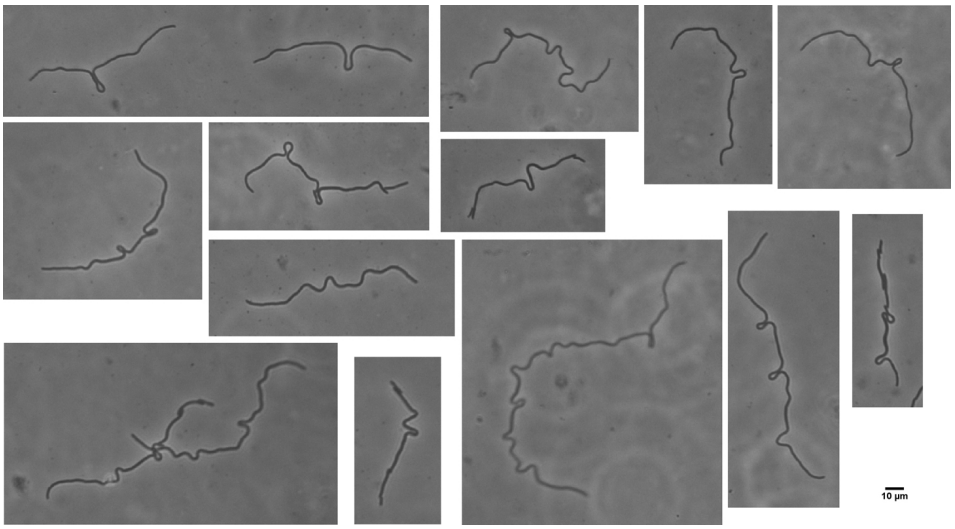

FIGURE 2 | Loop formation in the elongated cells after shift down. MNR2 eel cells from a 16h LBNS culture were plated on minimal medium slide cultures and photographed after 2.5 h. Scale bar indicates 10 μm for the entire figure. Loops form at some distance from the end and from each other but otherwise show no obvious pattern.

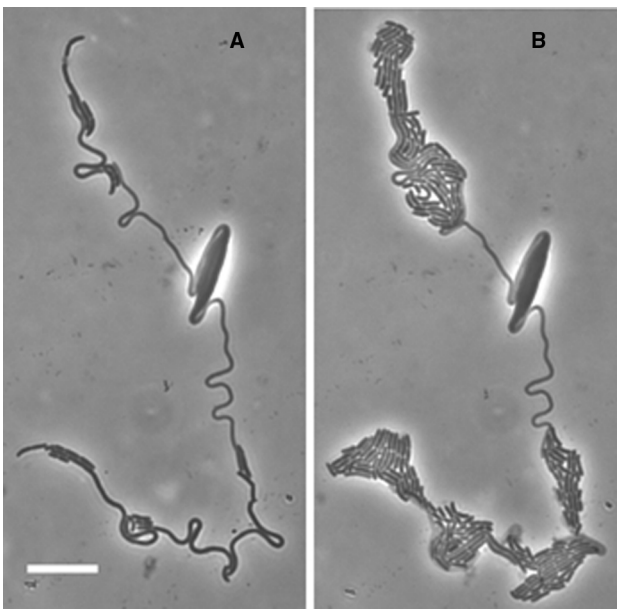

FIGURE 3 | Heterogeneity in the MNR2 elongated cells. A 16 h culture of *E. coli* MNR2 in LBNS plated on a glucose minimal medium slide culture at 37°C was photographed after 6.5 h **(A)**, then left at room temperature for 18 h and the same field was re-photographed **(B)**.

produce a few rods, and break up into segments of various lengths, and some even lyse. An example of this extreme heterogeneity is seen in **Figure 3**. However, the design of this experiment actually promotes heterogeneity. This experiment is indeed a return to conditions which allow division, but it is also a major metabolic shift down. While the cells can suddenly begin to activate PBP3 and divide, they are also suddenly deprived of nutrients and have to begin making all the compounds they need. They can do this at a few points, but not at many. This experiment is worth repeating with a shift from LBNS to LBmin, i.e., restoring high osmolality in the presence of all the nutrients in LB.

Filament Formation During Cell Division Arrest

Although the MNR2 eel cells we saw at low osmolality are the longest *E. coli* observed, conditional elongation in *E. coli* had been observed during the 1960s and 1970s, when it was characterized in mutants that were impaired in cell division. These mutants would continue elongating for a short time after division was blocked, but unlike the eel cells they would ultimately lyse and die.

Cell division requires the assembly of a complex division machinery. The process is initiated when FtsZ, the most well studied of the division proteins, polymerizes into a discrete structure, called the FtsZ ring or Z-ring, but likely much more complex than currently thought (Fu et al., 2010). Assembly of the Z-ring is essential for the recruitment of subsequent members of the division complex, including PBP3 (Errington et al., 2003). In conditions under which cells cannot form the Z-ring, PBP3 is not activated and they cannot form a crosswall, but they do grow into relatively short-lived elongated cells called filaments.

Many factors can disrupt the elongation-division cycle of *E. coli* and lead to formation of filaments. These include alterations in the stability or availability of the essential division proteins, especially FtsZ. Mutations in *ftsZ* or depletion of the protein due to DNA damage and subsequent triggering of the SOS response are both well-studied conditions that cause filamentation (Jones and Holland, 1984; Addinall et al., 1996). These differ from MNR2 eel cells, which are also blocked in cell division and elongate under adverse environmental conditions (in this case, low osmolality), but are viable and become much longer.

E. coli Filaments in *fts* Mutants

The *fts* (filamentation temperature sensitive) series of mutants were isolated by virtue of their inability to divide when grown on LBNS at 42°C and have allowed the elucidation of many of the steps in Z-ring formation (Lutkenhaus et al., 2012). Such temperature-sensitive (Ts) mutations have been isolated in many of the essential cell division genes, which gave rise to the nomenclature of *fts* for these genes. Most of these mutants share common traits when shifted to 42°C, in that they begin cell division, and reach different stages depending on the mutation and the gene affected, but none of them can complete the process (Taschner et al., 1988). Because FtsZ is the earliest division protein, *ftsZ* mutants abort division very early on, which typically results in so-called "smooth" filaments. Disrupting the later division proteins, such as in *ftsA*, *ftsQ*, or *ftsE* mutants, allows the cells to begin septation. Most such mutants can polymerize FtsZ but cannot assemble the full complex required for successful division, and these cells assemble many partial, usually regularly-spaced Z-rings along the length of the filaments (Addinall et al., 1996). This results in "rough" filaments that show clear, marked constrictions where these incomplete rings form (Taschner et al., 1988, Figure 3). Regardless of what stage is inhibited, the filaments remain viable for only a few hours. The *ftsZ84* mutant, one of the earliest and best studied, lyses and sees a drop in viability 3 h after the temperature shift (Ricard and Hirota, 1973).

Much work was done with *ftsZ84* over the decades, taking advantage of the conditional mutation to study and understand FtsZ function and the essential role the protein plays in cell division (Lutkenhaus et al., 2012). Although most of these studies focused on FtsZ itself and its molecular role in cell division, they did in the process reveal a lot of information about how *E. coli* functions (or does not) when it reaches much longer lengths than usual. Most of the *ftsZ*(Ts) mutants can function at permissive temperatures such as 30°C. Under these conditions, the *ftsZ84* mutant synthesizes DNA and segregates nucleoids regularly (Ma and Margolin, 1999). The cells grow as rods and divide normally, although a significant number of cells (about one-third) lack Z-rings entirely (Addinall and Lutkenhaus, 1996). Upon shifting to 42°C, regular nucleoid segregation continues, but now occurs over the entire length of the filament (Bi and Lutkenhaus, 1992; Ma and Margolin, 1999). However, cell division is blocked with remarkable speed. FtsZ rings in an *ftsZ84* mutant seem to disappear as early as 2 min after the temperature shift, even though some of these cells retain a sharply-demarcated septum when viewed by electron microscopy (Addinall et al., 1997, Figure 2). After 10 min, these are replaced by deeper, blunted constrictions, which never complete the process. This is consistent with division sites beginning to form, but due to the mutated FtsZ the cells cannot complete the process at 42°C and septation aborts prematurely, leaving these blunted constrictions to mark the site of their failure.

As *ftsZ84* filaments are left at 42°C, they continue elongating and show no signs of rings (Addinall et al., 1996). If left for several hours they eventually lyse and die (Ricard and Hirota, 1973), but this fate can be avoided by shifting the filaments back to a permissive temperature (such as 30°C) before enough damage has been done. When cells of an *ftsZ84* mutant are upshifted to 42°C for 2 min, then downshifted back to 30°C, they start forming new rings at unconstricted, future division sites, but they seem unable to reform a ring at a previously-constricted site that was aborted during the upshift (Addinall et al., 1997). The cell "remembers" that it chose a division site and started to constrict, but it either cannot remember that the constriction aborted prematurely, or it cannot promptly resume or restart the constriction, presumably because the topology of an aborted site is different and a partial septum is already there and prevents reassembly of the Z-ring complex. Unfortunately no study followed these filaments for a longer time after the downshift, and whether the cells are eventually capable of fully recovering and re-targeting a previous division site if given enough time remains unknown. The MNR2 eel cells, with their increased viability and lengths, could provide a useful tool to settle this question.

In vitro studies of the mutated FtsZ84 protein have revealed defects in its biochemical function even at 30°C, but these do not seem to affect its ability to support cell division under permissive conditions *in vivo*. FtsZ is a GTPase and a tubulin homolog (De Boer et al., 1992; RayChaudhuri and Park, 1992). Like most members of this superfamily, it polymerizes by binding GTP and immediately hydrolyzing it, then depolymerizes when GDP is released (Scheffers and Driessen, 2002). The polymer structure is very dynamic and the turnover of FtsZ is high as individual molecules are cycled in and out of the polymer (Sun and Margolin, 1998). FtsZ84 has greatly reduced GTPase activity as seen by biochemical assays, even at 30°C, yet complete Z-rings are readily seen in *ftsZ84* mutants and the cells can divide (Mukherjee et al., 2001). Likewise, the Z-ring of an *ftsZ84* mutant has a much slower turnover rate than wild-type, but does not affect its doubling time at 30°C (Stricker et al., 2002). The biochemical defects of the mutant protein, which are measurable under all conditions, only manifest in the cell itself under specific environmental conditions. Unfortunately the exact players that compensate for these defects at 30°C yet allow the formation of the elongated filaments at 42°C remain unknown.

However, a couple of factors that can affect filamentation in *ftsZ84* have been well characterized. The first is that mild overexpression (twofold to threefold) of *ftsZ84* can suppress filamentation and allow *ftsZ84* mutants to divide at 42°C, which indicates that an increase in the level of the mutated protein can compensate for its functional deficit (Phoenix and Drapeau, 1988; Lu et al., 2001). The second is that many of the *fts*(Ts) mutations do not filament when grown in medium of higher osmolality. The *ftsZ84* mutant filaments in LBNS, but when grown on LB (i.e., with sodium chloride) and at 42°C, *ftsZ84* cells divide, are alive and form colonies (Ricard and Hirota, 1973). The inhibition of cell division in the MNR2 eel cells is similarly dependant on low osmolality, though unlike the *fts*(Ts) mutants they elongate without needing a temperature shift (El-Hajj and Newman, 2015). Not all the temperature-sensitive mutants are affected by osmolality or salt; for example *ftsZ26* filament at 42°C in both LB and LBNS (Bi and Lutkenhaus, 1992).

Why an increase in osmotic pressure restores division in some mutants but not others is not fully understood. In the MNR2 eel cells, elongation correlates with a decrease in the cellular levels of FtsZ, which we have suggested is the reason these cells cannot form a functional Z-ring (El-Hajj and Newman, 2015), but no

such correlation has been drawn in any of the *fts*(Ts) mutants that we know of. On the contrary, in a number of *ftsZ*(Ts) mutants (including *ftsZ84*) grown in LBNS, the levels of FtsZ were *higher* at 42°C, when the cells filament, than they were at 30°C where these mutants could divide as the usual short rods (Addinall et al., 2005). *E. coli* grows within a large range of osmotic pressure but functions optimally between 300 to 500 mOsm (Cayley and Record, 2004). A change in osmotic pressure affects the cell at just about every level, from the composition of the lipid bilayer to protein-nucleic acid interactions and most enzymatic reactions (Kornblatt and Kornblatt, 2002). Low osmolality affects MNR2 and *ftsZ84* similarly, in that they both elongate, but the precise mechanism disrupted by this change in osmotic pressure is different and the cells become either filaments destined to die or eel cells that can keep elongating.

Filament Formation During the SOS Response

As we mentioned in the introduction to this review, one of the remarkable features of *E. coli* (as well as many other bacteria) is that its metabolism is very efficient. New cells are produced rapidly with no wasting of metabolites and with very few mutants. The SOS response is a general stress response that many bacteria undergo when exposed to environmental or chemical factors that lead to DNA damage, such as radiation or some antibiotics (Walker, 1996). It involves a global and comprehensive regulatory network aimed at temporarily halting replication and division while repairing the DNA lesions, which ensures that the mutations that led to triggering the response do not get passed on to daughter cells.

The mechanism underlying induction of the SOS response is well described (Erill et al., 2007). Most of the genes involved in triggering the response are regulated by the LexA repressor, which is normally bound to their promoter region and blocks their expression (d'Ari, 1985). Conditions that induce DNA damage (such as UV irradiation) lead to the formation of lesions in the DNA. During DNA replication, the DNA polymerase complex inevitably encounters these lesions and cannot get past them, which stalls the replication fork. This leads to the recruitment of RecA to the site of the lesion and its activation when it binds to the single-strand DNA generated by the interruption in replication (Sassanfar and Roberts, 1990). Activated RecA can promote the autolytic cleave of LexA (Horii et al., 1981), which dissociates it from the promoter region of the SOS genes and enables their active transcription. A host of genes are then expressed (Janion, 2008), many of which are involved in stabilizing the stalled replication fork or in repairing the lesion (Baharoglu and Mazel, 2014). In order to buy time for repairing the DNA damage, the cell delays septation through the SOS-induced cell division inhibitor SulA (Huisman et al., 1984).

SulA blocks cell division during the SOS response by interacting directly with FtsZ in a 1:1 (Higashitani et al., 1995). This forms a stable complex that prevents FtsZ subunits from polymerizing and effectively inhibits septation at its earliest stage (Trusca et al., 1998; Cordell et al., 2003). SulA inhibition of FtsZ polymerization is reversible (Maguin et al., 1986), which allows the cell to exit the SOS phase and resume normal division once the DNA damage has been dealt with. This is controlled by the Lon protease, which plays a role in the degradation of SulA, freeing the FtsZ monomers to polymerize and initiate a new division cycle (Schoemaker et al., 1984).

If Lon function is inhibited, SulA is no longer degraded and can continue to accumulate and to sequester FtsZ. This extends the division block of the SOS response, and as the cells continue to elongate they form aseptate, multinucleate filaments (Adler and Hardigree, 1965). These filaments are not viable and the cell division block eventually becomes irreversible; within 4 or 5 h of their formation, only 2% of the filaments can recover and form colonies (Adler and Hardigree, 1964). However, the block can be overcome by reactivating Lon in the filaments (Walker and Pardee, 1967), since SulA would then be degraded, freeing FtsZ to polymerize and reinitiate cell division (Schoemaker et al., 1984).

Early during their characterization, SOS-induced filaments were noted for being metabolically competent despite being inhibited in cell division. They continue to elongate, increase mass, and synthesize nucleic acids and proteins (Walker and Pardee, 1967). Despite triggering the SOS state in response to DNA damage, they replicate their chromosomes and distribute DNA continuously and regularly throughout their length (Adler and Hardigree, 1965). Why then do they lyse and die within a few hours, while the metabolically competent MNR2 eel cells survive and continue to elongate well past this time? The SOS response triggers the expression of diverse genes, many of which are not necessarily involved in cell division but in regulating other aspects of *E. coli* metabolism and physiology (Janion, 2008). This probably affects the filaments in ways that were not measured or observed but that disrupt their metabolism and eventually leads to their death. This would be advantageous from an evolutionary perspective—a filament where the SOS response stays induced for so long is one that cannot repair the DNA lesions that triggered it in the first place and its death ensures the mutations do not get propagated to daughter cells. One feature they still share with the MNR2 eel cells is that in both cases elongation is initiated by a decrease in the availability of FtsZ.

The cellular concentration of FtsZ is constant throughout the division cycle, and is set at a critical concentration below which division is hindered (Rueda et al., 2003; Weart and Levin, 2003). Division begins not by synthesizing more FtsZ but by assembling the heretofore soluble FtsZ into the Z-ring (Sun and Margolin, 1998), with eventual activation of PBP3. A decrease in FtsZ can prevent PBP3 activation and onset of division and lead to the formation of elongated cells, as seen when cells are partially or completely depleted of FtsZ (Dai and Lutkenhaus, 1991). In a typical *ftsZ*(Ts) mutant such as *ftsZ84*, the cells form filaments with no constrictions after transfer from 30°to 42°C (Addinall et al., 1996), where FtsZ84 function is inhibited. The filaments produce increased levels of FtsZ84, perhaps in an attempt to compensate for the inhibition in the activity of the mutant protein (Addinall et al., 2005). During the SOS response, the FtsZ molecule itself is intact, but its sequestration by SulA decreases the pool of available, active FtsZ, which also leads to filamentation (Lutkenhaus, 1983; Chen et al., 2012). A similar mechanism is used by OpgH, a moonlighting enzyme that acts as a nutrient-dependant regulator of cell size by sequestering FtsZ under nutrient-rich conditions (Hill et al., 2013). In the case of the MNR2 eel cells, FtsZ activity

is reduced because the levels of the proteins are much lower in medium of low osmolality, presumably lower than the critical concentration required for division (El-Hajj and Newman, 2015). A reduction in FtsZ function is therefore clearly correlated with division inhibition and elongation, but the differences underlying the exact mechanisms in each case also lead to different fates for the elongated cells.

Giant Bacteria

Although MNR2 grows as long as any bacterium when it is cultured in low-osmolality LBNS, it has no way of dividing in this medium. This distinguishes the *E. coli* long cells from naturally-occuring giant bacteria, which can divide despite reaching similar lengths. The giant bacteria have evolved complex mechanisms to survive and take advantage of this enormous size, which is indeed the norm for them.

When we think of bacteria, we tend to think of unicellular microorganisms 1–5 μm in length or diameter. Many of the "traditional" bacteria fall within this length, such as *E. coli*, *Salmonella*, *Vibrio, Bacillus*, and *Staphylococcus*. However, bacterial sizes encompass a much wider range. *Mycoplasma pneumoniae*, one of the smallest known bacteria, is only 0.2 μm in diameter. These cells are so small that, over the course of its evolution, the bacterium drastically reduced the size of its genome by loss of most of its metabolic pathways, locking it into an obligate parasitic lifestyle for the acquisition of most metabolites (Himmelreich et al., 1996). At the opposite end of the spectrum, *Epulopiscium fishelsoni* cells can reach lengths of 700 μm and widths of 80 μm (Angert et al., 1993). The largest bacterium known, *Thiomargarita namibiensis*, is a giant sulfur bacterium that forms linear chains of spherical-shaped cells with diameters of up to 750 μm, so large that individual cells can be seen without any optical enhancements (Schulz et al., 1999).

Thiomargarita and Giant Sulfur Bacteria

Giant bacteria need to deal with very different surface/volume considerations and have evolved elaborate transport and division systems in order to survive at sizes much larger than the more typical bacteria. Koch attempted to estimate the maximum size a cell could be if it relied exclusively on diffusion, and calculated this maximum as 300 μm (Koch, 1996). The diameter of *T. namibiensis* cocci frequently exceeds this and can reach values as high as 750 μm. They overcomes transport problems by organizing their cytoplasm around a large storage vacuole that takes up almost 98% of the cell's volume (Schulz et al., 1999). The actual cytoplasm is a thin spherical shell that wraps around this liquid vacuole and contains a large number of sulfur globules. This arrangement allows all points of the cytoplasm close proximity to both the extracellular space and the vacuole, which overcomes the diffusion size limit. Another giant sulfur bacterium was isolated in the Gulf of Mexico, with large spherical cells up to 375 μm in diameter. This *Thiomargarita*-like bacterium had a similar cellular structure consisting of a central storage vacuole surrounded by a spherical shell of cytoplasm, which also contained sulfur globules (Kalanetra et al., 2005).

Why do the *Thiomargarita* bacteria organize their cytoplasm in such a way, and why do they need such a large central vacuole? A very long cell with a small diameter, such as the MNR2 eel cells, can overcome surface/volume limitations while maintaining a much smaller biovolume. The central vacuole seems to be a feature of giant sulfur bacteria and had already been described in *Beggiatoa* (Nelson et al., 1989). *Beggiatoa* is motile and usually uses oxygen as an electron acceptor in its sulfur oxidation, but it can store nitrate in the vacuole and use it as a temporary alternative electron acceptor when oxygen is low and it needs to move to another, more oxygen-rich environment (Dunker et al., 2011). Both of the identified *Thiomargarita* bacteria are non-motile and their vacuoles are much larger than in *Beggiatoa*. They may have evolved these giant vacuoles as nitrate storage tanks to survive long periods of anoxia and of low environmental nitrate. Schulz and Jorgensen (2001) calculated that the vacuole of *T. namibiensis* could store enough nitrate for a cell to survive almost 2 months without an external supply of either oxygen or nitrate, but under laboratory conditions a cell can survive for well over a year.

Epulopiscium fishelsoni

Before the identification of *Thiomargarita*, the previous contender for largest bacterium was *Epulopiscium fishelsoni*, a symbiotic microorganism that spends the entirety of its life cycle within the gut of the surgeonfish (Fishelson et al., 1985). Reaching a length up to 700 μm and a width of 80 μm, the cell encloses a large volume of continuous cytoplasm, resulting in transport problems from outside and within the cell (Angert et al., 1993). *Epulopiscium fishelsoni* overcomes surface/volume limitations using extreme polyploidy; each cell has between 50,000 and 120,000 copies of the chromosome, with the exact number being directly proportional to the size of the cell (Mendell et al., 2008). As *Epulopiscium fishelsoni* cells get larger they replicate their chromosome to such high numbers to allow extremely high expression of transport pumps, as well as ribosomes, many of which are concentrated toward the center of the cell, away from the cell membrane. This is coupled to a large number of infoldings of the cell membrane, which is thought to enhance transport across the membrane and further into the center of the cell (Clements and Bullivant, 1991). Transport pumps on the cell membrane are similar to those in other bacteria, but they are much more kinetically active and have unusually high transport rate (Bresler and Fishelson, 2006), presumably to compensate for *Epulopiscium fishelsoni*'s much lower surface/volume ratio.

Epulopiscium does not divide like the typical *E. coli* using FtsZ and PBP3 as we described earlier. Instead, two daughter cells form inside the parent cell, each with its own cell membrane, and both completely enclosed within the cytoplasm of the parent (Angert, 2012). FtsZ does polymerize into a ring structure, not at midcell, but at the poles of the daughter cells instead (Angert and Clements, 2004). Eventually the daughter cells take over most of the cytoplasm of the parent and burst out, killing the parent in the process (Montgomery and Pollak, 1988). The growth of these daughter cells inside the parental cell shares some similarities with endospore formation in bacteria such as *Bacillus* (Errington, 1993), with one major difference: *Epulopiscium fishelsoni* daughter cells are not quiescent but fully active. This makes *Epulopiscium*

and its relatives unique in that they rely on viviparous reproduction with the formation of multiple internal offsprings, which are released by destroying the parental cell.

Desulfobulbaceae and Cable Filaments

Recently, a relative of *Desulfobulbus* was identified that blurs the line of what defines an individual bacterial cell. These Desulfobulbaceae form extremely long cable-like filaments in marine sediments, up to 1.5 cm long, twice that of the longest MNR2 eel cell (Pfeffer et al., 2012). Although an individual eel cell has no compartmentalization and a continuous cytoplasm, the Desulfobulbaceae filament consists of a linear chain of hundreds of cells, each only 3 μm long and each with its own inner membrane. However, all the cells within the filament are encased within the same outer membrane, which spans the entire 1.5 cm of length uninterrupted. Whether each filament is a single cell or a colony of hundreds of cells depends on whether we define the inner membrane or the outer membrane as enclosing a single cell. The cytoplasm of each short cell within the filament is unconnected to that of the adjacent cells, but each cell is connected to its neighbors by a filling that bridges the gap (Pfeffer et al., 2012). This organization allows high electron conductivity, which gives the Desulfobulbaceae filament the remarkable property of acting like an electric cable capable of conducting current across the layers of sediment where it normally grows. When followed over several weeks, the filaments grow and expand deeper into the sediments (Larsen et al., 2014; Schauer et al., 2014). The remarkable length of these filaments is thought to help them couple oxygen consumption, which requires contact with surface sediments, and the sulfide oxidation that occurs in deeper, anoxic layers.

Concluding Remarks

Escherichia coli normally exists as a small rod, but we have discussed many conditions that cause it to elongate when cell division is inhibited. Some of these are related to lowered activity of FtsZ, such as in *ftsZ*(Ts) mutants, or when FtsZ is sequestered by SulA during the SOS response. Many metabolic defects also interfere with cell division, including metabolism of amino acids such as serine and methionine, as well as disruptions SAM synthesis, which is required for most methylations. In the MNR2 eel cells, disruption of SAM metabolism linked to one or more unknown mutations has resulted in the longest *E. coli* cells observed. This might be due to the methylation of a key cell division activator being disrupted in this mutant.

We conclude from these and other examples that as long as it remains narrow, allowing efficient uptake and excretion of material, *E. coli* can arrange its metabolism to function and grow over large lengths of undivided protoplasm. It can place its DNA and ribosomes so as to produce mRNA and proteins, and organize its enzymes spatially to function efficiently. In these ways it is as efficient as the giant bacteria like *Thiomargarita*, which have evolved as very large cells and have specific mechanisms to live at these sizes. *E. coli* lacks the specific adaptation to divide but has no trouble surviving at such sizes.

What an ultra elongated *E. coli* cannot do that *Thiomargarita* can is divide! We suggest that long length presents no particular metabolic problems by itself. However, the lack of an efficient division system for its long variants keeps *E. coli* short.

Acknowledgments

We would like to thank Giri Narasinham for teaching us to analyze whole genome sequence data. ZE is grateful to Pat Gulick and Justin Powlowski for their financial support at Concordia University. EN wishes to thank Kalai Mathee for transferring the Newman lab from the downtown campus to the west end and organizing the new lab, Noel Guyves, Dean Solin, Jean Rosa, Marianne Chancerel, Jack Kornblatt, and Conrad Woldringh. ZE dedicates this review to Walid, Carmen, and Shadi El-Hajj for their continued support and love. EN dedicates this review to Harold Newman and Vijay Mathur without whom, nothing.

References

Addinall, S. G., Bi, E., and Lutkenhaus, J. (1996). FtsZ ring formation in *fts* mutants. *J. Bacteriol.* 178, 3877–3884.

Addinall, S. G., Cao, C., and Lutkenhaus, J. (1997). Temperature shift experiments with an *ftsZ84*(Ts) strain reveal rapid dynamics of FtsZ localization and indicate that the Z ring is required throughout septation and cannot reoccupy division sites once constriction has initiated. *J. Bacteriol.* 179, 4277–4284.

Addinall, S. G., and Lutkenhaus, J. (1996). FtsA is localized to the septum in an FtsZ-dependent manner. *J. Bacteriol.* 178, 7167–7172.

Addinall, S. G., Small, E., Whitaker, D., Sturrock, S., Donachie, W. D., and Khattar, M. M. (2005). New temperature-sensitive alleles of ftsZ in *Escherichia coli*. *J. Bacteriol.* 187, 358–365.

Adler, H. I., and Hardigree, A. A. (1964). Analysis of a gene controlling cell division and sensitivity to radiation in *Escherichia coli*. *J. Bacteriol.* 87, 720–726.

Adler, H. I., and Hardigree, A. A. (1965). Growth and division of filamentous forms of *Escherichia coli*. *J. Bacteriol.* 90, 223–226.

Angert, E. R. (2012). DNA replication and genomic architecture of very large bacteria. *Annu. Rev. Microbiol.* 66, 197–212. doi: 10.1146/annurev-micro-090110-102827

Angert, E. R., and Clements, K. D. (2004). Initiation of intracellular offspring in *Epulopiscium*. *Mol. Microbiol.* 51, 827–835. doi: 10.1046/j.1365-2958.2003.03869.x

Angert, E. R., Clements, K. D., and Pace, N. R. (1993). The largest bacterium. *Nature* 362, 239–241. doi: 10.1038/362239a0

Baharoglu, Z., and Mazel, D. (2014). SOS, the formidable strategy of bacteria against aggressions. *FEMS Microbiol. Rev.* 38, 1126–1145. doi: 10.1111/1574-6976.12077

Bi, E., and Lutkenhaus, J. (1992). Isolation and characterization of *ftsZ* alleles that affect septal morphology. *J. Bacteriol.* 174, 5414–5423.

Bresler, V., and Fishelson, L. (2006). Export pumps in *Epulopiscium fishelsoni*, the symbiotic giant gut bacterium in *Acanthurus nigrofuscus*. *Naturwissenschaften* 93, 181–184. doi: 10.1007/s00114-006-0084-3

Burman, J. D., Harris, R. L., Hauton, K. A., Lawson, D. M., and Sawers, R. G. (2004). The iron-sulfur cluster in the L-serine dehydratase TdcG from *Escherichia coli* is required for enzyme activity. *FEBS Lett.* 576, 442–444. doi: 10.1016/j.febslet.2004.09.058

Cayley, S., and Record, M. T. Jr. (2004). Large changes in cytoplasmic biopolymer concentration with osmolality indicate that macromolecular crowding may regulate protein-DNA interactions and growth rate in osmotically stressed *Escherichia coli* K-12. *J. Mol. Recognit.* 17, 488–496. doi: 10.1002/jmr.695

Chen, Y., Milam, S. L., and Erickson, H. P. (2012). SulA inhibits assembly of FtsZ by a simple sequestration mechanism. *Biochemistry* 51, 3100–3109. doi: 10.1021/bi201669d

Chien, A. C., Hill, N. S., and Levin, P. A. (2012). Cell size control in bacteria. *Curr. Biol.* 22, R340–R39. doi: 10.1016/j.cub.2012.02.032

Cicchillo, R. M., Baker, M. A., Schnitzer, E. J., Newman, E. B., Krebs, C., and Booker, S. J. (2004). *Escherichia coli* L-serine deaminase requires a [4Fe-4S] cluster in catalysis. *J. Biol. Chem.* 279, 32418–32425. doi: 10.1074/jbc.M404381200

Clements, K. D., and Bullivant, S. (1991). An unusual symbiont from the gut of surgeonfishes may be the largest known prokaryote. *J. Bacteriol.* 173, 5359–5362.

Cohn, M. (2014). The Institut Pasteur attic dwellers: their origins, their paths to discovery. *Res. Microbiol.* 165, 318–324. doi: 10.1016/j.resmic.2014.05.027

Cordell, S. C., Robinson, E. J., and Löwe, J. (2003). Crystal structure of the SOS cell division inhibitor SulA and in complex with FtsZ. *Proc. Natl. Acad. Sci. U.S.A.* 100, 7889–7894. doi: 10.1073/pnas.1330742100

Dai, K., and Lutkenhaus, J. (1991). *ftsZ* is an essential cell division gene in *Escherichia coli*. *J. Bacteriol.* 173, 3500–3506.

Dajkovic, A., Pichoff, S., Lutkenhaus, J., and Wirtz, D. (2010). Cross-linking FtsZ polymers into coherent Z rings. *Mol. Microbiol.* 78, 651–668. doi: 10.1111/j.1365-2958.2010.07352.x

d'Ari, R. (1985). The SOS system. *Biochimie* 67, 343–347. doi: 10.1016/S0300-9084(85)80077-8

De Boer, P., Crossley, R., and Rothfield, L. (1992). The essential bacterial cell-division protein FtsZ is a GTPase. *Nature* 359, 254–256. doi: 10.1038/359254a0

den Blaauwen, T. (2013). Prokaryotic cell division: flexible and diverse. *Curr. Opin. Microbiol.* 16, 738–744. doi: 10.1016/j.mib.2013.09.002

Driskell, L. O., Tucker, A. M., Winkler, H. H., and Wood, D. O. (2005). Rickettsial *metK*-encoded methionine adenosyltransferase expression in an *Escherichia coli metK* deletion strain. *J. Bacteriol.* 187, 5719–5722. doi: 10.1128/JB.187.16.5719-5722.2005

Du, S., and Lutkenhaus, J. (2014). SlmA antagonism of FtsZ assembly employs a two-pronged mechanism like MinCD. *PLoS Genet.* 10:e1004460. doi: 10.1371/journal.pgen.1004460

Dunker, R., Røy, H., Kamp, A., and Jørgensen, B. B. (2011). Motility patterns of filamentous sulfur bacteria, *Beggiatoa* spp. *FEMS Microbiol Ecol.* 77, 176–185. doi: 10.1111/j.1574-6941.2011.01099.x

El-Hajj, Z. W., and Newman, E. B. (2015). An *Escherichia coli* mutant that makes exceptionally long cells. *J. Bacteriol.* 197, 1507–1514.

El-Hajj, Z. W., Reyes-Lamothe, R., and Newman, E. B. (2013). Cell division, one-carbon metabolism and methionine synthesis in a metK-deficient *Escherichia coli* mutant, and a role for MmuM. *Microbiology* 159, 2036–2048. doi: 10.1099/mic.0.069682-0

Erill, I., Campoy, S., and Barbé, J. (2007). Aeons of distress: an evolutionary perspective on the bacterial SOS response. *FEMS Microbiol. Rev.* 31, 637–656. doi: 10.1111/j.1574-6976.2007.00082.x

Errington, J. (1993). *Bacillus subtilis* sporulation: regulation of gene expression and control of morphogenesis. *Microbiol. Rev.* 57, 1–33.

Errington, J., Daniel, R. A., and Scheffers, D. J. (2003). Cytokinesis in bacteria. *Microbiol. Mol. Biol. Rev.* 67, 52–65. doi: 10.1128/MMBR.67.1.52-65.2003

Fishelson, L., Montgomery, W. L., and Myrberg, A. A. (1985). A unique symbiosis in the gut of tropical herbivorous surgeonfish (Acanthuridae: Teleostei) from the red sea. *Science* 229, 49–51. doi: 10.1126/science.229.4708.49

Fu, G., Huang, T., Buss, J., Coltharp, C., Hensel, Z., and Xiao, J. (2010). *In vivo* structure of the *E. coli* FtsZ-ring revealed by photoactivated localization microscopy (PALM). *PLoS ONE.* 5:e12682. doi: 10.1371/journal.pone.0012680

Ghosal, D., Trambaiolo, D., Amos, L. A., and Löwe, J. (2014). MinCD cell division proteins form alternating copolymeric cytomotive filaments. *Nat. Commun.* 5, 5341. doi: 10.1038/ncomms6341

Greene, R. C., Hunter, J. S., and Coch, E. H. (1973). Properties of *metK* mutants of *Escherichia coli* K-12. *J. Bacteriol.* 115, 57–67.

Grover, N. B., and Woldringh, C. L. (2001). Dimensional regulation of cell-cycle events in *Escherichia coli* during steady-state growth. *Microbiology* 147, 171–181.

Hasnain, S., McClendon, C. L., Hsu, M. T., Jacobson, M. P., and Bandyopadhyay, P. (2014). A new coarse-grained model for *E. coli* cytoplasm: accurate calculation of the diffusion coefficient of proteins and observation of anomalous diffusion. *PLoS ONE* 9:e106466. doi: 10.1371/journal.pone.0106466

Higashitani, A., Higashitani, N., and Horiuchi, K. (1995). A cell division inhibitor SulA of *Escherichia coli* directly interacts with FtsZ through GTP hydrolysis. *Biochem. Biophys. Res. Commun.* 209, 198–204. doi: 10.1006/bbrc.1995.1489

Hill, N. S., Buske, P. J., Shi, Y., and Levin, P. A. (2013). A moonlighting enzyme links *Escherichia coli* cell size with central metabolism. *PLoS Genet.* 9:e1003663. doi: 10.1371/journal.pgen.1003663

Himmelreich, R., Hilbert, H., Plagens, H., Pirkl, E., Li, B. C., and Herrmann, R. (1996). Complete sequence analysis of the genome of the bacterium *Mycoplasma pneumoniae*. *Nucleic Acids Res.* 24, 4420–4449. doi: 10.1093/nar/24.22.4420

Hoppert, M., and Mayer, F. (1999). Principles of macromolecular organization and cell function in bacteria and archaea. *Cell Biochem. Biophys* 31, 247–284. doi: 10.1007/BF02738242

Horii, T., Ogawa, T., Nakatani, T., Hase, T., Matsubara, H., and Ogawa, H. (1981). Regulation of SOS functions: purification of *E. coli* LexA protein and determination of its specific site cleaved by the RecA protein. *Cell* 27, 515–522. doi: 10.1016/0092-8674(81)90393-7

Huisman, O., D'Ari, R., and Gottesman, S. (1984). Cell-division control in *Escherichia coli*: specific induction of the SOS function SfiA protein is sufficient to block septation. *Proc. Natl. Acad. Sci. U.S.A.* 81, 4490–4494. doi: 10.1073/pnas.81.14.4490

Janion, C. (2008). Inducible SOS response system of DNA repair and mutagenesis in *Escherichia coli*. *Int. J. Biol. Sci.* 4, 338–344. doi: 10.7150/ijbs.4.338

Jiang, H., Si, F., Margolin, W., and Sun, S. X. (2011). Mechanical control of bacterial cell shape. *Biophys. J.* 101, 327–335. doi: 10.1016/j.bpj.2011.06.005

Johnson, J. W., Fisher, J. F., and Mobashery, S. (2013). Bacterial cell-wall recycling. *Ann. N. Y. Acad. Sci.* 1277, 54–75. doi: 10.1111/j.1749-6632.2012.06813.x

Jones, C. A., and Holland, I. B. (1984). Inactivation of essential division genes, *ftsA*, *ftsZ*, suppresses mutations at sfiB, a locus mediating division inhibition during the SOS response in *E. coli*. *EMBO J.* 3, 1181–1186.

Kalanetra, K. M., Joye, S. B., Sunseri, N. R., and Nelson, D. C. (2005). Novel vacuolate sulfur bacteria from the Gulf of Mexico reproduce by reductive division in three dimensions. *Environ. Microbiol.* 7, 1451–1460. doi: 10.1111/j.1462-2920.2005.00832.x

Koch, A. L. (1996). What size should a bacterium be? A question of scale. *Annu. Rev. Microbiol.* 50, 317–348. doi: 10.1146/annurev.micro.50.1.317

Koch, A. L., and Woldringh, C. L. (1994). The metabolic inertness of the pole wall of a gram-negative rod. *J. Theor. Biol.* 171, 415–425. doi: 10.1006/jtbi.1994.1245

Kornblatt, J. A., and Kornblatt, M. J. (2002). The effects of osmotic and hydrostatic pressures on macromolecular systems. *Biochim. Biophys. Acta* 1595, 30–47. doi: 10.1016/S0167-4838(01)00333-8

Larsen, S., Nielsen, L. P., and Schramm, A. (2014). Cable bacteria associated with long-distance electron transport in New England salt marsh sediment. *Environ. Microbiol. Rep.* 7, 175–179. doi: 10.1111/1758-2229.12216

Lederer, F. L., Günther, T. J., Raff, J., and Pollmann, K. (2011). *E. coli* filament formation induced by heterologous S-layer expression. *Bioeng. Bugs* 2, 178–181. doi: 10.4161/bbug.2.3.15418

Lu, C., Stricker, J., and Erickson, H. P. (2001). Site-specific mutations of FtsZ—effects on GTPase and *in vitro* assembly. *BMC Microbiol.* 1:7. doi: 10.1186/1471-2180-1-7

Lutkenhaus, J. (1983). Coupling of DNA replication and cell division: *sulB* is an allele of *ftsZ*. *J. Bacteriol.* 154, 1339–1346.

Lutkenhaus, J., Pichoff, S., and Du, S. (2012). Bacterial cytokinesis: from Z ring to divisome. *Cytoskeleton (Hoboken)* 69, 778–790. doi: 10.1002/cm.21054

Ma, X., and Margolin, W. (1999). Genetic and functional analyses of the conserved C-terminal core domain of *Escherichia coli* FtsZ. *J. Bacteriol.* 181, 7531–7544.

Maguin, E., Lutkenhaus, J., and D'Ari, R. (1986). Reversibility of SOS-associated division inhibition in *Escherichia coli*. *J. Bacteriol.* 166, 733–738.

Mendell, J. E., Clements, K. D., Choat, J. H., and Angert, E. R. (2008). Extreme polyploidy in a large bacterium. *Proc. Natl. Acad. Sci. U.S.A.* 105, 6730–6734. doi: 10.1073/pnas.0707522105

Mendelson, N. H., Sarlls, J. E., Wolgemuth, C. W., and Goldstein, R. E. (2000). Chiral self-propulsion of growing bacterial macrofibers on a solid surface. *Phys. Rev. Lett.* 84, 1627–1630. doi: 10.1103/PhysRevLett.84.1627

Monette, A. (2006). *The Effects of cpx Genes on the Regulation of L-Serine Metabolism in Escherichia coli K-12.* M.Sc. thesis, Montreal: Concordia University.

Montgomery, W. L., and Pollak, P. E. (1988). *Epulopiscium fishelsoni* n.g., n.s., a protist of uncertain taxonomic affinities from the gut of an herbivorous reefish. *J. Protozool.* 35, 565–569. doi: 10.1111/j.1550-7408.1988.tb04153.x

Mukherjee, A., Saez, C., and Lutkenhaus, J. (2001). Assembly of an FtsZ mutant deficient in GTPase activity has implications for FtsZ assembly and the role of the Z ring in cell division. *J. Bacteriol.* 183, 7190–7197. doi: 10.1128/JB.183.24.7190-7197.2001

Nelson, D. C., Wirsen, C. O., and Jannasch, H. W. (1989). Characterization of large, autotrophic *Beggiatoa* spp. abundant at hydrothermal vents of the Guaymas Basin. *Appl. Environ. Microbiol.* 55, 2909–2917.

Newman, E. B., Budman, L. I., Chan, E. C., Greene, R. C., Lin, R. T., Woldringh, C. L., et al. (1998). Lack of *S*-adenosylmethionine results in a cell division defect in *Escherichia coli*. *J. Bacteriol.* 180, 3614–3619.

Pfeffer, C., Larsen, S., Song, J., Dong, M., Besenbacher, F., Meyer, R. L., et al. (2012). Filamentous bacteria transport electrons over centimetre distances. *Nature* 491, 218–221. doi: 10.1038/nature11586

Phoenix, P., and Drapeau, G. R. (1988). Cell division control in *Escherichia coli* K-12: some properties of the *ftsZ84* mutation and suppression of this mutation by the product of a newly identified gene. *J. Bacteriol.* 170, 4338–4342.

Potluri, L. P., Kannan, S., and Young, K. D. (2012). ZipA is required for FtsZ-dependent preseptal peptidoglycan synthesis prior to invagination during cell division. *J. Bacteriol.* 194, 5334–5342. doi: 10.1128/JB.00859-12

Rainwater, S., and Silverman, P. M. (1990). The Cpx proteins of *Escherichia coli* K-12: evidence that *cpxA*, *ecfB*, *ssd*, and *eup* mutations all identify the same gene. *J. Bacteriol.* 172, 2456–2461.

RayChaudhuri, D., and Park, J. T. (1992). *Escherichia coli* cell-division gene *ftsZ* encodes a novel GTP-binding protein. *Nature* 359, 251–254. doi: 10.1038/359251a0

Ricard, M., and Hirota, Y. (1973). Process of cellular division in *Escherichia coli*: physiological study on thermosensitive mutants defective in cell division. *J. Bacteriol.* 116, 314–322.

Rueda, S., Vicente, M., and Mingorance, J. (2003). Concentration and assembly of the division ring proteins FtsZ, FtsA, and ZipA during the *Escherichia coli* cell cycle. *J. Bacteriol.* 185, 3344–3351. doi: 10.1128/JB.185.11.3344-3351.2003

Sassanfar, M., and Roberts, J. W. (1990). Nature of the SOS-inducing signal in *Escherichia coli*. The involvement of DNA replication. *J. Mol. Biol.* 212, 79–96. doi: 10.1016/0022-2836(90)90306-7

Schaechter, M., Maaløe, O., and Kjeldgaard, N. O. (1958). Dependency on medium and temperature of cell size and chemical composition during balanced grown of *Salmonella typhimurium*. *J. Gen. Microbiol.* 19, 592–606. doi: 10.1099/00221287-19-3-592

Schauer, R., Risgaard-Petersen, N., Kjeldsen, K. U., Tataru Bjerg, J. J., Jørgensen, B. B., Schramm, A., et al. (2014). Succession of cable bacteria and electric currents in marine sediment. *ISME J.* 8, 1314–1322. doi: 10.1038/ismej.2013.239

Scheffers, D. J., and Driessen, A. J. (2002). Immediate GTP hydrolysis upon FtsZ polymerization. *Mol. Microbiol.* 43, 1517–1521. doi: 10.1046/j.1365-2958.2002.02828.x

Schoemaker, J. M., Gayda, R. C., and Markovitz, A. (1984). Regulation of cell division in *Escherichia coli*: SOS induction and cellular location of the SulA protein, a key to Lon-associated filamentation and death. *J. Bacteriol.* 158, 551–561.

Schulz, H. N., Brinkhoff, T., Ferdelman, T. G., Mariné, M. H., Teske, A., and Jorgensen, B. B. (1999). Dense populations of a giant sulfur bacterium in Namibian shelf sediments. *Science* 284, 493–495. doi: 10.1126/science.284.5413.493

Schulz, H. N., and Jorgensen, B. B. (2001). Big bacteria. *Annu. Rev. Microbiol.* 55, 105–137. doi: 10.1146/annurev.micro.55.1.105

Shao, Z., and Newman, E. B. (1993). Sequencing and characterization of the *sdaB* gene from *Escherichia coli* K-12. *Eur. J. Biochem.* 212, 777–784. doi: 10.1111/j.1432-1033.1993.tb17718.x

Stricker, J., Maddox, P., Salmon, E. D., and Erickson, H. P. (2002). Rapid assembly dynamics of the *Escherichia coli* FtsZ-ring demonstrated by fluorescence recovery after photobleaching. *Proc. Natl. Acad. Sci. U.S.A.* 99, 3171–3175. doi: 10.1073/pnas.052595099

Su, H., and Newman, E. B. (1991). A novel L-serine deaminase activity in *Escherichia coli* K-12. *J. Bacteriol.* 173, 2473–2480.

Sun, Q., and Margolin, W. (1998). FtsZ dynamics during the division cycle of live *Escherichia coli* cells. *J. Bacteriol.* 180, 2050–2056.

Taheri-Araghi, S., Bradde, S., Sauls, J. T., Hill, N. S., Levin, P. A., Paulsson, J., et al. (2015). Cell-size control and homeostasis in bacteria. *Curr. Biol.* 25, 385–391. doi: 10.1016/j.cub.2014.12.009

Taschner, P. E., Huls, P. G., Pas, E., and Woldringh, C. L. (1988). Division behavior and shape changes in isogenic *ftsZ*, *ftsQ*, *ftsA*, *pbpB*, and *ftsE* cell division mutants of *Escherichia coli* during temperature shift experiments. *J. Bacteriol.* 170, 1533–1540.

Trusca, D., Scott, S., Thompson, C., and Bramhill, D. (1998). Bacterial SOS checkpoint protein SulA inhibits polymerization of purified FtsZ cell division protein. *J. Bacteriol.* 180, 3946–3953.

Tucker, A. M., Winkler, H. H., Driskell, L. O., and Wood, D. O. (2003). *S*-adenosylmethionine transport in *Rickettsia prowazekii*. *J. Bacteriol.* 185, 3031–3035. doi: 10.1128/JB.185.10.3031-3035.2003

van der Ploeg, R., Verheul, J., Vischer, N. O., Alexeeva, S., Hoogendoorn, E., Postma, M., et al. (2013). Colocalization and interaction between elongasome and divisome during a preparative cell division phase in *Escherichia coli*. *Mol. Microbiol.* 87, 1074–1087. doi: 10.1111/mmi.12150

Walker, G. C. (1996). "The SOS response of *Escherichia coli*," in *Escherichia coli* and *Salmonella typhimurium*, Vol. 1, eds F. C. Neidharbt, R. III. Curtiss, J. L. Ingraham, E. C. C. Lin, K. B. Low, B. Magasanik, et al. (Washington, DC: American Society for Microbiology), 1400–1416.

Walker, J. R., and Pardee, A. B. (1967). Conditional mutations involving septum formation in *Escherichia coli*. *J. Bacteriol.* 93, 107–114.

Wang, S., Arends, S. J., Weiss, D. S., and Newman, E. B. (2005). A deficiency in *S*-adenosylmethionine synthetase interrupts assembly of the septal ring in *Escherichia coli* K-12. *Mol. Microbiol.* 58, 791–799. doi: 10.1111/j.1365-2958.2005.04864.x

Weart, R. B., and Levin, P. A. (2003). Growth rate-dependent regulation of medial FtsZ ring formation. *J. Bacteriol.* 185, 2826–2834. doi: 10.1128/JB.185.9.2826-2834.2003

Wei, Y., and Newman, E. B. (2002). Studies on the role of the metK gene product of *Escherichia coli* K-12. *Mol. Microbiol.* 43, 1651–1656. doi: 10.1046/j.1365-2958.2002.02856.x

Woldringh, C., Huls, P., Pas, E., Brakenhoff, G. J., and Nanninga, N. (1987). Topography of peptidoglycan synthesis during elongation and polar cap formation in a cell division mutant of *Escherichia coli* MC4100. *Microbiology* 133, 575–586. doi: 10.1099/00221287-133-3-575

Young, K. D. (2010). Bacterial shape: two-dimensional questions and possibilities. *Annu. Rev. Microbiol.* 64, 223–240. doi: 10.1146/annurev.micro.112408.134102

Zhang, X., El-Hajj, Z. W., and Newman, E. (2010). Deficiency in L-serine deaminase interferes with one-carbon metabolism and cell wall synthesis in *Escherichia coli* K-12. *J. Bacteriol.* 192, 5515–5525. doi: 10.1128/JB.00748-10

Zhang, X., and Newman, E. (2008). Deficiency in L-serine deaminase results in abnormal growth and cell division of *Escherichia coli* K-12. *Mol. Microbiol.* 69, 870–881. doi: 10.1111/j.1365-2958.2008.06315.x

Conflict of Interest Statement: The authors declare that the research was conducted in the absence of any commercial or financial relationships that could be construed as a potential conflict of interest.

Copyright © 2015 El-Hajj and Newman. This is an open-access article distributed under the terms of the Creative Commons Attribution License (CC BY). The use, distribution or reproduction in other forums is permitted, provided the original author(s) or licensor are credited and that the original publication in this journal is cited, in accordance with accepted academic practice. No use, distribution or reproduction is permitted which does not comply with these terms.

frontiers in Microbiology

PERSPECTIVE
published: 12 May 2015
doi: 10.3389/fmicb.2015.00455

The stoichiometric divisome: a hypothesis

Alexander J. F. Egan and Waldemar Vollmer**

The Centre for Bacterial Cell Biology, Institute for Cell and Molecular Biosciences, Newcastle University, Newcastle upon Tyne, UK

Dividing *Escherichia coli* cells simultaneously constrict the inner membrane, peptidoglycan layer, and outer membrane to synthesize the new poles of the daughter cells. For this, more than 30 proteins localize to mid-cell where they form a large, ring-like assembly, the divisome, facilitating division. Although the precise function of most divisome proteins is unknown, it became apparent in recent years that dynamic protein–protein interactions are essential for divisome assembly and function. However, little is known about the nature of the interactions involved and the stoichiometry of the proteins within the divisome. A recent study (Li et al., 2014) used ribosome profiling to measure the absolute protein synthesis rates in *E. coli*. Interestingly, they observed that most proteins which participate in known multiprotein complexes are synthesized proportional to their stoichiometry. Based on this principle we present a hypothesis for the stoichiometry of the core of the divisome, taking into account known protein–protein interactions. From this hypothesis we infer a possible mechanism for peptidoglycan synthesis during division.

Keywords: bacterial cell division, peptidoglycan, peptidoglycan synthesis, divisome and multiprotein complex

OPEN ACCESS

Edited by:
Arieh Zaritsky, Ben-Gurion University of the Negev, Israel

Reviewed by:
William Doerrler, Louisiana State University, USA
Miguel A. De Pedro, Consejo Superior de Investigaciones Científicas, Spain
Manjula Reddy, Centre for Cellular and Molecular Biology, India

****Correspondence:***
Alexander J. F. Egan and Waldemar Vollmer, The Centre for Bacterial Cell Biology, Institute for Cell and Molecular Biosciences, Newcastle University, Richardson Road, Newcastle upon Tyne NE2 4AX, UK
alexander.egan@ncl.ac.uk; w.vollmer@ncl.ac.uk

Specialty section:
This article was submitted to Microbial Physiology and Metabolism, a section of the journal Frontiers in Microbiology

Received: *25 March 2015*
Accepted: *27 April 2015*
Published: *12 May 2015*

Citation:
Egan AJF and Vollmer W (2015) The stoichiometric divisome: a hypothesis. Front. Microbiol. 6:455. doi: 10.3389/fmicb.2015.00455

Introduction

The peptidoglycan cell wall is an essential component of most bacteria, required for the maintenance of cell morphology and structural integrity (Weidel and Pelzer, 1964). Peptidoglycan (PG) forms a net-like, continuous layer, called the sacculus, surrounding the cytoplasmic membrane. Thus, a bacterial cell needs to increase the surface of its sacculus in order to grow and divide. Sacculus growth has to be well-controlled, because the accumulation of defects may lead to cell lysis; this is the case when antibiotics like β-lactams inhibit peptidoglycan synthesis. Remarkably, the growth of the single-layered sacculus in *E. coli* is accompanied by the release of as much as 50% of the total peptidoglycan material per generation by hydrolases (Goodell, 1985). What are the molecular mechanisms of sacculus growth? Höltje (1998) proposed that multi-enzyme complexes made of peptidoglycan synthases and hydrolases simultaneously synthesize new peptidoglycan and incorporate it into the sacculus, and remove old material, by a so-called 3-for-1 mechanism. Subsequent experimental evidence supported the multi-enzyme complex hypothesis. Genetic and biochemical data have demonstrated many protein–protein interactions between various peptidoglycan synthases, hydrolases, regulatory proteins, and cytoskeletal elements (reviewed in Typas et al., 2012; Egan and Vollmer, 2013). These have been observed in several species including, but not limited to, the Gram-positive *Bacillus subtilis*, *Staphylococcus aureus* and *Streptococcus pneumoniae* and the Gram-negative *Caulobacter crescentus* and *E. coli*, which will be the focus of this article.

In *E. coli*, cell division involves over 30 proteins, with twelve of these (the Fts proteins and ZipA) absolutely required for the process (Margolin, 2005). The assembly of essential proteins occurs in two steps; FtsZ, FtsA, ZipA, Zap proteins (A–E) and FtsEX assemble early at the future division

TABLE 1 | Synthesis rates of the late division proteins (and FtsA) and their ratios relative to PBP3 in MOPS minimal and complete media according to Li et al. (2014).

	MOPS minimal			MOPS complete		
Protein	**Copy number**	**∼ Ratio to PBP3**	**Molecules/complex[a]**	**Copy number**	**∼ Ratio to PBP3**	**Molecules/complex[a]**
PBP3	144	1.0	2	349	1.0	2
PBP1B	139	1.0	2	512	1.5	2/3
LpoB	954	6.6	2[b]	1490	4.3	2[b]
FtsN	269	1.9	4	871	2.5	4/5
FtsW	117	0.8	2	293	0.8	2
FtsQ	147	1.0	2	336	1.0	2
FtsL	201	1.4	2	416	1.2	2
FtsB	140	1.0	2	487	1.4	2
FtsK	213	1.5	3	508	1.5	3
FtsA	575	4.0	8	984	2.8	6

[a]*We have assumed that previously observed homodimerizations (e.g., PBP3, PBP1B) occur within the divisome.*
[b]*Despite the apparent excess of LpoB, we have assumed two molecules per complex given its stoichiometry with PBP1B is 1:1 (Egan et al., 2014).*

site, before any constriction is visible. Immediately before the onset of constriction the divisome matures through the incorporation of FtsK, FtsQ, FtsL, FtsB, FtsW, PBP3 (FtsI), and FtsN (Aarsman et al., 2005). By a largely unknown process these proteins, along with other accessory proteins, then facilitate the synthesis of the new cell poles of each daughter cell (reviewed in Typas et al., 2012; Egan and Vollmer, 2013). Although different methodologies have identified a large number of interactions between divisome proteins (Egan and Vollmer, 2013), for most of these the precise interaction sites are not known. Moreover, while the cellular copy number of some but not all divisome proteins have been reported over the years, the stoichiometry of proteins within the divisome is not known.

A recent study by Li et al. (2014) used ribosome profiling/footprinting to evaluate the genome-wide absolute protein synthesis rates and protein copy numbers in *E. coli*. Interestingly, they observed proportional synthesis of proteins present in multiprotein complexes. Proteins of 59 out of 64 cytosolic and membrane complexes (92%) with known stoichiometry were found to be synthesized proportionally to their stoichiometry. Based on this principle of proportional synthesis of proteins participating in complexes, and using the protein synthesis rates from Li et al. (2014), we suggest a hypothetical model for the core divisome complex in *E. coli* factoring in known protein–protein interactions. From this hypothetical stoichiometry model we suggest possible aspects of the mechanisms for PG synthesis during division.

Using the Ratios of Division Proteins to Suggest a Stoichiometry for the Complex

Our aim here was to model the complex formed by the late division proteins and FtsA, without FtsZ and other cytoplasmic or accessory components. PBP3 is the monofunctional peptidoglycan transpeptidase (TPase) essential for cell division in *E. coli* (Weiss et al., 1997), and there is no evidence that PBP3 is active elsewhere in the cell other than the division site. We therefore surmised PBP3 is a reasonable choice for use as the reference point for our considerations on divisome stoichiometry. To this end we calculated the ratios of absolute synthesis rates of each of the *E. coli* cell division proteins (FtsA, FtsK, FtsQ, FtsL, FtsB, PBP3 (*ftsI*), FtsW, FtsN, and PBP1B; Li et al., 2014) to the synthesis rate of PBP3 for cells grown in both minimal and complete media (MOPS media with either full or minimal supplement; **Table 1**). The ratios are similar at both conditions except for PBP1B and its interacting protein FtsN (Müller et al., 2007) which are both slightly more abundant in complete media for unknown reason. This increased abundance may reflect the fact that PBP1B is able to function outside of the divisome, presumably in cell elongation. PBP1B has been shown to be functionally redundant with the other major PG synthase of *E. coli*, PBP1A (Yousif et al., 1985; Denome et al., 1999). FtsN interacts with PBP1B in non-dividing cells (Müller et al., 2007) and hence might be associated with PBP1B at all times. An apparent disparity in synthesis rate was seen with the OM lipoprotein regulator of PBP1B, LpoB, which is in sixfold or fourfold excess over its cognate synthase in minimal and compete media, respectively. It was previously shown that PBP1B and LpoB proteins interact with a 1:1 stoichiometry (Egan et al., 2014). The reason for the excess of LpoB is unknown, but may be of regulatory consequence. LpoB is absolutely essential for PBP1B function in the cell (Paradis-Bleau et al., 2010; Typas et al., 2010), therefore, an excess of LpoB may increase the likelihood that PBP1B can be activated. However, we cannot exclude other mechanisms including, for example, enhanced turnover of LpoB in the cell, necessitating higher synthesis.

PBP3 interacts with PBP1B and both form, and are likely functional as, homodimers (Zijderveld et al., 1991; Bertsche et al., 2005, 2006; Sauvage et al., 2014). We therefore assume that there are two molecules of PBP3 and two molecules of PBP1B present in a functional peptidoglycan synthesis unit (or complex). Interestingly, most other late division proteins (except FtsK, FtsL, and FtsN) had ratios of approximately 1:1 with PBP3 and PBP1B. FtsL, whose ratio to PBP3 is 1.4:1, is part of the FtsQLB complex within the divisome (Buddelmeijer and Beckwith, 2004). FtsL is unstable in the absence of FtsB in both *B. subtilis* and *E. coli* (Daniel and Errington, 2000; Buddelmeijer et al., 2002), and FtsQ, FtsL, and FtsB appear to interact in equimolar stoichiometry; different models suggest a 1:1:1 or a 2:2:2 complex (Masson et al., 2009; Villanelo et al., 2011). We therefore assume two molecules FtsL per complex, equivalent to FtsQ and FtsB.

FtsN has been previously shown to self-associate (Di Lallo et al., 1999), but there are no published data on the stoichiometry of its interactions with PBP1B and PBP3 (Wissel and Weiss, 2004; Müller et al., 2007). Given its ratio of 2:1 to PBP3 (and PBP1B) FtsN may exist in the divisome as a tetramer, or as two separate dimers. FtsN is the last essential protein recruited to mid-cell, and its absence leads to the delocalization of the already assembled divisome components (Rico et al., 2010). Recent evidence suggests that FtsN is the ultimate regulator of septal PG synthesis. In addition to its interactions with PBP3 and PBP1B, FtsN interacts directly with the early divisome protein FtsA (Busiek et al., 2012). This interaction is thought to provide the final signal for the beginning of constrictive PG synthesis through both FtsA and the FtsQLB complex. It was recently shown that point mutations in *ftsA*, *ftsL*, and *ftsB* can bypass the need for FtsN and the altered proteins acted synergistically to restore cell division in the absence of FtsN, suggesting that FtsN signals for constriction via these proteins (Liu et al., 2015; Weiss, 2015). Of note, the copy number of ∼4500 FtsN molecules per cell determined previously by immunodetection (Ursinus et al., 2004) is significantly higher than the 260 (MOPS minimal)/870 (MOPS complete) molecules per cell determined by ribosome profiling (Li et al., 2014), suggesting that FtsN numbers might vary with strain and growth conditions, which were different in both studies.

FtsK is the first of the "late" divisome proteins, bridging the PG synthetic and cytoskeletal parts of the complex through interactions with FtsA and FtsQ (Chen and Beckwith, 2001; Buddelmeijer and Beckwith, 2004; Aarsman et al., 2005). FtsK has two domains, an N-terminal domain anchored in the inner membrane (IM) which is essential for cell division (Grenga et al., 2008; Dubarry et al., 2010) and a cytoplasmic C-terminal domain which hexamerizes to form a directional DNA pump to resolve chromosome dimers, which is essential in cells with catenated sister chromosomes (Aussel et al., 2002). These domains are linked by a 600 residue long flexible region (Löwe et al., 2008). A specific mutation in *ftsA* or overproduction of *ftsQ, ftsA*, and *ftsZ* can partially compensate for the loss of *ftsK*, suggesting that the essential role of FtsK in cell division may be ensuring divisome stability or spatial regulation (Geissler and Margolin, 2005). The N-terminal domain of FtsK was shown to form hexamers independently of the C-terminal domain and exist as such at midcell (Bisicchia et al., 2013). The mid-cell of predivisional or dividing cells contained 1–8 (average of 7) hexamers of FtsK (Bisicchia et al., 2013). The ratio of FtsK to PBP3 is 1.5:1, suggesting that there are three molecules of FtsK for every two of PBP3 and thus three FtsK molecules per complex. Therefore, the FtsK homohexamer appears to interact with two complexes. We therefore suggest that FtsK spatially co-ordinates two of the peptidoglycan synthesis complexes, which we term "synthesis nodes," with the FtsZ-FtsA cytoskeletal structures in the cytoplasm.

Figure 1A shows our hypothetical model for core divisome stoichiometry based on the determined protein ratios. The protein ratios suggest that there are two peptidoglycan synthesis nodes associated with an FtsK hexamer, when three may well be able to associate. The complex is likely highly dynamic, coalescing and dissociating repeatedly in the cell for separate rounds of PG synthesis. Remarkably, such a complex has a total of 42 membrane proteins together containing as many as 92 transmembrane helices. Hence, the impact of these on membrane properties is likely to be profound. Moreover, the divisome complex is likely to be even larger because we have not included accessory divisome components such as FtsEX, FtsP, ZipA or the peptidoglycan hydrolases.

Constrictive PG Synthesis by the Divisome

At given conditions the cell maintains a constant diameter during growth, prior to division (Koch, 1995; Höltje, 1998). Presumably, the elongasome complex operates to robustly maintain cell diameter and rod-shape. In contrast, the divisome employs a constrictive mode of PG synthesis during cell division to produce the new cell poles, altering the architecture of the cell envelope. There are parallels between the divisome and elongasome in terms of their constituent proteins (Typas et al., 2012), and it was recently suggested that the divisome has evolved from the elongasome (Szwedziak and Löwe, 2013). Both contain class A and class B PBPs, a SEDS protein implicated in lipid II flippase activity (Mohammadi et al., 2011) and IM proteins which are likely required for spatial coordination and proper complex assembly. FtsK and FtsQLB are key components of the divisome with no known analog in the elongasome. They could be in part responsible for mediating constrictive peptidoglycan synthesis, ultimately driven by FtsZ dynamics.

After modeling a potential stoichiometry of the divisome we attempted to reconcile how the peptidoglycan machinery may function. According to our stoichiometry model the whole complex with two nodes would theoretically be capable of synthesizing four glycan chains and it has eight transpeptidase active sites. The latter can link the new glycan chains with each other and attach them to the existing sacculus. Given that the cell produces two identical new cell poles for each daughter we extend Höltje's (1998) three-for-one model for the divisome. We suggest that each synthesis node works to produce and attach two new strands at two docking strands situated either side of another strand, coordinated spatially by FtsK and ultimately the cytoskeletal proteins. As with Höltje's (1998) model the hydrolysis of the docking strands allows for the insertion of the new strands into the existing layer, to progress the septum closure. Indeed, elegant labeling experiments showed that 30–50% of the newly synthesized PG is removed simultaneously or shortly after it is incorporated into the new septum (Uehara and Park, 2008). The insertion of new material and the inward growth of the septum occurs in a symmetrical pattern (**Figure 1B**). This mechanism also accounts for the aberrant septation observed in certain peptidoglycan hydrolase mutants. *E. coli* cells deficient in *N*-acetylmuramyl-L-alanine amidases undergo cytokinesis and form septal PG between two daughter cells, but are unable to separate from each other due to the defect in cleavage of this septal PG (Heidrich et al., 2001). This observation can be explained by successive deposition of new septal PG without removal of the docking strands.

What drives constrictive peptidoglycan synthesis during division? A current model is that the FtsZ cytoskeletal ring, the assembly of which represents the first stage in the division process

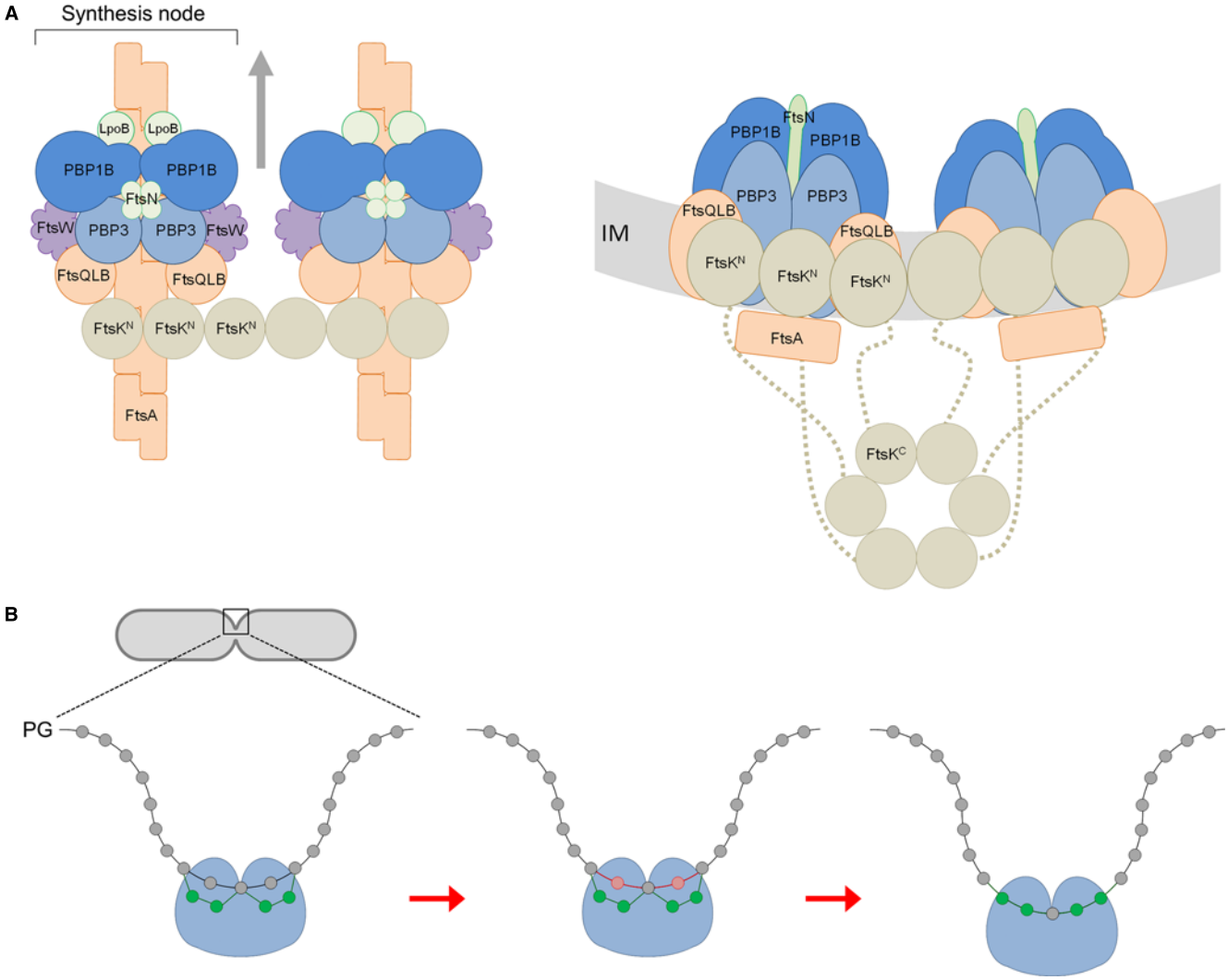

FIGURE 1 | A model for the divisome stoichiometry and its potential mechanism of action. (A) Proposed divisome complex with stoichiometry according to protein synthesis rates. Left: view from above, without the inner membrane (IM). Right: side view, including the C-terminal domain of FtsK and flexible linker region (dashed line). Proteins are represented as colored spheres/ovals; synthases (PBP1B and PBP3) in blue, regulators (LpoB, FtsN) in green, lipid II flippase (FtsW) in purple, and other core proteins in orange (FtsQLB, FtsA) or brown (FtsK). Proteins are shown roughly to scale with known protein–protein interactions accommodated (summarized in Egan and Vollmer, 2013). In this snap-shot of the dynamic machinery two PG synthesis nodes are co-ordinated with FtsA filaments and an FtsK hexamer. We have not attempted to reconcile FtsZ, ZipA, or Zap proteins for simplicity. The arrows indicate the direction of complex movement and glycan chain synthesis. **(B)** View of PG synthesis from the perpendicular axis of the cell. The divisome complex, featuring two synthesis nodes coordinated by FtsK and the cytoskeletal proteins is shown as a single entity for simplicity (blue ball). Each synthesis node produces and cross-links two new glycan strands to the existing sacculus either side of a central strand. These four new glycans (shown in green) are synthesized and attached beneath two existing (docking) strands (shown in red) adjacent to the this central strand, which are simultaneously removed through the action of PG hydrolases as first proposed by Höltje (1998).

(Bi and Lutkenhaus, 1991), exerts a constrictive force on the IM under consumption of guanosine triphosphate (GTP) (reviewed in Erickson et al., 2010; Meier and Goley, 2014). In support of this a membrane-anchored version of FtsZ alone was able to produce visible invaginations in tubular unilaminar vesicles in the presence of GTP, but it could not produce sufficient force for full constriction (Osawa et al., 2009). It is thought that the switch of FtsZ filaments from straight to curved conformations is the basis for constriction (Erickson et al., 2010). However, calculations based on the structural models of FtsZ filaments estimate the minimum diameter the Z-ring could achieve is between 50 and 250 nm, when considering additional factors such as the structures of FtsZ's membrane anchors FtsA and ZipA. Neither diameter would allow for complete scission of the cell (Erickson et al., 2010). Thus, it was suggested that PG synthesis may contribute to the constrictive force in the later stages of cytokinesis (Joseleau-Petit et al., 2007; Erickson et al., 2010). This is consistent with the fact that efficient constriction only begins after the divisome has matured through the recruitment of FtsK and the other late division proteins (Aarsman et al., 2005), but is hardly

occurring when the fully assembled FtsZ ring is still associated with the elongasome during pre-septal PG synthesis (de Pedro et al., 1997; Typas et al., 2012; van der Ploeg et al., 2013). The question of how PG synthesis by the divisome may contribute to constriction remains unclear. However, it is a reasonable assumption that the expansion of the septal PG due to the incorporation of new material at the tip of the inward growing septum exerts some force on other parts of the cell envelope.

In summary, we have modeled the stoichiometry of the complex responsible for peptidoglycan synthesis during division based on the average copy numbers of the core proteins in the cell and known interactions. We have assumed that the synthesis of the proteins within the complex is proportional, as observed in ~90% of known complexes of *E. coli*. However, we are aware that in the cell the divisome is likely to be highly dynamic, thus our model represents a single view of one of the core complexes, presumably its final assembly state. From this model we propose an update to Höltje's (1998) three-for-one model with regard to the functioning divisome, such that four strands are simultaneously incorporated while two are removed. We expect that our hypothetical model will be tested and improved in the coming years, as our understanding of the divisome's constituent proteins deepens.

Acknowledgment

This work was supported by the Wellcome Trust [101824/Z/13/Z].

References

Aarsman, M. E. G., Piette, A., Fraipont, C., Vinkenvleugel, T. M. F., Nguyen-Distèche, M., and den Blaauwen, T. (2005). Maturation of the *Escherichia coli* divisome occurs in two steps. *Mol. Microbiol.* 55, 1631–1645. doi: 10.1111/j.1365-2958.2005.04502.x

Aussel, L., Barre, F. X., Aroyo, M., Stasiak, A., Stasiak, A. Z., and Sherratt, D. (2002). FtsK is a DNA motor protein that activates chromosome dimer resolution by switching the catalytic state of the XerC and XerD recombinases. *Cell* 108, 195–205. doi: 10.1016/S0092-8674(02)00624-4

Bertsche, U., Breukink, E., Kast, T., and Vollmer, W. (2005). *In vitro* murein peptidoglycan synthesis by dimers of the bifunctional transglycosylase-transpeptidase PBP1B from *Escherichia coli*. *J. Biol. Chem.* 280, 38096–38101. doi: 10.1074/jbc.M508646200

Bertsche, U., Kast, T., Wolf, B., Fraipont, C., Aarsman, M. E. G., Kannenberg, K., et al. (2006). Interaction between two murein (peptidoglycan) synthases, PBP3 and PBP1B, in *Escherichia coli*. *Mol. Microbiol.* 61, 675–690. doi: 10.1111/j.1365-2958.2006.05280.x

Bi, E., and Lutkenhaus, J. (1991). FtsZ ring structure associated with division in *Escherichia coli*. *Nature* 354, 161–164. doi: 10.1038/354161a0

Bisicchia, P., Steel, B., Debela, M. H. M., Löwe, J., and Sherratt, D. (2013). The N-terminal membrane-spanning domain of the *Escherichia coli* DNA translocase FtsK hexamerizes at midcell. *MBio* 4, e00800-13. doi: 10.1128/mBio.00800-13

Buddelmeijer, N., and Beckwith, J. (2004). A complex of the *Escherichia coli* cell division proteins FtsL, FtsB and FtsQ forms independently of its localization to the septal region. *Mol. Microbiol.* 52, 1315–1327. doi: 10.1111/j.1365-2958.2004.04044.x

Buddelmeijer, N., Judson, N., Boyd, D., Mekalanos, J. J., and Beckwith, J. (2002). YgbQ, a cell division protein in *Escherichia coli* and *Vibrio cholerae*, localizes in co-dependent fashion with FtsL to the division site. *Proc. Natl. Acad. Sci. U.S.A.* 99, 6316–6321. doi: 10.1073/pnas.092128499

Busiek, K. K., Eraso, J. M., Wang, Y., and Margolin, W. (2012). The early divisome protein FtsA interacts directly through its 1c subdomain with the cytoplasmic domain of the late divisome protein FtsN. *J. Bacteriol.* 194, 1989–2000. doi: 10.1128/JB.06683-11

Chen, J. C., and Beckwith, J. (2001). FtsQ, FtsL and FtsI require FtsK, but not FtsN, for co-localization with FtsZ during *Escherichia coli* cell division. *Mol. Microbiol.* 42, 395–413. doi: 10.1046/j.1365-2958.2001.02640.x

Daniel, R. A., and Errington, J. (2000). Intrinsic instability of the essential cell division protein FtsL of *Bacillus subtilis* and a role for DivIB protein in FtsL turnover. *Mol. Microbiol.* 36, 278–289. doi: 10.1046/j.1365-2958.2000.01857.x

Denome, S. A., Elf, P. K., Henderson, T. A., Nelson, D. E., and Young, K. D. (1999). *Escherichia coli* mutants lacking all possible combinations of eight penicillin binding proteins: viability, characteristics, and implications for peptidoglycan synthesis. *J. Bacteriol.* 181, 3981–3993.

de Pedro, M. A., Quintela, J. C., Höltje, J. V., and Schwarz, H. (1997). Murein segregation in *Escherichia coli*. *J. Bacteriol.* 179, 2823–2843.

Di Lallo, G., Ghelardini, P., and Paolozzi, L. (1999). Two-hybrid assay: construction of an *Escherichia coli* system to quantify homodimerization ability *in vivo*. *Microbiology* 145, 1485–1490. doi: 10.1099/13500872-145-6-1485

Dubarry, N., Possoz, C., and Barre, F.-X. (2010). Multiple regions along the *Escherichia coli* FtsK protein are implicated in cell division. *Mol. Microbiol.* 78, 1088–1100. doi: 10.1111/j.1365-2958.2010.07412.x

Egan, A. J. F., Jean, N. L., Kumoutsi, A., Bougault, C. M., Biboy, J., Sassine, J., et al. (2014). Outer-membrane lipoprotein LpoB spans the periplasm to stimulate the peptidoglycan synthase PBP1B. *Proc. Natl. Acad. Sci. U.S.A.* 111, 8197–8202. doi: 10.1073/pnas.1400376111

Egan, A. J. F., and Vollmer, W. (2013). The physiology of bacterial cell division. *Ann. N. Y. Acad. Sci.* 1277, 8–28. doi: 10.1111/j.1749-6632.2012.06818.x

Erickson, H. P., Anderson, D. E., and Osawa, M. (2010). FtsZ in bacterial cytokinesis: cytoskeleton and force generator all in one. *Microbiol. Mol. Biol. Rev.* 74, 504–528. doi: 10.1128/MMBR.00021-10

Geissler, B., and Margolin, W. (2005). Evidence for a functional overlap among multiple bacterial cell division proteins: compensating for the loss of FtsK. *Mol. Microbiol.* 58, 596–612. doi: 10.1111/j.1365-2958.2005.04858.x

Goodell, E. W. (1985). Recycling of murein by *Escherichia coli*. *J. Bacteriol.* 163, 305–310.

Grenga, L., Luzi, G., Paolozzi, L., and Ghelardini, P. (2008). The *Escherichia coli* FtsK functional domains involved in its interaction with its divisome protein partners. *FEMS Microbiol. Lett.* 287, 163–167. doi: 10.1111/j.1574-6968.2008.01317.x

Heidrich, C., Templin, M. F., Ursinus, A., Merdanovic, M., Berger, J., Schwarz, H., et al. (2001). Involvement of *N*-acetylmuramyl-L-alanine amidases in cell separation and antibiotic-induced autolysis of *Escherichia coli*. *Mol. Microbiol.* 41, 167–178. doi: 10.1046/j.1365-2958.2001.02499.x

Höltje, J.-V. (1998). Growth of the stress-bearing and shape-maintaining murein sacculus of *Escherichia coli*. *Microbiol. Mol. Biol. Rev.* 62, 181–203.

Joseleau-Petit, D., Liébart, J.-C., Ayala, J. A., and D'Ari, R. (2007). Unstable *Escherichia coli* L forms revisited: growth requires peptidoglycan synthesis. *J. Bacteriol.* 189, 6512–6520. doi: 10.1128/JB.00273-07

Koch, A. L. (1995). *Bacterial Growth and Form*. New York, NY: Chapman & Hall.

Li, G.-W., Burkhardt, D., Gross, C., and Weissman, J. S. (2014). Quantifying absolute protein synthesis rates reveals principles underlying allocation of cellular resources. *Cell* 157, 624–635. doi: 10.1016/j.cell.2014.02.033

Liu, B., Persons, L., Lee, L., and de Boer, P. A. J. (2015). Roles for both FtsA and the FtsBLQ subcomplex in FtsN-stimulated cell constriction in *Escherichia coli*. *Mol. Microbiol.* doi: 10.1111/mmi.12906 [Epub ahead of print].

Löwe, J., Ellonen, A., Allen, M. D., Atkinson, C., Sherratt, D. J., and Grainge, I. (2008). Molecular mechanism of sequence-directed DNA loading and translocation by FtsK. *Mol. Cell* 31, 498–509. doi: 10.1016/j.molcel.2008.05.027

Margolin, W. (2005). FtsZ and the division of prokaryotic cells and organelles. *Nat. Rev. Mol. Cell Biol.* 6, 862–871. doi: 10.1038/nrm1745

Masson, S., Kern, T., Le Gouëllec, A., Giustini, C., Simorre, J.-P., Callow, P., et al. (2009). Central domain of DivIB caps the C-terminal regions of the FtsL/DivIC coiled-coil rod. *J. Biol. Biochem.* 284, 27687–27700. doi: 10.1074/jbc.M109.019471

Meier, E. L., and Goley, E. D. (2014). Form and function of the bacterial cytokinetic ring. *Curr. Opin. Cell Biol.* 26, 19–27. doi: 10.1016/j.ceb.2013.08.006

Mohammadi, T., van Dam, V., Sijbrandi, R., Vernet, T., Zapun, A., Bouhss, A., et al. (2011). Identification of FtsW as a transporter of lipid-linked cell wall precursors across the membrane. *EMBO J.* 30, 1425–1432. doi: 10.1038/emboj.2011.61

Müller, P., Ewers, C., Bertsche, U., Anstett, M., Kallis, T., Breukink, E., et al. (2007). The essential cell division protein FtsN interacts with the murein (peptidoglycan) synthase PBP1B in *Escherichia coli*. *J. Biol. Chem.* 282, 36394–36402. doi: 10.1074/jbc.M706390200

Osawa, M., Anderson, D. E., and Erickson, H. P. (2009). Curved FtsZ protofilaments generate bending forces on liposome membranes. *EMBO J.* 28, 3476–3484. doi: 10.1038/emboj.2009.277

Paradis-Bleau, C., Markovski, M., Uehara, T., Lupoli, T. J., Walker, S., Kahne, D. E., et al. (2010). Lipoprotein cofactors located in the outer membrane activate bacterial cell wall polymerases. *Cell* 143, 1110–1120. doi: 10.1016/j.cell.2010.11.037

Rico, A. I., García-Ovalle, M., Palacios, P., Casanova, M., and Vicente, M. (2010). Role of *Escherichia coli* FtsN protein in the assembly and stability of the cell division ring. *Mol. Microbiol.* 76, 760–771. doi: 10.1111/j.1365-2958.2010.07134.x

Sauvage, E., Derouaux, A., Fraipont, C., Joris, M., Herman, R., Rocaboy, M., et al. (2014). Crystal structure of penicillin-binding protein 3 (PBP3) from *Escherichia coli*. *PLoS ONE* 9:e98042. doi: 10.1371/journal.pone.0098042

Szwedziak, P., and Löwe, J. (2013). Do the divisome and elongasome share a common evolutionary past? *Curr. Opin. Microbiol.* 16, 745–751. doi: 10.1016/j.mib.2013.09.003

Typas, A., Banzhaf, M., van den Berg van Saparoea, B., Verheul, J., Biboy, J., Nichols, R. J., et al. (2010). Regulation of peptidoglycan synthesis by outer-membrane proteins. *Cell* 143, 1097–1109. doi: 10.1016/j.cell.2010.11.038

Typas, A., Banzhaf, M., Gross, C. A., and Vollmer, W. (2012). From the regulation of peptidoglycan synthesis to bacterial growth and morphology. *Nat. Rev. Microbiol.* 10, 123–136. doi: 10.1038/nrmicro2677

Uehara, T., and Park, J. T. (2008). Growth of *Escherichia coli*: significance of peptidoglycan degradation during elongation and septation. *J. Bacteriol.* 190, 3914–3922. doi: 10.1128/JB.00207-08

Ursinus, A., Van den Ent, F., Brechtel, S., de Pedro, M., Höltje, J.-V., Lowe, J., et al. (2004). Murein (peptidoglycan) binding property of the essential cell division protein FtsN from *Escherichia coli*. *J. Bacteriol.* 186, 6728–6737. doi: 10.1128/JB.186.20.6728-6737.2004

van der Ploeg, R., Verheul, J., Vischer, N. O. E., Alexeeva, S., Hoogendoorn, E., Postma, M., et al. (2013). Colocalization and interaction between elongasome and divisome during a preparative cell division phase in *Escherichia coli*. *Mol. Microbiol.* 87, 1074–1087. doi: 10.1111/mmi.12150

Villanelo, F., Ordenes, A., Brunet, J., Lagos, R., and Monasterio, O. (2011). A model for the *Escherichia coli* FtsB/FtsL/FtsQ cell division complex. *BMC Struct. Biol.* 11:28. doi: 10.1186/1472-6807-11-28

Weidel, W., and Pelzer, H. (1964). Bagshaped macromolecules—a new outlook on bacterial cell walls. *Adv. Enzymol. Relat. Areas Mol. Biol.* 26, 193–232.

Weiss, D. S. (2015). Last but not least: new insights into how FtsN triggers constriction during *Escherichia coli* cell division. *Mol. Microbiol.* 95, 903–909. doi: 10.1111/mmi.12925

Weiss, D. S., Pogliano, K., Carson, M., Guzman, L. M., Fraipont, C., Nguyen-Distèche, M., et al. (1997). Localization of the *Escherichia coli* cell division protein Ftsl (PBP3) to the division site and cell pole. *Mol. Microbiol.* 4, 671–681. doi: 10.1046/j.1365-2958.1997.5041869.x

Wissel, M. C., and Weiss, D. S. (2004). Genetic analysis of the cell division protein FtsI (PBP3): amino acid substitutions that impair septal localization of FtsI and recruitment of FtsN. *J. Bacteriol.* 186, 490–502. doi: 10.1128/JB.186.2.490-502.2004

Yousif, S. Y., Broome-Smith, J. K., and Spratt, B. G. (1985). Lysis of *Escherichia coli* by β-Lactam antibiotics: deletion analysis of the role of penicillin-binding proteins 1A and 1B. *J. Gen. Microbiol.* 131, 2839–2845. doi: 10.1099/00221287-131-10-2839

Zijderveld, C. A., Aarsman, M. E., den Blaauwen, T., and Nanninga, N. (1991). Penicillin-binding protein 1B of *Escherichia coli* exists in dimeric forms. *J. Bacteriol.* 173, 5740–5746.

Conflict of Interest Statement: The authors declare that the research was conducted in the absence of any commercial or financial relationships that could be construed as a potential conflict of interest.

Copyright © 2015 Egan and Vollmer. This is an open-access article distributed under the terms of the Creative Commons Attribution License (CC BY). The use, distribution or reproduction in other forums is permitted, provided the original author(s) or licensor are credited and that the original publication in this journal is cited, in accordance with accepted academic practice. No use, distribution or reproduction is permitted which does not comply with these terms.

frontiers in Microbiology

ORIGINAL RESEARCH
published: 11 June 2015
doi: 10.3389/fmicb.2015.00586

Cell age dependent concentration of *Escherichia coli* divisome proteins analyzed with ImageJ and ObjectJ

Norbert O. E. Vischer[1], Jolanda Verheul[1], Marten Postma[1,2], Bart van den Berg van Saparoea[1,3], Elisa Galli[4], Paolo Natale[5], Kenn Gerdes[4,6], Joen Luirink[3], Waldemar Vollmer[4], Miguel Vicente[5] and Tanneke den Blaauwen[1]**

[1] Bacterial Cell Biology, Swammerdam Institute for Life Sciences, Faculty of Science, University of Amsterdam, Amsterdam, Netherlands, [2] Molecular Cytology, Swammerdam Institute for Life Sciences, Faculty of Sciences, University of Amsterdam, Amsterdam, Netherlands, [3] Department of Molecular Microbiology, Institute of Molecular Cell Biology, VU University, Amsterdam, Netherlands, [4] Centre for Bacterial Cell Biology, Institute for Cell and Molecular Biosciences, Newcastle University, Newcastle upon Tyne, UK, [5] Centro Nacional de Biotecnología-Consejo Superior de Investigaciones Científicas, Madrid, Spain, [6] Department of Biology, University of Copenhagen, Copenhagen, Denmark

The rod-shaped Gram-negative bacterium *Escherichia coli* multiplies by elongation followed by binary fission. Longitudinal growth of the cell envelope and synthesis of the new poles are organized by two protein complexes called elongasome and divisome, respectively. We have analyzed the spatio-temporal localization patterns of many of these morphogenetic proteins by immunolabeling the wild type strain MC4100 grown to steady state in minimal glucose medium at 28°C. This allowed the direct comparison of morphogenetic protein localization patterns as a function of cell age as imaged by phase contrast and fluorescence wide field microscopy. Under steady state conditions the age distribution of the cells is constant and is directly correlated to cell length. To quantify cell size and protein localization parameters in 1000s of labeled cells, we developed 'Coli-Inspector,' which is a project running under ImageJ with the plugin 'ObjectJ.' ObjectJ organizes image-analysis tasks using an integrated approach with the flexibility to produce different output formats from existing markers such as intensity data and geometrical parameters. ObjectJ supports the combination of automatic and interactive methods giving the user complete control over the method of image analysis and data collection, with visual inspection tools for quick elimination of artifacts. Coli-inspector was used to sort the cells according to division cycle cell age and to analyze the spatio-temporal localization pattern of each protein. A unique dataset has been created on the concentration and position of the proteins during the cell cycle. We show for the first time that a subset of morphogenetic proteins have a constant cellular concentration during the cell division cycle whereas another set exhibits a cell division cycle dependent concentration variation. Using the number of proteins present at midcell, the stoichiometry of the divisome is discussed.

Keywords: non-destructive marking, divisome, image analysis, immunolocalization, FtsZ, PBP1B, LpoA, FtsN

OPEN ACCESS

Edited by:
Jaan Männik, University of Tennessee, USA

Reviewed by:
Jodi L. Camberg, University of Rhode Island, USA
Jie Xiao, Johns Hopkins School of Medicine, USA

****Correspondence:***
Norbert O. E. Vischer and Tanneke den Blaauwen, Bacterial Cell Biology, Swammerdam Institute for Life Sciences, Faculty of Science, University of Amsterdam, Science Park, 1098 XH Amsterdam, P. O. Box 94323, 1090 GE Amsterdam, Netherlands
n.o.e.vischer@uva.nl; t.denblaauwen@uva.nl

Specialty section:
This article was submitted to Microbial Physiology and Metabolism, a section of the journal Frontiers in Microbiology

Received: *28 January 2015*
Accepted: *28 May 2015*
Published: *11 June 2015*

Citation:
Vischer NOE, Verheul J, Postma M, van den Berg van Saparoea B, Galli E, Natale P, Gerdes K, Luirink J, Vollmer W, Vicente M and den Blaauwen T (2015) Cell age dependent concentration of Escherichia coli divisome proteins analyzed with ImageJ and ObjectJ. Front. Microbiol. 6:586. doi: 10.3389/fmicb.2015.00586

Introduction

Escherichia coli is a Gram-negative rod shaped bacterium that divides by binary fission. The new daughter cells will first elongate in length before a new division cycle is initiated at a cell age dependent on cell mass (Taheri-Araghi et al., 2015). Consequently, fast growing cells that are much longer than slowly growing cells initiate division almost immediately after birth. Large protein complexes that are termed elongasome and divisome synthesize and hydrolyze peptidoglycan during cell elongation and cell division, respectively (Egan and Vollmer, 2013; van der Ploeg et al., 2013). These protein complexes share some of their proteins (Mohammadi et al., 2007; White et al., 2010; van der Ploeg et al., 2013), and many of the proteins have their own enzymatic activities, which categorize the elongasome and divisome as hyperstructures (Norris et al., 2007). These hyperstructures are not assembled and then kept stable like the ribosomes, they are rather dynamic and can associate cell cycle dependent. It is therefore relevant for the understanding of the organization of both processes to determine their composition and cellular localization as a function of the bacterial cell division cycle age (cell age).

Observing Cells in Steady-State Growth

Escherichia coli grows exponentially making it possible to access cell age dependent information without the need for synchronizing the cells. In liquid medium growing cells that are repeatedly diluted in pre-warmed medium at an early exponential phase will develop a constant metabolism (Dennis and Bremer, 1974). From then on, the number of cells in the culture will increase just as fast as the total mass or optical density of the cells in the culture. As a result, both the average mass of the cells in the culture and their age frequency distribution, are constant, the hallmarks of steady state growth. Because the *E. coli* cell diameter is constant, it is possible to determine the age of an individual cell by its length. High quality phase contrast imaging in combination with image analysis allows the conversion of a length distribution to an age distribution of large numbers of cells comprising all ages. Precise spatio-temporal information on bacterial proteins during the cell cycle can be obtained using specific antibodies conjugated to fluorophores.

Coli-Inspector

A specialized software project (Coli-Inspector) was developed for the analysis of the morphometrical and fluorescence related properties of the immunolabeled proteins. Measurements included cell length, cell diameter, constriction sites, and spatial distribution of fluorescence along the cell axis. This information is extracted from sets of phase contrast and fluorescence images that are organized as hyperstacks. In order to acquire and manage this multitude of parameters across many images in an integrated way, we used ImageJ (Schneider et al., 2012) in combination with the ObjectJ plug-in.

ObjectJ focuses on the organization of image-analysis tasks using an integrated approach. Central to a task is a project file that dynamically links all related components together: a user-defined palette for non-destructive markers, color-coded hierarchical vector objects across many images that are linked to the project, qualifiers for creating subsets of results, and the macros that are in use. The project stores all previous analysis results and at any time the user has the flexibility to extract different sets of results from marked locations such as intensities and spatial parameters.

An important feature ensures that every step during the analysis is clearly visualized with the possibility to intercept or override automatic methods, which helps to eliminate artifacts at an early stage.

ObjectJ helps to keep the desktop clean by integrating all relevant information in the project file instead of creating additional files. In most cases, graphs and numerical output can be displayed transiently from the newest data set without the need to send files to an external (spread sheet) program, which means that the interconnection of cell data and their link to the images remains intact.

A special feature of Coli-Inspector is the creation of profile maps (**Figure 1**, Panel 5), which visualizes the spatio-temporal distribution and correlation of different fluorophores along the cell axis. Optionally, the profile map can arrange profiles for each cell in a way that the pole with the stronger fluorescence in the "leader channel" always points to the same side (**Figure 3**). Fluorescence in any other channel ("follower channel") is not correlated if the collective distribution along the cell axis remains symmetrical due to the random orientation during acquisition. This is illustrated by the immunolabeled Min system that prevents polar divisions.

Protein Localization Analysis

The Coli-Inspector project was tailored for spatio-temporal protein localization analysis and is, like ImageJ and ObjectJ, free and open source[1]. A user manual is available online.

Using the Coli-Inspector project, we determined the localization of PBP1B, PBP1A, PBP3, PBP5, LpoB, LpoA, FtsB, FtsK, FtsN, FtsZ, ZapA, ZapB, ZipA, MinC, and MinD as a function of cell age in the wild type strain MC4100 grown in minimal glucose medium at 28°C. All data are directly comparable because the cells were grown to the same steady state. Since every medium and growth temperature results in a different steady state, the timing of protein localization cannot be extrapolated to other growth rates and conditions. However, the general organization of morphogenesis is probably similar under at least a variety of laboratory conditions.

Using the steady state cell growth approach, we have previously shown that the maturation of the divisome occurs in two clearly separated steps (den Blaauwen et al., 1999; Aarsman et al., 2005; van der Ploeg et al., 2013). In the first step, the proto-ring is assembled at midcell. The tubulin homologue FtsZ polymerizes in a ring-like structure underneath the cytoplasmic membrane at midcell. FtsA and ZipA localize simultaneously with the Z-ring (Rueda et al., 2003) and tether the Z-ring to the cytoplasmic membrane. Other proteins such as ZapA help to organize the ring during its status nascendi (Mohammadi et al., 2009; Bisicchia et al., 2013a). ZapB binds

[1]https://sils.fnwi.uva.nl/bcb/objectj/

to itself, to ZapA and to FtsZ and seems to function as a sensor between the terminal region of the chromosome and the Z-ring (Espeli et al., 2012). In the second step with some time delay (Aarsman et al., 2005), all other cell division proteins are recruited, including FtsK, PBP3, PBP1B, FtsB, and FtsN. The role of these proteins will be further discussed in the result section.

The combination of steady state growth, the fluorescent immunolabeling of endogenous proteins, and the unique features of Coli-Inspector were used in this study to assess the cellular protein concentration of the above-mentioned morphogenetic proteins as a function of the bacterial cell age. Many proteins are present at a constant cellular, not necessarily uniformly localized, concentration. Interestingly, several proteins other than FtsZ [whose transcription is known to be regulated (Garrido et al., 1993)] appear to have a varying concentration.

The recent publication of Li et al. (2014) reports the number of molecules of each protein synthesized in one generation in *E. coli* as measured by ribosome profiling. These data allowed us to convert fluorescence arbitrary units into the number of protein molecules and to determine the number of proteins at midcell for each immunolabeled divisome protein. The resulting data were used to discuss the stoichiometry of the cell envelope synthetic machinery during the constriction process.

Materials and Methods

Growth Conditions and Media

Escherichia coli K12 cells were grown to steady state in glucose minimal medium (Gb1) containing 6.33 g of $K_2HPO_4.3H_2O$, 2.95 g of KH_2PO_4, 1.05 g of $(NH_4)_2SO_4$, 0.10 g of $MgSO_4.7H_2O$, 0.28 mg of $FeSO_4.7H_2O$, 7.1 mg of $Ca(NO_3)_2.4H_2O$, 4 mg of thiamine, 4 g of glucose and 50 μg of required amino acids per liter pH 7.0 at 28°C. MC4100 (LMC500) requires Lys for growth in minimal medium. Absorbance was measured at 450 nm with a 300-T-1 spectrophotometer (Gilford Instrument Laboratories Inc.). Steady state growth was achieved by dilution of an over night culture 1:1000 in fresh prewarmed medium of 28°C. The cells were allowed to grow up to a density of 0.2 and then diluted again in prewarmed medium. This procedure was repeated during 40 generations of exponential growth. The mass doubling time of MC4100 is 80 min under these conditions. The overnight dilution was calculated using the equation: $D = 2^{t/Td}\left(\frac{OD_{now}}{OD_{des}}\right)$, where D is the required dilution of the culture to obtain the desired optical density (OD_{des}) after t minutes, and Td is the mass doubling time in min. OD_{now} is the optical density of the culture to be diluted. The steady state cultures were fixed by addition of a mixture of formaldehyde (f.c. 2.8%) and glutaraldehyde (f.c. 0.04%) to the shaking water bath. This gives an osmotic shock that does not affect the localization of membrane or cytosolic proteins (Hocking et al., 2012; van der Ploeg et al., 2013). Unfortunately, periplasmic proteins that are freely diffusing are shocked toward the poles. Therefore, the procedure is not suitable for immunolabeling of periplasmic proteins and if used, their localization pattern should be verified using fluorescent protein (FP) fusions and live imaging.

Immunolabeling

Immunolabeling of the cells was performed as described (Buddelmeijer et al., 2013). Antisera were either pre-purified using cells of a deletion strain (**Table 1**) of the particular protein against which the antiserum was directed, or the specific IgG was purified using the native protein against which it was directed (Karczmarek et al., 2007; Typas et al., 2010). In brief, formaldehyde/glutaraldehyde fixed and Tx100/lysozyme permeabilized cells were incubated for 1 h at 37°C with purified polyclonal antibodies directed against FtsK, FtsN, FtsB, FtsZ, ZipA, MinC, MinD, PBP3, PBP5, PBP1B, PBP1A, LpoB, LpoA, ZapA, all diluted in blocking buffer. ZapB was immunolabeled with Fabs conjugated to Cy3. As secondary antibody, donkey anti-rabbit conjugated to Cy3 (Jackson Immunochemistry, USA) diluted 1:300 in blocking buffer (0.5% (wt/vol) blocking reagents (Boehringer, Mannheim, Germany) in PBS) was used, and the samples were incubated for 30 min at 37°C. For immunolocalization, cells were immobilized on 1% agarose in water slabs coated object glasses as described (Koppelman et al., 2004) and photographed with a Coolsnap *fx* (Photometrics) CCD camera mounted on an Olympus BX-60 fluorescence microscope through a 100x/N.A. 1.35 oil objective. Images were taken using the program ImageJ with MicroManager[2].

Image Analysis

Phase contrast and fluorescence images were combined into hyperstacks using ImageJ[3] and these were linked to the project file of Coli-Inspector running in combination with the plugin ObjectJ[4]. The images were scaled to 14.98 pixel per μm. The fluorescence background has been subtracted using the modal values from the fluorescence images before analysis. Major analysis steps are given in the Section "Results," and the full Coli-Inspector documentation can be found at https://sils.fnwi.uva.nl/bcb/objectj/examples. Slight misalignment of fluorescence with respect to the cell contours as found in phase contrast was corrected using Fast-Fourier techniques. The fluorescence image was translated in x–y direction so that fluorescence measured under all cell contours reached a maximum[5].

Data Analysis

Cells are assumed to have rotational symmetry, where the midline as detected from the cell contour in phase contrast represents the cell axis. Partial or entire cell volume is obtained by the integration of 1-pixel-thick disks with local diameter along the cell axis. Envelope area is obtained by contour rotation. Fluorescence values are derived from the second channel of the profile map, where each cell is represented as a vector (1-pixel wide column). Each pixel contains the entire fluorescence

[2]https://www.micro-manager.org

[3]http://imagej.nih.gov/ij/

[4]https://sils.fnwi.uva.nl/bcb/objectj/

[5]https://sils.fnwi.uva.nl/bcb/objectj/examples/AlignFluorChannels/AlignFluorChannels.htm

TABLE 1 | Used strains and their genotypes.

Strain name	Characteristics	Genotype	Source
MC4100	Wild type	F$^-$, *araD139, Δ(argF-lac)U169deoC1, flbB5301, ptsF25, rbsR, relA1, rpslL150, lysA1*	Taschner et al. (1988)
BW25113	Wild type	F$^-$, *Δ(araD-araB)567, ΔlacZ4787*(::rrnB-3), *λ$^-$, rph-1, Δ(rhaD-rhaB)568, hsdR514*	Baba et al. (2006)
PA340-678	ΔMreBCD	F$^-$, *argH1, thr-1, leuB6, ghd-1, gltB31, thi-1, lacY1, gal-6, xyl-7, ara-14, mtl-2, malA1, rpsL9, tonA2*	Wachi et al. (1987)
CS12-7	ΔPBP5	W1485 *rpoS rpH dacA::kan* 512-1	Potluri et al. (2010)
LMC1084	ΔMinCDE	PB114 Δ*minB*::Km(R), *dad*R1, *trpE61, trpA62, tna5, purB,L-*$^+$	de Boer et al. (1989)
BW25113 ΔlpoA	ΔLpoA	BW25113 Δ*lpoA*	Baba et al. (2006)
BW25113 ΔlpoB	ΔLpoB	BW25113 Δ*lpoB*	Baba et al. (2006)
JW3359 mrcA	ΔPBP1A	BW25113 Δ*mrcA*	Baba et al. (2006)
JW0145 mrcB	ΔPBP1B	BW25113 ΔmrcB	Baba et al. (2006)
LMC3143	ΔZapA	LMC500 Δ*zapA*	Mohammadi et al. (2009)
MC1000 ΔZapB	ΔZapB	Δ*zapB*Δ (*ara-leu*) Δ*lac rpsL*150	Ebersbach et al. (2008)
CH5/pCH32	ZipA depletion	PB103 *zipA::aph/aadA*$^+$ *repA*(Ts) *ftsZ*$^+$*zipA*$^+$ *recA::Tn10*	Hale and de Boer (1999)

of a 1-pixel-thick disk including light detected slightly outside the contour due to the point-spread function. The sum of all vector elements (pixels) is displayed as FluorTotal. The concentration of the fluorescence per cell (ConcTotal) or the concentration in the envelope (ConcWall) was calculated by dividing the FluorTotal by either the cell volume (for FtsZ, ZapA, and ZapB), or by the envelope area for all other proteins that are cytoplasmic membrane bound or inserted. In order to relate fluorescent light quantities to absolute numbers of protein molecules, the conversion factor *F* was calculated by dividing the integrated fluorescence by the number of proteins of the average cell. The number of involved protein molecules could then be calculated for an individual cell or even a part of it. Midcell was defined as the central part of the cell comprising 0.8 μm of the axis. From either cell part, midcell and remaining cell, the volume, the integrated fluorescence, and thus the concentration of fluorophores can be calculated. The difference of the two concentrations is multiplied with the volume of midcell. It yields FCPlus (surplus of fluorescence) and, via factor *F*, MolsFCPlus (surplus of protein molecules at the cell center). These values are positive or negative for higher or lower concentrations in the center, respectively. For age calculation, all cell lengths are sorted in ascending order. Then the equation

$$\text{age} = \ln(1 - 0.5^{*}\text{rank}/(\text{nCells} - 1))/\ln(0.5)$$

is used, where *rank* is a cell's index in the sorted array, *nCells* is the total amount of cells, and *age* is the cell's age expressed in the range 0.. 1. For explanation of the most important parameters used in this study see **Table 2**.

Results and Discussion

Coli-Inspector for Multi-Parameter Image Analysis

The settings and macro commands of the Coli-Inspector project, in combination with the ObjectJ plugin, made it possible to perform a large number of different experiments, each based on multi-parameter measurements of 1000s of cells. The "Qualifying" mechanism allowed addressing subsets of cells that then could be used for selective browsing, creating plots, or identifying artifacts. ObjectJ manages the interconnection of individual data structures via the "project file" without creating auxiliary files, which keeps the desktop clean. Only the project file (".ojj" extension), together with the hyperstacks to be analyzed (linked images), need to be in the same directory. It was not necessary to rely on an external spreadsheet program, which would have disconnected the results from the marked cells in the images. Coli-Inspector's specific macro commands appear in the ObjectJ menu in approximately the order they are typically invoked.

TABLE 2 | Overview of the most important parameters used for the analysis of the spatio-temporal localization of the immunolabeled proteins.

Parameter	Description	Unit
Age	Cell age based on cell length	(0–100) %
F	Conversion factor	proteins/FluorUnit
Fluortotal	Integrated fluorescence of cell	FluorUnit
Volume	Total cell volume (sum of disk volumes)	μm^3
ConcTotal	Concentration of fluorescent material in cell volume	FluorUnit/μm^3
CellWall	Area of cell envelope	μm^2
Area	Area of cell projection (contour as obtained from phase contrast image)	μm^2
ConcWall	Concentration of fluorescent material in cell envelope	FluorUnits/μm^2
MidCell Volume	Cell compartment ± 0.4 μm from cell center	μm^3
FCPlus	Surplus of fluorescence in cell center compared to the rest of the cell	FluorUnit
MolsCPlus	Molecules in Center surplus gives the number of molecules in the cell center that are in surplus compared to the rest of the cell (calculated from FCPlus * *F*)	molecules

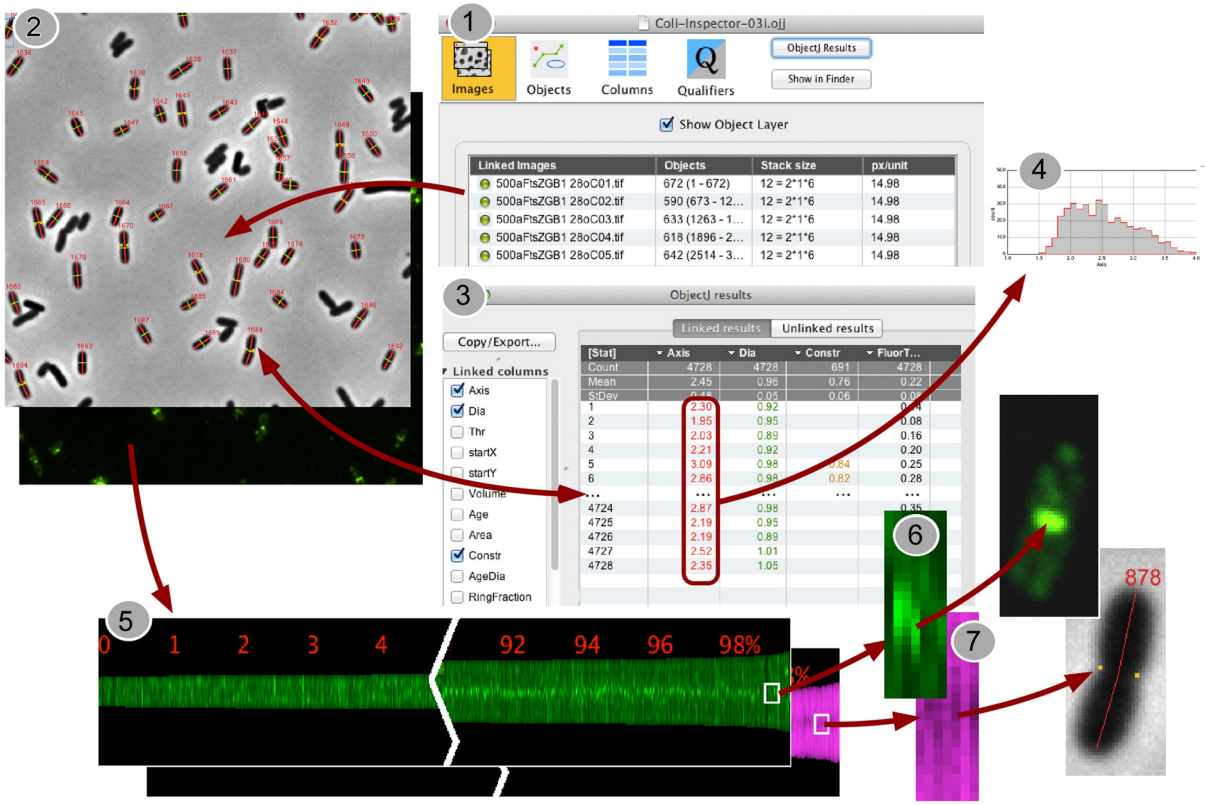

FIGURE 1 | Back-and-forth navigation between individual image processing steps. (1) In the project window "Coli-Inspector-03i.ojj," the panel for "Linked Images" is active and shows the double-clickable names of the images that are linked and thus intended to be analyzed. **(2)** Via embedded macro commands, the cells in all linked images can be marked as "composite objects," which consist of different markers for cell axes (red), cell diameters (green), and constriction sites (yellow dots). Markers are displayed transiently upon the images, while being stored and managed in the project file. **(3)** Calculated cell properties are displayed in the "ObjectJ Results Table" that is part of the project file. Each cell occupies one row. Any number of columns can be defined to store the desired morphometric or intensity related results. Result rows are bi-directionally linked to the corresponding cells for fast back-and-forth navigation. **(4)** ObjectJ result columns include column statistics and can be directly visualized as histograms. **(5)** A Map of Profiles is created that visualizes all cell profiles along their axes as 1-pixel-wide columns in a floating-point hyperstack. The height of a column corresponds to the cell length in pixels, and each pixel holds the local fluorescence (green) or the local diameter (magenta). Here, the profile map is sorted from short to long cells and, as steady state population, exponentially calibrated in age from 0 to 100%. Thus it visualizes the change of fluorescence distribution along the cell during cell cycle time (green), and the development of the constriction before the cell divides (magenta band becomes darker due to smaller diameter at the constriction site). **(6,7)** Clicking in the Map will expose the corresponding cell, which allows quickly locating artifacts or special phenomena.

When the project file is opened in ImageJ, four different panels appear and can be selected via icons: "Images," "Objects," "Columns," and "Qualifiers" (**Figure 1**, Panel 1). The image files must then be "linked" to the project, e.g., by dragging them from the project folder onto the "Images" icon or its panel. They must be 3D or 4D hyperstacks, where the third dimension contains "channels" for phase-contrast and fluorescence images (**Figure 1**, Panel 2). In the fourth dimension, different field views can be stored as "frames." Scaling is required in pixels per micrometer. This information is reflected in the "Images" panel under "stack size" and "px/unit," respectively. The images in the downloadable example project conform to these requirements.

Analysis of Cells

Typically, the user starts with the command "Mark Filaments" and checks whether rejections (e.g., due to clustered cells) in the first few images are plausible, and will then continue with full automatic analysis of all remaining images at a speed of ~500 cells per minute. Cells are analyzed by first calling ImageJ's particle analyzer and then by performing additional shape recognition. A perpendicular slit-shaped window is moved from the cell's center toward either end for detecting the possibly curved cell axis. Then a number of shape parameters are tested for accepting or rejecting the cell. In case of rejection, a temporary yellow text overlay above the cell displays the conflicting criterion, so the user can visually verify the efficiency of the current shape criteria.

In contrast to ImageJ, that does not support composite regions of interest, ObjectJ can handle hierarchical non-destructive objects (for marking cells) and can either address the entire object or subordinate parts of it ("items") for further analysis. If a cell is accepted, it is treated as a single object and is marked with a segmented line item of type "Axis"

(cell length in red), and a line item of type "Dia" (mean diameter in green, **Figure 1**, Panel 2). The corresponding numerical data will automatically appear in one row per cell in the ObjectJ "results table" (**Figure 1**, Panel 3). More items such as constriction markers can optionally be added later. Rather than using ImageJ's built-in overlay technique, which linearly stores the ROI information in the image file or in the ROI manager and which is optimized for single images, ObjectJ manages all information centrally by the project file. Populations that extend across many hyperstacks can be marked without putting any organizational burden upon the user. Manual detection of artifacts that are left over from imperfect shape recognition takes into account that they often appear at either end of the spectrum of property values (e.g., very thick or very thin cells). With a single keystroke any subpopulation could be browsed in the order of any sorted parameter such as length, diameter or derived result, refining the power of automatic classification with rapid visual inspection. Deletion of undesired objects can also be performed with a keystroke, removing all markers of the selected cell. The ObjectJ "results table" is then automatically updated and allows the observation of statistics or the creation of histograms via the contextual menu connected to each column title (**Figure 1**, Panel 4).

Map of Profiles

Additional information of the cell population is stored in the "Map of Profiles," which is a 32-bit (floating point) stack holding as many channels as the acquired images, and which is stored in the "project folder." For each cell, one slot is arranged containing a vertically centered pixel column whose height corresponds to the cell length. In case of fluorescence, a pixel in the Map contains the integrated brightness of a 1-pixel-thick disk at the corresponding axis position (**Figure 1**, Panel 6). In case of phase contrast, a pixel contains the local cell diameter. For example, the smaller diameter at a cell constriction site will be translated into less brightness and appear dark in the center (**Figure 1**, Panel 7).

Creating Sorted and Qualified Maps was useful to show the cells in growing order from left to right. As length is related to age, the development pattern during the cell cycle can be observed, such as the creation of the Z-ring (**Figure 1**, Panel 5) or the constriction process toward the end of the cell cycle.

Collective Profile

A collective profile is created from all cell profiles in a Map. They are first resampled to a normalized cell length of 100 data points, and then averaged to a single plot. Optionally, the collective profiles of several channels can be displayed in

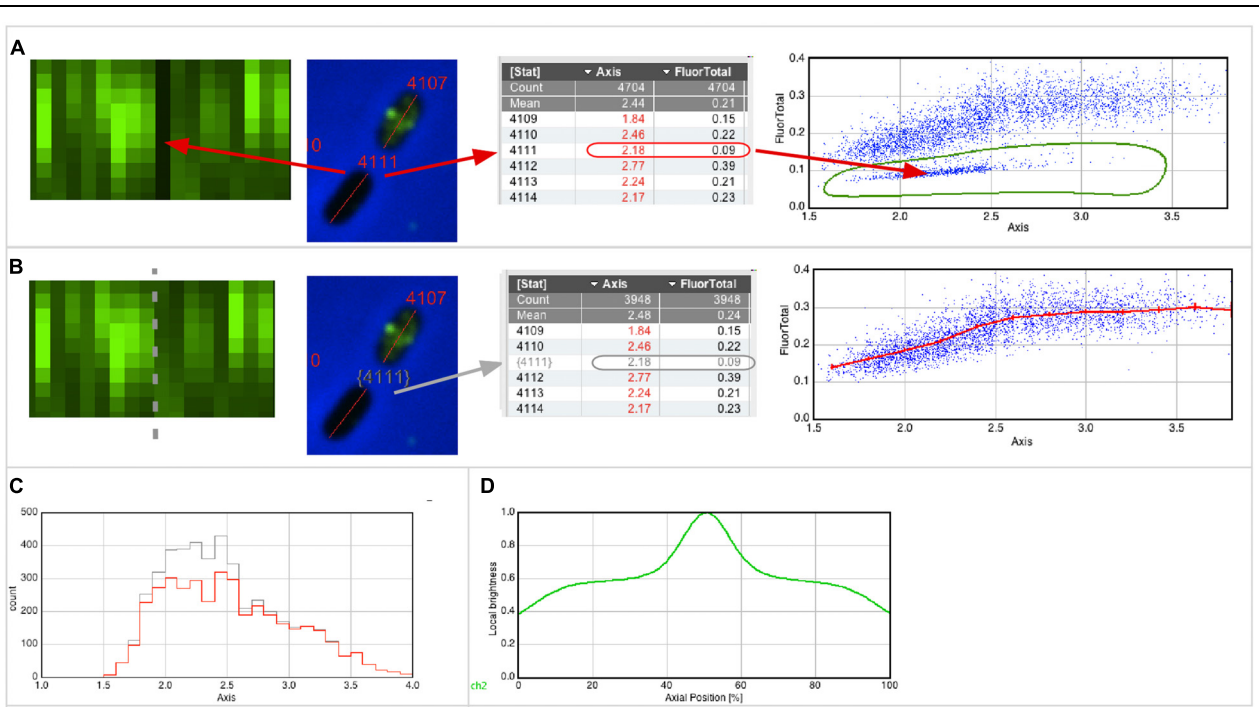

FIGURE 2 | Qualifying and plotting. (A) The Map of fluorescence (left) shows a vertical black line, indicating low fluorescence (FluorTotal = 0.09) for cell #4111 that obviously did not permeabilize properly. In the scatter plot (right), which shows fluorescence versus axis length, similar cells appear as a cloud of dots in the lower part. Using a hand-drawn region of interest (ROI), these cells can be easily enclosed and selected. **(B)** The software allows temporarily disqualifying those cells whose dots are in the hand-drawn ROI. Disqualified cells will appear with a gray number label both in their images and in the results table, and they do not contribute to statistics, plotting and sorting. The Map of fluorescence (left) can be updated to show qualified cells only, and can be sorted for axis length. The scatter plot (right) is redrawn to include qualified cells only, and shows a line through markers of the mean value of 0.25 μm length bin size with error bars of 95% confidence. **(C)** Distribution of cell lengths of all and qualified-only cells in gray and red, respectively. **(D)** Collective normalized profile of qualified cells, showing the fluorescence distribution versus the relative position along the cell axis.

the same graph. In case of a steady state population, the cell cycle time can be resolved in a number of age groups. For example, specifying 10 age groups will create a stack of 10 profiles that shows development stages during a typical cell cycle.

Integrated Data Analysis

The Map of Profiles is a useful intermediate data set. It can visualize the longitudinal fluorophore distribution depending on age, and it allows deriving results and plots that describe individual age groups. In general, due to the integrated concept of ObjectJ and its "Qualifying" feature, histograms and scatterplots of any subpopulation can be created inside ImageJ while keeping the link to the images intact.

For example, **Figure 2A** (left) shows that cell #4111 appears as a black slot in the Map, indicating very low fluorescence. The image of this cell, as well as its numerical properties, can be displayed with a single click (red arrows). When creating a scatter plot "Fluorescence vs. Axis," similar non-fluorescent cells appear as a separate cloud of points, which can be selected with a hand-drawn region of interest (ROI; **Figure 2A**, right). The low fluorescence could be explained with low inflow of fluorophores due to weak permeabilization (however, for experiments described here below, only cultures in which all cells were permeabilized were used). **Figure 2B** shows how these cells could be excluded from data analysis. Disqualifying cells uses gray color for labels and results (gray arrows) and excludes them from the statistics, plots (**Figure 2B**, right; **Figures 2C,D**) and optionally from the Map (**Figure 2B**, left). As long as non-qualified cells are not deleted from the results, the total population will appear in gray and the qualified population will appear in red in any histogram created from the result table (**Figure 2C**).

Asymmetrical Localization

A "collective profile" appears symmetrical due to the random up/down orientation of the cells in the Map (**Figure 2D**). However, cells that show an asymmetrical distribution of fluorescence along the cell axis, i.e., having a bright and a dark pole, are valuable candidates to further study the spatial correlation of different fluorophores. Therefore, a command is available to orient the cells in the map so that the bright pole

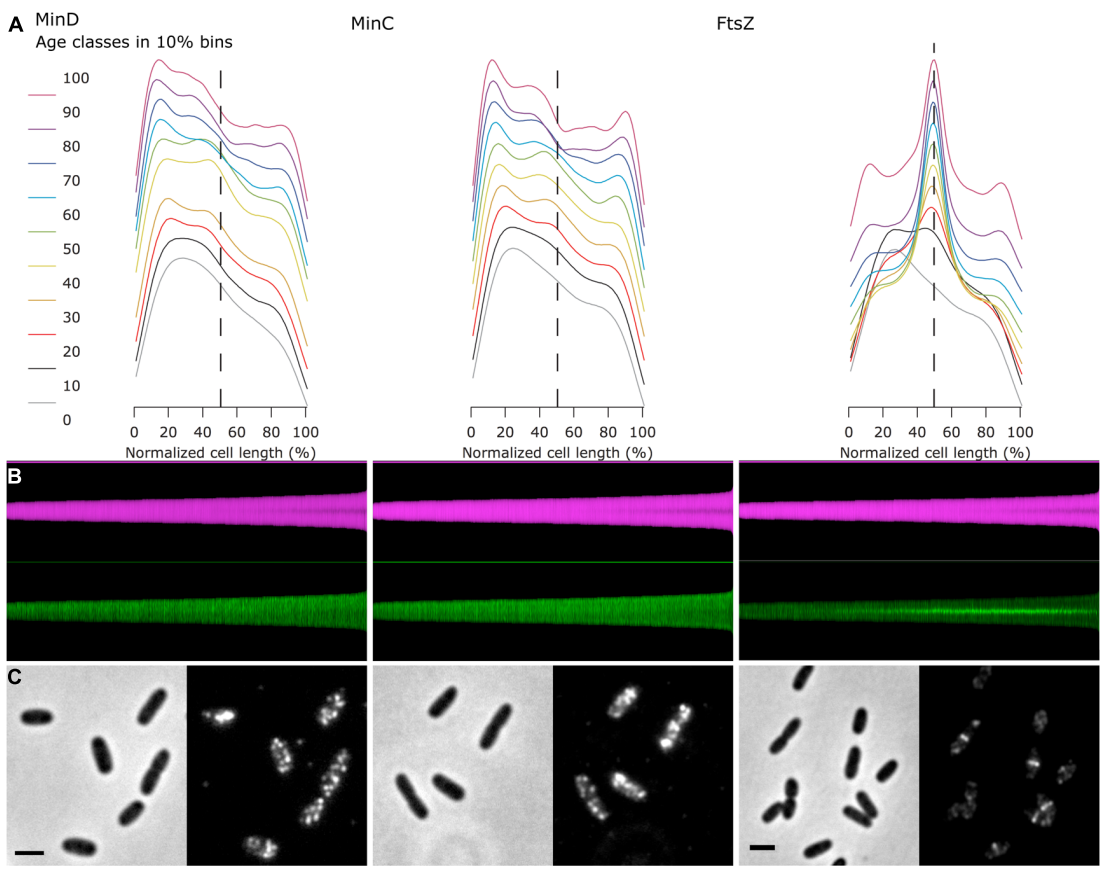

FIGURE 3 | Fluorescence profiles of immunolabeled endogenous MinC, MinD, and FtsZ show cell division cycle dependent localization. (A) For each of the three proteins, the fluorescence profiles along the cell axis are shown for 10 age classes. The profiles are asymmetric, as the brighter pole was oriented toward left before averaging. Plots are vertically stacked with an increment of 0.1 for better visualization. Dashed line indicates cell center. **(B)** Map of diameter profiles (magenta) and fluorescence profiles (green, bright pole upward). Cells are sorted for length, ascending from left to right. **(C)** Channel pairs of phase contrast (left) and fluorescence (immunolabeled proteins, right) are shown. The scale bar equals 2 μm.

in a chosen "leader channel" always points upward (**Figure 3B**). The asymmetry of that channel is thus preserved after averaging, which results in a collective profile with its median in the left half (**Figure 3A**). Any asymmetry in the profile of a "follower channel" indicates that fluorophore localization is correlated with the leader channel, whereas symmetry suggests an independent process. Collective profiles can also be created from individual age classes to resolve the fluorophore localization during the cell cycle (**Figure 3A**).

The Min System

As an example of the use of the asymmetrical profiles, the MinD and MinC proteins of the Min system of *E. coli* were immunolabeled. The Min system consists of three proteins (see for a review Lutkenhaus et al., 2012): first, the ATPase MinD that binds to the cytoplasmic membrane of the cell poles with an amphipathic helix when it is in the ATP bound form; second, the FtsZ polymerization inhibitor MinC that is recruited by MinD to the membrane; and third, MinE, which stimulates the ATPase activity of MinD. This stimulation of the ATPase activity by MinE causes the release of MinD and MinC from the membrane. Because the majority of the Min proteins are localized at one pole, the release of MinCD causes the proteins to move to the opposite cell pole, where they attach again to the inner membrane. The subsequent stimulation of the ATPase activity of MinD by MinE at this pole causes the cycle to start again, resulting in a regular oscillation of the three proteins from one pole to the other. As a result, FtsZ polymerization is inhibited near the cell poles. This oscillation behavior has been demonstrated *in vivo* using Min FPs fusions (Raskin and de Boer, 1997, 1999a,b) and also *in vitro* using the isolated Min proteins (Loose et al., 2011; Arumugam et al., 2014). Because of the oscillation, all Min proteins could theoretically end up in one of the daughter cells during division. However, *in vivo* studies using FP fusions to MinD (Juarez and Margolin, 2010), MinC and MinE (Ventura and Sourjik, 2011) have shown that the Min proteins become equally distributed between the new born daughter cells, because the oscillation wave is split in two before the closure of the septum. Assuming that the MinC and MinD proteins would on average be present at higher concentrations in the cell poles, we used this characteristic to demonstrate the use of Coli-Inspector's ability to sort cells according to age, together with the analysis of asymmetric fluorescence profiles.

For this purpose, wild type cells grown to steady state in minimal glucose medium at 28°C were labeled with anti-MinD, -MinC, and -FtsZ (**Figure 3**). Subsequently, the cells were measured and sorted according to cell length with fluorescent profiles, in which the brighter pole is always pointing upward (**Figure 3B**). In an average map of fluorescence profiles with random orientation of the brighter pole, the polar localization of the Min proteins would not be very obvious (**Figure 3C**), but after orienting the brighter poles pointing upward and plotting of the profiles in 10% age classes, the similar asymmetric polar localization of MinC and MinD becomes obvious (**Figure 3A**).

In conclusion, the Coli-Inspector features enable the comparison and verification of the localization behavior of the endogenous Min proteins with that of the FP-Min protein fusions. In addition, information about the age dependent localization pattern could be obtained.

Concentration of Cell Division Proteins During the Division Cycle

The Map of Profiles can be used to determine the amount of fluorescence present in an individual cell. From the morphological parameters, the volume or the surface area of each cell can be calculated and therefore the relative concentration of the immunolabeled protein can be determined. We analyzed the cellular concentration of many morphogenetic proteins as function of the division cycle (**Figure 4**) and noticed that most proteins have a constant concentration at all cell ages (**Table 3**). The genes coding for a number of the cytoplasmic steps of PG precursor synthesis and several of the cell division proteins such as *ftsL*, *ftsI* (*pbpB*), *ftsW*, *ftsQ*, *ftsA,* and *ftsZ* are expressed from one large operon called the *dcw* cluster (Vicente et al., 1998). Other genes such as *ftsN* and *ftsK* are in separated locations on the chromosome. Multiple promoters regulate the expression of *ftsZ*. The *ftsQ* p1gearbox promoter was reported to ensure the cell size dependent constant concentration of FtsQ, FtsA, and FtsZ under various growth conditions (Aldea et al., 1990; Sitnikov et al., 1996; Ballesteros et al., 1998). The ratio between the number of proteins produced per cell cycle in cells grown in rich medium and cells grown in poor medium is fairly constant for many of the morphogenetic proteins (Li et al., 2014). Therefore, these σ^S dependent promoter types might also be involved in the expression of other morphogenetic proteins. However, as far as we are aware not much is known about the promoter organization of their genes. Even less is known about the regulation of gene expression as a function of the cell cycle, which is clearly a gap in our present knowledge.

The constant cellular concentration of the immunolabeled proteins indicated that despite their transition from single, dimeric or subcomplex protein state to their presence in a multi-protein complex during the assembly of the division machinery, epitopes remained accessible to the antibodies. Antibody epitopes are usually directed at exposed and flexible regions of the protein, especially when the antibodies are developed against purified protein as it is the case for our sera. The proteins that had a variable concentration during the cell cycle will be discussed individually below.

When the number of proteins per average cell is known, it is possible to translate the fluorescent units of the immunolabeling into number of proteins. Knowing the number of proteins and their localization in the cell envelope gives the possibility to determine the number of proteins in the divisome or the stoichiometry of its subunits. The resolution of the microscope is not enough to restrict the localization measurements to the precise position of the septal ring. Therefore we used a much larger volume of midcell extended by 0.4 μm on either side of the center. Conceding that not all proteins in this volume are part of the septal ring, we calculated the number of molecules that were present in this volume above the general background of the same molecules in the cell

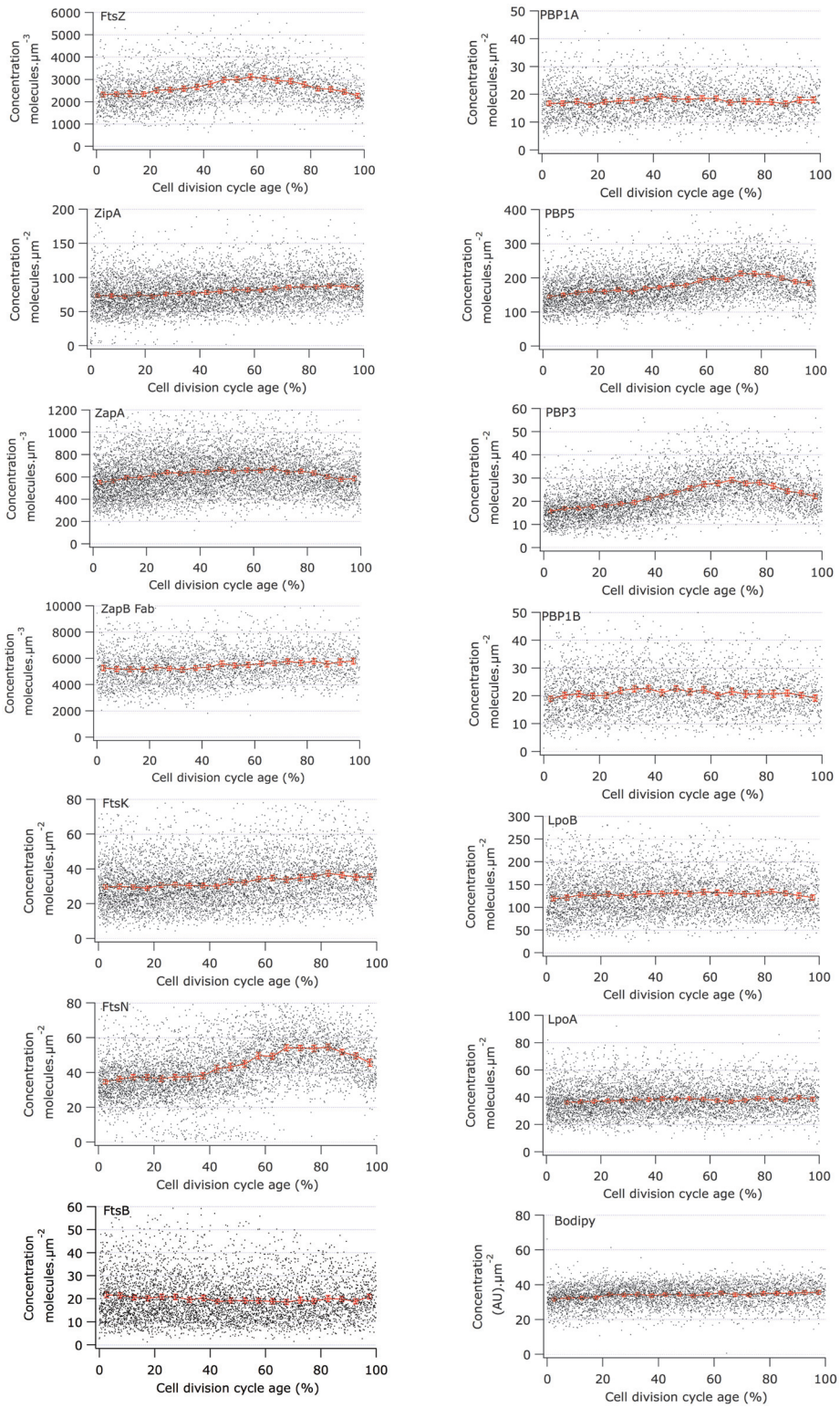

FIGURE 4 | Concentration of morphogenetic proteins as function of the bacterial cell division cycle. For each graph the concentration of the indicated protein is plotted against the cell age in %. The black dots are the data for each individual cell. The red line and markers are the mean value of 5% age bins and the error bars indicate the border of the 95% confidence interval. The concentration of FtsZ, ZapA, and ZapB is plotted per volume unit because these are cytoplasmic proteins. The concentration of all other proteins is plotted per area unit because they are cell envelope bound. The cell cycle age is plotted as percentage of the mass doubling time (80 min) of the to steady state grown MC4100 cells.

TABLE 3 | Immunolabeled proteins.

Protein	Function	Change in concentration (%)[a]	Number of cells	Anti-serum purification	Concentration based various techniques (source)[b]	Concentration based on (Li et al., 2014)
FtsZ	Z-ring	25	3528	Serum is specific	4800 ± 1300 (Mohammadi et al., 2009)	3335
FtsA	Membrane tether of FtsZ and divisome protein recruitment	n.d.	n.d.	n.d.	200 (Mukherjee and Donachie, 1990)	575
ZipA	Membrane tether of FtsZ and FtsA modulator.	10	6555	ZipA depleted		501
ZapA	Cross-links Z, binds ZapB	18	8378	ΔZapA	6100 ± 1000 (Mohammadi et al., 2009)	738
ZapB	Binds ZapA and MatP	20	5050	ΔZapB	∼13000 (Ebersbach et al., 2008)	7797
FtsK	Divisome activation and chromosome deconcatenation	10	6505	Affinity	∼100 (Bisicchia et al., 2013b)	213
FtsB	Binds FtsQ	10	5110	Affinity		140
PBP3	Transpeptidase	40	5499	Affinity	63 ± 12 (Dougherty et al., 1996)	144
FtsN	Divisome activator	40	5921	Serum is specific	4650 ± 1780 ref (Ursinus et al., 2004)	269
PBP1B	Glycosyl transferase and transpeptidase	10	3522	ΔPBP1B	123 ± 19 (Dougherty et al., 1996)1000 (Paradis-Bleau et al., 2010)	139
PBP1A	Glycosyl transferase and transpeptidase	10	3138	Affinity and ΔPBP1A	135 ± 24 (Dougherty et al., 1996) 500 (Paradis-Bleau et al., 2010)	116
LpoB	PBP1B activator	10	5177	ΔLpoB	2300 (Paradis-Bleau et al., 2010)	954
LpoA	PBP1A activator	10	5670	ΔLpoA	500 (Paradis-Bleau et al., 2010)	250
PBP5	DD-carboxypeptidase	30	5997	ΔPBP5	317 ± 69 (Dougherty et al., 1996)	1180
MinC[c]	FtsZ inhibitor	15	6110	ΔMinCDE	400 ± 80 (Szeto et al., 2001)	148
MinD[c]	MinC tethering to membrane	10	4315	ΔMinCDE	3000 (de Boer et al., 1991) 2000 (Shih et al., 2002)	644

[a]*An increase of 10% is to be expected for all samples as the controls eosine for cytoplasmic proteins and bodipy for membrane proteins, which are expected to have a constant concentration, also increase 10% in concentration during the cell division cycle. Therefore, the effective change in concentration will be for all proteins the given value-10%.* [b]*The numbers are derived from a variety of different strains an growth conditions and therefore not directly comparable to the numbers in the last column.* [c]*See Supplementary Figure S1 for the concentration of MinD, MinC and eosine as a function of the cell cycle age.*

(MolsCPlus). We did not choose the alternative method to simply include all molecules in the central volume because this most certainly would have resulted in an overestimation. To allow comparison, both sets of data are provided in the Supplementary Table S1.

Based on immunoblotting the average number of FtsZ molecules per cell was calculated to be 4800 ± 1300 ($n = 3$) in our wild type strain MC4100 grown to steady state in Gb1 at 28°C with a mass doubling time of 80 min (average cell volume is 1.35 ± 0.27 μm^3; Mohammadi et al., 2009). These are exactly the same conditions that have been used for the growth of the same strain in the present paper (see Materials and Methods). For MG1655 cells grown in MOPS minimal medium with a mass doubling time of 56 min (average cell volume is 1.43 ± 0.31 μm^3), the average number of FtsZ molecules was determined by ribosome profiling to be 3335 ± 1300 molecules (Li et al., 2014). The difference in average cell volume between these two strains and growth conditions is negligible given the 30% error (Li et al., 2014) in the determination of the number of proteins per average cell. This method seems to be relatively accurate and it has been performed for all proteins on a single strain grown under well-defined conditions. Therefore, we used the mean number of molecules per average cell determined by ribosome profiling (Li et al., 2014) for all calculations on the number of absolute molecules at midcell. Other data on the mean number of molecules found in the literature are often based on less reliable methods such as immunoblotting and are obtained from a large variety of growth conditions and strains (for comparison, the various measurements are presented in **Table 3**). Although Li et al. (2014) have taken the life-time of the proteins into account for their calculation of the number of proteins per cell, they could not correct for regulated protein degradations such as ClpX degradation of FtsZ (Camberg et al., 2009) or for fractions of proteins that are not active. Therefore, the absolute numbers presented here can be subject to variation.

The calculation of the volume or surface of the cells is based on the phase contrast images. To avoid over-interpretation of the results, we have also labeled the membrane with a fluorophore (bodipy-C12) and the cytosol with a fluorescent dye (eosine) and determined their cellular concentration as function of the cell cycle in fluorescence units. Both display an increase of

10% during the cell cycle (shown for bodipy in **Figure 4** and for eosine in Supplementary Figure S1). Consequently, only an increase of a protein concentration measured during the cell cycle of more than 10% was considered relevant. In addition, we argued that the concentration of a protein at the end of the cell cycle should be close to or decreasing toward the concentration of the protein in new-born cells. Changes in concentration that did not abide to this rule were not considered significant.

The Proto-Ring

Using immunolabeling and the Coli-Inspector macro, an increase of 15% in the cellular concentration of FtsZ was observed (**Figure 4**). Interestingly, 13% of the FtsZ molecules are degraded per generation (Camberg et al., 2009). Possibly, the number of molecules per cell is regulated by the two component protease ClpX that is known to be involved in the degradation (Camberg et al., 2011, 2014). The average number of 3335 FtsZ molecules per cell (Li et al., 2014) was used to calculate the concentration of FtsZ proteins at midcell. Between 60 and 80% of the cell age about 1100 ± 77 FtsZ molecules are present at midcell within 95% confidence borders (Supplementary Table S1). This is in agreement with the reported present of 30% of the total number of FtsZ molecules present at midcell (Stricker et al., 2002). Based on total internal reflection (TIR) PALM imaging, the Z-ring could consist of loosely organized protofilaments of limited size (Fu et al., 2010; Buss et al., 2013). The width of the Z-ring (110 nm) is largely invariant between different bacterial species and FtsZ expression levels (Fu et al., 2010; Jennings et al., 2011; Biteen et al., 2012). The length of the average protofilament in the ring could be about 120 nm or contain 27 FtsZ subunits (Stricker et al., 2002; Anderson et al., 2004; Chen and Erickson, 2005; Loose and Mitchison, 2014). With 1100 FtsZ molecules at midcell the Z-ring would consist of about 40 of these protofilaments. The number of FtsZ molecules/μm Z-ring at midcell increased up to 60% of the cell cycle age and thereafter remained constant at ∼450 molecules/μm till 90% of the cell cycle age (**Figure 5**; Supplementary Figure S1). The calculation of the circumference of the cell is based on the measured minimal midcell diameter (**Figure 5**) and the assumption that the three envelope layers constrict simultaneously. The resolution of the images was not good enough to use the minimal midcell diameter after 90% of the cell cycle for further calculations of the progression of the closure of the constriction. Summarizing, it can be concluded that the density of the Z-ring increases during the initial constriction and then stays constant.

ZipA and FtsA anchor FtsZ protofilaments to the cytoplasmic membrane (Ma et al., 1996; Mosyak et al., 2000; Yan et al., 2000; Hale and de Boer, 2002; Kuchibhatla et al., 2011). ZipA was recently shown to protect FtsZ against degradation by the ClpXP protease (Pazos et al., 2013a). ZipA is also thought to prevent self-interaction of FtsA because ZipA is not essential in an FtsA mutant that is not able to self-interact (Pichoff et al., 2012). The ZipA cellular concentration is constant during the cell division cycle (**Figure 4**) and ∼170 ± 15 molecules are observed at midcell (Supplementary Table S1). Assuming the

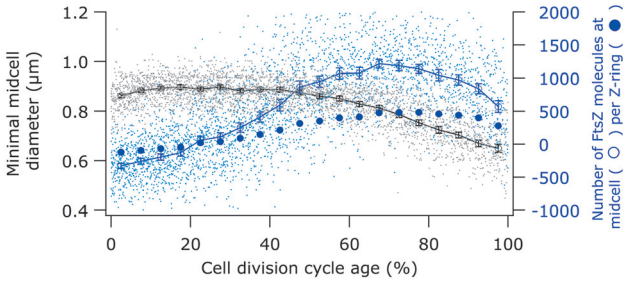

FIGURE 5 | Comparison of the timing of the constriction with the timing of the FtsZ localization at midcell. Black circles (legend on the left) show minimal cell diameter (constriction) versus cell age. Open blue circles (legend on the right) show "MolsCPlus," which is the number of extra FtsZ molecules at midcell compared to the number of FtsZ in the cell assuming an equal distribution of the molecules in the cytosol. Filled blue circles (legend on the right) show the mean number of FtsZ molecules per μm Z-ring. The bottom axis shows the cell division cycle age in percentage.

FtsA cellular concentration also to be constant (Rueda et al., 2003) and knowing that 30% of the FtsA molecules is present in the Z-ring (Pla et al., 1990), about 200 FtsA molecules would bind to the Z-ring. Consequently, each protofilament of 27 FtsZ residues would therefore be bound to the cell envelope by 4 ZipA molecules and 5 FtsA molecules. ZipA has a high affinity for FtsZ and interacts with the flexible C-terminus of FtsZ of which especially residue D373 is essential for the interaction (Haney et al., 2001). As FtsA binds with a lower affinity to the same flexible C-terminal domain of FtsZ (amino acids 367–383; Szwedziak et al., 2012), they will likely not bind simultaneously to the same FtsZ molecule. ZipA can form dimers (Skoog and Daley, 2012) and could therefore bind as dimer two FtsZ molecules in a single FtsZ protofilament but it could also bind two FtsZ protofilaments given its long and flexible cytoplasmic domain. In conclusion, together FtsA and ZipA could link every third FtsZ molecule to the cytoplasmic membrane.

The cellular concentration of ZapB was constant during the cell cycle (**Figure 4**). The cellular concentration of ZapA increased up to 30% cell age, stayed constant up to 70% cell age after which it decreased again to the level of new-born cells. The number of ZapA molecules at midcell did not mimic this change in concentration. ZapA is present at midcell with 150 ± 10 −170 ± 12 molecules between 67.5 and 92.5% of the cell age, indicating that while the total cellular ZapA concentration is already decreasing, the number of molecules at midcell is still increasing. The majority of the ZapA molecules is present as a tetramer in *E. coli* (Low et al., 2004; Small et al., 2007; Mohammadi et al., 2009; Pacheco-Gómez et al., 2013), which implies that every FtsZ protofilament can be cross-linked by a ZapA tetramer assuming that the ZapA tetramer can at least bind two protofilaments. ZapA does not bind the flexible C-terminal domain of FtsZ but binds to the core domain (den Blaauwen, unpublished results) allowing for mutual binding of ZapA and ZipA or FtsA. ZapB localized at midcell with 4200 ± 250 molecules between 72.5 and 92.5% of the

cell cycle. ZapB is a dimer and is dependent on its binding to ZapA (Galli and Gerdes, 2010) and possibly also on FtsZ (Pazos et al., 2013b) for its localization at midcell. Clearly, not enough ZapA molecules are present to bind all ZapB molecules [even if assuming the number of midcell ZapA molecules to be 1400 as determined by immunoblotting (Mohammadi et al., 2009)]. Galli and Gerdes (2010) could discriminate a fluorescent ZapB ring localizing inside the Z-ring by confocal microscopy. Given the axial resolution of the microscope a distance of about 200 nm would be required to resolve both structures. This is not compatible with a single ZapA tetramer connecting FtsZ and ZapB (**Figure 7**). ZapB is able to bind MatP, a protein that binds to specific sequences abundant in the terminal region of the chromosome (Mercier et al., 2008; Espeli et al., 2012). It would make sense if the ZapB molecules would extend toward the chromosome during the constriction process to verify whether the chromosomes are sufficiently separated. Recently, a high resolution microscopy study was published that confirms the presence of a layered network of FtsZ-ZapA-ZapB-MatP molecules (Buss et al., 2015). Interaction of ZapB with the chromosome might be communicated to the Z-ring and somehow stall the progress of the constriction to avoid cleavage of the nucleoids.

The Septal Synthesizing Complex

Protein Concentrations of PBP3 and FtsN Fluctuate

PBP3 is a transpeptidase that crosslinks peptides in peptidoglycan specifically during cell division at midcell (Adam et al., 1997; Weiss et al., 1999; Piette et al., 2004). PBP3 forms a subcomplex (Fraipont et al., 2011) with FtsW, which is possibly one of the peptidoglycan precursor lipid-II flippases (Ruiz, 2008; Mohammadi et al., 2011, 2014; Sham et al., 2014). PBP3 is essential for septal peptidoglycan synthesis, and its inhibition by aztreonam or its depletion results in a division arrest (Pogliano et al., 1997; Eberhardt et al., 2003). PBP3 interacts with PBP1B (Banzhaf et al., 2012), a bifunctional peptidoglycan synthesizing protein with glycosyl transferase activity to polymerize glycan strands and transpeptidase activity. The activity of PBP1B is stimulated by its interactions with LpoB (Paradis-Bleau et al., 2010; Typas et al., 2010) and FtsN (Müller et al., 2007). The cellular concentration of PBP1B and LpoB was constant during the cell division cycle of *E. coli* (**Figure 4**). Similarly, the bifunctional PBP1A involved in cell elongation as well as its regulator LpoA had a constant cellular concentration during the division cycle (**Figure 4**). Remarkably, the cellular concentration of PBP3 molecules increased as soon as it started to accumulate at midcell at 40% of the cell age until it reached a maximum at about 70% after which it returned to its level before midcell localization. The cellular concentration of PBP3 increased by 30% during it localization at midcell. At its maximum cellular concentration about 70 ± 6 PBP3 molecules were present at midcell. Assuming it to be a dimer (Fraipont et al., 2011; Sauvage et al., 2014), 35 ± 3 peptidoglycan synthesizing proteins complexes could be present in the Z-ring or approximately one per average FtsZ protofilament (see for images of the immunolocalization Supplementary Figure S2). Curiously, only maximally 18 ± 3 molecules of PBP1B were present at midcell above the cellular

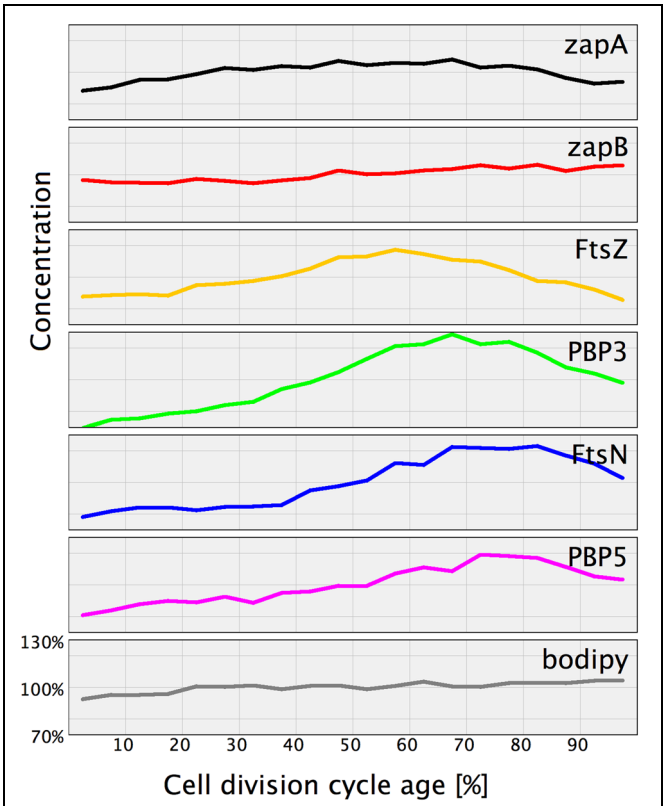

FIGURE 6 | Normalized protein concentration as function of cell age. For comparison the proteins that were found to have a cell age dependent concentration variation have been plotted in one graph. The concentration at the various cell cycle time points of each indicated protein was divided by the average concentration of that protein in the whole population. Subsequently, the concentration for the individual proteins was plotted against the cell division cycle age in percentage with an off sett on the *Y*-axes to enable individual visualization. For comparison the membrane stain bodipy-C12 and the ZapB protein that both have a constant concentration are included.

background, which is not sufficient to interact with each PBP3 dimer. The number of possible interactions is further reduced if PBP1B exists as a dimer (Zijderveld et al., 1991; Bertsche et al., 2005). Surprisingly, dimers of PBP1B or PBP1A, or a PBP1B-PBP1A complex were not observed using our in cell FRET assay with the fluorescent labeled proteins (Alexeeva et al., 2010; see Supplementary information and Table S2 and S3). The absence of FRET does not proof that PBP1B or 1A are monomers. However, evidence that the bifunctional PBPs are dimers *in vivo* is thus far lacking. The imbalance in the number of PBP molecules is not resolved by assuming that all molecules in the center cell volume are part of the divisome (Supplementary Table S1). Although PBP1B and PBP1A have been shown to be involved in cell division and cell elongation, respectively (Bertsche et al., 2006; Banzhaf et al., 2012), they can substitute for each other (Typas et al., 2010). Moreover, the elongasome and divisome have been reported to interact at least temporarily during septal synthesis (Vats et al., 2009; Fenton and Gerdes, 2013; van der Ploeg et al., 2013) and therefore, the 7 ± 2 PBP1A molecules present in surplus to the

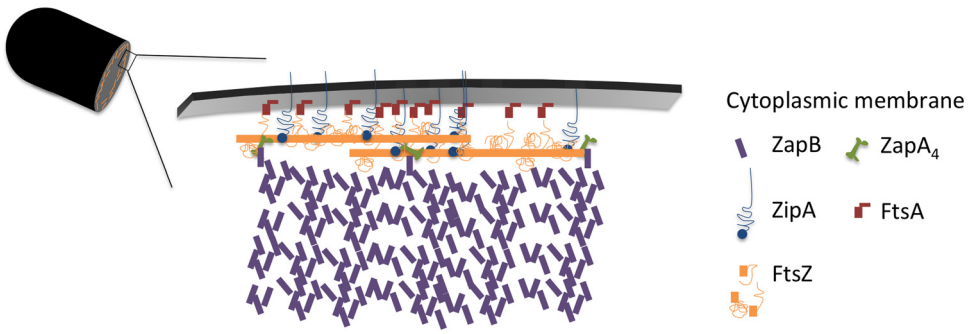

FIGURE 7 | Model of the proto-ring. Two FtsZ filaments in orange, each consisting of 27 residues with a length of 120 nm are connected to the cytoplasmic membrane by 4 ZipA molecules (blue) or 2 ZipA dimers that might cross-link 2 FtsZ protofilaments and 5 FtsA molecules (red). ZipA and FtsA compete for binding to the flexible C-terminal end of FtsZ. Each FtsZ protofilament is bound to a ZapA tetramer (green) that is potentially able to cross-link the protofilaments and which is also bound by ZapB (purple). About 100 ZapB molecules are available for each protofilament.

background of PBP1A molecules at midcell should be added to the septal peptidoglycan synthesizing complexes. The resulting 25 bifunctional PBP molecules (or 12.5 dimers) in the divisome are still not sufficient to saturate the 35 PBP3 dimers. Because of the multitude of interactions of PBP1B with other cell division proteins, occlusion of the epitopes of the polyclonal IgG might reduce the number of detectable PBP1B molecules at midcell resulting in an underestimation of protein numbers. However, if a subset of PBP1B molecules would become inaccessible because of association with divisome proteins one would expect the concentration of PBP1B to decrease in dividing cells unless the number of PBP1B molecules is upregulated during cell division like observed for FtsZ.

Two other proteins that are thought to be part of the core complex of the synthetic complex, FtsK and FtsB, were immunolabeled. FtsK has two functions, its integral membrane domain is needed to recruit the FtsQLB complex (Wang and Lutkenhaus, 1998), and it is involved in the coupling of the simultaneous constriction of the cytoplasmic membrane and the peptidoglycan layer (Berezuk et al., 2014). The cytoplasmic domain of FtsK is needed for its second function to position the *dif* sites near the terminus of the chromosomes to allow the XerCD recombinases (Löwe et al., 2008) to decatenate the chromosomes. The cytoplasmic domain consists of a long flexible linker and a DNA translocating γ-domain, which forms at least during ds-DNA translocation a double hexamer (Massey et al., 2006). Using a chromosomally encoded FtsK-YPet FP fusion between 24 and 36 FtsK molecules were observed at midcell during the constriction period in minimal medium grown cells (Bisicchia et al., 2013b). Because the measured number was mostly a multiplication of six, it was concluded that FtsK forms a hexamer at the site of constriction. In agreement with the data of (Bisicchia et al., 2013b), we observe between 50 ± 8 and 60 ± 8 FtsK molecules at midcell (Supplementary Table S1), which would be sufficient for 8–10 hexamers.

FtsB is part of the FtsQLB complex (Buddelmeijer and Beckwith, 2004; van den Berg van Saparoea et al., 2013) that interacts with many of the divisome proteins (Karimova et al., 2005, 2009; D'Ulisse et al., 2007). The interaction of this complex with FtsN was recently shown to activate cell division (Liu et al., 2015). FtsQ, FtsB, and FtsL are present with 147, 140, and 201 molecules per average cell, respectively (Li et al., 2014) and form a complex with a 1:1:1 stoichiometry (Luirink and den Blaauwen, unpublished results). Based on the immunolocalization of FtsB, about 20 ± 3 of these complexes will localize at midcell. Using the same method as for FtsK, Bisicchia et al. (2013b) detected between 36 and 66 FtsQ molecules at midcell in constricting cells using a chromosomally encode YPet-FtsQ FP fusion. Based on the periodicity of the numbers it was concluded that FtsQ, like FtsK, occurred as a hexamer. In our experience it is very difficult to obtain antibodies against the individual FtsQ, FtsL, FtsB, and FtsK proteins that give good and specific signal in cells (den Blaauwen and Luirink, unpublished results). Therefore, we cannot exclude that some of the FtsB epitopes are not accessible in the FtsQBL complex and that not all FtsB molecules present at midcell are detected. Based on our data and the data of (Bisicchia et al., 2013b) between 3 and 11 hexameric FtsQBL complexes could be present in the divisome. In view of a limited number of synthetic complexes, the observed 18 PBP1B plus 7 PBP1A molecules at midcell might not be an underestimation.

Taken our data and those of Bisicchia et al. (2013b) together 36–60 FtsK, 20–66 FtsQ, 25 PBP1A/B, and 70 PBP3 molecules could be present at midcell during constriction. If a hexameric configuration of FtsK is assumed, about 6–10 septal synthesizing complexes could be envisioned. The presence of 3–4 bifunctional peptidoglycan synthases per synthetic complex would allow the simultaneous insertion of 3–4 glycan strands. Such a mode of peptidoglycan synthesis would fit with the Höltje (1998) hypothesized model in which one glycan strand of the existing peptidoglycan layer is replaced by three new glycan strand or the "three for one model." The uncertainty in the number of proteins at midcell could easily be explained by the error in the measurement of the mean number of proteins in the cell (Li et al., 2014) and the error in the immunolocalization given the very low protein copy-numbers. A detailed PALM/STORM analysis of the stoichiometry of the divisome protein might be able to provide conclusive numbers.

The essential FtsN protein is a bitopic membrane protein with a short cytoplasmic domain that interacts with the IC domain of FtsA (Busiek and Margolin, 2014). Followed in the periplasm by an extended region that begins with three short helices of which the second is essential (Yang et al., 2004; Gerding et al., 2009). This region ends with a C-terminal SPOR domain that interacts with peptidoglycan (Ursinus et al., 2004) that may only be transiently present during the division process (Gerding et al., 2009). FtsN binds with its amino terminal 6 amino acids the IC domain of FtsA and keeps FtsA in a monomeric state that is able to recruit the peptidoglycan synthetic complex (Pichoff et al., 2014). The essential helix of FtsN is likely to affect the conformation of the FtsQBL complex because mutants in FtsL and FtsB can bypass FtsN (Liu et al., 2015). The SPOR domain (Duncan et al., 2013) is essential for self-enhanced localization at midcell of FtsN (Gerding et al., 2009; Rico et al., 2013). FtsN overexpression allows the bypass of ZipA because it fixes FtsA in the monomeric state by interacting with its IC domain. Overproduction of FtsN, but also the presence of the FtsL and FtsB mutants that can bypass FtsN, results in very short cells that initiate septal synthesis at a much earlier stage (Pichoff et al., 2014; Liu et al., 2015; Tsang and Bernhardt, 2015). This is possibly caused by a much faster recruitment of the late cell division proteins than in the wild type situation. By interacting with FtsA, by affecting FtsQLB, and by interacting with the peptidoglycan synthetic complex as well as with peptidoglycan, FtsN is likely able to monitor and secure the synchrony of the envelope synthesis.

The cellular concentration of FtsN is more or less constant up to 40% of the cell age before it starts to increase until it reaches a maximum at 90% of the cell age (**Figure 4** and see for images of the immunolocalization Supplementary Figure S2). The number of FtsN molecules at midcell also increased continuously until a maximum of about 150 ± 8 molecules is reached at 90% cell age (Supplementary Table S1). Consequently, the density of the number of FtsN molecules/μm Z-ring continues to increase at midcell at a cell age where the maximum number of FtsZ and PBP3 molecules is already declining, which agrees with its reported self enhanced localization during constriction (Gerding et al., 2009) and its self interaction (Di Lallo et al., 2003; Karimova et al., 2005; Alexeeva et al., 2010). The increase in cellular protein concentration for FtsN is, like for PBP3, ∼30% (**Figure 4**; **Table 2**).

That the number of FtsN molecules decreases much later than the number of FtsZ and PBP3 molecules at midcell is in agreement with the model of (Pichoff et al., 2014) in which the reduction of the number of FtsZ molecules at midcell leaves less FtsZ molecules available for the weakly FtsZ binding FtsA in competition with ZipA. The higher density of FtsN molecules will ensure that sufficient monomeric FtsA will be available to successfully compete with ZipA for the reduced number of FtsZ molecules.

The PBP5 Concentration Varies with Cell Age

PBP5 is the major DD-carboxypeptidase during exponential growth in *E. coli*. It Localizes at midcell in a substrate dependent fashion (Potluri et al., 2010). PBP5 started to accumulate at midcell at about 35% of the cell age, continued to accumulate and reached a maximum at 80% with 550 ± 32 molecules after which it decreased (Supplementary Table S1). This accumulation at midcell is partly due to a 20% increase in the PBP5 concentration during constriction (**Figure 4**). With its abundance at midcell, most pentapeptides that are not immediately used for the formation of peptide cross-links during septal peptidoglycan synthesis by PBP3/PBP1B and/or PBP1A/PBP2 will be converted to tetrapeptides by PBP5.

Of the immunolocalized proteins, FtsZ, PBP3, FtsN, and PBP5 increased their cellular concentration during constriction (**Figure 6**). Consequently, the excess of these proteins has to be removed by either proteolytic degradation or by regulation of their expression. It has been suggested by Camberg et al. (2011) that ClpXP may be involved in division by degrading other proteins than FtsZ. Maybe it also degrades PBP3 and FtsN, but not PBP5 which is periplasmic.

Conclusion

Immunolocalization analyzed as function of cell age allowed determination of the concentration of the labeled proteins and revealed that at least the concentration of FtsZ, ZapA, PBP3, FtsN, and PBP5 seem to be cell cycle regulated (**Figure 6**). Using the published mean number of proteins per cell, it was also possible to establish a stoichiometry for the proto-ring. For every protofilament of ∼27 FtsZ residues, 4 ZipA, 5 FtsA, 1 $ZapA_4$, and 105 ZapB molecules are available (**Figure 7**). Every second to fourth protofilament could also contain one peptidoglycan synthetic complex of which the composition might vary. When FtsN is included, it could bind 4 out of the 5 FtsA molecules that are present on an FtsZ protofilament. While cell division is in progress and the septum is closing, the number most divisome proteins, except FtsZ and PBP3, seem to be constant up to ∼90% cell age. This indicates that the molecule density of the divisome increases and that the amount of new envelope added to the closing septum is constant as was suggested in Wientjes and Nanninga (1989).

Acknowledgments

This paper is dedicated to the late Joachim-Volker Höltje (1941–2014). We are very grateful to the national BioResource Project-*E. coli* at the national institute of genetics, Japan for the creation of the KEIO collection (Baba et al., 2006; Yamamoto et al., 2009). We like to thank Larry Rothfield (Department of Molecular Biology and Biophysics University of Ct Health Center, Farmington, CT, USA) for his generous gift of antibodies against MinD of *E. coli*. MP was funded by a grant form the Netherlands Organization for Scientific Research (NWO-ALW VIDI 864.09.015), TB, JL, WV, MV, and PN were funded by the European Commission Contract

HEALTH-F3-2009-223431 (DIVINOCELL). MV and PN were also funded by the Ministerio de Ciencia e Innovación, Spanish Government Grants BIO2008-04478-C03-01 and BIO2011-28941-C03-01. WV was also funded by a Wellcome Trust Senior Investigator Award (WT101824AIA).

Supplementary Material

The Supplementary Material for this article can be found online at: http://journal.frontiersin.org/article/10.3389/fmicb.2015.00586/abstract

References

Aarsman, M. E. G., Piette, A., Fraipont, C., Vinkenvleugel, T. M. F., Nguyen-Distèche, M., and den Blaauwen, T. (2005). Maturation of the *Escherichia coli* divisome occurs in two steps. *Mol. Microbiol.* 55, 1631–1645. doi: 10.1111/j.1365-2958.2005.04502.x

Adam, M., Fraipont, C., Rhazi, N., Nguyen-Disteche, M., Lakaye, B., Frère, J. M., et al. (1997). The bimodular G57-V577 polypeptide chain of the class B penicillin-binding protein 3 of *Escherichia coli* catalyzes peptide bond formation from thiolesters and does not catalyze glycan chain polymerization from the lipid II intermediate. *J. Bacteriol.* 179, 6005–6009.

Aldea, M., Garrido, T., Pla, J., and Vicente, M. (1990). Division genes in *Escherichia coli* are expressed coordinately to cell septum requirements by gearbox promoters. *EMBO J.* 9, 3787–3794.

Alexeeva, S., Gadella, T. W. J., Verheul, J., Verhoeven, G. S., and den Blaauwen, T. (2010). Direct interactions of early and late assembling division proteins in *Escherichia coli* cells resolved by FRET. *Mol. Microbiol.* 77, 384–398. doi: 10.1111/j.1365-2958.2010.07211.x

Anderson, D. E., Gueiros-Filho, F. J., and Erickson, H. P. (2004). Assembly dynamics of FtsZ rings in *Bacillus subtilis* and *Escherichia coli* and effects of FtsZ-regulating proteins. *J. Bacteriol.* 186, 5775–5781. doi: 10.1128/JB.186.17.5775-5781.2004

Arumugam, S., Petrašek, Z., and Schwille, P. (2014). MinCDE exploits the dynamic nature of FtsZ filaments for its spatial regulation. *Proc. Natl. Acad. Sci. U.S.A.* 111, E1192–E1200. doi: 10.1073/pnas.1317764111

Baba, T., Ara, T., Hasegawa, M., Takai, Y., Okumura, Y., Baba, M., et al. (2006). Construction of *Escherichia coli* K-12 in-frame, single-gene knockout mutants: the Keio collection. *Mol. Syst. Biol.* 2, 2006.0008. doi: 10.1038/msb4100050

Ballesteros, M., Kusano, S., Ishihama, A., and Vicente, M. (1998). The ftsQ1p gearbox promoter of *Escherichia coli* is a major sigma S-dependent promoter in the ddlB-ftsA region. *Mol. Microbiol.* 30, 419–430. doi: 10.1046/j.1365-2958.1998.01077.x

Banzhaf, M., van den Berg van Saparoea, B., Terrak, M., Fraipont, C., Egan, A., Philippe, J., et al. (2012). Cooperativity of peptidoglycan synthases active in bacterial cell elongation. *Mol. Microbiol.* 85, 179–194. doi: 10.1111/j.1365-2958.2012.08103.x

Berezuk, A. M., Goodyear, M., and Khursigara, C. M. (2014). Site-directed fluorescence labeling reveals a revised N-terminal membrane topology and functional periplasmic residues in the *Escherichia coli* cell division protein FtsK. *J. Biol. Chem.* 289, 23287–23301. doi: 10.1074/jbc.M114.569624

Bertsche, U., Breukink, E., Kast, T., and Vollmer, W. (2005). In vitro murein peptidoglycan synthesis by dimers of the bifunctional transglycosylase-transpeptidase PBP1B from *Escherichia coli*. *J. Biol. Chem.* 280, 38096–38101. doi: 10.1074/jbc.M508646200

Bertsche, U., Kast, T., Wolf, B., Fraipont, C., Aarsman, M. E. G., Kannenberg, K., et al. (2006). Interaction between two murein (peptidoglycan) synthases, PBP3 and PBP1B, in *Escherichia coli*. *Mol. Microbiol.* 61, 675–690. doi: 10.1111/j.1365-2958.2006.05280.x

Bisicchia, P., Arumugam, S., Schwille, P., and Sherratt, D. (2013a). MinC, MinD, and MinE drive counter-oscillation of early-cell-division proteins prior to *Escherichia coli* septum formation. *mBio* 4:e00856-13. doi: 10.1128/mBio.00856-13

Bisicchia, P., Steel, B., Mariam Debela, M. H., Löwe, J., and Sherratt, D. (2013b). The N-terminal membrane-spanning domain of the *Escherichia coli* DNA translocase FtsK hexamerizes at midcell. *mBio* 4:e00800-13. doi: 10.1128/mBio.00800-13

Biteen, J. S., Goley, E. D., Shapiro, L., and Moerner, W. E. (2012). Three-dimensional super-resolution imaging of the midplane protein FtsZ in live *Caulobacter crescentus* cells using astigmatism. *Chemphyschem* 13, 1007–1012. doi: 10.1002/cphc.201100686

Buddelmeijer, N., Aarsman, M. E. G., and den Blaauwen, T. (2013). *Immunolabeling of Proteins in Situ in Escherichia coli K12 Strains. Bio-Protocoll,* 1–4. Available at: http://www.bio-protocol.org/wenzhang.aspx?id=852

Buddelmeijer, N., and Beckwith, J. (2004). A complex of the *Escherichia coli* cell division proteins FtsL, FtsB and FtsQ forms independently of its localization to the septal region. *Mol. Microbiol.* 52, 1315–1327. doi: 10.1111/j.1365-2958.2004.04044.x

Busiek, K. K., and Margolin, W. (2014). A role for FtsA in SPOR-independent localization of the essential *Escherichia coli* cell division protein FtsN. *Mol. Microbiol.* 92, 1212–1226. doi: 10.1111/mmi.12623

Buss, J., Coltharp, C., Huang, T., Pohlmeyer, C., Wang, S.-C., Hatem, C., et al. (2013). In vivo organization of the FtsZ-ring by ZapA and ZapB revealed by quantitative super-resolution microscopy. *Mol. Microbiol.* 89, 1099–1120. doi: 10.1111/mmi.12331

Buss, J., Coltharp, C., Shtengel, G., Yang, X., Hess, H., and Xiao, J. (2015). A multi-layered protein network stabilizes the *Escherichia coli* FtsZ-ring and modulates constriction dynamics. *PLoS Genet.* 11:e1005128. doi: 10.1371/journal.pgen.1005128

Camberg, J. L., Hoskins, J. R., and Wickner, S. (2009). ClpXP protease degrades the cytoskeletal protein, FtsZ, and modulates FtsZ polymer dynamics. *Proc. Natl. Acad. Sci. U.S.A.* 106, 10614–10619. doi: 10.1073/pnas.0904886106

Camberg, J. L., Hoskins, J. R., and Wickner, S. (2011). The interplay of ClpXP with the cell division machinery in *Escherichia coli*. *J. Bacteriol.* 193, 1911–1918. doi: 10.1128/JB.01317-10

Camberg, J. L., Viola, M. G., Rea, L., Hoskins, J. R., and Wickner, S. (2014). Location of dual sites in *E. coli* FtsZ important for degradation by ClpXP; one at the C-terminus and one in the disordered linker. *PLoS ONE* 9:e94964. doi: 10.1371/journal.pone.0094964

Chen, Y., and Erickson, H. P. (2005). Rapid in vitro assembly dynamics and subunit turnover of FtsZ demonstrated by fluorescence resonance energy transfer. *J. Biol. Chem.* 280, 22549–22554. doi: 10.1074/jbc.M500895200

D'Ulisse, V., Fagioli, M., Ghelardini, P., and Paolozzi, L. (2007). Three functional subdomains of the *Escherichia coli* FtsQ protein are involved in its interaction with the other division proteins. *Microbiology* 153, 124–138. doi: 10.1099/mic.0.2006/000265-0

de Boer, P. A., Crossley, R. E., and Rothfield, L. I. (1989). A division inhibitor and a topological specificity factor coded for by the minicell locus determine proper placement of the division septum in *E. coli*. *Cell* 56, 641–649. doi: 10.1016/0092-8674(89)90586-2

de Boer, P. A., Crossley, R. E., Hand, A. R., and Rothfield, L. I. (1991). The MinD protein is a membrane ATPase required for the correct placement of the *Escherichia coli* division site. *EMBO J.* 10, 4371–4380.

den Blaauwen, T., Buddelmeijer, N., Aarsman, M. E., Hameete, C. M., and Nanninga, N. (1999). Timing of FtsZ assembly in *Escherichia coli*. *J. Bacteriol.* 181, 5167–5175.

Dennis, P. P., and Bremer, H. (1974). Macromolecular composition during steady-state growth of *Escherichia coli* B-r. *J. Bacteriol.* 119, 270–281.

Di Lallo, G., Fagioli, M., Barionovi, D., Ghelardini, P., and Paolozzi, L. (2003). Use of a two-hybrid assay to study the assembly of a complex multicomponent protein machinery: bacterial septosome differentiation. *Microbiology* 149, 3353–3359. doi: 10.1099/mic.0.26580-0

Dougherty, T. J., Kennedy, K., Kessler, R. E., and Pucci, M. J. (1996). Direct quantitation of the number of individual penicillin-binding proteins per cell in *Escherichia coli*. *J. Bacteriol.* 178, 6110–6115.

Duncan, T. R., Yahashiri, A., Arends, S. J. R., Popham, D. L., and Weiss, D. S. (2013). Identification of SPOR domain amino acids important for septal localization, peptidoglycan binding, and a disulfide bond in the cell division protein FtsN. *J. Bacteriol.* 195, 5308–5315. doi: 10.1128/JB.00911-13

Eberhardt, C., Kuerschner, L., and Weiss, D. S. (2003). Probing the catalytic activity of a cell division-specific transpeptidase in vivo with beta-lactams. *J. Bacteriol.* 185, 3726–3734. doi: 10.1128/JB.185.13.3726-3734.2003

Ebersbach, G., Galli, E., Møller-Jensen, J., Löwe, J., and Gerdes, K. (2008). Novel coiled-coil cell division factor ZapB stimulates Z ring assembly and cell division. *Mol. Microbiol.* 68, 720–735. doi: 10.1111/j.1365-2958.2008.06190.x

Egan, A. J. F., and Vollmer, W. (2013). The physiology of bacterial cell division. *Ann. N. Y. Acad. Sci.* 1277, 8–28. doi: 10.1111/j.1749-6632.2012.06818.x

Espeli, O., Borne, R., Dupaigne, P., Thiel, A., Gigant, E., Mercier, R., et al. (2012). A MatP-divisome interaction coordinates chromosome segregation with cell division in *E. coli*. *EMBO J.* 31, 3198–3211. doi: 10.1038/emboj.2012.128

Fenton, A. K., and Gerdes, K. (2013). Direct interaction of FtsZ and MreB is required for septum synthesis and cell division in *Escherichia coli*. *EMBO J.* 32, 1953–1965. doi: 10.1038/emboj.2013.129

Fraipont, C., Alexeeva, S., Wolf, B., van der Ploeg, R., Schloesser, M., den Blaauwen, T., et al. (2011). The integral membrane FtsW protein and peptidoglycan synthase PBP3 form a subcomplex in *Escherichia coli*. *Microbiology* 157, 251–259. doi: 10.1099/mic.0.040071-0

Fu, G., Huang, T., Buss, J., Coltharp, C., Hensel, Z., and Xiao, J. (2010). In vivo structure of the *E. coli* FtsZ-ring revealed by photoactivated localization Microscopy (PALM). *PLoS ONE* 5:e12682. doi: 10.1371/journal.pone.0012680

Galli, E., and Gerdes, K. (2010). Spatial resolution of two bacterial cell division proteins: ZapA recruits ZapB to the inner face of the Z-ring. *Mol. Microbiol.* 76, 1514–1526. doi: 10.1111/j.1365-2958.2010.07183.x

Garrido, T., Sánchez, M., Palacios, P., Aldea, M., and Vicente, M. (1993). Transcription of ftsZ oscillates during the cell cycle of *Escherichia coli*. *EMBO J.* 12, 3957–3965.

Gerding, M. A., Liu, B., Bendezú, F. O., Hale, C. A., Bernhardt, T. G., and De Boer, P. A. J. (2009). Self-enhanced accumulation of FtsN at division sites and roles for other proteins with a SPOR domain (DamX, DedD, and RlpA) in *Escherichia coli* cell constriction. *J. Bacteriol.* 191, 7383–7401. doi: 10.1128/JB.00811-09

Hale, C. A., and de Boer, P. A. (1999). Recruitment of ZipA to the septal ring of *Escherichia coli* is dependent on FtsZ and independent of FtsA. *J. Bacteriol.* 181, 167–176.

Hale, C. A., and de Boer, P. A. J. (2002). ZipA is required for recruitment of FtsK, FtsQ, FtsL, and FtsN to the septal ring in *Escherichia coli*. *J. Bacteriol.* 184, 2552–2556. doi: 10.1128/JB.184.9.2552-2556.2002

Haney, S. A., Glasfeld, E., Hale, C., Keeney, D., He, Z., and de Boer, P. (2001). Genetic analysis of the *Escherichia coli* FtsZ.ZipA interaction in the yeast two-hybrid system. Characterization of FtsZ residues essential for the interactions with ZipA and with FtsA. *J. Biol. Chem.* 276, 11980–11987. doi: 10.1074/jbc.M009810200

Hocking, J., Priyadarshini, R., Takacs, C. N., Costa, T., Dye, N. A., Shapiro, L., et al. (2012). Osmolality-dependent relocation of penicillin-binding protein PBP2 to the division site in caulobacter crescentus. *J. Bacteriol.* 194, 3116–3127. doi: 10.1128/JB.00260-12

Höltje, J. V. (1998). Growth of the stress-bearing and shape-maintaining murein sacculus of *Escherichia coli*. *Microbiol. Mol. Biol. Rev.* 62, 181–203.

Jennings, P. C., Cox, G. C., Monahan, L. G., and Harry, E. J. (2011). Super-resolution imaging of the bacterial cytokinetic protein FtsZ. *Micron* 42, 336–341. doi: 10.1016/j.micron.2010.09.003

Juarez, J. R., and Margolin, W. (2010). Changes in the Min oscillation pattern before and after cell birth. *J. Bacteriol.* 192, 4134–4142. doi: 10.1128/JB.00364-10

Karczmarek, A., Martínez-Arteaga, R., Baselga, R. M.-A., Alexeeva, S., Hansen, F. G., Vicente, M., et al. (2007). DNA and origin region segregation are not affected by the transition from rod to sphere after inhibition of *Escherichia coli* MreB by A22. *Mol. Microbiol.* 65, 51–63. doi: 10.1111/j.1365-2958.2007.05777.x

Karimova, G., Dautin, N., and Ladant, D. (2005). Interaction network among *Escherichia coli* membrane proteins involved in cell division as revealed by bacterial two-hybrid analysis. *J. Bacteriol.* 187, 2233–2243. doi: 10.1128/JB.187.7.2233-2243.2005

Karimova, G., Robichon, C., and Ladant, D. (2009). Characterization of YmgF, a 72-residue inner membrane protein that associates with the *Escherichia coli* cell division machinery. *J. Bacteriol.* 191, 333–346. doi: 10.1128/JB.00331-08

Koppelman, C.-M., Aarsman, M. E. G., Postmus, J., Pas, E., Muijsers, A. O., Scheffers, D.-J., et al. (2004). R174 of *Escherichia coli* FtsZ is involved in membrane interaction and protofilament bundling, and is essential for cell division. *Mol. Microbiol.* 51, 645–657. doi: 10.1046/j.1365-2958.2003.03876.x

Kuchibhatla, A., Bhattacharya, A., and Panda, D. (2011). ZipA binds to FtsZ with high affinity and enhances the stability of FtsZ protofilaments. *PLoS ONE* 6:e28262. doi: 10.1371/journal.pone.0028262.g007

Li, G.-W., Burkhardt, D., Gross, C., and Weissman, J. S. (2014). Quantifying absolute protein synthesis rates reveals principles underlying allocation of cellular resources. *Cell* 157, 624–635. doi: 10.1016/j.cell.2014.02.033

Liu, B., Persons, L., Lee, L., and De Boer, P. A. J. (2015). Roles for both FtsA and the FtsBLQ subcomplex in FtsN-stimulated cell constriction in *Escherichia coli*. *Mol Microbiol.* 95, 945–970. doi: 10.1111/mmi.12906

Loose, M., Fischer-Friedrich, E., Herold, C., Kruse, K., and Schwille, P. (2011). Min protein patterns emerge from rapid rebinding and membrane interaction of MinE. *Nat. Struct. Mol. Biol.* 18, 577–583. doi: 10.1038/nsmb.2037

Loose, M., and Mitchison, T. J. (2014). The bacterial cell division proteins FtsA and FtsZ self-organize into dynamic cytoskeletal patterns. *Nat. Cell Biol.* 16, 38–46. doi: 10.1038/ncb2885

Low, H. H., Moncrieffe, M. C., and Löwe, J. (2004). The crystal structure of ZapA and its modulation of FtsZ polymerisation. *J. Mol. Biol.* 341, 839–852. doi: 10.1016/j.jmb.2004.05.031

Löwe, J., Ellonen, A., Allen, M. D., Atkinson, C., Sherratt, D. J., and Grainge, I. (2008). Molecular mechanism of sequence-directed DNA loading and translocation by FtsK. *Mol. Cell.* 31, 498–509. doi: 10.1016/j.molcel.2008.05.027

Lutkenhaus, J., Pichoff, S., and Du, S. (2012). Bacterial cytokinesis: From Z ring to divisome. *Cytoskeleton* (*Hoboken*) 69, 778–790. doi: 10.1002/cm.21054

Ma, X., Ehrhardt, D. W., and Margolin, W. (1996). Colocalization of cell division proteins FtsZ and FtsA to cytoskeletal structures in living *Escherichia coli* cells by using green fluorescent protein. *Proc. Natl. Acad. Sci. U.S.A.* 93, 12998–13003. doi: 10.1073/pnas.93.23.12998

Massey, T. H., Mercogliano, C. P., Yates, J., Sherratt, D. J., and Löwe, J. (2006). Double-stranded DNA translocation: structure and mechanism of hexameric FtsK. *Mol. Cell.* 23, 457–469. doi: 10.1016/j.molcel.2006.06.019

Mercier, R., Petit, M.-A., Schbath, S., Robin, S., El Karoui, M., Boccard, F., et al. (2008). The MatP/matS site-specific system organizes the terminus region of the *E. coli* chromosome into a macrodomain. *Cell* 135, 475–485. doi: 10.1016/j.cell.2008.08.031

Mohammadi, T., Karczmarek, A., Crouvoisier, M., Bouhss, A., Mengin-Lecreulx, D., and den Blaauwen, T. (2007). The essential peptidoglycan glycosyltransferase MurG forms a complex with proteins involved in lateral envelope growth as well as with proteins involved in cell division in *Escherichia coli*. *Mol. Microbiol.* 65, 1106–1121. doi: 10.1111/j.1365-2958.2007.05851.x

Mohammadi, T., Ploeger, G. E. J., Verheul, J., Comvalius, A. D., Martos, A., Alfonso, C., et al. (2009). The GTPase activity of *Escherichia coli* FtsZ determines the magnitude of the FtsZ polymer bundling by ZapA in vitro. *Biochemistry* 48, 11056–11066. doi: 10.1021/bi901461p

Mohammadi, T., Sijbrandi, R., Lutters, M., Verheul, J., Martin, N., den Blaauwen, T., et al. (2014). Specificity of the transport of Lipid II by FtsW in *Escherichia coli*. *J. Biol. Chem.* 289, 17707–17718. doi: 10.1074/jbc.M114.557371

Mohammadi, T., van Dam, V., Sijbrandi, R., Vernet, T., Zapun, A. E., Bouhss, A., et al. (2011). Identification of FtsW as a transporter of lipid-linked cell wall precursors across the membrane. *EMBO J.* 30, 1425–1432. doi: 10.1038/emboj.2011.61

Mosyak, L., Zhang, Y., Glasfeld, E., Haney, S., Stahl, M., Seehra, J., et al. (2000). The bacterial cell-division protein ZipA and its interaction with an FtsZ fragment revealed by X-ray crystallography. *EMBO J.* 19, 3179–3191. doi: 10.1093/emboj/19.13.3179

Mukherjee, A., and Donachie, W. D. (1990). Differential translation of cell division proteins. *J. Bacteriol.* 172, 6106–6111.

Müller, P., Ewers, C., Bertsche, U., Anstett, M., Kallis, T., Breukink, E., et al. (2007). The essential cell division protein FtsN interacts with the murein (peptidoglycan) synthase PBP1B in *Escherichia coli*. *J. Biol. Chem.* 282, 36394–36402. doi: 10.1074/jbc.M706390200

Norris, V., den Blaauwen, T., Doi, R. H., Harshey, R. M., Janniere, L., Jiménez-Sánchez, A., et al. (2007). Toward a hyperstructure taxonomy. *Annu. Rev. Microbiol.* 61, 309–329. doi: 10.1146/annurev.micro.61.081606.103348

Pacheco-Gómez, R., Cheng, X., Hicks, M. R., Smith, C. J. I., Roper, D. I., Addinall, S., et al. (2013). Tetramerization of ZapA is required for FtsZ bundling. *Biochem. J.* 449, 795–802. doi: 10.1042/BJ20120140

Paradis-Bleau, C., Markovski, M., Uehara, T., Lupoli, T. J., Walker, S., Kahne, D. E., et al. (2010). Lipoprotein cofactors located in the outer membrane activate bacterial cell wall polymerases. *Cell* 143, 1110–1120. doi: 10.1016/j.cell.2010.11.037

Pazos, M., Natale, P., and Vicente, M. (2013a). A specific role for the ZipA protein in cell division: stabilization of the FtsZ protein. *J. Biol. Chem.* 288, 3219–3226. doi: 10.1074/jbc.M112.434944

Pazos, M., Natale, P., Margolin, W., and Vicente, M. (2013b). Interactions among the early *Escherichia coli* divisome proteins revealed by bimolecular fluorescence complementation. *Environ. Microbiol.* 15, 3282–3291. doi: 10.1111/1462-2920.12225

Pichoff, S., Du, S., and Lutkenhaus, J. (2014). The bypass of ZipA by overexpression of FtsN requires a previously unknown conserved FtsN motif essential for FtsA-FtsN interaction supporting a model in which FtsA monomers recruit late cell division proteins to the Z ring. *Mol. Microbiol.* 95, 971–981. doi: 10.1111/mmi.12907

Pichoff, S., Shen, B., Sullivan, B., and Lutkenhaus, J. (2012). FtsA mutants impaired for self-interaction bypass ZipA suggesting a model in which FtsA's self-interaction competes with its ability to recruit downstream division proteins. *Mol. Microbiol.* 83, 151–167. doi: 10.1111/j.1365-2958.2011.07923.x

Piette, A., Fraipont, C., den Blaauwen, T., Aarsman, M. E. G., Pastoret, S., and Nguyen-Distèche, M. (2004). Structural determinants required to target penicillin-binding protein 3 to the septum of *Escherichia coli*. *J. Bacteriol.* 186, 6110–6117. doi: 10.1128/JB.186.18.6110-6117.2004

Pla, J., Dopazo, A., and Vicente, M. (1990). The native form of FtsA, a septal protein of *Escherichia coli*, is located in the cytoplasmic membrane. *J. Bacteriol.* 172, 5097–5102.

Pogliano, J., Pogliano, K., Weiss, D. S., Losick, R., and Beckwith, J. (1997). Inactivation of FtsI inhibits constriction of the FtsZ cytokinetic ring and delays the assembly of FtsZ rings at potential division sites. *Proc. Natl. Acad. Sci. U.S.A.* 94, 559–564. doi: 10.1073/pnas.94.2.559

Potluri, L., Karczmarek, A., Verheul, J., Piette, A., Wilkin, J.-M., Werth, N., et al. (2010). Septal and lateral wall localization of PBP5, the major D, D-carboxypeptidase of *Escherichia coli*, requires substrate recognition and membrane attachment. *Mol. Microbiol.* 77, 300–323. doi: 10.1111/j.1365-2958.2010.07205.x

Raskin, D. M., and de Boer, P. A. (1997). The MinE ring: an FtsZ-independent cell structure required for selection of the correct division site in *E. coli*. *Cell* 91, 685–694. doi: 10.1016/S0092-8674(00)80455-9

Raskin, D. M., and de Boer, P. A. (1999a). MinDE-dependent pole-to-pole oscillation of division inhibitor MinC in *Escherichia coli*. *J. Bacteriol.* 181, 6419–6424.

Raskin, D. M., and de Boer, P. A. (1999b). Rapid pole-to-pole oscillation of a protein required for directing division to the middle of *Escherichia coli*. *Proc. Natl. Acad. Sci. U.S.A.* 96, 4971–4976. doi: 10.1073/pnas.96.9.4971

Rico, A. I., Krupka, M., and Vicente, M. (2013). In the beginning *Escherichia coli* assembled the proto-ring: an initial phase of division. *J. Biol. Chem.* 288, 20830–20836. doi: 10.1074/jbc.R113.479519

Rueda, S., Vicente, M., and Mingorance, J. (2003). Concentration and assembly of the division ring proteins FtsZ, FtsA, and ZipA during the *Escherichia coli* cell cycle. *J. Bacteriol.* 185, 3344–3351. doi: 10.1128/JB.185.11.3344-3351.2003

Ruiz, N. (2008). Bioinformatics identification of MurJ (MviN) as the peptidoglycan lipid II flippase in *Escherichia coli*. *Proc. Natl. Acad. Sci. U.S.A.* 105, 15553–15557. doi: 10.1073/pnas.0808352105

Sauvage, E., Derouaux, A., Fraipont, C., Joris, M., Herman, R., Rocaboy, M., et al. (2014). Crystal structure of penicillin-binding protein 3 (PBP3) from *Escherichia coli*. *PLoS ONE* 9:e98042. doi: 10.1371/journal.pone.0098042

Schneider, C. A., Rasband, W. S., and Eliceiri, K. W. (2012). NIH Image to ImageJ: 25 years of image analysis. *Nat. Chem. Biol.* 9, 671–675. doi: 10.1038/nmeth.2089

Sham, L.-T., Butler, E. K., Lebar, M. D., Kahne, D., Bernhardt, T. G., and Ruiz, N. (2014). Bacterial cell wall. MurJ is the flippase of lipid-linked precursors for peptidoglycan biogenesis. *Science* 345, 220–222. doi: 10.1126/science.1254522

Shih, Y.-L., Fu, X., King, G. F., Le, T., and Rothfield, L. (2002). Division site placement in *E.coli*: mutations that prevent formation of the MinE ring lead to loss of the normal midcell arrest of growth of polar MinD membrane domains. *EMBO J.* 21, 3347–3357. doi: 10.1093/emboj/cdf323

Sitnikov, D. M., Schineller, J. B., and Baldwin, T. O. (1996). Control of cell division in *Escherichia coli*: regulation of transcription of ftsQA involves both rpoS and SdiA-mediated autoinduction. *Proc. Natl. Acad. Sci. U.S.A.* 93, 336–341. doi: 10.1073/pnas.93.1.336

Skoog, K., and Daley, D. O. (2012). The *Escherichia coli* cell division protein ZipA forms homodimers prior to association with FtsZ. *Biochemistry* 51, 1407–1415. doi: 10.1021/bi2015647

Small, E., Marrington, R., Rodger, A., Scott, D. J., Sloan, K., Roper, D., et al. (2007). FtsZ polymer-bundling by the *Escherichia coli* ZapA orthologue, YgfE, involves a conformational change in bound GTP. *J. Mol. Biol.* 369, 210–221. doi: 10.1016/j.jmb.2007.03.025

Stricker, J., Maddox, P., Salmon, E. D., and Erickson, H. P. (2002). Rapid assembly dynamics of the *Escherichia coli* FtsZ-ring demonstrated by fluorescence recovery after photobleaching. *Proc. Natl. Acad. Sci. U.S.A.* 99, 3171–3175. doi: 10.1073/pnas.052595099

Szeto, T. H., Rowland, S. L., and King, G. F. (2001). The dimerization function of MinC resides in a structurally autonomous C-terminal domain. *J. Bacteriol.* 183, 6684–6687. doi: 10.1128/JB.183.22.6684-6687.2001

Szwedziak, P., Wang, Q., Freund, S. M. V., and Löwe, J. (2012). FtsA forms actin-like protofilaments. *EMBO J.* 31, 2249–2260. doi: 10.1038/emboj.2012.76

Taheri-Araghi, S., Bradde, S., Sauls, J. T., Hill, N. S., Levin, P. A., Paulsson, J., et al. (2015). Cell-Size control and homeostasis in bacteria. *Curr. Biol.* 25, 385–391. doi: 10.1016/j.cub.2014.12.009

Taschner, P. E., Huls, P. G., Pas, E., and Woldringh, C. L. (1988). Division behavior and shape changes in isogenic ftsZ, ftsQ, ftsA, pbpB, and ftsE cell division mutants of *Escherichia coli* during temperature shift experiments. *J. Bacteriol.* 170, 1533–1540.

Tsang, M.-J., and Bernhardt, T. G. (2015). A role for the FtsQLB complex in cytokinetic ring activation revealed by an ftsL allele that accelerates division. *Mol. Microbiol.* 95, 925–944. doi: 10.1111/mmi.12905

Typas, A., Banzhaf, M., van den Berg van Saparoea, B., Verheul, J., Biboy, J., Nichols, R. J., et al. (2010). Regulation of peptidoglycan synthesis by outer-membrane proteins. *Cell* 143, 1097–1109. doi: 10.1016/j.cell.2010.11.038

Ursinus, A., van den Ent, F., Brechtel, S., de Pedro, M., Höltje, J.-V., Löwe, J., et al. (2004). Murein (peptidoglycan) binding property of the essential cell division protein FtsN from *Escherichia coli*. *J. Bacteriol.* 186, 6728–6737. doi: 10.1128/JB.186.20.6728-6737.2004

van den Berg van Saparoea, H. B., Glas, M., Vernooij, I. G. W. H., Bitter, W., den Blaauwen, T., and Luirink, J. (2013). Fine mapping the contact sites of *Escherichia coli* cell division proteins FtsB and FtsL on FtsQ protein. *J. Biol. Chem.* 288, 24340–24350. doi: 10.1074/jbc.M113.485888

van der Ploeg, R., Verheul, J., Vischer, N. O. E., Alexeeva, S., Hoogendoorn, E., Postma, M., et al. (2013). Colocalization and interaction between elongasome and divisome during a preparative cell division phase in *Escherichia coli*. *Mol. Microbiol.* 87, 1074–1087. doi: 10.1111/mmi.12150

Vats, P., Shih, Y.-L., and Rothfield, L. (2009). Assembly of the MreB-associated cytoskeletal ring of *Escherichia coli*. *Mol. Microbiol.* 72, 170–182. doi: 10.1111/j.1365-2958.2009.06632.x

Ventura, B. D., and Sourjik, V. (2011). Self-organized partitioning of dynamically localized proteins in bacterial cell division. *Mol. Syst. Biol.* 7, 1–13. doi: 10.1038/msb.2010.111

Vicente, M., Gomez, M. J., and Ayala, J. A. (1998). Regulation of transcription of cell division genes in the *Escherichia coli* dcw cluster. *Cell Mol. Life Sci.* 54, 317–324 doi: 10.1007/s000180050158

Wachi, M., Doi, M., Tamaki, S., Park, W., Nakajima-Iijima, S., and Matsuhashi, M. (1987). Mutant isolation and molecular cloning of mre genes, which determine cell shape, sensitivity to mecillinam, and amount of penicillin-binding proteins in *Escherichia coli*. *J. Bacteriol.* 169, 4935–4940.

Wang, L., and Lutkenhaus, J. (1998). FtsK is an essential cell division protein that is localized to the septum and induced as part of the SOS response. *Mol. Microbiol.* 29, 731–740. doi: 10.1046/j.1365-2958.1998.00958.x

Weiss, D. S., Chen, J. C., Ghigo, J. M., Boyd, D., and Beckwith, J. (1999). Localization of FtsI (PBP3) to the septal ring requires its membrane anchor, the Z ring, FtsA, FtsQ, and FtsL. *J. Bacteriol.* 181, 508–520.

White, C. L., Kitich, A., and Gober, J. W. (2010). Positioning cell wall synthetic complexes by the bacterial morphogenetic proteins MreB and MreD. *Mol. Microbiol.* 76, 616–633. doi: 10.1111/j.1365-2958.2010.07108.x

Wientjes, F. B., and Nanninga, N. (1989). Rate and topography of peptidoglycan synthesis during cell division in *Escherichia coli*: concept of a leading edge. *J. Bacteriol.* 171, 3412–3419.

Yamamoto, N., Nakahigashi, K., Nakamichi, T., Yoshino, M., Takai, Y., Touda, Y., et al. (2009). Update on the Keio collection of *Escherichia coli* single-gene deletion mutants. *Mol. Syst. Biol.* 5, 335. doi: 10.1038/msb.2009.92

Yan, K., Pearce, K. H., and Payne, D. J. (2000). A conserved residue at the extreme C-terminus of FtsZ is critical for the FtsA-FtsZ interaction in *Staphylococcus aureus*. *Biochem. Biophys. Res. Commun.* 270, 387–392. doi: 10.1006/bbrc.2000.2439

Yang, J.-C., van den Ent, F., Neuhaus, D., Brevier, J., and Löwe, J. (2004). Solution structure and domain architecture of the divisome protein FtsN. *Mol. Microbiol.* 52, 651–660. doi: 10.1111/j.1365-2958.2004.03991.x

Zijderveld, C. A., Aarsman, M. E., den Blaauwen, T., and Nanninga, N. (1991). Penicillin-binding protein 1B of *Escherichia coli* exists in dimeric forms. *J. Bacteriol.* 173, 5740–5746.

Conflict of Interest Statement: The authors declare that the research was conducted in the absence of any commercial or financial relationships that could be construed as a potential conflict of interest.

Copyright © 2015 Vischer, Verheul, Postma, van den Berg van Saparoea, Galli, Natale, Gerdes, Luirink, Vollmer, Vicente and den Blaauwen. This is an open-access article distributed under the terms of the Creative Commons Attribution License (CC BY). The use, distribution or reproduction in other forums is permitted, provided the original author(s) or licensor are credited and that the original publication in this journal is cited, in accordance with accepted academic practice. No use, distribution or reproduction is permitted which does not comply with these terms.

frontiers in Microbiology

ORIGINAL RESEARCH
published: 22 April 2015
doi: 10.3389/fmicb.2015.00346

Tetracycline hypersensitivity of an *ezrA* mutant links GalE and TseB (YpmB) to cell division

Pamela Gamba[1]*, *Eva Rietkötter*[1], *Richard A. Daniel*[1] and *Leendert W. Hamoen*[1,2]*

[1] Centre for Bacterial Cell Biology, Institute for Cell and Molecular Biosciences, Newcastle University, Newcastle upon Tyne, UK, [2] Bacterial Cell Biology, Swammerdam Institute for Life Sciences, University of Amsterdam, Amsterdam, Netherlands

OPEN ACCESS

Edited by:
Jaan Männik,
University of Tennessee, USA

Reviewed by:
Akos T. Kovacs,
Friedrich Schiller University of Jena, Germany
Mariana Pinho,
Instituto de Tecnologia Química e Biológica, Portugal

***Correspondence:**
Pamela Gamba,
Centre for Bacterial Cell Biology, Institute for Cell and Molecular Biosciences, Newcastle University, Richardson Road, NE2 4AX, Newcastle upon Tyne, UK
pamelagamba@gmail.com;
Leendert W. Hamoen,
Bacterial Cell Biology, Swammerdam Institute for Life Sciences, University of Amsterdam, Science Park 904, 1098 XH, Amsterdam, Netherlands
l.w.hamoen@uva.nl

Specialty section:
This article was submitted to Microbial Physiology and Metabolism, a section of the journal Frontiers in Microbiology

Received: 11 February 2015
Accepted: 08 April 2015
Published: 22 April 2015

Citation:
Gamba P, Rietkötter E, Daniel RA and Hamoen LW (2015) Tetracycline hypersensitivity of an ezrA mutant links GalE and TseB (YpmB) to cell division. Front. Microbiol. 6:346. doi: 10.3389/fmicb.2015.00346

Cell division in bacteria is initiated by the polymerization of FtsZ into a ring-like structure at midcell that functions as a scaffold for the other cell division proteins. In *Bacillus subtilis*, the conserved cell division protein EzrA is involved in modulation of Z-ring formation and coordination of septal peptidoglycan synthesis. Here, we show that an *ezrA* mutant is hypersensitive to tetracycline, even when the tetracycline efflux pump TetA is present. This effect is not related to the protein translation inhibiting activity of tetracycline. Overexpression of FtsL suppresses this phenotype, which appears to be related to the intrinsic low FtsL levels in an *ezrA* mutant background. A transposon screen indicated that the tetracycline effect can also be suppressed by overproduction of the cell division protein ZapA. In addition, tetracycline sensitivity could be suppressed by transposon insertions in *galE* and the unknown gene *ypmB*, which was renamed *tseB* (*t*etracycline sensitivity *s*uppressor of *ezrA*). GalE is an epimerase using UDP-glucose and UDP-N-acetylglucosamine as substrate. Deletion of this protein bypasses the synthetic lethality of *zapA ezrA* and *sepF ezrA* double mutations, indicating that GalE influences cell division. The transmembrane protein TseB contains an extracytoplasmic peptidase domain, and a GFP fusion shows that the protein is enriched at cell division sites. A *tseB* deletion causes a shorter cell phenotype, indicating that TseB plays a role in cell division. Why a deletion of *ezrA* renders *B. subtilis* cells hypersensitive for tetracycline remains unclear. We speculate that this phenomenon is related to the tendency of tetracycline analogs to accumulate into the lipid bilayer, which may destabilize certain membrane proteins.

Keywords: FtsZ, EzrA, tetracycline, FtsL, GalE, *Bacillus subtilis*

Introduction

Division of a bacterial cell involves the coordinated action of several proteins that localize at midcell and assemble in a multiprotein complex known as the divisome. The most crucial component of the division machinery is FtsZ, a structural homolog of eukaryotic tubulin (Lowe and Amos, 1998), which polymerizes into a ring-like structure at midcell when cell division is initiated (Bi and Lutkenhaus, 1991; Peters et al., 2007). In *B. subtilis*, the Z-ring is tethered to the membrane by FtsA (Wang et al., 1997; Ma and Margolin, 1999) and SepF (Duman et al., 2013), and functions as a scaffold for all other division proteins (for review, see Adams and Errington, 2009). Bundling of FtsZ protofilaments is stimulated by both SepF and the conserved protein ZapA

(Gueiros-Filho and Losick, 2002; Singh et al., 2008; Gundogdu et al., 2011; Pacheco-Gomez et al., 2013). Another conserved early cell division protein that binds to the Z-ring is EzrA, which will be discussed below. After the Z-ring has formed, the late cell division proteins are recruited (Gamba et al., 2009). The transmembrane proteins PBP 2B, FtsL, DivIB, and DivIC are interdependent for their recruitment to the Z-ring. PBP 2B is the transpeptidase that introduces cross-links into septal peptidoglycan (Daniel et al., 1996). The exact function of FtsL, DivIB, and DivIC is unclear. FtsL is efficiently degraded by the regulatory protease RasP through intramembrane proteolysis (Bramkamp et al., 2006), and presumably plays a regulatory role because of its marked instability (Daniel et al., 2006). DivIC is also an unstable protein (Robson et al., 2002). DivIB might have a role in the regulation of FtsL and DivIC stability (Daniel et al., 2006).

Several proteins modulate the assembly of the Z-ring in space and time. In *Bacillus subtilis*, the Min proteins prevent cell division at newly formed cell poles by inhibiting FtsZ bundling (Dajkovic et al., 2008; Gregory et al., 2008), and by promoting disassembly of the divisome after division is completed (van Baarle and Bramkamp, 2010). The nucleoid occlusion protein Noc binds to specific DNA sequences and prevents Z-ring assembly over the nucleoid, thereby coordinating cell division with DNA segregation (Wu and Errington, 2004; Wu et al., 2009; Adams et al., 2015). Cell division also responds to the metabolic status of the cell. The glucosyltransferase UgtP, involved in the synthesis of lipoteichoic acids, has been shown to accumulate at septa and to inhibit cell division in a growth-rate dependent manner (Weart et al., 2007; Chien et al., 2012). Recently, a link to central carbon metabolism has been established with the discovery that pyruvate levels can affect Z-ring formation (Monahan et al., 2014).

The early cell division protein EzrA is conserved in low G+C Gram-positive bacteria. The protein is anchored to the cell membrane by an N-terminal transmembrane domain and has a large cytoplasmic C-terminal domain that binds to FtsZ (Levin et al., 1999; Haeusser et al., 2004). Initially, it was assumed that EzrA negatively regulates Z-ring formation since an *ezrA* mutant shows an increased frequency of Z-rings in fast growth rate conditions, and purified EzrA inhibits bundling of FtsZ protofilaments (Haeusser et al., 2004; Chung et al., 2007; Singh et al., 2007). However, the function of EzrA is more complicated. Cells lacking EzrA are significantly longer than wild-type cells because of a delay in constriction (Levin et al., 1999; Kawai and Ogasawara, 2006), and deletion of the positive Z-ring regulators *zapA* or *sepF* in an *ezrA* background causes a severe block in cell division (Gueiros-Filho and Losick, 2002; Hamoen et al., 2006). A recent crystallographic study suggested that EzrA forms large semi-circular structures that can hook FtsZ filaments to the cell membrane. The large curved EzrA structures show some homology to the spectrin proteins which connect actin filaments in eukaryotes (Cleverley et al., 2014). Another activity of EzrA is the recruitment of the major transglycosylase/transpeptidase PBP 1 from the lateral wall to the division site (Claessen et al., 2008; Tavares et al., 2008).

Here we describe a peculiar phenotype of an *ezrA* mutant, the hypersensitivity to the antibiotic tetracycline. Detailed analysis of this phenomenon revealed that this sensitivity is not related to the classical inhibitory effect of tetracycline on protein translation. We show that overexpression of FtsL can suppress the tetracycline effect, and low levels of this key cell division regulator might be the reason for the phenotype. Using an extensive transposon screen we identified two new genes, *galE* and *ypmB,* which suppress the tetracycline sensitivity of an *ezrA* mutant when deleted. Interestingly, the absence of the UDP-galactose epimerase GalE restores also the lethal cell division defects of a *ezrA sepF* or *ezrA zapA* double mutant. Since a transposon insertion in the unknown *ypmB* gene suppresses the tetracycline induced defects of an *ezrA* mutant, the gene was renamed *tseB* (*t*etracycline sensitivity *s*uppressor of *ezrA*). TseB is a membrane protein with an extracellular protease domain, and is enriched at cell division sites. The absence of this protein causes a short cell phenotype, further suggesting a role in cell division.

Materials and Methods

Bacterial Strains and Growth Conditions

Strains and plasmids used in this study are listed in **Table 1**. *B. subtilis* strains were grown at 30°C or 37°C in Antibiotic medium no. 3 (PAB, Difco, or Oxoid), LB or competence medium (CM) (Hamoen et al., 2002). Agar (Bacteriological agar no. 1, Oxoid) was added to a final concentration of 1.5% to prepare solid media. When required, media were supplemented with 10 μg/ml tetracycline (unless stated otherwise), 5 mM $MgSO_4$, 22.5 μM EDTA, 22.5 μM phenanthroline, or 0.5 μg/ml anhydrotetracycline. If needed, xylose and IPTG were used as inducers at concentrations of 0.5–2%, and 1 mM, respectively. Selection of transformants was performed on nutrient agar (Oxoid), supplemented when required with 10 μg/ml tetracycline, 5 μg/ml chloramphenicol, 50 μg/ml spectinomycin, 5 μg/ml kanamycin or 0.5 μg/ml erythromycin with 25 μg/ml lincomycin. *E. coli* strains were grown in LB at 37°C and used as cloning intermediates.

Growth Assays on Agar Plates

Frozen stocks were streaked out to single colonies on nutrient agar plates supplemented as required and grown overnight at 37°C. To ensure an even distribution of cells on all the plates that had to be compared, fresh single colonies were picked and spread onto a short streak on a new nutrient agar plate. This primary streak was then crossed with a new sterile loop that was used to transfer the inoculum on a new plate and isolate single colonies. Then, for each of the other agar plates that had to be compared within the same experiment, the same procedure was repeated with a new sterile loop by crossing the primary streak on a different (yet adjacent) point.

Plasmid and Strain Construction

Molecular cloning, PCRs, and *E. coli* transformations were carried out by standard techniques. Oligonucleotides used in this study are listed in **Table 2**. To construct plasmid pPG6(mGFP), a fragment of 504 bp containing the *tseB* coding sequence was amplified from 168 chromosomal DNA with oligonucleotides PG77 and PG79, carrying the *Hind*III and *Xho*I restriction sites, respectively. The insert was then cloned into an equally cut pSG1729, resulting in plasmid pPG6. Plasmid pPG6 was then

TABLE 1 | Strains and plasmids used in this study.

Strain	Relevant features or genotype	Construction, source or reference
B. subtilis		
168	*trpC2*	Laboratory stock
BSB1	*trp+*	Nicolas et al., 2012
1356	*zapA-yshB::tet*	Feucht and Errington, 2005
2020	*amyE*::(P_{xyl}-*gfpmut1-ftsZ, spc*)	J. Sievers (unpublished)
3362	*ezrA::tet*	Hamoen et al., 2006
3828	*ftsL*::*pSG441 aphA-3* P_{spac}*-pbpB, amyE*::*cat* P_{xyl}-Δ*30-ftsL*	Bramkamp et al., 2006
4077	*ylmBC*::*(erm* P_{spac}*-ylmD), ezrA*::*tet*	Hamoen et al., 2006
814	Δ*ftsL-Pspac-pbpB kan, amyE*::*Pxyl-HA-ftsL cat*	Daniel and Errington, 2000
BG239	*thr-5, tet-4*	Wei and Bechhofer, 2002
KS273	*aprE*::*Pspac-zapA spc*	Surdova et al., 2013
LH28	*ezrA*::*cat*	L. Hamoen (unpublished)
SG82	*lacA*::*tet*	Laboratory stock
YK012	CRK6000 *ezrA*::*spc*	Kawai and Ogasawara, 2006
YK204	CRK6000 *sepF*::*spc*	Ishikawa et al., 2006
PG49	*ezrA*::*spc*	YK012 DNA → 168
PG100	*lacA*::*tet, ezra*::*cat*	LH28 DNA → SG82
PG112	*tet-4*	5kb *rpsJ* region from BG239 → 168
PG113	*tet-4, ezrA*::*spc*	5kb *rpsJ* region from BG239 → PG49
PG116	*tet-4, ezrA*::*cat*	5kb *rpsJ* region from BG239 → LH28
PG121	*ezrA*::*tet*, *tseB*:*TnYLB-1 kan*	pMarB integration into 3362
PG126	*ezrA*::*tet*, *zapA-TnYLB-1- yshB kan*	pMarB integration into 3362
PG129	*ezrA*::*tet*, *galE*:*TnYLB-1 kan*	pMarB integration into 3362
PG135	*tseB*:*TnYLB-1 kan*	PG121 DNA → 168
PG140	*zapA-TnYLB-1- yshB kan*	PG126 DNA → 168
PG143	*galE*:*TnYLB-1 kan*	PG129 DNA → 168
PG149	*aprE*::P_{spac}*-zapA, spc*	KS273 DNA → 168
PG158	*sepF*::*spc*	YK204 DNA → 168
PG160	*ezrA*::*tet, amyE*::P_{xyl}-Δ*30ftsL-cat*	3828 DNA → 3362
PG162	*ezrA*::*cat, aprE*::P_{spac}*-zapA spc*	PG149 DNA → LH28
PG164	*ezrA*::*cat, zapA-yshB*::*tet,* P_{spac}*-zapA*	1356 DNA → PG162
PG209	*ezrA*::*tet, amyE*::P_{xyl}*-gfp-ftsZ spc*	2020 DNA → 3362
PG234	*galE*::*kan*	This work
PG235	*tseB*::*kan*	This work
PG238	*ezrA*::*tet, galE*::*kan*	PG234 DNA → 3362
PG239	*ezrA*::*tet, tseB*::*kan*	PG235 DNA → 3362
PG251	*galE*::*spc*	This work
PG252	*tseB*::*spc*	This work
PG294	*ezrA*::*tet, galE*::*kan, sepF*::*spc*	YK204 DNA → PG238
PG296	*galE*::*kan, ylmBC*::*(erm* P_{spac}*-ylmD), ezrA*::*tet*	4077 DNA → PG238
PG305	Δ*ftsL-*P_{spac}*-pbpB kan, amyE*::P_{xyl}*-HA-ftsL cat, ezrA*::*tet*	3362 DNA → 814
PG307	*ezrA*::*cat, zapA-yshB*::*tet, aprE*::P_{spac}*-zapA spc, galE*::*kan*	PG234 DNA → PG164
PG325	*aprE*::P_{spac}*-tseB spc*	pPG16 → 168
PG327	*aprE*::P_{spac}*-galE spc*	pPG18 → 168
PG330	*tseB*::*kan, aprE*::P_{spac}*-tseB spc*	PG325 DNA → PG235
PG332	*ezrA*::*tet, galE*::*kan, aprE*::P_{spac}*-galE spc*	PG327 DNA → PG239
PG333	*ezrA*::*tet, tseB*::*kan, aprE*::P_{spac}*-tseB spc*	PG325 DNA → PG239
PG718	*trp+, amyE*::P_{xyl}*-gfp-tseB spc*	pPG6(mGFP) integration into BSB1
PG742	Δ*ftsL-Pspac-pbpB kan, amyE*::*Pxyl-HA-ftsL cat, lacA*::*tet*	SG82 DNA → 814
E. coli		
DH5α	F^-, *φ80lacZΔM15*, *Δ(lacZYAargF)U196*, *recA1*, *endA1*, *hsdR17*, (r_{K-}, m_{K+}), *phoA*, *supE44*, *λ*$^-$, *thi*$^-$*1*, *gyrA96*, *relA1*	Invitrogen

Plasmid	Relevant features or genotype	Construction, source or references
pAPNC213	*bla aprE' spc lacI* P_{spac}*'aprE*	Morimoto et al., 2002
pMarB	*bla erm* P_{ctc} *Himar1 kan* (TnYLB-1)	Le Breton et al., 2006
pSG1729	*bla amyE3' spc* P_{xyl}*-gfpmut1' amyE5'*	Lewis and Marston, 1999
pHT21	*kan*	Trieu-Cuot and Courvalin, 1983
pLOSS*	*spc*	Claessen et al., 2008
pPG6(mGFP)	*bla amyE3' spc* P_{xyl}*tseB-mgfpm1' amyE5'*	This work
pPG16	*bla aprE' spc lacI* P_{spac} *tseB'aprE*	This work
pPG18	*bla aprE' spc lacI* P_{spac} *galE'aprE*	This work

Unless stated otherwise, all strains were made in the 168 wild type background. Genes responsible for resistance to antibiotics are abbreviated as follows: bla, ampicillin; cat, chloramphenicol; erm, erythromycin; kan, kanamycin; spc, spectinomycin; tet, tetracycline.

used for a quick change mutagenesis reaction with oligonucleotides HS410 and HS411 in order to introduce the A206K mutation in the GFP coding sequence to reduce protein dimerization. The resulting plasmid was verified by sequencing and named pPG6(mGFP).

Plasmids pPG16 and pPG18 were derived from pAPNC213, which was digested with *Eco*RI and *Bam*HI, and ligated with PCR products digested with the same restriction enzymes. For plasmid pPG16, the *tseB* coding sequence, including the ribosome binding site, was amplified using oligonucleotides PG152 and PG159. For plasmid pPG18, the *galE* coding sequence and 70 bp of the upstream region was amplified with oligonucleotides PG70 and PG161.

TABLE 2 | Oligonucleotides used in this study.

Name	Restriction site	Sequence (5′–3′)
HS410		CCTGTCCACACAATCTAAACTTTCGAAAGATCCC
HS411		GGGATCTTTCGAAAGTTTAGATTGTGTGGACAGG
Km3	*Bam*HI	GGG**GGATCC**AAGACGAAGAGGATGAAG
Km4	*Eco*RI	CCC**GAATTC**AGAGTATGGACAGTTGCG
oIPCR1		GCTTGTAAATTCTATCATAATTG
oIPCR2		AGGGAATCATTTGAAGGTTGG
oIPCR3		GCATTTAATACTAGCGACGCC
PG57		TGATGGTGCTCCAGAAGAAC
PG58		ACAGAACCACGAACTGTAGG
PG70	*Eco*RI	GCC**GAATTC**TTATTCCGCACTCTTATACCCATT
PG77	*Hind*III	CGG**AAGCTT**TTAAGGCGTGATATTTTTGAGAA
PG79	*Xho*I	CGG**CTCGAG**ATGAGAAAAAAAGCATTAATATTTACCG
PG103	*Bam*HI	GAC**GGATCC**CTTCTCACCTACGTACGATA
PG120		TACCTTCCTGCAGCTGATTC
PG121		GAGCAGCTTACTGGAATCTC
PG122	*Hind*III	GATCAGT**AAGCTT**GACGAATTAGGGGGAGTTCAAG
PG128	*Bam*HI	GAA**GGATCC**CCTAAAAAATGACCTGTTTT
PG129		CTCCGTTCCTCCACTTGATG
PG130	*Eco*RI	ATA**GAATTC**GAATGGAGGCCTTCTCAATT
PG131		ATGATGATCGCCCGCGAAAC
PG134	*Nco*I	GAGT**CCATGG**TCAGAGTATGGACAGTTGCG
PG135	*Nco*I	GATC**CCATGG**GACGAATTAGGGGGAGTTCAAG
PG146	*Bam*HI	CCGA**GGATCC**AGGATGTACTTAAACGCTAACG
PG149	*Hind*III	GCC**AAGCTT**CAAGAGGACGCTTTATTCTTC
PG152	*Eco*RI	CGTC**GAATTC**TTAAGGCGTGATATTTTTGAGAA
PG159	*Bam*HI	ACCT**GGATCC**TCGGCCTTGCGCTGGATGAAGA
PG161	*Bam*HI	GGCA**GGATCC**CTATTAATAAACGATTAAACTTC
Spc-pLoss-Rev	*Eco*RI	GCAGCC**GAATTC**CAAGAGGACGCTTTATTCTTC

Recognition sites for restriction enzymes are indicated in bold.

Genes were deleted by replacing their coding sequences with antibiotic resistance cassettes. Approximately 3 kb upstream and downstream of the coding sequence of the gene of interest were amplified. For deletion of *galE*, oligonucleotides PG128-PG129 and PG130-PG131 were used. For *tseB* deletions, oligonucleotides PG120-PG135 and PG103-PG131 were used for a deletion with a *kan* cassette, while PG120-PG122 and PG103-PG121 were used to construct a deletion with a *spc* cassette. Relevant restriction sites were inserted into the primers. Ligation reactions were assembled with equimolar concentrations of each of the three PCR products, using about 1.5 μg of each 3 kb product in a total volume of 40 μl. Competent cells of *B. subtilis* were transformed with half of each ligation reaction. Transformants were selected on antibiotic plates and verified by PCR. Antibiotic resistance cassettes were amplified from plasmids: *kan* from pHT21 (oligonucleotides km3-km4 for *galE* and km3-PG134 for *tseB*), *spc* from pLOSS* (oligonucleotides PG146 and spc-pLoss-Rev for *galE*, PG146-PG149 for *tseB*).

An N-terminal GFP fusion to *tseB* was constructed by transforming pPG6(mGFP) plasmid into strain BSB1, generating strain PG718. The integration was obtained by a double crossover recombination event between the *amyE* regions located on the plasmid and the chromosomal *amyE* gene of strain 168. Transformants were selected on nutrient agar plates containing spectinomycin. Correct integration into the *amyE* gene was tested and confirmed by lack of amylase activity upon growth on plates containing 1% starch.

Microscopic Imaging

Samples were mounted on microscope slides coated with a thin layer of 1.2% agarose. Images were acquired with a Zeiss Axiovert 200 M or a Zeiss Axiovert 135 microscope coupled to a Sony Cool-Snap HQ cooled CCD camera (Roper Scientific), and using Metamorph imaging software (Universal Imaging). For membrane staining, cells were mounted on slides coated with 1% agarose supplemented with the membrane dye Nile Red (0.1 μg/ml, Molecular Probes) or by mixing 9 μl of cells with 1 μl of Nile Red solution (12.5 mg/ml) before spotting the sample on the agarose slide. Alternatively, cells were mixed with the membrane dye FM5-95 (Invitrogen), at a final concentration of 0.4 μg/ml. Nucleoids were stained by adding DAPI (0.02 μg/ml, Sigma) to the agarose slide. Images were analyzed and prepared for publication with ImageJ (http://rsb.info.nih.gov/ij/). For time-lapse microscopy, strain PG718 was grown in CM supplemented with 0.5% xylose at 30°C until cells reached exponential phase, and subsequently mounted onto a thin semisolid matrix made of CM supplemented with 0.5% xylose and 1.5% low-melting point agarose on a microscope slide. Slides were incubated in a temperature-controlled chamber (30°C) on a Deltavision RT automated microscope (Applied Precision). Phase contrast and GFP images were taken every 10 min.

Screen for Tetracycline-Insensitive Suppressor Mutants

Random transposon mutagenesis of strain 3362 (*ezrA*::*tet*) was carried out using the mariner transposable element TnYLB-1 as described (Le Breton et al., 2006). Plasmid pMarB was transformed into strain 3362 at 30°C. Individual colonies carrying the complete transposon plasmid were picked and grown in LB at 37°C for 8 h. Aliquots were frozen and stored at −80°C. Serial dilutions of each culture were plated on nutrient agar plates containing kanamycin or erythromycin and incubated at 50°C overnight to inhibit plasmid replication. The following morning, the clone with the highest ratio of kan^R/erm^R colonies on plates was chosen. Appropriate dilutions of the selected clone were plated on nutrient agar plates and incubated at 50°C to construct a library of about 70,000 colonies. Cells were scraped off the plates, aliquoted, and frozen. About 75,000 clones of the library were plated on PAB plates supplemented with 10 μg ml^{-1} tetracycline and incubated at 37°C for 20 h. Individual colonies were picked and checked for integration of the transposon (kan^R), loss of the plasmid (erm^S), presence of the *ezrA* deletion (tet^R), and checked under the microscope to see loss of the filamentous phenotype when streaked on PAB with tetracycline. Two rounds of backcrosses into strain 3362 were performed to confirm the linkage between transposon insertion and loss of

tetracycline hypersensitivity. Finally, the site of transposon insertion was determined by performing an inverse PCR amplification on the chromosomal DNA which had been previously digested with TaqI and ligated. Finally, PCR reactions were sequenced and the results aligned with the *B. subtilis* published genome sequence. Oligonucleotides for inverse PCR and sequencing were oIPCR1, −2 and −3 respectively, as described (Le Breton et al., 2006).

Cell Length Measurements

Cells were grown at 37°C in CM, LB, PAB, or PAB supplemented with 5 mM Mg^{2+}. At mid-exponential phase for LB medium or early stationary phase for other media, cells were sampled and stained with Nile Red prior to microscopic examination. At least 100–150 cells were measured in each experiment and all experiments were replicated at least three times. The mean cell length was calculated for each experiment and then averaged over three replicates. Wild type cell length was set as 100% and relative cell length was calculated for all other strains.

Western Blotting

For the detection of HA-FtsL shown in **Figure 4**, cells were grown overnight at 30°C in PAB with 5 mM $MgSO_4$, 0.5–2% xylose, 1 mM IPTG. Cultures were diluted to an O.D.600 of 0.1 in the same medium, grown for 2 h at 37°C and diluted again to 0.1 in warm medium. The exponentially growing cultures were incubated until an O.D.600 of 0.3 (**Figure 4A**) or 0.5 (**Figures 4B,C**) was reached. Cell pellets were resuspended in 100 µl of 1× NuPAGE LDS Sample Buffer (Invitrogen) with 5× Complete mini protease inhibitor (Roche) and broken by sonication. Relative protein concentrations were estimated by reading the A280 of all samples with a NanoDrop® ND-1000 spectrophotometer and equal amount of proteins were loaded on polyacrylamide gels. Proteins were transferred onto a PVDF membrane (GE Healthcare) by using either a wet or a semi-dry procedure and Western blotting was performed according to standard methods. In this study, a 1:10,000 dilution of rabbit polyclonal anti-FtsZ serum (laboratory stock), 1:10,000 dilution of rabbit polyclonal anti-PBP2B serum (laboratory stock), and a 1:1000 dilution of mouse monoclonal 12CA5 anti-HA antibody (Ivanov and Nasmyth, 2005) were used. Secondary antiserums, anti-rabbit-horseradish-peroxidase, and anti-mouse-horseradish-peroxidase (Sigma), were used at a dilution of 1:10,000.

For the immunodetection of ZapA shown in Figure S1, strains were grown at 37°C in PAB medium and samples were collected and flash frozen at O.D.600 ∼0.3. Cell pellets were resuspended in lysis buffer (100 mM Tris-Cl pH 7.5, 2 mM EDTA, supplemented with Roche Complete mini protease inhibitor) containing 5 µg/ml lysozyme, incubated 10 min at 37°C and then sonicated. Cell debris were removed by centrifugation. Relative protein concentrations were estimated with a Bio-Rad protein assay and equal amount of proteins were loaded on NuPAGE 4–12% Bis-Tris gradient gels which were run in MES buffer (Life Technologies). Proteins were transferred onto a Hybond-P PVDF membrane (GE Healthcare) by using a wet procedure and western blotting was performed according to standard methods. A 1:2000 dilution of rabbit polyclonal anti-ZapA serum was used. Anti-rabbit horseradish peroxidase-linked antiserum (Sigma) was used as secondary antibody at a dilution of 1:10,000. Protein bands were detected using an ImageQuant LAS 4000 mini digital imaging system (GE Healthcare).

Results

Tetracycline Hypersensitivity of an *ezrA* Mutant

A *B. subtilis ezrA* mutant forms normal colonies on plate. When we transformed an *ezrA* deletion into other *B. subtilis* backgrounds, sometimes very small colonies were obtained that contained filamentous cells. However, this result was not always reproducible. Eventually, it emerged that this filamentous phenotype was caused by insertion of the tetracycline resistance cassette *tetL* in *ezrA*, in combination with selection of transformants on selective PAB plates. Without tetracycline, an *ezrA* mutant forms normal colonies on PAB plates (**Figure 1A**). Despite the presence of a functional resistance cassette, the addition of tetracycline (10 µg/ml) results in very small colonies containing highly filamentous cells, (**Figures 1A,B**). Addition of 5 mM $MgSO_4$ to PAB plates with tetracycline restored normal growth and abolished filamentation (**Figures 1A,B**). When the *tetL* cassette was located at another locus (*lacA*), in an otherwise wild-type background, no effect on cell length or colony size was observed. Subsequent introduction of a different *ezrA* deletion (*ezrA*::*cat*) into this background resulted again in small colonies and strong filamentation on PAB plates with tetracycline (**Figures 1A,B**). For unknown reasons, we did not observe this filamentation phenotype in liquid PAB medium. Finally, hypersensitivity became apparent also on nutrient agar plates, but only when increased levels of tetracycline were used ($\geq$ 30 µg/ml).

To examine whether the effect of tetracycline was specific for an *ezrA* mutant, several division mutants were tested that carried a *tetL* cassette. No significant effect on colony size or cell length was observed when a *zapA*, *sepF*, *noc,* or *gpsB* mutant was grown on PAB plates with tetracycline (**Figure 1A** and data not shown), indicating that the effect is specific for *ezrA*.

Tetracycline Effect is Not Related to Protein Translation Inhibition

PAB medium contains relative low concentrations of Mg^{2+} (210 µM Murray et al., 1998). Interestingly, the growth defect of an *ezrA* mutant on PAB plates with tetracycline can be suppressed by the addition of Mg^{2+}. Tetracycline is a metal-ion chelator (Nelson, 1998) and might reduce the cellular Mg^{2+} concentrations to such levels that growth and cell division are affected in this growth medium. If this is the case then a similar phenotype should be observed with other magnesium chelators. However, neither the addition of EDTA nor phenanthroline, applied at the same molar concentrations as tetracycline (23 µM), had an effect on cell division (not shown).

The *tetL* cassette encodes the TetA transporter which exports tetracycline in a complex with divalent cations such as Mg^{2+} (Krulwich et al., 2001). To see whether the growth phenotype was linked to the presence of the TetA transporter, an alternative tetracycline resistance cassette was used. *tet-4* is a point

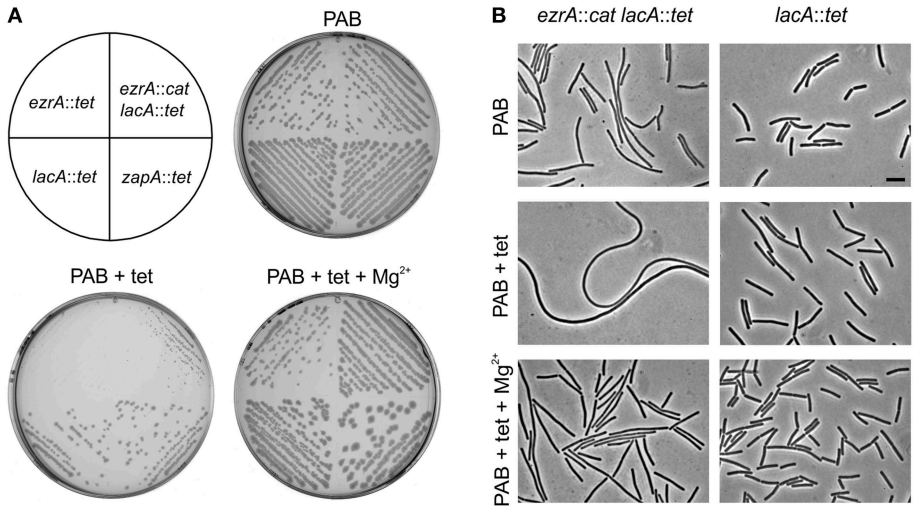

FIGURE 1 | Effect of tetracycline on *ezrA* mutants. (A) Growth of *ezrA*::*tet* (3362), *lacA*::*tet* (SG82), *ezrA*::*cat lacA*::*tet* (PG100), and *zapA-yshB*::*tet* (1356) strains on PAB plates with and without 10 μg/ml tetracycline (tet) and 5 mM $MgSO_4$ (Mg^{2+}). **(B)** Phase contrast images of cells taken from the PAB plates in **(A)**. Scale bar 5 μm.

mutation in the ribosomal protein S10 that reduces the sensitivity of the ribosome for tetracycline (Williams and Smith, 1979; Wei and Bechhofer, 2002). This mutation confers tetracycline resistance without affecting the concentration of the internal Mg^{2+} pool. The *tet-4* mutation provides a lower resistance to tetracycline compared to the *tetL* cassette, therefore strains were grown on PAB plates containing 2 μg/ml tetracycline (**Figures 2A,B**). Again, introduction of an *ezrA* mutation in the *tet-4* background caused hypersensitivity to tetracycline, indicating that this phenotype is not related to the TetA transporter.

The fact that the *tet-4* mutation is unable to prevent the tetracycline effect suggests that this phenomenon is not associated with the inhibition of protein translation. This was supported by the finding that 0.5 μg/ml anhydrotetracycline, a tetracycline analog that does not bind to the ribosome (Oliva and Chopra, 1992), also affects growth and cell division of *ezrA* mutants (**Figures 2C,D**).

Tetracycline Does Not Affect Z-Ring Formation

The tetracycline-induced filamentation of *ezrA* cells indicates a cell division problem. To examine whether this problem is caused by an inability to form Z-rings, a fluorescent GFP-FtsZ marker was introduced. The resulting strain PG209 (*ezrA*::*tet amyE*::*Pxyl-gfp-ftsZ*) was streaked on PAB plates containing 10 μg/ml tetracycline and 0.5% xylose to induce GFP-FtsZ. Cells were taken from colonies and mounted onto agarose covered microscope slides containing Nile Red and DAPI, to stain the cell membrane and nucleoid, respectively (**Figure 3**). The filamentous cells were very fragile and many cells lysed. Intact cells showed normal nucleoids and some Z-rings, but the fluorescent membrane stain indicated a clear lack of septation. This suggests that the block in cell division is not caused by a defect in FtsZ assembly, but occurs later in the division process.

Low FtsL Levels in *ezrA* Mutants

Kawai and Ogasawara have shown that an *ezrA* mutant is sensitive to reduced FtsL expression levels (Kawai and Ogasawara, 2006). FtsL is unstable and cleaved by the zinc metalloprotease RasP, which is involved in regulated intramembrane proteolysis (RIP) (Heinrich et al., 2008; Wadenpohl and Bramkamp, 2010). This proteolytic degradation plays an important regulatory role in the assembly of the late cell division proteins (Daniel et al., 2006). Possibly, FtsL levels become critically limiting for growth when an *ezrA* mutant is grown on PAB plates in the presence of tetracycline.

We first tested FtsL levels in an *ezrA* background, by using a strain that carries a deletion of the native *ftsL* gene and an ectopically located xylose-inducible HA-tagged *ftsL* fusion (strain 814, Daniel and Errington, 2000). The HA epitope tag enables convenient detection of cellular FtsL levels with Western blotting using sensitive HA-antibodies. Strain 814 was transformed with the *ezrA*::*tet* mutation, resulting in strain PG305. This strain showed an extremely slow growth rate when grown with 0.5% xylose in liquid PAB medium without antibiotics. In fact, no HA-FtsL could be detected under these conditions (**Figure 4A**). When the xylose concentration was increased to 2%, strain PG305 grew better, although still slower than strain 814, and a weak HA-FtsL band became visible (**Figure 4B**). Interestingly, strain PG305 showed normal growth with 0.5% xylose when 5 mM Mg^{2+} was added to the medium, although FtsL levels were still not restored to the levels observed in the parental strain 814 (**Figure 4C**). These data indicate that a deletion of *ezrA* results in reduced FtsL levels, which explains why an *ezrA* mutant is so sensitive for manipulation of the FtsL concentration.

As mentioned above, we observed hypersensitivity to tetracycline only on agar plates. Unfortunately, growth on solid medium hampers homogeneous sampling at specific growth phases. Therefore, we introduced a tetracycline resistance marker

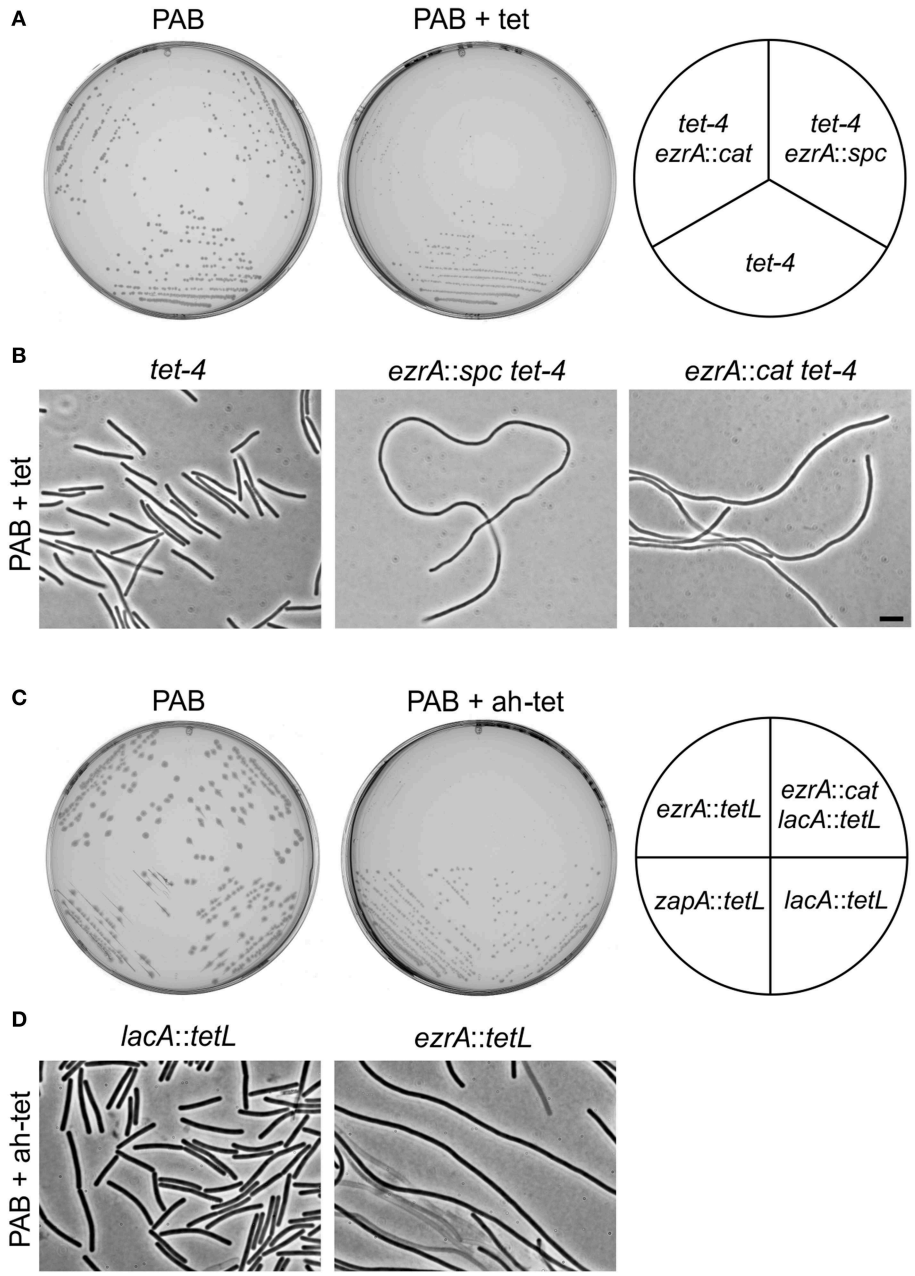

FIGURE 2 | Tetracycline-induced growth defects of *ezrA* mutants are unrelated to protein translation inhibition. (A) Growth of strains *tet-4* (PG112), *ezrA*::*cat tet-4* (PG116), *ezrA*::*spc tet-4* (PG113), on PAB plates supplemented with 2 μg/ml tetracycline (tet). **(B)** Phase contrast images of cells taken from the PAB plates in **(A)**. Scale bar 5 μm. **(C)** Effect of anhydrotetracycline. Growth of *ezrA*::*tet* (3362), *ezrA*::*cat lacA*::*tet* (PG100), *zapA-yshB*::*tet* (1356), and *lacA*::*tet* (SG82) strains on PAB plates with or without 0.5 μg/ml anhydrotetracycline (ah-tet). ZapA mutant strain was included as an additional control. **(D)** Phase contrast images of cells taken from the PAB plates in **(C)**.

into strain 814, obtaining strain PG742 and plated serial dilutions onto PAB plates in the presence of increasing concentrations of xylose, to allow for differential expression of FtsL. As shown in **Figure 4D**, higher levels of induction were required to allow colony formation in the presence of tetracycline, suggesting that FtsL levels become limiting under those conditions. These data would imply that the tetracycline-induced filamentation of an *ezrA* mutant can be suppressed by increasing FtsL levels in the cell. To test this, a xylose-inducible truncated copy of FtsL (Δ*30-ftsL*) was introduced into an *ezrA*::*tet* mutant. This variant of FtsL was chosen since removal of the first 30 amino acids of FtsL stabilizes the protein (Bramkamp et al., 2006). When the resulting strain PG160 was streaked on PAB plates with tetracycline and 1% xylose, cell

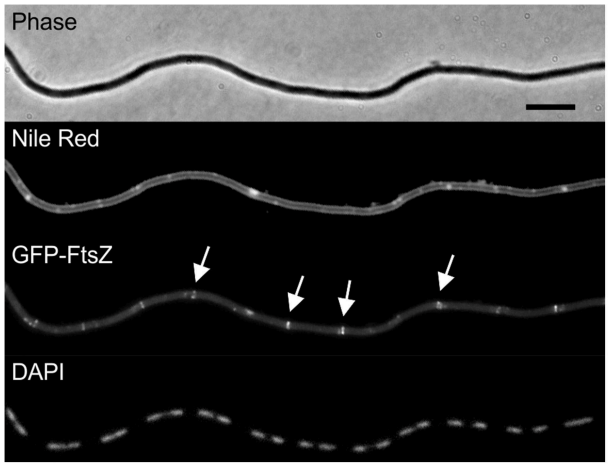

FIGURE 3 | Tetracycline does not prevent Z-ring formation. Strain PG209 (*ezrA*::*tet amyE*::*Pxyl-gfp-ftsZ*) was streaked on PAB plates containing 10 μg/ml tetracycline, and 0.5% xylose to induce GFP-FtsZ. Cells were stained with DAPI and Nile Red to visualize nucleoids and the cell membrane, respectively. Arrows highlight some of the Z-rings. Scale bar 5 μm.

division was indeed restored and normal colonies were obtained (**Figures 4E,F**).

Screen for Novel Suppressor Mutants

The mechanism by which tetracycline causes filamentation of an *ezrA* mutant is unclear. To examine whether other proteins are involved in the tetracycline effect, we screened a transposon library for mutants that would grow normally on PAB plates with tetracycline. Plasmid pMarB, carrying the *mariner* transposon TnYLB-1 (Le Breton et al., 2006), was introduced into strain 3362 (*ezrA*::*tet*), and after transposon mutagenesis approximately 70,000 colonies were screened. Several suppressor mutants that restored colony growth and rescued the division defect were selected. Further analyses showed that one suppressor strain contained a transposon inserted immediately after *zapA*. Two other suppressor mutants harbored transposon insertions into *galE*, which encodes an UDP-galactose epimerase (Estrela et al., 1991; Soldo et al., 2003), and two suppressor mutants contained transposon insertions in the unknown gene *ypmB*. A *galE* and *ypmB* null mutant were made by replacing the complete ORFs with a kanamycin resistance marker (strain PG234 and PG235), and transforming the deletions into strain 3362 (*ezrA*::*tet*). The resulting double mutants grow normally on PAB plates with tetracycline (**Figure 5**), confirming that the absence of either GalE or YpmB suppresses the tetracycline induced cell division defect.

ZapA Overexpression Suppresses Filamentation

zapA is the upstream gene in the bicistronic *zapA-yshB* operon. Since one of the suppressors contained a transposon insertion between *zapA* and *yshB*, and precisely one nucleotide upstream the start codon of *yshB,* it is possible that a reduced expression of YshB prevents the synthetic filamentous phenotype. To test this, an *ezrA* mutation was introduced into a strain that lacks the complete *zapA-yshB* operon and contains an ectopic copy of only *zapA* driven by the IPTG-inducible *Pspac* promoter. In the absence of IPTG, this strain formed small colonies and highly filamentous cells on PAB plates, even without tetracycline (**Figures 6A,B**). This is in agreement with a previous study which showed that a *zapA ezrA* double mutant forms very filamentous cells (Gueiros-Filho and Losick, 2002). However, the strain grew normally and showed no filamentation when IPTG was added to induce ZapA expression (**Figures 6A,B**), even in the presence of tetracycline (not shown). Thus, suppression of the tetracycline phenotype does not require the absence of YshB, since an *ezrA* mutant that overexpresses ZapA and that contains a normal copy of the *zapA-yshB* operon, also grows normally (**Figure 5**). It is likely that the transposon insertion somehow stabilizes *zapA* mRNA leading to increased ZapA levels in the cell. We therefore tested ZapA levels with Western blot and confirmed that the transposon insertion causes overexpression of ZapA in both 168 and *ezrA* backgrounds (Figure S1).

Deletion of *galE* Restores Cell Division

GalE is an epimerase that catalyzes the reversible conversion between UDP-galactose and UDP-glucose, as well as between UDP-N-acetylgalactosamine and UDP-N-acetylglucosamine (Krispin and Allmansberger, 1998; Soldo et al., 2003). A *galE* mutant is defective in exopolysaccharide synthesis which results in impaired biofilm formation (Chai et al., 2012). Moreover, the cell wall of a *galE* mutant is devoid of poly(glucose galactosamine 1-P), the so-called minor wall-teichoic acid (Freymond et al., 2006). Teichoic acids are phosphate-rich anionic glycopolymers which constitute a major component of the Gram-positive cell wall. Several physiological roles have been proposed for these polymers, including cation homoeostasis, antibiotic resistance, morphogenesis and cell division (Weidenmaier and Peschel, 2008; Schirner et al., 2009). Interestingly, an *ezrA* mutant is also more sensitive to chloramphenicol and ampicillin as well as to several other cell wall antibiotics (Figures S2, S3). General antibiotic sensitivity is a phenotype that is often observed in cell wall mutants, and in this case might be related to the role of EzrA in shuttling PBP 1 from the lateral wall to the division site (Claessen et al., 2008). Introduction of a *galE* mutation decreased antibiotic sensitivity of an *ezrA* mutant to wild type levels (Figure S3). Importantly, inactivation of *galE* alone showed no increased resistance to antibiotics compared to the wild type strain 168, suggesting that the suppression effect is not due to a general increased protection against antibiotics by means of an altered cell wall composition. Moreover, deletion of the sugar transferases GgaAB, which also impairs minor teichoic acid synthesis (Freymond et al., 2006), did not suppress the tetracycline phenotype.

Absence of GalE Restores Cell Division in *sepF ezrA* and *zapA ezrA* Double Mutants

A remaining question is whether the absence of GalE only suppresses the tetracycline effect or whether such mutation actually has a more direct role in cell division. Previously, it was shown that mutations in the lipoteichoic acid biosynthesis pathway reduces the activity of UgtP, thereby stimulating FtsZ polymerization (Weart et al., 2007). Since a *galE* mutation changes

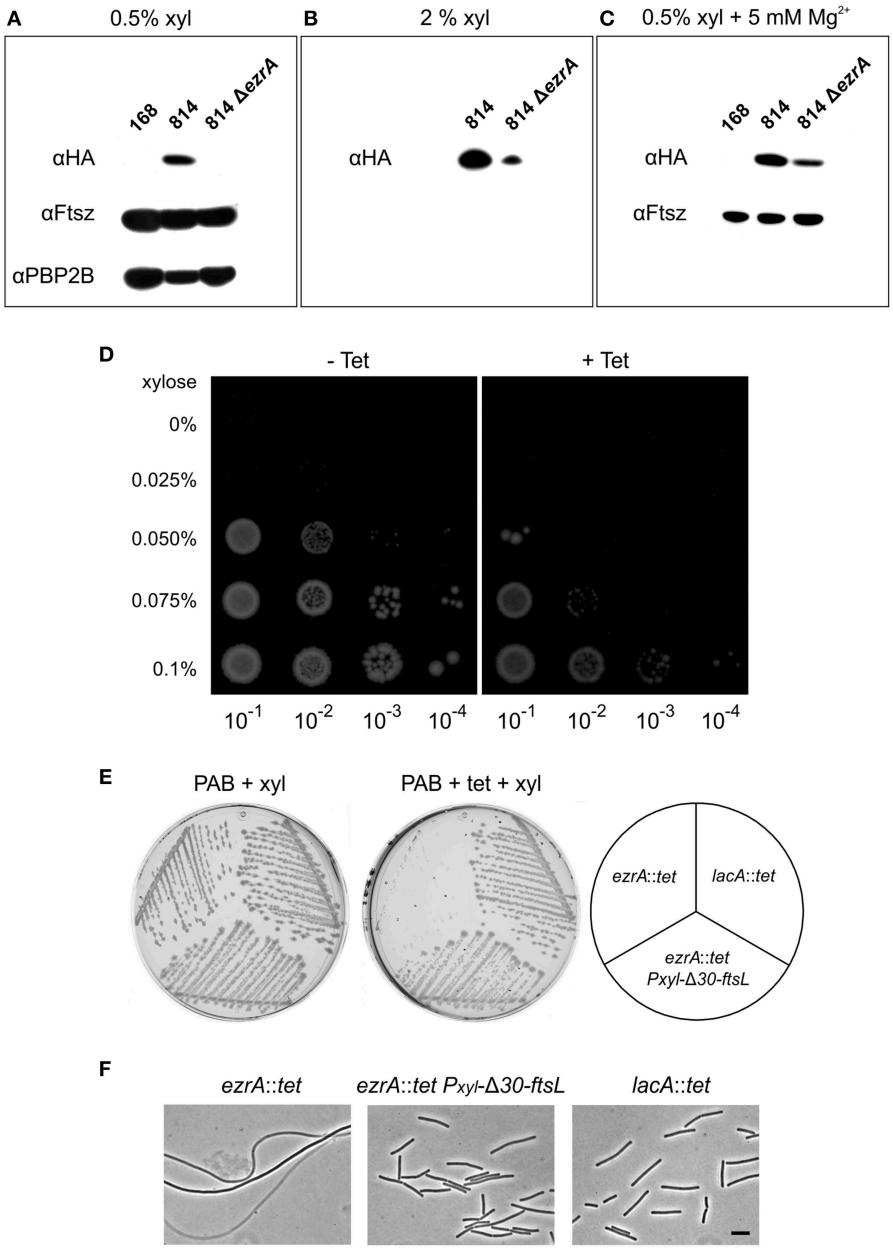

FIGURE 4 | FtsL overexpression suppresses the tetracycline effect. **(A)** Western blot of HA-FtsL, FtsZ, and Pbp2B from total protein extracts of strains 168 (wild type), 814 (Δ*ftsL-Pspac-pbpB, amyE*::*Pxyl-HA-ftsL*), and 814 Δ*ezrA* (PG305) grown at 37°C in PAB medium supplemented with 1 mM IPTG and 0.5% xylose. IPTG was added to express the essential *pbpB* gene downstream of the *ftsl-pbp2B* operon. **(B)** Western blot of HA-FtsL from total protein extracts of strains 814 and 814 Δ*ezrA* (PG305) grown in PAB medium with 1 mM IPTG and 2% xylose. **(C)** Western blot of HA-FtsL and FtsZ from total protein extracts of strains 168, 814, and 814 Δ*ezrA* (PG305) grown at 37°C in PAB medium supplemented with 5 mM $MgSO_4$, 20 μg/ml K-aspartate, 1 mM IPTG, and 0.5% xylose. Aspartate was included to circumvent any effect on the inactive downstream *aspB* gene. **(D)** Growth of strain PG742 (Δ*ftsL-Pspac-pbpB*, *amyE*::*Pxyl-HA-ftsL*, *lacA*::*tet*) on PAB plates supplemented with 1 mM IPTG, with increasing concentrations of xylose (0.025–0.1%) and with or without 10 μg/ml tetracycline. Serial dilutions of exponentially growing cells were plated and images were taken after overnight incubation at 37°C. **(E)** Growth of *ezrA*::*tet* (3362), *lacA*::*tet* (SG82), and *ezrA*::*tet amyE*::*Pxyl-Δ30-ftsL* (PG160) strains on PAB plates with 1% xylose, and with or without 10 μg/ml tetracycline, after overnight incubation at 37°C. **(F)** Phase contrast images of cells taken from the plates. Scale bar 5 μm.

the teichoic acid composition of the cell, this mutation might also influence cell division. To test this, the possible mitigating effect of a *galE* deletion on the cell division defect of a *zapA ezrA* double mutant was investigated. A strain lacking *ezrA*, and with *zapA* under control of an IPTG-inducible promoter (strain PG164), forms small colonies and filamentous cells in

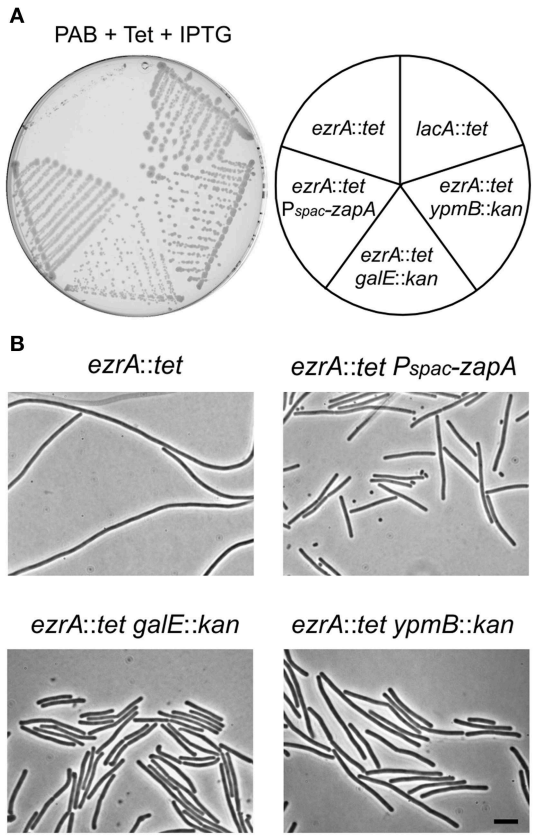

FIGURE 5 | Suppression of the tetracycline phenotype. (A) Growth of *ezrA*::*tet* (3362), *ezrA*::*tet aprE*::*Pspac-zapA* (PG273) *ezrA*::*tet galE*::*kan* (PG238), *ezrA*::*tet ypmB*::*kan* (PG239), *lacA::tet* (SG82) strains on a PAB plate with 10 μg/ml tetracycline and 1 mM IPTG for ZapA induction. **(B)** Phase contrast images of cells taken from the PAB plates in **(A)**. Scale bar 5 μm.

the absence of IPTG. When the *galE* deletion was introduced into this background, the resulting strain (PG307) grew much better without IPTG and filamentation was strongly reduced (**Figures 6A,B**).

Since a *galE* deletion restored cell division in the *zapA ezrA* double mutant, we were curious whether such deletion could also restore growth and cell division in the synthetic lethal *sepF ezrA* double mutant. *B. subtilis* strain 4077 contains an *ezrA* deletion and an IPTG-inducible *sepF* operon. This strain can only grow when IPTG is added to the growth medium (Hamoen et al., 2006). However, transformation of the *galE* mutation into this strain resulted in colony formation on PAB plates without IPTG (**Figure 6C**), and microscopic imaging showed that cell division was restored (**Figure 6D**). Consistent with this result, it was possible to make a viable *ezrA sepF galE* triple mutant (PG294), although this strain grows slower than the single mutants and shows a high degree of filamentation (Figure S4). Again, the effect of a *galE* deletion is not linked to the lack of minor teichoic acids as the Δ*ggaAB* mutant failed to suppress IPTG dependency of strain 4077 (not shown). Therefore, we must conclude that GalE activity affects the cell division process.

Deletion of *ypmB* (*tseB*) Suppresses the Tetracycline Effect

Two transposon suppressors were found in *ypmB*, and replacement of *ypmB* by a kanamycin resistant marker suppressed the tetracycline-induced growth inhibition and filamentation (**Figure 5**). However, *ypmB* is the second gene of a tri-cistronic operon and is preceded by *ypmA* and followed by *aspB*, which is involved in aspartate biosynthesis. To rule out a possible downstream effect, an ectopic IPTG-inducible copy of *ypmB* was introduced into the *ypmB ezrA* double mutant. The resulting strain PG333 forms only filamentous cells on tetracycline containing PAB plates when IPTG is present, indicating that the transposon suppression is due to the absence of a functional *ypmB* gene and not a consequence of downstream effects on *aspB* (Figure S5). Because of its role in the tetracycline sensitivity of an *ezrA* strain, this hypothetical gene was renamed *tseB* (*t*etracycline sensitivity *s*uppressor of *ezrA*).

When cell lengths of the different transposon mutants were measured in an otherwise wild type background, the insertion in *tseB* showed the greatest effect and produced significant shorter cells compared to the wild type strain, especially when grown in minimal competence medium (approximately 25% shorter) (**Figures 7A,B**). Minimal competence medium contains a relative high concentration of Mg^{2+} (6.6 mM), and the addition of magnesium to PAB medium further reduced the average cell length (**Figure 7B**). The addition of aspartic acid to the growth medium, which might be required if *aspB* was not expressed at sufficient levels, did not have an effect on this phenotype (not shown).

Secondary structure predictions of the 161 amino acid long TseB suggested that the protein has a large extracellular domain attached to the cell membrane by a single N-terminal transmembrane helix (SOSUI software, Hirokawa et al., 1998). To study the localization of TseB, an N-terminal GFP-TseB fusion was constructed using a monomeric variant of GFP. The reporter fusion was inserted into the *amyE* locus of a strain carrying also the wild type copy of *tseB* at the native locus. The GFP-TseB fusion is at least partially functional since it can complement the short cell phenotype of a *tseB* mutation in minimal medium (not shown). The GFP-TseB fusion shows clear membrane localization that is enriched at cell division sites in some cells (**Figure 7C**). In addition, the GFP signal appears to be almost absent from matured septa (**Figure 7C**, arrows). Time-lapse microscopy showed this dynamic localization more clearly, and confirmed the disappearance of the protein from septa late in the cell division process, presumably when septation is completed (**Figure 7D**).

Discussion

Hypersensitivity to Tetracycline

The finding that a cell division mutant is hypersensitive to antibiotics, and in particular to tetracycline, has not been reported before. It is as yet unclear why tetracycline causes a growth and division defect in an *ezrA* mutant while the tetracycline-resistance marker is present. Our data suggests that FtsL might be destabilized under these growth conditions (**Figure 4D**). This might lead to a severe division block when combined with an

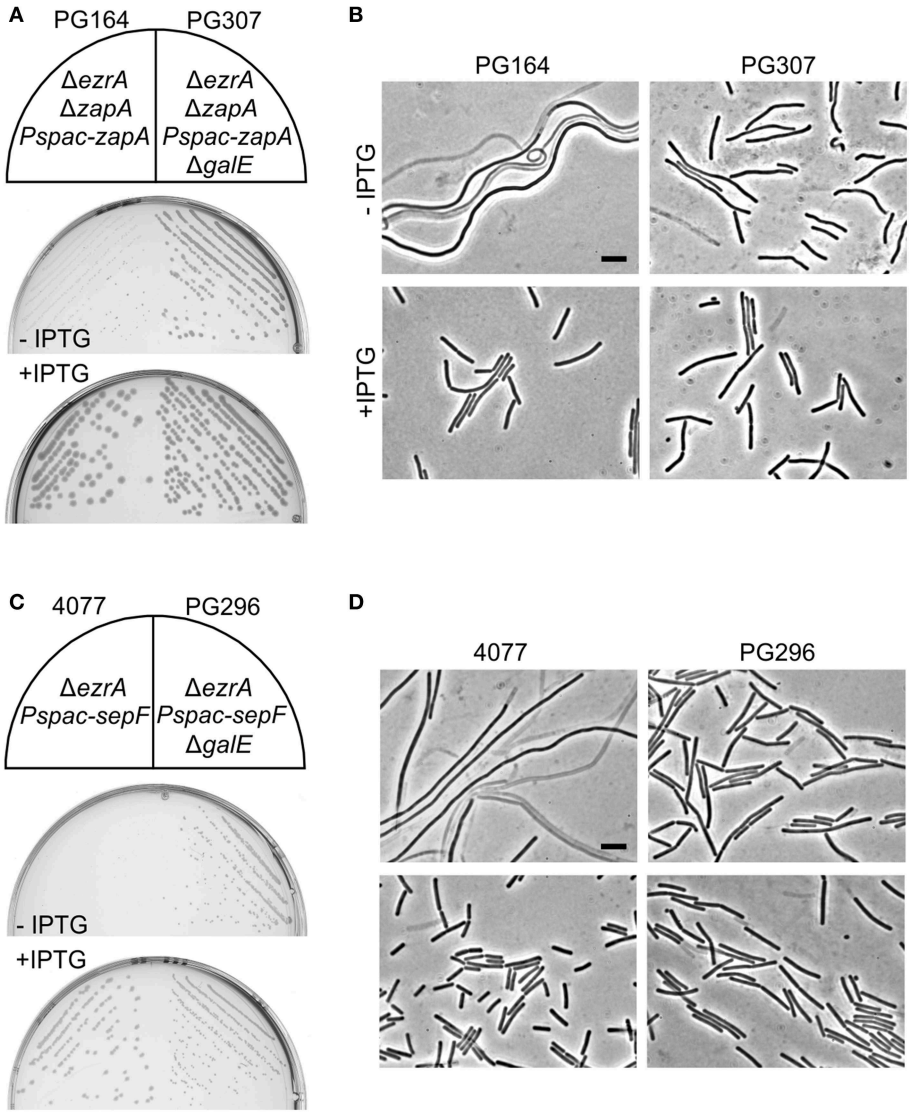

FIGURE 6 | Absence of GalE restores cell division in *zapA ezrA* and *sepF ezrA* double mutants. (A) Growth on PAB plates with or without 1 mM IPTG, and **(B)** related phase contrast microscopic images of strains PG164 (*zapA-yshB*::*tet*, *ezrA*::*cat, aprE*::P_{spac}*-zapA)* and PG307 (*zapA-yshB*::*tet*, *ezrA*::*cat, aprE*::P_{spac}*-zapA, galE*::*kan*). IPTG was used to induce ZapA. **(C)** Growth on nutrient agar plates with 0.5 μg/ml erythromycin, in the presence or absence of 1 mM IPTG, and **(D)** related phase contrast microscopic images of strains 4077 (*ylmBC*::P_{spac}*-ylmD-H, ezrA*::*tet)* and PG296 (*ylmBC*::P_{spac}*-ylmD-H, ezrA*::*tet, galE*::*kan*). Addition of IPTG induces the expression of *sepF* (= *ylmF*) and of the *ylmDEGH* genes. Scale bar 5 μm.

ezrA deletion, which has in itself a similar effect (**Figures 4A–C**). However, our transposon screen revealed that also ZapA overexpression can suppress the tetracycline effect. In contrast to FtsL, ZapA is an early cell division protein and forms links between FtsZ protofilaments promoting Z-ring assembly (Gueiros-Filho and Losick, 2002; Pacheco-Gomez et al., 2013). Possibly, this also promotes the stability of the late divisome components.

The fact the tetracycline hypersensitivity phenotype is only observed on PAB plates and not in liquid medium might have to do with localized depletion of Mg^{2+} ions that exacerbates the effect. Since Mg^{2+} suppresses the tetracycline induced phenotype, we initially assumed that the metal-ion chelating activity of tetracycline was responsible for the cell division defect. However, other metal chelators did not result in filamentation of an *ezrA* mutant. Interestingly, it is not the classical translation-inhibiting activity of tetracycline that is causing cell filamentation, since the *tet-4* ribosomal mutation did not mitigate the tetracycline effect, and anhydrotetracycline also caused filamentation. Tetracycline and anhydrotetracycline are lipophilic compounds that accumulate in the cell membrane, and it has been suggested that the bactericidal activity of anhydrotetracycline is caused by membrane de-energization (Chopra, 1994; Chopra and Roberts, 2001). Reduction of the membrane potential by tetracycline could explain its effects on cell division, since the cell

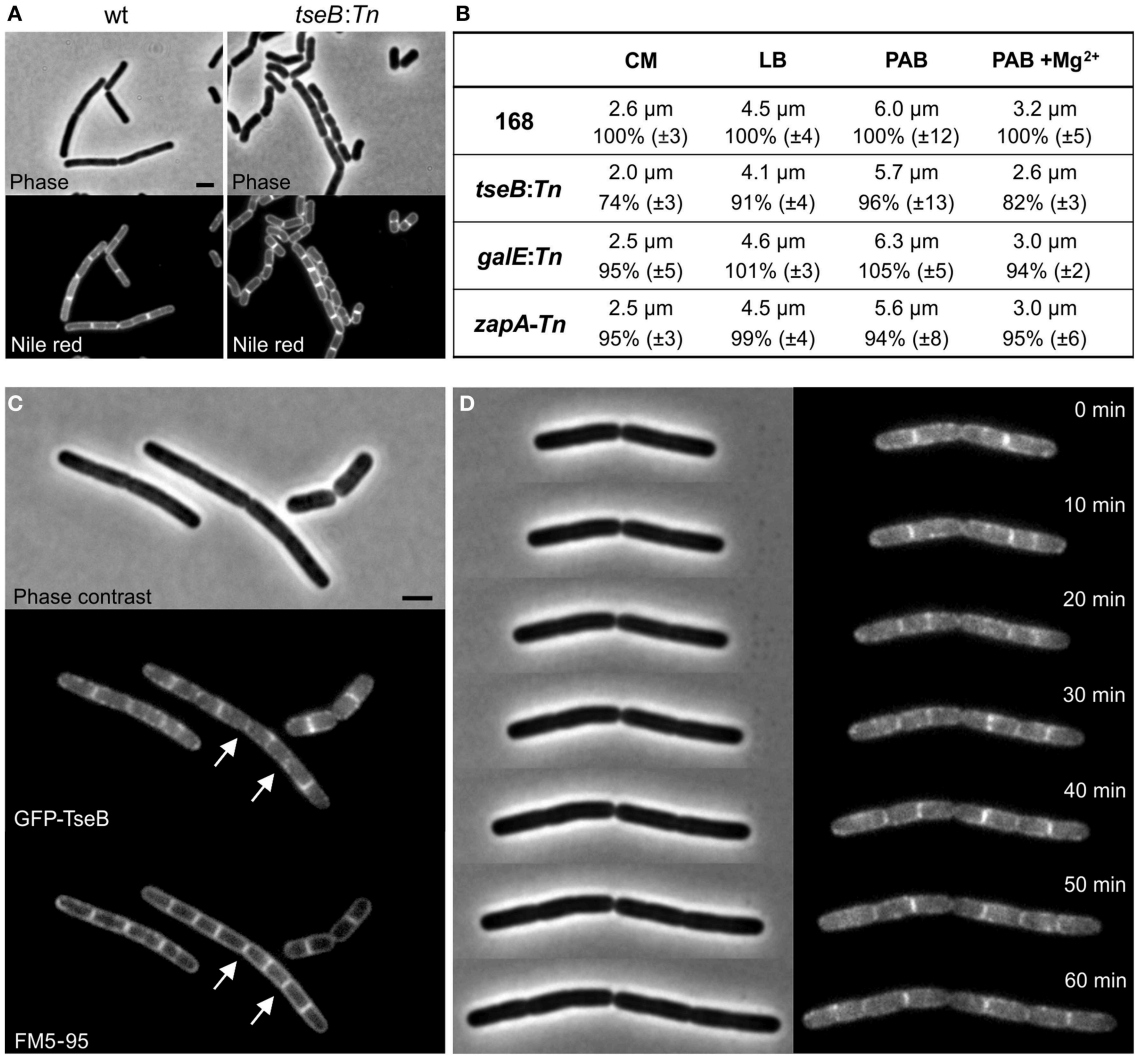

	CM	LB	PAB	PAB +Mg^{2+}
168	2.6 µm 100% (±3)	4.5 µm 100% (±4)	6.0 µm 100% (±12)	3.2 µm 100% (±5)
tseB:Tn	2.0 µm 74% (±3)	4.1 µm 91% (±4)	5.7 µm 96% (±13)	2.6 µm 82% (±3)
galE:Tn	2.5 µm 95% (±5)	4.6 µm 101% (±3)	6.3 µm 105% (±5)	3.0 µm 94% (±2)
zapA-Tn	2.5 µm 95% (±3)	4.5 µm 99% (±4)	5.6 µm 94% (±8)	3.0 µm 95% (±6)

FIGURE 7 | Phenotype of Δ*tseB* and localization of GFP-TseB. (A) Phase contrast and membrane stain (Nile red) images of wild type strain 168 and the *tseB* mutant strain PG135 (*tseB*:*TnYLB-1*) grown in competence medium at 37°C. Scale bar 2 µm. **(B)** Cell length measurements of the transposon mutants in different growth media. Strains 168, *tseB*:*TnYLB-1*(PG135), *galE*:*TnYLB-1* (PG143) and *zapA-TnYLB1-yshB* (PG140), were grown at 37°C in competence medium (CM), LB, PAB, or PAB supplemented with 5 mM Mg^{2+}. Averaged absolute and relative cell lengths are presented below in %, and standard deviations are shown in brackets. One hundred to one hundred and fifty cells were measured in each experiment in triplicate. **(C)** Localization of GFP-TseB. Strain PG718 (*amyE*::*Pxyl-mgfp-tseB*) was grown in competence medium at 30°C with 0.5% xylose to express GFP-TseB. GFP, membrane stain (FM5-95) and phase contrast images were taken during exponential growth. Scale bar 2 µm. Arrows highlight some of the septa in which the GFP signal is absent. **(D)** Time-lapse microscopy experiment showing dynamic localization of GFP-TseB. Strain PG718 (*amyE*::*Pxyl-mgfp-tseB*) was grown at 30°C on a microscope slide made of competence medium supplemented with 0.5% xylose. GFP and phase contrast images were taken every 10 min.

division proteins FtsA and MinD require the membrane potential for membrane localization and function (Strahl and Hamoen, 2010). However, we have been unable to detect a clear reduction in membrane potential (within 15 min) when *B. subtilis* cells were incubated with tetracycline. It has been shown that relative small amounts of tetracycline (1 µg/ml) can increase the membrane fluidity (Vincent et al., 2004). Possibly, this change in membrane fluidity will make certain transmembrane proteins more susceptible to proteolytic degradation, such as FtsL or other late division proteins. Interestingly, divalent cations are known to reduce membrane fluidity (Binder and Zschornig, 2002; Vest et al., 2004), and this might explain why the addition of Mg^{2+} suppresses the tetracycline effect.

Effect of GalE on Cell Division

A *galE* deletion suppresses the tetracycline effect and rescues the synthetic lethality of *zapA ezrA* and *sepF ezrA* double mutations. This, together with the fact that the lack of minor teichoic acids itself (Δ*ggaAB* mutant) did not suppress the cell division effect, suggests that GalE plays a more direct role in cell division. We

could not observe any division defect in a *galE* mutant, but the *galE* mutation improves the efficiency of division in *ezrA* mutant cells considerably. One possibility is that the absence of *galE* alters the levels of UDP-glucose, since GalE catalyzes the reversible production of UDP-glucose from UDP-galactose. UDP-glucose is the substrate for UgtP, the sugar transferase that is involved in lipoteichoic acid, which also regulates FtsZ assembly (Weart et al., 2007). Therefore, a *galE* deletion might indirectly influence the activity of UgtP. Interestingly, we were unable to test the *ugtP* mutant on PAB plates, since this strain showed strongly impaired growth and morphological defects (bulging) in PAB medium (not shown).

TseB Influences Cell Division

We have shown that TseB deletion suppresses the tetracycline effect and causes a short cell phenotype under certain growth conditions. The protein is attached to the membrane and contains an extra-cytoplasmic peptidase domain that is found in cell-wall associated regulatory metallopeptidases (Yeats et al., 2004). We hypothesize that the protein might be involved in the proteolytic degradation of extracellular proteins among which FtsL or others that affect the levels of FtsL. However, western blot experiments failed to consistently detect increased amounts of FtsL in a *tseB* mutant (not shown). Nevertheless, the short cell phenotype of a *tseB* mutant and the septal enrichment is compatible with a role in the division process. The protein is conserved within families belonging to the Bacillales and Lactobacillales orders (STRING database, Szklarczyk et al., 2011). Intriguingly, there is a significant co-occurrence in bacterial genomes among TseB, PBP2A and PbpH (STRING database, (Szklarczyk et al., 2011)). These two penicillin-binding proteins are required for cell wall synthesis during elongation (Wei et al., 2003) and were shown to be drivers for MreB dynamics (Dominguez-Escobar et al., 2011; Garner et al., 2011). Possibly, TseB is involved in the switch between septal and lateral cell wall synthesis, which could explain its connection to EzrA.

Acknowledgments

We thank the members of the Centre for Bacterial Cell Biology for helpful discussions. We are grateful to David Bechhofer for the gift of strain BG239, to Frederico Gueiros-Filho for providing the ZapA-antiserum and to Edward de Koning for help with FtsL western blots. PG was supported by a Marie Curie EST fellowship from the European Commission and by a Biological Sciences Research Council grant (BB/I004238/1) awarded to LH. ER was supported by a short term Marie Curie EST fellowship from the European Commission. LH is supported by NWO grant STW-Vici 12128.

Supplementary Material

The Supplementary Material for this article can be found online at: http://journal.frontiersin.org/article/10.3389/fmicb.2015.00346/abstract

References

Adams, D. W., and Errington, J. (2009). Bacterial cell division: assembly, maintenance and disassembly of the Z ring. *Nat. Rev. Microbiol.* 7, 642–653. doi: 10.1038/nrmicro2198

Adams, D. W., Wu, L. J., and Errington, J. (2015). Nucleoid occlusion protein Noc recruits DNA to the bacterial cell membrane. *EMBO J.* 34, 491–501. doi: 10.15252/embj.201490177

Bi, E. F., and Lutkenhaus, J. (1991). FtsZ ring structure associated with division in *Escherichia coli*. *Nature* 354, 161–164. doi: 10.1038/354161a0

Binder, H., and Zschornig, O. (2002). The effect of metal cations on the phase behavior and hydration characteristics of phospholipid membranes. *Chem. Phys. Lipids* 115, 39–61. doi: 10.1016/S0009-3084(02)00005-1

Bramkamp, M., Weston, L., Daniel, R. A., and Errington, J. (2006). Regulated intramembrane proteolysis of FtsL protein and the control of cell division in *Bacillus subtilis*. *Mol. Microbiol.* 62, 580–591. doi: 10.1111/j.1365-2958.2006.05402.x

Chai, Y., Beauregard, P. B., Vlamakis, H., Losick, R., and Kolter, R. (2012). Galactose metabolism plays a crucial role in biofilm formation by *Bacillus subtilis*. *MBio* 3, e00184–e00112. doi: 10.1128/mBio.00184-12

Chien, A. C., Zareh, S. K., Wang, Y. M., and Levin, P. A. (2012). Changes in the oligomerization potential of the division inhibitor UgtP co-ordinate *Bacillus subtilis* cell size with nutrient availability. *Mol. Microbiol.* 86, 594–610. doi: 10.1111/mmi.12007

Chopra, I. (1994). Tetracycline analogs whose primary target is not the bacterial ribosome. *Antimicrob. Agents Chemother.* 38, 637–640. doi: 10.1128/AAC.38.4.637

Chopra, I., and Roberts, M. (2001). Tetracycline antibiotics: mode of action, applications, molecular biology, and epidemiology of bacterial resistance. *Microbiol. Mol. Biol. Rev.* 65, 232–260. doi: 10.1128/MMBR.65.2.232-260.2001

Chung, K. M., Hsu, H. H., Yeh, H. Y., and Chang, B. Y. (2007). Mechanism of regulation of prokaryotic tubulin-like GTPase FtsZ by membrane protein EzrA. *J. Biol. Chem.* 282, 14891–14897. doi: 10.1074/jbc.M605177200

Claessen, D., Emmins, R., Hamoen, L. W., Daniel, R. A., Errington, J., and Edwards, D. H. (2008). Control of the cell elongation-division cycle by shuttling of PBP1 protein in *Bacillus subtilis*. *Mol. Microbiol.* 68, 1029–1046. doi: 10.1111/j.1365-2958.2008.06210.x

Cleverley, R. M., Barrett, J. R., Basle, A., Bui, N. K., Hewitt, L., Solovyova, A., et al. (2014). Structure and function of a spectrin-like regulator of bacterial cytokinesis. *Nat. Commun.* 5, 5421. doi: 10.1038/ncomms6421

Dajkovic, A., Lan, G., Sun, S. X., Wirtz, D., and Lutkenhaus, J. (2008). MinC spatially controls bacterial cytokinesis by antagonizing the scaffolding function of FtsZ. *Curr. Biol.* 18, 235–244. doi: 10.1016/j.cub.2008.01.042

Daniel, R. A., and Errington, J. (2000). Intrinsic instability of the essential cell division protein FtsL of *Bacillus subtilis* and a role for DivIB protein in FtsL turnover. *Mol. Microbiol.* 36, 278–289. doi: 10.1046/j.1365-2958.2000.01857.x

Daniel, R. A., Noirot-Gros, M. F., Noirot, P., and Errington, J. (2006). Multiple interactions between the transmembrane division proteins of *Bacillus subtilis* and the role of FtsL instability in divisome assembly. *J. Bacteriol.* 188, 7396–7404. doi: 10.1128/JB.01031-06

Daniel, R. A., Williams, A. M., and Errington, J. (1996). A complex four-gene operon containing essential cell division gene *pbpB* in *Bacillus subtilis*. *J. Bacteriol.* 178, 2343–2350.

Dominguez-Escobar, J., Chastanet, A., Crevenna, A. H., Fromion, V., Wedlich-Soldner, R., and Carballido-Lopez, R. (2011). Processive movement of MreB-associated cell wall biosynthetic complexes in bacteria. *Science* 333, 225–228. doi: 10.1126/science.1203466

Duman, R., Ishikawa, S., Celik, I., Strahl, H., Ogasawara, N., Troc, P., et al. (2013). Structural and genetic analyses reveal the protein SepF as a new membrane anchor for the Z ring. *Proc. Natl. Acad. Sci. U.S.A.* 110, E4601–E4610. doi: 10.1073/pnas.1313978110

Estrela, A. I., Pooley, H. M., De Lencastre, H., and Karamata, D. (1991). Genetic and biochemical characterization of *Bacillus subtilis* 168 mutants specifically blocked in the synthesis of the teichoic acid poly(3-O-beta-D-glucopyranosyl-N-acetylgalactosamine 1-phosphate): *gneA*, a new locus, is associated with UDP-N-acetylglucosamine 4-epimerase activity. *J. Gen. Microbiol.* 137, 943–950. doi: 10.1099/00221287-137-4-943

Feucht, A., and Errington, J. (2005). *ftsZ* mutations affecting cell division frequency, placement and morphology in *Bacillus subtilis*. *Microbiology* 151, 2053–2064. doi: 10.1099/mic.0.27899-0

Freymond, P. P., Lazarevic, V., Soldo, B., and Karamata, D. (2006). Poly(glucosyl-N-acetylgalactosamine 1-phosphate), a wall teichoic acid of *Bacillus subtilis* 168: its biosynthetic pathway and mode of attachment to peptidoglycan. *Microbiology* 152, 1709–1718. doi: 10.1099/mic.0.28814-0

Gamba, P., Veening, J. W., Saunders, N. J., Hamoen, L. W., and Daniel, R. A. (2009). Two-step assembly dynamics of the *Bacillus subtilis* divisome. *J. Bacteriol.* 191, 4186–4194. doi: 10.1128/JB.01758-08

Garner, E. C., Bernard, R., Wang, W., Zhuang, X., Rudner, D. Z., and Mitchison, T. (2011). Coupled, circumferential motions of the cell wall synthesis machinery and MreB filaments in *B. subtilis*. *Science* 333, 222–225. doi: 10.1126/science.1203285

Gregory, J. A., Becker, E. C., and Pogliano, K. (2008). *Bacillus subtilis* MinC destabilizes FtsZ-rings at new cell poles and contributes to the timing of cell division. *Genes Dev.* 22, 3475–3488. doi: 10.1101/gad.1732408

Gueiros-Filho, F. J., and Losick, R. (2002). A widely conserved bacterial cell division protein that promotes assembly of the tubulin-like protein FtsZ. *Genes Dev.* 16, 2544–2556. doi: 10.1101/gad.1014102

Gundogdu, M. E., Kawai, Y., Pavlendova, N., Ogasawara, N., Errington, J., Scheffers, D. J., et al. (2011). Large ring polymers align FtsZ polymers for normal septum formation. *EMBO J.* 30, 617–626. doi: 10.1038/emboj.2010.345

Haeusser, D. P., Schwartz, R. L., Smith, A. M., Oates, M. E., and Levin, P. A. (2004). EzrA prevents aberrant cell division by modulating assembly of the cytoskeletal protein FtsZ. *Mol. Microbiol.* 52, 801–814. doi: 10.1111/j.1365-2958.2004.04016.x

Hamoen, L. W., Meile, J. C., De Jong, W., Noirot, P., and Errington, J. (2006). SepF, a novel FtsZ-interacting protein required for a late step in cell division. *Mol. Microbiol.* 59, 989–999. doi: 10.1111/j.1365-2958.2005.04987.x

Hamoen, L. W., Smits, W. K., De Jong, A., Holsappel, S., and Kuipers, O. P. (2002). Improving the predictive value of the competence transcription factor (ComK) binding site in *Bacillus subtilis* using a genomic approach. *Nucleic Acids Res.* 30, 5517–5528. doi: 10.1093/nar/gkf698

Heinrich, J., Lunden, T., Kontinen, V. P., and Wiegert, T. (2008). The *Bacillus subtilis* ABC transporter EcsAB influences intramembrane proteolysis through RasP. *Microbiology* 154, 1989–1997. doi: 10.1099/mic.0.2008/018648-0

Hirokawa, T., Boon-Chieng, S., and Mitaku, S. (1998). SOSUI: classification and secondary structure prediction system for membrane proteins. *Bioinformatics* 14, 378–379. doi: 10.1093/bioinformatics/14.4.378

Ishikawa, S., Kawai, Y., Hiramatsu, K., Kuwano, M., and Ogasawara, N. (2006). A new FtsZ-interacting protein, YlmF, complements the activity of FtsA during progression of cell division in *Bacillus subtilis*. *Mol. Microbiol.* 60, 1364–1380. doi: 10.1111/j.1365-2958.2006.05184.x

Ivanov, D., and Nasmyth, K. (2005). A topological interaction between cohesin rings and a circular minichromosome. *Cell* 122, 849–860. doi: 10.1016/j.cell.2005.07.018

Kawai, Y., and Ogasawara, N. (2006). *Bacillus subtilis* EzrA and FtsL synergistically regulate FtsZ ring dynamics during cell division. *Microbiology* 152, 1129–1141. doi: 10.1099/mic.0.28497-0

Krispin, O., and Allmansberger, R. (1998). The *Bacillus subtilis galE* gene is essential in the presence of glucose and galactose. *J. Bacteriol.* 180, 2265–2270.

Krulwich, T. A., Jin, J., Guffanti, A. A., and Bechhofer, H. (2001). Functions of tetracycline efflux proteins that do not involve tetracycline. *J. Mol. Microbiol. Biotechnol.* 3, 237–246.

Le Breton, Y., Mohapatra, N. P., and Haldenwang, W. G. (2006). *In vivo* random mutagenesis of *Bacillus subtilis* by use of TnYLB-1, a mariner-based transposon. *Appl. Environ. Microbiol.* 72, 327–333. doi: 10.1128/AEM.72.1.327-333.2006

Levin, P. A., Kurtser, I. G., and Grossman, A. D. (1999). Identification and characterization of a negative regulator of FtsZ ring formation in *Bacillus subtilis*. *Proc. Natl. Acad. Sci. U.S.A.* 96, 9642–9647. doi: 10.1073/pnas.96.17.9642

Lewis, P. J., and Marston, A. L. (1999). GFP vectors for controlled expression and dual labelling of protein fusions in *Bacillus subtilis*. *Gene* 227, 101–110. doi: 10.1016/S0378-1119(98)00580-0

Lowe, J., and Amos, L. A. (1998). Crystal structure of the bacterial cell-division protein FtsZ. *Nature* 391, 203–206. doi: 10.1038/34472

Ma, X., and Margolin, W. (1999). Genetic and functional analyses of the conserved C-terminal core domain of *Escherichia coli* FtsZ. *J. Bacteriol.* 181, 7531–7544.

Monahan, L. G., Hajduk, I. V., Blaber, S. P., Charles, I. G., and Harry, E. J. (2014). Coordinating bacterial cell division with nutrient availability: a role for glycolysis. *MBio* 5, e00935–e00914. doi: 10.1128/mBio.00935-14

Morimoto, T., Loh, P. C., Hirai, T., Asai, K., Kobayashi, K., Moriya, S., et al. (2002). Six GTP-binding proteins of the Era/Obg family are essential for cell growth in *Bacillus subtilis*. *Microbiology* 148, 3539–3552.

Murray, T., Popham, D. L., and Setlow, P. (1998). *Bacillus subtilis* cells lacking penicillin-binding protein 1 require increased levels of divalent cations for growth. *J. Bacteriol.* 180, 4555–4563.

Nelson, M. L. (1998). Chemical and biological dynamics of tetracyclines. *Adv. Dent. Res.* 12, 5–11. doi: 10.1177/08959374980120011901

Nicolas, P., Mader, U., Dervyn, E., Rochat, T., Leduc, A., Pigeonneau, N., et al. (2012). Condition-dependent transcriptome reveals high-level regulatory architecture in *Bacillus subtilis*. *Science* 335, 1103–1106. doi: 10.1126/science.1206848

Oliva, B., and Chopra, I. (1992). Tet determinants provide poor protection against some tetracyclines: further evidence for division of tetracyclines into two classes. *Antimicrob. Agents Chemother.* 36, 876–878. doi: 10.1128/AAC.36.4.876

Pacheco-Gomez, R., Cheng, X., Hicks, M. R., Smith, C. J., Roper, D. I., Addinall, S., et al. (2013). Tetramerization of ZapA is required for FtsZ bundling. *Biochem. J.* 449, 795–802. doi: 10.1042/BJ20120140

Peters, P. C., Migocki, M. D., Thoni, C., and Harry, E. J. (2007). A new assembly pathway for the cytokinetic Z ring from a dynamic helical structure in vegetatively growing cells of *Bacillus subtilis*. *Mol. Microbiol.* 64, 487–499. doi: 10.1111/j.1365-2958.2007.05673.x

Robson, S. A., Michie, K. A., Mackay, J. P., Harry, E., and King, G. F. (2002). The *Bacillus subtilis* cell division proteins FtsL and DivIC are intrinsically unstable and do not interact with one another in the absence of other septasomal components. *Mol. Microbiol.* 44, 663–674. doi: 10.1046/j.1365-2958.2002.02920.x

Schirner, K., Marles-Wright, J., Lewis, R. J., and Errington, J. (2009). Distinct and essential morphogenic functions for wall- and lipo-teichoic acids in *Bacillus subtilis*. *EMBO J.* 28, 830–842. doi: 10.1038/emboj.2009.25

Singh, J. K., Makde, R. D., Kumar, V., and Panda, D. (2007). A membrane protein, EzrA, regulates assembly dynamics of FtsZ by interacting with the C-terminal tail of FtsZ. *Biochemistry* 46, 11013–11022. doi: 10.1021/bi700710j

Singh, J. K., Makde, R. D., Kumar, V., and Panda, D. (2008). SepF increases the assembly and bundling of FtsZ polymers and stabilizes FtsZ protofilaments by binding along its length. *J. Biol. Chem.* 283, 31116–31124. doi: 10.1074/jbc.M805910200

Soldo, B., Scotti, C., Karamata, D., and Lazarevic, V. (2003). The *Bacillus subtilis* Gne (GneA, GalE) protein can catalyse UDP-glucose as well as UDP-N-acetylglucosamine 4-epimerisation. *Gene* 319, 65–69. doi: 10.1016/S0378-1119(03)00793-5

Strahl, H., and Hamoen, L. W. (2010). Membrane potential is important for bacterial cell division. *Proc. Natl. Acad. Sci. U.S.A.* 107, 12281–12286. doi: 10.1073/pnas.1005485107

Surdova, K., Gamba, P., Claessen, D., Siersma, T., Jonker, M. J., Errington, J., et al. (2013). The conserved DNA-binding protein WhiA is involved in cell division in *Bacillus subtilis*. *J. Bacteriol.* 195, 5450–5460. doi: 10.1128/JB.00507-13

Szklarczyk, D., Franceschini, A., Kuhn, M., Simonovic, M., Roth, A., Minguez, P., et al. (2011). The STRING database in 2011: functional interaction networks of proteins, globally integrated and scored. *Nucleic Acids Res.* 39, D561–D568. doi: 10.1093/nar/gkq973

Tavares, J. R., De Souza, R. F., Meira, G. L., and Gueiros-Filho, F. J. (2008). Cytological characterization of YpsB, a novel component of the *Bacillus subtilis* divisome. *J. Bacteriol.* 190, 7096–7107. doi: 10.1128/JB.00064-08

Trieu-Cuot, P., and Courvalin, P. (1983). Nucleotide sequence of the *Streptococcus faecalis* plasmid gene encoding the 3′5″-aminoglycoside phosphotransferase type III. *Gene* 23, 331–341. doi: 10.1016/0378-1119(83)90022-7

van Baarle, S., and Bramkamp, M. (2010). The MinCDJ system in *Bacillus subtilis* prevents minicell formation by promoting divisome disassembly. *PLoS ONE* 5:e9850. doi: 10.1371/journal.pone.0009850

Vest, R. S., Gonzales, L. J., Permann, S. A., Spencer, E., Hansen, L. D., Judd, A. M., et al. (2004). Divalent cations increase lipid order in erythrocytes and susceptibility to secretory phospholipase A2. *Biophys. J.* 86, 2251–2260. doi: 10.1016/S0006-3495(04)74283-6

Vincent, M., England, L. S., and Trevors, J. T. (2004). Cytoplasmic membrane polarization in Gram-positive and Gram-negative bacteria grown in the absence and presence of tetracycline. *Biochim. Biophys. Acta* 1672, 131–134. doi: 10.1016/j.bbagen.2004.03.005

Wadenpohl, I., and Bramkamp, M. (2010). DivIC stabilizes FtsL against RasP cleavage. *J. Bacteriol.* 192, 5260–5263. doi: 10.1128/JB.00287-10

Wang, X., Huang, J., Mukherjee, A., Cao, C., and Lutkenhaus, J. (1997). Analysis of the interaction of FtsZ with itself, GTP, and FtsA. *J. Bacteriol.* 179, 5551–5559.

Weart, R. B., Lee, A. H., Chien, A. C., Haeusser, D. P., Hill, N. S., and Levin, P. A. (2007). A metabolic sensor governing cell size in bacteria. *Cell* 130, 335–347. doi: 10.1016/j.cell.2007.05.043

Wei, Y., and Bechhofer, D. H. (2002). Tetracycline induces stabilization of mRNA in *Bacillus subtilis*. *J. Bacteriol.* 184, 889–894. doi: 10.1128/jb.184.4.889-894.2002

Wei, Y., Havasy, T., McPherson, D. C., and Popham, D. L. (2003). Rod shape determination by the *Bacillus subtilis* class B penicillin-binding proteins encoded by *pbpA* and *pbpH*. *J. Bacteriol.* 185, 4717–4726. doi: 10.1128/JB.185.16.4717-4726.2003

Weidenmaier, C., and Peschel, A. (2008). Teichoic acids and related cell-wall glycopolymers in Gram-positive physiology and host interactions. *Nat. Rev. Microbiol.* 6, 276–287. doi: 10.1038/nrmicro1861

Williams, G., and Smith, I. (1979). Chromosomal mutations causing resistance to tetracycline in *Bacillus subtilis*. *Mol. Gen. Genet.* 177, 23–29. doi: 10.1007/BF00267249

Wu, L. J., and Errington, J. (2004). Coordination of cell division and chromosome segregation by a nucleoid occlusion protein in *Bacillus subtilis*. *Cell* 117, 915–925. doi: 10.1016/j.cell.2004.06.002

Wu, L. J., Ishikawa, S., Kawai, Y., Oshima, T., Ogasawara, N., and Errington, J. (2009). Noc protein binds to specific DNA sequences to coordinate cell division with chromosome segregation. *EMBO J.* 28, 1940–1952. doi: 10.1038/emboj.2009.144

Yeats, C., Rawlings, N. D., and Bateman, A. (2004). The PepSY domain: a regulator of peptidase activity in the microbial environment? *Trends Biochem. Sci.* 29, 169–172. doi: 10.1016/j.tibs.2004.02.004

Conflict of Interest Statement: The authors declare that the research was conducted in the absence of any commercial or financial relationships that could be construed as a potential conflict of interest.

Copyright © 2015 Gamba, Rietkötter, Daniel and Hamoen. This is an open-access article distributed under the terms of the Creative Commons Attribution License (CC BY). The use, distribution or reproduction in other forums is permitted, provided the original author(s) or licensor are credited and that the original publication in this journal is cited, in accordance with accepted academic practice. No use, distribution or reproduction is permitted which does not comply with these terms.

frontiers in Microbiology

ORIGINAL RESEARCH
published: 28 May 2015
doi: 10.3389/fmicb.2015.00516

MioC and GidA proteins promote cell division in *E. coli*

Mark Lies[1], *Bryan J. Visser*[2], *Mohan C. Joshi*[1], *David Magnan*[2] *and David Bates*[1,2]*

[1] *Molecular and Human Genetics, Baylor College of Medicine, Houston, TX, USA,* [2] *Integrative Molecular and Biomedical Sciences, Baylor College of Medicine, Houston, TX, USA*

The well-conserved genes surrounding the *E. coli* replication origin, *mioC* and *gidA*, do not normally affect chromosome replication and have little known function. We report that *mioC* and *gidA* mutants exhibit a moderate cell division inhibition phenotype. Cell elongation is exacerbated by a *fis* deletion, likely owing to delayed replication and subsequent cell cycle stress. Measurements of replication initiation frequency and origin segregation indicate that *mioC* and *gidA* do not inhibit cell division through any effect on *oriC* function. Division inhibition is also independent of the two known replication/cell division checkpoints, SOS and nucleoid occlusion. Complementation analysis indicates that *mioC* and *gidA* affect cell division *in trans*, indicating their effect is at the protein level. Transcriptome analysis by RNA sequencing showed that expression of a cell division septum component, YmgF, is significantly altered in *mioC* and *gidA* mutants. Our data reveal new roles for the gene products of *gidA* and *mioC* in the division apparatus, and we propose that their expression, cyclically regulated by chromatin remodeling at *oriC*, is part of a cell cycle regulatory program coordinating replication initiation and cell division.

Keywords: mioC, gidA, bacterial cell division, bacterial cell cycle, *oriC*, FIS, replication initiation, ymgF

OPEN ACCESS

Edited by:
Conrad L. Woldringh, University of Amsterdam, Netherlands

Reviewed by:
Hua Xiang, Chinese Academy of Sciences, China
Elena C. Guzmán, Universidad de Extremadura, Spain

***Correspondence:**
David Bates, Baylor College of Medicine, One Baylor Plaza, BCM225, Houston, TX 77030, USA
bates@bcm.edu

Specialty section:
This article was submitted to Microbial Physiology and Metabolism, a section of the journal Frontiers in Microbiology

Received: *04 March 2015*
Accepted: *09 May 2015*
Published: *28 May 2015*

Citation:
Lies M, Visser BJ, Joshi MC, Magnan D and Bates D (2015) MioC and GidA proteins promote cell division in E. coli Front. Microbiol. 6:516. doi: 10.3389/fmicb.2015.00516

Introduction

In all cells, DNA replication and cell division are temporally coordinated to maintain a one-to-one relationship between genome and cell duplication. Cell cycle regulation in bacteria is subject to additional stringency because division cycles can be as short as 20 min, thus cells must replicate and segregate a full genome equivalent within this timeframe. To date no mechanism has been identified in *E. coli* to link replication and division. Pioneering work by the Helmstetter lab (Cooper and Helmstetter, 1968) indicated that the bacterial cell cycle might be controlled solely by the frequency and timing of replication initiation. This idea stemmed from synchronized cell experiments, which showed that in *E. coli* B/r strains the periods of DNA replication and septum development were relatively constant (~40 and 20 min, respectively) with the remainder of the cell cycle defined as a flexible pre-initiation "B" period (Dix and Helmstetter, 1973). It was hypothesized that cell division was triggered by an unknown event occurring at the end of the replication period, presumably replication of an essential cell division gene (Dix and Helmstetter, 1973; Den Blaauwen et al., 1999). Supporting this view, replication termination and cell division occur at the same cell location (Bates and Kleckner, 2005; Wang et al., 2005), and there is even some sharing of machinery between the two processes (e.g., FtsK translocase, Wang et al., 2005, 2006; Burton et al., 2007).

However, two lines of evidence suggest that cell division is initiated independently of replication termination. First, all known physical interactions between replicating DNA and

the division apparatus are inhibitory. Specifically, midcell FtsZ polymerization is repressed by the presence of unsegregated DNA (Mulder and Woldringh, 1989; Moriya et al., 2010; Cambridge et al., 2014), partially dependent on direct inhibition from the nucleoid-bound SlmA protein in *E. coli* (Bernhardt and De Boer, 2005) or NOC in *B. subtilis* (Wu et al., 2009; Rodrigues and Harry, 2012). Second, most genetic and cytological data places initial FtsZ ring assembly steps very early in the replication period far in advance of termination (e.g., Addinall and Lutkenhaus, 1996; Yu et al., 1998; Harry et al., 1999). Inhibiting DNA replication prior to or soon after the initiation step imparts a strong cell division block independent of nucleoid occlusion, but once established, inhibition of replication elongation through drug treatment or temperature sensitive replisome mutant does not itself inhibit FtsZ ring assembly (Harry et al., 1999; Regamey et al., 2000; Arjes et al., 2014; Morigen et al., 2014). In such a cell, Z-rings form off-center in a nucleoid occlusion-dependent process, generating anucleate cells (Mulder and Woldringh, 1989).

One possible connection between replication initiation and cell division is through activated expression of a cell division regulator gene near the replication origin, *oriC*. The very highly conserved *gidA* gene, which is located immediately leftward of *oriC* (**Figure 1**), was previously implicated in cell division via a cell filamentation phenotype in *gidA* (glucose inhibited division) deletion mutants when grown in glucose-containing media (Von Meyenburg and Hansen, 1980). The mechanism of the division defect in *gidA* mutants is unclear. Wild-type *gidA*, also known as *mnmG*, encodes a protein that in combination with MnmE is involved in modification of specific tRNA molecules, (Bregeon et al., 2001; Moukadiri et al., 2009). This tRNA modification may be important to prevent deleterious ribosomal frameshift mutations. However, comparison of *mnmE* and *gidA* (*mnmG*) mutant phenotypes indicates that GidA has additional functions outside tRNA modificiation (Bregeon et al., 2001). The other well-conserved gene flanking the replication origin is *mioC*, located immediately rightward of *oriC* (**Figure 1**). *mioC* encodes a protein that has been implicated in biotin synthesis *in vitro* (Birch et al., 2000), but *mioC* mutants do not require biotin for growth in rich or minimal medium (D.B., unpublished). Thus, MioC protein has no established biological function.

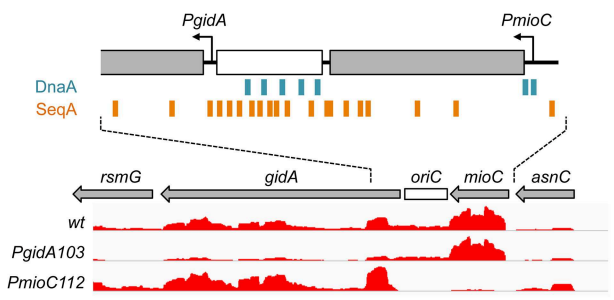

FIGURE 1 | Transcription in the *oriC* region. The minimal *oriC* (white box) and surrounding genes are shown, with transcription direction indicated by arrows. Binding sites for DnaA (blue boxes) and SeqA (orange boxes) overlap *mioC* and *gidA* promoters, respectively. Relative transcription in *wildtype* and *gidA* and *mioC* promoter mutants, as determined by RNA-sequencing is shown (height of red lines indicate relative reads per base pair).

Transcription of both *mioC* and *gidA* are thought to contribute to regulation of replication initiation, as *oriC* plasmids require both genes for replication (Lobner-Olesen et al., 1987; Asai et al., 1990; Bates et al., 1997). Since open reading frame deletions within either gene are generally not deleterious (Tanaka and Hiraga, 1985), it is thought that transcription through these genes affects replication initiation by changing origin topology (Asai et al., 1990). Based on the twin-domain supercoiling model (Liu and Wang, 1987), *gidA* transcription oriented away from *oriC* would introduced stimulatory negative supercoils, and *mioC* transcription oriented toward *oriC* would introduce inhibitory positive supercoils (**Figure 1**). This so-called "transcriptional activation" model is supported by the fact that *gidA* and *mioC* transcription is strongly cell-cycle specific, with stimulatory *gidA* transcription highest before initiation and *mioC* inhibitory transcription highest after initiation (Theisen et al., 1993; Su'etsugu et al., 2003). However, these effects seem to be specific to *oriC* plasmids. Preventing transcription from either gene on the chromosome has no measurable phenotype on the timing, rate or synchrony of replication initiation in otherwise wild-type cells under a variety of growth conditions (Lobner-Olesen and Boye, 1992; Bates et al., 1997; Asai et al., 1998; Molina et al., 1999). Only when multiple DnaA binding sites were deleted within *oriC*, was *gidA* transcription found to stimulate chromosomal initiation (Bates et al., 1997). These studies and the high sequence conservation of both *mioC* and *gidA* suggest that transcription near *oriC* may have once been an important initiation mechanism but, as we will argue here, may have later evolved other roles.

In a previous study, we observed that *mioC* and *gidA* promoter mutations in a *fis*$^-$ cell background resulted in extreme cell filamentation (Bates et al., 1997). Fis is a well-conserved and abundant nucleoid associated protein that is important for chromosome structure and transcriptional regulation of many genes, but has no known role in cell division (Skoko et al., 2006; Bradley et al., 2007; Browning et al., 2010). The expression of *fis* is stringent controlled and Fis levels rise dramatically after nutritional upshift reaching a maximum in mid-exponential phase (Mallik et al., 2006). Fis binds within the *oriC* sequence and likely has some role in replication initiation (Filutowicz et al., 1992) particularly under rapid growth conditions (Flatten and Skarstad, 2013). Because DNA/mass values (an indicator of replication efficiency) of *fis* mutant cells were not further reduced by *mioC* and *gidA* promoter mutations (Bates et al., 1997), we concluded that cell filamentation in the triple mutant resulted from some unknown feature of cell division regulation. Here, we further examine how these three genes affect DNA replication, chromosome segregation and cell division.

Materials and Methods

Bacterial Strains, Plasmids and Growth Conditions

All strains used in this work are derivatives of *E. coli* MG1655. Genotype, construction and sources of all strains are provided

in **Table S1**. Unmarked gene deletions in *sulA* (DB768) and *fis* (DB670) were created by amplifying a kanamycin resistance gene cassette flanked by Flp recognition sequences (FRT) from pKD4 (Cherepanov and Wackernagel, 1995), with 40 bp fragments on both ends homologous to the 5′ and 3′ ends of *sulA* or *fis* (primers listed in **Table S2**), then transferring the construct into the MG1655 chromosome by homologous recombination (Yu et al., 2000) selecting for kanamycin resistance. The *kan* gene was then deleted by expression of Flp from pCP20 (Cherepanov and Wackernagel, 1995) and curing the plasmid. The *ymgF::tet* deletion mutation was created by amplifying the tetracycline resistance gene from pBR322 with 40 bp fragments on both ends homologous to the 5′ and 3′ ends of *ymgF* (primers listed in **Table S2**), then transferring the construct into MG1655 by homologous recombination. A strain with in-frame *gidA* and *mioC* deletions was made by transferring a linearized *gidA122*Δ *mioC*Δ*121 asnA101::cat* fragment from the mutant *oriC* plasmid pDB123 (Bates et al., 1997) into MG1655 by homologous recombination. The *ymgF::tet* and *PsulA-GFP* mutations were introduced into various *PgidA PmioC fis* strains by P1 transduction. Wild-type *oriC* plasmid pDB101 is previously described (Bates et al., 1997). All strains were verified by PCR or sequencing.

For all experiments, cells were grown in LB medium supplemented with 0.1% glucose at 37°C. Unless otherwise stated, exponential growth was achieved by 1:1600 dilution of a saturated culture into fresh medium with shaking to OD600 absorbance of 0.2, at which point samples were removed for analysis. Antibiotics were added for selection in P1 transduction and to maintain plasmids at the following concentrations: ampicillin (50 μg/ml), chloramphenicol (50 μg/ml), tetracycline (20 μg/L) and kanamycin (55 μg/ml).

Flow Cytometry and qPCR

DNA content was measured in DAPI stained cells by flow cytometry as previously described (Joshi et al., 2013). For rifampicin runoff analysis, exponential cultures were treated with 150 μg/ml rifampicin to inhibit replication initiation and 10 μg/ml cephalexin to inhibit cell division, and incubated at 37°C with shaking for 1 h to allow completion of replication. All flow cytometry was performed on a Becton-Dickinson LSR II Cell Analyzer. *oriC* to *ter* ratios were determined by quantitative reat-time PCR (qPCR) using the $\Delta\Delta C_t$ method. Primers and details for qPCR are previously described (Joshi et al., 2011).

Phase and Fluorescence Microscopy (Cell Length, PI, DAPI, FM4-64, FISH)

For cell length determination, cells were fixed in 2.5% formaldehyde for 15 min at room temperature then 45 min on ice, followed by three washes in PBS pH7. Cell monolayers were created by applying fixed cells between a coverslip and an agarose-coated slide, then imaged by phase contrast. Cell length was determined in 500–600 cells per sample using MicrobeTracker software (Sliusarenko et al., 2011). For membrane permeability assays, live cells were washed three times in 0.85% NaCl and stained with 5 μM propridium iodide and imaged by fluorescence microscopy. The fraction of fluorescent (PI-positive) cells were quantified for 1000–1500 cells per sample by hand counting. Nucleoids and cell membranes were visualized in formaldehyde-fixed cell samples by simultaneous staining with 0.5 μg/ml 4′, 6′-diamidino-2-phenlyindole (DAPI) or 1 μg/ml FM4-64. FISH analysis of *oriC* and *ter* positioning was performed as previously described (Joshi et al., 2011).

Transcriptome Analysis

RNA for RNA-seq was isolated using acid phenol extraction and sequencing libraries were prepared using the Bacteria ScriptSeq kit (Epicentre). Briefly, rRNA was depleted from 5 μg total RNA using the Ribo-Zero Bacterial rRNA removal kit (Epicentre), followed by isopropanol precipitation of mRNA. Resulting mRNA was converted to terminal-tagged cDNA and 15 cycles of PCR were performed using ScriptSeq Set 1 index PCR primers (Illumina) to create the indexed cDNA libraries. These were quantified by Qubit fluorimetry and qPCR and diluted to a final concentration of 18 pM and pooled. Single-end sequencing was performed on an Illumina Next-generation MiSeq sequencer using a 150-cycle MiSeq Reagent Kit V3. Reads were aligned using Rockhopper software (McClure et al., 2013), using MG1655 as a reference genome. Transcript levels of *PmioC* (DB535) and *PgidA* (DB679) samples were normalized to a wild-type (DB510) sample. Statistical analysis and graphing were performed in Matlab (MathWorks).

Results

Blocking *mioC* and *gidA* Expression Inhibits Cell Division

In a previous study demonstrating that *mioC* and *gidA* transcription do not affect chromosomal replication initiation, we created promoter mutations in each of the genes (*PmioC112* and *PgidA103*) that resulted in severely decreased transcription as implied previously from ß-galactosidase assays (Bates et al., 1997) and verified here by RNA sequencing (**Figure 1**, red). Although *PmioC* and *PgidA* mutations did not affect the rate or timing of replication initiation (Bates et al., 1997), they did result in subtle increases in cell length, especially *PmioC* which was ∼35% longer than isogenic wild-type (**Figures 2A,C**; hatched columns). Continued cell growth in the absence of cell division was reflected in a disparity between mass (OD600) doubling time and cell number doubling time measured using a particle counter (**Figure 2C**; light and dark gray columns).

The addition of a *fis::kan* null mutation greatly exacerbates the cell elongation phenotype of the promoter mutations, with triple mutant *fis PmioC PgidA* exhibiting severe filamentation (**Figures 2B,D**; hatched columns). Although *fis*$^-$ cells have a reduced growth rate (∼50% of wt; **Figures 2C,D**), neither *PmioC* nor *PgidA* significantly enhanced the poor growth phenotype of the *fis* mutant (Bates et al., 1997; below) suggesting that the promoter mutations affected cell division directly and not through general growth effects. Similar cell elongation was observed in MG1655 (used here) and CM735 (not shown) strain backgrounds. Interestingly, despite a severe cell division phenotype in triple mutant cells, the strain is viable with fewer

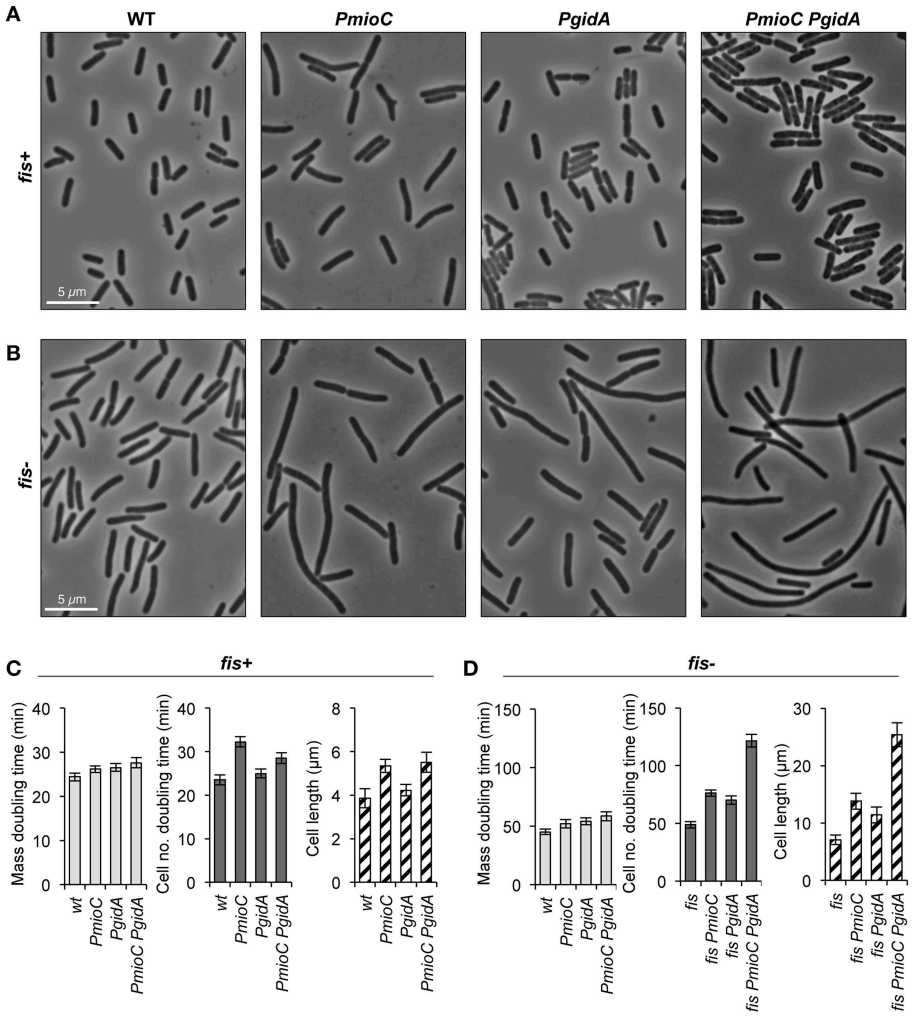

FIGURE 2 | *mioC* and *gidA* promoter mutants are elongated. Cells carrying promoter mutations (*PmioC*, *PgidA*) in a *fis*$^+$or *fis*$^-$ genetic background were diluted 1:1600 in LB medium at 37°C and assayed for growth and cell division. **(A,B)** Phase contrast images of cells at mid-exponential phase (OD600 = 0.2). **(C,D)** Above cultures were assayed for mass doubling time by optical density at 600 nm (light gray bars), cell number doubling time by flow counting in a Coulter particle counter (dark gray bars), and cell length at OD600 = 0.2 by direct microscopic observation (hatched bars, n = 500–600 cells). Values are means of 5 independent experiments ±1 standard deviation (SD).

than 1% of cells stainable with propidium iodide (data not shown). Survival is explained by the ability of filamentous cells to divide in late exponential and early stationary phase, with stationary phase cultures consisting of ∼normal length cells (**Figure S1**). Fis mediates expression of a diverse set of genes involved in all aspects of growth including translation, nutrient transport, carbon and energy metabolism, but relatively few genes involved in DNA replication and cell division (Bradley et al., 2007).

Cell Division Inhibition Is Independent of Both the SOS Response and Nucleoid Occlusion

An early stage of cell division is inhibited in triple mutant cells as indicated by the absence of division septa in filamented cells (**Figure 3A**, right). Further, we observed very few anucleate cells, which would occur frequently if FtsZ rings were repositioned by nucleoid occlusion in cells with unsegregated DNA (Bernhardt and De Boer, 2005). Supporting the idea that division was not inhibited by a chromosome segregation failure, nucleoid staining with DAPI showed that most filaments contained well-separated nucleoid bodies presumably composed of fully replicated chromosomes (**Figure 3A**, middle). Rare triple mutant cells exhibiting diffuse DAPI staining also frequently stained positive for propidium iodide, indicating that non-segregated nucleoids in those cells may have resulted from cell lysis. We further tested whether cell elongation in triple mutant cells was independent of nucleoid occlusion by introducing a *slmA*Δ mutation, which prevents the inhibition of midcell FtsZ rings over unsegregated DNA (Bernhardt and De Boer, 2005). We observed no significant decrease in cell length of quad mutant *slmA*Δ *fis PmioC PgidA* over *slmA*$^+$ *fis PmioC PgidA* cells (**Figures 3B,C**), nor was there an increase in frequency of

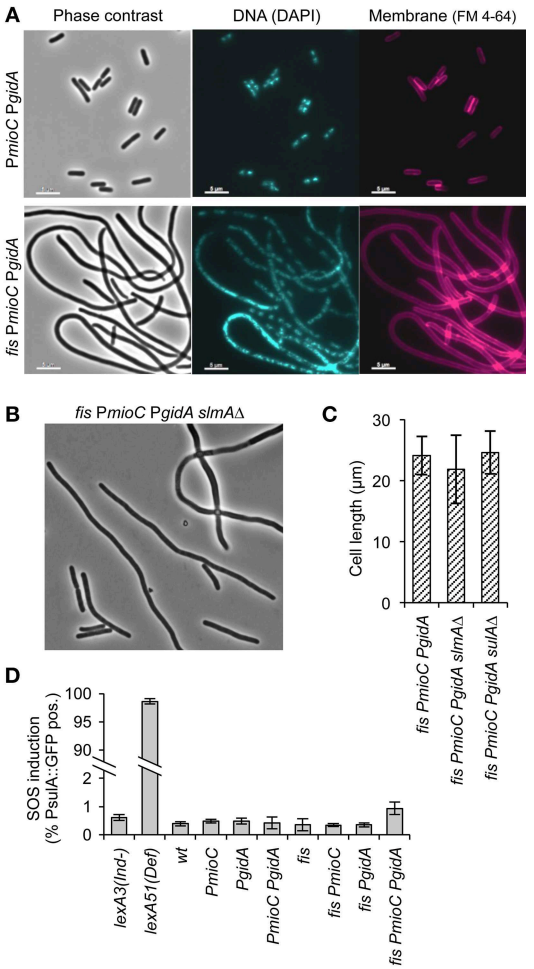

FIGURE 3 | Promoter mutants do not activate the SOS response or nucleoid occlusion. (A) DNA and membrane staining in a *PmioC PgidA* double mutant (top) or *PmioC PgidA fis* triple mutant (bottom) indicate an absence of division septa between segregated nucleoids. **(B)** Phase contrast image of a *PmioC PgidA fis slmA*Δ quad mutant. **(C)** Cell length of triple mutant (*PmioC PgidA fis*) cells in the presence or absence of a *slmA* or *sulA* deletion mutation. **(D)** SOS induction in *PmioC PgidA* and *fis* mutant combinations was measured by flow cytometry of strains carrying a *PsulA::GFP* reporter construct (Materials and Methods). Values are means of 3 independent experiments (±1 SD).

anucleate cells (not shown). This suggests that chromosome segregation was not significantly perturbed as the filamentous phenotype was not caused by nucleoid occlusion of the division plane.

We next asked whether cell elongation was dependent on the SOS response, which activates a large normally repressed regulon of cell cycle arrest and DNA repair genes that includes the potent cell division inhibitor, SulA (Huisman et al., 1984). To test if SOS was activated in elongating cells, we measured expression of a *PsulA*-GFP reporter gene inserted into the chromosome of all mutant strains (Shee et al., 2013). Cells were grown exponentially and GFP fluorescence was measured by flow cytometry. All mutant strains, including the filamentous triple mutant exhibited <1% of green cells during exponential growth (**Figure 3D**). Subsequent analysis of *PsulA*-GFP expression in triple mutant cells by microscopy, indicated that even among the longest cells (>15 μm), <5% were SOS-induced (not shown). In contrast, constitutively SOS induced *lexA51(Def)* cells were ∼98% GFP-positive, validating the assay. We further introduced a *sulA* deletion into the triple mutant, and found no difference in cell length compared to triple mutant *sulA*$^+$ cells (**Figure 3C**). We conclude that cell elongation observed in our mutants was independent of both the two cell division inhibitors SulA and SlmA.

Cell Elongation did not Result from Inefficient Chromosome Replication or Segregation

We previously reported that promoter mutations in *mioC* and *gidA* did not adversely affect the timing or efficiency of chromosomal replication (Bates et al., 1997). Even a subtle delay in replication could create an unbalanced cell cycle that results in delayed cell division. For example, blocking replication elongation by depleting dNTPs with hydroxyurea results in incomplete replication intermediates that block division independently of both SOS and SlmA (Cambridge et al., 2014). To confirm and extend our previous analysis of DNA replication, we measured DNA content and cell mass by flow cytometry in the mutant set. As expected, promoter single and double mutants in a *fis*$^+$ background exhibited a normal number of chromosomes and synchronous replication initiation, as shown by rifampicin runoff histograms (**Figure 4A**). In this method, which involves blocking replication initiation with rifampicin and cell division with cephalexin and allowing ongoing replication forks to complete, cells accumulate a number of fully replicated chromosomes equal to the number of origins present at the time of drug treatment. Under our growth conditions (LB/37°C), wild-type cells mostly contained either 4 or 8 origins (**Figure 4A**, left). This indicates that replication initiation occurred synchronously, with all origins in a cell firing ∼simultaneously, and thus containing 2^n origins where n is equal to any positive integer. Double *PmioC PgidA* mutants exhibited slightly more 8-origin cells than *wildtype*, but this difference was not statistically significant. Rifampicin runoff in *fis*$^-$ cells did not produce discernable chromosome peaks in our flow cytometry analysis, likely owing to asynchronous replication (Flatten and Skarstad, 2013) and uneven DAPI staining due to abnormal chromosome structure (Skoko et al., 2006).

The ratio of DNA per unit of cell mass in exponentially growing cells (without rifampicin treatment), is essentially constant in healthy populations, but differs strongly in strains with inefficient replication initiation or elongation (Stepankiw et al., 2009 and references therein). DNA/mass was unaffected by *mioC* or *gidA* promoter mutations in either *fis*$^+$ or *fis*$^-$ backgrounds as determined by DAPI and light scatter flow cytometry measurements (**Figure 4B**), implying that cell elongation did not result from a reduced replication initiation or elongation rate, which would decrease DNA/mass values. By comparison, temperature-sensitive *dnaA46* mutant cells grown at 30°C, which are about twice the length of identically-grown

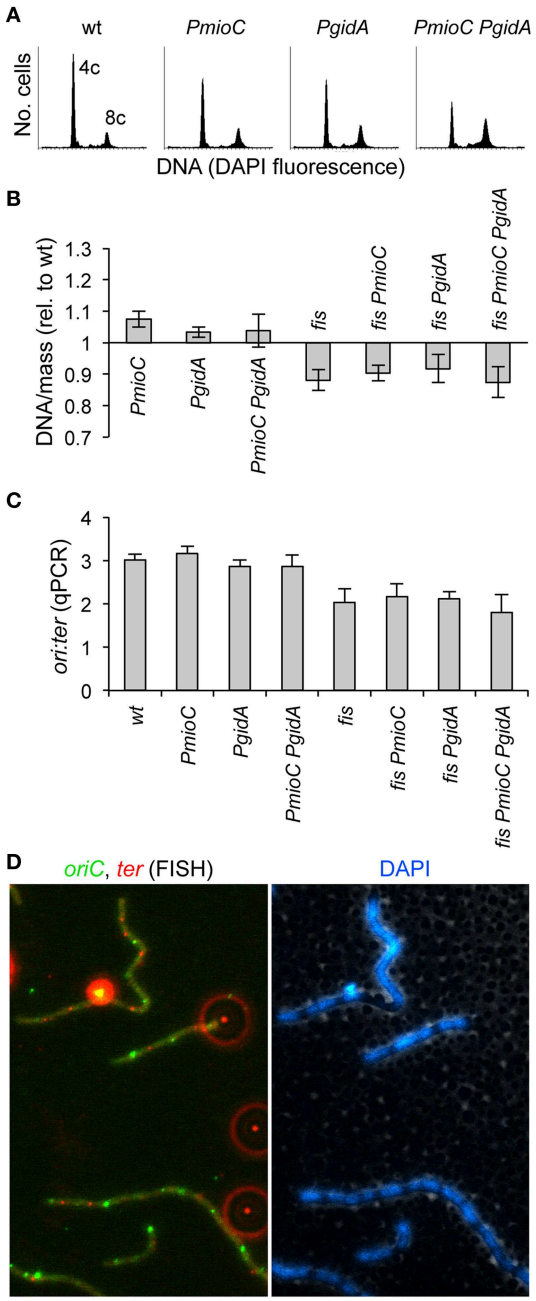

FIGURE 4 | Promoter mutations do not impair DNA replication or chromosome segregation. (A) Rifampicin runoff DNA histograms in *PmioC* and *PgidA* mutants indicate synchronous replication initiations. Numbers represent the number of chromosomes at the major peaks. **(B)** DNA/mass in exponentially growing cultures was measured by flow cytometry of DAPI stained cells (values are relative to *wildtype*). **(C)** The ratio of *oriC* sites to *ter* sites in above cells was measured by qPCR, indicating the rate of DNA replication and whether replication forks were blocked between *oriC* and *ter*. Values in **B,C** are means of 3 independent experiments (±1 SD). **(D)** The positions of *oriC* (green foci) and *ter* (red foci) in elongating triple mutant *PmioC PgidA fis* cells was analyzed by FISH (left panel). Bright extracellular foci (appearing as red halos) are multi-fluorescent beads added for image alignment. DAPI staining (right panel) indicates *ter* foci are located between segregated nucleoids, consistent with normal chromosome segregation (Text). See Material and Methods for details.

wild-type cells, exhibit a 30–40% reduced DNA/mass value (Boye et al., 1996).

We further looked for evidence of slowed replication elongation by measuring the *oriC* to *ter* rato in our mutants by quantitative PCR (qPCR). This assay would reveal for example any replication fork blockage late in the C period, which would likely not significantly affect overall DNA/mass values. Wild-type cells had an *ori*:*ter* ratio of ∼3, which was unchanged in single or double promoter mutants (**Figure 4C**). Similarly the *ori*:*ter* ratio in *fis*$^-$ cells (≈2) did not significantly change upon introduction of either or both *mioC* or *gidA* promoter mutations. To test whether chromosome segregation was impaired in our mutant, which could account for inhibited cell division (above), we examined the number and positions of *oriC* and *ter* copies by fluorescence *in situ* hybridization (FISH). This analysis showed evenly spaced *oriC* and *ter* foci in all strains, even in elongated triple mutant cells (**Figure 4D**). These data suggest that cell elongation present in triple mutant cells did not result from a reduction in the rate of replication initiation or blocked replication elongation or chromosome segregation.

The Division Block Is Mediated by a Lack of MioC and GidA Protein

The transcriptional activation model (Theisen et al., 1993) posits that *mioC* and *gidA* primarily function to modulate replication initiation via transcription-induced supercoiling changes at *oriC*. Given that all our tests indicate that *PmioC* and *PgidA* mutants have unperturbed chromosomal replication initiation, fork elongation, and chromosome segregation, it is a reasonable prediction that cell elongation in promoter mutants is due to an absence of MioC and GidA proteins, and not gene transcription *per se*. To test this idea, we created in-frame deletion mutants of both genes, in which most of the open reading frame was deleted but promoters were left in-tact (Materials and Methods). Transcription through the remaining open reading frame occurs at normal levels and an *oriC* plasmid containing both mutations could support plasmid replication (Bates et al., 1997). Cells carrying a *fis* mutation with both *mioC*Δ and *gidA*Δ in-frame deletions exhibited severe cell elongation (**Figure 5A**, gray), with average cell length within error of *fis PmioC PgidA* cells (**Figure 5A**, black). Examination of cell length through all three growth phases showed that both the *fis*$^+$ double mutant and the *fis*$^-$ triple mutant exhibited similar temporal patterns of elongation with maximal cell length occurring in late exponential phase (**Figure 5B**, gray and black lines). These results support the idea that *mioC* and *gidA* affect cell division by providing a division-related gene product, not by transcription-induced replication effects.

We next asked whether the cell division phenotype of triple mutant cells could be complemented *in trans* by exogenous GidA and MioC protein. Cells carrying *PmioC PgidA* and *fis*$^-$ mutations were transformed with two *oriC* plasmids, pDB101 carrying the wild-type *mioC* and *gidA* genes and promoter sequences, and pDB123 carrying the *mioC*Δ and *gidA*Δ in-frame deletions. Both of these plasmids fully support *oriC*-dependent plasmid replication (Bates et al., 1997). Triple mutant *fis PmioC PgidA* cells expressing GidA and MioC protein from pDB101

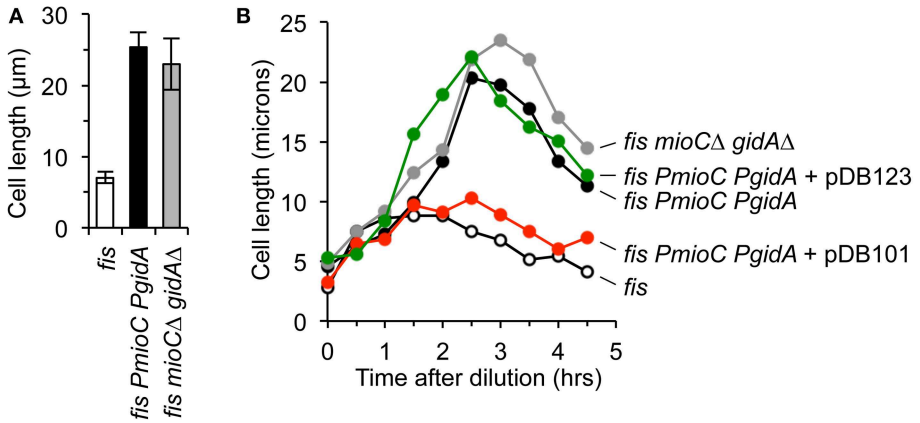

FIGURE 5 | The division phenotype of *mioC* and *gidA* mutants is complemented *in trans*. (A) Cell length in exponential cultures of *fis* parental, *fis* with *mioC* and *gidA* promoter mutations, and *fis* with *mioC* and *gidA* in-frame ORF deletions with active transcription, was measured by direct microscope observation (3 independent experiments, ±1 SD). **(B)** Cell length was measured over time through all three growth phases in the indicated mutants and plasmids. Complementation of the cell division phenotype in triple mutant cells (*fis PmioC PgidA*) occurred with a plasmid expressing MioC and GidA protein (pDB101), but not with a control plasmid carrying *mioC* and *gidA* ORF deletions (pDB123).

grew to a maximum length of ∼7–10 microns, similar to cells carrying a single *fis* mutation (**Figure 5B**, red and open circles). By comparison, *fis PmioC PgidA* cells transformed with the control plasmid that does not express MioC or GidA protein but has a functioning *oriC* (pDB123), elongated to a maximum of ∼22 μm (**Figure 5B**, green) with similar extent and kinetics as non-transformed triple mutants. We conclude that MioC and GidA are cell division regulatory proteins.

MioC and GidA Regulate Expression of a Cell Division gene, *ymgF*

Although neither MioC nor GidA are known to regulate transcription, both have been implicated in information transfer functions (Introduction) and it is possible that mutants have altered expression of one or more cell division-related genes. To test this, we measured the relative abundance of all the *E. coli* mRNAs in wild-type and *PmioC* and *PgidA* single mutant strains by next-generation RNA sequencing. Both mutants had several up-regulated and several down-regulated genes as shown by high and low ticks, with each tick representing a single gene (**Figures 6A,B**). Altered genes included various ontology groups including amino acid and carbon metabolism, transcription, membrane proteins, and small molecule transport (**Table S3**). One gene in particular, *ymgF*, was significantly under-expressed (3.3-fold less than *wt*) in the *PmioC* mutant and over-expressed (3.1-fold more than *wt*) in the *PgidA* mutant (**Figures 6A,B**, arrows). This gene was previously identified in a bacterial two-hybrid screen for factors that interact with the division septum component FtsL (Karimova et al., 2009). GFP-tagged YmgF localizes strongly to the division septum, and although a *ymgF* deletion does not confer a growth or cell division phenotype, overexpression of YmgF suppresses a temperature-sensitive *ftsQ* mutant (Karimova et al., 2009). YmgF is a 72 amino acid integral membrane protein, but little else is known about its function.

To test epistasis relationships between *mioC*, *gidA*, and *ymgF*, we examined cell length in our mutant set in the presence or absence of a *ymgF::kan* deletion mutation. Cell elongation in the *PmioC PgidA* double mutant was decreased by ∼20% after addition of *ymgF*Δ, with resulting cell lengths within error of wild-type cells (**Figure 6C**). This effect was greatly amplified in *fis*$^-$ derivatives, with nearly a nearly 3-fold reduction in cell length of quad mutant cells (*fis PmioC PgidA ymgF*Δ) compared to isogenic *ymgF*$^+$ cells, to approximately wild-type lengths (**Figure 6D**). These results suggest that the entirety of MioC's and GidA's effect on cell division is dependent on YmgF, and therefore they act upstream of YmgF to regulate division.

Discussion

MioC and GidA Promote Cell Division without Affecting Replication Initiation

We have shown that *mioC* and *gidA* mutants have a reduced capacity to divide, which is exacerbated by a *fis* deletion. Several data suggest that division inhibition did not result from late or inefficient DNA replication. (1) Mutations in *mioC* and *gidA* did not reduce the simultaneous firing of multiple origins in the same cell (initiation synchrony). (2) DNA contents (DNA/mass or number of origins) were not affected by a *mioC* or *gidA* mutation, even in the presence of a *fis* mutation. (3) Division inhibition did not involve SOS induction, which could have resulted from DNA damage caused by replication defects, as shown by an absence of PsulA-GFP expression in triple mutant *PmioC PgidA fis* cells and by normal *sulA* expression in *PmioC* and *PgidA* strains by transcription profiling. (4) Elongating *mioC* and *gidA* mutants showed no apparent chromosome segregation defects (e.g., that might result from late DNA replication) by DAPI analysis and by FISH analysis of *oriC* and *ter* numbers and locations. (5) Triple mutant cells continued to elongate in the presence of a *slmA* mutation, suggesting that division

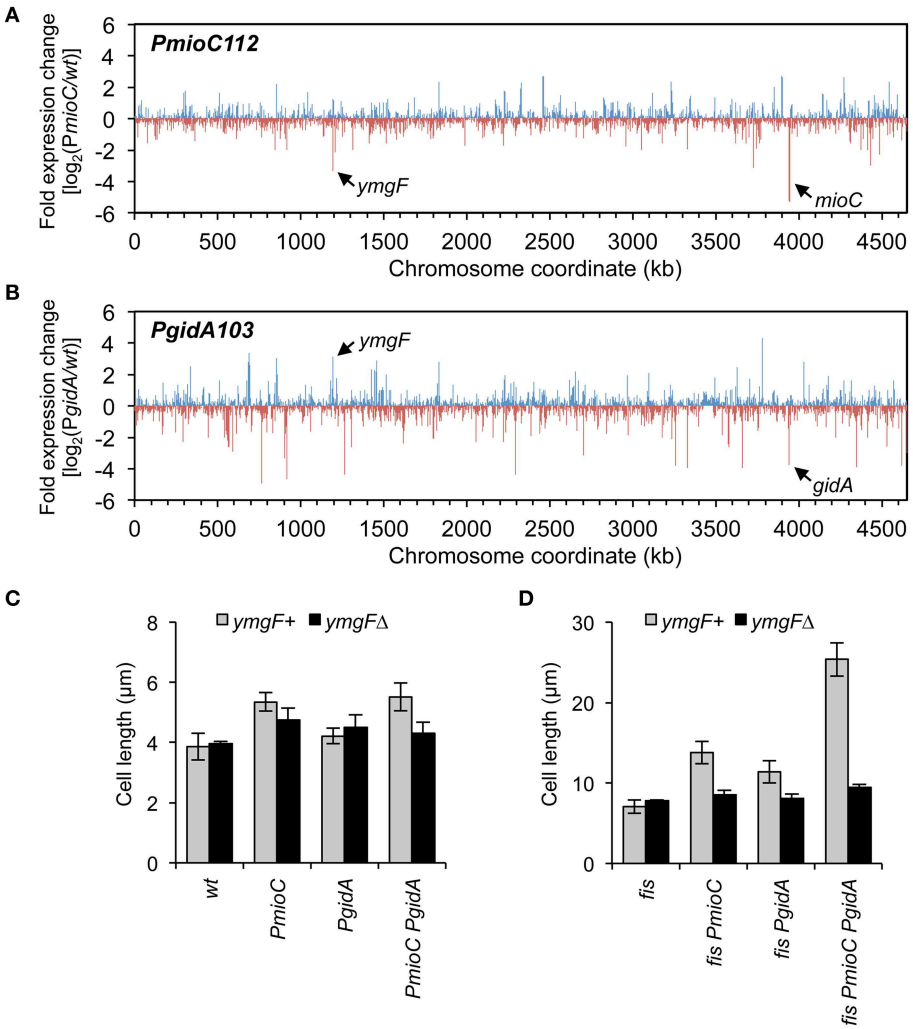

FIGURE 6 | Transcription profiling in *mioC* and *gidA* mutants. (A,B) Changes in gene expression across the *E. coli* genome in *mioC* **(A)** and *gidA* **(B)** promoter mutants relative to *wildtype* was determined by RNA sequencing (Materials and Methods). Blue and red ticks indicated positive or negative fold-changes of individual genes. The positions of *mioC* and *gidA*, and a strongly affected cell division gene, *ymgF*, are indicated. See **Table S3** for description of other affected genes. **(C,D)** The cell elongation phenotype of *gidA* and *mioC* mutants requires YmgF. Cell length was measured in exponentially growing *wildtype* and *mioC* and *gidA* promoter mutants in *fis*$^+$ **(C)** or *fis*$^-$ **(D)** genetic background, in the presence (black bars) or absence (gray bars) of a *ymgF*Δ mutation.

was not inhibited by nucleoid occlusion. (6) Finally, the cell division defect was shown to result from a lack of MioC and GidA protein, not a lack of *mioC* and *gidA* transcription, which has previously been implicated in replication initiation control (Introduction).

All of these results suggest that *mioC* and *gidA* affect cell division independently of any *cis*-mediated effects at *oriC*, and this is supported by work indicating that *mioC* and *gidA* do not affect chromosomal replication initiation (Lobner-Olesen and Boye, 1992; Bogan and Helmstetter, 1996; Bates et al., 1997). Possible subtle segregation defects capable of inhibiting division but undetected by DAPI or FISH analysis cannot be ruled out. Additionally, it was recently shown that unsegregated chromosomes can block cell division independently of SOS or SlmA (Cambridge et al., 2014), leaving open this possibility. Transcription analysis in *Salmonella gidA* mutants, which also exhibit cell elongation, indicated abnormal expression of several chromosome segregation genes including *mreB*, *mukB*, *xerC*, *parA*, and *parB* (Shippy et al., 2012). In our transcription analysis, none of these genes, nor any other known segregation gene, were significantly changed in either *PgidA* or *PmioC* strains, thus there may be a divergence of roles for GidA and MioC between the two organisms.

Expression of *mioC* and *gidA* are Cell Cycle Controlled

Transcription of many genes varies significantly during the cell cycle (Zhou et al., 1997), which in many cases is correlated in time and amplitude to the predicted replication of those genes, but in others, like *mioC* and *gidA*, transcription is

switch-like with abrupt on/off kinetics (Theisen et al., 1993; Ogawa and Okazaki, 1994; illustrated in **Figure 7A**). Both *mioC* and *gidA* transcription is thought to be mediated by the initiation proteins DnaA and SeqA, whose binding sites overlap the *mioC* and *gidA* promoters (**Figure 1A**). Binding of these proteins is primarily regulated by remodeling events that occur at *oriC* at the time of initiation (**Figure 7B**): (1) A cluster of GATC sites in the left end of *oriC* become hemimethylated after passage of the replication fork, which causes ∼20-fold increase in SeqA binding immediately adjacent to the *gidA* promoter (Slater et al., 1995; Nievera et al., 2006). Transcription of *gidA* is continually blocked until *oriC* is remethylated ∼1/3 of the cell cycle later (the sequestration period; Slater et al., 1995; Bogan and Helmstetter, 1997). (2) At the same time, *mioC* transcription is de-repressed by replication initiation, through removal of DnaA protein bound to two conserved DnaA boxes within the *mioC* promoter (Bogan and Helmstetter, 1996). DnaA rebinding is thought to be temporarily inhibited by titration of free DnaA to newly replicated binding sites, which are concentrated toward *oriC* on the *E. coli* chromosome (Kitagawa et al., 1998). (3) Remethylation of the GATC cluster in *oriC* and subsequent removal of SeqA protein (de-sequestration) de-repress the *gidA* promoter. (4) Finally, the cycle is completed by rebinding of the *mioC* promoter by DnaA protein, blocking its transcription. This cyclic expression of GidA and MioC protein allows us to develop a working model for a new replication-division linkage regulatory pathway (below).

General Model for Replication Initiation-Dependent Cell Division Control

The resulting *mioC* and *gidA* transcription pattern places maximal MioC expression about midway through DNA replication at which point GidA expression is at its lowest (**Figure 7A**). From our expression analysis, transcription of *ymgF*, encoding a division septum protein (Karimova et al., 2009), was ∼3-fold higher in *gidA* mutants and ∼3-fold lower in *mioC* mutants.

Joining these data, we predict that *ymgF* expression would reach a maximum about midway through DNA replication, or just after, very near the point at which FtsZ polymerization normally begins (e.g., Addinall and Lutkenhaus, 1996). During fast growth, replication initiation at multiple origins is synchronous, thus maintaining cyclic and coordinated *mioC, gidA, and ymgF* expression. Modulation of *ymgF* expression by MioC and GidA may involve a complex indirect mechanism, as neither protein are known transcription regulators (Introduction).

The weak division phenotype of *mioC* and *gidA* mutants (without an additional *fis* mutation) as well as a *ymgF*Δ mutant (Karimova et al., 2009), suggests that the affected division control mechanism is likely either redundant with other control mechanisms, or part of a division checkpoint that is utilized under specific growth phases, or both. Because Fis is a known regulator of replication initiation (Filutowicz et al., 1992; Flatten and Skarstad, 2013) with no known role in regulating division, we speculate that deletion of *fis* exacerbates the division phenotype of *gidA* and *mioC* mutants by delaying replication initiation. Late *oriC* firing (and *gidA* and *mioC* promoter remodeling) would normally lead to a corresponding late division cycle with adjusted (late) division, but there is no such adjustment in the *gidA mioC fis* triple mutant, thus severe elongation. Further research into if and how MioC, GidA, and YmgF interact to mediate cell division, as well as how Fis contributes to this mediation is essential.

The above model is consistent with the proposal by Nordstrom and colleagues that DNA replication and cell division are independently regulated processes that are temporally correlated through the actions of specific "cell cycle" checkpoints (Nordstrom et al., 1991; Boye and Nordstrom, 2003). This idea stemmed from observations that changes in the timing of DNA replication initiation brought about by manipulations of growth medium or temperature were not accompanied by closely corresponding changes in the timing of cell division (i.e., cell length; Bernander and Nordstrom, 1990; Boye et al., 1996).

Two-Trick Ponies?

Considering the substantial published data on *mioC* and *gidA* (not half of which is cited here) we speculate that these well-conserved genes have dual function, mediating

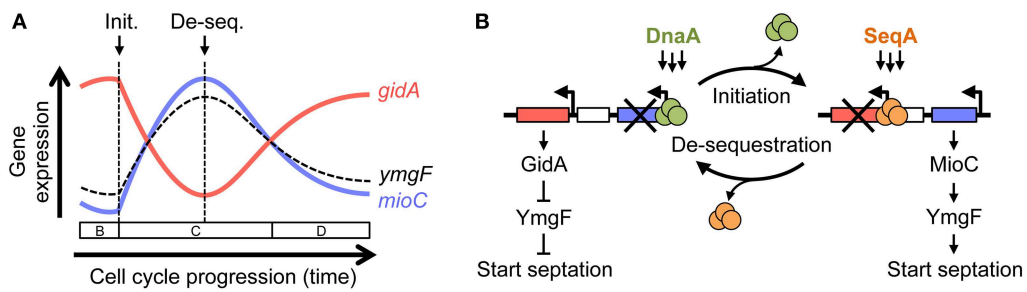

FIGURE 7 | A model for MioC and GidA-mediated linkage between replication initiation and cell division. (A) Schematic of *mioC* (blue) and *gidA* (red) transcription during the cell cycle from synchronized cell experiments (Theisen et al., 1993; Ogawa and Okazaki, 1994), and predicted expression of *ymgF* (dashed curve). Times of replication initiation and origin de-sequestration are indicated by arrows, with cell cycle pre-initiation (B period), replication (C period), and cell division (D period) shown above time line. **(B)** Cyclic inverse expression of *mioC* and *gidA* occur as a consequence of replication-dependent remodeling and subsequent remethylation (de-sequestration). See Discussion for detailed description.

cell division in response to replication initiation, and also activating *oriC* under exceptional circumstances. We previously showed that strains with a large deletion within the minimal *oriC* sequence required *gidA* transcription for viability (Bates et al., 1997), implying that *gidA* transcription stimulates open complex formation in these cells. Similarly, these genes may help drive initiation under conditions of low DnaA, temperature, or other suboptimal initiation conditions, and they may have been an essential component of a primordial initiation system (Asai et al., 1998). Transcription of *mioC* and *gidA* may also regulate initiation (and division) in non-steady state situations, in which the normal 1:1 ratio of initiation and division is temporarily circumvented to support multi-forked replication (in rich media there are division-less initiations in lag phase and initiation-less divisions in early stationary phase). This idea is supported by the fact that *mioC* is stringently controlled (Chiaramello and Zyskind, 1989). Interestingly, *mioC* transcription is affected by a putative cell division protein, MraZ, which binds a site overlapping the the *mioC* promoter DnaA box (Eraso et al., 2014). Cells overexpressing MraZ have ∼12-fold reduced *mioC* transcription, and exhibit severe cell elongation to the point of cell death, but MioC overexpression did not alleviate the cell division defect (Eraso et al., 2014), therefore the relationship between MraZ-mediated division inhibition and *mioC* repression is unclear. Additionally, *mioC* and *gidA* genes may be responsible for over-initiation of replication observed after thymine depletion (Martín et al., 2014). Thymine starvation results in stalled replication forks, and cells typically die from an abundance of stalled forks near *oriC*. Martín and colleagues showed that thymine-less death could be prevented by introducing promoter mutations in *mioC* and *gidA*, suggesting that these genes are part of a (sometimes futile) cell cycle response pathway to reinitiate replication when fork progression is impaired.

Acknowledgments

We thank Walter Messer, Daniel Ladant, Gouzel Karimova, Susan Rosenberg, Christophe Herman, and Bill Margolin for strains and plasmids. We also thank Sue Lovett, Jesus Eraso, Bill Margolin, Christophe Herman and Susan Rosenberg for discussion. All research was supported by National Institutes of Health (NIH) grant R01GM102679 to DB. This project was further supported by NIH grant DP1-CA174424 to Susan Rosenberg for next generation sequencing and by the Cytometry and Cell Sorting Core at Baylor College of Medicine with funding from NIH grants P30 AI036211, P30 CA125123, and S10 RR024574.

Supplementary Material

The Supplementary Material for this article can be found online at: http://journal.frontiersin.org/article/10.3389/fmicb.2015.00516/abstract

Figure S1 | Growth phase-specific cell elongation in *PmioC PgidA fis*. Cell length (open circles) and culture density (OD600, dashed line) were measured in *PmioC PgidA fis* triple mutant cells for 10 h after 1:1600 dilution into fresh LB medium. Maximal cell length occurs in mid-late exponential phase, with cells approaching normal cell length by late stationary phase.

Table S1 | *E. coli* strains.

Table S2 | Cloning primers.

Table S3 | Functional categorization of GidA and MioC regulated genes*.

References

Addinall, S. G., and Lutkenhaus, J. (1996). FtsA is localized to the septum in an FtsZ-dependent manner. *J. Bacteriol.* 178, 7167–7172.

Arjes, H. A., Kriel, A., Sorto, N. A., Shaw, J. T., Wang, J. D., and Levin, P. A. (2014). Failsafe mechanisms couple division and DNA replication in bacteria. *Curr. Biol.* 24, 2149–2155. doi: 10.1016/j.cub.2014.07.055

Asai, T., Bates, D. B., Boye, E., and Kogoma, T. (1998). Are minichromosomes valid model systems for DNA replication control? Lessons learned from *Escherichia coli*. *Mol. Microbiol.* 29, 671–675. doi: 10.1046/j.1365-2958.1998.00901.x

Asai, T., Takanami, M., and Imai, M. (1990). The AT richness and gid transcription determine the left border of the replication origin of the *E. coli* chromosome. *EMBO J.* 9, 4065–4072.

Bates, D. B., Boye, E., Asai, T., and Kogoma, T. (1997). The absence of effect of *gid* or *mioC* transcription on the initiation of chromosomal replication in *Escherichia coli*. *Proc. Natl. Acad. Sci. U.S.A.* 94, 12497–12502. doi: 10.1073/pnas.94.23.12497

Bates, D., and Kleckner, N. (2005). Chromosome and replisome dynamics in *E. coli*: loss of sister cohesion triggers global chromosome movement and mediates chromosome segregation. *Cell* 121, 899–911. doi: 10.1016/j.cell.2005.04.013

Bernander, R., and Nordstrom, K. (1990). Chromosome replication does not trigger cell division in *E. coli*. *Cell* 60, 365–374. doi: 10.1016/0092-8674(90)90588-6

Bernhardt, T. G., and De Boer, P. A. J. (2005). SlmA, a nucleoid-associated, FtsZ binding protein required for blocking septal ring assembly over chromosomes in *E. coli*. *Mol. Cell* 18, 555–564. doi: 10.1016/j.molcel.2005.04.012

Birch, O. M., Hewitson, K. S., Fuhrmann, M., Burgdorf, K., Baldwin, J. E., Roach, P. L., et al. (2000). MioC Is an FMN-binding protein that is essential for *Escherichia coli* biotin synthase activity *in vitro*. *J. Biol. Chem.* 275, 32277–32280. doi: 10.1074/jbc.M004497200

Bogan, J. A., and Helmstetter, C. E. (1996). *mioC* transcription, initiation of replication, and the eclipse in *Escherichia coli*. *J. Bacteriol.* 178, 3201–3206.

Bogan, J. A., and Helmstetter, C. E. (1997). DNA sequestration and transcription in the *oriC* region of *Escherichia coli*. *Mol. Microbiol.* 26, 889–896. doi: 10.1046/j.1365-2958.1997.6221989.x

Boye, E., and Nordstrom, K. (2003). Coupling the cell cycle to cell growth. *EMBO Rep.* 4, 757–760. doi: 10.1038/sj.embor.embor895

Boye, E., Stokke, T., Kleckner, N., and Skarstad, K. (1996). Coordinating DNA replication initiation with cell growth: differential roles for DnaA and SeqA proteins. *Proc. Natl. Acad. Sci. U.S.A.* 93, 12206–12211. doi: 10.1073/pnas.93.22.12206

Bradley, M. D., Beach, M. B., De Konig, A. P. J., Pratt, T. S., and Osuna, R. (2007). Effects of Fis on *Escherichia coli* gene expression during different growth stages. *Microbiology* 153, 2922–2940. doi: 10.1099/mic.0.2007/008565-0

Bregeon, D., Colot, V., Radman, M., and Taddei, F. (2001). Translational misreading: a tRNA modification counteracts a +2 ribosomal frameshift. *Genes Dev.* 15, 2295–2306. doi: 10.1101/gad.207701

Browning, D. F., Grainger, D. C., and Busby, S. J. (2010). Effects of nucleoid-associated proteins on bacterial chromosome structure and gene expression. *Curr. Opin. Microbiol.* 13, 773–780. doi: 10.1016/j.mib.2010.09.013

Burton, B. M., Marquis, K. A., Sullivan, N. L., Rapoport, T. A., and Rudner, D. Z. (2007). The ATPase SpoIIIE transports DNA across fused septal

membranes during sporulation in *Bacillus subtilis*. *Cell* 131, 1301–1312. doi: 10.1016/j.cell.2007.11.009

Cambridge, J., Blinkova, A., Magnan, D., Bates, D., and Walker, J. R. (2014). A replication-inhibited unsegregated nucleoid at mid-cell blocks Z-ring formation and cell division independently of SOS and the SlmA nucleoid occlusion protein in *Escherichia coli*. *J. Bacteriol.* 196, 36–49. doi: 10.1128/JB.01230-12

Cherepanov, P. P., and Wackernagel, W. (1995). Gene disruption in *Escherichia coli*: TcR and KmR cassettes with the option of Flp-catalyzed excision of the antibiotic-resistance determinant. *Gene* 158, 9–14. doi: 10.1016/0378-1119(95)00193-A

Chiaramello, A. E., and Zyskind, J. W. (1989). Expression of *Escherichia coli* dnaA and *mioC* genes as a function of growth rate. *J. Bacteriol.* 171, 4272–4280.

Cooper, S., and Helmstetter, C. E. (1968). Chromosome replication and the division cycle of *Escherichia coli* B/r. *J. Mol. Biol.* 31, 519–540. doi: 10.1016/0022-2836(68)90425-7

Den Blaauwen, T., Buddelmeijer, N., Aarsman, M. E., Hameete, C. M., and Nanninga, N. (1999). Timing of FtsZ assembly in *Escherichia coli*. *J. Bacteriol.* 181, 5167–5175.

Dix, D. E., and Helmstetter, C. E. (1973). Coupling between chromosome completion and cell division in *Escherichia coli*. *J. Bacteriol.* 115, 786–795.

Eraso, J. M., Markillie, L. M., Mitchell, H. D., Taylor, R. C., Orr, G., and Margolin, W. (2014). The highly conserved MraZ protein is a transcriptional regulator in *Escherichia coli*. *J. Bacteriol.* 196, 2053–2066. doi: 10.1128/JB.01370-13

Filutowicz, M., Ross, W., Wild, J., and Gourse, R. L. (1992). Involvement of Fis protein in replication of the *Escherichia coli* chromosome. *J. Bacteriol.* 174, 398–407.

Flatten, I., and Skarstad, K. (2013). The Fis protein has a stimulating role in initiation of replication in *Escherichia coli in vivo*. *PLoS ONE* 8:e83562. doi: 10.1371/journal.pone.0083562

Harry, E. J., Rodwell, J., and Wake, R. G. (1999). Co-ordinating DNA replication with cell division in bacteria: a link between the early stages of a round of replication and mid-cell Z ring assembly. *Mol. Microbiol.* 33, 33–40. doi: 10.1046/j.1365-2958.1999.01439.x

Huisman, O., D'ari, R., and Gottesman, S. (1984). Cell-division control in *Escherichia coli*: specific induction of the SOS function SfiA protein is sufficient to block septation. *Proc. Natl. Acad. Sci. U.S.A.* 81, 4490–4494. doi: 10.1073/pnas.81.14.4490

Joshi, M. C., Bourniquel, A., Fisher, J., Ho, B. T., Magnan, D., Kleckner, N., et al. (2011). *Escherichia coli* sister chromosome separation includes an abrupt global transition with concomitant release of late-splitting intersister snaps. *Proc. Natl. Acad. Sci. U.S.A.* 108, 2765–2770. doi: 10.1073/pnas.1019593108

Joshi, M. C., Magnan, D., Montminy, T. P., Lies, M., Stepankiw, N., and Bates, D. (2013). Regulation of sister chromosome cohesion by the replication fork tracking protein SeqA. *PLoS Genet.* 9:e1003673. doi: 10.1371/journal.pgen.1003673

Karimova, G., Robichon, C., and Ladant, D. (2009). Characterization of YmgF, a 72-residue inner membrane protein that associates with the *Escherichia coli* cell division machinery. *J. Bacteriol.* 191, 333–346. doi: 10.1128/JB.00331-08

Kitagawa, R., Ozaki, T., Moriya, S., and Ogawa, T. (1998). Negative control of replication initiation by a novel chromosomal locus exhibiting exceptional affinity for *Escherichia coli* DnaA protein. *Genes Dev.* 12, 3032–3043. doi: 10.1101/gad.12.19.3032

Liu, L. F., and Wang, J. C. (1987). Supercoiling of the DNA template during transcription. *Proc. Natl. Acad. Sci. U.S.A.* 84, 7024–7027. doi: 10.1073/pnas.84.20.7024

Lobner-Olesen, A., Atlung, T., and Rasmussen, K. V. (1987). Stability and replication control of *Escherichia coli* minichromosomes. *J. Bacteriol.* 169, 2835–2842.

Lobner-Olesen, A., and Boye, E. (1992). Different effects of *mioC* transcription on initiation of chromosomal and minichromosomal replication in *Escherichia coli*. *Nucleic Acids Res.* 20, 3029–3036. doi: 10.1093/nar/20.12.3029

Mallik, P., Paul, B. J., Rutherford, S. T., Gourse, R. L., and Osuna, R. (2006). DksA is required for growth phase-dependent regulation, growth rate-dependent control, and stringent control of fis expression in *Escherichia coli*. *J. Bacteriol.* 188, 5775–5782. doi: 10.1128/JB.00276-06

Martín, C. M., Viguera, E., and Guzmán, E. C. (2014). Rifampicin suppresses thymineless death by blocking the transcription-dependent step of chromosome initiation. *DNA Repair* 18, 10–17. doi: 10.1016/j.dnarep.2014.03.004

McClure, R., Balasubramanian, D., Sun, Y., Bobrovskyy, M., Sumby, P., Genco, C. A., et al. (2013). Computational analysis of bacterial RNA-Seq data. *Nucleic Acids Res.* 41:e140. doi: 10.1093/nar/gkt444

Molina, F., Jiménez-Sánchez, A., Zyskind, J. W., and Guzmán, E. C. (1999). Chromosomal insertions localized around *oriC* affect the cell cycle in *Escherichia coli*. *Biochimie* 81, 811–818. doi: 10.1016/S0300-9084(99)00216-3

Morigen, M., Flåtten, I., and Skarstad, K. (2014). The *Escherichia coli* datA site promotes proper regulation of cell division. *Microbiology* 160, 703–710. doi: 10.1099/mic.0.074898-0

Moriya, S., Rashid, R. A., Rodrigues, C. D., and Harry, E. J. (2010). Influence of the nucleoid and the early stages of DNA replication on positioning the division site in *Bacillus subtilis*. *Mol. Microbiol.* 76, 634–647. doi: 10.1111/j.1365-2958.2010.07102.x

Moukadiri, I., Prado, S., Piera, J., Velazquez-Campoy, A., Bjork, G. R., and Armengod, M.-E. (2009). Evolutionarily conserved proteins MnmE and GidA catalyze the formation of two methyluridine derivatives at tRNA wobble positions. *Nucleic Acids Res.* 37, 7177–7193. doi: 10.1093/nar/gkp762

Mulder, E., and Woldringh, C. L. (1989). Actively replicating nucleoids influence positioning of division sites in *Escherichia coli* filaments forming cells lacking DNA. *J. Bacteriol.* 171, 4303–4314.

Nievera, C., Torgue, J. J., Grimwade, J. E., and Leonard, A. C. (2006). SeqA blocking of DnaA-*oriC* interactions ensures staged assembly of the *E. coli* pre-RC. *Mol. Cell* 24, 581–592. doi: 10.1016/j.molcel.2006.09.016

Nordstrom, K., Bernander, R., and Dasgupta, S. (1991). The *Escherichia coli* cell cycle: one cycle or multiple independent processes that are co-ordinated. *Mol. Microbiol.* 5, 769–774. doi: 10.1111/j.1365-2958.1991.tb00747.x

Ogawa, T., and Okazaki, T. (1994). Cell cycle-dependent transcription from the gid and *mioC* promoters of *Escherichia coli*. *J. Bacteriol.* 176, 1609–1615.

Regamey, A., Harry, E. J., and Wake, R. G. (2000). Mid-cell Z ring assembly in the absence of entry into the elongation phase of the round of replication in bacteria: co-ordinating chromosome replication with cell division. *Mol. Microbiol.* 38, 423–434. doi: 10.1046/j.1365-2958.2000.02130.x

Rodrigues, C. D. A., and Harry, E. J. (2012). The min system and nucleoid occlusion are not required for identifying the division site in *Bacillus subtilis* but ensure its efficient utilization. *PLoS Genet.* 8:e1002561. doi: 10.1371/journal.pgen.1002561

Shee, C., Cox, B. D., Gu, F., Luengas, E. M., Joshi, M. C., Chiu, L. Y., et al. (2013). Engineered proteins detect spontaneous DNA breakage in human and bacterial cells. *Elife* 2:e01222. doi: 10.7554/eLife.01222

Shippy, D. C., Heintz, J. A., Albrecht, R. M., Eakley, N. M., Chopra, A. K., and Fadl, A. A. (2012). Deletion of glucose-inhibited division (*gidA*) gene alters the morphological and replication characteristics of Salmonella enterica Serovar typhimurium. *Arch. Microbiol.* 194, 405–412. doi: 10.1007/s00203-011-0769-7

Skoko, D., Yoo, D., Bai, H., Schnurr, B., Yan, J., McLeod, S. M., et al. (2006). Mechanism of chromosome compaction and looping by the *Escherichia coli* nucleoid protein fis. *J. Mol. Biol.* 364, 777–798. doi: 10.1016/j.jmb.2006.09.043

Slater, S., Wold, S., Lu, M., Boye, E., Skarstad, K., and Kleckner, N. (1995). E. *coli* SeqA protein binds *oriC* in two different methyl-modulated reactions appropriate to its roles in DNA replication initiation and origin sequestration. *Cell* 82, 927–936. doi: 10.1016/0092-8674(95)90272-4

Sliusarenko, O., Heinritz, J., Emonet, T., and Jacobs-Wagner, C. (2011). High-throughput, subpixel precision analysis of bacterial morphogenesis and intracellular spatio-temporal dynamics. *Mol. Microbiol.* 80, 612–627. doi: 10.1111/j.1365-2958.2011.07579.x

Stepankiw, N., Kaidow, A., Boye, E., and Bates, D. B. (2009). The right half of the *Escherichia coli* replication origin is not essential for viability, but facilitates multi-forked replication. *Mol. Microbiol.* 74, 467–479. doi: 10.1111/j.1365-2958.2009.06877.x

Su'etsugu, M., Emoto, A., Fujimitsu, K., Keyamura, K., and Katayama, T. (2003). Transcriptional control for initiation of chromosomal replication in *Escherichia coli*: fluctuation of the level of origin transcription ensures timely initiation. *Genes Cells* 8, 731–745. doi: 10.1046/j.1365-2443.2003.00671.x

Tanaka, M., and Hiraga, S. (1985). Negative control of *oriC* plasmid replication by transcription of the *oriC* region. *Mol. Gen. Genet.* 200, 21–26. doi: 10.1007/BF00383307

Theisen, P. W., Grimwade, J. E., Leonard, A. C., Bogan, J. A., and Helmstetter, C. E. (1993). Correlation of gene transcription with the time of initiation of chromosome replication in *Escherichia coli*. *Mol. Microbiol.* 10, 575–584. doi: 10.1111/j.1365-2958.1993.tb00929.x

Von Meyenburg, K., and Hansen, F. G. (1980). The origin of replication, *oriC*, of the *Escherichia coli* chromosome: genes near *oriC* and construction of *oriC* deletion mutations. *ICN-ULCA Symposia Mol. Cell. Biol.* 19, 137–159. doi: 10.1016/b978-0-12-048850-6.50022-3

Wang, S. C., West, L., and Shapiro, L. (2006). The bifunctional FtsK protein mediates chromosome partitioning and cell division in *Caulobacter*. *J. Bacteriol.* 188, 1497–1508. doi: 10.1128/JB.188.4.1497-1508.2006

Wang, X., Possoz, C., and Sherratt, D. J. (2005). Dancing around the divisome: asymmetric chromosome segregation in *Escherichia coli*. *Genes Dev.* 19, 2367–2377. doi: 10.1101/gad.345305

Wu, L. J., Ishikawa, S., Kawai, Y., Oshima, T., Ogasawara, N., and Errington, J. (2009). Noc protein binds to specific DNA sequences to coordinate cell division with chromosome segregation. *EMBO J.* 28, 1940–1952. doi: 10.1038/emboj.2009.144

Yu, D., Ellis, H. M., Lee, E. C., Jenkins, N. A., Copeland, N. G., and Court, D. L. (2000). An efficient recombination system for chromosome engineering in *Escherichia coli*. *Proc. Natl. Acad. Sci. U.S.A.* 97, 5978–5983. doi: 10.1073/pnas.100127597

Yu, X. C., Weihe, E. K., and Margolin, W. (1998). Role of the C terminus of FtsK in *Escherichia coli* chromosome segregation. *J. Bacteriol.* 180, 6424–6428.

Zhou, P., Bogan, J. A., Welch, K., Pickett, S. R., Wang, H. J., Zaritsky, A., et al. (1997). Gene transcription and chromosome replication in *Escherichia coli*. *J. Bacteriol.* 179, 163–169.

Conflict of Interest Statement: The authors declare that the research was conducted in the absence of any commercial or financial relationships that could be construed as a potential conflict of interest.

Copyright © 2015 Lies, Visser, Joshi, Magnan and Bates. This is an open-access article distributed under the terms of the Creative Commons Attribution License (CC BY). The use, distribution or reproduction in other forums is permitted, provided the original author(s) or licensor are credited and that the original publication in this journal is cited, in accordance with accepted academic practice. No use, distribution or reproduction is permitted which does not comply with these terms.

frontiers in
MICROBIOLOGY

ORIGINAL RESEARCH ARTICLE
published: 07 January 2015
doi: 10.3389/fmicb.2014.00738

Interaction sites of DivIVA and RodA from *Corynebacterium glutamicum*

Boris Sieger and Marc Bramkamp*

Biocenter – Ludwig-Maximilians-University Munich, Munich, Germany

Edited by:
Conrad L. Woldringh, University of Amsterdam, Netherlands (retired)

Reviewed by:
Sven Halbedel, Robert Koch Institute, Germany
Kevin D. Young, University of Arkansas for Medical Science, USA

***Correspondence:**
Marc Bramkamp, Biocenter – Ludwig-Maximilians-University Munich, Großhaderner Straße 2-4, 82152 Planegg-Martinsried, Munich, Germany
e-mail: marc.bramkamp@lmu.de

Elongation growth in actinobacteria is localized at the cell poles. This is in contrast to many classical model organisms where insertion of new cell wall material is localized around the lateral site. We previously described a role of RodA from *Corynebacterium glutamicum* in apical cell growth and morphogenesis. Deletion of *rodA* had drastic effects on morphology and growth, likely a result from misregulation of penicillin-binding proteins and cell wall precursor delivery. We identified the interaction of RodA with the polar scaffold protein DivIVA, thus explaining subcellular localization of RodA to the cell poles. In this study, we describe this interaction in detail and map the interaction sites of DivIVA and RodA. A single amino acid residue in the N-terminal domain of DivIVA was found to be crucial for the interaction with RodA. The interaction site of RodA was mapped to its cytoplasmic, C-terminal domain, in a region encompassing the last 10 amino acids (AAs). Deletion of these 10 AAs significantly decreased the interaction efficiency with DivIVA. Our results corroborate the interaction of DivIVA and RodA, underscoring the important role of DivIVA as a spatial organizer of the elongation machinery in *Corynebacterineae*.

Keywords: DivIVA, RodA, *Corynebacterium glutamicum*, protein–protein interactions, polar cell growth, FRET

INTRODUCTION

Corynebacterium glutamicum is a fast growing, facultative anaerobic, Gram positive *Actinobacterium* with high industrial importance in the production of amino acids (AAs; Ikeda and Nakagawa, 2003). For this purpose, fast growth rates and high cell densities are two major properties to ensure efficient production rates. Furthermore, *C. glutamicum* gained medical interest due to its mycobacteria-like cell wall and its phylogenetic relation to notorious pathogens such as *C. diphtheriae*, *Mycobacterium tuberculosis*, and *M. leprae* (Barh et al., 2011; Cayabyab et al., 2012). Members of the genus *Corynebacterium* are abundant species on the human skin and airways microbiome (Cowling and Hall, 1993; Zeeuwen et al., 2013). *C. glutamicum* and all other actinobacteria grow apically by insertion of new cell wall material at the cell poles (Locci and Schaal, 1980; Brown et al., 2011; Donovan and Bramkamp, 2014). Spatial localization of the cell wall machinery is governed by a coiled-coil protein, DivIVA (Letek et al., 2008; Sieger et al., 2013). This is in remarkable contrast to rod-shaped bacteria from other phyla such as firmicutes or proteobacteria. In these organisms a MreBCD-based cell wall synthetic machinery is acting along the lateral sites of the cell (Jones et al., 2001; Kruse et al., 2005). The processive enzymes, e.g. penicillin-binding proteins are, however, ubiquitous (Popham and Young, 2003). Furthermore, membrane integral proteins of the SEDS family are found in every cell wall synthetic cluster (Henriques et al., 1998; Pastoret et al., 2004). It is believed that an FtsW homolog is associated with septal cell wall synthesis, while RodA homologs are part of the elongation machinery (Pastoret et al., 2004; Real et al., 2008; Sieger et al., 2013). FtsW and RodA are associated with flipping the cell wall precursor lipid II (Ikeda and Nakagawa, 2003; Noirclerc-Savoye et al., 2003; Mohammadi et al., 2011). A new candidate for lipid II flipping, MurJ, has recently been described (Sham et al., 2014). Maybe, both enzymes may confer translocation of lipid II. However, based on earlier studies with *rodA* deletion mutants in *C. glutamicum*, it became evident that lack of RodA may also influence activity of the cognitive penicillin-binding proteins (Sieger et al., 2013).

In a previous study we identified RodA as being essential for growth and determination of cell shape (Sieger et al., 2013). DivIVA is frequently present in Gram positive species and generally composed of a highly conserved N-terminal domain, followed by two coiled-coil domains (Letek et al., 2009; **Figures 1A,B**). The N-terminal domain is involved in membrane attachment via exposed phenylalanine residues, positioned at the tip of intertwined loops as revealed by the crystal structure of the *Bacillus subtilis* DivIVA (Oliva et al., 2010). The coiled-coil domains are required for oligomerization and scaffold formation (Stahlberg et al., 2004; Lenarcic et al., 2009). DivIVA proteins lack an enzymatic function and polymerize into large oligomers in a nucleotide independent fashion (Muchova et al., 2002).

In the past decade several interaction partners of DivIVA have been identified. *B. subtilis* DivIVA anchors the Min system via MinJ to the cell poles, thus contributing to division site selection (Bramkamp et al., 2008; Patrick and Kearns, 2008). In addition, DivIVA interacts with RacA to attach the DNA to the prespore pole during *B. subtilis* sporulation (Ben-Yehuda et al., 2003; Wu and Errington, 2003). Further interaction partners are the division inhibitor Maf in competent *B. subtilis* cells (Briley et al., 2011), the transcriptional regulator ComN during promotion of natural competence (dos Santos et al., 2012) and SpoIIE for asymmetric

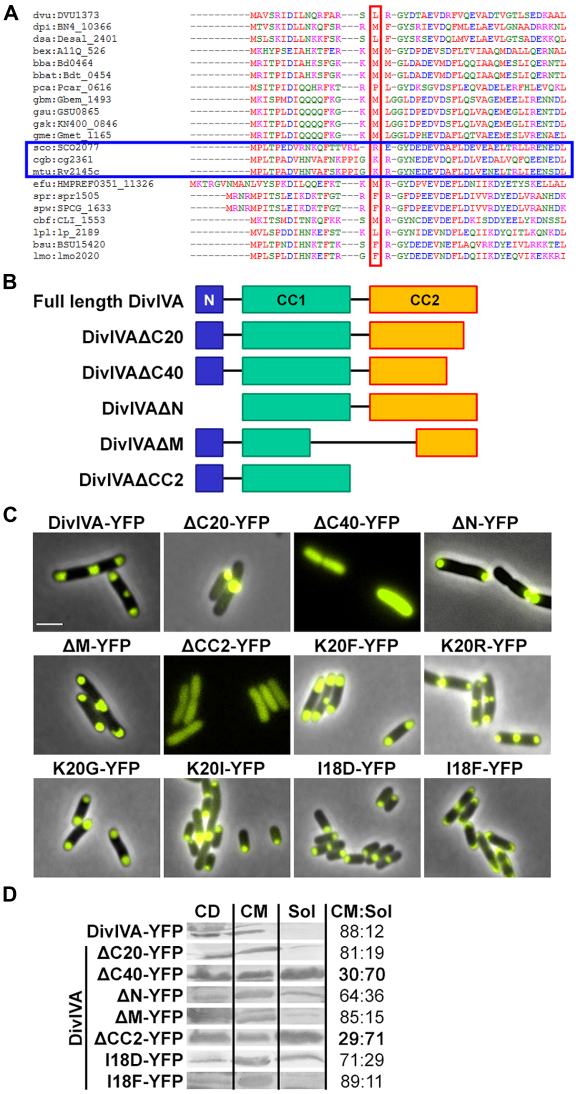

FIGURE 1 | (A) Sequence alignment of N-terminal domains of several DivIVA proteins. Marked in red are AA residues that correspond to the F17 residue located at the tip of intertwined loops, according to the *Bacillus subtilis* DivIVA crystal structure. Polar growing actinobacteria such as *Streptomyces*, *Corynebacterium*, and *Mycobacteria* have a positively charged residue at this position (marked with a blue box). In the case of *C. glutamicum*, the corresponding AA is the lysine K20. Dvu: *Desulfovibrio vulgaris*, Dpi: *Desulfovibrio piezophilus*, Dsa: *Desulfovibrio salexigens*, Bex: *Bdellovibrio exovorus*, Bba: *Bdellovibrio bacteriovorus*, Bbat: *Bdellovibrio bacteriovorus* Tiberius, Pca: *Pelobacter carbinolicus*, Gbm: *Geobacter bemidjiensis*, Gsu: *G. sulfurreducens* PCA, Gsk: *G. sulfurreducens* KN400, Gme: *G. metallireducens*, Sco: *Streptomyces coelicolor*, Cgb: *Corynebacterium glutamicum*, Mtu: *Mycobacterium tuberculosis*, Efu: *Enterococcus faecium* DO, Spr: *Streptococcus pneumoniae* R6, Spw: *S. pneumoniae* CGSP14, Cbf: *Clostridium botulinum* F, Lpl: *Lactobacillus plantarum* WCFS1, Bsu: *B. subtilis*, Lmo: *Listeria monocytogenes*. Sequences were obtained from KEGG database. **(B)** Topology models of full length DivIVA and several truncation mutants that were generated and used in this study. DivIVAΔC20 and DivIVAΔC40 lack 20 or 40 AAs of their C-terminal ends. DivIVAΔN lacks the N-terminal domain, DivIVAΔM lacks a middle part of 154 AAs (144-298) and DivIVACC2 lacks the second coiled coil domain. **(C)** Fluorescence microscopy images of DivIVA variants that were heterologously expressed in *Escherichia coli*. Full length DivIVA-YFP

(Continued)

FIGURE 1 | Continued
localizes to both cell poles and the septum. DivIVAΔC20-YFP lost its proper localization character and forms huge, presumably non-functional, aggregates at mostly one cell pole. DivIVAΔC40-YFP as well as DivIVACC2-YFP localize in the cytoplasm, likely due to misfolding or lack of oligomerization. DivIVAΔN-YFP localizes to the poles; however, not always to both cell poles. DivIVAΔM-YFP localizes similar to wild type DivIVA. The DivIVA point mutants K20F and K20R localize similar compared to wild type protein. Mutants K20G-YFP and K20I-YFP showed polar localization, partly to one pole, comparable to DivIVAΔN-YFP. Mutant I18D-YFP showed no alterations in localization and membrane binding, whereas mutant I18F-YFP gives rise to increased membrane association. I18 is likely involved in membrane binding due to its hydrophobic character. **(D)** Ratios of non-aggregated, membrane attached vs. soluble DivIVA mutants. Full length DivIVA-YFP is 88% membrane attached and similar values were obtained from DivIVAΔC20-YFP and DivIVAΔM-YFP. DivIVAΔN-YFP is 64% membrane attached, implicating defects in membrane attachment that were drastically reduced for DivIVAΔC40-YFP and DivIVACC2-YFP to 30% and 29%, respectively. Mutant I18D-YFP had a minor decrease in membrane binding (71%) whereas I18F-YFP had a similar membrane affinity compared to WT DivIVA-YFP (89%). CD, cell debris fraction; CM, cell membrane fraction; Sol, soluble fraction. All numbers are mean values of at least three independent experiments.

division during sporulation (Eswaramoorthy et al., 2014). Only recently, it was demonstrated how MinJ and RacA of *B. subtilis* bind to separate domains of DivIVA (van Baarle et al., 2013). RacA interacts with the 11 C-terminal AAs of DivIVA, whereas MinJ binds to the N-terminal lipid binding domain. Although many more interaction partners of DivIVA have been identified in several organisms, as reviewed by (Lin and Thanbichler, 2013; Laloux and Jacobs-Wagner, 2014), little is known about their interaction sites involved in protein–protein interaction.

Here we describe the identification of the RodA–DivIVA interaction sites, thereby corroborating earlier results that suggested an interaction of *C. glutamicum* DivIVA and RodA (Sieger et al., 2013). Mutational analysis and subsequent interaction studies using a Förster-Resonance Energy Transfer (FRET)-based assay reveals that DivIVA interacts with the C-terminal domain of RodA. The N-terminal domain, which is supposed to play a role in membrane association, is crucial for the interaction with RodA. The molecular mechanism seems to include electrostatic interactions, since a positive charge in DivIVA is essential for full protein–protein interaction.

EXPERIMENTAL PROCEDURES

GENERAL CLONING TECHNIQUES

General cloning was performed as described before (Sieger et al., 2013). Oligonucleotides were obtained from Sigma Aldrich and are listed in Table S1. Plasmids generated in this study are listed in **Table 1**. *C. glutamicum* strains are listed in **Table 2**. *Escherichia coli* strains that were transformed with the plasmids from **Table 1** for cloning and protein expression are not listed separately. Point mutants of DivIVA were generated via overlapping PCR using oligonucleotides carrying the desired point mutation. *E. coli* was grown in Luria Broth supplemented with 100 mg ml^{-1} carbenicillin (pETDuet-1) or 50 mg ml^{-1} kanamycin (pEKEX2). *C. glutamicum* was grown in Brain Heart Infusion (BHI; Oxoid) supplemented with 25 mg ml^{-1} kanamycin (pEKEX2). Protein expression was induced with 0.1 mM IPTG.

Table 1 | Plasmids.

No	Name	Description	Reference
	pETDuet-1		
EX001	pETDuet-1	*bla, PT7lacI-, PT7lacI-*	Novagen
BS001	Duet CFP	*bla, PT7lacI-eCFP, PT7lacI-*	Sieger et al. (2013)
BS002	Duet YFP	*bla, PT7lacI-, PT7lacI-eYFP*	Sieger et al. (2013)
BS003	Duet CFP YFP	*bla, PT7lacI-eCFP, PT7lacI-eYFP*	Sieger et al. (2013)
BS004	Duet DivIVA-YFP	*bla, PT7lacI-, PT7lacI-divIVA-eYFP*	Sieger et al. (2013)
BS005	Duet RodA-CFP	*bla, PT7lacI-rodA-eCFP, PT7lacI-*	Sieger et al. (2013)
BS006	Duet FtsW-CFP	*bla, PT7lacI-ftsW-eCFP, PT7lacI-*	Sieger et al. (2013)
BS007	Duet RodA-CFP DivIVA-YFP	*bla, PT7lacI-rodA-eCFP, PT7lacI-divIVA-eYFP*	Sieger et al. (2013)
BS008	Duet FtsW-CFP DivIVA-YFP	*bla, PT7lacI-ftsW-eCFP, PT7lacI-divIVA-eYFP*	Sieger et al. (2013)
BS025	Duet RodAΔC10-CFP	*bla, PT7lacI-rodAΔC10-eCFP PT7lacI-*	This study
BS026	Duet RodAΔC80-CFP	*bla, PT7lacI-rodAΔC80-eCFP, PT7lacI-*	This study
BS027	Duet RodA1/2-CFP	*bla, PT7lacI-rodA1/2-eCFP, PT7lacI-*	This study
BS028	Duet RodA2/2-CFP	*bla, PT7lacI-rodA2/2-eCFP, PT7lacI-*	This study
BS029	Duet RodAΔC10-CFP DivIVA-YFP	*bla, PT7lacI-rodA ΔC10-eCFP, PT7lacI-divIVA-eYFP*	This study
BS030	Duet RodAΔC80-CFP DivIVA-YFP	*bla, PT7lacI-rodA ΔC80-eCFP, PT7lacI-divIVA-eYFP*	This study
BS031	Duet RodA1/2-CFP DivIVA-YFP	*bla, PT7lacI-rodA1/2-eCFP, PT7lacI-divIVA-eYFP*	This study
BS032	Duet RodA2/2-CFP DivIVA-YFP	*bla, PT7lacI-rodA2/2-eCFP, PT7lacI-divIVA-eYFP*	This study
BS033	Duet DivIVAΔC20-YFP	*bla, PT7lacI-, PT7lacI-divIVAΔC20-eYFP*	This study
BS034	Duet DivIVAΔC40-YFP	*bla, PT7lacI-, PT7lacI-divIVAΔC40-eYFP*	This study
BS035	Duet DivIVAΔM-YFP	*bla, PT7lacI-, PT7lacI-divIVAΔM-eYFP*	This study
BS036	Duet DivIVAΔN-YFP	*bla, PT7lacI-, PT7lacI-divIVAΔN-eYFP*	This study
BS037	Duet DivIVAΔCC2-YFP	*bla, PT7lacI-, PT7lacI-divIVAΔCC2-eYFP*	This study
BS038	Duet RodA-CFP DivIVAΔC20-YFP	*bla, PT7lacI-rodA-eCFP, PT7lacI-divIVAΔC20-eYFP*	This study
BS039	Duet RodA-CFP DivIVAΔC40-YFP	*bla, PT7lacI-rodA-eCFP, PT7lacI-divIVAΔC40-eYFP*	This study
BS040	Duet RodA-CFP DivIVAΔM-YFP	*bla, PT7lacI-rodA-eCFP, PT7lacI-divIVAΔM-eYFP*	This study
BS041	Duet RodA-CFP DivIVAΔN-YFP	*bla, PT7lacI-rodA-eCFP, PT7lacI-divIVAΔN-eYFP*	This study
BS042	Duet RodA-CFP DivIVAΔCC2-YFP	*bla, PT7lacI-rodA-eCFP, PT7lacI-divIVAΔCC2-eYFP*	This study
BS043	Duet RodAE438G-CFP	*bla, PT7lacI-rodAE438G-eCFP, PT7lacI-*	This study
BS044	Duet RodAE438G-CFP DivIVA-YFP	*bla, PT7lacI-rodAE438G-eCFP, PT7lacI-divIVA-eYFP*	This study
BS045	Duet RodAK434G-CFP	*bla, PT7lacI-rodAK434G-eCFP, PT7lacI-*	This study
BS046	Duet RodAK434G-CFP, DivIVA-YFP	*bla, PT7lacI- rodAK434G-eCFP, PT7lacI-divIVA-eYFP*	This study
BS047	Duet RodAQ435G-CFP	*bla, PT7lacI-rodAQ435G-eCFP, PT7lacI-*	This study
BS048	Duet RodAQ435G-CFP, DivIVA-YFP	*bla, PT7lacI-rodAQ435G-eCFP, PT7lacI- divIVA-eYFP*	This study
BS049	Duet RodAS433G-S437G-CFP	*bla, PT7lacI-rodAS433G-S437G-eCFP, PT7lacI-*	This study
BS050	Duet RodAS433G-S437G-CFP, DivIVA-YFP	*bla, PT7lacI-rodAS433G S437G-eCFP, PT7lacI-divIVA-eYFP*	This study
BS051	Duet RodAmutC10-CFP	*bla, PT7lacI-mutC10-eCFP, PT7lacI-*	This study
BS052	Duet RodAmutC10-CFP, DivIVA-YFP	*bla, PT7lacI- mutC10-eCFP, PT7lacI-divIVA-eYFP*	This study
BS053	Duet DivIVAK20F-YFP	*bla, PT7lacI-, PT7lacI-divIVAK20F-eYFP*	This study
BS054	Duet RodA-CFP, DivIVAK20F-YFP	*bla, PT7lacI-rodA-eCFP, PT7lacI-divIVAK20F-eYFP*	This study
BS055	Duet DivIVAK20R-YFP	*bla, PT7lacI-, PT7lacI-divIVAK20R-eYFP*	This study
BS056	Duet RodA-CFP, DivIVAK20R-YFP	*bla, PT7lacI-rodA-eCFP, PT7lacI-divIVAK20R-eYFP*	This study
BS057	Duet DivIVAK20G-YFP	*bla, PT7lacI-, PT7lacI-divIVAK20G-eYFP*	This study
BS058	Duet RodA-CFP, DivIVAK20G-YFP	*bla, PT7lacI-rodA-eCFP, PT7lacI-divIVAK20G-eYFP*	This study

(Continued)

Table 1 | Continued

No.	Name	Description	Reference
BS059	Duet DivIVAK20I-YFP	*bla, PT7lacI-, PT7lacI-divIVAK20I-eYFP*	This study
BS060	Duet RodA-CFP, DivIVAK20I-YFP	*bla, PT7lacI-rodA-eCFP, PT7lacI-divIVAK20I-eYFP*	This study
BS061	Duet DivIVAI18D-YFP	*bla, PT7lacI-, PT7lacI-divIVAI18D-eYFP*	This study
BS062	Duet RodA-CFP, DivIVAI18D-YFP	*bla, PT7lacI-rodA-eCFP, PT7lacI-divIVAI18D-eYFP*	This study
BS063	Duet DivIVAI18F-YFP	*bla, PT7lacI-, PT7lacI-divIVAI18F-eYFP*	This study
BS064	Duet RodA-CFP, DivIVAI18F-YFP	*bla, PT7lacI-rodA-eCFP, PT7lacI-divIVAI18F-eYFP*	This study
	pEKEX2		
EX010	pEXEK2	*Escherichia coli – C. glutamicum* shuttle vector, Kan^R, P_{tac} *lacI*^{q}, pBL1 $oriV_{C.g.}$, pUC18 $oriV_{E.c.}$,	Eikmanns et al. (1991)
BS018	pEX2 RodA-GFP	Kan^R, P_{tac} *lacI*^{q}, pBL1 $oriV_{C.g.}$, pUC18 $oriV_{E.c.}$, *rodA-gfp*	Sieger et al. (2013)
BS053	pEX2 RodA1/2-GFP	Kan^R, P_{tac} *lacI*^{q}, pBL1 $oriV_{C.g.}$, pUC18 $oriV_{E.c.}$, *rodA1/2-gfp*	This study
BS054	pEX2 RodA2/2-GFP	Kan^R, P_{tac} *lacI*^{q}, pBL1 $oriV_{C.g.}$, pUC18 $oriV_{E.c.}$, *rodA2/2-gfp*	This study
BS055	pEX2 RodAΔC10-GFP	Kan^R, P_{tac} *lacI*^{q}, pBL1 $oriV_{C.g.}$, pUC18 $oriV_{E.c.}$, *rodAΔC10-gfp*	This study
BS056	pEX2 RodAΔC80-GFP	Kan^R, P_{tac} *lacI*^{q}, pBL1 $oriV_{C.g.}$, pUC18 $oriV_{E.c.}$, *rodAΔC80-gfp*	This study

Table 2 | Strains.

Number	Genotype/Description	Reference
C. glutamicum		
WT	ATCC 13032	Laboratory stock
Res 167	restriction deficient *C. glutamicum* mutant, otherwise considered WT	Tauch et al. (2002)
BSC001	WT, Δ*rodA*	Sieger et al. (2013)
BSC002	WT, DivIVA-mCherry, Δ*rodA*	Sieger et al. (2013)
BSC014	WT, Δ*rodA*, DivIVA-mCherry, carrying plasmid BS018	This study
BSC015	WT, Δ*rodA*, DivIVA-mCherry, carrying plasmid BS055	This study
BSC016	WT, Δ*rodA*, DivIVA-mCherry, carrying plasmid BS056	This study
BSC017	WT, Δ*rodA*, DivIVA-mCherry, carrying plasmid BS053	This study
BSC018	WT, Δ*rodA*, DivIVA-mCherry, carrying plasmid BS054	This study
E. coli		
DH5α	F^- φ80*lac*Z.M15(*lac*ZYA-*arg*F)U169 *rec*A1 *end*A1 *hsd*R17(r_k-, m_k+) *pho*A *sup*E44 *thi*-1 *gyr*A96 *rel*A1 λ^-	Invitrogen
BL21 (DE3)	F^- *ompT gal dcm lon hsd*S_B($r_B{}^-$ $m_B{}^-$) λ(DE3 [*lacI lacUV5*-T7gene1 *ind1 sam7 nin5*])	Invitrogen

MICROSCOPY

Microscopy was performed on a Zeiss Axio Observer Z1 microscope equipped with a Hamamatsu OrcaR^2 camera. A Plan-Apochromat 100x/1.4 Oil Ph3 objective (Zeiss) was used. YFP fluorescence was visualized with filter set 46 HE YFP shift free and CFP fluorescence with filter set 47 HE CFP shift free (Zeiss). Images were acquired with Zen software (Zeiss) or AxioVision 4.6 (Zeiss) and processed with Adobe Photoshop.

FRET

Quantitative FRET values (R_{CY}) were calculated as ratios from emission maxima of eCFP (480 nm) and eYFP (525 nm). FRET measurements were performed in late exponential growing *E. coli* cells after one washing step with 0.9% NaCl. 150 µl of cell suspension were loaded into a 96 well microtiter plate and subsequently measured in a Tecan Infinite M200 Pro plate reader. The excitation wavelength was 435 nm; emission was monitored in a range from 466 to 610 nm in 3 nm increments.

CELL FRACTIONATION

Analysis of protein localization was performed by cell fragmentation and subsequent centrifugation. Cells were lysed in a FastPrep homogenizer (MP) in five rounds at 5 ms^{-1}. Cell debris and aggregated proteins were removed by centrifugation at 14000 × *g* for 20 min and cell membranes were harvested at 90000 × *g* for 30 min. Together with the supernatant, samples were run on SDS PAGE and analyzed by immune-blotting. DivIVA-YFP mutants were blotted with an α-GFP antibody

and visualized using an α-rabbit-alkaline phosphatase secondary antibody.

RESULTS

TRUNCATION MUTANTS OF DivIVA REVEAL DISTINCT DOMAIN FUNCTIONS

Several truncation mutants of DivIVA were heterologously expressed to analyze importance of the individual domains for protein localization and protein–protein interactions. *C. glutamicum* DivIVA is composed of a short N-terminal domain (N) and two coiled-coil domains (CC1 and CC2; **Figure 1B**). The topology and subcellular localization of the mutants are shown in **Figure 1C**. It turned out that CC2 is responsible for proper folding or assembly of DivIVA oligomers, as deletion of 20 AAs (ΔC20) resulted in aggregation of a likely non-functional protein and deletion of 40 AAs (ΔC40) resulted in cytoplasmic appearance. Since CC2 has been reported to play a role in oligomerization in the *B. subtilis* DivIVA (Oliva et al., 2010), this would explain how DivIVA monomers lose their ability to localize to the cell poles. Deletion of the N-terminal domain had only a minor effect, where some cell poles were free of protein, likely due to reduced membrane attachment (**Figure 1D**). 64% of the DivIVA variant ΔN was still membrane associated in contrast to 88% of the wild type protein. Deletion of a middle part of DivIVA (ΔM, AA 144-298) had no effect on DivIVA localization and deletion of CC2 showed the same localization defect as ΔC40. Cell lysate fractionation confirmed the observation that DivIVA-ΔC40 and DivIVA-ΔCC2 fail to localize to the membrane. In these two mutants only 30% (ΔC40)/29% (ΔCC2) of non-aggregated protein remains membrane attached. Full length DivIVA-YFP, ΔC20, and ΔM are 88%/81%/85%, membrane associated (**Figure 1D**).

Data derived from the crystal structure of the *B. subtilis* DivIVA suggested a role for phenylalanine (F17, *B. subtilis* numbering) in membrane-binding. This residue is not conserved in most other species (**Figure 1A**). Members of the class *Actinobacteria* possess a positively charged residue (arginine, lysine) at the corresponding position (K20 in *C. glutamicum* and *M. tuberculosis*). Sequence alignments between various DivIVA sequences reveal that the actinobacterial DivIVA homologs contain sequence insertions compared to other DivIVA sequences and it may be that other hydrophobic AAs such as isoleucine at position 18 (*C. glutamicum* numbering) might fulfill a function analogous to the F17 from *B. subtilis* (**Figure 1A**). To approach this idea, I18 was mutated to an aspartate and a phenylalanine and both mutants were tested for membrane attachment. It turned out that I18D revealed a slight decrease in membrane binding (71%), whereas I18F had a similar membrane affinity compared to WT (89%; **Figure 1D**). Finally, we mutated the lysine residue situated at position 20 in *C. glutamicum* to analyze influence of localization and DivIVA–RodA interaction. The DivIVA variants K20F and K20R localized properly at the poles and septa (**Figure 1C**), suggesting that K20 is not essential for membrane binding.

PROTEIN–PROTEIN INTERACTIONS MEASURED BY FÖRSTER-RESONANCE ENERGY TRANSFER (FRET)

We established a FRET assay which allows visualization of protein–protein interaction in cell cultures after heterologous expression in *E. coli*. The proteins of interest are fused to CFP or YFP, respectively and expressed from plasmid pET-Duet1 (Novagen), which harbors two multiple cloning sites with two individual T7 promoters. **Table 3** shows ratios of emission maxima measured for several strains. Ratios were calculated by dividing emission maxima for CFP (525 nm) and YFP (480 nm), respectively; thereby giving a R_{CY} value that allows to judge about putative protein–protein interactions. We grouped the ratios into steps as indicated in **Table 3**, which illustrate the interaction situation of several proteins analyzed *in vivo*. R_{CY} values below 0.9 reflect a high CFP emission and low YFP emission, as obtained from strains expressing CFP or CFP-tagged proteins alone. A strain expressing soluble CFP and YFP also falls in this R_{CY} range (0.64) and demonstrates the reliability of the assay (Figure S1). Both fluorophores are evenly distributed in the cytosol; however, a FRET signal is not generated even under conditions of extreme overexpression. Values between 0.9 and 1.1 occur when CFP and YFP fluorescent fusions are present in the cell, where some of the fluorescence energy can be transferred from donor to acceptor upon random approximation of the fluorophores. This approximation can be due to topological circumstances, as it is the case for DivIVA and FtsW, a divisome specific RodA homolog. Similar ratios were obtained from other non-interacting examples such as DivIVA with BetP (a betaine carrier) or several RodA and DivIVA mutants (**Table 3**). In addition, a FRET-based ATP-sensor protein expressed from plasmid pRSETB AT1.03 (Imamura et al., 2009) served as a positive control. The ATP-sensor gave a strong FRET signal under physiological ATP levels ($R_{CY} = 1.25$). However, when the pRSETB AT1.03 cells were treated with CCCP to depolarize the membrane and thus reduce the ATP level in the cell, the R_{CY} values are 0.98 and are indicative for a loss of FRET. As another control we tested a previously described interaction partner of DivIVA, wild type ParB, and a non-interacting point mutant, ParBR21A. (Donovan et al., 2012). R_{CY} values were 1.16 for DivIVA–ParB interaction and 0.95 for DivIVA and ParBR21A (Figure S2; **Table 3**). Finally, when only YFP or YFP-tagged proteins were expressed, the emission spectra lack a CFP signal resulting in high R_{CY} values (>1.3).

A POSITIVELY CHARGED AMINO ACID IN THE N-TERMINUS OF DivIVA IS CRUCIAL FOR INTERACTION WITH RodA

We utilized the established FRET assay to map interaction sites between DivIVA and RodA. Therefore, we co-expressed the DivIVA truncation mutants with full length RodA in *E. coli* and evaluated the interaction microscopically (**Figure 2**). Here we show that DivIVAΔC20 is not able to enrich RodA at the poles. DivIVAΔC40 and CC2 both appear cytoplasmic and consequently do not interact with RodA. Interestingly, DivIVAΔN turned out to be unable to enrich RodA to the cell poles (**Figure 2**, forth column), thereby implicating the involvement of the N-terminal domain for RodA interaction. DivIVAΔM showed the same localization and interaction behavior as full length DivIVA (**Figure 2**, fifth column), thus suggesting that the middle domain is not involved in RodA interaction. We further analyzed the N-terminal domain by mutating the lysine residue at position 20 (K20). When we mutated K20 to a phenylalanine, RodA enrichment was completely abolished (**Figure 3**, left column). The FRET ratio of 0.93 is in the range

Table 3 | Classification and apportioning of FRET ratios into subgroups representing the interaction situation of the fusion proteins.

CFP/YFP ratio	Meaning	Examples			Reference
		Donor	Acceptor	Ratio	
<0.9	CFP fluorescence; no FRET	CFP	–	0.55	This study
		ParB-CFP	–	0.57	This study
		ParBR21A-CFP	–	0.57	This study
		RodA-CFP	–	0.60	Sieger et al. (2013)
		FtsW-CFP	–	0.62	Sieger et al. (2013)
		CFP	YFP	0.64	This study
		RodAmutC10-CFP	–	0.67	This study
		BetP-CFP	–	0.68	Sieger et al. (2013)
		RodAS433GS437G-CFP	–	0.68	This study
		RodAΔC10-CFP	–	0.73	This study
		RodAK434G-CFP	–	0.75	This study
		RodAQ435G-CFP	–	0.89	This study
0.9–1.1	Approximation of fluorophores; no enrichment or interaction	RodA-CFP	DivIVAΔC20-YFP	0.92	This study
		RodA-CFP	DivIVAK20F-YFP	0.93	This study
		ParBR21A-CFP	DivIVA-YFP	0.95	This study
		RodA-CFP	DivIVAK20G-YFP	0.96	This study
		RodA-CFP	DivIVAK20I-YFP	0.97	This study
		RodA-CFP	DivIVAΔN-YFP	0.97	This study
		pRSETB AT1.03	+CCCP (1 μg/ml)	0.98	Sieger et al. (2013)
		BetP-CFP	DivIVA-YFP	0.99	Sieger et al. (2013)
		RodAΔC80-CFP	DivIVA-YFP	0.99	This study
		RodAΔC10-CFP	DivIVA-YFP	1.03	This study
		RodAK434G-CFP	DivIVA-YFP	1.04	This study
		RodAQ435G-CFP	DivIVA-YFP	1.04	This study
		RodAS433GS437G-CFP	DivIVA-YFP	1.06	This study
		FtsW-CFP	DivIVA-YFP	1.09	Sieger et al. (2013)
1.1–1.3	Enrichment/interaction	RodAE438G-CFP	DivIVA-YFP	1.10	This study
		RodA-CFP	DivIVAK20R-YFP	1.11	This study
		RodA-CFP	DivIVAI18D-YFP	1.14	This study
		RodA-CFP	DivIVA-YFP	1.15	Sieger et al. (2013)
		ParB-CFP	DivIVA-YFP	1.16	This study
		RodAmutC10-CFP	DivIVA-YFP	1.17	This study
		RodA-CFP	DivIVAΔM-YFP	1.19	This study
		pRSETB AT1.03	- CCCP	1.25	Sieger et al. (2013)
		RodA-CFP	DivIVAI18F-YFP	1.27	This study
>1.3	YFP fluorescence; no FRET	–	YFP	2.55	This study
		–	DivIVA-YFP	4.43	This study
		–	DivIVAΔN-YFP	4.52	This study

of approximation without interaction (**Table 3**). Similar, mutations K20I and K20G abolished interaction of DivIVA with RodA (**Figure 3**, middle columns). To address whether the observed loss of interaction depends on the positive charge, we constructed a conservative replacement, K20R. Interestingly, the co-localization of RodA was restored in the K20R mutant, implicating that a positive charge is necessary for interaction with RodA (**Figure 3**, right column, white arrows; R_{CY} value of 1.11). DivIVA variants I18D

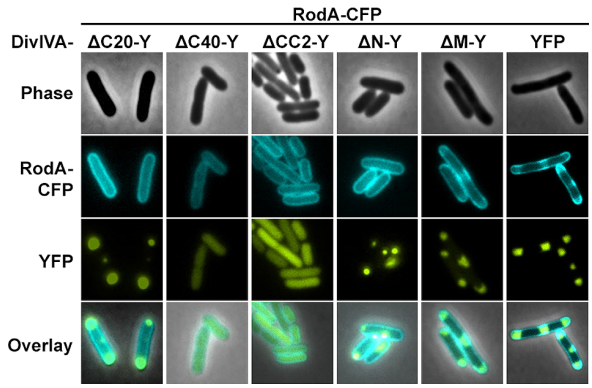

FIGURE 2 | Co-localization studies of DivIVA-YFP mutants with RodA-CFP from *C. glutamicum*. DivIVAΔC20-YFP is likely non-functional and thus cannot recruit RodA to the cell poles (first column). DivIVAΔC40-YFP and DivIVACC2-YFP, which appear cytoplasmic, cannot be interpreted in terms of co-localization with RodA (second and third column). DivIVAΔN-YFP does not to recruit RodA to the cell poles (fourth column), unlike DivIVAΔM-YFP (fifth column), and full length DivIVA-YFP (sixth column).

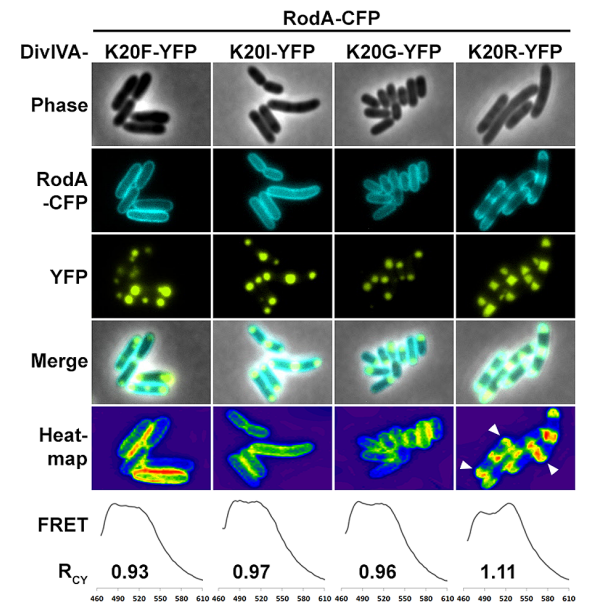

FIGURE 3 | Fluorescence microscopy of RodA-CFP and DivIVA-YFP mutants K20F-YFP, K20I-YFP, K20G-YFP, and K20R-YFP. K20F-YFP as well as K20I-YFP and K20G-YFP are not able to recruit RodA to the cells poles. However, the conservative amino acid replacement K20R-YFP allows for DivIVA–RodA interaction. Heat maps emphasize the co-localization (white arrows). R_{CY} values derived from FRET assays describe the ratio of CFP and YFP fluorescence maxima as an indication for FRET efficiency. The R_{CY}'s for RodA-CFP with non-interacting DivIVA-YFP mutants are 0.93 (K20F), 0.97 (K20I), and 0.96 (K20G). R_{CY} for interaction between RodA-CFP and DivIVAK20R-YFP is 1.11.

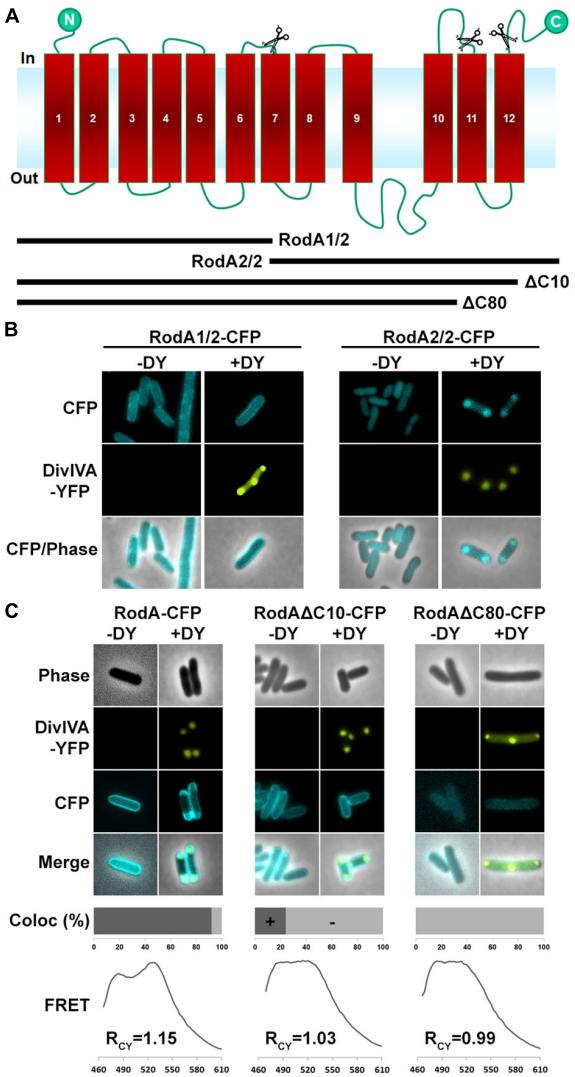

FIGURE 4 | (A) Topology model of RodA according to topology prediction (TMHMM). Scissors indicate truncation sites. The protein possesses 12 transmembrane domains and both ends are at the cytoplasmic site. **(B)** Fluorescence microscopy images of full length DivIVA-YFP and the two truncation mutants RodA1/2-CFP and RodA2/2-CFP. While individually expressed RodA1/2-CFP localizes to the membrane (first column), co-localization with DivIVA-YFP seems to be abolished (second column). RodA2/2-CFP lost completely its membrane localization and appears cytoplasmic (third column); however, when co-expressed with DivIVA, it is co-localized to DivIVA foci (forth column). **(C)** Localization of RodA-CFP, RodAΔC10-CFP, and RodAΔC80-CFP (-DY) and co-localization with DivIVA-YFP (+DY). Full length RodA co-localizes to 95% of all DivIVA foci, RodAΔC10-CFP co-localizes to 20%, and RodAΔC80-CFP does not co-localize with DivIVA-YFP. FRET measurements confirm these observations. R_{CY} values are 1.15 for full length RodA, 1.03 for RodAΔC10-CFP, and 0.99 for RodAΔC80-CFP.

and I18F did not show any alteration in RodA interaction (Figure S3). Both mutants were able to co-localize RodA-CFP, supporting the notion that not all mutations in that region interfere with RodA interaction.

RodA's C-TERMINUS IS INVOLVED IN INTERACTION WITH DivIVA

Next we aimed to identify the RodA interaction site with DivIVA. **Figure 4A** shows a topology model of RodA according to a topology prediction simulation (TMHMM; Arnold et al., 2006). The protein harbors 12 transmembrane domains and both termini

are facing the cytoplasm. To identify the interaction site with DivIVA we first divided the protein into two CFP-tagged halves and expressed them individually and together with DivIVA in *E. coli* (**Figure 4B**). It turned out that the N-terminal part (RodA1/2) localized to the membrane, however, it did not co-localize with DivIVA. The C-terminal part (RodA2/2) appeared cytoplasmic, but co-localized completely with DivIVA, implicating that the interaction site must be in the C-terminal half of the protein, although the truncated protein is apparently not inserted correctly into the membrane. We then made CFP-tagged truncations of 10 and 80 AAs from the C-terminus, ensuring cytoplasmic localization of the fluorophore. Whereas >90% of full length RodA-CFP co-localized with DivIVA foci ($R_{CY} = 1.15$), co-localization of RodAΔC10-CFP was reduced to approximately 20% ($R_{CY} = 1.03$) and completely abolished for RodAΔC80-CFP ($R_{CY} = 0.99$; **Figure 4C**). Apparently, the C-terminal 10 AAs contribute to the RodA–DivIVA interaction. We finally tested several point mutations in the C-terminal domain of RodA. We reasoned that maybe a negatively charged residue might interact with K20 that we identified within DivIVA to be responsible for interaction. In spite of this, the variant RodAE438G did not abolish interaction ($R_{CY} = 1.10$). RodAmut10C-CFP, a strain where all C-terminal 10 AAs of RodA were mutated into 10 AAs with similar residues (K → R, Q → N, A → G, $R_{CY} = 1.17$, **Figure 5**) preserved the interaction. However, point mutants K434G, Q435G, and the double mutant S433G–S437G decreased interaction with DivIVA ($R_{CY} = 1.04$, 1.04, and 1.05), implicating an essential role of these four AAs in DivIVA–RodA interaction (**Figure 5**).

To support the data obtained with the heterologous expression system, we checked subcellular localization and growth complementation of RodA mutants in *C. glutamicum*. Therefore, we applied fluorescence microscopy after homologous expression of the truncation mutants in Δ*rodA* (**Figure 6A**, strains BSC014-16). In addition we used a DivIVA-mCherry background as topological marker for the cell poles and septa. Whereas full length RodA-GFP localized to the cell poles in a DivIVA-dependent manner (yellow arrows; Sieger et al., 2013), RodAΔC10-GFP localized only to some poles and not always co-localized with DivIVA. Instead, most of the RodAΔC10-GFP formed random foci in the cell that did not co-localize with DivIVA (white arrows). These two observations corroborate the situation in *E. coli*, where only 20% of RodA ΔC10 foci co-localized with DivIVA, implicating loss of tight interaction. RodAΔC80-GFP appeared cytoplasmic and co-localization could not be observed, identical to the situation observed in *E. coli*. These observations were confirmed in a growth experiment on BHI-Agar plates (**Figure 6B**). Wild type and the complementation strain Δ*rodA*/RodA-GFP grew normal, whereas Δ*rodA*/RodAΔC10-GFP showed slight growth defects. All other strains (Δ*rodA*, Δ*rodA*/RodAΔC80-GFP, Δ*rodA*/RodA1/2-GFP, Δ*rodA* RodA2/2-GFP) were not able to support growth within 12 h of incubation at 30°C.

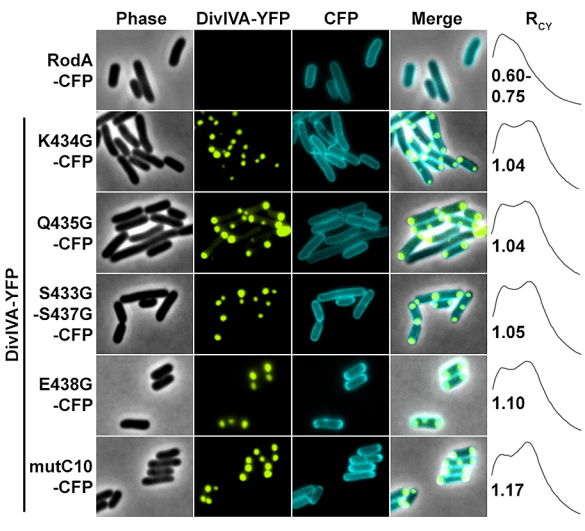

FIGURE 5 | Fluorescence microscopy images and R_{CY} values of RodA-CFP mutants expressed with DivIVA-YFP. When expressed individually all RodA-CFP point mutants showed membrane localization identical to wild type RodA-CFP, as shown exemplarily in the first row. Co-expression and localization with DivIVA-YFP reveals effects of RodA mutants K434G, Q435G and the double mutant S433G/S437G, implicating that these four AAs are essential for interaction with DivIVA (rows 2–4). Point mutant E438G has no effect on co-localization (fifth row), as well as mutant mutC10 where the last 10 AAs are changed to 10 AAs with similar residues (WT sequence: MSKQASEVAA → AVRNGIADGG). These observations are confirmed by R_{CY} measurements. A positive control with full-length proteins can be found in **Figure 2** and (Sieger et al., 2013).

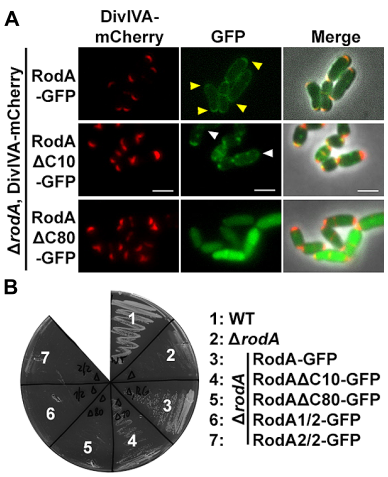

FIGURE 6 | (A) Fluorescence microscopy images of *C. glutamicum* DivIVA-mCherry, Δ*rodA* (BSC002), complemented with full length and truncated versions of RodA-GFP. RodA-GFP localizes DivIVA-like to the cell poles (first row, yellow arrows, strain BSC014). RodAΔC10-GFP forms random foci in the cell and several DivIVA foci are free of RodAΔC10-GFP, implicating reduced interaction (second row, white arrows, strain BSC015). RodAΔC80-GFP appears cytoplasmic, polar foci are not observed (third row, strain BSC016). Fluorescence images were taken at equal exposure times (250 ms for mCherry and 500 ms for GFP). Scale bars: 2 μm. **(B)** Growth experiment of WT, Δ*rodA* and complementation strains on Brain Heart Infusion agar. WT and full length complementation showed normal growth after 12 h at 30°C (Sieger et al., 2013). Complementation with RodAΔC10-GFP (strain BSC015) had a slight growth defect, reflecting the observation of reduced DivIVA interaction. Δ*rodA* (BSC001) as well as complementation strains RodAΔC80-GFP (BCS016), RodA1/2-GFP (BSC017), and RodA2/2-GFP (BSC018) could not develop colonies within 12 h.

DISCUSSION

Spatial and temporal organization is a major task in cell cycle regulation of all living species. Topological determinants like DivIVA are involved in spatial regulation of protein machineries such as the Min system in *B. subtilis* and *Listeria monocytogenes* (Bramkamp et al., 2008; Kaval et al., 2014) or the apical growth machinery in *C. glutamicum* (Letek et al., 2008; Sieger et al., 2013). Until now, it was unclear how the apical growth machinery is positioned in actinobacteria. Earlier studies suggested a link between DivIVA and penicillin-binding proteins (Letek et al., 2008), but recently, we could demonstrate the interaction between DivIVA and RodA in *C. glutamicum* (Sieger et al., 2013). However, the protein domains mediating interactions were not mapped. Here, we now identified the N-terminal domain of DivIVA as interaction partner of the C-terminal tail of RodA. We identified a positively charged residue (K20) in DivIVA to play a crucial role in this interaction. Loss of the positive charge at this position abolishes DivIVA–RodA interaction, while the conservative mutation, K20R, restores protein–protein interaction. The N-terminal domain of DivIVA is considered to be important for membrane-binding. The structure of the *B. subtilis* DivIVA reveals that the N-terminus folds into an intertwined-loop which exposes the hydrophobic residue F17. Mutational analysis shows that F17 is essential for membrane binding of the *B. subtilis* DivIVA. Moreover, the binding is backed by positive charged residues (R18; Oliva et al., 2010). Sequence alignments reveal that the N-terminal domain of DivIVA is highly homologous in most Gram positive bacteria. However, residue F17 from *B. subtilis* DivIVA is not conserved in actinobacteria. *Streptomyces*, *Corynebacterium,* and *Mycobacterium* species rather contain a positively charged residue at the corresponding site (**Figure 1A**). The actinobacterial DivIVA homologs contain sequence insertions and the hydrophobic residue mediating membrane association is thus likely I18 in case of *C. glutamicum.* Although mutation of such to an aspartate did not abolish membrane association compared to WT, localization of I18D in the heterologous host is slightly different compared to wild type (**Figure 1C**). Mutation of I18 to a phenylalanine, whose hydrophobic character is even more distinctive, restored polar localization of DivIVA and revealed wild type like membrane association. While membrane binding for the *B. subtilis* DivIVA has been studied in great detail, we know less about membrane binding properties of the actinobacterial proteins. Subcellular localization of *C. glutamicum* DivIVA shows some obvious differences compared to its *B. subtilis* homolog. While the *B. subtilis* DivIVA localizes tightly underneath the polar membrane (Edwards and Errington, 1997), forming a crescent-like structure lining the pole, the *C. glutamicum* protein localizes to the cell poles, but reaches into the cytoplasm (Letek et al., 2009; Donovan et al., 2012), forming a large complex, similar to the PopZ protein found in *C. crescentus* (Laloux and Jacobs-Wagner, 2013). It is therefore likely that membrane binding mechanisms are different in *B. subtilis* and *C. glutamicum* DivIVA proteins. Support to this notion comes from localization studies using truncated DivIVA (DivIVAΔN), lacking the N-terminal domain. Although, DivIVAΔN is significantly more soluble compared to the full length protein, about 64% of the protein is still membrane associated. Despite its role in membrane interaction, the N-terminal domain of DivIVA is essential for interaction with RodA. The positive charge at residue K20 is required for interaction. It is plausible that the exposed, N-terminal loop of DivIVA is required for interaction with a membrane integral protein such as RodA. A central domain of DivIVA has been shown earlier to promote interaction with the origin-binding protein ParB (Donovan et al., 2012), indicating the modular character of DivIVA which encompasses various domains to mediate protein–protein interaction to various partner proteins.

RodA is an integral membrane protein with 12 predicted transmembrane helices. This topology gives rise to several putative binding-sites that could mediate DivIVA binding. A first, rough truncation study where we expressed RodA in two halves indicated that the DivIVA interaction site is likely situated in the C-terminal part of RodA. Further truncation analysis revealed that the last 10 AAs, forming the C-terminal domain facing the cytoplasm are contributing to the RodA–DivIVA interaction. RodAΔC10 has a drastically reduced FRET interaction with DivIVA; however, expression of RodAΔC10 in *C. glutamicum* to some extent complements growth in a Δ*rodA* strain background. Only truncation of the last 80 AAs from the C-terminus completely abolishes localization and interaction with DivIVA. A similar situation has been reported for FtsW, a RodA homolog that is involved in cell division. FtsW interacts via its C-terminal end with FtsZ during cytokinesis of *M. tuberculosis* (Datta et al., 2002). We were able to pinpoint amino acid residues responsible for RodA–DivIVA interaction in RodA (K434G, Q435G, and the double mutant S433G–S437G), suggesting that the RodA C-terminal domain forms an interaction domain which is built by several amino acid residues.

In earlier work we have been showing that ParB interacts with DivIVA in *C. glutamicum.* We have mapped the interaction sites and identified a central region in DivIVA (AAs 144-229) as interaction site with ParB (Donovan et al., 2012). Thus, DivIVA exhibits several exclusive interaction domains allowing DivIVA to act as interaction hub for the connection of apical cell growth and chromosome orientation. The N-terminal region of *B. subtilis* DivIVA interacts with MinJ, a multispan transmembrane protein involved in cytokinesis and division site selection (van Baarle et al., 2013). Thus, DivIVA proteins have evolved to contain interaction motifs for several protein–protein interactions. In actinobacteria DivIVA proteins are essential, likely because they are involved in the spatio-temporal control of two essential cellular processes, cell elongation, and chromosome segregation. Consistent with the fundamental role of DivIVA in these bacteria, actinobacterial DivIVA proteins are larger, containing sequence insertions, when compared to their firmicute counterparts. Future analysis might focus on the regulation of the various protein–protein interactions. DivIVA has been identified as substrate of several protein kinases. Examples of DivIVA phosphorylation have been reported for *M. tuberculosis* (Kang et al., 2005), *Streptomyces coelicolor* (Hempel et al., 2012), and *Streptococcus pneumoniae* (Beilharz et al., 2012). Thereby, phosphorylation of DivIVA has major implications in cell growth or division (Fleurie et al., 2012). It is likely possible that a similar regulatory mechanisms determines chromosome segregation and cell elongation in *C. glutamicum.*

ACKNOWLEDGMENTS

The authors acknowledge financial support from the Deutsche Forschungsgemeinschaft (BR2915/6-1) and the Federal ministry of Education and Research (BMBF, 031A302B). We thank Karin Schubert for critical comments on the manuscript.

SUPPLEMENTARY MATERIAL

The Supplementary Material for this article can be found online at: http://www.frontiersin.org/journal/10.3389/fmicb.2014.00738/abstract

REFERENCES

Arnold, K., Bordoli, L., Kopp, J., and Schwede, T. (2006). The SWISS-MODEL workspace: a web-based environment for protein structure homology modelling. *Bioinformatics* 22, 195–201. doi: 10.1093/bioinformatics/bti770

Barh, D., Jain, N., Tiwari, S., Parida, B. P., D'afonseca, V., Li, L., et al. (2011). A novel comparative genomics analysis for common drug and vaccine targets in *Corynebacterium pseudotuberculosis* and other CMN Group of human pathogens. *Chem. Biol. Drug Des.* 78, 73–84. doi: 10.1111/j.1747-0285.2011.01118.x

Beilharz, K., Nováková, L., Fadda, D., Branny, P., Massidda, O., and Veening, J.-W. (2012). Control of cell division in *Streptococcus pneumoniae* by the conserved Ser/Thr protein kinase StkP. *Proc. Natl. Acad. Sci. U.S.A.* 109, E905–E913. doi: 10.1073/pnas.1119172109

Ben-Yehuda, S., Rudner, D. Z., and Losick, R. (2003). RacA, a bacterial protein that anchors chromosomes to the cell poles. *Science* 299, 532–536. doi: 10.1126/science.1079914

Bramkamp, M., Emmins, R., Weston, L., Donovan, C., Daniel, R. A., and Errington, J. (2008). A novel component of the division-site selection system of *Bacillus subtilis* and a new mode of action for the division inhibitor MinCD. *Mol. Microbiol.* 70, 1556–1569. doi: 10.1111/j.1365-2958.2008.06501.x

Briley, K. Jr., Prepiak, P., Dias, M. J., Hahn, J., and Dubnau, D. (2011). Maf acts downstream of ComGA to arrest cell division in competent cells of *B. subtilis*. *Mol. Microbiol.* 81, 23–39. doi: 10.1111/j.1365-2958.2011.07695.x

Brown, P. J. B., Kysela, D. T., and Brun, Y. V. (2011). Polarity and the diversity of growth mechanisms in bacteria. *Semin. Cell Dev. Biol.* 22, 790–798. doi: 10.1016/j.semcdb.2011.06.006

Cayabyab, M. J., Macovei, L., and Campos-Neto, A. (2012). Current and novel approaches to vaccine development against tuberculosis. *Front. Cell Infect. Microbiol.* 2:154. doi: 10.3389/fcimb.2012.00154

Cowling, P., and Hall, L. (1993). *Corynebacterium striatum*: a clinically significant isolate from sputum in chronic obstructive airways disease. *J. Infect.* 26, 335–336. doi: 10.1016/0163-4453(93)95823-2

Datta, P., Dasgupta, A., Bhakta, S., and Basu, J. (2002). Interaction between FtsZ and FtsW of *Mycobacterium tuberculosis*. *J. Biol. Chem.* 277, 24983–24987. doi: 10.1074/jbc.M203847200

Donovan, C., and Bramkamp, M. (2014). Cell division in Corynebacterineae. *Front. Microbiol.* 5:132. doi: 10.3389/fmicb.2014.00132

Donovan, C., Sieger, B., Krämer, R., and Bramkamp, M. (2012). A synthetic *Escherichia coli* system identifies a conserved origin tethering factor in Actinobacteria. *Mol. Microbiol.* 84, 105–116. doi: 10.1111/j.1365-2958.2012.08011.x

dos Santos, V. T., Bisson-Filho, A. W., and Gueiros-Filho, F. J. (2012). DivIVA-mediated polar localization of ComN, a posttranscriptional regulator of *Bacillus subtilis*. *J. Bacteriol.* 194, 3661–3669. doi: 10.1128/JB.05879-11

Edwards, D. H., and Errington, J. (1997). The *Bacillus subtilis* DivIVA protein targets to the division septum and controls the site specificity of cell division. *Mol. Microbiol.* 24, 905–915. doi: 10.1046/j.1365-2958.1997.3811764.x

Eikmanns, B. J., Kleinertz, E., Liebl, W., and Sahm, H. (1991). A family of *Corynebacterium glutamicum*/*Escherichia coli* shuttle vectors for cloning, controlled gene expression, and promoter probing. *Gene* 102, 93–98. doi: 10.1016/0378-1119(91)90545-M

Eswaramoorthy, P., Winter, P. W., Wawrzusin, P., York, A. G., Shroff, H., and Ramamurthi, K. S. (2014). Asymmetric division and differential gene expression during a bacterial developmental program requires DivIVA. *PLoS Genet.* 10:e1004526. doi: 10.1371/journal.pgen.1004526

Fleurie, A., Cluzel, C., Guiral, S., Freton, C., Galisson, F., Zanella-Cleon, I., et al. (2012). Mutational dissection of the S/T-kinase StkP reveals crucial roles in cell division of *Streptococcus pneumoniae*. *Mol. Microbiol.* 83, 746–758. doi: 10.1111/j.1365-2958.2011.07962.x

Hempel, A. M., Cantlay, S., Molle, V., Wang, S.-B., Naldrett, M. J., Parker, J. L., et al. (2012). The Ser/Thr protein kinase AfsK regulates polar growth and hyphal branching in the filamentous bacteria *Streptomyces*. *Proc. Natl. Acad. Sci. U.S.A.* 109, E2371–E2379. doi: 10.1073/pnas.1207409109

Henriques, A. O., Glaser, P., Piggot, P. J., and Moran, C. P. Jr. (1998). Control of cell shape and elongation by the rodA gene in *Bacillus subtilis*. *Mol. Microbiol.* 28, 235–247. doi: 10.1046/j.1365-2958.1998.00766.x

Ikeda, M., and Nakagawa, S. (2003). The *Corynebacterium glutamicum* genome: features and impacts on biotechnological processes. *Appl. Microbiol. Biotechnol.* 62, 99–109. doi: 10.1007/s00253-003-1328-1

Imamura, H., Nhat, K. P., Togawa, H., Saito, K., Iino, R., Kato-Yamada, Y., et al. (2009). Visualization of ATP levels inside single living cells with fluorescence resonance energy transfer-based genetically encoded indicators. *Proc. Natl. Acad. Sci. U.S.A.* 106, 15651–15656. doi: 10.1073/pnas.0904764106

Jones, L. J. F., Carballido-López, R., and Errington, J. (2001). Control of cell shape in bacteria: helical, actin-like filaments in *Bacillus subtilis*. *Cell* 104, 913–922. doi: 10.1016/S0092-8674(01)00287-2

Kang, C. M., Abbott, D. W., Park, S. T., Dascher, C. C., Cantley, L. C., and Husson, R. N. (2005). The *Mycobacterium tuberculosis* serine/threonine kinases PknA and PknB: substrate identification and regulation of cell shape. *Genes Dev.* 19, 1692–1704. doi: 10.1101/gad.1311105

Kaval, K. G., Rismondo, J., and Halbedel, S. (2014). A function of DivIVA in *Listeria monocytogenes* division site selection. *Mol. Microbiol.* 94, 637–654. doi: 10.1111/mmi.12784

Kruse, T., Bork-Jensen, J., and Gerdes, K. (2005). The morphogenetic MreBCD proteins of *Escherichia coli* form an essential membrane-bound complex. *Mol. Microbiol.* 55, 78–89. doi: 10.1111/j.1365-2958.2004.04367.x

Laloux, G., and Jacobs-Wagner, C. (2013). Spatiotemporal control of PopZ localization through cell cycle-coupled multimerization. *J. Cell Biol.* 201, 827–841. doi: 10.1083/jcb.201303036

Laloux, G., and Jacobs-Wagner, C. (2014). How do bacteria localize proteins to the cell pole? *J. Cell Sci.* 127, 11–19. doi: 10.1242/jcs.138628

Lenarcic, R., Halbedel, S., Visser, L., Shaw, M., Wu, L. J., Errington, J., et al. (2009). Localisation of DivIVA by targeting to negatively curved membranes. *EMBO J.* 28, 2272–2282. doi: 10.1038/emboj.2009.129

Letek, M., Fiuza, M., Ordonez, E., Villadangos, A. F., Flardh, K., Mateos, L. M., et al. (2009). DivIVA uses an N-terminal conserved region and two coiled-coil domains to localize and sustain the polar growth in *Corynebacterium glutamicum*. *FEMS Microbiol. Lett.* 297, 110–116. doi: 10.1111/j.1574-6968.2009.01679.x

Letek, M., Ordonez, E., Vaquera, J., Margolin, W., Flardh, K., Mateos, L. M., et al. (2008). DivIVA is required for polar growth in the MreB-lacking rod-shaped actinomycete *Corynebacterium glutamicum*. *J. Bacteriol.* 190, 3283–3292. doi: 10.1128/JB.01934-07

Lin, L., and Thanbichler, M. (2013). Nucleotide-independent cytoskeletal scaffolds in bacteria. *Cytoskeleton* 70, 409–423. doi: 10.1002/cm.21126

Locci, R., and Schaal, K. P. (1980). Apical growth in facultative anaerobic actinomycetes as determined by immunofluorescent labeling. *Zentralbl. Bakteriol. A.* 246, 112–118. doi: 10.1016/S0172-5599(80)80102-7

Mohammadi, T., Van Dam, V., Sijbrandi, R., Vernet, T., Zapun, A., Bouhss, A., et al. (2011). Identification of FtsW as a transporter of lipid-linked cell wall precursors across the membrane. *EMBO J.* 30, 1425–1432. doi: 10.1038/emboj.2011.61

Muchova, K., Kutejova, E., Scott, D. J., Brannigan, J. A., Lewis, R. J., Wilkinson, A. J., et al. (2002). Oligomerization of the *Bacillus subtilis* division protein DivIVA. *Microbiology* 148, 807–813.

Noirclerc-Savoye, M., Morlot, C., Gerard, P., Vernet, T., and Zapun, A. (2003). Expression and purification of FtsW and RodA from *Streptococcus pneumoniae*, two membrane proteins involved in cell division and cell growth, respectively. *Protein Expr. Purif.* 30, 18–25. doi: 10.1016/S1046-5928(03)00051-2

Oliva, M. A., Halbedel, S., Freund, S. M., Dutow, P., Leonard, T. A., Veprintsev, D. B., et al. (2010). Features critical for membrane binding revealed by DivIVA crystal structure. *EMBO J.* 29, 1988–2001. doi: 10.1038/emboj.2010.99

Pastoret, S., Fraipont, C., Den Blaauwen, T., Wolf, B., Aarsman, M. E. G., Piette, A., et al. (2004). Functional analysis of the cell division protein FtsW of *Escherichia coli*. *J. Bacteriol.* 186, 8370–8379. doi: 10.1128/jb.186.24.8370-8379.2004

Patrick, J. E., and Kearns, D. B. (2008). MinJ (YvjD) is a topological determinant of cell division in *Bacillus subtilis*. *Mol. Microbiol.* 70, 1166–1179. doi: 10.1111/j.1365-2958.2008.06469.x

Popham, D. L., and Young, K. D. (2003). Role of penicillin-binding proteins in bacterial cell morphogenesis. *Curr. Opin. Microbiol.* 6, 594–599. doi: 10.1016/j.mib.2003.10.002

Real, G., Fay, A., Eldar, A., Pinto, S. M., Henriques, A. O., and Dworkin, J. (2008). Determinants for the subcellular localization and function of a nonessential SEDS protein. *J. Bacteriol.* 190, 363–376. doi: 10.1128/jb.01482-07

Sham, L. T., Butler, E. K., Lebar, M. D., Kahne, D., Bernhardt, T. G., and Ruiz, N. (2014). Bacterial cell wall. MurJ is the flippase of lipid-linked precursors for peptidoglycan biogenesis. *Science* 345, 220–222. doi: 10.1126/science.1254522

Sieger, B., Schubert, K., Donovan, C., and Bramkamp, M. (2013). The lipid II flippase RodA determines morphology and growth in *Corynebacterium glutamicum*. *Mol. Microbiol.* 90, 966–982. doi: 10.1111/mmi.12411

Stahlberg, H., Kutejova, E., Muchova, K., Gregorini, M., Lustig, A., Muller, S. A., et al. (2004). Oligomeric structure of the *Bacillus subtilis* cell division protein DivIVA determined by transmission electron microscopy. *Mol. Microbiol.* 52, 1281–1290. doi: 10.1111/j.1365-2958.2004.04074.x

Tauch, A., Kirchner, O., Loffler, B., Gotker, S., Puhler, A., and Kalinowski, J. (2002). Efficient electrotransformation of *Corynebacterium diphtheriae* with a mini-replicon derived from the *Corynebacterium glutamicum* plasmid pGA1. *Curr. Microbiol.* 45, 362–367. doi: 10.1007/s00284-002-3728-3

van Baarle, S., Celik, I. N., Kaval, K. G., Bramkamp, M., Hamoen, L. W., and Halbedel, S. (2013). Protein–protein interaction domains of *Bacillus subtilis* DivIVA. *J. Bacteriol.* 195, 1012–1021. doi: 10.1128/JB.02171-12

Wu, L. J., and Errington, J. (2003). RacA and the Soj-Spo0J system combine to effect polar chromosome segregation in sporulating *Bacillus subtilis*. *Mol. Microbiol.* 49, 1463–1475. doi: 10.1046/j.1365-2958.2003.03643.x

Zeeuwen, P. L., Kleerebezem, M., Timmerman, H. M., and Schalkwijk, J. (2013). Microbiome and skin diseases. *Curr. Opin. Allergy Clin. Immunol.* 13, 514–520. doi: 10.1097/ACI.0b013e328364ebeb

Conflict of Interest Statement: The authors declare that the research was conducted in the absence of any commercial or financial relationships that could be construed as a potential conflict of interest.

Received: 15 October 2014; accepted: 05 December 2014; published online: 07 January 2015.

Citation: Sieger B and Bramkamp M (2015) Interaction sites of DivIVA and RodA from Corynebacterium glutamicum. Front. Microbiol. ***5****:738. doi: 10.3389/fmicb.2014.00738*

This article was submitted to Microbial Physiology and Metabolism, a section of the journal Frontiers in Microbiology.

Copyright © 2015 Sieger and Bramkamp. This is an open-access article distributed under the terms of the Creative Commons Attribution License (CC BY). The use, distribution or reproduction in other forums is permitted, provided the original author(s) or licensor are credited and that the original publication in this journal is cited, in accordance with accepted academic practice. No use, distribution or reproduction is permitted which does not comply with these terms.

frontiers in Microbiology

ORIGINAL RESEARCH
published: 17 June 2015
doi: 10.3389/fmicb.2015.00607

Multi-color imaging of the bacterial nucleoid and division proteins with blue, orange, and near-infrared fluorescent proteins

*Fabai Wu, Erwin Van Rijn, Bas G. C. Van Schie, Juan E. Keymer† and Cees Dekker**

Department of Bionanoscience, Kavli Institute of Nanoscience, Delft University of Technology, Delft, Netherlands

OPEN ACCESS

Edited by:
Conrad L. Woldringh, University of Amsterdam, Netherlands

Reviewed by:
Joe Lutkenhaus, University of Kansas Medical Center, USA
Yu-Ling Shih, Institute of Biological Chemistry – Academia Sinica, Taiwan

***Correspondence:**
Cees Dekker, Department of Bionanoscience, Kavli Institute of Nanoscience, Delft University of Technology, Lorentzweg 1, 2628CJ Delft, Netherlands
c.dekker@tudelft.nl

†Present address:
Juan E. Keymer, Institute of Ecology and Biodiversity and Department of Ecology, School of Biological Sciences, Pontifical Catholic University, Santiago, Chile

Specialty section:
This article was submitted to Microbial Physiology and Metabolism, a section of the journal Frontiers in Microbiology

Received: *30 March 2015*
Accepted: *02 June 2015*
Published: *17 June 2015*

Citation:
Wu F, Van Rijn E, Van Schie BGC, Keymer JE and Dekker C (2015) Multi-color imaging of the bacterial nucleoid and division proteins with blue, orange, and near-infrared fluorescent proteins. Front. Microbiol. 6:607. doi: 10.3389/fmicb.2015.00607

Studies of the spatiotemporal protein dynamics within live bacterial cells impose a strong demand for multi-color imaging. Despite the increasingly large collection of fluorescent protein (FP) variants engineered to date, only a few of these were successfully applied in bacteria. Here, we explore the performance of recently engineered variants with the blue (TagBFP), orange (TagRFP-T, mKO2), and far-red (mKate2) spectral colors by tagging HU, LacI, MinD, and FtsZ for visualizing the nucleoid and the cell division process. We find that, these FPs outperformed previous versions in terms of brightness and photostability at their respective spectral range, both when expressed as cytosolic label and when fused to native proteins. As this indicates that their folding is sufficiently fast, these proteins thus successfully expand the applicable spectra for multi-color imaging in bacteria. A near-infrared protein (eqFP670) is found to be the most red-shifted protein applicable to bacteria so far, with brightness and photostability that are advantageous for cell-body imaging, such as in microfluidic devices. Despite the multiple advantages, we also report the alarming observation that TagBFP directly interacts with TagRFP-T, causing interference of localization patterns between their fusion proteins. Our application of diverse FPs for endogenous tagging provides guidelines for future engineering of fluorescent fusions in bacteria, specifically: (1) The performance of newly developed FPs should be quantified *in vivo* for their introduction into bacteria; (2) spectral crosstalk and inter-variant interactions between FPs should be carefully examined for multi-color imaging; and (3) successful genomic fusion to the 5′-end of a gene strongly depends on the translational read-through of the inserted coding sequence.

Keywords: fluorescent proteins, bacterial cell division, bacterial chromosome, MinD, HU, FtsZ, TagRFP-T, TagBFP

Introduction

The use of fluorescent proteins (FPs) has greatly advanced our understanding of the subcellular architecture of bacteria. Soon after the first cloning of the green fluorescence protein (*gfp*) gene from *Aequorea victoria* (Prasher et al., 1992) and its first application as fluorescence marker *in vivo* (Chalfie et al., 1994), it was successfully adopted to visualize essential proteins involved in cell division and division-site selection in bacteria, such as FtsZ/FtsA (Ma et al., 1996) and MinE/MinD/MinC (Raskin and de Boer, 1997, 1999; Hu and Lutkenhaus, 1999). The results from these studies planted the significant notion that the intracellular environment of bacteria is not

only structured, but also extremely dynamic. Other hallmarks include cytoskeletal filaments responsible for cell shape maintenance (Jones et al., 2001; Ausmees et al., 2003; Domínguez-Escobar et al., 2011; Garner et al., 2011; van Teeffelen et al., 2011), and polarly localized proteins involved in chemotaxis, virulence and metabolism (Sourjik and Berg, 2000; Charles et al., 2001; Lindner et al., 2008; Li and Young, 2012). Recently, several large fluorescent-fusion libraries have been constructed for *Escherichia coli* and *Caulobacter crescentus*, allowing genome-scale, quantitative studies of protein localization, which is especially powerful when accompanied by the development of a quantitative analysis toolbox (Kitagawa et al., 2006; Werner et al., 2009; Taniguchi et al., 2010; Kuwada et al., 2015).

Two decades of efforts have expanded the spectrum of FPs to a full range, showing strong promise for multi-color imaging. However, the application of many FPs for live cell imaging of bacteria have been hindered by various factors. Most prominently, the fast synthesis and degradation of protein in bacteria (in contrast to eukaryotes) demands fast-folding of FPs. This is clearly indicated by the fact that mutations improving the folding properties of EGFP generation (which resulted in SBFP2, SCPF3A, SGFP2, and SYFP2), enhanced their effective brightness by several folds in bacteria, while this was much less the case when expressed in mammalian cells (Kremers et al., 2006, 2007). Also, the orange FPs mOrange and mKO were not visible in live *E. coli* due to slow maturation, with the latter only visible after an overnight incubation after fixation (Alexeeva et al., 2010). The fast-folding properties of some FPs such as Venus, mCherry, and sfGFP have shown advantages for functional fusions (Osawa and Erickson, 2005; Bendezú et al., 2009; Dinh and Bernhardt, 2011), and have been broadly used. On the other hand, these fast-folding FPs do not always provide the native protein localization patterns (Landgraf et al., 2012). Furthermore, the degree of oligomerization, the brightness, the photostability, as well as the spectral separation between FPs are properties no less essential for successful capture of native events at the demanded spatial and temporal resolution. However, thus far, these factors have been barely quantified in live bacteria.

Here, we set out to expand the spectrum of FPs for live cell imaging in *E. coli* by labeling the cytosol, the nucleoid, as well as the division proteins. HU-2, encoded by *hupA* gene, is a subunit of nucleoid-associated proteins HU, which serves as a marker for the nucleoid that was previously shown to colocalize with DAPI when fused to GFP (Wery et al., 2001). Fluorescently labeled LacI has been used as an operator-repressor system to label specific genomic loci by targeting repeated *lacO* sequences (Lau et al., 2003). Combining the HU-2 and LacI labels allows us to localize a genomic locus in the context of the global nucleoid structure. For imaging division, we focus on FtsZ proteins, which polymerize to initiate a cytokinetic ring, and whose localization is regulated by the nucleoid and MinCDE proteins (Ma et al., 1996; Hu and Lutkenhaus, 1999; Raskin and de Boer, 1999; Bailey et al., 2014; Du and Lutkenhaus, 2014). To visualize the latter, we constructed a fusion gene at the endogenous *minD* locus for expressing sfGFP-MinD proteins, which oscillate between the two cell halves of the rod-shape *E. coli* and form a time-averaged concentration gradient that have a maxima at the cell poles and minimum at the mid-cell (Raskin and de Boer, 1999).

Expanding from the FPs derived from jellyfish *A. victoria*, we examine the performances of the monomeric FPs at the blue (TagBFP), orange (TagRFP-T and mKO2), far red (mKate2), and near-infrared (dimeric eqFP670) spectral colors. All FPs used in this study are listed in **Table 1**. The latter proteins are derivatives of the FPs from the sea anemone *Entacmaea quadricolor* and *Fungia concinna*, known for their brightness, photostability, and relatively fast maturation (Shaner et al., 2008; Subach et al., 2008; Shcherbo et al., 2009, 2010; Sun et al., 2009; Morozova et al., 2010). By quantitatively comparing the brightness, photostability, and spectral properties of these proteins to other proteins with

TABLE 1 | Properties of the fluorescent proteins (FPs) used in this study.

FP*	λ_{ex} (nm)	λ_{em} (nm)	QY	EC	Brightness	Oligomerization	Reference	Codon
EBFP2	383	448	0.56	32000	18	Monomer	Ai et al. (2007)	n.a.
SBFP2	383	448	0.47	34000	16	Monomer	Kremers et al. (2007)	n.a.
TagBFP	402	457	0.63	52000	32.8	Monomer	Subach et al. (2008)	Mammal
mCerulean	433	475	0.62	43000	26.7	Monomer	Rizzo et al. (2004)	n.a.
TagCFP	458	480	0.57	37000	21	Monomer	Evrogen	Mammal
TagGFP2	483	506	0.6	56500	33.9	Monomer	Evrogen	Mammal
sfGFP	485	510	0.65	83300	54.1	Monomer	Pedelacq et al. (2006)	Bacteria
TagYFP	508	524	0.62	50000	31	Monomer	Evrogen	Mammal
mYPet	517	530	0.77	104000	80.1	Monomer	Nguyen and Daugherty (2005)	n.a.
mKO2	551	565	0.62	63800	39.6	Monomer	Lee et al. (2013)	Yeast
TagRFP-T	555	584	0.41	81000	33.2	Monomer	Shaner et al. (2008)	Mammal
mCherry	587	610	0.22	72000	15.8	Monomer	Shaner et al. (2004)	n.a.
mKate2	588	633	0.4	62500	25	Monomer	Shcherbo et al. (2009)	Mammal
eqFP670	605	670	0.06	15700	0.9	Dimer	Shcherbo et al. (2010)	Mammal
TagRFP657	611	657	0.1	34000	3.4	Monomer	Morozova et al. (2010)	Bacteria

**The properties are: $\lambda_{ex}/\lambda_{em}$, wavelengths for excitation/emission maxima; QE, quantum yield; EC, extinction coefficient; brightness are calculated from QE and EC; reported oligomerization property; and codon usage for the versions used in this study.*

the same spectral colors, we find that these proteins function well as cytosolic labels and/or C-terminal tags, and that they provide strong advantages in brightness, photostability, and spectral separation compared to other FPs that are currently in use for bacteria. Furthermore, our approach to tag the *minD* gene at its endogenous locus revealed a detrimental effect of the coding sequence on N-terminal fusions. Finally, we combined these FP tags in bacterial strains to assess their suitability for multi-color imaging. Together, Our data provide guidelines for an optimal strategy in choosing new FPs for multi-color imaging in bacteria.

Materials and Methods

Plasmid and Strain Construction

The plasmids were constructed using Gateway cloning kit (Invitrogen, catalog # 11789013, 11791019) and Infusion EcoDry kits (Clonetech, catalog # 638912), Coding sequences of *tagYFP*, *tagGFP2*, *tagRFP-T*, *ebfp2*, *tagBFP*, *hupA*, *minDE*, and *aph frt* were respectively amplified from the pTagYFP-C1, pTagGFP2-C1, pTagRFP-T, pBAD-EBFP, pTagBFP-C1, W3110 genome, W3110 genome, and pKD13, and inserted into the Gateway entry vectors through BP reactions as described in the Gateway protocol. These and previously described entry vectors in Wu et al. (2015) were then combined through Gateway LR reaction to produce destination vectors pERB006, pFWB007, pBVS32, pFWB009, pBVS36, and pBVS37. For constructing pFWM006, we amplified the backbone of pBVS3 with P_{lac} and *aph*, the *hupA* fragment from pFWB006, and the *mKO2* fragment from pyomKO2, and combined these into one plasmid through a three-fragments Infusion reaction. For construction of pFWM007, we amplified the backbone of pBVS3 with *Plac* and *aph*, the *hupA* fragment from pFWB006, and the *sBFP2* fragment from pSBFP2-C1, and combined these into one plasmid through a three-fragment Infusion reaction. Plasmid pFWZ7 was constructed through an ligation reaction (Infusion kit) with four PCR-amplified fragments, which were the backbone of pFB174 with arabinose promoter and chloramphenicol resistance gene, an *ftsZ* (5′ sequence, 1–999 bp) fragment with an 18 base overhang coding the flexible linker GSGSGS, a GGSGSS flexible linker plus *ftsZ* (3′ sequence, 991–1052 bp) plus *aph frt* sequence amplified from strain FW1370, two synthesized oligos containing the tetracysteine (TC) peptide coding sequence and the two flanking flexible linkers. The TC coding sequence was then replaced by *tagRFP-T*, *sfGFP*, and *tagCFP* to produce plasmid pFWZ4, pFWZ5, and pFWZ6 through two-fragment Infusion reactions. pFWZ0 was constructed through Gibson assembly of pFB174 backbone and the *ftsZ::aph frt* sequence amplified from strain FW1370. All plasmids are listed in **Table 2**.

The genomic insertions were constructed using λ Red recombination (Datsenko and Wanner, 2000) and shuffled between strains using P1 transduction as described previously (Wu et al., 2015). The PCR fragments from plasmids pERB006, pFWM007, pFWB006, pBVS32, pFW009, pFWM006, pBVS3, and pBVS4 were electroporated into the electro-competent cells of W3110 containing pKD46, to result in strains FW1722,

TABLE 2 | Plasmids used in this study.

Plasmids	Descriptions	Reference
pKD13	*aph frt* (Amp^R)	Datsenko and Wanner (2000)
pKD46	P_{ara}*::gam bet exo* (Amp^R)	Datsenko and Wanner (2000)
pCP20	*Pr-flp* (Amp^R Cm^R)	Datsenko and Wanner (2000)
pDonR P4-P1R	Gateway plasmid entry 1	Invitrogen
pDonR 211	Gateway plasmid entry 2	Invitrogen
pDonR P2R-P3	Gateway plasmid entry 3	Invitrogen
pDEST R4-R3	Gateway destination vector	Invitrogen
pTagBFP-C1	P_{cmv}*::TagBFP* (Kan^R)	Evrogen
pTagCFP-C1	P_{cmv}*::TagCFP* (Kan^R)	Evrogen
pTagYFP-C1	P_{cmv}*::TagYFP* (Kan^R)	Evrogen
pTagGFP2-C1	P_{cmv}*::TagGFP2* (Kan^R)	Evrogen
pmKate2-C1	P_{cmv}*::mKate2* (Kan^R)	Evrogen
pTagRFP-T	P_{T7}*::tagRFP-T* (Amp^R)	Shaner et al. (2008)
pNirFP-N1	P_{cmv}*::eqFP670* (Kan^R)	Evrogen
pBAD-EBFP2	P_{ara}*::ebfp2-6xhis* (Amp^R)	Addgene, Michael Davidson
pSBFP2-C1	P_{cmv}*::sbfp2* (Amp^R)	Kremers et al. (2007)
pyomKO2	*pFA6a-link-yomKO2* (Kan^R)	Lee et al. (2013)
pFX40	P_{lac}*::yfp-minD minE* (Amp^R)	Shih et al. (2002)
pKD3ftsQAZ	*PftsQAZ* (Amp^R)	Dai and Lutkenhaus (1991)
pFB174	P_{ara}*::mreBCD* (Cm^R)	Bendezú and de Boer (2008)
pBVS3	P_{lac}*::yfp-minD minE::aph frt* (Kan^R, Amp^R)	Wu et al. (2015)
pBVS4	P_{lac}*::sfgfp-minD minE::aph frt* (Kan^R, Amp^R)	Wu et al. (2015)
pERA001	Gateway destination vector with P_{rha} (Tet^R)	This work
pERB006	*pERA001::hupA-ebfp2::aph frt* (Kan^R, Amp^R)	This work
pFWM007	P_{lac}*::hupA-sbfp2::aph frt* (Kan^R, Amp^R)	This work
pFWB006	*pDEST::hupA-tagBFP::aph frt* (Kan^R, Amp^R)	This work
pBVS32	*pDEST::leuB'-Pj23100::tagRFP-T::aph frt-leuB"* (Kan^R, Amp^R)	This work
pEcTagRFP657	*E. coli codon-optimized TagRFP657 gene*	This work
pERB004	*pERA001::leuB'-Pj23100::tagRFP657::aph frt-leuB"* (Kan^R, Tet^R)	This work
pERB005	*pERA001::Pt7::tagRFP657::aph frt* (Kan^R,Tet^R)	This work
pFWB009	*pDEST::hupA-tagRFP-T::aph frt* (Kan^R, Amp^R)	This work
pFWM006	P_{lac}*::hupA-mKO2::aph frt* (Kan^R, Amp^R)	This work
pFWB019	*pDEST::hupA-mKate2::aph frt* (Kan^R, Amp^R)	This work

(Continued)

TABLE 2 | Continued

Plasmids	Descriptions	Reference
pBVS36	*pDEST:: TagYFP-MinDE::aph frt* (Kan^R, Amp^R)	This work
pBVS37	*pDEST:: TagGFP2-MinDE::aph frt* (Kan^R, Amp^R)	This work
pFWZ0	P_{ara}*::ftsZ::aph frt* (Kan^R, Cm^R)	This work
pFWZ4	P_{ara}*::ftsZswtagRFP-T::aph frt* (Kan^R, Cm^R)	This work
pFWZ5	P_{ara}*::ftsZswsfGFP::aph frt* (Kan^R, Cm^R)	This work
pFWZ6	P_{ara}*::ftsZswtagCFP::aph frt* (Kan^R, Cm^R)	This work
pFWZ7	P_{ara}*::ftsZswTC::aph frt* (Kan^R, Cm^R)	This work

FW1951 and FW1344, FW1401, FW1464, FW2455, FW1462, FW1534. The PCR fragments of pFWM007, pFWM006, and pFWB019 were amplified to replace the *mCherry* in strain RRL189 through λ Red recombination to result in strains FW1965, FW2417, and FW2450. The PCR fragments of pBVS3, pBVS36, and pBVS37 were used to replace the Δ*minD minE::cat sacB* in strain FW1363 through λ Red recombination to result in strains FW1480, FW1248, FW1393. Note that in strain FW1363 the *minC* gene is intact. The above listed strains were cured of kanamycin resistance using pCP20 as described in Datsenko and Wanner (2000), and listed in **Table 2**. To confirm the functionality of YFP-MinD, *Plac::yfp-minDE* was transduced from FW1462 into FW1363 to yield strain FW1463. For multi-color imaging, *hupA-tagBFP* from FW1344 was transduced into strain FW1554 to yield 1561; Δ*leuB::eqFP670* was transduced from FW1489 into FW1554 to yield FW1559; Δ*leuB::tagRFP-T* was transduced from FW1401 into FW1359 to yield FW1406; *hupA-mYPet* from FW1551 was transduced into a strain with *aph* cured from FW1965 to yield FW2480; *Plac::yfp-minDE* was transduced from FW1462 into FW1459 to yield strain FW1503; pFWZ4 was transformed into strain FW1559. All strains used are listed in **Table 3**.

Growth Conditions

For genetic engineering, *E. coli* cells were incubated in Lysogeny broth (LB) supplemented, when required, with 100 μg/ml ampicillin (Sigma-Aldrich), 50 μg/ml kanamycin (Sigma-Aldrich), or 34 μg/ml chloramphenicol (Sigma-Aldrich) for plasmid selection, or with 25 μg/ml kanamycin, 20 μg/ml chloramphenicol, or 0.2% sucrose for selection of the genomic insertions of gene cassettes. For imaging strains with fluorescent foci with LacI fusions, we grew cells in liquid M9 minimum medium (Fluka Analytical) supplemented with 2 mM $MgSO_4$, 0.1 mM $CaCl_2$, 0.4% glycerol (Sigma-Aldrich), and 0.01% protein hydrolysate amicase (PHA; Fluka Analytical). For imaging other strains, we grew cells either in liquid M9 minimum medium supplemented with 2 mM $MgSO_4$, 0.1 mM $CaCl_2$, 0.4% glucose (Sigma-Aldrich), and 0.25% PHA, or in LB medium. For imaging, overnight cultures were back diluted into the fresh medium described above to an OD (600 nm, same below) of 0.01 in falcon tubes until an OD of 0.4–0.6 for M9 medium with 0.25% PHA

TABLE 3 | Bacterial strains used in this study.

Strains	Descriptions	Reference
W3110	F-, lambda-, IN(rrnD-rrnE)1, rph-1	Hayashi et al. (2006)
FW1363	W3110, Δ*minD minE::sacB cat*	Wu et al. (2015)
FW1247	W3110, Δ*leuB::Pj23100 tagBFP::aph frt*	Wu et al. (2015)
FW1268	W3110, Δ*leuB::Pj23100 tagBFP::frt*	This work
FW1722	W3110, *hupA-ebfp2::aph frt*	This work
FW2486	W3110, *hupA-ebfp2::frt*	This work
FW1951	W3110, *hupA-sbfp2::aph frt*	This work
FW2485	W3110, *hupA-sbfp2::frt*	This work
FW1344	W3110, *hupA-tagBFP::aph frt*	This work
FW1359	W3110, *hupA-tagBFP::frt*	This work
FW1561	W3110, Δ*minD minE::exorbs2-sfgfp-minD minE::frt, hupA-tagbfp::aph frt*	This work
RRL189	AB1157, *ori1::lacOx240::hygR, ter3::tetOx240::accC1* Δ*galK::tetR-mCerulean::frt,* Δ*leuB::lacI-mCherry::frt*	Reyes-Lamothe et al. (2008)
FW1965	AB1157, *ori1::lacOx240::hygR, ter3::tetOx240::accC1* Δ*galK::tetR-mCerulean::frt,* Δ*leuB::lacI-sbfp2::aph frt*	This work
FW1551	W3110, *hupA-mYPet::aph frt*	This work
FW2480	AB1157, *ori1::lacOx240::hygR, ter3::tetOx240::accC1* Δ*galK::tetR-mCerulean::frt,* Δ*leuB::lacI-sbfp2::frt, hupA-mYpet::aph frt*	This work
FW1401	W3110, Δ*leuB::Pj23100 tagRFP-T::aph frt*	This work
FW1459	W3110, Δ*leuB::Pj23100 tagRFP-T::frt*	This work
FW1489	W3110, Δ*leuB::Pj23100 eqFP670::aph frt*	Wu et al. (2015)
FW2095	W3110, Δ*leuB::Pj23100 eqFP670::frt*	This work
FW1464	W3110, *hupA-tagRFP-T::aph frt*	This work
FW1495	W3110, *hupA-tagRFP-T::frt*	This work
FW2455	W3110, *hupA-mKO2::aph frt*	This work
FW2495	W3110, *hupA-mKO2::frt*	This work
FW2417	*AB1157, ori1::lacOx240::hygR, ter3::tetOx240::accC1* Δ*galK::tetR-mCerulean::frt,* Δ*leuB::lacI-mKate2::aph frt*	This work
FW2450	AB1157, *ori1::lacOx240::hygR, ter3::tetOx240::accC1* Δ*galK::tetR-mCerulean::frt,* Δ*leuB::lacI-mKO2::aph frt*	This work
FW1248	W3110, Δ*minD minE::tagYFP-minD minE::aph frt*	This work
FW1393	W3110, Δ*minD minE::tagGFP2-minD minE::aph frt*	This work
BN1406	W3110, *hupA-tagBFP::frt,* Δ*leuB::Pj23100 tagRFP-T::aph frt*	This work
FW1480	W3110, Δ*minD minE::yfp-minD minE::aph frt*	This work

(Continued)

TABLE 3 | Continued

Strains	Descriptions	Reference
FW1462	W3110, Δ*lacZYA::rbsexo1-yfp-minD minE::aph frt*	This work
FW1463	W3110, Δ*minD minE::sacB cat*, Δ*lacZYA::rbsexo1-yfp-minD minE::aph frt*	This work
FW1503	W3110, Δ*leuB::Pj23100 tagRFP::frt*, Δ*lacZYA::rbsexo1-yfp-minD minE::aph frt*	This work
FW1534	W3110, Δ*lacZYA::rbsexo2-sfGFP-minD minE::aph frt*	This work
FW1537	W3110, Δ*minD minE::rbsexo2-sfGFP-minD minE::aph frt*	This work
FW1541	W3110, Δ*minD minE::rbsendo-sfgfp-minD minE::aph frt*	Wu et al. (2015)
FW1554	W3110, Δ*minD minE::rbsexo2-sfgfp-minD minE::frt*	This work
FW1559	W3110, Δ*minD minE::rbsexo2-sfgfp-minD minE::frt*, Δ*leuB::eqFP670::aph frt*	This work
FW1370	W3110, *ftsZ::aph frt::envA*	This work
JKD7-1	W3110, Δ*ftsZ::aph*	Dai and Lutkenhaus (1991)

and LB, and OD of 0.1 for M9 medium with 0.01% PHA. The growth conditions for the FtsZ complementation assay are as described in Osawa and Erickson (2005). 0.002% arabinose was used for the induction of ectopic FtsZswTagRFP-T fusion from the plasmids in the presence of the endogenous *ftsZ*.

Microscopy

Fluorescence imaging was carried out using Nikon Ti-E microscope with 100X CFI Apo TIRF objective with an NA of 1.49. All fluorescent probes were excited using a Nikon Intensilight, except for the photo-bleaching of lacI foci, which was excited by SpectraX LED single-spectrum light sources (Lumencor) with SpectraX filter sets (Lumencor). For imaging with Nikon Intensilight, the $\lambda_{ex}/\lambda_{bs}/\lambda_{em}$ wavelengths of the filter cubes are as follows: SBFP2 and EBFP2 (363–391/425/435–485 nm), TagBFP (395–415/420/435–485 nm), mCerulean (426–446/455/460–500 nm), sfGFP (450–490/495/500–550 nm), mYpet and FlAsH (490–510/515/520–550 nm), TagRFP-T and mKO2 (530–560/562/570–620 nm), mCherry and mKate2 (540–580/585/592–668 nm), eqFP670 (589–625/649/655–1200 nm). For imaging with SpectraX, the excitation filters for orange and red proteins are respectively 555/25 nm (center/width, same below) and 575/22 nm. The multiband emission filters are respectively 435/26 – 510/40 – 595/40 – 705/72 nm, and 465/25 – 545/30 – 630/60 nm. The fluorescence signal was recorded by an Andor EMCCD camera (iXon Ultra 885), with an EM gain of 100. While our emission filter for the eqFP670 extends to the infrared region, eqFP670 does not fluoresce beyond 850 nm, which is well-within the detection range for most EMCCD cameras, including the one used in this study.

Image Analysis

Analysis of fluorescent microscopy images was carried out using Matlab with our customized programs. The background intensity was subtracted for all images individually. For identification of fluorescent LacI foci or nucleoid, the images were Gaussian blurred for subtraction, and a threshold for the expected object size and intensity was applied to eliminate noise. The intensities of the identified objects were then collected for statistics. For the photobleaching data, the mean per-pixel intensity of each nucleoid was calculated independently. To compare the photostability of more than two FPs in the main figure, the total intensities of all identified objects were summed and divided by the total number of pixel for all found objects in the first image, in order to take the completely bleached objects at the later stage of the bleaching period into account. In the latter case, the sum fluorescence intensity of the FPs in individual objects was plotted only in the supplementary figures. The standard deviation values of the intensities were not shown in the main figures for the convenience of display, and are instead plotted in supplementary figures. The matlab scripts used for these measurements can be found at http://ceesdekkerlab.tudelft.nl/downloads/.

The signal-to-noise ratio (SNR) of the cytosolic FPs is calculated using $SNR_{cell} = (I_{cell}\text{-}I_{bg})/SD_{bg}$. We use the standard deviation value of the cell-free region as a measure of background noise (SD_{bg}). We use the difference between the mean intensity of a cell (I_{cell}) and the mean background intensity (I_{bg}) as a measure of signal. The mean and SD values of the SNR calculated from all cells are used for plotting.

Results

A Bright Blue Fluorescent Protein for Multi-Color Imaging in Bacteria

The blue variants of the fluorescent proteins (BFPs) have seen few applications in bacteria due to their low brightness and short excitation wavelength (see **Table 1**). In principle, if a BFP would be sufficiently bright, it can be imaged with excitation light that is weak enough to avoid photodamage to the cells. It was recently reported that the purified monomeric mTagBFP (commercial name TagBFP) has a brightness that is similar to EGFP and 1.8 times that of EBFP2 (Subach et al., 2008). To examine its performance in bacteria, we first transformed a high-copy plasmid carrying the *tagBFP* gene under a T3 promoter into an *E. coli* strain, and indeed we observed bright blue fluorescence upon excitation through a customized filter set in a Nikon Intensilight. Furthermore, we engineered a new construct into the *leuB* locus in the *E. coli* genome, yielding strain FW1268, where the expression of *tagBFP* gene is driven by a synthetic constitutive promoter and a synthetic ribosome-binding site (RBS). The fluorescence signal of the expressed TagBFP is indeed sufficient for full cell labeling of bacteria (**Figure 1A**), indicating that TagBFP may have the brightness and maturation rate suitable for labeling proteins expressed at their endogenous level.

To compare the performance of TagBFP to other BFP variants as fluorescent tags in bacteria, we fused either *tagBFP*, *eBFP2,* or *sBFP2* genes to the 3′-end of the endogenous *hupA* gene, and

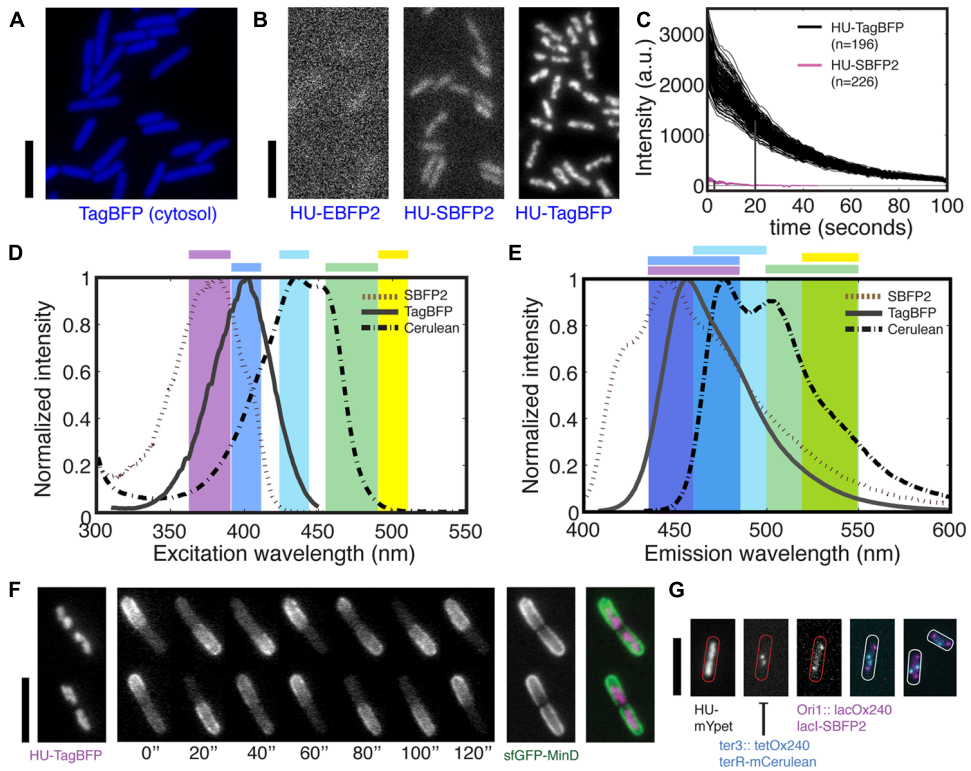

FIGURE 1 | Bright blue fluorescent proteins for multi-color imaging in bacteria. (A) TagBFP is bright when expressed from a genomic copy under a constitutive promoter for cytosolic label in live *Escherichia coli* cell. **(B)** Fluorescent images of HU-2 tagged by three blue fluorescent protein (BFP) variants in live *E. coli* during exponential growth. **(C)** Brightness and photostability of HU-TagBFP and HU-SBFP2 in live *E. coli* cells under the constant exposure to the Nikon Intensilight with the respective filter sets. Each line represents the average intensity of one nucleoid. The index n indicates the numbers of nucleoids examined. The vertical lines indicate the bleaching halftime. **(D)** Excitation spectra of SBFP2, TagBFP, and Cerulean (a CFP), and the ranges of bandpass filters (shown in color) used for the excitation of blue, cyan, green, and yellow FPs. Note that different filters were used for SBFP2 and TagBFP due to their different excitation peak. **(E)** Emission spectra of SBFP2, TagBFP, and Cerulean, and the ranges of bandpass filters used for collecting the fluorescent light emitted by blue, cyan, green, and yellow FPs. **(F)** Endogenous fusions HU-TagBFP and sfGFP-MinD are combined for dual-color imaging. From left to right: a HU-TagBFP image, an sfGFP-MinD time series, a per-pixel standard deviation (SD) image of sfGFP-MinD calculated over time, and a false-color overlay of HU2-TagBFP and sfGFP-MinD. **(G)** Three-colors imaging of chromosome and chromosomal loci using HU2 label and two operator-repressor systems. Shown are three individual images followed by an overlay of the latter two, and an extra example. All scale bars indicate 5 μm.

examined their performance (**Figures 1B,C**). For imaging, we used two customized filter sets for the different excitation peaks of the EBFP2/SBFP2 (379 nm) and TagBFP (402 nm; **Figure 1D**), and the same emission filter (**Figure 1E**). Importantly, direct FP fusions to the C-termini of genes at their endogenous loci have been confirmed to maintain the endogenous expression level of these genes (Taniguchi et al., 2010).

HU-TagBFP outperforms HU-EBFP2 and HU-SBFP2 to a surprising extent in live bacteria, as shown in **Figure 1B**. It shows a 20 times higher fluorescence intensity than HU-SBFP2, showing clear chromosome morphologies for 200 ms exposure to half of the maximum excitation intensity provided by Nikon Intensilight. Note that the intensities of the Intensilight do vary for the different spectral range. Unexpectedly, HU-SBFP2 was threefold brighter in the stationary growth phase, despite that HU-2 was shown to be four times more abundant in the exponential phase (Ali Azam et al., 1999). Such an increase in brightness in the stationary phase was not observed in any of the other HU-2 fluorescent fusions. We hypothesize that the increase in brightness is due to a slower turnover of HU-SBFP2 proteins at stationary phase, allowing the proteins to successfully mature and fluoresce. Next to their higher brightness, the HU-TagBFP also shows superior photostability. The above constructs were used to compare the photostability of HU-TagBFP and HU-SBFP2 under the constant exposure to the same excitation light as imaged for **Figure 1B**. HU-TagBFP showed a bleaching half-time of 18 s, in contrast to the 6-s half-time for HU-SBFP2, see **Figure 1C**. In other words, the fluorescence signal of HU-TagBFP would only drop 50% after acquiring 90 images with the settings for **Figure 1B**. The initial intensity of the 196 nucleoids is measured to equal 2671 ± 354 (mean ± SD, a.u.), i.e., the HU-TagBFP concentration has a standard deviation that is only 13% of the mean value across the cell population during exponential growth in LB.

TagBFP's excitation/emission spectra are well-separable from green and yellow fluorescent proteins (GFPs and YFPs) for multi-color imaging (**Figures 1D,E**). Taking advantage of the narrow

excitation profile of TagBFP and its excitation peak at 402 nm, we customized a filter set to maximize the excitation efficiency and to collect the majority of the emitted light (**Figures 1D,E**). This filter set can be combined with regular commercial filter sets for GFP or YFP for two-colors imaging. Here, we illustrate such a combination by transducing the endogenous *hupA-tagBFP* fusion construct into a strain with a bright endogenous *sfGFP-minD* fusion (for details see **Figure 4**), yielding strain FW1561. Shown in **Figure 1F**, these two fluorescent probes successfully captured both the localizations of the nucleoids and the MinD oscillations, which together define the mid-cell for the localization of the cytokinesis machinery.

A potential combination of BFPs with cyan fluorescent proteins (CFPs) can further increase the options for multi-color imaging. Despite the higher brightness of TagBFP compared to SBFP2, it has more spectral overlap with CFP and thus is found less suitable for this application. As shown in **Figures 1D,E**, SBFP2 can be well-separated from common CFPs through customized filters, whereas the overlap between TagBFP and the CFPs is larger. Note that our current emission filter range for SBFP2 can be further adjusted to a 410–460 nm range to avoid crosstalk with CFPs. The combination of SBFP2 and SCFP3A was previously shown in Hela cells, where SBFP2 was highly expressed in the cytosol (Kremers et al., 2007). However, the limited subsequent usage in bacteria and our not fully satisfactory results for the HU-SBFP2 fusion lowered our expectations for the extent of its applications. Nevertheless, we suggest that, SBFP2 may find its application in protein co-localization studies if the morphology is not overly complicated. Here, for example, we replaced the mCherry in a LacI fusion (strain RRL189 Reyes-Lamothe et al., 2008), resulting in a LacI-SBFP2 fusion that targets the 240 *lacO* repeats in the origin region of the *E. coli* genome (strain FW1965). In this strain, the expression of the LacI-SBFP2 is constitutive. We found that it can be co-imaged with *ter* foci label TetR-mCerulean (cyan) and chromosome label HupA-mYpet (yellow; strain FW2480) (**Figure 1G**). Notably, the LacI-SBFP2 foci are much dimmer than the original LacI-mCherry fusion, requiring 2-s exposure time with Nikon Intensilight, thus less suitable for time-lapse imaging in dynamics studies. Alternatively, Everogen has produced TagCFP (Ex/Em = 457/480 nm) which can be combined with TagBFP, but we did not persue this route due to its potential spectral crosstalk with YFPs, and that our FtsZ-TagCFP fusion did not fluoresce.

Bright and Photostable Fluorescent Proteins in the Orange-Red, Far-Red, and Near-Infrared Spectral Range

By applying the same procedure above to characterize the performance of TagRFP-T and eqFP670 (commercial name NirFP) as cytosolic labels, we found that they perform superiorly in brightness and photostability for the orange and near-infrared spectral range, respectively (**Figure 2A**). Despite the fact that these two proteins are excited with long-wavelength and hence less phototoxic compared to GFP, frequent time-lapse imaging of strains FW1459 and FW2095, with the same setting for **Figure 2A** at a frame rate of 5 s for 5 min did lead to cell growth arrest although no significant photobleaching was observed (data not shown), indicating that the photostability is not a limiting factor for imaging live cells using these FPs. Note that this is an overexposure test for whether the photostability is sufficiently high when imaging is carried out at a lower rate where photodamage is avoided. The trade-off between photodamage, fluorescence signal, and temporal resolution requires moderation of the settings to specific cases.

Notably, despite the fact that the near-infrared dimer eqFP670 was reported to have a brightness that is only 8% of EGFP as well as a modest maturation speed (Shcherbo et al., 2010), we were able to visualize the cells using either a regular far-red filter set or a customized near-infrared filter set (**Figures 2B,C**). This is largely owing to the almost full collection of far-red emission lights, while a smaller part of the emitted light is collected for the other proteins to avoid cross-talk. By contrast, a monomeric derivative TagRFP657 (excitation/emission peaks at 611/657 nm), which was produced for flow cytometer applications is not visible in our constructs even when placed under either the same synthetic promoter as above or a T7 promoter in a plasmid with pBR322 origin (pERB004 and pERB005). This agrees with the invisibility of TagRFP657 in a previous attempt in yeast (Lee et al., 2013). These facts thus make eqFP670 the most red-shifted protein applicable to bacteria so far, although we note that it's dimeric property limits its application for protein fusions.

TagRFP-T and eqFP670 have the spectral properties that allow multi-color imaging at the red-shifted spectral range. While TagRFP-T has been reported as a red FP, its excitation and emission spectra are more blue shifted compared to conventional RFPs such as mCherry (Shaner et al., 2008). By comparing the spectral data of TagRFP-T and eqFP670, we propose that TagRFP-T can be imaged solely at the orange spectral range for excellent separation from GFPs/YFPs as well as from eqFP670, provided that latter is imaged at the near-infrared spectral range (**Figures 2B,C**). These customized filter sets allow us to measure the relative brightness of the two proteins in live cells (as shown in **Figure 2A**) from yellow to near-infrared spectral region (**Figure 2D**). Both TagRFP-T and eqFP670 are invisible with a YFP filter, while they show an equal brightness when imaged with a regular far-red filter used for mCherry. As expected from the spectral data, TagRFP-T does not show any bleed-through into the near-infrared spectral range. In the orange spectral range, TagRFP-T exhibits an over 10 times higher signal-to-noise ratio than the small bleed-through signal from eqFP670. The bleed-through from the eqFP670 into the orange spectral range is difficult to avoid due to the long tail of its excitation spectrum into the shorter wavelength. From these data, we conclude that the combination of TagRFP-T and eqFP670 is excellent for multi-color imaging at the orange and near-infrared spectral range.

As TagRFP-T was reported to be the most photostable FP at the red-shifted spectrum (Shaner et al., 2008), we set out to examine its performance as a fluorescent tag in live bacteria. We fused the 3′-end of *hupA* gene to *tagRFP-T* as well as to another recently reported FP gene, *mKO2*, which is expected to encode

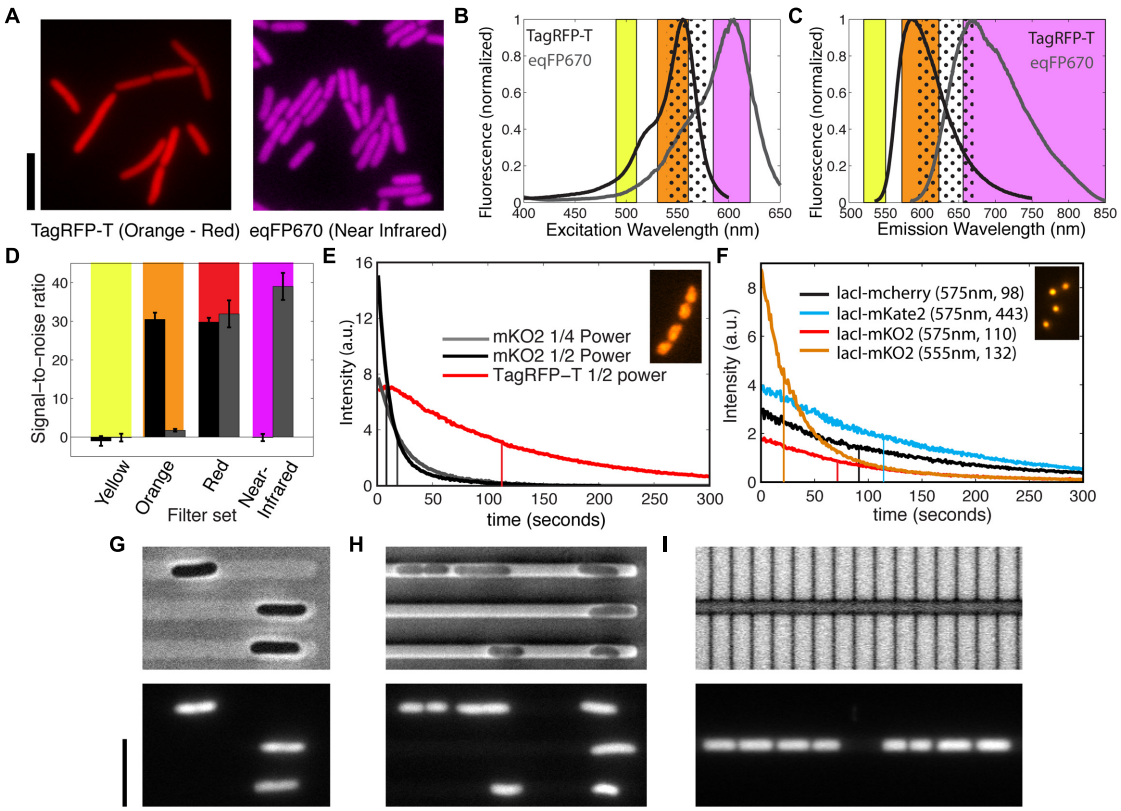

FIGURE 2 | Bright and photostable fluorescent proteins in the orange-red, far-red, and near-infrared spectral range. (A) *E. coli* showing the fluorescence of cytosolic TagRFP-T (using orange filter set) and cytosolic eqFP670 (using near-infrared filter set) when expressed from a genomic copy under a constitutive promoter for cell body label in live *E. coli*. Scale bars, 5 μm. **(B,C)** Excitation and emission spectra of TagRFP-T and eqFP670, and the ranges of bandpass filters for the excitation and emission at yellow, orange, far-red, and near-infrared spectral range. These spectral ranges are as specified in the methods section for mYpet, TagRFP-T, mCherry, and eqFP670. The dotted regions indicate far-red filters. **(D)** Signal-to-noise ratios of TagRFP-T (black bar) and eqFP670 (gray bar) expressed in the strains shown in **(A)**, when imaged with different filter cubes shown in **(B,C)**. Here, the noise is defined by the standard deviation of the background intensity, and the signal is the difference between the fluorescence intensity of the cell and the mean background intensity. **(E)** Photobleaching of HU-mKO2 and HU-TagRFP-T in live *E. coli* cells under the constant exposure to the Nikon Intensilight at different power as indicated with the orange filter set. Inset shows a false-color image of nucleoids labeled by HU-TagRFP-T. Vertical lines indicate the bleaching halftime. **(F)** Photobleaching of chromosomal ori foci (Ori1::lacOx240) labeled by LacI-mcherry, LacI-mKate2, and LacI-mKO2 under the constant exposure to the SpectraX LED light source (1/4 power) with far-red or orange filter sets. The intensity values are the mean intensities of all the loci, i.e., the total intensity of detected loci divided by the initial number of detected loci. The indicated numbers for each probe are, respectively, the excitation wavelength and the number of spots measured. The inset shows a fluorescence image of the lacI-mKO2 foci. Vertical lines indicate the bleaching halftime. **(G–I)** Effect of microstructures made from different materials on the single-cell identifications in bright-field imaging (top panels) and using fluorescent microscopy of cytosolic labels (bottom panels). **(G)** *E. coli* cells in agarose-based microstructures, as described in Takeuchi et al. (2005). **(H)** *E. coli* cells between PDMS structures and an agarose pad, as described in Wu et al. (2015). **(I)** *E. coli* cells between silicon structures and PDMS, as described in Männik et al. (2012). The *E. coli* cells in **(G–I)** are strain BN1590 and fluorescent imaging was done in the near-infrared channel. The bright-field images in **(G,H)** were obtained through phase-contrast microscopy, whereas in **(I)** it was a regular wide-field image obtained through reflective light. Scale bar is 5 μm.

a bright, fast-folding orange/red FP (**Figure 2E**). Indeed, these two fluorescent probes show excellent brightness as an HU-2 tag in live bacteria, clearly improving the performance of orange proteins mKO and mOrange, which were previously shown to be invisible in live cells as fluorescent tags to FtsZ (Alexeeva et al., 2010). Under the same microscope and camera settings, HU-mKO2 appear to be 2.2 times as bright as TagRFP-T, but 15 times less photostable (**Figure 2E**, Supplementary Figure S1). Even when the exposure of HU-mKO2 was tuned to result in the same initial intensity as HU-TagRFP-T, it showed a 17-s bleaching half-time, in contrast to the 102 s for TagRFP-T. Thus, comparing these two proteins, mKO2 is more suitable for imaging proteins at low abundance, whereas TagRFP-T is more suitable for long-term time-lapse imaging.

Besides TagRFP-T and eqFP670, a far-red monomeric FP mKate2 was derived from the same origin. It showed more emission at the far-red spectral range and 57% higher brightness than mCherry (Shcherbo et al., 2009). Its photostability was shown to be similar to mCherry for purified proteins and 2.5-fold enhanced when expressed in yeast after codon optimization (Shcherbo et al., 2009; Lee et al., 2013). Here, we compare its brightness and photostability in bacteria by replacing the *lacI-mCherry* construct in strain RRL189 (see above for LacI-SBFP2 fusion) with *lacI-mKate2*. Shown in **Figure 2F**, the average

intensity of the fluorescent foci of LacI-mKate2 is 25% enhanced with the same excitation/emission filters as compared to regular far-red proteins. The photostability of the two proteins is similar. In both cases after 300 s of exposure, 95% of all spots were still detectable through our automated software, showing that LacI-mCherry or LacI-mKate2 are both excellent candidates for operator-repressor system in time-lapse imaging. Furthermore, we engineered a LacI-mKO2 fusion based on strain RL189, and its foci are five times brighter in the orange spectral range than in the red spectral range (**Figure 2F**, Supplementary Figure S2). The photobleaching half-time of LacI-mKO2 is, however, 2.5 times shorter at the orange spectral range, likely due to the strong light absorbance.

Our comparison between all the orange-red and far-red fluorescent fusion tested here shows that TagRFP-T is indeed superior in photostability, agreeing with the quantitative data from the purified proteins and from fluorescent fusions in yeast (Shaner et al., 2008; Lee et al., 2013). Its far-red derivative mKate2 is indeed brighter than mChrrey in bacteria, but less significantly as previously reported in purified form and as fusion tag in yeast, which can be resulted from a slower maturation of mKate2 compared to mCherry.

Expanding the spectral range of fluorescence proteins for cytosolic label is also advantageous for studies using microstructures. Microstructures and microfluidics are emerging tools for studying bacterial physiology (Wang et al., 2010; Männik et al., 2012; Hol and Dekker, 2014; Wu et al., 2015). While these tools provide many advantages in manipulating the chemical and physical environment, they can impose challenges for imaging. In particular, the materials for the confining microstructures can make a great difference for visualizing cell body without fluorescence. For example, the structures made from agarose gel are transparent and allow phase contrast microscopy to visualize cell boundaries, owing to the fact that an agarose gel has lower refractive index (1.33, same as water) than bacteria (∼1.4; **Figure 2G**). By contrast, polydimethylsiloxane (PDMS), the most commonly used polymer for microfluidic applications, has a reflective index of around 1.4, which is almost identical to that of a bacterial cell. When imaging bacteria in between PDMS structures and agarose, the cell boundaries display much less contrast (**Figure 2H**). This type of interference between the microfluidic channel boundary and the bacterial boundary is even worsened for PDMS–PDMS interfaces. Furthermore, silicon structures are non-transparent, thus only allowing bright-field or DIC microscopy, in reflection rather than transmission, and bacteria in ∼micron-sized channels are difficult to distinguish (**Figure 2I**). In all these scenarios, the availability of cytosolic labels at the near-infrared (eqFP670) spectral range becomes particularly useful as a third or fourth color (**Figures 2G–I**, bottom panels).

A Bright and Photostable FtsZswTagRFP-T Fusion for Multi-Color Imaging of Cell Division

As shown above, TagRFP-T can be spectrally well-separable from the near-infrared protein eqFP670 as well as from GFPs/YFPs. This can potentially lead to three-colors imaging at the long-wavelength regime, where phototoxicity can be reduced by avoiding near-UV excitations (such as necessary for CFPs or BFPs). Such an approach is in fact essential when frequent time-lapse imaging is required for tracking dynamic protein localizations over long time. Here, we describe the construction of new FtsZ and MinD fusions for time-lapse imaging of division site selection in *E. coli* with high temporal resolution.

An FtsZ molecule has a globular structure composed of independently folded N-terminal and C-terminal domains both essential for polymerization, followed by an unstructured flexible linker, and a conserved C-terminal tail responsible for interacting with its membrane-bound partners FtsA and ZipA as well as lateral interactions between FtsZ polymers (**Figure 3A**; Oliva et al., 2004; Osawa and Erickson, 2005; Shen and Lutkenhaus, 2009; Erickson et al., 2010; Buske and Levin, 2013). Biochemical and genetic studies also indicated that the C-terminal tail is the primary target of two negative regulators of FtsZ polymerization, MinC and SlmA (Shen and Lutkenhaus, 2009; Du and Lutkenhaus, 2014). So far, none of the realized fluorescent fusions of FtsZ have been shown to be fully functional, indicating that both the C-terminal tail and the globular domain are sensitive to spatial perturbations. Two close-to-functional examples are an EYFP-FtsZ fusion at temperatures below 28°C though with a very small fraction of cleaved FtsZ (Alexeeva et al., 2010), and an FtsZswVenus fusion (where Venus is inserted into the unstructured linker region of FtsZ) that rescued FtsZ deletion at 42°C after several rounds of passage likely involving mutations in the genome (Osawa and Erickson, 2005).

Since directed replacement and random insertion assays both indicated that the unstructured linker region of FtsZ can be perturbed to some extent (Osawa and Erickson, 2005; Buske and Levin, 2013), we set out to probe the possibilities of inserting other fluorescent tags at the amino acid 333 of FtsZ by adopting the strains and selection processes for FtsZswVenus (see Osawa and Erickson, 2005 and Materials and Methods; **Figure 3A**). We hoped that a FP derived from another origin could perform differently during the folding of the sandwich fusion, thus have potential to success in sandwich fusion. In order to confirm the suitability of the custom-designed flexible linkers and insertion site, we first inserted a tetracysteine (TC) sequence (FLNCCPGCCVEP) flanked by the short flexible linkers (GSGSGS-TC-GGSGSS) into the *ftsZ* gene, yielding pFWZ7. This TC tag can later be labeled by Fluorescein Arsenical Hairpin (FlAsH; Griffin et al., 1998). When induced with 0.2% arabinose, the construct pFWZ7 was able to both co-exist with the native FtsZ, and rescue the lethal effect of FtsZ deletion (**Figure 3B**). Under this growth condition, however, the Δ*ftsZ* strain with pFWZ7 always showed a significant fraction of filamentous cells (30% in biomass). To label the FtsZswTC with the FlAsH dye, we optimized the protocol for live cell staining in *E. coli*. By incubating an exponentially growing bacterial culture in LB with 2 μM FlAsH dye for 3 h followed by a gentle wash step with EDT_2 buffer, we were able to observe the fluorescence of Z-rings localizing at the cell middle in the regular rod-shaped cells (**Figure 3B**). By contrast, the filamentous cells show patches of fluorescence over the whole cell body, indicating that the filamentation is mainly caused by the overproduction of FtsZswTC, which disrupted the ratio between FtsA and FtsZ.

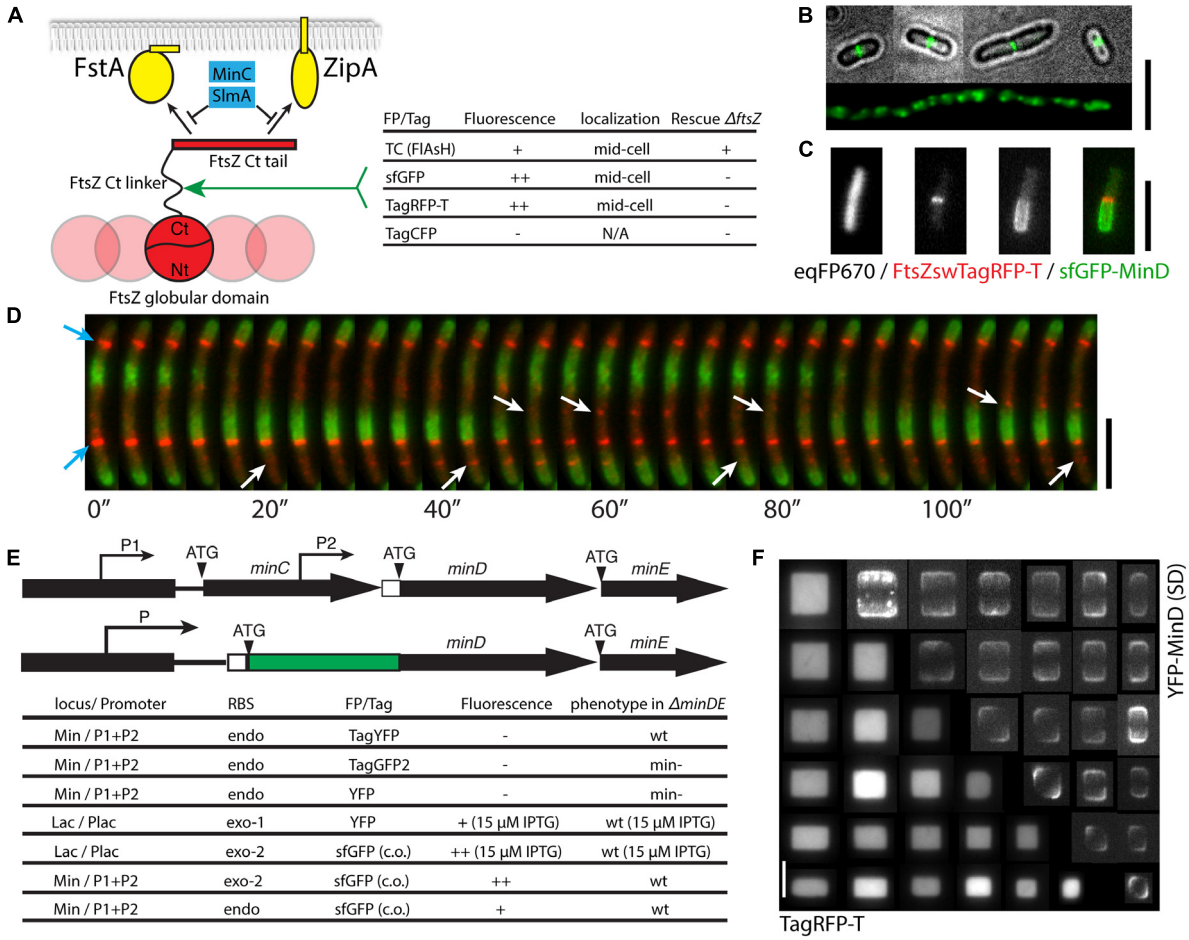

FIGURE 3 | Multi-color imaging of cell division at the green, yellow, orange, and near-infrared spectral range. (A) A sandwich fusion strategy for labeling FtsZ and the effectiveness of using various fluorescent tags or proteins. These fluorescent probes were inserted within the flexible linker between the extreme C-terminal tail of FtsZ that is responsible for the direct interactions with FtsA, ZipA, MinC and SlmA, and the globular structure responsible for polymerization. **(B)** Fluorescence microscopy images of a strain expressing FtsZswTC labeled by the FlAsH dye (in green). The top four cells show regular rod-shaped cells (cell boundary shown in gray scale) with central Z-ring (green), while the bottom one is part of a filamentous cell in the same culture showing overexpressed FtsZ fusion proteins (green). **(C)** A combination of near infrared, orange-red and green FPs for three-colors imaging (strain FW1559 with pFWZ4, induced with 0.0002% arabinose). The FtsZswTagRFP-T was expressed from an ectopic copy under the arabinose promoter P_{BAD}. **(D)** Time-lapse images showing the dynamics of FtsZswTagRFP-T and sfGFP-MinD in an elongated cell (strain FW1554 with pFWZ4, induced with 0.0002% arabinose) treated with cephalexin. Blue arrows show stable Z-rings; white arrows indicate the locations where FtsZ proteins polymerize and depolymerize. All scale bars indicate 5 μm. **(E)** Schematic and table showing the effectiveness of the fluorescent labeling of MinD at different genomic loci with different promoters and RBSs. Note that for simplicity, the RBSs of MinC and MinE are not shown. P, promoter; ATG, start codon; the white box denotes the RBS; exo, exogenous; endo, endogenous. **(F)** Fluorescent images of strain FW1503 co-expressing cytosolic TagRFP-T and YFP-MinD used in a cell shaping experiment, where single cells grow into the shapes of nanofabricated chambers, as described in Wu et al. (2015). This shows that orange-red and yellow FPs can be combined for multi-color imaging. The bottom left show cytosolic eqFP670 fluorescence and the top right images are YFP-MinD standard-deviation image calculated from the 25 images taken in 2 min.

It was shown previously that an overexpression of only FtsZ or only FtsA can lead to a filamentous phenotype (Dai and Lutkenhaus, 1992). In order to confirm that filamentation is caused by an incorrect protein expression level, we engineered pFWZ0 (Para::ftsZ) and transformed into the Δ*ftsZ* strain, which rescued the cell growth upon induction but also showed a similar morphological heterogeneity. We were, however, unable to reduce the proportion of filamentous cells by lowering arabinose concentration, likely due to the inherent all-or-none expression pattern of P_{BAD} promoter. Because the FlAsH tag showed very weak fluorescence and poor photostability, we did not proceed further to optimize the construct for homogeneous induction or insertion into the genome.

We further replaced the TC peptide in the pFWZ7 construct with sfGFP, TagRFP-T, and TagCFP, which are derived from three different protein origins (**Figure 3A**). The FtsZswsfGFP and FtsZswTagRFP-T were able to form fluorescent Z-rings with or without the existence of native, untagged FtsZ, but they were not able to rescue the lethal effect of FtsZ deletion. The FtsZswTagCFP, on the other hand, did not fluoresce and was not

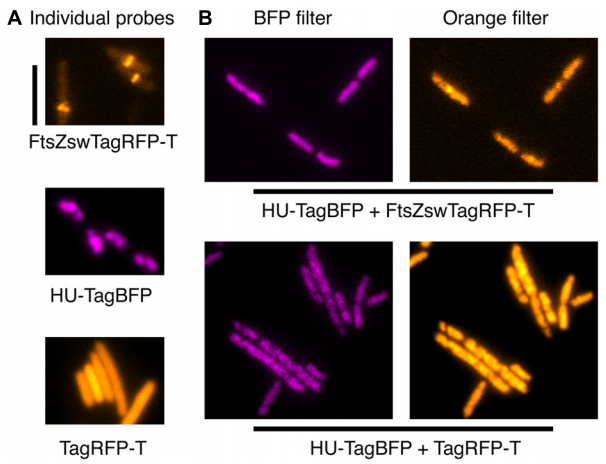

FIGURE 4 | HU-TagBFP interferes with the localizations of TagRFP-T and FtsZswTagRFP-T. (A) False-color images of the individual fluorescent fusions. **(B)** The recruitment of both the FtsZswTagRFP-T and cytosolic TagRFP-T by the HU-TagBFP to the nucleoid, when these probes were combined. Scale bar at the top left indicates 5 μm.

investigated further. Nevertheless, the former two constructs can serve as alternative ectopic FtsZ probes in addition to the existing ones.

The FtsZswTagRFP-T is bright and photostable, and can be combined with eqFP670 and sfGFP-MinD for three-colors imaging (**Figure 3C**). The superior brightness and photostability of both FtsZswTagRFP-T and sfGFP-MinD allowed us to probe the dynamic relations between the localization of FtsZ and MinD with a frame rate of 1–4 s for 2 min. **Figure 3D** shows that FtsZ filaments can be assembled and disassembled within a time frame of 20–30 s, in a pattern which anti-correlates with sfGFP-MinD localization patterns. Besides the above-mentioned advantages, the use of FtsZswTagRFP-T also results in less phototoxicity due to its long excitation/emission wavelength, in contrast to the previous YFP-MinD/FtsZ-CFP combination (Shih et al., 2005).

The Endogenous *minD* Fusion Reveals the Importance of Codon-Dependent Translational Read-Through for N-Terminal Fusions

Min proteins in *E. coli* oscillate between the two cell poles, forming a time-averaged concentration gradient of MinC, an FtsZ antagonist, with a minimum at the cell middle to allow Z-ring formation (**Figure 1F**). Without the Min system, *E. coli* often divide asymmetrically, producing anucleated minicells. The Min operon is composed of *minC*, *minD,* and *minE* genes which are positioned sequentially in the genome, with one promoter in front of MinC that drives the transcription of all three genes, and another promoter embedded in the *minC* gene to only drive MinD and MinE expression (de Boer et al., 1989; **Figure 3E**). Co-transcription of *minD* and *minE* ensures the ratio of their protein products to be rather constant, which is essential for the localization patterns of all Min proteins. Previously, *gfp-minDE* and *yfp-minDE* constructs were shown to be able to complement the Δ*minDE* phenotype when placed under the lac promoter in medium copy plasmids and induced with low concentrations of IPTG (Raskin and de Boer, 1999; Shih et al., 2002). These constructs were widely used for studying the Min protein dynamics. However, it is difficult to match inducible expression to native protein levels at all physiological conditions, and the lac promoter is known to show inhomogeneity and leaky expression.

We set out to engineer a strain where the expression of a MinD fusion will be driven by the endogenous promoter and RBS such that the expression level of the fusion will most closely reflect the native status (**Figure 3E**; Wu et al., 2015). We first constructed a few N-terminal *minD* fusion constructs that are followed by the *minE* gene and a kanamycin resistance gene. The tags are TagYFP and TagGFP2, purchased from Evrogen for their claimed photostability and fast-folding property, and YFP, from the original construct mentioned above. Unfortunately, when inserted into the *min* locus replacing a Δ*minDE::sacB-cat* cassette, none of them resulted in a strain that showed fluorescence, and only TagYFP-MinD appeared to be functional in complementing the minicell phenotype. The non-functional endogenous *yfp-minD* fusion must be caused by an insufficient expression level rather than the functionality of the fusion proteins, since YFP-MinD fusion was proven functional and fluorescent when expressed from a plasmid. On the other hand, TagYFP-MinD appeared to be expressed and functional but do not fluoresce. We next inserted the Plac::yfp-minDE construct and a new *Plac::sfGFP-minDE* construct into the genomic *lac* operon, keeping the RBS from the original plasmids, and these cells showed YFP-MinD/sfGFP-MinD oscillations, when induced using 15 μM IPTG in both wild-type and Δ*minDE* background. The sfGFP used here is a codon-optimized version. This further confirms that the difficulty in the endogenous fusion of *minD* is caused by the translational read-through when the endogenous *minD* RBS is combined with the other FP genes.

To test whether the endogenous *minD* RBS can be functional when combined with codon-optimized version of the *sfGFP* gene, we first replaced the RBS of the *Plac::sfGFP-MinD* construct with the *minD* RBS, which successfully result in sfGFP-MinD oscillations under IPTG induction. Finally, we replaced the Δ*minDE::sacB-cat* region with the *sfGFP-minDE* construct either with only the endogenous *minD* RBS or with an exogenous RBS from the plasmid behind the endogenous *minD* RBS. Both strains appeared to completely rescue the minicell phenotype (**Figure 3E**). The sfGFP-MinD fusion under the endogenous RBS was expressed at a level almost identical to the wild-type (Wu et al., 2015).

The endogenous fusion of the *sfGFP-minD*, in combination with cytosolic eqFP670 label, allowed us to study the Min pattern formation in diverse cell shapes defined by microstructures (Wu et al., 2015). By inoculating the *E. coli* cells into microchambers, we were able to mold them into defined shapes across a large range of sizes. Studying sfGFP-MinD oscillation patterns in these cells revealed that Min proteins are able to orient their oscillations according to the symmetry and scale of the cell boundary, and scale their concentration gradients with the cell dimension within a length range of 3–6 microns (Wu et al., 2015). Here,

we show that also the ectopically expressed YFP-MinD fusion (in a wild-type *minDE*$^+$ background, strain FW1503) can be combined with cytosolic TagRFP-T (strain FW1503) for the same applications, yielding the same localization patterns as sfGFP-MinD (**Figure 3F**). This confirms that the effect of symmetry and scale on the Min pattern formation is intrinsic and not dependent on the FPs, and verifies that the previous studies with modest YFP-MinD levels indeed represent well the native Min protein behavior. However, strain FW1503 appeared to be more sensitive to osmotic shock due to unknown reasons and thus less suitable for quantitative studies or for producing cells larger than 4.5 μm × 4.5 μm × 1 μm using the same shaping method.

TagBFP Directly Interacts with TagRFP-T

From the characteristics of all FPs above, we expected that TagBFP and TagRFP-T would be excellent, mutually exclusive partners for multi-color imaging, in combination with the broadly available bright GFPs/YFPs variants. Thus, we transformed pFWZ4 (FtsZswTagRFP-T) into strain FW1359 for co-imaging of FtsZ and chromosome. To our surprise, we observed patchy blobs in the orange channel, which colocalize with the fluorescence signals from the TagBFP channel (**Figure 4**). It appears that the HU-TagBFP recruites FtsZswTagRFP-T to the nucleoid. To confirm such a strong interaction between TagBFP with TagRFP-T, we transduced a *tagRFP-T* cassette into strain FW1359, and found that HU-TagBFP is also able to recruit the freely diffusing cytosolic TagRFP-T molecules to the nucleoid (**Figure 4**). Moreover, this recruitment induced elongated cell morphology and chromosome-segregation defects (**Figure 4**).

Discussion

We have introduced recently developed blue (TagBFP), orange (TagRFP-T and mKO2), red (mKate2), and near-infrared FPs (eqFP670) into localization studies in bacteria. These proteins generally showed the superior brightness and photostability in bacteria, consistent with previous reports of their *in vitro* behavior. This indicates that their folding properties are not the limiting factor for their general application in bacteria, contrasting earlier versions of proteins in the blue and orange spectral range, such as EBFP2 and mOrange. The near-infrared protein eqFP670 exhibited a strong brightness under our imaging conditions, presenting itself as an excellent candidate for cell body labeling for long-term and/or frequent imaging. Its extremely far-red excitation at 610 nm can minimize phototoxicity during imaging compared to all other FPs presented here. The addition of these FPs now leads to the ability to re-shuffle optimal choices of fluorescent probes *in vivo* for various combinations of colors. At the far-red spectral range, mKate2 showed a 25% improvement over mCherry. Since the latter is often chosen for its super-fast folding property, it is yet to be determined whether mKate2 and TagRFP-T can outperform mCherry in all aspects, such as for tagging periplasmic proteins.

For single-color imaging with high temporal resolution, TagRFP-T appears to be an excellent probe for bacterial studies. Besides its extremely strong photostability, it is excited with a much longer wavelength compared to the common GFPs. Using TagRFP-T reduces the phototoxicity compared to GFPs, allowing imaging at higher frequency and intensity. Adding to a previous study which successfully used its ancestor TagRPF as N-terminal tag (Alexeeva et al., 2010), we showed here that the brightness and photostability of TagRF-T is not perturbed by fusions to proteins either in the middle or at their C terminus, thus proving that TagRFP-T can be generally applicable in protein fusions.

For two-colors imaging, we have shown that a combination of TagRFP-T and sfGFP can allow imaging at high frequency without significant photobleaching. For three-colors protein tagging, TagBFP/GFP/mKO2 can be a good alternative to the commonly used set of CFP/YFP/mCherry. In particular, cyan FPs are mostly dimmer and less photostable than GFPs, whereas TagBFP is a fast-folding, bright and photostable variant. However, we note that the excitation spectrum of TagBFP is closer to the UV range compare to that of CFPs, which imposes a trade off between brightness and phototoxicity in time-lapse imaging. When a fourth color is required, one can add eqFP670 to the former combination (**Table 4**), whereas SBFP2 can supplement the latter. However, eqFP670 is a dimer, and thus often unsuitable for protein tagging, while SBFP2 shows a very low brightness, thus requiring either high expression levels, or strong excitation at around 380 nm.

For five-colors imaging, it is possible to combine SBFP2/mCerulean/mYPet/TagRFP-T/eqFP670 (see **Table 5**). Note that the above-mentioned limitations regarding the brightness of SBFP2 and the dimer property of eqFP670 are evident. The brightness in the blue/cyan spectrum can be improved by either engineering a bright FP that is more

TABLE 4 | Suggestions of four-colors combinations and excitation/emission filter sets.

Four-colors				
FPs	**TagBFP**	**sfGFP**	**mKO2**	**eqFP670**
Excitation filter (nm)	395–415	450–490	530–560	589–625
Beamsplitter (nm)	420	495	562	649
Emission filter (nm)	435–485	500–550	570–620	655–1200
Detected color	Blue	Green	Orange	Near-infrared

TABLE 5 | Suggestions of five-colors combinations and excitation/emission filter sets.

Five-colors					
FPs	**SBFP2**	**mCerulean**	**mYPet**	**TagRFP-T**	**eqFP670**
Excitation filter (nm)	353–391	426–446	490–510	530–560	589–625
Beamsplitter (nm)	400	455	515	562	649
Emission filter (nm)	410–460	460–500	520–550	570–620	655–1200
Detected color	Blue	Cyan	Yellow	Orange	Near-infrared

blue-shifted than TagBFP, or by engineering a cyan FP with a narrower excitation/emission spectrum that reduces spectral cross-talk with TagBFP. Regarding monomeric near-infrared or infrared FPs, there have been reports of newly evolved versions with an improved brightness (Yu et al., 2014). They were, however, mainly developed for deep-tissue imaging, and are yet to be tested for fluorescent tagging in bacteria for their brightness and folding properties.

The observed direct interaction between TagBFP and TagRFP-T prohibits the combination of these two proteins in the same cell. While the dimerization or aggregation of monomeric FPs at high concentration has been recognized (Snaith et al., 2010), the possibility of two monomeric proteins interacting with each other is not commonly tested. For example, by constructing a library of individual fluorescent fusions to the same protein in yeast, Lee et al. (2013) proposed the combination of the above two proteins for multi-color imaging. Our findings emphasize that the evolution of future fluorescent probes should take the interspecies interactions into account.

Our efforts to produce HU-2, FtsZ, and MinD fusion proteins for fully replacing the endogenous ones exemplify the multi-faceted challenge regarding fluorescent tagging, which naturally depend on the structural properties of the native proteins and the transcriptional/translational read-through at their genomic loci. The fact that a short TC peptide insertion into the unstructured region of FtsZ successfully rescued the lethal effect of Δ*ftsZ* but not in the case of sfGFP and TagRFP-T agrees with the finding that the unstructured region of the FtsZ has a limited tolerance to the size of a insertion (Buske and Levin, 2013). For visualizing MinD, we showed that it is possible to carry out N-terminal fusions at an endogenous genetic locus, albeit typically requiring independent sampling effort for individual genes due to the sensitivity of the transcription and translation read-through at the coding sequence close to the RBS (Kudla et al., 2009). Regarding a valid representation of a native localization pattern, a previous example showed that, while the super-fast folders sfGFP and mCherry were shown to be particularly advantageous in N-terminal or sandwich fusions and studies in periplasm (Bendezú et al., 2009; Dinh and Bernhardt, 2011; Wu et al., 2015), they were shown to form non-native foci when fused to ClpXP (Landgraf et al., 2012). Here we assessed the advantage of the recently developed FPs for studies in bacteria based on quantitative comparisons on a number of targets. We suggest that their performance as fluorescent tags be further tested in comparison to the native proteins in other future studies.

The expansion and detailed study of the FP reported in this paper will help imaging cell division in bacteria. The understanding of the processes involved in chromosome organization and cell division in bacteria has seen great development owing to the use of FPs. Current challenges in microscopy imaging of these processes lie in increasing the spatiotemporal resolution, uncovering the native behavior, and simultaneously inspecting the multiple interacting sub-components. We expect that our quantitative evaluation of novel FPs and the fusion strategies will facilitate tackling these challenges.

Author Contributions

FW, JK, and CD conceived the experiments, FW, EVR, and BVS did the experiments, FW analyzed the data, FW and CD wrote the paper.

Acknowledgments

We thank Louis Kuijpers, Margot Guurink, and Kevin Felter for their assistance in part of the strain construction. We thank Roger Tsien and Hugo Snippert for the pTagRFP-T plasmid, Dorus Gadella for the pSBFP2-C2 plasmid and the spectral information of SBFP2, Conrad Woldringh for HupA plasmids which we used for initial inspection of HU labels, Masaki Osawa for the JKD7-1 strain and pKD3ftsQAZ, Rodrigo Reyes-Lamothe, and David Sherratt for the strain RRL189 and a mYpet construct, Sriram Krishnan for a mYpet construct, Yu-Ling Shih for pFX40, and Piet de Boer for pFB174. This work was partly supported by the Netherlands Organisation for Scientific Research (NWO/OCW) as part of the Frontiers of Nanoscience program, NanoNextNL program 3B (FW), and European Research Council NanoforBio No. 247072 (CD).

Supplementary Material

The Supplementary Material for this article can be found online at: http://journal.frontiersin.org/article/10.3389/fmicb.2015.00607/abstract

References

Ai, H.-W., Shaner, N. C., Cheng, Z., Tsien, R. Y., and Campbell, R. E. (2007). Exploration of new chromophore structures leads to the identification of improved blue fluorescent proteins. *Biochemistry* 46, 5904–5910. doi: 10.1021/bi700199g

Alexeeva, S., Gadella, T. W. J., Verheul, J., Verhoeven, G. S., and Den Blaauwen, T. (2010). Direct interactions of early and late assembling division proteins in *Escherichia coli* cells resolved by FRET. *Mol. Microbiol.* 77, 384–398. doi: 10.1111/j.1365-2958.2010.07211.x

Ali Azam, T., Iwata, A., Nishimura, A., Ueda, S., and Ishihama, A. (1999). Growth phase-dependent variation in protein composition of the *Escherichia coli* nucleoid. *J. Bacteriol.* 181, 6361–6370.

Ausmees, N., Kuhn, J. R., and Jacobs-Wagner, C. (2003). The bacterial cytoskeleton: an intermediate filament-like function in cell shape. *Cell* 115, 705–713. doi: 10.1016/S0092-8674(03)00935-8

Bailey, M. W., Bisicchia, P., Warren, B. T., Sherratt, D. J., and Männik, J. (2014). Evidence for divisome localization mechanisms independent of the min system and SlmA in *Escherichia coli*. *PLoS Genet.* 10:e1004504. doi: 10.1371/journal.pgen.1004504

Bendezú, F. O., and de Boer, P. A. J. (2008). Conditional lethality, division defects, membrane involution, and endocytosis in mre and mrd shape mutants of *Escherichia coli*. *J. Bacteriol.* 190, 1792–1811. doi: 10.1128/jb.01322-07

Bendezú, F. O., Hale, C. A., Bernhardt, T. G., and De Boer, P. A. J. (2009). RodZ (YfgA) is required for proper assembly of the MreB actin cytoskeleton and cell shape in *E. coli*. *EMBO J.* 28, 193–204. doi: 10.1038/emboj.2008.264

Buske, P. J., and Levin, P. A. (2013). A flexible C-terminal linker is required for proper FtsZ assembly in vitro and cytokinetic ring formation in vivo. *Mol. Microbiol.* 89, 249–263. doi: 10.1111/mmi.12272

Chalfie, M., Tu, Y., Euskirchen, G., Ward, W., and Prasher, D. (1994). Green fluorescent protein as a marker for gene expression. *Science* 263, 802–805. doi: 10.1126/science.8303295

Charles, M., Pérez, M., Kobil, J. H., and Goldberg, M. B. (2001). Polar targeting of *Shigella* virulence factor IcsA in Enterobacteriacae and *Vibrio*. *Proc. Natl. Acad. Sci. U.S.A.* 98, 9871–9876. doi: 10.1073/pnas.171310498

Dai, K., and Lutkenhaus, J. (1991). ftsZ is an essential cell division gene in *Escherichia coli*. *J. Bacteriol.* 173, 3500–3506.

Dai, K., and Lutkenhaus, J. (1992). The proper ratio of FtsZ to FtsA is required for cell division to occur in *Escherichia coli*. *J. Bacteriol.* 174, 6145–6151.

Datsenko, K. A., and Wanner, B. L. (2000). One-step inactivation of chromosomal genes in *Escherichia coli* K-12 using PCR products. *Proc. Natl. Acad. Sci. U.S.A.* 97, 6640–6645. doi: 10.1073/pnas.120163297

de Boer, P. A. J., Crossley, R. E., and Rothfield, L. I. (1989). A division inhibitor and a topological specificity factor coded for by the minicell locus determine proper placement of the division septum in *E. coli*. *Cell* 56, 641–649. doi: 10.1016/0092-8674(89)90586-2

Dinh, T., and Bernhardt, T. G. (2011). Using superfolder green fluorescent protein for periplasmic protein localization studies. *J. Bacteriol.* 193, 4984–4987. doi: 10.1128/jb.00315-311

Domínguez-Escobar, J., Chastanet, A., Crevenna, A. H., Fromion, V., Wedlich-Söldner, R., and Carballido-López, R. (2011). Processive movement of MreB-associated cell wall biosynthetic complexes in bacteria. *Science* 333, 225–228. doi: 10.1126/science.1203466

Du, S., and Lutkenhaus, J. (2014). SlmA antagonism of FtsZ assembly employs a Two-pronged mechanism like MinCD. *PLoS Genet.* 10:e1004460. doi: 10.1371/journal.pgen.1004460

Erickson, H. P., Anderson, D. E., and Osawa, M. (2010). FtsZ in bacterial cytokinesis: cytoskeleton and force generator all in one. *Microbiol. Mol. Biol. Rev.* 74, 504–528. doi: 10.1128/MMBR.00021-10

Garner, E. C., Bernard, R., Wang, W., Zhuang, X., Rudner, D. Z., and Mitchison, T. (2011). Coupled, circumferential motions of the cell wall synthesis machinery and MreB filaments in *B. subtilis*. *Science* 333, 222–225. doi: 10.1126/science.1203285

Griffin, B. A., Adams, S. R., and Tsien, R. Y. (1998). Specific covalent labeling of recombinant protein molecules inside live cells. *Science* 281, 269–272. doi: 10.1126/science.281.5374.269

Hayashi, K., Morooka, N., Yamamoto, Y., Fujita, K., Isono, K., Choi, S., et al. (2006). Highly accurate genome sequences of *Escherichia coli* K-12 strains MG1655 and W3110. *Mol. Syst. Biol.* 2, 2006.0007. doi: 10.1038/msb4100049

Hol, F. J. H., and Dekker, C. (2014). Zooming in to see the bigger picture: microfluidic and nanofabrication tools to study bacteria. *Science* 346:1251821. doi: 10.1126/science.1251821

Hu, Z., and Lutkenhaus, J. (1999). Topological regulation of cell division in *Escherichia coli* involves rapid pole to pole oscillation of the division inhibitor MinC under the control of MinD and MinE. *Mol. Microbiol.* 34, 82–90. doi: 10.1046/j.1365-2958.1999.01575.x

Jones, L. J. F., Carballido-López, R., and Errington, J. (2001). Control of cell shape in bacteria: helical, actin-like filaments in *Bacillus subtilis*. *Cell* 104, 913–922. doi: 10.1016/S0092-8674(01)00287-2

Kitagawa, M., Ara, T., Arifuzzaman, M., Ioka-Nakamichi, T., Inamoto, E., Toyonaga, H., et al. (2006). Complete set of ORF clones of *Escherichia coli* ASKA library (a complete set of *E. coli K*-12 ORF archive): unique resources for biological research. *DNA Res.* 12, 291–299. doi: 10.1093/dnares/dsi012

Kremers, G.-J., Goedhart, J., Van Den Heuvel, D. J., Gerritsen, H. C., and Gadella, T. W. J. (2007). Improved green and blue fluorescent proteins for expression in bacteria and mammalian cells. *Biochemistry* 46, 3775–3783. doi: 10.1021/bi0622874

Kremers, G.-J., Goedhart, J., Van Munster, E. B., and Gadella, T. W. J. (2006). Cyan and yellow super fluorescent proteins with improved brightness, protein folding, and FRET förster radius. *Biochemistry* 45, 6570–6580. doi: 10.1021/bi0516273

Kudla, G., Murray, A. W., Tollervey, D., and Plotkin, J. B. (2009). Coding-sequence determinants of gene expression in *Escherichia coli*. *Science* 324, 255–258. doi: 10.1126/science.1170160

Kuwada, N. J., Traxler, B., and Wiggins, P. A. (2015). Genome-scale quantitative characterization of bacterial protein localization dynamics throughout the cell cycle. *Mol. Microbiol.* 95, 64–79. doi: 10.1111/mmi.12841

Landgraf, D., Okumus, B., Chien, P., Baker, T. A., and Paulsson, J. (2012). Segregation of molecules at cell division reveals native protein localization. *Nat Meth.* 9, 480–482. doi: 10.1038/nmeth.1955

Lau, I. F., Filipe, S. R., Søballe, B., Økstad, O.-A., Barre, F.-X., and Sherratt, D. J. (2003). Spatial and temporal organization of replicating *Escherichia coli* chromosomes. *Mol. Microbiol.* 49, 731–743. doi: 10.1046/j.1365-2958.2003.03640.x

Lee, S., Lim, W. A., and Thorn, K. S. (2013). Improved blue, green, and red fluorescent protein tagging vectors for *S. cerevisiae*. *PLoS ONE* 8:e67902. doi: 10.1371/journal.pone.0067902

Li, G., and Young, K. D. (2012). Isolation and identification of new inner membrane-associated proteins that localize to cell poles in *Escherichia coli*. *Mol. Microbiol.* 84, 276–295. doi: 10.1111/j.1365-2958.2012.08021.x

Lindner, A. B., Madden, R., Demarez, A., Stewart, E. J., and Taddei, F. (2008). Asymmetric segregation of protein aggregates is associated with cellular aging and rejuvenation. *Proc. Natl. Acad. Sci. U.S.A.* 105, 3076–3081. doi: 10.1073/pnas.0708931105

Ma, X., Ehrhardt, D. W., and Margolin, W. (1996). Colocalization of cell division proteins FtsZ and FtsA to cytoskeletal structures in living *Escherichia coli* cells by using green fluorescent protein. *Proc. Natl. Acad. Sci. U.S.A.* 93, 12998–13003. doi: 10.1073/pnas.93.23.12998

Männik, J., Wu, F., Hol, F. J. H., Bisicchia, P., Sherratt, D. J., Keymer, J. E., et al. (2012). Robustness and accuracy of cell division in *Escherichia coli* in diverse cell shapes. *Proc. Natl. Acad. Sci. U.S.A.* 109, 6957–6962. doi: 10.1073/pnas.1120854109

Morozova, K. S., Piatkevich, K. D., Gould, T. J., Zhang, J., Bewersdorf, J., and Verkhusha, V. V. (2010). Far-Red fluorescent protein excitable with red lasers for flow cytometry and superresolution STED nanoscopy. *Biophys. J.* 99, L13–L15. doi: 10.1016/j.bpj.2010.04.025

Nguyen, A. W., and Daugherty, P. S. (2005). Evolutionary optimization of fluorescent proteins for intracellular FRET. *Nat. Biotechnol.* 23, 355–360. doi: 10.1038/nbt1066

Oliva, M. A., Cordell, S. C., and Lowe, J. (2004). Structural insights into FtsZ protofilament formation. *Nat. Struct. Mol. Biol.* 11, 1243–1250. doi: 10.1038/nsmb855

Osawa, M., and Erickson, H. P. (2005). Probing the domain structure of FtsZ by random truncation and insertion of GFP. *Microbiology* 151, 4033–4043. doi: 10.1099/mic.0.28219-0

Pedelacq, J.-D., Cabantous, S., Tran, T., Terwilliger, T. C., and Waldo, G. S. (2006). Engineering and characterization of a superfolder green fluorescent protein. *Nat. Biotechnol.* 24, 79–88. doi: 10.1038/nbt1172

Prasher, D. C., Eckenrode, V. K., Ward, W. W., Prendergast, F. G., and Cormier, M. J. (1992). Primary structure of the *Aequorea victoria* green-fluorescent protein. *Gene* 111, 229–233. doi: 10.1016/0378-1119(92)90691-H

Raskin, D. M., and de Boer, P. A. J. (1997). The MinE ring: an FtsZ-Independent cell structure required for selection of the correct division site in *E. coli*. *Cell* 91, 685–694. doi: 10.1016/S0092-8674(00)80455-9

Raskin, D. M., and de Boer, P. A. J. (1999). Rapid pole-to-pole oscillation of a protein required for directing division to the middle of *Escherichia coli*. *Proc. Natl. Acad. Sci. U.S.A.* 96, 4971–4976. doi: 10.1073/pnas.96.9.4971

Reyes-Lamothe, R., Possoz, C., Danilova, O., and Sherratt, D. J. (2008). Independent positioning and action of *Escherichia coli* replisomes in live cells. *Cell* 133, 90–102. doi: 10.1016/j.cell.2008.01.044

Rizzo, M. A., Springer, G. H., Granada, B., and Piston, D. W. (2004). An improved cyan fluorescent protein variant useful for FRET. *Nat. Biotechnol.* 22, 445–449. doi: 10.1038/nbt945

Shaner, N. C., Campbell, R. E., Steinbach, P. A., Giepmans, B. N. G., Palmer, A. E., and Tsien, R. Y. (2004). Improved monomeric red, orange and yellow

fluorescent proteins derived from *Discosoma* sp. red fluorescent protein. *Nat. Biotechnol.* 22, 1567–1572. doi: 10.1038/nbt1037

Shaner, N. C., Lin, M. Z., Mckeown, M. R., Steinbach, P. A., Hazelwood, K. L., Davidson, M. W., et al. (2008). Improving the photostability of bright monomeric orange and red fluorescent proteins. *Nat. Methods* 5, 545–551. doi: 10.1038/nmeth.1209

Shcherbo, D., Murphy, C. S., Ermakova, G. V., Solovieva, E. A., Chepurnykh, T. V., Shcheglov, A. S., et al. (2009). Far-red fluorescent tags for protein imaging in living tissues. *Biochem. J.* 418, 567–574. doi: 10.1042/BJ20081949

Shcherbo, D., Shemiakina, I. I., Ryabova, A. V., Luker, K. E., Schmidt, B. T., Souslova, E. A., et al. (2010). Near-infrared fluorescent proteins. *Nat. Methods* 7, 827–829. doi: 10.1038/nmeth.1501

Shen, B., and Lutkenhaus, J. (2009). The conserved C-terminal tail of FtsZ is required for the septal localization and division inhibitory activity of MinC(C)/MinD. *Mol. Microbiol.* 72, 410–424. doi: 10.1111/j.1365-2958.2009.06651.x

Shih, Y.-L., Fu, X., King, G. F., Le, T., and Rothfield, L. (2002). Division site placement in *E.coli*: mutations that prevent formation of the MinE ring lead to loss of the normal midcell arrest of growth of polar MinD membrane domains. *EMBO J.* 21, 3347–3357. doi: 10.1093/emboj/cdf323

Shih, Y.-L., Kawagishi, I., and Rothfield, L. (2005). The MreB and Min cytoskeletal-like systems play independent roles in prokaryotic polar differentiation. *Mol. Microbiol.* 58, 917–928. doi: 10.1111/j.1365-2958.2005.04841.x

Snaith, H. A., Anders, A., Samejima, I., and Sawin, K. E. (2010). "New and old reagents for fluorescent protein tagging of microtubules in fission yeast: experimental and critical evaluation," in *Methods in Cell Biology*, Chap. 9, eds C. Lynne and T. Phong (Waltham, MA: Academic Press), 147–172. doi: 10.1016/s0091-679x(10)97009-x

Sourjik, V., and Berg, H. C. (2000). Localization of components of the chemotaxis machinery of *Escherichia coli* using fluorescent protein fusions. *Mol. Microbiol.* 37, 740–751. doi: 10.1046/j.1365-2958.2000.02044.x

Subach, O. M., Gundorov, I. S., Yoshimura, M., Subach, F. V., Zhang, J., Grüenwald, D., et al. (2008). Conversion of red fluorescent protein into a bright blue probe. *Chem.Bbiol.* 15, 1116–1124. doi: 10.1016/j.chembiol.2008.08.006

Sun, Y., Booker, C. F., Kumari, S., Day, R. N., Davidson, M., and Periasamy, A. (2009). Characterization of an orange acceptor fluorescent protein for sensitized spectral fluorescence resonance energy transfer microscopy using a white-light laser. *J. Biomed. Opt.* 14:054009. doi: 10.1117/1.3227036

Takeuchi, S., Diluzio, W. R., Weibel, D. B., and Whitesides, G. M. (2005). Controlling the shape of filamentous cells of *Escherichia coli*. *Nano Lett.* 5, 1819–1823. doi: 10.1021/nl0507360

Taniguchi, Y., Choi, P. J., Li, G.-W., Chen, H., Babu, M., Hearn, J., et al. (2010). Quantifying *E. coli* proteome and transcriptome with single-molecule sensitivity in single cells. *Science* 329, 533–538. doi: 10.1126/science.1188308

van Teeffelen, S., Wang, S., Furchtgott, L., Huang, K. C., Wingreen, N. S., Shaevitz, J. W., et al. (2011). The bacterial actin MreB rotates, and rotation depends on cell-wall assembly. *Proc. Natl. Acad. Sci. U.S.A.* 108, 15822–15827. doi: 10.1073/pnas.1108999108

Wang, P., Robert, L., Pelletier, J., Dang, W. L., Taddei, F., Wright, A., et al. (2010). Robust growth of *Escherichia coli*. *Curr. Biol.* 20, 1099–1103. doi: 10.1016/j.cub.2010.04.045

Werner, J. N., Chen, E. Y., Guberman, J. M., Zippilli, A. R., Irgon, J. J., and Gitai, Z. (2009). Quantitative genome-scale analysis of protein localization in an asymmetric bacterium. *Proc. Natl. Acad. Sci. U.S.A.* 106, 7858–7863. doi: 10.1073/pnas.0901781106

Wery, M., Woldringh, C. L., and Rouviere-Yaniv, J. (2001). HU-GFP and DAPI co-localize on the *Escherichia coli* nucleoid. *Biochimie* 83, 193–200. doi: 10.1016/S0300-9084(01)01254-8

Wu, F., Van Schie, B., Keymer, J. E., and Dekker, C. (2015). Symmetry and scale orient Min protein patterns in bacterial shape sculptures. *Nat. Nanotechnol.* doi: 10.1038/nnano.2015.126

Yu, D., Gustafson, W. C., Han, C., Lafaye, C., Noirclerc-Savoye, M., Ge, W.-P., et al. (2014). An improved monomeric infrared fluorescent protein for neuronal and tumour brain imaging. *Nat. Commun.* 5:3626. doi: 10.1038/ncomms4626

Conflict of Interest Statement: The authors declare that the research was conducted in the absence of any commercial or financial relationships that could be construed as a potential conflict of interest.

Copyright © 2015 Wu, Van Rijn, Van Schie, Keymer and Dekker. This is an open-access article distributed under the terms of the Creative Commons Attribution License (CC BY). The use, distribution or reproduction in other forums is permitted, provided the original author(s) or licensor are credited and that the original publication in this journal is cited, in accordance with accepted academic practice. No use, distribution or reproduction is permitted which does not comply with these terms.

frontiers in Microbiology

REVIEW
published: 14 April 2015
doi: 10.3389/fmicb.2015.00306

Spatial coordination between chromosomes and cell division proteins in *Escherichia coli*

Jaan Männik[1,2]* *and Matthew W. Bailey*[1]

[1] Department of Physics and Astronomy, University of Tennessee, Knoxville, TN, USA, [2] Department of Biochemistry and Molecular and Cellular Biology, University of Tennessee, Knoxville, TN, USA

To successfully propagate, cells need to coordinate chromosomal replication and segregation with cell division to prevent formation of DNA-less cells and cells with damaged DNA. Here, we review molecular systems in *Escherichia coli* that are known to be involved in positioning the divisome and chromosome relative to each other. Interestingly, this well-studied micro-organism has several partially redundant mechanisms to achieve this task; none of which are essential. Some of these systems determine the localization of the divisome relative to chromosomes such as SlmA-dependent nucleoid occlusion, some localize the chromosome relative to the divisome such as DNA translocation by FtsK, and some are likely to act on both systems such as the Min system and newly described Ter linkage. Moreover, there is evidence that *E. coli* harbors other divisome-chromosome coordination systems in addition to those known. The review also discusses the minimal requirements of coordination between chromosomes and cell division proteins needed for cell viability. Arguments are presented that cells can propagate without any dedicated coordination between their chromosomes and cell division machinery at the expense of lowered fitness.

Keywords: nucleoid, divisome, Z-ring, cell division, *Escherichia coli*, protocell, nucleoid occlusion

OPEN ACCESS

Edited by:
Julie A. Maupin-Furlow, University of Florida, USA

Reviewed by:
Alex Dajkovic, Institut National de la Recherche Agronomique, France
Harold Erickson, Duke University, USA
Piet A. De Boer, Case Western Reserve University, USA

***Correspondence:**
Jaan Männik, Department of Physics and Astronomy, University of Tennessee, 401 Nielsen Physics Building, Knoxville, TN 37996, USA
jmannik@utk.edu

Specialty section:
This article was submitted to Microbial Physiology and Metabolism, a section of the journal Frontiers in Microbiology

Received: *27 January 2015*
Accepted: *27 March 2015*
Published: *14 April 2015*

Citation:
Männik J and Bailey MW (2015) Spatial coordination between chromosomes and cell division proteins in Escherichia coli. Front. Microbiol. 6:306. doi: 10.3389/fmicb.2015.00306

Introduction

In most bacteria, the main macromolecular structure that is responsible for coordinating cell division with other cellular processes, including replication and segregation of chromosomes, is the Z-ring (Margolin, 2005; Adams and Errington, 2009; de Boer, 2010; Lutkenhaus et al., 2012). The Z-ring is organized by linear FtsZ-(proto)filaments that in *Escherichia coli* are anchored to the cell plasma membrane by FtsA and ZipA linker proteins. The assembly and disassembly of protofilaments can happen rapidly on the time-scale of seconds (Erickson et al., 2010). This dynamic nature of the Z-ring makes it susceptible to regulation by numerous protein factors that can tip the balance between the assembly and disassembly of filaments.

Formation of the Z-ring is the first step in bacterial cytokinesis. Once the Z-ring has formed it becomes a scaffold for over 30 other proteins that form a divisome complex (Liu et al., 2015). The divisome carries out septal envelope synthesis that leads to the pinching off of one daughter cell from the other. In wild-type *E. coli*, pinching off occurs very accurately in the middle of the mother cell between two separated daughter nucleoids (Trueba, 1982; Den Blaauwen et al., 1999; Männik et al., 2012). In mutant cells, the inaccurate placement of the Z-ring relative to nucleoids can lead to cells lacking chromosomal DNA completely, i.e., minicells (Adler et al., 1967) or to cells that have an incomplete set of genetic material, i.e., have guillotined nucleoids (Niki et al., 1991;

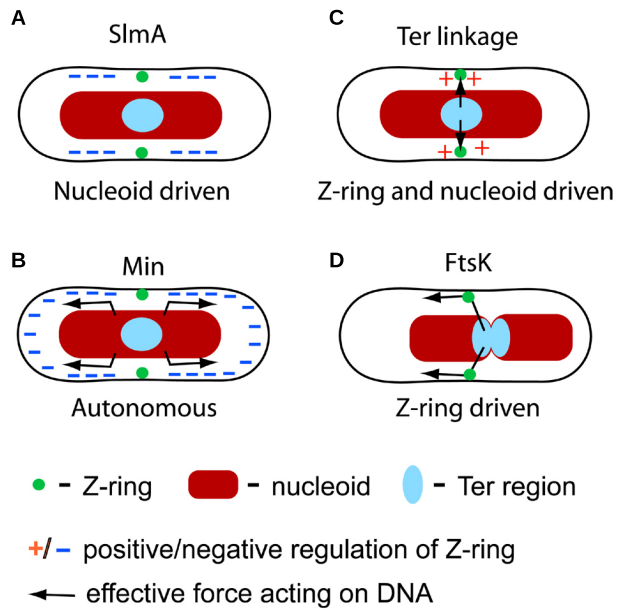

FIGURE 1 | Four molecular mechanisms that have been identified in spatial coordination between the chromosome and divisome in *E. coli*. **(A)** SlmA-mediated nucleoid occlusion is a nucleoid driven mechanism which negatively regulates Z-ring formation in the vicinity of the chromosome except at the replication terminus region. **(B)** The Min system is independent of the nucleoid but it has been implicated in segregating and separating nucleoids. The Min system negatively regulates Z-ring formation at cell poles. **(C)** The Ter linkage is involved in determining the location of the Z-ring by a positive regulatory mechanism. The linkage is also involved in holding the Ter region fixed relative to the divisome. **(D)** FtsK translocase pumps DNA across the divisome in a directed manner leading to repositioning of chromosomes.

Cook and Rothfield, 1999; Hendricks et al., 2000). *E. coli* cells have developed a number of molecular systems to prevent this outcome. These systems include nucleoid occlusion (NO), the Min system, the Ter linkage, and FtsK translocase (**Figure 1**). There is evidence that other mechanisms may also be involved. Here, we will review the aforementioned known molecular systems and discuss some hypothetical ones that have been implicated in spatially coordinating the divisome and chromosome. We will limit our discussion to *E. coli*; coordination systems in other bacterial species show divergent molecular origins (Adams et al., 2014; Monahan et al., 2014). We will expand our scope in the last part of this review where we will discuss the minimal requirements for the coordination between cell division proteins and chromosomes that are necessary for the survival of any cell.

Nucleoid Occlusion

The early discussion of coordination between cell division and chromosome replication/segregation centered on the idea of NO (Hussain et al., 1987; Mulder and Woldringh, 1989; Woldringh et al., 1990; Wu and Errington, 2011). The idea of NO is based on observations that constrictions in dividing cells were excluded from the regions occupied by the nucleoids. Woldringh and others proposed that the inhibitory effect of the nucleoid is mediated by short range interactions stemming from the nucleoid which are related to transcription and translation (Woldringh et al., 1991). Zaritsky and Woldringh (2003) further refined the idea proposing that molecular crowding of the inner surface of the plasma membrane in the vicinity of the nucleoid was responsible for this inhibitory effect. These authors hypothesized that crowding results from the transertion process. In transertion, nascent membrane proteins are synthesized concurrently with yet ongoing transcription of their mRNA and are inserted into the cell plasma membrane while their translation occurs (Norris, 1995; Woldringh, 2002). Altogether, this process links DNA to the inner membrane by a molecular chain that includes RNA polymerase, nascent mRNA, ribosome, and nascent protein. The nascent protein is hypothesized to insert itself into the plasma membrane by its N-terminal domain while still being translated. Taking that approximately 1/3 of all proteins in *E. coli* are membrane proteins, the number of transertional linkages should be considerable at any given point of the cell cycle and could lead to significant membrane crowding (Woldringh, 2002). Zaritsky and Woldringh (2003) hypothesized that crowding could be lower in membrane areas adjacent to the replication terminus region because of the smaller density of highly expressed membrane targeted genes. This assumption suggests that Z-ring assembly is least inhibited in membrane regions adjacent to the replication terminus in accord with experimental observations.

The effect of transertion-related crowding on Z-ring formation was experimentally studied (Sun and Margolin, 2004). These authors observed that severing transertional linkages by blocking transcription with rifampicin treatment indeed allowed Z-rings to form over the nucleoids. Conversely, severing transertional linkages by blocking translation with chloramphenicol caused nucleoid compaction and exclusion of Z-rings from the membrane regions in the proximity of nucleoids. Furthermore, in SecA(ts) cells where protein insertion was thermally inactivated, the NO effect was still present even though the nucleoids did not segregate properly. The two latter observations therefore were not in accord with the transertion-based crowding ideas. To explain their data, the authors concluded that the nucleoid structure and packing density most likely plays a role in excluding the Z-rings from the regions adjacent to the nucleoid. Z-rings could localize "over" the expanded nucleoids but not over the compact ones. This idea has been supported by other measurements where nucleoid packing was altered (Sun and Margolin, 1998). So far, it remains unclear how the nucleoid packing density can influence Z-ring positioning especially during chloramphenicol treatment when the compacted nucleoid resides far from the cell membrane. Indirect effects of chloramphenicol and rifampicin treatment in these experiments could not be ruled out. In that light, more experiments are warranted to explore further the role of membrane crowding on Z-ring positioning.

SlmA Mediated Nucleoid Occlusion

A major development in the understanding of NO came with the discovery of the SlmA protein from a synthetically lethal screen (Bernhardt and de Boer, 2005). Cells that lacked both *slmA* and *minCDE* were not able to divide in rich medium and gave rise to filamentous cells, indicating a defect in septation. The same

authors also observed that some Z-rings could localize over unsegregated nucleoids in *slmA minCDE* cells suggesting SlmA played a role in Z-ring positioning. This role was also visible from studies of *slmA dnaA* cells in rich medium where a closing septum appeared in the middle of the nucleoid mass presumably because of the lack of a functional NO system (Bernhardt and de Boer, 2005). Spatial positioning of the Z-ring by SlmA is thought to result from a specific binding pattern of SlmA on *E. coli* chromosomal DNA. SlmA specific binding sites are distributed over the chromosome with a notable exception at the replication terminus region (Cho et al., 2011; Tonthat et al., 2011). Such a distribution, together with the inhibitory action of SlmA, can generate the NO effect, i.e., Z-rings do not assemble over chromosomal DNA except near the replication terminus region. Note that the replication terminus region, which positions itself at mid-cell in the later part of cell cycle, is in the vicinity of the membrane region where the Z-ring typically assembles (**Figure 1A**).

Two possible molecular mechanisms by which SlmA inhibits the formation of the Z-ring have been proposed. One model posits that SlmA causes depolymerization of FtsZ protofilaments (Cho et al., 2011; Cho and Bernhardt, 2013; Du and Lutkenhaus, 2014). *In vitro* assays show that depolymerization of FtsZ only occurs at a significant rate when SlmA is bound to DNA in its specific binding sites (Cho et al., 2011). Consequently, depolymerization of protofilaments takes place everywhere in the nucleoid except at the replication terminus region. Further characterization of the depolymerization process shows that it occurs in two steps (Du and Lutkenhaus, 2014). In the first step, DNA-bound SlmA attaches to the highly conserved C-terminal tail of FtsZ. In this binding, SlmA competes with other FtsZ regulators (MinC, ClpX) and interaction partners (ZipA, FtsA, ZapD). In the second step, further interactions occur that lead to protofilament breakage. The resulting breakage appears to minimally affect the GTPase activity of FtsZ (Cho et al., 2011).

In an alternative model, it was proposed that DNA-bound SlmA does not depolymerize protofilaments but instead captures them and renders them incapable of Z-ring formation (Tonthat et al., 2011, 2013). The authors showed that SlmA binds to its specific binding sites as a dimer of dimers. Once the initial nucleation has occurred, the dimers can cooperatively spread on DNA. Tonthat et al. (2011, 2013) proposed that these higher order SlmA structures capture FtsZ filaments. However, so far microscopy of FtsZ fusion proteins has not confirmed any co-localization between FtsZ protofilaments and extended SlmA structures within the cell.

While characterization of SlmA at the molecular level has been extensive, understanding its role and function at the cellular level is still limited. How could SlmA that is bound to chromosomal DNA inhibit Z-ring formation at the cell membrane? Models described in (Du and Lutkenhaus, 2014) and (Tonthat et al., 2013), although different in their interaction mechanism between SlmA and FtsZ, both assume that DNA-bound SlmA comes into proximity of the cell membrane to influence the localization of the Z-ring. However, DNA-bound SlmA within the nucleoid makes only limited contacts with the membrane and therefore would interact infrequently with membrane-bound FtsZ. Transertional linkages may help to facilitate these contacts (Tonthat et al., 2013) but the existing microscopy data indicates that SlmA is localized within the nucleoid rather than in the vicinity of the cell surface (Bernhardt and de Boer, 2005). Alternatively, Bernhardt and de Boer (2005) proposed that depolymerization of protofilaments can happen within the nucleoid. The latter mechanism would lead only to a weak site-selective effect of SlmA on Z-ring localization. Existing experimental data (Männik et al., 2012) indeed shows that SlmA does not convey a strong site-selective effect on Z-ring location in fast growth conditions. How effectively SlmA inhibits Z-ring formation in various growth conditions remains yet to be characterized.

Although SlmA mediated NO has received the most attention recently, there is strong evidence that additional mechanisms beyond SlmA can lead to a NO effect in *E. coli*. It was observed that cell division proteins are positioned in accordance with NO in cells lacking SlmA. The NO effect was distinctly present even when the shapes and sizes of these cells were strongly perturbed (Männik et al., 2012). It was also observed that a replication-inhibited and unsegregated nucleoid at mid-cell blocks Z-ring formation independent of the SlmA and SOS response (Cambridge et al., 2014). How these inhibitory effects of nucleoids are mediated at a molecular level is currently not known, but from these data it is clear that the SlmA-related mechanism is not the only one that realizes NO in *E. coli* cells.

The Min System

The three Min proteins, MinC, MinD, and MinE, form a well-understood geometric positioning system for the Z-ring in *E. coli* that defines the cell's geometric middle and prevents polar septations (Lutkenhaus, 2007, 2012; Shapiro et al., 2009; Moseley and Nurse, 2010). Fluorescent tagging of Min proteins has shown that MinC, MinD, and MinE exhibit remarkable oscillatory behavior in *E. coli* cells, moving back and forth between the two poles with a typical oscillatory period from 30 s to 1 min (Raskin and de Boer, 1999). Of these three proteins, only MinD and MinE are necessary to set up the oscillations while MinC, which follows and binds to MinD, acts as an inhibitor for Z-ring formation (Lutkenhaus, 2007). MinC binding to membrane-attached MinD activates its inhibitory function (Lutkenhaus, 2012). Due to the oscillations, the destabilizing effect of MinC on Z-ring formation is the strongest at the cell poles, where the time-averaged concentration of MinD-bound MinC is the highest. This negative regulation prevents minicelling at the poles. However, the Min system appears also to play a role in the precise localization of the Z-ring at midcell (Guberman et al., 2008).

In its inhibitory action, MinC resembles SlmA. MinC also binds to the conserved C-terminal domain of FtsZ and its subsequent interactions lead to breakage of the FtsZ polymer. GTPase activity of FtsZ is required for the MinC mediated breakage but at the same time MinC does not lead to increased GTPase activity of FtsZ (Dajkovic et al., 2008; Shen and Lutkenhaus, 2010). Measurements using *in vivo* reconstituted assays show how these two perhaps contradictory findings can be reconciled (Arumugam et al., 2014). Arumugam et al. (2014) propose that MinC dimers cap FtsZ filament ends. They also observe that FtsZ filaments lose monomers throughout its length. Such loss leads to breaks and gaps in the filament. In the absence of MinC these breaks could be annealed

by the addition of new monomers but in the presence of MinC capping this would not occur and filaments become destabilized. The same authors also propose that MinC binding to FtsZ hinders protofilament bundling, which leads to further weakening of the Z-ring. Because of the several observed similarities between SlmA and MinC, it is tempting to speculate that a similar scenario also can be realized when SlmA depolymerizes FtsZ filaments.

Extensive modeling has been carried out to capture the oscillatory behavior of the Min system based on continuum models and stochastic simulations. For a cross-section of this work spanning from early to current models see (Meinhardt and de Boer, 2001; Kruse, 2002; Huang et al., 2003; Fange and Elf, 2006; Kerr et al., 2006; Halatek and Frey, 2012; Bonny et al., 2013). The oscillatory movement of MinD and MinE in the cell emerges in all of these models due to the ATP and MinE-modulated attachment of MinD to the plasma membrane. The computational models are able to semi-qualitatively reproduce experimentally measured oscillation patterns and oscillation periods. Although different models introduce slight variations in reactions occurring between MinD and MinE, they all can be categorized in mathematical terms as reaction-diffusion systems that exhibit Turing instability (Turing, 1952). Arguably the Min system in *E. coli* is the best studied example where the Turning instability mechanism leads to the formation of a dynamic pattern in a living organism.

The Min system functions autonomously from the nucleoid as shown convincingly in *in vitro* reconstituted assays (Loose et al., 2008; Ivanov and Mizuuchi, 2010; Schweizer et al., 2012). The same conclusion also can be drawn based on experiments with cells that lack nucleoids but have a functioning Min system. Remarkably, in these cells the Z-ring also can be placed relatively accurately in the middle of the cell (Sun and Margolin, 1998; Yu and Margolin, 1999; Pazos et al., 2014). Taking that the two daughter chromosomes separate from each other approximately at mid-cell in normal growth conditions, this system alone is perhaps sufficient to coordinate chromosomes and cell division proteins in *E. coli*. However, if the cell shape becomes aberrant (Männik et al., 2012) then the Min system and NO can define different locations for the cell division plane. In conflicting cases, it appears that the NO mechanism dominates over the Min system (Männik et al., 2012).

While the Min system is not directly involved in coordinating the Z-ring and chromosomes, an indirect involvement is possible (**Figure 1B**). Several authors have pointed out that deletion of the Min system leads to a small defect in chromosome segregation and in the separation of daughter nucleoids in *E. coli* (Mulder et al., 1990; Akerlund et al., 2002; Di Ventura et al., 2013; Jia et al., 2014). Di Ventura et al. (2013) have proposed that MinD, which is a homolog of ParA, binds to DNA. These authors propose that MinD oscillation and DNA binding provides a Brownian-ratchet mechanism for DNA segregation and separation (Di Ventura et al., 2013). Further experimental support to this interesting idea is still warranted.

The Ter Linkage

The Min system and NO are negative regulators for cell division proteins, i.e., they inhibit Z-ring formation in certain locations of the cell. Recent research strongly suggests that there exists also a positive regulation mechanism in *E. coli*, which guides cell division proteins toward the replication terminus region of the chromosome (Bailey et al., 2014; **Figure 1C**). The presence of a positive regulation mechanism became evident in studies of cells that lacked both the Min system and SlmA-mediated NO. In these cells, the Z-ring positioned itself over the centers of segregating nucleoids instead of localizing at the cell poles or gaps between the nucleoids. The effect was particularly striking in cephalexin-treated cells that show many well separated nucleoids. Time-lapse measurements of *slmA min* cells showed that formation of the Z-ring commenced shortly after the arrival of the replication terminus region to the nucleoid center, even though transient associations of the Z-ring and the replication terminus region could be seen before the replication terminus centralized.

A different piece of evidence shows that the replication terminus region is anchored to the Z-ring (Espeli et al., 2012). The replication terminus region of *E. coli* chromosome forms a compact entity, termed the Ter macrodomain, which is organized by MatP proteins (Mercier et al., 2008; Dupaigne et al., 2012). MatP, like SlmA, is a DNA-binding protein. Interestingly, binding sites of these two proteins in *E. coli* chromosomal DNA are completely complementary—MatP specific binding sites, 23 total, can be found only in an 800 kb stretch around the *dif* sequence (located at 32.24′) in the replication terminus region while SlmA binding sites are located, essentially, everywhere else. Work by Espeli et al. (2012) has shown that the anchoring of the Ter region to the Z-ring occurs due to the MatP C-terminal interaction with the Z-ring associated protein ZapB (Espeli et al., 2012), which indirectly interacts with FtsZ through ZapA (Galli and Gerdes, 2010). The anchor, which we refer as the Ter linkage, connects the replication terminus region to the Z-ring through a chain of DNA-MatP-ZapB-ZapA-FtsZ. Only the nearest components in the Ter linkage are thought to interact (**Figure 2A**). The function of the linkage is not fully established but it appears to guarantee that the positioning of the chromosomes relative to the divisome does not change after the Z-ring has formed.

There are thus two sequential processes occurring that coordinate the Z-ring and the replication terminus region (**Figure 2B**). First, a signal from the replication terminus region promotes assembly of the Z-ring in its immediate vicinity. Second, after the Z-ring has formed the replication terminus region becomes linked to the Z-ring by a connection involving MatP, ZapB, and ZapA. Interestingly, ZapA and ZapB, and to lesser degree MatP, are also needed in the first step (Bailey et al., 2014). How exactly MatP, ZapB, and ZapA promote Z-ring formation in the vicinity of the Ter macrodomain is not known. It is possible that positive regulation itself is not a direct consequence of MatP, ZapA, and ZapB but results from some other molecular system that associates with the replication terminus region. MatP, ZapA, and ZapB may help to reinforce this signal by linking the source of the signal to the nascent Z-ring and strengthening its effect. At this point, the hypothesis has not been tested and the mechanistic details of the positive regulation are yet to be established.

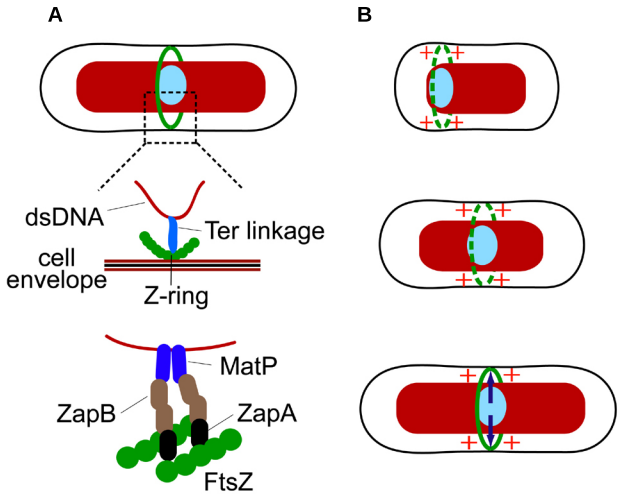

FIGURE 2 | The Ter linkage coordinates localization of both the Z-ring and the Ter macrodomain region of the chromosome. (A) A putative connection between the DNA in the Ter region and the Z-ring via the Ter linkage. Schematics from top to bottom show progressive zoom-ins of the Ter region (light blue ellipse) and the Z-ring (green circles). ZapB in the linkage could form filaments or even filament networks. **(B)** Cell-cycle dependent processes involving the Ter linkage. Top: in the beginning of cell cycle the Ter macrodomain region is localized at the nucleoid periphery close to the new pole of the cell. Positive regulation from the Ter region promotes transient Z-rings to form in its vicinity. Middle: as the cell cycle progresses, the Ter region moves to the center of the nucleoid. It has been hypothesized that the motion is related to replication of the Ter region (Espeli et al., 2012). The positive signal from the Ter region continues to promote Z-ring formation in its vicinity. Bottom: as the Z-ring fully forms the Ter region becomes attached to the Z-ring through a link involving MatP, ZapB, and ZapA (indicated by arrows).

Effect of the Divisome on the Nucleoid—the FtsK Translocase

So far the discussion has focused on mechanisms where the nucleoid directly or indirectly determines the localization of cell division proteins. The opposite processes, in which the divisome affects positioning of the nucleoid, or at least part of it, are also present in *E. coli*. The Ter linkage, discussed in previous section, is one example where the divisome exerts its effect on the nucleoid. However, the Ter linkage appears to maintain rather than to actively re-arrange the chromosomal organization and positioning. Contrarily, DNA translocase FtsK (Begg et al., 1995) allows the divisome to actively re-arrange the *E. coli* chromosome in an ATP-dependent manner (**Figure 1D**). As is the case with the Ter linkage, the activity of FtsK seems to affect the Ter region of the chromosome (Deghorain et al., 2011; Stouf et al., 2013). Since the Ter region comprises about 20% of the total *E. coli* chromosome its re-arrangements have global implications to chromosome organization.

FtsK translocation activity leads to positioning of chromosomal *dif* site in the divisome during late stages of the cell cycle. The *dif* site is a 28 bp sequence in the replication terminus region where chromosome dimers are resolved by the XerCD recombinase. FtsK is capable of pumping DNA on both chromosome arms toward the *dif* site. The directionality in pumping is due to KOPS (FtsK orienting/polarizing sequence), which are oriented in opposite directions on the left and right arms of the *E. coli* chromosome. FtsK loads onto DNA at KOPS sites in a specific orientation. Unidirectional pumping by FtsK then leads to the movement of the *dif* site toward the divisome irrespective of which chromosome arm FtsK was loaded upon (Sherratt et al., 2010). Loading and translocation can only occur *in vivo* when FtsK is localized in the divisome where it forms hexameric units (Bisicchia et al., 2013). The translocation through the barrel in the FtsK hexameric assembly takes place at a rate of about 5 kb/s and stops when FtsK reaches the *dif* site (Sherratt et al., 2010). FtsK translocation activity releases most DNA-binding proteins from the translocated region of the chromosome (Lee et al., 2014). Among others, MatP proteins are also released. The latter leads to dissociation of the Ter linkage at late stages of cytokinesis (Stouf et al., 2013). It is likely that the Ter linkage facilities the activity of FtsK by maintaining this chromosomal region physically in the proximity of the divisome.

FtsK activity on DNA is not limited to translocation. At *dif* sites, FtsK is responsible for activation of the XerCD system that resolves chromosome dimers. FtsK has also been implicated in activating Topo IV (parC), which removes chromosome catenates (Espeli et al., 2003).

Minimal Requirements for Coordination

Interestingly, none of the four molecular systems that have been discussed in this review are strictly essential in *E. coli*. One can delete *slmA* and *minCDE* together with either *matP*, *zapA*, or *zapB* from *E. coli* but the cells still remain viable in slow growth conditions (Bailey et al., 2014). Moreover, even though FtsK is essential, its DNA translocating domain (C-terminal domain) is not (Sherratt et al., 2010). Is it possible that *E. coli* harbors some additional molecular system that coordinates its divisome and chromosome, and this yet to be discovered system is indispensable? As discussed above, there is strong evidence that the NO effect can occur without SlmA. Although the molecular bases of this mechanism remains unknown it could be an essential mechanism. Alternatively, it is possible that there are no indispensable mechanisms that coordinate cell division and chromosome segregation in *E. coli*. One can ask what minimal coordination is needed between cell division proteins and chromosomes for any cell (not only *E. coli*) to propagate. For propagation of a sizeable cell population, the ultimate limit appears to be that on average more than half of the nucleoids need to survive cell division undamaged and emerge in newborn daughter cells (note that small cell populations can go extinct even when more than half of the nucleoids survive cell division). One way to fulfill this requirement in cells that lack any dedicated coordination mechanism between cell division and chromosomes is to increase cell size. If the division plane is placed randomly in the cell then the probability to produce viable daughter cells increases as the cell size increases (**Figure 3**). Multinucleoid cells are more likely to produce two viable daughters upon random placement of the division plane at the expense of losing some genetic material. However, rod-shaped bacterial cells with two nucleoids can also give rise to a viable population when their sizes are sufficiently large. In the latter case, it is assumed

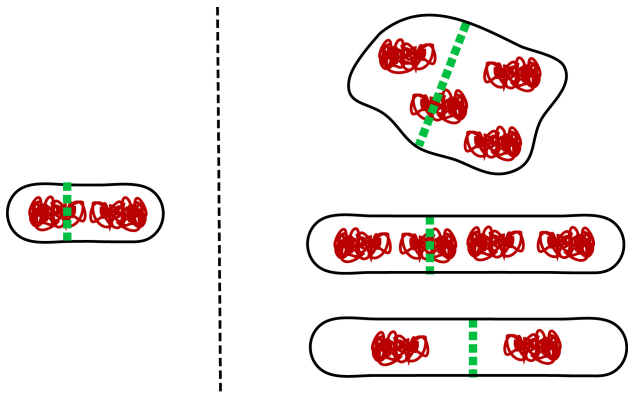

FIGURE 3 | Larger cell size mitigates lack of spatial coordination between cell division machinery and genetic information. A small cell (left) requires a sophisticated apparatus to coordinate cell division and chromosomes. For larger cells (right) the requirements for coordination are more relaxed. This applies in particular for multi-nucleoid cells where despite some genetic material being damaged during division the majority of daughter cells still receive a full complement of genes and remain viable. At least in rod shapes, long diploid cells can also give rise to viable population even when their division plane placement is random.

that the physical size of the nucleoid does not depend on cell size and nucleoids are randomly placed in the cell before division. It remains to be proven if viable populations also can emerge in other cell geometries under these assumptions. Interestingly, as the systems depicted in **Figure 1** are progressively deleted from *E. coli*, the cells become larger (longer) but remain viable in slow growth conditions (Bailey et al., 2014) in accordance with this hypothesis.

Although large cells can cope with random placement of division planes, their fitness is very low because these cells lose a substantial amount of resources when they produce unviable cells or guillotine nucleoids. Mechanisms that coordinate cell division proteins and chromosomes are thus essential for cellular fitness. These mechanisms are highly efficient in modern bacteria. The probability that wild type *E. coli* produces minicells has been estimated to be less than 0.03% (Niki et al., 1991). It is, however, plausible that early protocells did not have any dedicated coordination systems. This argument is supported by findings that different bacterial species have evolved very different molecular mechanisms that coordinate divisomes and chromosomes (Monahan et al., 2014). As a corollary to this discussion, the lack of these coordination systems would imply that early protocells were perhaps larger than present day bacteria. Alternatively, early protocells might have had mechanisms that provided some coordination between division planes and chromosomes but which were not specifically dedicated for the task. For example, in a rod-shaped bacterial cell, membrane mechanics dictates that divisions which partition a mother cell into two equal halves are energetically more favorable than asymmetric divisions (Shlomovitz and Gov, 2009). Also, it is likely that chromosomes could be pushed mechanically away as the division septum closes preventing them from being guillotined or that chromosomes could provide enough mechanical hindrance to prevent the septum from closing in cells that lack strong cell wall. These mechanisms could still be present in modern *E. coli* even though their influence is overridden by the more efficient molecular systems such as Min, SlmA, Ter linkage, and FtsK.

Concluding Remarks

As this review emphasizes, there are several modular pathways coordinating chromosomal positioning with cell division in *E. coli*, which are redundant, at least, in slow growth conditions. Moreover, there is evidence that, in addition to the mechanisms known so far, there are other types of coordination which have not been described yet. All the mechanisms lead to increased cellular fitness but are not essential for cell viability. Perhaps surprisingly, one of the conclusions of this review is that the *E. coli* cell can cope with very limited coordination between cell division proteins and chromosomes.

Acknowledgments

The authors thank Anna Jennings, Jaana Männik, and Conrad Woldringh for valuable comments on the manuscript. The work was supported in part by University of Tennessee start-up funds and NSF research grant MCB-1252890.

References

Adams, D. W., and Errington, J. (2009). Bacterial cell division: assembly, maintenance and disassembly of the Z ring. *Nat. Rev. Microbiol.* 7, 642–653. doi: 10.1038/nrmicro2198

Adams, D. W., Wu, L. J., and Errington, J. (2014). Cell cycle regulation by the bacterial nucleoid. *Curr. Opin. Microbiol.* 22, 94–101. doi: 10.1016/j.mib.2014.09.020

Adler, H. I., Fisher, W. D., Cohen, A., and Hardigre, A. (1967). Miniature *Escherichia coli* cells deficient in DNA. *Proc. Natl. Acad. Sci. U.S.A.* 57, 321–326. doi: 10.1073/pnas.57.2.321

Akerlund, T., Gullbrand, B., and Nordstrom, K. (2002). Effects of the Min system on nucleoid segregation in *Escherichia coli*. *Microbiology* 148, 3213–3222.

Arumugam, S., Petrasek, Z., and Schwille, P. (2014). MinCDE exploits the dynamic nature of FtsZ filaments for its spatial regulation. *Proc. Natl. Acad. Sci. U.S.A.* 111, E1192–E1200. doi: 10.1073/pnas.1317764111

Bailey, M. W., Bissichia, P., Warren, B. T., Sherratt, D. J., and Männik, J. (2014). Evidence for divisome localization mechanisms independent of the Min system and SlmA in *Escherichia coli*. *PLoS Genet.* 10:e1004504. doi: 10.1371/journal.pgen.1004504

Begg, K. J., Dewar, S. J., and Donachie, W. D. (1995). A new *Escherichia coli* cell-division gene, ftsK. *J. Bacteriol.* 177, 6211–6222.

Bernhardt, T. G., and de Boer, P. A. J. (2005). SlmA, a nucleoid-associated, FtsZ binding protein required for blocking septal ring assembly over chromosomes in *E. coli*. *Mol. Cell* 18, 555–564. doi: 10.1016/j.molcel.2005.04.012

Bisicchia, P., Steel, B., Debela, M. H. M., Loewe, J., and Sherratt, D. (2013). The N-terminal membrane-spanning domain of the *Escherichia coli* DNA translocase FtsK hexamerizes at midcell. *mBio* 4, e00800–e00813. doi: 10.1128/mBio.00800-13

Bonny, M., Fischer-Friedrich, E., Loose, M., Schwille, P., and Kruse, K. (2013). Membrane binding of MinE allows for a comprehensive description of min-protein pattern formation. *PLoS Comput. Biol.* 9:e1003347. doi: 10.1371/journal.pcbi.1003347

Cambridge, J., Blinkova, A., Magnan, D., Bates, D., and Walker, J. R. (2014). A replication-inhibited unsegregated nucleoid at mid-cell blocks Z-ring formation

and cell division independently of SOS and the SlmA nucleoid occlusion protein in *Escherichia coli*. *J. Bacteriol.* 196, 36–49. doi: 10.1128/JB.01230-12

Cho, H. B., and Bernhardt, T. G. (2013). Identification of the SlmA active site responsible for blocking bacterial cytokinetic ring assembly over the chromosome. *PLoS Genet.* 9:e1003304. doi: 10.1371/journal.pgen.1003304

Cho, H. B., McManus, H. R., Dove, S. L., and Bernhardt, T. G. (2011). Nucleoid occlusion factor SlmA is a DNA-activated FtsZ polymerization antagonist. *Proc. Natl. Acad. Sci. U.S.A.* 108, 3773–3778. doi: 10.1073/pnas.1018674108

Cook, W. R., and Rothfield, L. I. (1999). Nucleoid-independent identification of cell division sites in *Escherichia coli*. *J. Bacteriol.* 181, 1900–1905.

Dajkovic, A., Lan, G., Sun, S. X., Wirtz, D., and Lutkenhaus, J. (2008). MinC spatially controls bacterial cytokinesis by antagonizing the scaffolding function of FtsZ. *Curr. Biol.* 18, 235–244. doi: 10.1016/j.cub.2008.01.042

de Boer, P. A. J. (2010). Advances in understanding *E. coli* cell fission. *Curr. Opin. Microbiol.* 13, 730–737. doi: 10.1016/j.mib.2010.09.015

Deghorain, M., Pages, C., Meile, J.-C., Stouf, M., Capiaux, H., Mercier, R., et al. (2011). A defined terminal region of the *E. coli* chromosome shows late segregation and high FtsK activity. *PLoS ONE* 6:e22164. doi: 10.1371/journal.pone.0022164

Den Blaauwen, T., Buddelmeijer, N., Aarsman, M. E. G., Hameete, C. M., and Nanninga, N. (1999). Timing of FtsZ assembly in *Escherichia coli*. *J. Bacteriol.* 181, 5167–5175.

Di Ventura, B., Knecht, B., Andreas, H., Godinez, W. J., Fritsche, M., Rohr, K., et al. (2013). Chromosome segregation by the *Escherichia coli* Min system. *Mol. Syst. Biol.* 9, 686. doi: 10.1038/msb.2013.44

Dupaigne, P., Tonthat, N. K., Espeli, O., Whitfill, T., Boccard, F., and Schumacher, M. A. (2012). Molecular basis for a protein-mediated DNA-bridging mechanism that functions in condensation of the *E. coil* chromosome. *Mol. Cell* 48, 560–571. doi: 10.1016/j.molcel.2012.09.009

Du, S. S., and Lutkenhaus, J. (2014). SlmA antagonism of FtsZ assembly employs a two-pronged mechanism like MinCD. *PLoS Genet.* 10:e1004460. doi: 10.1371/journal.pgen.1004460

Erickson, H. P., Anderson, D. E., and Osawa, M. (2010). FtsZ in bacterial cytokinesis: cytoskeleton and force generator all in one. *Microbiol. Mol. Biol. Rev.* 74, 504–528. doi: 10.1128/MMBR.00021-10

Espeli, O., Borne, R., Dupaigne, P., Thiel, A., Gigant, E., Mercier, R., et al. (2012). A MatP-divisome interaction coordinates chromosome segregation with cell division in *E. coli*. *EMBO J.* 31, 3198–3211. doi: 10.1038/emboj.2012.128

Espeli, O., Lee, C., and Marians, K. J. (2003). A physical and functional interaction between *Escherichia coli* FtsK and topoisomerase IV. *J. Biol. Chem.* 278, 44639–44644. doi: 10.1074/jbc.M308926200

Fange, D., and Elf, J. (2006). Noise-induced Min phenotypes in *E coli*. *PLoS Comput. Biol.* 2:637–648. doi: 10.1371/journal.pcbi.0020080

Galli, E., and Gerdes, K. (2010). Spatial resolution of two bacterial cell division proteins: ZapA recruits ZapB to the inner face of the Z-ring. *Mol. Microbiol.* 76, 1514–1526. doi: 10.1111/j.1365-2958.2010.07183.x

Guberman, J. M., Fay, A., Dworkin, J., Wingreen, N. S., and Gitai, Z. (2008). PSICIC: noise and asymmetry in bacterial division revealed by computational image analysis at sub-pixel resolution. *PLoS Comput. Biol.* 4:e1000233. doi: 10.1371/journal.pcbi.1000233

Halatek, J., and Frey, E. (2012). Highly canalized MinD transfer and MinE sequestration explain the origin of robust MinCDE-protein dynamics. *Cell Rep.* 1, 741–752. doi: 10.1016/j.celrep.2012.04.005

Hendricks, E. C., Szerlong, H., Hill, T., and Kuempel, P. (2000). Cell division, guillotining of dimer chromosomes and SOS induction in resolution mutants (dif, xerC, and xerD) of *Escherichia coli*. *Mol. Microbiol.* 36, 973–981. doi: 10.1046/j.1365-2958.2000.01920.x

Huang, K. C., Meir, Y., and Wingreen, N. S. (2003). Dynamic structures in *Escherichia coli*: spontaneous formation of MinE rings and MinD polar zones. *Proc. Natl. Acad. Sci. U.S.A.* 100, 12724–12728. doi: 10.1073/pnas.2135445100

Hussain, K., Begg, K. J., Salmond, G. P. C., and Donachie, W. D. (1987). ParD—a new gene coding for a protein required for chromosome partitioning and septum localization in *Escherichia coli*. *Mol. Microbiol.* 1, 73–81. doi: 10.1111/j.1365-2958.1987.tb00529.x

Ivanov, V., and Mizuuchi, K. (2010). Multiple modes of interconverting dynamic pattern formation by bacterial cell division proteins. *Proc. Natl. Acad. Sci. U.S.A.* 107, 8071–8078. doi: 10.1073/pnas.0911036107

Jia, S., Keilberg, D., Hot, E., Thanbichler, M., Sogaard-Andersen, L., and Lenz, P. (2014). Effect of the Min system on timing of cell division in *Escherichia coli*. *PLoS ONE* 9:e103863. doi: 10.1371/journal.pone.0103863

Kerr, R. A., Levine, H., Sejnowski, T. J., and Rappel, W. J. (2006). Division accuracy in a stochastic model of Min oscillations in *Escherichia coli*. *Proc. Natl. Acad. Sci. U.S.A.* 103, 347–352. doi: 10.1073/pnas.0505825102

Kruse, K. (2002). A dynamic model for determining the middle of *Escherichia coli*. *Biophys. J.* 82, 618–627. doi: 10.1016/S0006-3495(02)75426-X

Lee, J. Y., Finkelstein, I. J., Arciszewska, L. K., Sherratt, D. J., and Greene, E. C. (2014). Single-molecule imaging of FtsK translocation reveals mechanistic features of protein-protein collisions on DNA. *Mol. Cell* 54, 832–843. doi: 10.1016/j.molcel.2014.03.033

Liu, B., Persons, L., Lee, L., and de Boer, P. A. J. (2015). Roles for both FtsA and the FtsBLQ subcomplex in FtsN-stimulated cell constriction in *Escherichia coli*. *Mol. Microbiol.* 95, 945–970. doi: 10.1111/mmi.12906

Loose, M., Fischer-Friedrich, E., Ries, J., Kruse, K., and Schwille, P. (2008). Spatial regulators for bacterial cell division self-organize into surface waves in vitro. *Science* 320, 789–792. doi: 10.1126/science.1154413

Lutkenhaus, J. (2007). Assembly dynamics of the bacterial MinCDE system and spatial regulation of the Z ring. *Annu. Rev. Biochem.* 76, 539–562. doi: 10.1146/annurev.biochem.75.103004.142652

Lutkenhaus, J. (2012). The ParA/MinD family puts things in their place. *Trends Microbiol.* 20, 411–418. doi: 10.1016/j.tim.2012.05.002

Lutkenhaus, J., Pichoff, S., and Du, S. (2012). Bacterial cytokinesis: from Z ring to divisome. *Cytoskeleton* 69, 778–790. doi: 10.1002/cm.21054

Männik, J., Wu, F., Hol, F. J. H., Bissichia, P., Sherratt, D. J., Keymer, J. E., et al. (2012). Robustness and accuracy of cell division in *Escherichia coli* in diverse cell shapes. *Proc. Natl. Acad. Sci. U.S.A.* 109, 6957–6962. doi: 10.1073/pnas.1120854109

Margolin, W. (2005). FtsZ and the division of prokaryotic cells and organelles. *Nat. Rev. Mol. Cell Biol.* 6, 862–871. doi: 10.1038/nrm1745

Meinhardt, H., and de Boer, P. A. J. (2001). Pattern formation in *Escherichia coli*: a model for the pole-to-pole oscillations of Min proteins and the localization of the division site. *Proc. Natl. Acad. Sci. U.S.A.* 98, 14202–14207. doi: 10.1073/pnas.251216598

Mercier, R., Petit, M.-A., Schbath, S., Robin, S., El Karoui, M., Boccard, F., et al. (2008). The MatP/matS site-specific system organizes the terminus region of the *E. coli* chromosome into a macrodomain. *Cell* 135, 475–485. doi: 10.1016/j.cell.2008.08.031

Monahan, L. G., Liew, A. T. F., Bottomley, A. L., and Harry, E. J. (2014). Division site positioning in bacteria: one size does not fit all. *Front. Microbiol.* 5:19. doi: 10.3389/fmicb.2014.00019

Moseley, J. B., and Nurse, P. (2010). Cell division intersects with cell geometry. *Cell* 142, 189–193. doi: 10.1016/j.cell.2010.07.004

Mulder, E., Elbouhali, M., Pas, E., and Woldringh, C. L. (1990). The *Escherichia coli* MinB mutation resembles GyrB in defective nucleoid segregation and decreased negative supercoiling of plasmids. *Mol. Gen. Genet.* 221, 87–93. doi: 10.1007/BF00280372

Mulder, E., and Woldringh, C. L. (1989). Actively replicating nucleoids influence positioning of division sites in *Escherichia coli* filaments forming cells lacking DNA. *J. Bacteriol.* 171, 4303–4314.

Niki, H., Jaffe, A., Imamura, R., Ogura, T., and Hiraga, S. (1991). The new gene MukB codes for a 177 kD protein with coiled-coil domains involved in chromosome partitioning of *Escherichia coli*. *EMBO J.* 10, 183–193.

Norris, V. (1995). Hypothesis—chromosome separation in *Escherichia coli* involves autocatalytic gene expression, transertion and membrane-domain formation. *Mol. Microbiol.* 16, 1051–1057. doi: 10.1111/j.1365-2958.1995.tb02330.x

Pazos, M., Casanova, M., Palacios, P., Margolin, W., Natale, P., and Vicente, M. (2014). FtsZ placement in nucleoid-free bacteria. *PLoS ONE* 9:e91984. doi: 10.1371/journal.pone.0091984

Raskin, D. M., and de Boer, P. A. J. (1999). Rapid pole-to-pole oscillation of a protein required for directing division to the middle of *Escherichia coli*. *Proc. Natl. Acad. Sci. U.S.A.* 96, 4971–4976. doi: 10.1073/pnas.96.9.4971

Schweizer, J., Loose, M., Bonny, M., Kruse, K., Moench, I., and Schwille, P. (2012). Geometry sensing by self-organized protein patterns. *Proc. Natl. Acad. Sci. U.S.A.* 109, 15283–15288. doi: 10.1073/pnas.1206953109

Shapiro, L., McAdams, H. H., and Losick, R. (2009). Why and how bacteria localize proteins. *Science* 326, 1225–1228. doi: 10.1126/science.1175685

Shen, B., and Lutkenhaus, J. (2010). Examination of the interaction between FtsZ and MinCN in *E. coli* suggests how MinC disrupts Z rings. *Mol. Microbiol.* 75, 1285–1298. doi: 10.1111/j.1365-2958.2010.07055.x

Sherratt, D. J., Arciszewska, L. K., Crozat, E., Graham, J. E., and Grainge, I. (2010). The *Escherichia coli* DNA translocase FtsK. *Biochem. Soc. Trans.* 38, 395–398. doi: 10.1042/BST0380395

Shlomovitz, R., and Gov, N. S. (2009). Membrane-mediated interactions drive the condensation and coalescence of FtsZ rings. *Phys. Biol.* 6:046017. doi: 10.1088/1478-3975/6/4/046017

Stouf, M., Meile, J.-C., and Cornet, F. (2013). FtsK actively segregates sister chromosomes in *Escherichia coli*. *Proc. Natl. Acad. Sci. U.S.A.* 110, 11157–11162. doi: 10.1073/pnas.1304080110

Sun, Q., and Margolin, W. (1998). FtsZ dynamics during the division cycle of live *Escherichia coli* cells. *J. Bacteriol.* 180, 2050–2056.

Sun, Q., and Margolin, W. (2004). Effects of perturbing nucleoid structure on nucleoid occlusion-mediated toporegulation of FtsZ ring assembly. *J. Bacteriol.* 186, 3951–3959. doi: 10.1128/JB.186.12.3951-3959.2004

Tonthat, N. K., Arold, S. T., Pickering, B. F., Van Dyke, M. W., Liang, S. D., Lu, Y., et al. (2011). Molecular mechanism by which the nucleoid occlusion factor, SlmA, keeps cytokinesis in check. *EMBO J.* 30, 154–164. doi: 10.1038/emboj.2010.288

Tonthat, N. K., Milam, S. L., Chinnam, N., Whitfill, T., Margolin, W., and Schumacher, M. A. (2013). SlmA forms a higher-order structure on DNA that inhibits cytokinetic Z-ring formation over the nucleoid. *Proc. Natl. Acad. Sci. U.S.A.* 110, 10586–10591. doi: 10.1073/pnas.1221036110

Trueba, F. J. (1982). On the precision and accuracy achieved by *Escherichia coli* cells at fission about their middle. *Arch. Microbiol.* 131, 55–59. doi: 10.1007/BF00451499

Turing, A. M. (1952). The chemical basis of morphogenesis. *Philos. Trans. R. Soc. B* 237, 37–72. doi: 10.1098/rstb.1952.0012

Woldringh, C. L. (2002). The role of co-transcriptional translation and protein translocation (transertion) in bacterial chromosome segregation. *Mol. Microbiol.* 45, 17–29. doi: 10.1046/j.1365-2958.2002.02993.x

Woldringh, C. L., Mulder, E., Huls, P. G., and Vischer, N. (1991). Toporegulation of bacterial division according to the nucleoid occlusion model. *Res. Microbiol.* 142, 309–320. doi: 10.1016/0923-2508(91)90046-D

Woldringh, C. L., Mulder, E., Valkenburg, J. A. C., Wientjes, F. B., Zaritsky, A., and Nanninga, N. (1990). Role of the nucleoid in the toporegulation of division. *Res. Microbiol.* 141, 39–49. doi: 10.1016/0923-2508(90)90096-9

Wu, L. J., and Errington, J. (2011). Nucleoid occlusion and bacterial cell division. *Nat. Rev. Microbiol.* 10, 8–12. doi: 10.1038/nrmicro2671

Yu, X. C., and Margolin, W. (1999). FtsZ ring clusters in min and partition mutants: role of both the Min system and the nucleoid in regulating FtsZ ring localization. *Mol. Microbiol.* 32, 315–326. doi: 10.1046/j.1365-2958.1999.01351.x

Zaritsky, A., and Woldringh, C. L. (2003). Localizing cell division in spherical *Escherichia coli* by nucleoid occlusion. *FEMS Microbiol. Lett.* 226, 209–214. doi: 10.1016/S0378-1097(03)00580-9

Conflict of Interest Statement: The authors declare that the research was conducted in the absence of any commercial or financial relationships that could be construed as a potential conflict of interest.

Copyright © 2015 Männik and Bailey. This is an open-access article distributed under the terms of the Creative Commons Attribution License (CC BY). The use, distribution or reproduction in other forums is permitted, provided the original author(s) or licensor are credited and that the original publication in this journal is cited, in accordance with accepted academic practice. No use, distribution or reproduction is permitted which does not comply with these terms.

frontiers in Microbiology

REVIEW
published: 13 May 2015
doi: 10.3389/fmicb.2015.00478

The Min system and other nucleoid-independent regulators of Z ring positioning

*Veronica W. Rowlett and William Margolin**

Department of Microbiology and Molecular Genetics, University of Texas Medical School at Houston, Houston, TX, USA

Rod-shaped bacteria such as *E. coli* have mechanisms to position their cell division plane at the precise center of the cell, to ensure that the daughter cells are equal in size. The two main mechanisms are the Min system and nucleoid occlusion (NO), both of which work by inhibiting assembly of FtsZ, the tubulin-like scaffold that forms the cytokinetic Z ring. Whereas NO prevents Z rings from constricting over unsegregated nucleoids, the Min system is nucleoid-independent and even functions in cells lacking nucleoids and thus NO. The Min proteins of *E. coli* and *B. subtilis* form bipolar gradients that inhibit Z ring formation most at the cell poles and least at the nascent division plane. This article will outline the molecular mechanisms behind Min function in *E. coli* and *B. subtilis*, and discuss distinct Z ring positioning systems in other bacterial species.

Keywords: bacterial cell division, divisome, Min system, FtsZ, Z-ring positioning

OPEN ACCESS

Edited by:
Arieh Zaritsky, Ben-Gurion University of the Negev, Israel

Reviewed by:
Marc Bramkamp, Ludwig-Maximilians-University Munich, Germany
Imrich Barak, Institute of Molecular Biology, Slovak Academy of Sciences, Slovakia
Liz Harry, University of Technology, Sydney, Australia
Orietta Massidda, Università di Cagliari, Italy

***Correspondence:**
William Margolin, Department of Microbiology and Molecular Genetics, University of Texas Medical School at Houston, 6431 Fannin, Houston, TX 77030, USA
william.margolin@uth.tmc.edu

Specialty section:
This article was submitted to Microbial Physiology and Metabolism, a section of the journal Frontiers in Microbiology

Received: *27 March 2015*
Accepted: *30 April 2015*
Published: *13 May 2015*

Citation:
Rowlett VW and Margolin W (2015) The Min system and other nucleoid-independent regulators of Z ring positioning. Front. Microbiol. 6:478. doi: 10.3389/fmicb.2015.00478

Introduction

In bacteria, several proteins assemble at the cell center (midcell) to form the divisome, or cell division machine (Martos et al., 2012). At the start of divisome formation, FtsZ, a homolog of eukaryotic tubulin, polymerizes and forms a ring-like structure, the Z ring, at midcell (Bi and Lutkenhaus, 1991). The Z ring functions as a scaffold for cell division proteins and is an obvious target for regulating the site of cytokinesis. Decades of research in *E. coli* and *B. subtilis* have led to insights into the molecular mechanisms of NO and the Min system, which negatively regulate Z ring formation by preventing Z rings from forming over nucleoids or at cell poles, respectively. However, it is likely that other regulators contribute to Z ring positioning in these bacteria (Rodrigues and Harry, 2012). Recently, unique negative and positive regulators of Z ring formation have been identified in bacteria that lack NO and/or Min systems, highlighting the diversity of division site selection mechanisms.

Minicells and the Min System

Several decades ago, Adler et al. (1967) identified small, nucleoid free *E. coli* cells described as minicells. These minicells do not divide, but remain metabolically active for hours. Minicells also form in *B. subtilis* and other bacteria (Reeve et al., 1973). Historically, purified minicells were used to produce radiochemically pure proteins from high-copy plasmids that partition into minicells and could be selectively labeled in purified minicell preparations (Roozen et al., 1971). More recently, minicells have been useful for viewing cell surface structures by cryo-electron tomography (Liu et al., 2012; Hu et al., 2013) and are also being developed as safe cellular systems for antigen delivery to tumor cells (MacDiarmid and Brahmbhatt, 2011; Carleton et al., 2013).

In *E. coli*, Min proteins localize to the cell poles and function to prevent Z rings from forming near those poles (**Figure 1**; Bramkamp and van Baarle, 2009). In *B. subtilis*, the Min system has a

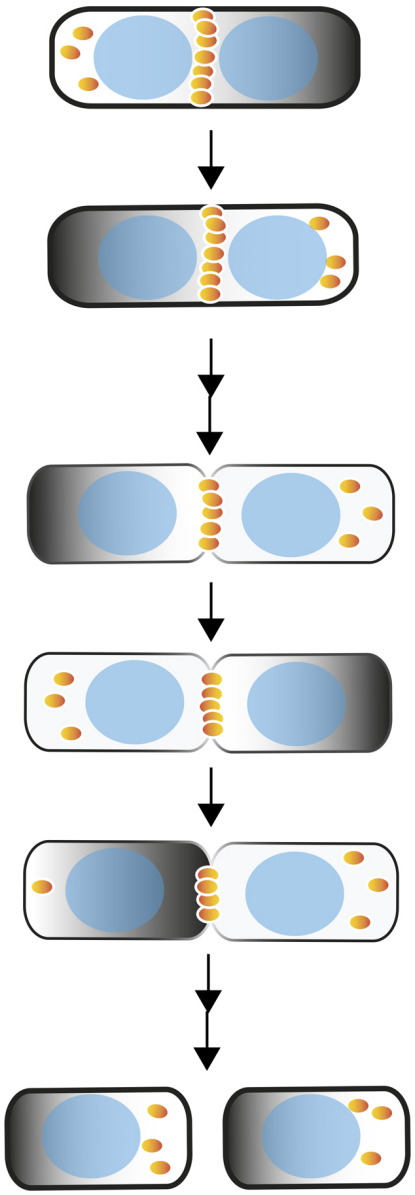

FIGURE 1 | Negative spatial regulation of Z ring positioning in *E. coli* by the Min system. Shown are Min oscillations (dark gradients), dynamics of FtsZ (orange spheres) and eventual assembly as a Z ring at the midpoint of a wild-type cell through the process of cell division and partitioning of the Min system to daughter cells. Nucleoids are depicted as blue ovals; passage of time in seconds is represented by an arrow, passage of time in minutes by a double arrow.

somewhat different role (see next section). When Min proteins are deleted or non-functional, Z rings are able to form both at correct midcell locations and at cell poles, resulting in minicells and cells of heterogeneous length, as not all Z rings are functional to complete division (de Boer et al., 1989; Yu and Margolin, 1999). One of the Min proteins, MinC, directly interacts with FtsZ and inhibits FtsZ polymerization (Hu et al., 1999; Dajkovic et al., 2008; Shen and Lutkenhaus, 2009, 2010). As described below, MinC also interacts with partner proteins that localize it to cell poles, creating a gradient of MinC that is highest at cell poles and lowest at midcell (Monahan and Harry, 2012).

Min Systems of *B. subtilis* and *E. coli*

In *B. subtilis*, DivIVA localizes the Min proteins to the poles of the cell (Cha and Stewart, 1997; Edwards and Errington, 1997). DivIVA functions as a generic cell-pole targeting protein, as it senses negative membrane curvature in a wide variety of species, including fission yeast (Edwards et al., 2000; Lenarcic et al., 2009). As a result, DivIVA relocalizes from cell poles to the new septum because of its sharp curvature. MinJ acts as an adaptor protein between polarly-targeted DivIVA and MinD, efficiently recruiting MinD to cell poles, where it binds the cytoplasmic membrane via its C-terminal amphipathic helix (Szeto et al., 2002). MinD binds MinC directly, and by doing so recruits the Z ring inhibitor MinC to the cell poles (Bramkamp et al., 2008; Patrick and Kearns, 2008). The Min system of *B. subtilis* was originally believed to migrate to existing cell poles to form a static bipolar gradient, with polar MinC inhibiting assembly of Z rings only at cell poles. However, more recent evidence indicates that Min proteins are recruited to midcell prior to septation and formation of new cell poles (Gregory et al., 2008). It is thought that localization of Min proteins to midcell prevents more than one Z ring from forming there, and plays a role in establishing a new bipolar gradient in daughter cells (Gregory et al., 2008; van Baarle and Bramkamp, 2010). The Min system thus does not seem to identify midcell as much as promote efficient use of the midcell site (Rodrigues and Harry, 2012).

The Min system in *E. coli* differs from that of *B. subtilis* because *E. coli* lacks DivIVA and instead contains a third Min protein, MinE. Because they lack DivIVA, *E. coli* cells need to establish a MinC bipolar gradient without the benefit of a polar targeting protein. As in *B. subtilis*, *E. coli* MinD directly binds the membrane and directly binds MinC (de Boer et al., 1991; Hu and Lutkenhaus, 2003). The MinE protein is critical for targeting the MinCD complex to the cell poles (see below). MinE forms a ring and causes MinD to be removed from one pole and migrate to the opposite pole (Raskin and de Boer, 1997; Hu et al., 2002). The dynamics between MinD and MinE create an oscillating system, in which MinC is a passenger (**Figure 2**; Hu and Lutkenhaus, 1999; Raskin and de Boer, 1999a,b). As a result of the oscillation, where most of the time is spent at the cell poles with only a short transit (typically 10 s) between them, the average position of MinC over time is at the poles and not at midcell, which leaves midcell as the least inhibited location for FtsZ assembly (**Figure 1**).

Although it is fairly well understood how the Min systems of *E. coli* and *B. subtilis* position Z rings during vegetative growth, relatively little is known about the requirements for placement of Z rings near the cell poles in preparation for asymmetric septation in *B. subtilis* and other Gram positive endospore-forming bacilli such as clostridia. A clue comes from the reconstitution of *E. coli*'s oscillating Min system in *B. subtilis*. Fluorescently-tagged MinD and MinE from *E. coli* oscillate from cell pole to cell pole when produced in *B. subtilis* cells deleted for native *minD* (Jamroškovič et al., 2012), consistent with the self-contained nature of the MinDE oscillator (Ramirez-Arcos et al., 2002). Interestingly, this artificial oscillation inhibited sporulation,

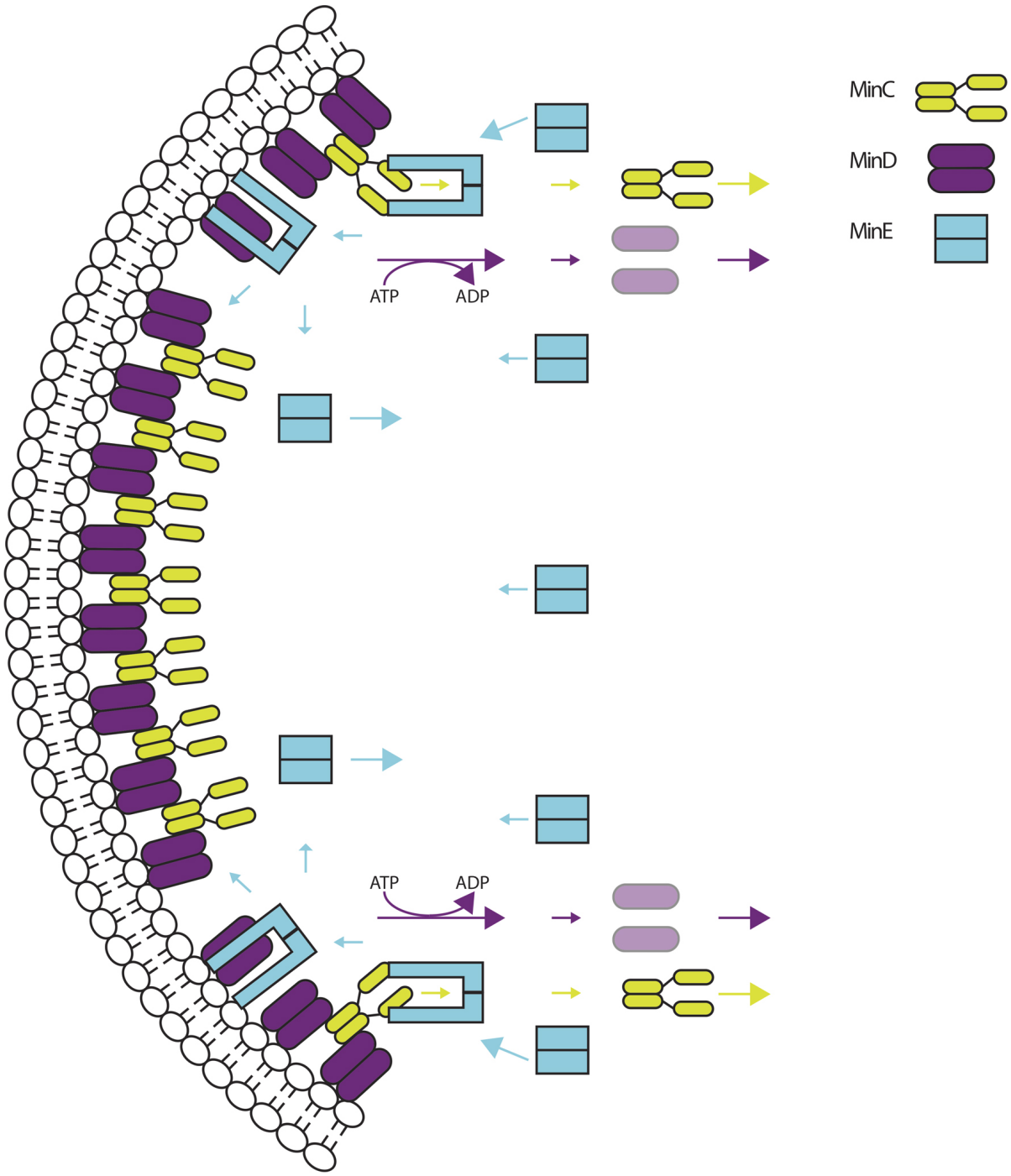

FIGURE 2 | The molecular mechanism of Min oscillation. Membrane-bound complexes of MinC (chartreuse) and MinD (purple) are targeted by MinE (cyan). MinE dimers change conformation and bind MinD and the membrane, displacing MinC and stimulating the ATPase activity of MinD and its removal from the membrane. MinC and MinD-ADP move toward the opposite pole and begin another cycle of oscillation. MinE can stay membrane bound to remove more MinCD complexes, or change conformation and follow MinD to the opposite pole. Adapted from Rowlett and Margolin (2013).

likely by preventing the assembly of Z rings near cell poles that is a hallmark of endospore formation in *B. subtilis*. This suggests that a constitutive oscillatory Min regime, while optimal for medial cell division in cells like *E. coli* that only grow vegetatively, may be problematic in cells that need to switch to asymmetric division for endospore formation (Barák, 2013). The presence of both MinDE and MinDJ/DivIVA in spore-forming clostridia may point to an ancestral Min system that exploited the advantages of each system, perhaps for switching from a vegetative oscillatory mode to a sporulation-induced static mode.

Molecular Mechanism of Min Oscillation in *E. coli* Cells

The MinC protein has two distinct domains that synergistically inhibit polymerization of FtsZ. The N-terminal half of the protein is sufficient to antagonize the longitudinal interactions of FtsZ subunits within a protofilament, whereas the C-terminal half inhibits the lateral interactions between FtsZ protofilaments (Hu and Lutkenhaus, 2000; Shiomi and Margolin, 2007; Shen and Lutkenhaus, 2009, 2010). The C-terminus of MinC binds to MinD, which is required for the full inhibition of FtsZ lateral interactions, and is important for MinC dimerization (Hu and Lutkenhaus, 2000, 2003). MinD is a ParA family ATPase that contains a C-terminal membrane targeting sequence (MTS) as mentioned above (de Boer et al., 1991; Hu and Lutkenhaus, 2003). When bound to ATP, MinD dimerizes and associates with the membrane (Szeto et al., 2002; Hu and Lutkenhaus, 2003). MinC and MinD form copolymers of alternating MinC and MinD dimers that are similar to eukaryotic septins (Ghosal et al., 2014; Conti et al., 2015). MinCD complexes are removed from the membrane by MinE (Raskin and de Boer, 1997).

In *E. coli* cells lacking MinE, MinCD binds to the membrane and inhibits Z ring formation throughout the cell, resulting in lethal filamentation (de Boer et al., 1989). Thus, MinE is essential for the MinCD complex to assume its role as a spatial regulator. MinE packs many activities into its compact 88 amino acid size. First, it harbors an amphipathic helix at its N-terminus that serves as an MTS, and direct membrane interaction is important for its function (Ma et al., 2003; Hsieh et al., 2010). Earlier mathematical models did not account for this membrane binding, but more recent models have (Schweizer et al., 2012; Bonny et al., 2013). Upon recognizing MinD, dimers of MinE change conformation, bind MinD, displace MinC, and stimulate the ATPase activity of MinD, causing monomerization of MinD and its removal from the membrane (**Figure 2**; Raskin and de Boer, 1997; Hu et al., 2002; Suefuji et al., 2002; Lackner et al., 2003; Loose et al., 2011; Park et al., 2011). Once dislodged from the membrane, MinD-ATP is regenerated from MinD-ADP by ADP-ATP exchange and immediately re-binds the membrane (Huang et al., 2003). However, it will tend to bind the membrane far from its most recent complex, because the MinE complex that recently removed it can remain on the membrane via its MTS (Loose et al., 2011; Park et al., 2011). This allows MinE to remove other bound complexes of MinCD at the original site, including those that recently re-bound, before changing back to its original conformation and migrating to the opposite pole (Park et al., 2011).

In support of this molecular mechanism, MinE always lags behind MinD. Because MinD-ATP binds to the membrane cooperatively, newly formed MinD-ATP will form a large complex as far away as possible from the original site, which happens to be the opposite pole of a normal sized *E. coli* cell. MinE, with no substrate remaining at the original site, diffuses through the cytoplasm, and possibly the membrane, until it binds to the edge of the newly assembled MinD complex at the opposite pole. *In vivo*, this is observed as a ring of MinE at the edge of the polar zone of MinD. Because the MinD polar zones are large and extend far from the cell pole, MinE rings are often observed near midcell, where they then follow the edge of the MinD polar zone as it shrinks toward the pole (Raskin and de Boer, 1997).

While Min proteins oscillate between cell poles, proteins that are recruited in the early stages of cell division, including FtsZ, ZipA, ZapA, and ZapB, also oscillate oppositely from the Min system with the same period as the Min system (Thanedar and Margolin, 2004; Bisicchia et al., 2013; Tonthat et al., 2013). ZipA and FtsA function to tether the Z ring to the inner membrane (Pichoff and Lutkenhaus, 2005), and ZipA has also been shown to bundle FtsZ protofilaments *in vitro* (Hale and de Boer, 1999; Hale et al., 2000). ZapA recruits ZapB to the Z ring and these proteins function to stimulate and stabilize Z ring formation (Gueiros-Filho and Losick, 2002; Galli and Gerdes, 2010; Buss et al., 2013). As ZipA and ZapA bind to FtsZ directly, and ZapB binds to ZapA, all three proteins are dependent on the Z ring for their localization. Therefore, their counter-oscillatory behavior is likely caused by the periodic assembly and disassembly of Z ring precursor complexes in response to oscillating waves of MinC (Thanedar and Margolin, 2004; Bisicchia et al., 2013).

Other Factors Influencing Min Oscillation

The oscillation of Min proteins can vary in response to changes in growth conditions, protein levels, and the cell cycle. For example, increased temperatures will shorten the period of Min oscillation from about a minute to several seconds (Touhami et al., 2006). Higher levels of MinD relative to MinE reduce MinD ATPase activity and lengthen the oscillation period, whereas lower MinD:MinE ratios increase MinD ATPase activity and shorten the period (Raskin and de Boer, 1999b; Hu et al., 2002), which is consistent with MinE as the driver of MinD dynamics. During later stages of cell division when the division septum is closing, MinD begins to "pause" at midcell prior to the formation of two separate oscillating systems, one in each daughter cell (Juarez and Margolin, 2010). Intriguingly, MinD is often observed to localize at opposite sides of the developing septum prior to doubling. This phenomenon is likely a result of the doubling in pole-to-pole distance prior to division. The pausing of MinD at midcell is likely required for equal partitioning of MinD into daughter cells and has been simulated mathematically (Di Ventura and Sourjik, 2011). This behavior might also prevent new Z rings from forming adjacent to existing rings, similar to the septal localization observed for Min proteins in *B. subtilis* as described above (Gregory et al., 2008; van Baarle and Bramkamp, 2010). This idea is supported by evidence that MinC also exhibits similar septal pausing (Hu and Lutkenhaus, 1999).

In addition to the pausing phenomenon, Min oscillation is strongly influenced by cell geometry. *E. coli* cells of normal length have a pole-to-pole pattern of Min localization, which is constrained by the essentially one-dimensional cellular rod shape (Raskin and de Boer, 1999b). If cells become elongated, such as in division-defective mutants, oscillation no longer extends from one pole to the other because the pole-to-pole distance becomes too long. Instead, the pattern changes to multiple (2 or more) oscillating units, some of which form traveling waves, in which MinD alternates from traveling through the membrane to traveling through the cytoplasm between poles (Raskin and de

Boer, 1999b; Hu and Lutkenhaus, 2001; Bonny et al., 2013). The result is that zones of MinCD appear and disappear throughout the filamentous cell with ~7 μm spacing (Raskin and de Boer, 1999b; Meinhardt and de Boer, 2001). It is likely that these MinCD zones help restrict where Z rings form distal to cell poles within these filaments.

Min proteins also respond to changes in cell shape, indicating that oscillation is not restricted to a symmetrical pattern. For example, in *E. coli* cells such as *rodA* mutants that grow and divide as spheres, MinD and MinE will migrate from one location to another on the cell periphery in a seemingly disorganized pattern, although there is a strong bias for migration down a long axis (Corbin et al., 2002). This behavior has been simulated by mathematical models (Huang and Wingreen, 2004). Such round cell mutants divide in alternating perpendicular planes, much like Staphylococci except only in two dimensions instead of three; if the Min system is inactivated in these mutant cells, their division becomes highly irregular (Begg and Donachie, 1998; Corbin et al., 2002). When round cells divide, they pinch and form a long axis, thus establishing Min oscillations parallel to the growing septum. This pattern will then define the midpoint of future perpendicular Z ring or arc (Pas et al., 2001), which explains how this alternating division pattern can occur (Corbin et al., 2002). Other evidence for geometric control of Min oscillation comes from branched *E. coli* cells, where Min proteins travel in a clockwise or counterclockwise direction between cell branches (Varma et al., 2008).

Membrane curvature and/or phospholipid composition likely serve as physical cues for localization of DivIVA and MinD (Barák and Muchová, 2013). The anionic phospholipid cardiolipin contributes to membrane curvature, and is enriched both at cell poles and the septum of dividing *E. coli* and *B. subtilis* cells (Mileykovskaya and Dowhan, 2000; Kawai et al., 2004). Phosphatidylglycerol is also enriched at *E. coli* cell poles and may contribute to the anionic nature of polar membranes, which seems to be important for binding of MinD and MinE (Mileykovskaya et al., 2003; Mazor et al., 2008; Renner and Weibel, 2012; Oliver et al., 2014; Vecchiarelli et al., 2014). In mutants lacking phosphatidylethanolamine (PE), MinD does not oscillate in organized zones but instead assembles and disassembles dynamically at peripheral foci throughout the cell, probably because the levels of anionic phospholipids are too high (Mileykovskaya et al., 2003). Cells lacking PE also divide poorly and exhibit spiral FtsZ patterns (Mileykovskaya et al., 1998), but is not yet known if these effects result from perturbations of the Min system or of other proteins that affect FtsZ assembly and function. In *B. subtilis*, on the other hand, specific phospholipids do not seem to be involved in the polar targeting by DivIVA (Lenarcic et al., 2009).

Cell-free Reconstitution of Min Protein Dynamics

The Min system has been an attractive subject for generating mathematical models to better understand Min protein dynamics (Kruse et al., 2007; Bonny et al., 2013). Such models of the Min system have both confirmed *in vivo* data, and have been used to predict patterns later confirmed using *in vivo* experiments (Bonny et al., 2013). These models implied that MinD and MinE were sufficient for the oscillatory behavior, and as proof of this, purified MinD and MinE were shown to self-organize into wave patterns on supported lipid bilayers (SLBs) in the presence of ATP (Loose et al., 2008). MinD first binds ATP and forms a homogenous layer on the bilayer, and when MinE is added, planar waves form, with MinD at the leading edge and MinE at the trailing edge (Loose et al., 2008). This nicely mimics the lagging behavior of MinE observed in *E. coli* cells (Hale et al., 2001). Reconstitution of FtsZ and MinC on SLBs uncovered the molecular mechanism of MinC inhibition of FtsZ by demonstrating that MinC can both bind FtsZ to prevent monomers from incorporating into polymers, and remove monomers from existing polymers (Arumugam et al., 2014). When FtsZ was reconstituted on the SLBs with MinDE, with and without MinC, MinC was shown to be required for spatial organization of FtsZ on MinDE waves (Arumugam et al., 2014). Most convincingly, MinCDE oscillation from pole to pole was reconstituted in rod-shaped compartments covered with membranes, as was FtsZ assembly at the midpoint of those compartments (**Figure 3C**; Zieske and Schwille, 2013, 2014).

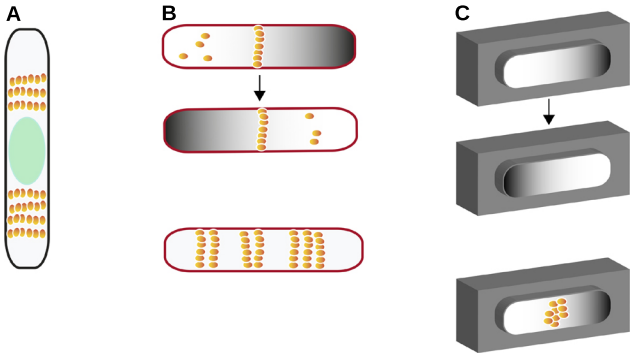

FIGURE 3 | Different model systems for investigating nucleoid-independent Z ring positioning in *E. coli*. (A) Multiple Z rings in cells lacking both Min and topoisomerase IV with large nucleoid-free regions on either side of unpartitioned nucleoid (green oval). **(B)** (top) Min oscillations and FtsZ positioning in nucleoid-free maxicells (outlined in red); (bottom) Z ring positioning in maxicells containing FtsZ that is unresponsive to MinC. **(C)** Cell-free oscillation of MinCDE in artificial cell-like compartments coated with a lipid bilayer before (top and middle) and after addition of purified FtsZ (bottom). FtsZ is depicted as orange spheres.

The Min System Acts Independently of the Nucleoid but May Influence Chromosome Partitioning

Certain chromosome partitioning mutants of *E. coli*, such as those inactivating Topoisomerase IV or the MukBEF condensing complex, result in a relatively high percentage of anucleate cells (Hiraga et al., 1991; Stewart and D'Ari, 1992; Hayama and Marians, 2010). Importantly, Z rings are positioned near the center of anucleate cells, indicating that chromosomes, though active for NO, are not essential for Z ring positioning (Sun et al., 1998). Indeed, mathematical models for Min-mediated centering of the Z ring assume that Min proteins are sufficient without any other macromolecules needed. Moreover, Min oscillations occur independently of nucleoid structural changes (Sun and Margolin,

2001), and Z rings can be centered by the Min system alone in the reconstitution experiments described above. Finally, *E. coli* maxicells, which are generated by UV-mediated destruction of the chromosome and are thus nucleoid-free, retain an oscillating Min system and also support Z ring formation at midcell. This supports the *in vitro* reconstitution data and suggests that the Min system alone can restrict Z rings to midcell in *E. coli* (**Figure 3B**; Pazos et al., 2014).

One question in the field is what advantages might the ATP-burning Min oscillation confer upon *E. coli*, considering that the *B. subtilis* Min system does not oscillate. Several studies have suggested that *E. coli* cells lacking Min systems have defects in chromosome partitioning (Bernander et al., 1989; Åkerlund et al., 1992, 2002). As the driving forces for chromosome partitioning in *E. coli* are unknown, this brings up the possibility that the Min oscillation somehow aids this process. Recent evidence suggests that MinD can bind chromosomal DNA directly, and therefore tether the chromosome to the membrane (Di Ventura et al., 2013), which might influence chromosome partitioning (Schofield et al., 2010).

Even when it is not oscillating, the *B. subtilis* Min system is also linked to chromosome replication. Another ParA family ATPase called Soj binds to chromosomal DNA and the DnaA initiator protein to activate DNA replication. However, Soj is also present as an inactive form that binds to MinD at cell poles, which prevents Soj activation of DNA replication (Murray and Errington, 2008).

Additional Regulators of Z ring Positioning in *E. coli* and *B. subtilis*

Recent evidence suggests that spatial regulators of Z ring positioning other than NO and Min exist in *E. coli* and *B. subtilis*. In *E. coli* cells, deletions of the Min system and SlmA, the mediator of NO, are synthetically lethal when cells are grown in rich medium (Wu and Errington, 2004; Bernhardt and de Boer, 2005). Removing both systems results in too many potential locations for Z rings to form **Figure 3A**, preventing assembly of a single coherent ring at midcell (Yu and Margolin, 1999; Bernhardt and de Boer, 2004). However, in minimal medium, cells that lack Min proteins and NO can survive and divide quite well, although the reason for the growth medium-dependence is not clear (Bernhardt and de Boer, 2005). Upon further investigation, cells lacking both NO and Min had more precise Z ring placement and produced fewer minicells than cells that only lacked Min (Bailey et al., 2014). These findings suggest that when both systems are not present, other factors contribute to Z ring positioning (Cambridge et al., 2014).

These factors may involve the nucleoid itself. For example, a positive regulatory system that involves the Ter macrodomain region of the chromosome has been implicated in Z ring positioning, as it occupies the center of the nucleoid during Z ring positioning (Bailey et al., 2014). In this system, MatP serves to connect the Ter macrodomain to the divisome through interaction with ZapB (Espéli et al., 2012), and this network is involved in regulating septal constriction (Buss et al., 2015). Cells that lack all known systems still exhibit a bias for Z rings localizing to midcell, although with lower precision and accuracy, indicating that other overlapping factors help to position Z rings (Bailey et al., 2014). *B. subtilis* cells that lack NO and Min proteins also precisely position Z rings, but Z ring formation is delayed, indicating their importance for Z ring formation at the proper time of the cell cycle (Rodrigues and Harry, 2012). Positive markers for Z ring formation in *B. subtilis* cells are also hypothesized (Moriya et al., 2010). In their "midcell potentiation" model, Moriya et al. (2010) proposed that as chromosome replication progresses, it acts along with NO and other factors to license midcell for Z-ring assembly. Essential chromosomal DNA replication proteins such as DnaX of *E. coli* (Bates and Kleckner, 2005) and DnaB of *B. subtilis* (Imai et al., 2000) localize at or near midcell. What first attracts these proteins to midcell is a key unanswered question.

Negative Spatial Regulation of Z ring Formation in *Caulobacter*

Like many other bacterial species, *Caulobacter crescentus* lacks both NO and Min systems, but contains a protein that restricts Z ring formation to midcell (Thanbichler and Shapiro, 2006). MipZ is a member of the ParA-like family of ATPases that includes MinD, and is conserved in α-proteobacteria (Thanbichler and Shapiro, 2006). In *C. crescentus,* MipZ binds to the chromosomal replication origin (*oriC*) and forms a complex with proteins that are involved in chromosome partitioning. Prior to replication and partitioning, *oriC* and bound MipZ are at one cell pole, and FtsZ is at the opposite pole, farthest from MipZ. Upon chromosome replication, the duplicated *oriC* migrates to the opposite cell pole, forming a bipolar gradient (Thanbichler and Shapiro, 2006). Unlike MinD, MipZ is able to directly interact with FtsZ and inhibit polymer formation, therefore the bipolar gradient of MipZ permits assembly of FtsZ at midcell, at the lowest MipZ concentration (Thanbichler and Shapiro, 2006; Kiekebusch et al., 2012). In contrast to *E. coli*, this seems to be a mechanism to position the Z ring in response to both spatial and cell cycle cues without the need for a separate NO system.

Positive Spatial Regulators of Z ring Formation

Until a few years ago, the known spatial regulators of the Z ring all acted to prevent Z ring formation at undesirable sites such as the cell poles or over the nucleoid. This negative regulation was satisfying because it generally exploited cell poles, which are a defined part of the cell that were once division sites, and did not need to invoke a midcell marker. Recently, however, several proteins that positively regulate Z ring formation have been identified in bacterial species that lack NO and/or Min systems. These proteins locate to the midcell division site and promote Z ring formation there, the very opposite of the Min/NO mechanism. The first reported example of a positive regulation system is the SsgA-SsgB pair in *Streptomyces coelicolor* (Willemse et al., 2011). SsgA-like proteins are present only in actinomycetes and are involved in forming multiple sporulation septa (Traag and van Wezel, 2008). *S. coelicolor* is able to grow vegetatively as mycelia in the absence of cell division, which enabled this study to be done in the absence of FtsZ. Notably, SsgA and SsgB localize to division sites between nucleoids in an *ftsZ* null mutant, indicating

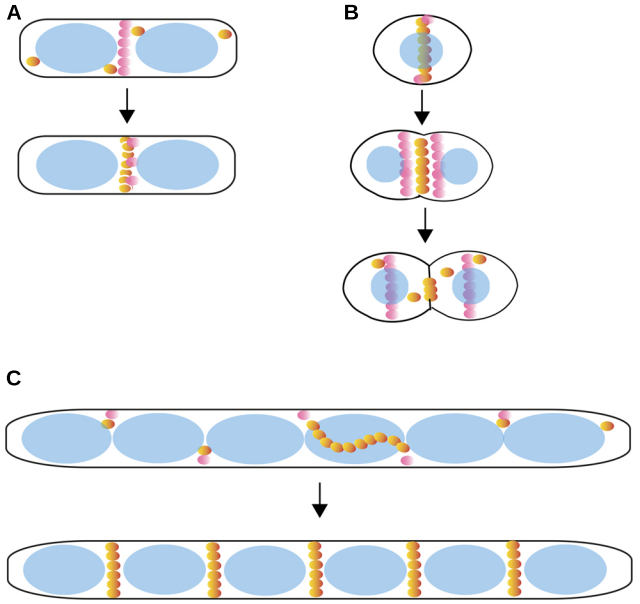

FIGURE 4 | Positive control of Z ring positioning. Shown are models for positive spatial regulation of Z rings by PomZ in *Myxococcus xanthus* **(A)**; MapZ/LocZ in *Streptococcus pneumoniae* **(B)**; SsgB in *Streptomyces* aerial mycelia that are developing into spores **(C)**. A sample cell cycle progression is shown for each. The above regulators are represented by pink spheres, FtsZ as orange spheres, and nucleoids as blue ovals.

that their localization is independent of FtsZ (McCormick et al., 1994; Willemse et al., 2011). SsgA recruits SsgB to midcell, where SsgB likely promotes FtsZ polymerization into discrete Z rings and serves as a membrane tether for the rings (Willemse et al., 2011). During formation of aerial spores, multiple Z rings are recruited to SsgB foci, ultimately forming sporulation septa (**Figure 4C**).

In another example of what seems to be positive regulation, PomZ, a ParA family ATPase, positions Z rings in the ∂-proteobacterial species known for its ability to swarm and produce fruiting bodies, *Myxococcus xanthus* (Treuner-Lange et al., 2013). *M. xanthus* cells lacking PomZ have classic defects in cell division that are hallmarks of aberrant Z ring positioning, including filamentation and the formation of minicells (Treuner-Lange et al., 2013). PomZ localizes to midcell prior to, and in the absence of, FtsZ **Figure 4A**). However, a direct interaction between PomZ and FtsZ has not yet been observed, indicating that other unidentified proteins are involved in bridging this connection and/or positioning the Z ring (Treuner-Lange et al., 2013).

Rod-shaped Actinobacteria have less precise Z ring placement when compared to *E. coli* and *B. subtilis* (reviewed in Donovan and Bramkamp, 2014). Although lacking Min and NO homologs, *Corynebacterium glutamicum* produces a homolog of ParA, PldP, which may play a role in localizing the Z ring (Donovan et al., 2010). PldP localizes to midcell early in the cell cycle, and inactivation of PldP results in an increased variation in cell length as well as minicell formation (Donovan et al., 2010). Further work is required to confirm the role of PldP in Z ring positioning.

Until recently, the only known spatial regulators of FtsZ were in naturally rod-shaped species, and it was unknown how new Z rings formed in cocci. However, a transmembrane protein in *Streptococcus pneumoniae*, called either LocZ (Localizing at mid-cell of FtsZ) or MapZ (Mid-cell-anchored protein Z) has been found to localize to midcell and contribute to Z ring positioning, cell shape, and division (Fleurie et al., 2014; Holečková et al., 2014). Cells lacking LocZ/MapZ are viable, but have cell shape defects and form minicells (Holečková et al., 2014). MapZ/LocZ localizes as rings at new division sites prior to the arrival of FtsZ (**Figure 4B**), and it was shown that MapZ interacts directly with FtsZ (Fleurie et al., 2014; Holečková et al., 2014). Once the midcell Z ring forms, MapZ/LocZ gradually move from midcell to the cell quarters, the sites of the next division (Fleurie et al., 2014; Holečková et al., 2014). Together, the evidence suggests that this regulator may stimulate FtsZ assembly at midcell. Homologs of LocZ/MapZ are present in streptococci, lactococci, and enterococci, suggesting that these species regulate Z ring positioning by a similar mechanism (Fleurie et al., 2014; Holečková et al., 2014). There has been no published report of FtsZ assembly *in vitro* from streptococci, perhaps because this FtsZ assembles poorly without a stimulatory factor.

Conclusion and Perspectives

The wide varieties of Z ring positioning systems identified in recent years highlight the complexity and diversity of bacteria (Monahan et al., 2014). The two systems that are best understood are the negative regulators of Z ring placement, NO and Min. Further studies will be required to elucidate the mechanism of recently identified systems, and to identify factors that contribute to Z ring positioning that are currently unknown. A common theme among many known Z ring positioning systems is the involvement of ParA-like proteins, which are also involved in chromosome segregation (Lutkenhaus et al., 2012). Another important question for further study is how positive regulators of Z ring positioning are recruited to midcell, particularly as the midpoint of a rod shaped cell does not feature any known molecular marker. In the cases of PomZ and MapZ/LocZ, it remains possible that their positioning at midcell is indirectly orchestrated by negative regulatory factors that depend on cell poles as cues. On the other hand, there is evidence that round cells such as *Staphylococcus aureus* may directly use spatial cues derived from previous septation events. Prior division septa result in orthogonal belts of distinct cell wall material that encircle the cell, acting to mark those sites for several generations. It is thought that the intersection of these belts mark the site for new cell division events (Turner et al., 2010). NO also has a role in Z ring placement in *S. aureus*, as loss of NO perturbs Z ring placement (Veiga et al., 2011). It remains to be determined how widespread this type of mechanism is and which proteins help mediate assembly of Z rings in these systems.

Acknowledgments

The authors are grateful for support from grant GM61074 from the National Institutes of Health and from the University of Texas Graduate School of Biomedical Sciences.

References

Adler, H. I., Fisher, W. D., Cohen, A., and Hardigree, A. A. (1967). Miniature *Escherichia coli* cells deficient in DNA. *Proc. Natl. Acad. Sci. U.S.A.* 57, 321–326.

Åkerlund, T., Bernander, R., and Nordström, K. (1992). Cell division in *Escherichia coli minB* mutants. *Mol. Microbiol.* 6, 2073–2083. doi: 10.1111/j.1365-2958.1992.tb01380.x

Åkerlund, T., Gullbrand, B., and Nordström, K. (2002). Effects of the Min system on nucleoid segregation in *Escherichia coli*. *Microbiology* 148, 3213–3222.

Arumugam, S., Petrášek, Z., and Schwille, P. (2014). MinCDE exploits the dynamic nature of FtsZ filaments for its spatial regulation. *Proc. Natl. Acad. Sci. U.S.A.* 111, E1192–E1200. doi: 10.1073/pnas.1317764111

Bailey, M. W., Bisicchia, P., Warren, B. T., Sherratt, D. J., and Männik, J. (2014). Evidence for divisome localization mechanisms independent of the Min system and SlmA in *Escherichia coli*. *PLoS Genet.* 10:e1004504. doi: 10.1371/journal.pgen.1004504

Barák, I. (2013). Open questions about the function and evolution of bacterial Min systems. *Front. Microbiol.* 4:378. doi: 10.3389/fmicb.2013.00378

Barák, I., and Muchová, K. (2013). The role of lipid domains in bacterial cell processes. *Int. J. Mol. Sci.* 14, 4050–4065. doi: 10.3390/ijms14024050

Bates, D., and Kleckner, N. (2005). Chromosome and replisome dynamics in *E. coli*: loss of sister cohesion triggers global chromosome movement and mediates chromosome segregation. *Cell* 121, 899–911. doi: 10.1016/j.cell.2005.04.013

Begg, K. J., and Donachie, W. D. (1998). Division planes alternate in spherical cells of *Escherichia coli*. *J. Bacteriol.* 180, 2564–2567.

Bernander, R., Merryweather, A., and Nordström, K. (1989). Overinitiation of replication of the *Escherichia coli* chromosome from an integrated runaway-replication derivative of Plasmid R1. *J. Bacteriol.* 171, 674–683.

Bernhardt, T. G., and de Boer, P. A. J. (2004). Screening for synthetic lethal mutants in *Escherichia coli* and identification of EnvC (YibP) as a periplasmic septal ring factor with murein hydrolase activity. *Mol. Microbiol.* 52, 1255–1269. doi: 10.1111/j.1365-2958.2004.04063.x

Bernhardt, T. G., and de Boer, P. A. J. (2005). SlmA, a nucleoid-associated, FtsZ binding protein required for blocking septal ring assembly over chromosomes in *E. coli*. *Mol. Cell* 18, 555–564. doi: 10.1016/j.molcel.2005.04.012

Bi, E., and Lutkenhaus, J. (1991). FtsZ ring structure associated with division in *Escherichia coli*. *Nature* 354, 161–164. doi: 10.1038/354161a0

Bisicchia, P., Arumugam, S., Schwille, P., and Sherratt, D. (2013). MinC, MinD, and MinE drive counter-oscillation of early-cell-division proteins prior to *Escherichia coli* septum formation. *mBio* 4, e00856–13. doi: 10.1128/mBio.00856-13

Bonny, M., Fischer-Friedrich, E., Loose, M., Schwille, P., and Kruse, K. (2013). Membrane binding of MinE allows for a comprehensive description of Min-protein pattern formation. *PLoS Comput. Biol.* 9:e1003347. doi: 10.1371/journal.pcbi.1003347

Bramkamp, M., Emmins, R., Weston, L., Donovan, C., Daniel, R. A., and Errington, J. (2008). A novel component of the division-site selection system of *Bacillus subtilis* and a new mode of action for the division inhibitor MinCD. *Mol. Microbiol.* 70, 1556–1569. doi: 10.1111/j.1365-2958.2008.06501.x

Bramkamp, M., and van Baarle, S. (2009). Division site selection in rod-shaped bacteria. *Curr. Opin. Microbiol.* 12, 683–688. doi: 10.1016/j.mib.2009.10.002

Buss, J., Coltharp, C., Huang, T., Pohlmeyer, C., Wang, S.-C., Hatem, C., et al. (2013). *In vivo* organization of the FtsZ-ring by ZapA and ZapB revealed by quantitative super-resolution microscopy. *Mol. Microbiol.* 89, 1099–1120. doi: 10.1111/mmi.12331

Buss, J., Coltharp, C., Shtengel, G., Yang, X., Hess, H., and Xiao, J. (2015). A multi-layered protein network stabilizes the *Escherichia coli* FtsZ-ring and modulates constriction dynamics. *PLoS Genet.* 11:e1005128. doi: 10.1371/journal.pgen.1005128

Cambridge, J., Blinkova, A., Magnan, D., Bates, D., and Walker, J. R. (2014). A replication-inhibited unsegregated nucleoid at mid-cell blocks Z-ring formation and cell division independently of SOS and the SlmA nucleoid occlusion protein in *Escherichia coli*. *J. Bacteriol.* 196, 36–49. doi: 10.1128/JB.01230-12

Carleton, H. A., Lara-Tejero, M., Liu, X., and Galán, J. E. (2013). Engineering the type III secretion system in non-replicating bacterial minicells for antigen delivery. *Nat. Commun.* 4, 1590. doi: 10.1038/ncomms2594

Cha, J.-H., and Stewart, G. C. (1997). The divIVA minicell locus of *Bacillus subtilis*. *J. Bacteriol.* 179, 1671–1683.

Conti, J., Viola, M. G., and Camberg, J. L. (2015). The bacterial cell division regulators MinD and MinC form polymers in the presence of nucleotide. *FEBS Lett.* 589, 201–206. doi: 10.1016/j.febslet.2014.11.047

Corbin, B. D., Yu, X.-C., and Margolin, W. (2002). Exploring intracellular space: function of the Min system in round-shaped *Escherichia coli*. *EMBO J.* 21, 1998–2008. doi: 10.1093/emboj/21.8.1998

Dajkovic, A., Lan, G., Sun, S. X., Wirtz, D., and Lutkenhaus, J. (2008). MinC spatially controls bacterial cytokinesis by antagonizing the scaffolding function of FtsZ. *Curr. Biol.* 18, 235–244. doi: 10.1016/j.cub.2008.01.042

de Boer, P. A. J., Crossley, R. E., Hand, A. R., and Rothfield, L. I. (1991). The MinD protein is a membrane ATPase required for the correct placement of the *Escherichia coli* division site. *EMBO J.* 10, 4371–4380.

de Boer, P. A. J., Crossley, R. E., and Rothfield, L. I. (1989). A division inhibitor and a topological specificity factor coded for by the minicell locus determine proper placement of the division septum in *E. coli*. *Cell* 56, 641–649. doi: 10.1016/0092-8674(89)90586-2

Di Ventura, B., Knecht, B., Andreas, H., Godinez, W. J., Fritsche, M., Rohr, K., et al. (2013). Chromosome segregation by the *Escherichia coli* Min system. *Mol. Syst. Biol.* 9, 686. doi: 10.1038/msb.2013.44

Di Ventura, B., and Sourjik, V. (2011). Self-organized partitioning of dynamically localized proteins in bacterial cell division. *Mol. Syst. Biol.* 7, 457. doi: 10.1038/msb.2010.111

Donovan, C., and Bramkamp, M. (2014). Cell division in Corynebacterineae. *Front. Microbiol.* 5:132. doi: 10.3389/fmicb.2014.00132

Donovan, C., Schwaiger, A., Krämer, R., and Bramkamp, M. (2010). Subcellular localization and characterization of the ParAB system from *Corynebacterium glutamicum*. *J. Bacteriol.* 192, 3441–3451. doi: 10.1128/JB.00214-10

Edwards, D. H., and Errington, J. (1997). The *Bacillus subtilis* DivIVA protein targets to the division septum and controls the site specificity of cell division. *Mol. Microbiol.* 24, 905–915. doi: 10.1046/j.1365-2958.1997.3811764.x

Edwards, D. H., Thomaides, H. B., and Errington, J. (2000). Promiscuous targeting of *Bacillus subtilis* cell division protein DivIVA to division sites in *Escherichia coli* and fission yeast. *EMBO J.* 19, 2719–2727. doi: 10.1093/emboj/19.11.2719

Espéli, O., Borne, R., Dupaigne, P., Thiel, A., Gigant, E., Mercier, R., et al. (2012). A MatP–divisome interaction coordinates chromosome segregation with cell division in *E. coli*. *EMBO J.* 31, 3198–3211. doi: 10.1038/emboj.2012.128

Fleurie, A., Lesterlin, C., Manuse, S., Zhao, C., Cluzel, C., Lavergne, J. -P., et al. (2014). MapZ marks the division sites and positions FtsZ rings in *Streptococcus pneumoniae*. *Nature* 516, 259–262. doi: 10.1038/nature13966

Galli, E., and Gerdes, K. (2010). Spatial resolution of two bacterial cell division proteins: ZapA recruits ZapB to the inner face of the Z-ring. *Mol. Microbiol.* 76, 1514–1526. doi: 10.1111/j.1365-2958.2010.07183.x

Ghosal, D., Trambaiolo, D., Amos, L. A., and Löwe, J. (2014). MinCD cell division proteins form alternating copolymeric cytomotive filaments. *Nat. Commun.* 5, 5341. doi: 10.1038/ncomms6341

Gregory, J. A., Becker, E. C., and Pogliano, K. (2008). *Bacillus subtilis* MinC destabilizes FtsZ-rings at new cell poles and contributes to the timing of cell division. *Genes Dev.* 22, 3475–3488. doi: 10.1101/gad.1732408

Gueiros-Filho, F. J., and Losick, R. (2002). A widely conserved bacterial cell division protein that promotes assembly of the tubulin-like protein FtsZ. *Genes Dev.* 16, 2544–2556. doi: 10.1101/gad.1014102

Hale, C. A., Meinhardt, H., and de Boer, P. A. J. (2001). Dynamic localization cycle of the cell division regulator MinE in *Escherichia coli*. *EMBO J.* 20, 1563–1572. doi: 10.1093/emboj/20.7.1563

Hale, C. A., Rhee, A. C., and de Boer, P. A. J. (2000). ZipA-induced bundling of FtsZ polymers mediated by an interaction between C-terminal domains. *J. Bacteriol.* 182, 5153–5166. doi: 10.1128/JB.182.18.5153-5166.2000

Hale, C., and de Boer, P. A. J. (1999). Recruitment of ZipA to the septal ring of *Escherichia coli* is dependent on FtsZ and independent of FtsA. *J. Bacteriol.* 181, 167–176.

Hayama, R., and Marians, K. J. (2010). Physical and functional interaction between the condensin MukB and the decatenase topoisomerase IV in *Escherichia coli*. *Proc. Natl. Acad. Sci. U.S.A.* 107, 18826–18831. doi: 10.1073/pnas.1008140107

Hiraga, S., Niki, H., Imamura, R., Ogura, T., Yamanaka, K., Feng, J., et al. (1991). Mutants defective in chromosome partitioning in *E. coli*. *Res. Microbiol.* 142, 189–194. doi: 10.1016/0923-2508(91)90029-A

Holečková, N., Doubravová, L., Massidda, O., Molle, V., Buriánková, K., Benada, O., et al. (2014). LocZ is a new cell division protein involved in proper

septum placement in *Streptococcus pneumoniae*. *mBio* 6, e01700–e01714. doi: 10.1128/mBio.01700-14

Hsieh, C.-W., Lin, T.-Y., Lai, H.-M., Lin, C.-C., Hsieh, T.-S., and Shih, Y.-L. (2010). Direct MinE-membrane interaction contributes to the proper localization of MinDE in *E. coli*. *Mol. Microbiol.* 75, 499–512. doi: 10.1111/j.1365-2958.2009.07006.x

Hu, B., Margolin, W., Molineux, I. J., and Liu, J. (2013). The bacteriophage T7 virion undergoes extensive structural remodeling during infection. *Science* 339, 576–579. doi: 10.1126/science.1231887

Hu, Z., Gogol, E. P., and Lutkenhaus, J. (2002). Dynamic assembly of MinD on phospholipid vesicles regulated by ATP and MinE. *Proc. Natl. Acad. Sci. U.S.A.* 99, 6761–6766. doi: 10.1073/pnas.102059099

Hu, Z., and Lutkenhaus, J. (1999). Topological regulation of cell division in *Escherichia coli* involves rapid pole to pole oscillation of the division inhibitor MinC under the control of MinD and MinE. *Mol. Microbiol.* 34, 82–90. doi: 10.1046/j.1365-2958.1999.01575.x

Hu, Z., and Lutkenhaus, J. (2000). Analysis of MinC reveals two independent domains involved in interaction with MinD and FtsZ. *J. Bacteriol.* 182, 3965–3971. doi: 10.1128/JB.182.14.3965-3971.2000

Hu, Z., and Lutkenhaus, J. (2001). Topological regulation of cell division in *E. coli*: spatiotemporal oscillation of MinD requires stimulation of its ATPase by MinE and phospholipid. *Mol. Cell* 7, 1337–1343. doi: 10.1016/S1097-2765(01)00273-8

Hu, Z., and Lutkenhaus, J. (2003). A conserved sequence at the C-terminus of MinD is required for binding to the membrane and targeting MinC to the septum. *Mol. Microbiol.* 47, 345–355. doi: 10.1046/j.1365-2958.2003.03321.x

Hu, Z., Mukherjee, A., Pichoff, S., and Lutkenhaus, J. (1999). The MinC component of the division site selection system in *Escherichia coli* interacts with FtsZ to prevent polymerization. *Proc. Natl. Acad. Sci. U.S.A.* 96, 14819–14824. doi: 10.1073/pnas.96.26.14819

Huang, K. C., Meir, Y., and Wingreen, N. S. (2003). Dynamic structures in *Escherichia coli*: spontaneous formation of MinE rings and MinD polar zones. *Proc. Natl. Acad. Sci. U.S.A.* 100, 12724–12728. doi: 10.1073/pnas.2135445100

Huang, K. C., and Wingreen, N. S. (2004). Min-protein oscillations in round bacteria. *Phys. Biol.* 1, 229–235. doi: 10.1088/1478-3967/1/4/005

Imai, Y., Ogasawara, N., Ishigo-Oka, D., Kadoya, R., Daito, T., and Moriya, S. (2000). Subcellular localization of DNA-initiation proteins of *Bacillus subtilis*: evidence that chromosome replication begins at either edge of the nucleoids. *Mol. Microbiol.* 36, 1037–1048. doi: 10.1046/j.1365-2958.2000.01928.x

Jamroškovič, J., Pavlendová, N., Muchová, K., Wilkinson, A. J., and Barák, I. (2012). An oscillating Min system in *Bacillus subtilis* influences asymmetrical septation during sporulation. *Microbiology* 158, 1972–1981. doi: 10.1099/mic.0.059295-0

Juarez, J. R., and Margolin, W. (2010). Changes in the Min oscillation pattern before and after cell birth. *J. Bacteriol.* 192, 4134–4142. doi: 10.1128/JB.00364-10

Kawai, F., Shoda, M., Harashima, R., Sadaie, Y., Hara, H., and Matsumoto, K. (2004). Cardiolipin domains in *Bacillus subtilis* marburg membranes. *J. Bacteriol.* 186, 1475–1483. doi: 10.1128/JB.186.5.1475-1483.2004

Kiekebusch, D., Michie, K. A., Essen, L.-O., Löwe, J., and Thanbichler, M. (2012). Localized dimerization and nucleoid binding drive gradient formation by the bacterial cell division inhibitor MipZ. *Mol. Cell* 46, 245–259. doi: 10.1016/j.molcel.2012.03.004

Kruse, K., Howard, M., and Margolin, W. (2007). An experimentalist's guide to computational modelling of the Min system. *Mol. Microbiol.* 63, 1279–1284. doi: 10.1111/j.1365-2958.2007.05607.x

Lackner, L. L., Raskin, D. M., and de Boer, P. A. J. (2003). ATP-dependent interactions between *Escherichia coli* Min proteins and the phospholipid membrane *in vitro*. *J. Bacteriol.* 185, 735–749. doi: 10.1128/JB.185.3.735-749.2003

Lenarcic, R., Halbedel, S., Visser, L., Shaw, M., Wu, L. J., Errington, J., et al. (2009). Localisation of DivIVA by targeting to negatively curved membranes. *EMBO J.* 28, 2272–2282. doi: 10.1038/emboj.2009.129

Liu, J., Hu, B., Morado, D. R., Jani, S., Manson, M. D., and Margolin, W. (2012). Molecular architecture of chemoreceptor arrays revealed by cryoelectron tomography of *Escherichia coli* minicells. *Proc. Natl. Acad. Sci. U.S.A.* 109, E1481–E1488. doi: 10.1073/pnas.1200781109

Loose, M., Fischer-Friedrich, E., Herold, C., Kruse, K., and Schwille, P. (2011). Min protein patterns emerge from rapid rebinding and membrane interaction of MinE. *Nat. Struct. Mol. Biol.* 18, 577–583. doi: 10.1038/nsmb.2037

Loose, M., Fischer-Friedrich, E., Ries, J., Kruse, K., and Schwille, P. (2008). Spatial regulators for bacterial cell division self-organize into surface waves *in vitro*. *Science* 320, 789–792. doi: 10.1126/science.1154413

Lutkenhaus, J., Pichoff, S., and Du, S. (2012). Bacterial cytokinesis: from Z ring to divisome. *Cytoskeleton* 69, 778–790. doi: 10.1002/cm.21054

Ma, L.-Y., King, G., and Rothfield, L. (2003). Mapping the MinE site involved in interaction with the MinD division site selection protein of *Escherichia coli*. *J. Bacteriol.* 185, 4948–4955. doi: 10.1128/JB.185.16.4948-4955.2003

MacDiarmid, J. A., and Brahmbhatt, H. (2011). Minicells: versatile vectors for targeted drug or si/shRNA cancer therapy. *Curr. Opin. Biotechnol.* 22, 909–916. doi: 10.1016/j.copbio.2011.04.008

Martos, A., Jiménez, M., Rivas, G., and Schwille, P. (2012). Towards a bottom-up reconstitution of bacterial cell division. *Trends Cell Biol.* 22, 634–643. doi: 10.1016/j.tcb.2012.09.003

Mazor, S., Regev, T., Mileykovskaya, E., Margolin, W., Dowhan, W., and Fishov, I. (2008). Mutual effects of MinD-membrane interaction: I. Changes in the membrane properties induced by MinD binding. *Biochim. Biophys. Acta.* 1778, 2496–2504. doi: 10.1016/j.bbamem.2008.08.003

McCormick, J. R., Su, E. P., Driks, A., and Losick, R. (1994). Growth and viability of *Streptomyces coelicolor* mutant for the cell division gene *ftsZ*. *Mol. Microbiol.* 14, 243–254. doi: 10.1111/j.1365-2958.1994.tb01285.x

Meinhardt, H., and de Boer, P. A. J. (2001). Pattern formation in *Escherichia coli*: a model for the pole-to-pole oscillations of Min proteins and the localization of the division site. *Proc. Natl. Acad. Sci. U.S.A.* 98, 14202–14207. doi: 10.1073/pnas.251216598

Mileykovskaya, E., and Dowhan, W. (2000). Visualization of phospholipid domains in *Escherichia coli* by using the cardiolipin-specific fluorescent dye 10-N-nonyl acridine orange. *J. Bacteriol.* 182, 1172–1175. doi: 10.1128/JB.182.4.1172-1175.2000

Mileykovskaya, E., Fishov, I., Fu, X., Corbin, B. D., Margolin, W., and Dowhan, W. (2003). Effects of phospholipid composition on MinD-membrane interactions *in vitro* and *in vivo*. *J. Biol. Chem.* 278, 22193–22198. doi: 10.1074/jbc.M302603200

Mileykovskaya, E., Sun, Q., Margolin, W., and Dowhan, W. (1998). Localization and function of early cell division proteins in filamentous *Escherichia coli* cells lacking phosphatidylethanolamine. *J. Bacteriol.* 180, 4252–4257.

Monahan, L. G., and Harry, E. J. (2012). Identifying how bacterial cells find their middle: a new perspective. *Mol. Microbiol.* 87, 231–234. doi: 10.1111/mmi.12114

Monahan, L. G., Liew, A. T. F., Bottomley, A. L., and Harry, E. J. (2014). Division site positioning in bacteria: one size does not fit all. *Front. Microbiol.* 5:19. doi: 10.3389/fmicb.2014.00019

Moriya, S., Rashid, R. A., Rodrigues, C. D. A., and Harry, E. J. (2010). Influence of the nucleoid and the early stages of DNA replication on positioning the division site in *Bacillus subtilis*. *Mol. Microbiol.* 76, 634–647. doi: 10.1111/j.1365-2958.2010.07102.x

Murray, H., and Errington, J. (2008). Dynamic control of the DNA replication initiation protein DnaA by Soj/ParA. *Cell* 135, 74–84. doi: 10.1016/j.cell.2008.07.044

Oliver, P. M., Crooks, J. A., Leidl, M., Yoon, E. J., Saghatelian, A., and Weibel, D. B. (2014). Localization of anionic phospholipids in *Escherichia coli* cells. *J. Bacteriol.* 196, 3386–3398. doi: 10.1128/JB.01877-14

Park, K.-T., Wu, W., Battaile, K. P., Lovell, S., Holyoak, T., and Lutkenhaus, J. (2011). The Min oscillator uses MinD-dependent conformational changes in MinE to spatially regulate cytokinesis. *Cell* 146, 396–407. doi: 10.1016/j.cell.2011.06.042

Patrick, J. E., and Kearns, D. B. (2008). MinJ (YvjD) is a topological determinant of cell division in *Bacillus subtilis*. *Mol. Microbiol.* 70, 1166–1179. doi: 10.1111/j.1365-2958.2008.06469.x

Pas, E., Einav, M., Woldringh, C. L., and Zaritsky, A. (2001). Perpendicular planes of FtsZ arcs in spheroidal *Escherichia coli* cells. *Biochimie* 83, 121–124. doi: 10.1016/S0300-9084(00)01219-0

Pazos, M., Casanova, M., Palacios, P., Margolin, W., Natale, P., and Vicente, M. (2014). FtsZ placement in nucleoid-free bacteria. *PLoS ONE* 9:e91984. doi: 10.1371/journal.pone.0091984

Pichoff, S., and Lutkenhaus, J. (2005) Tethering the Z ring to the membrane through a conserved membrane targeting sequence in FtsA. *Mol. Microbiol.* 55, 1722–1734. doi: 10.1111/j.1365-2958.2005.04522.x

Ramirez-Arcos, S., Szeto, J., Dillon, J. R., and Margolin, W. (2002). Conservation of dynamic localization among MinD and MinE orthologues: oscillation of *Neisseria gonorrhoeae* proteins in *Escherichia coli*. *Mol. Microbiol.* 46, 493–504. doi: 10.1046/j.1365-2958.2002.03168.x

Raskin, D. M., and de Boer, P. A. J. (1997). The MinE ring: an FtsZ-independent cell structure required for selection of the correct division site in *E. coli*. *Cell* 91, 685–694. doi: 10.1016/S0092-8674(00)80455-9

Raskin, D. M., and de Boer, P. A. J. (1999a). MinDE-dependent pole-to-pole oscillation of division inhibitor MinC in *Escherichia coli*. *J. Bacteriol.* 181, 6419–6424.

Raskin, D. M., and de Boer, P. A. J. (1999b). Rapid pole-to-pole oscillation of a protein required for directing division to the middle of *Escherichia coli*. *Proc. Natl. Acad. Sci. U.S.A.* 96, 4971–4976. doi: 10.1073/pnas.96.9.4971

Reeve, J. N., Mendelson, N. H., Coyne, S. I., Hallock, L. L., and Cole, R. M. (1973). Minicells of *Bacillus subtilis*. *J. Bacteriol.* 114, 860–873.

Renner, L. D., and Weibel, D. B. (2012). MinD and MinE interact with anionic phospholipids and regulate division plane formation in *Escherichia coli*. *J. Biol. Chem.* 287, 38835–38844. doi: 10.1074/jbc.M112.407817

Rodrigues, C. D. A., and Harry, E. J. (2012). The Min system and nucleoid occlusion are not required for identifying the division site in *Bacillus subtilis* but ensure its efficient utilization. *PLoS Genet.* 8:e1002561. doi: 10.1371/journal.pgen.1002561

Rowlett, V. W., and Margolin, W. (2013) *Curr. Biol.* 23, 553–556. doi: 10.1016/j.cub.2013.05.024

Roozen, K. J., Fenwick, R. G. Jr, and Curtis, R. III. (1971). Synthesis of ribonucleic acid and protein in plasmid-containing minicells of *Escherichia coli* K-12. *J. Bacteriol.* 107, 21–33.

Schofield, W. B., Lim, H. C., and Jacobs-Wagner, C. (2010). Cell cycle coordination and regulation of bacterial chromosome segregation dynamics by polarly localized proteins. *EMBO J.* 29, 3068–3081. doi: 10.1038/emboj.2010.207

Schweizer, J., Loose, M., Bonny, M., Kruse, K., Mönch, I., and Schwille, P. (2012). Geometry sensing by self-organized protein patterns. *Proc. Natl. Acad. Sci. U.S.A.* 109, 15283–15288. doi: 10.1073/pnas.1206953109

Shen, B., and Lutkenhaus, J. (2009). The conserved C-terminal tail of FtsZ is required for the septal localization and division inhibitory activity of MinCc/MinD. *Mol. Microbiol.* 72, 410–424. doi: 10.1111/j.1365-2958.2009.06651.x

Shen, B., and Lutkenhaus, J. (2010). Examination of the interaction between FtsZ and $MinC^{N}$ in *E. coli* suggests how MinC disrupts Z rings. *Mol. Microbiol.* 75, 1285–1298. doi: 10.1111/j.1365-2958.2010.07055.x

Shiomi, D., and Margolin, W. (2007). The C-terminal domain of MinC inhibits assembly of the Z ring in *Escherichia coli*. *J. Bacteriol.* 189, 236–243. doi: 10.1128/JB.00666-06

Stewart, P. S., and D'Ari, R. (1992). Genetic and morphological characterization of an *Escherichia coli* chromosome segregation mutant. *J. Bacteriol.* 174, 4513–4516.

Suefuji, K., Valluzzi, R., and RayChaudhuri, D. (2002). Dynamic assembly of MinD into filament bundles modulated by ATP, phospholipids, and MinE. *Proc. Natl. Acad. Sci. U.S.A.* 99, 16776–16781. doi: 10.1073/pnas.262671699

Sun, Q., and Margolin, W. (2001). Influence of the nucleoid on placement of FtsZ and MinE rings in *Escherichia coli*. *J. Bacteriol.* 183, 1413–1422. doi: 10.1128/JB.183.4.1413-1422.2001

Sun, Q., Yu, X.-C., and Margolin, W. (1998). Assembly of the FtsZ ring at the central division site in the absence of the chromosome. *Mol. Microbiol.* 29, 491–503. doi: 10.1046/j.1365-2958.1998.00942.x

Szeto, T. H., Rowland, S. L., Rothfield, L. I., and King, G. F. (2002). Membrane localization of MinD is mediated by a C-terminal motif that is conserved across eubacteria, archaea, and chloroplasts. *Proc. Natl. Acad. Sci. U.S.A.* 99, 15693–15698. doi: 10.1073/pnas.232590599

Thanbichler, M., and Shapiro, L. (2006). MipZ, a spatial regulator coordinating chromosome segregation with cell division in *Caulobacter*. *Cell* 126, 147–162. doi: 10.1016/j.cell.2006.05.038

Thanedar, S., and Margolin, W. (2004). FtsZ exhibits rapid movement and oscillation waves in helix-like patterns in *Escherichia coli*. *Curr. Biol.* 14, 1167–1173. doi: 10.1016/j.cub.2004.06.048

Tonthat, N. K., Milam, S. L., Cinnam, N., Whitfill, T., Margolin, W., and Schumacher, M. A. (2013). SlmA forms a higher-order structure on DNA that inhibits cytokinetic Z-ring formation over the nucleoid. *Proc. Natl. Acad. Sci. U.S.A.* 110, 10586–10591. doi: 10.1073/pnas.1221036110

Touhami, A., Jericho, M., and Rutenberg, A. D. (2006). Temperature dependence of MinD oscillation in *Escherichia coli*: running hot and fast. *J. Bacteriol.* 188, 7661–7667. doi: 10.1128/JB.00911-06

Traag, B. A., and van Wezel, G. P. (2008). The SsgA-like proteins in actinomycetes: small proteins up to a big task. *Antonie Van Leeuwehoek* 94, 85–97. doi: 10.1007/s10482-008-9225-3

Treuner-Lange, A., Aguiluz, K., van der Does, C., Gómez-Santos, N., Harms, A., Schumacher, D., et al. (2013). PomZ, a ParA-like protein, regulates Z-ring formation and cell division in *Myxococcus xanthus*. *Mol. Microbiol.* 87, 235–253. doi: 10.1111/mmi.12094

Turner, R. D., Ratcliffe, E. C., Wheeler, R., Golestanian, R., Hobbs, J. K., and Foster, S. J. (2010). Peptidoglycan architecture can specify division planes in *Staphylococcus aureus*. *Nat. Commun.* 1, 26. doi: 10.1038/ncomms1025

van Baarle, S., and Bramkamp, M. (2010). The MinCDJ system in *Bacillus subtilis* prevents minicell formation by promoting divisome disassembly. *PLoS ONE* 5:e9850. doi: 10.1371/journal.pone.0009850

Varma, A., Huang, K. C., and Young, K. D. (2008). The Min system as a general cell geometry detection mechanism: branch lengths in Y-shaped *Escherichia coli* cells affect Min oscillation patterns and division dynamics. *J. Bacteriol.* 190, 2106–2117. doi: 10.1128/JB.00720-07

Vecchiarelli, A. G., Li, M., Mizuuchi, M., and Mizuuchi, K. (2014). Differential affinities of MinD and MinE to anionic phospholipid influence Min patterning dynamics *in vitro*. *Mol. Microbiol.* 93, 453–463. doi: 10.1111/mmi.12669

Veiga, H., Jorge, A. M., and Pinho, M. G. (2011). Absence of nucleoid occlusion effector Noc impairs formation of orthogonal FtsZ rings during *Staphylococcus aureus* cell division. *Mol. Microbiol.* 80, 1366–1380. doi: 10.1111/j.1365-2958.2011.07651.x

Willemse, J., Borst, J. W., de Waal, E., Bisseling, T., and van Wezel, G. P. (2011). Positive control of cell division: FtsZ is recruited by SsgB during sporulation of Streptomyces. *Genes Dev.* 25, 89–99. doi: 10.1101/gad.600211

Wu, L. J., and Errington, J. (2004). Coordination of cell division and chromosome segregation by a nucleoid occlusion protein in *Bacillus subtilis*. *Cell* 117, 915–925. doi: 10.1016/j.cell.2004.06.002

Yu, X.-C., and Margolin, W. (1999). FtsZ ring clusters in min and partition mutants: role of both the Min system and the nucleoid in regulating FtsZ ring localization. *Mol. Microbiol.* 32, 315–326. doi: 10.1046/j.1365-2958.1999.01351.x

Zieske, K., and Schwille, P. (2013). Reconstitution of pole-to-pole oscillations of Min proteins in microengineered polydimethylsiloxane compartments. *Angew. Chem. Int. Ed.* 52, 459–462. doi: 10.1002/anie.201207078

Zieske, K., and Schwille, P. (2014). Reconstitution of self-organizing protein gradients as spatial cues in cell-free systems. *Elife* 3, e03949. doi: 10.7554/eLife.03949.026

Conflict of Interest Statement: The authors declare that the research was conducted in the absence of any commercial or financial relationships that could be construed as a potential conflict of interest.

Copyright © 2015 Rowlett and Margolin. This is an open-access article distributed under the terms of the Creative Commons Attribution License (CC BY). The use, distribution or reproduction in other forums is permitted, provided the original author(s) or licensor are credited and that the original publication in this journal is cited, in accordance with accepted academic practice. No use, distribution or reproduction is permitted which does not comply with these terms.

frontiers in Microbiology

ORIGINAL RESEARCH
published: 10 July 2015
doi: 10.3389/fmicb.2015.00662

Simultaneous regulation of cell size and chromosome replication in bacteria

*Po-Yi Ho and Ariel Amir**

School of Engineering and Applied Sciences, Harvard University, Cambridge, MA, USA

Bacteria are able to maintain a narrow distribution of cell sizes by regulating the timing of cell divisions. In rich nutrient conditions, cells divide much faster than their chromosomes replicate. This implies that cells maintain multiple rounds of chromosome replication per cell division by regulating the timing of chromosome replications. Here, we show that both cell size and chromosome replication may be simultaneously regulated by the long-standing initiator accumulation strategy. The strategy proposes that initiators are produced in proportion to the volume increase and is accumulated at each origin of replication, and chromosome replication is initiated when a critical amount per origin has accumulated. We show that this model maps to the incremental model of size control, which was previously shown to reproduce experimentally observed correlations between various events in the cell cycle and explains the exponential dependence of cell size on the growth rate of the cell. Furthermore, we show that this model also leads to the efficient regulation of the timing of initiation and the number of origins consistent with existing experimental results.

Keywords: replication initiation, cell cycle, cell size regulation, multiple forks, mathematical modeling

OPEN ACCESS

Edited by:
Arieh Zaritsky, Ben-Gurion University of the Negev, Israel

Reviewed by:
Charles Edward Helmstetter, Florida Institute of Technology, USA
Joao D. Xavier, Memorial Sloan Kettering Cancer Center, USA
Avinoam Rabinovitch, Ben-Gurion University of the Negev, Israel

****Correspondence:***
Ariel Amir, School of Engineering and Applied Sciences, Harvard University, 29 Oxford Street, Cambridge, 02138 MA, USA
arielamir@seas.harvard.edu

Specialty section:
This article was submitted to Microbial Physiology and Metabolism, a section of the journal Frontiers in Microbiology

Received: *31 March 2015*
Accepted: *17 June 2015*
Published: *10 July 2015*

Citation:
Ho P and Amir A (2015) Simultaneous regulation of cell size and chromosome replication in bacteria. Front. Microbiol. 6:662. doi: 10.3389/fmicb.2015.00662

1. Introduction

Bacterial cells are extremely proficient in regulating and coordinating the different processes of the cell cycle. The Cooper-Helmstetter model proposes a molecular mechanism that couples two such processes, the replication of the chromosome and the division of the cell (Cooper and Helmstetter, 1968). In the model, cell division occurs a constant duration after the initiation of chromosome replication. The model implies a tight coordination between replication initiation and cell division such that in cells able to double faster than their chromosomes can replicate, multiple rounds of replications proceed simultaneously (Yoshikawa et al., 1964; Cooper and Helmstetter, 1968). To answer how cells regulate the timing of initiation, it was proposed that replication initiation factors accumulate to a critical amount per origin of replication to trigger the initiation of replication (Helmstetter et al., 1968). Since the conception of the above model, many experiments and models have attempted to capture the molecular mechanisms responsible for the initiation of multiple rounds of replication. However, no model has been completely satisfactory (Donachie and Blakely, 2003).

As a result of the coupling between replication and division, the average cell size per origin is approximately a constant independent of the growth rate of the cell (Donachie, 1968). Furthermore, it is now understood that a common size regulation strategy for organisms including bacteria and budding yeast is the incremental model in which division occurs upon the addition of a constant

size dependent on the growth rate of the cell (Amir, 2014; Campos et al., 2014; Soifer et al., 2014; Taheri-Araghi et al., 2015). However, the molecular mechanisms responsible for the incremental model of size control remain in question.

Our main result in this work is to show that the initiator accumulation strategy not only regulates size according to the incremental model, but also regulates simultaneously the timing of initiation and the number of origins of replication. The strategy says that replication initiates upon the accumulation of a critical amount of replication initiation factors per origin. We emphasize the importance of the partitioning of replication initiation factors amongst origins, which we show is essential in order for the multiple replication forks to be adequately regulated. We show, analytically and numerically, that this strategy robustly regulates both cell size and the number of origins. Agreement between existing experiments and predictions of the above model reveals essential features that must be captured in any molecular mechanisms coordinating replication initiation and cell division. Finally, we make distinct predictions regarding the distribution of cell sizes at initiation of replication.

2. Methods

2.1. Multiple Origins Accumulation Model

We consider the regulation strategy in which replication initiates upon the accumulation of a critical amount of replication initiation factors, or "initiators," per origin of replication (Helmstetter et al., 1968). We assume that the initiators are expressed via an autorepressor model, as seen in **Figure 1** (Sompayrac and Maaloe, 1973). In this model, a protein is expressed such that its concentration c remains constant and independent of the growth rate of the cell, which is plausible to achieve through autorepression. Therefore, an increase in the volume of the cell corresponds to a proportional increase in the copy number of this autorepressing protein. A second protein is the initiator and is expressed under the same promoter as the first, but in contrast to the first protein, it is *localized* at the origins of replication. For simplicity, we assume that the initiators are equally partitioned amongst the origins. Initiation then occurs when a critical copy number per origin N_{critical} of the localized initiators is reached, after which the initiators are assumed to degrade. Under these assumptions, the copy number of the initiator effectively measures the increase in volume since initiation.

More precisely, if a cell initiated a round of replication at volume v_i into O number of origins, the amount of initiators $N_{\text{initiators}}$ immediately after initiation is zero. To initiate the next round of replication, the cell must accumulate ON_{critical} initiators, but because the initiator is expressed under the same promoter as the autorepressor, the cell must also accumulate ON_{critical} autorepressors. Because the concentration of the autorepressor is constant, this implies that the cell must accumulate a corresponding volume $\Delta = N_{\text{critical}}/c$ per origin, independent of the growth rate, to trigger the next initiation.

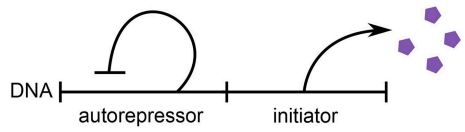

FIGURE 1 | Schematic of the autorepressor model of initiator expression. An autorepressor is expressed such that its concentration remains constant and independent of the growth rate of the cell. The initiator is expressed in proportion to the autorepressor, but is localized at the origins of replication. Adapted from Sompayrac and Maaloe (1973).

Thus, on a phenomenological level, the above biophysical model maps to the following regulation strategy for initiation,

$$v_i^{\text{tot,next}} \approx v_i + O\Delta, \tag{1}$$

Equation (1) says that if a cell initiated a round of replication at cell volume v_i into O number of origins, then the cell will attempt to initiate another round of replication at total volume $v_i^{\text{tot,next}}$, which is the sum of the volumes of all cells in the lineage since the initiation event at v_i (typically two cells). This is not to be confused with the threshold model in which cells initiate upon reaching a threshold volume proportional to the number of origins, $v_i^{\text{next}} \propto O$. For the rest of this manuscript, O will denote the number of origins *after* initiation at cell volume v_i but *before* initiation at total cell volume $v_i^{\text{tot,next}}$.

We assume an exponential mode of growth for cell volume with a constant doubling time τ and a corresponding constant growth rate $\lambda = \ln 2/\tau$ (Godin et al., 2010). From Equation (1) and the exponential mode of growth, durations between initiations are

$$t_i = \frac{1}{\lambda} \ln\left(1 + \frac{O\Delta}{v_i}\right) + \xi, \tag{2}$$

where ξ represents some noise in the initiation process. An initiation event will trigger a division event after a constant duration $C + D$, where C and D are respectively, the constant duration required to replicate the chromosome and the constant duration between replication termination and division (Cooper and Helmstetter, 1968). We will refer to Equation (1) as the multiple origins accumulation model (i.e., initiators are accumulated per origin). **Figure 2** illustrates this regulation strategy. We note that the strategy described here is mathematically equivalent to the "replisome" model of Bleecken (1971) (not to be confused with the current use of the term replisome).

Finally, we will not take into account additional biological mechanisms that act at the level of the initiation of chromosome replication, such as *oriC* sequestration, Dam methylation, and the "eclipse" phenomenon (Bogan and Helmstetter, 1997; Zaritsky et al., 2007; Campbell and Kleckner, 2010). While these mechanisms are important to prevent rapid re-initiations, by themselves they are insufficient in ensuring an appropriately coordinated coupling between chromosome replication and cell division, which is the main focus of our work.

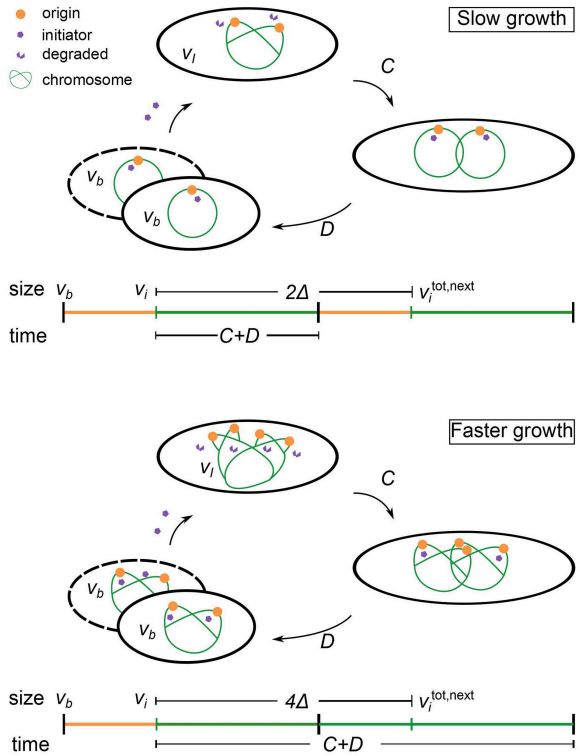

FIGURE 2 | Schematic of the regulation strategy of the multiple origins accumulation model. See text for the details of the model. Slow growth denotes $0 < \frac{C+D}{\tau} < 1$. Faster growth denotes $1 < \frac{(C+D)}{\tau}$. In the above example, $\frac{(C+D)}{\tau} < 2$.

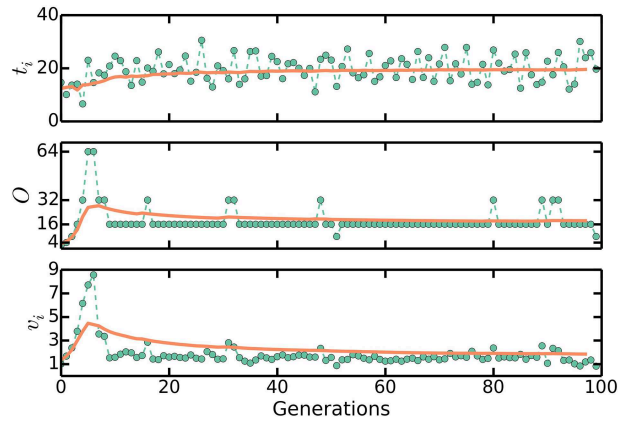

FIGURE 3 | t_i, O, and v_b approaching stationary distributions in numerical simulations of the multiple origins accumulation model. First, we initialize a population of N cells with uniformly distributed cell ages. Durations between initiations of replication are calculated as Equation (2) and the noise in the initiation process is assumed to be normally distributed. In an initiation event, the number of origins in a cell is doubled. The corresponding division event occurs after a constant time $C + D$. In a division event, the number of origins in a cell, along with the size of the cell, is halved, and two identical cells are generated. There are no division events without the corresponding initiation events. Following this procedure, a population of cells will robustly reach a stationary distribution of cell sizes and number of origins per cell regardless of initial conditions. The plots here track one lineage of cells. Solid lines are moving averages. Here, $C + D = 70$ mins, $\tau = 20$ mins, and $\sigma_\tau = 4$ mins. These are biologically realistic choices. We set $\Delta = 1/2^{(C+D)/\tau}$ so that $\langle v_b \rangle \approx 1$.

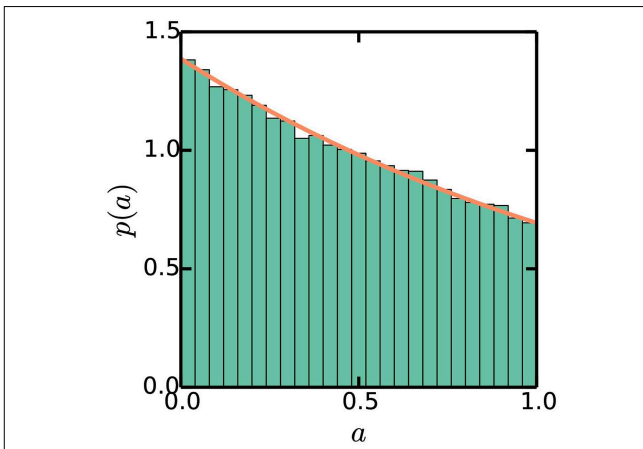

FIGURE 4 | Stationary exponential distribution of cell ages. Simulations are the same as **Figure 3**. The line plots $p(a) = (\ln 2)\, 2^{1-a}$, as described in the Appendix.

2.2. Numerical Simulations

We can numerically simulate the multiple origins accumulation model given $C + D$, τ, and Δ as experimentally measurable parameters. First, we initialize a population of N cells with uniformly distributed cell ages. Durations between initiations are calculated as Equation (2) and the noise in the initiation process is assumed to be normally distributed with standard deviation σ_τ, though the precise nature of the noise does not affect any of our conclusions. It is assumed that in an initiation event, the number of origins in a cell is doubled. The corresponding division event occurs after a constant time $C+D$. In a division event, the number of origins in a cell, along with the size of the cell, is halved, and two identical cells are generated. We neglect the stochasticity arising from asymmetric divisions, which do not significantly affect any of the results. There are no division events without the corresponding initiation events. Following this procedure, a population of cells will robustly reach stationarity regardless of initial conditions, as seen in **Figures 3**, **4**.

3. Results

3.1. Multiple Origins Accumulation Robustly and Efficiently Regulates the Number of Origins of Replication

An important measurable consequence of the tight coupling between replication initiation and cell division is the average number of origins of replication per cell. It has been theoretically shown that the average number of origins per cell is

$$\langle O \rangle = 2^{(C+D)/\tau}. \tag{3}$$

The derivations leading up to Equation (3), summarized in Appendix, hinge on assuming an *efficient process*: the population is growing exponentially and reaches a stationary distribution of cell ages, implying that there are no delays due to

chromosome replication. These assumptions are independent of any molecular mechanisms for initiation and thus should be fulfilled by any efficient mechanism. We will show that the multiple origins accumulation model reproduces Equation (3).

The multiple origins accumulation model regulates initiation via negative feedback on the volume at initiation described by Equations (1) and (2). The feedback enables cells to maintain a stationary average volume at initiation and a stationary average duration between initiations despite noise in the initiation process. Specifically, if a cell initiated replication at volume $v_i = O\Delta$, then the duration to the next initiation event is

$$t_i(O) \approx \frac{1}{\lambda}\ln\left(1+\frac{O\Delta}{O\Delta}\right) = \tau. \quad (4)$$

But if a cell initiated replication at a slightly larger volume $v_i = O\Delta + \delta v$, the duration to the next initiation event is

$$t_i'(O) \approx \frac{1}{\lambda}\ln\left(1+\frac{O\Delta}{O\Delta+\delta v}\right) \lesssim \tau. \quad (5)$$

Equations (4) and (5) say that a cell that initiated at a slightly larger volume than average tend to initiate again faster than average so that its volume at next initiation is again near the average. Similar reasoning says that cells that initiated at slightly smaller volumes tend to initiate again slower than average. In this way, cells maintain a stationary average volume at initiation and a stationary average duration between initiations.

Furthermore, the feedback enables cells to maintain a balanced cell cycle, in which there is on average one and only one initiation event per cell cycle. In the case of negligible noise, a balanced cell cycle implies that cells will initiate at cell age (Bremmer and Dennis, 1996)

$$a_i = 1 + \lfloor\frac{C+D}{\tau}\rfloor - \frac{C+D}{\tau}, \quad (6)$$

where $a = 0$ represents cell birth, $a = 1$ represents cell division, and $\lfloor\rfloor$ is the mathematical floor operator (largest integer smaller or equal to the argument). But in the case of realistic noise, a cell may initiate an extra round of replication if the noise is negative enough, $\xi/\tau \lesssim \lfloor(C+D)/\tau\rfloor - (C+D)/\tau$, which corresponds to an extra initiation at volume $v_i' = 2O\Delta - \delta v$. The multiple origins accumulation model is robust to these stochastic events because a cell that initiated an extra round of replication will initiate again after

$$t_i(2O) \approx \frac{1}{\lambda}\ln\left(1+\frac{2O\Delta}{2O\Delta-\delta v}\right) \gtrsim \tau. \quad (7)$$

In other words, cells with extra rounds of replication will initiate slower than those without so that the stationary average duration between initiations is maintained. The cell cycle following the extra initiation will typically not have any initiations, so that the initiation following the extra initiation will occur at approximately the average volume at initiation. A cell that missed a round of replication will return to a balanced initiation process in the analogous manner. In this way, the multiple origins accumulation model is able to efficiently maintain a balanced cell cycle in fast growth conditions. In contrast, the model simulated by Campos et al. (2014) is not robust to the noise in the initiation process, because in their model, the incremental volume needed to trigger initiation is not partitioned between origins. We will elaborate on this in Section 3.3.

The multiple origins accumulation model is therefore able to robustly regulate the timing of initiations in face of extra initiations. Extra initiations can occur not only because of noise in the initiation process, but also because of a shift in the growth rate of the cell such as that found in a shift-up experiment, in which a population of cells is abruptly switched from one nutrient condition to a richer nutrient condition allowing for faster growth. The increase in growth rate corresponds to a decrease in the duration between initiations. Therefore, cell in a shift-up experiment will initiate extra rounds of replication in the cycle immediately following the shift-up, but as we have seen, the multiple origins accumulation model is able to appropriately regulate the timing of initiations to reflect the new growth rate. Simulations of the multiple origins accumulation model reached stationary distributions of cell ages, durations between initiations, cell sizes, and number of origins per cell, regardless of initial conditions or the magnitude of the noise ξ in Equation (2), as seen in **Figures 3**, **4**. Simulations also show that the number of origins is regulated as in Equation (3), as seen in **Figure 5**. The above considerations show that the multiple origins accumulation model regulates the number of origins robustly and efficiently in face of noise in the initiation process.

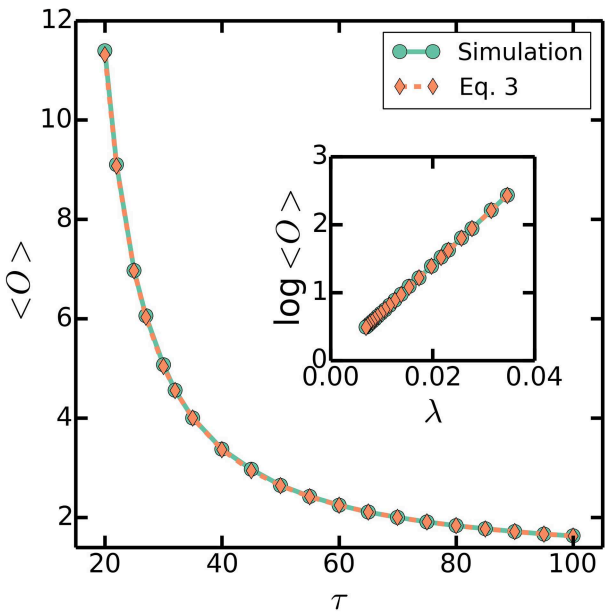

FIGURE 5 | $\langle O \rangle$ as a function of τ. Simulations are the same as **Figure 3**, with a varying τ = 20–100 mins, a fixed $C + D$ = 70 mins, and $\sigma_\tau/\tau = 0.2$. Dashed line plots (Equation 3). Similarly, inset plots $\log\langle O \rangle$ as a function of λ.

3.2. Multiple Origins Accumulation Robustly Regulates Cell Size

It was recently shown that the multiple origins accumulation model of replication initiation reduces to the incremental model of size regulation (Amir, 2014)

$$v_d \approx v_b + v_0. \tag{8}$$

Equation (8) says that if a cell is born with volume v_b, then the cell will attempt to divide at volume v_d, where v_0 is the constant incremental volume from birth to division. In fact, v_0 can be expressed in terms of known parameters. First, if a cell initiated replication at volume v_i, then the corresponding division event will occur at total volume $v_d^{\text{tot}} = v_i 2^{(C+D)/\tau}$. But there will have been $\log_2 O$ division events since initiation at v_i, so that the corresponding volume at birth is

$$v_b = \frac{v_d^{\text{tot}}}{O} = \frac{v_i 2^{(C+D)/\tau}}{O}. \tag{9}$$

In a balanced cell cycle, the next initiation event will occur at total volume $v_i^{\text{tot,next}} \approx v_i + O\Delta$ and the corresponding division event will occur at total volume $v_d^{\text{tot,next}} = v_i^{\text{tot,next}} 2^{(C+D)/\tau}$. Similarly, there will have been $\log_2 O$ division events since initiation at v_i^{next}, so that the corresponding volume at division is

$$v_d = \frac{v_d^{\text{tot,next}}}{O} = \frac{v_i 2^{(C+D)/\tau}}{O} + \Delta 2^{(C+D)/\tau}. \tag{10}$$

Therefore,

$$v_d - v_b \approx \Delta 2^{(C+D)/\tau}. \tag{11}$$

Within the multiple origins accumulation model, this derivation is valid for any $C + D$ and τ (Amir, 2014).

The incremental model of size regulation predicts distributions, correlations, correlation coefficients, and scalings consistent with existing measurements (Amir, 2014; Campos et al., 2014; Soifer et al., 2014; Taheri-Araghi et al., 2015). In particular, the average cell volume at birth

$$\langle v_b \rangle \approx \Delta 2^{(C+D)/\tau}. \tag{12}$$

Equation (12) says that the average cell volume at birth is exponentially dependent on the growth rate, a well-known and well-tested result for *E. coli* and *B. subtilis* (Schaechter et al., 1958; Sharpe et al., 1998; Taheri-Araghi et al., 2015). Simulations of the multiple origins accumulation model also confirm this result, as seen in **Figure 7**. Thus, the multiple origins accumulation model robustly regulates cell size.

3.3. Master Accumulation Predictions are Inconsistent with Existing Experiments

Consider the regulation strategy

$$v_i^{\text{tot,next}} \approx v_i + \Delta. \tag{13}$$

Equation (13) says that if a cell initiated a round of chromosome replication at cell volume v_i with O number of origins of replication, then the cell will attempt to initiate another round of replication at total volume $v_i^{\text{tot,next}}$, where Δ is a constant volume independent of the growth rate. This is an incremental model of size control applied at initiation. If we assume the same mode of initiator expression as before, then the regulation strategy described by Equation (13) corresponds to replication initiation upon accumulation of a critical amount of initiators *without* partitioning of initiators between origins. Instead, a plausible molecular picture is that of initiators accumulating at a "master" origin, whose initiation triggers the cascade initiation of other origins (Lobner-Olesen et al., 1994). We will therefore refer to Equation (13) as the master accumulation model. In contrast to the multiple origins accumulation model described above, here in the master accumulation model, the total volume at next initiation does not depend on the number of origins present in the cell.

As before, we assume an exponential mode of growth with a constant doubling time τ. The durations between initiations are therefore

$$t_i(O) = \frac{1}{\lambda} \ln\left(1 + \frac{\Delta}{v_i}\right) + \xi, \tag{14}$$

where ξ represents some noise in the initiation process. Again as before, an initiation event will trigger a division event after a constant duration $C + D$. Equation (14) differs from Equation (2) by a missing factor of O. As we show below, the factor of O is essential in regulating appropriately the timing of initiations.

However, essential in regulating appropriately the timing of initiations and the master accumulation model does not reproduce the well-known exponential scaling of cell size with growth rate. The derivation follows and is similar to that of the multiple origins accumulation model. First, if a cell initiated replication at volume v_i, then the corresponding division event will occur at total volume $v_d^{\text{tot}} = v_i 2^{(C+D)/\tau}$. But there will have been $\log_2 O$ division events since initiation at v_i, so that the corresponding volume at birth is

$$v_b = \frac{v_d^{\text{tot}}}{O} = \frac{v_i 2^{(C+D)/\tau}}{O}. \tag{15}$$

In a balanced cell cycle, the next initiation event will occur at total volume $v_i^{\text{tot,next}} \approx v_i + \Delta$ and the corresponding division event will occur at total volume $v_d^{\text{tot,next}} = v_i^{\text{tot,next}} 2^{(C+D)/\tau}$. Similarly, there will have been $\log_2 O$ division events since initiation at v_i^{next}, so that the corresponding volume at division is

$$v_d = \frac{v_d^{\text{tot,next}}}{O} = \frac{v_i 2^{(C+D)/\tau}}{O} + \frac{\Delta 2^{(C+D)/\tau}}{O}. \tag{16}$$

Therefore,

$$v_d - v_b = \frac{\Delta 2^{(C+D)/\tau}}{O}. \tag{17}$$

This derivation is valid for any $C + D$ and τ. However, from Equation (3), O should scale exponentially with the growth rate like $2^{(C+D)/\tau}$ so that

$$\langle v_b \rangle \approx v_d - v_b \sim \Delta. \tag{18}$$

Equation (18) says that the average cell size is a constant roughly independent of the growth rate, a prediction contradicting the well-tested exponential scaling with growth rate for the model organisms mentioned above.

Furthermore, the above reasoning assumes that the master accumulation model can maintain a balanced cell cycle. But the master accumulation model cannot robustly maintain a balanced cell cycle in face of noise as Equation (14) demonstrates. Specifically, if a cell initiated replication at volume $v_i = \Delta$, then the duration to the next initiation event is

$$t_i(O) \approx \frac{1}{\lambda} \ln\left(1 + \frac{\Delta}{\Delta}\right) = \tau. \tag{19}$$

But the cell may proceed to initiate an extra round of replication if the noise is negative enough, $\xi/\tau \lesssim \lfloor (C+D)/\tau \rfloor - (C+D)/\tau$, which corresponds to an extra round of initiation at volume $v_i' = 2\Delta - \delta v$. The next initiation will then occur after

$$t_i(2O) \approx \frac{1}{\lambda} \ln\left(1 + \frac{\Delta}{2\Delta - \delta v}\right) \gtrsim \log_2\left(\frac{3}{2}\right)\tau. \tag{20}$$

Implying that:

$$t_i(2O) \lesssim t_i(O) \tag{21}$$

Equation (21) says that cells with more origins will initiate faster than those with less, giving rise to cells with average durations between birth and division not equal to τ. In other words, the master accumulation model does not robustly regulate the initiation process to maintain a balanced cell cycle. Indeed, simulations of the master accumulation model do not converge to a balanced cell cycle. Likewise, Campos et al. (2014) carried out simulations of the master accumulation model and obtained "widely abnormal cell size distributions." Given the above inconsistent predictions, the master accumulation model can be ruled out as a possible regulation strategy for replication initiation.

3.4. Multiple Origins Accumulation Suggests That Variations in $C + D$ Are Small

In claiming that the master accumulation model gives incorrect correlations between growth rate dependent variables, Campos et al. (2014) simulated the master accumulation model and reported negative correlations between cell size at birth v_b and cell size differences between birth and division Δv, whereas none is observed experimentally. In contrast to claims in Campos et al. (2014), the negative correlations do not provide evidence against the multiple origins accumulation model nor the master accumulation model. Instead, the negative correlations provide evidence that variability in the durations from initiation to division $C + D$ should be small. Indeed, the multiple origins accumulation model, because of its reduction to the incremental model of size control, predicts no correlations between v_b and Δv, *given* that variations in $C + D$ are small compared to variations in τ. Simulations assuming that durations from initiation to the corresponding division are normally distributed with mean $C + D$ and standard deviation σ_{C+D} show that the correlations between v_b and Δv become increasingly negative as σ_{C+D}/σ_τ increases, as seen in **Figure 6**. **Figure 6** shows that as long as $\sigma_{C+D}/\sigma_\tau < 0.3$, the correlations between v_b and Δv will be close to zero. This is intuitive because when σ_{C+D} is small compared to σ_τ, fluctuations in cell sizes at birth arise due to variations in cell sizes at initiation, but these variations are negatively fed back into the multiple origins accumulation model as explained in Section 3.1. On the other hand, when σ_{C+D} is comparable to σ_τ, some fluctuations in cell sizes at birth arise due to variations in durations between initiation and division, but these variations are not accounted for by the multiple origins accumulation model. Variations of this nature give rise to the negative correlations between v_b and Δv.

3.5. Multiple Origins Accumulation Predicts Proportionality between Cell Size and the Number of Origins Per Cell

The simultaneous regulation of cell size and the number of origins per cell in the multiple origins accumulation model gives rise to a strict relationship between the two variables. In the multiple origins accumulation model, the average cell volume at birth (Equation 12) is exponentially dependent on the growth rate, while the average number of origins per cell (Equation 3) also scales exponentially with the growth rate. Therefore, we have that

$$\langle v_b \rangle \approx \Delta \langle O \rangle \tag{22}$$

That is, the multiple origins accumulation model predicts that given a fixed volume increment per origin Δ, the average volume at birth and the average number of origins per cell will scale appropriately with respect to a varying $(C + D)/\tau$ to give rise to the above approximate proportionality. The critical size regulation strategy proposed by Donachie assumed this proportionality (Donachie, 1968), but is inconsistent with measured correlations in *E. coli* because thresholding size at any point in the cell cycle washes away the memory of the initial conditions, and therefore leads to a vanishing correlation coefficient between size at birth and size at division - contrary to measurements; on the other hand, multiple origins accumulation predicts this proportionality, and is consistent with measured correlations (Amir, 2014; Campos et al., 2014; Soifer et al., 2014; Taheri-Araghi et al., 2015). Simulations of the multiple origins accumulation model confirm that cell size is indeed approximately proportional to the number of origins per cell, as seen in **Figure 7**. We emphasize that the approximate proportionality is a property predicted by the multiple origins accumulation model. In contrast, other strategies that do not regulate the number of origins, such as the master accumulation model, would not predict it.

3.6. Multiple Origins Accumulation Predicts Bimodal Cell Sizes at Initiation

In addition to the approximate proportionality between cell size and the number of origins per cell, the multiple origins accumulation model predicts that the distribution of cell sizes at initiation will be approximately bimodal because cells will

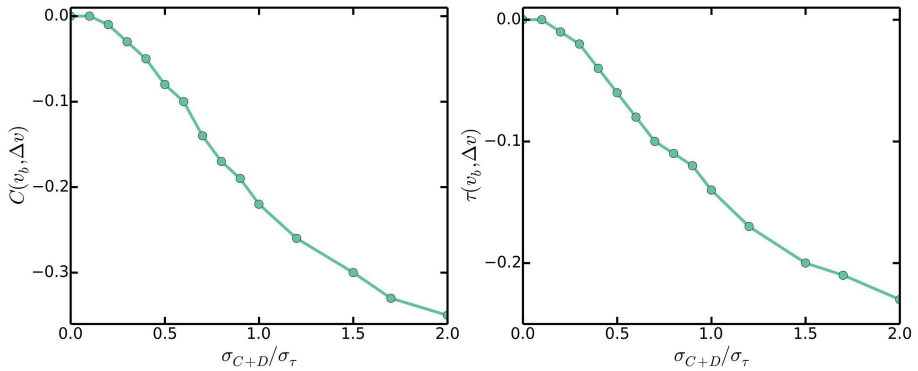

FIGURE 6 | Pearson (left) and Kendall (right) correlations between cell sizes at birth v_b and cell size differences between birth and division Δv against σ_{C+D}/σ_τ.

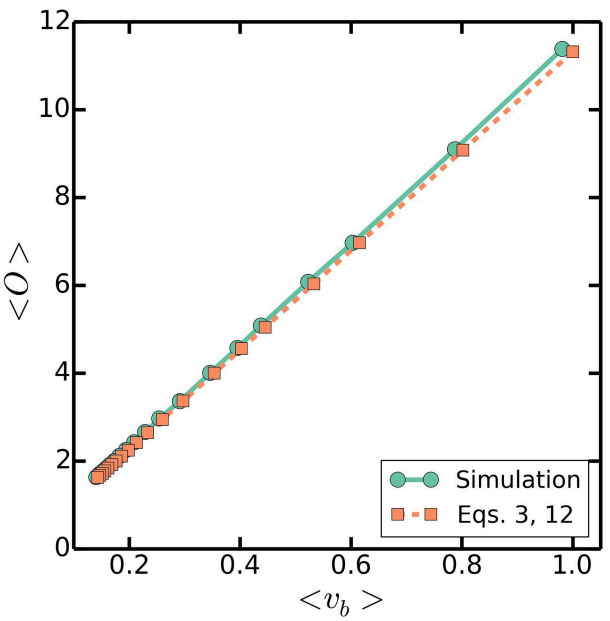

FIGURE 7 | $\langle O \rangle$ against $\langle v_b \rangle$. Simulations are as in **Figure 3**, with a varying $\tau = 20 - 100$ mins, a fixed $C + D = 70$ mins, and $\sigma_\tau/\tau = 0.2$. Dashed line plots (Equations 3 and 12).

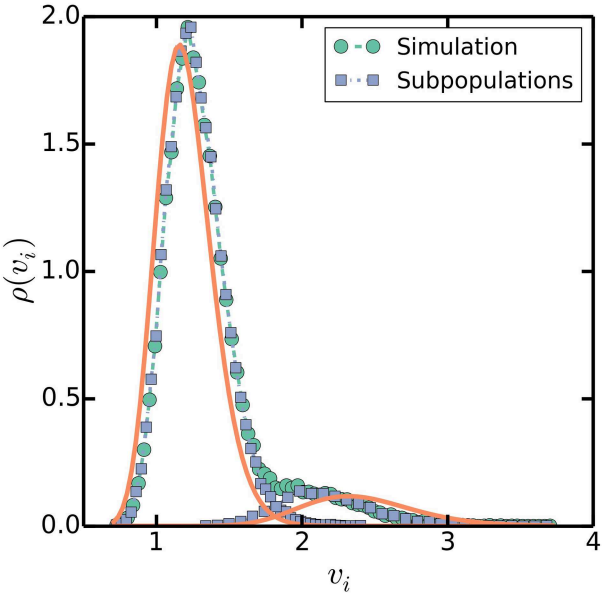

FIGURE 8 | Distribution of volumes at initiation. Simulations are as in **Figure 3**, with $\tau = 100$ mins, $C + D = 70$ mins, and $\sigma_\tau = 20$ mins as a specific, slow growth example. Square symbols separate volumes at initiation into two subpopulations, one whose cells initiated the predicted number of rounds of replication at volumes near $l_0\Delta$, and another whose cells initiated extra rounds of replication near twice that volume $2l_0\Delta$. Solid lines plot lognormal distributions with means $l_0\Delta$ and $2l_0\Delta$ and variances $\sigma_{v_i}^2 = 4\sigma_\tau^2/3\tau^2$ (Amir, 2014).

initiate extra rounds of replication when the noise is large enough. Simulations show that the distribution of cell sizes at initiation is indeed bimodal, with one large peak corresponding to a subpopulation whose cells initiated the expected number of rounds of replication and a smaller subpopulation whose cells initiated extra rounds of replication, as seen in **Figure 8**. Naively, because the distribution of cell sizes is lognormal in the multiple origins accumulation model, the distribution of cell sizes at initiation should be approximately the sum of two lognormal distributions with means $O_0\Delta$ and $2O_0\Delta$, where $O_0 = 2^{\lfloor (C+D)/\tau \rfloor}$, and the ratio between the frequencies of the two peaks equal to the probability that $\xi/\tau \lesssim \lfloor (C+D)/\tau \rfloor - (C+D)/\tau$. However, the value $O_0\Delta$ overestimates the average sizes at initiation of cells that initiated extra rounds of replication because of correlations between the volumes at initiation and the probability for extra rounds of replication. The correlations arise from Equation (2), which says that a smaller volume at initiation correlates with a larger probability for extra rounds of replication during the current cell cycle. The bimodal distribution of cell sizes at initiation highlights how the multiple origins accumulation model, without invoking other mechanisms, can robustly maintain a balanced cell cycle despite noise in the initiation process and is an experimentally testable prediction of our model.

3.7. Multiple Origins Accumulation Predictions Are Consistent with Experiments on Mutants

Existing experiments on mutants of *E. coli* and *B. subtilis* produced results consistent with the predictions of the multiple origins accumulation model. Experiments have shown by manipulating the cell size of *E. coli* via mutations that a decrease in ν is correlated with a decrease in $C + D$ and that a decrease in ν is also correlated with a decrease in $\langle O \rangle$ (Hill et al., 2012). In the language of the multiple origins accumulation model, ν is controlled by Δ and $(C + D)/\tau$. We assume that the mutations left unchanged the replication initiation mechanism in *E. coli*., so that Δ is a constant throughout. But τ remained approximately constant with changes in ν, so a decrease in ν must correspond to a decrease in $C + D$. One particular measurement reported for *E. coli* cells an average doubling time $\tau \approx 25$ mins for wildtype and mutant cells, $C + D \approx 40$ mins $+ 20$ mins for wildtype cells, and $(C + D)' \approx 30$ mins $+ 20$ mins for mutant cells (Hill et al., 2012). Given these values and Equation (12), the relative change in cell sizes corresponding to the reported difference in the durations from initiation to division should be $2^{((C+D)'-(C+D))/\tau} \approx 0.75$. That is, the mutant cells should be 0.75 times the size of the wildtype cells. This is in excellent agreement with the 25% decrease in volume reported. Moreover, the size at initiation did not change for these smaller mutants, consistent with our model which predicts the size at initiation to depend only on Δ and not on $C + D$. In contrast, in the case of *B. subtilis*, $C + D$ in smaller mutant cells remained constant, suggesting that Δ is the quantity which was changed. Based on this interpretation, our model would predict that both size at initiation and at birth would change proportionally. Indeed, it was found that both the average mutant cell size and the mutant cell size at initiation both decreased by approximately 35% (Hill et al., 2012). The above experiments also observed the predicted approximate proportionality between cell size and the number of origins per cell in both *E. coli* and *B. subtilis* (Hill et al., 2012). It remains to be shown that cell sizes at initiation fall into an approximate bimodal distribution. The agreement between experimental results and the predictions made by the multiple origins accumulation model speaks to the importance of regulating simultaneously cell size and the number of origins.

4. Discussion

The multiple origins accumulation model proposes that replication initiates upon the accumulation of a critical amount of initiators per origin. If the initiators are expressed as in the autorepressor model, this strategy corresponds to Equation (1), which in turn reduces to the incremental model of size control, which predicts distributions, correlations, and scalings consistent with existing measurements. Specifically, the average cell size scales exponentially with the growth rate of the cell, Equation (12), as does the average number of origins per cell, Equation (3). The model robustly regulates both cell size and the number of origins per cell such that cell size is approximately proportional to the number of origins per cell, Equation (22). These predictions are consistent with existing experiments on *E. coli* and *B. subtilis* (Hill et al., 2012). A proportionality between ploidy and cell size has also been observed in other organisms, including yeast (Marshall et al., 2012). The multiple origins accumulation model is a general regulation strategy that may illuminate the source of the approximate proportionality between cell size and the number of origins across organisms.

An essential feature of the multiple origins accumulation model is the tight coupling between chromosome replication and cell division. The differences between the multiple origins accumulation model and the master accumulation model emphasizes this coupling and the importance of regulating the timing of initiation. By negatively regulating cell size in response to the number of origins via Equation (1), the multiple origins accumulation model is able to maintain a balanced cell cycle and achieve robustness in face of noise in the initiation process. However, the master accumulation model described by Equation (13) is a regulation strategy without such a feedback mechanism. The master accumulation model is unable to maintain a balanced cell cycle and does not predict the exponential scaling of cell size. This suggests that regulation strategies must account for the number of origins per cell in order to regulate appropriately the frequency of division.

The coupling between the number of origins to the division frequency could be demonstrated via a shift-up experiment. It was found for *E. coli* that cells maintain their rate of division for a duration of $C + D$ after a shift-up, a phenomenon known as rate maintenance (Kjeldgaard et al., 1958; Cooper, 1969). The multiple origins accumulation model naturally accounts for rate maintenance, because division always occurs at time $C + D$ after initiation (chromosome replication rate is independent of growth rate). Furthermore, the model offers a robust mechanism to regulate, after a transient, the number of origins per cell appropriately with the new growth rate via Equation (3). The existence of a rate maintenance period implies that division is coupled to replication initiation, and the incremental model applied at birth and division is a valid phenomenological description only at stationarity. Instead, it is the underlying molecular mechanism of replication initiation that dictates the frequency of division.

Although the multiple origins accumulation model captures many aspects of the coupling between replication and division, experiments with minichromosomes suggest that the molecular mechanism is more complicated. Minichromosomes are plasmids containing the *oriC* sequence coding for chromosomal origins. In general, minichromosomes initiate replications in coordination with chromosomes and do not affect the growth properties of the cell, such as the doubling time or the average cell size (Leonard and Helmstetter, 1986). However, if more than $\sim$ 40 minichromosomes are present in a cell, replication initiation is no longer synchronous, the doubling time increases, the average number of origins per cell decreases, and the average cell size decreases (Lobner-Olesen, 1999). Another experiment inserted a second origin into *E. coli* chromosome and observed again that the extra origin does not affect the growth properties of the cell (Wang et al., 2011). These result points to a more complicated molecular mechanism than accumulation of

initiators per origin. Several mechanisms have been suggested, but none has been completely satisfactory. For example, the master accumulation mechanism discussed in Section 3.3 is ruled out for being unable to robustly regulate the number of origins. Another plausible regulation strategy is one in which replication initiates when a critical ratio of active to inactive initiators is reached (Donachie and Blakely, 2003). The validity of this strategy remains to be tested.

The molecular mechanism underlying the regulation of replication initiation is yet to be unraveled, but here we have given significant constraints regarding the potential mechanisms. Specifically, this work and previous works have shown that the molecular mechanism in question should satisfy both the incremental model of size control and the mathematical form of the multiple origins accumulation model described by Equation (1), so that the predicted distributions, correlations, and scalings remain intact and consistent with existing experiments.

Author Contributions

PH and AA developed the theoretical model and conducted the mathematical analysis.

Acknowledgments

The authors thank Lydia Robert and Nancy Kleckner for useful discussions.

References

Amir, A. (2014). Cell size regulation in bacteria. *Phys. Rev. Lett.* 112, 208102. doi: 10.1101/004457

Bleecken, S. (1971). "Replisome"-controlled initiation of DNA replication. *J. Theor. Biol.* 32, 81–92.

Bogan, J. A., and Helmstetter, C. (1997). DNA sequestration and transcription in the *oriC* region of *Escherichia coli*. *Mol. Microbiol.* 26, 889–896.

Bremer, H., and Churchward, G. (1977). An examination of the Cooper-Helmstetter theory of DNA replication in bacteria and its underlying assumptions. *J. Theor. Biol.* 69, 645–654.

Bremmer, H., and Dennis, P. (1996). "Modulation of chemical composition and other parameters of the cell by growth rate," in *Escherichia coli and Salmonella*, ed F. C. Neidhardt (Washington DC: ASM Press), 1553–1569.

Campbell, J. L., and Kleckner, N. (2010). Cells *oriC* and *dnaA* gene promoter are sequestered from *dam* methyltransferase following the passage of the chromosomal replication fork. *Cell* 62, 967–979. doi: 10.1016/0092-8674(90)90271-F

Campos, M., Surovtsev, I. V., Kato, S., Paintdakhi, A., Beltran, B., Ebmeier, S. E., et al. (2014). A constant size extension drives bacterial cell size homeostasis. *Cell* 159, 1433–1446. doi: 10.1016/j.cell.2014.11.022

Cooper, S. (1969). Cell division and DNA replication following a shift to a richer medium. *J. Mol. Biol.* 43, 1–11.

Cooper, S., and Helmstetter, C. (1968). Chromosome replication and the division cycle of *Escherichia coli* b/r. *J. Mol. Biol.* 31, 519–540.

Donachie, W. D. (1968). Relationship between cell size and time of initiation of DNA replication. *Nature* 219, 1077–1079.

Donachie, W. D., and Blakely, G. (2003). Coupling the initiation of chromosome replication to cell size in *Escherichia coli*. *Curr. Opin. Microbiol.* 6, 146–150. doi: 10.1016/S1369-5274(03)00026-2

Godin, M., Delgado, F. F., Son, S., Grover, W. H., Bryan, A. K., Tzur, A., et al. (2010). Using buoyant mass to measure the growth of single cells. *Nat. Methods* 7, 387–390. doi: 10.1038/nmeth.1452

Helmstetter, C., Cooper, S., Pierucci, O., and Revelas, E. (1968). On the bacterial life sequence. *Cold Spring Harb. Symp. Quant. Biol.* 33, 809–822.

Hill, N., Kadoya, R., Chattoraj, D., and Levin, P. (2012). Cell size and the initiation of DNA replication in bacteria. *PLoS Genet.* 8:e1002549. doi: 10.1371/journal.pgen.1002549

Kjeldgaard, N., Maaloe, O., and Schaechter, M. (1958). The transition between different physiological states during balanced growth of *Salmonella typhimurium*. *J. gen. Microbiol.* 19, 607–616.

Leonard, A., and Helmstetter, C. (1986). Cell cycle-specific replication of *Escherichia coli* minichromosomes. *Proc. Natl. Acad. Sci. U.S.A.* 83, 5101–5105.

Lobner-Olesen, A. (1999). Distribution of minichromosomes in individual *Escherichia coli* cells: implications for replication control. *EMBO J.* 18, 1712–1721.

Lobner-Olesen, A., Hansen, G., Ramussen, K. V., Martin, B., and Kuempel, P. L. (1994). The initiation cascade for chromosome replication in wild-type and *dam* methyltransferase deficient *Escherichia coli* cells. *EMBO J.* 13, 1856–1862.

Marshall, W. F., Young, K., Swaffer, M., Wood, E., Nurse, P., Kimura, A., et al. (2012). What determines cell size? *BMC Biol.* 10:101. doi: 10.1186/1741-7007-10-101

Powell, E. (1956). Growth rate and generation time of bacteria, with special reference to continuous culture. *J. gen. Microbiol.* 15, 492–511.

Robert, L., Hoffmann, M., Krell, N., Aymerich, S., Robert, J., and Doumic, M. (2014). Division in *Escherichia coli* is triggered by a size-sensing rather than a timing mechanism. *BMC Biol.* 12:17. doi: 10.1186/1741-7007-12-17

Schaechter, M., Maaloe, O., and Kjeldgaard, N. (1958). Dependency on medium and temperature of cell size and chemical composition during balanced growth of *Salmonella typhimurium*. *J. gen. Microbiol.* 19, 592–606.

Sharpe, M. E., Hauser, P. M., Sharpe, R. G., and Errington, J. (1998). *Bacillus subtilis* cell cycle as studied by fluorescence microscopy: constancy of cell length at initiation of DNA replication and evidence for active nucleoid partitioning. *J. Bacteriol.* 180, 547–555.

Soifer, I., Robert, L., Barkai, N., and Amir, A. (2014). Single-cell analysis of growth in budding yeast and bacteria reveals a common size regulation strategy. *ArXiv e-prints* 1410.4771.

Sompayrac, L., and Maaloe, O. (1973). Autorepressor model for control of DNA replication. *Nature* 241, 133–135.

Taheri-Araghi, S., Bradde, S., Sauls, J. T., Hill, N. S., Levin, P. A., Paulsson, J., et al. (2015). Cell-size control and homeostasis in bacteria. *Curr. Biol.* 25, 385–391. doi: 10.1016/j.cub.2014.12.009

Wang, X., Lesterlin, C., Reyes-Lamothe, R., Ball, G., and Sheratt, D. J. (2011). Replication and segrgation of an *Escherichia coli* chromosome with two replication origins. *Proc. Natl. Acad. Sci. U.S.A.* 108, E243–E250. doi: 10.1073/pnas.1100874108

Yoshikawa, H., O'Sullivan, A., and Sueoka, N. (1964). Sequential replication of the *Bacillus subtilis* chromosome, III. regulation of initiation. *Proc. Natl. Acad. Sci. U.S.A.* 52, 973–980.

Zaritsky, A., Vischer, N., and Rabinovitch, A. (2007). Changes of initiation mass and cell dimensions by the 'eclipse'. *Mol. Microbiol.* 63, 15–21. doi: 10.1111/j.1365-2958.2006.05501.x

Conflict of Interest Statement: The authors declare that the research was conducted in the absence of any commercial or financial relationships that could be construed as a potential conflict of interest.

Copyright © 2015 Ho and Amir. This is an open-access article distributed under the terms of the Creative Commons Attribution License (CC BY). The use, distribution or reproduction in other forums is permitted, provided the original author(s) or licensor are credited and that the original publication in this journal is cited, in accordance with accepted academic practice. No use, distribution or reproduction is permitted which does not comply with these terms.

Appendix

Derivations of the Average Number of Origins per Cell

The average number of origins per cell has been calculated previously in two distinct derivations (Cooper and Helmstetter, 1968; Bremer and Churchward, 1977). The two derivations seemed to make different assumptions to arrive at the same conclusions, bringing into question the necessity of the underlying assumptions. Here, we reproduce the two derivations and show that both derivations in fact make the same assumptions.

The model of the cell cycle under consideration is due to Cooper and Helmstetter (1968). In this model, replication initiation occurs on average every doubling time τ. An initiation event then triggers a division event after a constant duration $C + D$, where C and D are respectively, the constant duration required to replicate the chromosome and the constant duration between replication termination and division. Given C, D, and τ, we want to find the average number of origins per cell. The average number of origins per cell is defined as $\langle O\rangle = \langle O_{\text{total}}/N\rangle$, where O_{total} is the total number of origins in a population of cells, N is the number of cells in that population, and brackets denote the ensemble average.

First, we reproduce the derivation due to Cooper and Helmstetter (1968). To calculate the average number of origins per cell, we must first define the probability distribution underlying the ensemble average. In an asynchronous population of exponentially growing cells, the cells must be exponentially distributed in the cell cycle for ensemble averages to be stationary with respect to time (Powell, 1956). Defining cell age $a = 0$ at birth and $a = 1$ at division, the exponential distribution of cell ages is

$$p(a) = \left(\ln 2\right) 2^{1-a}. \tag{23}$$

We can now calculate the desired ensemble averages. For example, if $0 < \frac{C+D}{\tau} < 1$, then a cell younger than $\left(\tau - (C+D)\right)/\tau$ will not be replicating its chromosome and will have only one origin, whereas a cell older than $\left(\tau - (C+D)\right)/\tau$ will be replicating its chromosome and will have two origins. We have assumed that the amount of time a cell spends with more than two origins is negligible, which is plausible for weak noise in the initiation process. The average number of origins per cell in an asynchronous, exponentially growing population is then

$$\begin{aligned}\langle O\rangle &= \ln 2\left[\left(\int_0^{\frac{\tau-(C+D)}{\tau}} 2^{1-a}da\right) + 2\left(\int_{\frac{\tau-(C+D)}{\tau}}^{1} 2^{1-a}da\right)\right]\\ &= \left[\left(2 - 2^{(C+D)/\tau}\right) + 2\left(2^{(C+D)/\tau} - 1\right)\right]\\ &= 2^{(C+D)/\tau}.\end{aligned} \tag{24}$$

Similarly if $1 < \frac{C+D}{\tau} < 2$, then a cell must initiate replication not only for its daughter cells, but also for its granddaughter cells. In this case, a cell with cell age less than $\left(2\tau - (C+D)\right)/\tau$ will not be replicating its chromosome for its granddaughters and will have only two origins, whereas a cell with cell age more than $\left(2\tau - (C+D)\right)/\tau$ will be replicating its chromosome for its granddaughters and will have four origins. Again, we have assumed weak noise.

Thus, we see that

$$p(O = O_0) = \ln 2\int_0^{\Delta T} 2^{1-a}da, \tag{25}$$

$$p(O = 2O_0) = \ln 2\int_{\Delta T}^{1} 2^{1-a}da, \tag{26}$$

where $O_0 = 2^{\lfloor (C+D)/\tau\rfloor}$, and $\Delta T = \left(\lfloor (C+D)/\tau\rfloor + 1\right)\tau - (C+D)$. Simplification gives

$$\langle O\rangle = 2^{(C+D)/\tau}, \tag{27}$$

which generalizes (Equation 24) and is valid for any $C + D$ and τ. The two assumptions made in this derivation are that the population is growing exponentially and that the population has reached a stationary distribution of cell ages.

Next, we reproduce the derivation due to Bremer and Churchward (1977). Assuming exponential growth, the number of cells must grow exponentially as $N \propto 2^{t/\tau}$. Similarly, the total number of origins must grow at the same exponential rate so that $O_{\text{tot}} \propto 2^{t/\tau}$. But an initiation event triggers a division event after a constant duration $C + D$, so the number of cells must on average lag behind the total number of origins by $2^{(C+D)/\tau}$. The average number of origins per cell must then be $\langle O\rangle = \langle O_{\text{tot}}/N\rangle = 2^{(C+D)/\tau}$. Although the distribution of cell ages was not explicitly involved in this derivation, the assumption of a stationary ensemble average under exponential growth is satisfied if and only if the distribution of cell ages is exponential (Powell, 1956).

The exponential distribution of cell ages is not always realized in experimental setups. For example, single-cell experiments that track a lineage of cells, such as those in Taheri-Araghi et al. (2015), will follow a different distribution, as discussed in Robert et al. (2014). Experiments that track a single cell will follow a uniformly distributed cell age. In that case, Equation (27) is replaced by

$$\langle O\rangle = O_0\left(1 + \frac{C+D}{\tau} - \lfloor\frac{C+D}{\tau}\rfloor\right). \tag{28}$$

Simulations tracking a population of cells with uniformly distributed cell ages confirm this result. The differences between Equations (27) and (28) do not significantly change the predictions of the multiple origins accumulation model.

frontiers in Microbiology

REVIEW
published: 29 May 2015
doi: 10.3389/fmicb.2015.00515

Size sensors in bacteria, cell cycle control, and size control

Lydia Robert [1, 2, 3]*

[1] UMR1319 Micalis, Institut National de la Recherche Agronomique, Jouy-en-Josas, France, [2] UMR Micalis, AgroParisTech, Jouy-en-Josas, France, [3] Laboratoire Jean Perrin (Université Pierre et Marie Curie-Centre National de la Recherche Scientifique UMR8237), Université Pierre et Marie Curie, Paris, France

Bacteria proliferate by repetitive cycles of cellular growth and division. The progression into the cell cycle is admitted to be under the control of cell size. However, the molecular basis of this regulation is still unclear. Here I will discuss which mechanisms could allow coupling growth and division by sensing size and transmitting this information to the division machinery. Size sensors could act at different stages of the cell cycle. During septum formation, mechanisms controlling the formation of the Z ring, such as MinCD inhibition or Nucleoid Occlusion (NO) could participate in the size-dependence of the division process. In addition or alternatively, the coupling of growth and division may occur indirectly through the control of DNA replication initiation. The relative importance of these different size-sensing mechanisms could depend on the environmental and genetic context. The recent demonstration of an incremental strategy of size control in bacteria, suggests that DnaA-dependent control of replication initiation could be the major size control mechanism limiting cell size variation.

Keywords: size control, bacterial cell cycle, replication initiation, incremental model, DnaA, FtsZ, MinCD

OPEN ACCESS

Edited by:
Conrad L. Woldringh, University of Amsterdam, Netherlands

Reviewed by:
Piet A. De Boer, Case Western Reserve University, USA
Manuel Loic Campos, Howard Hughes Medical Institute at Yale, USA

***Correspondence:**
Lydia Robert, Laboratoire Jean Perrin (Université Pierre et Marie Curie-Centre National de la Recherche Scientifique UMR8237), UPMC, 75005 Paris, France
lydia.robert@upmc.fr

Specialty section:
This article was submitted to Microbial Physiology and Metabolism, a section of the journal Frontiers in Microbiology

Received: *27 February 2015*
Accepted: *09 May 2015*
Published: *29 May 2015*

Citation:
Robert L (2015) Size sensors in bacteria, cell cycle control, and size control. Front. Microbiol. 6:515. doi: 10.3389/fmicb.2015.00515

1. Introduction

All dividing cells have to coordinate different steps of the cell cycle, such as DNA replication, chromosome segregation, and cytokinesis. In eukaryotes, cell cycle control has been widely studied and the overall logic is well-understood (Murray and Hunt, 1993). The orderly progression in the eukaryotic cycle relies on a biochemical engine composed of cyclins and cyclin-dependendent kinases (CDKs). The periodic activity of cyclin-CDK complexes regulates the cell cycle transitions such as the initiation of DNA replication or the entry into mitosis (Murray and Hunt, 1993). In addition, specific control mechanisms, often called checkpoints, ensure that late events do not occur before the completion of earlier events (Hartwell and Weinert, 1989). In contrast, the logic of the bacterial cell cycle, even though intensively studied for more than half a century, remains unclear. Bacteria do not possess any cyclins or CDKs. Numerous regulatory mechanisms have been discovered and characterized in details, such as the control of DNA replication initiation (Katayama et al., 2010) or the SOS response, which inhibits division in case of DNA damage or replication arrest (Simmons et al., 2008). However, how these different mechanisms are organized and connected to ensure an orderly progression into the cycle remains unclear (Haeusser and Levin, 2008).

In many organisms, progression through the cycle is coupled with cellular growth. In the budding yeast *Saccharomyces cerevisiae*, the duration of the G1 phase depends on the cell size at birth, smaller cells spending a longer time in G1 (Johnston et al., 1977; Di Talia et al., 2007; Turner et al., 2012). Likewise, in the fission yeast *Schizosaccharomyces pombe*, mitotic entry is delayed in smaller cells (Fantes, 1977; Sveiczer et al., 1996). In bacteria, cell cycle progression was

as well-assumed to be under size control. In 1968, building on the seminal physiological studies of Schaechter et al. (1958) and Cooper and Helmstetter (1968) on *Salmonella typhimurium* and *Escherichia coli*, Donachie showed that at the population level, the average initiation mass, i.e., the ratio of cell mass to the number of replication origins is constant regardless of the growth rate and culture medium (Donachie, 1968). This lead him to propose a size control mechanism at the single cell level, in which the cell initiates DNA replication when it reaches a critical size, and divides a constant time after initiation. Although widely accepted for decades, this model became controversial in recent years (Voorn et al., 1993; Wold et al., 1994; Boye et al., 1996; Bates and Kleckner, 2005; Chien et al., 2012; Hill et al., 2012). Nevertheless, definitive evidence for size control in bacteria was provided by recent studies using quantitative data on single cell growth and division in both *E. coli*, *Bacillus subtilis*, and *Caulobacter crescentus* (Campos et al., 2014; Osella et al., 2014; Robert et al., 2014; Soifer et al., 2014; Taheri-Araghi et al., 2015).

However, no size-sensing module has been identified so far, and the molecular basis of size control stays unclear. Cells could sense their length,volume or mass. Here I use cell size as a catch-all descriptor and describe how cell size could be sensed through different pathways involved in the control of cytokinesis, chromosome segregation or replication initiation. Importantly, the potential size-sensing mechanisms are not mutually exclusive and size control could be implemented redundantly at several cell cycle stages. Such redundancy has been evidenced in the fission yeast *S. pombe*. In addition to the major size control acting at mitosis entry (Fantes and Nurse, 1977), a second size control mechanism acts at the G1/S transition (Fantes and Nurse, 1978). This second size-control is usually invisible since the G2/M control produces cells whose size at birth already exceeds the requirement of the G1/S control. Nevertheless, this second mechanism can be revealed when the primary G2/M control is perturbed, such as in the *wee1* mutant (Fantes and Nurse, 1978). *S. cerevisiae* has also been proposed to exhibit an usually invisible size-control, acting at the G2/M transition (Murray and Hunt, 1993; Turner et al., 2012). Several size checkpoints could as well-exist in bacteria, where the cytokinesis, the chromosome segregation and the initiation of replication might all depend on cell size. As in yeast, the most stringent of these size control mechanisms would be responsible for the limitation of the variations of the cell size in bacteria. Interestingly, recent experimental results on size control in bacteria argue against the current critical size paradigm and suggest an incremental strategy: division does not occur at a critical size but rather when a constant size has been added to the size at birth (Campos et al., 2014; Soifer et al., 2014; Taheri-Araghi et al., 2015). Such phenomenological description sheds a new light on the mechanism limiting cell size variations. Therefore, after a description of all the potential size-sensing mechanisms involved in the control of cytokinesis, chromosome segregation and replication initiation, I will discuss which of these mechanisms could be responsible for the limitation of cell size variations, in light of this incremental principle.

2. The Min System: a Geometric Size-Sensor Controlling Cytokinesis?

A critical event in the bacterial division process is the polymerization of the tubulin-like protein FtsZ into an annular structure called the Z ring, which locates the division site and recruits the numerous proteins required to carry out cytokinesis (Bi and Lutkenhaus, 1991; Addinall and Holland, 2002; Margolin, 2005; Harry et al., 2006). In *E. coli* and *B. subtilis*, the positioning of the Z ring has been widely studied. It is generally assumed to rely on two inhibitory systems: Nucleoid Occlusion (NO) and the Min system (Lutkenhaus, 2007; Wu and Errington, 2011). The latter is based on the protein complex MinCD, an inhibitor of FtsZ polymerization that concentrates at the cell ends, and is therefore essential to prevent polar divisions (Adler et al., 1967; De Boer et al., 1989; Lutkenhaus, 2007). In *E. coli*, the localization pattern of MinCD emerges from remarkable oscillations of the complex from pole to pole, which create over time a gradient of concentration showing a minimum around mid-cell (Hu and Lutkenhaus, 1999; Raskin and de Boer, 1999; Hale et al., 2001). In contrast, in *B. subtilis* MinCD does not oscillate and the gradient is static (Lutkenhaus, 2007). In both organisms, the concentration of the MinCD complex along the cell axis may vary with cell length and MinCD has therefore been proposed to serve as a size ruler (Raskin and de Boer, 1999). Nevertheless, there is no experimental evidence yet allowing confirming or invalidating this hypothesis.

The function and localization of MinCD is very similar to those of the Pom1 kinase in the fission yeast *S.pombe* (Padte et al., 2006; Huang et al., 2007). This kinase exhibits a gradient of concentration in the cell, with maxima at cell ends and a minimum around mid-cell. This localization allows Pom1 to prevent the assembly of the division septum at the cell ends. It was also recently suggested to serve as a size sensing device responsible for size control at mitotic entry. The work of two different teams published in 2009 established that Pom1 is a dose-dependent inhibitor of mitosis, whose concentration at the cell middle decreases when the cells elongate (Martin and Berthelot-Grosjean, 2009; Moseley et al., 2009). Pom1 was shown to regulate the G2/M transition by inhibiting mitotic activators localized at the middle of the cells. The following model of size-dependent G2/M transition was proposed: when the cells are short, the high concentration of Pom1 at mid-cell where it can interact with mitotic regulators inhibits mitotic entry. When the cell grows, this inhibition progressively weakens as the concentration of Pom1 at mid-cell decreases. Pom1 was therefore proposed to be a dedicated size sensor involved in cell cycle control. This discovery appeared promising for understanding the molecular basis of size control. Nevertheless, a few years later, one of the team involved in this discovery presented evidence that Pom1 is in fact not the size sensor but rather a modulator that affects the link between the measured size and the division probability, thus changing the size threshold at mitosis (Novák, 2013; Wood and Nurse, 2013). This conclusion was supported by the behavior of the *pom1*Δ mutant, which is shorter but exhibits a wild type correction for cell size fluctuations, compressing or extending the duration of the

cycle according to the cell's size at birth (Wood and Nurse, 2013).

Bacteria possess some geometric sensors similar to Pom1. In *E. coli* and *B. subtilis*, the potential Pom1-like geometric sensor is the MinCD complex. In *C. crescentus*, which has no MinCD orthologs, a gradient of the inhibitor of FtsZ polymerization MipZ emanates from the cell poles after the segregation of the replication origins (Goley et al., 2007). The mechanism that was proposed for size-sensing through Pom1 could in principle apply to its bacterial counterparts: cell elongation could lead to a decrease of MinCD/MipZ concentration in the cell middle, thus triggering the formation of the Z ring. Alternatively, these regulators could be, like Pom1, modulators of cell size at division.

3. FtsZ, a Size Sensor?

In the fission yeast, very recent results suggest that the cdr2 mitotic activator regulated by Pom1 could be the size sensor controlling mitotic entry (Pan et al., 2014). Cdr2 is localized in a band of cortical nodes at mid-cell, where it accumulates when the cell elongates. Pan et al. therefore proposed that a critical cdr2 concentration is attained when the cell reaches a critical size and triggers mitotic entry. The bacterial FtsZ protein, the target of MinCD regulation, has also been proposed to act as a size sensor (Chien et al., 2012). In this model, division would occur when the amount of FtsZ inside the cell reaches a threshold. In support of this hypothesis, FtsZ levels are known to modulate the size at division in *E. coli* (Chien et al., 2012). In *C. crescentus*, FtsZ expression and degradation are regulated during the cell cycle. As a consequence, the concentration oscillates during the cycle with a maximum at the onset of constriction, after which FtsZ is degraded (Quardokus et al., 1996; Kelly et al., 1998). This dynamics is in agreement with division being triggered by a critical level of FtsZ. In contrast, in *E. coli* and *B. subtilis*, FtsZ is constitutively expressed and its concentration is constant throughout the cycle. Its total amount is therefore proportional to cell size.

The capacity of the yeast protein Cdr2 to serve as a size-sensor mainly relies on its localization, so that the local concentration at mid-cell increases when cells elongate. Similarly, specific localization of FtsZ could be responsible for a size-dependent local concentration at mid-cell. In addition to ring structures, FtsZ can assemble into helices in *E. coli* and *B. subtilis* (Ben-Yehuda and Losick, 2002; Thanedar and Margolin, 2004; Harry et al., 2006). FtsZ has also been shown to oscillate from one pole to the other, out of phase with the Min system (Thanedar and Margolin, 2004; Bisicchia et al., 2013). The Z ring may therefore form from the reorganization of moving helices. However, helical structures of FtsZ have still to be confirmed. In particular, such helical structures can be artifacts of fluorescent fusions, as demonstrated for the MreB protein (Domínguez-Escobar et al., 2011; Van Teeffelen et al., 2011; Swulius and Jensen, 2012). Therefore, the localization of FtsZ is still unclear, but some size-dependence of the local concentration at mid-cell is possible, leading to a critical size for Z ring formation. Importantly, in *E. coli* and *B. subtilis* the ring is known to form well before constriction (Den Blaauwen et al., 1999). In addition, recent data suggests that at the single cell level, the timing of its formation is independent of the timing of constriction and the cell length at birth (Tsukanov et al., 2011). It is therefore possible that once the ring is formed, the amount of FtsZ it contains increases up to a threshold where the ring becomes able to recruit all the downstream components of the divisome and constrict. In this case, division timing could depend on cell size through FtsZ accumulation inside the ring.

4. Chromosome Segregation: a Size-Dependent Event?

Chromosome segregation occurs in three steps: separation of the newly replicated origins, bulk chromosome segregation and separation of the replicated termini (Wang et al., 2013). Bulk chromosome segregation appears as an important transition, leading to the appearance of a DNA free space at mid-cell and relief of the division inhibition mediated by Nucleoid Occlusion (NO). NO prevents the formation of the Z ring in the vicinity of the chromosome (Mulder and Woldringh, 1989; Wu and Errington, 2011). The mechanism of NO is not fully elucidated yet but some molecular bases have been provided by the discovery of the Noc protein of *B. subtilis* and SlmA protein of *E. coli*, which associate with DNA and inhibit FtsZ polymerization (Wu and Errington, 2004; Bernhardt and De Boer, 2005). Interestingly, these NO proteins bind to specific DNA sequences that decorate a large portion of the chromosome but are absent from the Ter region (Wu and Errington, 2011). Therefore, NO proteins are largely removed from mid-cell following bulk chromosome segregation.

The mechanism underlying bulk chromosome segregation are still unclear but entropic forces have been proposed to either drive or facilitate segregation (Jun and Wright, 2010; Di Ventura et al., 2013). Such forces can in theory segregate mixed chains of polymers in a situation of confinement. A single *E. coli* chromosome is more than 1 mm in length and has to be compacted more than 1000-fold to fit inside the cell (Wang et al., 2013). Replicated chromosomes are thus confined inside the cell, whose shape and size will determine the intensity of the entropic forces. Importantly, if segregation is entropy-driven, it should be easier in longer cells. During cell elongation, the intensity of the entropic forces increases, which could lead to size-dependent segregation. In agreement with this hypothesis, experimental results on cell cycle progression in single cells suggest that the timing of nucleoid splitting depends on cell growth rather than on replication progression (Bates and Kleckner, 2005). Therefore, if driven by entropic forces, the very act of segregation could be a size-dependent signal, transmitted to the division machinery through the relief of NO.

Interestingly, the MinCD gradient has recently been shown to be involved in chromosome segregation (Di Ventura et al., 2013). MinD was shown to bind DNA and tether it to the cell membrane. The Min system therefore provides a gradient of membrane sites for DNA attachment. Computer simulations showed that entropic forces alone could not ensure full chromosome segregation. In contrast, full segregation would be possible

if chromosomes repeatedly bind to membrane-associated sites forming a gradient emanating from the pole, such as provided by MinD. The concentration of MinD along the cell axis is likely to depend on cell length, as was demonstrated for Pom1 in the fission yeast (Martin and Berthelot-Grosjean, 2009; Moseley et al., 2009). Its involvement in segregation suggests another potential size-dependence for chromosome segregation.

5. The Initiation of Replication: Size-Sensing Through DnaA?

In the long-standing model of bacterial cell cycle initially proposed by Donachie, the coordination between growth, replication and division is mainly achieved through the control of replication initiation : the cell grows until reaching a critical size at which point replication is initiated and division occurs at a fixed time after initiation (Donachie, 1968). Donachie proposed that replication initiation could be controlled by a positive regulator, which accumulates proportionally to cell size and triggers initiation when reaching a critical amount. This critical amount would therefore correspond to a critical size. Later, DnaA was identified as the initiator protein in bacteria and has therefore been the natural candidate for Donachie's positive regulator (Løbner-Olesen et al., 1989).

I will focus here on *E. coli*, where replication initiation has been most studied and best characterized. In *E. coli*, the initiator DnaA is active when bound with ATP and inactive when bound with ADP. Active DnaA binds to specific DNA sequences in the replication origin region, leading to unwinding of the DNA sister strands in a neighboring AT-rich region and loading of the replisome (Katayama et al., 2010). This initiation event is tightly controlled in order to occur once and only once in each cell cycle. In particular, several mechanisms ensure the inactivation of DnaA following initiation, in order to prevent immediate reinitiation. These mechanisms include seqA-dependent sequestration of OriC and transcriptional repression of the *dnaA* gene (Campbell and Kleckner, 1990), titration of DnaA to the datA chromosomal locus (Kitagawa et al., 1996), and DnaA inactivation through RIDA, a replication-coupled mechanism involving a complex of Hda, ADP, and the DNA polymerase sliding clamp (Kato and Katayama, 2001; Katayama et al., 2010). All these mechanisms ensure that replication initiation occurs only once in the cell cycle. After this wave of inactivation, the newly produced DnaA, which is rapidly converted to ATP-DnaA (Messer, 2002), accumulates in the cell until the next initiation event. In addition, some reactivation mechanisms convert ADP-DnaA to ATP-DnaA (Katayama et al., 2010). A mechanism involving cardiolipin, a membrane phospholipid, has been suggested (Sekimizu and Kornberg, 1988), and two specific DNA sequence, DARS1 and DARS2, have been demonstrated to promote the conversion of ADP-DnaA to ATP-DnaA (Fujimitsu et al., 2009).

As an outcome, the cellular level of ATP-DnaA oscillates during the cell cycle, with a maximum at the time of initiation (Kurokawa et al., 1999). Initiation has therefore been proposed to occur when the amount of ATP-DnaA reaches a threshold. Interestingly, when DnaA is overexpressed several folds, the initiation timing is only slightly perturbed (Atlung et al., 1987; Kurokawa et al., 1999). In these conditions, it was shown that the proportion of the ATP and ADP-bound forms is unchanged (Kurokawa et al., 1999). Since these two forms might compete for binding DNA, initiation could be triggered when the ratio of ATP-DnaA to ADP-DnaA reaches a threshold (Donachie and Blakely, 2003). Thus, a simple model of initiation control, developed in Donachie and Blakely (2003), postulates that DnaA is synthesized constitutively, so that its total amount is proportional to cell mass, and immediately binds ATP (Messer, 2002). The ratio of ATP to ADP bound DnaA therefore would increase in parallel with cell size, until it reaches a threshold and triggers initiation of replication, leading to the inactivation of DnaA. In this model, the constitutive expression of DnaA and its immediate binding to ATP leads to an amount of active DnaA and a ratio of the active to inactive form both increasing linearly with cell size after replication initiation. It is still unclear how this linear relation could be affected by the reactivation of DnaA during the cycle, which is not taken into account in this simple model.

6. Recent Revision of the Critical Size Paradigm of Size Control: the Incremental Model

In both yeast and bacteria, substantial correlations are observed at the single cell level between size at birth and size at division (Campos et al., 2014; Soifer et al., 2014; Taheri-Araghi et al., 2015). Such correlations argue against the classical model of cell size control in which division occurs at a critical size, up to some noise, with no memory of the size at birth. Indeed both yeasts and bacteria show some memory between one generation and the next: the cell's size at division is correlated to its size at birth, i.e., to the size at division of its mother.

Such a memory could in principle be the result of epigenetic inheritance of some molecules involved in the determination of the critical size. Gene expression naturally undergoes random fluctuations whose time scale is usually larger than a generation time. Such slow fluctuations can therefore generate correlations between the abundance of a protein in a cell and in its daughter (Rosenfeld et al., 2005; Longo and Hasty, 2006). When considering a molecular pathway involved in size measurement and control of cell cycle progression, such simple epigenetic memory would be likely to introduce some correlations throughout generations, such as between the size at division of a cell and its daughter's. The simple critical size model can be modified to take such memory into account. For instance an additional structuring variable can be added in the equations of the so-called sloppy size control model, using a division rate depending not only on the cell size but also on its size at birth (Osella et al., 2014). Using another mathematical framework, size at division can be described using an autoregressive model (Amir, 2014).

Strikingly, in very different organisms such as *E. coli*, *B. subtilis*, *C. crescentus*, and *S. cerevisiae*, the dependence of size

at division on size at birth is the same, a linear relationship with slope one (Campos et al., 2014; Soifer et al., 2014; Taheri-Araghi et al., 2015). It is worth noting that the case of *C. crescentus* is currently debated, since another dependence have been suggested by Iyer-Biswas et al., who proposed that the size at division is a multiple ($\approx$1.8) of the size at birth, indicating a timer mechanism of division control (Iyer-Biswas et al., 2014). Nevertheless, the data obtained by Iyer-Biswas et al. was then analyzed independently by Jun et al. in a way similar to the analysis performed in *E. coli*, *B. subtilis*, and *S. cerevisiae*, giving a linear relationship with slope $\approx$1.2 (Jun and Taheri-Araghi, 2015). The linear relationship with slope one is precisely the prediction of the so-called incremental model, where a cell tries to add a constant volume between birth and division (Sompayrac and Maaløe, 1973; Voorn et al., 1993; Amir, 2014). Therefore, even though some memory can be caused by slow fluctuations in gene expression, the value of the memory exhibited by the size at division through the successive generations and its conservation among several very divergent organisms suggest a more profound revision of the classical critical size model: the cell does not divide at a critical size but tries to add a constant size to its size at birth.

7. Candidate Sensors for an Incremental Measure of Cell Size and Possible Mechanisms Limiting Cell Size Variations

7.1. Control of Cytokinesis and Chromosome Segregation

Although the interpretation of the experimental data in terms of the incremental model cannot conclude on the underlying molecular mechanisms, it offers a phenomenological description and sheds a new light on the possible mechanisms limiting cell size variations. As detailed in the previous sections, several mechanisms may be responsible for the size-sensing and the size-dependent control of cytokinesis, chromosome segregation and DNA replication initiation. Among these mechanisms, one may lead to the limitation of cell size variations. This mechanism should implement an incremental strategy.

Potential geometric sensors such as MinCD are unlikely to implement an incremental strategy: they could link the instantaneous division probability with the current cell size but could hardly measure a size increment since birth. Importantly, Campos et al. showed that a Δ*minC* mutant of *E. coli* also exhibits an incremental strategy of size control, therefore demonstrating that the Min system does not play a crucial role in sensing the size increment (Campos et al., 2014).

Likewise, the process of chromosome segregation may be size-dependent but is unlikely to be related to a size increment. Entropic forces potentially driving or facilitating segregation could depend on the instantaneous cell size and geometry but hardly on the difference between the instantaneous size and the size at a previous cell cycle event. Likewise, the potential involvement of MinCD in segregation would rather create a dependence on the instantaneous cell size than on a size increment.

In *E. coli* and *B. subtilis*, the concentration of FtsZ is constant during the cell cycle. Its total amount is therefore proportional to cell size and not to the size increment since birth. FtsZ is thus unlikely to be a size increment sensor in these organisms. The situation is different for *C. crescentus*, where FtsZ is degraded at the onset of constriction (Quardokus et al., 1996; Kelly et al., 1998). The FtsZ-dependent size measure would therefore be reset at the end of the cycle when FtsZ is degraded. FtsZ levels could therefore in principle be correlated to the increment of size since birth in this organism.

Therefore, in *E. coli* and *B. subtilis* the limitation of cell size variations seems unlikely to result from size control at the level of cytokinesis or chromosome segregation. In contrast, in *C. crescentus* FtsZ could perform a measure of size increment.

7.2. Control of Replication Initiation

The incremental model postulates a constant size increment between two successive events of the cell cycle, such as between birth and division or between an initiation event and the next one. Interestingly, Campos et al. studied the possibility that the size increment could be applied at a cell cycle event other than division, such as replication initiation (Campos et al., 2014). They performed simulations of such a "phase-shifted" model and found that it was not compatible with their data on *E. coli* and *C. crescentus*. In particular, their model produced a negative correlation between the size increment (between birth and division) and the size at birth, whereas no such correlation exists in the data. Nevertheless, recent work by Ho and Amir (in this Frontiers Research Topic: The Bacterial Cell: Coupling between Growth, Nucleoid Replication, Cell Division and Shape) shows that this correlation strongly depends on the variability in the durations from replication initiation to division. If this variability is small compared to the variability in the duration of the whole cell cycle (less than 30 percent), then the correlation is close to zero, as experimentally observed. Campos et al. also report that their phase-shifted model produces abnormal cell size distributions. Nevertheless, using a different phase-shifted model, Ho and Amir show that cell size can be robustly regulated. Therefore, the results of the simulations of the "phase shifted" model of Campos et al. cannot be used to rule out the possibility of size control at the level of replication initiation.

When *E. coli* cells are shifted from a poor medium to a rich medium, the rate of mass increase immediately changes whereas the rate of cell division is maintained at the pre-shift value for a lag of approximately 60 min, corresponding to the constant C + D period (Kjeldgaard et al., 1958; Cooper, 1969). This phenomenon, called rate maintenance supports the hypothesis of size control acting at the level of replication initiation (Cooper, 1969), such as proposed in Donachie's model (Donachie, 1968; Donachie and Blakely, 2003). Also in support of this hypothesis, cell size is exponentially dependent on growth rate (Schaechter et al., 1958), with an exponent of 60 min (i.e., C + D period). This relation can be easily derived in the framework of the incremental model when the size increment is added between two successive replication initiation events, as shown in Amir (2014). If initiation is triggered by the size-dependent amount of active

DnaA, its subsequent inactivation would reset the size measure at each initiation event. Donachie's model could therefore be revisited to account for the incremental strategy: initiation would be triggered not at a critical size but when a critical size has been added since the last initiation event (see **Figure 1**). Division would follow a constant time after initiation, through an as-yet unknown mechanism. As mentioned above, in addition to the ATP-DnaA formed by *de novo* DnaA expression, ADP-DnaA can be partly reactivated during the cycle. How the amount of ATP-DnaA varies with cell mass between two initiation events is therefore not completely clear. In addition, initiation may be triggered by other DnaA-dependent variables, such as the ratio of the active to inactive forms (Donachie and Blakely, 2003). It is still unclear what is the triggering signal for initiation and how it is linked to cell size. Nevertheless, the inactivation of DnaA following initiation is crucial in initiation control and appears as an interesting basis for the implementation of an incremental size measure. The incremental model can satisfyingly describe *E. coli*, *B. subtilis*, and *C. crescentus* as well as the budding yeast *S. cerevisiae*. The conservation of this size control strategy among widely divergent organisms is striking and suggests some common organizing principle. Interestingly, even though the molecular mechanisms involved in replication initiation are different among these organisms, common control principles can be found. For instance the negative regulation of OriC after initiation is common to *E. coli*, *B. subtilis*, and *C. crescentus* (Katayama et al., 2010). Also, the principle of RIDA, which inactivates DnaA in *E. coli* in a replication-coupled manner through the action of the polymerase sliding clamp, is widely conserved (Katayama et al., 2010). The clamp-mediated inactivation of initiation proteins has also been demonstrated in *B. subtilis* (Soufo et al., 2008), *C. crescentus* (Collier and Shapiro, 2009), and in several eukaryotic organisms (Arias and Walter, 2006; Nishitani et al., 2006; Katayama et al., 2010). For all these organisms the initiation potential may therefore fluctuate in the cell in a way similar to the DnaA-related signal in *E. coli*. This may lead to a common size control strategy, such as described by the incremental model.

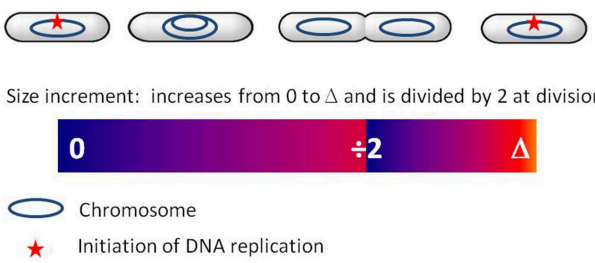

FIGURE 1 | Incremental model for cell size control at replication initiation in bacteria (see also Amir, 2014). For simplicity, a slowly growing *E. coli* cell is represented. The colored bar represents the dynamics of the size increment S through the cell cycle. After initiation of replication, S increases until division. At division, *S* is shared between the two daughter cells. In each daughter cell, S then increases up to the critical value Δ, leading to replication initiation and resetting of the size increment ($S = 0$).

8. Conclusion

The identification of a size-sensing molecule has been a long lasting quest and has proven surprisingly difficult, as evidenced by the recent controversy on the role of Pom1 in the fission yeast. This might indicate that size-sensing is generally not the function of a single molecule but is rather a systems-level property. In other words, several proteins inside a regulatory pathway may participate to the size-dependence of a cell cycle event. As an example, in *E. coli* the local concentrations of MinCD and FtsZ at mid-cell might both change when the cell elongates and could in concert determine the size-dependence of cytokinesis. Importantly, numerous cell cycle regulators exhibit specific localization patterns, such as CtrA and MipZ in *C. crescentus*, MinCD, SlmA, DnaA in *E. coli* (Bernhardt and De Boer, 2005; Goley et al., 2007; Lutkenhaus, 2007; Boeneman et al., 2009; Nozaki et al., 2009). Such subcellular localization can readily result in size-dependent local concentration. When a protein is constitutively expressed, its total amount is proportional to cell size. If such a protein is localized in a subcellular volume that does not change proportionally to the total volume when the cell grows, its local concentration is size-dependent. As a simple example, if the subcellular volume is constant, the protein concentration is proportional to the total cell volume. Several regulators in a single pathway can be localized, in particular since some events such as cytokinesis are spatially controlled, and several size-dependent signals may therefore co-exist, leading to a complex size control of the event.

Here I described several regulatory pathways that could lead to size-dependent regulation of replication initiation, chromosome segregation and cytokinesis. In principle they could all be responsible for cell size control, i.e., for the observed dependence of the interdivision time on the size at birth at the single cell level. Old physiology experiments, in particular demonstrating the "rate maintenance" phenomenon (Kjeldgaard et al., 1958; Cooper, 1969), suggest that size control in *E. coli* acts primarily at the level of replication initiation (Cooper, 1969). In agreement with this hypothesis, the dynamics of DnaA activity could potentially explain the observed incremental strategy for size control. The inactivation of DnaA following initiation could reset some DnaA-dependent signal which could therefore be linked to a size increment. In addition, the widely conserved principles underlying replication initiation control are in agreement with the common incremental strategy found in three divergent bacteria, as well as in a unicellular eukaryotic organism. In the budding yeast, size control is known to act primarily at the Start transition, i.e., the onset of replication, with a modulation of the G1 duration according to cell size at birth (Johnston et al., 1977; Turner et al., 2012). Experimental data are also compatible with size control acting slightly earlier, for instance at the level of origin licensing (Soifer et al., 2014). In contrast, in *S. pombe*, size control is known to act primarily at the G2/M transition (Fantes and Nurse, 1977; Turner et al., 2012). Interestingly, a recent analysis of single cell growth and division in this organism indicate that it does not follow the incremental model (Nobs and Maerkl, 2014), suggesting that the incremental strategy could be a property of the size

control provided by the regulatory mechanisms of replication initiation. It would be interesting to study at the single cell level the *wee1* mutant of *S. pombe*, which exhibits size control at the G1/S transition and determine whether size control follows an incremental strategy. In bacteria, DnaA-dependent initiation may provide the principal mechanism limiting cell size variations. Other cell cycle transitions may be size dependent, such as cytokinesis or chromosome segregation, leading to secondary size control mechanisms that could be revealed in specific environmental or genetic contexts, as demonstrated in yeasts.

Acknowledgments

I am grateful to Marina Elez, Ariel Amir, and Sven van Teeffelen for critical reading and to the reviewers for useful comments.

References

Addinall, S. G., and Holland, B. (2002). The tubulin ancestor, FtsZ, draughtsman, designer and driving force for bacterial cytokinesis. *J. Mol. Biol.* 318, 219–236. doi: 10.1016/S0022-2836(02)00024-4

Adler, H., Fisher, W. D., Cohen, A., and Hardigree, A. A. (1967). Miniature *Escherichia coli* cells deficient in DNA. *Proc. Natl. Acad. Sci. U.S.A.* 57, 321–326.

Amir, A. (2014). Cell size regulation in bacteria. *Phys. Rev. Lett.* 112:208102. doi: 10.1103/PhysRevLett.112.208102

Arias, E. E., and Walter, J. C. (2006). PCNA functions as a molecular platform to trigger Cdt1 destruction and prevent re-replication. *Nat. Cell Biol.* 8, 84–90. doi: 10.1038/ncb1346

Atlung, T., Løbner-Olesen, A., and Hansen, F. G. (1987). Overproduction of DnaA protein stimulates initiation of chromosome and minichromosome replication in *Escherichia coli*. *Mol. Gen. Genet.* 206, 51–59.

Bates, D., and Kleckner, N. (2005). Chromosome and replisome dynamics in *E. coli*: loss of sister cohesion triggers global chromosome movement and mediates chromosome segregation. *Cell* 121, 899–911. doi: 10.1016/j.cell.2005.04.013

Ben-Yehuda, S., and Losick, R. (2002). Asymmetric cell division in *B. subtilis* involves a spiral-like intermediate of the cytokinetic protein FtsZ. *Cell* 109, 257–266. doi: 10.1016/S0092-8674(02)00698-0

Bernhardt, T. G., and De Boer, P. A. J. (2005). Slma, a nucleoid-associated, FtsZ binding protein required for blocking septal ring assembly over chromosomes in *E. coli*. *Mol. Cell* 18, 555–564. doi: 10.1016/j.molcel.2005.04.012

Bi, E. F., and Lutkenhaus, J. (1991). Ftsz ring structure associated with division in *Escherichia coli*. *Nature* 354, 161–164.

Bisicchia, P., Arumugam, S., Schwille, P., and Sherratt, D. (2013). MinC, MinD, and MinE drive counter-oscillation of early-cell-division proteins prior to *Escherichia coli* septum formation. *mBio* 4:e00856–13. doi: 10.1128/mBio.00856-13

Boeneman, K., Fossum, S., Yang, Y., Fingland, N., Skarstad, K., and Crooke, E. (2009). *Escherichia coli* DnaA forms helical structures along the longitudinal cell axis distinct from MreB filaments. *Mol. Microbiol.* 72, 645–657. doi: 10.1111/j.1365-2958.2009.06674.x

Boye, E., Stokke, T., Kleckner, N., and Skarstad, K. (1996). Coordinating dna replication initiation with cell growth: differential roles for DnaA and SeqA proteins. *Proc. Natl. Acad. Sci. U.S.A.* 93, 12206–12211.

Campbell, J. L., and Kleckner, N. (1990). *E. coli oriC* and the dnaA gene promoter are sequestered from dam methyltransferase following the passage of the chromosomal replication fork. *Cell* 62, 967–979.

Campos, M., Surovtsev, I. V., Kato, S., Paintdakhi, A., Beltran, B., Ebmeier, S. E., et al. (2014). A constant size extension drives bacterial cell size homeostasis. *Cell* 159, 1433–1446. doi: 10.1016/j.cell.2014.11.022

Chien, A.-C., Hill, N. S., and Levin, P. A. (2012). Cell size control in bacteria. *Curr. Biol.* 22, R340–R349. doi: 10.1016/j.cub.2012.02.032

Collier, J., and Shapiro, L. (2009). Feedback control of DnaA-mediated replication initiation by replisome-associated HdaA protein in *Caulobacter*. *J. Bacteriol.* 191, 5706–5716. doi: 10.1128/JB.00525-09

Cooper, S. (1969). Cell division and dna replication following a shift to a richer medium. *J. Mol. Biol.* 43, 1–11.

Cooper, S., and Helmstetter, C. E. (1968). Chromosome replication and the division cycle of *Escherichia coli*. *J. Mol. Biol.* 31, 519–540.

De Boer, P. A., Crossley, R. E., and Rothfield, L. I. (1989). A division inhibitor and a topological specificity factor coded for by the minicell locus determine proper placement of the division septum in *E. coli*. *Cell* 56, 641–649.

Den Blaauwen, T., Buddelmeijer, N., Aarsman, M. E., Hameete, C. M., and Nanninga, N. (1999). Timing of FtsZ assembly in *Escherichia coli*. *J. Bacteriol.* 181, 5167–5175.

Di Talia, S., Skotheim, J. M., Bean, J. M., Siggia, E. D., and Cross, F. R. (2007). The effects of molecular noise and size control on variability in the budding yeast cell cycle. *Nature* 448, 947–951. doi: 10.1038/nature06072

Di Ventura, B., Knecht, B., Andreas, H., Godinez, W. J., Fritsche, M., Rohr, K., et al. (2013). Chromosome segregation by the *Escherichia coli* min system. *Mol. Syst. Biol.* 9:686. doi: 10.1038/msb.2013.44

Domínguez-Escobar, J., Chastanet, A., Crevenna, A. H., Fromion, V., Wedlich-Söldner, R., and Carballido-López, R. (2011). Processive movement of MreB-associated cell wall biosynthetic complexes in bacteria. *Science* 333, 225–228. doi: 10.1126/science.1203466

Donachie, W. D. (1968). Relationship between cell size and time of initiation of dna replication. *Nature* 219, 1077–1079.

Donachie, W. D., and Blakely, G. W. (2003). Coupling the initiation of chromosome replication to cell size in *Escherichia coli*. *Curr. Opin. Microbiol.* 6, 146–150. doi: 10.1016/S1369-5274(03)00026-2

Fantes, P., and Nurse, P. (1977). Control of cell size at division in fission yeast by a growth-modulated size control over nuclear division. *Exp. Cell Res.* 107, 377–386.

Fantes, P. A. (1977). Control of cell size and cycle time in *Schizosaccharomyces pombe*. *J. Cell Sci.* 24, 51–67.

Fantes, P. A., and Nurse, P. (1978). Control of the timing of cell division in fission yeast: cell size mutants reveal a second control pathway. *Exp. Cell Res.* 115, 317–329.

Fujimitsu, K., Senriuchi, T., and Katayama, T. (2009). Specific genomic sequences of *E. coli* promote replicational initiation by directly reactivating ADP-DnaA. *Genes Dev.* 23, 1221–1233. doi: 10.1101/gad.1775809

Goley, E. D., Iniesta, A. A., and Shapiro, L. (2007). Cell cycle regulation in *Caulobacter*: location, location, location. *J. Cell Sci.* 120, 3501–3507. doi: 10.1242/jcs.005967

Haeusser, D. P., and Levin, P. A. (2008). The great divide: coordinating cell cycle events during bacterial growth and division. *Curr. Opin. Microbiol.* 11, 94–99. doi: 10.1016/j.mib.2008.02.008

Hale, C. A., Meinhardt, H., and de Boer, P. A. (2001). Dynamic localization cycle of the cell division regulator MinE in *Escherichia coli*. *EMBO J.* 20, 1563–1572. doi: 10.1093/emboj/20.7.1563

Harry, E., Monahan, L., and Thompson, L. (2006). Bacterial cell division: the mechanism and its precison. *Int. Rev. Cytol.* 253, 27–94. doi: 10.1016/S0074-7696(06)53002-5

Hartwell, L. H., and Weinert, T. A. (1989). Checkpoints: controls that ensure the order of cell cycle events. *Science* 246, 629–634.

Hill, N. S., Kadoya, R., Chattoraj, D. K., and Levin, P. A. (2012). Cell size and the initiation of DNA replication in bacteria. *PLoS Genet.* 8:e1002549. doi: 10.1371/journal.pgen.1002549

Hu, Z., and Lutkenhaus, J. (1999). Topological regulation of cell division in *Escherichia coli* involves rapid pole to pole oscillation of the division inhibitor MinC under the control of MinD and MinE. *Mol. Microbiol.* 34, 82–90.

Huang, Y., Chew, T. G., Ge, W., and Balasubramanian, M. K. (2007). Polarity determinants Tea1p, Tea4p, and Pom1p inhibit division-septum assembly at cell ends in fission yeast. *Dev. Cell* 12, 987–996. doi: 10.1016/j.devcel.2007.03.015

Iyer-Biswas, S., Wright, C. S., Henry, J. T., Lo, K., Burov, S., Lin, Y., et al. (2014). Scaling laws governing stochastic growth and division of single bacterial

cells. *Proc. Natl. Acad. Sci. U.S.A.* 111, 15912–15917. doi: 10.1073/pnas.1403232111

Johnston, G. C., Pringle, J. R., and Hartwell, L. H. (1977). Coordination of growth with cell division in the yeast Saccharomyces cerevisiae. *Exp. Cell Res.* 105, 79–98.

Jun, S., and Taheri-Araghi, S. (2015). Cell-size maintenance: universal strategy revealed. *Trends Microbiol.* 23, 4–6. doi: 10.1016/j.tim.2014.12.001

Jun, S., and Wright, A. (2010). Entropy as the driver of chromosome segregation. *Nat. Rev. Microbiol.* 8, 600–607. doi: 10.1038/nrmicro2391

Katayama, T., Ozaki, S., Keyamura, K., and Fujimitsu, K. (2010). Regulation of the replication cycle: conserved and diverse regulatory systems for DnaA and *oriC*. *Nat. Rev. Microbiol.* 8, 163–170. doi: 10.1038/nrmicro2314

Kato, J.-I., and Katayama, T. (2001). Hda, a novel DnaA-related protein, regulates the replication cycle in *Escherichia coli*. *EMBO J.* 20, 4253–4262. doi: 10.1093/emboj/20.15.4253

Kelly, A. J., Sackett, M. J., Din, N., Quardokus, E., and Brun, Y. V. (1998). Cell cycle-dependent transcriptional and proteolytic regulation of FtsZ in *Caulobacter*. *Genes Dev.* 12, 880–893.

Kitagawa, R., Mitsuki, H., Okazaki, T., and Ogawa, T. (1996). A novel DnaA protein-binding site at 94.7 min on the *Escherichia coli* chromosome. *Mol. Microbiol.* 19, 1137–1147.

Kjeldgaard, N., Maaløe, O., and Schaechter, M. (1958). The transition between different physiological states during balanced growth of *Salmonella typhimurium*. *J. Gen. Microbiol.* 19, 607–616.

Kurokawa, K., Nishida, S., Emoto, A., Sekimizu, K., and Katayama, T. (1999). Replication cycle-coordinated change of the adenine nucleotide-bound forms of dnaa protein in *Escherichia coli*. *EMBO J.* 18, 6642–6652.

Løbner-Olesen, A., Skarstad, K., Hansen, F. G., von Meyenburg, K., and Boye, E. (1989). The DnaA protein determines the initiation mass of *Escherichia coli* K-12. *Cell* 57, 881–889.

Longo, D., and Hasty, J. (2006). Dynamics of single-cell gene expression. *Mol. Syst. Biol.* 2:64. doi: 10.1038/msb4100110

Lutkenhaus, J. (2007). Assembly dynamics of the bacterial minCDE system and spatial regulation of the Z ring. *Annu. Rev. Biochem.* 76, 539–562. doi: 10.1146/annurev.biochem.75.103004.142652

Martin, S. G., and Berthelot-Grosjean, M. (2009). Polar gradients of the DYRK-family kinase Pom1 couple cell length with the cell cycle. *Nature* 459, 852–856. doi: 10.1038/nature08054

Margolin, W. (2005). Ftsz and the division of prokaryotic cells and organelles. *Nat. Rev. Mol. Cell Biol.* 6, 862–871. doi: 10.1038/nrm1745

Messer, W. (2002). The bacterial replication initiator DnaA. DnaA and *oriC*, the bacterial mode to initiate dna replication. *FEMS Microbiol. Rev.* 26, 355–374. doi: 10.1016/S0168-6445(02)00127-4

Moseley, J. B., Mayeux, A., Paoletti, A., and Nurse, P. (2009). A spatial gradient coordinates cell size and mitotic entry in fission yeast. *Nature* 459, 857–860. doi: 10.1038/nature08074

Mulder, E., and Woldringh, C. L. (1989). Actively replicating nucleoids influence positioning of division sites in *Escherichia coli* filaments forming cells lacking DNA. *J. Bacteriol.* 171, 4303–4314.

Murray, A. W., and Hunt, T. (1993). *The Cell Cycle: an Introduction*. New York, NY: Oxford University Press.

Nishitani, H., Sugimoto, N., Roukos, V., Nakanishi, Y., Saijo, M., Obuse, C., et al. (2006). Two E3 ubiquitin ligases, SCF-Skp2 and DDB1-Cul4, target human Cdt1 for proteolysis. *EMBO J.* 25, 1126–1136. doi: 10.1038/sj.emboj.7601002

Nobs, J.-B., and Maerkl, S. J. (2014). Long-term single cell analysis of *S. pombe* on a microfluidic microchemostat array. *PLoS ONE* 9:e93466. doi: 10.1371/journal.pone.0093466

Novák, B. (2013). Pom1 is not the size ruler. *Cell Cycle* 12, 3463–3464. doi: 10.4161/cc.26818

Nozaki, S., Niki, H., and Ogawa, T. (2009). Replication initiator DnaA of *Escherichia coli* changes its assembly form on the replication origin during the cell cycle. *J. Bacteriol.* 191, 4807–4814. doi: 10.1128/JB.00435-09

Osella, M., Nugent, E., and Lagomarsino, M. C. (2014). Concerted control of *Escherichia coli* cell division. *Proc. Natl. Acad. Sci. U.S.A.* 111, 3431–3435. doi: 10.1073/pnas.1313715111

Padte, N. N., Martin, S. G., Howard, M., and Chang, F. (2006). The cell-end factor Pom1p inhibits Mid1p in specification of the cell division plane in fission yeast. *Curr. Biol.* 16, 2480–2487. doi: 10.1016/j.cub.2006.11.024

Pan, K. Z., Saunders, T. E., Flor-Parra, I., Howard, M., and Chang, F. (2014). Cortical regulation of cell size by a sizer cdr2p. *Elife* 3:e02040. doi: 10.7554/eLife.02040

Quardokus, E., Din, N., and Brun, Y. V. (1996). Cell cycle regulation and cell type-specific localization of the FtsZ division initiation protein in *Caulobacter*. *Proc. Natl. Acad. Sci. U.S.A.* 93, 6314–6319.

Raskin, D. M., and de Boer, P. A. (1999). Rapid pole-to-pole oscillation of a protein required for directing division to the middle of *Escherichia coli*. *Proc. Natl. Acad. Sci. U.S.A.* 96, 4971–4976.

Robert, L., Hoffmann, M., Krell, N., Aymerich, S., Robert, J., and Doumic, M. (2014). Division in *Escherichia coli* is triggered by a size-sensing rather than a timing mechanism. *BMC Biol.* 12:17. doi: 10.1186/1741-7007-12-17

Rosenfeld, N., Young, J. W., Alon, U., Swain, P. S., and Elowitz, M. B. (2005). Gene regulation at the single-cell level. *Science* 307, 1962–1965. doi: 10.1126/science.1106914

Schaechter, M., MaalOe, O., and Kjeldgaard, N. O. (1958). Dependency on medium and temperature of cell size and chemical composition during balanced growth of *Salmonella typhimurium*. *Microbiology* 19, 592–606.

Sekimizu, K., and Kornberg, A. (1988). Cardiolipin activation of DnaA protein, the initiation protein of replication in *Escherichia coli*. *J. Biol. Chem.* 263, 7131–7135.

Simmons, L. A., Foti, J. J., Cohen, S. E., and Walker, G. C. (2008). The SOS regulatory network. *Ecosal Plus* 2008, 1–48. doi: 10.1128/ecosalplus.5.4.3

Soifer, I., Robert, L., Barkai, N., and Amir, A. (2014). *Single-cell analysis of growth in budding yeast and bacteria reveals a Common size regulation strategy*. Available online at: http://arxiv.org/abs/1410.4771

Sompayrac, L., and Maaløe, O. (1973). Autorepressor model for control of dna replication. *Nature* 241, 133–135.

Soufo, C. D., Soufo, H. J. D., Noirot-Gros, M.-F., Steindorf, A., Noirot, P., and Graumann, P. L. (2008). Cell-cycle-dependent spatial sequestration of the DnaA replication initiator protein in *Bacillus subtilis*. *Dev. Cell* 15, 935–941. doi: 10.1016/j.devcel.2008.09.010

Sveiczer, A., Novak, B., and Mitchison, J. M. (1996). The size control of fission yeast revisited. *J. Cell Sci.* 109(Pt 12), 2947–2957.

Swulius, M. T., and Jensen, G. J. (2012). The helical MreB cytoskeleton in *Escherichia coli* MC1000/pLE7 is an artifact of the N-terminal yellow fluorescent protein tag. *J. Bacteriol.* 194, 6382–6386. doi: 10.1128/JB.00505-12

Taheri-Araghi, S., Bradde, S., Sauls, J. T., Hill, N. S., Levin, P. A., Paulsson, J., et al. (2015). Cell-size control and homeostasis in bacteria. *Curr. Biol.* 25, 385–391. doi: 10.1016/j.cub.2014.12.009

Thanedar, S., and Margolin, W. (2004). Ftsz exhibits rapid movement and oscillation waves in helix-like patterns in *Escherichia coli*. *Curr. Biol.* 14, 1167–1173. doi: 10.1016/j.cub.2004.06.048

Tsukanov, R., Reshes, G., Carmon, G., Fischer-Friedrich, E., Gov, N., Fishov, I., et al. (2011). Timing of Z-ring localization in *Escherichia coli*. *Phys. Biol.* 8:066003. doi: 10.1088/1478-3975/8/6/066003

Turner, J. J., Ewald, J. C., and Skotheim, J. M. (2012). Cell size control in yeast. *Curr. Biol.* 22, R350–R359. doi: 10.1016/j.cub.2012.02.041

Van Teeffelen, S., Wang, S., Furchtgott, L., Huang, K. C., Wingreen, N. S., Shaevitz, J. W., et al. (2011). The bacterial actin MreB rotates, and rotation depends on cell-wall assembly. *Proc. Natl. Acad. Sci. U.S.A.* 108, 15822–15827. doi: 10.1073/pnas.1108999108

Voorn, W., Koppes, L., and Grover, N. (1993). Mathematics of cell division in *Escherichia coli*: comparison between sloppy-size and incremental-size kinetics. *Curr. Top. Mol. Gen.* 1, 187–194.

Wang, X., Llopis, P. M., and Rudner, D. Z. (2013). Organization and segregation of bacterial chromosomes. *Nat. Rev. Genet.* 14, 191–203. doi: 10.1038/nrg3375

Wold, S., Skarstad, K., Steen, H. B., Stokke, T., and Boye, E. (1994). The initiation mass for dna replication in *Escherichia coli* K-12 is dependent on growth rate. *Eur. Mol. Biol. Organ. J.* 13, 2097–2102.

Wood, E., and Nurse, P. (2013). Pom1 and cell size homeostasis in fission yeast. *Cell Cycle* 12, 3417–3425. doi: 10.4161/cc.26462

Wu, L. J., and Errington, J. (2004). Coordination of cell division and chromosome segregation by a nucleoid occlusion protein in *Bacillus subtilis*. *Cell* 117, 915–925. doi: 10.1016/j.cell.2004.06.002

Wu, L. J., and Errington, J. (2011). Nucleoid occlusion and bacterial cell division. *Nat. Rev. Microbiol.* 10, 8–12. doi: 10.1038/nrmicro2671

Conflict of Interest Statement: The author declares that the research was conducted in the absence of any commercial or financial relationships that could be construed as a potential conflict of interest.

Copyright © 2015 Robert. This is an open-access article distributed under the terms of the Creative Commons Attribution License (CC BY). The use, distribution or reproduction in other forums is permitted, provided the original author(s) or licensor are credited and that the original publication in this journal is cited, in accordance with accepted academic practice. No use, distribution or reproduction is permitted which does not comply with these terms.

frontiers in Microbiology

ORIGINAL RESEARCH
published: 08 December 2015
doi: 10.3389/fmicb.2015.01349

Self-Consistent Examination of Donachie's Constant Initiation Size at the Single-Cell Level

Sattar Taheri-Araghi [1, 2]*

[1] Department of Physics, University of California, San Diego, La Jolla, CA, USA, [2] Department of Physics and Astronomy, California State University, Northridge, Northridge, CA, USA

How growth, the cell cycle, and cell size are coordinated is a fundamental question in biology. Recently, we and others have shown that bacterial cells grow by a constant added size per generation, irrespective of the birth size, to maintain size homeostasis. This "adder" principle raises a question as to when during the cell cycle size control is imposed. Inspired by this question, we examined our single-cell data for initiation size by employing a self-consistency approach originally used by Donachie. Specifically, we assumed that individual cells divide after constant C + D minutes have elapsed since initiation, independent of the growth rate. By applying this assumption to the cell length vs. time trajectories from individual cells, we were able to extract theoretical probability distribution functions for initiation size for all growth conditions. We found that the probability of replication initiation shows peaks whenever the cell size is a multiple of a constant unit size, consistent with the Donachie's original analysis at the population level. Our self-consistent examination of the single-cell data made experimentally testable predictions, e.g., two consecutive replication cycles can be initiated during a single cell-division cycle.

Keywords: cell size, adder principle, cell cycle, chromosome replication, critical initiation size, single-cell analysis

OPEN ACCESS

Edited by:
Jaan Männik, University of Tennessee, USA

Reviewed by:
Vic Norris, University of Rouen, France
Christine Jacobs-Wagner, The Howard Hughes Medical Institute, USA
Marco Cosentino Lagomarsino, University Pierre et Marie Curie, France

***Correspondence:**
Sattar Taheri-Araghi
sattar.taheri@csun.edu

Specialty section:
This article was submitted to Microbial Physiology and Metabolism, a section of the journal Frontiers in Microbiology

Received: *06 April 2015*
Accepted: *16 November 2015*
Published: *08 December 2015*

Citation:
Taheri-Araghi S (2015) Self-Consistent Examination of Donachie's Constant Initiation Size at the Single-Cell Level. Front. Microbiol. 6:1349. doi: 10.3389/fmicb.2015.01349

1. INTRODUCTION

The coordination between growth and the cell cycle is a fundamental aspect of cellular physiology. The classic work of Schaechter, Maaløe and Kjelgaard established the "growth law," which states that the average size of bacterial cells in steady-state growth condition scales exponentially with the respective average growth rate (Schaechter et al., 1958). This is one of the first quantitative principles in bacterial physiology. Another important quantitative principle is the bacterial cell cycle model, whose two cornerstone assumptions are (i) in balanced growth the duration of replication (C period) of *Escherichia coli* chromosome is constant independent of the growth condition and (ii) cell divides after a constant time (C + D period) has elapsed since replication initiation (Cooper and Helmstetter, 1968; Helmstetter, 1968; Cooper, 1969).

In an important work, Donachie studied the consequences of the growth law and the cell cycle model together (Donachie, 1968). He concluded that, if both models are correct, the size of the cell per origin at the moment replication is initiated should be constant for all growth conditions. Furthermore, if the two models are correct, then the growth law can be expressed using the measured C + D as

$$m(T) = m_0 2^{(C+D)/T}, \quad (1)$$

where m is the average cell size and T is average cell doubling time. In other words, Donachie was able to make experimentally testable predictions by self-consistently examining the relationship between two different assumptions. Furthermore, conversely, the predicted relationship can be used to estimate C + D using size m and the average doubling time T, which can be measured and tested independently. In Appendix A, we present another example of self-consistency check, i.e., by self-consistently combining the initiator model (Cooper, 1969; Helmstetter, 1969) and the cell cycle model, we can show that the growth law emerges.

In recent years, single-cell experiments have significantly improved our understanding of growth and cell-size control in bacteria [For a review see Taheri-Araghi et al. (2015b) and discussions therein]. Single-cell data reveal information about fluctuations, heterogeneity and correlations between measurable parameters, which are masked in population measurements. In particular, we and others have shown that bacteria employ an "adder" principle to maintain size homeostasis during steady-state growth (Campos et al., 2014; Taheri-Araghi et al., 2015a). That is, cells grow by a constant size from birth to division, irrespective of the birth size. This automatically ensures that deviations in cell-size are corrected within a few generations. The adder principle however raises an important issue of when during the cell cycle size control is imposed.

This work presents a single-cell version of Donachie's analysis to our data in Taheri-Araghi et al. (2015a). We assume that C + D is constant for all cells. Using this assumption, we retrace C + D minutes backward in time from each cell division to extract a hypothetical initiation size of individual cells. We then ask if these assumptions lead to constant initiation size at the single-cell level. We found that, if the C + D period is indeed constant for all cells, the constant initiation size is consistent with the adder principle at the single-cell level. Another prediction of our self-consistent analysis is that a cell can initiate two rounds of replication between birth and division. These predictions can be tested experimentally to verify the validity of the assumptions.

2. MATERIALS AND METHODS

2.1. Experimental Data on Growth and Division of *E. coli*

We used experimental data of cell length vs. time for seven different growth conditions for *E. coli* reported in Taheri-Araghi et al. (2015a). The media, average generation time, and average newborn size of cells are listed in **Table 1**. For the details of the experiments and growth media see Taheri-Araghi et al. (2015a) and its Supplementary Material. For the details of the single-cell growth experiment see Wang et al. (2010).

2.2. Retracing Length vs. Time Data to Infer Initiation Size

We apply the cell cycle model by Helmstetter and Cooper (Cooper and Helmstetter, 1968; Helmstetter, 1968; Cooper, 1969) to infer the initiation size. That is, we assume that individual cells initiate replication C + D minutes prior to cell division (**Figure 1A**). We estimate C + D self-consistently by fitting the population average size vs. growth data from Taheri-Araghi et al. (2015a) to Equation (1). The fitting outcome is that C + D = 69 min.

TABLE 1 | Name of the growth conditions, average generation time, and average cell size at birth.

Name of growth media	Generation time (minutes)	Size at birth (μm^3)
TSB	17.1	2.73
Synthetic Rich	22.5	1.64
Glucose+12 a.a.	26.7	1.04
Glucose+6 a.a.	30.2	0.80
Glucose	37.7	0.59
Sorbitol	50.8	0.46
Glycerol	51.3	0.42

Since we do not have direct experimental data on the actual fluctuations of C and D periods, we cannot quantify the error arising from the retracing method. However, we can add noise to C + D extracted by fitting data to Equation (1), and use it to check robustness of our conclusions. In Appendix B, we present a detailed discussion on the effect of noise in C + D. We find that the predictions of our analysis are robust to random fluctuations in the C and D periods, unless the added noise is larger than $\gtrsim$ 20% of the generation time (**Figure A2**).

We provide a final self-consistency check that our single-cell analysis agrees with the population level results in Appendix C.

3. RESULTS AND DISCUSSION

3.1. Distribution of Inferred Initiation Size Shows Distinct Peaks, Consistent with Donachie's Constant Initiation Size Model

We computed distributions of hypothetical initiation size by retracing the single-cell length vs. time data for seven different growth conditions (**Figure 1B**). All distributions showed peaks. An obvious question is whether these peaks are multiples of constant initiation size as Donachie inferred from population data. To answer this question, we overlaid the distributions (**Figure 1D**).

Indeed, we found that the peaks of the inferred initiation size distributions collapse onto each other, with the peak positions increase in exponent of 2 from the position of the left-most peak. We then calculated inferred initiation size per replication origin (**Figure 1E**). Distributions from various growth conditions collapse on each other in the form of single-peak distributions. This is consistent with the model that replication initiates whenever the cell size per origin reaches a constant critical size, regardless of the growth condition (Donachie, 1968; Pritchard, 1968). (In Appendix D we show how the number of replication origins is calculated.)

A prediction of our self-consistent analysis is the possibility of double initiations. For significant fractions of subpopulations of cells, retracing by constant C + D predicted two initiations

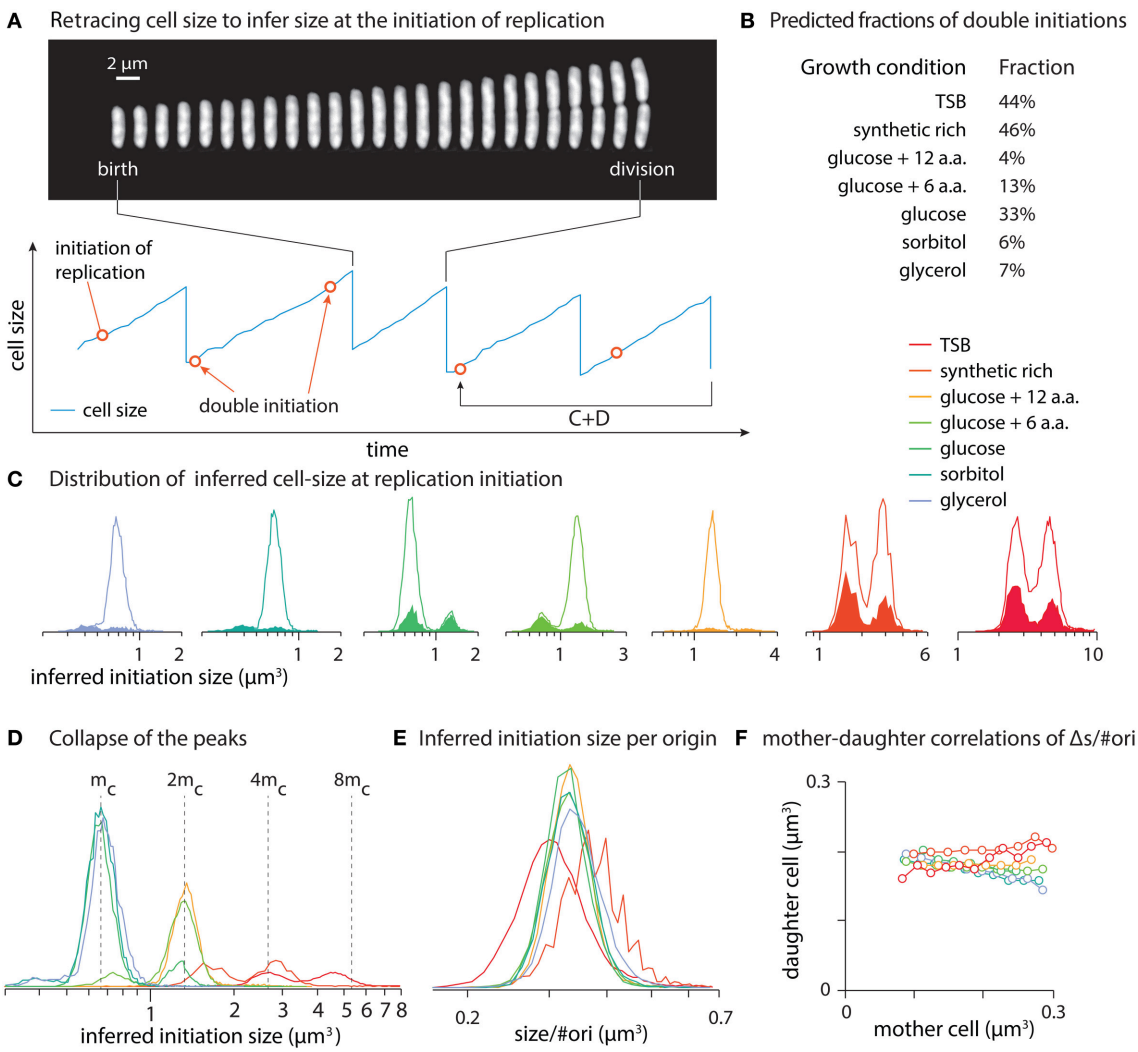

FIGURE 1 | (A) Retracing cell size C + D minutes prior to cell divisions to infer size at initiation of replication. Constancy of C + D predicts some cells have two initiations in one division cell cycle. **(B)** Fractions of initiations that occur in generations with double initiations. **(C)** Distributions of hypothetical initiation size can be bimodal. Each panel refers to one growth condition where filled area show the distribution of double initiations and solid lines show the distribution of all hypothetical initiation sizes. **(D)** The peaks of the distributions in C collapse onto each other. **(E)** Inferred initiation size per origin of replication from various growth condition collapse onto each other. **(F)** Mother-daughter correlations of $\Delta s/\#ori$ (growth per origin of replication), based on inferred initiation moments. Panel **(A)** is reproduced from Taheri-Araghi et al. (2015a) with permission from Elsevier.

separated by growth of a constant size per origin between them within a single generation (**Figures 1B–E**). This is not what is expected from the basic assumptions of the cell cycle control, which requires one-to-one correspondence between replication cycle and division cycle (Mitchison, 1971). Since this prediction seemingly violates a basic assumption, direct experimental test at the single-cell level will be important.

3.2. Conditions for Consistency of Constant (C + D) Model with Adder Principle

Another important question is whether the Helmstetter-Cooper model based on constant C + D is consistent with the adder principle. The organized pattern of inferred initiation size in **Figures 1D,E** can support such consistency. Unfortunately, with our current data we cannot answer whether replication starts at a critical size or after the cell grows for a constant size per origin from previous initiation. However, we can test if the constant C + D assumption and the adder principle are consistent by mother-daughter correlations. In **Figure 1F**, we show that there are no significant correlations between the mother and the daughter cells in terms of added size per origin ($\Delta s/\#ori$), as expected by the adder principle. That is, growth of the daughter cell by a constant $\Delta s/\#ori$ between initiation events is independent of the mother. Since $\Delta s/\#ori$ has been estimated by the constant C + D assumption, our analysis suggest that the two assumptions are mutually consistent.

Growth by a constant size per origin is consistent with the classic initiator model by Helmstetter and Cooper, stating that chromosome replication starts once the accumulation of initiators reach a critical threshold level (Cooper, 1969; Helmstetter, 1969). A feedback mechanism was proposed by Sompayrac and Maaloe (1973) to maintain initiator level proportional to cell size. We showed in Appendix A how the initiator and the cell cycle model by Helmstetter and Cooper can lead to the growth law.

While the initiator model seems plausible for the coordination of cell size and the replication cycle, there are experimental data that cannot be explained by the initiator model. For example, it has been shown that both an ectopic origin and the original wildtype origin initiate simultaneously without significant changes in growth kinetics (Wang et al., 2011). Another example is synchronous replication of minichromosomes that carry similar origin of replication in cells (Messer et al., 1978; Leonard and Helmstetter, 1986). In these examples, the relationship between size and number of origins do not follow the wild-type. At this point, we do not have sufficient experimental evidence to confirm the initiator model and the critical size for initiation and its link to the adder principle. Nevertheless, one way to reconcile a consistency between adder and constant C + D is to have an adder-like behavior for cell size at the initiation of chromosome replication.

3.3. Future Work

In this work, we applied Donachie's self-consistent analysis to the single cell data we reported recently. With the assumption that C + D is constant for individual cells, our analysis makes two predictions that can be directly tested experimentally in the future work: (i) double initiations of chromosome replication in one division cycle, and (ii) growth by a constant size between two consecutive replication initiations. Single-cell level test of these predictions will clarify whether our assumption of constancy of C + D is valid. Cell-size dependency or large fluctuations of C + D can change these predictions.

Several recent models discussed various size control routes in bacteria (Amir, 2014; Campos et al., 2014; Iyer-Biswas et al., 2014a,b; Kennard et al., 2014; Osella et al., 2014; Taheri-Araghi et al., 2015a). An interesting, unresolved question is how size control principles align with the cell cycle control. For a conclusive answer, we need direct experimental data on the progression of cell cycle in individual cells.

Finally, while adder principle appears general for all bacterial organisms tested so far, eukaryotes are not perfect adder (Jun and Taheri-Araghi, 2015). Further insights on the molecular mechanism of the adder principle can be gained through experimental tests in which we can perturb the perfect adder. Previously, perturbation of cell division machinery has been experimentally linked to variations of cell size (Weart et al., 2007; Chien et al., 2012; Hill et al., 2013). The timing of replication initiation was also linked to cell size, where *E. coli* mutants of smaller size delay initiation until they reach the appropriate initiation size (Hill et al., 2012). Interestingly, a modest over expression of DnaA-ATP can recover the replication initiation timing. We believe experiments on wild-type or size mutants in which the rate of accumulation of possible initiators can be temporarily decoupled from cell size (with overexpression or inhibition of their expression) will reveal valuable information on the regulation of cell size and the coordination of the cell cycle with cell size.

FUNDING

This work was supported by Paul G. Allen Foundation, the Pew Charitable Trusts, and the National Science Foundation CAREER Award (MCB-1253843) to Suckjoon Jun.

ACKNOWLEDGMENTS

This work was accomplished under guidance of Suckjoon Jun. The theoretical tools and analysis were developed through discussions with members of the Jun Lab in the University of California, San Diego. We thank Massimo Vergassola, Terrence Hwa, Steven D. Brown, and John T. Sauls for critical reading of the manuscript and stimulating discussions.

REFERENCES

Amir, A. (2014). Cell size regulation in bacteria. *Phys. Rev. Lett.* 112, 208102. doi: 10.1103/PhysRevLett.112.208102

Campos, M., Surovtsev, I. V., Kato, S., Paintdakhi, A., Beltran, B., Ebmeier, S. E., et al. (2014). A constant size extension drives bacterial cell size homeostasis. *Cell* 159, 1433–1446. doi: 10.1016/j.cell.2014.11.022

Chien, A. C., Hill, N. S., and Levin, P. A. (2012). Cell size control in bacteria. *Curr. Biol.* 22, R340–R349. doi: 10.1016/j.cub.2012.02.032

Cooper, S. (1969). Cell division and DNA replication following a shift to a richer medium. *J. Mol. Biol.* 43, 1–11. doi: 10.1016/0022-2836(69)90074-6

Cooper, S., and Helmstetter, C. E. (1968). Chromosome replication and the division cycle of *Escherichia coli* B/r. *J. Mol. Biol.* 31, 519–540. doi: 10.1016/0022-2836(68)90425-7

Donachie, W. D. (1968). Relationship between cell size and time of initiation of DNA replication. *Nature* 219, 1077. doi: 10.1038/2191077a0

Helmstetter, C. E. (1969). "Regulation of chromosome replication and cell division in *Escherichia coli*," in *The Cell Cycle,* eds G. M. Padilla, G. L. Whitson, and I. L. Cameron (New York, NY; London: Academic Press), 15–35.

Helmstetter, C. E. (1968). DNA synthesis during the division cycle of rapidly growing *Escherichia coli* B/r. *J. Mol. Biol.* 31, 507–518. doi: 10.1016/0022-2836(68)90424-5

Hill, N. S., Buske, P. J., Shi, Y., and Levin, P. A. (2013). A moonlighting enzyme links *Escherichia coli* cell size with central metabolism. *PLoS Genet.* 9:e1003663. doi: 10.1371/journal.pgen.1003663

Hill, N. S., Kadoya, R., Chattoraj, D. K., and Levin, P. A. (2012). Cell size and the initiation of DNA replication in bacteria. *PLoS Genet.* 8:e1002549. doi: 10.1371/journal.pgen.1002549

Iyer-Biswas, S., Crooks, G. E., Scherer, N. F., and Dinner, A. R. (2014a). Universality in stochastic exponential growth. *Phys. Rev. Lett.* 113, 028101. doi: 10.1103/PhysRevLett.113.028101

Iyer-Biswas, S., Wright, C. S., Henry, J. T., Lo, K., Burov, S., Lin, Y., et al. (2014b). Scaling laws governing stochastic growth and division of single bacterial

cells. *Proc. Natl. Acad. Sci. U.S.A.* 111, 15912–15917. doi: 10.1073/pnas.1403232111

Jun, S., and Taheri-Araghi, S. (2015). Cell-size maintenance: universal strategy revealed. *Trends Microbiol.* 23, 4–6. doi: 10.1016/j.tim.2014.12.001

Kennard, A. S., Osella, M., Javer, A., Grilli, J., Nghe, P., Tans, S., et al. (2014). Individuality and universality in the growth-division laws of single *E. coli* cells. ArXiv :1411.4321.

Leonard, A., and Helmstetter, C. E. (1986). Cell cycle-specific replication of *Escherichia coli* minichromosomes. *Proc. Natl. Acad. Sci. U.S.A.* 83, 5101–5105. doi: 10.1073/pnas.83.14.5101

Messer, W., Bergmans, H. E., Meijer, M., Womack, J. E., Hansen, F. G., and von Meyenburg, K. (1978). Mini-chromosomes: plasmids which carry the *E. coli* replication origin. *Mol. Gen. Genet.* 162, 269–275. doi: 10.1007/BF00268852

Mitchison, J. (1971). *The Biology of the Cell Cycle*. Cambridge, UK: Cambridge University Press.

Osella, M., Nugent, E., and Cosentino Lagomarsino, M. (2014). Concerted control of *Escherichia coli* cell division. *Proc. Natl. Acad. Sci. U.S.A.* 111, 3431–3435. doi: 10.1073/pnas.1313715111

Pritchard, R. H. (1968). Control of DNA synthesis in bacteria. *Heredity* 23, 467–476.

Schaechter, M., Maaløe, O., and Kjeldgaard, N. O. (1958). Dependency on medium and temperature of cell size and chemical composition during balanced growth of *Salmonella typhimurium*. *J. Gen. Microbiol.* 19, 592–606. doi: 10.1099/00221287-19-3-592

Sompayrac, L., and Maaloe, O. (1973). Autorepressor model for control of DNA replication. *Nat. New Biol.* 241, 133–135. doi: 10.1038/newbio241133a0

Taheri-Araghi, S., Bradde, S., Sauls, J. T., Hill, N. S., Levin, P. A., Paulsson, J., et al. (2015a). Cell-size control and homeostasis in bacteria. *Curr. Biol.* 25, 385–391. doi: 10.1016/j.cub.2014.12.009

Taheri-Araghi, S., Brown, S. D., Sauls, J. T., McIntosh, D. B., and Jun, S. (2015b). Single-cell physiology. *Annu. Rev. Biophys.* 44, 123–142. doi: 10.1146/annurev-biophys-060414-034236

Wang, P., Robert, L., Pelletier, J., Dang, W. L., Taddei, F., Wright, A., et al. (2010). Robust growth of *Escherichia coli*. *Curr. Biol.* 20, 1099–1103. doi: 10.1016/j.cub.2010.04.045

Wang, X., Lesterlin, C., Reyes-Lamothe, R., Ball, G., and Sherratt, D. J. (2011). Replication and segregation of an *Escherichia coli* chromosome with two replication origins. *Proc. Natl. Acad. Sci. U.S.A.* 108, E243–E250. doi: 10.1073/pnas.1100874108

Weart, R. B., Lee, A. H., Chien, A.-C., Haeusser, D. P., Hill, N. S., and Levin, P. A. (2007). A metabolic sensor governing cell size in bacteria. *Cell* 130, 335–347. doi: 10.1016/j.cell.2007.05.043

Conflict of Interest Statement: The author declares that the research was conducted in the absence of any commercial or financial relationships that could be construed as a potential conflict of interest.

Copyright © 2015 Taheri-Araghi. This is an open-access article distributed under the terms of the Creative Commons Attribution License (CC BY). The use, distribution or reproduction in other forums is permitted, provided the original author(s) or licensor are credited and that the original publication in this journal is cited, in accordance with accepted academic practice. No use, distribution or reproduction is permitted which does not comply with these terms.

APPENDIX A

Consistency Between the Initiator Model, Growth Law and Critical Initiation Size

In this appendix we model a nutrient shift experiment where the timing of the initiation of chromosome replication and, thus, cell divisions are calculated based on the initiator model proposed and tested by Helmstetter and Cooper (Cooper, 1969; Helmstetter, 1969). We derive an analytical solution for cell size and the cell cycle of bacteria that experience a nutrient shift. From that, we show that the growth law and the critical size model emerge from the initiator model.

Below is the list of the assumptions of the model:

- Chromosome replication initiates once the initiators accumulate to a critical level. When a round of replication starts, initiators get destroyed.
- There is a constant time gap, $C+D$, between each initiation of replication and cell division.
- During steady-state and nutrient-shift the timing of initiations of replication are given by:
  - (i) In steady-state: period of initiators accumulation up to the threshold is T, equivalent to cells' generation time.
  - (ii) During nutrient shift from doubling times T_1 to T_2: If shift occurs at t_1 minutes after the last initiation, next initiation happens at t_1+t_2, where $t_1/T_1+t_2/T_2 = 1$ (Cooper, 1969).
- The cell grows exponentially and the size increase rate changes promptly upon a nutrient shift.

To begin with, consider a cell growing in steady-state condition with doubling time T_1. At time T_s after a division, the nutrient condition changes. The new condition imposes an eventual doubling time of T_2 in the final steady-state. Here we choose the reference of the time, $t = 0$, the birth of the cell in which nutrient shift happened (**Figure A1**). Thus, nutrient shift happens at $t = T_s$ during a cell cycle that the cell was expected to divide at $t = T_1$. The time of planned division at T_1 can change or remain unchanged depending on the timing of T_s with respect to rounds of chromosome replications. We take three steps to proceed with the calculation:

(i) We find the timing of initiations of chromosome replication, both before nutrient shift and after nutrient shift.
(ii) From the timing of replication initiations, we find timing of cell divisions, assuming every initiation results in a cell division after $C + D$ minutes.
(iii) From the timing of cell division we calculate cell size considering that size increases exponentially with a rate instantaneously proportional to nutrient condition.

Since multiple cell cycles can overlap in bacteria, we assume at the time of nutrient shift, T_s, there are n cell cycles overlapping ($n = 0, 1, 2, ...$). The case $n = 0$ refers to the cells in slow growth condition if nutrient shift happens in the gap between the birth and initiation of chromosome replication (B period). There is a relationship between n, T_1, T_s, and $C + D$, the shorter the T_1 the larger the n can be. Also, n can vary depending on when the nutrient shift happens during the cell cycle. Without loss of generality, we choose not to elaborate further on this relationship as the final results can be expressed in terms of T_1, T_2, and $C+D$.

Timing of Chromosome Replications

Since there is a one-to-one correspondence between initiation of replication and cell division, the time gap between the n rounds of ongoing cell cycles at $t = T_s$ must be the generation time in the pre-shift condition, T_1. As the first cell division after $t = 0$ was scheduled at T_1, the "oldest" of the n overlapping cell cycles must have started at $T_1 - (C + D)$. The rest of them started every T_1 minutes thereafter. The initiation times of these n cell cycles are, thus, the following series:

$$T_1 - (C + D), 2T_1 - (C + D), ..., nT_1 - (C + D). \quad \text{(A1)}$$

Let's consider the next chromosome replication (the first after nutrient shift) starts at $t = T_r$, which depends on both time of nutrient shift, T_s, and generation time in the second growth condition, T_2. Next rounds of replication after T_r initiate every T_2 minutes. Thus, the timing of replication initiation after the nutrient shift is simply:

$$T_r, T_r + T_2, T_r + 2T_2, ... \quad \text{(A2)}$$

The time T_r can be calculated based on the third assumption of the model that we discussed earlier. Until the moment of nutrient shift, T_s, initiators have been accumulating since the start of the last round of replication, $t = nT_1-(C+D)$, with the rate of $1/T_1$. [e.g., $3T_1 - (C + D)$ in **Figure A1**] From $t = T_s$ until $t = T_r$, initiators accumulate at rate $1/T_2$. The following equation can be solved for T_r,

$$\frac{1}{T_1}\left[T_s - nT_1 + (C + D)\right] + \frac{1}{T_2}(T_r - T_s) = 1, \quad \text{(A3)}$$

which yields

$$T_r = (n + 1)T_2 + T_s - \frac{T_2}{T_1}(T_s + C + D). \quad \text{(A4)}$$

Timing of Cell Divisions

Each initiation of chromosome replication leads to a cell division after a time gap of $(C + D)$. From Equations (A1) and (A2) and **Figure A1**, the cell division times from ongoing cell cycles and the ones starting after nutrient shift are:

$$\underbrace{T_1, 2T_1, ..., (n-1)T_1, nT_1,}_{\text{divisions from ongoing cell cycles}}$$
$$\underbrace{T_r + (C + D), T_r + (C + D) + T_2, T_r + (C + D) + 2T_2, ...}_{\text{divisions from cell cycles that start after nutrient shift}} \quad \text{(A5)}$$

Cell-Size after the Nutrient Shift

Let's consider $m(T_1)$ denotes the newborn cell size during steady-state growth with generation time T_1. We aim to calculate $m(T_2)$,

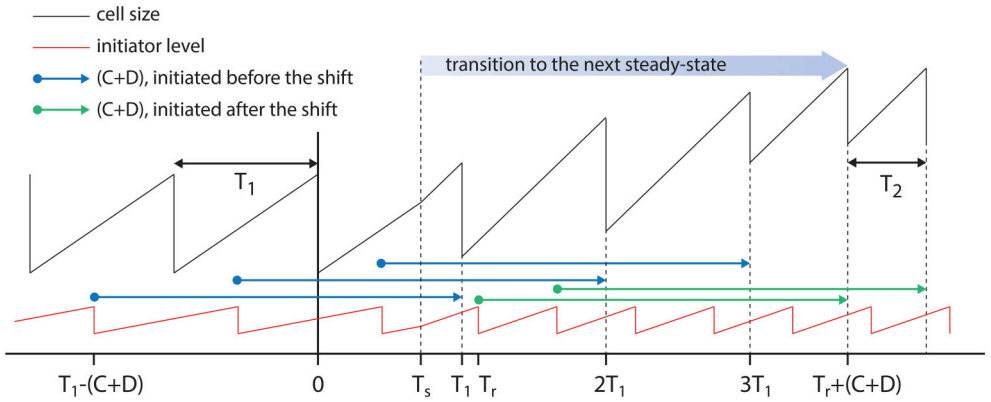

FIGURE A1 | Cell cycle and nutrient shift. Here $n = 3$ cell cycles overlap at the moment of nutrient shift, $t = T_S$. In this example $T_1 > T_2$ and thus $m(T_1) < m(T_2)$. The three rounds of cell cycle started before nutrient shift lead to divisions at T_1, $2T_1$, and $3T_1$ (blue arrows). The first initiation of replication after the nutrient shift, sets up the start of the new steady-state (green arrows starting at T_r).

the newborn cell size at steady-sate with generation time T_2. Cells reach steady-state after the division at $T_r + (C + D)$, where the gap between cell divisions is T_2 and the size increase rate is $1/T_2$. Thus, the cell size after that division is the newborn cell-size in the new steady state, $m(T_2)$.

From $t = 0$ until $t = T_s$ cell size increases exponentially with rate $1/T_1$ (pre-shift rate). Upon nutrient shift, the rate of cell size increase changes instantaneously to $1/T_2$. The division at $t = T_r + (C + D)$ (corresponding to start of the new steady-state) is the $(n+1)th$ division after $t = 0$ (see Equation A5). Thus, the newborn cell size is given by

$$m(T_2) = \frac{1}{2^{n+1}} m(T_1) 2^{T_s/T_1} \times 2^{(T_r+C+D-T_s)/T_2}, \qquad \text{(A6)}$$

where the first factor on the right-hand-side counts $(n + 1)$ divisions, the second term refers to the growth from birth at $t = 0$ until nutrient shift at $t = T_s$, and the third accounts for the size increase from the nutrient shift, $t = T_s$, until division at $t = T_r + C + D$.

Substituting T_r from Equation (A4) in Equation (A6), we get

$$m(T_2) = m(T_1) 2^{-(C+D)/T_1} \times 2^{(C+D)/T_2} \qquad \text{(A7)}$$

Equation (A7) denotes that if cells grow in any steady-state condition with generation time T, newborn cell size is exponentially related to T,

$$m(T) = m_\circ 2^{(C+D)/T}. \qquad \text{(A8)}$$

This is the growth law (Schaechter et al., 1958), with the exponent being $(C + D)$ if the relationship presented in the base of two. The exponent is consistent with Donachie's constant size at initiation of chromosome replication, as we elaborate below.

Cell-Size at Initiation of Replication

Consider that cells growing in a steady-state condition with generation time T and that up to N cell cycles overlap $(N = 1, 2, 3...)$. That means from an initiation of chromosome replication until the cell division (this corresponds to a gap of $(C + D)$) we have N cell division events. For slowest growth conditions where cell cycles do not overlap we have $N = 1$. If $m_c(T)$ refers to cell size at which initiation occurs, the newborn cell size after the corresponding cell division is

$$\frac{1}{2^N} m_c(T) 2^{(C+D)/T} = m(T), \qquad \text{(A9)}$$

where the first factor accounts for N divisions and the rest accounts for growth for $(C+D)$ minutes. Substituting $m(T)$ from Equation (A8), we obtain

$$m_c(T) = 2^N m_\circ. \qquad \text{(A10)}$$

Since 2^N is the total number of replication forks when N cell cycle overlap, Equation (A10) shows that cell size per origin of replication at the initiation of replication is constant, independent of growth condition. This is the Donachie's observation in 1968 by combining the growth law and Helmstetter-Cooper model.

APPENDIX B

Noise and Uncertainty in Retracing Analysis

One may question the effect of noise in C + D in retracing analysis and the extent it influences the distributions reported in **Figure 1**. The retracing analysis has an intrinsic "reading error." Since we do not have experimental data on the fluctuations of the durations of C and D periods for individual cells, we cannot completely avoid or quantify this reading error. However, in this appendix we present how we can choose a constant C + D to minimize the error. Here, we show that adding any noise to retracing time, C + D, merely adds *extra* reading error and does not capture actual fluctuations of C and D periods.

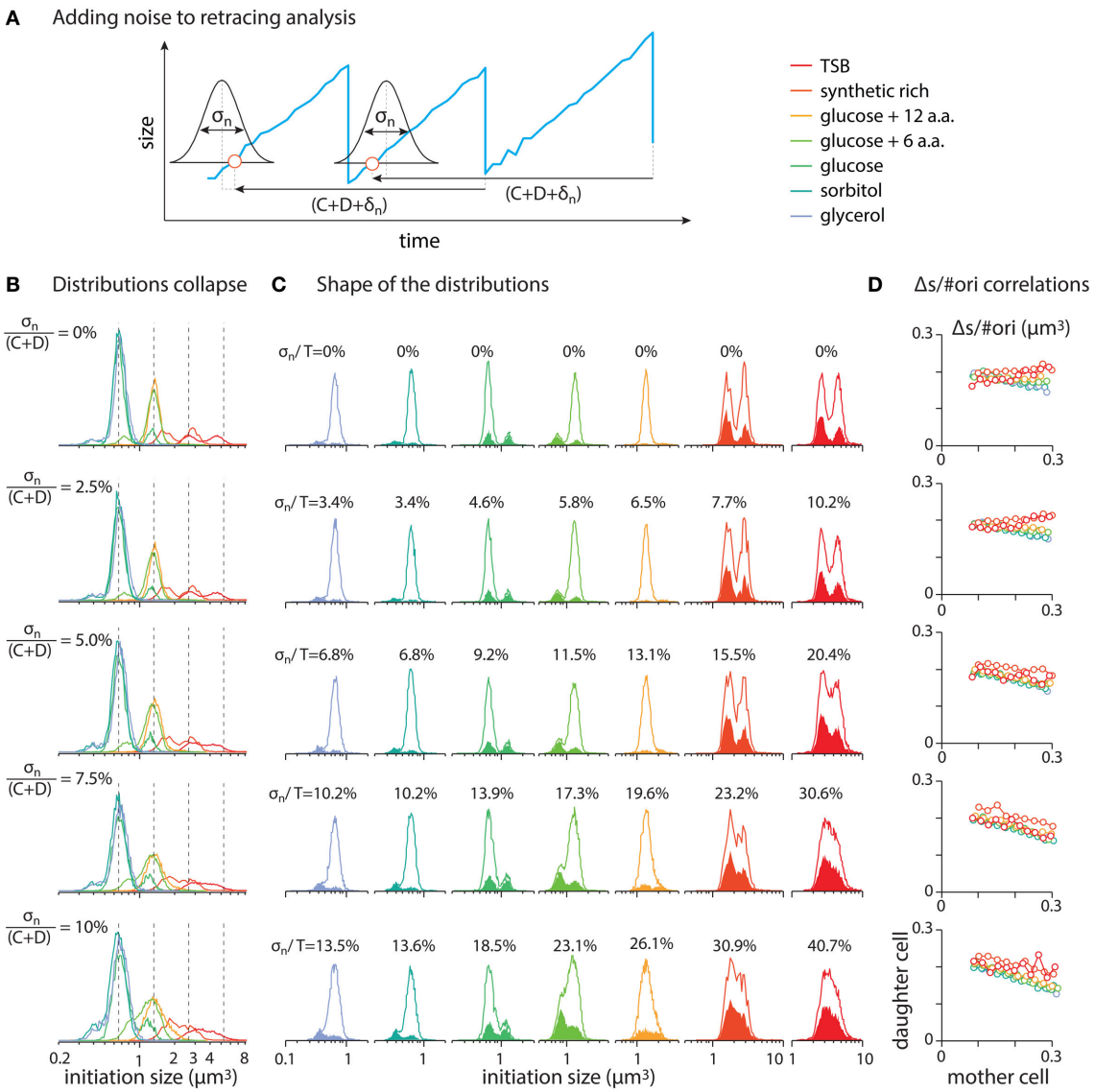

FIGURE A2 | (A) To test the effect of noise in the analysis, a Gaussian noise δ_n with standard deviation of standard deviation of σ_n is added to the retracing time. **(B)** Various levels of noise is tested with standard deviations, σ_n, chosen at 0, 2.5, 5, 7.5, and 10% of C + D. **(C)** Solid lines refer to the distribution from whole cell population and filled area refer to cells with double initiations in a division cycle. Standard deviation, σ_n, in each row is the same as the one in the corresponding row in **(B)**. The ratio of the standard deviations, σ_n, to the average doubling time, T, is noted on the left side of each sub panel. **(D)** Mother-daughter correlations of $\Delta s/\#ori$ with noise added in retracing.

There are two different points that should not be mixed:

(i) The actual fluctuations in C and D periods.
(ii) The noise that can be possibly added to retracing time, C + D.

The reading error, defined as the difference between the actual moment of initiation and the inferred moment, is a result of the combination of (i) and (ii). Regarding the point (i), we believe that there are fluctuations in C and D periods. However, to date, we do not have any experimental data measuring and addressing these fluctuations at a single-cell level. Regarding the point (ii), retracing is an indirect method of estimating initiation time and size. Adding noise to retracing time can test the extent the outcome is robust with respect to noise.

Let's consider the actual fluctuations of C + D periods (combined) have the standard deviation of σ_a. In the case that we do not include noise in retracing time, the inferred readings miss these actual fluctuations. Thus, the readings error has the standard deviation of σ_a as well. Now consider that we add a noise in retracing time such that initiation times are estimated C + D + δ_n prior to cell divisions. Here δ_n is a stochastic variable. Let's assume the standard deviation of (C + D + δ_n) is σ_n. The noise δ_n is independent of fluctuations in C and D periods. Thus, this

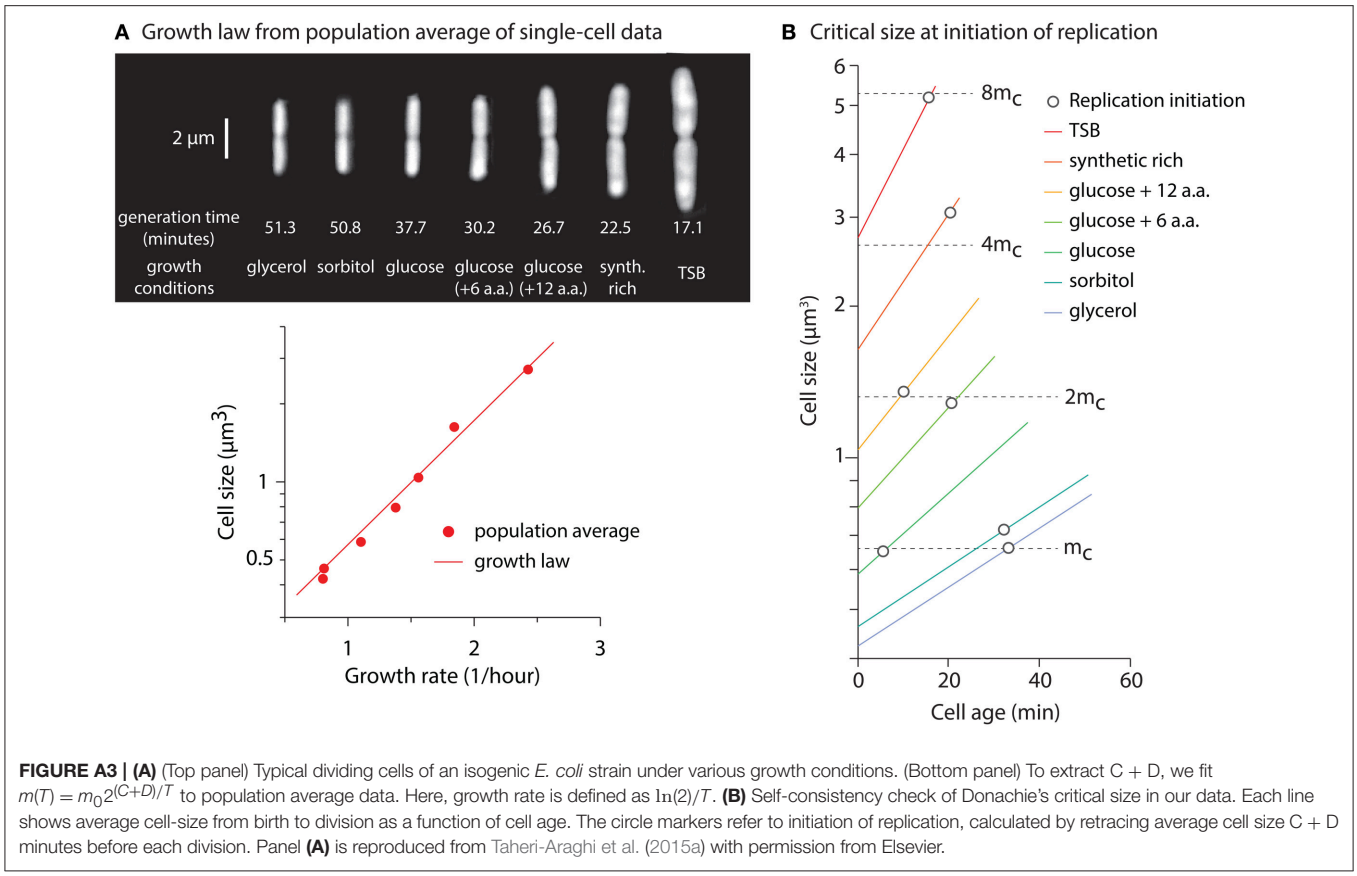

FIGURE A3 | (A) (Top panel) Typical dividing cells of an isogenic *E. coli* strain under various growth conditions. (Bottom panel) To extract C + D, we fit $m(T) = m_0 2^{(C+D)/T}$ to population average data. Here, growth rate is defined as $\ln(2)/T$. **(B)** Self-consistency check of Donachie's critical size in our data. Each line shows average cell-size from birth to division as a function of cell age. The circle markers refer to initiation of replication, calculated by retracing average cell size C + D minutes before each division. Panel **(A)** is reproduced from Taheri-Araghi et al. (2015a) with permission from Elsevier.

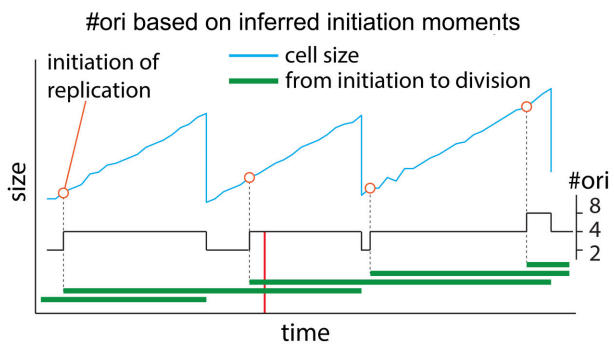

FIGURE A4 | Number of origins of replication, #*ori*, based on inferred initiation moments. If *N* replication cycles overlap at any time point (green horizontal lines in the graph) during cell cycle, the total number of origins at that time point is $\#ori = 2^N$.

type of noise does not capture the actual fluctuations, but only adds more uncertainty to the reading of inferred initiation size and time.

If both actual fluctuations of C + D and added noise are Gaussian, we can calculate the standard deviation of the reading error. If the actual initiation points happen $(C + D + \delta_a)$ prior to cell divisions, the retracing analysis reads those initiations at $(C + D + \delta_n)$. (δ_a and δ_n are independent stochastic variables). Thus, the reading error is given by:

$$error = (C + D + \delta_n) - (C + D + \delta_a). \quad (A11)$$

Since δ_n and δ_a are independent Gaussian variables, the standard deviation of the error is given by

$$\sigma^2_{error} = \sigma^2_n + \sigma^2_a. \quad (A12)$$

Therefore, to minimize the error in retracing analysis, we should minimize the noise in $C + D + \delta_n$ in the analysis. For this reason using a constant C + D is a better choice for this study.

To visualize the effect of noise in the analysis, we added Gaussian noise in retracing time and tracked the changes in the distributions of the inferred initiation sizes. As expected, the noise widens the distributions and beyond certain points, it influences the bimodal shape of the distributions. Various levels of noise is tested with standard deviations, σ_n, chosen at 0%, 2.5%, 5%, 7.5%, and 10% of C + D. **Figure A2B**, shows distributions of the initiation size for various level of noise, as noted on the left side of each panel.

Figure A2C depicts the distributions of inferred initiation size for individual growth conditions. The solid lines in each panel refer to the distributions from whole cell population and the filled area refer to cells with double initiations in

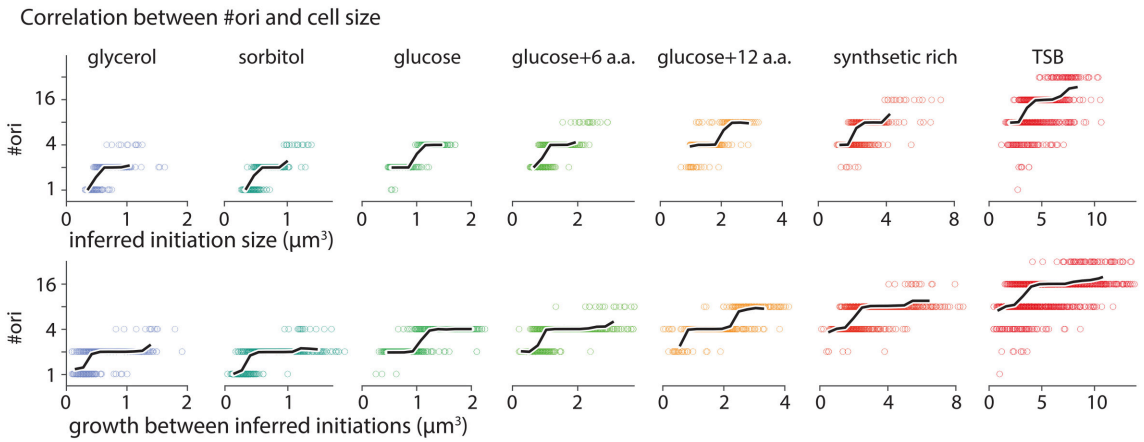

FIGURE A5 | Correlation between *#ori* and cell size. Number of origins, *#ori*, as a function of cell size at inferred initiation points (top panels) and as a function of growth between two consecutive initiations (bottom panel). *#ori* is a discrete parameter taking only values in exponents of two (*#ori* = 1, 2, 4,...). However, it shows a positive correlation with cell size. Black lines present *average* *#ori* as a function of inferred initiation size and growth between replication initiations.

one division cycle. The level of noise, σ_n, in each row of **Figure A2C** is the same as the one in the corresponding row in **Figure A2B**. The numbers on top of each distribution show the ratio of the standard deviation, σ_n, of the noise to the average doubling time in each growth condition, σ_n/T. For noises with $\sigma_n/T \gtrsim 20\%$, the widening of the distributions are such that peaks of the bimodal distributions start to overlap. However, the prediction of double initiations are robust with respect to the shape of the distributions (see filled area in panels of **Figure A2C**).

In **Figure A2D**, we show the effect of added noise in the mother-daughter correlations of $\Delta s/\#ori$. We do not see significant correlations between mother and daughter cells. However, at high level of added noise, the correlations tends to slightly tilt toward negative values since a random noise affects the value of $\Delta s/\#ori$ oppositely in two consecutive generations.

In conclusion, for the retracing analysis used in this work, a constant value for retracing time C + D minimizes the analysis error. Our test on the distributions of the inferred initiation cell size shows that the shape of distributions are more or less conserved if the noise in the retracing time is up to $\sim$ 20% of the generation time. Beyond this threshold the shape of the distributions start to change.

APPENDIX C

Consistency Check between Population Average and Single-Cell Analysis

In this appendix, we reproduce the Donachie's analysis on the *average* cell-size data from our single-cell measurements. To this end, we use C + D extracted from fitting average data to Equation (1) (**Figure A3A**), where C + D = 69 min. As expected, applying retracing analysis reproduces Donachie's critical size model (**Figure A3B**). This analysis is solely for a secondary self-consistency check of critical size model on our single-cell data (i.e., given the method used here, we do not expect any result otherwise).

Figure A3B shows cell size from birth to division as a function of cell age for seven different growth conditions. The circle markers refer to the moment of the replication initiation. Since C + D is longer than the generation times for the growth conditions in the study, each initiation size essentially refers to cell size in previous generations. The initiation size of different growth conditions can be clustered such that the initiation size per replication origin is constant and independent of growth condition. For the slowest condition, $m_c = 0.66\,\mu m^3$ and for the rest, critical initiation size increases by factors of two [1].

APPENDIX D

Calculating Number of Origin of Replication Based on Initiation Times

Based on inferred moments of initiation, one can mathematically calculate the number of origins during the cell cycle. A graphical example is presented in **Figure A4**. The graph shows cell size and the inferred moments of initiation as a function of time. The horizontal green lines show replication cycles from initiation of replications until the corresponding cell divisions. In slowest growth conditions, where we have either zero or one replication cycle going on in the cell ($N = 0$ or 1), we know that $\#ori = 1$ or 2 (not shown in the figure). In fast growth conditions, N (>1) replication cycles can overlap. At any initiation of replication, number of overlapping cell cycles, N, increases by one and number of origins of replication, *#ori*, increases by a factor of two. At any cell division, number of overlapping cell cycles, N, decreases by one and *#ori* decreases by a factor of two. Thus, since

[1] As a consistency check we can also extract $m_\circ$ from **Figure A3A** using Equation (1) and compare it with m_c through Equation (A10). We find $m_\circ = 0.168\mu m^3$. In the slowest condition in the study, $N = 2$ cell cycles overlap. $m_c = 0.66\mu m^3 \sim 2^2 m_\circ$. This agrees with Equation (A10) that states $m_c = 2^N m_\circ$.

for $N = 0$, $\#ori = 1$ and for $N = 1$, $\#ori = 2$ and since increasing N by one increases *#ori* by a factor of two, we conclude if N replication cycles overlap at any moment, *#ori* at that moment is given by $\#ori = 2^N$. For instance, at the moment shown with the red vertical line in **Figure A4**, $N = 2$ replication cycles overlap (two horizontal green lines cross the red line). Thus, the total number of *#ori* at that moment is $2^N = 4$. This can be applied to any moment throughout the cell cycle to calculate *#ori* as a function of time.

To examine correlation between *#ori* and cell size, we plotted *#ori* calculated at inferred initiation points as a function of initiation cell size (**Figure A5** top panels) and as a function of growth between initiations (**Figure A5** bottom panels). *#ori* is a discrete quantity taking only values in exponents of two (*#ori* =1, 2, 4,...). There is, however, a positive overall correlation between computed *#ori* and cell size as depicted by black lines in each panel of **Figure A5** (black lines show *average #ori* as a function of corresponding size or growth). The positive correlation arises from the fact that size and generation time are negatively correlated and that shorter generation time results in more overlapping replication cycles, thus larger *#ori*. The parameter $\Delta s/\#ori$ that is used in **Figure 1F** is calculated based on growth between inferred initiation points per *#ori* during that growth period.

Advantages of publishing in Frontiers

OPEN ACCESS
Articles are free to read, for greatest visibility

COLLABORATIVE PEER-REVIEW
Designed to be rigorous – yet also collaborative, fair and constructive

FAST PUBLICATION
Average 85 days from submission to publication (across all journals)

COPYRIGHT TO AUTHORS
No limit to article distribution and re-use

TRANSPARENT
Editors and reviewers acknowledged by name on published articles

SUPPORT
By our Swiss-based editorial team

IMPACT METRICS
Advanced metrics track your article's impact

GLOBAL SPREAD
5'100'000+ monthly article views and downloads

LOOP RESEARCH NETWORK
Our network increases readership for your article

Frontiers
EPFL Innovation Park, Building I • 1015 Lausanne • Switzerland
Tel +41 21 510 17 00 • Fax +41 21 510 17 01 • info@frontiersin.org
www.frontiersin.org

Find us on